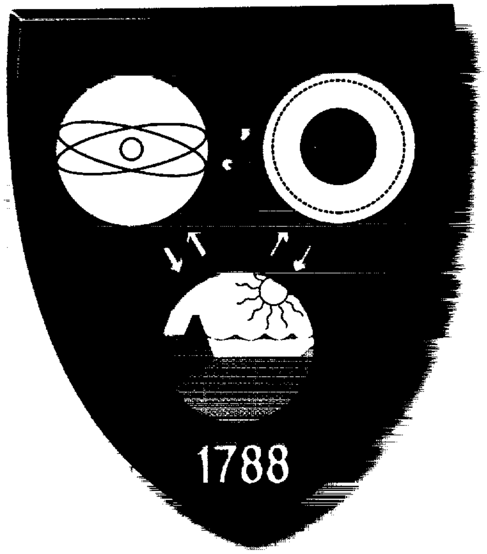

Ninth Annual V. M. Goldschmidt Conference

Harvard University
Cambridge, Massachusetts

August 22–27, 1999

Ninth Annual
V. M. Goldschmidt Conference

August 22–27, 1999

Harvard University
Cambridge, Massachusetts

Hosted by

Department of Earth and Planetary Sciences
Harvard University

Sponsored by

Geochemical Society
European Association of Geochemistry
Lunar and Planetary Institute
Harvard University
National Aeronautics and Space Administration

Lunar and Planetary Institute 3600 Bay Area Boulevard Houston TX 77058-1113

LPI Contribution No. 971

Compiled in 1999 by
LUNAR AND PLANETARY INSTITUTE

The Institute is operated by the Universities Space Research Association under Contract No. NASW-4574 with the National Aeronautics and Space Administration.

Material in this volume may be copied without restraint for library, abstract service, education, or personal research purposes; however, republication of any paper or portion thereof requires the written permission of the authors as well as the appropriate acknowledgment of this publication.

Abstracts in this volume may be cited as

Author A. B. (1999) Title of abstract. In *Ninth Annual V. M. Goldschmidt Conference*, p. XX. LPI Contribution No. 971, Lunar and Planetary Institute, Houston.

This volume is distributed by

ORDER DEPARTMENT
Lunar and Planetary Institute
3600 Bay Area Boulevard
Houston TX 77058-1113, USA
Phone: 281-486-2172
Fax: 281-486-2186
E-mail: order@lpi.jsc.nasa.gov

Mail order requestors will be invoiced for the cost of shipping and handling.

Preface

This volume contains abstracts that have been accepted for presentation at the Ninth Annual V. M. Goldschmidt Conference, August 22–27, 1999, hosted by the Department of Earth and Planetary Sciences, Harvard University, Cambridge, Massachusetts. The program committee consisted of C. Agee *(NASA Johnson Space Center),* T. Bowers *(Gradient Corporation),* S. Bowring *(Massachusetts Institute of Technology),* F. Frey *(Massachusetts Institute of Technology),* J. Hayes *(Woods Hole Oceanographic Institution),* H. Holland *(Harvard University),* S. Jacobsen *(Harvard University),* W. McDonough *(Harvard University),* R. Murray *(Boston University),* R. Rudnick *(Harvard University),* N. Shimizu *(Woods Hole Oceanographic Institution),* D. Schrag *(Harvard University),* and M. VanBaalen *(Harvard University).*

Administration and publication support for this meeting were provided by the staff of the Publications and Program Services Department at the Lunar and Planetary Institute.

Contents

Quantifying Precambrian Crustal Extraction: The Root is the Answer
D. Abbott, D. Sparks, C. Herzberg, W. Mooney, A. Nikishin, and Y. Zhang 1

Amphibole-veined Lithospheric Mantle Sources for Recent Alkaline Basalts in the Northern Canadian Cordillera
A.-C. Abraham, D. Francis, and M. Polvé 1

Stable Isotopes in Deep-Sea Corals: A New Mechanism for "Vital Effects"
J. Adkins, E. Boyle, and W. Curry 2

The Solubility of Iron-Magnesium Chlorite in Hydrothermal Solutions
S. U. Aja 2

Highly Siderophile Elements in Mantle Sulfides: *In Situ* Laser Ablation Microprobe Inductively Coupled Plasma Mass Spectrometry Analysis
O. Alard, W. L. Griffin, J. P. Lorand, S. Jackson, and S. Y. O'Reilly 3

The Early Evolution of the Earth and Mars from Hafnium-Neodymium-Isotopic Systematics
F. Albarède, J. Blichert-Toft, J. D. Vervoort, J. Gleason, and M. T. Rosing 3

Ion Probe Micrometer Scale Stable Isotopic Ratios of Aerosol Microparticles
J. Aléon, M. Chaussidon, and B. Marty 4

Spherical Fly-Ash Particles as Markers for Contemporary Deposition of Atmospheric Pollutants
T. Alliksaar 4

Soluble Salts in Pathologies of Granitic Monuments of Braga (Northwestern Portugal)
C. A. S. Alves and M. A. Sequeira Braga 5

Characterization of Saline Pollution Affecting the Angra Do Heroísmo Cathedral: A Trachytic Monument of Terceira Island (Azores-Portugal)
C. A. S. Alves, M. A. Sequeira Braga, and A. Trancoso 6

The Osmium-Isotopic Message in the Lesser Antilles Arc Lavas
S. Alves, P. Schiano, and C. J. Allègre 6

Vertical and Horizontal Distributions of Neodymium-isotopic Ratio of the Northwestern Pacific, Sea of Okhotsk, and Japan Sea
H. Amakawa, D. S. Alibo, and Y. Nozaki 7

Opal as a Uranium-Lead Geochronometer
Yu. Amelin and L. A. Neymark 8

Lutetium-Hafnium and Uranium-Lead Systematics of Early-Middle Archean Single Zircon Grains
Yu. Amelin, D.-C. Lee, and A. N. Halliday 8

The Extraterrestrial Mass Flux on the Early Earth
A. D. Anbar, G. L. Arnold, S. J. Mojzsis, and K. J. Zahnle 9

Iron-isotopic Fractionation Studies Using Multiple Collector Inductively Coupled Plasma Mass Spectrometry
A. D. Anbar, C. Zhang, J. Barling, J. E. Roe, and K. H. Nealson 10

Particle-mediated Surface Water Export: Comparison of Estimates from Uranium-238–Thorium-234 Disequilibria and Sediment Traps in a Continental Shelf Region
P. S. Andersson, Ö. Gustafsson, P. Roos, D. Broman, and A. Toneby 10

Potassium-rich Clinopyroxenes as Mantle Conveyors of Crustal Components
L. André, V. S. Shatsky, K. De Corte, N. V. Sobolev, and J. Navez 11

Hydration Mechanisms and Structural Characterization of Simplified Glasses (Comparison Between Basaltic and Radioactive Waste Glasses)
F. Angeli, Th. Charpentier, D. Boscarino, G. Della Mea, and J.-C. Petit 11

X-Ray Absorption Spectroscopy Investigation of Arsenite and Arsenate Adsorption on Gamma Aluminum Oxide
Y. Arai, E. J. Elzinga, and D. L. Sparks 12

Experimental Study of Gold Solubility in Hydrochloric Acid-bearing Water Vapor
S. M. Archibald and A. E. Williams-Jones 12

Hafnium-isotopic Compositions of Komatiites
N. T. Arndt and J. Blichert-Toft 13

Contrasting Extracellular Enzymatic Hydrolysis Rates and Substrate Specificities in Bottom Water and Surface Sediments: Implications for Organic Matter Remineralization and Carbon Preservation
C. Arnosti 13

Protactinium-Thorium-Uranium Fractionation During Mantle Melting: Inferences from Continental Basalt Data
Y. Asmerom, H. Cheng, T. Tesfay, B. Bierman, and R. L. Edwards 14

Control of Oceanic New Production in the Equatorial Pacific by Iron
A. K. Aufdenkampe, J. J. McCarthy, M. Rodier, and J. W. Murray 14

Alteration of Oceanic Troctolites by Magmatic Fluids in Ocean Drilling Program Hole 735B?
W. Bach, Y. Niu, J. C. Alt, and S. E. Humphris 15

Early Chemical and Petrographic Changes During Peat-to-Lignite Transformations
A. M. Bailey, A. D. Cohen, W. H. Orem, W. C. Riese, and S. Thibodeaux 16

Bioavailability and Chemical Composition of Thermally Altered *Pinus Resinosa* (Red Pine) Wood
J. A. Baldock 16

Geochemical Signatures in the Early Proterozoic Oceanic Sediments: Case History from the Aravalli Supergroup of Southcentral Rajasthan, India
D. M. Banerjee and P. Bhattacharya 17

X-Ray Photoelectron Spectroscopy Study of Reductive Dissolution of Birnessite by Oxalate
D. M. Banerjee and H. W. Nesbitt 17

Microbial Populations Sustained by Dissolution of Iron Silicates
J. F. Banfield, S. A. Welch, C. M. Santelli, K. J. Edwards, and P. L. Bond 17

Accelerated Weathering of Feldspar Under Elevated $PCO_2(g)$ at 25°C and 1 atm
S. A. Banwart and A. Berg 18

Use of Radium-226 for Groundwater Dating
F. Barbecot, L. Dever, and C. Hillaire-Marcel 18

Dating Climatic Events in the Eastern Mediterranean Region Using Cave Deposits
M. Bar-Matthews, A. Ayalon, and A. Kaufman 19

Basalts in Mongolia: Evidence for Contribution from a Widespread Hydrous Lithospheric Source
T. L. Barry, P. D. Kempton, A. D. Saunders, M. S. Pringle, G. Davies, and B. F. Windley 19

Geochemistry of Xenolithic Eclogites from West Africa
M. G. Barth, R. L. Rudnick, I. Horn, W. F. McDonough, M. J. Spicuzza, J. W. Valley, and S. E. Haggerty 20

Laboratory Examination of Microbial Perturbations in a Geological Disposal Site for Radioactive Waste
K. Bateman, P. Coombs, K. Hama, V. L. Hards, A. E. Milodowski, J. M. West, P. D. Wetton, and H. Yoshida 20

Intraplate Magmatism of the Kola Structure, Baltic Shield Bayanova
T. B. Bayanova 21

The Role of Iron Metabolizing Organisms in the Iron Geochemical Cycle Revealed by Iron-Isotopic Measurements
B. L. Beard and C. M. Johnson 21

Mobility and Accumulation of Platinum-Group Metals and Select Trace Metals in the Poland Kupferschiefer
A. Bechtel, S. Oszczepalski, A. M. Ghazi, W. C. Elliott, and B. D. Chatham 22

Rhenium and Osmium Loss from Subducted Oceanic Basalt and the Rhenium Budget of the Continents
H. Becker 22

Secular Carbon-isotopic Variations and Changing Environment in the Early Paleoproterozoic
A. Bekker and J. A. Karhu 22

Solubility and Reaction Rates of Aluminum Solid Phases Under Hydrothermal Conditions
P. Bénezeth, D. A. Palmer, and D. J. Wesolowski 23

Crust-Mantle Evolution in the Early Archean: A View from a 3.8-Ga Terrane of Southern West Greenland
V. C. Bennett, A. P. Nutman, C. R. L. Friend, and M. D. Norman 24

Mackinawite Stability at High Temperatures
L. G. Benning, C. L. Cahill, S. M. Clark, H. L. Barnes, and J. B. Parise 24

Growth Morphologies on Pyrite Surfaces
L. G. Benning, A. L. Owsley, and H. L. Barnes 25

Sulfate-reducing Bacteria and Mackinawite Stability
L. G. Benning, R. T. Wilkin, and K. O. Konhauser 26

The Dissolved and Particulate Loads of Rains Constrained by Lead, Strontium Isotopes, and Major and Trace Elements
D. Ben Othman, J. M. Luck, P. Telouk, and F. Albarède 26

Physicochemical Characterization of Carbonaceous Particles: Factors for Assessing Biological Activity
K. A. BéruBé, S. A. Murphy, T. P. Jones, F. D. Pooley, B. J. Williamson, and R. J. Richards 27

Using Brown Coal as an Organic Fertilizer
O. S. Bezuglova 28

High-Iridium Concentration in Alkaline Rocks of Deccan and Implications to Cretaceous-Tertiary Boundary Enhancement
N. Bhandari, P. N. Shukla, and A. D. Shukla 28

Acid Dissolution Rates of 2:1 Phyllosilicate Clay Minerals Measured with *In Situ* Atomic Force Microscopy
B. R. Bickmore, D. Bosbach, M. F. Hochella Jr., and L. Charlet 28

On a Jurassic Transcontinental Seaway, Thermohaline Circulation, and Oxygen-18
C. J. Bjerrum, D. R. Gröcke, S. P. Hesselbo, H. C. Jenkyns, S. M. Olsen, G. Shaffer, and F. Surlyk 29

Quantitative Analysis of Experimental Microbe-Mineral Interactions Using Vertical Scanning White Light Interferometry
R. E. Blake and A. Lüttge 29

New Constraints from Hafnium Isotopes on the Source of Hawai'ian Basalts
J. Blichert-Toft, F. A. Frey, and F. Albarède 30

Quantitative Determination of Smectite Surface Areas by the Sorption of Polyvinylpyrrolidone
A. E. Blum, D. D. Eberl, and D. W. Rutherford 30

The Paleozoic Evolution of the Western Margin of Gondwana Reconstructed with Neodymium and Lead Isotopes
B. Bock, H. Bahlburg, G. Wörner, and U. Zimmermann 31

Evolution of the Southeast Asian Continent from Uranium-Lead and Hafnium Isotopes in Single Grains of Zircon and Baddeleyite from Large Rivers
F. Bodet and U. Schärer 31

Microbial Degradation of Organic Matter in Sediments of the Arabian Deep Sea
A. Boetius, M. Nitsche, T. Ferdelman, K. Lochte, and O. Pfannkuche 32

Applicability of the Uranium-isotopic Model as a Prospecting Technique in Guarany Aquifer, South America
D. M. Bonotto 33

The Implications of Dissolved Uranium in Deep Groundwaters from Guarany Aquifer, South America, for the Disposal of Radioactive Wastes
D. M. Bonotto 33

Arsenic Sorption on Metal Sulfides
B. C. Bostick and S. E. Fendorf 34

Seasonal Dynamics in the Biogeochemistry, Stable Isotopic Geochemistry, and Microbial Community Structure of Temperate Intertidal Sediments
M. E. Böttcher, B. Hespenheide, C. Beardsley, E. Llobet-Brossa, A. Schramm, A. Wieland, G. Böttcher, B. Schnetger, U.-G. Berninger, R. Rossello-Mora, R. Amann, and O. Larsen 34

Lithium-Isotopic Compositions of Mariana Arc Lavas: Implications for Crust-Mantle Recycling
C. Bouman and T. R. Elliott 35

High-Precision Uranium-Lead Geochonological Constraints on Early Animal Evolution
S. A. Bowring, M. W. Martin, and K. L. Davidek 35

Diffusion of Argon from Melt Inclusions in Quartz Phenocrysts
J. W. Boyce, M. Grove, and M. R. Reid 36

Lead Isotopes as Tracers for Environmental Pollution at a Former Uranium Mining Site in Eastern Germany
G. Bracke and M. Satir 36

Migration of Rare Earth Elements at the Natural Fission Reactor of Bangombé Shown Using Fissiongenic Isotopic Ratios
G. Bracke, F. Gauthier-Lafaye, and H. Hidaka 37

Platinum-190/Osmium-186– and Rhenium-187/Osmium-187–isotopic Systematics of Abyssal Peridotites
A. D. Brandon, J. E. Snow, R. J. Walker, J. W. Morgan, and T. D. Mock 37

Effects of the Hydrosphere on the Evolution of Basaltic Magmas
M. E. Brandriss and D. K. Bird 38

Bacteria-promoted Dissolution of a Common Soil Silicate
S. L. Brantley, L. J. Liermann, and B. E. Kalinowski 39

Evolution of Temperature Control on Alkenone Biosynthesis
S. C. Brassell 39

Chemical Composition of Silurian Seawater: Preliminary Results from Environmental Scanning Electron Microscopy–Energy Dispersive Spectroscopy Analyses of Fluid Inclusions in Marine Halites
S. T. Brennan, T. K. Lowenstein, M. N. Timofeeff, and L. A. Hardie 40

A Polyphasic Approach to Study the Diversity and Vertical Distribution of Sulfur-Oxidizing *Thiomicrospira* Species in Coastal Sediments of the German Wadden Sea
T. Brinkhoff, C. M. Santegoeds, K. Sahm, J. Kuever, and G. Muyzer 40

The Temporal Evolution of the Oligocene-Recent Izu-Bonin Arc: The Tephra Perspective
C. J. Bryant, R. J. Arculus, and S. M. Eggins 41

Halogen Geochemistry of the Mantle Determined from Globally Distributed Diamond Samples
R. Burgess and J. W. Harris 41

Optimizing Ochre Accretion at the Source
S. P. Burke, S. A. Banwart, A. Jarvis, and P. L. Younger 42

Bubble-by-Bubble Degassing of Mid-Ocean-Ridge Basalt Magmas
P. G. Burnard 42

Sensitivity and Isotopic Discrimination in a Nier-type Source as a Function of Pressure: Implications for Argon and Helium Analysis
P. G. Burnard and K. A. Farley 43

Aerosol Carbon in the Remote Atmosphere
P. R. Buseck, M. Pósfai, L. Jia, and J. R. Anderson 44

Framboidal Pyrite Formation by the Oxidation of Iron(II) Monosulfide by Hydrogen Sulfide
I. B. Butler and D. Rickard 44

Iron Sulfide Oxidation in an Anoxic Chemostated Reaction System
I. B. Butler, S. T. Grimes, and D. Rickard 45

Microscale Trace-Element and Sulfur-isotopic Distributions in Hydrothermal Sulfides
I. B. Butler, R. W. Nesbitt, and A. E. Fallick 45

Formation of the Thiospinel, Greigite, Through the Oxidation of Iron(II) Monosulfide in the Presence of Aldehydes
I. B. Butler, D. Rickard, and A. Oldroyd 46

In Situ X-Ray Diffraction of Troilite Under Reduced, Anoxic Hydrothermal Conditions
C. L. Cahill, L. G. Benning, S. M. Clark, and J. B. Parise 47

Controls on Ocean pH and Alkalinity: Atmospheric Carbon Dioxide and Carbonate Sediments
K. Caldeira and R. A. Berner 47

Platinum-Group-element Microanalysis of Ordinary Chondrite Metal Grains by Laser Ablation Inductively Coupled Plasma Mass Spectrometry
A. J. Campbell and M. Humayun 48

Vertical and Latitudinal Variation of Geochemical Composition of Marine Particles Off Tasmania: Role of Advective, Biological, and Authigenic Processes
D. Cardinal, T. Cattaldo, M. Elskens, F. Dehairs, and L. André 49

Online Matrix Separation for Analysis of Rare Earth Elements Using Inductively Coupled Plasma Mass Spectrometry: Applications to Continental Waters
J. Carignan and D. Yeghicheyan 49

Oxygen Isotopes of Eclogites from the Orapa Kimberlite (Botswana): Possible Origins
P. Cartigny, K. S. Viljoen, and G. Wörner 50

Reconstructing the Paleotopography of Mountain Belts from the Isotopic Composition of Authigenic Minerals
C. P. Chamberlain and M. A. Poage 50

Eruption of the British Tertiary Volcanic Province in Approximately Two Million Years During Chron 26R
L. M. Chambers and M. S. Pringle 51

The Society Plume: Isotopes and Trace Elements Along the Chain
C. Chauvel, H. Guillou, S. Blais, G. Guille, R. Maury, and M. Caroff 51

Neodymium-Hafnium-isotopic Compositions of Aluminum-depleted and Aluminum-undepleted Komatiites of the Komati Formation (South Africa)
V. Chavagnac, S. W. Parman, R. W. Carlson, J. C. Dann, T. L. Grove, and S. A. Bowring 52

Effect of Oxalate on the Siderophore-promoted Dissolution of Goethite
S.-F. Cheah and G. Sposito 53

Isotopic Systematics in Portales Valley
J. H. Chen, D. A. Papanastassiou, and G. J. Wasserburg 53

Fluid Inclusion Evidence for High Copper Content of Ore-forming Fluid for Xifanping Porphyry Copper Deposit, Sichuan Province, China
P. Chen, R. Wang, X. Chen, and S. Xu 54

Determination of Melanterite-Rozenite and Chalcanthite-Bonattite Equilibria by the Humidity Buffer Technique at 0.1 MPa
I.-M. Chou, R. R. Seal II, and B. S. Hemingway 54

Use of Isotopic Tracers in the Quantification of Mining-derived Metals in Bed Sediments, Animas River Watershed, Colorado
S. E. Church, D. M. Unruh, and D. L. Fey 55

High-Precision Lead-isotopic Record of the Last 350 ka from an Iron-Manganese Crust (121 DK) from the Northeast Atlantic
C. Claude-Ivanaj, W. Abouchami, S. J. G. Galer, A. Koschinsky, and A. W. Hofmann 55

Oxygen-isotopic Fractionation Between Magnetite and Water
D. R. Cole, J. W. Valley, M. J. Spicuzza, and J. Horita 56

Stable Isotopic Fractionation Associated with Anaerobic Degradation of Chlorinated Hydrocarbons
M. L. Coleman, T. J. McGenity, and M. C. P. Isaacs 56

Accurate and Precise Isotopic Ratio Measurements of NBS 981 Lead by Multiple Collector Inductively Coupled Plasma Mass Spectrometry: Why are the Ratios Different from Thermal Ionization Mass Spectrometry Measurements?
K. D. Collerson and Z. A. Palacz 57

Ion Association in Sodium Chloride Brines at High Temperatures and Pressures: Results from Molecular Dynamics Simulations
M. D. Collings and D. M. Sherman 57

The Dominance of the Riverine Particulate Phosphorus Flux in Supplying Phosphate to the Oceans and a 10,000-Year Residence Time for Phosphorus
A. S. Colman and H. D. Holland 58

Isotopic Evidence for Groundwater Flow and Biodegradation of Organic Solvents at the Test Area North Site, Idaho National Engineering and Environmental Laboratory
M. E. Conrad, D. J. DePaolo, D. L. Song, and E. Neher 58

Reactive Melt Migration Beneath the Mid-Atlantic Ridge: Evidence from ODP Leg 153 Gabbros
L. A. Coogan, P. D. Kempton, and A. D. Saunders 59

Evidence for the Origin of Oceanic Oxide Gabbros by Channelized Melt Flow Through the Lower Crust
L. A. Coogan, C. J. MacLeod, S. J. Edwards, and H. J. B. Dick 60

Residence of Magma at Kilauea Volcano, Hawai'i: Internal Thorium-230–Radium-226 Isochron Dating of the 1955 East Rift Eruption
K. M. Cooper, M. R. Reid, R. C. Roback, M. T. Murrell, and D. A. Clague 60

Application of Charge-Radius Concepts to Trace Elements in Igneous and Metamorphic Zircon
D. H. Cornell, A. Scherstén, P. Hoskin, and J. Lindsay 61

At Least Three Carbon-Isotopic Excursions/Glaciations in the Neoproterozoic: Carbon-isotopic Chemostratigraphy of Neoproterozoic-Cambrian Strata, Southern Great Basin, USA
F. A. Corsetti and A. J. Kaufman 62

Trace Metals in Sedimentary Iron Sulfides: Preliminary Results
C. F. Cottnam, I. B. Butler, and D. Rickard 62

A Single-Site Model for Metal Adsorption Over a Range of Surface Coverages
L. J. Criscenti and D. A. Sverjensky 63

The Origin of Minewater Contamination from the Carboniferous Coal Measure Sequence in the United Kingdom
S. J. Croxford, S. A. Banwart, and J. C. Cripps 63

Controls on Metal Transport in Sediment-Covered Ridge-Crest Hydrothermal Systems: Experimental and Theoretical Constraints
A. C. Cruse and J. S. Seewald 64

Interlaboratory Data on Elemental and Isotopic Carbon in the Carbonaceous Particle Reference Material, NIST SRM 1649A
L. A. Currie, B. A. Benner Jr., R. Cary, E. R. M. Druffel, T. I. Eglinton, P. C. Hartmann, J. D. Kessler, D. B. Klinedinst, G. A. Klouda, J. V. Marolf, C. A. Masiello, A. Pearson, J. G. Quinn, C. M. Reddy, J. F. Slater, and S. A. Wise 64

Thermal Optical Isotopic Analysis of Elemental Carbon in Carbonaceous Particles
L. A. Currie and J. D. Kessler 65

Sea-Level and Deep-Ocean Temperature Changes Since the Last Interglacial from Combined Protactinium-231 and Thorium-230 Dating of Corals
K. B. Cutler, R. L. Edwards, F. W. Taylor, H. Cheng, J. Adkins, C. D. Gallup, and G. S. Burr 65

The Neodymium-isotopic Composition in a Boreal River: A Reflection of Selective Weathering and Colloidal Transport
R. Dahlqvist, P. S. Andersson, and J. Ingri 66

Occurrence of Trace Elements in Coal Ash and Sludge Amended Soils in India
S. Datta, B. Hart, M. A. Powell, W. S. Fyfe, and S. Tripathy 66

Hafnium-isotopic Time Series in Iron-Manganese Crusts: A Comparison Between ε_{Hf} and ε_{Nd} Variations
K. David, M. Frank, N. S. Belshaw, and R. K. O'Nions 67

Crystal Isotopic Stratigraphy Using Laser Ablation
J. P. Davidson, F. J. Tepley III, Z. Palacz, and S. Meffan-Main 67

The Effect of Magnesium as an Impurity on Calcite Growth: A Model System for Biomineralization
K. J. Davis, P. M. Dove, and J. J. De Yoreo 68

Proterozoic Underplating of the Archean Wyoming Craton and Medicine Hat Block During Assembly of Western Laurentia
W. J. Davis and G. M. Ross 68

Carbon-isotopic and Nitrogen Analysis of Carbonado by Secondary Ion Mass Spectrometry
S. De, P. J. Heaney, E. P. Vicenzi, and J. Wang 69

Variations in the Isotopic Composition of Marine Calcium over the Last 160 Million Years
C. L. De La Rocha and D. J. DePaolo 69

Paleozoic Plume in the Northeastern Baltic Shield: Duration from Rubidium-Strontium Data
A. A. Delenitsyn, O. V. Gogol, and T. B. Bayanova 70

Strontium Isotopes, Alkalinity Fluxes, and Carbon Dioxide Consumption: Is There a General Relationship?
L. A. Derry and C. France-Lanord 70

Nature of Fluxes from Subducted Slab to Mantle Wedge in the Lesser Antilles Arc: Origin of M- and C-series Basalts
J. D. Devine, W. M. White, P. Copeland, and D. R. Gravatt 71

Carbon-isotopic Records and Extinction-triggered Ecological Collapse
S. D'Hondt 71

The Nature of Intrusion and Melt Transport in the Lower Ocean Crust at an Ultraslow Spreading Ridge
H. J. B. Dick, J. H. Natland, J. Kinoshita, P. Robinson, C. MacLeod, A. Kvassnes, and the MODE '98 Leg IV, JR31, and ODP Leg Scientific Parties 71

Carbon-isotopic Biogeochemistry of Aerobic Biodegradation of Aromatic Hydrocarbons
E. J. M. Diegor, T. A. Abrajano, T. Patel, L. Stehmeier, and J. Gow 72

Development of a High-Pressure Digestion Technique and a Data Acquisition and Reduction Procedure and Their Application to the Inductively Coupled Plasma Mass Spectrometry Analysis of Urban Sediments and Soils
W. G. Diegor, H. P. Longerich, T. A. Abrajano, and I. Horn 72

Interaction of Silicic Acid with Iron Oxides
M. Dietzel 73

Geochemical and Rare-Earth-element Characteristics of Ferruginous Siliceous Rocks of Bikou Group, Qinling, China: Implications for Ancient Seafloor Hydrothermal Fluid Processes
Z. J. Ding, C. Q. Liu, H. Y. Li, and Z. S. Yang 74

Partial Molar Volumes of Siderophile Elements in Melts: Implications for the Pressure-dependence of Metal-Silicate Partitioning
D. B. Dingwell, P. Courtial, C. Holzapfel, J. Gottsmann, A. Holzheid, and H. Palme 74

The Geochemistry and Petrology of an Urban Canal Bed Mud
J. S. Dodd, A. E. Milodowski, D. J. Large, N. J. Fortey, and S. J. Kemp 75

Some Comparative Geochemistry of Oceanic and Continental Igneous Rocks
B. R. Doe 75

Zinc Adsorption on Iron(II)/Iron(III) Substrates Produced by Microbial Reduction of High-Surface-Area Goethite
R. J. Donahoe, K. D. Kirk, and E. Y. Graham 75

Nitrogen-isotopic Values as a Proxy for Land-Use Patterns in the Connecticut River Watershed
T. A. Douglas, C. P. Chamberlain, and R. R. Harrington 76

Nature and Origin of the Lower Crust of Cratonic Europe: Xenolith Suites from the Baltic Shield and East European Platform
H. Downes, A. J. W. Markwick, and P. D. Kempton 77

Presidential Address: Formation and Primordial Differentiation of the Earth
M. J. Drake 77

On the Early Differentiation of Mars
G. Dreibus 78

Rare Earth Elements in Oceanic Phillipsites
A. V. Dubinin 78

Kinetics and Surface Microstructural Evolution of Microbially Mediated Sulfide Dissolution: Implications for Modeling Acid Mine Drainage Generation
K. J. Edwards, M. M. McGuire, R. J. Hamers, and J. F. Banfield 79

Oxygen-isotopic Evidence on the Origin of Chemical Variation in the Sources of Normal-Mid-Ocean-Ridge Basalts
J. M. Eiler, P. Schiano, N. Kitchen, and E. M. Stolper 79

Uranium-Thorium-Protactinium Constraints on Melting Beneath the Mariana Arc
T. Elliott and G. Koetsier 80

Fundamental Studies of Pyrite Oxidation in Gaseous and Aqueous Environments
A. R. Elsetinow, D. R. Strongin, and M. A. A. Schoonen 80

Crystallization, Replacement, Assimilation, Melting, and Infiltration Processes that Form the Plutonic Foundation of the Oceanic Crust
D. Elthon 80

The Search for the Protostome-Deuterostome Ancestor: Conflict Between Paleontological and Molecular Data
D. H. Erwin 81

Some Abyssal Peridotites Are Old!
S. Esperança, S. E. Sichel, M. F. Horan, R. J. Walker, T. Juteau, and R. Hekinian 81

Experimental Methods for Determining the Rates of Contaminant Release from Spoil Material and Deep Mines
K. A. Evans and S. Banwart 82

Hydrothermal Source of Radiogenic Strontium to Himalayan Rivers
M. J. Evans, L. A. Derry, and S. P. Anderson 82

Hydrogen-isotopic Fractionation Between Amorphous Silica and Water and Its Implication in the Formation of Epithermal Quartz
K. Faure and Y. Matsuhisa 83

The Iodine-129 System and Its Potential for Dating Organic Material
U. Fehn 83

Isotopic Exchange Energetics and Mechanisms of Silica in Water from *Ab Initio* Calculations
M. A. Felipe, J. D. Kubicki, and D. M. Rye 83

Probing the Electrical Double-Layer Structure at the Rutile-Water Interface with X-Ray Standing Waves
P. Fenter, L. Cheng, S. Rihs, M. Machesky, P. Geissbühler, M. J. Bedzyk, and N. C. Sturchio 84

A New Approach of Determining the $Fe^{3+}/\Sigma Fe$ in Minerals and Glasses with the Electron Microprobe
M. Fialin and C. Wagner 85

Stratabound Copper Occurrences at the Base of the Miocene in Northwestern Sardinia, Italy
M. Fiori 85

Paragenetic Assemblage of High Sulfidation Epithermal Gold Deposit of Furtei, Sardinia, Italy
M. Fiori and S. M. Grillo 85

Isotopic Evidence of Historic and Chronic Inputs of Contaminant Lead in San Francisco Bay
A. R. Flegal, D. J. Steding, and C. E. Dunlap 86

Molecular-Scale Studies of Arsenic and Selenium Sorption on Hydrous Manganese Oxides
A. L. Foster, G. E. Brown Jr., and G. A. Parks 86

The Permian-Triassic Boundary in Australia: Organic Carbon-isotopic Anomalies Relate to Organofacies, Not a Biogeochemical "Event"
C. B. Foster, G. A. Logan, and R. E. Summons 87

The Timing of Prograde Metamorphism in the Himalaya
G. L. Foster, D. Vance, C. I. Prince, P. Kinny, and N. B. W. Harris 88

Copper Biomineralization: Toward Quantifying the Effects of Bacteria on Precipitation
D. A. Fowle, J. B. Fein, K. M. Kemner, B. A. Bunker, S. Kelly, and M. Boyanov 88

How the Himalayan-Tibet Uplift Affects the Carbon Cycle
C. France-Lanord, A. Galy, and L. A. Derry 89

A More Chondritic Archean Mantle?
D. Francis 89

Lead- and Neodymium-isotopic Evolution of Water Masses at the Indonesian Seaway During the Last 35 Million Years
M. Frank and R. K. O'Nions 90

Southern Ocean Response to Lead- and Neodymium-isotopic Changes in the Northwest Atlantic During the Last 10 Million Years
M. Frank and R. K. O'Nions 90

Unraveling the Tectono-Metamorphic History in the Isua Supracrustals (West Greenland): Mineral Lead Stepwise Leaching Evidence for Early- and Late Archean Metasomatic-Metamorphic Events
R. Frei, M. T. Rosing, E. J. Krogstad, M. Storey, and F. Albarède 91

Sustainable Development: The Role of Geochemistry
W. S. Fyfe 92

The Effect of a Water-rich Subduction Component on Melt Production in Mantle Peridotite
G. A. Gaetani and T. L. Grove 92

Olivine-hosted Melt Inclusions Remember the Magma Chamber, Not the Mantle
G. A. Gaetani and E. B. Watson 93

Cosmochemical Determinism in the Formation of Habitable Planets
E. J. Gaidos 93

Climate and Geochemical Modeling of Proterozoic Glaciations
E. J. Gaidos and J. L. Kirschvink 94

Molecular Inferences in the Origin of Oxidant-associated Enzymes
E. J. Gaidos, K. H. Nealson, P. Jayakumar, and J. L. Kirschvink 94

New Thorium-230 Data from Barbados Fossil Corals: The Beginning and End of Stage 5e and the Timing and Amplitude of Event 6.5
C. D. Gallup, H. Cheng, R. Speed, and R. L. Edwards 94

High-Precision Magnesium-isotopic Ratio Measurement by Multiple Collector Inductively Coupled Mass Spectrometry: A New Tool in Cosmochemistry and Geochemistry
A. Galy, L. Halicz, N. S. Belshaw, E. D. Young, and R. K. O'Nions 95

Complexation of Metals with Aqueous Sulfide in an Anaerobic Treatment Wetlands, Butte, Montana
C. H. Gammons 95

Are Oceanic Nitrogen and Phosphorus Cycles Linked by Denitrification and Phosphogenesis in Upwelling Margins?
R. S. Ganeshram, T. F. Pedersen, and S. E. Calvert 96

Phosphate and Arsenate Complexation at the Surface of Goethite in 0.7 M Sodium Chloride Solution
Y. Gao and A. Mucci 96

Evidenced Redox Disequilibrium from Iron and Arsenic Behavior in Tailing Lecheate (Cheni Site, France)
O. Gaskova, M. Azaroual, F. Bodenan, and E. Gaucher 97

Subcontinental Mantle Below Eifel, Germany: Constraints by Noble Gases
C. Gautheron, M. Moreira, J. Kunz, J. L. Joron, M. Kurz, and C. J. Allègre 97

Icelandic Mantle Structure or Basalt Seasonality?
M. A. M. Gee, M. F. Thirlwall, R. N. Taylor, and B. J. Murton 98

Mineral Formation and Redox-Sensitive Trace Elements in a Near-Surface Hydrothermal Alteration System
A. U. Gehring, P. M. Schosseler, and P. G. Weidler 99

Hyperthermophilic Microorganisms in Arsenic-rich Hot Springs
T. M. Gihring, G. K. Druschel, and J. F. Banfield 99

The Effect of pH and Oxygen Fugacity on Metal Mobility by Metal-Carboxylate Complexes
T. H. Giordano 99

Black Carbon in Terra Preta Soils of the Brazilian Amazon Region
B. Glaser, G. Guggenberger, L. Haumaier, and W. Zech 100

Muong Nong-type Australasian Tektites: Implications Regarding the Parent Material and Source Area
B. P. Glass 100

How Did the Growth of Continents Influence the Chemical and Isotopic Evolution of Precambrian Oceans?
Y. Goddéris, J. Veizer, and L. M. François 100

Evidence for Radium-Barium Fractionation in Mid-Ocean-Ridge Basalt Plagioclase: Implications for Geochronology and Mantle Melting
S. J. Goldstein, K. W. W. Sims, K. M. Cooper, M. T. Murrell, and A. J. Nunn 101

Strontium Isotopes in South Atlantic Detritus: A Surface Current Proxy and Tracer of Agulhas Leakage
S. L. Goldstein, S. R. Hemming, S. Kish, and R. Rutberg 101

From a Hot Spot to a Cold Spot: Spatial Correlogram Analysis of Helium-isotopic Variations Along the Southeast Indian Ridge
D. W. Graham, F. J. Spera, J. E. Lupton, and D. M. Christie 102

Environmental Applications of Multiple Collector Inductively Coupled Plasma Mass Spectrometry: Measurement of Lead-isotopic Ratios in Precipitation Samples from the Great Lakes and Everglades Regions
J. R. Graney, J. N. Christensen, G. J. Keeler, A. N. Halliday, M. S. Landis, and J. T. Dvonch 103

Measurements of Sulfur-32,33,34 in Allan Hills 84001 and Nakhla Sulfides by Multicollector Secondary Ion Mass Spectrometry: Implications for Crustal-Atmospheric Exchange and Biogenic Activity on Mars
J. P. Greenwood, S. J. Mojzsis, C. D. Coath, and J. T. Wasson 103

Mapping the Subcontinental Lithosphere with Garnet Populations
W. L. Griffin, S. Y. O'Reilly, N. I. Fisher, J. Friedman, C. G. Ryan, and E. van Achterbergh 104

The Hafnium-isotopic Composition of Cratonic Mantle: Laser Ablation Microprobe Multiple Collector Inductively Coupled Plasma Mass Spectrometry Analysis of Zircon Megacrysts in Kimberlites
W. L. Griffin, N. J. Pearson, E. A. Belousova, S. E. Jackson, E. van Achterbergh, S. Y. O'Reilly, and S. R. Shee 104

Hafnium, Lead, and Strontium Isotopes in LIMA from the Jagersfontein Kimberlite: *In Situ* Analysis by Laser Ablation Microprobe Multiple Collector Inductively Coupled Plasma Mass Spectrometry
W. L. Griffin, N. J. Pearson, M. Zhang, S. Y. O'Reilly, and Z. Wang 105

Estimation of Sorption of Trace Metals to Natural Sediments
J. Griffioen and P. Venema 106

Subaqueous Sulfur Eruptions at Waiotapu, New Zealand
S. T. Grimes, D. Rickard, P. Browne, and S. Simmons 106

Experimental Pyritization of Plant Cells
S. T. Grimes, D. Rickard, D. Edwards, A. Oldroyd, L. Axe, and K. Davies 107

Strontium-isotopic Distribution in the Broadlands-Ohaaki Geothermal System, New Zealand
S. T. Grimes, D. Rickard, C. Hawkesworth, P. van Calsteren, and P. Browne 107

Denitrification During the Toarcian Oceanic Anoxic Event as Recorded by Nitrogen-isotopic Ratios of Bulk Marine Organic Matter
D. R. Gröcke and H. C. Jenkyns 108

Stable Isotopic and Carbon/Nitrogen Ratios of Fossil Wood from the Mesozoic: Insights into Ocean-Atmosphere Links
D. R. Gröcke, S. P. Hesselbo, H. C. Jenkyns, G. Taylor, S. A. Robinson, and H.-J. Schöffel 109

Strontium-isotopic Calibration of Ammonite Subzones in the Jurassic and Early Cretaceous
D. R. Gröcke, S. P. Hesselbo, J. Mutterlose, H. C. Jenkyns, R. L. Hall, and S. M. Robinson 110

Novel Copper Oxide Reaction Products of Thermally Altered *Pinus Resinosa* Wood
J. A. Gudeman, J. Baldock, and J. I. Hedges 110

Advances in Lead Isotopes in the Health Field
B. L. Gulson 111

Experimental Measurements of Acid-Base Buffering Properties and Metal Sorption by Lichens
J. R. Haas 111

Two-Step Laser Mass Spectrometry: A Tool for the Chemical Characterization and Source Assignment of Black Carbon
O. P. Haefliger, R. Zenobi, and T. D. Bucheli 112

High-Precision Calcium-isotopic Ratio Measurement by Multiple Collector Inductively Coupled Mass Spectrometry: Preliminary Data of Calcium-isotopic Ratios in Carbonates
L. Halicz, A. Galy, N. S. Belshaw, and R. K. O'Nions 113

Uranium in Karst Water in the Guizhou Province, China
G. L. Han and C. Q. Liu 113

Osmium-, Neodymium-, and Strontium-isotopic Systematics in Young, Fertile, and Weakly Metasomatized Spinel Peridotite Xenoliths from Northern Queensland, Australia
M. R. Handler and V. C. Bennett 114

Black Shale Weathering and the Mobility of Osmium Isotopes, Rhenium, and Platinum Group Elements
R. E. Hannigan and B. Peucker-Ehrenbrink 114

Speciation and Bioavailability of Iron in Lake Kinneret
Y. Hareli, Y. Erel, C. Rosin, and A. Sukenik 115

The Release of Lead and Rare Earth Elements During Granitoid Dissolution
Y. Harlavan and Y. Erel 115

Variations in Helium-3/Helium-4 (R/R_a) Ratios in an Active Rift Zone: Hengill Complex, Iceland
D. Harrison, P. Burnard, and G. Turner 115

A Helium-isotopic Test for the Origin of Plume Mantle Under the Northern East Scotia Ridge
D. W. Harrison, P. T. Leat, and G. Turner 116

Intracrustal Processing of Volcanic Arcs as Shown by Osmium-Neodymium-Strontium-isotopic Variations in the Southern Cascade Range
G. L. Hart, C. M. Johnson, S. B. Shirey, M. A. Clynne, C. R. Bacon, and R. L. Christiansen 117

Partitioning of Pyrogenic and Petrogenic Polycyclic Aromatic Hydrocarbons in Narragansett Bay Sediments
P. C. Hartmann and J. G. Quinn 117

Reactivity of Bulk Organic Matter in Aquifer Sediments
N. Hartog and J. Griffioen 118

Nitrogen- and Carbon-isotopic Systematics Within Siberian Diamonds: Constraints from Secondary Ion Mass Spectrometry and Fourier Transform Infrared Studies
E. Hauri, D. G. Pearson, G. Bulanova, and H. J. Milledge 118

Crustal Recycling or Core-Mantle Interaction? Stable Isotopic Signatures of Hawai'ian Basalts
E. Hauri, P. Tomascak, and J. Lassiter 118

A History of Ocean Salinity During the Phanerozoic, Based on Sedimentary Cycling
W. W. Hay, S. Floegel, and C. N. Wold 119

Does Surface Structure Influence H^+ and OH^- Adsorption on Silicates in an Aqueous Medium? An Example Based on Albite and Albite Glass
R. Hellmann 119

Molybdenum(VI) Speciation and Kinetics in Sulfidic Waters
G. R. Helz and B. E. Erickson 120

Osmium-isotopic Analysis by Dynamic Multiple Collector Inductively Coupled Plasma Mass Spectrometry Using Iridium-191 Signal Normalization
N. G. Hemming, S. L. Goldstein, and R. G. Fairbanks 120

Neodymium-isotopic Constraints on Deep Ocean Circulation During the Late Quaternary
S. R. Hemming and S. L. Goldstein 121

Lead-isotopic Measurements of Sanidine Monitor Standards: Implications for Provenance Analysis and Tephrochronology
S. R. Hemming and E. T. Rasbury 121

The Foundation Seamounts (South Pacific): Geochemical Evidence of Past and Present Ridge-Hotspot Interactions?
C. Hémond, C. W. Devey, and M. Maia 122

Stability of Allanite to High Pressure-Temperature: Implications for Light Rare-Earth-element Budget in Subducted Crust
J. Hermann 122

Experimental Constraints on Continental Rocks in Ultra-High-Pressure Metamorphism
J. Hermann and D. H. Green 123

Cumulate Processes and Geochemical Differentiation Within Oceanic Layer 3
J. Hertogen 124

Extraterrestrial Helium-3 Flux Recorded in Marine Sediments in the North Pacific at ODP Sites 885/886 over the Past 4 Million Years
S. M. Higgins, R. F. Anderson, F. Marcantonio, M. Stute, and P. Schlosser 124

Helium-isotopic Investigations of Source Mixing in the Icelandic Mantle
D. R. Hilton, K. Gronvold, C. G. Macpherson, and P. R. Castillo 125

Acetate and C1 Compounds are Largely Ignored by Methanogens in Northern Wetlands
M. E. Hines, K. N. Duddleston, R. B. Reich, and R. P. Kiene 125

A New Approach to the Study of Anaerobic Methane-Oxidizing Consortia in Marine Sediments: Biomarker and Phylogenetic Evidence
K.-U. Hinrichs, E. F. DeLong, and J. M. Hayes 126

Experimental Study of Partial Melts of Clinopyroxenite and the Origin of Ultracalcic Melt Inclusions
M. M. Hirschmann and P. Schiano 126

Thermodynamics of Molecular Hydrogen in Anaerobic Microbial Ecosystems
T. M. Hoehler, M. J. Alperin, D. B. Albert, and C. S. Martens 127

Tropical Carbonate $\delta^{13}C$ Record of a Neoproterozoic Snowball Earth
P. F. Hoffman, G. P. Halverson, D. P. Schrag, G. Soffer, and A. J. Kaufman 127

Tracing Water Flowpaths During a Storm Event Using Strontium-87/Strontium-86 Ratios
J. F. Hogan and J. D. Blum 127

In Situ Hafnium-, Uranium/Lead-, and Lead/Lead-isotopic Analyses of Zircons and Baddeleyite by Laser Ablation Multiple Collector Inductively Coupled Plasma Mass Spectrometry
I. Horn, W. F. McDonough, and R. L. Rudnick 128

Multinuclear Nuclear Magnetic Resonance Investigation of the Structure and Dynamics of Surface and Interlayer Species of Hydrotalcite-like Compounds
X. Hou and R. J. Kirkpatrick 129

Oxygen-isotopic Fractionation in the System of Quartz-NaCl-$CaCl_2$-Water at High Pressure and High Temperature
G. Hu and R. N. Clayton 129

Nonreactive Solute Dispersion in Triassic Sandstone: Laboratory Simulation and an Application to the Field
W. Huang and D. N. Lerner 130

Bioremediation of Petrochemical Contaminants in Unsaturated Soil
W. Huang, D. N. Lerner, and G. Li 130

El Niño During the Last Interglacial Period Recorded by a Fossil Coral from Indonesia
K. A. Hughen, D. P. Schrag, S. B. Jacobsen, and W. Hantoro 130

Lithium and Its Isotopes in River Water and Suspended Material
Y. Huh, L.-H. Chan, and J. M. Edmond 131

A Nickel Carbonate Elegy
W. Hummel 131

Timescale of Aqueous Activity in the Early Solar System
I. D. Hutcheon, L. Browning, K. Keil, A. N. Krot, D. L. Phinney, M. Prinz, and M. K. Weisberg 132

Experimental Verification of Stratification Formation in Solidifying Medium Under the Action of Standing Wave
V. L. Il'chenko 133

The Systematic Evolution of the Lanthanide Tetrad Effect in Peraluminous Granite Suites
W. Irber 133

Geochronology of High-Grade Metamorphism in New Zealand
T. R. Ireland 133

Age of the Lithospheric Mantle Beneath and Around the Slave Craton: A Rhenium-Osmium-isotopic Study of Peridotite Xenoliths from the Jericho and Somerset Island Kimberlites
G. J. Irvine, M. G. Kopylova, R. W. Carlson, D. G. Pearson, S. B. Shirey, and B. A. Kjarsgaard 134

Quantitative Laser Ablation Microprobe Inductively Coupled Plasma Mass Spectrometry Analysis of Trace Elements in Diamonds
S. E. Jackson, R. M. Davies, W. L. Griffin, S. Y. O'Reilly, and B. Doyle 135

Determination of High-Precision Isotopic Ratios by Laser Ablation Multiple Collector Inductively Coupled Plasma Mass Spectrometry
S. E. Jackson, W. L. Griffin, and N. J. Pearson 135

Isotopes and Methods for Modeling of Geochemical Cycles
S. B. Jacobsen 136

Toward a Consistent Early Solar System Chronology
S. B. Jacobsen 137

Strontium-, Carbon-, and Oxygen-isotopic Variations of Neoproterozoic Seawater
S. B. Jacobsen and A. J. Kaufman 137

On the Search for Neodymium-142 in Terrestrial Rocks
E. Jagoutz and R. Jotter 138

Temperature, Pressure, and Rhenium-Osmium Age Systematics of Off-Craton Peridotite Xenoliths from the Namaqua-Natal Belt, Western South Africa
P. E. Janney, R. W. Carlson, S. B. Shirey, D. R. Bell, and A. P. le Roex 139

A Novel Reactor to Determine the Rate of Pyrite Oxidation in Air
J. K. Jerz and J. D. Rimstidt 139

Elemental Geochemistry of Dolomitite Weathering Profile and Its Implication for Composition of the Upper Continental Crust
H. B. Ji, S. J. Wang, Z. Y. Ouyang, and D. Q. Zhou 140

Isotopic Signatures Across the Frasnian-Famennian Boundary: Evidence for Enhanced Productivity, Water Column Anoxia, and Variations in Seawater Temperature
M. M. Joachimski 141

Late Quaternary Paleoenvironments and the Extinction of the Australian Megafauna
B. J. Johnson, G. H. Miller, M. L. Fogel, and J. W. Magee 141

Fate of Cyanide Used in Processing of Gold Ores: New Evidence from Isotopic Measurements
C. A. Johnson, D. J. Grimes, and R. O. Rye 141

Development of Selenium Stable Isotopes for Environmental Applications
T. M. Johnson, M. J. Herbel, and T. D. Bullen 142

Comparative Magma Oceanography
J. H. Jones 143

The Earliest Known Occurrences of Charcoal in the Fossil Record
T. P. Jones and N. P. Rowe 143

The Role of Lower Crustal Delamination in the Genesis of Continental Crust
M. Jull and P. Kelemen 144

Melt Generation and Transport: Constraints from the Deglaciation of Iceland
M. Jull, D. McKenzie, J. Maclennan, L. Slater, and K. Gronvold 144

The Effect of Hydrogen Bonding on the Structure and Properties of Aqueous Hydrothermal Fluids: Computer Simulation Studies
A. G. Kalinichev 145

Computer Simulations of the Interlayer Structure and Dynamics of Mixed-Metal Layered Hydroxides
A. G. Kalinichev, R. J. Kirkpatrick, and R. T. Cygan 145

Mechanisms of Pyrite Oxidation Revealed from *In Situ* Measurements of Dissolved Oxygen, Eh, and pH of Solutions in a Closed System
G. Kamei and H. Ohmoto 146

The Genesis of Siderite in Archean and Paleoproterozoic Oceans
A. J. Kaufman 146

Lanthanide Tetrad Effects in Rare-Earth-Element Fractionation Among Particulate, Colloidal, and Solution Forms in River Water
I. Kawabe, I. Ohnishi, T. Sakakibara, and K. Yamomoto 147

Creation, Modification, and Destruction of Continental Lithosphere in the Neogene Central Andes
S. M. Kay and R. W. Kay 147

Comparison of Chemical Variation in Gabbros from Ophiolites, Oceanic Crust, and Continental, Igneous Layered Intrusions
P. B. Kelemen 148

Speculation on Consequences of Delamination of Ultramafic Plutonic Rocks from the Lower Crust and Implications for the Genesis of the Continental Crust
P. B. Kelemen and M. Jull 148

Updated Review of Melt-Extraction Processes in the Upper Mantle Beneath Oceanic Spreading Ridges and Intraplate Volcanic Centers
P. B. Kelemen, G. Hirth, and M. Spiegelman 149

Mantle Flow and Geochemical Heterogeneity
J. B. Kellogg and R. J. O'Connell 150

Garnet Granulite Xenoliths from the Northern Baltic Shield: The Lower Crust of a Paleoproterozoic LIP
P. D. Kempton, H. Downes, L. Neymark, E. V. Sharkov, R. Zartman, and J. Wartho 150

The Depleted Components of Mantle Plumes: A Strontium-Neodymium-Lead-Hafnium Study of the North Atlantic Rifted Margin
P. D. Kempton, J. G. Fitton, A. D. Saunders, G. M. Nowell, R. Taylor, and B. S. Hardarson 150

Halogen and Noble Gas Evidence for the Age and Origin of Mineralizing Fluids in Copper-Porphyry Deposits
M. Kendrick, R. Burgess, R. Pattrick, and G. Turner 151

Melt Inclusions in Subduction-related Basalts: An Example from the Mariana Arc
A. J. R. Kent and T. Elliot 152

Mercury Sorption to Iron- and Aluminun-(Hydr)Oxides and Speciation in Natural Samples
C. S. Kim, G. E. Brown Jr., and J. J. Rytuba 152

Major- and Trace-Element Geochemistry of Siliceous Shale, Middle Miocene Onnagawa Formation (13–6 Ma), Japan: Causes for Variations in Primary Productivity and Redox
S. K. Kimura and N. S. Shikazono 153

Structure and Dynamics of Surface and Interlayer Species: A Combined Nuclear Magnetic Resonance and Molecular Modeling Perspective
R. J. Kirkpatrick, P. Yu, X. Hou, A. Kalinichev, and R. T. Cygan 154

Continental Growth and Environments of Archean Continental Crust: An Example of the Coastal Pilbara Terrain, Western Australia
S. Kiyokawa, A. Taira, T. Byrne, and Y. Sano 154

Horizontal Distributions of Inorganic and Organic Sulfur in Estuarine Surface Sediments from Toyama Bay, Japan
Y. Kiyosu, I. Yamaguchi, and K. Katsuyama 155

Oxygen-isotopic Analyses of Diagenetic Cherts and the Temperature History of the Earth
L. P. Knauth 155

Salinity History of Seawater
L. P. Knauth 156

Fractionated Crust of Mars as an Adequate Response to Its Body Wave Warping
G. G. Kochemasov 156

Intrusion Stratification as a Response to Changes in the Earth's Rotation Rate with Various Periods
G. G. Kochemasov 157

Constraints on Diagenetic Age Disturbance: Combined Uranium-Protactinium and Uranium-Thorium Ages of the Key Largo Formation, Florida Keys, USA
G. Koetsier, T. Elliott, and C. Fruijtier 157

Redistribution of Trace Elements During Garnet to Spinel Peridotite Facies Transformations
K. T. Koga, N. Shimizu, and T. L. Grove 158

Stability of Hydrosulfide Complex $AuHS^0$ in Gold-bearing Solutions
G. R. Kolonin, G. A. Pal'yanova, and G. P. Shironosova 158

Microbial-Silica Interactions in Modern Hot Spring Sinter
K. O. Konhauser, V. R. Phoenix, and D. G. Adams 159

The Isotopic Composition of Conodonts and Brachiopods as Proxies for Evolution of Triassic Seawater
C. Korte, J. Veizer, and H. Kozur 160

Isotopic Structure and Crust-forming Events of the Cental Asia: Evidence for Extensive Continental Crust Growth in the Phanerozoic
V. P. Kovach, V. I. Kovalenko, V. V. Yarmolyuk, A. B. Kotov, I. K. Kozakov, and E. B. Salnikova 160

Effect of Desferrioxamine-B and DFOMTA on the Adsorption of Lead and Europium on the Goethite Surface
S. M. Kraemer, J. Xu, K. N. Raymond, and G. Sposito 160

The Influence of Soil-respired Carbon Dioxide on Mineral Weathering and Soil Water Geochemistry: Results from Natural and Experimental (Elevated Carbon Dioxide) Temperate Forest Ecosystems
T. C. W. Ku, L. M. Walter, J. M. Budai, G. W. Kling, D. R. Zak, and E. L. Williams 161

Molecular Modeling of Soot and Interactions with Polycyclic Aromatic Hydrocarbons
J. D. Kubicki 161

Isotopic Age of Main Geological Events of the Kolmozero-Voronja Greenstone Belt, Kola Peninsula, Russia
N. M. Kudryashov 162

Black Carbon and the Global Carbon and Oxygen Cycle
T. A. J. Kuhlbusch 163

An Analytical Method for the Determination of Different Carbon Fractions in Soils
T. A. J. Kuhlbusch, R. G. Zepp, and S. E. Trumbore 163

Rare Gases Constrain Mantle Mixing in the Réunion Hot Spot
J. Kunz and C. J. Allègre 164

Trace-Element Redistribution and Asian Dust Accumulation in a Hawai'ian Soil Chronosequence
A. C. Kurtz, L. A. Derry, and O. A. Chadwick 165

Dynamics of the Galapagos Hotspot from Helium-isotopic Geochemistry
M. D. Kurz, J. M. Curtice, A. E. Saal, and D. Geist 165

Influence of Pressure on the Diffusivity of Carbon and Oxygen in Calcite
T. C. Labotka, D. R. Cole, and L. R. Riciputi 165

Osmium-isotopic and Abundance Variations in Mexican Arc Lavas: Constraints on Partitioning of Osmium in Arc and Non-Arc Settings
J. C. Lassiter and J. F. Luhr 166

Trace-Element Analysis of Sulfide and Silicate Phases with High-Resolution Secondary Ion Mass Spectrometry
G. D. Layne and N. Shimizu 167

Delamination of Continental Lithosphere Beneath an Active Margin? Thermobarometric and Rhenium-Osmium-isotopic Constraints from Sierra Nevadan Xenoliths
C.-T. Lee, Q. Z. Yin, J. T. Chesley, R. L. Rudnick, W. F. McDonough, G. H. Brimhall Jr., and S. B. Jacobsen 167

Metasediments in the Lower Crust: Tectonic Origin Inferred Form *In Situ* Hafnium-isotopic Analyses of Zircons in a Metasedimentary Xenolith
C.-T. Lee, Q. Z. Yin, I. Horn, R. L. Rudnick, and W. F. McDonough 168

Natrocarbonatite Petrogenesis: Limestone-Trona (Evaporite) Volatile-fluxing and Syntectic Reactions Revisited
D. R. Lentz 168

Chlorine-isotopic Fractionation in a Sequence of Black Shales
S. M. Lev and R. D. Vocke Jr. 169

Geochemistry of the Shuiquangou Gold-bearing Alkaline Metasomatic Complex in Northwest Hebei, China
H. Y. Li, Z. S. Yang, Z. M. Gao, Z. J. Ding, and T. Y. Luo 170

Hydroxyl Behavior in Oxyhydroxide Phases (MOOH, M = Al, Fe, Mn) Based on Periodic Molecular Orbital Calculations
J.-J. Liang and R. T. Cygan 170

Uranium-Thorium-Radium-Barium Systematic of Baltic Ferromanganese Concretions
V. Liebetrau, A. Eisenhauer, N. Gussone, G. Wörner, and B. T. Hansen 171

An Isotopic Study of Groundwater in Granitic Terrains (Northwest Portugal)
A. S. Lima, M. O. Silva, P. M. Carreira, and D. Nunes 171

Trace-Element Chemistry and Petrogenesis of Peridotite and Pyroxenite Xenoliths from Pliocene Basanites of the Dzhilinda River, Vitim Volcanic Field
K. D. Litasov, Yu. D. Litasov, A. S. Mekhonoshin, and V. G. Mal'kovets 172

Melt Pockets in Mantle Xenoliths from Alkali Basalts of Vitim and Udokan Volcanic Fields, East Siberia
K. D. Litasov, V. V. Sharygin, Yu. D. Litasov, and S. Z. Smirnov 173

Variations in Concentrations of Dissolved Trace Elements in River Water of Guizhou, China
C. Q. Liu and G. L. Han 173

The Continental Exhalation of Copper Deposits from Red Clastic Formation in the Lanping-Simao Basin, Western Yunnan, China
J. Liu, C. Liu, C. Li, J. Pan, and T. Zhang 174

The Characteristics of Ore-bearing Chert from Cambrian Gold Deposits and Their Sedimentary Environmental Implications in Western Qinling Mountains, China
J. Liu, C. Liu, J. Liu, and T. Gu 174

Characteristics of Mantle Metasomatism and Geochemical Mechanism of Petrogenesis and Mineralization of Alkali-rich Porphyries
X. Liu, Z. Gao, J. Liu, X. Zhan, C. Li, and W. Su 174

Xenolith Evidence for Tectonic Underplating of Sedimentary Rocks and Layered Compositions of the Lower Crust at the Northern Margin of the North China Craton
Y. S. Liu and S. Gao 175

Osmium-isotopic Compositions of Horoman Ultramafic Complex in Hokkaido, Japan
Y. Z. Liu and T. Tanaka 175

Terminal Proterozoic Benthic Microbial Mats and Their Environmental Significance
G. A. Logan, C. R. Calver, P. Gorjan, R. E. Summons, J. M. Hayes, and M. R. Walter 176

Evaluating Secular Changes in Seawater Chemistry
T. K. Lowenstein, M. N. Timofeeff, L. A. Hardie, and S. T. Brennan 176

Assessment of Human Impact on a Coastal Embayment, Cebu, Philippines: Analysis of Bay Water and Sediments
A. R. Lucero Jr., M. E. S. Lupo, and P. C. Momongan 177

Zinc and Copper Isotopes as Tracers of Metal Origin in the Dissolved and Particulate Loads of Rain
J. M. Luck, D. Ben Othman, F. Albarède, and P. Telouk 177

How Well Can We Really Do Timescale Geochronology with Zircon Uranium-Lead?
K. R. Ludwig, R. Mundil, and P. R. Renne 178

How Alkali Basalts Ascending in Melt Conduits Can Affect Melting in Adjacent Peridotite
C. C. Lundstrom 178

Electrochemistry and Structure of Yttria-stabilized Zirconia Membranes for Potentiometric Measurements in Hydrothermal Systems
S. N. Lvov, G. C. Ulmer, X. Y. Zhou, S. M. Ulyanov, L. G. Benning, D. E. Grandstaff, M. Manna, E. Vicenzi, and H. L. Barnes 179

Sulfur Geochemistry of the Mesoproterozoic Bylot Supergroup, Northern Baffin and Bylot Islands, Canada: Local and Global Implications
T. W. Lyons and L. C. Kah 179

Mineralogy and Geochemistry of the Lateritic Profiles in South Jiangxi, China: Implications for Source-Area Weathering and Provenance
Y. J. Ma and C. Q. Liu 180

Seasonal Migration of Redox Boundary and Its Influence on Water Quality in Lake Lugu, Yunnan, China
Y. J. Ma and C. Q. Liu 180

Variability of Mercury and Phosphorus in Everglades Peat Cores: Implications for Mercury Mobility
A. W. Macfarlane and C. Arfstrom 181

Seasonal Changes in Lake Michigan Sediment Microbial Activity: A Model for "Top-Down" Control of Carbon Conversion
B. J. MacGregor, M. Maurer, B. Baker, D. P. Moser, K. H. Nealson, and D. A. Stahl 181

Magma Transport and Storage in the Melt Lens and Underlying Crystal Mush at Fast-Spreading Ridges: Constraints from the Oman Ophiolite
C. J. MacLeod, G. Yaouancq, R. M. Thomas, L. A. Coogan, and M. J. O'Hara 182

Timing of Mammal-like Reptile Extinctions and the Use of Carbon Isotopes in the Study of the Permian/Triassic Boundary
K. G. MacLeod, P. L. Koch, R. H. M. Smith, M. J. de Wit, and N. A. Rakotosolofo 183

Calcium-Aluminum-rich Inclusions in Chondrite Meteorites: The Case for Local Production in the Solar Nebula
G. J. MacPherson 183

Contamination of the Bushveld Complex Through Progressive Partial Melting of Crustal Wall Rocks
W. Maier, N. T. Arndt, E. Curl, and M. Ohnenstetter 184

Experimental Study of Pyrite Oxidation by Dissolved Oxygen: Oxidation Model Based on Surface Observations
M. Manaka and H. Ohmoto 184

What Do We Learn from Peaks of Uranium and Manganese in Deep Sea Sediments?
A. Mangini 185

Accessory Minerals and Trace-Element Fractionation in Granites
J. Mareels, M. Verhaeren, and J. Hertogen 185

Sill Stack Mush Column Magmatism
B. D. Marsh 185

The Polycyclic Aromatic Hydrocarbons and Biomarkers in Carbonaceous Matter of Kimberlite Pipe "Mir" and Hosted Sedimentary Rocks
D. Kh. Martikhaeva, E. A. Razvozzhaeva, A. G. Polozov, and A. E. Vorontsov 186

Paleogeographic Reconstruction of a Paleocene Carboniferous Basin (Los Cuervos Formation, Táchira State, Venezuela) by Using Trace-Element Content and Geostatistical Analysis of Coals
M. Martínez, M. Escobar, and C. López 186

Identification of Microbial Methane Deposits Via Core Analysis
A. M. Martini, L. M. Walter, J. C. McIntosh, and J. M. Budai 187

Goldschmidt's Legacy: Brian Mason's Contributions to Geochemistry and Meteoritics
U. B. Marvin 187

Black Carbon (Carbon-14) in the Santa Monica Basin: Riverine Delivery and Sedimentary Accumulation
C. A. Masiello, E. R. M. Druffel, and S. Griffin 188

A New Method for *In Situ* High-Precision Sulfur-isotopic Ratio Measurements by Laser Ablation Multiple Collector Inductively Coupled Plasma Mass Spectrometry
P. R. D. Mason, C.-J. de Hoog, and S. Meffan-Main 188

The "Lomagundi" Carbon-isotopic Anomaly Revisited: Extremely High $\delta^{13}C$ Excursion in Continental and Marine Carbonate Rocks of the Circa 2.1-Ga Magondi Supergroup, Zimbabwe
S. Master, B. Th. Verhagen, and J. D. Kramers 189

Comparison of Depth Profiles for Light Rare-Earth-element Tetrad Effect in Representative Oceans
A. Masuda and J. Shimoda 189

Rhenium-Osmium Evidence for Crustal Influences on Porphyry Copper Sulfides and Duration of Mineralization
R. Mathur, J. Ruiz, and F. Munizaga 190

Hafnium-isotopic Constraints on the Source of Kerguelen Archipelago Lavas
N. Mattielli, J. Blichert-Toft, D. Weis, D. Damasceno, J. S. Scoates, F. A. Frey, F. Albarède, and A. Giret 190

Dissolution of Aluminum-substituted Goethites by an Aerobic *Pseudomonas Mendocina Var.* Bacteria
P. A. Maurice, Y.-J. Lee, and L. Hersman 191

The Sulfide Capacities of Haplobasaltic and Basaltic Silicate Melts at 1400°C and 1 Bar
J. A. Mavrogenes and H. St. C. O'Neill 191

Tracing the Fate of Anthropogenic Nitrogen in Large Watersheds by Isotopic Techniques
B. Mayer and C. Heinzer 192

Sulfur- and Rhenium-Osmium-isotopic Systematics in Precambrian Seafloor Massive Sulfides
T. E. McCandless, R. D. Mathur, C. J. Eastoe, and A. Kontinen 192

New Developments in *In Situ* Analyses: Harvard University's Laser Ablation Inductively Coupled Plasma Mass Spectrometry (Quad and Multicollector) Laboratory
W. F. McDonough, R. L. Rudnick, and I. Horn 193

Surface Chemistry of Sulfide Minerals During Oxidative Dissolution
M. M. McGuire, K. J. Edwards, J. F. Banfield, and R. J. Hamers 193

Chemical and Isotopic Evidence for Pleistocene Recharge to Silurian-Devonian Aquifers, Illinois Basin
J. C. McIntosh, L. M. Walter, J. M. Budai, and A. M. Martini 194

Geochemical Evidence for Sedimentary Silica on Mars
S. M. McLennan 194

Copper-Chloride Complexing in Hydrothermal Brines
D. C. McPhail, J. Brugger, W. Liu, L. Spiccia, and J. Black 195

Three Palaeoproterozoic Positive Isotopic Excursions of Carbonate Carbon-13/Carbon-12: Still a Paradox
V. A. Melezhik and A. E. Fallick 196

Isotopic Composition of Concretionary Sulfides from the 2000-Ma Noneuxinic Basin, Pechenga Greenstone Belt, Northwest Russia
V. A. Melezhik, L. N. Grinenko, and A. E. Fallick 196

Evolution of Mineral and Glass Surface Roughness with Dissolution
N. P. Mellott, S. L. Brantley, and C. G. Pantano 196

Source Discrimination of Atmospheric Aerosols at Alert, Arctic Canada During 1994–1995 Using a Year-Long Record of Lead-isotopic and Trace-Element Data
G. Mercier, C. Gariépy, L. A. Barrie, and A. Simonetti 197

Anomalous Xenon in the Precambrian Nuclear Reactor in Okelobondo (Gabon): A Possible Connection to the Fission Component in the Terrestrial Atmosphere
A. P. Meshik, K. Kehm, and C. M. Hohenberg 198

H_2O Characteristics of Mantle Endmembers: Evidence from Mid-Ocean-Ridge Basalts and Ocean Island Basalts
P. J. Michael 198

Experimental Study of Cassiterite Solubility in Hydrogen-Chloride-bearing Water Vapor
A. A. Migdisov and A. E. Williams-Jones 199

The Mass-dependent Oxygen-isotopic Fractionation Line: New Measurements and the Need for a Reporting Consensus
M. F. Miller, I. A. Franchi, and C. T. Pillinger 200

The Riverine Discharge of Black Carbon into Coastal Sediments of the Gulf of Mexico
S. Mitra, T. S. Bianchi, and B. A. McKee 200

Rare-Earth-Element and Strontium-isotopic Study of the Middle Permian Limestone-Dolostone Sequence in Kuzuu Area, Central Japan
N. Miura, Y. Asahara, and I. Kawabe 201

Geochronological Studies of the Oldest Known Marine Sediments
S. J. Mojzsis and T. M. Harrison 201

Geochemistry of the Thermal Waters and Associated Trace Elements in Falcon State, Venezuela
R. L. Montero, M. Martínez, W. G. Meléndez, and G. Garbán 202

Noble Gas Constraints on Degassing Processes
M. M Moreira and P. Sarda 202

Kinetics of ^{40}Ar, H_2O, H_2 Release During Glauconite Hydrothermal Transformation
I. M. Morozova, A. V. Maslenikov, and L. K. Levsky 203

Uranium-Lead Zircon System During the Alkaline Metasomatism: Natural and Experimental Modeling
I. M. Morozova, N. G. Rizvanova, and L. K. Levsky 203

Oxygen-Sulfur-isotopic Measurement in Continuous Flow Mode: Application to the Origin of Dissolved Sulfates in Himalayan Rivers Using Elemental Analyzer Stable Isotope Ratio Mass Spectrometry
J. Morrison, C. France-Lanord, and A. C. Pierson-Wickmann 203

Suboxic Nitrification in Recent Sediments from a Scottish Sea Loch
R. J. G. Mortimer, M. D. Krom, P. Hayes, and I. M. Davies 204

Isotopic Evolution of Kauai Shield-stage Lavas
S. Mukhopadhyay, J. C. Lassiter, S. W. Bogue, and K. A. Farley 204

Comparison Between Black Carbon Distribution in Alpine Lacustrine and Coastal Marine Sediments
G. Muri, B. Cermelj, J. Faganeli, and A. Brancelj 205

Differential Weathering of Granitic Quarry Samples and Monument Stones
M. Nasraoui, N. Clauer, and M. I. Prudêncio 205

Differentiation by Deformation in the Ocean Crust
J. H. Natland and H. J. B. Dick 206

Origin of Deep-seated Hydrothermal Brines in Northern Germany: Geochemistry of Gases and Isotopes
D. Naumann, J. Erzinger, and E. Faber 206

Role of Water in Energetics of Zeolites and Layered Materials
A. Navrotsky 207

Probing the Interiors of the Terrestrial Planets: Data from the Moon and Mars
C. R. Neal, J. C. Ely, and J. C. Jain 207

The Ontong Java Plateau: Evidence of a Deep Earth Origin
C. R. Neal, J. C. Ely, A. L. Birkhold, J. C. Jain, J. J. Mahoney, and R. A. Duncan 208

Geochronological Constraints on the Source of Continental Rocks from the Kerguelen Plateau, ODP Site 1137, Elan Bank
K. E. Nicolaysen, D. Weis, F. A. Frey, S. A. Bowring, M. F. Coffin, and the Leg 183 Shipboard Scientific Party 208

Trace-Element Variations in Mantle Wedge Peridotites Above Modern Subduction Zones
Y. Niu, R. L. Fisher, and J. W. Hawkins 209

Platinum-Group-element and Rhenium Abundances in Hawai'ian Picrites: Compositional Variations in the Mantle Plume and Possible Secondary Mobility
M. D. Norman, V. C. Bennett, and M. O. Garcia 210

Hydrocarbon Speciation in Carbon-Oxygen-Hydrogen Fluids During Serpentinization
C. Normand and A. E. Williams-Jones 210

Hafnium-isotopic Systematics of Kimberlites, Lamproites, and Megacrysts: Implications for Mantle Reservoirs and the Composition of Bulk Silicate Earth
G. M. Nowell, D. G. Pearson, and P. D. Kempton 211

Hafnium-Isotopic Analysis of Kimberlite Megacrysts by Laser Ablation and Solution Mode Plasma Ionization Multicollector Mass Spectrometry: Evidence for a Contribution from a Deep Mantle Component in Kimberlites and Megacryst Magmas?
G. M. Nowell, D. G. Pearson, P. D. Kempton, R. W. Carlson, D. Bell, and R. E. Zartmann 212

The Effect of Growth Rate, $(U/Ca)_{aq}$, and Mg^{2+} on Uranyl Ion Coprecipitation with Calcite
M. Nugent and R. J. Reeder 213

Geological Constraints on Interpreting Early Archean Mineral and Whole-Rock Isotopic Data: Case History from the Itsaq Gneiss Complex, Greenland
A. P. Nutman, V. C. Bennett, and C. R. L. Friend 213

Evaluation of Human Impact on Lacustrine Environments and Ecosystems in the Twentieth Century by Using Stable Isotopic Ratios of Fish Specimens
N. O. Ogawa, H. Oda, T. Nakamura, N. Ohkouchi, N. S. Smirnova-Zalumi, V. V. Smirnov, N. G. Melnik, N. A. Bondarenko, T. Koitabashi, and E. Wada 214

Organic Carbon and Nitrogen Isotopes as Source Indicators of Organic Matter Preserved in Sediments of the Gulf of Trieste (North Adriatic)
N. Ogrinc, G. Fontolan, J. Faganeli, and S. Covelli 214

Sulfur-isotopic Records Around Livello Bonarelli Black Shale at the Cenomanian-Turonian Boundary
N. Ohkouchi, Y. Kajiwara, and A. Taira 214

Carbon-isotopic Records of Marine and Terrestrial Biomarkers in the Southern Ocean Sediments
N. Ohkouchi, K. Kawamura, N. Takemoto, M. Ikehara, and T. Nakatsuka 215

Does Siderite Constrain the pCO_2 and pO_2 Levels of the Archean Atmosphere?
H. Ohmoto 215

Experimental Study of Distribution Coefficients of Rare Earth Elements Between Iron-Manganese Deposits and Seawater in View of Rare-Earth-Element(III)-Carbonate Complexation Constants
A. Ohta and I. Kawabe 216

A Chemical Weathering Study of a Small Mountainous Granitic Watershed (Estibère, France): Water Chemistry, Soil and Rock Mineralogy, and Strontium-87/Strontium-86-isotopic Composition
P. Oliva, B. Dupré, M. Remaury, T. Gauquelin, F. Martin, and J. Darrozes 216

The Effect of Melt Composition on the Activity Coefficients of Some Siderophile Element Components (FeO, NiO, CoO, MoO_2, MoO_3, and WO_2) in Melts in the CMAS System
H. St. C. O'Neill and S. M. Eggins 217

Atmospheric CO_2 Levels During the Late Miocene and the Expansion of C_4 Grasses
M. Pagani, K. H. Freeman, and M. A. Arthur 218

New Geochemical (Major- and Trace-Element, Including Rare-Earth-element) Data from Pronto Mine and Ville Marie Weathering Profiles in Ontario and Québec, Canada: Elemental Mobility During Paleoproterozoic Weathering of Archean Granitic Basement
A. Panahi and G. M. Young 218

Molecular Simulation of Methane Hydrate Structure and Dynamics in Montmorillonite Interlayers
S.-H. Park and G. Sposito 218

The Role of H_2O in Controlling the Composition of High-Degree Mantle Melts
S. W. Parman and T. L. Grove 219

Laser Ablation Plasma Ionization Multicollector Mass Spectrometry: A New Method for Intracrystal Uranium-Thorium-Lead Geochronology Using Microsampling Techniques
R. Parrish, M. Horstwood, G. Nowell, S. Noble, H. Timmermann, P. Shaw, and I. Bowen 219

Crustal Growth Mechanisms: The Role of Transform Continental Margins
P. J. Patchett and C. G. Chase 220

Radiogenic Isotopes and Clastic Sediments
P. J. Patchett, G. M. Ross, J. D. Vervoort, J. Blichert-Toft, and F. Albarède 220

Open System Models of Lead-isotopic Evolution of the Earth
D. Paul and W. M. White 221

Greenhouse Warming by CH_4 in the Archean Atmosphere
A. A. Pavlov and J. F. Kasting 222

Radiocarbon Evidence for Autotrophic Metabolism in Marine Planktonic *Archaea*
A. Pearson, T. I. Eglinton, and J. M. Hayes 222

Isotope Dilution Inductively Coupled Plasma Mass Spectrometry Analyses of Rhenium-Osmium Isotopes and Platinum Group Elements Via Solvent-Extraction and Anion-Exchange Preconcentration and a Desolvating Nebulizer
D. G. Pearson and S. J. Woodland 222

The Deep Sources of Plumes: Rhenium-Osmium–Platinum-Osmium-isotopic and Platinum-Group-Element Systematics of High Helium-3/Helium-4 West Greenland Picrites
D. G. Pearson, L. M. Larsen, R. J. Walker, S. J. Woodland, A. K. Pedersen, R. W. Carlson, and S. B. Shirey 223

Magmatic Processes Operating in the Lowermost Oceanic Crust: Examples from the Leka Ophiolite Complex (Norway)
R. B. Pedersen and B. Tikoff 223

Dissolution and Growth of the Alumina Minerals Gibbsite, Diaspore, and Boehmite Studied Using Atomic Force Microscopy
C. D. Peskleway, G. S. Henderson, and F. J. Wicks 224

Platinum-Group-element Concentrations and Osmium-isotopic Ratios in Loess: A Proxy for the Eroding Upper Continental Crust?
B. Peucker-Ehrenbrink and B. M. Jahn 224

Photosynthesis Influences Silica Biomineralization
V. R. Phoenix, K. O. Konhauser, and D. G. Adams 225

The Osmium Budget of Himalayan River Sediments and Soils: Importance of Black Shale Erosion
A.-C. Pierson-Wickmann, L. Reisberg, and C. France-Lanord 225

Microbial Communities in Charcoal from Wildfire and the Underlying Humus
J. Pietikainen, O. Kiikkila, and H. Fritze 226

Uranium-238–Thorium-230–Radium-226 Disequilibria in Historical Kilauea Volcano Lavas: Mantle Melting Within the Hawai'ian Plume
A. J. Pietruszka, K. H. Rubin, and M. O. Garcia 226

A Hafnium-isotopic Composition Record of the Central Indian Ocean from Ferromanganese Crusts
A. M. Piotrowski, D-C. Lee, A. N. Halliday, J. N. Christensen, and J. R. Hein 227

Constraints from Thorium/Lanthanum on the Evolution of the Continents
T. Plank 228

An Earth-System Science Approach to Understanding, Predicting, Mitigating, and Remediating Metal Mobility from Mines and Unmined Mineral Deposits
G. S. Plumlee and M. J. Logsdon 228

Rhenium-Osmium-isotopic Systematics of Several Deccan Alkaline Complexes
A. Poirier, L. Reisberg, A. Simonetti, C. Gariépy, and S. L. Goldstein 228

Chemical Structure of the Refractory Organic Fraction Isolated from a Forest Soil (Lacadee, Southwest France): Black Carbon Contribution and Analytical Bias
N. Poirier, C. Largeau, J.-N. Rouzaud, S. Derenne, A. Mariotti, and J. Balesdent 229

Boninite-like Volcanic Rocks in the 3.7–3.8-Ga Isua Greenstone Belt (Central Tectonic Domain), Southwest Greenland
A. Polat, A. W. Hofmann, M. Rosing, and J. Myers 229

Geochemistry of 3.7–3.8-Billion-Year-Old Pillow Basalt Cores and Rims from the Isua Greenstone Belt (Northwestern Tectonic Domain) Greenland: Implications for Geodynamic Settings
A. Polat, A. W. Hofmann, J. Myers, and P. W. U. Appel 230

A Commercial Celestine Ores in Iron-Ore Deposits of the Siberian Platform
A. G. Polozov, T. N. Moroz, N. A. Palchik, L. V. Miroshnichenko, O. Yu. Belozerova, I. M. Romanenko, and P. F. Benedyuk 230

Transformation of Basalt on Contact to Salts in the Siberian Platform Sedimentary Cover
A. G. Polozov, O. A. Proidakova, G. P. Sandimirova, and E. V. Smirnova 231

Charred Organic Matter in Black Soils of Saskatchewan
E. V. Ponomarenko and D. W. Anderson 232

Kinetics of the Abiotic Reduction of Colloidal MnO_2 by Nitrite
J. I. Popp and G. W. Luther III 232

Organic Carbon and Sulfide Sulfur-isotopic Studies from the Oxygen/Sulfur and Sulfur/Deuterium Boundary Sediments in Poland
E. Porebska, Z. Sawlowicz, and H. Strauss 232

Spatial Distribution of Chromium in Northeast Arabian Sea Sediments
C. Prakash Babu, H.-J. Brumsack, and B. Schnetger 233

Biogeochemistry of the Cauvery Flood Plain Sediments, Southern India: Implications to Their Origin and Farming
G. K. Prasad and V. Rajamani 233

Iodine-Xenon Dating: Sensitive Chronometer for Reprocessing in the Primitive Solar System
O. V. Pravdivtseva and C. M. Hohenberg 234

A Fast Thermal Method For Black Carbon Analysis of Natural Samples
K. M. Prentice and J. I. Hedges 234

Platinum Group Elements in the 2.8-Ga Kostomuksha Greenstone Belt
I. S. Puchtel and M. Humayun 234

Clay Characterization with an Electron Microprobe: An Archaeological Example Using Coarse Pottery from the Aztec Cultural Horizon in Morelos, Mexico
G. Purcell, D. Wark, and S. Adhya 235

Mechanism of Adsorption of Cadmium onto Goethite and Hydrous Ferric Oxide in the Presence of Selenite
K. V. Ragnarsdottir, L. Spadini, and A. Manceau 235

Characterization and Origin of an Ultrapotassic Aluminous A-type Granitoid from Southwestern India
H. M. Rajesh 236

Fatty Acids in Particulates from Conception Bay, Newfoundland: Molecular and Carbon-isotopic Variations Across the 1996 Spring Bloom
C. S. Ramos, C. Parrish, T. Quibuyen, and T. Abrajano 236

The Fate of Sorbed Arsenic and Chromium During Early Diagenetic Transformations of Iron Oxides: Insights from Extended X-Ray Absorption Fine Structure Spectroscopy
S. R. Randall, D. M. Sherman, and K. V. Ragnarsdottir 237

Characterization of Colloids of Environmental and Geochemical Interest Using Field-Flow Fractionation Inductively Coupled Plasma Mass Spectrometry
J. F. Ranville, R. Beckett, and D. J. Chittleborough 237

New Insights into the Seismotectonics of Deep-seated Intrusions
A. S. P. Rao 238

New Insights into the Tectonics of Proterozoic Anorthosites
A. S. P. Rao 239

Microbial and Chemical Redox Reactions of Iron in Depth Profiles of Paddy Soil
S. Ratering and S. Schnell 239

Osmium Isotopes as Tracers of Sewage Dispersal in the Marine Environment
G. Ravizza, C. B. Tuit, and M. H. Bothner 240

Carbon-isotopic Characteristics of Pyrogenic Polycyclic Aromatic Hydrocarbons and Black Carbon in Aquatic Sediments: Development of Methods
C. M. Reddy and T. I. Eglinton 240

Chlorine-isotopic Ratios of Semivolatile Chlorinated Organic Compounds
C. M. Reddy, L. J. Heraty, B. D. Holt, N. C. Sturchio, T. I. Eglinton, K. A. Maruya, and J. L. Lake 241

Carbon Black from Automobile Tires
C. M. Reddy, H. Takada, and H. Kumata 242

X-Ray Absorption Fine Structure Study of the Incorporation Modes of Uranyl Species into Calcite and Aragonite
R. J. Reeder, M. Nugent, and G. M. Lamble 242

In Situ Uranium-Lead Ages of Zircons from the Bishop Tuff: No Evidence for Long Crystal Residence Times
M. R. Reid and C. D. Coath 243

Progress Report on High-Resolution Comparison of Argon/Argon and Uranium/Lead Systems
P. R. Renne, R. Mundil, K. Min, and K. R. Ludwig 243

Chronostratigraphy of the Sagantole Formation, Afar, Ethiopia, and the Age of Ardipithecus Ramidus
P. R. Renne, G. WoldeGabriel, W. K. Hart, G. Heiken, and T. D. White 244

Neodymium and Lead Isotopes in Atlantic Iron-Manganese Crusts: Panama Gateway and Intensification of Northern Hemisphere Glaciation
B. C. Reynolds, M. Frank, and R. K. O'Nions 244

Thorium-230 and Carbon-14 Dating of Speleothems from the Bahamas: Implications for Calibration of the Radiocarbon Timescale
D. A. Richards, J. W. Beck, D. J. Donahue, P. L. Smart, and R. L. Edwards 245

Old Zircon Megacrysts from Young Northwest Territories Kimberlites
S. H. Richardson, R. E. Zartman, and J. A. Carlson 245

A Pyrite Grand Unified Theory
D. Rickard 246

Experimental Constraints on the Behavior of Rhenium and Osmium During Mantle Melting and Magmatic Differentiation
K. Righter 246

Core Formation and Wet Terrestrial Accretion
K. Righter and M. J. Drake 247

Micrometer Scale Variations of $\delta^{18}O$ in Corals
C. Rollion-Bard, M. Chaussidon, C. France-Lanord, and E. Bard 247

Boron-isotopic Analysis in Sediments by Ion Microprobe: Implications for Weathering and the Oceanic Boron Budget
E. F. Rose, M. Chaussidon, and C. France-Lanord 248

Deposition and Storage of Spheroidal Carbonaceous Particles in European Mountain Lakes and Their Catchments
N. L. Rose, E. Shilland, H. Yang, P. G. Appleby, T. Berg, L. Camarero, M. Gabathuler, K. Hanselmann, R. Harriman, K. Koinig, L. Lien, U. Nickus, B. Steiner Trad, E. Stuchlík, H. Thies, and M. Ventura 249

Continental Crust as a Consequence of Collision Geodynamics: Some Precambrian and Phanerozoic Examples
O. M. Rosen and V. S. Fedorovsky 249

Salt Seepage into Lake Kinneret, Israel: Can $\delta^{37}Cl$ Help?
J. M. Rosenbaum, A. Nishri, M. Stiller, and M. Gophen 250

The Response of Marine Sediment Bacteria to Organic Carbon Input
R. Rosselló-Mora, B. Thamdrup, H. Schäfer, and R. Amann 250

Quantifying Elemental Sulfur (S^0), Bisulfide (HS^-), and Polysulfides (S_x^{2-}) Using a Cyclic Voltammetry Method
T. F. Rozan, S. M. Theberge, and G. W. Luther III 251

Trace-Element Characterization of Metamorphic Zircons
D. Rubatto, I. S. Williams, and D. Günther 251

Evidence for a Mafic, Rutile-bearing Reservoir in the Earth
R. L. Rudnick, M. Barth, W. F. McDonough, and I. Horn 252

Assessing Reactive Surface Area During Mica Dissolution with X-Ray Photoelectron Spectroscopy and Real-Time, *In Situ* Atomic Force Microscopy Observations
E. Rufe and M. F. Hochella Jr. 252

Osmium Concentrations and Isotopic Composition of the Lower Crust in Mexico
J. Ruiz, J. T. Chesley, and K. Righter 253

Modern Formation Processes for Fossil Brines in the Great Australian Bight
J. L. Russell and the ODP Leg 182 Shipboard Science Party 253

Major- and Trace-Element Abundance Data in the Circa 2.2-Ga Hekpoort Paleosol
R. Rye 253

Ammonium Partitioning and Nitrogen-isotopic Fractionation During High-Temperature Metamorphic Fluid-Rock Interactions
S. J. Sadofsky and G. E. Bebout 254

Quantum Chemical Model for Apatite Mineralization on Silica Bioceramics
N. Sahai and J. A. Tossell 255

Greenstone-Granite Belts of the Hearne Domain, Nunavut, Canada: Evolution of Juvenile Neoarchean Oceanic Crust
H. A. Sandeman, B. Cousens, W. J. Davis, S. Hanmer, T. Peterson, J. Ryan, and S. Tella 255

Rhenium and Osmium System in Ophiolitic Complexes: Implications for Chromitite Formation and Ophiolite Paragenesis
R. A. Santos, K. Suzuki, B. Takano, Y. Tatsumi, Y. Miyata, and Y. Nozaki 255

Seawater pH Control on the Boron-isotopic Composition of Calcite: Inorganic Coprecipitation Experiments
A. Sanyal, M. Nugent, R. J. Reeder, and J. Bijima 256

Compound-Specific Hydrogen-isotopic Measurements of Lacustrine Organic Matter: A Novel Tool for Paleoclimatology
P. E. Sauer, J. M. Hayes, T. I. Eglinton, A. L. Sessions, and A. Schimmelmann 256

Dissolution of Analcite Under Conditions of Alkaline pH
D. Savage, C. Rochelle, M. Mihara, Y. Moore, A. Milodowski, K. Bateman, and D. Bailey 257

Comparision of Evolution of Samarium-Neodymium and Rubidium-Strontium Systems in Metamorphic Country Rocks in Contact Zones of Intrusions: Eldora Stock, Colorado (USA) and Ozernaja Varaka, Kola Peninsula (Russia)
V. M. Savatenkov and L. K. Levsky 258

Scavenging of Cobalt and Nickel by Iron Hydroxide in Submarine Hydrothermal Plumes: Experimental Modeling
A. V. Savenko 258

Analysis of Microbial Diversity in Sediments from the Benguela Upwelling System Showing Anaerobic Methane Oxidation
H. Schäfer, H. Fossing, T. G. Ferdelman, and G. Muyzer 258

Influence of Temperature on Nickel Sorption on Clay Mineral and Oxide Surfaces
K. G. Scheckel and D. L. Sparks 259

Uptake Mechanisms of Radionuclides on Clay Surfaces as Determined by X-Ray Absorption Spectroscopy
M. A. Scheidegger, R. Dähn, B. Baeyens, and M. H. Bradbury 259

Calcium-rich Silica-undersaturated Melts in Island Arcs
P. Schiano, J. M. Eiler, and E. M. Stolper 260

Quantification of Organic Particles from Fossil Fuel Combustion in Soils
M. W. I. Schmidt, H. Knicker, P. G. Hatcher, and I. Kögel-Knabner 260

Char from Vegetation Fires in Soils?
M. W. I. Schmidt, J. O. Skjemstad, and I. Kögel-Knabner 261

An Empirical Assessment of "Ultra" High-Precision Uranium-Lead Zircon Geochronology: Zircon and Sphene Systematics of the Fish Canyon Tuff
M. D. Schmitz and S. A. Bowring 262

The Evolution of Cratonic Geotherms: Uranium-Lead Thermochronometric Constraints from Lower Crustal Xenoliths, Lesotho, Southern Africa
M. D. Schmitz and S. A. Bowring 263

Methane-based Biosynthesis in Florida Escarpment Abyssal Brine Seeps
M. Schoell, R. J. Hwang, C. K. Paull, and C. S. Martens 263

The Effect of Visible Light and Phosphate on the Kinetics of Pyrite Oxidation by Dissolved Molecular Oxygen
M. A. A. Schoonen and D. R. Strongin 264

Strontium Isotopes in Neoproterozoic Cap Carbonates from Namibia: Evidence for Intense Chemical Weathering in the Aftermath of a Snowball Earth
D. P. Schrag, P. F. Hoffman, G. P. Halverson, S. A. Bowring, and K. Abbasi 264

Uranium-Series Dating of Lake Carbonates: The Lessons from Lake Lisan (Paleo-Dead Sea)
A. Schramm, M. Stein, and S. L. Goldstein 265

Fluid Evolution in Shear-Zone Hosted Mesothermal Gold Deposits: Examples from the Yilgarn Craton and Lachlan Fold Belt, Australia
P. K. Seccombe, S. C. Dick, and Z. Jiang 265

Highly Radiogenic Upper Crustal Rocks of Central Idaho and Its Bearing on Ore Genesis
K. P. Selvam, A. W. Macfarlane, G. Sen, and V. J. Salters 266

Hydrogen Isotope Ratio Monitoring Gas Chromatography Mass Spectrometry
A. L. Sessions, T. W. Burgoyne, A. Schimmelmann, and J. M. Hayes 266

Ancient-depleted Mantle Under a Modern Spreading Center: Osmium Evidence from Hydrothermal Fluids from Juan De Fuca Ridge
M. Sharma, A. W. Hofmann, G. J. Wasserburg, and D. A. Butterfield 267

The Carbon Dioxide/Helium-3 Systematics of Plume-, Mid-Ocean-Ridge Basalt-, and Arc-type Lavas from the Manus Back-Arc Basin
A. M. Shaw, D. R. Hilton, C. G. Macpherson, and J. M. Sinton 268

Elemental Fractionation and Equilibrium Processes
D. M. Shaw 268

A High-Precision Benthic Foraminiferal Strontium/Calcium Record over the Past 35,000 Years
C.-C. Shen, S. R. Emerson, D. W. Hastings, T. Lee, C.-H. Chiu, and G. T. Shen 269

New Insights of Sulfide Ore Genesis from an Osmium-Strontium-isotopic Study of Chinkuashi Gold-Copper Deposit in Taiwan
J. J. Shen, L. P. Tan, C. H. Chen, C. Y. Lan, and C. H. Chen 269

Ion Solvation and Molecular Dynamics at the Goethite/Water Interface
D. M. Sherman 269

Thermodynamics of Strontium, Barium, and Lead Solid Solution in $CaSO_4$: Results from Atomistic Simulations
D. M. Sherman 270

Rare-Earth-Element Fractionation and Neodymium-isotopic Variation in Pacific Hydrothermal Plumes and Metalliferous Sediments
R. M. Sherrell, G. Ravizza, M. P. Field, and J. Blusztajn 271

Brown Coal as a Detoxicant of Soils Polluted with Heavy Metals
A. V. Shestopalov, O. S. Bezuglova, and I. V. Morozov 271

Carbon Dioxide Flux Due to Hydrothermal Venting from Back-Arc Basin and Island Arc and Its Influence on Global Carbon Dioxide Cycle
N. S. Shikazono and H. K. Kashiwagi 272

Geochemical Consequences of Partial Melting at the Core-Mantle Boundary
N. Shimizu, K. Hirose, and Y. Fei 272

Large Lead-isotopic Variations in Olivine-Hosted Melt Inclusions in a Basalt from the Mid-Atlantic Ridge
N. Shimizu, A. V. Sobolev, G. D. Layne, and O. P. Tsamerian 273

Carbon Cycles Studies with Fatty-Acid Biomarkers and a Mixed Layer Model
K. H. Shin, S. Noriki, N. Tanaka, and M. Ikeda 273

Rhenium-Osmium- and Oxygen-isotopic Systematics of Diamondiferous and Non-Diamondiferous Eclogites from the Roberts Victor Kimberlite, South Africa
S. B. Shirey, U. Wiechert, R. W. Carlson, J. J. Gurney, and L. Van Heerden 273

Trace Elements and Carbon-isotopic Composition of Inclusion-free Diamonds
A. A. Shiryaev, N. N. Dogadkin, and E. M. Galimov 274

X-Ray Investigation of the Principle Nitrogen-related Defects in Diamonds and Their Models
A. A. Shiryaev, Yu. A. Klyuev, A. M. Naletov, and A. T. Dembo 275

The Estuarine Chemistry of Rare Earth Elements: Comparison of the Amazon, Fly, Sepik, and Gulf of Papua Systems
E. R. Sholkovitz and R. Szymczak 276

Anomalous Lead Isotopes and Sources of Leads in the Upper Mississippi Valley Zinc-Lead District, USA
A. A. Sicree and H. L. Barnes 276

Thermodynamic Modeling of Bromine Partition Between Seawater and Its Solids
M. G. Siemann and M. Schramm 276

Inferences from Uranium-series Disequilibra on Magma Origin and Migration Beneath the Izu Arc
O. Sigmarsson, J. B. Gill, P. Holden, and C. C. Lundstrom 277

Modeling Crustal Growth Using Samarium-Neodymium Database of Shales
F. Simien, E. Lewin, C. J. Allègre, and A. N. Dia 277

Variation in the Sources and Fluxes of Atmospheric Pollutants Proximal to Montréal (Québec), Canada as Inferred from a Year's Lead- and Strontium-isotopic Record for Precipitations
A. Simonetti, C. Gariépy, L. Poissant, and J. Carignan 278

Geochemistry of Flood Plain Sediments of the Kaveri River, Southern India
P. Singh and V. Rajamani 278

Regional Rocky Mountain Climate Change Recorded by Oxygen Isotopes of Holocene Ferricretes
D. J. Sjostrom, M. A. Poage, C. P. Chamberlain, and G. Furniss 279

The Determination of Charcoal in Soils
J. O. Skjemstad, L. J. Janik, and J. A. McGowan 280

The Nature, Distribution, and Impact of Charcoal in Soils
J. O. Skjemstad, L. J. Janik, and L. R. Spouncer 280

Dissolution Mechanisms of Hydrogen in β-Mg_2SiO_4 (Wadsleyite) Using Hydrogen-1 Magic-Angle Spinning Nuclear Magnetic Resonance
A. E. Slesinger, B. J. Wood, and S. C. Kohn 280

The Nature and Reactivity of Combustion Soots
D. M. Smith and A. R. Chughtai 281

Geoavailability of Metals in a Mine-Waste Material
K. S. Smith, G. P. Meeker, R. W. Leinz, S. J. Sutley, H. L. O. Huyck, and G. A. Desborough 281

Rare-Earth-element and Trace-Element Trends in the Everglades as Tracers for Sedimentary Processes
J. E. Sonke and V. J. M. Salters 281

$CaCO_3$ Dissolution in Equatorial Deep-Sea Sediments During Interglacial-Glacial Transitions
J. Specht and A. Mangini 282

Isotopic Modeling of the Significance of Sulfate Reduction for Phenol Attenuation in a Polluted Aquifer
M. Spence, S. Bottrell, S. Thornton, and D. Lerner 282

Strontium-isotopic Ratios Trace Natural Alkaline Addition to Coal Mine Drainage
S. L. Stafford, R. C. Capo, B. W. Stewart, A. Reynolds, and R. S. Hedin 283

Major Trends in the Mineralogy of Carbonate Skeletons Reflect Oscillations in Mid-Ocean-Ridge Spreading Rates and Seawater Chemistry
S. M. Stanley and L. A. Hardie 283

The Pan African Plume Event and the Growth of Gondwana
M. Stein 284

In Situ Zircon Trace-Element Analysis by High-Mass Resolution Secondary Ion Mass Spectrometry
R. A. Stern 284

Analysis of Volatile Organic Compounds over Octopus Spring, Yellowstone National Park, Using Open-Path Fourier Transform Infrared Spectroscopy
D. L. Stoner, J. G. Jolley, K. S. Miller, D. J. Fife, and W. F. Bauer 285

Mapping and Cataloging Microbial Biodiversity Within Its Geochemical Environment
D. L. Stoner, M. C. Miller, L. J. White, J. A. Brizzee, R. L. Lee, and R. C. Rope 285

The Role of Garnet-Pyroxenite in the Source of Hawai'ian Basalts: Hafnium-Neodymium-Thorium-isotopic Evidence
A. Stracke, V. J. M. Salters, K. W. W. Sims, and J. Blichert-Toft 285

The Sulfur-isotopic Composition of Precambrian Sediments: Seawater Chemistry and Biological Evolution
H. Strauss 286

Rare-Earth-Element Geochemistry of Ferromanganese Concretions from the Barents Sea and the White Sea
S. V. Strekopytov, E. L. Vinogradova, and A. V. Dubinin 286

Stable Isotopic Investigations of the Chlorinated Aliphatic Hydrocarbons
N. C. Sturchio, L. J. Heraty, B. D. Holt, L. Huang, and T. A. Abrajano 287

Marine Sediments: A Black Carbon Reservoir and Record of Combustion
D. Suman 288

2-Methylhopanoids: Biomarkers for Cyanobacteria and for Oxygenic Photosynthesis
R. E. Summons, L. L. Jahnke, J. M. Hope, and G. A. Logan 288

Molecular Modeling of Cesium-Smectite Hydrates
R. A. Sutton and G. Sposito 289

The Influence of Sulfides on Soluble Iron(III) in Anoxic Sediment Porewaters
M. Taillefert, S. M. Theberge, V. Hover, and G. W. Luther III 289

Oxygen-isotopic and Rare-Earth-Element Compositions of Quartz Veins Within Xingzi Group of Lushan, Southeast China: Implications for the Origin Metamorphic Fluids
H. F. Tang and C. Q. Liu 289

Making Continental Crust by Crustal Delamination in Subduction Zones, and Complementary Accumulation of the EMI Component in the Deep Mantle
Y. Tatsumi 290

Formation of Soil from Weathered Granite: Insights into Inorganic and Biogeochemical Processes from Mineralogical, Microbiological, and Bulk Chemical Analyses
A. E. Taunton, S. A. Welch, and J. F. Banfield 290

The Dependence of Plagioclase Dissolution and Strontium Release Rates on Solution Saturation State
A. S. Taylor, J. D. Blum, and A. C. Lasaga 291

Diamond: Just Another Metamorphic Mineral?
L. A. Taylor, G. A. Snyder, and A. Camacho 291

On the Difficulties of Making Earth-like Planets
S. R. Taylor 292

Measurement of Fluxes and Concentrations of Heavy Metals in Sediment Porewaters Using Diffusive Gradients in Thin Films
P. R. Teasdale, W. Davison, and J. Hamilton-Taylor 292

X-Ray Spectroscopy Investigations of Lead(II) Distributions Within Biofilms Formed on Metal-Oxide Surfaces
A. S. Templeton, T. P. Trainor, J. D. Ostergren, S. J. Traina, A. M. Spormann, S. R. Sutton, M. Newville, and G. E. Brown Jr. 293

The Fundamentals of Calcite Mineralization: Surface Processes of Spiral Growth
H. H. Teng, P. M. Dove, and J. J. De Yoreo 294

Kinetics of Calcite Growth: Analysis of Surface Processes and Relationships to Macroscopic Rate Laws
H. H. Teng, P. M. Dove, and J. J. De Yoreo 294

A Century-long Record of Anthropogenic Nutrient Loading Provided by $\delta^{15}N$ Values in Sediment from a Eutrophic Lake
J. L. Teranes and S. M. Bernasconi 295

Distribution and Mobility of Lead in Roadside Soils
N. Teutsch, Y. Erel, and L. Halicz 296

Identifying Metal Sulfide Complexes in Freshwaters Using Laser Desorption Mass Spectroscopy
S. M. Theberge, T. F. Rozan, and G. W. Luther III 296

Oxygen-isotopic Systematics of Reykjanes Ridge Mid-Ocean-Ridge Basalts: Constraints on the Origin and Composition of Icelandic Plume Mantle
M. F. Thirlwall, R. N. Taylor, D. P. Mattey, C. G. Macpherson, M. A. M. Gee, and B. J. Murton 296

Protactinium-231/Uranium-235–Thorium-230/Uranium-238 Systematics of Young Volcanic Rocks from Central America: Contrasting Behavior Related to Subduction Fluxes?
R. B. Thomas, M. M. Hirschmann, H. Cheng, R. L. Edwards, and M. K. Reagan 297

A Multimethod Approach to Correlating Bentonites from the Silurian of the Welsh Basin
J. Thorogood, N. J. G. Pearce, C. A. Bendall, D. K. Loydell, R. Cave, and J. A. Evans 298

Strontium and Neodymium Isotopes in Apatites: Their Application to the Study of Bentonites from the Welsh Basin
J. Thorogood, N. J. G. Pearce, J. A. Evans, D. K. Loydell, and R. Cave 298

Chemical Composition of Cretaceous Seawater: Results from Environmental Scanning Electron Microscopy–Energy Dispersive X-Ray Spectrometry Analyses of Fluid Inclusions in Marine Halites
M. N. Timofeeff, T. K. Lowenstein, and L. A. Hardie 299

Chemical Composition of Permian Seawater: Results from Environmental Scanning Electron Microscopy–Energy Dispersive Spectroscopy Analysis of Fluid Inclusions in Marine Halites
M. N. Timofeeff, T. K. Lowenstein, and L. A. Hardie 299

Stratigraphic Records of Black Carbon from Lake Sediments as Archives of Continental Environmental Change
W. Tinner and F. S. Hu 300

Lithium-isotopic Geochemistry of Mono Lake, California
P. B. Tomascak, N. G. Hemming, and S. R. Hemming 301

Gold Adsorption on Goethite and Humic Acid-coated Goethite
T. Tosiani 301

Theoretical Evidence for Copper Thioarsenite Complexing
J. A. Tossell 302

Argon in Mid-Ocean-Ridge Basalts and Loihi Glasses and Implications for the Evolution of the Earth's Mantle
M. Trieloff, M. Falter, and E. K. Jessberger 302

How Does Quartzite Weather? A Geochemical Study of Proterozoic Quartzite in the Semiarid Regions of Delhi, India
J. K. Tripathi and V. Rajamani 303

Non-Conservative Molybdenum Behavior in Seawater
C. B. Tuit and G. E. Ravizza 303

Experimental Study of the Alteration Process of Basaltic Glass Under High Partial Pressure of Carbon Dioxide
S. Utsunomiya and T. Murakami 304

Carbonatites at 200 Kilometers: Quenched Melt Inclusions in Megacrystalline Lherzolite Xenoliths, Slave Craton, Canada
E. van Achterbergh, W. L. Griffin, K. Kivi, N. J. Pearson, and S. Y. O'Reilly 304

GLITTER: Online Interactive Data Reduction for the Laser Ablation Inductively Coupled Plasma Mass Spectrometry Microprobe
E. van Achterbergh, C. G. Ryan, and W. L. Griffin 305

Hydrogeochemistry of Madeira Island
C. H. Van der Weijden, J. P. G. Loch, and F. A. L. Pacheco 306

High-Resolution Lead and Neodymium Records of Northeast Indian Ocean Sediments over the Past 150 ka: Fluctuations in the Monsoon and Himalayan Weathering Associated with Northern Hemisphere Glaciation
D. Vance and K. W. Burton 306

Precise Lead-isotopic Analysis by Multiple Collector Inductively Coupled Plasma Mass Spectrometry: Long-Term Reproducibility and Comparison with Double-Spike Measurements
D. Vance and P. van Calsteren 307

Distribution of Carbon Among Organic-Mineral Fractions of Vertisols and Zonal Soils as Influenced by Biogeochemical Conditions
A. Ya. Vanyushina, L. S. Travnikova, and R. C. O. Gaiego 308

Dissolved Organics in Formation Waters from the Pannonian Basin, Hungary
I. Varsanyi, Z. Karpati, J. M. Matray, L. O. Kovacs, and A. Klopp 308

Investigation of the Role of Natural Organic Matter in the Sorption of Copper in an Oxisoil Profile
F. V. Vasconcelos, B. D. H. Honeyman, D. M. Macalady, and J. R. Ranville 309

Isotopic Geochemistry of Shark Teeth as Indicators of Environmental Conditions
T. W. Vennemann, E. Hegner, G. Cliff, and G. W. Benz 310

Hafnium-Isotopic Composition of the Crust and Mantle During the Archean: Constraints on Crust-Mantle Evolution
J. D. Vervoort, P. J. Patchett, F. Albarède, J. Blichert-Toft, M. E. Barley, T. S. Blake, C. W. Brauhart, M. G. Green, and R. J. Thériault 310

Low $\delta^{18}O$ Despite Involvement of Subducted Continental Material in the Banda Arc
P. Z. Vroon, D. Lowry, M. J. van Bergen, A. Boyce, and D. Mattey 311

Geochemistry of Carbon and Oxygen Isotopes of Carbonatites from the Western Part of the Altay-Sayan Folding System
V. V. Vrublevsky, B. G. Pokrovsky, V. N. Kuleshev, I. F. Gertner, V. P. Parnachov, and G. N. Anoshin 311

Improvement of Low-Level Trace-Element Analysis with the Electron Microprobe for Recording Mantle Processes
C. Wagner and M. Fialin 312

Platinum-Rhenium-Osmium Distribution at 10 GPa in Iron-Nickel-Sulfur-Phosphorus
D. Walker 313

The $\alpha_0 * K_0$ = Constant Form Fits Hot Compression of B2 KCl, Rhombohedral $KClO_3$, Orthorhombic $KClO_4$, and O_2 Gas to 96 kbar Calibrated Against B1 NaCl
D. Walker, S. M. Clark, M. C. Johnson, and R. L. Jones 313

Surprisingly Small Oxygen-2 Gas Volumes from 22–96 kbar at 600°C Are Confirmed from Decomposition of Orthorhombic $KClO_4$
D. Walker, S. M. Clark, M. C. Johnson, and R. L. Jones 314

Osmium-isotopic Constraints on the Early Evolution of the Mantles of the Earth, Moon, and Mars
R. J. Walker, B. Asuquo, H. M. Prichard, and A. D. Brandon 315

Osmium-186–Osmium-187 Isotope Systematics of Manganese Nodules and Marine Sediments
R. J. Walker, S. R. Hemming, H. Becker, and M. Hodgson 315

Improving the Accuracy of Potassium-Argon Determinations on Organoclays
J. M. Wampler, W. C. Elliott, S. K. Sears, and S. Shata 316

Spectroscopic Probes of Degradation Reactions Promoted by Metal Oxide Surfaces
D. Wang, W. E. Dubbin, J. Y. Shin, M. Zavarin, M. A. Cheney, T. G. Spiro, and G. Sposito 317

Geochemistry and Metallization of Mylonite-hosted Gold Deposit in the South China
H. N. Wang, J. Chen, J. F. Ji, and C. Y. Sun 317

Molecular Modeling of the Interlayer Structure and Dynamics in Hydrotalcite
J. Wang, A. G. Kalinichev, R. J. Kirkpatrick, R. T. Cygan, and X. Hou 318

Carbonate Rock Weathering and Pedogenesis in the South of China
S. J. Wang, H. B. Ji, Z. Y. Ouyang, and D. Q. Zhou 318

Geochemistry of the Ore Fluid in the Jinjitai Carbonate Rock-hosted Gold Deposit, Sichuan, China
X. C. Wang and Z. R. Zhang 318

Geochemistry of the Triassic Basalt in the Luhuo-Daofu Region, Southwestern China, and Its Tectonic Significance
X. C. Wang and Z. R. Zhang 319

First Data on Rare-Earth-Element Distributions in the Changjiang Estuary: Relatively Low Concentrations and Conservative Behavior at Low-Salinity Regions
Z.-L. Wang, C.-Q. Liu, and J. Zhang 319

Bacterially Promoted Calcium Carbonate Precipitation and Solid-Phase Capture of Strontium and UO_2
L. A. Warren, N. Parmar, and F. G. Ferris 320

Chromium(III) Sorption and Oxidation on Manganite (γ-MnOOH) as Observed with Fluid-Cell Atomic Force Microscopy and X-Ray Photoelectron Spectroscopy
R. M. Weaver and M. F. Hochella Jr. 321

Racemization Isochrons for the United States Atlantic Coastal Plain Quaternary: Independent Calibration and Geochemical Implications of Results from Marginal Marine Units, Central Florida
J. F. Wehmiller, L. L. York, D. S. Jones, and R. W. Portell 321

Evidence for a Continental Component at Elan Bank from Leg 183-Site 1137 on the Kerguelen Plateau
D. Weis, J. Barling, D. Damasceno, F. A. Frey, K. E. Nicolaysen, and the Leg 183 Shipboard Scientific Party 321

Tracing Sources of Channel and North Sea Pollution Aerosols Above the Straits of Dover Using Lead-isotopic Geochemistry
D. Weis, K. Deboudt, and P. Flament 322

Role of Microorganisms and Microbial Metabolites in Apatite and Biotite Dissolution Kinetics
S. A. Welch, A. E. Taunton, and J. F. Banfield 322

Oxygen-isotopic Composition of Conodont Apatite: A Potential Proxy for Paleozoic Marine Water Temperatures and Salinities
B. Wenzel, W. Buggisch, M. M. Joachimski, P. Königshof, and C. Lécuyer 323

Phosphate-Oxygen-isotopic Microanalysis by Infrared Laser Isotope Ratio Monitoring Gas Chromatography Mass Spectrometry
B. Wenzel, M. M. Joachimski, J. Rauch, and W. Buggisch 323

Magnetite Surface Protonation to 290°C from Acid/Base Titrations with *In Situ* pH Measurement
D. J. Wesolowski, M. L. Machesky, D. A. Palmer, and L. M. Anovitz 324

Development of Quaternary Pedogenic Calcite and Dolomite on the Island of Hawai'i
C. E. Whipkey, R. C. Capo, and O. A. Chadwick 324

Hafnium-isotopic Geochemistry of the Galapagos
W. M. White and J. Blichert-Toft 325

The Coordination Chemistry of Siderophores Within Soils
C. F. Whitehead and A. T. Stone 326

Geochemistry of Eclogites from Alp De Trescolmen, Adula Nappe, Central Alps, Switzerland
R. A. Wiesli, L. A. Taylor, J. W. Valley, M. J. Spicuzza, G. A. Snyder, A. Camacho, and M. Kurasawa 326

Partitioning of Trace Metals in Anoxic Black Sea Sediments
R. T. Wilkin and M. A. Arthur 327

The Chemical and Mineralogical Response of Allanite to Hydrothermal Alteration, Casto Granite, Idaho
S. A. Wood and A. Ricketts 328

The Effect of Fulvic Acid on the Extent and Rate of Dissolution of Obsidian
S. A. Wood, L. M. Anovitz, J. M. Elam, D. R. Cole, L. R. Riciputi, and P. Bénezeth 329

Determination of the Solubility of Crystalline Neodymium $(OH)_3$ in Sodium Triflate Solutions from 30° to 250°C with *In Situ* pH Measurement
S. A. Wood, D. A. Palmer, D. J. Wesolowski, and P. Bénezeth 329

Platinum Group Elements in Subduction Zone Magmas: Anion Exchange Preconcentration Inductively Coupled Plasma Mass Spectrometry Analyses of Lesser Antilles and Izu-Bonin Magmas
S. J. Woodland, D. G. Pearson, J. A. Pearce, and M. F. Thirlwall 330

An Experimental Study of Copper(I) Chloride Solubility in Water Vapor at Temperatures from 360° to 400°C and Water-Vapor Saturated Pressure
Z. Xiao, A. E. Williams-Jones, and C. H. Gammons 331

Using Linear Free-Energy Relationship to Predict Stability Constants of Aqueous Metal Complexes/Chelates
H. Xu and Y. Wang 331

Nitrous Oxide Emissions from Agricultural Soil in Guizhou Province, Southwestern China
W. B. Xu, Y. T. Hong, X. H. Chen, and C. S. Li 331

Quantification of Quench Rates in Water, Air, and Liquid Nitrogen
Z. Xu and Y. Zhang 332

Geochemical and Isotopic Constraints for the Evolution of the Slave Province
K. Yamashita and R. A. Creaser 332

Possible Relations of Felsic Magmas to Ore Metals in Volcanogenic Massive Sulfide Deposits: Geochemical Evidence from the Bathurst Mining Camp, Iberian Pyrite Belt, Abitibi Belt, and the Hokuroku District
K. Yang and S. D. Scott 333

Milankovitch Theory Reviewed from Arid Closed-Basin Lacustrine Calcite in Death Valley, California
W. Yang and T. K. Lowenstein 333

Fractal Analysis of Gold Grade in Cangshang Gold Deposit, Northwestern Jiaodong, China
Z. S. Yang, H. Y. Li, Z. M. Gao, Z. J. Ding, and T. Y. Luo 333

Comparison of Size-Exclusion Chromatographic Gels for the Characterization of Polymeric Silica
D. M. Yates and P. J. Heaney 334

The Niobium-92-Zirconium-92 p-Process Chronometer
Q. Z. Yin, I. Horn, W. F. McDonough, J. Zipfel, S. B. Jacobsen, and R. L. Rudnick 334

Precise and Accurate Calibration of Osmium Spike
Q. Z. Yin, C.-T. Lee, W. F. McDonough, I. Horn, R. L. Rudnick, and S. B. Jacobsen 335

Molybdenum- and Tungsten-isotopic Signatures in the Early Solar System
Q. Z. Yin, K. Yamashita, and S. B. Jacobsen 335

Comparison Between Field and Laboratory Rates of Rhyolite Weathering
T. Yokoyama and J. F. Banfield 336

Source Tracing of Archeological Copper Smelting Ore by *In Situ* Isotopic Measurements by Laser Ablation Inductively Coupled Plasma Mass Spectrometry Using Quadrupole and Multicollector Techniques
S. M. M. Young, I. Horn, D. Miller, J. Cantle, F. Keenan, and I. Bowen 337

Geologic Assessment of the Biogeochemical Feedback Response to the Climatic and Chemical Perturbations of the Late Paleocene Thermal Maximum
J. C. Zachos and G. R. Dickens 337

Carbon Dioxide Cycling: Climate, Impacts, and the Faint Young Sun
K. J. Zahnle and N. H. Sleep 338

Dynamical Signatures of Living Systems
M. Zak 338

Hydrologic Constraints on the Localization of Sediment-hosted Gold Ore Bodies of Southwestern Guizhou, China
C.-B. Zhang and Z.-R. Zhang 339

Subchronic Toxicity of Rare Earth Elements and Estimated Daily Intake Allowance
H. Zhang, W. F. Zhu, and J. Feng 339

Could the Late Permian, Deep Ocean Have Been Anoxic?
R. Zhang, M. J. Follows, J. Grotzinger, and J. C. Marshall 339

Experimental Determination of the Dependence of Water Speciation on Controlled Cooling Rate
Y. Zhang and Z. Xu 339

Comparative Studies of Rare Earth Elements in Groundwaters and Aquifer Materials from the Southern Great Basin
X. Zhou, K. H. Johannesson, K. J. Stetzenbach, C. Guo, and I. M. Farnham 340

Natural Variations of Iron and Copper Isotopes Determined by Plasma Source Mass Spectrometry: Applications to Geochemistry and Cosmochemistry
X. K. Zhu, N. S. Belshaw, Y. Guo, and R. K. O'Nions 341

Tertiary Seawater Chemistry: Implications from Fluid Inclusions in Halite
H. Zimmermann 341

Stability of Polycyclic Aromatic Hydrocarbons in the Solar Nebula
M. Yu. Zolotov and E. L. Shock 341

Abstracts

QUANTIFYING PRECAMBRIAN CRUSTAL EXTRACTION: THE ROOT IS THE ANSWER.

D. Abbott[1], D. Sparks[2], C. Herzberg[3], W. Mooney[4], A. Nikishin[5], and Y. Zhang[6], [1]Lamont-Doherty Earth Observatory, USA, [2]Texas A&M University, College Station TX 77843, USA, [3]Rutgers University, New Brunswick NJ 08903, USA, [4]U.S. Geological Survey, Menlo Park CA 94025, USA, [5]Geological Faculty, Moscow State University, Moscow 119899, Russia, [6]University of California–Santz Cruz, Santa Cruz CA 95064, USA.

We use two different methods to estimate the total amount of continental crust that was extracted by the end of the Archean and the Proterozoic. The first method uses the sum of seismic thickness of the crust, the eroded thickness of the crust, and the trapped melt within the lithospheric root to estimate total crustal volume. This method finds an average equivalent thickness of Archean crust of 69 ± 9 km and an average equivalent thickness of Proterozoic crust of 61 ± 11 km. Much of this crust never reached the surface, but remained within the continental root as congealed, iron rich komatiitic melt. The second method uses experimental estimates of percentage of partial melting versus the length of the melt column to estimate the amount of crust extracted through time. This method finds that the average equivalent thickness of Archean crust was 63 ± 5 km, and the average equivalent thickness of Early Proterozoic crust was 44 ± 2 km. It is likely that some of this crust remained trapped within the lithospheric root and that some of the Early Proterozoic crust contains recycled Archean age crust. Overall, we find that 31–53% of continental crust was extracted by the end of the Archean, most likely by 2.7 Ga. Between 54 and 84% of continental crust was extracted by the end of the Early Proterozoic, most likely by 1.8–2.0 Ga. Our results are most consistent with geochemical models that call upon large amounts of recycling of early extracted continental crust. We call upon trapped Fe-rich melt within the lithospheric root to solve the iron problem, rather than lithospheric delamination.

AMPHIBOLE-VEINED LITHOSPHERIC MANTLE SOURCES FOR RECENT ALKALINE BASALTS IN THE NORTHERN CANADIAN CORDILLERA.

A.-C. Abraham[1,2], D. Francis[1], and M. Polvé[2], [1]Department of Earth and Planetary Sciences, McGill University, 3450 University Street, Montréal, Québec H3A 2A7, Canada (abraham@geosci.lan.mcgill.ca), [2]Unité Mixte de Recherche–Centre National de la Recherche Scientifique 5563, Université Paul Sabatier, 38 rue des 36 Ponts, 31400 Toulouse, France.

Primitive Tertiary to recent alkaline volcanic rocks in the Northern Canadian Cordillera define two compositional end members, olivine nephelinite (NEPH) and hypersthene normative olivine basalts (Hy-NORM). NEPH are Si-undersaturated rocks (ne >15 wt%) that define an end member characterized by large enrichments in incompatible trace elements, but isotopically depleted in term of their Sr, Nd, and Pb composition. They have low concentrations of large ion lithophile elements (LILE) compared to other incompatible elements such as Nb, Th, U, and the light rare earth elements (LREE) [1]. The Hy-NORM end member is characterized by the lowest trace-element concentrations, but still exhibit a general enrichment in the most incompatible elements. Hy-NORM always have higher Pb-isotopic ratios than NEPH, and their $^{87}Sr/^{86}Sr$ and $^{143}Nd/^{144}Nd$ signatures vary with the tectonic block through which they have erupted [1].

The relative behavior of LILE and LREE in NEPH requires the presence of a K-bearing phase in their mantle sources [2]. Incongruent melting of amphibole (1 Amph = 0.45 Liq + 0.45 Cpx + 0.1 Sp) produces liquids consistent with both major and trace-element concentrations of the most Nb-rich NEPH of each individual center (Fig. 1). The NEPH end member may represent amphibole-rich veins that developed in the sublithospheric mantle by the migration of asthenospheric fluids. Their depleted isotopic signatures coupled with high contents of Rb, Sm, Th, and U indicate that this enrichment is relatively recent.

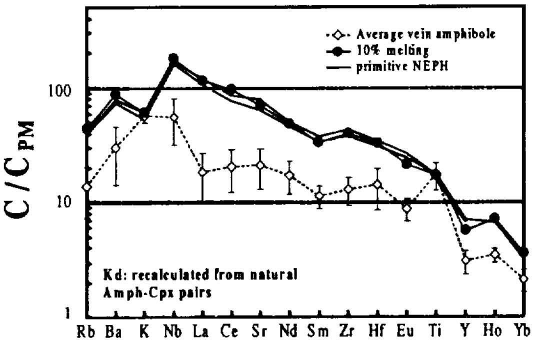

Fig. 1. Trace-element concentrations normalized to primitive mantle.

Primitive Hy-NORM from the northern Canadian Cordillera have major-element signatures similar to other small alkaline centers erupted on phanerozoic continental margins [e.g., 3]. They are characterized by high SiO_2, FeO, Ti_2O, and low CaO, similar to primitive OIB olivine tholeiites as opposed to MORB olivine tholeiites. They have, however, higher Al_2O_3 than primitive OIB, and have higher Na_2O contents than both OIB and MORB (Fig. 2). The SiO_2 content indicates a last equilibration at relatively low pressure, between 10 and 15 kbar [4] consistent with the absence of garnet in the amphibole melting reaction. Hirose and Kushiro [4] showed that FeO and Al_2O_3 are strongly dependent on the composition of the source. The high-FeO content of the Hy-NORM might be explained by the existence of a source more Fe-rich than pyrolite under the Northern Cordillera (Fig. 2).

The high Na_2O contents may indicate that primitive Hy-NORM were generated by low degrees of partial melting or might be a source signature, characteristic of phanerozoic continental mantle. The Al_2O_3 and CaO contents of the most primitive lavas suggest, however, that clinopyroxene was exhausted in their residue, implying relatively large degrees of partial melting. Although the Sr-Nd-Pb-isotopic signatures of the Hy-NORM depend on the tectonic block through which they erupted, they cannot be explained by contamination by the upper crust [1]. The terrane dependence of the major, trace and isotopic compositions of primitive Hy-NORM is consistent with their derivation from distinct lithospheric roots.

References: [1] Abraham et al., in preparation. [2] Francis D. and Ludden J. (1995) *J. Petrol., 36,* 1171–1191. [3] Zhang M. and O'Reilly S. Y. (1997) *Chem. Geol., 136,* 33–54. [4] Hirose K. and Kushiro I. (1993) *EPSL, 114,* 477–489.

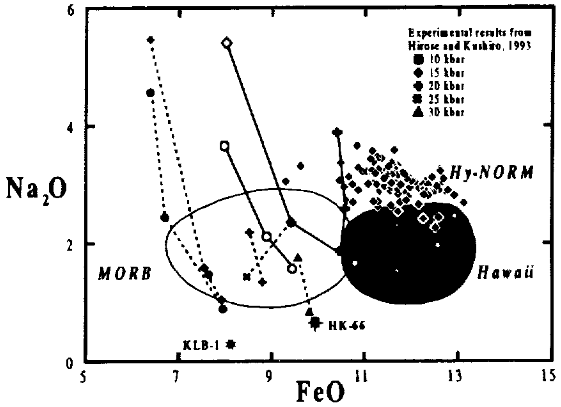

Fig. 2. Na_2O vs. FeO for primitive Hy-NORM compared to primitive OIB and MORB olivine tholeiites.

STABLE ISOTOPES IN DEEP-SEA CORALS: A NEW MECHANISM FOR "VITAL EFFECTS."

J. Adkins[1], E. Boyle[2], and W. Curry[3], [1]Lamont-Doherty Earth Observatory, Columbia University, Route 9W, Palisades NY 10964, USA, [2]Department of Earth and Planetary Sciences, Massachussetts Institute of Technology, Cambridge MA 02139, USA, [3]Department of Geology and Geophysics, Woods Hole Oceanographic Institution, Woods Hole MA 02543, USA.

Several studies have established that the aragonitic skeletons of deep-sea corals are out of equilibrium for the stable isotopes of C and O. Values of $\delta^{13}C$ and $\delta^{18}O$ in deep-sea corals are linearly correlated across a range of more than 12‰ for C and 4‰ for O. However, the heaviest isotopic values, within a single specimen, can obtain inorganic equilibrium. As deep-sea corals grow in a temporally stable temperature, salinity and $\delta^{13}C$ of DIC environment, the trend in $\delta^{13}C$ and $\delta^{18}O$ values must be related to the biomineralization mechanism itself. Recent work has related potential changes in this "vital effect" to climate variations in the past [1]. In our work, we establish a regular pattern of $\delta^{13}C$ and $\delta^{18}O$ in the coral *Desmophyllum cristagalli* and propose new mechanism for the cause of this vital effect.

The radially symmetric species *D. cristagalli* has thin septa that are attached around an outer rim by "innerseptal" aragonite. In general the thin septa, growing toward the center of the coral, are isotopically heavier than the thicker material around the outside. Microsampling of the aragonite shows that the stable isotopes are strongly correlated with the coral's banding pattern. On a photographic negative image, optically dense white bands are further out of equilibrium than dark bands. These dark bands, in the thinnest portion of the septa, are at $\delta^{18}O$ equilibrium, to the degree that this value is known. All of the microsampled specimens show a break in the linear relationship between $\delta^{18}O$ and $\delta^{13}C$ at the lightest values. In this region, $\delta^{13}C$ reaches a maximum depletion while $\delta^{18}O$ continues to decrease.

This break in slope is an important clue that a previous mechanism for isotopic disequilibrium in corals, based on kinetic fractionation effects, might be incorrect. In two landmark papers, McConnaughey proposed that the slow step of CO_2 hydration in the extra cellular calcifying fluid (ECF) fractionates C and O and that this isotopic signature is preserved more strongly in fast precipitating aragonite [2]. Using the same picture of the ECF as McConnaughey, we propose a thermodynamic mechanism that allows for a slope break at the lightest values and still works in the presence of Ca ATPase, an enzyme found in corals that catalyzes CO_2 hydration. Because bicarbonate and carbonate ions can not diffuse across the ECF membrane, isotopically light $CO_2(aq)$ is an important source of C to the aragonite skeleton. This light C mixes with ambient DIC, which has several "leaky" pathways into the ECF. Carbon dioxide diffusion is driven by a pH gradient that is actively maintained by the coral to increase the alkalinity of the ECF. This pH increase also decreases the $\delta^{18}O$ of the aragonite by the pH effect originally documented by McCrea [3] and further examined in more detail by others [4,5]. In this model, the stable isotopes are coupled because the increased pH of the ECF (dominating the $\delta^{18}O$ signal) also controls the relative importance of CO_2 diffusion (dominating the $\delta^{13}C$ signal) into the calcifying region. This mechanism may have wider application in biological carbonates as many organisms have very similar slopes of $\delta^{13}C$ vs. $\delta^{18}O$.

References: [1] Smith et al. (1997). [2] McConnaughey (1989). [3] McCrea (1950). [4] Usdowski et al. (1991). [5] Zeebe (1999).

THE SOLUBILITY OF IRON-MAGNESIUM CHLORITE IN HYDROTHERMAL SOLUTIONS.

S. U. Aja, Department of Geology, Brooklyn College of the City University of New York, 2900 Bedford Avenue, Brooklyn NY 11210, USA.

Introduction: Solid mixtures of kaolinite and natural chlorites (±quartz) and/or chlorite-gibbsite have been equilibrated in aqueous 1.0 M NaCl, 0.001 or 0.005 M $MgCl_2$ solutions at 25°, 125°, 175°, and 200°C and saturated vapor pressures. Reversibility of fluid-mineral equilibria was demonstrated by approaching final solution compositions from high and low log $a^{1/2}_{Mg^{2+}}/a_{H^+}$ and from silica under- and supersaturation. At the end of the experiments, the solutions were separated using immiscible displacement techniques [1] and analyzed by determining pH, Eh, and the concentrations of various metal ions (Na, Mg, Fe, Si, Ti, Ni, Cr, and Al). The measured compositions were recalculated to activities at temperatures using EQ3/6 (v. 7.2a; [2]). The chlorite compositions and run products were also examined by ATEM [3].

Results and Discussion: Fluid-mineral equilibria involving natural trioctahedral chlorites may be modeled by presuming a binary solid solution having clinochlore and chamosite as phase components such that the equilibrium reaction becomes

$$\begin{gathered}(Mg_5Al)(AlSi_3)O_{10}(OH)_8 + 5Fe^{+2} \rightleftharpoons \\ (Fe^{+2}{}_5Al)(AlSi_3)O_{10}(OH)_8 + 5Mg^{+2}\end{gathered} \qquad (1)$$

This presupposes that Al^{+3}, Fe^{+3}, and $SiO_{2,aq}$ (in addition to $Cr^{3+}{}_{(aq)}$, $Ni^{2+}{}_{(aq)}$, and $Mn^{2+}{}_{(aq)}$) are fixed at constant activities and that the levels of Mg and Fe^{+2} are controlled by the appropriate phase components. However, this is more likely to be true for experiments conducted under elevated conditions as opposed to those conducted under low temperatures. Furthermore, a graphical analysis of the solution data indicated that the chlorites reacted with a fixed composition during the course of the experiment. That is, natural chlorites may be presumed to behave thermodynamically as 1-component phases during isothermal, isobaric experiments and thus the thermodynamic properties of mixing the endmember components to yield the starting bulk composition are fixed. But being that some of the above species were not buffered, the solution data were interpreted using the equilibrium constant approach. The reaction between kaolinite and the Mg-rich chlorite at 25°, 125°, and 175° was modeled using equations 2, 3, and 4 respectively [3].

$$\begin{gathered}(Mg_{8.303}Fe^{2+}{}_{0.861}Fe^{3+}{}_{0.343}Al_{2.264}Ca_{0.019}Mn_{0.017}Ni_{0.014}Cr^{3+}{}_{0.007}) \\ (Si_{5.750}Al_{2.250})O_{20}(OH)_{16} + 12.989\ H^+ + 0.215\ O_{2(g)} \rightleftharpoons \\ Al_2Si_2O_5(OH)_4 + 8.303Mg^{2+} + 2.514Al(OH)^-{}_4 + \\ 1.204\ Fe(OH)^-{}_4 + 0.017Mn^{2+} + 0.019Ca^{2+} + 0.014Ni^{2+} + \\ 0.007Cr^{3+} + 3.75SiO_{2(aq)} + 5.058H_2O\end{gathered} \qquad (2)$$

$$\begin{gathered}(Mg_{8.303}Fe^{2+}{}_{0.861}Fe^{3+}{}_{0.343}Al_{2.264}Ca_{0.019}Mn_{0.017}Ni_{0.014}Cr^{3+}{}_{0.007}) \\ (Si_{5.750}Al_{2.250})O_{20}(OH)_{16} + 16.601\ H^+ \rightleftharpoons \\ Al_2Si_2O_5(OH)_4 + 8.303Mg^{2+} + 2.514Al(OH)^-{}_4 + \\ 1.204\ Fe(OH)^-{}_4 + 0.017Mn^{2+} + 0.019Ca^{2+} + 0.014Ni^{2+} + \\ 0.007Cr^{3+} + 3.75SiO_{2(aq)} + 9.272H_2O + 0.086\ O_{2(g)}\end{gathered} \qquad (3)$$

$$\begin{gathered}(Mg_{8.303}Fe^{2+}{}_{0.861}Fe^{3+}{}_{0.343}Al_{2.264}Ca_{0.019}Mn_{0.017}Ni_{0.014}Cr^{3+}{}_{0.007}) \\ (Si_{5.750}Al_{2.250})O_{20}(OH)_{16} + 16.707\ H^+ + 0.215\ O_{2(g)} \rightleftharpoons \\ 2.257Al_2Si_2O_5(OH)_4 + 8.303Mg^{2+} + 0.602\ Fe_2O_3 + 0.017Mn^{2+} + \\ 0.019Ca^{2+} + 0.014Ni^{2+} + 0.007Cr^{3+} + 1.263SiO_{2(aq)} + 9.272H_2O\end{gathered} \qquad (4)$$

The equilibrium constants thus calculated have been summarized in Table 1.

TABLE 1. Log K for Mg chlorite-kaolinite reaction.

Reaction	Log K
2	52.43 ± 7.50
3	62.33 ± 6.89
4	79.06 ± 2.60

In order to evaluate the mixing properties for chlorite solid solutions, the Mg/H activity ratios measured at 25°C were compared with values predicted for (endmember) clinochlore-kaolinite equilibria; the comparison indicates that the experimentally measured assemblage is more stable. At quartz saturation, for instance, the predicted value of log $a^{1/2}_{Mg}{}^{2+}/a_H{}^+$ is 5.4 orders of magnitude higher than the measured value for the clinochlore-kaolinite compatibility. Apparently, the Gibbs energy of mixing (ΔG°_{mix}) for Fe-Mg chlorite solid solutions may be significantly larger than currently presumed in the literature.

Acknowledgments: We thank the donors of the Petroleum Research Fund, administered by the American Chemical Society, for their support of this work.

References: [1] Aja et al. (1991) *GCA, 55,* 1353–1364. [2] Wolery (1993) LLNL, UCRL-MA-110662. [3] Aja S. U. and Small J. S. (1999) *Eur. J. Mineral.*, in press.

HIGHLY SIDEROPHILE ELEMENTS IN MANTLE SULFIDES: *IN SITU* LASER ABLATION MICROPROBE INDUCTIVELY COUPLED PLASMA MASS SPECTROMETRY ANALYSIS.

O. Alard[1], W. L. Griffin[1], J. P. Lorand[2], S. Jackson[1], and S. Y. O'Reilly[2], [1]Key Centre for Geochemical Evolution and Metallogeny of Continents, Department of Earth and Planetary Sciences, Macquarie University, Sydney, NSW 2109, Australia (oalard@laurel.ocs.mq.edu.au), [2]Laboratoire de Mineralogie, Museum National d'Histoire Naturelle, European Space Agency–Centre National de la Recherche Scientifique 7058, 61 Rue Buffon, 75005 Paris, France.

The geochemistry of the siderophile and chalcophile elements potentially carries large amounts of information on processes in mantle-derived rocks. In particular, the platinum group elements (PGE), which are classified with Au and Re as highly sideophile elements (HSE) may be even more useful than the more commonly used REE. Sulfide phases are thought to be the main hosts for the HSE in mantle rocks; PGE contents on the order of tens of ppm have been reported for sulfide inclusions in peridotite-paragenesis diamonds [1] and for sulfide fractions from the Lherz orogenic massif [2]. However these two studies have yielded contrasting chondrite-normalized PGE patterns; sulfides in diamond have high IPGE (Os, Ir, and Ru) contents and $Pd/Ir_N < 1$, and "massif" sulfides have lower IPGE contents and $Pd/Ir_N > 1$.

We have determined the HSE (PGE + Au) contents of single mantle sulfide grains using a custom-built Nd:YAG UV laser-ablation microprobe linked to a Perkin Elmer Sciex ELAN6000 ICPMS. We have investigated peridotite xenoliths in alkali basalts from Eastern Australia and the Massif Central (France); kimberlite-hosted garnet peridotites (South Africa); orogenic peridotites from Lherz (Pyrenees, France); and an abyssal peridotite from the Kane area (Atlantic).

The PGE contents of the sulfides are highly variable; e.g., Os ranges from 0.5 to 100 ppm and Pd from 0.4 to 83 ppm. The concentrations of IPGE in sulfide are roughly inversely correlated with whole-rock S content. None of the PGE patterns of sulfides, whether enclosed in other phases or interstitial, is chondritic. Mantle-normalized PGE patterns can be divided into two basic types: (1) pattern A (Fig. 1) which displays high IPGE content and decreasing normalized contents toward Pd and Au, leading to $Pd/Ir_N < 1$; and (2) pattern B (Fig. 1) which is characterized by low IPGE contents and $Pd/Ir_N > 1$. The two patterns can be observed in different sulfide grains in the same sample. Sulfides having pattern A are MSS and are generally enclosed in primary silicate phases (e.g., olivine, garnet); they occur in all sample types. The B pattern is found in interstitial sulfides, which commonly are Cu-rich compared to the silicate-enclosed ones from the same sample. For instance, in sample AR-10 (New England, Australia), which has 330 ppm of S and $Al_2O_3 \approx 2.5\%$, angular sulfides within metasomatic patches have typical B patterns.

Both patterns may display negative Pt anomalies ($Pt/Pd_N < 1$ and $Pt/Ru_N < 1$). These anomalies can be very pronounced as in lherzolite 84-1 from Lherz which has Pt/Pd_N and Pt/Ru_N as low as 0.02 and 0.04 respectively. However, the whole rock Pt/Pd_N and Pt/Ru_N are 0.5, 0.5 respectively [3], and the discrepancy may imply that Pt is hosted by a phase(s) other than sulfide. We have occasionally observed Pt peaks at the begining or end of sulfide ablation runs in serpentinized rocks, suggesting that Pt may occur as discrete phase(s) at the margins of sulfide grains, perhaps within altered sulfide or in silicates. However, we have not yet observed any nugget effect for PGEs other than Pt in mantle sulfides [cf. 4–5], even in the most PGE-rich ones. This suggests that PGEs are highly soluble in base metal sulfides under mantle conditions.

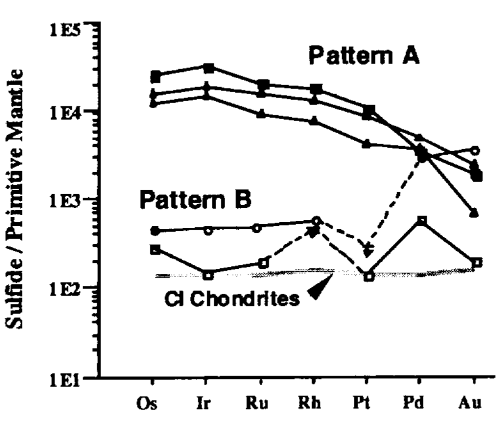

Fig. 1. Primitive-mantle normalized PGE patterns. Primitive mantle and CI chondrite values are from [6].

On the basis of petrographic observations and experimental work [e.g., 7] we interpret sulfides with A patterns as residual MSS while sulfides displaying B patterns may represent trapped sulfide liquids. The complementary nature of these two patterns suggests that they are related through a single process, the partial melting of a "primitive" sulfide with a chondritic pattern: A sulfides represent the restite while B sulfides are related to the partial melt. Since many of the mantle samples studied here display both patterns, we suggest that many of the "typical" chondritic mantle patterns found in whole-rock PGE analyses may reflect a mixing between several sulfide generations. *In situ* analysis is required to understand these patterns.

References: [1] Bulanova G. P. et al. (1996) *GCA, 124,* 111–125. [2] Pattou L. et al. (1996) *Nature, 379,* 712–715. [3] Lorand J. P. et al. (1999) *J. Petrol.,* in press. [4] Tredoux et al. (1997) *EAG Workshop 97.* [5] Balhaus C. (1997) *EAG Workshop 97.* [6] McDonough and Sun (1995) *Chem. Geol., 120,* 225–253. [7] Li et al. (1996) *GCA, 60,* 1231–1238.

THE EARLY EVOLUTION OF THE EARTH AND MARS FROM HAFNIUM-NEODYMIUM-ISOTOPIC SYSTEMATICS.

F. Albarède[1], J. Blichert-Toft[1], J. D. Vervoort[2], J. Gleason[1], and M. T. Rosing[3], [1]Ecole Normale Supérieure de Lyon, 69007 Lyon, France (albarede@ens-lyon.fr), [2]University of Arizona, Tucson AZ 85721, USA, [3]Geologisk Museum, 1350 Copenhagen, Denmark.

Mantle convection on terrestrial planets should be geochemically traceable. Three planets (Earth, Mars, and the Moon) are accessible to geochemical observation. Their wide range of depth and gravity makes the extent of mineral stability fields very different, notably for garnet and perovskite. These two minerals can be adequately traced for their strong fractionation of two pairs of parent and daughter isotopes, $^{147}Sm/^{144}Nd$ and $^{176}Lu/^{177}Hf$, through the isotopic composition of Nd and Hf.

Neodymium- and Hf-isotopic data on shergottites [1] show that basaltic material was extracted very early to produce the enriched crust and the depleted mantle of Mars. The martian crust differs from the lunar highlands by a lesser plagioclase abundance, a result of the stronger gravity. The persistence of isotopic anomalies associated with extinct radionuclides [2] suggests that, just as for the Moon, the early chemical differentiation of the martian mantle survived since 4.4–4.2 Ga, thereby casting doubt on the persistence of vigorous convection in the mantle of this planet.

On Earth, the oldest coherent piece of ancient crust is in Isua, Greenland, and is 3.8 b.y. old. Although some mobility of the elements of the radiogenic systems is undoubtedly present, the integrated Sm/Nd and Lu/Hf ratios of the mantle source of Isua volcanics and felsic rocks fall between the modern values of the terrestrial mantle and those of the poorly mixed lunar and martian mantles [3–5]. This observation depends very little on the age assumed for these rocks.

This isotopic pattern reveals that, in contrast to the Moon and Mars, the terrestrial mantle has nearly reached convective steady-state. Extraction of basaltic melts both at ridge crests and hot spots plus flushing at subduction zones result in the formation of continental crust and mantle heterogeneities. This fractionation induced by phase changes is balanced by convective mixing. Some memory of the initial chemical stratification is, however, still noticeable in the mantle source of Archean basalts. The relative strength of the Lu/Hf and Sm/Nd fractionation and the contrast between the melt and inferred source values of these ratios (the "Hf paradox" of [6]) indicates the ubiquitous role of garnet as an essential mineral left behind by melt extraction. Garnet was a very likely residual phase during the cooling of magma oceans of the Earth and Mars. Garnet seems also to be a residual phase of modern as well as Archean basalt extraction [5].

Alternatively, evidence for nonchondritic values of the terrestrial mantle in the Archean may call the chondritic paradigm into question [7]. Whether the Sm/Nd and Lu/Hf ratios of the bulk Earth equal those of ordinary chondrites echoes the discrepancy found for O isotopes between this group of meteorites and terrestrial material [8]. The Earth may have formed from a mixture of meteorites from different classes or from a particular reservoir of nebular material with Sm/Nd and Lu/Hf ratios different from those observed in ordinary chondrites. An alternative possibility is that the giant impact that formed the Moon blasted off irreversibly the Hadean crust and its inventory of lithophile elements and left the planet with Sm/Nd and Lu/Hf ratios higher than in the initial material. Making these ratios significantly larger in the BSE than in chondrites so that the Archean mantle is not excessively depleted has, however, the perturbing consequence of moving the entire modern array of oceanic basalts into the enriched quadrant. This in turn begs the question: Where is the missing complement of such an "enriched" source of oceanic basalts? The BSE values for the Sm-Nd and Lu-Hf systems as they are now [9] therefore seem to be reasonably well determined.

The persistence of transient chemical heterogeneities for ~0.8 b.y. after planetary accretion is consistent with the thermal relaxation of the Earth [10] and reflects that both heat loss and chemical equilibration keep pace with plume extraction and plate tectonics. The question of whether any memory of the primordial differentiation has been preserved in the modern deep mantle is important for mantle tomography.

References: [1] Blichert-Toft J. et al. (1999) *EPSL*, submitted. [2] Harper J. et al. (1995) *Science, 267,* 213–217. [3] Lee D.-C. and Halliday A. N. (1997) *Nature, 388,* 854–857 [4] Vervoort J. D. and Blichert-Toft J. (1998) *GCA*, in press. [5] Blichert-Toft J. et al. (1999) *GCA*, in press. [6] Salters V. J. M. and Hart S. R. (1989) *Nature, 342,* 420–422. [7] Vervoort J. D. et al. (1999) *EPSL, 168,* 79–99. [8] Clayton R. N. (1993) *Ann. Rev. Earth Planet. Sci., 21,* 115–149. [9] Blichert-Toft J. and Albarède F. (1997) *EPSL, 148,* 243–258. [10] Schubert G. et al. (1979) *JGR, 85,* 2531–2538.

ION PROBE MICROMETER SCALE STABLE ISOTOPIC RATIOS OF AEROSOL MICROPARTICLES.

J. Aléon, M. Chaussidon, and B. Marty, Centre de Recherches Pétrographiques et Géochimiques–Centre National de la Recherche Scientifique, 15 rue Notre Dame des Pauvres, 54500 Vandoeuvre-lès-Nancy, France (aleon@crpg.cnrs-nancy.fr; chocho@crpg.cnrs-nancy.fr; bmarty@crpg.cnrs-nancy.fr).

Aerosols are involved in photochemical reactions, in clouds microphysics and in the atmospheric radiative budget. The knowledge of their characteristics is therefore required to have a better approach of global atmospheric understanding. Stable isotopic ratios can be used as a powerful tool to determine the circulations of primary aerosols such as mineral dust [1] or to constrain the chemical processes occuring during the formation of secondary aerosols such as sulfates or sulfuric acid droplets [2]. The O-isotopic ratios of quartz from mineral dust can be used to determine the proportions of magmatic and metamorphic quartz of high-temperature origin and of sedimentary quartz of low-temperature origin. Sulfur- and O-isotopic ratios in volcanic sulfates, if available at the scale of single grains, will provide new informations on the oxidative processes occuring in a volcanic plume.

Up to now isotopic data have been obtained for bulk aerosol samples which might obscure isotopic signals since classical techniques for O-isotopic analyses, for instance, require more than 10^8 individual micrometer-sized grains.

We developed a technique to analyze $^{18}O/^{16}O$ and $^{34}S/^{32}S$ ratios in individual micrometer-sized aerosol particles with a high sensitivity Cameca IMS 1270 ion probe. Quartz grains are chemically separated from the samples [3] and then incrusted into an In foil prior to analysis. The solubility of sulfates and their submicrometer size lead to additional difficulties for the sample preparation. Filter fibers with aerosol particles are hand picked from the filters and one by one incrusted into an In foil. A gold grid is then pressed on the sample to ensure that the preparation is conductive.

In the imaging mode a 5 pA Cs^+ primary beam focused down to <1 μm is rastered over zones of 25 × 25 μm on the quartz samples. Quantitative O-isotopic images are then acquired on an electron multiplier. A software has been developed to process these images in order to recognize automatically individual particles and to compute their isotopic ratios (Fig. 1). The particles when located by image analysis can also analyzed in the ponctual mode. The ion intensity obtained for ^{18}O on a single micrometer-sized particle allows to reach a 1σ reproducibility better than 3–5‰ for $\delta^{18}O$, which gives the possibility to separate for instance low T quartz from high T quartz.

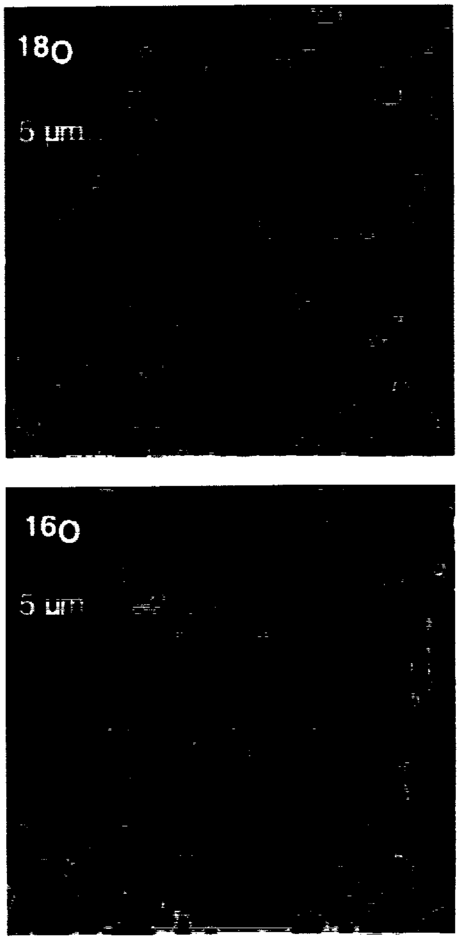

Fig. 1. Oxygen-16 and ^{18}O images of micrometer-sized quartz grains mounted in In.

For sulfates a 0.2 to 0.3 nA Cs^+ primary beam is used in a rastering mode. Sulfur-32 and ^{34}S isotopes are counted on an electron multiplier and a reproducibility of 1‰ can be achieved for $\delta^{34}S$. Preliminary results obtained on 1986 Etna samples, filters collected by aircraft by Le Cloarec in the plume of the volcano at several distances from the craters, show for instance only a few per mil variations.

References: [1] Clayton R. N. et al. (1972) *JGR, 77,* 3907–3915. [2] Castleman A. W. et al. (1974) *Tellus, 26,* 222–234. [3] Syers J. K. et al. (1968) *GCA, 32,* 1022–1025.

SPHERICAL FLY-ASH PARTICLES AS MARKERS FOR CONTEMPORARY DEPOSITION OF ATMOSPHERIC POLLUTANTS.

T. Alliksaar, Institute of Ecology, Tallinn University of Educational Sciences, Kevade Street 2, Tallinn 10137, Estonia (tiiu@eco.edu.ee).

Introduction: Fossil-fuel combustion is one of the most important anthropogenic sources of several pollutants affecting ecosystems. Most of the chemical compounds reflecting atmospheric pollution are to a varying extent liable to transformation and do not leave good and reliable records, especially when annual average or long-term distribution of pollutants is studied. Due to their composition, spherical fly-ash particles, formed during the high tem-

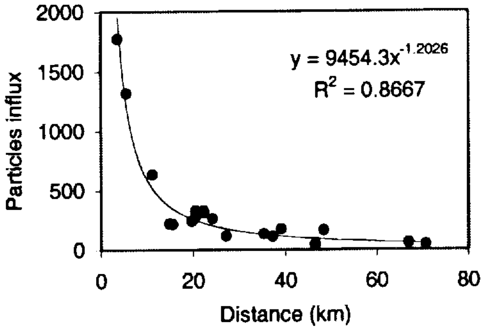

Fig. 1. Spherical fly-ash particles influx (no. cm^{-2} per 4 months) in snow samples compared with the distance (kilometers) from the main power plants of northeastern Estonia.

perature combustion of fossil fuels, are chemically resistant and preserve well in environment. This makes them stable markers for the historical monitoring of atmospheric deposition of pollutants.

In order to find out the spread and deposition of airborne pollutants fly-ash particles were analyzed in snow samples of northeastern Estonia. This area is the main region of energy production in Estonia where local fossil fuel, oil shale, is used. The results of snow samples were compared with fly-ash particle concentration data obtained earlier from lake surface sediments covering the last 5–10 years as well as from upper sediment cores.

Results and Discussion: Some earlier studies [1,2] have demonstrated that lake sediments can be used successfully for investigating spatial distribution of atmospheric pollutants. The results from Estonian lake surface sediments showed that the concentration of fly-ash particles follows mainly the location of industrial areas but at the same time is also influenced by sediment processes (e.g., accumulation rate, distribution, resedimentation, etc.) and trophic status of the lakes [3]. Therefore particle concentrations in adjacent lakes were found to be very variable (5–20× differences) even though these lakes should receive similar fly-ash particle inputs from the atmosphere.

Analyzing the upper part of sediment cores additional information for the estimation of particles influx can be obtained. As usually fly-ash particle distribution curve in the sediments follows the historical record of fuel combustion in the region, it is possible to date recent lake sediments by particle counting. In this way sediment accumulation rate as well as particle influx values can be assessed. Despite the general trend in particle deposition the influxes per sediment surface unit vary 2–3× in the lakes within a short distance [4].

The results from snow samples characterise better the distribution of pollution sources since problems accompanied with in-lake processes are excluded. The fly-ash particle influx values in snow water are decreasing with an increase of the distance from the main power plants in northeastern Estonia (Fig. 1). Similar exponential growth in particles deposition rate within 10 km from the pollution sources has been observed by other researchers too [e.g., 5]. At the same time, deposition fluxes of atmospheric pollutants are highly dependent on the weather conditions and the landscape structure (the openness, topography, the surface roughness, etc.) [6]. Despite that the variations in particle deposition in snow-cover of adjacent sampling sites are negligible.

The combined analysis of fly-ash particles in sediments and snow-cover show that they can be used for environmental monitoring as well as for validation of air-pollution models (both dispersion and deposition). Paleogeographical approach in this investigation enables to describe multiyear average values of particles deposited in the ecosystem and estimate the changes in time. As fly-ash particles are emitted together with several micro- and macrocomponents they can be used as general indicators for deposition of air pollutants from fossil fuel combustion.

References: [1] Wik M. and Renberg I. (1991) *Ambio, 20,* 289–292. [2] Rose N. L. (1996) *Environ. Pollut., 91,* 245–252. [3] Alliksaar T. and Punning J-M. (1998) *Water, Air and Soil Pollut., 106,* 219–239. [4] Punning J-M. et al. (1997) *Oil Shale, 14,* 347–362. [5] Wik M. and Renberg I. (1996) *J. Paleolimnol., 15,* 193–206. [6] Kaasik M. et al. (1999) *Water, Air and Soil Pollut.,* in press.

SOLUBLE SALTS IN PATHOLOGIES OF GRANITIC MONUMENTS OF BRAGA (NORTHWEST PORTUGAL).

C. A. S. Alves and M. A. Sequeira Braga, Centro de Ciências do Ambiente, Departimento Ciências da Terra, Universidade do Minho, 4700-320 Braga, Portugal (casaix@dct.uminho.pot).

Introduction: This study aims to characterize the soluble salts that occurs on pathologies of granitic buildings of Braga (northwest Portugal) and to discuss the possible pollution sources. Three sites of Braga were studied: Largo do Paço architectonic complex (14th–18th centuries), Biscainhos Museum, and Assembleia Distrital building. These two last buildings were part of the old Biscainhos Palace (17th–18th centuries), but, for administrative reasons and due to their different history of use, are considered as separate units.

Materials and Methods: Samples of granular disintegration, scales and flakes affecting granitic stones and efflorescences on several building materials were collected. These pathologies were studied by optical microscopy, XRD, SEM/EDS, and chemical analysis of the aqueous extract by AAS and ion chromatography.

Results and Discussion: Several saline minerals were found in the efflorescences and their distribution seems to indicate different pollution sources. Gypsum occurs associated with the diverse saline minerals (generally in minor quantities) and, therefore, it is not mentioned in the following discussion of the efflorescence mineralogy. Niter is the dominant, and very frequently unique saline mineral, in most of the Biscainhos Museum and in a restricted zone of the Largo do Paço complex, reflecting organic contributions from domestic animals (and their alimentation) that were present in the past. In the Assembleia Distrital building, where there was a salt storehouse, there are great amounts of halite efflorescences, but they are limited to a column in the entrance hall and the adjacent stair. Around this place the mineralogy of the efflorescences changes to trona and thenardite (sometimes with minor aphthitalite) and the presence of these minerals extends to the adjacent zones of the Biscainhos Museum. This mineralogical evolution could be explained by the interaction between the solutions from the salt deposit and the wall rendering mortar. Darapskite and nitratite occur in zones of

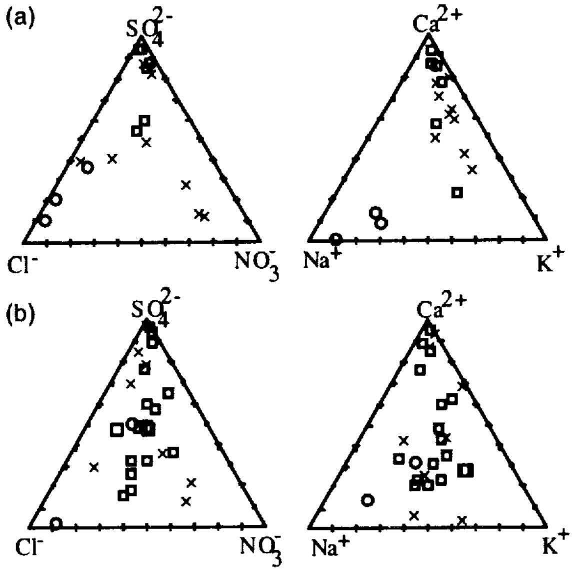

Fig. 1. Proportions of main anions and cations (in meq) in the aqueous extract of samples from the Largo do Paço complex and Biscainhos Museum sheltered (□) and unsheltered places (×) and from the Assembleia Distrital building (○). **(a)** Scales and flakes; **(b)** granular disintegration.

contact between the salt system characterized by niter and the salt system originated from the old salt storehouse. Alkaline sulfates and carbonates (mainly thenardite, but also aphthithalite, syngenite, and trona) are dominant in a limited zone of the Largo do Paço, and their formation seems linked to the cement mortar used in restorations performed in the present century. In the Largo do Paço complex, the presence of halite, with nitratite and niter, appears to be associated with human organic contributions. The limited occurrence of magnesium sulfates seems related to the same salt system.

The samples of scales and flakes from several sheltered places of the Largo do Paço complex and Biscainhos Museum are characterized by the presence of gypsum aggregates in the surface of separation from the stone, regardless of the diversity of saline minerals that occurs in the efflorescences also found in those places. The aqueous extract composition of these scales and flakes show a trend toward the sulfate and calcium poles (Fig.1a - □). In the samples from the unsheltered places of this buildings it is much rarer to found gypsum aggregates and there is a major scattering of the aqueous extract composition (Fig. 1a - ×). The scales and flakes from inside the Assembleia Distrital building are characterized by the presence of halite, as main saline mineral, in the surface of separation from the stone. The aqueous extract composition of these samples show a trend toward the sodium and chloride poles (Fig. 1a - ○).

The characterization of granular disintegration samples is more difficult, due to the interference from granite minerals and to the great dispersion of the aqueous extract composition (Fig. 1b).

Conclusions: The variety of the soluble salts indicates that several pollution sources contribute to the saline pollution in the studied monuments. The type and distribution of the soluble salts show that human-related pollution sources are much more important than natural ones.

Acknowledgments: This work is supported by PRAXIS XXI 1/2.1/ CSH/254/95.

CHARACTERIZATION OF SALINE POLLUTION AFFECTING THE ANGRA DO HEROÍSMO CATHEDRAL: A TRACHYTIC MONUMENT OF TERCEIRA ISLAND (AZORES, PORTUGAL).

C. A. S. Alves[1], M. A. Sequeira Braga[1], and A. Trancoso[2], [1]Centro de Ciências do Ambiente, Departimento Ciências da Terra, U.M. 4700-320 Braga, Portugal (casaix@dct.uminho.pt), [2]Instituto Nacional de Engenharia e Tecnologia Industrial, Estrada do Paço do Lumiar, 1649-038 Lisboa, Portugal.

Introduction: The trachytic stones of the façades of the Angra do Heroísmo Cathedral present intense deterioration in the form of granular disintegration, scales and flakes (stone pathologies) that occurs from near the ground to the top of the façades. These stones were in times covered with a mortar rendering. Inside the church, the stones are well preserved but there are saline efflorescences that occurs on wall rendering mortar (leading to the disruption of the wall painting), in mortar joints between stones, in a tile panel (in the mortar joints between tiles and in places of the tiles were the glazing has peeled off) and in a trachytic stone that was covered with cement. These decay features are typically associated with salt pollution. The present study aims to characterize the soluble salts and to discuss the contamination sources.

Materials and Methods: Several samples of the stone pathologies were collected at different heights (0.6–4.6 m) and in the different façades. Studies were carried out by SEM/EDS and chemical analysis of the main constituents of the soluble extract. The cations were determined by flame atomic absorption spectrometry and the anions by ion chromatography The saline efflorescences were studied by optical microscopy (immersion method), X-ray diffraction, and SEM/EDS.

Results and Discussion: The chemical analysis of the soluble extract show an enrichment on soluble salts in the samples from the monument (0.1405–1.552% soluble salt content) when compared with a sample from a trachyte quarry (0.028% soluble salt content). In the monument, there is a certain trend for the higher stone samples to have greater soluble salt contents.

Plotting of the results in a diagram of meq proportions of main anions and cations (Fig. 1) show that the soluble content of the samples are near the Na-Ca line and near the chloride-sulfate line, with a clear trend towards the chloride and Na poles, which are the main ions in most of the samples. The levels of the different ions do not define clear trends with the height of the samples. However, there is a weak tendency for the levels of chloride, sulfate, and Na to increase with the height of the samples. SEM observations showed the presence of halite and gypsum in samples of the stone's pathologies.

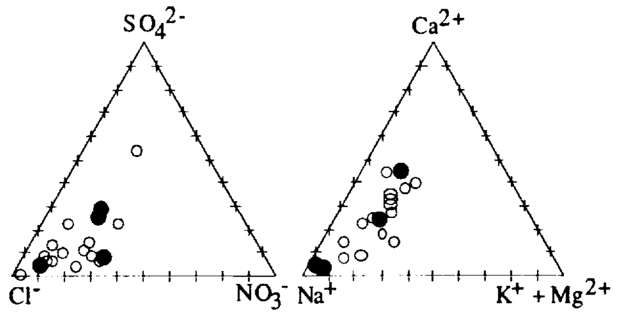

Fig. 1. Proportions of main anions and cations (in meq) in the soluble extract of samples of granular disintegration (●) and scales and flakes (○).

Mirabilite ($Na_2SO_4*10H_2O$) is the most common saline mineral in the efflorescences that occur inside the monument, being identified in wall rendering mortar (with traces of gypsum in one sample), mortar joints between stones, and between tiles. A sodium carbonate [probably natron (Na_2CO_3 $10H_2O$))] was identified in efflorescences occurring in the tiles panel. Halite and gypsum were identified in the efflorescence found on a trachytic stone covered with cement.

The predominance of Na and chloride in the stone pathologies could be justified by contamination from rainwater with a main oceanic component. However, some ions (nitrate, Ca, sulfate, and K) have ratios to chloride higher than those found in the rainwater from the neighbor Pico island [1]. These higher ratios could be debt to contributions from other saline sources (namely the mortar rendering that covered the stones and car pollution).

The mineralogy of the efflorescences inside the church showed a clear sodic domain, but there seem to be an evolution from NaCl to Na_2O_4S and carbonate. This evolution was already observed in granitic monuments of Braga (northwest Portugal) and could be associated with the composition of the wall rendering mortar. The efflorescence found in the trachytic stone, even that covered with cement, could be more closely related to the rainwater that infiltrate the church, and thus would be explained the presence of halite and gypsum in this efflorescence.

Conclusions: The distribution of the pathologies, along all the height of the façades, and the mineralogical and chemical results suggest that rainwater is the main saline pollution source on the Angra do Heroísmo Cathedral. The pollution by rainwater and the high precipitation registered in the Terceira Island explain the difference of durability between the stones on façades and inside the monuments and show the high susceptibility of trachytic stones to natural agents.

Acknowledgments: This work is supported by PRAXIS XXI 2/2.1/ CSH/254/95.

References: [1] Louvat P. and Allègre C. J. (1998) *Chem. Geol., 148,* 177–200.

THE OSMIUM-ISOTOPIC MESSAGE IN THE LESSER ANTILLES ARC LAVAS.

S. Alves, P. Schiano, and C. J. Allègre, Laboratoire de Géochimie et Cosmochimie, Institut de Physique du Globe de Paris, 4 place Jussieu, 75252 Paris Cedex 05, France (alves@ipgp.jussieu.fr).

Introduction: Numerous geochemical studies have suggested a large role of subducted sediments in the source of Antilles lavas, and generally infer that the proportion of the sediment component increases southward, in agreement with the increasing thickness of the sedimentary column at the trench [e.g., 1]. Marine sediments, and old oceanic and continental crust have much more radiogenic Os-isotopic compositions than peridotites, because of the seawater signature for the sediments ($^{187}Os/^{188}Os$ = 1.059 [2]), and of the high Re/Os ratios in melts relative to mantle residues for the crust. As a consequence, recycling or assimilating such radiogenic materials is likely to increase the Os-isotopic ratios of island arc magmas.

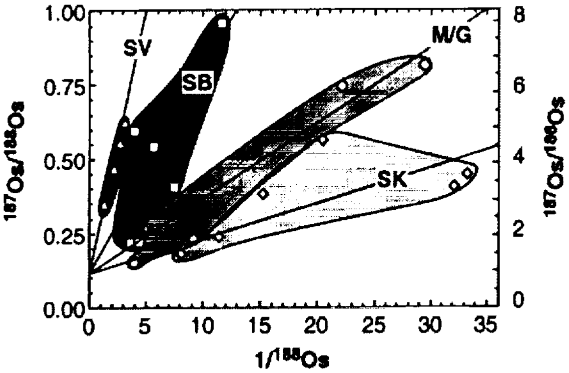

Fig. 1. Osmium-187/osmium-186 vs. $1/^{188}Os$ for Lesser Antilles volcanics. Each symbol is for a single island.

Results: We measured Os-isotopic ratios and Re and Os concentrations in 15 recent volcanic rocks from the Lesser Antilles inner arc. Our samples have basaltic to andesitic compositions and come from Saba (SB), St. Kitts (SK), Guadeloupe (G), Martinique (M), and St. Vincent (SV) islands, lying from north to south of the arc.

The Os and Re contents range from 0.2 to 5.6 ppt, and 70 to 460 ppt respectively, and completely overlap the ranges previously found for Java and Japan calc-alkaline basalts [3,4]. Osmium-isotopic compositions of the samples also display a large variation. Osmium-187/osmium-188 ratios range from 0.149 to 0.957, and are comparable to those of Java and Japan calc-alkaline lavas. Several analyses of some samples revealed that the Os content and isotopic ratio can also vary significantly within a single rock.

Discussion: We have reported the results in a $^{187}Os/^{188}Os$ vs. $1/^{188}Os$ diagram (Fig. 1). The data show that the islands (except St. Kitts) are represented by positive linear trends, starting at a common unradiogenic Os-rich end, and spreading out to several radiogenic compositions. These linear correlations likely reflect binary mixtures between radiogenic components and the unradiogenic peridotitic upper mantle. Binary mixtures appear as common feature of Os isotopes [see 5], especially for arc lavas [3,4].

In a $^{207}Pb/^{204}Pb$ vs. $^{206}Pb/^{204}Pb$ diagram, the data define a positive correlation extending from Atlantic MORBs toward the sediment field. This relationship is interpreted as an increasing proportion of recycled sediments in the mantle sources southward. However, no clear relationship is observed between Os isotopes and the geographic location of the islands.

Also, fractional crystallization coupled (or not) with assimilation of continental material cannot account alone for the covariations between Os contents and isotopic ratios, in particular because no simple relationship is observed between Os and the other elements, even for the islands taken separately.

In fact, radiogenic end members of Fig. 1 can be considered as source components. Turner et al. [1] have suggested that in Lesser Antilles northern islands, where the sediment contribution is low, lavas are marked by the contribution to the mantle source of an aqueous fluid characterized by trace elements and isotopic ratios compatible with an origin from altered oceanic crust. Accordingly, SB and SK have high Ba/Th ratios and low Pb-isotopic ratios, consistent with such a fluid addition. However, Fig. 1 shows that these islands have clearly distinct Os-isotopic signatures. Moreover, SV and M, which are both enriched in radiogenic Pb, also display strongly contrasted Os mixing trends. These observations suggest that the Os mixing correlations for Caribbean islands are decoupled from the Pb isotopes.

References: [1] Turner S. et al. (1996) *EPSL, 142,* 191–207. [2] Levasseur S. et al. (1998) *Science, 282,* 272–274. [3] Alves S. et al. (1999) *EPSL, 168,* 65–77. [4] Alves S. et al. (1999) *EUG10 Conf.,* Strasbourg.

VERTICAL AND HORIZONTAL DISTRIBUTIONS OF NEODYMIUM-ISOTOPIC RATIO OF THE NORTHWESTERN PACIFIC, SEA OF OKHOTSK, AND JAPAN SEA.

H. Amakawa, D. S. Alibo, and Y. Nozaki, Ocean Research Institute, University of Tokyo, Nakano-ku 1-15-1, Tokyo, Japan.

Introduction: Since Piepgras and Wasserburg (1980) first reported the Nd-isotopic ratio of seawaters, it has been applied as a tracer for studying global or basin-wide ocean circulation. Previous studies revealed interoceanic differences in Nd-isotopic ratios, which suggest a relatively shorter residence time of Nd (~1000 yr) compared with the mixing time of ocean water (~2000 yr), although the residence time of Nd estimated from the river flux well exceeds 5000 yr [1]. To circumvent the discrepancy in the residence time, several ideas are proposed, which can be classified into two categories: Nd flux from the estuarine sediment and that from the particle-water exchange. The northwestern Pacific Ocean, which shows high weathering rates, seems to be a clue for understanding such processes. However, only a small number of Nd-isotopic data for seawaters are available for this region to date. Here, we report the Nd-isotopic composition of seawaters collected from the northwestern Pacific Ocean together with the Sea of Okhotsk and Japan Sea above oceanic regions for understanding the oceanographic factors controlling the distribution of the Nd-isotopic ratio.

Results: In Fig. 1, the depth profiles of ε_{Nd} values of the Pacific Ocean (CM5), Sea of Okhotsk (CM6), and Japan Sea (CM20) are shown. The range in ε_{Nd} value of CM5 is the almost same as that of the previously reported ones of the northwestern Pacific Ocean (TPS 24-271-1) [2]. A maximum around 1000 m observed in the profile of TPS 24-271-1 is much more clearly identified in CM5. Although the number of data is limited, CM6 shows a similar depth profile as CM5. The sill depth between the Pacific Ocean and Sea of Okhotsk is more than 2000 m. Thus, the maximum around 1000 m seems to be congruent for both oceanic regions. However, the source of radiogenic Nd is not clear yet. CM20 of the Japan Sea site shows a fairly uniform isotopic composition below 500 m, i.e., within the Japan Sea Proper Water. The residence time of the Japan Sea Proper Water is estimated to be several hundred years [3,4]. Thus, the residence time of Nd is deduced to be longer than that of the Japan Sea Proper Water.

As shown in Fig. 2, each oceanic region shows distinctive Nd-isotopic ratios for surface samples. The Japan Sea shows the lowest ε_{Nd} (–8.9 to –7.2), which implies the relatively larger flux of Nd from continental crust compared with the other oceanic regions. The range in ε_{Nd} for the Pacific samples (–5.6 to –2.2) is much wider than that of the Japan Sea samples. On the west coast of the Japan islands, the Kuroshio and Oyashio currents flow. The Kuroshio current with low ε_{Nd} value (–6 to –5) flows in the Pacific Ocean south of 35°N. The low ε_{Nd} value might be due to the large input of continental Nd while flowing at the south of the Japan islands. On the other hand, the Oyashio Current with high ε_{Nd} value (>–3) flows in the Pacific Ocean north of 40°N along the Kurile Islands with high ε_{Nd} value (+7 to +10).

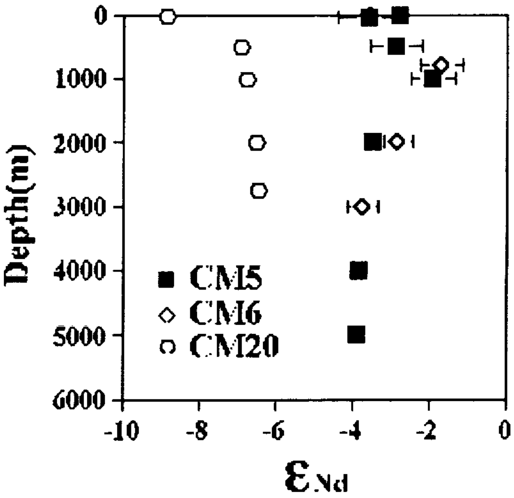

Fig. 1. Depth profiles of Nd-isotopic ratio.

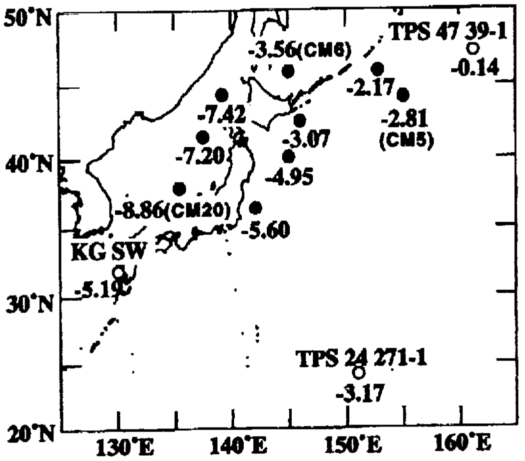

Fig. 2. The distribution of Nd-isotopic ratio of surface seawater. Closed circles = this study; open circles = reported data).

This might result in various Nd-isotopic ratios of surface seawater in the northwestern Pacific.

References: [1] Goldstein and Jacobsen (1988) *EPSL, 87,* 249–265. [2] Piepgras and Jacobsen (1988) *GCA, 52,* 1373–1381. [3] Gamo and Horibe (1983) *J. Ocenogr. Soc. Japan, 39,* 220–230. [4] Harada and Tsunogai (1986) *EPSL, 77,* 236–244.

OPAL AS A URANIUM-LEAD GEOCHRONOMETER.

Yu. Amelin[1] and L. A. Neymark[2], [1]Department of Earth Sciences, Royal Ontario Museum, Toronto ON, M5S 2C6, Canada (yuria@rom.on.ca), [2]Mail Stop 963, Pacific Western Technologies, Denver Federal Center, Denver CO 80225, USA (lneymark@usgs.gov).

Introduction: Records of ancient water flow in arid environments are preserved in precipitated from groundwater mineral crusts, composed largely of calcite and amorphous silica (opal and chalcedony). These minerals have been dated by the ^{14}C and $^{230}Th/U$ methods [1]; however these methods are limited to ages ≤50 ka and ≤500 ka respectively. The U-Pb system in opal and chalcedony allows dating in the age range from ~50 ka to millions of years and older [2,3]. For opals younger than ~500 ka it is possible to apply combined U/Pb and $^{230}Th/U$ dating to the same materials, thus allowing better evaluation of closed system conditions, determination of initial $^{234}U/^{238}U$ ratios, and examination of continuous vs. episodic growth of opal [4].

Recently, U/Pb dating of opal has been used to study paleohydrology at Yucca Mountain, Nevada, a potential site for high-level radioactive waste repository [3,4]. Further application of this geochronometer requires evaluation of its robustness in a series of experiments with large homogeneous opal samples, some of which may subsequently be used as standard samples. We have selected three large (~1–20 g) opal samples from the mineral collection of the Royal Ontario Museum and studied their U-Pb and ^{230}Th-U systems.

Samples and Methods: Two of the analyzed opal samples are visually homogeneous; one of them (E1989) is clear, another one (M21277) is translucent. The third sample (M21006) comprises a translucent opal matrix with clear opal veins. All three samples show relatively bright green fluorescence in shortwave UV light.

Combined U/Pb- and $^{230}Th/U$-isotopic determinations [4] were made from single small (1.5–8.1 mg) digestions spiked with a mixed ^{205}Pb-^{229}Th-^{233}U-^{236}U tracer solution of high-isotopic purity. Uranium, Th, and Pb concentrations and $^{234}U/^{238}U$, $^{230}Th/^{238}U$, $^{206}Pb/^{238}U$, and $^{207}Pb/^{235}U$ ratios were determined simultaneously. Procedure blanks were 1.0–1.5 pg Pb, and about 2 pg ^{238}U and ^{232}Th.

Results: Uranium concentrations vary from 2.2 to 850 ppm, Th from 0.015 to 350 ppb, and common Pb from 7 to 500 ppb. The $^{238}U/^{204}Pb$ ratios are from 8.8×10^4 to 2.8×10^6. Variations of U concentrations of 2–4× are observed in all three samples. In all cases fractions with brighter fluorescence in UV light have higher U concentrations.

Lead-isotopic compositions are radiogenic with measured $^{206}Pb/^{204}Pb$ between 100 and 1000, and $^{207}Pb/^{204}Pb$ between 20.2 and 62. The $^{207}Pb/^{235}U$ ages of two homogeneous opals are 15.3 Ma for E1989 and 2.20 Ma for M21277 and are reproducible between fractions. Errors of $^{207}Pb/^{235}U$ ages are between 1.4–5.6% (2σ). The heterogeneous sample M21006 yielded a $^{207}Pb/^{235}U$ age of 8.83 ± 0.07 Ma for the matrix, and 2.71 ± 0.02 Ma for the vein.

All fractions have $^{206}Pb/^{238}U$ ages slightly older than $^{207}Pb/^{235}U$ ages. This reverse discordance may indicate that all studied opals precipitated from water with elevated $^{234}U/^{238}U$ activity ratio. The measured $^{230}Th/^{238}U$ and $^{234}U/^{238}U$ ratios in all fractions are in secular equilibrium, thus suggesting that the U-Th (and presumably U-Pb) isotopic systems have not been disturbed during the last 500 ka.

Discussion: The results of this study, together with previously published data from Yucca Mountain [3,4] and the earlier study by Ludwig et al. [2] suggest that opal is a promising U-Pb and U-series chronometer. Using these methods in combination is essential for both "young" samples with disequilibrium $^{230}Th/^{238}U$ and $^{234}U/^{238}U$, and "old" ones in secular equilibrium. In the latter case the classical concordia diagram cannot be used as a check for closed system behavior because of unknown initial excess of ^{234}U.

Ages of "old" opals can be determined from $^{207}Pb/^{235}U$ ratios that are not affected by initial U-isotopic disequilibrium. The $^{207}Pb/^{235}U$ ratios are much more sensitive to common Pb correction than the $^{206}Pb/^{238}U$ ratios, therefore low analytical blank and finding opals with low common Pb are crucial. One problem that remains to be solved is finding low-U/Pb mineral phases cogenetic with opal, which Pb-isotopic composition can be used for the common Pb correction.

The first data from the three large opal samples suggest that some of these or similar samples can be possibly used as interlaboratory standards if U-Pb dating of opal becomes a commonly used technique.

References: [1] Paces J. B. et al. (1996) *GSA Abstr. with Progr. 28,* A-139. [2] Ludwig K. R. et al. (1980) *EPSL, 46,* 221–232. [3] Neymark L. A. et al. (1998) *Mineral. Mag., 62a,* 1077–1078. [4] Neymark L. A. et al. (1997) *Eos Trans. AGU, 46,* F788.

LUTETIUM-HAFNIUM AND URANIUM-LEAD SYSTEMATICS OF EARLY-MIDDLE ARCHEAN SINGLE ZIRCON GRAINS.

Yu. Amelin[1], D.-C.Lee[2], and A. N. Halliday[3], [1]Department of Earth Sciences, Royal Ontario Museum, Toronto ON, M5S 2C6, Canada (yuria@rom.on.ca), [2]Department of Geological Sciences, University of Michigan, Ann Arbor MI 48109, USA (dclee@umich.edu), [3]Department of Earth Sciences, Eidgenössische Technische Hochschule, Zürich, CH-8092, Switzerland (halliday@erdw.ethz.ch).

Introduction: The Lu-Hf system in zircon is an excellent isotopic tracer of mantle depletion and crustal growth recorded in ancient rocks. It was successfully used to examine the degree of early Archean mantle depletion [1,2] and appears to give tighter constraints than the Sm-Nd system in whole rock samples. High sensitivity MC-ICP-MS permits precise analysis of Hf from single zircon grains [3], which was impossible to do previously using TIMS.

One problem that remained unresolved in previous studies is the complexity of zircon populations, which adds uncertainty to initial Hf ratios. Multiple episodes of zircon growth and ancient Pb loss, common in early Archean rocks, result in $^{207}Pb/^{206}Pb$ ages that are variable between and within zircon grains. Using biased age values produces inaccurate $\varepsilon_{Hf}(T)$ by as much as 2.2–2.5 ε-units per 100 m.y.

Results: We have studied zircons from 15 rocks from four early-middle Archean areas. In order to evaluate the role of heterogeneity of zircon populations and to obtain the most reliable $\varepsilon_{Hf}(T)$, we have analyzed several abraded zircon grains (from two to eight) from each sample for both Lu-Hf and U-Pb. Hafnium-isotopic analyses with precision better than 1–1.5 ε-units (2σ) were obtained from grains weighing 0.003–0.010 mg. The $\varepsilon_{Hf}(T)$ values are calculated using $^{207}Pb/^{206}Pb$ ages of the same grains measured by ID-TIMS.

Itsaq Gneiss Complex, Western Greenland. Three gneiss samples from the Isua area contain zircons with little discordance (0–5%) and $^{207}Pb/^{206}Pb$ ages of ~3690 Ma. Their $\varepsilon_{Hf}(T)$ are relatively uniform (internal variations less than 1.5 ε-units) and have average values from 1.3 to 2.7. One of the samples also yielded 3730 Ma grains with $\varepsilon_{Hf}(T) = 2$. An augen gneiss sample from the Nuuk area yielded 3620–3600-Ma zircon grains with $\varepsilon_{Hf}(T)$ between 1.6 and 3.0.

Acasta Gneiss Complex, Northwestern Canada. Uranium-lead zircon data (0–15% discordant) from four tonalitic and amphibolitic gneisses and a granite form scattered linear arrays with upper concordia intercepts at 3600–3540 Ma, and lower intercepts at 1000–2100 Ma. Older grains with $^{207}Pb/^{206}Pb$ ages up to 3790 Ma are present in some samples. The Hf-isotopic systematics of the Acasta gneisses is far more complex than that of zircons from other studied areas. The $\varepsilon_{Hf}(T)$ values have internal variations of 3–5 ε-units. In two samples $\varepsilon_{Hf}(T)$ correlates with degree of discordance. The predominant zircon populations have $\varepsilon_{Hf}(T)$ between 0 and –3. In addition, two amphibolite samples contain zircon grains with $\varepsilon_{Hf}(T) = -4.6$ to –5.

Barberton Mountain Land, South Africa. Zircons from tonalitic-trondhjeimitic gneisses are characterized by large and variable discordance of 3–40%. Discordia lines with excess scatter have upper intercepts of 3520–3510 Ma for two gneisses of the pre-Onverwacht stage, and 3440 Ma for two gneisses of the Onverwacht stage. Lower intercepts close to zero suggest that recent Pb loss (due to tropical weathering?) is the main cause of discordance. $\varepsilon_{Hf}(T)$ in some samples vary with discordance. The $\varepsilon_{Hf}(T)$ values of the gneisses, based on least discordant zircon grains, are between 1.5 and 3.6.

Pilbara Craton, Western Australia. Two samples of felsic volcanics contain uniform 3450 Ma zircon populations with little discordance (0–7%). Their $\varepsilon_{Hf}(T)$ are internally homogeneous with average values of 1.9 and 4.3. The third felsic volcanic rock is 3320 Ma old with $\varepsilon_{Hf}(T) = 1.9$.

Discussion: Application of U-Pb and Lu-Hf methods to the same zircon grains and analysis of small samples (single grains or grain fragments) are crucial for finding closed geochemical systems and thereby obtaining reliable Hf-isotopic data from early Archean rocks.

Our data suggest that the Itsaq, Barberton, and Pilbara complexes were formed by a crust derived from depleted mantle. These complexes grew over 100–200-m.y. periods mainly by addition of juvenile crust, while reworking of older crust was less significant. The higher $\varepsilon_{Hf}(T)$ values in the 3520–3440-Ma Barberton and Pilbara rocks compared to the 3690-Ma Itsaq gneisses is consistent with uniform or increasing mantle depletion during the early Archean.

In contrast, the Acasta gneiss complex was probably formed of very old crust (>3800–4000 Ma) that was extensively reworked by several events at 3750–3540 Ma [4]. This supports the similarity between the Acasta gneiss complex and the source of 4200–3400-Ma Jack Hills detrital zircons [3].

References: [1] Vervoort J. D. et al. (1996) *Nature, 379,* 624–627. [2] Vervoort J. D. and Blichert-Toft J. (1999) *GCA,* in press. [3] Amelin Yu. et al. (1999) *Nature,* in press. [4] Bowring S. A. and Williams I. S. (1999) *CMP, 134,* 3–16.

THE EXTRATERRESTRIAL MASS FLUX ON THE EARLY EARTH.

A. D. Anbar[1], G. L. Arnold[1], S. J. Mojzsis[2], and K. J. Zahnle[3], [1]Department of Earth and Environmental Sciences, University of Rochester, Rochester NY 14627, USA (anbar@earth.rochester.edu), [2]Department of Earth and Space Sciences, Institute for Geophysics and Planetary Physics, Center for Astrobiology, University of California, Los Angeles, Los Angeles CA 90095, USA, [3]NASA Ames Research Center, Moffett Field CA 94035, USA.

We have measured Ir and Pt in ancient metasediments to obtain the first direct constraints on the extraterrestrial mass flux at the Earth's surface before 3.8 Ga (the Hadean era). The craters of the Moon record an intense "late heavy bombardment" (LHB), beginning as early as 4.15 Ga and terminating ~3.85 ± 0.05 Ga. Recent geochemical studies of metasediments and other supracrustal rocks from Akilia Island, in southern West Greenland, appear to extend both the record of marine sedimentation and the record of metabolically-sophisticated life to >3.8 Ga [1,2].

Extreme Ir and Pt enrichment is possible in the Akilia metasediments due to the heightened LHB extraterrestrial mass flux (M_{LHB}). Based on the lunar crater record, the mass flux from impactors during the ~300-m.y. LHB was ~10^{-4} gm cm^{-2} yr^{-1}, or ~10^3× the rate over the past 1 b.y. The mass flux from interplanetary dust particles (IDP) is more difficult to constrain, but may have been as much as 150× the present level. Because of the enrichment of Ir and other PGE in chondritic material relative to the Earth's crust, sediments deposited during this time could have Ir concentrations ~10^3× higher than Paleozoic equivalents (as high as ~1 ppm in the case of slowly accumulating deep sea sediments).

We analyzed samples from three locations in a 5-m-thick layer of the Akilia Island meta-chert/BIF unit. Iridium and Pt concentrations ([Ir] and [Pt]) were also determined in the metamorphosed equivalents of pyroxenite, a peridotite/komatiite and a tholeiitic basalt from flows interlayered and in knife-edge contact with the metasediments. Sample sizes were 5–20 g. Measurements were made by isotope dilution ICP-MS, following addition of spike to powdered samples and NiS fire assay preconcentration [3].

Despite the potential for enrichment, [Ir] and [Pt] are consistently very low in the metasediments. In most samples, [Ir] and [Pt] are below the procedural detection limits of ~2 ppt and ~30 ppt, respectively. However, [Ir] and [Pt] in the mafic and ultramafic samples are typical of these lithologies, which indicates that Ir and Pt were largely retained in rocks of the Akilia association despite amphibolite to granulite facies metamorphism.

To reconcile the observations with the lunar record using a simple model of two-component mixing between Ir-free background sediment accumulating at rate S, and extraterrestrial Ir, S >30 g cm^{-2} yr^{-1} (~100,000 m $m.y.^{-1}$, lithified) is required. Such rates strain credulity. For BIF, S <0.3 g cm^{-2} yr^{-1} is probable [4], indicating an extraterrestrial mass flux <10^{-6} g cm^{-2} yr^{-1}.

The observations *can* be reconciled with the lunar record using plausible sedimentation rates if we account for the mass distribution of the impactor population, which approximates a power law. A consequence is that most of the mass flux is delivered by the largest impactors, which are also the least frequent [5]. Hence

$$\frac{M_S}{M_{LHB}} = \left(\frac{\Delta\tau_S}{\Delta\tau_{LHB}}\right)^{\frac{1}{b}-1} \qquad (1)$$

where M_S is the median extraterrestrial mass flux reflected in sedimentary Ir, $\Delta\tau_S$ is the window of time "sampled" by the sediment, $\Delta\tau_{LHB}$ is the duration of the LHB, and b is an empirical scaling parameter (0.6 < b < 0.8). A relationship between S and [Ir] is obtained by combining equation (1) with the simple two-component mixing model (Fig. 1). For samples of the size studied here, the observations are satisfied if S >0.02 g cm^{-2} yr^{-1} (~70 m $m.y.^{-1}$).

These findings have important implications for the search for evidence of life at the Earth's surface in the Hadean. During the ~300-m.y. LHB, the interval between impacts large enough to sterilize the surface environment and disrupt sedimentary processes would have been ~10^7–10^8 yr. Extensive

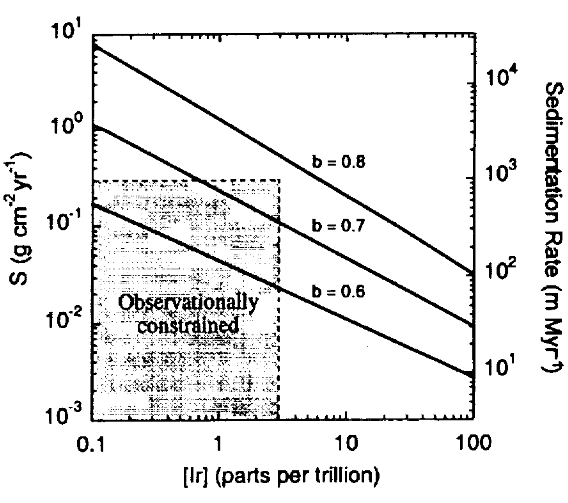

Fig. 1. Sediment accumulation vs. [Ir].

sedimentary sequences could have accumulated during these intervals if $S > 0.02$ g cm^{-2} yr^{-1}. Such intervals are also long enough to envision recolonization of the surface by microorganisms living in deep sea refugia. Thus, conditions were favorable for the deposition of sediments with all the geochemical characteristics of those found on Akilia Island during most of the late Hadean.

References: [1] Mojzsis S. J. et al. (1996) *Nature, 384,* 55–59. [2] Nutman A. P. et al. (1997) *GCA, 61,* 2475–2484. [3] Ravizza G. and Pyle D. (1997) *Chem. Geol., 141,* 251–268. [4] Morris R. C. (1993) *Precambrian Res., 60,* 243–286. [5] Tremaine S. and Dones L. (1993) *Icarus, 106,* 335–341.

IRON-ISOTOPIC FRACTIONATION STUDIES USING MULTIPLE COLLECTOR INDUCTIVELY COUPLED PLASMA MASS SPECTROMETRY.

A. D. Anbar[1,3], C. Zhang[2], J. Barling[1], J. E. Roe[3], and K. H. Nealson[4], [1]Department of Earth and Environmental Sciences, University of Rochester, Rochester NY 14627, USA (anbar@earth.rochester.edu), [2]Department of Geological Sciences, University of Missouri, Columbia MO 65211, USA, [3]Department of Chemistry, University of Rochester, Rochester NY 14627, USA, [4]Jet Propulsion Laboratory and Division of Geological and Planetary Sciences, California Institute of Technology, Pasadena CA 91125, USA.

Introduction: The importance of Fe biogeochemistry has stimulated interest in Fe-isotopic fractionation. Recent studies using thermal ionization mass spectrometry (TIMS) and a "double spike" demonstrate the existence of biogenic Fe-isotopic effects [1,2]. Here, we assess the utility of multiple-collector inductively-coupled plasma mass spectrometry (MC-ICP-MS) with a desolvating sample introduction system for Fe-isotopic studies, and present data on Fe biominerals produced by a thermophilic bacterium.

Analytical Approach: The utility of MC-ICP-MS to study transition metal isotopic fractionations has been demonstrated for Cu [3,4], Zn [3], and Mo [4]. The advantages of MC-ICP-MS over TIMS include high ionization efficiency, simplified sample preparation, the ability to compare samples and standards at similar operating conditions, and increased sample throughput. In addition, instrumental mass bias can be corrected by using an internal "elemental spike" [3,4]. This simplifies sample preparation and data reduction compared to an isotopic "double spike," and offers better precision than external standardization.

A major obstacle to the use of MC-ICP-MS for Fe-isotopic studies is the isobaric interference by ArO^+ and ArN^+ at masses 56 and 54, respectively. The key to the method presented here is the use of a membrane desolvation system to minimize these interferences.

Here, Fe samples and standards are "spiked" with a Cu standard prior to MC-ICP-MS analysis using a VG Plasma54. Samples are introduced to the plasma using a Cetac, Inc., Aridus I desolvation system. Intensities of ArO^+ and ArN^+ (typically <1 mV) are determined at the beginning of each session, and the stored results used for interference corrections during subsequent data acquisition. A microconcentric nebulizer is used in the Aridus I to reduce the uptake rate to <100 μL/min. Data are collected in two cycles (^{63}Cu and ^{65}Cu, followed by ^{54}Fe, ^{56}Fe, ^{57}Fe, and ^{58}Fe), because the mass spread from mass 54 to 65 is too large for simultaneous collection. Beam intensities from ^{54}Fe and ^{56}Fe are typically >300 mV and >5,000 mV, respectively, using solutions of concentration ~1 ppm.

After correction for instrumental mass bias using the internal "Cu spike" [3,4], the isotopic composition of samples and standards is compared using the "δ" notation ($\delta^{5X}Fe = (^{5X}Fe/^{54}Fe)_{sample}/(^{5X}Fe/^{54}Fe)_{std} - 1) \times 10^3‰$). To validate the precision of δ determinations, we analyzed a gravimetric standard prepared from a JMC Fe ICP standard solution enriched by a known amount in ^{54}Fe. The method was then applied to samples of unknown isotopic composition, including amorphous Fe oxyhydroxide used as an Fe source for a cultured thermophilic Fe-reducing bacterium, as well as $FeCO_3$ (siderite) produced extracellularly during growth of this microorganism.

Results and Discussion: MC-ICP-MS coupled to a desolvation system permits $\delta^{56}Fe$ measurements with an *external* precision of ~ ±0.15‰ (1σ) on samples containing ~1 μg of Fe. This assessment is based on 35 analyses of the ^{54}Fe-enriched standard compared to the isotopically-normal JMC standard over a period of several months ($\delta^{56}Fe = -11.74 \pm 0.17‰$). The agreement with the actual value, $\delta^{56}Fe = -11.77‰$, indicates that the effects of residual ArO^+ and ArN^+ are small, and that the "elemental spike" approach does not introduce systematic inaccuracy in δ determinations. The precision of $\delta^{57}Fe$ is somewhat worse, because of the low abundance of ^{57}Fe.

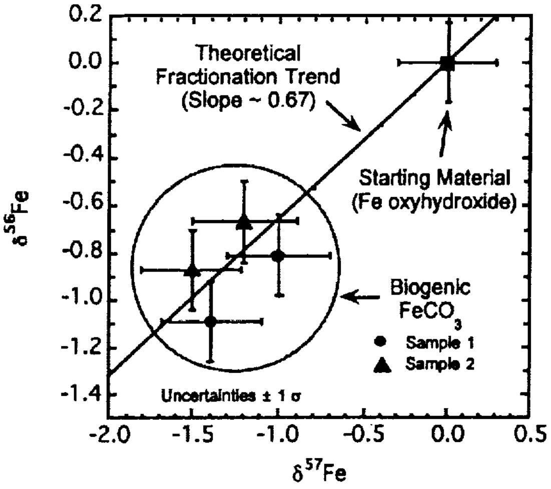

Fig. 1. Isotopic composition of biogenic siderite.

In an initial study of biogenic Fe minerals, the isotopic composition of two samples of extracellular $FeCO_3$ produced during early microbial growth was found to be shifted from the composition of the starting material by ~0.43‰/amu (Fig. 1). The correspondence between the measurements and the mass-dependent fractionation trend indicates that the data are unaffected by isobaric interferences. The magnitude of the observed fractionation is consistent with previous studies of mesophilic microorganisms [1,2]. These results demonstrate the utility of MC-ICP-MS for Fe-isotopic studies, and suggest new avenues of research.

References: [1] Beard B. L. et al. (1998) *GSA Abstr. with Prog. 30,* A156. [2] Bullen T. D. and McMahon P. M. (1997) *Eos Trans. AGU, 78,* S173. [3] Maréchal C. N. et al. (1999) *Chem. Geol., 156,* 251–273. [4] Anbar A. D. et al. (1998) *Mineral. Mag, 62A,* 53–54.

PARTICLE-MEDIATED SURFACE WATER EXPORT: COMPARISON OF ESTIMATES FROM URANIUM-238–THORIUM-234 DISEQUILIBRIA AND SEDIMENT TRAPS IN A CONTINENTAL SHELF REGION.

P. S. Andersson[1], Ö. Gustafsson[2], P. Roos[3], D. Broman[2], and A. Toneby[2], [1]Laboratory for Isotope Geology, Swedish Museum of Natural History, Box 50007, 104 05 Stockholm, Sweden (per.andersson@nrm.se), [2]Institute of Applied Environmental Research, Stockholm University, 104 05 Stockholm, Sweden (orjan.gustafsson@itm.su.se; dag.broman@itm.su.se; anders.toneby@itm.su.se), [3]Department of Radiation Physics, Lund University, 221 85 Lund, Sweden (per.roos@radfys.lu.se).

The continental shelf is recognized as an important regime for vertical export of particles and associated constituencies. Accurate methods for quantifying vertical particle transport are thus essential to marine biogeochemistry.

A commonly used method for estimating vertical fluxes in surface waters is sediment traps. However, the quality of flux estimates from sediment traps have been questioned based on several suspected artifacts such as hydrodynamic biases, preservation problems and the presence of "swimmers" [e.g., 1]. More recently, the ^{234}Th ($t_{1/2} = 24.1$ d) in the water column, that show deficiencies relative to equilibria with ^{238}U, related to uptake onto sinking particles, has been applied as an indicator of particle flux [2,3]. Comparison of the ^{234}Th deficit in the upper waters with the excess ^{234}Th in the sediment trap yields a technique suitable for "calibration" of sediment trap collection efficiency. So far, this "calibration method" has only been tested in the open ocean environment [2].

In an ongoing study planned for two years, we sample at a biweekly to monthly interval the ^{238}U-^{234}Th disequilibrium for calibration of sediment traps in a continental shelf region. The study site, Landsort deep (BY-31, N58°35'; E18°14', depth = 449 m), located in the northwest Baltic Sea about 40 km offshore, has been used for a long-time (>100 yr for some data) as a monitoring station for various physical and biogeochemical parameters.

Sediment traps of a commonly used design [4] with straight cylinders, 10 cm diameter and a height/width ratio of 5, were deployed below the mixed surface layer at 40 m depth. Samples for water column ^{234}Th analysis were collected, in the middle of the mixed layer, by filtering large volumes (200–1200 L) of water through a 0.2-μm polypropylene filter to separate particles and, through two identical cartridges impregnated with Mn-oxide to extract filterpassing Th. The ^{234}Th activities were determined within one week of sampling using radiochemical methods [3].

Preliminary data from July to October 1998 suggest a consistent overtrapping of about a factor 10 relative to ^{238}U-^{234}Th derived flux estimates. During this period both the ^{238}U-^{234}Th disequilibria and the ^{234}Th on the particle fraction decreased. This trend also followed a decrease in the particulate organic C (POC) concentration.

Comparison of the ^{238}U-^{234}Th disequilibria in the water column with that in sediment traps will be presented and interpreted in terms of the physical and biogeochemical environment.

References: [1] Gardner W. D. (1996) *U.S. JGOFS Rpt.*, http://www-ocean.tamu.edu/JGOFS/contents.html. [2] Buesseler K. O. (1991) *Nature, 353,* 420. [3] Gustafsson Ö. G. et al. (1998) *Cont. Shelf Res., 18,* 805–829. [4] Broman D. et al. (1990) *Coast. Shelf Sci., 30,* 429–436.

POTASSIUM-RICH CLINOPYROXENES AS MANTLE CONVEYORS OF CRUSTAL COMPONENTS.

L. André[1], V. S. Shatsky[2], K. De Corte[3,1], N. V. Sobolev[2], and J. Navez[1], [1] Section of Mineralogy-Petrography-Geochemistry, Royal Museum for Central Africa, B-3080, Tervuren, Belgium (lucandre@africamuseum.be), [2]United Institute of Geology, Geophysics and Mineralogy, Russian Academy of Sciences, Siberian Division, Novosibirsk, 630090, Russia, [3]Department of Geology and Soil Science, University of Ghent, Krijgslaan, 281, B-9000, Ghent, Belgium.

Introduction: A sediment recycled at 5–9 GPa within the mantle is likely to be composed of clinopyroxene, garnet, phengite and/or orthoclase and coesite. During partial melting, orthoclase and phengite should disappear producing K-rich siliceous melts with cpx-garnet-rich residues. Because recent crystallographic, petrologic, and experimental studies converge to demonstrate that cpx could be a host for K within the same pressure interval, these cpx-rich residues might be appropriate conveyers to transfer K and some other lithophile elements (Rb, Sr, Cs, Ba, and Pb) deeper into the mantle. To investigate this question, we determine trace elements on specimens from the two reported varieties of K-rich cpx: K-rich diopsides from the ultra-high-pressure (UHP) Kokchetav Massif and K-rich omphacites inclusions from lamproitic diamonds. The Laserprobe ICP-MS was used to achieve *in situ* microanalyses.

Results: All Kokchetav K-rich cpx correspond to high MgO diopsides with low jadeite and Ti-Cr contents. Their K_2O content is extremely variable: 0.2–1.3 wt. In comparison to K-poor lithospheric mantle diopsides, the K-rich diopsides have much higher crustal-like Rb, Cs, and Pb concentrations (two orders of magnitude), similar Ba and light rare-earth contents, but lower Sr contents. This results in unusal K/Rb (>500), Rb/Cs (1–17), Ba/Rb (0.2–4), and Ce/Pb (0.08–1.5), which are much lower than the uniform values of upper continental crust material. The two large (50–100 μm) analyzed omphacite inclusions in diamonds from the Proterozoic (1180 Ma) Argyle lamproites compare very closely to the Kokchetav cpx by their low Ba contents associated with high crustal-like Rb, Cs, Pb enrichments and low Rb/Cs, Ba/Rb, Ce/Pb.

Discussion: Experiments [1,2] suggest that K-rich cpx are stable only in the presence of K-rich fluids (probably above 20 wt%). Considering the large number of factor that could control the partition of K (and likely, most other alkali elements) between clinopyroxenes and a K-rich fluid, this amazing geochemical similitude probably recovers some convergent features in the genesis of both pyroxenes. Whatever the origin of this common signature, the Argyle data demonstrates that crustal-like K, Rb, Cs, Pb concentrations could be stored by K-rich cpx, somewhere close to the source of lamproitic magmas. Phengite breakdown is proposed to be the source of these K-rich fluids. Indeed, the frequent recognition of phengite as inclusions in the Kokchetav garnet, sometimes coexisting with K-rich diopside, demonstrates that both minerals were stable together, at some stage during the prograde UHP metamorphism, in agreement with experimental results. Because phengite melting process should make phengite-derived trace (Rb-Cs-Ba-Pb) elements available for repartition between dolomite (Ba), K-rich cpx (Rb, Cs, Pb), and a K-rich fluid (Rb-Cs-Pb), it could account for the unusual Rb/Cs, Ba/Rb, and Ce/Pb. In particular, the larger substitution of Rb and Cs over Ba into the K-diopside is probably linked to the equilibrium with dolomites into which Ba is preferentially partitioned.

Subduction of K-cpx-rich rocks, formed either as residues from phengite melting in the down-going slab or through the percolation of K-rich fluids within eclogitic bodies, is proposed as a mechanism to recycle supracrustal K, Rb, Cs, Pb, Sr, and Nd to the mantle, up to a pressure where cpx gradually enters into solid solution with the garnet phase. Nevertheless, the narrow range of Rb/Cs, Ba/Rb, Ce/Pb values in oceanic basalts precludes any large contamination of ordinary mantle by subducted K-cpx-rich materials with low Rb/Cs, Ba/Rb, and Ce/Pb. The low Rb/Cs of K-cpx that appears complementary to MORB-OIB mantle values with respect to the primitive mantle, is in agreement with the existence of some recycled K-cpx rich rocks in the mantle. Indeed, it could help to close the global balance of Rb and Cs with the lithospheric mantle, the depleted mantle, and the continental crust. Although these arguments emphasize storage of "MORB-OIB" and "K-cpx rich rocks" reservoirs in two essentially unmixed regions from the mantle, our results support the idea of occasional exchanges between these reservoirs as an explanation for the OIB isotopic features. K-cpx has Rb/Sr 1–20 fold higher than the primitive mantle values (0.03), but U/Pb-Th/Pb 100× lower than the mantle ratios (0.114 and 0.46). Minor admixture of a Proterozoic K-cpx-rich rock component (such as the Argyle omphacites) to the OIB source would therefore destroy the magmatic derived correlation between these ratios, with the capacity of causing the well-known lack of correlation for Sr-Pb isotopes in OIB.

References: [1] Harlow G. E. (1997) *Am. Mineral., 82,* 259–269. [2] Luth R. W. (1997) *Am. Mineral., 82,* 1198–1209.

HYDRATION MECHANISMS AND STRUCTURAL CHARACTERIZATION OF SIMPLIFIED GLASSES (COMPARISON BETWEEN BASALTIC AND RADIOACTIVE WASTE GLASSES).

F. Angeli[1], Th. Charpentier[1], D. Boscarino[1], G. Della Mea[2], and J.-C. Petit[1], [1]Commissariat à l'Energie Atomique, DSM/DRECAM, Service de Chimie Moléculaire, CEA/Saclay, 91191 Gif sur Yvette, France, [2]Università di Trento and INFN/LNL, Via Romea 4, 35020 Legnaro-Padova, Italy.

Introduction: The alteration mechanisms of radioactive waste glasses must be assessed over periods of time that are completely out of reach of the laboratory experiments. Natural analogs, such as basaltic glasses, have been proposed and investigated to circumvent this major difficulty [1]. The durability of both materials has been compared extensively, with particular attention given to the chemical interactions between the solid and the attack solution. Nevertheless, the influence of the vitreous structure might be another important factor for the comprehension of the glass reactivity in aqueous solution.

In order to study the relations between the structure and the reactivity in aqueous solution, several aluminosilicate and aluminoborosilicate glasses (containing the main components of the French nuclear waste glass, R7T7, and of a basaltic glass) have been synthesized. The local structure has been studied using ^{23}Na and ^{27}Al 3Q MAS NMR spectroscopy. All glasses contain Al as network former and Na as network modifier, which can be used in NMR as probes of their local environment. We obtained data concerning the distributions of bond distances and bond angles. This information on glasses allows to have a new insight in their different degree of disorder. Afterwards, the glasses have been leached at 90°C in acid and neutral pH for ~10 h. Resonant nuclear reaction analyses with energetic ion beams (RNRA) have been used to study the hydration and the ion exchange process by measuring the H (^{1}H[^{15}N,γ]^{12}C) and Na (^{23}Na[p,α]^{20}Ne) profiles of leached glasses and to detect the surface enrichment or depletion. These results on simplified glasses are linked with previous studies on natural and technological glasses [2]. Thus, it is possible to determine the influence of each oxide on the structure and the reactivity. In fact, the penetration of the hydration front in the first step of the alteration is closely connected to the glass composition and structure. This type of result is an interesting approach permitting to understand the reasons of an analogy during the alteration between different glasses.

References: [1] Petit J.-C. (1992) *Geochem. Explor., 46,* 1. [2] Petit J.-C. et al. (1990) *GCA, 54,* 1941.

X-RAY ABSORPTION SPECTROSCOPY INVESTIGATION OF ARSENITE AND ARSENATE ADSORPTION ON GAMMA ALUMINUM OXIDE.

Y. Arai, E. J. Elzinga, and D. L. Sparks, Department of Plant and Soil Sciences, University of Delaware, Newark DE 19717-1303, USA (ugarai@udel.edu).

Arsenic (As) is found in the environment as a result of natural geologic events and anthropogenic inputs. The current U.S. standard of maximum As concentration level in drinking water is 50 ppb. However, the expected new standard (2 ppb) in the near future raises serious concerns about protecting human and ecological health. The fate and transport in soil/water environments highly depend on the oxidation state [primary As(III) or As(V)]. In acid to alkaline environments, oxyanions can be adsorbed onto variable-charge mineral surfaces by inner-sphere adsorption via ligand exchange and /or outer-sphere adsorption via electrostatic interaction. Hayes and coworkers proposed an indirect method distinguishing inner- from outer-sphere complexes by examining ionic strength (I) effects on adsorption envelopes [1]. Inner-sphere complexes are not greatly affected by I, whereas the presence of outer-sphere complexes is indicated by a shift in the pH with a change in I due to competitive adsorption with counter anions. Several researchers have investigated As adsorption mechanisms on clay minerals using *in situ* spectroscopic techniques. Extended X-ray adsorption fine structure (EXAFS) and ATR-FTIR spectroscopic studies showed the formation of both binuclear bridging and monodentate As(V) complexes on ferrihydrite and goethite [2,3]. Combined studies (ATR-FTIR, electrophoretic mobility measurement, and titration sorption) also suggested inner-sphere adsorption mechanisms of As(V) and As(III) on ferrihydrite [4].

Few spectroscopic studies have been conducted to elucidate oxyanion adsorption mechanisms at mineral/water interfaces as a function of pH and I. The objective of this study was to investigate the pH and I effect on As(III) and As(V) adsorption mechanisms at the γ-Al_2O_3-water interface using X-ray absorption spectroscopy (XAS).

Materials and Methods: All experiments were conducted at 22°–25°C in a N_2-filled glove box. Standards and reagent solutions were prepared in boiled purified water. Five g L^{-1} of γ-Al_2O_3 suspension were preequilibrated for 5 d in 0.01 or 0.8 M $NaNO_3$ solution at pH = 3–8, and then were reacted with As(III or V) over the same pH range and the same I for 20 h. XAS data was collected on beamline X-11A at the National Synchrotron Light Source (NSLS), Brookheaven National Laboratory, Upton, NY. EXAFS spectra were quantitatively analyzed using Winxas 1.1. and FEFF 6.0.

Results and Discussion: Arsenic(V) adsorption on γ-Al_2O_3 was insensitive to changes in I between pH = 3–8, whereas As(III) adsorption increased with increasing pH and decreasing I in this pH range. Based on the theory proposed by Hayes et al. [1], innersphere complexes for As(V) and outer-sphere complexes for As(III) can be formed. Inner-sphere As(V) adsorption is evidenced by our XAS data, which show (1) a significant difference between XANES spectra of As(V)(aq) and that of adsorbed As(V), and (2) the presence of an Al shell in the radial structure functions (RSF) of adsorbed As(V) at any pH and I. For As(III), an Al shell is present in the RSFs of all samples, indicating that innersphere complexes are formed. The As(III) XANES spectra, however, show that outersphere complexes are also formed, and that the importance of outersphere As(III) complexes increased with decreasing pH and I. Overall data of As(III) suggest that both inner- and outer-sphere adsorption coexist, but inner-sphere adsorption increases as pH and I increase.

References: [1] Hayes K. F. et al. (1988) *J. Colloid. Interface. Sci., 125,* 717–726. [2] Fendorf S. et al. (1997) *Environ. Sci. Technol., 31,* 315–320. [3] Waychunas G. A. et al. (1993) *GCA, 53,* 2251–2269. [4] Suarez D. L. et al. (1998) in *Mineral Water-Interfacial Reactions Kinetics and Mechanisms* (D. L. Sparks and T. J. Grundl, eds.), pp. 136–178, American Chemical Society, Washington, DC.

EXPERIMENTAL STUDY OF GOLD SOLUBILITY IN HYDROCHLORIC ACID-BEARING WATER VAPOR.

S. M. Archibald and A. E. Williams-Jones, Department of Earth and Planetary Sciences, McGill University, Montréal, Québec H3A 2A7, Canada (sandy@eps.mcgill.ca).

Introduction: Two-phase fluid separation (boiling) is a common feature of hydrothermal systems and is an important factor in the formation of metallic mineral deposits. It has long been assumed that metal fractionation is primarily due to the liquid phase, and the effect of boiling is to remove volatiles, thus saturating the liquid phase with ore minerals. Several workers have postulated that the vapor phase may, in fact, be a favorable medium for carrying metals in sufficient concentrations to form economic mineralization [1,2]. Investigations of volcanic fumaroles, such as those of Volcan Momotombo, Nicaragua, have shown that concentrations of up to 24 ppb Au are present in the vapor [3]. Given the fact that HCl is a common volatile component in volcanic gases, and Au mineralization is intimately associated with volcanic edifices, a study was undertaken to investigate the vapor transport of Au. The aim of this study is to obtain thermodynamic data that will be used to determine the dominant species of Au transport in a HCl-bearing water.

Theory: The reaction whereby Au is transported as a H_2O-HCl vapor complex can be expressed by

$$Au^{gas} + m\ HCl^{gas} + n\ H_2O^{gas} = AuCl_m\,(H_2O)_n^{gas} + H_2^{gas}$$

where m and n define the solvation number of the Cl and H_2O species respectively. Armellini and Tester [4] used a similar method to describe NaCl solubility in water vapor. Values of m and n may be calculated from the concentration of Au in the vapor phase using the relationships

$$\left(\frac{\partial \log P_{AuCl\,(H_2O)}}{\partial \log P_{HCl}}\right)_{T,\,P_{O_2},\,P_{H_2O}} = m$$

$$\left(\frac{\partial \log P_{AuCl\,(H_2O)}}{\partial \log P_{H_2O}}\right)_{T,\,P_{O_2},\,P_{HCl}} = n - \frac{m}{2}$$

Experimental Method: The experiments were performed in a Ti screw seal autoclave and involved measuring the solubility of pure Au in an H_2O-HCl-bearing vapor. The autoclaves were loaded with preweighted quartz ampoules, one containing Au wire (99.99% purity), and another containing a known mass of MoO_2-MoO_3 powder. The log f_{O_2} of the reaction was held constant at –22.8 (300°C) by the MoO_2-MoO_3 buffer. Solutions of HCl were pipetted to the bottom of the autoclaves, the concentrations of which were equivalent to pH values between 3.4 and 1.7. To ensure that the system was undersaturated with respect to liquid, and that any Au would be dissolved as a vapor species, the amount of solution added was carefully calculated.

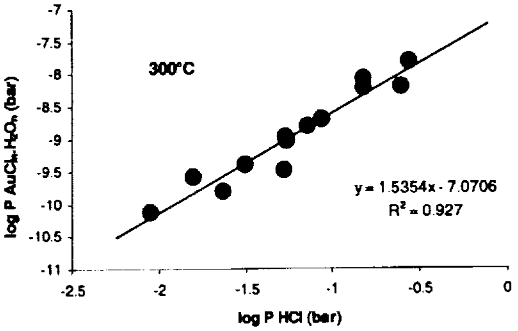

Fig. 1.

The autoclaves were sealed and placed in a preheated fan oven until equilibrium was reached (>13 d). After each run, the autoclave was removed from the oven and quenched in a container with water (300°–~40°C), followed by cooling with compressed air. The autoclaves were then opened and washed several times using 3–5 mL of aquaregia. The concentration of Au in the final solution was determined by instrumental neutron activation analysis (INAA).

Preliminary Results: Figure 1 illustrates the concentration of Au in water vapor at 300°C as a function of P_{HCl} at constant P_{H_2O} (m = 1.5). A similar diagram can be drawn for constant P_{HCl} and variable P_{H_2O} at 300°C (n = 3.75).

Based on our preliminary data, we conclude that Au most probably occurs in the gaseous form $AuCl(H_2O)_3$. Initial experimental results at 360°C suggest that this species is also dominant at that temperature. The calculated partial pressures of AuCl are several orders of magnitude higher than those for the water-free system calculated using the data of James and Hager [5].

References: [1] Hendley R. W. and McNabb A. (1974) *Econ. Geol., 73,* 1–20. [2] Heinrich C. A. et al. (1992) *Econ. Geol., 87,* 1566–1583. [3] Gemmell J. B. (1987) *J. Volcanol. Geotherm. Res., 33,* 161–181. [4] Armellini F. J. and Tester J. W. (1993) *Fluid Phase Equilibria, 84,* 123–142. [5] James S. E. and Hager J. P. (1977) *Metall. Trans. B., 9B,* 501–508.

HAFNIUM-ISOTOPIC COMPOSITIONS OF KOMATIITES.

N. T. Arndt[1] and J. Blichert-Toft[2], [1]Géosciences, Université de Rennes 1, 35042 Rennes Cedex, France, [2]Ecole Normale Supérieure de Lyon, 46 Allée d'Italie, 69364 Lyon Cedex 7, France.

Komatiites are ultramafic magmas that form through melting at high pressures of unusually hot parts of the mantle. Many of the oldest komatiites have low Al_2O_3/TiO_2 and depleted HREE, features that are attributed to garnet fractionation at some stage during their formation. It is unclear, however, whether this fractionation took place at the time of melting, or well before, perhaps during the crystallization of an early magma ocean. Hafnium-isotopic compositions that are well suited to treat such problems, had hitherto been difficult to measure in komatiites, but this problem has been resolved with the development of magnetic-sector inductively coupled plasma mass spectrometry (ICP-MS).

We report here the Hf-isotopic compositions of 10 komatiites. Four are Al-depleted komatiites from the 3.45-Ga Barberton greenstone belt in South Africa; the others are Al-undepleted komatiites from 2.7-Ga and 1.9-Ga belts in Canada and Zimbabwe. We also measured compositions of three tholeiites, one from Barberton and two from the 1.9-Ga Canadian belt, to provide information about the composition of ambient Precambrian mantle.

All komatiites have high initial $^{176}Hf/^{177}Hf$ ratios. All initial ε_{Hf} values are positive and fall in the range 2.2 to 7.8. Almost this entire range is also present in 3.45-Ga Barberton komatiites (2.2–7.3). $\varepsilon_{Hf(T)}$ correlates with $\varepsilon_{Nd(T)}$ and defines a crude linear array that coincides with compositions of both modern oceanic basalts (Fig. 1) and of Phanerozoic to Archean juvenile crustal rocks. The composition of bulk silicate Earth (BSE) estimated from analyses of various types of meteorites [1] plots below this array.

To explain the moderately to highly positive initial ε_{Hf} values of 3.45-Ga Barberton komatiites, the source must have had high Lu/Hf for a considerable time. This implies old material *enriched* in garnet, a result contrary to earlier models in which the low Al_2O_3/TiO_2 and low Lu/Hf of this type of komatiite was said to be inherited directly from a part of the mantle that was *depleted* in garnet. The source may have been the lower, garnet-rich cumulate portion of a solidified magma ocean, not the garnet-depleted upper portion assumed in older models. The low Al_2O_3/TiO_2 and low Lu/Hf of this type of komatiite, in contrast, are features of the primary magmas, not of their mantle source: the fractionation of Al_2O_3/TiO_2 and Lu/Hf must then have resulted from residual garnet left in the source during the melting that formed the komatiites.

To explain the bias to high initial ε_{Hf} values of the komatiites and virtually all other terrestrial rocks (Fig. 1), we consider two alternatives.

1. Accepted values for the Hf-isotopic composition of bulk silicate Earth (BSE) are inappropriate and the actual composition has slightly higher $^{176}Hf/^{177}Hf$ and lower $^{176}Lu/^{177}Hf$. When calculated using these values, ε_{Hf} values of early komatiites are closer to zero and consistent with ε_{Nd} values. The problem with this interpretation is that the proposed composition lies off the chondritic meteorite isochron, which implies that the Earth had a different age, or accreted from material with composition different from that of the meteorites.

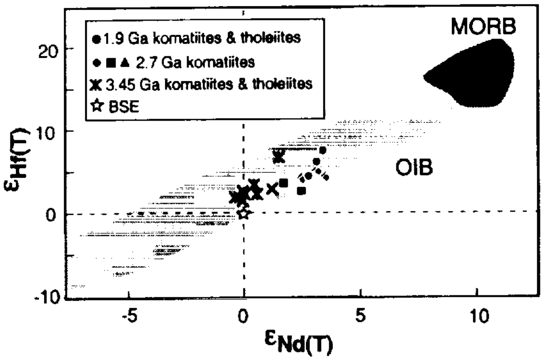

Fig. 1.

2. A hidden reservoir with low Lu/Hf, whose presence in the mantle had been postulated [1] to explain the difference in composition between oceanic basalts and BSE, must have formed at a very early stage in Earth history.

References: [1] Blichert-Toft J. and Albarède F. (1997) *EPSL, 148,* 243–258.

CONTRASTING EXTRACELLULAR ENZYMATIC HYDROLYSIS RATES AND SUBSTRATE SPECIFICITIES IN BOTTOM WATER AND SURFACE SEDIMENTS: IMPLICATIONS FOR ORGANIC MATTER REMINERALIZATION AND CARBON PRESERVATION.

C. Arnosti, Campus Box 3300, Department of Marine Sciences, 12-7 Venable Hall, University of North Carolina, Chapel Hill NC 27599, USA (arnosti@marine.unc.edu).

Introduction: Microbial remineralization of organic macromolecules is initiated via activities of extracellular enzymes, since bacteria must hydrolyze substrates larger than ~600 daltons prior to transport into the cell [1]. The structural specificities of these extracellular enzymes, as well as the rates at which they function, therefore significantly affect remineralization of organic matter in marine environments. Little is known, however, about the structural specificities and activities of microbial extracellular enzymes. Recent molecular biological investigations, however, suggest that the microbial communities found in sediments may differ fundamentally from communities living in the water column [2]. The extracellular enzymes utilized by these communities may therefore also differ. Potential hydrolysis rates and substrate specificities of extracellular enzymes in bottom water and surface sediments of Skagerrak (North Sea-Baltic Sea transition) were directly compared in order to ascertain the extent to which chemical structure may affect enzymatic hydrolysis rates, and to investigate possible differences in substrate specificities among water-column and sedimentary microbial communities.

Methods: Six different fluorescently-labeled (FLA-) polysaccharides were synthesized using the method of Glabe et al. [3] as modified by Arnosti [4]. The polysaccharides included pullulan (a polymer of maltotriose), laminarin (β-linked glucose), xylan (β-linked xylose), fucoidan (sulfated fucose polysaccharide), arabinogalactan (polymer of galactose and arabinose), and chondroitin sulfate (sulfated polymer of N-actyl-galactoseamine and glucuronic acid). These polysaccharides were selected as substrates because they span a range of chemical compositions, and their component monomers are common in marine environments [e.g., 5–7].

Monomer-equivalent concentrations (i.e., complete hydrolysis would yield the same concentration of monomers) of single FLA-polysaccharides were added to triplicate vials containing 20 mL of homogenized surface sediments, or 15 mL of bottom water. At each time point, sediment samples were centrifuged to obtain a porewater sample; the sediments were subsequently rehomogenized and reincubated. One milliliter of each bottom water sample was filtered through a 0.2-μm-pore-size filter and then frozen. Samples were analyzed via low-pressure gel permeation chromatography with fluorescence detection to determine the molecular weight distribution of the FLA-polysaccharides, i.e., the extent of substrate hydrolysis at each time point.

Results and Discussion: All of the polysaccharides were measurably hydrolyzed in sediments over the course of the experiment. Potential hydrolysis rates differed by factors of 10–100 among the set of six polysaccharides both in seawater and in sediments. The relative order of potential hydrolysis rates in sediments was distinctly different from that of the bottom water samples. In surface sediments, pullulan hydrolysis was extremely rapid, and relative hydrolysis rates decreased in the order pullulan $\gg$ laminarin > chondroitin sulfate $\gg$ xylan > arabinogalactan $\gg$ fucoidan. In bottom water, in contrast, pullulan, arabinogalactan, and fucoidan were barely hydrolyzed, while chondroitin sulfate, xylan, and laminarin were hydrolyzed relatively rapidly. Hydrolysis rates decreased in the order chondroitin sulfate $\gg$ xylan > laminarin $\ggg$ arabingalactan $\equiv$ pullulan $\equiv$ fucoidan.

The differences among the relative hydrolysis rates may reflect fundamental differences in seawater and sedimentary microbial communities with disparate extracellular enzymatic capabilities. Some polysaccharides may preferentially survive passage through the water column, and subsequently fuel benthic metabolism. The contrasting hydrolysis rates of the two glucose polysaccharides (pullulan and laminarin) in seawater and sediments demonstrate the importance of polysaccharide secondary and tertiary structure in determining hydrolysis rates. Such structural differences are not easily explored with currently utilized analytical methods.

The slow hydrolysis of fucoidan both in bottom water and in sediments is intriguing in light of the fact that deoxysugar-containing sulfated polysaccharides, a description which fits fucoidan, may be important and persistent components of transparent exopolymer particles (TEP) [8–9]. In addition, carbohydrates constitute an estimated 25–50% of dissolved organic C (DOC) [10]. Since bulk DOC is geochemically "old," some fraction must survive several ocean mixing cycles [11]. The macromolecular structure of these carbohydrates, and factors which may contribute to their resistance, remain unknown, since most analyses of marine carbohydrates yield only monomer composition [e.g., 5–7]. Slow hydrolysis in seawater and sediments may provide the opportunity for physical/chemical transformations to occur, which may further increase recalcitrance towards microbial remineralization.

References: [1] Weiss M. S. et al. (1991) *Science, 254,* 1627–1630. [2] Llobet-Brossa E. et al. (1998) *Appl. Environ. Microbiol., 64,* 2691–2696. [3] Glabe C. G. et al. (1983) *Anal. Biochem., 130,* 287–294. [4] Arnosti C. (1996) *Organic Geochem., 25,* 105–115. [5] Mopper K. (1977) *Mar. Chem., 5,* 585–603. [6] Cowie G. L. and Hedges J. I. (1984) *GCA, 48,* 2075–2087. [7] Skoog A. and Benner R. (1997) *Limnol. Oceanogr., 42,* 1803–1813. [8] Mopper K. et al. (1995) *Dp. Sea Res., 42,* 47–73. [9] Zhou J. et al. (1998) *Limnol. Oceanogr., 43,* 1860–1871. [10] Benner R. et al. (1992) *Science, 255,* 1561–1564. [11] Williams P. M. and Druffel E. R. M. (1987) *Nature, 330,* 246–248.

PROTACTINIUM-THORIUM-URANIUM FRACTIONATION DURING MANTLE MELTING: INFERENCES FROM CONTINENTAL BASALT DATA.

Y. Asmerom[1], H. Cheng[2], T. Tesfay[1], B. Bierman[1], and R. L. Edwards[2], [1]Department of Earth and Planetary Sciences, University of New Mexico, Albuquerque NM 87131, USA (asmerom@unm.edu), [2]Department of Geology and Geophysics, University of Minnesota, Minneapolis MN 55455, USA.

The trace-element and isotopic composition of basalts reflect compositional characteristics of their mantle source and processes that took place during melting and subsequent evolution. Elemental and isotopic variations in basalts may in turn be used to make inferences about mantle composition and dynamics. In this regard, the U-series nuclides provide unique opportunity, because, among other things, (1) the initial parent/daughter nuclide ratio of the source is known, (2) it is possible to constrain chronology of elemental fractionation, and (3) in the case of Th-U, in many instances it is possible to infer Th/U fractionation during melting by looking at Th-isotopic variations that are immune to changes due to post-melting mineral fractionation. The use of multiple U-series nuclides, such as the ^{231}Pa-^{235}U and ^{230}Th-^{238}U pairs, provide even more robust constraints not possible with one system.

Continental basalts provide may sample both the asthenospheric and lithospheric mantle, depending on their geodynamic settings. In old continental crust setting it is possible to delineate asthenospheric and lithospheric mantle sources using Nd-isotopic variations in basalts. In agreement with previous work [1,2], mineral-melt partitioning is the *initial* primary control on Th-U fractionation. Basalts derived from spinel lherzolite source, clinopyroxene as the controlling mineral, show no Th-U fractionation, without exception. This is supportive of experimental data showing that $D_U^{CPX}/D_{Th}^{CPX} = \sim 1$ [3] and powerfully constrained by combined Pa-U and Th-U data [4]. Basalts derived from the asthenosphere show large ^{230}Th over ^{238}U enrichment, similar to enriched MORB. Unlike mid-ocean ridges, however, asthenospheric mantle melting under continents, and most likely under ocean islands, is strongly modulated by the lithosphere.

Protactinium-231 over ^{235}U enrichment [(^{231}Pa/ ^{235}U) ~1.2–2.4] is present on all samples we have measured, regardless of the mantle source and inferred source mineralogy. Although there are no experimental partitioning data for Pa, it is expected to be much more incompatible than U and Th during both spinel lherzolite and garnet peridotite melting. For alkali basalts, those derived from the asthenosphere show larger Pa over U enrichments than those derived from the lithosphere. We suspect the difference reflects the extra Pa over U enrichment in the asthenospheric mantle-derived lavas due to dynamic melting ingrowth [5–7]. For lithospheric mantle-derived lavas, alkali basalts show larger Pa over U enrichments, compared to their tholeiitic counterparts, consistent with degree of melting, having important control on Pa-U fractionation. The large ^{231}Pa over ^{235}U enrichment seen in lithospheric mantle tholeiitic lavas is surprising. The tholeiitic composition may primarily reflect shallow depth melting, instead of high degree of melting within the lithosphere. It is also possible that melting within the lithospheric mantle may involve enrichment processes not fully appreciated as of now.

References: [1] Asmerom Y. and Edwards R. L. (1995) *EPSL, 134,* 1–7. [2] Asmerom Y. (1999) *EPSL, 166,* 163–175. [3] Salters V. J. M. and Longhi J. (1999) *EPSL, 166,* 15–30. [4] Asmeron et al., in review. [5] McKenzie D. (1985) *EPSL, 72,* 81–91. [6] Williams R. W. and Gill J. B. (1989) *GCA, 53,* 1607–1619. [7] Spiegelman M. and T. Elliott (1993) *118,* 1–20.

CONTROL OF OCEANIC NEW PRODUCTION IN THE EQUATORIAL PACIFIC BY IRON.

A. K. Aufdenkampe[1], J. J. McCarthy[2], M. Rodier[3], and J. W. Murray[1], [1]Mail Code Z, School of Oceanography, University of Washington, Seattle WA 98195-7940, USA (anthonya@ocean.washington.edu), [2]Mail Code Z, Harvard University, 26 Oxford Street, Cambridge MA 02138, USA, [3]Institut de Recherche pour le Développement, Station Marine d'Endoume, 13007 Marseille, France.

Introduction: Oceanic primary production stimulated by newly available nutrients — or new production [1] — directly drives the biological pump of organic C export to the deep ocean [2]. Therefore, understanding what controls the magnitude and variability of new production is of great importance to oceanographers and global C modelers alike.

We present here results of a reanalysis of nine cruises to the equatorial Pacific that directly measured new production using ^{15}N methods. We show that multiple linear regression (MLR) is successful at predicting nearly eighty percent of the observed variability in new production using commonly measured water properties. To address the fundamental biogeochemical causes of variability in new production, we also develop a simple mass balance model of coupled N and Fe fluxes within the euphotic zone.

Multiple Linear Regression Model: Multiple linear regression analysis is particularly well suited to determining which subset of variables best explains the variability in another. This statistical method was performed for nine cruises to the equatorial Pacific: WEC88 [3], WEC8803-B [4], US JGOFS EqPac Surveys [5] I and II and Time Series [6] I and II, France JGOFS FluPac [7] and OliPac [8], and Zonal Flux [9]. Of dozens of variables tested, nitrate and ammonia inventories, rates of primary production, and average euphotic zone temperatures were most important to predicting new production, with a multiple R^2 of 0.79.

The success of MLR methods at predicting new production is a large step toward the goal of extending shipboard measurements to larger spatial and temporal scales with remotely sensed data. However, despite substantial previous evidence in support of each of the independent variables, the MLR

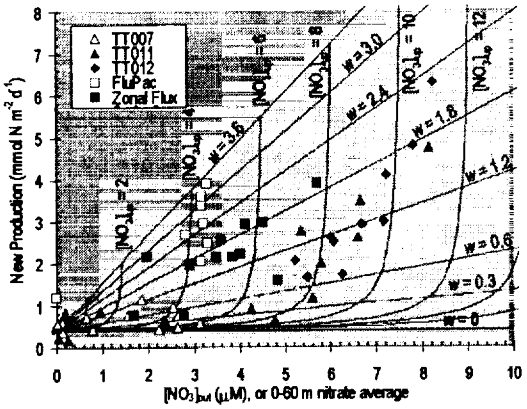

Fig. 1. New Production as a function of exported nitrate for five equatorial Pacific cruises. Lines represent contours derived from the N:Fe mass balance model. $[NO_3]_{up}$ in units of µM, and w in m d^{-1}.

method does not address the fundamental biogeochemical causes for new production variability. In addition, much of the remaining "unexplained" variability in the MLR can be traced to differences between cruises in their partial regression slopes of nitrate.

Coupled Nitrogen/Iron Mass Balance Model: Iron is widely acknowledged as the limiting nutrient in HNLC regions [10], and mass balance requirements define new production as equal to the flux of the limiting nutrient into the ecosystem. Based on simple, one-box mass balance equations for N and Fe, new production (NP) was formulated as a function of the average concentration of advectively exported nitrate $[(NO_3)_{out}]$. An important consequence of these equations is that the form of the function depends strongly upon the mode of physical forcing to the system. When comparing stations with large differences in the depth of the nitricline, yet with relatively similar upwelling velocities (w), NP is a linear function of $(NO_3)_{out}$ (Fig. 1). However, where the concentration of nitrate upwelled from the base of the euphotic zone $[(NO_3)_{up}]$ remains constant and w varies, NP vs. $(NO_3)_{out}$ is a hyperbolic function with a vertical asymptote of constant $(NO_3)_{out}$. Observed NP to nitrate relationships for individual cruises fit the model quite well when the modes of physical forcing for each cruise is taken into account (Fig. 1).

Conclusion: Modeling results from both statistical and biogeochemical approaches show that variability in new production within the equatorial Pacific is both understandable and predictable.

References: [1] Dugdale R. C. and Goering J. J. (1967) *L&O, 12,* 196–206. [2] Eppley R. W. and Peterson B. J. (1979) *Nature, 282,* 677–680. [3] Wilkerson F. P. and Dugdale R. C. (1992) *JGR, 97,* 669–679. [4] Pena M. A. et al. (1992) *MEPS, 80,* 265–274. [5] McCarthy J. J. et al. (1996) *DSR-II, 43,* 1065–1093. [6] Wheeler P. A. and Barber R. T. (1994) http://www1.whoi.edu/jgofs.html. [7] Navarette C. (1998) Ph.D. thesis, Université Paris VI, 313. [8] Raimbault P. et al. (1999) *JGR, 104,* 3341–3356. [9] Le Borgne R. et al. (1999) *Oceanol. Acta, 22,* 57–66. [10] Landry M. R. et al. (1997) *L&O, 42,* 405–418.

ALTERATION OF OCEANIC TROCTOLITES BY MAGMATIC FLUIDS IN OCEAN DRILLING PROGRAM HOLE 735B?

W. Bach[1], Y. Niu[2], J. C. Alt[3], and S. E. Humphris[1], [1]Woods Hole Oceanographic Institution, 360 Woods Hole Road, Woods Hole MA 02543, USA, [2]University of Queensland, Brisbane, Australia, [3]University of Michigan, Ann Arbor MI, USA.

Ocean Drilling Program (ODP) Hole 735B represents a section through 1.5 km of lower oceanic crust formed at the very slow spreading Southwest Indian Ridge. The section is dominated by gabbroic lithologies with abundant veins and veinlets of both igneous and metamorphic origins. Besides pronounced hydrothermal alteration (reaction of rock with seawater-derived fluids) in the upper 600 m of the hole, there is also evidence for the presence of magmatic fluids as revealed by O- and H-isotopic compositions of amphiboles spatially and genetically associated with veins and pockets of felsic material from the upper 500 m of the hole [1]. Moreover, fluid inclusions in apatite hosted in felsic material represent trapped magmatic vapor and brines [2]. These observations suggest that exsolution of magmatic fluids may be a common process in the magmatic evolution of the lower oceanic crust. So far, evidence for the presence of deuteric fluids was confined to late-stage magmatic material and hence it was uncertain whether the magmatic fluids can migrate and redistribute trace elements in the lower crust.

Here we present new data that suggest — for the first time — that magmatic fluids are not just confined to felsic material but may be able to flow through fracture networks leading to pervasively alteration of basement rocks. This process could have important consequences for the redistribution of elements in the lower oceanic crust. Our interpretation is based on a detailed documentation of bulk rock and mineral compositional variations of a dark, amphibole/plagioclase/phlogopite/chlorite-bearing vein, the associated centimeter-wide alteration halo and a decimeter-sized alteration patch all hosted by undeformed and fresh troctolite at a depth between 510 and 520 m below sea floor. The halo and the patch are 60–80% recrystallized with olivine being completely replaced by amphibole, phlogopite and chlorite, and plagioclase being partly replaced by secondary calcic and sodic plagioclase, amphibole, and prehnite. Neither the vein nor the alteration halo or patch show phases that are typically associated with felsic veins and rocks impregnated by late-stage silicic melts (quartz, apatite, and zircon).

Of particular significance is the presence of secondary calcic plagioclase (which has not been previously described from Hole 735B) associated with hornblendes. Secondary calcic plagioclase can form by reaction of rock with aqueous fluids at high temperatures (>500°C) [3]; impregnation with silicic melt would form sodic plagioclase. The hornblendes usually form euhedral crystals and seems to have crystallized earlier than fibrous actinolite commonly intergrown with phlogopite (both K- and Na-rich) and chlorite. Ion-microprobe measurements of REE concentrations reveal that the early euhedral hornblendes have patterns similar to magmatic hornblendes (LREE depleted, negative Eu anomaly, total REE several hundred parts per million) whereas the later fibrous actinolites have patterns similar to hydrothermal vent fluids (LREE enriched, positive Eu anomaly, total REE few tens of parts per million). There is little textural evidence to support equilibrium between the hornblendes and the calcic plagioclase, but the observation that they are always spatially closely associated suggests they were formed during the same recrystallization event. The magmatic REE pattern of the hornblendes and the high anorthite content of the plagioclase leads us to believe the recrystallizing agent was a magmatic fluid. Very briny fluid inclusions in plagioclase are common and may represent trapped magmatic fluids.

Our hypothesis of interaction of the rocks with magmatic fluids is supported by the bulk rock composition of the samples. The altered rocks show 8 to 40 fold enrichments in Cs, Rb, Th, U, Nb, Ta, K, REE (except Eu), Sn, Y, and Be. Such enrichments are difficult to explain by hydrothermal alteration. Results from ODP Hole 504B show that high degrees of hydrothermal alteration at temperatures between 400° and 500°C result in depletion — not enrichment — of these elements in the rock [4]. Introduction of magmatic fluids is the most likely process responsible for the trace-element enrichments in the altered troctolites. We believe that the enrichment was imposed by reaction of the rock with a magmatic fluid — not a melt — because there is no petrographic evidence for the presence of felsic or oxide-rich material, and the major-element composition of the altered rocks does not show the characteristic changes in major-element composition observed in rocks impregnated by late-stage melts.

The compositional variability of secondary minerals suggests that there was a large range in mineralization temperatures very likely associated with variations in fluid composition. The deuteric alteration (~500°–700°C) is followed by alteration at lower temperatures (<400°C) and the formation of chlorite, actinolite, albite, and prehnite during which seawater-derived fluids were probably involved. This retrograde overprint makes bulk rock stable isotopic data difficult to interpret. The O- and H-isotopic data of altered and fresh rocks are consistent with deuteric alteration but do not unequivocally confirm it. Oxygen- and H-isotopic data of mineral separates will be obtained to test our hypothesis

References: [1] Stakes D. S. (1991) *Stable Isotope Geochem.*, 77–90. [2] Kelley D. S., *JGR, 101,* 2943–2962. [3] Vanko D. A. and Laverne C., *EPSL, 162,* 27–43. [4] Bach W. et al., *Proc. ODP Sci. Results, 148,* 39–55.

EARLY CHEMICAL AND PETROGRAPHIC CHANGES DURING PEAT-TO-LIGNITE TRANSFORMATIONS.

A. M. Bailey[1], A. D. Cohen[2], W. H. Orem[3], W. C. Riese[4], and S. Thibodeaux[5], [1]Department of Geology, University of Southwest Louisiana, Lafayette LA 70504, USA (ambailey@usl.edu), [2]Department of Geological Sciences, University of South Carolina, Columbia SC 29208, USA (cohen@geol.sc.edu), [3]U.S. Geological Survey, 956 National Center, Reston VA 22092, USA (borem@usgs.gov), [4]Vastar Resources Inc., Houston TX 77079, USA (rriese1@vastar.com), [5]Burlington Resources, Farmington NM 87499, USA (sthibodeaux@br-inc.com).

Introduction: Peat layers have special significance as chemically active horizons in the evolution of deltaic and other shoreline-related sediments, and as the source of fossil fuels. Laboratory simulations provide a means to study changes in various kinds of peat layers undergoing diagenesis and allow a better understanding of inorganic, petrographic, and organic transformations that may occur during and after burial.

Experimental: Well-characterized peats are being subjected to stepwise increasing temperatures and pressures from 30°C and 300 psi to 60°C and 2100 psi in open systems over periods of two weeks. This is followed by two weeks at 60°C and 2100 psi, conditions that are found to produce a lignite-like material. Solutions extracted during experiments are being monitored by ICP and IC for changes in inorganic and organic constituents, and organic and petrographic changes in the solids are being determined by Pyr. GC/FT-IR/FID and GC/MS and microscopy.

Results: Solution data show that major-element and organic acid/anion concentrations vary with initial peat type and systematically with step within experiments for a given peat [1]. Data (corrected for porewater contributions) suggest several processes may be responsible for these systematic variations, including desorption, increased solubility with increased temperatures and pressures, and enhanced solubility with complexation.

Significant changes are observed in the solids. Petrographically, new textures and macerals are produced [2]. Compressions of from 83 to 88% produce dark brown to black, shiny, flattened pellets exhibiting microscopic banding and vertical and horizontal microcracks. Vertical cracks are observed primarily in gelinitic bands; whereas, horizontal cracks tend to form at microband boundaries. In transmitted light all vitrinite precursors show some changes in color to orange or red; however, some of these precursors are found to contain darker, minute particles derived from microorganisms ("pseudomicrinites") that only became prominent after maturation. Fusinite precursors are only found in peats derived from fire-prone environments. Liptinites display a slight increase in red/green fluorescence during coalification and some flow of components into nearby cracks. Positive changes in reflectance of huminitic macerals occur during experiments.

Organic changes can also be observed [3]. Pyr. GC/FT-IR/FID and GC/MS show significant decreases in cellulosic constituents and relative increases in lignitic constituents for some coalified peat types. Other studies [4] using ^{13}C NMR and elemental analysis reveal limited bulk changes in peats processed to 60°C and 2100 psi, primarily a decrease in O-containing organic compounds. Increasing temperatures and pressures to 125°C and 3000 psi produce more bulk changes including continued loss of cellulose and other O-containing compounds, and a decrease in H-rich compounds, probably volatile aliphatic compounds and fatty acids. Similar decreases in cellulose have been noted by others [5].

Summary: In summary, results show extensive inorganic and petrographic transformations and some organic transformations for peats brought to 60°C and 2100 psi over four weeks. An open system appears to promote these changes. Conditions of 125°C and 3000 psi promote additional bulk organic chemical changes.

References: [1] Bailey A. M. et al., *Chem. Geol.*, in review. [2] Cohen A. D. and Bailey A. M. (1997) *Int. J. Coal Geol., 34,* 163–194. [3] Rollins M. S. et al. (1991) *Org. Geochem., 17,* 451–465. [4] Bailey A. M. et al. (1994) *GSA Abstr. with Prog., 25,* A96. [5] Orem W. H. et al. (1996) *Org. Geochem., 24,* 111–125.

BIOAVAILABILITY AND CHEMICAL COMPOSITION OF THERMALLY ALTERED *PINUS RESINOSA* (RED PINE) WOOD.

J. A. Baldock, Commonwealth Scientific and Industrial Research Organisation Land and Water, PMB 2, Glen Osmond, SA 5064, Australia (jeff.baldock@adl.clw.csiro.au).

Introduction: The presence of charcoal and charred plant residues has been demonstrated in soils and sediments. In this study the bioavailability of C in unaltered and thermally altered wood was compared with that of glucose and cellulose. The chemistry of the unaltered and thermally altered wood was characterised using a variety of solid-state ^{13}C nuclear magnetic resonance (NMR) analyses. Bioavailability of C in the heated wood was related to changes in the chemical composition.

Materials and Methods: *Pinus resinosa* (Red Pine) wood was collected from the bole of living trees. Sapwood was separated from bark and heartwood, dried at 70°C, ground and heated to temperatures of 150°, 200°, 250°, 300°, and 350°C. Heating was continued until no further mass loss was measured. Total mass loss during heating was determined. Total organic C contents of unheated (70°C) and heated wood were determined.

Bioavailability of organic C (OC) in the unheated and heated wood samples was determined in a laboratory incubation experiment. To a sand matrix containing no OC, an appropriate mass of glucose, cellulose, unaltered wood, or thermally altered wood was added to give an OC content of 10 g C g^{-1} sample. The sand/OC mixtures were amended with a nutrient solution and inoculated with microorganisms extracted from a decomposing *Pinus resinosa* log. The concentration of N in nutrient solution was set to produce a C:N ratio of 15 in the incubated samples, and a volumetric water content of 0.29 cm^3 cm^{-3}. The samples were incubated in the dark at 25°C for 120 d.

Solid-state ^{13}C NMR analyses were completed using a Varian Unity 200 NMR spectrometer operating at a ^{13}C frequency of 50.3 MHz. Conventional cross-polarization and Bloch decay NMR analyses were completed using the unaltered and thermally altered wood samples. The NMR observability of OC in each sample, relative to that in glycine, was determined to allow quantitative interpretations.

Results and Discussion: *Bioavailability of C in the wood samples.* Organic C in the unaltered wood was less available than OC in glucose or cellulose, but was more available than OC in the thermally altered samples (Fig. 1). With increasing heating temperature and degree of thermal alteration, the bioavailability of wood OC decreased. At temperatures ≥200°C, little thermally altered OC was available to microorganisms over the 120-d incubation period.

Solid-state NMR analyses. The distribution of OC in alkyl, O-alkyl, aromatic, and carbonyl structures was similar for the two ^{13}C NMR analyses (Fig. 2). With increasing extent of thermal alteration, O-alkyl C content decreased while aromatic C content increased. The proportion of total OC observed in the cross-polarization analysis decreased from 90 to 30% with increasing thermal alteration; however, that associated with the Bloch decay analysis remained high (>85%) for all samples (Fig. 2). The decreased bioavailability of the wood samples was related to a conversion from an organic material dominated by O-alkyl C (carbohydrates) to one dominated by aromatic C. The different observability of OC in the two NMR analyses

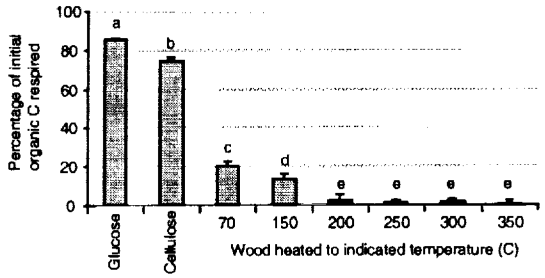

Fig. 1. Bioavailability of OC in glucose, cellulose, unaltered wood, and thermally altered wood. Error bars present standard deviations with n = 6. Mean values with different letters are different at α = 0.05.

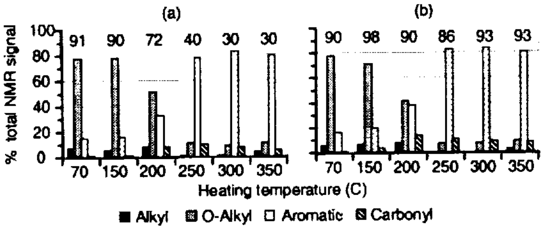

Fig. 2. Chemical composition of the unaltered and thermally altered wood using **(a)** cross-polarization and **(b)** Bloch decay ^{13}C NMR analyses. Values given above each set of bars represent the measured observability of the OC contained in the sample.

suggested that the aromatic C was in structures devoid of protons in the thermally altered wood.

GEOCHEMICAL SIGNATURES IN THE EARLY PROTEROZOIC OCEANIC SEDIMENTS: CASE HISTORY FROM THE ARAVALLI SUPERGROUP OF SOUTHCENTRAL RAJASTHAN, INDIA.

D. M. Banerjee[1] and P. Bhattacharya[2], [1]Department of Geology, University of Delhi, Delhi-110007, India, [2]Division of Land and Water Resources, Royal Institute of Technology, SE-100 44 Stockholm, Sweden.

Although source area discrimination of graywackes and arenites of the Early Proterozoic Aravalli supergroup of southcentral Rajasthan has been made possible using major- and trace-element (viz. Al_2O_3/SiO_2 ratios, FM traces and REEs) analyses [1], the associated shales and low-grade metamorphosed argillites are better candidates for such studies [2]. Effect of low-grade metamorphism on REEs appear to be minimal in fine-grained sediments like shales and phyllites [3]. Around Udaipur in Rajasthyan, in the type area of the Aravalli supergroup, three major meta-argillite assemblages have been distinguished, the Debari Argillite, Girwa Valley Argillite and Jharol Argillite. Major-, trace-, and REEs in these rocks have been analyzed from several well constrained profiles. Taking into account the effects of modifying factors like grain size, adsorption, elemental mobility, and source-area weathering, a series of source area discrimination diagrams were plotted. These studies show that the Debari Argillite represent the early phase of the sedimentation in the Aravalli sea and reflect a passive margin tectonic setting that shows a gradual change in character to an active margin setup. The overlying Girwa Valley Argillite closely associated with the graywackes (with relict fragments of andesite) also reflects an active continental margin to a continental island arc type setting. Major-element chemistry of the youngest unit of silty arenite in the argillite succession suggests a passive margin although FM trace-element ratios indicate tectonic setting similar to that of Girwa Valley Argillite. Debari argillites show marked LREE depletion, marked positive Eu anomaly, strong, negative Ce anaomaly and a granitic gneiss as the source area. The Girwa Valley Argillite show steep REE profile with strong LREE enrichment, strong negative Eu anomaly, and moderate Ce depletion with dacitic and andesitic source terrain. Jharol Argillites show characters similar to Girwa Valley Argillite barring cases where positive Eu and strong negative Ce anomalies have been recorded. The source terrain is interpreted as granitic gneiss. Such intricate flippings of provenance documented by the changes in the chemical ratios in the rocks have been explained by the progressive unroofing of the Late Archean and Early Proterozoic basement complex followed by complex opening and closing of microplate margins resulting into erosion and subduction of the upper-crust material in different stages of plate adjustment.

References: [1] Banerjee D. M. and Bhattacharya P. (1984) *Precambrian Res., 67,* 11–35. [2] Sholkovitz E. R. (1988) *Am. J. Sci., 288,* 236–281. [3] Condie K. C. (1991) *GCA, 55,* 2527–2531.

X-RAY PHOTOELECTRON SPECTROSCOPY STUDY OF REDUCTIVE DISSOLUTION OF BIRNESSITE BY OXALATE.

D. M. Banerjee and H. W. Nesbitt, Department of Earth Sciences, University of Western Ontario, London ON, N6A 5B7, Canada (dipban@julian.uwo.ca).

Reductive dissolution of synthetic 7 Å-birnessite $[MnO_{1.7}(OH)_{0.25}$ or $MnO_{1.95}]$ by Na-oxalate produces a Mn(III) intermediate reaction product (here represented as $MnOOH^*$) which subsequently reacts with sorbed $(COO)_2^{-2}$ to form an unreactive Mn(III)-oxalate surface complexes at the solution-mineral interface according to the reactions:

$$2MnO_2 + (COO)_2^{-2} + 2H^+ = 2MnOOH^* + 2CO_2 \qquad (1)$$

$$2MnOOH^* + (COO)_2^{-2} = 2[MnOOH\text{-}COO]^- \qquad (2)$$

X-ray Photoelectron Spectroscopy (XPS) results from $Mn2p_{3/2}$, C1s and O1s spectra of reacted surfaces reveal that initially rapid production of CO_2 via reaction (1) results in accumulation of CO_2 at the reaction interface. After about 15 min, the reaction rate decreases to the point where desorption keeps pace with accumulation (no appreciable change in adsorbed CO_2 content between 15 min and 2.5 h). The rate of CO_2 production continues to decrease with time until after 10 h of reaction CO_2 is not detected at the reaction surface. Reduction of Mn(IV) of birnessite to Mn(III) indicates that MnO_2-oxalate redox reaction proceeds as transfer of one electron per metal center.

There is no XPS evidence for reduction of Mn(III) of the solid to Mn(II) in the presence of oxalate. Whereas this reaction proceeds in presence of arsenite, oxalate inhibits this step, probably through formation of a strong Mn(III)-oxalate surface complex (either monodentate or bidentate). This postulate is consistent with Mn^{3+}(aq) stabilization by oxalate in aqueous solutions. Further study using X-ray absorption spectroscopy (XAS) is required for a better understanding of the structure of the surface complexes.

Rate of release of soluble Mn(II) to dilute oxalate solutions (5×10^{-4} M) is lower by an order of magnitude compared with rate of release to aerated, distilled water at similar pH. Apparently, the process of proton promoted dissolution of the soluble Mn(II) component of birnessite in distilled water is impeded by the addition of oxalate. This is probably due to the formation of a binuclear, bidentate surface complex between Mn(II,III) and adsorbed oxalate ions.

MICROBIAL POPULATIONS SUSTAINED BY DISSOLUTION OF IRON SILICATES.

J. F. Banfield, S. A. Welch, C. M. Santelli, K. J. Edwards, and P. L. Bond, Department of Geology and Geophysics, University of Wisconsin–Madison, 1215 West Dayton Street, Madison WI 53706, USA (jill@geology.wisc.edu).

Introduction: It is widely accepted that oxidation of Fe provides metabolic energy for microorganisms living in acidic solutions and that microbial catalysis of Fe oxidation controls the rate of dissolution of sulfide minerals in most terrestrial and marine environments. However, the potential importance of ferrous Fe released by silicate mineral dissolution as a microbial energy source has received scant attention. In part, this may be attributed to the paucity of data supporting the existence of prokaryotes able to catalyze Fe oxidation at near neutral pH. The recent isolation of a diversity of species capable of Fe oxidation at circumneutral pH under microaerophilic conditions [1,2] raises the intriguing possibility that Fe-based lithotrophy may sustain (and may have sustained) microbial populations in a variety of Earth (and possibly extraterrestrial) environments. Recently, we verified that under some conditions, iron silicate dissolution can support substantial microbial populations [3]. In this paper we suggest a method to predict cell numbers that may be sustained by dissolution or Fe-bearing minerals in rocks in fairly typical near-surface environments.

Approach, Methods, and Analysis: It should be possible to predict the number of cells that can be supported by oxidation of ferrous Fe from (1) the typical rate at which cells metabolize Fe, and (2) the mineral dissolution rate. From the data of Edwards et al. [4,5] we estimate that cell-normalized rates for Fe oxidation range between ~9×10^{-17}–3×10^{-18} mol $Fe^{2+}cell^{-1}$ s^{-1}). This range is comparable with our measured rate of aqueous oxidation of ferrous Fe by *Thiobacillus ferrooxidans* of 6×10^{-18} mol $Fe^{2+}cell^{-1}$ s^{-1}. The dissolution rate of fayalite, measured at pH 2 in variously oxidized control solutions, was ~1.5×10^{-11} moles Fe^{2+} cm^{-2} s^{-1}, comparable with the published abiotic, anoxic rate [6]. Based on this, we predict that dissolution of fayalite crystals (0.1 $m^2\ g^{-1}$ surface area) should sustain ~10^9 cells. Field-emission, low-voltage scanning electron microscope-based determinations of surface-attached cell populations and planktonic cell counts are consistent with this prediction. Furthermore, almost complete oxidation of aqueous ferrous to ferric iron in microbial experiments, compared to negligible ferric iron in the abiotic control, indicates close to maximum utilization of ferrous iron.

The relevance of microorganisms supported by pH 2 dissolution of fayalite is quite limited. However, based on published dependencies of dissolution rates on temperature, mineral composition, particle size, and pH, we can estimate populations that may be sustained by dissolution of typical rocks. The extrapolation is probably insensitive to variations in cell oxidation rates due to species and temperature. Optimal growth rates for acidophilic Fe-oxidizing organisms in Fe-rich environments vary by less than a factor of 5 between 20°–70°C [7]. However, Fe oxidation rates should vary with concentration of dissolved Fe, as predicted for enzymatic reactions that obey Michaelis-Menton kinetics. Despite this, reported growth rates of Fe-oxidizing neutralophiles (under conditions where aqueous Fe concentrations must be orders of magnitude lower than for acidic environments) are comparable to those of acidophiles [1]. Estimates below do not account for variation in Fe oxidation rates per cell, so predicted cell numbers are minimum estimates. Measurements of the Fe oxidation rates for the new neutralophiles are needed to allow incorporation of this potentially significant effect.

The amount of Fe released by dissolution of Fo_{90} is ~3 orders of magnitude less than fayalite [6] Reaction in circumneutral water will further decrease the rate, and thus sustainable populations, by 2 orders of magnitude [6] (implying ~10^4 cells g^{-1}). Granite containing ~10% typical biotite dissolving in pH 5.8 solutions [8] should be able to sustain ~10^4 cells g^{-1}. The number of lithotrophs supported by Fe oxidation will increase with decrease in particle size, increased solution acidity, decreased metabolism rates, and increased Fe concentration in the silicate minerals. Populations of cells supported by Fe lithotrophy involving ocean floor basalt (2°–4°C) are possible if metabolism rates are suppressed relative to those reported here.

References: [1] Emerson D. and Moyer C. (1997) *Appl. Environ. Micro., 63,* 4784–4792. [2] Sobolev D. and Roden E. E. (1990) *Am. Soc. Micro. 99th General Meeting,* 451. [3] Santelli C. M. et al., in preparation. [4] Edwards K. J. et al. (1998) *Am. Mineral., 83,* 1444. [5] Edwards K. J. et al., *GCA,* submitted. [6] Westrich H. R. et al. (1993) *Am. J. Sci., 293;* Casey W. H. et al. (1993) *Chem. Geol., 105.* [7] Norris P. R. (1990) in *Microbial Mineral Recovery* (H. L. Erlich and C. L. Brierley, eds.), McGraw-Hill, NY. [8] Malmstrom M. and Banwart S. (1997) *GCA, 61,* 2779.

ACCELERATED WEATHERING OF FELDSPAR UNDER ELEVATED $PCO_2(g)$ AT 25°C AND 1 atm.

S. A. Banwart[1] and A. Berg[2], [1]Department of Civil Engineering, Sir Frederick Mappin Building, Mappin Street, Sheffield, S1 3JD, England (k.evans@sheffield.ac.uk), [2]Department of Inorganic Chemistry, The Royal Institute of Technology, Stockholm 100 44, Sweden (astrid.berg@swipnet.se).

Carbon dioxide is generally assumed to play a potentially important role in the weathering of minerals at low temperature and pressure, through suppression of pH, and the known impact of increased proton activity to accelerate the weathering of primary silicate minerals. This hypothesis can be questioned on the basis that the upper range of tabulated soil $PCO_2(g)$ (10^{-2}–$10^{-1.5}$ atm [1]) only results in suppression of pH to values slightly below pH 5, while significant acceleration of silicate weathering due to protons generally occurs only at lower pH [2].

An alternative role of CO_2 in soil environments is to accelerate mineral weathering through the impact of the adsorbed carbonate ligand to lower the activation energy for release of Al ions from the mineral lattice [3]. This effect is similar to that proposed for low weight organic ligands such as oxalate to accelerate mineral dissolution [2], and is hypothesized due to the structural similarity between the carbonate ligand and carboxylic acids.

Results from recent laboratory studies of anorthite dissolution, using flow-through reactors at 25°C and 1 atm total pressure, show a significant increase in mineral weathering rate at elevated concentrations of $CO_2(g)$ [4]. The rate of Al release from the mineral follows a fractional order empirical rate law of the form rate = $k[CO_3^{2-}]$ ($k = 5.9 \pm 1.0 \times 10^{-8}\ l\ m^{-2}\ h^{-1}$; units at 1 mol $[CO_3^{2-}]$).

This empirical rate law is consistent with a ligand-accelerated surface reaction mechanism where rapid and reversible formation of surface Al-carbonato complexes precedes a relatively slower and rate-limiting irreversible release of Al from the mineral lattice. The observed dependence of reaction rate on pH and $PCO_2(g)$ is consistent with a first-order rate dependence on the surface concentration of the Al-carbonato complex; rate = $k\{>AlCO_3^-\}$ ($k = 0.25 \pm 0.1 \times 10^{-3}\ h^{-1}$; surface concentration in units mol m^{-2}). The experimental data also allow the stability constant for formation of the surface complex to be estimated: $>AlOH_2^+ + CO_2(g) \rightleftharpoons >AlCO_3^- + 2H^+$ ($\log K = 5.3 \pm 1.0$).

Organic ligands and protons are generally assumed to provide the greatest impact on weathering rates in soil environments. Comparison of the rate data reported above, with similar data for organic-ligand accelerated weathering of plagioclase, shows that the effect of carbonate ligands can be as strong, or stronger, under elevated $PCO_2(g)$ [4]. This effect is most pronounced at neutral and near-basic pH, where adsorption of low-weight organic ligands is limited. Under elevated $PCO_2(g)$ in this pH range, however, carbonate ion activity increases dramatically due to the pH effects on the aqueous speciation of inorganic C. This in turn drives formation of the surface Al-carbonato complex, and results in accelerated release of Al from the mineral.

There are several potential implications for weathering in natural environments. Current hypotheses on weathering processes before the advent of land plants suggests that microbial respiration in the unsaturated zone resulted in elevated $PCO_2(g)$ [5]. Although it could be argued that the impact on weathering through pH suppression would be minimal, an alternative weathering mechanism in this environment is carbonate ligand-accelerated weathering at neutral or basic pH. In addition to a potential impact on weathering in modern soils and the vadose zone, carbonate-promoted weathering could play a possible role in submarine basalt weathering considering the ocean carbonate concentration near 0.2 mM.

At circumneutral pH and elevated $PCO_2(g)$, carbonate-promoted weathering can result in acceleration of plagioclase dissolution to an extent that is observed in laboratory weathering studies of organic acids in the near-acid pH range. The commonly termed phrase "carbonation weathering" should therefore be extended to include not only the postulated effect of elevated $PCO_2(g)$ to accelerate weathering through suppression of pH, but also the possibility of carbonate-ligand accelerated weathering at circumneutral pH.

References: [1] Appelo C. A. J. and Postma D. (1993) *Geochemistry, Groundwater and Pollution,* A. A. Balkema, Rotterdam. [2] Blum A. E. and Stillings L. L. (1995) in *Chemical Weathering Rates of Silicate Minerals,* Reviews in Mineralogy, Vol. 31, pp. 291–351, Min. Soc. Am., Washington, DC. [3] Bruno J. et al. (1992) *GCA, 56,* 1139–1147. [4] Berg A. and Banwart S. (1999) *Chem. Geol.,* in press. [5] Keller C. K. and Wood B. D. (1993) *Nature, 364,* 223–225.

USE OF RADIUM-226 FOR GROUNDWATER DATING.

F. Barbecot[1], L. Dever[1], and C. Hillaire-Marcel[2], [1]Laboratoire d'Hydrologie et de Géochimie Isotopique, Université Paris-Sud, Orsay, France, [2]Centre de Recherche en Géochimie Isotopique et en Géochronologie, Université du Québec à Montréal, Montréal, Québec, Canada.

Radium-226 can be used as a tracer of groundwater residence time within the aquifer, and be compared to radiocarbon ages. Such an approach is based on a geochemical model taking into account that (1) the initial ^{226}Ra coming from carbonate dissolution in the recharge area, and (2) the ^{226}Ra *in situ* production in the aquifer itself.

Calculation of ^{226}Ra ages can be obtained by

$$^{226}Ra_m = {}^{226}Ra_I \times e^{(-\lambda t)} + {}^{226}Ra_P \times (1 - e^{(-\lambda t)})$$

where $^{226}Ra_{m,\ I,\ P}$ is the measured ^{226}Ra, initial ^{226}Ra, and *in situ* ^{226}Ra contents respectively, λ is the disintegration constant for ^{226}Ra ($4.279 \times 10^{-4}\ y^{-1}$), and t is the ^{226}Ra age of the sample.

The initial ^{226}Ra mineralization can be estimated in the recharge area on a water sample with high-^{14}C content (82.3 ± 0.6 pMC) that is considered a representative of early water mineralization. The initial ^{226}Ra content, corrected from radioactive decay according to the $A^{14}C$ value, has thus been estimated at ~1.12 ± 0.01 to 1.66 ± 0.04 dpm L^{-1}.

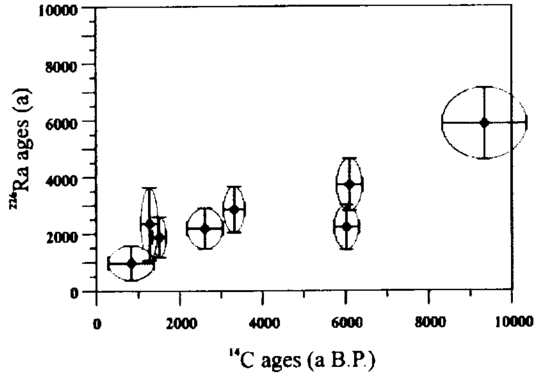

Fig. 1.

For each sample a correction based on the TDIC contents has been performed in order to take into account the variation of pedoclimatic conditions during the aquifer recharge stage.

The ^{226}Ra *in situ* production through time can be estimated from an "old" groundwater (~20 ka) where initial ^{226}Ra content can be neglected with respect to the *in situ* production. The ^{226}Ra *in situ* production takes place in the aquifer matrix through recoil effect, decay of adsorbed ^{230}Th, and water-carbonates interaction. The ^{226}Ra *in situ* production is estimated to 0.3615 ± 0.005 dpm L^{-1}.

The ^{226}Ra *in situ* production can also be calculated via the ^{226}Ra-excess value with respect to U (0.27 dpm L^{-1}).

According to these geochemical models, ^{226}Ra ages can be compared to ^{14}C ages.

The slope of the correlation (<1) may indicate either that the ^{226}Ra *in situ* production has been underestimated, or that models used to calculate ^{14}C ages do not take into account all the retardation factors occurring in the system.

However, the very good correlation existing between ^{226}Ra ages and ^{14}C ages indicates that ^{226}Ra could be very useful for the validation of the radiocarbon ages for late Holocene groundwater.

DATING CLIMATIC EVENTS IN THE EASTERN MEDITERRANEAN REGION USING CAVE DEPOSITS.

M. Bar-Matthews[1], A. Ayalon[1], and A. Kaufman[2], [1]Geological Survey of Israel, 30 Malkhei Israel Street, 95501 Jerusalem, Israel, [2]Department of Environmental Sciences, Weizmann Institute of Science, 76100 Rehovot, Israel.

The most accurate and extensive continental paleoclimate record of the eastern Mediterranean region is obtained from carbonate cave deposits (speleothems) in Israel, sampled at locations close to the eastern Mediterranean coastline. The speleothems were continuously deposited during the last 180 k.y. Detailed C- and O-isotopic profiles combined with TIMS ^{230}Th-^{234}U dating enable the accurate determination of the ages of climatic events in the region, and the correlation of local with regional and major climatic events.

The time period of the last 180 ka includes the six marine isotopic stages for which a number of climatic events can be recognized in the region. The most dry and coolest and events are associated with glacial stages III and II, at 46, 35, and 19 k.y.; similar, but less extreme conditions, prevailed during stage VI at 155 and 140 ka. In contrast, warmer and wetter periods occurred during stage VI, at 175 and 153–145 ka, during stages III and II at 54 and 36 k.y., and during deglaciation, between 17 and 12 ka. Deluge periods are observed during interglacial stage V, between 124 and 120 ka, (with a peak at 122 k.y.), and during the early Holocene between 10 and 7 ka, with a peaks at 8.5 and 7 ka. Less extreme, but still very wet periods occurred also between 108 and 100 ka, and between 85 and 80 ka. Quasiperiodic changes, at millennial timescales occurred during the glacial and the Holocene periods.

The O-isotopic record recorded by speleothems primarily reflect changes in the amount of rainfall, and the O-isotopic composition of precipitation, which is directly related to the isotopic composition of the atmospheric moisture above the eastern Mediterranean Sea. Thus, dating isotopic events using speleothems provides an accurate reflection of regional and global climatic events.

BASALTS IN MONGOLIA: EVIDENCE FOR CONTRIBUTION FROM A WIDESPREAD HYDROUS LITHOSPHERIC SOURCE.

T. L. Barry[1], P. D. Kempton[2], A. D. Saunders[1], M. S. Pringle[3], G. Davies[4], and B. F. Windley[1], [1]Geology Department, Leicester University, Leicester, LE1 7RH, UK (tlb2@leicester.ac.uk), [2]Isotope Geosciences Laboratory, National Research Council, Keyworth, Nottingham, NG12 5GG, UK, [3]Scottish Universities Research and Reactor Centre, Argon Isotope Facility, Scottish Enterprise Technology Park, Rankine Avenue, East Kilbride, G75 0QF, Scotland, [4]Hoofd Afdeling Massapectrometry, Vrije Universeit Amsterdam, 1081 HV Amsterdam, The Netherlands.

Until recently little has been know about the widespread volcanism of Mongolia. Early Cenozoic basalts erupted ~30 Ma (new ^{40}Ar/^{39}Ar dates) in the Gobi desert of southern Mongolia, are geochemically very similar to younger lavas (6–0.005 Ma) erupted in the Hangai dome of central Mongolia. Trace-element patterns for all the basalts are convex-upward, LREE-enriched [La/Tb = 6.4–7.1 (Gobi); 4.0–8.8 (Hangai)] and strongly heavy REE-depleted [Tb/Yb = ~3.0 (Gobi); <4.3 (Hangai)] suggesting interaction with garnet.

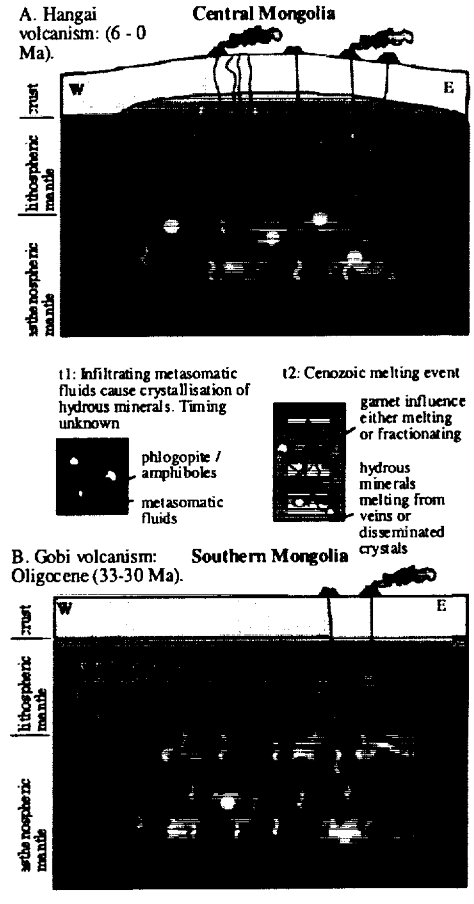
A. Hangai volcanism: (6 - 0 Ma).
Central Mongolia
W
E
crust
lithospheric mantle
asthenospheric mantle
t1: Infiltrating metasomatic fluids cause crystallisation of hydrous minerals. Timing unknown
phlogopite / amphiboles
metasomatic fluids
t2: Cenozoic melting event
garnet influence either melting or fractionating
hydrous minerals melting from veins or disseminated crystals
B. Gobi volcanism: Oligocene (33-30 Ma).
Southern Mongolia
W
E
crust
lithospheric mantle
asthenospheric mantle

Fig. 1. Schematic representation showing melt regime for Cenozoic Mongolian volcanism. **(a)** The complex setting for melt generation in the Hangai area. Some of the magmatism suggests a greater influence of hydrous mineral melting, possibly relfecting the abundance of mantle veins at a given time. **(b)** Melting of a hydrous mineral-bearing source led to small degree melts.

Chemical and isotopic (Sr, Nd, Pb, Hf, and He) studies were undertaken on both Gobi and Hangai alkali basalts to establish magmatic sources and melting processes. Fractional crystallization appears to have had only moderate influences on composition and cannot explain all the variations seen. AFC modeling incorporating compositions of analyzed crustal xenoliths indicate that the basalts have not been affected by crustal contamination. However, both Gobi and Hangai lavas are enriched in K, Nb, Sr and P. This may reflect the breakdown of hydrous phases in the lithospheric mantle during a Cenozoic melting event. The initial enrichment of the source may have occurred at any time; both ancient and modern metasomatic amphiboles occur within Cenozoic hosted mantle xenoliths [e.g., 1]. Low $^{143}Nd/^{144}Nd$ values (0.512265–0.512313) for Gobi basalts and some Hangai basalts (>0.512431) supports an old enrichment event, however this is unlikely the case for all samples, where enrichment may have recently precluded melt generation. In support of a hydrous mineral-bearing mantle under Mongolia are the occurrences of phlogopite megacrysts in the Cenozoic basalts, as well as previously documented amphibole-bearing mantle xenoliths [1]. The isotopes indicate that the mantle beneath Mongolia is heterogeneous with not only an enriched lithospheric component, but also a depleted lithospheric mantle reservoir, characterized by low $^{206}Pb/^{204}Pb$ ratios (>17.0620). In addition, an asthenospheric component may have contributed to overall melt compositions, as suggested by slightly higher $^{3}He/^{4}He$ ratios (<10.8 ± 31%) than MORB, and $^{87}Sr/^{86}Sr$ and $^{143}Nd/^{144}Nd$ ratios close to bulk silicate earth.

The Hangai and Gobi basalts were previously regarded as plume-related, representing part of a large diffuse Cenozoic volcanic province which includes Bartoy and Vitim near Baikal, Russia. It is apparent that the same melting process has occurred over a large area (>>600 km) and throughout a long period of time (>30 Ma), suggesting that vast areas of the Mongolian lithospheric mantle has been metasomatically enriched at some time. In our model, a thermal anomaly underlying Mongolia need only be slightly hotter than ambient mantle temperatures, because preferential melting of hydrous-bearing assemblages in the lithosphere could lead to alkalic melt generation. A high heat-flux plume is not required.

References: [1] Ionov D. A. et al. (1992) *Contrib. Mineral. Petrol., 111,* 235–247.

GEOCHEMISTRY OF XENOLITHIC ECLOGITES FROM WEST AFRICA.

M. G. Barth[1], R. L. Rudnick[1], I. Horn[1], W. F. McDonough[1], M. J. Spicuzza[2], J. W. Valley[2], and S. E. Haggerty[3], [1]Department of Earth and Planetary Sciences, Harvard University, 20 Oxford Street, Cambridge MA 02138, USA (barth@eps.harvard.edu), [2]Department of Geology and Geophysics, University of Wisconsin–Madison, Madison WI 53706, USA, [3]Department of Geology, University of Massachusetts, Amherst MA 01003, USA.

Xenolithic eclogites (bimineralic rocks composed of garnet and omphacite) from kimberlite pipes document equilibration at upper-mantle pressures and temperatures. However, the origin of their protoliths and the subsequent metamorphic evolution of these bimineralic rocks are less certain. Xenolithic eclogites have been variously interpreted as crystallized high-pressure magmas or their cumulates, or as fragments of recycled oceanic crust, which may or may not have been through a melting episode associated with subduction. Trace-element and stable isotopic geochemistry are powerful tools with which to investigate the concealed evolutionary record of eclogites and to constrain possible precursors. For this reason, we have measured the O-isotopic ratios of clean mineral separates of garnets, omphacite, and kyanite in xenolithic eclogites from the Koidu kimberlite pipe, Sierra Leone, by laser fluorination techniques. Trace-element compositions of garnets, omphacites, rutiles, and ilmenites have been determined by laser ablation inductively coupled plasma-mass spectrometery (ICP-MS) from which whole-rock compositions have been reconstructed.

The Koidu eclogites fall into two groups, based on their major-element chemistry: high-MgO (>16 wt% MgO) and low-MgO (6–13 wt% MgO). The high-MgO group shows diverse trace-element patterns and mantlelike $\delta^{18}O$. LREE-enriched patterns in some of these samples are inconsistent with a cumulate or restite origin. Therefore, these samples may represent crystallized picritic melts, which may or may not include minor cumulate phases. However, the diversity of incompatible trace-element patterns is difficult to explain with a simple crystallization model and suggests a more complex origin. In this abstract we concentrate on the low-MgO group, which shows evidence for being fragments of subducted oceanic crust.

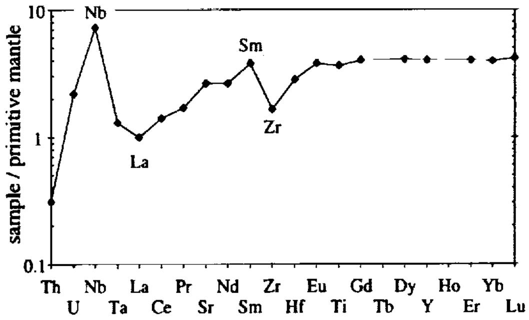

Fig. 1. Primitive mantle-normalized diagram of the median of the reconstructed low-MgO Koidu eclogites.

Oxygen-isotopic data obtained on garnets show variable isotopic compositions, with several samples having both isotopically lighter and heavier values than the mantle range. Additional garnet, omphacite, and kyanite separates are being measured and will be reported at the meeting.

The 11 low-MgO eclogites analyzed to date are all LREE depleted. The jadeite-poor eclogites (<30% jadeite component in clinopyroxene) have very similar LREE-depleted patterns, whereas the jadeite-rich eclogites have more variable LREE-depleted patterns. The kyanite-bearing samples show pronounced positive Eu anomalies.

High-field strength elements are largely contained in accessory rutile, for which modes have been calculated from Ti mass balance between the measured whole-rock and mineral compositions. The majority of reconstructed eclogite whole-rock compositions show superchondritic Nb/La ratios (Fig. 1, median Nb/La = 5) but subchondritic Zr/Sm ratios (median = 12).

The presence of Eu anomalies and the deviation of $\delta^{18}O$ from mantle values in the low-MgO eclogites suggest a low-pressure protolith such as altered oceanic crust. The more heterogeneous REE patterns of the jadeite-rich samples are consistent with more intense hydrothermal alteration (e.g., albitization) of the oceanic precursor than of the jadeite-poor samples. The LREE depletions, flat HREE patterns, and positive Nb anomalies require an episode of partial melting (or dehydration) of rutile-bearing garnet amphibolite or eclogite during subduction. A protolith with a flat trace-element pattern — similar to enriched mid-ocean ridge basalt or oceanic plateau basalt — loses LREE during partial melting/dehydration while Nb and the HREE stay in the residue due to the high-partition coefficients of rutile and garnet, respectively (Fig. 1). The complementary silicic melt (or fluid) would show Nb and HREE depletions, as observed in tonalite-trondhjemite-granodiorite suites, which make up large portions of the crust in Archean cratons. Therefore, the Koidu eclogites may represent fragments of processed oceanic crust that are residues from Archean continental crust formation.

LABORATORY EXAMINATION OF MICROBIAL PERTURBATIONS IN A GEOLOGICAL DISPOSAL SITE FOR RADIOACTIVE WASTE.

K. Bateman[1], P. Coombs[1], K. Hama[2], V. L. Hards[1], A. E. Milodowski[1], J. M. West[1], P. D. Wetton[1], and H. Yoshida[2], [1]British Geological Survey, Keyworth, Nottingham, NG12 5GG, UK, [2]Japan Nuclear Cycle Development Institute, Tono Geoscience Centre, 959-31, Jorinji Izumi, Toki, Gifu 509-51 Japan.

Introduction: Microbial activity can have a significant impact on geochemical processes as it can influence mineral dissolution and precipitation, pH, alkalinity, and redox. Detailed studies into the subsurface microbiology of Äspö [1] had revealed the presence of many different bacteria in the deep groundwaters including Fe- and sulfate-reducing bacteria, the implications of which are discussed in detail in an earlier study [2]. A series of experiments were conducted as part of a BGS-JNC collaborative program to study the rock-water and microbial interactions.

Experiments: Results from previous work [3] using batch systems showed that microbes potentially have complex effects on the geochemistry of the system. The experiments discussed here were designed to represent more realistic conditions, by using flowing systems. Both columns and mixed-flow reactors were used in these experiments. The experiments were conducted within an anaerobic chamber with a controlled $N_2/H_2/CO_2$ atmosphere. A series of experiments were conducted in which crushed Äspö Diorite was reacted with Äspö groundwater flowing into the system. Half the experiments were inoculated with a mixture of sulfate-reducing bacteria (SRB) and Fe-reducing bacteria (IRB). Fluid was continuously analyzed for chemical and microbial changes during the experiments. The fluid pH and flow rate were also monitored. The reacted solid residues from the experiments were examined for mineralogical and petrographic changes at the end of the experiments.

Results: The column experiments were run for about two weeks before the columns with bacteria added became blocked and flow fluid ceased. The mixed-flow experiments were ran anaerobically for three months, after which two of the experiments were allowed to run aerobically for a further three months.

Microbiology results. Bacterial populations were sustained throughout the experiments.

Mineralogy results. Some evidence of biofilm development was observed during analysis of residues from the column experiments. However, the mixed-flow experiments showed no clear evidence (or preservation) of biofilm development.

Scanning electron microscopy (SEM) observation of the solid residues from the mixed-flow experiments showed no significant evidence for reaction when compared to the starting material. However, there was a loss of fine-grained (i.e., <5 µm) material, which originally adhered to grain surfaces in the starting material. There was also evidence for the formation of minor amounts of smectite on primary mineral surfaces; smectite was not present in the starting materials. X-ray diffraction analysis (XRD) supported the identification of smectite in the residues. Mineralogical observations indicate that minor conversion of chlorite and chloritised biotite fines present within the crushed diorite has produced smectite and mixed-layer chlorite-smectite. The degree of alteration was greater in the experiments when bacteria were present, but no difference in reaction was seen between the anaerobic experiments, and those that were initially anaerobic and subsequently run aerobically. This suggests that the smectite formation occurred under anaerobic conditions, with little subsequent alteration under aerobic conditions.

The observations are consistent with those of the column experiments. The columns with bacteria became blocked very rapidly, and minor amounts of smectite were observed in the reaction residues examined after this period. Experiments without bacteria did not block up. These results are consistent with bacterially enhanced smectite formation being responsible for the blocking of the column experiments. However, additional research is required to confirm whether or not this hypothesis is correct. If bacterial action is indeed shown to be responsible for the enhanced rate of smectite formation, the chemical mechanism needs to be established by further work.

Chemistry results. Little evidence for rock-water interactions is seen in the chemical analysis data for all the experiments. There are some slight initial increases observed for some elements (i.e., Si, Al) but this is probably the result of the reestablishment of equilibrium between the groundwater and the crushed rock as no further trends are observed. Modeling of the fluids showed them to be saturated with respect to clay minerals. Possibly, the observed mineralogical changes reflect alteration occurring in microbially mediated microenvironments close to mineral surfaces. Consequently, these changes may be too small to be detected in the chemical analysis of the bulk fluid.

Acknowledgments: This work is published with the permission of the Director of the British Geological Survey and JNC.

References: [1] Pedersen and Karlsson (1995) *SKB Technical Rpt. 95-10.* [2] Banwart S. (1995) *SKB Technical Rpt. 95-26.* [3] Bateman et al. (1998) *Mineral. Mag., 62A,* 124–125.

INTRAPLATE MAGMATISM OF THE KOLA STRUCTURE, BALTIC SHIELD BAYANOVA.

T. B. Bayanova, Geological Institute of the Kola Science Centre, Fersman str. 14, Apatity, Murmansk reg., 184200, Russia.

The oldest dikes in Fennoscandinavia are the metagabbronorite dikes of Kirgora. Uranium-lead dating of two dikes, which cut the BIF formation of the Olenegorsk ore field, yielded 2739 ± 10 and 2738 ± 6 Ma. All zircon fractions are in the upper part of the concordia plot; one point of altered baddeleyite lies in the lower part, showing an age of 330 ± 28 Ma, and reflects the age of Paleozoic alkaline magmatism 360–380 Ma [1], which is widespread in the eastern Baltic Shield. The U-Pb age on apatite from one of the dikes is 1960 ± 30 Ma, which we interpret as Svecofennian metamorphic events.

Zircons from garnet metaanorthosite of the Achinsky, Tsaga, and Medvezhje-Schuchieozersky massifs (Keivy Structure) have Archean U-Pb ages of 2678 ± 16, 2659 ± 3, and 2663 ± 7, respectively.

The Kola belt of layered PGE-bearing intrusions formed in the interval between 2.5–2.45 Ga, and the duration of formation of individual intrusions is about 50 Ma. The U-Pb zircon age of gabbronorite from the lower layers of PGE-bearing reefs in the Fedorovo-Pansky Massif is 249 ± 1.5 Ma. The age of gabbropegmatite is 2470 ± 9 Ma. The U-Pb age on baddeleyite and zircon from anorthosite of the upper layers of the ore-bearing reefs is 2447 ± 12 Ma. The gabbronorite of Mt.Generalskaya (basement of Pechenga Structure) yielded a U-Pb age on zircon of 2496 ± 10 Ma, and the anorthosite 2447 ± 12 Ma. Baddeleyite analyzed from the anorthosite of the Imandra lopolith gave a U-Pb age of 2437 ± 11 Ma. A very coeval U-Pb age 2434 ± 7 Ma was obtained for zircons from the pegmatoid gabbronorite of the drusite Kovdozersky Massif located in the Belomorian mobile belt.

A lamprophyre dike of the Pechenga structure has a U-Pbage of 1711 ± 12 Ma.

Three fractions ofrecrystallized baddeleyite and one zircon fraction were studied from the Tiksheozero carbonatite. The U-Pb age obtained, 1650 ± 5 Ma, is in agreement with Sm-Nd and Rb-Sr mineral isochron data, 1.7 Ga [2], and probably reflects the Svecofennian metamorphic events. Previously, we obtained a Pb-Pb age on two populations of zircon: 2500 ± 55 and 2480 ± 40 Ma [3]. These Archean ages can be interpreted either as the emplacement age or the age of zircon xenocrysts.

Acknowledgments: This study was financially supported by the Russian Foundation for Fundamental Investigations, grant 98-05-64321.

References: [1] Kramm et al. (1993). [2] Belyatsky and Tikhomirova (1993). [3] Bayanova et al. (1995).

THE ROLE OF IRON METABOLIZING ORGANISMS IN THE IRON GEOCHEMICAL CYCLE REVEALED BY IRON-ISOTOPIC MEASUREMENTS.

B. L. Beard and C. M. Johnson, Department of Geology and Geophysics, University of Wisconsin–Madison, 1215 West Dayton Street, Madison WI 53706, USA.

Introduction: Metabolic processing of Fe by bacteria is a ubiquitous phenomenon and includes organisms that reduce Fe [e.g., 1], and organisms that oxidize Fe [e.g., 2]. The important role that these organisms play in controlling Fe geochemical cycling is just now becoming recognized [3], but their importance in the geologic past is speculative because identification of metabolic processing is often veiled by the long expanse of geologic time. In order to gain a better understanding of how microbial life may have shaped our planet we have developed a biosignature that identifies metabolic processing of Fe using the isotopic composition of Fe.

A double-spike technique that uses conventional thermal ionization mass spectrometry has been developed, Fe-isotopic compositions can be measured to a precision of 0.2 to 0.3‰ for the $^{56}Fe/^{54}Fe$ ratio [4]. Iron-isotopic variations are reported as $\delta^{56}Fe‰ = [^{56}Fe/^{54}Fe_{sample}/^{56}Fe/^{54}Fe_{standard} - 1]10^3$, the $^{56}Fe/^{54}Fe$ ratio of the standard is equal to 15.7028, the measured ratio of a variety of terrestrial and lunar igneous rocks.

Controlled laboratory experiments using the Fe-reducing bacteria *Shewanella putrefaciens* grown on a ferrihydrite substrate indicates that metabolically reduced Fe has a $\delta^{56}Fe$ value that is 1.3‰ less than that of the starting ferrihydrite composition. In contrast, inorganic Fe has a constant Fe-isotopic composition; the Fe-isotopic composition measured for a variety of terrestrial and lunar rocks (peridotite to rhyolite) is invariant ($\delta^{56}Fe = 0$). The constant isotopic composition of inorganic Fe provides an ideal baseline for evaluating the importance of metabolically processed Fe in the geologic past.

The isotopic composition of Fe has been measured from a variety of sedimentary environments, including Precambrian banded Fe formations and Fe-Mn nodules. The range in Fe-isotopic compositions from these sedimentary environments is large (the measured range in $\delta^{56}Fe$ values is 2.5‰, a factor of 10 greater than the analytical uncertainty), and suggests that Fe-metabolizing bacteria have played an important role in the Fe geochemical cycle for much of Earth's history. For example, Fe-isotopic compositional variations measured in individual layers of Precambrian banded Fe formations vary systematically. Dark colored, Fe-rich layers have near zero $\delta^{56}Fe$

values, whereas, light colored, Fe-poor layers have positive δ^{56}Fe values. The rhythmic variations in Fe-isotopic compositions measured in banded Fe formations is consistent with production of the fine scale layering in banded Fe formations by diagentic alteration by Fe-reducing bacteria, as originally proposed by Nealson and Meyers [5].

Variations in Fe-isotopic compositions measured in Fe-Mn nodules is correlated with major-element nodule compositions. Nodules with compositions consistent with formation by diagentic pore fluids have negative δ^{56}Fe values (–1.62 to –0.96), consistent with the strong role proposed for metal-reducing bacteria which may mobilize metals in pore fluids. In contrast, nodules that have compositions consistent with formation by hydrogenous accretion have variable δ^{56}Fe values (–1.24 to +0.17). Iron-isotopic compositions for nodules formed by hydrogenous accretion are correlated with productivity levels in the oceans. Nodules from the low productivity, ice-covered Arctic Ocean have δ^{56}Fe values of ~–0.3, as compared to nodules from the higher productivity Pacific Ocean that have δ^{56}Fe values of ~–1.2.

Bacterial processing of Fe produces measurable Fe-isotopic fractionations and the present data on inorganic Fe indicates that nonenzymatic processes do not produce measurable Fe-isotopic fractionations. Therefore, the isotopic composition of Fe may be uniquely suited as a biosignature for evaluating the role of Fe metabolizing organisms in the geologic past, and as a tool for evaluating if life existed on other planets. Iron-isotopic variations measured for naturally occurring samples indicate that variations in Fe-isotopic compositions are preserved in nature and these variations are best interpreted as being a result of biological processes. Current work is focusing on evaluating the magnitude of inorganic Fe-isotopic fractionation through the use of reaction columns and electrochemistry, the scope of biological fractionation of Fe in controlled experiments using a variety of substrates and Fe-metabolizing organisms, and determining the variation in Fe-isotopic compositions in the solar system by analysis of meteoritic material.

References: [1] Nealson and Saffarini (1994) *Annu. Rev. Microbiol., 48,* 311–343. [2] Emerson and Moyer (1997) *Appl. Environ. Mircobiol., 63,* 4784–4792. [3] Nealson (1997) *Annu. Rev. Earth Planet. Sci., 25,* 403–434. [4] Beard and Johnson (1999) *GCA,* in press. [5] Nealson and Meyers (1990) *Am. J. Sci., 288,* 35–45.

MOBILITY AND ACCUMULATION OF PLATINUM-GROUP METALS AND SELECT TRACE METALS IN THE POLAND KUPFERSCHIEFER.

A. Bechtel[1], S. Oszczepalski[2], A. M. Ghazi[3], W. C. Elliott[3], and B. D. Chatham[3], [1]Universität Bonn, Bonn, Germany, [2]Poland Geological Survey, Warsaw, Poland, [3]Georgia State University, Atlanta GA 30303, USA (wcelliott@gsu.edu).

The mobility and accumulation of the platinum group metals (PGM), and select trace metals were measured from Kupferschiefer collected from core throughout the Poland Zechstein Basin. PGM were measured using inductively coupled plasma mass spectrometry (ICPMS) and ion exchange preconcentration methods. The PGM, base metals (Cu, Ag) increase in concentration toward the Rote Fäule, a zone of postdepositional oxidation. The areal pattern of PGM and trace element abundances argue for their mobilization and migration outward from the Rote Fäule into the reduced Cu-mineralized Kupferschiefer. Metals having low solubilities (Pt, Pd, Au, and REE) are most abundant at the Rote Fäule and in the Transition zone between the Rote Fäule and the reduced Cu-mineralized Kupferschiefer (e.g., Pt = 202–537 ppb). Metals having higher solubilities (e.g., Ag, Cu, Pb, Co, and Re) are more abundant in the Cu-mineralized Kupferschiefer (Ag = 47–55 ppm and Re = 541–948 ppb) compared to the Rote Fäule (Ag = 3–4 ppm and Re = 113–211 ppb). These results are consistent with recent models describing the Kupferschiefer mineralization. The sources of these metals are enigmatic. They are thought to be mobilized from the underlying Rotliegendes, the Variscan basement or from the Kupferschiefer by oxidizing brines released during intracontinental rifting in the Triassic period.

RHENIUM AND OSMIUM LOSS FROM SUBDUCTED OCEANIC BASALT AND THE RHENIUM BUDGET OF THE CONTINENTS.

H. Becker, Department of Geology, University of Maryland, College Park MD 20742, USA (hbecker@geol.umd.edu).

Introduction: It has been noted that the moderate Re enrichment in the continental crust (CC) complements the Re depletion observed in the subcontinental lithospheric mantle (SCLM), resulting in an overall chondritic modern ^{187}Os/^{188}Os of both reservoirs combined [1]. The complementary behavior of these two reservoirs with respect to Re can be compared with the complementary behavior of mildly incompatible minor and major elements such as Ca, Al, and Fe [2]. However, CC and SCLM cannot be balanced with respect to highly incompatible elements [2]. This implies that either the complementary relationship between those reservoirs for mildly incompatible elements, such as Re, is accidental or multistage processes result in differential extraction of elements according to their incompatibility during CC formation. The preferential extraction of fluid-mobile incompatible elements from subducted oceanic crust in subduction zones over the last 2–3 b.y., and incorporation into CC via arc magmatism, may provide a partial solution for this paradox [3]. Altered basalts lose a large fraction of their Re during dehydration in subduction zones. If this process operated over the last 3–3.5 b.y. it may account for a large fraction of Re in the CC.

Methods: Rhenium and Os abundances were measured by isotope dilution/N-TIMS on 2–3 g of powdered sample using Carius tube digestion in reverse aqua regia, solvent extraction for Os and anion exchange chemistry for Re. Duplicate analyses, some of them including predigestion in HF-HCl-Ethanol, yielded in some cases good in others poor reproducibility of concentrations. Poor reproducibility of concentrations in some samples is attributed to heterogeneous distibution of sulfides.

Rhenium and Osmium in Subducted Metabasalts: In MORB, Re shows good correlations with mildly incompatible elements [4]. Metabasalts metamorphosed in paleosubduction zones (eclogites, blueschists and high-pressure mafic granulites), however, do not show these correlations because of Re loss. These rocks lost ~60% of their Re (abundances 2.5–1689 ppt, median 331 ppt Re) compared to ~860 ppt for MORB with Y abundances comparable to the metabasalts. Rhenium is lost either by dissolution of sulfides in aqueous fluids during dehydration, or during alteration of the protoliths near the ocean ridges. In contrast, Os abundances (0.96–909 ppt, median 6 ppt Os) in the metabasalts are comparable to those in MORB, and possible losses or gains of Os are evidently minor.

Rhenium Budget of the Continental Crust: On a long-term basis, the loss of Re from oceanic crust in subduction zones may contribute significantly to the budget of Re in the CC. Estimates for the Re abundance of upper CC range between 200 and 500 ppt, with a preferred estimate of 400 ppt [5]. Lower CC may have a factor of 2 lower Re abundance compared to upper CC [6]. Thus, values between 300 and 400 ppt may be good approximations for the bulk CC.

The amount of Re extracted from 7.1 km of oceanic crust over 3–3.5 b.y. at efficiencies comparable to the median value obtained from the metabasalts (~60%) comprises $1.2–1.4 \times 10^{17}$g. This represents 14–16× or 19–22× the amount of Re in CC, if the latter contains 400 ppt or 300 ppt Re, respectively. The mismatch in this mass balance suggests that most of the Re (>90–95%) in oceanic crust is recycled back into the mantle [1]. The Re abundance in the CC approximately matches the loss of ~60% Re ($\sim 3.3–9.6 \times 10^{15}$ g Re) from the most altered portion of oceanic crust (uppermost 0.2–0.5 km), if subduction occurred over the last 3–3.5 b.y., and if past production rates of oceanic crust were comparable to present-day production rates. Uncertainties in these estimates are large enough that basaltic underplating [6] and accretion of mafic terranes may provide additional, significant contributions of Re to the continents.

The hypothesis that a significant proportion of Re in the continents may have been derived from dehydration or melting of oceanic basalt needs more corroborative evidence. The relatively high Re abundance estimated for the bulk upper continental crust requires that some juvenile continental rocks, such as modern calcalkaline rocks or Archean continental rocks (e.g., tonalite-trondhjemite-granodiorite suite), have sufficiently high Re abundances. Since no data are available on such rocks and Re abundance data on other upper crustal rocks are scarce, more work on evolved crustal rocks is necessary.

References: [1] Martin C. E. et al. (1991) *Austral. J. Earth Sci., 38,* 569–576. [2] Silver P. G. et al. (1988) *Annu. Rev. Earth Planet. Sci., 16,* 477–541. [3] Miller D. M. et al. (1994) *Nature, 368,* 514–520. [4] Schiano P. et al. (1997) *EPSL, 150,* 363–379. [5] Esser B. K. and Turekian K. K. (1993) *GCA, 57,* 3093–3104. [6] Saal A. E. et al. (1998) *Nature, 393,* 58–61.

SECULAR CARBON-ISOTOPIC VARIATIONS AND CHANGING ENVIRONMENT IN THE EARLY PALEOPROTEROZOIC.

A.

Bekker[1] and J. A. Karhu[2], [1]Department of Geological Sciences, VPI & SU, Blacksburg VA 24061, USA (abekker@vt.edu), [2]Geological Survey of Finland, FIN-02150 Espoo, Finland.

Analysis of sedimentary successions from several basins allows us to suggest the following temporal relationship between secular C-isotopic and environmental changes in the early Paleoproterozoic.

BIFs were deposited at ~2.45 Ga on the continental margins of the São Francisco, Kaapvaal, and Pilbara cratons. The carbonate units (Gandarela Formation, Brazil and Tongwane Formation, South Africa) overlying BIFs but preceding the ~2.4-Ga glacial epoch (GE) have C-isotopic ratios that are similar to those in sedimentary carbonates of the present-day oceans [1,2]. Uraniferous/pyritiferous conglomerates that were deposited at the base of ~2.45-Ga-old rift successions of Fennoscandia and North America indicate that O level in the atmosphere was still low.

The Duitschland Formation, Chuniespoort Group, South Africa provides evidence for negative to positive $\delta^{13}C_{carb}$ shifts between glacial events [2]. In North America the Huronian and Snowy Pass Supergroups contain shales and cap carbonates overlying diamictites. They have negative $\delta^{13}C_{carb}$, enriched $\delta^{13}C_{org}$, and decreased $\Delta\delta$ values. The observed relationship between biogeochemical C cycling and climatic changes during the Paleoproterozoic glacial epoch (GE) is similar to one in the Neoproterozoic [3]. Sedimentary units deposited at the end of the GE show the first indications of O level rise in the atmosphere. Evidence has been provided by REE concentrations [4], the increase in S-isotopic fractionation [5,6], and the appearance of Cu stratiform deposits [7] and red beds [8,9].

The GE was followed on the Fennoscandian and Canadian Shields by deposition of mature Al-rich quartzites with chemical and mineralogical signatures indicating warm arid climate and deep weathering. Several carbonate successions (Mooidraai Formation, South Africa [4], and Randville Formation, Michigan and Wisconsin, USA) stratigraphically above the last expression of the GE have $\delta^{13}C$ values varying between 0 and +4‰. These data suggest that after the GE the C-isotopic composition of the ocean was similar or slightly enriched in ^{13}C relative to the present-day ocean.

Carbonate successions with an age between 2.2 and 2.1 Ga are highly enriched in ^{13}C with average $\delta^{13}C$ values ranging from 7‰ to 12‰ [10]. This C isotope excursion is clearly postglacial and constrained to have started earlier than 2.22 Ga in Fennoscandian and Canadian shields. Sedimentary successions with an age between 2.2 and 2.1 Ga contain evidence for warm arid climate including pseudomorphs after sulfate and halite, B-enrichment, magnesite and red beds, and they are devoid of BIFs. The fractionation between inorganic and organic C in ^{13}C-enriched carbonates of this age is close to 30‰ [10].

Carbon-isotopic excursion ended between 2.11 and 2.06 Ga [10]. Carbon-isotopic values of carbonates deposited shortly after the end of the C-isotopic excursion range between 0 and +3‰ in the Lower Albanel Formation, QE [11] and Nash Fork Formation, WY. The end of the excursion coincides with deposition of Mn-carbonates, phosphorites, BIFs, organic-rich shales, the oldest fossils of possible eukaryotic origin, and decrease in stromatolite abundance. Postexcursion black shales from Fennoscandia and from the Francevillian basin, Gabon contain organic C with highly depleted $\delta^{13}C_{org}$ values (below −40‰). Environmental changes at the end of the C-isotopic excursion are compatible with an overturn of a stratified ocean with anoxic deep waters rich in Mn, P, Fe, and ^{12}C-enriched CO_2. This overturn could have been related to a change in paleogeography due to the opening of the Manikewan and Svecofennian oceans at ~2.1 Ga and the associated sea level rise.

Climatic changes and biogeochemical C cycling seem to have been coupled on a short-term scale during the Paleoproterozoic glacial epoch. The pattern is similar to that observed during the Neoproterozoic glacial epoch. It also appears that at the end of the C-isotopic excursion, at 2.1 Ga tectonics may have been a major factor controlling the biogeochemical cycling of C.

References: [1] Schidlowski M. et al. (1976) *N. Jb. Mineral. Mh., 8,* 344–353. [2] Bekker A. et al. (1998) *Eos Trans. AGU, 79,* F412–413. [3] Kaufman A. J. et al. (1997) *Proc. Natl. Sci. USA, 94,* 6600–6605. [4] Bau M. et al., *Mineral. Mag., 62A,* 127–128. [5] Cameron E. M. (1982) *Nature, 296,* 145–148. [6] Hattori K. et al. (1982) *Science, 221,* 549–551. [7] Kirkham R. V. (1989) *Geol. Ass. Can. Spec. Pap. 36,* 3–38. [8] Rainbird R. H. and Donaldson J. A. (1987) *Can. J. Earth Sci., 25,* 710–724. [9] Eriksson P. G. and Cheney E. S. (1992) *Precambrian Res., 54,* 257–269. [10] Karhu J. A. and Holland H. D. (1996) *Geology, 24,* 867–870. [11] Karhu J. A. (1993) *Geol. Surv. Finland Bull. 371.* [12] Mirota M. D. and Veizer J. (1994) *GCA, 58,* 1735–1745.

SOLUBILITY AND REACTION RATES OF ALUMINUM SOLID PHASES UNDER HYDROTHERMAL CONDITIONS.

P. Bénézeth, D. A. Palmer, and D. J. Wesolowski, Chemical and Analytical Sciences Division, Oak Ridge National Laboratory, P.O. Box 2008, Oak Ridge TN 37831-6110, USA.

Introduction: Experimental studies involving equilibrium solubility and dissolution/precipitation rates were initiated on boehmite (AlOOH) using a hydrogen-electrode concentration cell (HECC). This cell provides continuous, accurate *in situ* pH measurements of solid/solution mixtures to 295°C with provision for either removing solution samples for analysis of the metal content, or adding either of two titrants. This cell has been recently used to measure the solubility of minerals such as brucite, boehmite, zincite, and magnetite.

The ability to perturb pH_m isothermally by addition of acidic or basic titrant opens the door for studies of the kinetics of dissolution/precipitation, even for relatively fast reactions. By monitoring the change in pH_m with time, detailed kinetic information can be obtained without the need for sampling.

Results and Discussion: The solubility of pure synthetic boehmite (AlOOH) has been measured in NaCl brines over a wide range of pH_m (2–10), temperature (100°–290°C), and ionic strength (0.03–5 molal NaCl). As an example, Fig. 1 shows the results of multiple titrations obtained at 150°C (0.1 molal NaCl), performed both from acidic and basic solutions using the appropriate titrants. These results show that the solubility of boehmite is reproducible and also reversible, from both over and undersaturation. The solid curve in this figure represents the solubility calculated from a fit of the data using a general least-squares program.

Studies of the dissolution/precipitation rates of boehmite were initiated in neutral to basic solutions at 100°–290°C. The equilibrium solubilities obtained after each addition of acid (inverted triangles, Fig. 1) or base (triangles, Fig. 1) are in excellent agreement with the solubility curve obtained previously. These results show also that the rates of both the dissolution/precipitation reactions are extremely fast at high temperature.

For the dissolution steps at 100°C, the pH_m vs. time data indicated a smooth exponential approach to equilibrium. The rate of dissolution was converted from pH_m vs. time to total Al molality vs. time. This reaction obeys the simple rate law: $d[Al(OH)_4^-]/dt = k_{diss}C - k_{prec}C_{mH+}m_{Al(OH)_4^-}$, where C is the ratio of boehmite surface area to mass of solution, k_{diss} and k_{prec} are the zero-order and second-order rate constants for dissolution and precipitation. A plot of rate [d(Al)/dt] vs. $[H^+][Al(OH)_4^-]$ proved to be linear and the logarithm of the ratio of the dissolution/precipitation rate constants for both steps is within 0.1 log units of the corresponding equilibrium constant for the boehmite/aluminate reaction determined previously.

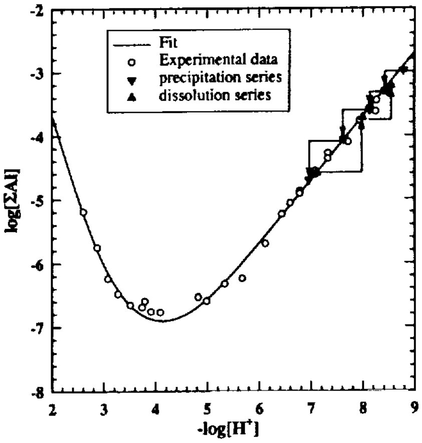

Fig. 1. Solubility and kinetics of precipitation/dissolution of boehmite at 150°C and 0.1 molal NaCl.

We are extending this work to include gibbsite, kaolinite and more complex aluminosilicate phases.

Acknowledgments: This research was sponsored by the Office of Basic Energy Sciences and the Office of Energy Efficiency and Renewable Energy, U.S. Department of Energy, under contract DE-AC05-96OR22464 with Oak Ridge National Laboratory, managed by Lockheed Martin Energy Research Corporation.

CRUST-MANTLE EVOLUTION IN THE EARLY ARCHEAN: A VIEW FROM A 3.8-Ga TERRANE OF SOUTHERN WEST GREENLAND.

V. C. Bennett[1], A. P. Nutman[1], C. R. L. Friend[2], and M. D. Norman[3], [1]Research School of Earth Sciences, Australian National University, Canberra ACT 0200, Australia (vickie.bennett@anu.edu.au), [2]Department of Geology, Oxford Brookes University, Headington, Oxford, UK, [3]Centre for Ore Deposit Research, University of Tasmania, Hobart TAS 7001, Australia.

Introduction: The rare remnants of early Archean crust provide our only direct record of the origins of the earliest continents, hydrosphere and biosphere. Key questions are the relative roles of modern style, subduction driven plate tectonics, as opposed to other forms of crustal crust genesis, e.g., underplating, delamination, melting of tectonically thickened basaltic crust, in the early Earth. Understanding early crust formation processes is required to constrain the development of mantle and crustal reservoirs and the role of volatiles in the early Earth, with attendant implications for early life environments. Here we report Nd-isotopic compositions, U-Pb zircon ages and major and trace element data from an exceptionally well-preserved area of early Archean crust in the Itsaq gneiss complex of southwest Greenland.

Within the early Archean terranes of southwest Greenland, two areas have been the primary target of numerous previous studies; these are the Isua supracrustal belt, and the coastal areas south of Nuuk comprising 3.55–>3.85 Ga gneisses and supracrustal assemblages. Our ongoing studies focus on a previously less-studied area of gneisses south of the Isua supracrustal belt (ISB). The gneisses in this region contrast significantly with those in the coastal area in having experienced lower metamorphic grade in the early Archean (amphibolite vs. granulite) and in containing several low strain areas where the granitoids are single phase, homogenous meta-igneous rocks, rather than the banded grey gneisses and migmatites typifying most early Archean terranes. Associated with the felsic rocks are large enclaves of layered gabbros, spinel peridotites, BIF, and amphibolites which are also locally exceedingly well preserved.

Results: Detailed cathodoluminescence and SHRIMP U-Pb zircon isotopic studies document ~3.81-Ga and ~3.78-Ga tonalite and quartzdiorite suites south of the ISB [1]. These rocks are characterized by simple zircon populations dominated by prismatic grains with micrometer-scale oscillatory zoning parallel to their crystal faces, arguing for a magmatic crystallization origin, and with no resorbtion and no inherited cores. In contrast, in the southern coastal region affected by granulite facies metamorphism, zircon populations range from complex to simple, depending whether the gneisses were derived from single igneous phases or migmatites. Initial Nd-isotopic compositions fall in a narrow range from $\varepsilon_{Nd} = 2\text{–}3$ requiring derivation from a depleted mantle source confirming previous studies [2]. Trace-element concentrations of the high Al, sodic tonalites were determined by laser ICP-MS analysis of fusion disks, avoiding potential dissolution problems. The older tonalite suite possess subparallel REE patterns, with LREE enrichments (La/Y - n = 11–34; avg. = 17), low total REE contents, small positive Eu anomalies and high Sr/Y implicating the role of garnet. The ~30-m.y. younger tonalites have lower Sr at a given silica, negative Eu anomalies, and higher contents of incompatible elements.

Discussion: Trace-element modeling demonstrates that these characteristics can be accounted for by large degrees (>30%) of partial melting of an eclogitic source. However many aspects of these melts cannot be achieved simply by closed system melting of an unmodified basaltic precursor. In particular the high Ba/Th, Ba/Nb, La/Nb, and low Nb/Th, Ce/Pb, Nb/Ta, and Rb/Cs ratios of these tonalites are analogous to those of modern arc magmas and suggest the presence of an aqueous phase. The geochemistry and inferred source mineralogy of these samples is similar to some modern arc suites, i.e., adakites, but not necessarily originating in the same tectonic setting. Significant differences compared with modern arc suites and with other Archean tonalites are the notably lower overall trace element contents at a given silica content, which can be modeled by derivation from a LREE depleted basaltic komatiite. Large spinel peridotite bodies within the tonalites yield unradiogenic measured Os-isotopic compositions from olivine and spinel separates requiring a ~3.8-Ga mantle extraction age [3]. The moderately fertile compositions are distinct from those of Archean cratonic xenoliths, e.g., Siberia and argue that these peridotites are likely relicts of early Archean oceanic mantle, yet they are found in the present continental lithosphere, further highlighting the diversity of processes evident by 3.8 Ga.

The implicated substantial role for fluids in early crustal genesis reinforces the significance of water in the formation of the oldest continental crust and complements the case made on the basis of the age of waterlain sediments within the Itsaq gneiss complex for a substantial hydrosphere at >3.85 Ga [4].

References: [1] Nutman et al., in press. [2] Bennett et al. (1993) *EPSL, 119,* 299–317. [3] Bennett et al., *GCA,* submitted. [4] Nutman et al. (1997) *GCA, 61,* 2475–2484.

MACKINAWITE STABILITY AT HIGH TEMPERATURES.

L. G. Benning[1,*], C. L. Cahill[2], S. M. Clark[3], H. L. Barnes[1], and J. B. Parise[2,4], [1]Department of Geosciences, Pennsylvania State University, University Park PA 16802, USA (*present address: School of Earth Sciences, University of Leeds, Leeds LS2 9JT, UK; l.benning@earth.leeds.ac.uk), [2]Department of Chemistry, State University of New York, Stony Brook NY 11794, USA, [3]Daresbury Laboratory, Warrington, UK, [4]Department of Geosciences, State University of New York, Stony Brook NY 11784, USA.

Introduction: Low-temperature Fe monosulfides (mackinawite, greigite) are essential precursors in sedimentary pyrite formation processes [e.g., 1–5], and thus are very important for the understanding of the global Fe, S, and C geochemical cycles. At higher temperatures it is generally accepted that troilite and pyrrhotite (with a multitude of structural types) are the stable Fe-S phases. However, the stability fields and the relationships between mackinawite, troilite and pyrrhotite structure types at temperatures below 200°C are not well defined. This study explores the upper temperature limit of freshly prepared mackinawite equilibrated with reduced, H_2S-rich solutions using synchrotron radiation. This method allows *in situ* real-time observation of reaction mechanism under anoxic conditions on a time- and temperature-dependent scale.

Methods: *In situ* energy dispersive X-ray diffraction (XRD) experiments were performed on beamline 16.4 at the Daresbury Laboratories, UK. The reaction cell used in these experiments was a modification of the design by Evans [6]. Due to the requirements for sample preparation (fastidiously anoxic conditions) quartz tubes sealed under vacuum were used instead of the Parr steel autoclave. This change in methodology warranted anaerobic conditions and reduced the problems with signal to noise ratio previously encountered when using steel reactors [7]. The samples were prepared in a glove box under

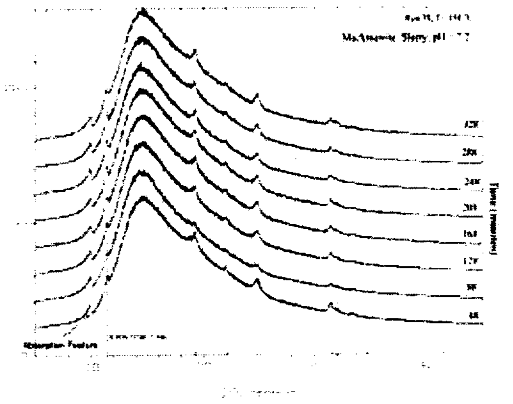

Fig. 1. Real time *in situ* XRD at 150°C. Y-axis is relative intensity.

a constant positive pressure of O_2-free N following the methodologies employed and described in detail in [5]. In short, samples were prepared in glass reactors in which a deoxygenated $Fe(NH_4)_2(SO_4)_2\ 6H_2O$ solution (prepared from O_2-free doubly distilled water) was saturated with H_2S gas. The pH of these solutions was adjusted to values between 4 and 7.5 with O_2-free NaOH solution. This adjustment promoted the immediate formation of a black Fe monosulfide precipitate. Samples of such slurries were loaded in the glove box into individual quartz tubes. The tubes were evacuated, removed from the glove box, frozen in liquid N, and sealed. After sealing, the tubes were dropped into a Cu heating block at preset temperatures (100°–250°C) and the collection of the *in situ* energy dispersive XRD spectra was started. X-ray diffraction scans were collected every 10–240 s (depending on temperature) and the results were converted to angular dispersive data at the constant stepsize of 0.01° and $\lambda = 1.0$ Å. The data were reduced for easy comparison with the JCPDS and ICSD databases. This experimental method supported an investigation of reaction mechanisms but not a thorough structural study.

Results and Discussion: The first X-ray scan in most experiments showed a poorly ordered mackinawite structure, that with time and increasing temperature transformed into a well ordered mackinawite. The figure below shows an experiment for up to 6.5 h at 150°C, which revealed that mackinawite is stable under these conditions without transforming into another monosulfide.

When the temperature was raised above 187°C mackinawite rapidly transformed to troilite. The assignment of the correct structure type was, however, not easily achieved, as the experimental conditions were not optimal to distinguish among the variety of possible high temperature FeS phases [see also 8].

Acknowledgments: We wish to thank the NSF [EAR 95-26762 (LGB, HLB) and DMR 97-13375 (JBP)] and the Mineralogical Society of America (CLC) for financial support for this study. In addition, we wish to thank the Material Research Laboratory at Daresbury for their help during the course of these experiments.

References: [1] Rickard D. T. (1969) *Stock. Contrib. Geol., 20,* 49–66. [2] Berner R. A. (1970) *Am. J. Sci., 268,* 1–23. [3] Schoonen M. A. A. and Barnes H. L. (1991) *GCA, 55,* 1495–1504. [4] Wilkin and Barnes (1996) *GCA, 60,* 4167–4179. [5] Benning L. G. et al. (1999a) *Chem. Geol.,* in press. [6] Evans J. S. O. et al. (1994) *Rev. Sci. Inst., 66,* 2442–2445. [7] Cahill C. L et al. (1999) *Chem. Geol.,* in press. [8] Cahill C. L. et al., this volume.

GROWTH MORPHOLOGIES ON PYRITE SURFACES.

L. G. Benning[1,*], A. L. Owsley[1,2], and H. L. Barnes[1], [1]Department of Geosciences, Pennsylvania State University, University Park PA 16802, USA (*present address: School of Earth Sciences, University of Leeds, Leeds LS2 9JT, UK; l.benning@earth.leeds.ac.uk), [2]Department of Geology and Geophysics, Yale University, New Haven CT 06520, USA.

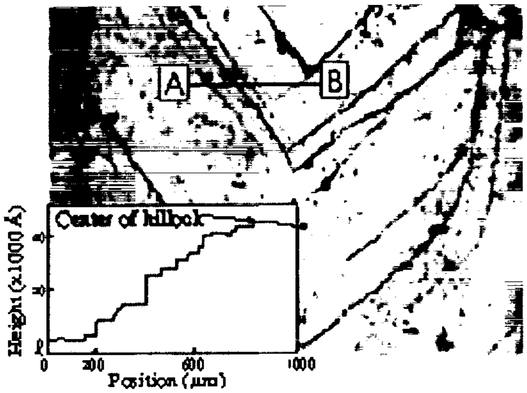

Fig. 1. Phase contrast microphotograph with the profilometer trace of one side of a growth hillock.

Fig. 2. Atomic force microscopy trace on the rise of a hillock on a {100} face.

Surfaces of natural pyrite crystals have been extensively studied and an intrinsic dependence of their structure on morphology and growth mechanisms has been demonstrated [1–4]. Apparently, the main factors controlling crystal morphology and growth are supersaturation, temperature, and, incorporated impurities. At conditions close to equilibrium, spiral growth dominates the growth rate, while at higher supersaturation, two-dimensional nucleation on preexisting surfaces controls the growth mechanism [1]. Technological advancements [e.g., development of special phase-contrast interferometry (PCI), scanning tunneling microscopy (STM), and atomic force microscopy (AFM)] have improved the resolution of surface structure measurements [3,5–7]. Although intensive studies on surface structures of natural pyrite have been carried out [e.g., 1–3], *in situ* growth experiments have been lacking. For various other minerals experimentally grown from solution, *in situ* growth rates (R), hillock slopes (p) and step advancing rates (v) have been measured as a function of known saturation state (σ) [e.g., 3–6] and, in general, a linear relation between R, p, v, and (σ) has been established. Evaluating these parameters on natural samples makes this function much less tractable because saturation states are unknown. However, surface topography permits the precise measurement of step height/width and slopes of spiral hillocks. Therefore, in this study, striation densities, step dimensions and hillock slopes for the {100} face of pyrite have been measured in an attempt to further explore pyrite growth mechanism.

Macroscopic smooth pyrite crystals from Navajun, Spain, were initially studied using scanning electron microscopy (SEM, Phillips, SX-20) and a thorough surface survey (including relative height and width measurements) revealed a dual distribution of the height and width of striations for cubic {100} faces.

To numerically assess hillock slopes, topographic and higher resolution techniques were required. Therefore, several samples, were evaluated on a 10–1000-μm scale with a surface profilometer (SP, Alpha-500, Tencor) (Fig. 1) and on a micrometer- to nanometer-scale with an atomic force microscope (AFM, DI-3100) (Fig. 2) [8].

The measurements of step height, width, and angle of profiles traces taken over hillocks were used to calculate the hillock slopes (p) [2,5]. Neighboring hillock growth-centers caused the growth of asymmetric pyramids with slopes differing by a factor of 2–7 on the two sides. On the other hand, elongated pyramids indicate highly anisotropic growth conditions, and the slopes vary by a factor of up to 10. An estimate of growth rates requires an independent estimate of the saturation state. Additional measurements are in progress, both to improve methods of characterizing the shapes of pyrite surfaces and to better understand the causes that produce these shapes [8].

Acknowledgments: We wish to thank NSF [EAR 95-26762] for financially supporting this study. The assistance from the Nanofabrication and Materials Characterization Laboratory at PSU is gratefully acknowledged.

References: [1] Sunagawa I. (1981) *Bull. Mineral., 104,* 81–87. [2] Endo Y. (1978) *Bull. Japan Geol. Surv., 25,* 1–64. [3] Sunagawa I. and Endo Y. (1970) *IMA Vol. 1970,* 63–84. [4] Sunagawa I. et al. (1995) *Prog. Cryst. Gr. and Char., 30,* 153–190. [5] Tsukamoto K. (1993) in *Morph. & Growth Unit of Cryst.* (I. Sunagava, ed.), pp. 451–478. [6] Tsukamoto K. (1989) *Farad. Discuss., 95.* [7] Pina C. M. et al. (1998) *Nature, 395,* 483–486. [8] Benning et al., in preparation. [9] Owsley A. L (1998) thesis, Pennsylvania State Univ.

SULFATE-REDUCING BACTERIA AND MACKINAWITE STABILITY.

L. G. Benning[1,2], R. T. Wilkin[1], and K. O. Konhauser[2], [1]Pennsylvania State University, Department of Geosciences, University Park PA 16802, USA, [2]School of Earth Sciences, University of Leeds, Leeds LS2 9JT, UK (benning@earth.leeds.ac.uk).

Introduction: The formation of sedimentary Fe monosulfides (mackinawite, greigite) and pyrite is strongly interlinked with bacterial sulfate reduction, and thus with the global geochemical Fe, S, and C cycles [1,2]. The inorganic formation and stability of FeS phases at T <100°C has been extensively studied due to their vital importance in the sedimentary pyrite formation processes [e.g., 1–6]. However, whether sulfate-reducing bacteria (SRB) are actively [7–8] or passively [3,9–11] involved in this process is equivocal. The main goal of this investigation was, therefore, to study the formation and long-term stability of FeS phases in the presence of ubiquitous SRBs.

Methods: A cultures of the SRB *Desulfovibrio desulfuricans* (ATCC # 29578) was grown in fastidiously anaerobic, minimal seawater-type medium supplemented with lactate. Culture tubes with fresh, sterile media were inoculated and equilibrated at 34°C. In the nutrient-deficient medium, growth was slower than predicted [9] and maximum growth was reached after 10–14 d [10]. The bacterial stock solution was used to inoculate fresh sterile media that subsequently was injected with 1 mL of Fe^{2+} or Fe^{3+} solution. This step promoted the immediate precipitation of a black Fe sulfide phase. At various time intervals bacterial growth rates, fluid and solid composition and bacterial and precipitate morphologies were monitored. Growth rates were determined by measuring the number of cells per milliliter of solution using a flow cytometer after treating with BacLight DNA dye. The solution composition was monitored for $pH_{25°C}$ (H_2S-tolerant glass electrode), $\Sigma Fe_{(aq)}$ [inductively-coupled plasma mass spectroscopy (ICPMS)], $\Sigma SO_{4(aq)}$ (ion chromatograph) and $\Sigma S_{(aq,\ reduced)}$ (S-coulometer). The solids were characterized using X-ray diffraction (XRD), scanning electron microscopy (SEM-EDS), and transmission electron microscopy (TEM). The ratio between iron monosulfides (acid-volatile sulfides, AVS; mackinawite and greigite) and pyrite (Cr reducible S) was determined via a sequential extraction method using an S-coulometer [see 6,10].

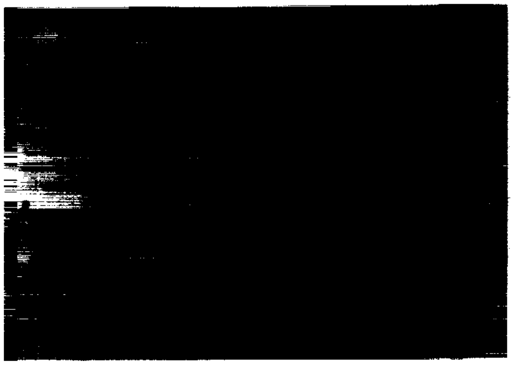

Fig. 1. The *D. desulfuricans* cells are Os-stained, with minor amounts of Fe (EDS). The stain arises from the use of 1% Os_2O_4, a postfixative agent used to cross link lipids in the membrane. Note that no sulfide phases are directly associated with the cells.

Results and Discussion: For all cultures (at maximum growth stage) a total cell count of 1–2 × 10^8/mL was determined. The consumption rate of SO_4 corresponds to the production rate of H_2S with a maximum H_2S concentration reached after approximately two weeks [10]. X-ray diffraction and SEM-EDS analysis of the solids revealed that even after six months the main solid reaction product is mackinawite. In some tubes greigite was present; however, it is assumed that the redox-state of these tubes was compromised (partial oxidation during sampling) because in several parallel experiments this was not observed. Pyrite did not form in any experiment even after six months of reaction time. These results were also corroborated by TEM analysis, which revealed both intact and lysed cells (Fig. 1).

The instantaneous precipitation of Fe monosulfides and the SEM/TEM analysis show that the formation of Fe monosulfides follows a purely inorganic pathway. Even six months of aging and reaction between the initial precipitate and the H_2S produced by the SRBs during sulfate reduction yields only mackinawite as sole stable phase. This fact is in accordance with most inorganic experimental studies [e.g., 1–6]. It is therefore concluded that in seawater-type media spiked with aqueous Fe species, the sole role of *D. desulfuricans* (in terms of Fe sulfide formation) is to produce bisulfide ions necessary for the precipitation of the monosulfide phases. They do not, however, catalyze monosulfide conversion, i.e., pyrite formation.

References: [1] Berner R. A. (1970) *Am. J. Sci., 268,* 1–23. [2] Goldhaber M. B. and Kaplan I. R. (1974) *The Sea, 5,* 569–655. [3] Rickard D. T. (1969) *Stock. Contrib. Geol., 20,* 49–66. [4] Schoonen M. A. A. and Barnes H. L. (1991) *GCA, 55,* 1495–1504. [5] Wilkin R. T. and Barnes H. L. (1996) *GCA, 60,* 4167–4179. [6] Benning L. G. et al. (1999) *Chem. Geol.,* in press. [7] Issatschenko B. L. (1929) *Int. Rev. Ges. Hydrobiol., 22,* 99–101. [8] Ravin D. and Southam G. (1997) *GSA Abstr. with Prog., 29,* A363. [9] Postgate J. R. (1984) Cambridge Univ. [10] Benning L. G. et al. (1999) *Proc. GES-5, Balkema,* in press. [11] Herbert R. B. et al. (1998) *Chem. Geol., 144,* 87–97.

THE DISSOLVED AND PARTICULATE LOADS OF RAINS CONSTRAINED BY LEAD, STRONTIUM ISOTOPES, AND MAJOR AND TRACE ELEMENTS.

D. Ben Othman[1], J. M. Luck[1], P. Telouk[2], and F. Albarède[2], [1]Unité Mixte de Recherche 5569, Hydrosciences (cc 057), Université Montpellier 2, 34095 Montpellier, France (d.benothman@dstu.univ-montp2.fr), [2]Géologie, Ecole Normale Supérieure de Lyon, 69364 Lyon, France.

Fluxes to the atmosphere of metals such as Cd, Pb, and Zn due to anthropogenic activities greatly exceed those linked to natural erosion, even in areas remote from cities or industry. Lead is a well-suited tracer of the origins of metals, thanks to its natural isotopic variations in rocks and mineralizations used by man.

Continental and marine rains from southern France were analyzed for their major-element, trace-element, and Pb-, Sr-isotopic compositions (both for dissolved and particulate loads). Detailed investigation was also carried out on three sequential rains, and on weak acid leaches ("leach") and HF/HNO_3 dissolution ("HF-residue") on the particulates according to the procedure of Hamelin et al. [1]. Low amounts of Pb recovered from those leaches were isotopically analyzed on the VG Plasma 54 at the ENS Lyon. Some data on local natural and anthropic end members are also presented [2], as are data on loesses (Fig. 1).

Among the possible sources of Pb — natural and anthropic — the road/gasoline appears to be the dominant one (Fig. 1). However, $^{207/204}Pb$ variations parallel to the industrial domain suggest the presence of at least two different sources toward the radiogenic values.

Detailed investigations on sequential rains indicate that (1) Mn, Cu, and somewhat Pb correlate with each other in the dissolved load, while Zn seems decoupled, and the interelement ratios are very similar in the various rains; (2) Zn, Cd, and Cu are well correlated during each rain event in the adsorbed part on the surface of particulates; (3) more than 85% of the Pb in the particulate is located in this leachable fraction; (4) this leachable Pb has systematically, although not drastically, lower isotopic values ($^{206/204}Pb$ = 17.70, close to road/gasoline values 17.5–17.6) than the corresponding Pb in the HF-residue (Fig. 2); (5) the Pb isotopes in the HF-residue are far from having rock or loess values; this would indicate that the "refractory" component is

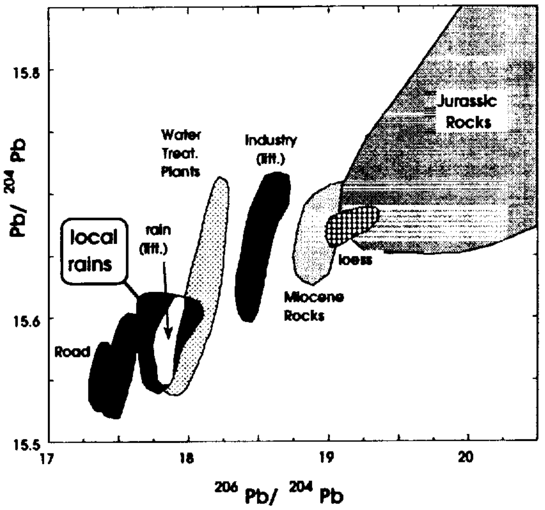

Fig. 1.

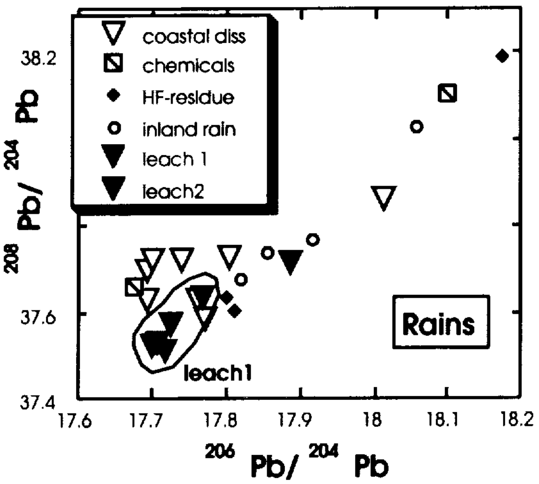

Fig. 2.

still strongly influenced by Pb from industrial emissions, contrary to the results obtained on Atlantic aerosols [1], whose residual Pb plotted in the sediment isotopic domain.

References: [1] Hamelin B. et al. (1989) *JGR, 94,* 16216–16243. [2] Luck J. M. and Ben Othman D. (1998) *Chem. Geol., 150,* 263–282.

PHYSICOCHEMICAL CHARACTERIZATION OF CARBONACEOUS PARTICLES: FACTORS FOR ASSESSING BIOLOGICAL ACTIVITY.

K. A. BéruBé[1], S. A. Murphy[1], T. P. Jones[1], F. D. Pooley[2], B. J. Williamson[3], and R. J. Richards[1], [1]School of Biosciences, P.O. Box 911, Cardiff University, Museum Avenue, Cardiff CF1 3US, UK, [2]School of Engineering, P.O. Box 917, Cardiff University, Museum Avenue, Cardiff CF1 3US, UK (berube@cardiff.ac.uk), [3]Department of Earth Sciences, Bristol University, Queen's Road, Bristol BS8 1JR, UK.

Introduction: Particulate matter with an aerodynamic diameter of ≤10 µm (PM10) is a widespread pollutant in urban air. Numerous epidemiological studies have found a relationship between particulate air pollution and increased cardiovascular and respiratory morbidity and mortality. Urban PM10 is a highly heterogeneous mixture that varies within and between cities, and with season, weather conditions and time of day. In the UK, it has been estimated that 20–80% of primary PM10 emissions can be attributed to diesel exhaust particles (DEP) [1], which in turn contributes between 80–95% of airborne particulate elemental C (PEC) [2]. The cause of adverse health effects with PM10 at low airborne mass concentrations (<30 µg/m^3 air) remains a mystery. The relative contribution(s) of particle mass, size, chemical composition, or combination of these factors, to these adverse effects is unknown. Current research has focused on the chemical composition and morphological properties of particles as a means to understanding their toxicity [3,4].

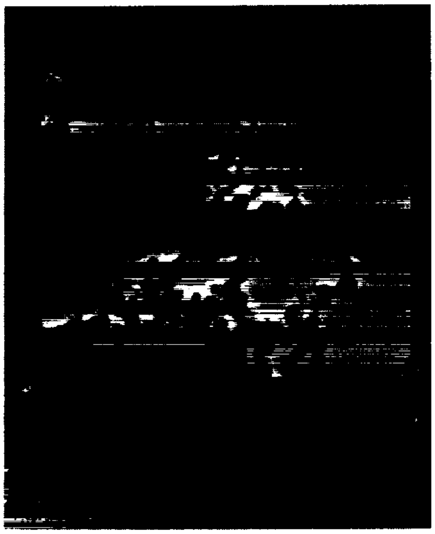

Fig. 1. Transmission electron micrograph of carbonaceous particles. Magnification 50,000×. Average particle size is 30 nm in diameter. Urban airborne sample collected via a PM10 selective-inlet head and prepared for TEM by impaction onto pioloform (0.8%) coated TEM (100 mesh) grids as described in [3].

Particle Characterization: The physical and chemical characteristics of particles must be understood when attempting to elucidate particle reactivity. Due to the highly heterogeneous nature of urban PM10, the study of their toxic effects requires the use of less complex carbonaceous "control" samples. Toxicologists have used manufactured carbon black (CB) particles to represent the refractory C of urban PM10 and DEP. A detailed physicochemical examination of commonly used CBs was undertaken. The techniques used included transmission electron microscopy (TEM), field emission scanning electron microscopy, image analysis, electron probe X-ray microanalysis, X-ray diffraction, and inductively coupled plasma mass and atomic emission spectrometry.

Conclusions: The aggregation properties of particles change from open-spaced aggregates with high reactive surface areas (RSA) to compact aggregates with reduced RSA, as a result of the wetting procedures used to prepare particles for biological assays. The different degrees of aggregation between low and high ordered CBs may affect their distributions within a biological system. The process of wetting promoted the dissolution of inorganic elements producing a wider spectrum of elements available for reaction. The presence of poorly ordered graphite within the CBs make them potentially more reactive and may increase their ability to accumulate metal ions and other toxic compounds. The overall implication of these findings is that each type of CB may produce different degrees of toxicity in biological systems. It is also probable that the changes seen from "dry" to "wet" laboratory samples of CB occur in humid and/or wet climates or upon deposition in the lung environment.

References: [1] Department of Environment (1995) *Particles,* HMSO, London. [2] Colebeck I. (1995) *Airborne Particulate Matter,* Springer, Berlin. [3] BéruBé K. A. et al. (1999) *Atmos. Environ, 33,* 1599–1614. [4] Murphy S. A. et al. (1998) *Life Sci., 62(19),* 1789–1799.

USING BROWN COAL AS AN ORGANIC FERTILIZER.

O. S. Bezuglova, Department of Soil Science, Rostov State University, B. Sadovaya Street, 105, Rostov-on-Don, 344006, Russia (besuglov@ic.ru).

Introduction: Degradation of arable soils leads to humus losses, changing of its composition, destruction of soil sructure, and decrease of their fertility. Reducing of traditional sources of organic matter makes the search for the new types of fertilizers an urgent issue. Brown coals (BC) have proved to be perspective in this relation.

Materials and Methods: The effect of BC and fertilizers based on its derivatives on ordinary calcareous chernozem and alluvial soil was investigated during field experiments with irrigation and dry farming. The BC-based fertilizers mentioned are ballast humates and BC-15 fertilizer, obtained through the original technology [1] using biologically active matters.

The BC of the Alexandria Coal-field (Ukraine), characterized by high content of humic acids served as a base. In both forms of fertilizers, humin makes the prevailing part: in BC it makes 87% of organic C, and in coal-humates its content is 2× lower. Humic acids extraction makes almost half of the whole organic matter. Percentage of the fulvic acids in coal-humates is increased 3.5–4× as much in comparison with BC, but is still very low. Coupled with natrium hydroxide BC changes correlation between the hydrolyzing and nonhydrolyzing parts: in coal it makes 0.15; in coal-humates the extent of organic matter hydrolization capacity is increased 7–8× as much. The pH of BC in water suspension makes 5.1 on an average. For coal-humates the alkaline environment with pH ~10 on average is characteristic. The BC and the coal-humates have ash content 40–45%.

In the irrigated crop rotation the fertilizers' doses were: BC (0.5–2 t ha^{-1}); NH$_4$-humate (0.25–1 t ha^{-1}); and Na-NH$_4$-humate (0.125–0.5 t ha^{-1}). Without irrigation the following doses were used: BC (1.0 t ha^{-1}); Na-humate 0.5–1.0 t ha^{-1}); and BC (15–1.0 t ha^{-1}).

Results and Discussion: Under irrigation, the BC fertile the cereals, maize, and soya crops — 15–30% increase in the year of applying in the fertilizer. Using humates made the crops 20–50% higher. Under conditions of dry-farming technology, the BC fertile the haricot bean crop capacity 590 kg ha^{-1} higher, Na-humate = 850 kg ha^{-1} higher, and BC-15 = 1020 kg ha^{-1} higher. This is caused by the fertilizers' influence on nutrient elements correlation in the environment and on their taking up by plant roots.

The humus matters system participation in the regulation of this process causes no doubt. The fertilizers under study provide humus state composition changing in the most important periods of plants' development, which testifies constant inflow of humus available forms. It causes the processes of humification and changing the content of soil organic matter (SOM) intensifying, especially when using the BC in the native form and BC-15. BC-15 in low doses manifests the qualities of biologically active combinations. It intensifies the hydrolysis of SOM and provides the stabilization of humus state. The BC exerts its maximum influence on the humus state of the soil in the third year after applying it in, and BC-15 in the second to third year after applying.

The BC-based fertilizers improve the nutritive regime of the soils at the expense of increasing microbial activity. The influence on these processes exerted by the fertilizers obtained through alkali treatment is time limited and, as for the aftereffect, they practically don't affect the dynamics of soil N. BC-15 exerts prolonged effect on the processes of ammonification-nitrification of the soil in favorable conditions of damping as well as in extremely droughty ones. The fertilizers also improve of soil P nutriment.

The BC and coal-humates have improved the soil structure conditions the case of irrigation as well as on the dry farming. The BC-15 provides for the best aggregating effect both in the extreme damping condition as well as in close to the optimum ones. The BC provides the soil aggregation under the favorable hydro-term regime in the year of applying, and in the droughty condition it does in the second to third year after applying. In extreme damping conditions the aggregating effect of the natrium coal-humates with doses of 0.5–0.25 t ha^{-1} is manifested, however in normal conditions it exerts practically no influence. Coal-humates in the double dose aggravates the structure condition, mainly at the expense of increasing the content of cloddy fractions.

Conclusion: Thus, the know-how fertilizer BC-15 exerts remarkable soft and even influence on biological activity of soils, the dynamics and content of SOM, as well as on the nutritive regime. By optimizing conditions, it fertile for the agricultural crop capacity increase.

References: [1] Bezuglova O. S. et al., The Coal-humic fertilizer. Invention patent No. 2111195. Invention priority June 19, 1996. Registered in the state register of inventions May 20, 1998.

HIGH-IRIDIUM CONCENTRATION IN ALKALINE ROCKS OF DECCAN AND IMPLICATIONS TO CRETACEOUS-TERTIARY BOUNDARY ENHANCEMENT.

N. Bhandari, P. N. Shukla, and A. D. Shukla, Physical Research Laboratory, Ahmedabad 380009, India.

The Deccan volcano sedimentary sequence at Anjar, Kutch contains nine basalt flows and several thick intertrappean sediment beds. The third intertrappean bed has been shown to contain three well-stratified layers having high-Ir and -Os concentrations, the highest values being 1302 pg/g and 1778 pg/g respectively. The ^{39}Ar-^{40}Ar ages of six basalts (F2 to F8) are close to 65 Ma. The three flows below the Ir-enriched intertrappean bed (IT III) show normal magnetic polarity whereas all except one of the upper basalts show reverse magnetic polarity. The data can be taken to indicate that the sequence covers the polarity zones 31N to 27R. The results thus support the view that Deccan volcanism occurred on a time span longer than a million years. The paleontological evidence in this sediment bed, being the uppermost horizon containing dinosaurian fossils, the geochronological and paleomagnetic data on the lava flows sandwiching this bed and the geochemical anomalies suggest that this intertrappean bed encompasses the Cretaceous-Tertiary (K/T) boundary.

Chemical analysis of the nine basalt flows indicates that all, except the uppermost flow F-9, are alkaline. In their major and trace-element composition (including the REE), the alkali basalts resember ocean island basalts (OIB). Similarities of many diagnostic trace-element ratios (e.g., Sm/Nd, Ba/Nb, Y/Nb, and Zr/Nb) with the Réunion Island basalts are consistent with their Réunion plume origin. The uppermost basalt is tholeiitic and chemically resembles the "uncontaminated" Ambenali type of Deccan Traps. Many of these alkaline flows show high concentrations of Ir, the highest value being 178 pg/g in flow 2.

The carbonatites, associated alkaline rocks and basalts of Amba Dongar alkaline complex in Chota Udaipur also have Ir concentration ranging up to 74 pg/g. Some of these values are more than an order of magnitude higher than theconcentration in tholeiitic basalts of Deccan, which typically have about 10 pg Ir/g. Many of these high-Ir rocks have formatino ages close to 65 Ma, similar to the K/T boundary event and may have contributed some Ir to the boundary clay layer.

Alkaline rocks of Deccan occur in Saurashtra, in the Cambay Basin and in the Narmada-Son Belt. However, they volumetrically constitute only a minor phase and therefore, in spite of their higher concentratino, their Ir contribution is too small to account for the anomalously high global inventory observed in the K/T boundary clays. Local enhancement of Ir in Deccan sediments can, however, arise if a significant part of the Ir can escape into the atmosphere, but it is not even sufficient to give rise to the Ir enhancement seen in the Anjar intertrappean sediments.

ACID DISSOLUTION RATES OF 2:1 PHYLLOSILICATE CLAY MINERALS MEASURED WITH *IN SITU* ATOMIC FORCE MICROSCOPY.

B. R. Bickmore[1], D. Bosbach[2], M. F. Hochella Jr.[1], and L. Charlet[3], [1]Department of Geological Sciences, 4044 Derring Hall, Virginia Polytechnic Institute and State University, Blacksburg VA 24061, USA (bbickmore@vt.edu; hochella@vt.edu), [2]Institut für Mineralogie, Universität Münster, Corrensstrasse 24, 48149 Münster, Germany (bosbach@nwz.uni-muenster.de), [3]Environmental Geochemistry Group, LGIT, B.P. 53, F-38041 Grenoble Cedex 9, France (laurent.charlet@obs.ujf-grenoble.fr).

Introduction: The chemical weathering of silicate minerals is of fundamental importance to the global cycling of elements, as well as the proton budget, in surface environments. The dissolution of 2:1 phyllosilicates is of particular importance because of their ubiquity, especially in soils.

At least two factors combine to make 2:1 phyllosilicate dissolution data difficult to interpret. First, the 2:1 crystal structure is strongly anisotropic, resulting in an uneven distribution of reactive sites over the surfaces of these minerals. During most of the dissolution process, by far the most reactive portion of the surface is at the edges, rather than the basal planes [1]. It is difficult to quantify the amount of edge surface area in a given sample, and without such data it is impossible to cast dissolution rates in a form that is comparable from sample to sample.

Second, many 2:1 phyllosilicates occur primarily as clays, i.e., platy particles <2 μm in diameter and 1 or more nanometers in height. Due to the charging characteristics of the surfaces of these minerals, they tend to flocculate, depending upon solution conditions. This creates the possibility that bulk dissolution experiments are diffusion-controlled, which would preclude the inference of mechanistic information regarding the surface reaction.

Recently, we have developed methods to immobilize clay minerals under aqueous solutions for analysis with atomic force microscopy (AFM) [2]. In our ongoing acid-dissolution experiments, we fix clay-size particles of 2:1 phyllosilicates on muscovite substrates coated with a monolayer of polyethyleneimine, a cationic polyelectrolyte. We are able to obtain three-dimensional images of single clay particles as they dissolve in acid solutions, and extract data regarding both dissolution rates and mechanisms. This approach sidesteps the problems mentioned above, because both total and edge surface areas (TSA and ESA) can be measured, and flocculation cannot occur.

Results: Acid-dissolution experiments are being carried out on hectorite, biotite, phlogopite, and montmorillonite clays. As expected, all the minerals studied appear to dissolve inward from the edge surface, with essentially no participation of the basal surfaces during the timescale of these experiments. So far we have obtained a rate for hectorite dissolution at pH 2 of 6.1×10^{-9} mol m^{-2} s^{-1} hectorite (normalized to ESA), or 1.6×10^{-10} mol m^{-2} s^{-1} hectorite (normalized to TSA) [3].

Discussion: The TSA-normalized rate is more than 4 orders of magnitude faster than that obtained by Zysset and Schindler [4] for montmorillonite (8.5×10^{-15} mol montmorillonite m^{-2} s^{-1}), whereas one would expect hectorite (a trioctahedral smectite) to dissolve at most 1–2 orders of magnitude faster than montmorillonite (a dioctahedral smectite) [5]. However, two other studies have published ESA-normalized rates for 2:1 phyllosilicates which can be directly compared to the ESA-normalized rate obtained for hectorite. Rufe and Hochella [6] used AFM to measure phlogopite etch pit growth at pH 2 and obtained a rate of 5.0×10^{-10} mol phlogopite m^{-2} s^{-1}. Turpault and Trotignon [1] measured the dissolution of macroscopic biotite flakes using bulk solution analysis, and a recalculation of their data yields an ESA-normalized rate of 3.0×10^{-7} mol biotite m^{-2} s^{-1} at pH 1.08. Clearly the hectorite rate is realistic when compared with reactive surface area normalized rates of similar minerals. We suspect that the montmorillonite dissolution rates published by Zysset and Schindler [4] reflect diffusion-controlled reaction due to flocculation.

Conclusion: *In situ* AFM provides a unique method to unambiguously determine surface reaction-controlled dissolution rates of 2:1 phyllosilicate clays. Not only are rate measurements made under conditions where diffusion is not the rate-limiting factor, but the reactive surface area can be directly measured at the same time. This allows for direct comparison of the dissolution rates of 2:1 phyllosilicates with different structures and formulas, as well as for certain mechanistic inferences.

References: [1] Turpault M.-P. and Trotignon L. (1994) *GCA, 58,* 2761–2775. [2] Bickmore B. R. et al. (1999) *Clays Clay Mineral.,* in press. [3] Bosbach D. et al., in preparation. [4] Zysset M. and Schindler P. W. (1996) *GCA, 60,* 921–931. [5] Kalinowski B. E. and Schweda P. (1996) *GCA, 60,* 367–385. [6] Rufe E. and Hochella M. F. (1999) *Science,* submitted.

ON A JURASSIC TRANSCONTINENTAL SEAWAY, THERMOHALINE CIRCULATION, AND OXYGEN-18.

C. J. Bjerrum[1], D. R. Gröcke[2], S. P. Hesselbo[2], H. C. Jenkyns[2], S. M. Olsen[1], G. Shaffer[1], and F. Surlyk[3], [1]Danish Center for Earth System Science, Niels Bohr Institute for Astronomy, Physics and Geophysics, University of Copenhagen, Juliane Maries Vej 30, DK-2100 Copenhagen, Denmark (cjb@dcess.ku.dk), [2]Department of Earth Sciences, University of Oxford, Parks Road, Oxford OX1 3PR, UK, [3]Geological Institute, University of Copenhagen, Denmark.

The marine geochemical and paleobiogeographic record from "greenhouse" transcontinental seaways can be used as a proxy for the paleo-state of global thermohaline circulation. Such a coupling is possible since the mean meridional flow within the seaways probably was governed by the density difference between adjacent oceans. Numerical ocean model results show that Jurassic meridional transcontinental seaways functions dynamically as a long straits. The possible feedback between the Jurassic thermohaline circulation and a transcontinental seaway is investigated with a conceptual nonlinear dynamic ocean-atmosphere box model where $\delta^{18}O$ is included as a tracer.

As in other ocean models several stable steady states of thermohaline circulation exist, where deep-water formation takes place in the northern or in the Tethys ocean box. Deep-water formation at northern high latitudes is associated with northward seaway currents, because the hydrostatic sea level is higher in the Tethys box than in the north. Deep-water formation in the Tethys box or at southern high latitudes conversely is associated with a southward seaway currents.

Model results on carbonate $\delta^{18}O$ in relation to the meridional thermohaline circulation and atmospheric moisture transport will be presented.

Preliminary model support is found in the literature on the Upper Jurassic rock record from the proto-North Atlantic seaway. Both northward and southward seaway currents can be inferred at different times in the Jurassic from a crude temporal covariation of ammonite faunal province boundaries and "secular" stable isotope.

QUANTITATIVE ANALYSIS OF EXPERIMENTAL MICROBE-MINERAL INTERACTIONS USING VERTICAL SCANNING WHITE LIGHT INTERFEROMETRY.

R. E. Blake[1] and A. Lüttge[2], [1]Department of Geology and Geophysics, Yale University, New Haven CT, USA (blake@hess.geology.yale.edu), [2]Department of Geology and Geophysics, Rice University, Houston TX, USA (aluttge@ruf.rice.edu).

Interest in the interactions between microorganisms and mineral surfaces has greatly intensified in recent years. Although many studies have appeared showing high-resolution images of bacteria and other microorganisms in association with mineral surfaces using optical, electron, confocal, atomic force and other microscopic techniques, few of these studies have reported direct quantitative measurements of reacted mineral surfaces, or of the kinetics of specific microbially-mediated processes. Reactions involving microorganisms at the relatively low-temperatures of most microbial habitats, also involve the action of microbial enzymes and, therefore, are almost certainly dominated by kinetic rather than thermodynamic and equilibrium effects. Thus, precise and accurate determination of the kinetics of microbially mediated reactions of mineral surfaces is crucial to the interpretation and modeling of the contribution of microbial metabolism to geochemical processes.

Where microbially mediated reactions of minerals have been quantified, for example, during some mineral dissolution and metal oxidation studies [e.g., 1–3], reaction rates have usually been based on analyses of bulk solution chemistry and normalization to the total surface area of reacting minerals as measured by gas adsorption (BET). As with abiotic dissolution kinetics experiments, the proper handling of surface area is problematic. A large degree of uncertainty is associated with measurements of bulk BET surface area, and the contribution of actual reactive surface area is not known. Determination of the actual reactive surface area and specific reactive sites on mineral surfaces becomes even more important for microbially-mediated processes where reaction is often localized in microenvironments between bacterial cell walls and mineral surfaces at the site of cell attachment, or may involve a combination of enzymatic and abiotic/inorganic mechanisms with variable effects on the mineral surface depending on solution chemistry, bacterial strain, and growth conditions (e.g., Fe^{2+} oxidation).

The new analytical technique of vertical scanning white light interferometry (VSWLI) [4], applied herein, complements existing surface analytical techniques by allowing quantitative analysis of surface dynamics during mineral dissolution and growth, and direct determination of reaction rates without the need for measurement of surface area. Reaction rates are determined from the retreat or advance of the actual mineral surface over time, and not from changes in bulk solution chemistry. Importantly, this allows accurate determination of mineral dissolution rates under conditions that result in very low concentrations of dissolved products, or where dissolved components are incorporated into bacterial biomass or trapped via complexation with organic polymers (e.g., glycocalyx). By introducting an internal reference onto the mineral surface, absolute rates may be determined in addition to measurements of the relative changes in surface features. In additon to quantification of mineral surface reactions, VSWLI offers several advantages that are especially critical to the study of microbe-mineral interactions, specifically, a large areal field of view (up to 730 × 580 μm) and a large vertical scan range (up to ~1 mm), with near atomic-scale vertical resolution (~2 nm) for surface features up to 100 μm high. These features complement other surface imaging and analytical techniques such as AFM, which offers higher resolution for detailed atomic-scale measurements, but a relatively small area of view.

We are using VSWLI in quantitative experimental investigations of reaction rates and interactions between bacterial cells and the surfaces of various minerals which may serve as important sources of nutrients, or in energy transfer (electron donors/acceptors), during heterotrophic and lithotrophic growth of microorganisms in nature including phosphate, Fe-oxide, and sulfide minerals. Results of initial culture experiments employing mineral phosphate as a sole P source for bacterial growth show highly localized and preferential colonization/reaction at only certain types of surface features such as fractures and microcracks by *Acinetobacter* ADP1. Microbes may be attracted to these features due to their higher surface energy. Specific coating and treatment of mineral surfaces allows resolution of single cells of *Acinetobacter* as well as associated etch pits using VSWLI, and the evolution of individual, microbially induced features such as pits may be followed over extended periods of time. Investigations of single cells and reaction rates of individual features are especially important in quantifying the spatially heterogeneous processes of microbial cell attachment and interaction with mineral surfaces. Results from additional microbial growth experiments will be presented and rates obtained from microbial and abiotic control systems will be compared.

References: [1] Ullman W. J. et al. (1996) *Chem. Geol., 132,* 11–17. [2] Edwards K. J. et al. (1998) *Am. Mineral., 83,* 1444–1453. [3] Nordstrom D. K. and Southam G. (1997) *Rev. Mineral., 35,* 361–390. [4] Lüttge A. et al. (1999) *Am. J. Sci.,* in press.

NEW CONSTRAINTS FROM HAFNIUM ISOTOPES ON THE SOURCE OF HAWAI'IAN BASALTS.

J. Blichert-Toft[1], F. A. Frey[2], and F. Albarède[1], [1]Ecole Normale Supérieure de Lyon, 69364 Lyon Cedex 7, France (jblicher@ens-lyon.fr; albarede@ens-lyon.fr), [2]Massachusetts Institute of Technology, Cambridge MA 02139, USA (fafrey@mit.edu).

Oxygen isotopes in Hawai'ian basalts [1] have recently contributed decisively to the issue of whether recycled lithospheric material is present in their mantle source or, as hinted by He isotopes, this hot spot erupts magmas from an essentially primitive mantle. Osmium isotopes [2] added the information that the low-$\delta^{18}O$ basalts are probably derived from the lower part of ancient oceanic crusts (gabbros), whereas the high-$\delta^{18}O$ basalts show the imprint of the upper part of the same crusts (pillow basalts and/or sediments). The following problems remain: (1) Can we identify a pelagic sediment component that would indicate that the lithospheric component is of oceanic origin (as opposed to continental)? (2) Can we exclude that the lithospheric components are not acquired upon ascent of Hawai'ian basalts through the modern Pacific lithosphere? (3) Can we obtain an indication of the age of the recycled material?

We report new Hf-isotopic compositions obtained by plasma source mass spectrometry (Plasma 54) [3] for basalts from a range of Hawai'ian volcanos for which a variety of other isotopic compositions are available from the literature. Whereas the mantle-crust array has a slope of 1.6 and a positive intercept of between 1 and 3 ε_{Hf} [4] the global Hawai'ian trend has a slope of about 1.0 and an intercept of 5 ε_{Hf} with a highly significant correlation coefficient R^2 of 0.92. When the Hawai'ian volcanos are inspected individually, Mauna Kea lavas contain the most radiogenic Hf and Nd, while Koolau lies at the other extreme. Individual correlations are found for Haleakala and Koolau with a slope (0.8 with an R^2 of 0.98) even shallower than that of the overall Hawai'ian trend. Hawai'ian basalts as a group, and Hawai'ian volcanos individually, therefore form arrays that point towards unradiogenic Nd and Hf compositions that plot distinctly above the mantle-crust array, and towards a component with a long-term relatively high Lu/Hf ratio, i.e., in the field of pelagic sediments [5] and deep-sea Fe-Mn nodules [6]. The volcano whose lavas contain most of this pelagic component is Koolau, for which high La/Nb and $^{187}Os/^{188}Os$ ratios and high $\delta^{18}O$ have been identified [1,2,7]. This signature was previously used to argue for oceanic crust as a source component.

A smooth hyperbolic array relates all the Hawai'ian basalts in an ε_{Hf} vs. $^{206}Pb/^{204}Pb$ plot. The curvature of this binary mixing array is strong enough that the asymptotes and the Pb/Hf ratio of the potential end members are nicely defined. The "sedimentary" end member (Koolau) has relatively unradiogenic Pb ($^{206}Pb/^{204}Pb = 17.8$) and can be tentatively assigned an age of 1 Ga. The second component (Kea) represents ancient lower oceanic crust. Its ε_{Hf} of +13 indicates that it cannot be modern Pacific crust. The Pb/Hf ratios that can be derived from the probable position of the end-members on the mixing array is consistent with the signature of the various components of an ancient oceanic crust.

Strontium isotopes add one more piece of information in that individual Hawai'ian volcanos define distinct trends in Hf-Sr-isotopic space that fan out towards the sedimentary end member with Koolau samples being amongst the most radiogenic in Sr. This fanning, which is also observed in Sr-Nd space, may reflect slight differences in the nature of the sediment involved, its depositional age, and the extent of Rb/Sr fractionation at subduction zones.

The contribution of Hf isotopes to the debate on the origin of Hawai'ian basalts is significant: (1) the presence of a pelagic sediment component requires that the recycled material was once oceanic lithosphere, (2) emplacement of plume material takes place without entrainment of modern asthenosphere or lithosphere [8], (3) the curvature of the Hf-Pb plot makes it possible to assign an age to the recycled component, and (4) there is no room so far in the isotopic space for a primitive component in the source of Hawai'ian basalts.

References: [1] Eiler J. M. et al. (1996) *EPSL, 144,* 453–468. [2] Lassiter J. C and Hauri E. H. (1998) *EPSL, 164,* 483–496. [3] Blichert-Toft J. et al. *Contrib. Mineral. Petrol., 127,* 248–260. [4] Vervoort J. D. et al. (1999) *EPSL, 168,* 79–99. [5] White W. M. et al. (1986) *EPSL, 79,* 46–54. [6] Albarède F. et al. (1998) *GRL, 25,* 3895–3898. [7] Roden M. F. et al. (1994) *GCA, 58,* 1431–1440. [8] Farnetani C. G. and Richards M. A. (1996) *EPSL, 136,* 251–267.

QUANTITATIVE DETERMINATION OF SMECTITE SURFACE AREAS BY THE SORPTION OF POLYVINYLPYRROLIDONE.

A. E. Blum[1], D. D. Eberl[1], and D. W. Rutherford[2], [1]U.S. Geological Survey, 3215 Marine Street, Boulder CO 80303, USA (aeblum@usgs.gov; ddeberl@usgs.gov), [2] U.S. Geological Survey, P.O. Box 25046, Denver Federal Center, Denver CO 80303, USA (dwruther@usgs.gov).

Introduction: Smectitic minerals may have a dramatic, sometimes dominate, effect on the physical and chemical properties of soils and sediments because of their high surface areas, high cation exchange capacities and swelling properties. However, the quantification of smectite minerals in sediments has remained problematic.

The Problem: Smectite particles are a single unit cell (1 nm) thick when dispersed in solution, and this is the surface area that controls the physical and chemical properties of smectites in saturated environments. However, completely dispersed smectite particles have no (001) X-ray diffraction (XRD) peak, since a single unit cell does not have any repeat distance [1]. The a-b plane can generate XRD peaks [particularly (060)], but these overlap with illites and micas, which are always ubiquitous in natural samples. Smectites when dried form XRD coherent aggregates that generate the commonly observed (001) diffraction peaks. However, both the efficiency of "stacking" and the orientation in the X-ray beam are highly variable in complex mixtures, making quantification of smectites by XRD very inaccurate.

During adsorption of inert gases in a dry environment, (i.e., N_2 BET) the gas does not access the "internal" surface, and therefore underestimates the smectite surface area. Smectites may also be quantified by measurement of the cation exchange capacity. However, the fixed charge of smectites can vary by almost a factor of two, leading to a similar error in extrapolating cation exchange capacity to quantify smectite abundance.

Recent work [2] has shown sorption of ethylene glycol monoethyl ether (EGME) is highly dependent on the exchangeable cation and layer charge

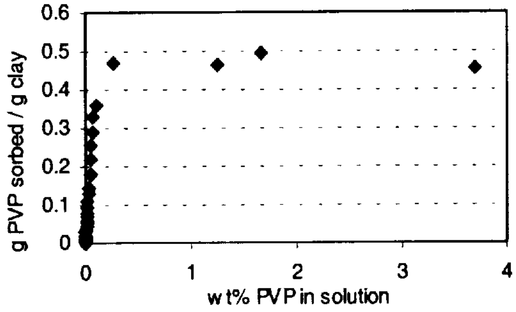

Fig. 1.

TABLE 1.

Sample	Surface Area (m^2/g)	g PVP Sorbed/g Clay	nm^2/molecule PVP
Belle Fouche smectite	755*	0.473	24.4
Cheto smectite	747*	0.593	20.9
Hectorite smectite	670*	0.510	21.8
Wyoming smectite	755*	0.530	23.7
RM30 illite	66†	0.058	19.0
Fumed SiO_2 (pH 9.2)	208‡	0.126	27.5
Fumed SiO_2 (pH 4.4)	208‡	0.125	27.7

* Calculated assuming 1-nm crystals, using muscovite molar volume and normalizing to formula weight from chemical analysis.

† Calculated from size distribution determined by XRD [3].

‡ N_2 BET.

as well as void sizes and organic C content, making EGME subject to greater uncertainty than simple cation exchange. Sorption of polyvinylpyrrolidone (PVP) avoids many of these problems.

Experimental Technique: A sample amount of 0.5 g is ultrasonically dispersed in 16 mL of water. Sodium- or Li-saturated clays are used to facilitate dispersion. Four milliliters of 10 wt% PVP (MW 10,000) are added and shaken overnight. The sample is centrifuged at 16,000 rpm for 2 h, a portion of the solution is decanted and weighed, dried at 105°C, and reweighed. PVP concentration in solution is determined by weight. Reproducibility is about ±2%.

Results: PVP sorption is constant at >0.3 wt% PVP in solution, and experiments target a final PVP concentration in solution of 0.5–1%.

PVP sorption appears to be independent of layer charge in smectites. Each PVP molecule covers ~21 nm^2. When PVP sorption on RM30 illite and fumed SiO_2 are normalized to surface area, they show a similar sorption density. The large sorption area, insensitivity to smectite layer charge, and the insensitivity of SiO_2 to pH (i.e., surface charge) suggests that PVP sorption is not localized at specific charged sites, but is more generalized, with significant stereochemical control and/or Van der Waals attractions.

References: [1] Eberl D. D. et al. (1998) *Clays Clay Mineral., 46,* 87–97. [2] Chiou C. T. and Rutherford D. W. (1997) *Clays Clay Mineral., 45,* 867–880. [3] Eberl D. D. et al. (1996) *USGS Open-File Rpt. 96-171,* 44 pp.

THE PALEOZOIC EVOLUTION OF THE WESTERN MARGIN OF GONDWANA RECONSTRUCTED USING NEODYMIUM AND LEAD ISOTOPES.

B. Bock[1], H. Bahlburg[2], G. Wörner[1], and U. Zimmermann[3], [1]Geochemisches Institut, Goldschmidtstrasse 1, 37077 Göttingen, Germany (bbock@ugcvax.dnet.gwdg.de), [2]Geol.-Pal. Institut, Corrensstrasse 24, 48149 Münster, Germany, [3]Geol.-Pal. Institut, Im Neuenheimer Feld 234, 69129 Heidelberg, Germany.

The Paleozoic development of the western margin of Gondwana is still not well understood. Some models call for subduction and accretion of exotic terranes during the Ordovician, even a continent-continent collision has been proposed, whereas other models propose an ensialic development of that margin during the Paleozoic. We investigated the presence or absence of terrane boundaries, of more juvenile additions and evidence for arc magmatism with Nd and Pb isotopes. We analyzed samples of the Late Proterozoic to Early Cambrian Puncoviscana Formation and the Upper Cambrian Meson Group to establish a record of the margin prior to Ordovician magmatic activity. The ε_{Nd} (450 Ma) values of the Puncoviscana Formation are uniform and range from –6.8 to –7.6 (n = 7). The samples of the Meson Group show a larger range in ε_{Nd} (450 Ma) from –5.4 to –9.7 (n = 4). This range can be explained by the lithology of the samples (quartzites) which have low REE abundances and are likely to be affected by mineral sorting processes. The calculated average crustal residence ages of both formations range from 1.7 to 1.6 Ga. The Cambrian St. Rosa de Tastil granitoid has an ε_{Nd} (450 Ma) of –5.4, only slightly less negative than the ε_{Nd} of the Puncoviscana Formation into which it intruded. Ordovician sedimentary rocks of the eastern part of the northern Puna have ε_{Nd} values indistinguishable from the underlying units with ε_{Nd} (450 Ma) of –6.1 to –8.9. A pillow basalt that intruded into these sedimentary rocks has a juvenile signature with ε_{Nd} of 3.6. Its geochemical compositions allows us to interpret it as an intraplate basalt, most likely emplaced during extension. Samples of the Silurian (?) Faja Eruptiva de la Puna Oriental have uniform ε_{Nd} values of –5.7 and are within analytical error identical to the value of the older St. Rosa de Tastil granitoid. Therefore, the volcaniclastic rocks deposited during the Arenig in the western part of the Puna (volcanosedimentary successions) are overlain by the Puna Turbidite complex. Some rocks of the volcanosedimentary successions show clear input of a juvenile component (ε_{Nd} 450 Ma = –1.3) whereas others lack this juvenile component (ε_{Nd} 450 Ma as low as –7.8). All samples of the Puna Turbidite complex lack the juvenile component (ε_{Nd} 450 Ma) of –7.0 ± 1) and appear to be derived from crust that is indistinguishable from the sources of the underlying units or those units themselves. Some Middle Ordovician samples of the eastern part of the Northern Puna carry ε_{Nd} (450 Ma) values of –9 indicating derivation from slightly older sources than the older sedimentary rocks. However, late Paleozoic rocks from N Chile carry slighlty more juvenile compositions with an average ε_{Nd} 450 Ma of –4.5. This is similar to the values we measured on Ordovician granitoids of the Complejo Igneo-Sedimentario del Cordon de Lila and also to the Faja Eruptiva de la Puna Oriental. Moreover, Rapela et al. [1] measured comparable ε_{Nd} values on rocks of the Sierra de Cordoba. Therefore, this shift towards slightly more juvenile Nd compositions relative to the tight range observed within the Puncoviscana Formation and the Puna Turbidite complex does not necessitate detritus derived from exotic sources, but may indicate a local shift of sources within western Gondwana. Our data show evidence for only minor crustal growth during the Ordovician. No addition of an exotic component is recognized as is expected if a terrane had been added to the Gondwana margin. Neodymium-isotopic compositions of the sedimentary rocks can be mostly explained by reworking older crustal material of Gondwana origin. These interpretations are consistent with the homogeneity of our Pb data. The samples show neither the relatively high $^{207}Pb/^{204}Pb$ ratios of the Arequipa Antofalla Terrane [2] nor the relatively unradiogenic compositions observed for the Argentine Precordillera [3].

References: [1] Rapela C. W. et al. (1998) *Geol. Soc. London Spec. Pub. 142,* 181–217. [2] Tosdal R. M. (1996) *Tectnophys., 15,* 827–842. [3] Mahlburg Kay S. et al. (1996) *J. Geol., 104,* 637–648.

EVOLUTION OF THE SOUTHEAST ASIAN CONTINENT FROM URANIUM-LEAD AND HAFNIUM ISOTOPES IN SINGLE GRAINS OF ZIRCON AND BADDELYITE FROM LARGE RIVERS.

F. Bodet and U. Schärer, Laboratoire de Géochronologie, Université Paris 7 and IPG-Paris, 2 place Jussieu, 75251 Paris Cedex 05, France (bodet@ipgp.jussieu.fr; scharer@ipgp.jussieu.fr).

To decipher the evolution of the southeast Asian continent, 202 single zircon and baddeleyite grains were studied by the U-Pb chronometer, and 128 of the precisely dated grains were analyzed for Hf isotopes. This is the first attempt to simultaneously measure the two isotopic systems in single grains from large rivers to resolve the age spectra of the crust and to elucidate source

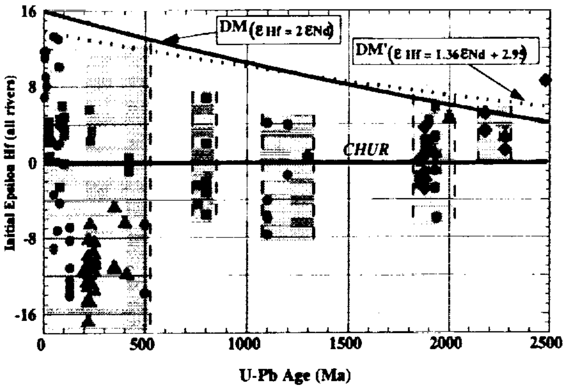

Fig. 1. Summary diagrams of $\varepsilon_{\mathrm{Hf_i}}$ vs. U-Pb ages for all zircon and baddeleyite grains. For comparison two alternative Hf-depletion curves (DM and DM') are given for the mantle, using the formalisms from [1] and [3].

characteristics of magmas involved in continental growth and recycling. Analyses of a maximum of zircons and baddeleyites (>70%) from five sand samples from the Mekong, Irrawaddy, and Red River permit identification of four different Proterozoic crustal growth events occurring at ~2.2 Ga, 1.9 Ga, 1.1 Ga (Grenville orogeny), and 0.8 Ga (Yangtze orogeny). Although a single 2.5-Ga-old baddeleyite grain was identified, Archean rocks seem to be totally absent in the ~1.3 × 10^6 km^2 large region sampled by the three rivers. Basement rocks of this region are entirely covered by Phanerozoic sediments. The U-Pb data also substantiate granitoid magmatism during the Pan-African, Caledonian, Indosinian, and Himalayan orogenies, all including to different degrees juvenile crust formation and crustal recycling, with the exception of essentially crustal derived Pan-African granites. For the Himalayan orogeny, mantle-melt input in the Irrawaddy region (Myanmar) was particularly important.

Hafnium analyses, adapted for single grain measurements, followed the methods established by [1] using modified values from [2] for planetary references. Initial $\varepsilon_{\mathrm{Hf_i}}$ signatures for zircon and baddeleyite range between +13.3 and −16.7, plotting in both the domains of LILE depleted and enriched reservoirs, relative to a chondritic evolution of the mantle (Fig. 1). Approximately half of the grains crystallized in magmas derived from significantly depleted mantle sources, and about 15% formed in magmas showing slightly depleted or enriched signatures ($\varepsilon_{\mathrm{Hf_i}}$: −1.37 to +1.59, 18 grains). The remaining zircons and baddeleyites yield strongly negative $\varepsilon\mathrm{Hf_i}$ documenting the incorporation of important amounts of crustal melts in magma genesis. The Paleoproterozoic events at 2.2 and 1.9 Ga seem to have produced the dominant mass of the southeast Asian continent, whereas the other orogenic cycles are characterized by substantial melting of continental material, formed during the two Paleoproterozoic events. This pattern is distinct for the three river systems demonstrating that the crustal segments sampled by the Red River, Mekong, and Irrawaddy have evolved in different continental settings, corroborating the successive accretion of variously evolved terranes to the South China block, most likely fragmented from Gondwanaland.

Analogously to the Nd notation [4] Hf model ages calculated for upper and average continental crust (Lu/Hf: 0.055 and 0.100 [5]) are up to 0.8 Ga, and 1.8 Ga older than the measured U-Pb crystallization ages. This discrepancy cannot be ascribed to uncertainties of model curves for time integrated LILE and Hf depletion of the upper mantle and therefore, the average Lu/Hf ratios of the southeast Asian continental crust must have been significantly different from those measured worldwide in fine-grained sediments. By allowing a period of 100 m.y. to produce zircon and baddeleyite-bearing intrusions during orogenic cycles, an average Lu/Hf-ratio of 0.014 ± 0.011 can be derived for the evolution of the bulk crust, leading to better agreement between U-Pb and Hf model ages.

References: [1] Patchett et al. (1981) *Contrib. Mineral. Petrol., 78,* 279–297. [2] Blichert-Toft J. and Albarède F. (1997) *EPSL, 148,* 243–258. [3] Vervoort et al. (1999) *EPSL, 168,* 79–99. [4] De Paolo D. J. and Wasserburg G. J. (1976) *GRL, 3,* 249–252. [5] Taylor S. R. and McLennan S. M. (1985) *Blackwell Scientific Publ.,* 312 pp.

MICROBIAL DEGRADATION OF ORGANIC MATTER IN SEDIMENTS OF THE ARABIAN DEEP SEA.

A. Boetius[1], M. Nitsche[1], T. Ferdelman[2], K. Lochte[1], and O. Pfannkuche[3], [1]Baltic Sea Research Institute, Seestrasse 15, 18119 Rostock-Warnemünde, Germany, [2]Max-Planck-Institute for Marine Microbiology, Celsiusstrasse 1, 28359 Bremen, Germany, [3]GEOMAR, Wischhofstrasse 1-3, 24148 Kiel, Germany.

In deep-sea sediments, bacterial degradation of OM plays the most important role in the turnover of elements and determines biogeochemical gradients in the sediment. Since bacteria can take up only small molecules through the cell membrane, they produce enzymes to hydrolyze the deposited OM extracellularly. The two main factors believed to protect OM from its enzymatical decomposition are (1) chemical resistance of organic substances, either due to their humification or due to the lack of O necessary for their complete degradation; and (2) physical resistance due to the sorption of organic substances to the mineral surfaces. Here we present new data on the distribution and microbial degradation of organic compounds in deep-sea sediments, which indicate that the preservation of OM could also be caused by the suppression or absence of certain benthic organisms.

In an investigation of microbial diagenesis of OM in sediments of the Arabian deep sea, we sampled an area in the open northwestern Arabian Sea (WAST, 16°13'N, 60°16'E, 4050 m water depth) which is characterized by high productivity in the surface waters and high POC flux to the seafloor. The bottom waters in this area are oxic. Compared to the stations in the central Arabian Sea (<0.5% TOC), sediments at station WAST are enriched in total organic C (>2% TOC). Several labile organic substances like pigments, proteins, lipids, and carbohydrates are present in high concentrations, comparable to what is usually found in much shallower marine sediments <500 m water depth. The vertical profiles of the concentrations of these organic substrates show their accumulaton in >5 cm sediment depth, where O and nitrate is depleted, but sulfate is abundant (Fig. 1). Microbial activity at

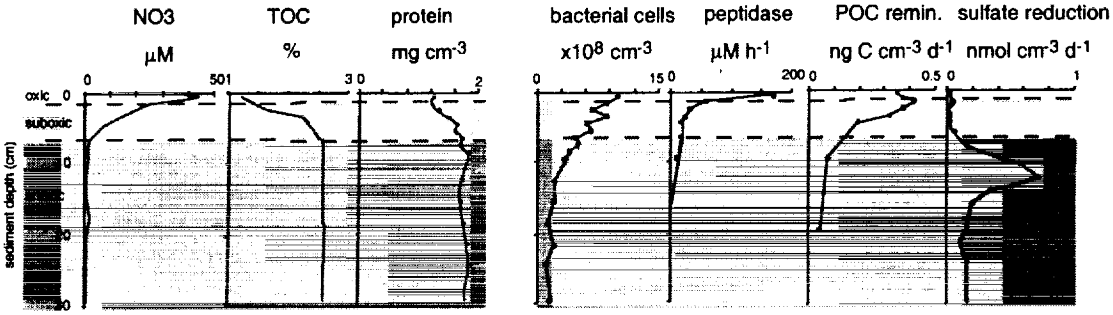

Fig. 1. Redox conditions, distribution of organic compounds, and microbial activity at WAST.

WAST is high in the upper 0–5 cm of the sediments. But most strikingly, microbial production and degradation of ^{14}C-labeled OM strongly decline in the zone of enriched OM concentrations >5 cm sediment depth. Sulfate reduction is very low in these sediments and limited to a narrow layer 2–5 cm below the nitrate penetration depth. This indicates that the decline in the activity of decomposers is limiting the supply of specific organic substrates required by the sulfate reducers.

A five-week-long degradation experiment revealed that the organic compounds that accumulate in the sediments of WAST cannot be degraded further by the autochtonous benthic bacteria, not even when the sediments were fully oxygenated. In contrast, the addition of fresh protein at similar concentrations as in the sediment led to a substantial increase in microbial activity and biomass within 1–2 weeks. A test of the enzymatic degradability of the sedimentary proteins in the 5–10 cm layer showed that up to 20% of the material is hydrolysable by proteases. However, the natural protease activity of the microbial assemblage in this layer was very low compared to other deep-sea stations (Fig. 1). To compare the decomposition potentials of bacteria and other benthic organisms, we measured the degradation of sedimentary proteins by deep-sea holothurians, which were able to reduce the sedimentary protein by 50% during its passage through the gut. Obviously these deposit feeders have very efficient ways of concentrating and digesting sedimentary proteins. However, in the area of WAST, the composition of the megafauna was completely different from other stations in the Arabian Sea. Ophiurids were abundant, but holothurians were nearly absent.

We do not know yet for which reasons this place in the western Arabian Sea differs so much from other regions of the abyssal plain. The paradoxon of high OM concentrations in the sediments and very low sulfate reduction rates has been observed in the larger area of the Oman margin. At WAST, the differences in the occurence and activity of benthic organisms could cause the incomplete degradation of organic matter in the sediments, because factors like depletion of electron acceptors, input of refractory terrigeneous material or burial due to high sedimentation rates can be ruled out. However, several turbidites were found in the sediments of WAST, including a young one of around 2K in the upper 0–30 cm. Also, station WAST is subject to extreme seasonal variation of POC input. It is possible that such considerable disturbances acting upon this environment on different timescales effect the distribution and activity of the benthic fauna and thus the preservation of OM in the sediments.

APPLICABILITY OF THE URANIUM-ISOTOPIC MODEL AS A PROSPECTING TECHNIQUE IN GUARANY AQUIFER, SOUTH AMERICA.

D. M. Bonotto, Departamento de Petrologia e Metalogenia, Instituto de Geociências e Ciências Exatas, Universidade Estadual Paulista, Av. 24-A, No. 1515, C.P. 178, 13506-900-Rio Claro-SP, Brazil (dbonotto@dpm.igce.unesp.br).

Introduction: Uranium-238 and its radiogenic daughter ^{234}U have been considered as very useful isotopes for the hydrogeochemical prospection of concealed U deposits, where the data for dissolved U content in groundwaters and $^{234}U/^{238}U$ activity ratio (AR) are plotted on a two-dimensional diagram containing several areas of associative significance [1–3]. In terms of dissolved U content, the main defined categories characterize: oxidized aquifer bathing strata with "normal" U mineral content (values between 1 and 10 ppb); oxidized aquifer bathing strata enhanced in U mineral content (values >10 ppb); reduced aquifer or strata with low U mineral content (values lower than 1 ppb). In terms of AR data, ground waters having values between 1 and 2 define "normal" world-wide situations, whereas it was also suggested the possibility of occurrence of processes related to the formation (values >2), or remobilization (values <1) of an accumulation of U. In this paper, the data on the isotopic concentrations of dissolved U in groundwater samples from Guarany aquifer, South America, were used to evaluate the applicability of the modeling in the area.

Sampling and Results: The Guarany aquifer of Triassic-Jurassic age extends over some 839,000 km² within the Paraná sedimentary basin [4], has an average thickness of 300–400 m, and is composed of silty and shaly sandstones of fluvial-lacustrine origin (the Pirambóia and Rosário do Sul Formations in Brazil and Buena Vista Formation in Uruguay), and variegated quartzitic sandstones accumulated by eolian processes under desertic conditions (the Botucatu Formation in Brazil, Misiones Formation in Paraguay, and Tacuarembó Formation in Uruguay and Argentina). The sampling of the Guarany aquifer was performed at 67 localities in São Paulo, Mato Grosso do Sul, Paraná, Santa Catarina and Rio Grande do Sul States in Brazil, where 77 groundwater samples (19–20 kg) were collected, stored in polyethylene bottles, and submitted to standard analytical procedures for determinations of the U content and AR [5]. Table 1 summarizes the range of the obtained values.

TABLE 1. Results of measurements realized for 77 groundwater samples from Guarany aquifer.

Parameter	Unit	Value	
		Minimum	Maximum
Uranium	ppb	0.004	15.36
$^{234}U/^{238}U$ AR	—	1.01	27.88

Discussion: The U content and AR values show great variability, where samples in all classification categories are present. A high dissolved U content value was found in one sample (15 ppb), which may be indicative of an previously unreported U accumulation though not necessarily of economic size and grade. Areas of stagnant alkaline waters where inflow is greatly restricted and residence time is long are common in the studied aquifer, but in spite of the alkaline character of the sample having high value of U content, it is not probable some relationship between the stagnancy of the water and its U content, because other samples having strong alkaline facies don't exhibit high U content. The pH and Eh data for the studied ground waters define oxidizing, reducing and intermediate conditions, with several samples being properly classified according to the U-isotopic data, whereas other don't adjust to any defined category, being plotted in fields not representing the actual redox conditions. Other factors responsible for the classification of the samples in different categories are: enhancement of ^{234}U in solution in accordance with an increase of the dissolution of Ca from the rock matrices; the occurrence of anthropogenic impacts affecting the oxidation-reduction conditions and modifying the presence of elements and compounds in solution, inclusive U; the effect of the temperature on the solubility of carbonates like calcite, since the precipitation of Ca^{2+} may occur at higher temperatures, affecting the values of the ARs. Therefore, the great complexity of the analyzed natural system suggests that several factors may be affecting the representation of the data on the U content vs. AR fence diagram, and that some caution be used on interpreting the high U content value measured for one sample.

Acknowledgments: The author thanks the International Atomic Energy Agency (IAEA Research Contract No. 9723/Regular Budget Fund) and CNPq (Conselho Nacional de Desenvolvimento Científico e Tecnológico)-Brasil for financial support of this investigation.

References: [1] Cowart J. B. and Osmond J. K. (1980) *U.S. DOE, Rpt. GJBX-119(80),* 112 pp. [2] Osmond J. K and Cowart J. B. (1981) *U.S. DOE, Rpt. GJBX-364(81),* 126 pp. [3] Chatam J. R. et al. (1981) *U.S. DOE, Rpt. GJBX-129(81),* 216 pp. [4] Araújo L. M. et al. (1995) *UFPR Rpt.*, 16 pp. [5] Osmond J. K. and Cowart J. B. (1976) *Atm. Energy Rev., 14,* 621–679.

THE IMPLICATIONS OF DISSOLVED URANIUM IN DEEP GROUNDWATERS FROM GUARANY AQUIFER, SOUTH AMERICA, FOR THE DISPOSAL OF RADIOACTIVE WASTES.

D. M. Bonotto, Departamento de Petrologia e Metalogenia, Instituto de Geociências e Ciências Exatas, UNESP, Av. 24-A, No. 1515, C.P. 178, 13506-900-Rio Claro-SP, Brazil (dbonotto@dpm.igce.unesp.br).

Introduction: Uranium isotopes are present at high-level wastes (HLW) from power reactors [1,2], and since the water is the carrier of any radionuclide release and equaly the last barrier before entry to the biosphere, it is important to evaluate the hydrogeochemical behavior of dissolved U in natural systems with the purpose of establishing analogies to the assessment of radioactive waste disposal sites. Deep burial of HLW in impermeable rocks at sedimentary basins is one option that has been considered, and, therefore, estimates of leach rates at such environments are useful for modeling purposes. In this paper, the data on the concentration of dissolved U in groundwater samples from Guarany aquifer of Triassic-Jurassic age, South America, were tentatively used for predicting the performance of a hypothetical repository.

Sampling and Results: The sampling of the Guarany aquifer was performed at 67 localities in São Paulo, Mato Grosso do Sul, Paraná, Santa Catarina and Rio Grande do Sul States in Brazil, where 77 groundwater samples (19–20 kg) were collected, stored in polyethylene bottles, and depending on the requirements of the analysis, they were unfiltered, filtered through a 0.45-µm membrane, unpreserved, or preserved with HCl. Standard analytical techniques were used for obtaining the composition of the major and minor elements in waters, for example, methyl orange end-point titration, potentiometry, flame photometry, ion selective electrode and inductively-coupled plasma emission, whereas α-spectrometry was utilized for determining the U isotopes [3]. The available data describing the wells allowed to estimate the geostatic pressure (GP) [4], which was used as an independent variable and defined several significant linear relationships relating the groundwater flow from the border of the basin toward its central part, in the direction of the dip of the geological units, i.e., temperature vs. GP (r = 0.93), dissolved O_2 vs. log GP (r = –0.65), pH vs. log GP (r = 0.75), Eh vs. log GP (r = –0.56), log Na^+ vs. log GP (r = 0.62), log $HCO_3^- + CO_3^{2-}$ vs. log GP (r = 0.62), log Cl^- vs. log GP (r = 0.61), log SO_4^{2-} vs. log GP (r = 0.55), log F^- vs. log GP (r = 0.72), log ionic strength vs. log GP (r = 0.64), log CO_2 partial presssure vs. log GP (r = –0.67), and log U vs. log GP (r = 0.33).

Discussion: An increase of temperature (up to 70°C) and basicity (up to pH = 9.9) were verified at the greater depths the aquifer reaches, conditions that are favorable to the U dissolution [1,2], with the highest value of dissolved U corresponding to 15 $\mu g L^{-1}$. An estimate of the outflow through the only visible outlet in this aquifer is 100–200 × 10^6 $m^3 a^{-1}$ [5], and, therefore, it is possible to consider 2250 kg as the annual mass of U transport. The Guarany aquifer underlies an area of about 839,000 km^2 in the Paraná Basin [6], and since its average thickness corresponds to 300–400 m [5], its volume can be estimated as 2.9 × 10^5 km^3. Because the typical U content and density of the rock matrixes of this aquifer are, respectively, 1.58 µg g^{-1} and 2 g cm^{-3}, it is possible to calculate 9.3 × 10^{11} kg as the total U source term in the Paraná basin. Thus, an estimate of 2.4 × 10^{-9} a^{-1} is obtained for the removal rate of U by groundwater solubilization, which is very reasonable when compared with values obtained for Th in the Poços de Caldas analog study [7]. Considering the waste inventory, the Nuclear Regulatory Commission [1] proposed that a rate of release of 10^{-7} a^{-1} will prevent any significant amounts of radiation from reaching the environment, although a rate of 10^{-5} a^{-1} also is suggested due to the existing technology for waste package and engineered backfill. Therefore, the results of this modeling represent the worst case, where waste is emplaced in a highly permeable host rock with no engineered barriers to restrict the mobilization of U, and, even under such conditions, it was possible to obtain an appropriate removal rate. Groundwater travel times of 10 k.y. to 1 m.y. and above are needed to allow for decay of most fission products and transuranics and if lower permeable formations assuring these conditions are guaranteed, then, sedimentary basins are important sites for the geological disposal of radioactive wastes.

Acknowledgments: The author thanks the International Atomic Energy Agency (IAEA Research Contract No. 9723/Regular Budget Fund) and CNPq (Cons. Nac. Des. Cient. Tec.)-Brazil for financial support of this investigation.

References: [1] Brookins D. G. (1984) *Geochemical Aspects of Radioactive Waste Disposal*, Springer-Verlag, 347 pp. [2] Roxburgh I. S. (1987) *Geology of High-level Nuclear Waste Disposal: An Introduction*, Chapman and Hall, 229 pp. [3] Osmond J. K. and Cowart J. B. (1976) *Atm. Energy Rev., 14,* 621–679. [4] Castany G. (1982) *Principles et méthodes de l'hydrogéologie,* Dunod, 238 pp. [5] Gilboa Y. et al. (1976) *J. Hydrol., 29,* 165–179. [6] Araújo L. M. et al. (1995) *UFPR Rpt.,* 16 pp. [7] Bonotto D. M. (1998) *J. S. Am. Earth Sci., 11,* 389–405.

ARSENIC SORPTION ON METAL SULFIDES.

B. C. Bostick[1] and S. E. Fendorf[1], [1]Department of Geological and Environmental Sciences, Stanford University, Stanford CA 94305-2115, USA.

Introduction: Arsenic is a redox-sensitive toxic element. Partitioning of As into the solid phase is desirable as it limits the bioavailability and transport of As to other areas. Arsenic sorption to many oxide minerals suggests that it partitions strongly with the solid phase [1,2]. However, As sorption to sulfide minerals, including pyrite and mackinawite, formed in anoxic environments is not well understood. Chemical extractions suggest that As and other elements associate strongly with iron sulfides [3,4], either as coprecipitates, sorbed species, or homogeneous precipitates. Unfortunately, a mechanistic understanding of the complexes is seldom achieved. The sorption of Ag^+ [5], Hg^{2+} [6], and Cd^{2+} [7,8] on pyrite indicate the formation of metal sulfide surface precipitates, suggesting that sorption of these cations on pyrite occurs by a different mechanism than is postulated for metal (hydr)oxides [9]. The sorption of anions including As has received very little attention. Here we investigate the nature of As surface complexes on iron sulfide minerals. A better understanding of these systems is necessary to determine how sorption to sulfide minerals affects their bioavailability and transport.

Methods: Solution studies were used to characterize the sorption envelopes for arsenite and arsenate sorption on synthetic mackinawite, pyrite, and galena. The surface complexes that formed through sorption were studied using X-ray absorption fine-structure spectroscopy (XAFS) and Raman spectroscopy. Electron microscopy provided information about changes in the morphology and analysis of bulk phases.

Results and Conclusions: All of the metal sulfide minerals studied exhibited similar sorption characteristics. Sorption was rapid and appreciable at near-neutral conditions and obeyed a BET isotherm, suggesting that the sorbed of As species includes the formation of surface precipitates. XAFS analyses indicate that the sorbed arsenite was coordinated to 3 S atoms at a distance of 2.41 Å. The presence of S in the coordination sphere means that As sorption on these metal sulfide minerals results in the formation of thioarsenic surface complexes. Under all surface coverages examined, the second coordination sphere contained Fe and As at a distance of approximately 3.95 Å, much longer than those of As(III) sulfide minerals. The presence of As in the second shell suggests that clusters are forming of the metal sulfide at all surface coverages studied. These surface clusters contain similar atomic distances to those of a thioarsenate trimer proposed by Helz et al. [10], and may help explain the characteristic isotherms for sorption. Combined, these data indicate that anion sorption to sulfide minerals may not be correctly modeled as simple ligand exchange reactions.

References: [1] Waychunas G. A. et al. (1993) *GCA, 57,* 2251–2269. [2] Manning B. et al. (1998) *Environ. Sci. Technol., 32,* 2383–2388. [3] Jacobs L. et al. (1985) *GCA, 49,* 1433–1444. [4] Morse J. W. et al. (1987) *Earth Sci. Rev., 24,* 1–42. [5] Scaini M. J. et al. (1995) *GCA, 59,* 2733–2747. [6] Hyland M. M. et al. (1990) *GCA, 54,* 117–130. [7] Bostick B. C. et al. (1998) *GCA,* submitted. [8] Parkman R. H. et al. (1999) *Am. Mineral., 84,* 407–419. [9] James R. O. and McNaughton M. G. (1977) *GCA, 41,* 1549–1555. [10] Helz G. R. et al. (1995) *GCA, 59,* 4591–4604.

SEASONAL DYNAMICS IN THE BIOGEOCHEMISTRY, STABLE ISOTOPIC GEOCHEMISTRY, AND MICROBIAL COMMUNITY STRUCTURE OF TEMPERATE INTERTIDAL SEDIMENTS.

M. E. Böttcher[1], B. Hespenheide[1], C. Beardsley[1], E. Llobet-Brossa[1], A. Schramm[1], A. Wieland[1], G. Böttcher[2], B. Schnetger[3], U.-G. Berninger[4], R. Rossello-Mora[1], R. Amann[1], and O. Larsen[1], [1]Max-Planck-Institut für Marine Microbiology, Celsiusstrasse 1, D-28359 Bremen, Germany (mboettch@mpi-bremen.de), [2]Geological Survey, Pampowerstrasse 66, D-19061 Schwerin, Germany, [3]Institute for Chemistry and Biology of the Marine Environment, University of Oldenburg, P.O. Box 2503, D-26111 Oldenburg, Germany, [4]Institut für Meereskunde, Duesternbrooker Weg 20, D-24105 Kiel, Germany.

An intergrated study, combining biogeochemical, stable isotopic, microsensor, sedimentological, phase-analytical, and molecular ecological methods, was carried out during a 1-yr period to investigate the seasonal dynamics of biogeochemical reactions (e.g., Mn, Fe, and sulfate reduction, sulfide reoxidation) in temperate intertidal sediments from the North Sea. A muddy sediment (site D; TOC about 3 wt%) was compared to a sandy sediment (site W; TOC about 0.1 wt%). Special attention has been paid to the influence of temperature as a process-controlling variable and the vertical abundance of bacteria, crustaceans, nematodes, heterotrophic flagelates, and ciliates.

Besides major, minor, and several trace elements (XRF), sediment cores were analyzed down to 20 cm depth for grain-size distribution (laser deflection), mineral composition (FTIR spectroscopy; X-ray diffraction), TOC (elemental analysis; LECO), and water content (gravimetry). Pore waters were analyzed for pH, ΣCO_2, NH_4^+, and salinity and the ICP-OES was used to measure major, minor ions, and selected trace elements (e.g., Mn^{2+}, Fe^{2+}). Leaching with Na-dithionite gave an estimate of the solid (reactive) Fe and Mn pools. The different sulfur pools (sulfate, hydrogen sulfide, AVS, pyrite, S^0, organic S) were quantified by different methods and isotopically ($^{34}S/^{32}S$) characterized (C-irmMS). Sulfate reduction rates were measured by the $^{35}SO_4^{2-}$ tracer technique. The O penetration depth was measured with microsensors. The type of organic matter available for microbial degradation was characterized by the C/N and C-isotopic ratios (C-irmMS). The downcore variation in the bacterial community structure was quantified using *in situ* hybridization techniques and specific oligonucleotide probes. Crustaceans, nematodes, heterotrophic flagelates, and ciliates were counted after DAPI staining.

The sediments at site D were characterized by bioturbating activities through the whole investigated depth with seasonal variations. Total organic C contents of the sediments ranged between 1 and 3.3% and were related to the abundance of clay minerals, indicating sorption process on mineral processes to be responsible for organic matter burial. The downcore variation of the C-isotopic composition of organic matter reflected the preferrential microbial degradation of labile (marine) organic matter compared to a more resistent (terrestrial) organic matter fraction. The sediments above 9 cmbsf contained an excess of TOC compared to the relationship between TOC and pyrite S proposed for normal marine sediments. In April, the O penetration depth reached down to 4.6 mm in the light and 1.2 mm in the dark. The corresponding abundance of hetrotrophic flagellates, ciliates, and crustaceans appeared to by partially controlled by the O penetration depth. Although suboxic conditions were indicated by the presence of dissolved Fe(II) and Mn(II) down to about 15 cm depth at site D, bacterial sulfate reduction rates up to more than 1000 nmol cm^{-3} d^{-1} were measured. A strong downcore decrease in all analyzed bacterial groups was found with a maximum activity at ~2 cm sediment depth. Up to 80% of the total cells detected by DAPI-staining hybridized with the rRNA targeted oligonucleotide probe EUB specific for the domain bacteria. Sulfate-reducing bacteria showed high abundance (up to 14% of total cells. Calculated cell-specific sulfate reduction rates are at the lower end of results observed in experiments with pure cultures. Depth integrated sulfate reduction rates showed a clear positive temperature dependence during the time of investigation. The microbial dissimilatory sulfate reduction led to a significant discrimination of ^{34}S and ^{32}S between the most stable reduced S fraction, pyrite, and dissolved porewater sulfate. Although, most observed isotope fractionation factors are within the range found in experiments with pure cultures of sulfate-reducing bacteria (ε between −4 and −46‰), the sometimes-enhanced isotope fractionation requires the consideration of a complex S cycle involving the reoxidation of H_2S, followed by the disproportionation of intermediate S species (e.g., S^0, $S_2O_3^{2-}$). Liberation of H_2S from the sediment into the water column or the atmosphere can be neglected in the time of investigation due to the well developed Fe and Mn reduction zones. The superimposition of a maximum of the sulfate reduction rate and dissolved Fe(II) and Mn(II) is likely due to Fe and Mn reduction coupled to the the oxidation of H_2S.

At site W, the bacterial activity was closely related to the availability of fresh marine organic matter leading to a disturbance of the typical steady-state biogeochemical zonation. Depth integrated sulfate reduction rates were found to be influenced by both temperaure and the availability of reactive organic matter.

LITHIUM-ISOTOPIC COMPOSITIONS OF MARIANA ARC LAVAS: IMPLICATIONS FOR CRUST-MANTLE RECYCLING.

C. Bouman and T. R. Elliott, Faculty of Earth Sciences, Vrije Universiteit, De Boelelaan 1085, 1081 HV Amsterdam, The Netherlands (bouc@geo.vu.nl; ellt@geo.vu.nl).

The process of subduction recycles material that carries a continental crust component (seawater and pelagic sediments) back into the mantle. Generally, two recycled components, subducted sediments and a "fluid" from the altered oceanic crust, are recognized. These components, together with contributions from the mantle wedge, shape the composition of arc lavas. For a number of elements, however, there is some difficulty in distinguishing the "fluid" from the mantle wedge; as for many chemical discriminants, the altered crust looks similar to mantle wedge material. Resolving this ambiguity is important in assessing element mass balance at convergent margins. Lithium-isotopic systematics of arc lavas have the potential to distinguish between contributions from the mantle wedge and altered oceanic crust. Lithium-7/lithium-6 ratios are only fractionated by low-temperature processes; variations in $^7Li/^6Li$ ratios thus imply the involvement of recycled material from the subducted slab, rather than mantle wedge.

Lithium-isotopic compositions of recent volcanics from the Mariana Islands have been determined to assess the potential of this tracer. Previous studies on the Marianas [e.g., 1] have indentified variable additions of a sediment melt with, for example, low $^{143}Nd/^{144}Nd$ and high Th/Nb, and a near-constant aqueous fluid flux, that produce large ^{238}U excesses in the sediment poor mantle wedge [1]. Samples from four different Mariana Islands (Guguan, Agrigan, Pagan, and Uracus) have been selected for this study, ranging from a sediment-rich (i.e., high Th/Nb) to a sediment-poor end member; the latter most clearly displaying the fluid signature (i.e., large ^{238}U excesses).

Lithium-isotopic ratios ($^7Li/^6Li$) have been analyzed by thermal ionization mass spectrometry using Li_3PO_4 loaded on double Re filaments. δ^7Li values of the Mariana arc lavas show variations between 4 and 8.5‰ relative to L-SVEC standard, with reproducibility of 1.5‰ (2σ). The Li-isotopic compositions of the most likely contributing components, fresh MORB (and by inference upper mantle), altered MORB and pelagic sediments range from +1.5 to +4.6‰ [3,4], +7.5 to +14‰ [3] and −2 to +8‰ [4] respectively.

Lithium concentrations in the Mariana lavas were determined using Isotope Dilution Mass Spectrometry and are between 5.63 to 7.81 ppm, compared to 3.6 to 6 ppm for fresh MORB [3,4], 8 to 75 ppm for altered MORB [3], and 30 to 100 ppm for pelagic sediments [4,5]. High Li concentrations result in high ratios of Li relative to elements with similar incompatibility, e.g., Yb. Mariana lavas have Li/Yb between 2.65 and 3.24.

Combined modeling of Li/Yb- and Li-isotopic compositions for upper mantle, pelagic sediment and aqueous fluid allows us to make a simple mass balance. This suggests an input of a sedimentary component resulting in relatively light Li-isotopic compositions and a large aqueous fluid flux (~30% × total Li in sediment-poor end member) producing relatively heavy isotope compositions in the process of Mariana arc magmatism. We find δ^7Li values as heavy as observed at the Izu volcanic front [4], which is also likely related to the input of altered oceanic crust. However, in the Marianas there is also a pelagic sedimentary component inferred from the low δ^7Li value of one volcanic island (Uracus). Additional Li-isotopic analyses on subducted sediment at the Mariana arc will help to refine the mass balance.

References: [1] Elliott T. R. et al. (1997) *JGR, 102,* 14991–15019. [2] Ryan J. G. et al. (1987) *GCA, 51,* 1727–1741. [3] Chan L. H. et al. (1992) *EPSL, 108,* 151–160. [4] Moriguti T. and Nakamura E. (1998) *EPSL, 163,* 167–174. [5] You C.-F. et al. (1995) *Geology, 23,* 37–40.

HIGH-PRECISION URANIUM-LEAD GEOCHRONOLOGICAL CONSTRAINTS ON EARLY ANIMAL EVOLUTION.

S. A. Bowring[1], M. W. Martin[1], and K. L. Davidek[1], [1]Department of Earth, Atmospheric and Planetary Sciences, Massachusetts Institute of Technology, 77 Massachusetts Avenue, Cambridge MA 02139, USA (sbowring@mit.edu).

The past five years have seen intensive efforts by paleontologists, evolutionary and developmental biologists, and geologists to better understand the first appearance and subsequent explosive diversification of animals. At the same time, the recognition and exploitation of thin air-fall ashbeds interlayered with fossil-bearing rocks has allowed the establishment of a high-precision temporal framework of animal evolution. Low laboratory blanks and ultrasmall sample analyses can lead to analytical uncertainties that translate to age uncertainties of <1 m.y. Although still in its infancy, this framework, when combined with integrated paleontological, chemostrati-graphic, and geological data will allow evaluation of models that invoke both intrinsic and extrinsic triggers for the Cambrian radiation.

New geochronological data from late Neoproterozoic rocks indicate Ediacaran fossils range from at least 572 Ma (Newfoundland) to 543 Ma (Namibia) and perhaps into the Cambrian. Complex trace fossils occur at least as far back as 555 Ma (White Sea). The number and complexity of trace fossils increases dramatically up to the Cambrian explosion that occurs over approximately a 10-m.y. interval (530–520 Ma). While the Neoproterozoic timescale has been extensively modified in the past six years, one of the remarkable but under appreciated conclusions is that the lower Cambrian is over 30 Ma in duration (543–510 Ma), while the middle and upper Cambrian (510–490 Ma) are only 10 m.y. in duration.

While we have made progress, there is much to do. Critical to understanding the role of extrinsic factors in animal evolution is high-precision calibration of the global chemostratigraphic (C and Sr) data. This will allow detailed evaluation of whether sudden isotopic excursions reflect globally synchronous events at the 100–300-ka level or are a reflection of local basinal changes. Outstanding questions remaining to be addressed include the following: (1) What is the duration and number of late Neoproterozoic glacial events and their relationship to diversity in the fossil record? (2) Is the negative $\delta^{13}C$ excursion at the Cambrian-Precambrian boundary globally synchronous and does it signal the extinction of Ediacaran and the creation of ecological niches for the ensuing Cambrian explosion? (3) Can the molecular clock approach for determining divergence times be tested using the temporally well calibrated upper Cambrian and Ordovician fossil record? (4) Can we use the fossil record to quantify rates of morphologic change?

Continued integration of high-precision geochronology with biological and paleontological studies will allow new insights into the history of early animal evolution. We believe that in 10 years or less this approach should allow discussion of the late Neoproterozoic-Cambrian record at the 100–300-ka level.

DIFFUSION OF ARGON FROM MELT INCLUSIONS IN QUARTZ PHENOCRYSTS.

J. W. Boyce, M. Grove, and M. R. Reid, Department of Earth and Space Sciences, University of California, Los Angeles, 3806 Geology Building, 595 Charles E. Young Drive East, Los Angeles CA 90095-1567, USA.

Glass inclusions in quartz phenocrysts from the ~760-ka Bishop Tuff that yield $^{40}Ar/^{39}Ar$ apparent ages >1 m.y. older than the eruption age have been used to support hypotheses for long-term storage of magma beneath the Long Valley area [1]. This interpretation depends upon the magnitude and relative importance of diffusion and solubility, as well as the internal distribution of melt inclusions, in determining Ar permeability through quartz at magmatic conditions. While appropriate Ar diffusion data for coarsely crystalline β-quartz are lacking, ionic porosity calculations indicate ~10^{-14} cm^2/s diffusivities at 720°C. This corresponds to a diffusive length scale of 5 mm for 1 Ma. Assuming no accumulation of Ar in the magma and that Ar solubility in quartz is not rate-limiting, this implies that quantitative Ar-loss from the melt inclusions would be achieved in <10^4 yr.

We have undertaken diffusion studies of glass inclusion-hosted, nucleogenic ^{39}Ar in quartz phenocrysts from the Bishop Tuff. The geometry, distribution, and total volume percent of glass inclusions contained within these phenocrysts has been characterized by serial sectioning followed by backscattered electron imaging. We find that in the materials we have selected for our experiments, glass inclusions represent ~1 vol% of phenocrysts and are generally situated <0.5 mm from grain boundaries. Preliminary short duration (30–100 min), low temperature (350°–1000°C) step-heating experiments we have performed with neutron-irradiated, 2-mm-diameter euhedral quartz phenocrysts resulted in liberation of only a very small fraction (~1%) of the total nucleogenic ^{39}Ar contained within the inclusions. While the negligible degree of Ar loss we observe is consistent with predictions based upon the ionic porosity model for a length scale of 500 μm, the results are somewhat surprising considering the large fraction of glass inclusions proximal to fractures within the host quartz. This may imply that the solubility of Ar in the viscous rhyolite melt is high enough to retain ^{39}Ar, even under *in vacuo* conditions. Similar behavior affects step-heating experiments involving sanidine. Available kinetic data for phase relations in the system SiO_2, indicate that under our experimental conditions, β-quartz is expected to persist metastably above 900°C with only minor amounts of highly disordered SiO_2 forming after weeks of heating at temperatures as high as 1200°C [2]. Longer-duration heating experiments in the 800°–1000°C range are planned to confirm the retentive character of the inclusions.

References: [1] van den Bogaard P. and Shirnick C. (1995) *Geology, 23,* 759–762. [2] Roberts A. L. (1959) in *Kinetics of High Temperature Processes* (Kingery, ed.), pp. 222–227.

LEAD ISOTOPES AS TRACERS FOR ENVIRONMENTAL POLLUTION AT A FORMER URANIUM MINING SITE IN EASTERN GERMANY.

G. Bracke[1] and M. Satir[2], [1]Centre de Géochimie de la Surface, CNRS-ULP-EOST, UMR 7517, 1 rue Blessig, F-67084 Strasbourg, France (bracke@illite.u-strasbg.fr), [2]Department of Mineralogy, Petrology and Geochemistry, University of Tübingen, Wilhelmstrasse 56, D-72074 Tübingen, Germany (satir@uni-tuebingen.de).

Introduction: Uranium mining in eastern Germany by WISMUT lead to severe devastation of the environment resulting in the one of world's largest tailing sites and waste rock piles [1]. Uranium mining was stopped with reunification of Germany in 1990. Remediation and rehabilitation of the mining sites has been conducted since then.

A study using Pb isotopes was carried out in order to elucidate the possible sources, pathways and sinks of environmental contamination. Several major sources (e.g., geological background, leaded gasoline, coal burning, dye manufactures, smelters, atmospheric deposition, and U mining) were taken into account. Pathways and sinks such as river sediments, soil, water, and atmospheric deposition were investigated for Pb content and isotopic composition.

Results: The Pb-isotopic compositions of possible sources define three distinct fields in a $^{206}Pb/^{207}Pb$ vs. $^{208}Pb/^{207}Pb$ plot (see Fig. 1). These fields were assigned to anthropogenic sources (field I), geologic background (field II), and U mining/mineralization (field III).

The Pb used for gasoline in former eastern Germany originated mainly from Russian deposits. Its Pb-isotopic composition was determined using unprocessed Pb and residues in old exhaust pipes and are also plotted in field I.

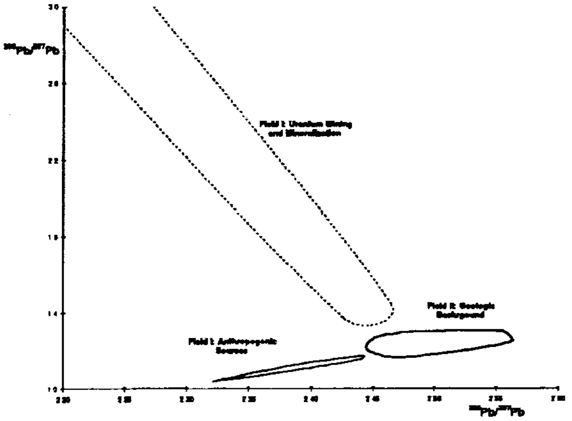

Fig. 1.

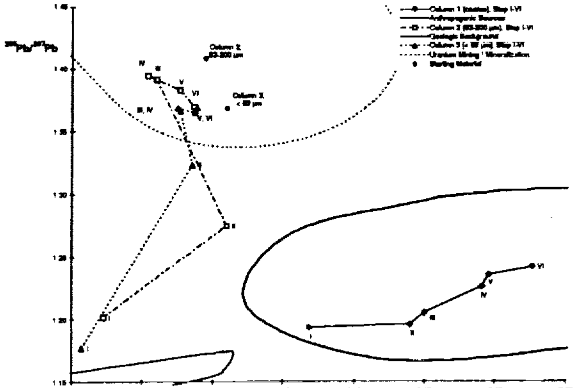

Fig. 2.

The main pollutants for Pb were anthropogenic. This is indicated by the Pb-isotopic composition of the river sediments, soils, and atmospheric deposition that plot in field I for most samples. Lead contamination caused by U mining/mineralization was detected in tailing pond sediments and mine waters only and had low Pb concentrations (less than 1 ppb Pb in water).

Sequential leaching experiments [2] were carried out on sediment from a tailing pond representing the residue of the ore processing. Radiogenic Pb having higher $^{206}Pb/^{207}Pb$ than the starting material was more soluble in the first step of the extraction procedure. It represented only a minor part of the total Pb content.

Column extraction experiments were carried out on different grain sizes of waste rock in addition. These showed that Pb having an isotope composition close to anthropogenic field is more soluble within the initial steps (see Fig. 2)

Conclusions: Uranium mining did not lead to significant environmental pollution by Pb. Only a small amount of radiogenic Pb was soluble.

Anthropogenic sources such as leaded gasoline and dye manufacturers are responsible for most contamination at the U mining sites. This type of Pb is more soluble as shown by column extraction experiments.

Despite the declining use of leaded gasoline in Europe leaded gasoline is still the main source for Pb pollution in atmospheric deposition.

References: [1] Bracke G. (1998) Tübinger Geowissenschaftliche Arbeiten 5/98, ISBN 3-8265-3777-7. [2] Zeien H. and Brümmer G. (1989) Mitteilungen der Deutschen Bodenkundlichen Gesellschaft 59/1, 505–510.

MIGRATION OF RARE EARTH ELEMENTS AT THE NATURAL FISSION REACTOR OF BANGOMBÉ SHOWN USING FISSIONGENIC ISOTOPIC RATIOS.

G. Bracke[1], F. Gauthier-Lafaye[1], and H. Hidaka[2], [1]Centre de Géochimie de la Surface, CNRS-ULP-EOST, UMR 7517, 1 rue Blessig, F-67084 Strasbourg, France (bracke@illite.u-strasbg.fr; gauthier@illite.u-strasbg.fr), [2]Hiroshima University, Kagamiyama 1-3-1, Higashi-Hiroshima 739, Japan (hidaka@ue.ipc.hiroshima-u.ac.jp).

Introduction: The natural nuclear fission reactors are located in the U deposits of Gabon. This very stable geological system has remained unfolded and unmetamorphosed for 2 b.y. Sixteen reactor zones have been discovered since 1972 but only the reactor zone in Bangombé is located ~11 m below the surface and is exposed to supergene weathering. This is in contrast to the other reactor zones that are located much deeper. The reactor core has a thickness of 10–20 cm. The Bangombé reactor provides an unique opportunity to study the behavior and migration pathways of fission products in rocks, clays, and minerals as a natural analog of a waste-disposal site, which has been affected by supergene weathering. A study using Pb- and REE-isotopes was carried out on this site to trace migration and weathering effects.

Results: Lead-lead and U-Pb dating gives ages of 1.97 Ga for the reactor zone. An iron-oxide crust just above the reactor zone has a similar age. This relates the formation of this zone to reactor operation and not to recent weathering .

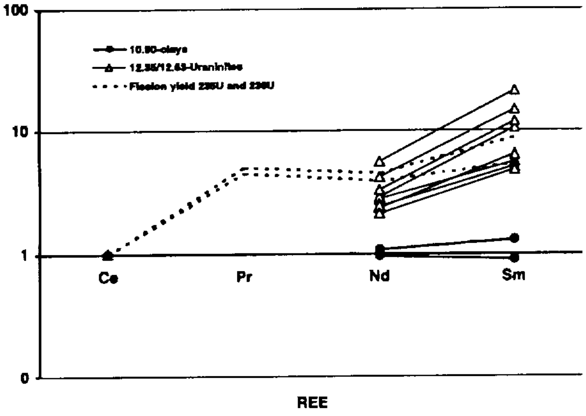

Fig. 1. Rare-earth-element patterns (SHRIMP).

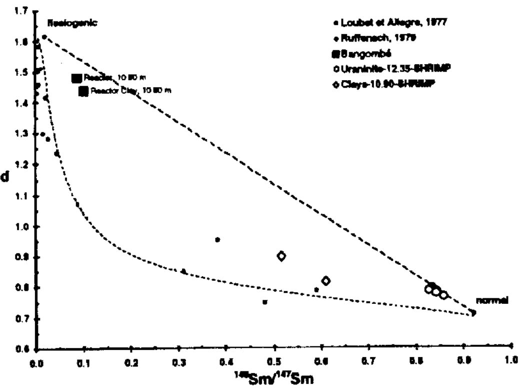

Fig. 2. Neodymium- and Sm-isotopic compositions of reactor zone 2, 10, and Bangombé.

Nevertheless, the effects of weathering have been found in clays of the altered zone by using rare earth elements (REE patterns). The clays are successively enriched in light REE and depleted in heavy REE with depth relative to source rock. Fissiongenic isotopes have not been found in the altered zone.

Below the reactor zone, an uraninite vein at 12.35 m was found inside a nodule of organic matter. Lead-lead and U-Pb dating revealed an age of 766 ± 85 Ma (SHRIMP). This indicates clearly a recrystallization of uraninite. Uranium-235 was not depleted in the uraninite. This uraninite vein was also investigated for Ce, Nd, and Sm and their isotope compositions. The Nd and Sm concentrations are enriched in the uraninite relative to Ce (Fig. 1). This is consistent with the higher fission yield of Nd and Sm. Surprisingly, Nd and Sm concentrations relative to Ce are not enriched in the clays at 10.90 m that are close to the reactor core.

The isotope compositions of Nd and Sm, obtained by SHRIMP, provide additional proof for fission products. Samples from the Bangombé reactor zone plot on a mixing line from fissiongenic to normal Nd and Sm using a $^{143}Nd/^{146}Nd$ vs. $^{149}Sm/^{147}Sm$ plot (Fig. 2). Sample data from reactor zones 2 and 10 and their surrounding rocks obtained by whole-rock analysis [1,2] define a curve due to the effects of neutron capture (^{149}Sm) and fission yield (^{143}Nd).

The difference between the reactor zone of Bangombé and reactor zones 2 and 10 is attributed to migration and retention of REE. Clays from the Bangombé reactor zone analyzed by SHRIMP plot close to the curve indicating fission. Clays analyzed as whole rock samples (<2 µm) plot close to the mixing line.

Discussion and Conclusions: The presence of fissiongenic Nd and Sm in the uraninite at 12.35 m can be explained by migration and subsequent retention in uraninite. This is supported by Pb-Pb dating of the uraninite, which reveals a recrystallization event at 766 ± 86 Ma and by the fact that ^{235}U is not depleted.

Clays from the reactor zone contain fissiongenic and normal Nd and Sm. Normal Nd and Sm may have been added by weathering although whole-rock analysis of the <2-µm fraction may include REE-bearing accessory minerals.

Clays analyzed by SHRIMP on a microscale contain Nd and Sm whose isotope compositions have been produced by a neutron flux *in situ*. This lead mainly to depletion of ^{149}Sm and to low fission yields.

References: [1] Loubet M. and Allegré C. J. (1977) *GCA, 41,* 1539–1548. [2] Ruffenach J. C. et al. (1976) *EPSL, 30,* 94–108.

PLATINUM-190/OSMIUM-186- AND RHENIUM-187/OSMIUM-187-ISOTOPIC SYSTEMATICS OF ABYSSAL PERIDOTITES.

A. D. Brandon[1], J. E. Snow[2], R. J. Walker[1], J. W. Morgan[1], and T. D. Mock[3], [1]Isotope Geochemistry Laboratory, Department of Geology, University of Maryland, College Park MD 20742, USA (brandon@geol.umd.edu), [2]Max-

Planck Institut für Chemie, Abteilung Geochemie, Postfach 3060, D-55020 Mainz, Germany, [3]Department of Terrestrial Magnetism, Carnegie Institution of Washington, 5241 Broad Branch Road NW, Washington DC 20015, USA.

Seven drilled-core abyssal peridotite samples from the Kane Transform area (KT), all from the same discrete block, have $^{187}Os/^{188}Os$ ranging from 0.122671 ± 8 to 0.127600 ± 2 and $^{186}Os/^{188}Os$ ranging from 0.119834 ± 4 to 0.119837 ± 2. The $^{186}Os/^{188}Os$ data are indistinguishable from one another, from previously reported ophiolite-derived Os-Ir alloys and chromitites, and from the Allende carbonaceous chondrite (0.119831 ± 6). This shows that the depleted, convecting upper mantle is relatively homogenous with respect to $^{186}Os/^{188}Os$ and that this ratio is generally independent of variation in $^{187}Os/^{188}Os$. To account for this, the Pt/Os of the bulk upper mantle must have remained within ±30% of chondritic most of Earth history. The lack of measurable, large-scale Pt/Os fractionation in the upper mantle is coupled with the fact that fertile continental lithosphere peridotites, unaltered MORB samples, and the most radiogenic abyssal peridotite samples converge to $^{187}Os/^{188}Os$ of about 0.126 to 0.130. These observations support previous arguments that the highly siderophile element budget of the upper mantle was controlled by the addition of a late veneer after core separation, consisting of materials with Pt/Os and Re/Os similar to enstatite or ordinary chondrites.

The Pt/Os ratio in the abyssal peridotite database from the literature varies by more than ±30% from chondritic. These variations may be the result of melt-rock reactions, which should be prevalent at mid-ocean ridges, or from partial melting. Melt-rock reaction will increase Pt/Os in the reacted peridotite because basaltic melts have high Pt/Os as a result of Pt being less compatible than Os during melting. Conversely, partial melting will decrease Pt/Os in the residue for the same reasons. A correlation exists between Pt/Os and $^{187}Os/^{188}Os$ in the KT abyssal peridotites (Fig. 1). Melt-rock reaction models following Rehkamper et al. [1] can successfully create this correlation by reacting material with the lowest Pt/Os and $^{187}Os/^{188}Os$ in Fig. 1, with a melt having $^{187}Os/^{188}Os$ of 0.14–0.16 and melt-rock ratios of 2–12. It is unlikely, however, that large volumes of melt with such radiogenic $^{187}Os/^{188}Os$ are prevalent at mid-ocean ridges. An alternative explanation is that the correlation in Fig. 1 can be accounted for by partial melting. We suggest the following model: At some time in the past, melting occurred in which Re and Pt were preferentially removed with the liquid relative to Os, leaving a residue with subchondritic Re/Os and Pt/Os. *In situ* decay of ^{187}Re to the present yields $^{187}Os/^{188}Os$ signature that is correlated with Pt/Os, as shown in Fig. 1. Viable partial melting models require that melting occurred ≥1 b.y. ago to match the correlation.

The ancient melting event recorded in the KT abyssal peridotites is much too old to have occurred recently at a mid-ocean ridge. Furthermore, a recent melting event at a ridge would have likely destroyed the systematics observed in Fig. 1 for the ancient melting event. Therefore, we suggest that this block of abyssal peridotite is unrelated to melting at a recent mid-ocean ridge and must instead be an isolated package of ancient variably melt depleted peridotite that has resisted convective mixing until recently stabilized as a portion of the oceanic lithosphere. If this is true for other abyssal peridotites, it indicates that some or all are unrelated to recent MORB genesis. This mechanism may be important for creating some sections of oceanic mantle lithosphere, as ancient melt depletion events are recorded by nonradiogenic $^{187}Os/^{188}Os$ in many abyssal peridotites.

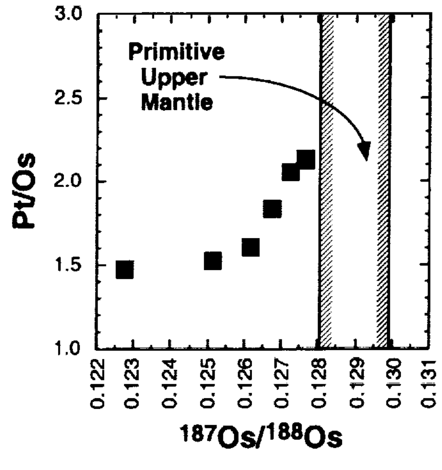

Fig. 1. Platinum/osmium vs. $^{187}Os/^{188}Os$ for the Kane Transform abyssal peridotites. The estimated range in $^{187}Os/^{188}Os$ for present-day primitive upper mantle is shown [2].

References: [1] Rehkamper et al. (1999) *EPSL*, submitted. [2] Meisel et al. (1996) *Nature, 383,* 517.

EFFECTS OF THE HYDROSPHERE ON THE EVOLUTION OF BASALTIC MAGMAS.

M. E. Brandriss[1] and D. K. Bird[2], [1]Department of Geology, Smith College, College Lane, Northampton MA 01063, USA (mbrandri@science.smith.edu), [2]Department of Geological and Environmental Sciences, Stanford University, Stanford CA 94305–2115, USA (bird@pangea.stanford.edu).

Overview: In layered gabbros of the Kap Edvard Holm Complex in East Greenland, gabbroic magmas were contaminated with water via the dehydration and partial assimilation of metabasaltic country rock xenoliths. This water was derived ultimately from the hydrosphere, which supplied meteoric water to the hydrothermal system that altered and hydrated the metabasalts under greenschist facies conditions. This alteration produced abundant hydrous secondary minerals such as chlorite, actinolite, and epidote. Contamination of the gabbroic magma by this hydrous oxidized material dramatically altered phase relationships in the crystallizing pluton, producing an abrupt transition from layered olivine gabbro to massive semiconformable layers of ultramafic rock and magnetite-rich oxide gabbro. The changes in mineral modes were not accompanied by significant changes in mineral compositions, implying that the main effect of contamination was simply to alter the relative stabilities of major cumulus phases [1]. The contamination of mafic magmas by dehydration of metabasaltic country rocks may thus alter liquid lines of descent, providing a mechanism by which hydrothermal solutions derived from seawater and/or meteoric water can fundamentally alter the evolution of basaltic magmas in the shallow crust.

Field Relations in the Study Area: The Kap Edvard Holm Complex consists mainly of layered olivine gabbros that intruded Precambrian gneisses and Tertiary greenschist-facies metabasalts during Eocene rifting prior to opening of the North Atlantic. Near the western part of the complex, the gabbros host large tabular xenoliths of metabasaltic country rock that were dehydrated and partially melted during stoping and heating [2]. As hydrous fluids and melts were expelled from the xenoliths, they percolated through and reacted with the host gabbroic cumulates, producing small, irregular, discordant replacive bodies of ultramafic rock and oxide gabbro clustered around xenolith margins. The ultramafic bodies represent zones in which plagioclase was resorbed by hydrous contaminated liquids that migrated through the partially solidified cumulates, the plagioclase having been destabilized relative to the mafic minerals as a result of the high concentrations of water. The oxide gabbros formed when these hydrous liquids crystallized within the cumulus pile.

Larger ultramafic and oxide gabbro bodies are present as semiconformable sheets within the layered gabbro sequence, with oxide gabbro lying directly above ultramafic rock. These sheets, up to several meters thick and extending for hundreds of meters along strike, are locally discordant to layering in the overlying gabbros and must therefore have grown within an existing cumulus pile. Contacts with the layered gabbros appear to be replacive rather than intrusive, suggesting that the bodies grew metasomatically as the hydrous liquids infiltrated and reacted with the cumulates. The large ultramafic and oxide gabbro sheets are mineralogically and texturally similar to the small discordant bodies near xenoliths and are themselves in a zone in which xenoliths are abundant. It is therefore concluded that the large sheets likewise formed as a result of hydrous contamination of "ordinary" gabbroic magma.

Mineral Compositions: A striking feature of the ultramafic and oxide gabbro bodies is that their constituent minerals are nearly identical in composition to those of the surrounding layered olivine gabbros. The Mg# of augite ranges from 0.74 to 0.78 and the Fo content of olivine ranges from 70 to 74, with no systematic differences among the various rock types. Plagioclase compositions are slightly more variable (mostly An_{54}–An_{68}), but the differences among rock types are small and the overlap in plagioclase compositions is extensive. The similarity of mineral compositions reflects derivation of all of the rock types from a single parental magma in which phase relations were shifted dramatically by the addition of small amounts of hydrous, oxidized contaminants. The resulting destabilization of plagioclase and stabilization of magnetite caused ultramafic and magnetite-rich rocks to form close together in the fractionation sequence. This is quite different from the behavior characteristic of tholeiitic magma systems, in which ultramafic cumulates are typically quite primitive (as observed commonly in ophiolites) and oxide-rich gabbros are substantially more evolved (e.g., Hole 735B on the Southwest Indian Ridge [3]). We therefore hypothesize that contamination of mafic magmas by hydrothermally altered basaltic crust can fundamentally alter liquid lines of descent, shifting them from tholeiitic trends of Fe enrichment toward calc-alkaline trends of Fe depletion and silica enrichment.

References: [1] Brandriss M. E. and Bird D. K. (1999) *J. Petrol., 40,* in press. [2] Brandriss M. E. et al. (1996) *Am. J. Sci., 296,* 333–393. [3] Dick H. J. B. et al. (1991) *Proc. ODP, 118,* 439–538.

BACTERIA-PROMOTED DISSOLUTION OF A COMMON SOIL SILICATE.

S. L. Brantley, L. J. Liermann, and B. E. Kalinowski, Department of Geosciences, Pennsylvania State University, University Park PA 16802, USA.

Introduction: Iron, Mn, Zn, Ni, Cu, Co, and Mo are each used in bacterial enzymes, coenzymes, and cofactors by common anaerobic and aerobic soil bacteria. While it is well known that bacteria excrete siderophores to extract Fe from their environment, it is not understood how these siderophores attack minerals to provide the Fe(III), nor is it understood how bacteria extract micronutrients other than Fe. In this work we investigated the dissolution of hornblende, a well-known "garbage mineral" that contains many of these micronutrients, in the presence of bacteria.

Bacterial Isolates: For all experiments, we isolated fresh bacteria from soil. In these isolations, we used inocula from a soil in the Adirondack mountains (New York, USA) containing hornblende. Two isolates were chosen because of their ability to live in Fe-poor medium in the presence of hornblende. Based upon partial sequencing of the 16s rRNA gene, we concluded the two isolates are of the genera *Streptomyces* and *Arthrobacter*.

Effect of Bacteria on Hornblende Dissolution: Two strategies for mobilizing Fe from hornblende are used by both species [1]: (1) the bacteria created acidic biofilms, and (2) excreted siderophores.

Bacteria were grown on the surface of hornblende in minimal medium for several days. Values of pH within microbial biofilms were measured with microelectrodes. Both hornblende crystal and synthesized hornblende glass were investigated. The values of the pH difference, $pH_{bulk\ medium} - pH_{mineral\text{-}water\ interface}$, were larger in unbuffered ($\Delta pH \leq 0.6$) than buffered medium ($\Delta pH \approx 0.04$). Growth of the *Arthrobacter* sp. also resulted in a larger pH difference between bulk and biofilm than the *Streptomyces* sp. by up to a factor of 10.

Under constant pH conditions, the streptomyces and arthrobacter increased the Fe release rate from hornblende over the first week up to 5–10× over abiotic controls respectively [1]. Two different catecholate siderophores produced by the isolates are presumed to cause this Fe release enhancement.

Effect of Deferoxamine Mesylate on Dissolution: Dissolution of hornblende was also analyzed in the presence of deferoxamine mesylate (DFAM), a hydroxamate siderophore derivative. Deferoxamine is also produced by streptomycetes. Addition of DFAM increased the dissolution rate according to the rate equation, $R = (8.8 \times 10^{-13})\ C^{0.5}$ where R is the release rate of Fe (mol m^{-2} s^{-1}) and C is the concentration (mol L^{-1}) of DFAM.

Surface Chemistry: X-ray photoelectron spectroscopy (XPS) of hornblende planchets after dissolution in the presence of *Arthrobacter* sp. revealed a substantial drop in the Fe/Si ratio of the hornblende surface after removal of the bacteria (ratio ≈0.1) as compared to samples treated in media without bacteria (ratio ≈0.2). We were not able to unequivocally interpret XPS of hornblende surfaces incubated with *Streptomyces* sp.

Summary: Bacteria isolated from an Adirondack soil were shown to extract Fe from the hornblende surface in minimal medium. These bacteria could (1) create acidic microenvironments in biofilms, (2) enhance Fe release over sterile control experiments, (3) produce catecholates, and (4) deplete the hornblende surface of Fe.

References: [1] Liermann L. J. et al. (1999) *GCA*, submitted.

EVOLUTION OF TEMPERATURE CONTROL ON ALKENONE BIOSYNTHESIS.

S. C. Brassell, Biogeochemical Laboratories, Department of Geological Sciences, Indiana University, Bloomington IN 47405-1403, USA (simon@indiana.edu).

Diagnostic Biomarkers: The ability to synthesize several molecular constituents of sedimentary organic matter is recognized to be confined to particular organisms [1]. Thus, the first appearances of such source-specific components can be expected to parallel the timing of the evolution of their presumed biological sources, their diversification, or their expansion to become significant contributors to preserved biomass [2,3]. For example, oleanane and 4,23,24-trimethyl-steranes occur as a prominent constituent of Cretaceous and Permian sediments respectively, consistent with the diversification of their putative source organisms, namely angiosperms [4] and dinoflagellates [5,6]. However, the connection between biomarker and biological source is not always established. The pronounced increase in 24-norcholestanes in the Cretaceous has been attributed to the evolution of diatoms [7], but this relationship has yet to be confirmed.

Origins and Utility of Alkenones: One of the most biologically restricted, but geologically significant, biomarkers are C_{37} to C_{39} di- and tri-unsaturated alkenones. These compounds are widespread in modern ocean sediments but occur in only a few living species of Haptophyta [8]. The proven value of alkenone unsaturation and C-isotopic composition as proxies for sea surface temperatures [9] and pCO_2 [10] prompts consideration of the timing of their first appearance and the development of their regulation of unsaturation as a response to temperature. The earliest occurrence of alkenones is in Albian sediments from the Blake-Bahama basin [11]. However, they differ from modern alkenone distributions in terms of their C number range (up to C_{41} and possibly C_{42}), carbonyl positions (odd-numbered alken-2-ones and even-numbered alken-3-ones), and presence as only di-unsaturated components [12].

Alkenones in Paleogene Sediments: Alkenones were found in suites of Eocene and Oligocene sediments with >0.2% organic C contents from six Atlantic sites (Fig. 1). The low concentrations of alkenones in some samples

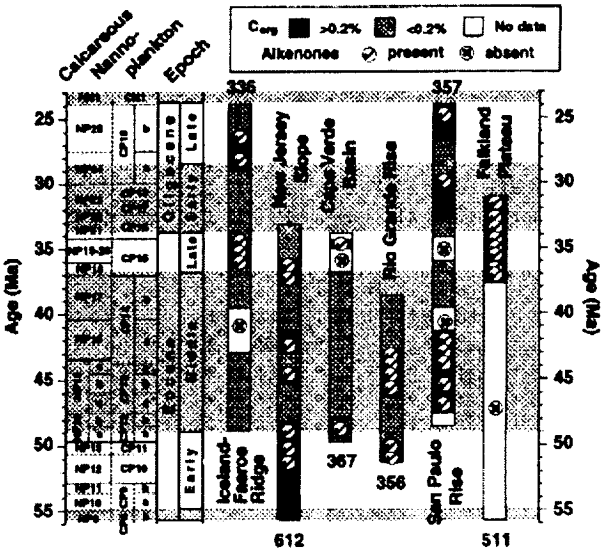

Fig. 1. Alkenones in Eocene and Oligocene sediments.

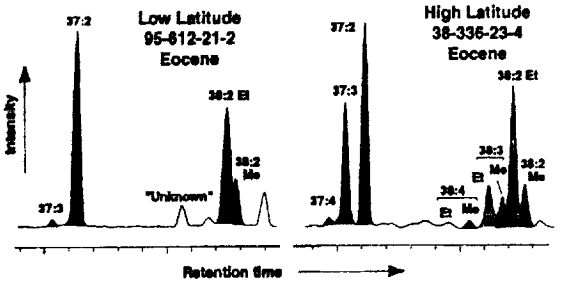

Fig. 2. GC traces of alkenones in Eocene sediments.

raises concerns about partial degradation and the primary character of their distributions [13]. However, the abundance of alkenones in other samples attests to the indigeneity of their distributions. Some distributions differ from those of modern counterparts containing no alkadienones, but both C_{38} and C_{39} alken-2-ones, complemented by other, as yet unidentified components structurally related to alkenones. Perhaps these distributions record variations in the biosynthetic pathways of alkenone-producing organisms during the Paleogene. By contrast, the alkenones in sediments from high latitudes closely resemble those characteristic of contemporary species and sediments (Fig. 2). Thus, the biosynthetic characteristics of alkenones in modern coccolithophorids appear to be inherited from alkenone-producing species adapted to colder waters during the Paleogene.

References: [1] Brassell S. C. et al. (1983) *Biochem. Soc. Trans., 11,* 575–586. [2] Summons R. E. and Walter M. R. (1990) *Am. J. Sci., 290A,* 212–244. [3] Brassell S. C. (1994) *ACS Symp. Ser. 562,* 2–30. [4] Moldowan J. M. et al. (1994) *Science, 265,* 768–771. [5] Summons et al. (1987) *GCA, 51,* 3075–3082. [6] Summons et al. (1992) *GCA, 56,* 2437–2444. [7] Holba A. G. et al. (1998) *Geology, 26,* 783–786. [8] Conte M. H. et al. (1994) in *The Haptophye Algae* (J. G. Green and B. S. C. Leadbetter, eds.), pp. 351–377, Oxford. [9] Brassell S. C. (1993) in *Organic Geochemistry* (M. H. Engel and S. Macko, eds.), pp. 699–738, Plenum. [10] Jasper J. P. and Hayes J. M. (1990) *Nature, 347,* 462–464. [11] Farrimond P. et al. (1986) *Org. Geochem., 10,* 897–903. [12] Marlowe I. T. et al. (1990) *Chem. Geol., 88,* 349–375. [13] Hoefs M. J. L. et al. (1998) *Paleoceanogr., 13,* 42–49.

CHEMICAL COMPOSITION OF SILURIAN SEAWATER: PRELIMINARY RESULTS FROM ENVIRONMENTAL SCANNING ELECTRON MICROSCOPY-ENERGY DISPERSIVE SPECTROSCOPY ANALYSES OF FLUID INCLUSIONS IN MARINE HALITES.

S. T. Brennan[1], T. K. Lowenstein[1], M. N. Timofeeff[1], and L. A. Hardie[2], [1]Department of Geological Sciences and Environmental Studies, State University of New York–Binghamton, Binghamton NY 13902, USA (lowenst@binghamton.edu; bf21297@binghamton.edu; bg20824@binghamton.edu), [2]Department of Earth and Planetary Sciences, Johns Hopkins University, Baltimore MD 21218, USA (hardie@gibbs.eps.jhu.edu).

Fluid inclusions in marine halites from the Upper Silurian Salina Group analyzed using the environmental scanning electron microscopy-energy dispersive X-ray spectrometry (ESEM-EDS) method show that Silurian seawater was different in major-element chemistry than modern seawater, enriched in Ca and K, and depleted in Mg and SO_4. The ESEM-EDS technique involves chemical analysis of individual primary fluid inclusions >30 µm in size. Thirty-three fluid inclusions from three borehole cores within the Michigan Basin (State USA 1-3, Wyandotte Chemical Corp., and MCGC Willow Cavern) analyzed via ESEM-EDS were compared with 18 earlier fluid inclusion analyses from the Salina Group [1].

In the Middle Silurian, the Michigan Basin was a normal marine setting with abundant reefs, including an extensive barrier reef system that rimmed the basin [2]. During the Upper Silurian, a relative drop in sea level cut off the Michigan Basin from the open ocean [2]. Seawater, likely impounded in this restricted basin by the barrier reefs, became concentrated and precipitated evaporites [3,4]. The Salina Group contains several hundred meters of halite, and tens of meters of sylvite (KCl) [4,5]. These thick evaporite units are part of large-scale marine carbonate-evaporite stratigraphic sequences, which suggests that the Salina halite is marine in origin [2–4]. The Salina halites contain primary sedimentary structures and textures (layered carbonate-anhydrite-halite cycles, ripple marks, and halite chevrons) diagnostic of precipitation from shallow waters [3,4].

Results from the ESEM-EDS analyses of fluid inclusions were obtained for Mg, K, and Ca; Na and Cl were computed for halite saturation using the Harvie-Moller-Weare (H-M-W) computer program [6]. SO_4 was always below detection. The first issue to address when interpreting the results is whether the surface water trapped inside inclusions is seawater. The geology of the Michigan Basin indicates that the evaporite parent waters were probably seawater. Furthermore, if the plots of the fluid inclusion chemistries from the four sample locations each fall along a single evaporation path, then the parent water in the four geographically separated locations had a uniform chemistry. Although the geology of the Michigan Basin suggests a marine seawater origin for the Salina salts, chemical analyses of fluid inclusions in halite from other deposits of the same age would greatly strengthen the case for a seawater parentage.

The results from our ESEM-EDS analyses and the data of [1] plotted on molality diagrams show a well-defined evaporation path for the major elements in fluid inclusions from the Salina halite. This consistent evaporation path confirms that the fluid inclusions analyzed are primary and formed from evaporating surface waters, likely seawater. Recently, Hardie [7] predicted changes in the chemical composition of Phanerozoic seawater controlled by relative changes in the amount of river influx and mid-ocean ridge hydrothermal water flux. Hardie's predicted Silurian seawater (enriched in Ca and K and depleted in Mg, Na, and SO_4 relative to modern seawater) was evaporated using the H-M-W computer program. Hardie's predicted Silurian seawater follows an evaporation pathway compatible with the major-element chemical composition of fluid inclusions in Silurian halite. We adjusted Hardie's predicted Silurian seawater composition (particularly K) to improve the correlation with the chemical compositions of the fluid inclusions.

The H-M-W computer program was used to calculate Silurian seawater chemistry, based on the observed evaporation pathway and assuming the m_{Cl} in the Silurian was equal to modern seawater. These calculations show that relative to modern seawater, Silurian seawater was enriched ~30% in K and depleted ~40% in Mg. Silurian Ca was much greater than modern seawater concentrations but exact values cannot be assigned without knowledge of the SO_4 concentrations in Silurian seawater. Gypsum precipitates before halite as seawater evaporates. As gypsum precipitates, Ca and SO_4 are removed in equal molar amounts until one of the species is consumed. Therefore, as all of the SO_4 was consumed, the initial concentration of SO_4 is unknown. Assuming an initial SO_4 concentration equal to modern seawater, Silurian seawater was enriched ~300% in Ca, relative to modern seawater. If Silurian SO_4 was half the modern concentration then, relative to modern seawater, Silurian seawater was enriched ~200% in Ca. These results support the hypothesis that seawater has undergone significant changes in major element composition in the past.

References: [1] Das N. et al. (1990) *GCA, 54,* 319–327. [2] Nurmi R. D. and Friedman G. M. (1977) *AAPG Stud. in Geol., 5,* 23–52. [3] Dellwig L. F. (1955) *JSP, 25,* 1–14. [4] Dellwig L. F. and Evans R. (1969) *AAPG Bull., 53,* 949–956. [5] Matthews R. D. and Egelson G. C. (1974) *4th Symp. on Salt,* 15–34. [6] Harvie C. E. et al. (1984) *GCA, 48,* 723–751. [7] Hardie L. A. (1996) *Geology, 24,* 279–283.

A POLYPHASIC APPROACH TO STUDY THE DIVERSITY AND VERTICAL DISTRIBUTION OF SULFUR-OXIDIZING *THIOMICROSPIRA* SPECIES IN COASTAL SEDIMENTS OF THE GERMAN WADDEN SEA.

T. Brinkhoff[1,2], C. M. Santegoeds[1], K. Sahm, J. Kuever[1], and G. Muyzer[3], [1]Max-Planck-Institut für Marine Microbiology, Celsiusstrasse 1, D-28359 Bremen, Germany, [2]Institute for the Chemistry and Biology of the Marine Environment, University of Oldenburg, P.O. Box 2503, D-26111 Oldenburg, Germany (thorsten.brinkhoff@icbm.uni-oldenburg.de), [3]Netherlands Institute for Sea Research, P.O. Box 59, NL-1790 AB Den Burg, Texel, The Netherlands.

Abstract: The use of ribosomal RNA as a molecular marker to detect and identify particular bacteria in their natural habitat [1] and to explore microbial diversity without the need of cultivation [e.g., 3] is now routinely used in microbial ecological studies. In some of these studies, the molecular approach was combined with microbiological methods in an attempt to iso-

late the relevant microorganisms [e.g., 5]. In other studies molecular biological techniques were used in combination with geochemical techniques, or with the application of microsensors [e.g., see 2], to characterize environmental parameters. However, the combination of molecular biological techniques, microbiological methods, and geochemical techniques or microsensors has only been used in a few studies [e.g., 7,8]. Yet this combination of techniques and concepts of different disciplines is necessary to obtain a better understanding of the interactions between microorganisms and their natural environment, which is the aim of microbial ecology. Here we describe the use of a comprehensive approach to study the functional role of different closely related *Thiomicrospira* strains in one habitat, the intertidal mud flat.

Thiomicrospira species are chemolithoautotrophic bacteria, that use reduced S compounds as energy source and CO_2 as C source; they are obligate aerobes [6]. Recently, four *Thiomicrospira* strains were isolated from a coastal mud flat of the German Wadden Sea [4]. To investigate the functional role of these closely related bacteria, we applied a polyphasic approach in which molecular biological and microbiological methods were combined with microsensor measurements. The microsensor measurements showed an O penetration in the sediment to a depth of about 2.0 mm. The pH decreased from 8.15 in the overlaying water to a minimum pH of 7.3 at a depth of 1.2 mm. Further down in the sediment, the pH increased to about 7.8 and remained constant. Most probable number (MPN) counts of chemolithoautotrophic S-oxidizing bacteria revealed nearly constant numbers along the vertical profile, ranging from 0.93 to 9.3×10^5 cells per gram sediment. A specific PCR was used to detect the presence of *Thiomicrospira* cells in these MPN counts, and to obtain their 16S rRNA sequences. The number of *Thiomicrospira* cells did not decrease with depth. It was found that *Thiomicrospira* was not a dominant S-oxidizing bacterium in this habitat. Denaturing gradient gel electrophoresis (DGGE) of PCR-amplified 16S rDNA fragments followed by hybridization analysis with a genus specific oligonucleotide probe showed the diversity of *Thiomicrospira* strains in the MPN cultures. Sequence analysis of the highest MPN dilutions in which *Thiomicrospira* was detected, revealed the presence of four clusters of several closely related sequences. Only one out of the 10 retrieved *Thiomicrospira* sequences was related to known isolates from the same habitat. Slot-blot hybridization of rRNA isolated from different sediment layers showed that, in contrast to the number of *Thiomicrospira* cells, the *Thiomicrospira*-specific rRNA decreased rapidly below the oxic layer of the sediment. The study indicates the enormous sequence diversity of closely related microorganisms present in one habitat, which so far has only been found by sequencing of molecular isolates. In addition, it gives indication that most of the *Thiomicrospira* populations in the sediment were quiescent.

References: [1] Amann R. I. et al. (1995) *Microbiol. Rev., 59,* 143–169. [2] Amann R. I. and Kühl M. (1998) *Current Opinion in Microbiology, 1,* 352–358. [3] Barns S. M. et al. (1994) *Proc. Natl. Acad. Sci. USA, 91,* 1609–1613. [4] Brinkhoff T. and Muyzer G. (1997) *Appl. Environ. Microbiol., 63,* 3789–3796. [5] Grosskopf R. et al. (1998) *Appl. Environ. Microbiol., 64,* 960–969. [6] Kuenen J. G. et al. (1992) in *The Prokaryotes* (A. Balows et al., eds.), pp. 2638–2657, Springer, Berlin, Germany. [7] Ramsing N. B. et al. (1996) *Appl. Environ. Microbiol., 62,* 1391–1404. [8] Teske A. et al. (1996) *Appl. Environ. Microbiol., 62,* 1405–1415.

THE TEMPORAL EVOLUTION OF THE OLIGOCENE-RECENT IZU-BONIN ARC: THE TEPHRA PERSPECTIVE.

C. J. Bryant, R. J. Arculus, and S. M. Eggins, Department of Geology, Australian National University, Canberra, ACT 0200 Australia (colleen.bryant@anu.edu.au; richard.arculus@anu.edu.au; stephen.eggins@anu.edu.au).

Intraoceanic arc systems like the Izu-Bonin (IB) are ideal locations in which to examine how the processes involved in arc magma genesis vary with time and with tectonic evolution. Tephra studies are crucial to this quest, due to the fragmentary temporal lava record.

Tectonic and Magmatic Evolution: The IB records a cyclic history of arc and backarc basin development since its inception at ~50 Ma. Early volcanism was dominated by boninitic magmas, with lesser tholeiitic magmas becoming more prominent with time. Extension at ~31–32 Ma led to backarc spreading in the Mariana arc but forearc rifting in the IB. Rift volcanism (site 793) was characterized by transitional boninitic-tholeiitic geochemical compositions [1] and was coeval with eruption of volcanic arc lavas (site 792). Backarc rifting (Shikoku Basin), initiated at ~25 Ma, continued until 5–17 Ma. This was associated with a reduction in volcanism (17–27 Ma), possibly with a hiatus spanning 20–23 Ma [2]. Incipient backarc extension was reestablished at ~2 Ma.

Temporal Evolution: Oligocene-Recent IB tephras are almost exclusively low-K tholeiites, and have low abundances of all incompatible elements, including LILE, LREE, HFSE, Th, U, and Pb. However, there are clearly discernable temporal geochemical variations within this interval.

Sparse Oligocene tephra horizons (24–31 Ma) recovered from ODP site 782 (leg 125) are chemically heterogeneous, potentially reflecting primary geochemical heterogeneity, the effects of alteration and reworking and derivation from multiple eruptive sources. The most chemically coherent (i.e., cogenetic) tephras, at 27 and 24 Ma, have low incompatible element abundances, and are strongly depleted in LREE with respect to HREE. The latter are equivalent to those observed for site 792 arc lavas. Both groups are geochemically distinct from the Oligocene volcanogenic turbidites [1], which have higher TiO_2 and total FeO (greater than normally observed between cogenetic lavas and tephras), and higher HREE and flatter REE patterns. Given their greater similarity with site 793 lavas and Eocene-Early Oligocene boninites and tholeiites, Oligocene turbidites are more likely derived from rift volcanism or represent reworking of older arc materials.

The 15–18-Ma tephras erupted at the resumption of volcanism (cessation of backarc spreading) are the most enriched IB tephras, particularly in those elements typically regarded as being slab-derived (i.e., Rb, Cs, Ba, Th, and U). In contrast, 2–15-Ma tephras represent the most incompatible element-poor tephras erupted in the post-boninitic history of the IB arc, with most depleted compositions being erupted immediately after the enriched 15–18-Ma tephras. The abundances of Th, U, and Nb increase, and Cs and Y decrease throughout the 2–15-Ma interval. All 2–15-Ma tephras have strongly LREE-depleted REE patterns. The <2-Ma tephras are almost indistinguishable from the 2–15-Ma ashes.

Variations in the Mantle Component: Due to their low solubility in aqueous fluids, HFSE/HREE ratios have been used to monitor mantle sources and processes (e.g., increases in Nb/Zr may reflect increased mantle fertility or lower degree of partial melting). Variations in HFSE/HREE in IB tephras broadly correlate with the temporal variations in incompatible element abundances. The highest Nb/Zr ratios are observed in the 15–18-Ma tephras, whereas the lowest occur in subsequent 2–15-Ma glasses.

Mantle fertility was low throughout the Oligocene. With the initiation of backarc spreading, the magmatic flux decreased, possibly ceasing completely between 20–23 Ma. The higher Nb/Zr ratios in 15–18-Ma tephras are consistent with smaller degrees partial melting, produced as arc magmatism reestablished itself. The decrease in Nb/Zr ratios at ~15 Ma probably marks the return to "normal" degrees of melting., with the decrease in Nb/Zr from the Oligocene reflecting real decreases in mantle fertility due to melt extraction in the backarc. The subsequent increase in Nb/Zr throughout the 2–15 Ma is consistent with a gradual increase in mantle fertility. By 2 Ma, the Nb/Zr ratios had returned to their pre-backarc spreading values. Although this interpretation is broadly in accord with that proposed by [1], the extent of depletion is argued to be not as large as that previously proposed. The 24 and 27 Ma tephras have appreciably higher Nb/Zr ratios than Oligocene turbidites. This may be linked to their boninite-like characteristics, noting that although boninites are considered to be derived from more depleted sources than tholeiites, they typically have higher Nb/Zr and Nb/Yb ratios. Therefore, these ratios may not be an accurate monitor of mantle fertility in the Oligocene turbidites.

Overall, the geochemical variability resulting from backarc-basin development is small compared to that observed in intraoceanic magmas worldwide.

References: [1] Gill J. B. et al. (1994) *Lithos., 33,* 135–168. [2] Taylor B. (1992) *Proc. ODP, Sci. Results, 126,* 627–651.

HALOGEN GEOCHEMISTRY OF THE MANTLE DETERMINED FROM GLOBALLY DISTRIBUTED DIAMOND SAMPLES.

R. Burgess[1] and J. W. Harris[2], [1]Department of Earth Sciences, University of Manchester, Oxford Road, Manchester M13 9PL, UK (ray.burgess@man.ac.uk), [2]Division of Earth Sciences, University of Glasgow, Glasgow G12 8QQ, UK.

Introduction: Evidence that diamond genesis is related to mantle fluids, containing high concentrations of volatiles, comes from the study of microinclusions in fibrous cubic diamond and the coats on octahedral diamond. These fluid inclusions provide the deepest samples of upper mantle fluids available for study, and their characterization is important for establishing the chemical and isotopic composition of mantle volatiles, investigating the transport of incompatible elements in the mantle, and understanding the genesis of diamonds.

Samples and Methods: Fifteen coated stones from four kimberlites in the Northwest Territories, Canada are compared with eight cubes from Jwaneng, Botswana and 13 "Congo tops" from the Democratic Republic of Congo. Coated stones from the Aikhal kimberlite, Siberia are currently being prepared for analysis. Noble gases, K, and halogens (Cl, Br, and I) were determined using extension of the ^{40}Ar-^{39}Ar technique. Gases were extracted from diamonds using six temperature steps over the interval 900°–2150°C.

Results: *Release patterns.* Two gas releases are observed at 1200°–1600°C and 2050°–2150°C respectively. The cause of the low-temperature release, which accounts for 15–30% of the total, is unknown at present; however, the high-temperature release occurs at diamond graphitization.

Argon-40, potassium, and chlorine relationships. Argon-40* and K are poorly correlated. Apparent ages are all higher than host kimberlite ages and most are above 4.5 Ga. In contrast, individual diamonds show good correlations between ^{40}Ar* and Cl, but there are variations in ^{40}Ar*/Cl values between stones. Canadian and African diamonds show a similar range in ^{40}Ar*/Cl of 506–1358 × 10^{-6} molar (M), but with different mean values of 965 ± 273 × 10^{-6} M and 831 ± 218 × 10^{-6} M respectively.

Halogens. Halogens are poorly correlated in Canadian diamonds with large variations in Br/Cl (1.3–63.0 × 10^{-3} M) and I/Cl (9.8–1703.5 × 10^{-6} M) even between diamonds from the same kimberlite. Halogens in African diamonds show a better correlation with a mean Br/Cl = 1.56 ± 0.25 × 10^{-3} M and most I/Cl between 20–70 × 10^{-6} M. Iodine/bromine for both African and Canadian diamonds are similar at 5–70 × 10^{-3} M. Concentrations of halogens, K, and noble gases are up to 30× higher in Canadian stones, probably because of a higher density of fluid inclusions.

Discussion: There is overlap between the range in halogen ratios of African diamonds with the lowest values of Canadian stones (Fig. 1). They are comparable with estimates of MORB based on existing data (Br/Cl = 1.03–1.22 × 10^{-3} M; I/Cl = 48–71 × 10^{-6} M [1,2]); Br/Cl ratios in diamonds are close to the seawater value at 1.53 × 10^{-3} M. High Br/Cl values in Canadian diamonds are associated with highest I/Cl and there is an overall trend away from MORB-like halogen signature toward I- and Br-rich and Cl-poor fluids. This extends from Leslie through Grizzly and Fox to the highest values in Koala diamonds (Fig. 1). This trend may represent mixing between a mantle fluid similar to that in African stones and a second Br- and I-rich fluid. Some crustal fluids have high Br/Cl and I/Cl ratios but their involvement in the diamond formation process at depths of 150 km requires a deep circulating process. An alternative mechanism that may explain the variation is the crystallization of a Cl-bearing phase such as apatite. Low Br/Cl ratios of 0.1–1 × 10^{-3} M have been determined in apatite from mantle peridotites [3], which is the correct sense for generating residual fluids with high Br/Cl.

References: [1] Jambon A. et al. (1995) *Chem. Geol., 126,* 101–117. [2] Schilling J. G. et al. (1996) *Phil. Trans. R. Soc. Lond., A297,* 147–178. [3] Ionov D. A. et al. (1997) *Chem. Geol., 141,* 153–184.

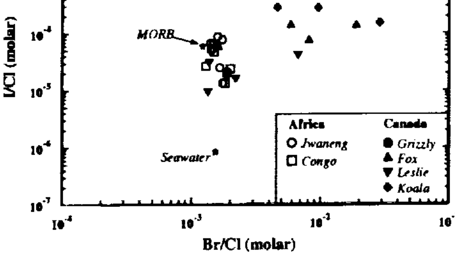

Fig. 1. Iodine/chlorine vs. Br/Cl for African and Canadian diamonds. Bromine/chlorine range for mantle apatite is from [3].

OPTIMIZING OCHRE ACCRETION AT THE SOURCE.

S. P. Burke[1], S. A. Banwart, A. Jarvis, and P. L. Younger, [1]Groundwater Protection and Restoration Group, Department of Civil Engineering, University of Sheffield, Mappin Street, Sheffield S1 3JD, UK.

Unregulated minewater discharges represent a significant environmental problem in mining regions throughout the world. In the absence of funds for active chemical treatment, passive systems using wetlands is one option where land is available. This study explores the possibility of harnessing ferrous iron adsorption and surface catalyzed oxidation to remove dissolved Fe loads from coal mine discharges. This geochemical process is particularly suited to the circumneutral, high-Fe waters present in coal mines. This scheme would allow ochre accretion and metal ion adsorption on artificial surfaces anchored in a reactor receiving the discharge, rather than impacting the ecology of receiving streams.

To assist in understanding Fe removal rates, a geochemical model has been developed to conceptualize the adsorption and oxidation processes involved in "ochre accretion." This model has been calibrated using field data and is being used to support the design of a pilot reactor scheme to clean up pumped discharges from abandoned coal mines in northeast England.

Initial modeling shows that Fe(II) in a minewater discharge can be removed through surface-catalyzed oxidation within a reactor. Treatment, however, is dependent on the chemistry of the inflowing minewater and several parameters of the reactor design. Optimum ochre accretion occurs where circumneutral minewaters with modest concentrations of Fe(II) are present with a suitable residence time and surface area present in the reactor. The model shows that the master variables alkalinity and pH have a profound influence on ochre accretion. Since Fe(II) adsorption is strongly pH dependent in the near-acid pH range, alkalinity present in the discharge helps maintain reactor pH, and thus adsorption and surface-catalyzed oxidation rates, above the threshold for Fe(II) adsorption.

BUBBLE-BY-BUBBLE DEGASSING OF MID-OCEAN-RIDGE BASALT MAGMAS.

P. G. Burnard, Department of Earth Sciences, Manchester University, Manchester M13 9PL, UK (present address: Mail Code 100-23, Department of Geological and Planetary Sciences, California Institute of Technology, Pasadena CA 91125, USA; peteb@gps.caltech.edu).

Introduction: As a batch of magma ascends through the crust, bubbles in the magma will grow due to decompression and CO_2 diffusion until they are quenched during eruption. As a result, vesicles of different sizes in basaltic glass record the history of volatile evolution; larger vesicles predate small vesicles and will preserve less fractionated volatiles. In order to trace the evolution in volatile compositions during MORB magma processes, the He, Ar, and CO_2 compositions of individual vesicles in two mid-Atlantic Ridge glasses (AMK 3379, AMK 3376) have been determined by laser decrepitation.

Vesicle Compositions: All vesicles had high ^{40}Ar/^{36}Ar, in the range 2000–30,000, consistent with contamination of vesicle-trapped volatiles with high ^{40}Ar/^{36}Ar by a ^{36}Ar-bearing atmospheric component. Contamination of the magma prior to eruption would result in a correlation between vesicle size and ^{40}Ar/^{36}Ar; no such correlation is present in the data, therefore variable addition of a posteruptive surficial contaminant is thought to result in the range in ^{40}Ar/^{36}Ar observed.

Argon/helium and Ar/CO_2 are not constant, but vary from vesicle to vesicle (Fig. 1) in both sections analyzed. In one of the sections (AMK 3376), Ar/He and Ar/CO_2 increase with increasing vesicle size. This is consistent with younger vesicles being formed from the residue of gas trapped in older vesicles. The vesicles in the other section (AMK 3339) were all too small to ascertain the relationship (if any) between vesicle size and composition.

The composition of vesicle-trapped volatiles in AMK 3376 are consistent with gas loss by Rayleigh distillation with relative Ar-CO_2 and He-CO_2 solubilities (α_{Ar,CO_2} and α_{He,CO_2}) of 0.5 and 5 respectively. Carbon dioxide was less soluble during degassing of this melt (relative to Ar or He) than expected; experimentally determined He, Ar, and CO_2 solubilities predict α_{Ar,CO_2} = 0.2 and α_{He,CO_2} = 2 (solubilities from [1,2]). The volatiles trapped in AMK 3339 vesicles cannot be produced by equilibrium degassing in an axial magma chamber, but probably reflect complex gas loss processes involving loss of volatiles by diffusion in addition to solubility-controlled degassing.

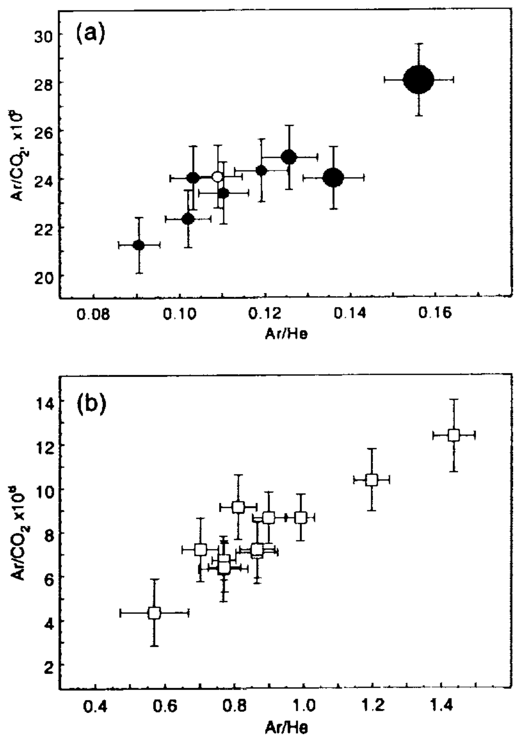

Fig. 1. (a) Helium-argon-carbon dioxide composition of individual AMK 3376 vesicles. Symbols sizes are proportional to vesicle volumes, which are in the range 0.5–3 μcm^3. Volume of the white symbol is not known (two vesicles were close together). Argon/helium and Ar/CO$_2$ increase with increasing vesicle volume. (b) Helium-argon-carbon dioxide compositions of individual AMK 3339 vesicles. The vesicles in this section were smaller and had a much more restricted range in vesicle volumes (0.08–0.31 μcm^3) than AMK 3376. Probably as a consequence, there was no correlation between vesicle volume and the composition of its trapped volatiles.

Vesicle Internal Pressures: The pressure inside the vesicles can be determined from knowledge of the vesicle volumes, which were estimated from the vesicle's area in thick section. The majority of vesicles had internal pressures between 0.25 and 0.4 kbar, consistent with the eruption pressure of 0.3 kbar. However, two vesicles from AMK 3376 and three from AMK 3339 have much higher VIPs, up to at least 1 kbar. Either these high pressures are artifacts of the technique, or the basalts were erupted at high pressures and then instantaneously quenched in order to preserve the high VIPs.

References: [1] Carroll M. R. and Stolper E. M. (1993) *GCA, 57,* 5039–5052. [2] Dixon J. E. (1997) *Am. Mineral., 82,* 368–378.

SENSITIVITY AND ISOTOPIC DISCRIMINATION IN A NIER-TYPE SOURCE AS A FUNCTION OF PRESSURE: IMPLICATIONS FOR ARGON AND HELIUM ANALYSIS.

P. G. Burnard and K. A. Farley, Mail Code 100-23, Department of Geological and Planetary Sciences, California Institute of Technology, Pasadena CA 91125, USA (peteb@gps.caltech.edu).

Ionization of noble gases in many modern mass spectrometers is achieved by electron bombardment in "Nier-type" ion sources. Neutral species in the spectrometer are ionized by an electron beam that strips an electron (or electrons) from molecules or atoms, producing positive ions. Applying a magnetic field to the source using small external magnets increases the electron path. The ions are extracted by a series of lower voltage focusing and accelerating plates before magnetic sector mass analysis (Fig. 1).

The sensitivity of Nier-type sources depends on the element (i.e., He, Ne, Ar, etc.) and isotope (i.e., ^{40}Ar, ^{39}Ar, ^{36}Ar, etc.) being ionized. There are variations in the ^{3}He/^{4}He discrimination (i.e., $(^3He/^4He)_{measured}/(^3He/^4He)_{real}$) as a function of He pressure [1]. We report variations in the focusing characteristics of MAP 215 noble-gas mass spectrometers that can account for some of the discrimination variations, and comment on the implications for future operation of noble-gas mass spectrometers with Nier-type sources.

The spectrometer sensitivity as a function of halfplate voltage at different He pressures is shown in Fig. 2. Large He signals (lower panel, Fig. 2) produce well-defined peaks with coincident maxima for both ^{3}He and ^{4}He. However, the shape of the ^{3}He and ^{4}He peaks is not identical: the ^{3}He signal falls more rapidly than the ^{4}He signal at halfplate voltages less than the optimum setting. At low He pressures, the ^{3}He and ^{4}He peaks are broader with noncoincident maxima. Furthermore, the position of the maxima is dependent on the He pressure in the spectrometer. Similar peak shapes and pressure-dependent migrations in the halfplate optimum voltage occur for Ar isotopes.

Isotopic discrimination as a function of pressure will result from these halfplate peakshapes. For example, maximizing spectrometer sensitivity using a 480-mV ^{4}He signal will result in a halfplate "voltage" of ≈90 V and negligible ^{3}He/^{4}He discrimination (Fig. 2). However, this halfplate "setting" will

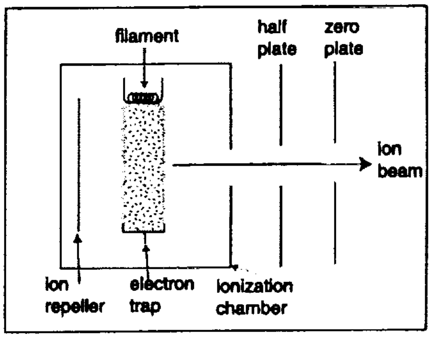

Fig. 1. Schematic section through a Nier-type source. The ionization chamber and halfplate voltages were 3 kV and 2.4 kV, respectively, with a trap current of 500 μA and electron potential of 58 eV.

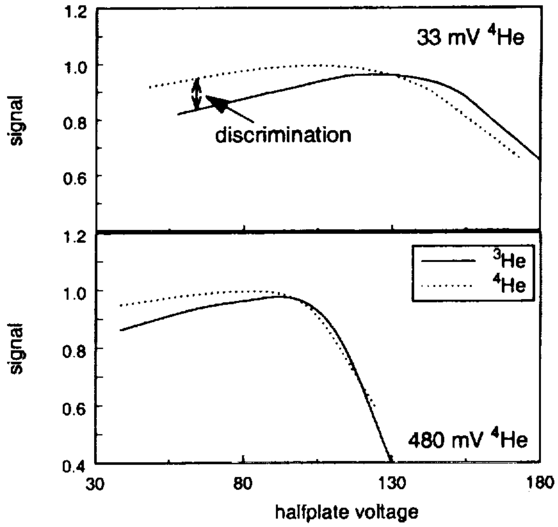

Fig. 2. Halfplate control on ^{3}He (ion multiplier) and ^{4}He (faraday cup) signals as a function of He pressure. Helium-3/helium-4 ratio = 22 × 10^{-6}. Signals normalized to maximum = 1. One halfplate "setting" (≡0.1 turns on the halfplate fine focus knob) = 9.6 V on the halfplate. Bias is the same for all measurements. The He-isotopic discrimination is the difference between the ^{4}He and ^{3}He lines.

not be optimized for a 33-mV ^4He signal, resulting in a loss of sensitivity and a significant discrimination of ≈10%. Furthermore, measuring more than 480 mV of ^4He at a halfplate "voltage" of 90 V will result in a catastrophic decrease in sensitivity. At these pressures, the ^4He peak shifts to even lower halfplate voltages (e.g., 1000-mV ^4He results in an optimum "setting" of ≈6); measuring 1000-mV ^4He at a "voltage" of 90 V will miss the peak.

The same arguments apply to Ar sensitivity and discrimination as a function of pressure. These experiments demonstrate the need to calibrate noble-gas mass spectrometers over the range in pressures measured in samples; calibration with a single standard gas aliquot will result in errors in both sensitivity and discrimination. Optimizing halfplate voltages can reduce the corrections for gas pressure.

References: [1] M. Honda et al. (1993) *GCA, 57,* 859–874.

AEROSOL CARBON IN THE REMOTE ATMOSPHERE.

P. R. Buseck[1], M. Pósfai[2], L. Jia[1], and J. R. Anderson[3], [1]Departments of Geology and Chemistry/Biochemistry, Arizona State University, Tempe AZ 85287, USA, [2]Department of Earth and Environmental Sciences, University of Veszprém, Veszprém, P.O. Box 158, H8201, Hungary, [3]Environmental Fluid Dynamics Program, Arizona State University, Tempe AZ 85287, USA.

It is widely accepted that biomass burning in many parts of the globe produces vast quantities of C that are injected into the troposphere. It is equally well known that power plants generate major quantities of carbonaceous aerosols; emissions from automobiles are most highly concentrated in urban regions and near major highways. The role of airplanes is less well established.

During transmission electron microscopic studies of aerosols from a variety of oceanic regions, both remote and within a few hundred kilometers of major populated regions, we have found carbonaceous particles to be widespread. Even in samples collected south of Tasmania (as part of the international Aerosol Characterization Experiment, ACE-1) we found that many sulfate particles contain small enclosed grains of soot. The area is far from any sources of biomass burning. The soot is characterized by typical globular structures of onion-like wrapped graphitic layers.

Only one fourth of the soot particles contain K, an indicator of likely biomass burning origin. We found similar aggregates (internal mixtures) in samples from the North Atlantic, Equatorial Pacific, and Indian Oceans, and from over continental areas. The origin of much of this atmospheric C is difficult to determine; a possible source is commercial aircraft flying at high altitudes. Such particles are small and, moreover, produced in the free troposphere; thus, they can stay aloft longer than the larger particles injected by biomass burning, vehicle exhaust, and power plants. The soot may provide a reactive surface for sulfate formation; once inside the sulfate, the absorption of visible light by soot is enhanced because of multiple refraction within the sulfate particle. Other types of C-bearing species in the remote troposphere include coatings on the surfaces of sulfates. Further study will be required to determine whether these presumably organic coatings are absorbing in the visible range, i.e., whether, according to the operational definition, they are true "black carbon" aerosols.

FRAMBOIDAL PYRITE FORMATION BY THE OXIDATION OF IRON(II) MONOSULFIDE BY HYDROGEN SULFIDE.

I. B. Butler[1] and D. Rickard, [1]Department of Earth Sciences, Cardiff University, Park Place Cardiff, CF1 3YE, Wales, UK (butlerib@cardiff.ac.uk).

Introduction: The ubiquity of framboidal pyrite occurrences in modern and ancient sedimentary environments and in low to medium temperature ore deposits suggests a robust formation mechanism able to operate under a range of physico-chemical conditions. Furthermore, the appearance of framboidal pyrite subjacent to the onset of anoxia in sediments and water columns is consistent with a formation mechanism which is geologically instantaneous. Finally, the highly spatially ordered microarchitecture present in many examples of framboidal pyrite (e.g., Fig. 1a) implies a formation mechanism which permits self-organization of individual microcrystals during framboid formation.

Experimental Results: Pyrite framboids have been synthesised via the oxidation of FeS (mackinawite) by H_2S [1,2] in aqueous solutions at pH 6, Eh >–250mV, and temperatures above 60°C in the absence of O_2 (Fig. 1b). Under these conditions, at Eh <–250mV, single crystals of pyrite are formed. The reaction proceeds via dissolution of solid FeS and subsequent reaction of an aqueous FeS cluster complex with H_2S [3]. Circular structures on the surface of individual microcrysts indicate crystal growth via the development of screw dislocations. Greigite (Fe_3S_4), which has been heavily implicated in framboid formation models [4,5] was not formed in any experimental runs.

Geological Implications: The oxidation of FeS by H_2S

$$FeS_{(mk)} + H_2S_{(aq)} = FeS_{2(py)} + H_{2(aq)}$$

is by far the most rapid pyrite forming reaction so far identified [1,3]. The involvement of an aqueous FeS cluster complex in the reaction facilitates transport and reaction, allowing the development of comparatively coarse grained framboidal pyrite textures from the extremely fine-grained dispersed FeS reactant in sedimentary environments. We suggest that the apparent Eh dependence of the reaction may be a supersaturation effect related to position within the pyrite stability field in Eh-pH space. The appearance of framboids close to the initiation of bacterial sulfate reduction in anoxic sediments and water columns may be unrelated to the presence of electron acceptors other than H_2S as has been previously supposed.

The size and form of the pyrite products of our reactions (both euhedral and framboidal) point to a nucleation vs. crystal growth rate control over the nature of the pyrite texture. Framboidal pyrite appears to formed under conditions favourable for rapid, cascade-style nucleation, but leading to slow, possibly substrate-limited growth. Single crystals indicate slow nucleation and normal crystal growth without substrate limitation. The results suggest that the framboidal texture results from rapid nucleation in environments where

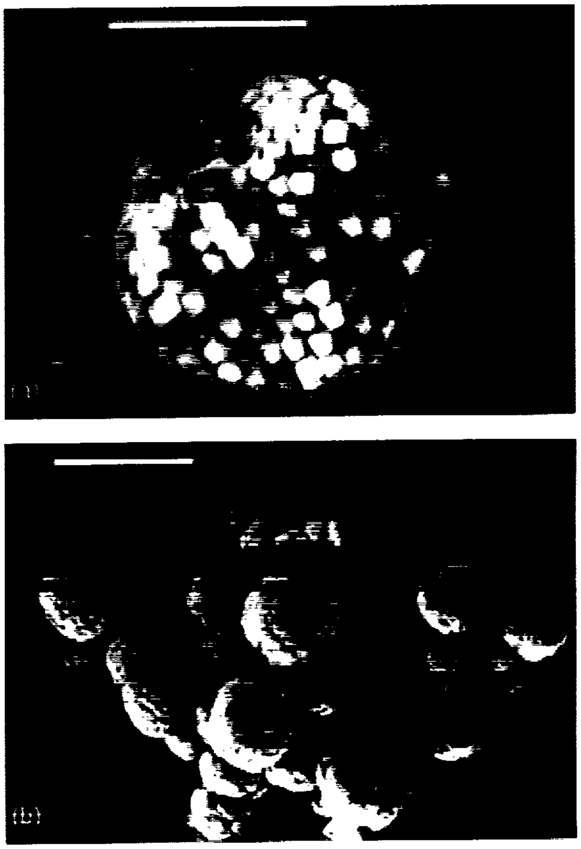

Fig. 1.

pyrite is strongly supersaturated. Where pyrite is metastable, or only slightly supersaturated, rapid pyrite nucleation is inhibited and single crystals form. The results demonstrate that pyrite framboids can form in the absence of molecular O_2, magnetic (e.g., greigite) intermediates, or biological intervention.

References: [1] Rickard D. (1997) *GCA, 63,* 115–134. [2] Butler I. B. and Rickard D., in preparation. [3] Rickard D. and Luther G. W. III (1997) *GCA, 63,* 135–147. [4] Sweeney R. E. and Kaplan I. R. (1973) *Econ. Geol., 68,* 618–634. [5] Wilkin R. T. and Barnes H. L. (1997) *GCA, 61,* 323–339.

IRON SULFIDE OXIDATION IN AN ANOXIC CHEMOSTATED REACTION SYSTEM.

I. B. Butler, S. T. Grimes, and D. Rickard, Department of Earth Sciences, Cardiff University, Park Place, Cardiff, CF1 3YE, Wales, UK (butlerib@cardiff.ac.uk).

Introduction: A consequence of using batch systems in iron sulfide experimentation is that K_{sp} for metastable phases, such as amorphous, precipitated or mackinawite-like iron(II) monosulfides (FeS) is unavoidably exceeded (Ksp'(FeSam) = 10^{-3} [1]), and it appears as though [FeS] is a necessary precursor for the formation of more stable, but less soluble, phases such as pyrite. Preliminary results from a chemostated continuous flow reactor reported here have provided evidence of the extreme sensitivity of [FeS] to oxidation by O_2 and have consequences for understanding transformations at ambient temperatures in the iron sulfide system.

Experimental: We constructed a sulfide chemostat system to investigate iron sulfide chemistry under strictly controlled pH, Eh, [Fe^{2+}], and [S-II] conditions, maintained by electrode monitoring and automated process control. The reaction of precipitated FeS in the presence of 10 mM aqueous H_2S at pH = 6–6.5 was studied in the absence of detectable O_2 for 2–4 weeks at 25°–40°C. The product was either the preservation of the original precipitated FeS or slow development of the thiospinel, greigite (Fe_3S_4) dependent on whether the O_2-free analytical grade N_2 had been passed through a fresh Zr-metal scrubber or not (Fig. 1). That is, up to two-thirds of the FeS- Fe(II) is oxidized to Fe(III), while the S(-II) remains unaffected, at O_2 concentrations between that of the O_2-free N_2 and the Zr-ZrO_2 buffer. The oxidation of FeS to Fe_3S_4 has been shown to be a solid-state reaction [2] that may involve dioxygen [3].

Discussion: The definition of "anoxic" refers to (≤0.1 ppm $O_{2(aq)}$) [4] where conventional analytical methods fail to detect free O_2. Unfortunately, most proprietary, analytical-grade gases appear to contain free O_2 around this level. For example, the BOC O-free N used in this experimentation may contain up to 16 ppm O_2. In batch reactors, these low concentrations do not represent a significant quantity of reactant. However, in continuous-flow reactors, this represents a constant supply of reactant O_2, which can cause oxidative transformations of FeS to Fe_3S_4 [3].

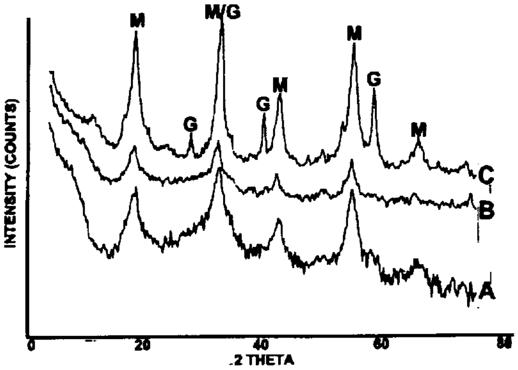

Fig. 1. X-ray diffraction analysis (XRDA) results for (plot A) initial FeS precipitated in reaction vessel; (plot B) FeS precipitate after 18 d at 25°C with 0.01 M H_2S, pH 6.5, in the absence of O_2; and (plot C) greigite products present in FeS aged for 15 d at 40°C with 0.01 M H_2S, pH 6.5, in the absence of measurable O_2.

The product of the Zr scrubbing was identified as baddleyite (ZrO_2) by X-ray diffraction analysis (XRDA). At equilibrium at 300°C the Zr/ZrO_2 buffer limits O_2 concentrations in the N_2 gas to f_{O_2} = 10–90 atm. Typical gas-flow rates through the pressurized chemostated reactor are of the order of 1–10 cm^3 min^{-1}, representing a total of 3 × 10^{-4} to 3 × 10^{-5} mol of O_2 over a period of two weeks, if O_2 is present at ~10 ppm. For reactions like

$$4FeS + ½O_2 + 2H^+ = Fe_3S_4 + Fe^{2+} + H_2O$$

0.5 mol O_2 are required for each mole of Fe_3S_4 produced. Therefore a maximum 6 × 10^{-4} moles Fe_3S_4 might be formed at 100% efficiency under these conditions, which is more than an order of magnitude less than the observed quantities. However, scrubbing the gas with hot Zr metal granules quantitatively removes O_2, and greigite is not formed in the reaction.

Conclusions: The results demonstrate that O_2 plays a significant role in greigite formation even at nonstoichiometric levels. We propose that O_2 catalyzes nucleation and growth of greigite by activating the FeS surface in reactions such as [5,6]

$$3FeS + H_2S = Fe_3S_4 + H_2$$

and

$$4FeS + 2H^+ = Fe_3S_4 + Fe^{++} + H_2$$

References: [1] Davison W. et al. (1988) *Pure Appl. Chem., 60,* 1535–1548. [2] Pósfai M. et al. (1998) *Science, 280,* 880–883. [3] Wilkin R. T. and Barnes H. L. (1996) *GCA, 60,* 4167–4179. [4] Berner R. (1980) Princeton Univ., 241 pp. [5] Rickard D. (1997) *GCA, 63,* 115–134 [6]. Butler I. B. et al., this volume.

MICROSCALE TRACE-ELEMENT AND SULFUR-ISOTOPIC DISTRIBUTIONS IN HYDROTHERMAL SULFIDES.

I. B. Butler[1], R. W. Nesbitt[2], and A. E. Fallick[3], [1]Department of Earth Sciences, Cardiff University, Park Place, Cardiff, CF1 3YE, Wales, UK (butlerib@cardiff.ac.uk), [2]School of Ocean and Earth Sciences, Southampton Oceanography Centre, University of Southampton, Southampton, SO14 3ZH, UK, (r.w.nesbitt@soc.soton.ac.uk), [3]Isotope Geosciences Unit, Scottish Universities Research and Reactor Centre, East Kilbride, G75 0QF, Scotland, UK.

Introduction: The interaction of ~350°C hydrothermal fluid and 2°C seawater during black smoker activity generates steep physicochemical gradients that control mineralogical and trace-element zoning in hydrothermal precipitates. Hydrothermal sulfides from the Broken Spur vent site (29°10'N, MAR) have been characterized using laser sampling methods to determine fine-scale trace-element and S-isotopic distributions. A combination of high-sensitivity inductively coupled plasma mass spectrometry (ICP-MS) and ultraviolet (UV) (266 nm) laser ablation (resolution = 30 mm) provides detection limits of <100 ppb for trace elements in sulfide. Infrared (1064 nm) laser extraction of S as SO_2, and isotopic analysis using gas-phase mass spectrometry allows sampling resolutions of better than 1 mm with an analytical precision of $\delta^{34}S$ = ±0.3‰ CDT [1,2].

Trace Metals: Laser ablation-inductively coupled plasma mass spectrometry (LA-ICPMS) analysis of the chalcopyrite wall of a black smoker chimney, demonstrates nonrandom V, Ag, In, Te, Ba, Au, Pb, and U distributions (see Fig. 1) [3]. Enrichments of In and Te in the inner zone of the wall are attributed to lattice incorporation during high-temperature sulfide precipitation. Enrichments of U and V within the outer part of the wall are caused by seawater incursion and redox immobilization of metals on sulfide surfaces. Enrichments of Au, Ag, Pb, and Ba in the outer wall may be related to hydrothermal fluid-seawater mixing. However, comparison of distribution data with reaction-transport models suggests a possible pH control on precipitation. Distribution data, combined with textural studies, indicate a progressive change of flow regimes in the chimney wall. Initial outward fluid advection causes chalcopyrite precipitation, anhydrite replacement and per-

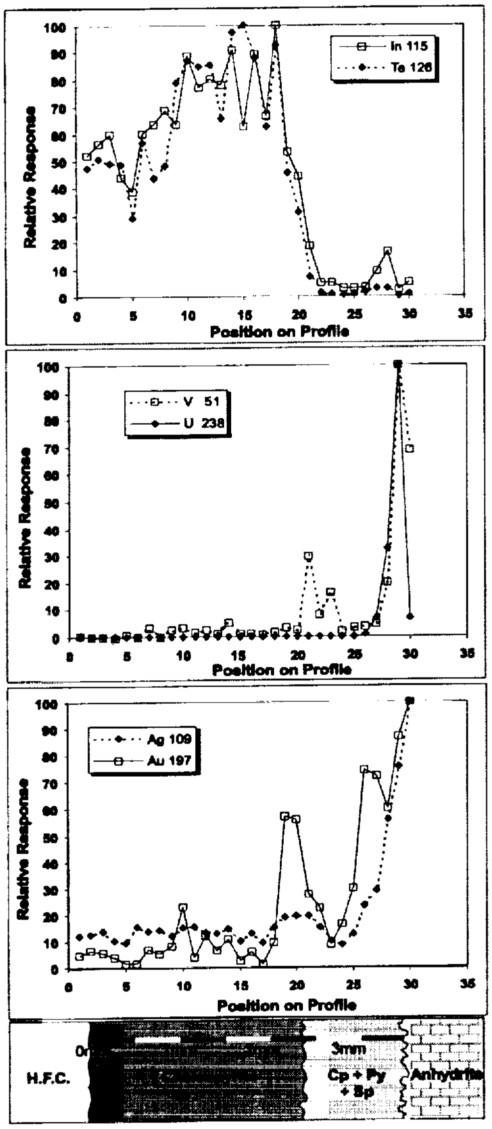

Fig. 1.

meability reduction. This permits later inward advection of seawater into the outer part of the chimney wall.

Sulfur Isotopes: A mature, diffuser structure shows complex mineralogical zoning [4], with the central pyrrhotite core surrounded by a collomorphic marcasite crust. Sulfur-isotopic data show a range of $\delta^{34}S = -4.55‰$ to $+4.8‰$ ($N = 20$). The data show distinct zoning, with core and outer crust materials showing ^{32}S depleted signatures, and mid-crust material showing ^{32}S enriched signatures. The ^{32}S enriched signatures cannot be modeled by mixing of hydrothermal fluid ($\delta^{34}S \approx 0‰$) and reduced seawater sulfate ($\delta^{34}S = 21‰$). Thus, ^{32}S enriched signatures may result from (1) bacterial sulfate reduction in the outer zones of the diffuser, or (2) isotopic fractionation by sulfide precipitation from an evolving fluid.

References: [1] Kelley S. P. and Fallick A. E. (1992) *GCA, 54,* 883–888. [2] Fallick A. E. et al. (1992) *Chem. Geol., 101,* 53–61. [3] Butler I. B. and Nesbitt R. W. (1999) *EPSL, 167,* 335–345. [4] Butler I. B. et al. (1998) *J. Geol. Soc. Lond., 155,* 773–785.

FORMATION OF THE THIOSPINEL, GREIGITE, THROUGH THE OXIDATION OF IRON(II) MONOSULFIDE IN THE PRESENCE OF ALDEHYDES.

I. B. Butler, D. Rickard, and A. Oldroyd, Department of Earth Sciences, Cardiff University, Park Place, Cardiff, CF1 3YE, Wales, UK (butlerib@cardiff.ac.uk).

Introduction: The conversion of Fe(II) monosulfide to the thiospinel, greigite (Fe_3S_4) involves the oxidation of two-thirds of the Fe(II) in FeS to Fe(III) in Fe_3S_4. At the same time, the S(-II) remains unoxidized. This may be written

$$4FeS + 2H^+ = Fe_3S_4 + Fe^{++} + H_2 \qquad (1)$$

which has a negative ΔG^0_r at 25°C. In contrast, the oxidation of FeS by H_2S to form pyrite involves the oxidation of S(-II) in FeS to S(-I) in FeS_2 while the Fe(II) remains unoxidized. With H_2S as the oxidizing agent [1], this may be written

$$FeS + H_2S = FeS_2 + H_2 \qquad (2)$$

Whereas reaction (1) appears to be a solid-state reaction [2], reaction (2) involves a solution stage [1,3]. The oxidation of FeS appears to proceed through two contrasting processes to different products. Recently Rickard et al. [4], using aldehyde catalysts, identified the process as a novel sulfide mineral switch with significance for microbial iron sulfide formation. Here we present further data on the processes responsible for the production of greigite by oxidation of FeS.

Experimental Results: Magnetic, crystalline greigite has been synthesized via the reaction of precipitated FeS in the presence of microscopic nonstoichiometric quantities of aliphatic and aromatic aldehydes (methaldehyde, ethaldehyde, and benzaldehyde) at temperatures of 100°C, in the absence of detectable $O_{2(aq)}$ ($<10^{-6}$ M) and any added S(-II). Benzaldehyde

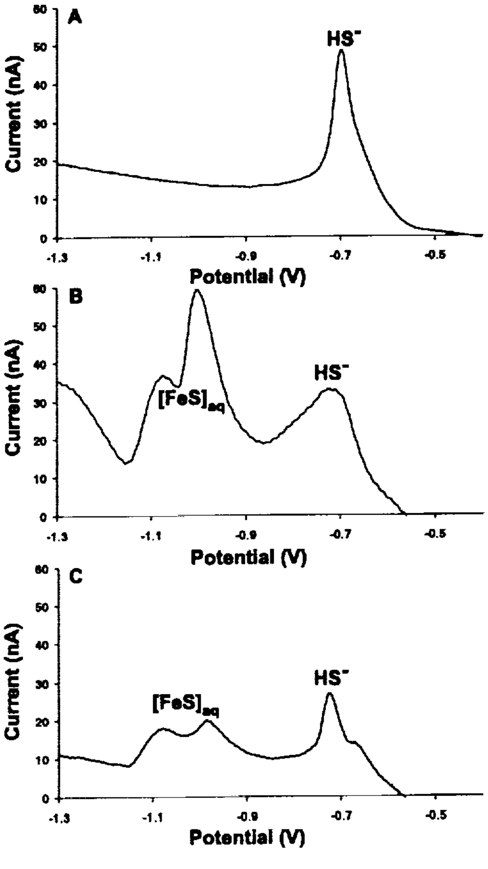

Fig. 1.

was most reactive to FeS, and ethaldehyde was least reactive. Short chain aliphatic ketones are unreactive to FeS. When the reaction of FeS and aldehydes competes with the oxidation of FeS by H_2S [4], a mixture of greigite and pyrite results. The ratio of the two products is proportional to the quantity of aldehyde added to the batch system.

Dissolution of FeS results in the formation of an $FeS_{(aq)}$ cluster complex that acts as an intermediate during pyrite formation [2,3]. The reactivity of this complex toward aldehydes has been investigated using square-wave voltammetry. Aqueous sulfide in 0.55 M, pH 7, NaCl solution is characterized by a single peak at a potential of –0.7 V (Fig. 1a). Addition of $Fe^{2+}_{(aq)}$ results in the formation of the electrode reactive $FeS_{(aq)}$ cluster complex, with a doublet at –1 to –1.1 V (Fig. 1b). Titration of the $FeS_{(aq)}$ with methaldehyde causes a reduction of the FeS doublet intensity (Fig. 1c) and, ultimately, complete removal of the species from the solution [2].

Conclusions: In the absence of added S(-II) the $FeS \rightarrow Fe_3S_4$ transformation is a solid-state reaction involving the removal of Fe from FeS. The reaction stoichiometry suggests that H^+ is involved in the process. Aldehydes act as catalysts in the reaction and inhibit formation of $[FeS]_{(aq)}$, limiting pyrite formation. Reactivity of carbonyls towards FeS (benzaldehyde > methaldehyde > ethaldehyde >>> ketone) appears to be controlled by the geometry of electron-withdrawing groups attached to the carbonyl C that affect the electrophilic character of the carbonyl group. The results demonstrate that FeS can undergo auto-oxidation in laboratory and natural aqueous systems, which may explain some conflicting experimental results.

References: [1] Rickard D. (1997) *GCA, 63,* 115–134. [2] Pósfai M. et al. (1998) *Science, 280,* 880–883. [3] Rickard D. and Luther G .W. (1997) *GCA, 63,* 135–147. [4] Rickard D. et al., in preparation.

IN SITU X-RAY DIFFRACTION OF TROILITE UNDER REDUCED, ANOXIC HYDROTHERMAL CONDITIONS.

C. L. Cahill[1], L. G. Benning[2], S. M. Clark[3], and J. B. Parise[1,4], [1]Department of Chemistry, State University of New York–Stony Brook, Stony Brook NY 11794, USA (christopher.cahill@sunysb.edu), [2]Pennsylvania State University, Department of Geosciences, University Park PA 16802, USA (present address: School of Earth Sciences, University of Leeds, Leeds LS2 9JT, UK), [3]Daresbury Laboratory, Warrington, UK, [4]Department of Geosciences, State University of New York–Stony Brook, Stony Brook NY 11794, USA.

Introduction: Under reduced, anoxic hydrothermal conditions, FeS (mackinawite) has been shown to persist to at least 180°C [1]. This result is highly dependant on O level in the reaction solution. An analogous study was undertaken for FeS (troilite, hexagonal, √3a, 2c cell) in order to examine its reaction pathway under similar conditions.

Experimental: The reaction cell used for these experiments is a modification of a design by Evans [2]. Rather than a steel Parr bomb-type autoclave, reactions take place in sealed quartz tubes. This has the advantage of advanced sample preparation as well as a cleaner signal. A Cu resistance heater block controls sample temperature, while stirring is possible via a magnetic stirring motor. The troilite starting material (hexagonal, √3a, 2c) [3] was prepared as follows: under an inert atmosphere, equimolar amounts of Fe and S were annealed at 860°C for two weeks. This material was then loaded into a quartz reaction tube and covered with an aqueous slurry of reduced FeS/H_2S under fastidiously anoxic conditions. After sealing, the tubes were dropped into the sample heating block at 150°C. *In situ* energy-dispersive XRD (Station 16.4; Daresbury Laboratory) spectra were collected every 30 s during the course of the experiment. Energy dispersive diffraction data were converted to angular dispersive at a constant stepsize of 0.01° and λ = 1.0 Å. Such was done in order to readily compare data to the JCPDS and ICSD as this was not a thorough structural study, but rather an investigation of reaction mechanism.

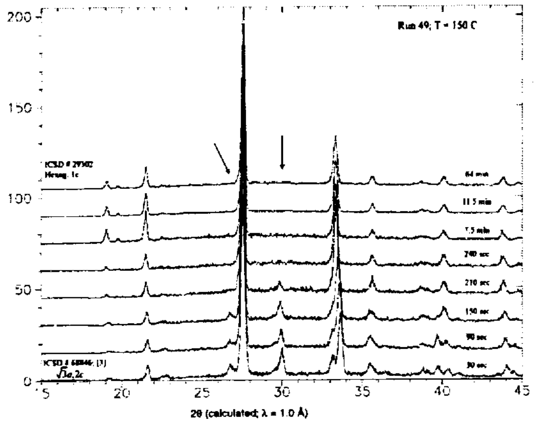

Fig. 1.

Results: The figure shows that, at 150°C, the hexagonal √3a, 2c cell transforms to the NiAs structure type (hexagonal, 1c). Several runs at various pH and controlled oxidation level are consistent with this observation. There is no evidence of the previously observed orthorhombic MnP structure [4]. These experimental conditions, however, are not optimized to detect the subtle diffraction phenomena responsible for such.

Acknowledgments: We thank the NSF [DMR 97-13375 (JBP) and EAR 95-26762 (LGB)] and the Mineralogical Society of America for financial support (CLC). We are grateful to the Materials Research Laboratory at Daresbury for their support and use of their facilities.

References: [1] Benning L. G., this volume. [2] Evans J. S. O. et al. (1994) *Rev. Sci. Inst., 66,* 2442–2445. [3] Keller-Besrest F. and Collin G. (1990) *J. Sol. State. Chem., 84,* 194–210. [4] King H. E. and Prewitt C. T. (1982) *Acta Cryst., B38,* 1877–1887.

CONTROLS ON OCEAN pH AND ALKALINITY: ATMOSPHERIC CARBON DIOXIDE AND CARBONATE SEDIMENTS.

K. Caldeira[1] and R. A. Berner[2], [1]Climate System Modeling Group, Lawrence Livermore National Laboratory, 7000 East Avenue, L-103, Livermore CA 94550, USA (kenc@llnl.gov), [2]Department of Geology and Geophysics, Yale University, New Haven CT 06520-8109, USA (berner@hess.geology.yale.edu).

Introduction: On a multimillion-year timescale, atmospheric CO_2 is controlled by the balance between (1) CO_2 supplied from magmatism, metamorphism, diagenesis, and organic C oxidation during weathering, and (2) CO_2 consumed by silicate-rock weathering (and subsequent C sediment deposition) and organic C burial in sediments. The atmospheric CO_2 content largely determines the mean partial pressure of CO_2 in the surface ocean. Because the ocean has been in contact with carbonate sediments throughout its history, it has generally remained near saturation with respect to calcite or some other carbonate mineral. The alkalinity of the oceans adjusts to meet the twin constraints of surface ocean pCO_2 and surface- or deep-ocean carbonate-mineral saturation state. Here, we quantify the relationship between atmospheric CO_2 and ocean pH, based on these principals, and quantify the extent to which this relationship can be affected by variation in ocean temperature, major cation content, calcite lysocline depth, organic and carbonate C productivity, controlling mineralogy, and other factors. We conclude that assumption of constant calcite-saturation state (or constant carbonate-ion concentration) provides a more reliable guide to paleo-pCO_2 than the assumption of constant ocean alkalinity. These results can be used to make predictions of atmospheric CO_2 content from paleo-pH proxies, and estimate uncertainties in those predictions.

Carbonate Chemistry: The partial pressure of CO_2 dissolved in water is related to the concentration of aqueous CO_2 [CO_2(aq)] via the expression

$$[CO_2(aq)] = \alpha \, pCO_2 \qquad (1)$$

Hence, the [CO_2(aq)] of the solution near equilibrium is largely determined by the pCO_2 of the overlying atmosphere and the temperature of the solution. CO_2(aq) can hydrate (i.e., join with H_2O) to form H_2CO_3. It is experimentally difficult to distinguish between CO_2(aq) and H_2CO_3, so the sum of their concentrations is often reported, designated as [H_2CO_3*].

Inorganic C in the solution may also appear in the form of bicarbonate (HCO_3^-) and carbonate (CO_3^{2-}), and the partitioning of inorganic C among these forms is controlled by the H ion concentration of the ocean

$$[H^+]\ [HCO_3^-] = k_1\ [H_2CO_3^*] \tag{2}$$

$$[H^+]\ [CO_3^{2-}] = k_2[HCO_3^-] \tag{3}$$

Also

$$[H^+]\ [OH^-] = k_w\ [H_2O] \tag{4}$$

Constant Alkalinity: Total alkalinity (ΣAlk) is the positive charge balanced by the negative charge on the weak acids. For a carbonic acid solution, electrical neutrality requires:

$$[\Sigma Alk] = [HCO_3^-] + 2\ [CO_3^{2-}] + [OH^-] - [H^+] \tag{5}$$

Solving equations (1–5) for pCO_2 as a function of pH, under the assumption of constant alkalinity, yields:

$$pCO_2 = h\ (h^2 - k_w + h)\ [\alpha\ k_1\ (h + 2\ k_2)]^{-1} \tag{6}$$

where A = [ΣAlk].

Constant Calcite Saturation State: We can represent the condition of calcite saturation by:

$$[Ca^{2+}]\ [CO_3^{2-}] = k_{sp} \tag{7}$$

If we consider that alkalinity is provided by Ca^{2+} and other ions, we can write

$$A = A_0 + 2\ [Ca^{2+}] \tag{8}$$

that is, alkalinity (A) is the sum of non-Ca alkalinity (A_0) plus the alkalinity provided by Ca (= 2 [Ca^{2+}]). We can then solve equations (1–5), (7), and (8) for pCO_2 as a function of pH, yielding:

$$\begin{gathered} pCO_2 = (h\ (h^2 - k_w + h\ A_0) + \\ h\ k_2^{-1/2}[k_2\ (h^2 - k_w + h\ A_0)^2 + 8\ k_{sp}\ h^2\ (h + 2\ k_2)^{1/2}] \\ [2\ \alpha\ k_1\ (h + 2\ k_2)]^{-1} \end{gathered} \tag{9}$$

Result: Equations (6) and (9), using parameter values typical of seawater, are plotted in Fig. 1., demonstrating the difference between assuming a constant alkalinity vs. constant calcite saturation state when estimating pCO_2 from a pH measurement or proxy.

Other Factors and Issues: Other factors have changed through Earth history, such as ocean temperature, the ratio of Ca^{2+} to Mg^{2+}, the controlling mineralogy of the ocean, biological productivity, and possibly borate concentration. These and other factors can change the relationship between measured pH and inferred atmospheric CO_2 content. These relationships will be quantified using a geochemical ocean model, and applied to the interpretation of paleo-pH proxies. Implications for the global alkalinity cycle and the evolution of ocean alkalinity will be discussed.

References: [1] Stumm and Morgan (1981).

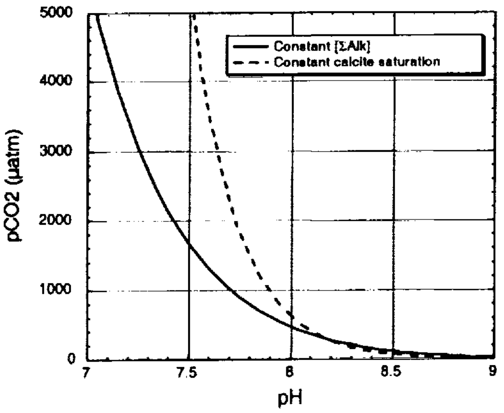

Fig. 1.

PLATINUM-GROUP-ELEMENT MICROANALYSIS OF ORDINARY CHONDRITE METAL GRAINS BY LASER ABLATION INDUCTIVELY COUPLED PLASMA MASS SPECTROMETRY.

A. J. Campbell and M. Humayun, Department of the Geophysical Sciences, University of Chicago, 5734 S. Ellis Avenue, Chicago IL 60637, USA (acampbel@midway.uchicago.edu).

Introduction: Platinum-group-element abundances in metal grains in ordinary chondrites have been measured using laser-ablation inductively coupled plasma mass spectrometery (LA-ICP-MS). An effort was made to determine the microdistribution of Re and Os in ordinary chondrite metal, knowledge of which is critical to the interpretation of ^{187}Re-^{187}Os ages and of chondrite genesis [1]. Relative abundances of Re, Os, Ir, and Pt in metallic grains in the Weston H4 and Soko-Banja LL4 chondrites are reported here.

Experimental: Specimens were polished and examined by scanning electron microscopy (SEM) to select grains for microanalysis by LA-ICP-MS. Inclusion-free, single-phase regions of metallic grains were chosen. Six grains of Weston metal, seven in Soko-Banja, and three in Allegan H5 have been analyzed to date.

A CETAC LSX-200 laser ablation peripheral was used for solid-sample introduction into a magnetic sector ICP mass spectrometer, the Finnigan MAT Element [2]. Each point on the sample was analyzed by three successive 15-pulse laser bursts; the laser-ablated pit produced was ~50 µm in diameter and 25 µm deep. The isotopes monitored were ^{57}Fe, ^{59}Co, ^{60}Ni, ^{102}Ru, ^{103}Rh, ^{105}Pd, ^{187}Re, ^{192}Os, ^{193}Ir, ^{195}Pt, and ^{197}Au. Instrumental sensitivity factors for each isotope were determined by measuring signal intensity from the ataxite Hoba, which has known concentrations of the elements of interest [3]. In the analyses discussed below, a smaller mass range, ^{187}Re to ^{195}Pt, was analyzed to enhance the precision (typically 3.5%) with which relative abundances of the HPGEs were determined. In this mode of analysis the absolute concentrations were determined using external calibration of the signal intensities, which was accurate only to within a factor of 1.5 or better.

Results and Discussion: Weston matrix kamacite grains were found to contain siderophile elements in approximately chondritic relative proportions, within a factor of 2. Soko-Banja matrix metal was observed to have a wider

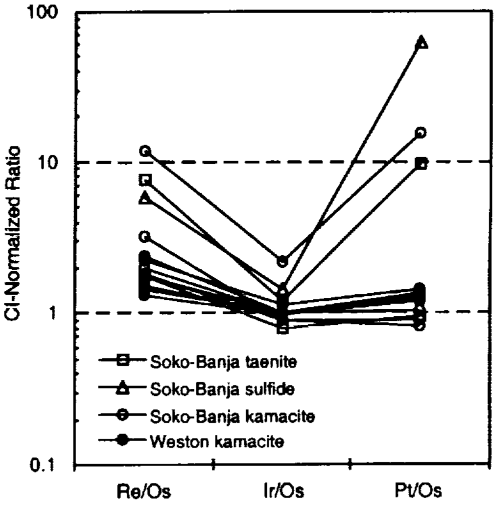

Fig. 1. HPGE ratios in Soko-Banja LL4 and Weston H4 matrix metal grains.

range of PGE concentrations; for example, Os concentrations ranged from about 0.08× chondritic to 16× chondritic. In Allegan, chondrule metal and matrix metal showed similar PGE concentrations.

The relative HPGE abundances are presented in Fig. 1, which shows CI-normalized Re/Os, Ir/Os, and Pt/Os ratios for different matrix metal grains in Soko-Banja and Weston. Errors are smaller than the symbols in this figure for most data, except ~20% errors on the three Soko-Banja grains that show high Re/Os ratios, and that had low PGE concentrations.

The normalized Ir/Os (0.98–1.15) and Pt/Os (1.19–1.46) ratios in Weston show a limited range of values among the six analyses in Fig. 1. The normalized Re/Os ratios in Weston, in contrast, have a broader range of 1.33–2.39. All of the Re/Os values in Weston kamacite are well above the CI value; this is consistent with the observation by Chen et al. [1] that Re is enriched with respect to Os in the metal fraction of ordinary chondrites, and suggests the presence of a low-Re/Os phase not yet identified.

Four of the Soko-Banja metal analyses in Fig. 1 exhibit patterns similar to those observed in Weston. The Ir/Os and Pt/Os ratios cluster around CI values, and the Re/Os values are systematically superchondritic and show a greater range. The other three grains in Soko-Banja had higher Re/Os, Ir/Os, and Pt/Os ratios, and low PGE concentrations. This PGE signature is understandable for the sulfide grain, but it is unusual for kamacite and taenite to exhibit low PGE concentrations and PGE patterns similar to those observed in sulfide (Fig. 1). It is conceivable that these metal grains were produced by decomposition of sulfides, and that they retained the original sulfide PGE signatures. An analogous dephosphidization of a metallic grain has been documented in CAI metal [4]. However, no further evidence of such a history for the Soko-Banja grains was obtained from petrographic study of the sample.

References: [1] Chen J. H. et al. (1998) *GCA, 62,* 3379–3392. [2] Campbell A. J. and Humayun M. (1999) *Anal. Chem., 71,* 939–946. [3] Campbell A. J. and Humayun M. (1999) *LPS XXX,* Abstract #1974. [4] Campbell A. J. et al. (1999) *LPS XXX,* Abstract #1609.

VERTICAL AND LATITUDINAL VARIATION OF GEOCHEMICAL COMPOSITION OF MARINE PARTICLES OFF TASMANIA: ROLE OF ADVECTIVE, BIOLOGICAL, AND AUTHIGENIC PROCESSES.

D. Cardinal[1], T. Cattaldo[2], M. Elskens[2], F. Dehairs[2], and L. André[1], [1]Department of Geology, Royal Museum for Central Africa, Leuvensesteenweg 13, B 3080 Tervuren, Belgium (geochim@africamuseum.be), [2]Department of Analytical Chemistry, Vrije Universiteit Brussel, ANCH, Pleinlaan 2, 1050 Brussels, Belgium (fdehairs@vub.ac.be).

Introduction: For a better understanding of global change, the quantification of its biological activity variations trough past in the Southern Ocean is essential. To reconstruct past productivity, Ba in sediment has been proposed as a proxy [e.g., 1]. However, the link between particulate Ba and productivity remains unclear. Moreover, lateral advection can disturb the vertical particles flux, especially in margin areas [2]. To assess particulate Ba (Ba$_p$) settling trough water column and latitude in the Southern Ocean, we focused our study on the comparison of Ba with elements used as indicators of oceanic processes (e.g., Al, Th, REEs for advection, and Ca, P, and Sr for surface biology).

Material and Methods: A latitudinal transect (42°S–54°S; 141°E) off Tasmania was studied during SAZ-98 cruise (R/V Aurora Australis). Suspended matter was sampled using 12-L Niskin bottles in the upper water column (surface to 600 m) and filtered in Perspex filtration units on polycarbonate filters (0.4 µm). Filtered material was dissolved by a tri-acid digestion of filters in Teflon beakers overnight at 90°C. REEs, Ba, Sr, U, Zr, and Th were then analyzed by inductively coupled plasma mass spectrometry (ICPMS) (VG PQ2 Plus) and major elements (except Si) by inductively coupled plasma-atomic emission spectrometry (ICP-AES) (Thermogroup Iris).

Results and Discussion: Some general features have been identified. Particulate Ba (Ba$_p$) vs. depth has the usual pattern observed in such samples: it increases from surface to subsurface up to a broad maximum (~200–400 m) and then remains constant or slightly decreases [e.g., 3]. This pattern emphasizes a clear decoupling between Ba and all other elements. Depletion of particulate Ce is higher for surface samples (i.e., lower Ce anomaly) and slowly disappears through depth to reach 1. It highlights the more detritic nature of particles at depth due to mineralization of biogenic particles in the upper water column. For the same reason, biogenic major elements (e.g., K, P, Mg, Na, and Ca) contents have lower concentrations in deeper samples compared to surface samples. The profile at 45°S forms an exception in that here there is a strong signal of detritic matter at depth (see further below).

We also observe a latitudinal trend, with lower Ca and higher Ba-bio (particulate Ba corrected from Ba of detritral origin) from north to south. Latitudinal variations of mesopelagic Ba-bio (weighted average Ba-bio concentration between 150 and 600 m), are in good agreement with new production as evidenced by f-ratio (ratio of NO_3 uptake to the uptake of all N sources).

However, locally element distribution can differ considerably from these general patterns. This is the case at 45°S. This station is of particular interest as it is situated within the Subtropical Front Zone and is close to Tasmania. An enhancement of detrital element contents (Al, Fe, REEs, Zr, and Th) at 45°S deeper samples is paralleled by a higher content of Ba-bio. We suspect that Ba does not come exclusively from biological productivity in local surface water but is supplied from elsewhere by advection. Presence or absence of advective input is indicated by the comparison of Ba-bio/Th ratio with Ba-bio content [3]: an increase of the latter without an increase of the former identifies advective supply of Ba-bio.

Conclusion: Correlation between Ba$_p$ and biological productivity in the area studied is quite good. It confirms the usefulness of Ba as an oceanic paleoproductivity proxy. Nevertheless, the comparison of Ba with other elements can identify some local features such as lateral advection. Thus, looking at the distribution of elemental particle compositions gives better insight into the different mechanisms controlling sedimentation process.

References: [1] Dymond J. et al. (1992) *Paleoceanogr., 7,* 163–181. [2] Fagel N. et al. (1999) *GCA,* accepted. [3] Dehairs F. et al. (1997) *Deep-Sea Res. II, 44,* 497–516.

ONLINE MATRIX SEPARATION FOR ANALYSIS OF RARE EARTH ELEMENTS USING INDUCTIVELY COUPLED PLASMA MASS SPECTROMETRY: APPLICATIONS TO CONTINENTAL WATERS.

J. Carignan and D. Yeghicheyan, Centre de Recherches Pétrographiques et Géochimiques–Centre National de la Recherche Scientifique, 15 rue Notre Dame des Pauvres, BP 20, 54501 Vandoeuvre-les-Nancy, France (carignan@crpg.cnrs-nancy.fr).

The dissolved (water sample filtered to <0.45 µm) REE content in continental waters may be highly variable but is generally very low, ranging between a few parts per trillion to hundreds of parts per trillion. Analytically, the parts-per-trillion level for REE is easily reached with the new generation of inductively coupled plasma mass spectrometers (ICP-MS). The main analytical problems are matrix effects and, mostly, isobaric refractory oxides that may form in the plasma torch. In the case of natural waters, the most important mass interference is Ba oxide (BaO). As the Ba/Eu and Ba/Sm ratios may reach 50,000 in some river waters, the interfering BaO may contribute to more than 95% of the signal on ^{153}Eu and ^{152}Sm masses.

We have compared results obtained on river waters using a direct injection of the sample in the ICP-MS (with subsequent corrections for interferences) with results obtained on the same samples using an "online" matrix separation. For the direct injection samples, solutions having 100 ppb Ba and 10 ppt REE were used as control for the accuracy of the interference corrections calculated for Sm and Eu. If the corrected value for the standard solution exceeded 20% away from the true value (10 ppt), results from the sample injected between the two controls were rejected. The RSD for Eu concentration for all the results obtained on the standard solution is better than 15%, and the accuracy is acceptable (average corrected concentration of 10.6 ppt). RSD values (n = 3–4) for river water samples vary between 10 and 75% for concentrations of 0.7–3 ppt Eu and 2–20 ppt Sm. RSD values for other REE generally range from 1 to 10%.

The "online" matrix extraction is performed with a computer-controlled peristaltic pump and valves using liquid chromatography. Conditioning of the column, sample loading (2 mL), washing, and elution of REE are done automatically. External calibration is used (500 ppt REE solution) and is

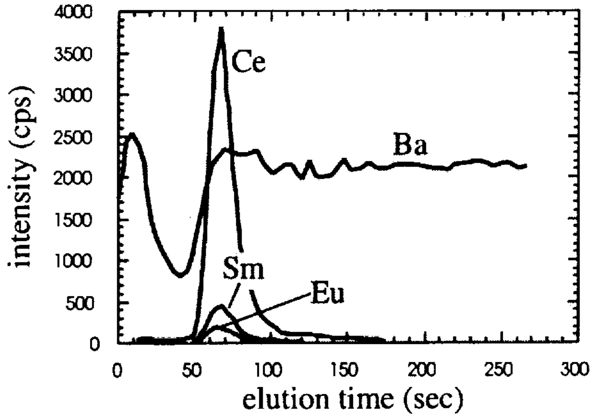

Fig. 1. Elution of REE and Ba after matrix separation.

repeated every three to four samples. The drift between each calibration is negligible. The depollution of the column from one sample to another is better than 99.3% for all REE and the whole procedure lasts for 15 min.

Elution peaks show that between 99.7 and 100% of the Ba is eliminated during the washing of the column (Fig. 1). The remaining Ba, if present, introduces a BaO interference of less than 5 counts/s, corresponding to sub-parts-per-trillion Eu and Sm. This contribution is less important than the standard deviation obtained for Eu and Sm concentrations and is considered negligible in most cases. A standard solution containing 10 ppt REE and 200 ppb Ba yielded relatively good accuracy for both Sm (9.76) and Eu (9.33). Furthermore, Sm (60 ppt) and Eu (8 ppt) concentrations measured for a natural river water standard (SLRS-4) containing 12.2 ppb Ba and for a SLRS-4 sample doped with Ba (~200 ppb equivalent) overlap within error (5–10%). For other river water samples, the RSD values for Eu concentrations ranging from 1 to 8 ppt vary from 5 to 20%.

Results obtained by direct injection and by matrix separation compare within error (5–15%) for most REE, including Sm and Eu. However, while most samples show a negative Eu anomaly when looking at data obtained from the direct injection method, these anomalies are much smaller or absent with data obtained from the matrix extraction method.

The online matrix separation before REE analysis with ICP-MS is a rapid method with very low sample consumption (2 mL) compared to the direct injection method (5–15 mL). The absence of BaO interference on Sm and Eu leads to more accurate measurements of these elements for sample having very high Ba/Sm and Ba/Eu ratios such as river waters.

OXYGEN ISOTOPES OF ECLOGITES FROM THE ORAPA KIMBERLITE (BOTSWANA): POSSIBLE ORIGINS.

P. Cartigny[1], K. S. Viljoen[2], and G. Wörner[1], [1]Geochemiches Institut der Universität Göttingen, Goldschmidtstrasse 1, 37077 Göttingen, Germany (pcharti@ugcvax.dnet.gwdg.de; gwoerne@gwdg.de), [2]De Beers Geoscience Center, P.O. Box 82232, Southdale 2135, South Africa (fviljoen@mhs7.tns.co.za).

Introduction: Xenoliths in kimberlites are our best window into the deep (i.e., >150 km) subcontinental mantle. Although generally rare, eclogites, bimineralic rocks constituted of omphacitic pyroxene and garnet, are ubiquitous. There is no consensus concerning their origin(s) and it was suggested that eclogites either represent pieces of Archean-recycled oceanic crust [e.g., 1] or mantle-derived melts [e.g., 2]. It was also suggested that eclogites are the residue after extraction of melts of tonalite-trondhjemite-granodiorite (TTG) composition that make part of the Archean crust [e.g., 3]. Recycled ocean- crust-derived eclogites were also invoked to account for the characteristics of the missing reservoir required for elemental and isotopic mass balance between depleted mantle and crust [4].

In understanding the origin of eclogites, O stable isotopic composition plays the central role. It is generally argued that eclogites have $\delta^{18}O$ values (from 2 to 90 vs. SMOW) that fall outside the *mantle* range (i.e., 5.5 ± 0.5‰). On the contrary, this $\delta^{18}O$-range is similar to that produced during hydrothermal alteration of the oceanic crust. However, if the range quoted above is valid for a mine like Roberts Victor, other mines yield more restricted $\delta^{18}O$ ranges, generally below 3‰, most of the $\delta^{18}O$ values being contained within the mantle-range [e.g., 1,5].

In fact, there are limited O-isotopic data coupled with major- and trace-element chemistry, most being generally obtained on one type of eclogite (i.e., eclogites of group I with or without diamond or of group II).

Samples and Methods: In order to better constrain O-isotopic variability in eclogites, we selected a series of 120 eclogites from Orapa (Botswana). Orapa is known to display samples covering a great range of $\delta^{18}O$ values [6]. The sample set is composed of eclogites belonging to group 1 (Na_2O in gt >0.09 wt% [7], 33 diamond-bearing and 56 non-diamond-bearing rocks) and group 2 (Na_2O in gt <0.09 wt% [7], non-diamond-bearing, 31 samples). Non-diamond-bearing samples are generally 2–3 cm in size, diamond-bearing samples being smaller. Samples are generally very fresh, allowing, in most cases, O isotopes of both clinopyroxenes and garnets to be investigated. Oxygen isotopes are analyzed by continuous-flow mass spectrometry, after extraction with UV-laser ablation [8] (spot around 300 μm), a technique allowing intrasample heterogeneity and isotopic equilibrium between minerals to be investigated.

Results: Major-element analyses have now been obtained on the whole eclogite collection. Eclogite chemistry is best reflected in the garnet composition. Diamondiferous eclogites show striking similarities with diamond inclusions. Nondiamondiferous group I and, even more, group II eclogites are more Ca-rich than diamondiferous samples. High-MgO eclogites (up to 17 wt% MgO) are present in every (i.e., including diamondiferous), type of eclogites.

Oxygen isotopes were measured on single mineral grains from 25 eclogites (diamond and non-diamond-bearing) eclogites. $\delta^{18}O$ values range from 5.0 to 8.30, most (i.e., 80%) being contained within the mantle range and no obvious low $\delta^{18}O$ values (<5.0‰) have been measured yet. Whereas several analyses of a single mineral grain gave reproducible $\delta^{18}O$ values, analyses of different grains from the same nodule suggest variations of about 1‰. Such an heterogeneity is surprising if one assumes that the nodules stayed billions of years at mantle temperatures. We therefore try to consider if a secondary process could affect eclogite $\delta^{18}O$ values. To better constrain this question we are presently obtaining trace-element data by laser-ablation ICP-MS. Also, a zonation cannot be rigorously demonstrated within the present set of data; accordingly, $\delta^{18}O$ values are going to be measured directly along profiles on thick sections.

Garnet $\delta^{18}O$ values roughly correlate negatively with Mg numbers. In other words, high MgO-eclogites yield mantlelike $\delta^{18}O$ values. Such a correlation is surprising since low hydrothermal alteration that produces the ^{18}O-enrichment is rather associated with Mg enrichment. It could be suggested that the Orapa kimberlite sampled several populations of eclogites nodules. It is expected that the analysis of trace-element data will allow to reveal or rule out the possibility of any genetical link between high and low MgO eclogites.

References: [1] Jacob D. et al. (1994) *GCA, 58,* 1151–1154. [2] Fung A. and Haggerty S. H., *JGR, 100,* 20451–20473. [3] Ireland T. et al. (1994) *EPSL, 128,* 199–213. [4] Blichert-Toft J. and Albarède F. (1997) *EPSL, 148,* 243–258. [5] Barth M. et al. (1997) *7th Intl. Kimberlites Conf. Ext. Abstr.,* Vol. 52–54. [6] Deines et al. (1991) *GCA, 55,* 515–524. [7] McCandless T. and Gurney J. J. (1989) in *Kimberlites and Related Rocks, Vol 2,* 827–832. [8] Wiechert U. and Hoefs J., *GCA, 59,* 4093–4101.

RECONSTRUCTING THE PALEOTOPOGRAPHY OF MOUNTAIN BELTS FROM THE ISOTOPIC COMPOSITION OF AUTHIGENIC MINERALS.

C. P. Chamberlain[1] and M. A. Poage[1], [1]Department of Earth Sciences, Dartmouth College, Hanover NH, USA.

The paleotopography of mountain belts can be reconstructed from the O-isotopic composition of authigenic minerals. The development of topography often creates strong rain shadows on the lee side of mountain belts, which in turn creates large isotopic depletions of ^{18}O and D in precipitation. The magnitude of the "rain shadow effect" is strongly correlated to topography. Our analysis of O isotopes from surface waters throughout the globe show a linear relationship between net elevation and the change in $\delta^{18}O$ of surface waters ($R^2 = 0.79$).

Using this relationship we have investigated both the timing and magnitude of elevation change in the Southern Alps of New Zealand, the Sierra Nevada Mountains of California, and the Himalayas. Our studies of O isotopes of kaolinites from New Zealand show a 6‰ decrease at the Early Pliocene, which corresponds to an ~2-km elevation change in the Southern Alps at this time. Oxygen isotope of smectites from the Sierra Nevada Mountains show little or no change in isotopic composition for the past 16 m.y. that suggests the Sierra Nevada Mountains have been a long-standing topographic feature.

ERUPTION OF THE BRITISH TERTIARY VOLCANIC PROVINCE IN APPROXIMATELY TWO MILLION YEARS DURING CHRON 26R.

L. M. Chambers[1] and M. S. Pringle[2], [1]Department of Geology and Geophysics, University of Edinburgh, West Mains Road, Edinburgh EH9 3JW, Scotland, UK (chamberl@glg.ed.ac.uk), [2]Scottish Universities Research and Reactor Centre, Scottish Enterprise Technology Park, East Kilbride G75 0QF, Scotland, UK (m.pringle@surrc.gla.ac.uk).

Introduction: New Ar/Ar ages on volcanic rock from the British Tertiary Volcanic Province (BTVP) suggest that the entire BTVP erupted in less than ~2 m.y. between 60.6 and 58.5 Ma, rather than in 11 m.y. between 63 and 52 Ma, as previously understood. According to existing geomagnetic reversal timescales (GRTS) [e.g., 1], this in entirely within Chron 26R.

Oldest Products: Stratigraphic constraints indicate that sanidine-bearing tuffs near the bottom of the lava sequence on the small isles of Muck and Eigg are among the oldest exposed products of the BVTP. Previous Ar/Ar work [2], based on two sanidine crystals separated from the tuffs, suggested an age of ~62.5 Ma, within Chron 27R. However, our analysis of nearly 60 individual sanidine crystals (e.g., Fig. 1), suggests instead that the tuffs are 60.6 ± 0.1 Ma with no sign of xenocrystic contamination. Even correcting for differences in standard ages used in the two studies, we suggest that the reported ages of [2] are too old, perhaps because of incomplete cleanup during analysis of their Ar/Ar standard, hornblende Mmhb-1.

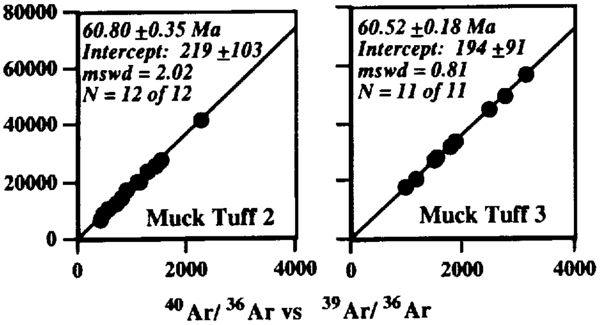

Fig. 1. Typical isochrons of sanidine from Muck.

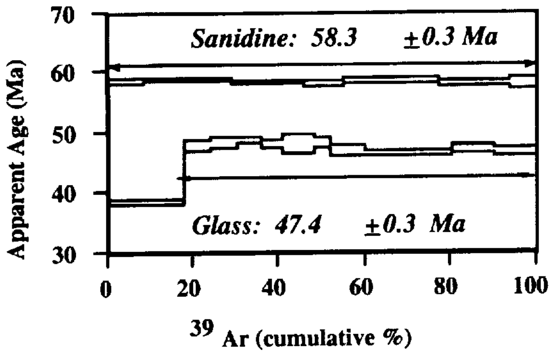

Fig. 2. Age spectra of the Sgurr of Eigg pitchstone.

Youngest Products: A post-erosional pitchstone from the Sgurr of Eigg had been thought to represent the youngest product produced by the BVTP, based on a feldspar and whole-rock (glass) Rb/Sr isochron age of 52.1 ± 1.0 Ma [3]. However, Ar/Ar age spectra on individual sanidine and petrographically fresh glass fragments (e.g., Fig. 2) show that the glass, at ~47 Ma, seems significantly younger than the sanidine, at ~58 Ma. We interpret the sanidine age as the best estimate of the crystallization age of the pitchstone. The younger glass Ar/Ar and Rb/Sr apparent ages are then the result of postcrystallization devitrification and alteration, may have no specific geologic significance, and indicate caution in relying on Ar/Ar ages of even apparently fresh glass without independent age control.

Geomagnetic Reversal Timescale Implications: Previous paleomagnetic studies have found a minimum of 7, and possibly 9, reversals in the BTVP sequence. Based on the Ar/Ar age constraints, at least some of these reversals must represent true normally magnetized cryptochrons within Chron 26R. If the current GRTS is correct, then the normally magnetized center 2 and 3 intrusive complexes of the Isle of Mull, as well as the early and late granites of the Western Red Hills (WRH) of the Isle of Skye, would have crystallized within the short (<20 k.y.?) periods of cryptochrons 26R.1r and 26R.2r, ~58.4 and 59.0 Ma. However, we consider it more likely that these complexes would have crystallized during the longer, normally magnetized period of Chron 26N, necessitating a significant revision of the GRTS. Also, the reversely magnetized Loch Ainort granite in the WRH sequence would then represent a reversely magnetized cryptochron within Chron 26N.

Absolute Calibration: The Ar/Ar ages reported here are relative to 27.92 Ma for the USGS sanidine standard 85G003; analyses of Cretaceous-Tertiary (K/T) boundary tektites during the course of this study average 64.8 ± 0.1 Ma. An initial comparison of our Ar/Ar ages with newly available U/Pb ages for the BVTP [e.g., 4] suggests that little inter-isotopic system correction is necessary. This is not consistent with other studies (based on, for example, calibration of Ar/Ar relative to astronomical time) that imply that the K/T boundary is as old as 66.0 Ma. Further work comparing modern Ar/Ar sanidine and U/Th/Pb zircon and titanite ages from products of the BVTP seems a very promising avenue for calibrating at least Ar/Ar and U/Th/Pb time.

References: [1] Cande and Kent (1995) *JGR, 100,* 6093–6095. [2] Pearson et al. (1996) *J. Geol. Soc. London, 153,* 815–818. [3] Dickin and Jones (1981) *J. Geol. Soc. London, 140,* 691–700. [4] Hamilton et al. (1998) *Nature, 394,* 260–263.

THE SOCIETY PLUME: ISOTOPES AND TRACE ELEMENTS ALONG THE CHAIN.

C. Chauvel[1,2], H. Guillou[3], S. Blais[2], G. Guille[4], R. Maury[5], and M. Caroff[5], [1]Laboratoire de Géodynamique des Chaînes Alpines, Institut Dolomieu, 15 rue M. Gignoux, F-38031 Grenoble Cédex, France (cchauvel@ujf-grenoble.fr), [2]Géosciences Rennes, Beaulieu, 35042 Rennes Cedex, France, [3]LSCE, 91198 Gif-sur-Yvette Cedex, France, [4]CEA/DASE, BP 12 91680 Bruyères-le-Châtel, France, [5]Domaines Océaniques, UBO, BP 809, 29285 Brest, France.

The Society Islands are famous for their radiogenic Sr-isotopic compositions that define the EM II component in plumes. However, previous work [e.g., 1–3] has shown that isotopic compositions in the Society islands in fact vary widely and that all islands are not characterized by elevated $^{87}Sr/^{86}Sr$. To better understand the composition of the plume and its origin, a systematic study including major and trace elements, isotopes, and dating of the various islands was necessary. We present new data obtained for Maupiti, Raiatea, Bora Bora, and Huahine islands, which all belong to the oldest volcanic events along the chain. These new data, used in conjunction with data already published in the literature, help understanding the nature of the EM II component present in many intraplate volcanism and its relationship to other compositions sampled by plumes.

New isotopic data obtained for basalts from the four islands have a wide range of compositions: $^{87}Sr/^{86}Sr$ ranges from 0.7038 to 0.7058, $^{143}Nd/^{144}Nd$

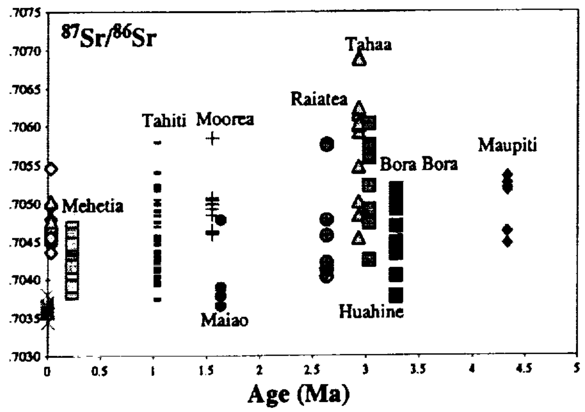

Fig. 1.

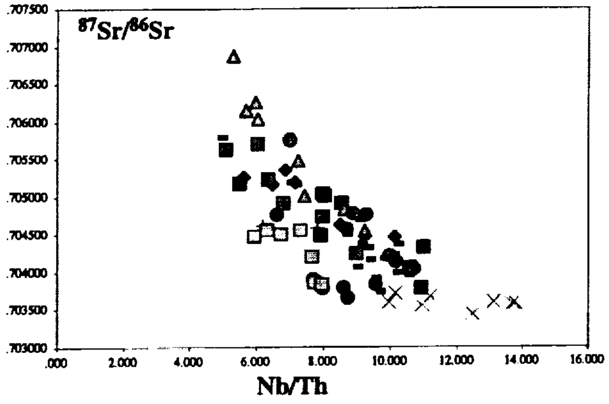

Fig. 2.

from 0.51266 to 0.51298, and $^{206}Pb/^{204}Pb$ from 18.80 to 19.20. In addition, variations are almost as large within a single island as between islands. This suggests that the plume source is isotopically heterogeneous at the scale of a single island. However, no obvious systematic evolution through time along the whole chain can be seen. The only general tendency is that the youngest island, Mehetia, and the active seamounts, have a smaller range of isotopic compositions than the older islands (see Fig. 1).

New trace-element data confirm the systematically low Ce/Pb ratios of the Society lavas. In Maupiti, Ce/Pb are very low and cluster around 17. Bora Bora basalts as well as Raiatea and Huahine basalts have higher and more variable ratios ranging from 18 to 28. Niobium/thorium ratios are also low with values generally less than 10. These values correlate with $^{87}Sr/^{86}Sr$ suggesting that the source component enriched in radiogenic Sr has very low Nb/Th (≈5).

The chemical trends defined by the Society islands can be generally interpreted in terms of melting of an heterogeneous plume source because the variability of trace-element ratios and isotopic compositions is as large at the island scale as at the chain scale. The main characteristics of the radiogenic Sr end member of the source are low Ce/Pb (<17), low Nb/Th (<6), but also low Sm/Hf (<1.3). These characteristics are typical of continental crust material and probably originate from sediment in the source. The existence of low Sm/Hf ratio associated to the elevated $^{87}Sr/^{86}Sr$ and low Nb/Th suggests, in addition, that the sediments have a detrital origin and that their trace-element pattern is controlled by the presence of zircon.

The oldest islands have the most extreme compositions, closest to EMII. This might indicate that the sediment component of the source region has been slowly consumed as melting proceeded in the plume.

References: [1] White W. M. and Hofmann A. W. (1982) *Nature, 296,* 821–825. [2] White W. M. and Duncan R. A. (1996) in *Earth Processes Reading the Isotopic Code* (A. Basu and S. Hart, eds.), pp. 183–206, Geophysical Monograph 95, American Geophysical Union, Washington. [3] Hémond C. et al. (1994) *Chem. Geol., 115,* 7–45.

NEODYMIUM-HAFNIUM-ISOTOPIC COMPOSITIONS OF ALUMINUM-DEPLETED AND ALUMINUM-UNDEPLETED KOMATIITES OF THE KOMATI FORMATION (SOUTH AFRICA).

V. Chavagnac[1], S. W. Parman[1], R. W. Carlson[2], J. C. Dann[1], T. L. Grove[1], and S. A. Bowring[1], [1]Department of Earth, Atmospheric and Planetary Sciences, Massachussetts Institute of Technology, Cambridge MA 02139, USA (vchava@mit.edu; jcdann@mit.edu; tlgrove@mit.edu; sbowring@mit.edu), [2]Department of Terrestrial Magnetism, Carnegie Institution of Washington, Washington DC 20015, USA (carlson@dtm.ciw.edu).

Introduction: Komatiites are high-magnesium igneous rocks that provide an opportunity to look at the primary chemical features of the oldest preserved mafic-ultramafic sequences of the Earth. They bear information on the conditions of melt generation in the Archean mantle. The 3.45-Ga Barberton komatiites are characterized by low Al_2O_3/TiO_2 ratios and HREE depletion that are typical features of the Al-depleted type [1]. Their special chemical signatures have been previously interpreted as the consequences of either garnet depletion [2,3] or garnet fractionation during the melting [1,4]. We report new geochemical and Sm-Nd-isotopic analyses on all units of the Komati Formation from the Barberton greenstone belt in order to (1) examine the primary chemical features of the Archean mantle, (2) constrain the Nd-Hf-isotopic compositions of the Archean mantle, and (3) determine the conditions and tectonic setting of melt generation. Samples were selected to maximize the abundance of original igneous minerals.

Geological Setting: The Barberton greenstone belt is on the eastern edge of the Kaapvaal Craton (South Africa). It is subdivided into three lithostratigraphic units: (1) the Onverwacht group, (2) the Fig Tree group, and (3) the Moodies group [5]. Our samples are peridotitic komatiite from several units of the Komati Formation in the Lower Onverwacht group. The metamorphic grade ranges from upper greenschist to amphibolite facies.

Results: Komatiites from the first unit are characterized by high Al_2O_3/TiO_2 ratios (>15), low CaO/Al_2O_3 ratios (~1.1–1.5), and chondritic HREE contents ($(Gd/Yb)_N$ ~1) in contrast to the Al_2O_3/TiO_2 ratios ~10, and the $(Gd/Yb)_N$ >1.4 reported by [6]. The second and fourth units show Al-depletion

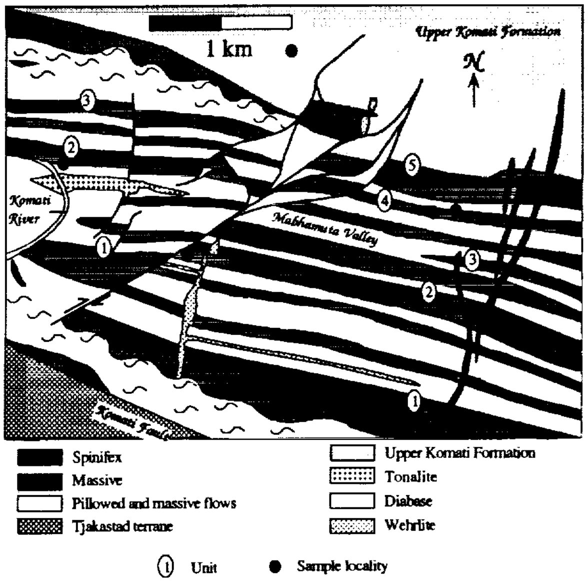

Fig. 1.

(Al_2O_3/TiO_2 ~10), highly variable CaO/Al_2O_3 ratios (0.2–2.8), and fractionated HREE patterns ($(Gd/Yb)_N$ ~1.4). The concentrations of incompatible elements indicate that the second and fourth units are depleted in Th, Zr, Hf, Nb, and LREE ($(La/Sm)_N$ ~0.8–1.1) whereas the first unit presents nearly chondritic $(La/Sm)_N$ ratios (~1–1.1) and small negative Hf/Hf*, Zr/Zr*, and Nb/Nb* anomalies.

Samarium-147/neodymium-144 ratios of all komatiite whole rocks range from 0.1755 to 0.1988 related to the variations in $^{143}Nd/^{144}Nd$ ratios between 0.512265 to 0.512746. Initial ε_{Nd} values vary from 1.2 to 2.4, with one exception at –1.4. The $\varepsilon_{Nd}(3.45)$ range is slightly smaller than previous Nd-isotopic studies of the Barberton komatiites and our values begin at the high end of previous studies and extend to higher initial ε_{Nd}. Lutetium-hafnium isotopic measurements of komatiites are in progress.

Discussion: First, similar trace-element patterns on each unit indicate that alteration and metamorphism effects have been minor. Second, Nb concentrations do not correlate with $(La/Sm)_N$ ratios sugggesting that crustal contamination may not have influenced the compositions of samples. Finally, $\varepsilon_{Nd}(3.45)$ do not correlate with CaO/Al_2O_3, Al_2O_3/TiO_2, and $(Gd/Yb)_N$ ratios indicating that the geochemical features are not related to mantle source composition, crustal contamination or possible input from slab-derived fluid-melt. Instead, the compositional characteristics reflect variable conditions-degrees of partial melting. Hafnium-isotopic compositions may help to determine whether the observed range in initial Nd-isotopic compositions reflect source heterogeneity or alteration-metamorphism.

References: [1] Sun S. S. and Nesbitt R. W. (1978) *CMP, 65,* 301–325. [2] Cawthorn R. G and Strong (1975) *EPSL, 23,* 369–375. [3] Ohtani et al. (1989) *CMP, 103,* 263–269. [4] Green D. H. (1975) *GCA, 3,* 15–18. [5] Lowe D. R. (1994) *Geology, 14,* 1099–1102. [6] Lahaye Y. et al. (1995) *Chem. Geol., 126,* 43–65.

EFFECT OF OXALATE ON THE SIDEROPHORE-PROMOTED DISSOLUTION OF GOETHITE.

S.-F. Cheah and G. Sposito, Ecosystem Sciences Division, Department of Environmental Science, Policy, and Management, Hilgard Hall #3110, University of California at Berkeley, Berkeley CA 94720-3110, USA (sfcheah@nature.berkeley.edu; gsposito@nature.berkeley.edu).

Introduction: Siderophores are Fe-specific ligands synthesized by microorganisms to acquire Fe under aerobic conditions. The effect of siderophores on iron oxide/oxyhydroxide dissolution (Fe release) kinetics in the presence of other natural organic ligands is not known. Such information is important for an understanding of biogeochemical cycling of Fe and as fundamental background information essential for determination of the effect of siderophores on metal transport. In this study, we investigated the influence of oxalic acid on the dissolution kinetics of goethite in the presence of a trihydroxamate siderophore, Desferrioxamine B (DFO-B). DFO-B is a siderophore synthesized by fungi and bacteria, and oxalic acid is one of the most common biologically produced organic acids in soil environments.

It has been generally assumed that ligand promoted dissolution in multiple ligand systems proceeds via independent pathways, summarized by the following equation [1]:

$$R_{total} = R_H + R_{ligand\ 1} + R_{ligand\ 2} + R_{ligand\ 3} + \cdots$$

Mineral dissolution in systems containing more than one ligand (other than OH^-) has been studied only in a small number of systems. In at least two of the systems studied, the presence of a second ligand led to synergistic effects in dissolution [2,3]. For these systems, the dissolution reactions do not proceed via independent pathways. Further research into multiple ligand system is therefore important for understanding surface reaction dynamics and mechanisms. It is also important to enhance our ability to describe dissolution reactions in natural environments, where the presence of multiple ligands is the norm.

Experimental: Continuous-flow stirred-tank reactors were used in the dissolution experiments. The reactors were immersed in a constant temperature water bath at 25°C, with the entire apparatus wrapped in aluminum foil to exclude light during the experiments. A 0.025-µm mixed cellulose acetate filter (Millipore) was placed at the bottom of each reactor to contain the goethite sample. The concentration of the goethite suspension was 10.0 g/L. Stirring speed was determined using a stroboscope and was maintained at approximately 500 rpm. The reactor flow rate was controlled using a variable speed peristaltic pump. The composition of the influent solution was 0.01 M $NaClO_4$, 5 mM MOPS buffer, and fixed ligand concentrations. The effluent pH was measured with an ORION ROSS combination electrode. Total dissolved Fe in the effluent solution was measured using inductively coupled plasma-atomic emission spectrometry (ICP-AES). The dissolution rate is then calculated as

$$R_{net} = 1/m \times [Fe]_{out} \times q/V$$

where m = mass of goethite; q = reactor flow rate; V = volume of reactor (V/q = residence time of the solution in the reactor); and $[Fe]_{out}$ is the Fe concentration in the effluent solution.

Results and Discussion: At pH of ~5, and in DFO-B alone, the goethite dissolution rate roughly paralleled the adsorption isotherm of DFO-B on goethite. This correspondence indicates that the dissolution rate is a function of adsorbed DFO-B concentration and that dissolution is via a ligand-promoted dissolution mechanism. In oxalic acid alone, the dissolution rates were negligible below 100 µM and began to increase linearly above 100 µM. This result suggests that, for oxalate, a critical concentration of ligand on the surface is necessary for ligand-promoted dissolution to be effective. In systems containing both oxalic acid and DFO-B, the dissolution rates were significantly higher than those obtained by simply adding the goethite dissolution rates for each ligand alone. This result suggests a synergistic effect between the two ligands in promoting goethite dissolution. We shall be conducting ligand adsorption experiments to help interpret our dissolution results.

Acknowledgments: S.-F. Cheah expresses gratitude to S. Kraemer for technical advice. Support by DOE grant DE-FG03-96ER14667 is appreciated.

References: [1] Zinder B. et al. (1986) *GCA, 50,* 1861–1869. [2] Banwart S. et al. (1989) *Colloid Surfaces, 39,* 303–309. [3] Kraemer S. M. et al. (1998) *ES&T, 32,* 2876–2882.

ISOTOPIC SYSTEMATICS IN PORTALES VALLEY.

J. H. Chen, D. A. Papanastassiou, and G. J. Wasserburg, Mail Code 170-25, Charles Arms Laboratory, Division of Geological and Planetary Sciences, California Institute of Technology, Pasadena CA 91125, USA (jchen@gps.caltech.edu).

Portales Valley is a recent meteorite fall consisting of a unique combination of an ordinary chondrite (H6) and of cross-cutting FeNi veins [1,2]. We have reported Re-Os and Pd-Ag data on Portales Valley (PV) and compared the isotope systematics with those of iron meteorites and of ordinary chondrites [3–7]. The unusual presence of massive FeNi veins in PV provides a unique opportunity to compare the Re-Os systematics in FeNi with lithophile parent-daughter systems. We present additional Re-Os on massive FeNi veins and new Rb-Sr, Sm-Nd, and U-Pb data on whole-rock (WR) samples of the chondritic portion.

Rhenium-Osmium: The ordinary chondrite Re-Os data plot close to the well-defined iron isochron, although the deviations found for ordinary chondrites are slightly larger than found for the irons. The Re-Os whole-rock isochron of irons gives the time of fractional crystallization of metal segregating into cores and pods in early planetary bodies. All "massive" metal from three different PV slabs plots within the area for H-chondrites, and slightly below the iron meteorite isochron. The data show a distinct range in $^{187}Os/^{188}Os$ and $^{187}Re/^{188}Os$, along the iron isochron, and are consistent with early formation. In contrast, the silicate-rich material and thin metal veins lie far to the right of this isochron and along a horizontal line, indicating recent redistribution of Re-Os in the chondrite breccia.

Palladium-Silver: Silver-107 excesses ($^{107}Ag^*$) are present in a wide range of iron and stony-iron meteorites with high Pd/Ag [7]. In chondrites and group IA irons, all with low Pd/Ag ratios, no $^{107}Ag^*$ is present. We determined Pd-Ag in a massive metal vein of PV [4]. Palladium-108/silver-109 in PV (~240) is close to those for group II irons, which show $^{107}Ag^*$, but in PV ^{107}Ag is normal (–0.2 ± 2.8‰). Portales Valley metal has a solar Pd/Ni and ~10^2 lower Ag/Ni. This indicates that the parent source of PV metal did not have live ^{107}Pd when it formed and that the Pd/Ag enrichment in PV metal occurred late (~10 Ma) relative to the IIAB, IIIAB, and IVA irons, consistent with the absence of ^{142}Nd effects (see below).

Rubidium-Strontium and Samarium-Neodymium: A WR silicate sample away from metal veins was prepared. The sample was leached gently in warm, dilute HCl (10 min). In contrast to mesosiderites, the leach does not contain large fractions (only 1–3%) of these elements, and indicates that the sample did not contain significant phosphates. The silicate-rich WR is an open system for Rb-Sr (T_{BABI} = 5.22 AE). Rubidium/strontium and ^{87}Sr/^{86}Sr are consistent with chondritic values, but the Sr concentration is a factor of ~5 higher than in typical chondrites. Neodymium and Sm are also highly enriched, but Sm/Nd ($f_{Sm/Nd} = -0.74$) is highly depleted relative to chondrites. Consistent with low Sm/Nd, ^{143}Nd/^{144}Nd in PV is $\varepsilon = -21.5$ εu, far below the chondritic present value (ε^{143}Nd = 0). We calculate, for Sm-Nd, T_{CHUR} = 3.37 AE. There is no evidence for ^{142}Nd effects. In summary, the silicate portion of PV is highly fractionated in lithophiles and not a typical chondritic material. The data also show open-system behavior, extending to young times.

Uranium-Thorium-Lead: A portion of the silicate-rich WR sample was leached with warm dilute HCl and HBr (L1) and then HNO_3 (L2). The residue has not been analyzed. L1 and L2 have similar and moderately radiogenic Pb-isotopic composition (α ~29). L1 has high (~47); L2 has low (~0.9). The data define a ^{207}Pb/^{206}Pb age of ~4.51 AE, indicative of early formation.

In summary, Re-Os and U-Pb suggest an early formation for the metal and the chondrite-dominated portion. Palladium-silver and ^{146}Sm-^{142}Nd indicate slightly late formation, and Rb-Sr and ^{147}Sm-^{143}Nd require a much younger event, associated with substantial Rb/Sr and Sm/Nd fractionation and large enrichments in the lithophile elements. For the formation of PV, we require the injection of molten metal with the preservation of a range of Re/Os but without significant Re/Os fractionation for events after ~4.5 AE. Based on Sm-Nd we also require melting of a portion of the chondritic silicates and strong enrichment of lithophile elements. The low Sm/Nd would be consistent with the preferential melting and injection of feldspar-rich material. This event would postdate the Sm-Nd T_{CHUR} model age and could be recent. A relatively recent event would be consistent with preserving the Pb-Pb model age. This scenario can provide a consistent formation at recent times by impact melting and injection of both the metal and silicate portions. The only significant conflict is the relatively old (4.5 AE) ^{40}Ar-^{39}Ar age determination [8].

Acknowledgments: This work is supported by NASA, NAG5-8251, division Contribution No. 8643(1034).

References: [1] Kring D. A. et al. (1999) *LPS XXX,* Abstract #1618. [2] Ruzicka A. et al. (1999) *LPS XXX,* Abstract #1616. [3] Rubin A. E. and Ulff-Møller F. (1999) *LPS XXX,* Abstract #1125. [4] Chen J. H. et al. (1999) *LPS XXX,* Abstract #1472. [5] Shen J. J. et al. (1996) *GCA, 60,* 2887. [6] Chen J. H. et al. (1998) *GCA, 62,* 3379. [7] Chen J. H. and Wasserburg G. J. (1996) *Geophys. Monogr., 95,* 1. [8] Pinault L. J. et al. (1999) *LPS XXX,* Abstract #2048.

FLUID INCLUSION EVIDENCE FOR HIGH COPPER CONTENT OF ORE-FORMING FLUID FOR XIFANPING PORPHYRY COPPER DEPOSIT, SICHUAN PROVINCE, CHINA.

P. Chen, R. Wang, X. Chen, and S. Xu, State Key Laboratory of Mineral Deposits, Nanjing University, Nanjing 210093, China

The porphyry Cu deposit is located in the western margin of the Yangtze Plate. Copper mineralizations are related to biotite adamellites intruding in the Permian and Triassic clastic rocks. Ore minerals are mainly chalcopyrite, molybdenite, chalcocite, bornite, and pyrite. Hydrothermal alterations of quartz + sericite + sulfide assemblage are closely associated with Cu mineralizations. The contact zone is a main location of mineralization.

The samples for fluid inclusion analyses were collected from the endocontact part of No. 80 intrusive body. Gangue quartz contains a lot of fluid inclusions, which are mainly multiphase fluid inclusions with daughter minerals, coexisting with a few vapor inclusions. The sizes of the multiphase fluid inclusions are in general 6–15 µm in length and 4–12 µm in width. They often contain two types of daughter minerals. One is transparent halite with cube shape. The other is an opaque mineral identified as chalcopyrite with tetrahedron shape. We have measured the volume of various phases for tens of multiphase fluid inclusions, and calculated the volume percentages of individual phase. They are respectively 11–17% vapor, 44–51% liquid, 33–40% halite, and ~2% chalcopyrite. Because the change of phase percentages is very slight in different samples, it is suggested that the solid daughter minerals should not be formed by accidental trap, but by normal precipitation of fluid after being trapped with decreasing temperature. Vapor-phase disappearance temperatures of the multiphase fluid inclusions ranged from 230° to 330°C on the Linkam TH 600 Stage and halite dissolved in the range 470° to 590°C. Equivalent NaCl content ranged from 55 to 65 wt% NaCl.

Some multiphase fluid inclusions were opened to make the samples for electron microprobe analysis. The identification of daughter mineral phases was made under a microprobe of JXA-8800M at Key National Laboratory of Mineral Deposit, Nanjing University. X-ray images show that the daughter minerals of tetrahedron- and ball-shape only contain Cu, Fe, and S. Microprobe analysis obtains S in the range 31.738–31.904 wt%, Fe 28.614–29.005 wt%, and Cu 39.041–39.648 wt%. Therefore, we suggest that these daughter minerals should be chalcopyrites. In the light of the estimated phase volume data and the density values of all the phases (chalcopyrite: 4.2 g/cm^3; halite: 2.16 g/cm^3; saturated NaCl solution: 1.2 g/cm^3; vapor density: negligible), we obtained the Cu contents of about 20,000 × 10^{-6}. Therefore, the ore-forming fluid is highly enriched in ore-material, which is higher than Cu content of 4000–16,000 × 10^{-6} of the fluid of the Cu-bearing breccia pipes, Mexico [1].

The discovery of Cu sulfides in C- and Cl-bearing bubbles in phenocryst-hosted melt inclusions shows that Cu resides in a vapor phase in some shallow magma chambers [2]. The high Cu content of ore-forming fluid for Xifanping porphyry copper deposit suggests that when magmas intrude at shallow levels of Earth's crust, Cu mainly partitions into a brine.

References: [1] Sawkins F. J. and Scherkenbach D. A. (1981) *Geology, 9,* 37–40. [2] Lowenstern J. B. et al. (1991) *Science, 252,* 1405–1409.

DETERMINATION OF MELANTERITE-ROZENITE AND CHALCANTHITE-BONATTITE EQUILIBRIA BY THE HUMIDITY BUFFER TECHNIQUE AT 0.1 MPa.

I.-M. Chou, R. R. Seal II, and B. S. Hemingway, U.S. Geological Survey, Reston VA 20192, USA (imchou@usgs.gov).

Introduction: Efflorescent sulfate salts are important constituents of acid mine drainage systems. The ability to geochemically model the behavior of efflorescent salts in aqueous systems is hindered by a limited and poor understanding of their phase equilibria and thermodynamic properties. By using the humidity buffer technique [1–5], we determined the equilibrium relative humidity (RH) and refined the thermodynamic relations for two dehydration reactions: (1) melanterite (Mel) = rozenite (Roz) + 3 H_2O, and (2) chalcanthite (Cha) = bonattite (Bon) + 2 H_2O.

Experimental Method and Results: A weighed amount of sample (either Mel-Roz or Cha-Bon mixtures) was loaded in a plastic container (1 cm outside diameter and 2 cm tall), which was partially immersed in a humidity buffer, a binary-saturated solution [1–5] in a glass container sealed by a rubber stopper with a septum. Small holes through the cap of the sample chamber allow the vapor phase of the sample to equilibrate with that of the buffer system at a fixed temperature (T). The head space of the sample-buffer system was evacuated before immersing the assembly in a water bath. The sample Ts were measured by a Pt-resistance probe (accurate to ±0.02°C and controlled to ±0.03°C). The direction of reaction was revealed by the sample mass change (precise to ±0.05 mg). Experimental results are listed in Table 1.

Thermodynamic Analysis: For both reactions,

$$\Delta G_r^0 = -RT \ln K = -nRT \ln (f_{H_2O})$$

$$\Delta G_r^0 = -nRT \ln [(f^*_{H_2O}) \times (\%RH)/100]$$

where DG_r^0 is the standard Gibbs free energy of reaction, K = equilibrium constant, R = gas constant,; T = absolute T, f_{H_2O} = equilibrium H_2O fugacity, $f^*_{H_2O}$ = fugacity of pure H_2O, and n = 3 and 2 for reactions (a) and (b) respectively. The derived thermodynamic data are compared with previous data in Table 2.

Discussion: The thermodynamic data reported in [1,3] for reactions (a) and (b) were improved in this study by adding several reversal points

TABLE 1. Experimental results at 0.1 MPa.

Humidity Buffer	T(°C)[1]	$f^*_{H_2O}$ (bar)[2]	%RH[3]	ln K
(a) Mel ($FeSO_4$ $7H_2O$)-Roz ($FeSO_4$ $4H_2O$) equilibria				
NaBr $2H_2O$	(21.30)	0.02535	58.74	–12.622
$CuCl_2$ $2H_2O$	(32.65)	0.04937	(68.40)	–10.164
$NaNO_3$	36.13 ± 0.51	0.05991	71.82	–9.438
NaCl	41.04 ± 0.35	0.07804	74.65	–8.529
KCl	48.30 ± 0.33	0.11347	81.38	–7.147
(b) Cha ($CuSO_4$ $5H_2O$)-Bon ($CuSO_4$ $3H_2O$) equilibria				
$MgCl_2$ $6H_2O$	[24.06 ± 0.02]	0.02997	32.85	–9.242
NaI $2H_2O$	[31.47 ± 0.07]	0.04619	36.00	–8.193
NaBr $2H_2O$	51.41 ± 0.08	0.13243	50.69	–5.402
KI	68.02 ± 0.09	0.28624	62.16	–3.453

[1] Equilibrium T. Data in parentheses from [3]; data in brackets from [1].

[2] Calculated from [6].

[3] Calculated from [2]. Data in parentheses from [5].

TABLE 2. Derived thermodynamic data (298.15 K).

ΔG_r^0 (kJ/mol)	ΔH_r^0 (kJ/mol)	ΔS_r^0 (J/K mol)	Reference
(a) Mel ($FeSO_4$ $7H_2O$)-Roz ($FeSO_4$ $4H_2O$) Equilibria			
29.231	159.39	436.6	This study
29.308	156.02	439.3	[3]
28.870	159.97	439.7	[7]
26.080	157.17	439.7	[8]
40.124	175.811	445.261	[9]
(b) Cha ($CuSO_4$ $5H_2O$)-Bon ($CuSO_4$ $3H_2O$) Equilibria			
22.593	111.73	299.0	This study
22.589	112.46	301.4	[1]
22.641	111.70	298.7	[10]
22.878	111.79	298.2	[8]

(Table 1). Our data for reaction (a) are in good agreement with several earlier humidity measurements near room T [11–13] and with the predicted values [7], but are very different from those reported in [8,9,14]. Our results for reaction (b) agree very well with all published data [1,8,10]. Our data are also consistent with our previous direct humidity measurements for both reactions at various T and 0.1 MPa. [15].

References: [1] Malinin A. A. et al. (1977) *Zhur. Fiz. Khim, 51,* 1557. [2] Greenspan L. (1977) *J. Res. NBS, A. Phys. Chem., 81A,* 89–96. [3] Malinin A. A. et al. (1979) *Russ. J. Phys. Chem., 53,* 755. [4] Chou I.-M. et al. (1998) *Eos Trans. AGU, 79,* S364. [5] Young J. F. (1967) *J. Appl. Chem., 17,* 241–245. [6] Haar L. et al. (1994) *NBS/NRC Steam Tables,* 320 pp. [7] Hemingway B. S., in preparation. [8] Dekock C. W. (1982) *Bur. Mines IC-8910,* 45 pp. [9] Pribylov K. P. (1969) *Russ. J. Inorg. Chem., 14,* 168–169. [10] Wagman D. D. et al. (1982) *J. Phys. Chem. Ref. Data, 11,* 291 pp. [11] Cohen E. (1900) *Arches. Neerl. Sci., 5,* 295. [12] Schumb W. C. (1923) *J. Am. Chem. Soc., 45,* 342–354. [13] Parkinson K. J. and Day W. (1981) *J. Exp. Bot., 127,* 411–418. [14] Ehlers E. G. and Stiles D. V. (1965) *Am. Mineral., 50,* 1457–1461. [15] Chou I.-M. et al. (1998) *GSA Abstr. with Progr., 30,* A-129.

USE OF ISOTOPIC TRACERS IN THE QUANTIFICATION OF MINING-DERIVED METALS IN BED SEDIMENTS, ANIMAS RIVER WATERSHED, COLORADO.

S. E. Church[1], D. M. Unruh[2], and D. L. Fey[1], [1]Mail Stop 973, U.S. Geological Survey, P.O. Box 25046, Denver CO 80225, USA (schurch@usgs.gov; dfey@usgs.gov), [2]Mail Stop 963, U.S. Geological Survey, P.O. Box 25046, Denver CO 80225, USA (dunruh@usgs.gov).

The U.S. Geological Survey study of the impact of inactive historical mines on the Animas River watershed, Colorado, is a large, multidisciplinary study that has as its focus the impact of past mining activities on the riparian habitat and the biologic and human health in the watershed. Individual scientific studies undertaken within the Animas River watershed are available on the Internet (http://amli.usgs.gov/amli). In this report, we provide an interpretation of the Pb-isotopic and geochemical data from the colloidal phase of the bed sediments to quantify the downstream dispersion of metal contamination from the Silverton mining district located in the headwaters of the Animas River watershed. Metals were extracted from the bed sediments using a warm (50°C) 2-M HCl-1% H_2O_2 solution for 3 h followed by inductively coupled plasma-atomic emission spectrometry (ICP-AES) analysis. Total digestion analysis of the residual phases indicated that silicate- and sulfide-bound metals are not extracted by this leach with the exception of galena. More than 80% of the Pb extractable from the bed sediments of the Animas River at Durango, Colorado, located more than 75 km downstream, was derived from the Silverton mining district. Using a ratioing technique (extractable metals/Pb), we demonstrate that different metals are differentially partitioned from the water into the colloidal phase and deposited on the sediment bed as a function of both velocity and distance downstream from Silverton, Colorado [1].

We also have sampled premining fluvial sediments from terrace remnants in the Animas River watershed to establish premining geochemical background concentrations for ore and ore-related metals in bed sediments in the watershed. Concentrations of Cu, Pb, Zn, As, Cd, and Ag in the sediments preserved in these remnant terraces were significantly elevated above crustal abundance values prior to mining. Comparisons of premining metal loads in the bed sediments with conditions today indicate a substantial increase in metal loads has occurred over the past 100 years.

Finally, we have analyzed the Sr-isotopic compositions of the fluvial sediments to calculate the detrital sediment loads added by major tributary streams to the Animas River. The Animas River drainage system is an ideal geologic setting for this experiment because (1) the Sr-isotopic compositions of the lavas in the San Juan caldera are relatively uniform, (2) the Animas River canyon traverses a pre-Cambrian crystalline terrane that has a radiogenic Sr-isotopic signature, and (3) the lower part of the Animas River cuts through a sedimentary sequence draining rocks of Paleozoic through Tertiary age, which contributes a large portion of the sediment load of the Animas River. These three datasets provide the basis for a quantitative assessment of the impact of historical mining activities on the Animas River watershed and provide a scientific basis for evaluation of effective remediation strategies.

References: [1] Church S. E. et al. (1997) *U.S. Geological Survey Open-File Rpt. 97-151,* 136 pp.

HIGH-PRECISION LEAD-ISOTOPIC RECORD OF THE LAST 350 KA FROM AN IRON-MANGANESE CRUST (121 DK) FROM THE NORTHEAST ATLANTIC.

C. Claude-Ivanaj[1], W. Abouchami[1], S. J. G. Galer[1], A. Koschinsky[2], and A. W. Hofmann[1], [1]Max-Planck-Institut für Chemie, Postfach 3060, 55020 Mainz, Germany (ivanaj@mpch-mainz.mpg.de), [2]Freie Universität Berlin, FR Rohstoff-und Umweltgeologie, Malteserstrasse, 74-100, 12249 Berlin, Germany.

Introduction: Hydrogenous Fe-Mn crusts have recently been extensively studied as they have been shown to record seawater changes in Pb and Nd-isotopic composition in relation with paleoclimate and ocean circulation changes [1–3]. Here, we report high-resolution Pb-isotopic measurements obtained using a Pb triple spike [4–5] on a Fe-Mn crust from the northeast Atlantic — crust 121 DK (tropic seamount, 24°53'N, 21°42'W), which sits at 2000 m depth in eastern north Atlantic deep water (ENADW). Age-depth relationships in crust 121 DK have been determined by TIMS U-Th [6]. Here, we examine the short-term Pb-isotopic variations over the last 350 k.y., corresponding to a depth of 1 mm. The advantage of using the Pb triple spike (TS) method [5,7] is that it allows resolution of small isotopic variations to a precision of ~100 ppm. Recently, Abouchami et al. [7] used the TS method and showed that there are systematic and gradual changes in all three Pb isotope ratios in crust 121 DK over the past 14 m.y., with an increased influence of a source of radiogenic Pb since 3–4 Ma.

Results: The U-Th data obtained previously [6] have shown that there has been a significant change in growth rate over the past 350 k.y. Approximately 110 ± 30 k.y. ago, the growth rate changed from 2.4 ± 0.1 mm/Ma to 4.7 ± 0.1 mm/Ma. This time coincides, within the limits of our sampling resolution with the transition from marine stage 6 to 5 (130 ka).

The high precision Pb-isotopic data allow us to resolve very small changes in all three isotope ratios. Lead-isotopic ratios range from 18.942 to 18.965, 15.697 to 15.704, and 39.058 to 39.072 for the ^{206}Pb/^{204}Pb, ^{207}Pb/^{204}Pb, and ^{208}Pb/^{204}Pb ratios, respectively. Despite the small range of isotopic variations, we can clearly resolve outside of analytical error a gradual secular increase in ^{206}Pb/^{204}Pb ratios from 350 ka to the end of stage 6. Subsequently, this increase was arrested and reversed itself by stage 2. In ^{206}Pb/^{204}Pb-^{207}Pb/^{204}Pb and ^{206}Pb/^{204}Pb-^{208}Pb/^{204}Pb space, the data define linear arrays consistent with the long-term record of 121DK of [7].

Discussion and Conclusions: 1. In both Pb-Pb isotope spaces, our data display linear arrays which can be interpreted as reflecting binary mixing between a high ^{206}Pb/^{204}Pb and a low ^{206}Pb/^{204}Pb component. The gradual increase of Pb-isotopic ratios toward the present day indicates a strengthening of the radiogenic Pb end-member influence which continues until the end of stage 6. Rather striking is that this appears to hold true over the last 3 m.y. as our samples plot on the trend of the dataset from [7]. These authors suggested that the Pb-isotopic variations over the past 3 m.y., reflect a progressively increasing contribution of more radiogenic NADW conveyed from the western to the eastern Atlantic basin, and a corresponding decrease in the proportion of less radiogenic Southern Component Water. However, this long-term progression in water mass mixing appears to have been arrested at the end of stage 6. Subsequently, we observe a slight decrease in the three Pb-isotopic ratios at stage 2. However, in both Pb-Pb-isotopic spaces, the younger samples still plot on a trend that cannot be distinguished from the overall long-term 3 Ma to present trend. It appears, therefore, that the same two water masses are still contributing to the net Pb-isotopic composition, but the progressive change in proportions of the two components has stopped and after about 50 ka started to reverse itself.

2. The change in growth rate occurs at ~110 ± 30 ka, and this makes crust 121 DK comparable to crust VA 13-2 in the Pacific Ocean, where a two-fold increase in growth rate occurs at a similar time (90 ka). Moreover, this change in VA 13-2 is also simultaneously associated with a secular Pb-isotopic decrease [1]. Although it is obvious that the two crusts display very different Pb-isotopic signatures, which reflect different sources of Pb, in both crusts the Pb decrease starts really to be significant from marine stage 2 onward. These two crusts are at present the only ones for which such high-time-resolution Pb-isotopic data are available, and it is therefore too early to generalize this observation as a global phenomenon.

References: [1] Abouchami W. et al. (1997) *GCA, 61,* 3957–3974. [2] Christensen J. N. et al. (1997) *Science, 277,* 913–918. [3] O'Nions R. K. et al. (1997) *EPSL, 155,* 15–28. [4] Galer S. J. G. and Abouchami W. (1998) *Mineral. Mag., 62A,* 491–492. [5] Galer S. J. G. (1999) *Chem. Geol., 157,* 255–274. [6] Claude-Ivanaj C. et al. (1998) *Mineral. Mag., 62A,* 335–336. [7] Abouchami W. et al. (1999) *GCA,* in press.

OXYGEN-ISOTOPIC FRACTIONATION BETWEEN MAGNETITE AND WATER.

D. R. Cole[1], J. W. Valley[2], M. J. Spicuzza[2], and J. Horita[1], [1]Geochemistry Group, Chemical and Analytical Sciences Division, Oak Ridge National Laboratory, Oak Ridge TN 37831-6110, USA (coledr@ornl.gov), [2]Department of Geology and Geophysics, University of Wisconsin–Madison, Madison WI 53706, USA (valley@geology.wisc.edu).

Introduction: Despite the improvements in analytical, experimental, and computational methods, there are still a significant number of rock-forming minerals for which isotopic fractionation data are limited or in disagreement. This is particularly true for magnetite and hematite, important accessory minerals occurring in a wide range of geological environments. Knowledge of the iron oxide-water O-isotopic fractionation factors can be used as geothermometers or to determine fluid sources. We have measured the O-isotopic fractionation factors between magnetite-water over the temperature ranges of 300°–800°C.

Methods: We selected three reaction pathways to investigate the O-isotopic fractionation between magnetite and water. These include (1) oxidation of iron powder in either pure water or dilute NaCl solution at NiNiO, (2) reduction of hematite through reaction with water or dilute acetic acid (HAC) at NiNiO, and (3) reaction of water or dilute NaCl with either fine-grained magnetite or hematite at NiNiO. Effective use of acetic acid is limited to temperatures up to ~400°C, whereas magnetite-water and hematite-water interactions become prohibitively slow below ~400°C. Therefore, we were forced to deal with chemical reactions that do not produce favorable overlaps or continuity in the fractionation data as a function of temperature.

Oxygen-isotopic exchange experiments in the systems hematite-water, hematite-water-HAc, and magnetite-water-NaCl were conducted at a variety of temperatures and generally 1 kbar using the partial exchange method, i.e., reaction of oxide with three or four isotopically different waters [1]. Because magnetite was the only O-bearing phase formed in the Fe-water-NaCl experiments, we assumed the run product would be in equilibrium with the fluid, thus negating the need for three or four isotopic waters. Each run product was characterized with X-ray diffraction (XRD), scanning electron microscopy (SEM), and, on a limited basis, high-resolution transmission electron microscopy (HRTEM) and Mössbauer spectrometry. Bulk oxide powers were analyzed by CO$_2$-laser-fluorinaton [2]. Large, magnetite single crystals from experiments involving reaction of hematite with 0.5 m HAc at 350°C were analyzed using a modified Cameca 4f ion microprobe [3].

Results and Discussion: Examination by SEM indicates the formation of well-crystallized octahedra and dodecahedra of magnetite with grain sizes as large as 100–200 µm, particularly in experiments where dilute HAc was used. Analyses of single crystals using the ion microprobe indicates that (1) crystals from a given run are homogeneous at the ±1‰ level, and (2) differences between the final average δ^{18}O of magnetite (multiple spots on 3–5 grains/capsule) and run solution are the same regardless of the initial starting water values, suggesting equilibrium was achieved. The agreement between fractionations determined from single crystals and from the partial exchange bulk method from the same experiments was very good, e.g., –8.60‰ vs. –8.21‰ at 350°C, 1 kbar respectively.

The most consistently well-behaved results were obtained from magnetite-0.5 m NaCl experiments conducted between 500° and 800°C for durations ranging from 235 h (800°C) to as long as 1798 h (600°C). Scanning electron microscope observations indicate that considerable grain growth occurred during these experiments with some grains attaining diameters in excess of 100 µm. Nearly 100% exchange was obtained at 600°, 700°, and 800°C; and over 90% at 500°C. We obtained the following fractionation factors: –5.54, –6.32, –6.79, and –7.79‰ for 800°, 700°, 600°, and 500°C, respectively. Oxygen-isotopic fractionations derived from Fe to magnetite oxidation at 700° and 800°C agree very closely with these results. Our high-temperature results are in good agreement with those estimated from other techniques [e.g., 4–5].

Below 500°C, the fractionations are based primarily on experiments where hematite was converted to magnetite. From 450° to 300°C, we observe a rather weak dependency on temperature, with the fractionation data passing through an apparent minimum at ~400°C. A minimum in the magnetite-water fractionation curve in this temperature range was predicted by theoretical studies, but at a somewhat lower temperature –200°C [6].

Acknowledgments: Funded by the Geosciences Program, Office of Basic Energy Sciences, DOE.

References: [1] Northrop D. and Clayton R. (1966) *J. Geol., 74,* 174–196. [2] Valley J. W. et al. (1995) *GCA, 59,* 5223–5231. [3] Fortier S. (1995) *GCA, 59,* 3871–3875. [4] Downs W. (1981) *GCA, 45,* 2065–2072. [5] Rowe M. W. et al. (1994) *GCA, 58,* 1064–1067. [6] Becker R. H. and Clayton R. N. (1966) *GCA, 40,* 1153–1165.

STABLE ISOTOPIC FRACTIONATION ASSOCIATED WITH ANAEROBIC DEGRADATION OF CHLORINATED HYDROCARBONS.

M. L. Coleman, T. J. McGenity, and M. C. P. Isaacs, Postgraduate Research Institute for Sedimentology, University of Reading, Whiteknights, Reading RG6 6AB, UK (m.l.coleman@reading.ac.uk).

Introduction: Chlorinated organic compounds, especially industrial solvents, are significant pollutants. It would be valuable to estimate the extent to which natural degradation processes have operated in a polluted site and thereby their *rate* of operation. With such information it would be possible to make an informed choice between natural attenuation and engineered solutions. We present here, initial results of a program to develop a method to monitor progress of the attenuation processes. Anaerobic microbial degradation is one of the major attenuation processes.

Experimental Methods: We used tetrachloroethene as the model solvent and two different pure cultures of reductively dehalogenating bacteria that have been shown to link PCE-metabolism to growth in a respiratory process. The two species, *Dehalospirilum multivorans* and *Dehalobacter restrictus*, were grown with H (*D. multivorans* only) or pyruvate (both species) as the electron donor and both degrade tetrachloroethene to cis-dichlorethene. The bacterial cultures were grown anaerobically in aqueous medium with a reservoir of tetrachloroethene dissolved in hexadecane (10% v/v solution) that formed a separate organic phase floating on the medium. A large number of parallel experiments and controls were set up and culture tubes were sacrificed and sampled at regular intervals during growth.

Results: We showed that there was no isotopic exchange between dissolved chlorinated solvent and chloride in solution. Therefore, the Cl-isotopic compositions of solvent and chloride in successive samples represent the cumulative progress of the dehalogenation process. Our preliminary data indicate that there is a significant isotopic fractionation factor associated with dehalogenation by both organisms. Δsolvent-inorganic chloride is ~–5‰ ($\alpha = 0.995$).

Discussion: The progress of the dehalogenation suggests that the fractionation factor does not change significantly during the reaction and the data can be modeled as a Rayleigh fractionation process. It seems likely that the basic cause of the isotopic changes represent a kinetic fractionation process similar in sense to those experienced by other stable isotopic elements (e.g., S). We have also conducted aerobic dehalogenation experiments. It is interesting to note that the Cl-isotopic fractionation factor for *aerobic* degradation of dichloromethane quoted by Sturchio et al. [1] is 0.9962 not very different from our figure for the *anaerobic* process.

Conclusion: These data provide important quantitative constraints to models of transport and attenuation of chlorinated solvents.

Acknowledgments: This work was supported by a grant from the United Kingdom Natural Environment Research Council to MLC and TJMcG (GST/02/2083).

References: [1] Sturchio N. C. et al. (1998) *Environ. Sci. Technol., 32,* 3037–3042.

ACCURATE AND PRECISE ISOTOPIC RATIO MEASUREMENTS OF NBS 981 LEAD BY MULTIPLE COLLECTOR INDUCTIVELY COUPLED PLASMA MASS SPECTROMETRY: WHY ARE THE RATIOS DIFFERENT FROM THERMAL IONIZATION MASS SPECTROMETER MEASUREMENTS?

K. D. Collerson[1] and Z. Palacz[2], [1]Department of Earth Sciences, University of Queensland, Brisbane, Queensland 4072, Australia (k.collerson@mailbox.uq.edu.au), [2]Micromass, Floats Road, Wythenshawe, Manchester, M23 9LE Zenon, UK (palacz@micromass.co.uk).

High-precision, Tl-normalized, Pb-isotopic ratio measurements of NBS 981 using multiple collector inductively coupled plasma mass spectrometers (MC-ICP-MS), have shown that reproducibilities are comparable with data from thermal ionization mass spectrometers (TIMS). However, accuracy of the measurements is not comparable with the double- or triple-spike TIMS techniques. Without exception, all MC-ICP-MS data have lower ratios for ^{208}Pb/^{206}Pb, ^{207}Pb/^{206}Pb, ^{208}Pb/^{204}Pb, ^{207}Pb/^{204}Pb, and ^{206}Pb/^{204}Pb by ~5–10× 2σ isotope ratio reproducibilities, when normalized with (IUPAC) ^{205}Tl/^{203}Tl = 2.3871. A disturbing and very important observation is that all MC-ICP-MS instruments appear to yield exactly the same isotopic compositions. To overcome this problem some authors have used different values of ^{205}Tl/^{203}Tl for fractionation correction to produce more accurate data. However the results still do not satisfactorily agree with the TIMS data, particularly for ratios involving ^{208}Pb.

We have analyzed NBS 981 using a single-focusing, hexapole-interfaced MC-ICP-MS (MICROMASS Isoprobe). This instrument uses a collision cell instead of an energy analyzer to reduce the ion energy of the ion beam to ~1 eV. A 50-ppb solution of NBS 981 with 5 ppb Tl was used for the experiments. Total Pb ion signals of 12 V were obtained using a CETAC MCN6000 desolvating nebulizer. At an aspiration rate of 40 μL/min, the total amount of Pb used per analysis was ~10 ng, with an ion/atom efficiency of 1 ion per 130 atoms. Collector efficiencies were unity.

Using an exponential fractionation correction and ^{205}Tl/^{203}Tl = 2.3871, Pb-isotopic ratios were identical to other MC-ICP-MS results, despite using a significantly lower sample concentration and more importantly totally different ion energy optics. The isotopic ratios were (±1σ) ^{208}Pb/^{206}Pb 2.165921 ± 72 ppm, ^{207}Pb/^{206}Pb 0.914423 ± 88 ppm, ^{206}Pb/^{204}Pb 16.9304 ± 152 ppm, ^{207}Pb/^{204}Pb 15.4815 ± 122 ppm, and ^{208}Pb/^{204}Pb 36.6692 ± 166 ppm. Data collection method was the same as TIMS with baselines measured at ±0.5 amu for each isotope, and the average of the two intensities subtracted from the peak.

Unlike TIMS, ICP uses a solution introduction system that may be subject to memory from previous samples and to impurities in the Ar gas supply, e.g., Hg. Thus an alternative baseline correction method, more appropriate to ICP-MS than TIMS was employed. This involved measuring the reagent/MCN6000 blank, gas/instrument blank as an "on peak zero," prior to introduction of the sample and subsequent measurement of the ±0.5-amu baseline. The on peak zero and ±0.5-amu baselines were combined and subtracted from the ion signal. Over the course of two days 45 analyses of the standard yielded (±1σ) ^{208}Pb/^{206}Pb 2.166486 ± 84 ppm, ^{207}Pb/^{206}Pb 0.914603 ± 120 ppm, ^{206}Pb/^{204}Pb 16.937 ± 194 ppm, ^{207}Pb/^{204}Pb 15.491 ± 160 ppm, ^{208}Pb/^{204}Pb 36.694 ± 200 ppm. These results are identical within error to double-spiked TIMS data [e.g., 1] (^{208}Pb/^{206}Pb 2.16701 ± 200 ppm (±1σ), ^{207}Pb/^{206}Pb 0.914585 ± 146 ppm, ^{206}Pb/^{204}Pb 16.9356 ± 133 ppm, ^{207}Pb/^{204}Pb 15.4891 ± 192 ppm, ^{208}Pb/^{204}Pb 36.7006 ± 308 ppm). These data demonstrate that accurate and precise isotopic ratios of Pb can be obtained using an unmodified Tl-isotopic composition and an exponential fractionation correction, providing attention is paid to correct blank subtraction.

References: [1] Todt et al. (1996).

ION ASSOCIATION IN SODIUM CHLORIDE BRINES AT HIGH TEMPERATURES AND PRESSURES: RESULTS FROM MOLECULAR DYNAMICS SIMULATIONS.

M. D. Collings and D. M. Sherman Department of Earth Sciences, University of Bristol, Bristol BS8 1RJ, UK (dave.sherman@bris.ac.uk).

Introduction: Sodium chloride brines are involved in the transport of metals and the formation of hydrothermal ore deposits. Moreover, such brines may control the electrical conductivity of crustal rocks. With increasing temperature, the dielectric constant of water decreases; in sodium chloride brines, this promotes the formation of NaCl ion pairs and NanClm clusters. At even higher temperatures, NaCl-water mixtures separate into two phases. The decreased dissociation of NaCl in aqueous solutions affects the ability of brines to transport metals. Moreover, ion-pair and cluster formation will also lower the electrical conductivity of crustal fluids. It is essential, therefore, that we understand the high-temperature thermodynamics of the NaCl-H_2O system. To date, our understanding of the equations of state and speciation of NaCl-H_2O fluids is based on the Born-model extrapolation developed by Helgeson and coworkers [1] or on the Pitzer model formulation [2].

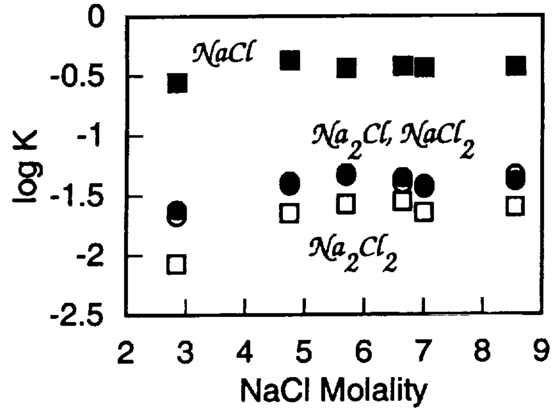

Fig. 1. Calculated dissociation constants of NaCl clusters at 600 K and 1 kbar.

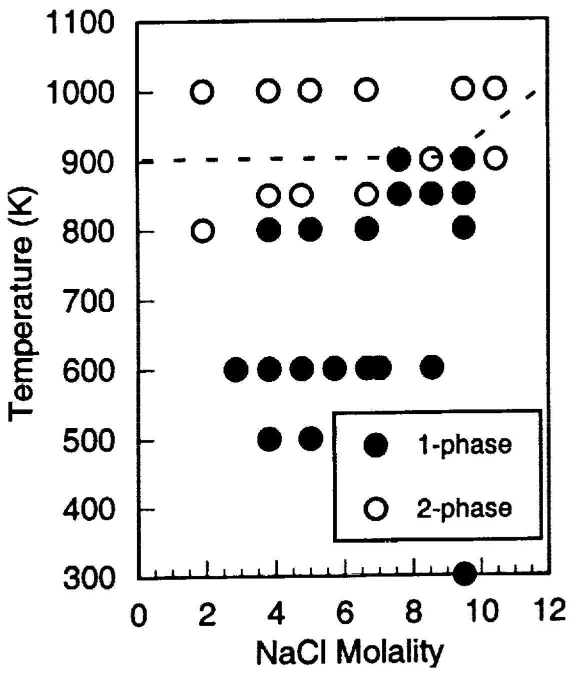

Fig. 2. Calculated phase diagram for the NaCl-water system at 1 kbar. Dashed boundary corresponds to that of [2].

In the work reported here, we present an atomistic approach to NaCl-H_2O solution thermodynamics using classical molecular dynamical simulations. From these calculations, we determined the speciation of NaCl brines as a function of temperature and pressure. We also determined the phase diagram of the NaCl-water system and the equation of state of NaCl-water mixtures.

Molecular Dynamics Calculations: For the calculations, we used the SPC/E model for water developed by Berendsen et al. [3]. The SPC/E model accurately reproduces the thermodynamic and dielectric properties of water, at least along the liquid-vapor coexistence curve [4]. The Na-O, Cl-O, and Cl-Cl short range potentials of Smith and Dang [5] were used; these potentials were shown by Brodholdt [6] to give a very accurate description of the density of NaCl-water mixtures.

Ion Association: In solutions from 2.0 to 8.0 molal, we find that the dominant species are Na+, Cl–, NaCl, Na_2Cl, $NaCl_2$ and Na_2Cl_2. We have determined a set of dissociation constants for these ion clusters which, within our uncertainty, are independent of composition, at least above 4 m NaCl (Fig. 1) This suggests that we can evaluate the solution thermodynamics of NaCl-H_2O mixtures without resorting to a Pitzer formulation.

Phase Separation: At 1 kbar, the calculated phase diagram of NaCl-H_2O mixtures shows a phase separation near 900 K that is approximately independent of composition over the range 1–10 molal (Fig. 2) This is in good agreement with the equation of state of Anderko and Pitzer [2]. We find, however, that to reliably demonstrate phase separation, MD runs must be at least 0.5 ns. Further calculations are needed to refine the phase boundary.

References: [1] Oelkers E. H. and Helgeson H. C. (1993) *GCA, 61,* 1359–1412. [2] Anderko A. and Pitzer K. S. (1993) *GCA, 57,* 1657–1680. [3] Berendsen H. J. C. et al. (1987) *J. Chem. Phys., 91,* 6269–6271. [4] Guissani Y. and Guillot B. (1993) *J. Chem. Phys., 98,* 8221–8235. [5] Smith D. E. and Dang L. X. (1994) *J. Chem. Phys., 100,* 3757–3766. [6] Brodholdt J. P. (1998) *Chem. Geol., 151,* 11–19.

THE DOMINANCE OF THE RIVERINE PARTICULATE PHOSPHORUS FLUX IN SUPPLYING PHOSPHATE TO THE OCEANS AND A 10,000-YEAR RESIDENCE TIME FOR PHOSPHORUS.

A. S. Colman[1] and H. D. Holland[2], [1]Department of Geology and Geophysics, Yale University, P.O. Box 208109, New Haven CT 06520-8109, USA (albert.colman@yale.edu), [2]Department of Earth and Planetary Sciences, Harvard University, 20 Oxford Street, Cambridge MA 02138, USA (holland@eps.harvard.edu).

We have calculated the diffusive phosphate flux from marine sediments for 193 published pore water phosphate profiles that met stringent criteria for quality control [1]. The relationships between these phosphate fluxes, sedimentation rate, and the rate of organic matter deposition were used to estimate the global diagenetic flux of phosphate from marine sediments to the oceans. The pore water phosphate profile data are confirmed by data from benthic flux chambers and from depth profiles of solid P concentrations in marine sediments.

Our best estimate of the preanthropogenic diffusive flux of phosphate from sediments to the oceans is 12×10^{11} mol/yr. Based on a compilation of data on the reactivity of P phases in riverine particulate matter and the burial efficiency of particulate P, we estimate that roughly 3.2×10^{11} mol/yr of this diagenetic release of P to the oceans derives from riverine reactive particulate P. Meybeck [2] estimated the preanthropogenic global riverine particulate P flux to the oceans to be 6.5×10^{11} mol/yr and the global riverine dissolved P flux to the oceans to be 0.32×10^{11} mol/yr. Our calculations therefore indicate that about half of the particulate P entering the oceans from rivers is released as dissolved phosphate and participates fully in the marine biogeochemical cycle of P. Furthermore, roughly 90% of the dissolved P inputs to the oceans from the continents are mediated by diagenetic release from riverine particulate P phases subsequent to deposition of those particulates in marine sediments. Using these values, we calculate the residence time for P in the oceans to be ~10,000 yr. This is slightly shorter than recent estimates for the residence time for phosphate in the oceans [e.g., 3,4] and is consistent with the recent trend toward higher estimates for removal fluxes of phosphate from the oceans as authigenic carbonate fluorapatite, as authigenic REE-minerals, and scavenged by MOR hydrothermal plume particles.

An important consequence of the dominance of particulates in the supply of bioavailable phosphate to the oceans is that phosphate inputs to the oceans can be significantly altered by changes in the efficiency with which phosphorus is diagenetically released from riverine reactive particulate phases. Changes in the distribution of sediment deposition between regions of high sedimentation and low sedimentation rates, or between high productivity regions and oligotrophic regions, or between reduced sediments and oxidized sediments could influence the release of particulate P into the dissolved phase. Changes in climate, sea level, and tectonic activity could therefore influence P release to the oceans, and their effects could be decoupled from the records of purported proxies for chemical weathering such as Sr and Os isotopes [5–7]. Our understanding of the marine biogeochemical cycles of other particle reactive species may require similar revision as we learn more about the effects of diagenetic overprinting on weathering fluxes.

References: [1] Colman A. S. and Holland H. D. (1999) in *Marine Authigenesis: From Microbial to Global* (C. R. Glenn et al., eds.), *SEPM Spec. Publ. No. 65,* in press. [2] Meybeck M. (1982) *Am. J. Sci., 282,* 401–450. [3] Ruttenberg K. C. (1993) *Chem. Geol., 107,* 405–409. [4] Filippelli G. M. and Delaney M. L. (1996) *GCA, 60,* 1479–1495. [5] Filippelli G. M. and Delaney M. L. (1994) *Paleoceanogr., 9,* 643–652. [6] Ruttenberg K. C. (1995) *Nature, 372,* 224–225. [7] Föllmi K. B. (1995) *Geology, 23,* 859–862.

ISOTOPIC EVIDENCE FOR GROUNDWATER FLOW AND BIODEGRADATION OF ORGANIC SOLVENTS AT THE TEST AREA NORTH SITE, IDAHO NATIONAL ENGINEERING AND ENVIRONMENTAL LABORATORY.

M. E. Conrad[1], D. J. DePaolo[1,2], D. L. Song[3], and E. Neher[4], [1]Mail Stop 70A-3363, E. O. Lawrence Berkeley National Laboratory, Berkeley CA 94720, USA (msconrad@lbl.gov), [2]Department of Geology and Geophysics, University of California, Berkeley CA 94720, USA (depaolo@socrates.berkeley.edu), [3]Department of Civil and Environmental Engineering, University of California at Berkeley, Berkeley CA 94720, USA (dlsong@uclink4.berkeley.edu), [4]Mail Stop 3954, Woodruff Annex Complex, Idaho National Engineering and Environmental Laboratory, P.O. Box 1625, Idaho Falls ID 83415, USA (neheer@inel.gov).

Introduction: The Test Area North (TAN) site at the Idaho National Engineering and Environmental Laboratory is located on the northern edge of the Snake River Plain in eastern Idaho. The geology of the site consists of basaltic lava flows with sedimentary interbeds. Between 1955 and 1972, a wide variety of waste materials, including low-level radioactive isotopes, sewage and chlorinated solvents, were injected into a 310-foot-deep well below the water table at the TAN site. The result of this activity is a 2-km plume. The primary contaminant of concern at the TAN site is trichloroethane (TCE).

Results and Discussion: To study the regional hydrology of the TAN site and to assess natural levels of biological activity in the groundwater, samples were collected from monitoring wells at the TAN site and regional groundwater wells. The $\delta\Delta$ and $\delta^{18}O$ values of the water, $^{87}Sr/^{86}Sr$ of dissolved Sr, and the $\delta^{13}C$ values of dissolved inorganic C compounds (DIC) for these samples were analyzed. In addition, in conjunction with an experiment designed to test the efficacy of injecting lactate to enhance biodegradation of TCE, we have been monitoring the $\delta^{13}C$ values of TCE, lactate and potential byproducts of anaerobic microbial metabolism of TCE and lactate.

Regional groundwater flow patterns. The Sr-isotopic data for the regional groundwater samples indicate that there are three distinct sources of water in the TAN area; regional flow through the Snake River aquifer ($^{87}Sr/^{86}Sr$ <0.710), the Birch Creek drainage to the north of the TAN site ($^{87}Sr/^{86}Sr$ ~0.712), and the Big Lost River drainage that feeds playa lakes to the west of TAN ($^{87}Sr/^{86}Sr$ ~0.7104). The $\delta\Delta$ and $\delta^{18}O$ values of the Big Lost River water indicate that this groundwater component is also strongly evaporated.

In the TAN plume area, the predominant source of groundwater (which is also evaporated and has $^{87}Sr/^{86}Sr$ values in the 0.7102 to 0.7105 range) appears to be the Big Lost River water. To the east and south of the plume, there is apparently some mixing with the regional groundwater, causing the direction of the plume to bend to the south. The Birch Creek water is predominant below a relatively continuous interbed that extends beneath the TAN site (and acts as an impermeable barrier to migration of the contaminants).

Evidence for natural attenuation of contaminants. The $\delta^{13}C$ values of groundwater DIC in samples from the TAN monitoring wells (–10‰ to –12‰) are 2–3‰ lower than the surrounding groundwaters. On a longitudinal cross section of the TAN plume, the lower $\delta^{13}C$ values correlate well with the TCE concentrations in the water. This is probably an indication that the contaminants in the plume are being biologically degraded, although it is possible that the source of the low $\delta^{13}C$ C is not entirely the TCE. Biodegradation of other contaminants, such as the sewage, would probably also lead to lower $\delta^{13}C$ values for the DIC.

The Sr-isotopic ratios of the plume provide additional evidence that the TCE is being naturally degraded in the plume. On a plot of TCE concentrations vs. $^{87}Sr/^{86}Sr$ ratios, most of the data fall below a straight mixing line, indicating that some other process besides dilution is contributing to the decreased TCE concentrations at the distal end of the plume. The most likely explanation for the loss of TCE is biodegradation; however, it is also possible that extensive volatilization of TCE could produce the same trend.

Monitoring of enhanced bioremediation. Since the beginning of this year, high concentrations of lactate have been pumped into the injection well in an attempt to accelerate biodegradation of TCE in the source area of the plume. In response to this activity, increased concentrations of intermediary byproducts of anaerobic reductive dechlorination of TCE, including cis-dichloroethylene (cis-DCE), vinyl chloride (VC), and ethylene, have been detected in the groundwater. Preliminary $\delta^{13}C$ analyses have been done on the TCE (–22‰ to –26‰), the cis-DCE (–18‰ to –22‰), VC (–37‰), and ethene (–47‰). The cause of the observed variations in the $\delta^{13}C$ values of the compounds is not yet clear.

The $\delta^{13}C$ value of the injected lactate is –11‰. The $\delta^{13}C$ values of byproducts of degradation of the lactate have been –5‰ to –8‰ for acetate, –12‰ to –14‰ for proprionate, and –15‰ to –18‰ for butyrate. In addition, the $\delta^{13}C$ values of groundwater DIC have increased from around –10‰ to +4‰, indicating derivation of DIC under methanogenic conditions.

The increased concentrations of byproducts of TCE and lactate degradation clearly indicate that biologic activity has been stimulated in the plume. However, the nature of this activity is complicated. The preliminary isotope data (sampling will continue until the end of the study in November 1999) may potentially be useful for determining which metabolic pathways are important for TCE degradation.

REACTIVE MELT MIGRATION BENEATH THE MID-ATLANTIC RIDGE: EVIDENCE FROM ODP LEG 153 GABBROS.

L. A. Coogan[1], P. D. Kempton[2], and A. D. Saunders[3], [1]Department of Earth Sciences, Cardiff University, Cardiff, Wales CF1 3YE, UK (cooganla@cardiff.ac.uk), [2]Isotope Geoscience Laboratories, National Environmental Research Council, Keyworth, Nottingham, UK (p.kempton@nigl.nerc.ac.uk), [3]Department of Geology, University of Leicester, Leicester, UK (ads@le.ac.uk).

Introduction: Models for subridge magma chambers are generally dominated by extensive regions of crystal mush [e.g., 1]. Here we provide evidence for the extensive post cumulus modification of gabbros recovered by ODP drilling near the Mid-Atlantic Ridge consistent with this model. The evidence comes from textural associations, correlations between textural and mineral chemical characteristics and modeling *in situ* mineral trace-element data.

ODP Hole 923A, ~10 km south of the Kane Fracture Zone [2], is dominated by two lithologies: (1) primitive plagioclase-olivine cumulates enclosed in clinopyroxene (Cr-diopside), and (2) more evolved plagioclase-clinopyroxene (brown augite) ± olivine ± orthopyroxene cumulates that show abundant grain size variations. Following shipboard nomenclature these are termed poikilitic olivine gabbros and brown-px gabbros respectively. Poikilitic olivine gabbros have consistently more primitive mineral compositions than brown-px gabbros in terms of Mg# of mafic phases and plagioclase An content [e.g., 3].

Correlations Between Texture and Composition: The degree of textural equilibrium of poikilitic olivine gabbros correlates with the modal proportion of clinopyroxene and trace-element composition of the clinopyroxene. More equilibrated samples have lower modal clinopyroxene abundances, and the clinopyroxene has higher incompatible trace-element abundances. In brown-px gabbros the grain size (1–10 mm) correlates with the grain shape and mafic phase Mg# such that coarser samples have more granular textures and lower mafic phase Mg#s. This is irrespective of whether grain size variation is sharp or gradational. Furthermore, textures suggest a reaction relationship exists in brown-px gabbros between olivine and clinopyroxene. Commonly olivine occurs as ragged irregularly shaped crystals within both the cores and rims of clinopyroxene. These phases also show a close spatial association to one another, commonly appearing to form composite grains. We interpret these observations as recording the reaction: melt + olivine to clinopyroxene.

Geochemical Modeling: Trace-element zoning profiles in clinopyroxenes have been determined by ion probe. Clinopyroxenes are strongly zoned in incompatible trace elements with abundances increasing dramatically toward crystal rims. Furthermore, highly incompatible elements (such as Zr) are fractionated from moderately incompatible elements (e.g., Y), such that the Zr/Y ratio increases from core to rim. These geochemical characteristics are seen in clinopyroxene in both poikilitic olivine gabbros and brown-px gabbros. The same trend is observed in the entire dataset as in single crystals, although with more scatter. The data cannot be modeled as fractional or equilibrium crystallization. Instead, we model it using the assimilation and fractional crystallization (AFC) equations of [4], with rates of assimilation to crystallization of 0.7–0.9.

Model for the Evolving Crystal Mush: These observations are interpreted in terms of processes in a subridge gabbroic crystal mush. Reaction between a migrating interstitial melt and the crystal assemblage it passes through leads to the interstitial melt following an AFC evolutionary path. In poikilitic olivine gabbro cumulates the densification of the primary crystal mush prior to clinopyroxene saturation was through compaction, leading to increasingly equilibrated textures. Clinopyroxene saturation inhibited further compaction and cemented the porosity. Higher incompatible trace-element abundances in clinopyroxene, where it occurs as a low percentage of the assemblage, reflects the evolution of the interstitial melt with increasing crystal/melt ratios. In brown-px gabbro cumulates the primary cumulate was more significantly modified by reaction with interstitial melt than in poikilitic olivine gabbros. Higher melt fluxes led to coarser grain sizes (Ostwald ripening) and more granular textures (a closer approach to textural equilibration). Higher amounts of reaction with interstitial melt also led to lower mafic phase Mg#s.

Fluid Dynamics: If the grain size variations reflect variable fluxes of interstitial melt, as suggested above, this is equivalent to channelized flow. Clogging of melt channelways by crystallization is expected in this scenario [5]. This can be avoided, however, if the concomitant crystal coarsening and a closer approach to textural equilibration leads to increased permeability.

Implications: The strong evidence for porous melt flow suggests that this may be an important mechanism for melt transport in the lower crust beneath slow spreading ridges. Return of evolved interstitial melt to an eruptable melt body could have a significant effect on the composition of erupted magmas. If the interstitial melt evolves along an AFC fractionation trend, this will be more significant than in standard boundary layer fractionation models [e.g., 6].

References: [1] Sinton J. and Detrick R. (1992) *JGR, 97,* 197–216. [2] Cannat M. et al. (1995) *Init. Rpt. ODP Leg 153.* [3] Coogan L. (1998) Ph.D. thesis, Univ. Leicester. [4] DePaolo D. (1981) *EPSL, 53,* 189–202. [5] Kelemen P. et al. (1995) *JGR, 100,* 475–496. [6] Langmuir C. (1989) *Nature, 340,* 199–205.

EVIDENCE FOR THE ORIGIN OF OCEANIC OXIDE GABBROS BY CHANNELIZED MELT FLOW THROUGH THE LOWER CRUST.

L. A. Coogan[1], C. J. MacLeod[1], S. J. Edwards[2], and H. J. B. Dick[3], [1]Department of Earth Sciences, Cardiff University, Cardiff, Wales CF1 3YE, UK (cooganla@cardiff.ac.uk; macleod@cardiff.ac.uk), [2]Department of Earth and Environmental Sciences, University of Greenwich, UK (s.j.edwards@greenwich.ac.uk), [3]Woods Hole Oceanographic Institution, Woods Hole MA 02543, USA (hdick@whoi.edu).

Introduction: Oxide-rich gabbro horizons within gabbro (*sl*) are a common constituent of lower crustal rocks dredged and drilled from slow spreading mid-ocean ridges [1–4]. We have investigated one such horizon in a drill core (BGS24) recovered during the *James Clark Ross* cruise JR31 survey of Atlantis Bank (southwest Indian Ridge) in March–May 1998.

Petrology of Core BGS-24: The oxide-rich portion of this core occurs between ~20 cm and 50 cm-bsf (below the seafloor). The host for the oxide gabbro is a moderately- to highly-deformed olivine gabbro. Only the upper contact between the olivine gabbro and oxide gabbro has been studied. The increase in modal oxide abundance at 20 cmbsf correlates with (1) a disappearance of olivine, (2) a coarsening of clinopyroxene, (3) the incoming of cumulus orthopyroxene, (4) a decrease in modal plagioclase, and (5) a decrease in the strength of the deformation fabric.

In thin section the textural relationships between oxides (ilmenite and magnetite) and clinopyroxene and plagioclase are complex. Plagioclase and clinopyroxene have clearly been partially resorbed prior to oxide precipitation. For example, optically continuous clinopyroxene occurs as discrete patches within oxides. Furthermore, both clinopyroxene and plagioclase crystals are commonly intricately embayed with smoothly curved boundaries when adjacent to oxides.

Geochemistry of Core BGS-24: Electron and ion microprobe analyses of ilmenite and clinopyroxene have been performed across the boundary from olivine gabbro to oxide gabbronorite. Dramatic compositional shifts occur at the boundary between oxide-poor olivine gabbro and oxide-rich gabbronorite.

Ilmenite shows steps in the abundance of MgO, Cr, Co, Mn, V, Zr, Hf, Nb, and Ta at the change from olivine gabbro to oxide gabbronorite. Of these elements only Mg is higher in the oxide gabbronorites. Steps also occur in ratios such as Zr/Nb. Clinopyroxene does not show such distinctive steps in element abundances between lithologies as ilmenite but gradients do occur. In contrast to ilmenite, clinopyroxene has a higher Mg# in the olivine gabbros than the oxide gabbronorites. Clinopyroxene is almost unzoned in the oxide gabbronorites but strongly zoned in the olivine gabbro host rock.

Gradients in element abundances also occur both across the modal boundary (e.g., V in clinopyroxene), and within just the oxide gabbronorite. For example, Cr in clinopyroxene decreases smoothly from ~150 ppm to <20 ppm from the olivine gabbro into the oxide gabbronorite. Zirconium and Nb abundances in ilmenite increase systematically with depth in the oxide gabbronorite but are subconstant and higher in ilmenite in the adjacent olivine gabbro.

Interpretation: The modal, textural, and geochemical characteristics described above are interpreted to have been generated as melt migrated through a decimeter-centimeter-scale channel in a crystal mush similar to as has been proposed by earlier workers [2,3]. Reaction between the migrating melt and the surrounding wall rock was complex. Modal metasomatism resulted in the replacement of olivine by orthopyroxene and the dissolution of plagioclase and clinopyroxene and growth of oxides. These reactions can explain the, otherwise unexpected, higher MgO content of ilmenite in the oxide gabbronorite, in which clinopyroxene has a lower Mg#. This is explained by the buffering of the melt MgO, by the replacement of orthopyroxene by olivine, and by the dissolution of clinopyroxene. The invading melt must have had a higher Si-activity than melt in equilibrium with the olivine gabbro, leading to olivine replacement by orthopyroxene. This reaction may have produced the increase in the activity of Fe in the melt necessary for oxide saturation. Complete fluxing of the oxide gabbronorite is indicated by the lack of zoning in clinopyroxene.

Lack of large increases in ratios such as P/Nd in clinopyroxene in oxide gabbronorites suggest the metasomatising melt was not formed by immiscible separation.

Element abundance gradients in the host olivine gabbro (e.g., Cr in clinopyroxene) are interpreted as the result of cryptic metasomatism of the wall rock during melt flow. This may have been caused either by diffusion through interstitial melt in the wall rock, or advection of melt perpendicular to the main melt flux direction. Significant melt flux through the proto-oxide gabbronorite is required to drive the reaction and cryptically metasomatize the wall rock.

Trace- and major-element modeling will be presented with the aim of investigating the composition of the metasomatizing melt and constraining the melt flux.

References: [1] Robinson P. T. et al. (1989) *Proc. Init. Rpt. ODP Leg 118.* [2] Dick H. J. B. et al. (1991) *Proc. Sci. Res. Leg 118.* [3] Natland J. H. et al. (1991) *Proc. Sci. Res. Leg 118.* [4] Cannat M. et al. (1995) *Proc. Init. Rpt. ODP Leg 153.*

RESIDENCE OF MAGMA AT KILAUEA VOLCANO, HAWAI'I: INTERNAL THORIUM-230–RADIUM-226 ISOCHRON DATING OF THE 1955 EAST RIFT ERUPTION.

K. M. Cooper[1,2], M. R. Reid[1], R. C. Roback[2], M. T. Murrell[2], and D. A. Clague[3], [1]Department of Earth and Space Sciences, University of California, Los Angeles, 595 Charles Young Drive East, Los Angeles CA 90095, USA (kcooper@ess.ucla.edu), [2]Mail Stop J514, Los Alamos National Laboratory, CST-7, Los Alamos NM 87545, USA, [3]Monterey Bay Aquarium Research Institute, P.O. Box 628, 7700 Sandholdt Road, Moss Landing CA 95039, USA.

Introduction: Magma residence times are difficult to quantify, but have been estimated by a variety of methods. For Kilauea Volcano in Hawai'i, calculations based on geophysical estimates of reservoir volume combined with supply rate yield residence times from 100 yr [1] to 3000 yr [2], whereas estimates based on geochemical variations in erupted lavas are 30–180 yr [3], and an estimate based on crystal size distribution is ~10 yr [4]. This range of tens to thousands of years represents very large uncertainties in timescales of magma transport and differentiation. We undertook a different approach to determining residence times by comparing the relative magnitudes of disequilibria between ^{230}Th and its immediate daughter ^{226}Ra ($t_{1/2}$ = 1600 yr) in mineral and groundmass separates from lavas. The magnitude of disequilibrium in minerals is a function of the initial fractionation of Ra from Th and of the time elapsed since crystal growth. Because no long-lived isotope of Ra exists, we use Ba as a chemical proxy for inherited Ra in the minerals. By considering theoretical differences in partitioning behavior of Ra and Ba, we can account for fractionation effects, allowing us to obtain an internally consistent age of crystallization. We present here results from the early stage of the 1955 East Rift eruption of Kilauea and a minimum residence time derived from the ^{226}Ra-^{230}Th disequilibria.

Results: We measured Ra, Ba, and Th concentrations and Th- and U-isotopic ratios in pyroxene, plagioclase, and groundmass separates from the 1955 lava by thermal ionization mass spectrometers (TIMS) at Los Alamos National Laboratory. Our measurements of Ra and Th concentrations in these separates are among the lowest ever reported. Uranium-238 and ^{234}U are in secular equilibrium, as expected for unaltered volcanic rocks. An upper limit of 545 yr for fractionation of Ra from Th in the pyroxene can be calculated by assuming that the measured ^{226}Ra is entirely the result of *in situ* decay of ^{230}Th. The ^{226}Ra/Ba ratio of pyroxene is ~6× larger than that measured in plagioclase; unless this difference is due to Ra/Ba fractionation during crystallization, it must reflect relative changes in ^{226}Ra due to radioactive decay since crystallization. The apparent age of 448 ± 10 yr for the plagioclase-pyroxene mineral isochron would represent a volume-averaged age of crystallization of these minerals.

However, the groundmass does not lie on the pyroxene-plagioclase isochron. Taken at face value, this might indicate that the phenocrysts did not grow from the melt represented by the groundmass, but petrographic and geochemical evidence from the early 1955 lavas are consistent with equilibrium between the groundmass and plagioclase and pyroxene phenocrysts. A theoretical analysis of Ra and Ba partition coefficients based on the model of [5] suggests that a more likely explanation for the discrepancy is that Ra and Ba were fractionated during crystal growth. Our calculations predict that D_{Ba} should be 5–50× larger than D_{Ra} in plagioclase and pyroxene. The precise values of these partition coefficients are sensitive primarily to temperature and crystal composition. Within a reasonable range of magma temperatures (from initial coprecipitation of pyroxene and plagioclase from Kilauea magmas at 1160°–1170°C to eruption temperatures for the early 1955 lavas of ~1100°C) and crystal compositions, the apparent discrepancy between groundmass and phenocryst compositions can be explained entirely by predicted Ra-Ba fractionation.

Based on our calculated partition coefficients, differential fractionation of Ra and Ba accounts for only a minor component of the observed differences in ^{226}Ra/Ba in the pyroxene and plagioclase separates, and, in fact, would predict higher ^{226}Ra/Ba in plagioclase than pyroxene. Thus, the higher ^{226}Ra/Ba in pyroxene must reflect *in situ* decay. When Ra/Ba fractionation in the three components are simultaneously considered, the data are consistent with crystallization of pyroxene and plagioclase from a magma represented by the groundmass composition at a mean age of 530–540 yr before present.

Discussion: The minimum residence time for the early 1955 magma implied by this analysis is therefore ~500 yr, substantially longer than most previous estimates of residence time for Kilauea magmas. Because the age obtained represents an average age of crystallization, a significant volume of crystals likely formed much earlier than 500 yr before eruption. If crystal growth rates were constant, crystallization of plagioclase and pyroxene would have begun ~1000 yr before eruption. Assuming a steady-state system and combining 500-yr minimum residence time with a magma supply rate of 0.08–0.11 km^3/yr [1] would imply that the volume of interconnected magma in the reservoir is >40 km^3 (as compared to typical estimates of ~11 km^3 [e.g., 1]) and/or that the magma supply rate is lower than previous estimates. Using our residence estimate and the temperature interval for pyroxene + plagioclase crystallization discussed above, we calculate an average cooling rate of <0.14°C/yr; if crystallization began at 1000 yr, the cooling rate would be 0.07°C/yr. The average temperature of the primary magma entering the reservoir has been estimated at 1346°C [2]; if our calculated cooling rates are similar to cooling rates early in the storage history of the magmas, 1000–2700 yr of residence would be required prior to the beginning of pyroxene-plagioclase crystallization.

References: [1] Decker R. W. (1987) *U.S. Geological Survey Prof. Paper 1350,* 997–1018. [2] Clague D. A. (1996) *AGU Chapman Conf.* (Tenerife, Canary Islands), 20–21. [3] Pietruszka A. J. and Garcia M. O. (1999) *EPSL, 167,* 311–320. [4] Mangan M. T. (1990) *J. Volcanol. Geotherm. Res., 44,* 295–302. [5] Blundy J. and Wood B. (1994) *Nature, 372,* 452–454.

APPLICATION OF CHARGE-RADIUS CONCEPTS TO TRACE ELEMENTS IN IGNEOUS AND METAMORPHIC ZIRCON.

D. H. Cornell[1], A. Scherstén[1], P. Hoskin[2], and J. Lindsay[3], [1]Gothenburg University, Box 460, SE 40530, Sweden (cornell@geo.gu.se), [2]Australian National University, Canberra, Australia (paul.hoskin@anu.edu.au), [3]GeoForschungs-Zentrum, Potsdam, Germany (kiwi@gfz-potsdam.de).

Introduction: Zircon, $ZrSiO_4$, is a geochronological archive because of its trace-element content and stability. Despite startling advances in imaging and dating polyphase zircon grains, the attribution of dates to igneous or metamorphic events still suffers from a lack of theoretical explanations for zircon's unique trace-element behavior and internal structure [1].

Igneous Zircon: Igneous zircon is often characterized by oscillatory zonation in cathodoluminescence (CL) or backscattered electron images. It commonly has ~100–1000 ppm U and Th, with Th/U >0.2, compositionally typified by zircon from a 4–5 Ma Andean crystal-poor rhyolite ignimbrite [2] (Fig. 1). Glass, zircon, apatite, and monazite in this rock were analyzed by laser ablation inductively coupled plasma mass spectrometry (LA-ICP-MS) with 25–50-µm spot size and depth. Partition coefficients (Kd) are valid for igneous zircon growth.

The REE^{3+} cations together with Sc define a 0.9-Å peak, the optimal size for ions entering the Zr site. A parallel curve through 4+ Th, Zr, and Hf is consistent with this interpretation, their 100-fold higher Kd reflect a charge balance problem for 3+ cations entering the Zr site, incompletely compensated by P^{5+}-Si^{4+} substitution. The positive Ce anomaly, typical of magmatic zircon, is due to the local oxidation of Ce^{3+} to Ce^{4+} entering zircon [3], driven by the charge balance requirement and the near-optimal size of Ce^{4+}. Despite the high Kd predicted for U by the 4+ curve, it plots below the 3+ curve in most magmatic zircon. Why? (1) Oxidation to U^{6+}(0.81Å), although possible by analogy with Ce, would not decrease its theoretical Kd. (2) The CL oscillations seen in igneous zircon are due to an intrinsic bright CL signal, modulated by variable U (350–915 ppm in TOC3 zircon), quenching the CL as it exceeds 3–400 ppm [1]. (3) Magmatic zircon commonly has small U-rich, CL-dark cores. (4) Intermediate and mafic rocks, with lower U levels than rhyolite or granite, have CL-dark, high-U zircon reflecting more efficient supply of U (higher T, lower viscosity). These observations suggest that U partition into magmatic zircon is retarded kinetically. High theoretical Kd and low U levels in magma relative to Zr (TOC3: U 10, Zr 70, Th 19 ppm), and relatively slow diffusion of U from the surrounding magma, results in depletion-replenishment cycles in the magma around growing zircons.

Metamorphic Zircon: Metamorphic zircon may be recognized in CL images, overgrowing or cutting across igneous growth zonation. It is usually CL-homogeneous and may be either bright or dark, depending on U content.

Figure 2 features a domain of CL-bright reworked 940-Ma zircon in a CL-dark 1680-Ma magmatic grain from the Borås tonalite (the magmatic

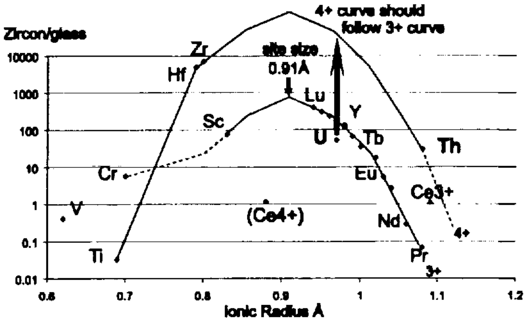

Fig. 1. Onuma Diagram for Andean rhyolite pumice TOC3 from the Altiplano-Puna volcanic complex [2]. Radii all for six-fold coordination after Whittaker and Muntus (1970).

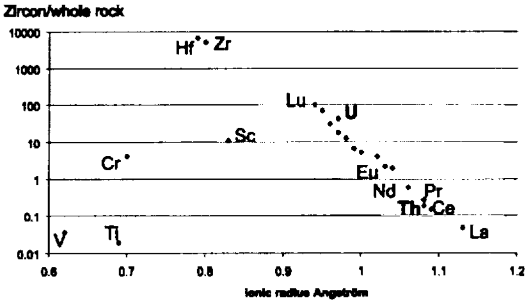

Fig. 2. Onuma diagram for metamorphic zircon in Borås Intrusion tonalite AA9635, Sweden, analysis by ion probe and LA-ICP-MS.

zircon shows features similar to Fig. 1). Its composition is typical of both new and completely reworked metamorphic and also pegmatite zircon and reflects equilibrium with hydrous fluid rather than growth from silicate magma (the whole rock is used for convenience). The disapperance of Ce anomaly and coherence of Th and Ce with the REE^{3+} curve shows that charge-balance considerations were unimportant. This may reflect substitution of [OH]$^-$ for O in the zircon lattice, providing charge-balance flexibility. Uranium also plots close to the curve; metamorphic zircon generally has the low Th/U ratios that crystal-chemical theory predicts for equilibrium zircon. The fluid-dominated system presents no kinetic problems to the attainment of equilibrium.

This crystal-chemical approach provides a theoretical basis for the distinction and dating of different types of zircon.

References: [1] Cornell D. H. et al. (1997) *Terra Nova, 9,* 450. [2] Lindsay J. et al. (1999) *J. Conf. Abstr., 4,* 414. [3] Hinton R. W. and Upton G. G. J. (1991) *GCA, 55,* 3287–3302.

AT LEAST THREE CARBON-ISOTOPIC EXCURSIONS/GLACIATIONS IN THE NEOPROTEROZOIC: CARBON-ISOTOPIC CHEMOSTRATIGRAPHY OF NEOPROTEROZOIC-CAMBRIAN STRATA, SOUTHERN GREAT BASIN, USA.

F. A. Corsetti[1] and A. J. Kaufman[2], [1]Department of Geological Sciences, Preston Cloud Research Laboratory, University of California, Santa Barbara CA 93106, USA (corsetti@magic.geol.ucsb.edu), [2]Department of Geology, University of Maryland, College Park MD 20742, USA.

Neoproterozoic sedimentary rocks record very large changes in the C-isotopic composition of seawater (>14‰ PDB), many times greater than most excursions seen in younger sediments [1]. In Neoproterozoic time, intensely negative C-isotopic excursions were apparently associated with widespread glaciations ~700–750 Ma and 560–600 Ma [1,2]. However, the number and form of C-isotopic excursions and glaciations found in Neoproterozoic strata between ~750 Ma and ~548 Ma are currently debated [2–6]. Some researchers interpret at least four post ~750-Ma glacially-influenced negative C-isotopic excursions [1–3,6]. Others find no more than two major negative C-isotopic anomalies in any one stratigraphic section, and extrapolate only two glacial events [4,5].

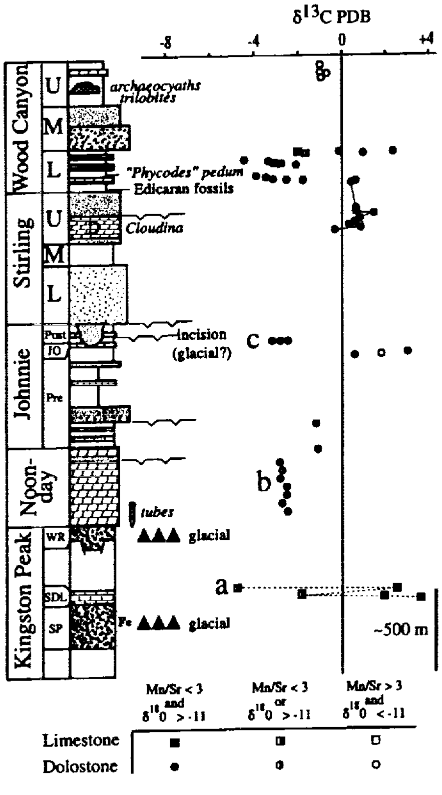

Fig. 1. Carbon-isotopic composition of microsampled primary marine phases vs. stratigraphic position. Note the presence of *three* negative isotopic excursions (a, b, c) in association with glacial or presumed glacial deposits.

In Death Valley, California, we have identified three negative C-isotopic excursions in a continuous Neoproterozoic sequence. Two older excursions (within the Sourdough Limestone member of the Kingston Peak Formation, and the overlying Noonday Dolomite) are in direct association with glacially derived strata (a and b in Fig. 1, recently confirmed by others). The oldest glacial deposits contain iron-formation, similar to many "Sturtian" glacial deposits in other localities [1]. A third profoundly negative excursion (in the overlying Johnnie Formation) is found in association with deeply incised valleys indicative of major relative sea level change (c in Fig. 1, also suggestive of glacial character), and was apparently not sampled by previous workers [e.g., 5]. Nonmarine sediments (the Stirling Quartzite) overly the strata containing the third excursion, precluding the potential preservation of a fourth excursion, as predicted by others. The Precambrian-Cambrian Boundary is constrained by the presence of *Phycodes (Treptichnus) pedum* in the overlying Wood Canyon Formation, and confirmed by the presence of a negative isotopic excursion, as seen in many other pre-C-C boundary sections.

Thus, we suggest that there were *at least* three negative C-isotopic excursions in Neoproterozoic time associated with glaciations, casting doubt on the claim of only two excursions/glaciations.

References: [1] Kaufman A. J. and Knoll A. H. (1995) *Precambrian Res., 73,* 27–49. [2] Kaufman A. J. et al. (1997) *Proc. Natl. Acad. Sci., 94,* 6600–6605. [3] Hoffman P. F. et al. (1998) *Science, 281,* 1342–1346. [4] Kennedy M. J. et al. (1998) *Geology, 26,* 1059–1063. [5] Prave A. (1999) *Geology, 27,* 289–384. [6] Saylor B. Z. et al. (1998) *J. Sed. Res., 68,* 1223–1235.

TRACE METALS IN SEDIMENTARY IRON SULFIDES: PRELIMINARY RESULTS.

C. F. Cottnam, I. B. Butler, and D. Rickard, Department of Earth Sciences, Cardiff University, Park Place, Cardiff CF1 3YE, Wales, UK (cottnam@cardiff.ac.uk).

Introduction: Anoxia are important in sediments and the water columns of restricted basins. The biosphere extends well below the present-day surface and, in these anoxic environments, sulfides control the bioavailability and mobility of metals by formation of sulfide minerals and aqueous complexes [1,2] and by sorption of metals with sulfide minerals. Iron sulfides are by far the most common sulfide minerals formed in sedimentary environments, and the association of high concentrations of metals such as Cu, Co, Ni, Hg, Pb, Au, etc., with iron sulfide minerals is well documented [e.g., 3,4], with concentrations of >10 wt% reported for metals in sedimentary mackinawite [4]. Both coprecipitation and adsorption mechanisms have been proposed as the means of trace metal incorporation with sulfide materials.

Experimental: Coprecipitation and adsorption of metals (Co, Ni, Cu, Pb, and Zn) at low temperature (25°C) with precipitated Fe(II) monosulfide have been experimentally investigated. For coprecipitation experiments two methods were utilized: (1) direct precipitation of mixed Fe and metal solutions by addition to sulfide solution, and (2) electrolytic corrosion of metal doped Fe wire in the presence of $H_2S_{(aq)}$. Surface adsorption of metals on iron sulfides was studied by measurement of uptake of metals onto preprecipitated Fe(II) monosulfide (disordered mackinawite) at low (μM) concentration.

Results: In coprecipitation experiments, it was found that nucleation of metal sulfides with FeS resulted in the formation of discrete sulfide mineral phases that were identifiable using Debye-Scherrer X-ray diffraction (XRD) methods. The precipitation kinetics of FeS have been shown [5] to follow standard Eigen-Wilkins kinetics where the rate of substitution of H_2S for H_2O is a function of water loss for the aquocation, $-k_w$. Experimental evidence [5,6] suggested that the relative rates of CuS and ZnS formation are also consistent with this mechanism. It is therefore proposed that the rates of formation of first row transition metal sulfides are a function of $-k_w$. The water loss rate constant for the first row transition aquometal ions (Cu-Fe) varies from 1×10^7 (Fe(II)) to 8×10^8 (Cu(II)). The rate of precipitation of the sulfides via the Eigen-Wilkins mechanism is then in the order CuS (fastest) > ZnS > CoS > NiS > FeS (slowest). Thus high weight percent concentrations if metals in association with natural sedimentary mackinawite cannot be the result of coprecipitation of metals with the FeS phase, since each first row transition metal sulfide forms at a different rate, but Cu-Ni sulfides before FeS. In the case of MnS this forms slower than FeS and Mn could be incorporated in FeS by a coprecipitation mechanism (consistent with the observations of Raiswell and Plant [4]). No information is available about the mechanism of PbS, HgS, and AuS precipitation from aqueous solution and therefore $-k_w$ cannot be used as a rate proxy at this time.

Adsorption experiments demonstrate the rapid and efficient adsorption of metals from solution by precipitated FeS. Adsorption of metals present at μM concentrations over the duration of the experiment resulted in the concentration of metals to weight percent levels without nucleation of discrete sulfide phases. We conclude that the association of high trace-metal concentrations with FeS in sediments is primarily the result of adsorption of metals from solution at low concentrations.

Future Directions: The behavior of metals associated with sedimentary FeS during pyrite formation is not well understood. The nature of the reaction pathway is expected to affect the metal loading of the pyrite and the bioavailability of metals. Experimental studies of metal incorporation during pyrite formation reactions will aid predictions of the medium term behavior of pollutant metals in landfill sites, anoxic sediments, and constructed wetlands.

References: [1] Luther G. W. III and Ferdelman T. G. (1993) *Environ. Sci. Technol., 27,* 1154–1163. [2] Luther G. W. III et al. (1996) *Environ. Sci. Technol., 30,* 671–679. [3] Huerta-Diaz M. A. and Morse J. W. (1992) *GCA, 56,* 2681–2702. [4] Raiswell R. and Plant J. (1980) *Econ. Geol., 75,* 684–699 [5] Rickard D. (1995) *GCA, 59,* 4367–4380. [6] Rickard D. et al. (1995) in *ACS Symposium Series, Vol. 612* (M. Vairaramurthy and M. Schoonen, eds.), pp. 168–193, ACS. [7] Sweeney R. E. and Kaplan I. R. (1973) *Econ. Geol., 68,* 618–634. [8] Rickard D. (1975) *Am. J. Sci., 275,* 636–652. [9] Rickard D. (1997) *GCA, 61,* 115–134. [8] Wilkin R. and Barnes H. L. (1996) *GCA, 60,* 4167–4179.

A SINGLE-SITE MODEL FOR METAL ADSORPTION OVER A RANGE OF SURFACE COVERAGES.

L. J. Criscenti and D. A. Sverjensky, Department of Earth and Planetary Sciences, Johns Hopkins University, Baltimore MD 21218, USA (crisc_lj@jhuvms.hcf.jhu.edu; sver@jhu.edu).

The rate of metal migration in the subsurface environment depends on the metal concentrations adsorbed by minerals. Metal adsorption over a range of surface coverages is often depicted as isotherms, in which the equilibrium concentrations of adsorbed and aqueous metal are compared on a log-log diagram. If data are collected over a range of metal concentrations, the isotherms are curvilinear, with slopes of 1 at low concentrations and slopes less than 1 at higher concentrations. Before the development of surface complexation models, the Langmuir equation, which accounts for adsorption to one surface site type, was used to describe the isotherm at low surface coverages. As the isotherm slope decreases, it was inferred that the metal adsorbs to more than one site type [1].

This interpretation has been incorporated into surface complexation studies without an adequate investigation of the effects of surface charge and potential on calculated isotherms. Previous workers have shown that a single-site triple layer model (TLM) can predict Co adsorption over a range of surface coverages [2] and that the curvature of isotherms calculated with a single-site TLM differs depending on the choice of complex [3]. It is proposed here that metal adsorption over a wide range of surface coverages can be described by a single-site TLM and that the observed differences in adsorption isotherm curvature reflect the formation of different types of metal surface complexes.

In this study, the Extended TLM [4] is used to develop a model for metal adsorption. In previous work [5], metal adsorption edges over a range of ionic strengths were fitted using one or two surface complexes. A large variety of complexes (e.g., $>SOHM^{2+}-NO_3^-$, $>SOM^+$, $>SOHM^{2+}$) were found for different metal-solid-electrolyte systems. These complexes and associated equilibrium constants can be used to predict adsorption over a range of metal concentrations. For example, the complex and log K found to fit ionic strength data [6] for Co adsorption onto magnetite (Fig. 1a) successfully predict adsorption for Co concentrations from 10^{-9} to 10^{-4} M. (Fig. 1b).

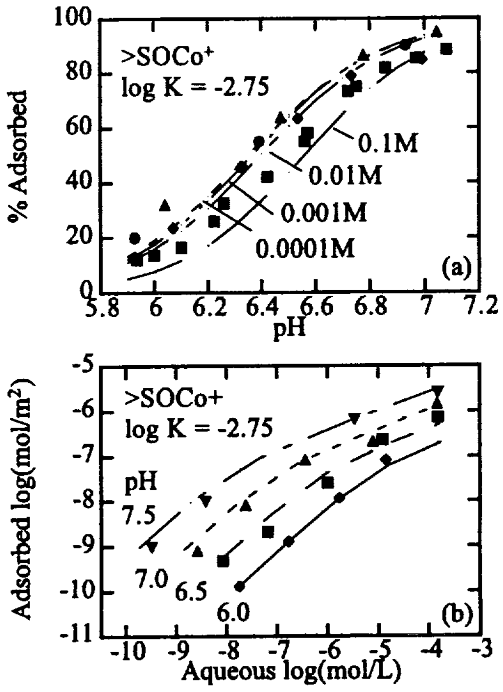

Fig. 1. Cobalt adsorption onto magnetite. Data from [6].

Surface complex stoichiometries and equilibrium constants can also be determined by fitting a suite of adsorption isotherms at different pH values. Within the context of a TLM, an isotherm equation is given by

$$C_{sc} = \frac{N_s \Pi\left(\frac{a_r}{a_p}\right) K \times 10^{(-z\Psi_o - v\Psi_\beta/2RT)}}{1 + \Pi\left(\frac{a_r}{a_p}\right) K \times 10^{(-z\Psi_o - v\Psi_\beta/2RT)}}$$

where C_{sc} is the concentration of the complex, N_s is the total site density, a_r and a_p are the activities of the aqueous reactants and products, K is the equilibrium constant, z, v, Ψ_o, and Ψ_β are the charges and electrostatic potentials of the complex on the 0 and β-planes of the TLM, R is the gas constant, and T is temperature.

The electrostatic potential term influences the shape of the isotherm. On a positive surface, the larger this term, the more metal adsorption is suppressed. As a result, the Langmuir portion of the isotherm decreases and the Freundlich portion (slope <1) increases. The maximum concentration of metal adsorbed and the spacing between adsorption isotherms at different pH also depends on the type of complex and the electrostatic potential term in the isotherm equation.

Using this information, metal surface complexes have been found to fit adsorption data for a wide variety of metals (Co, Cd, Cu, Pb, and Zn) onto different solids (goethite, hematite, HFO, corundum, quartz, silica, rutile, and magnetite) from different electrolytes (KNO_3, $NaNO_3$, NaCl, and $NaClO_4$). Metal surface coverages ranging from 10^{-9} mol/m^2 to 10^{-4} mol/m^2 can be fit and predicted successfully with a single-site TLM if the appropriate metal adsorption reactions are chosen.

References: [1] Benjamin (1979) Ph.D. thesis. [2] Katz and Hayes (1995) *JCIS, 170,* 477–490. [3] Robertson and Leckie (1997) *JCIS, 188,* 444–472. [4] Sahai and Sverjensky (1997) *GCA, 61,* 2827–2848. [5] Criscenti and Sverjensky (1999) *Am. J. Sci.*, in review. [6] Tamura et al. (1983) *JCIS, 92,* 303–314.

THE ORIGIN OF MINEWATER CONTAMINATION FROM THE CARBONIFEROUS COAL MEASURE SEQUENCE IN THE UNITED KINGDOM.

S. J. Croxford[1], S. A. Banwart[1], and J. C. Cripps[2], [1]Department of Civil Engineering, Sir Frederick Mappin Building, Mappin Street, Sheffield S1 3JD, UK (cip98sjc@sheffield.ac.uk), [2]Department of Earth Science, Dainton Building, Brook Hill, Sheffield S3 7HF, UK (j.cripps@sheffield.ac.uk).

Since the late 1970s, more than 75% of British coal mines have been decommissioned. The abandonment of these mines and associated operations has resulted in a rapid rise in groundwater levels within the affected areas. This rise in groundwater levels may result in the reestablishment of ancient springs as well as the development of new discharges from abandoned mines and associated structures. Water discharges generated through rebound are liable to be contaminated with a series of chemicals associated with the weathering of worked coal measure rocks. These contaminants can be detrimental to the local subterranean and surface environment. Therefore, it is essential to understand the development of these contaminated minewaters within various oxidizing and reducing conditions. Once these processes have been understood it maybe possible to produce a predictive model for the potential contaminant life span of a particular coal or mine field. Such research could also be adapted to consider other potentially contaminating environments, including ore and mineral mining, and associated spoil tips, opencast mining and industrial contaminated land.

In order to be able to develop a predictive model, it is essential that chemical weathering processes of mined coal measure sequences be understood. Hence, a series of laboratory batch reactor and column experiments are currently being constructed to determine the initial origin of minewater contamination and to ascertain the rate of chemical weathering under set laboratory conditions. These experiments will initially concentrate on a Carboniferous Coal Measure sequence selected from the Rawdon Colliery site, Moira, Leicestershire, England, from which a selection of unweathered and partially weathered rocks of different lithologies have been obtained. The samples comprised two Pyritic coal seams (P38 and P39 Coal), a siltstone, ironstone, two seatearths, and two mudstones. These samples were identified and classified for their initial chemical and physical properties prior to being incorporated into a simple preliminary experiment. This initial experiment was designed to determine the immediate reactively of the rocks in an aqueous solution. The initial pH measurement varies from highly acidic (pH 2.35) with the pyritic coals to circumneutral (pH 6.2) with the ironstone. Following completion of these initial tests, representative samples from each lithology were placed in batch reactors and submerged in a 1×10^{-2} molar NaCl solution. Atmospheric air was pumped through the batch reactors at a constant rate and pH and temperature levels were regularly monitored. Subsampling of the solid and liquid phases was periodically conducted to determine the progression of chemical reactions within the two phases.

Following completion and evaluation of these experiments, column tests will be conducted to study the chemical reactions that take place in unsaturated, oxidizing environments. Again, initial characterization of the samples together with monitoring of the chemical and mineralogical changes will be undertaken. Once these tests are concluded it is proposed that laboratory data will be compared with field data to test whether the chemistry of the initial and long-term discharges conform to predictions based on a known geometry, groundwater recovery, and sequence mineralogy.

CONTROLS ON METAL TRANSPORT IN SEDIMENT-COVERED RIDGE-CREST HYDROTHERMAL SYSTEMS: EXPERIMENTAL AND THEORETICAL CONSTRAINTS.

A. C. Cruse and J. S. Seewald, Mail Stop 4, Department of Marine Chemistry and Geochemistry, Woods Hole Oceanographic Institution, Woods Hole MA 02543, USA (acruse@whoi.edu; jseewald@whoi.edu).

Introduction: Hydrothermal activity at sediment-covered spreading centers such as Middle Valley and Guaymas Basin involves the chemical interaction of seawater with organic-bearing sediments and basaltic rocks. In general, fluids in these environments contain elevated concentrations of dissolved metals (Fe, Mn, Zn, and Cu) relative to seawater and are responsible for the formation of seafloor massive sulfide deposits. The presence of sedimentary organic matter has a potentially strong impact on metal transport by controlling pH and redox. Due to the complexity of natural systems, the reactions by which organic matter influences metal transport remain unclear. Presently, it is also uncertain as to the extent that sediments act as a source of dissolved metals relative to underlying basalts.

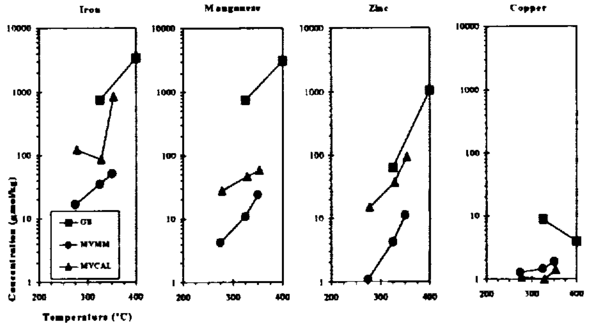

Fig. 1. Dissolved metal concentrations vs. temperature for sediment alteration experiments. Note log scale for concentration.

Reaction Mechanism: In order to assess the role of sediment alteration during metal mobilization, we conducted a set of hydrothermal experiments reacting fluids of seawater chlorinity with unaltered organic-lean Middle Valley and organic-rich Guaymas Basin sediments at 275°–400°C and 350–400 bars (experiments MVMM and GB respectively). Metal concentrations (Fe, Mn, and Zn) in both experiments increased with increasing temperature, although metal concentrations in GB were up to an order of magnitude greater than in MVMM (Fig. 1).

Variations in major-element fluid chemistry and observed alteration assemblages in GB suggest that precipitation of calcite represents an effective means to generate acidity under hydrothermal conditions, provided sources of Ca and CO_2 are available. During sediment alteration, albitization of anorthite represents an abundant Ca source while alteration of organic matter produces large amounts of CO_2. To test this mechanism, a second Middle Valley alteration experiment (MVCAL) was conducted in which excess calcite was added to maintain saturation. Metal concentrations in MVCAL were intermediate between those observed in MVMM and GB (Fig. 1). Fluid speciation calculation suggests that *in situ* pH conditions during GB were lower than during MVCAL, consistent with substantially greater amounts of organically-derived CO_2 released during alteration of organic-rich Guaymas Basin sediment.

Dissolved Cu concentrations in all three experiments remained at or near detection limits. Dissolved H_2 concentrations in all experiments were high, indicative of the reducing conditions caused by the presence of organic matter. Our results are consistent with other experimental work demonstrating that Cu mobility is strongly influenced by redox conditions [1].

Comparison with Basalt: Comparison of these data with results from similar basalt alteration experiments [2] reveals that at a given temperature basalt alteration results in dissolved Fe, Mn, and Zn concentrations intermediate between the two sedimentary endmembers. Copper concentrations were generally higher during basalt alteration relative to sediment alteration due to the more oxidizing conditions during fluid-basalt interaction. Our results indicate that sediments can be highly effective sources of metals to hydrothermal fluids, provided sufficient organic matter is present to generate requisite CO_2. The range of dissolved metal concentrations observed in fluids from active vents at Guaymas Basin and Middle Valley are consistent with those observed in our experiments and suggest equilibration with overlying sediments during ascent from deep-seated reaction zones to the seafloor.

References: [1] Seyfried W. E. Jr. and Ding K. (1993) *GCA, 57,* 1905–1917. [2] Seewald J. S. and Seyfried W. E. Jr. (1990) *EPSL, 101,* 388–403.

INTERLABORATORY DATA ON ELEMENTAL AND ISOTOPIC CARBON IN THE CARBONACEOUS PARTICLE REFERENCE MATERIAL, NIST SRM 1649A.

L. A. Currie[1], B. A. Benner Jr.[1], R. Cary[2], E. R. M. Druffel[3], T. I. Eglinton[4], P. C. Hartmann[5], J. D. Kessler[1], D. B. Klinedinst[1], G. A. Klouda[1], J. V. Marolf[1], C. A. Masiello[3], A. Pearson[4],

J. G. Quinn[5], C. M. Reddy[4], J. F. Slater[6], and S. A. Wise[1], [1]National Institute of Standards and Technology, Gaithersburg MD 20899, USA, [2]Sunset Laboratories Inc., 2221 Yew Street, Forest Grove OR 97116, USA, [3]Department of Earth System Science, University of California, Irvine, Irvine CA 92697, USA, [4]Department of Marine Chemistry and Geochemistry, Woods Hole Oceanographic Institution, Woods Hole MA 02543, USA, [5]Graduate School of Oceanography, University of Rhode Island, Narragansett RI 02882, USA, [6]Climate Change Research Center, University of New Hampshire, Durham NH 03824, USA.

Because of increased interest in the marine and atmospheric sciences in elemental carbon (EC) or black carbon (BC) or soot carbon (SC), and the difficulties in analyzing or even defining this pervasive component of particulate C, it has become increasingly important to have reference materials for intercomparison and quality control. The NIST "urban dust" standard reference material SRM 1649a is useful in this respect, in part because it comprises a considerable array of inorganic and organic species, and because it exhibits a large degree of isotopic heterogeneity. Certain organic fractions, for example, have ^{14}C contents reflecting essentially fossil sources (aliphatic fraction), whereas others contain significant amounts of biomass C (polar fraction: 43% modern C).

Although the "Washington urban dust" was collected from the Washington DC atmosphere more than 20 years ago, it is only within the past five years that a significant increase has been seen in C-isotopic and -elemental data for this SRM. Notable exceptions were the use of this SRM, together with its partner from St. Louis (SRM 1648), in a revealing EC intercomparison in the early 1980s, and ^{13}C and ^{14}C data for total and aromatic fractions, published in 1984. During 1998, SRM 1649 was repackaged and recertified as SRM 1649a, with the issuance of a Certificate of Analysis dated November 19, 1998. In contrast to previous certificates, this one devoted an entire page to "Reference values for carbon composition of SRM 1649a" including concentration data for total C and six different subclasses, and isotopic data (^{13}C, ^{14}C) for four of these. Also, for the first time ^{14}C speciation in individual PAH was listed.

During the past two years, informal intercomparisons have been under way among several laboratories represented by the coauthors of this paper, using SRM 1649a and other environmental SRMs, with a special focus on the elemental carbon concentration, and ^{13}C and ^{14}C *in* EC. A summary will be given of these new data, together with an indication of method dependence, which is considerable. (EC results range from ~0.02 to 0.13 g/g.) The new data will also have an opportunity to find a place in an expanded C-isotopic and -elemental table in a revised (1999) Certificate of Analysis. A primary goal of the poster presentation of the recent interlaboratory data on EC and C isotopes in EC and other significant fractions is to create a forum for discussion of the merits of the several chemical and thermal EC methods, especially as they relate to the subsequent determination of meaningful reference values for ^{13}C and ^{14}C. A secondary goal is to consider the need for establishing a broader, more formal framework for intercomparison, with extension to other environmental carbonaceous reference materials, as appropriate.

THERMAL OPTICAL ISOTOPIC ANALYSIS OF ELEMENTAL CARBON IN CARBONACEOUS PARTICLES.

L. A. Currie and J. D. Kessler, National Institute of Standards and Technology, Gaithersburg MD 20899, USA.

Elemental carbon (EC), also referred to as black carbon (BC) or soot carbon (SC), is one of the most interesting and important, yet one of the most metrologically elusive forms of C in the environment. Its importance springs from its unique role as a tracer of fire (incomplete combustion), especially in the flaming stage, and from its potential impact on climate *via* radiation forcing. Carbon-isotopic data for EC has special utility for the discrimination of source fuels, on the basis of photosynthetic cycle (^{13}C) and "age" (fossil, biomass; ^{14}C).

The essential problem with EC is that it is *not* a unique substance, but rather a continuum, so that analysis and isolation necessarily rely upon operational physicochemical definitions. This problem is compounded for isotopic measurements of EC, because it must be isolated prior to measurement by isotope ratio mass spectrometry (IRMS, ^{13}C) and/or accelerator mass spectrometry (AMS, ^{14}C). For studies involving tiny samples from remote atmospheres and polar ice cores, for example, one faces a further complication from impurities and blanks associated with some of the more vigorous chemical methods of EC isolation. We present here the results of a new approach to EC-isotopic measurement, using the special characteristics of the thermal optical transmission (TOT) method of EC assay, combined with a batch technique for capturing TOT fractions for subsequent isotopic analysis by IRMS and/or AMS. Special merits for low-level measurements of this purely thermal technique for EC isolation are (1) minimal blanks and impurities, and (2) discrimination of EC from pyrolyzed C via continuous monitoring of sample transmission.

The results will be demonstrated with isotopic data for a series of fractions, culminating in EC, isolated from NIST SRM 1649a, the urban dust carbonaceous particle standard reference material. The resulting ^{14}C data for the organic and elemental fractions of this isotopically heterogeneous material illustrate the utility of the approach, which is perhaps the forerunner of particulate ^{14}C speciation by continuous flow TOT/AMS. Ultimately, with online splitting to both types of mass spectrometer, one would have the capability of producing three dimensional dual isotopic thermograms.

SEA-LEVEL AND DEEP-OCEAN TEMPERATURE CHANGES SINCE THE LAST INTERGLACIAL FROM COMBINED PROTACTINIUM-231 AND THORIUM-230 DATING OF CORALS.

K. B. Cutler[1], R. L. Edwards[1], F. W. Taylor[2], H. Cheng[1], J. Adkins[3], C. D. Gallup[4], and G. S. Burr[5], [1]Department of Geology and Geophysics, University of Minnesota, Minneapolis MN 55455, USA (bank0026@tc.umn.edu), [2]Institute for Geophysics, University of Texas at Austin, Austin TX 78759, USA, [3]Lamont-Doherty Earth Observatory, Columbia University, Route 9W, Palisades NY 10954, USA, [4]Department of Geology, University of Maryland, College Park MD 20742, USA, [5]Department of Physics, National Science Foundation Accelerator Facility for Radioisotope Analysis, University of Arizona, Tucson AZ 85721, USA.

We use high-precision ^{231}Pa dating techniques to test the accuracy of ^{230}Th ages of fossil corals [1] and thereby establish the timing and amplitude of sea-level changes since the last interglacial. Corals from Papua New Guinea, Barbados, and elsewhere have been used since the 1960s to reconstruct sea-level history based on coral elevation, age, and local tectonic uplift rate. The ability to pinpoint the time of sea-level events was substantially improved in the late 1980s with the advent of high-precision ^{230}Th methods for dating corals. Despite these advances, the timing of sea-level changes has remained somewhat controversial due to the possibility of diagenesis and subsequent alteration of the coral age. Now, with similar techniques and comparable precision possible for ^{231}Pa dating, we have an independent check on ^{230}Th ages, which adds considerable confidence to sea-level histories established from samples that record concordant ages.

We dated nearly 30 coral samples from Papua New Guinea and Barbados with high-precision ^{230}Th and ^{231}Pa dating methods. The results were added to the existing bank of coral-based sea-level data and all data were screened based on the precision in sample age, proximity of the initial δ^{234}U value to the modern marine value, and degree to which the local diagenetic processes are constrained. Our data were subjected to an additional filter, ^{230}Th and ^{231}Pa age-concordancy. The resulting data were used to obtain a sea-level record.

Our data confirm a number of well established aspects of the sea-level curve, and also resolve some discrepancies. Furthermore, our data places new constraints on rates of sea-level change for specific portions of the curve. Sea level dropped rapidly between marine O-isotopic stages 5e to 5d, 5c to 5b, 5a to 4, and 3 to 2. The most rapid drop took place during the 5a to 4 transition, when sea level dropped at a rate of 9.2 m/k.y. for 5 k.y. Thus, almost 40% of glacial maximum ice volume was accommodated in 5 k.y. Additionally, our data yields the height of sea level during stage 5b, revealing that sea level dropped about 44 m between stages 5c and 5b, and rose about 49 m between stages 5b and 5a.

Each of the four periods of rapid sea-level drop correspond in time to intervals of unusually low northern hemisphere summer insolation [2], suggesting a fairly direct relationship between orbital forcing and climate during these intervals. Conventional wisdom suggests that long periods are required to reach maximum glaciation during a glacial cycle. Our data suggest that in fact ice buildup is at times very rapid. Thus, we argue that long intervals of time are required to reach maximum glaciation because the conditions amenable to glacial growth, i.e., very low insolation values, occur for only brief periods of time.

Protactinium-231 dating has also given insight to the nature of diagenesis at sample sites in New Guinea. Samples of the same age but with different degrees of alteration, and thus varying degrees of discordancy between the ^{231}Pa and ^{230}Th ages, were plotted on a (^{231}Pa/^{235}U) and (^{230}Th/^{234}U) concordia diagram. The results revealed that the local diagenetic processes usually involved significant Pa loss accompanied by a much smaller change, by loss or gain, in the Th budget.

Finally, a plot of sea level vs. deep-Pacific δ^{18}O reveals that a significant deep-ocean temperature shift occurred subsequent to 5e and during Termination I, consistent with the conclusions of earlier workers [3]. In addition, our sea-level record, combined with constraints from δ^{18}O measurements on stage 2 pore fluids [4], indicate that the cooling subsequent to 5e was smaller than the Termination I warming. The temperature residual is linearly correlated with sea level between stages 5c and 2. We observe a similar pattern in the deep Atlantic, but find a larger temperature signal.

References: [1] Pickett D. A. et al. (1994) *Anal. Chem., 66,* 1044–1049; Edwards et al. (1997) *Science, 276,* 782–786. [2] Berger A. (1978) *Quat. Res., 9,* 139–167. [3] Chappell J. and Shackleton N. J. (1986) *Nature, 324,* 137–140; Fairbanks R. G. and Matthews R. K. (1978) *Quat. Res., 10,* 181–196. [4] Schrag D. P. et al. (1996) *Science, 272,* 1930–1932.

THE NEODYMIUM-ISOTOPIC COMPOSITION IN A BOREAL RIVER: A REFLECTION OF SELECTIVE WEATHERING AND COLLOIDAL TRANSPORT.

R. Dahlqvist[1], P. S. Andersson[1], and J. Ingri[2], [1]Laboratory for Isotope Geology, Swedish Museum of Natural History, Box 50007, 104 05 Stockholm, Sweden (ralf.dahlqvist@nrm.se; per.andersson@nrm.se), [2]Department of Geology and Geochemistry, Stockholm University, 106 91 Stockholm, Sweden (johan.ingri@geo.su.se).

Selective weathering of till in northern Scandinavia has caused a fractionation of the REE. The glacial ice left the area about 8700 yr ago. Since then between 69% and 84% of the light REE and between 54% and 79% of the heavy REE has been depleted from the E-horizon, the most weathered part of the soil horizon, in the well-developed spodosols that dominate the area [1]. Thus, light REE is depleted faster than heavy REE, which results in increased Sm/Nd ratios with time in the spodosol profile.

The change in Sm/Nd ratios during selective weathering can potentially cause a change in the Nd-isotopic composition [ε_{Nd}(0)] of the released Nd. The uppermost humus layer show more negative ε_{Nd}(0) compared to bulk soil, whereas the depleted E-horizon have higher ε_{Nd}(0) compared to the bulk soil [2]. The interpretation is that part of the Nd released from the E-horizon has been redistributed to the humus layer by uptake of plants. As a result, the water transported Nd does not necessarily have to reflect the ε_{Nd}(0) of the bedrock or bulk soil.

Considering this, we have studied the river water transport of Nd by analyzing concentration (C_{Nd}) and ε_{Nd}(0) in a boreal river, the Kalix River, in northern Sweden. The soils in the Kalix River drainage basin (24,000 km^2) are dominated by till, mainly derived from granitic material. The water has been sampled at the river mouth on a weekly basis during 1991–1992, by *in situ* filtering through 0.45-μm filters.

The C_{Nd} show large seasonal variations generally correlated with discharge. The C_{Nd} vary from ~500 pmol/L during winter and summer to 1800 pmol/L during peak discharge in the spring (Fig. 1). This is in strong contrast to the major elements, e.g., Na, Ca, Mg, K, and Cl, which are diluted by meltwater during spring discharge. The increased C_{Nd} with discharge correlates with organic C (TOC) concentration and the suspended load. Ultrafiltration data indicate that the REE in the river is transported in colloidal material rich in C and Fe [3].

In contrast to the C_{Nd} no significant temporal variation is observed for the ε_{Nd}(0), with variations from –27.1 to –24.8 (Fig. 1). The ε_{Nd}(0) in all samples were lower than in the unweathered till and bedrock, which have typical values for the area of –-22.5 [1]. The ε_{Nd}(0) of the five samples are more similar to the significantly, lower values found in humus and plant material [2].

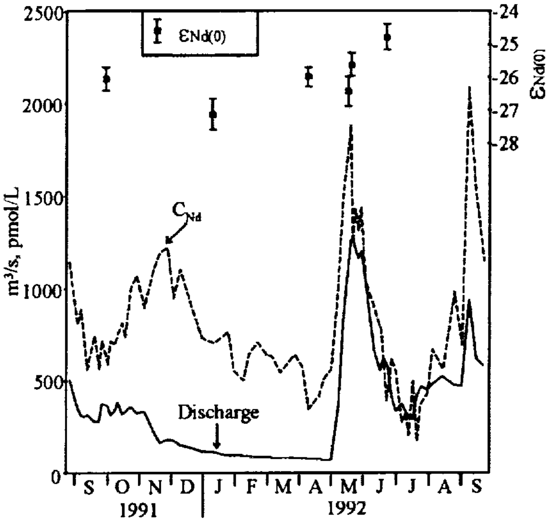

Fig. 1. Annual variation of discharge (m^3/s) Nd concentration (pmol/L) and ε_{Nd}(0) (2s errors) at the river mouth of the Kalix River, northern Sweden.

The river-transported Nd shows no direct correlation with the average age of the bedrock in the catchment area, which is about 1.9 Ga. Instead the composition is similar to that measured in plants and organic material. This suggests that selective weathering in the E-horizon combined with plant uptake and degradation governs the ε_{Nd}(0) of the Nd transported in the Kalix River. It is also clear that the river transport of Nd is strongly associated with colloidal material mainly derived from the upper soil horizons in the Kalix River catchment.

References: [1] Ohlander B. et al. (1996) *Appl. Geochem., 11,* 93–99. [2] Ohlander B. et al. (1998) *Mineral. Mag., 62A,* 1104–1105. [3] Ingri J. et al. (1999) *Chem. Geol.,* submitted.

OCCURRENCE OF TRACE ELEMENTS IN COAL ASH AND SLUDGE AMENDED SOILS IN INDIA.

S. Datta[1], B. Hart[1], M. A. Powell[1], W. S. Fyfe[1], and S. Tripathy[2], [1]Department of Earth Sciences, University of Western Ontario, London N6A 5B7, Canada (sdatta@julian.uwo.ca), [2]Department of Geology and Geophysics, Indian Institute of Technology, Kharagpur, India.

Removal of soil nutrients due to climatic and geological settings in many parts of India has resulted in low biomass production. This work involves the utilization of waste materials such as coal fly ash and sewage sludge for remineralizing these soils and increasing their bioproductivity. The amendments (fly ash and sludge/waterweed in ratios of 1:1 or 1:2 with soils) become an "artificial soil" and provide benefits not included when using NPK fertilizers. This method of utilization is favored over standard disposal methods that ultimately involve local waterways.

Red/lateritic (pH 5.3–6.4) and black (pH 8.0–8.3) soils from the state of Madhya Pradesh and saline-alkali soils (pH 10.3) from the Indo-Gangetic Plains of Uttar Pradesh are being remineralized using the waste mixtures. Sampling was carried out over a total of 100 ha from the two sites and was based on a regular square grid with intervals set at 100 m. Baseline and first year monitoring samples were collected from the upper 15 cm and lower 45–60 cm. X-ray diffraction (XRD) coupled with scanning electron microscopy/energy dispersive X-ray spectrometry (SEM/EDS) studies have been used to identify the relative proportions of important silicate phases including quartz, Na-Ca feldpars, mica, and clays (kaolinite, montmorillonite), Fe-Al oxide-hydroxides (hematite, goethite, gibbsite, and ferrihydrite), and salts (halite, sylvite, and gypsum) in the baseline soils. These data were compared to the major-element oxides as determined by X-ray fluorescence (XRF). A detailed trace-element analysis by inductively coupled plasma optical emission spectrometry (ICP-OES) (aqua-regia extraction) was done on all the soil, ash, and sludge samples. Potentially phytotoxic elements such as Cr, As, Pb, Ni, and Co, and plant nutrients including Cu, Zn, K, and Mo have been considered in this study. These metals have been correlated with the mineral phases in the soil.

X-ray photoelectron spectroscopy (XPS) shows the major-element distribution (O, C, Ca, Mg, K, Si, Cl, and Na) in the upper few nanometers of soil and mixtures. The surface chemical characteristics of these soils before and after interaction with the ash-sludge mixture were studied by XPS. The major species identified were of Fe (Fe^{+2}, Fe^{+3}, FeOOH), Al (Al_2O_3, AlOOH) and Mg (Mg^{+2}, $Mg(OH)_2$). XPS studies show the trace elements in the soils under different redox conditions. The relative capacity of the soil components to adsorb/precipitate the potentially toxic trace elements or increase the mobility of the elements availability to the plants has been assessed.

Contour plots of the lateral distribution of toxic metals show good correlation among the metals but no correlation with soil physical parameters such as pH, organic matter or cation exchange capacity.

First-year monitoring samples show some changes in physico-chemical characteristics but no significant changes in the trace-metal concentration. Preliminary data show a major increase in organic matter content and neutralization of soil acidity for the laterites.

HAFNIUM-ISOTOPIC TIME SERIES IN IRON-MANGANESE CRUSTS: A COMPARISON BETWEEN ε_{Hf} AND ε_{Nd} VARIATIONS.

K. David[1], M. Frank[2], N. S Belshaw[2], and R. K. O'Nions[2], [1]Department of Earth Sciences, University of Oxford, Parks Road, OX1 3PR, Oxford, UK (karined@earth.ox.ac.uk), [2]Department of Earth Sciences, University of Oxford, Parks Road, OX1 3PR, Oxford, UK.

Introduction: In contrast to other radiogenic isotopic systems used in marine geochemistry such as U-Th-Pb and Sm-Nd, the behavior of the Lu-Hf system is not totally well understood. The potential of Hf as a water mass tracer remains uncertain. However, the use of Hf is interesting due to the large range of isotopic signatures of the major sources of Hf in seawater and its potential to record hydrothermal inputs [1,2]. At present only, Hf-isotopic results obtained from Fe-Mn crusts and nodules are available to provide insights about Hf in seawater [2,3].

The aim of this study is to pursue questions of Hf sources to the oceans and its behavior as a water mass tracer.

Present-day Hafnium-isotopic Variations in the World's Oceans: In order to reconstruct the present-day Hf-isotopic distribution in the world's oceans, we measured the surface layers of 23 hydrogenetic Fe-Mn crusts recovered from seamounts in the Atlantic, Indian, and Pacific Oceans and for which Nd and Pb isotopes were already available [4].

By using a revised ion exchange chemistry [5], we measured Hf-isotopic ratios on a new generation of multiple collector plasma source mass spectrometer (Nu-Instruments) with a 2σ external reproducibility of 35 ppm (0.35 ε units).

The significant interoceanic and intraoceanic Hf-isotopic variations reflect an incomplete mixing of the isotopically diverse sources of Hf in the oceans. In agreement with previous studies, the results show a present-day provinciality that reflects the relative importance of continental and hydrothermal inputs of Hf into the different ocean basins [2,3]. This assumption is reinforced by the observation of strong correlations between Hf, Nd, and Pb isotopes for all crusts. The unradiogenic Hf signature of the Atlantic Ocean (average value $\varepsilon_{Hf}(0) = 0.4$) is explained by the introduction of Hf from the erosion of old continental material while the radiogenic signal of Hf in the Pacific Ocean (average value $\varepsilon_{Hf}(0) = 4.5$) is derived from younger continental and hydrothermal inputs of Hf. In contrast, the intermediate Hf of the Indian Ocean (average value $\varepsilon_{Hf}(0) = 3.6$) does not show evidence of the Himalayan erosion.

However, our data do not contradict the previous assumption that an eolian contribution should be taken into account in the balance of dissolved Hf in seawater in order to explain the more radiogenic Hf-isotopic composition of Fe-Mn crusts and Mn nodules than expected from their Nd-isotopic signatures with respect to the terrestrial array [3].

26-Ma Hafnium-isotopic Variations in the Central Pacific Ocean: A Hf isotope profile has been obtained for a central Pacific Ocean Fe-Mn crust (VA13/2, 4830 m). This crust was already dated using Co and ^{10}Be chronometers and Pb and Nd isotope profiles were reported [6,7]. Significant Hf isotopic variations of 2.5 ε units are found and Pb and Hf isotope variations are decoupled over the last 26 Ma. The overall Nd and Hf patterns display variations in ε_{Hf} that are 1.5× greater than those in ε_{Nd}. Coherent variations of the Hf and Nd isotope profiles are only observed for the last 14 m.y. Prior to 14 Ma, the similar patterns of Nd and Hf isotopes are offset by 2 m.y.

We conclude, therefore, that ε_{Hf} and ε_{Nd} were coupled in the deep Pacific Ocean over the last 14 m.y. in contrast to results obtained from other Pacific crusts [8]. These results suggest similar residence times for Hf and Nd. The apparent decoupling between Hf and Nd isotopes observed for the oldest part of the crust cannot be explained by a diffusion process but may reflect a smaller eolian input in the budget of Hf in the Pacific Ocean. This could also imply different residence times for Hf and Nd.

References: [1] White W. M. et al. (1986) *EPSL, 79,* 46–54. [2] Godfrey L. V et al. (1997) *EPSL, 151,* 91–105. [3] Albarède F. et al. (1998) *GRL, 25,* 3895–3898. [4] Von Blanckenburg F. et al. (1996) *GCA, 60,* 4957–4963. [5] David et al. (1999) *Chem. Geol., 157,* 1–12. [6] Frank M. et al. (1999) *GCA,* in press. [7] Ling H. F. et al. (1997) *EPSL, 146,* 1–12. [8] Lee D.-C. et al. (1998) *Mineral. Mag., 62A,* 870–871.

CRYSTAL ISOTOPIC STRATIGRAPHY USING LASER ABLATION.

J. P. Davidson[1], F. J. Tepley III[1], Z. Palacz[2], and S. Meffan-Main[2], [1]Department of Earth and Space Sciences, University of California, Los Angeles, Los Angeles CA 90095, USA (davidson@ess.ucla.edu), [2]Micromass UK, Floats Road, Wythenshawe, Manchester, M23 9LZ, UK.

Introduction: Recently it has been realized that many young volcanic rocks are characterized by Sr-isotopic disequilibrium among mineral components. This has been interpreted as reflecting open system differentiation processes. Core-to-rim Sr isotope profiles of plagioclase feldspars obtained through microdrilling can be used to record progressive changes in the composition of the melt from which the crystal grew.

A serious disadvantage to this approach is the time needed to microdrill crystal samples, process through low blank chemistry, and analyze via TIMS. The problem is compounded by the large number of analyses needed from a given sample to characterize and quantify open-system behavior. Laser ablation coupled to a multicollector inductively coupled plasma mass spectrometer (ICP-MS) sector instrument circumvents many of these problems and offers great potential for future petrogenetic investigations.

Methodology: We used a CETAC LSX 200 laser coupled to a Micromass Isoprobe™ instrument to characterize the Sr-isotopic compositions of feldspars from trachyandesite samples of the 1982 El Chichòn eruption, Chiapas, Mexico. These rocks have been previously shown to display a large range in inter- and intracrystal mineral isotope compositions [1,2], particularly among the plagioclase feldspars (although bulk rock ^{87}Sr/^{86}Sr is relatively uniform between samples). Laser ablation is able to reproduce the data already produced by microdrilling (Fig. 1), and is not compromised by the potential chemical blank interference. A critical comparison between the methods (Fig. 1) suggests the following: (1) Precisions are typically a factor of ~5 worse for laser ablation and clearly vary with Sr concentration — the El Chichòn feldspars are ~1600 ppm — but we have also analyzed feldspars with ~500 ppm Sr with ±~100 ppm. However, the total amount of sample used for laser "spots" is half that used for for microsampling. (2) Spatial resolution is comparable — of the order 100–300 µm. As with microsampling, for laser ablation there is an inevitable trade-off between spot size and ion beam intensity (for a given Sr concentration), which controls precision.

Limitations: An additional problem with laser ablation is the potential for Rb interference, which cannot be accurately corrected due to fractionation effects at the site of ablation (the ICP source itself has the great advantage of generating species-independent mass fractionations). While this does not affect the data of Fig. 1, since the feldspars have Rb/Sr ratios <0.005, we have investigated the effects using glass standards prepared from feldspars with added RbCl to vary the Rb/Sr ratio, and have found that a linear correction can be applied provided Rb/Sr ratios are not >0.2. This correction

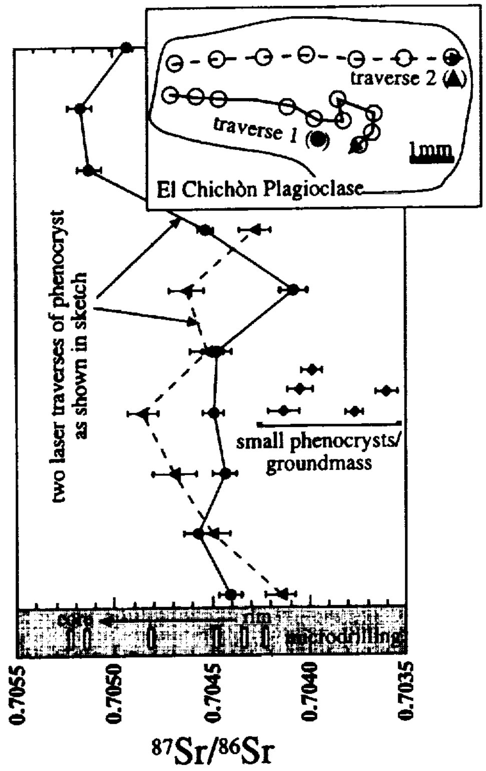

Fig. 1. Comparison of laser ablation and microdrilling on a feldspar crystal from El Chichòn. Laser ablation sites (~200 μm) are indicated along two traverses, distinguished by different symbols on the graph. Error bars (laser) and bar thicknesses (microdrill) indicate 2σ precision. There is a consistent general decrease in $^{87}Sr/^{86}Sr$ from core to rim shown by both methods — and ratios are clearly distinct from those of smaller plagioclase crystals in the rock (shown on graph), and the whole-rock value (~0.7041).

provides a reasonably accurate, but not very precise $^{87}Sr/^{86}Sr$ ratio, as uncorrected $^{87}Sr/^{86}Sr$ are >6.

References: [1] Davidson J. P. and Tepley F. III (1997) *Science, 275,* 826–829. [2] Tilling R. I. and Arth J. G. (1994) *IAVCEI Congress,* Middle East Technical University Department of Geological Engineering, Spec. Publ. 2.

THE EFFECT OF MAGNESIUM AS AN IMPURITY ON CALCITE GROWTH: A MODEL SYSTEM FOR BIOMINERALIZATION.

K. J. Davis[1], P. M. Dove[1], and J. J. De Yoreo[2], [1]School of Earth and Atmospheric Sciences, Georgia Institute of Technology, Atlanta GA 30332, USA (kdavis@eas.gatech.edu; dove@eas.gatech.edu), [2]Department of Chemistry and Materials Science, Lawrence Livermore National Laboratory, Berkeley CA 94550, USA.

Introduction: Calcium carbonate ($CaCO_3$) mineralization is currently the focus of intense research due to its importance in both geological and biological environments. The incorporation of Mg^{2+} into magnesian carbonates has been of particular interest due to its influence on the dominant carbonate polymorph precipitated from seawater [1] and its implications for understanding paleoclimates [2]. Further, Mg^{2+} is an important impurity in biomineralizing environments due to its ubiquity and to the ability of organisms to exert control over the amount of Mg^{2+} incorporated into carbonate materials through the complicated processes of biomineralization [3]. In turn, the extent to which Mg^{2+} is incorporated may have an influence upon the exquisite morphologies expressed by the carbonate minerals that are crystallized [4,5]. A complete understanding of the macroscopic processes that govern calcium carbonate formation in the presence of Mg^{2+}, with its implications for both biological and geological processes, may only be achieved through a microscopic understanding of the mechanisms involved.

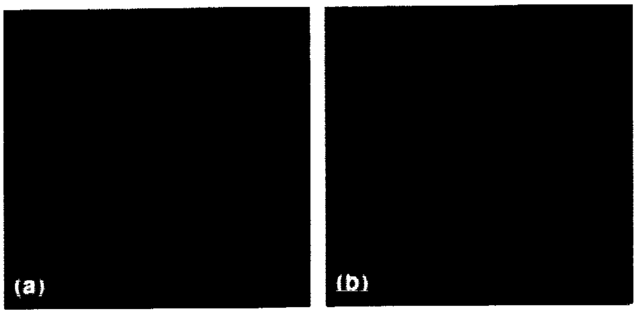

Fig. 1. (a) Calcite growth spiral grown in pure system (field of view = 3 × 3 μm). (b) Calcite growth spiral grown in $[Mg^{2+}]/[Ca^{2+}]$ approaching 0.3 (field of view = 3 × 3 μm).

In this study, contact-mode fluid-cell atomic force microscopy (AFM) was used to investigate the effect of Mg^{2+} on calcite growth kinetics in a flow-through environment. Kinetic parameters fundamental to calcite mineralization, such as step velocity ($v_{\pm}$) and overall growth rate (R), were measured through *in situ* observation of individual growth spirals, as a function of supersaturation and Mg^{2+} impurity levels. Significant changes in hillock morphology and favored crystallographic direction were also observed. Findings from this study are the first to document the *microscopic* role of magnesium in mediating calcite growth kinetics and to compare the results to existing crystal growth impurity models.

Results: Individual step velocities ($v_{\pm}$) for both the (+) and (–) vicinal faces were observed to be unaffected by Mg^{2+} impurities at $[Mg^{2+}]/[Ca^{2+}]$ up to 0.2, despite the finding that steps along the (–) direction appear to be pinned by an impurity fence. At $[Mg^{2+}]/[Ca^{2+}]$ of 0.3 and higher, step velocities along both directions decreased rapidly, coinciding with steps along all directions experiencing significant pinning by impurities. Terrace widths were not found to deviate significantly as a function of the Mg^{2+} content of the solution, indicating that under the conditions of this study Mg^{2+} failed to greatly change the step-edge surface energy or lattice strain of the spiral through incorporation.

The morphology of the spiral hillocks was also observed to be altered by the presence of Mg^{2+}. The (+/–) corners separating the (+) and (–) vicinal faces appear to erode as a function of Mg^{2+} eventually leading to a rounded hillock characterized by a lack of clear crystallographic directions at higher $[Mg^{2+}]/[Ca^{2+}]$.

Conclusions: This study is the first to demonstrate the microscopic effect of Mg^{2+} on the kinetics of calcite growth under the framework of crystal growth impurity models. Under the conditions of this study, Mg^{2+} was shown to primarily retard calcite growth through physical pinning of advancing steps rather than through changes in surface energy and lattice strain associated with incorporation. Further, preferential interaction of Mg^{2+} with different kink sites along certain crystallographic directions was demonstrated through the observed effect on hillock morphology. The results of this study yield some insight into how Mg^{2+} affects the fundamental kinetic parameters associated with calcite growth and its ability to direct the morphology of macroscopic carbonate crystals.

References: [1] Berner R. A. (1975) *GCA, 39,* 489–504. [2] Stanley S. M. and Hardie L. A. (1998) *Palaeo., 144,* 3–19. [3] Weber J. N. (1969) *Am. J. Sci., 267,* 537–566. [4] Howson M. R. et al. (1987) *Chem. Geol., 64,* 79–87. [5] Folk R. L. (1974) *J. Sed. Petrol., 44,* 40–53.

PROTEROZOIC UNDERPLATING OF THE ARCHEAN WYOMING CRATON AND MEDICINE HAT BLOCK DURING ASSEMBLY OF WESTERN LAURENTIA.

W. J. Davis[1] and G. M. Ross[2], [1]Geological Survey of Canada, 601 Booth Street, Ottawa ON, K1A 0E8, Canada,

[2]Geological Survey of Canada, 3303 33 Street Northwest Calgary, AB, T2L 2A7, Canada.

The recent Deep Probe seismic refraction survey across western Laurentia identified an anomalous, intermediate velocity (7–7.3 km/s) lower-crustal layer up to 25 km thick beneath the Archean Wyoming craton and Medicine Hat Block (MHB; [1]) The crust in these areas is also relatively thicker (50 km) than adjacent Proterozoic and Archean crustal blocks to the south and north (40 km). Lower-crustal xenoliths recovered from Eocene minette dikes in the Medicine Hat block north of the Wyoming craton include a significant population of garnet-clinopyroxene-plagioclase ± quartz mafic granulites that have equilibration pressures corresponding to crustal depths of 35–40+ km, consistent with derivation from the intermediate lower crustal velocity layer identified by the refraction survey.

The mafic granulites range in composition from 46–49% SiO_2 with Mg# of 40–58 and are characterized by broadly basaltic compositions with low K_2O contents, variable but low Na_2O (0.5–3%) and generally low TiO_2 contents (<1.0–2.4%). Three different REE profiles are documented: (1) flat to slightly LREE-enriched, (2) LREE-enriched, and (3) LREE-depleted compositions. None of the profiles exhibit significant Eu/Eu* (0.84–0.97). Types 1 and 3 exhibit moderate negative Nb anomalies relative to Th and La; whereas the LREE-enriched sample has high Nb, and a sinusoidal pattern peaking at La-Ce. The compositions are compatible with crystallization from basaltic melt (± cumulate). Mafic granulites of similar composition occur in minettes in the Great Falls Tectonic Zone along the northern margin of the Wyoming craton [2,3].

Zircon geochronology of the mafic granulites indicate dominantly Paleoproterozoic metamorphic ages between 1820 and 1700 (one sample has Archean metamorphic zircon). ε_{Nd} values at 1.8 Ga are all strongly negative ranging from −4.8 to −10, with Mesoarchean depleted mantle model ages. The Nd-isotopic compositions can be modeled as mixtures between evolved Archean crustal sources (Wyoming-MHB crust) and Proterozoic magmas, although an entirely Archean protolith cannot be eliminated. If the mafic granulites originate by magmatic intrusion in the lower crust, then the incorporation of considerable amounts of older crustal Nd (30–50%) into the magmas is required, as frequently reported for lower crustal mafic granulite xenoliths.

Integration of the refraction data with xenolith geochemistry suggests that the intermediate velocity layer developed beneath the Wyoming craton and MHB during the late collisional phase of assembly of western Laurentia, probably as a result of magmatic intrusion into the lower crust/upper mantle. Contemporaneous igneous rocks are rare in the upper crust and the origin of the mafic granulite layer, and its restriction to the Wyoming/MHB block remains uncertain. The development of the lower crust in the Proterozoic resulted in modal metasomatism (glimmerites) but apparently did not destroy lithospheric mantle of Archean age as recorded by Re-Os model ages for Wyoming lithosphere [4].

References: [1] Henstock et al. (1998) *GSA Today, 8,* 1–5. [2] Joswiak D. (1992) M.S. thesis, Univ. of Washington. [3] Collerson et al. (1988) *Terra Cognita, 8,* 270. [4] Carlson R. W and Irving A. J. (1994) *EPSL, 126,* 457–472.

CARBON-ISOTOPIC AND NITROGEN ANALYSIS OF CARBONADO BY SECONDARY ION MASS SPECTROMETRY.

S. De[1], P. J. Heaney[2], E. P. Vicenzi[3], and J. Wang[4], [1]Department of Geosciences, Princeton University, Princeton NJ 08544, USA (barna@geo.princeton.edu), [2]Department of Geosciences, Pennsylvania State University, University Park PA 16802, USA, [3]Princeton Materials Institute, Princeton University, Princeton NJ 08544, USA, [4]Department of Terrestrial Magnetism, Carnegie Institution of Washington, Washington DC 20015, USA.

Carbonado, a polycrystalline variety of diamond, is characterized by unusual C-isotopic compositions with bulk $\delta^{13}C$ values clustered tightly between −23‰ and −30‰ (relative to PDB). These values are significantly lighter than harzburgitic diamond (with a range in $\delta^{13}C$ from −1‰ to −10‰ with a single mode at −6‰) and fall near the lower extreme for eclogitic diamond (ranging from +3‰ to −34‰ with two modes at −5‰ and −12‰) [1]. In combination with textural and inclusion data, these isotopic compositions have led scientists to question whether carbonado originated in the mantle or in the crust.

Previous studies of carbonado have revealed a bimodal grain-size distribution that correlates with cathodoluminescent emissions [2]. We believe that these textures result from a two-step growth process, and we have obtained additional chemical evidence that supports the identification of two distinct crystal populations. Spot analyses using secondary ion mass spectrometry (SIMS) reveal a bimodal distribution of $\delta^{13}C$ values of −24‰ and −26‰. SIMS analyses also demonstrate that this $\delta^{13}C$ distribution coincides with bimodal variations in N abundance, and both of these chemical zonations correlate with cathodoluminescence emission signatures. However, a one-dimensional analysis of self-diffusion of C in diamond suggests that isotopic homogenization occurs extremely slowly, even under upper mantle conditions. Accordingly, the chemical partitioning observed in carbonado does not preclude mantle-based hypotheses for its origin, at least with respect to diffusional homogenization. Any model that accounts for the origin of carbonado must explain covariance among C isotopes, N abundances, cathodoluminescent emissions, and grain-size distributions.

References: [1] Kirkley M. B. (1998) in *The Nature of Diamonds* (G. Harlow, ed.), pp. 48–71. [2] Magee C. W. and Taylor W. R. (1998) *7th Intl. Kimberlite Conf. Ext. Abstr.,* 527–528.

VARIATIONS IN THE ISOTOPIC COMPOSITION OF MARINE CALCIUM OVER THE LAST 160 MILLION YEARS.

C. L. De La Rocha[1] and D. J. DePaolo[1,2], [1]Berkeley Center for Isotope Geochemistry, Department of Geology and Geophysics, University of California at Berkeley, Berkeley CA 94720-4767, USA (delaroch@uclink4.berkeley.edu), [2]Earth Sciences Division, E. O. Lawrence Berkeley National Laboratory, Berkeley CA 94720, USA (depaolo@socrates.berkeley.edu).

Introduction: The global Ca cycle has received little attention relative to biogeochemical cycles such as C and N, even though there is an intimate link between the Ca and C cycles and evidence for significant variations in the Ca content of ocean waters over geologic time. The formation and weathering of $CaCO_3$, for instance, play important roles in the control of atmospheric CO_2 concentrations [1–4]. Ca^{2+} concentrations have been theorized to vary from near zero from 4–1 Ga [5] to 30 µM at times over the last 550 m.y. [6,7], whereas the modern day value is 10 µM [8]. Deposition of carbonates does not occur uniformly over the history of the oceans, suggesting smaller scale but still significant fluctuations in Ca concentrations. Massive carbonate deposition occurred during the late Cretaceous, for instance, atop carbonate-poor sediments [9]. Such variations in the Ca budget of the oceans may be recorded in the Ca-isotopic composition of marine carbonates.

Calcium-isotopic Natural Abundances as a Potential Tracer of the Global Calcium Cycle: The Ca-isotopic composition ($\delta^{44}Ca$) of marine biogenic carbonates should record information concerning the global Ca cycle if $\delta^{44}Ca$ of marine biogenic carbonates reflects the $\delta^{44}Ca$ of the seawater from which they were precipitated. Due to high concentrations of Ca^{2+} in the surface waters of the ocean relative to other nutrients (e.g., µM levels for Ca vs. µM concentrations for N, P, and Si), biological uptake of Ca for biomineral formation never draws down Ca^{2+} concentrations by more than a few percent. This, coupled with a minor degree of isotopic fractionation (on the order of −1.3‰) during the biomineralization of $CaCO_3$ by coccolithophorids and foraminifera, leaves variations in $\delta^{44}Ca$ of dissolved Ca in the oceans as the major potential source of $\delta^{44}Ca$ variations in biogenic carbonates.

Variations in marine Ca $\delta^{44}Ca$ may be brought about by changing the relative balance among and between the inputs and outputs of Ca to and from the ocean. Sources of Ca for the ocean are the weathering of continental rocks and ocean floor basalt [1,10] and the primary sink is the biological fixation of Ca into sediments [11]. Continental weathering inputs are delivered to the ocean via rivers, groundwater, and the dissolution of dust deposited at the sea surface [11]. Presently, little is known of the isotopic composition of the various inputs and outputs of Ca in the ocean. The available data [12] do suggest differences in the $\delta^{44}Ca$ of the various inputs and outputs capable of producing significant variations in marine Ca $\delta^{44}Ca$ over million-year timescales.

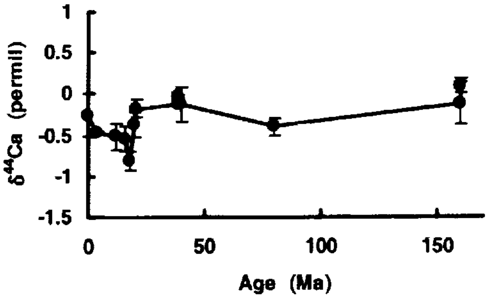

Fig. 1. δ^{44}Ca of marine sediments over the last 160 m.y.

δ^{44}Ca Variations Over the Last 160 Million Years: We report evidence for significant variations in the isotopic composition of Ca of biogenic carbonates, and hence of marine Ca, over the last 160 m.y. (Fig. 1). δ^{44}Ca of bulk carbonate sediments and separated foraminifera suggest marine Ca δ^{44}Ca variations on the order of 1‰ within the last 40 m.y. and over timescales as short as 3 m.y. Such variations could be brought about, for instance, by changes in the flux or δ^{44}Ca of Ca delivered to the oceans via rivers, groundwater, or mid-ocean-ridge hydrothermal emissions.

References: [1] Berner R. A. et al. (1983) *Am. J. Sci., 283,* 641–683. [2] Raymo M. E. et al. (1988) *Geology, 16,* 649–653. [3] Sundquist E. T. (1993) *Science, 259,* 934–941. [4] Holligan P. M. and Robertson J. E. (1996) *Global Change Biol., 2,* 85–95. [5] Kemp S. and Degens E. T. (1985) *Chem. Geol., 53,* 95–108. [6] Hardie L. A. (1996) *Geology, 24,* 279–283. [7] Stanley S. M. and Hardie L. A. (1998) *Palaeogeogr., Palaeoclimatol., Palaeoecol., 144,* 3–19. [8] Broecker W. S. and Peng T.-H. (1982) *Tracers in the Sea.* [9] Kennett J. P. (1982) *Marine Geol.* [10] Gieskes J. M. and Lawrence J. R. (1981) *GCA, 25,* 1687–1703. [11] Milliman J. D. (1993) *Global Biogeochem. Cycles, 7,* 927–957. [12] Skulan et al. (1997) *GCA, 61,* 2502–2510.

PALEOZOIC PLUME IN THE NORTHEASTERN BALTIC SHIELD: DURATION FROM RUBIDIUM-STRONTIUM DATA.

A. A. Delenitsyn, O. V. Gogol, and T. B. Bayanova, Geological Institute of Kola Science, Center of the Russian Academy of Sciences, Apatity, Murmansk Reg., 184200, Russia.

Northeastern part of the Baltic Shield includes more than 40 alkaline massifs, the largest of which are Khibiny and Kovdor. A Rb-Sr age of Khibiny ijolite is 371 ± 6 Ma and a U-Pb baddeleyite age is 382 ± 3 Ma. These ages fall into the interval of 360–380 Ma [1].

We have analyzed ultrabasic and alkaline syenites from the Kurga massif by Rb-Sr and U-Pb methods. A Rb-Sr isochron (WR and minerals) yielded an age of 404 ± 8 Ma; a concordant U-Pb age on two zircon points is 387 ± 7 Ma [2].

The Seblyavr alkaline ultrabasic massif with carbonatites has been also studied by the Rb-Sr and U-Pb methods. The Rb-Sr isochron (WR and minerals) gave an age of 406 ± 6 Ma; a concordant U-Pb age on two baddeleyite points is 378 ± 4 Ma. The U-Pb zircon and baddeleyite ages of the alkaline massifs are slightly younger than the Rb-Sr mineral and WR ages. We can explain this age difference by a suggestion that zircon and baddeleyite were formed at a postmagmatic stage of formation of the alkaline massifs.

Therefore, basing on precise Rb-Sr (WR and minerals) and U-Pb (baddeleyite and zircon) isotope data, we can conclude that the duration of the Paleozoic plume in the northeastern Baltic Shield is more than 40 m.y.

Acknowledgments: All investigations were funded by grant RFFI 98-05-64321, Russia.

References: [1] Kramm et al. (1993). [2] Arzamastsev et al. (1997).

STRONTIUM ISOTOPES, ALKALINITY FLUXES, AND CARBON DIOXIDE CONSUMPTION: IS THERE A GENERAL RELATIONSHIP?

L. A. Derry[1] and C. France-Lanord[2], [1]Department of Geological Sciences, Cornell University, Ithaca NY 14853, USA (lad9@cornell.edu), [2]Centre de Recherches Pétrographiques et Géochimiques–Centre de la Recherche Scientifique, BP 20, 54501 Vandoeuvre-lès-Nancy, France (cfl@crpg.cnrs-nancy.fr).

Alkalinity Generation: The interaction of the atmosphere with exposed silicate rocks generates riverine alkalinity and can remove CO_2 from the ocean-atmosphere reservoir. A number of studies have used the isotopic composition of Sr in the oceans as a proxy for changes in the alkalinity flux generated by weathering, and used this data to estimate CO_2 consumption by the silicate weathering sink over time. This approach is appealing because the Sr-isotopic evolution of the oceans is well known over the last 800 m.y., and the geochemical behavior of Sr is closely related to Ca. Its underlying assumptions include that the Sr-isotopic budget of the oceans reflects the weathering production of alkalinity in the form of Ca ions:

$$CaCO_3 + CO_2 + H_2O \leftrightarrow Ca^{++} + 2HCO_3^- \qquad (1)$$

$$CaSiO_3 + 2CO_2 + 3H_2O \leftrightarrow Ca^{++} + 2HCO_3^- + H_4SiO_4 \qquad (2)$$

The other key assumption is that reaction 1 should contribute relatively unradiogenic Sr from carbonates, while reaction 2 is associated with radiogenic Sr derived from rocks with a high time integrated Rb/Sr (or K/Ca) ratio. Only reaction 2 has a long-term impact on CO_2 with a net consumption of 1 mol of CO_2 upon formation of sedimentary carbonate:

$$Ca^{++} + 2HCO_3^- \leftrightarrow CaCO_3 + CO_2 + H_2O \qquad (3)$$

If the silicate alkalinity flux is composed of Ca^{++} (or Mg^{++}), then to the extent that Sr isotopes can be used to distinguish between carbonate and silicate weathering sources (reactions 1 or 2), the isotopic mass balance of Sr could be used to constrain the silicate weathering sink for C.

Strontium Isotopes and Carbon Dioxide: In fact, the link between the Sr-isotopic composition of the riverine flux and alkalinity is not straightforward. Recent work has shown that Himalayan rivers, which heavily influence the $^{87}Sr/^{86}Sr$ of the Cenozoic ocean, derive a substantial but still uncertain fraction of radiogenic Sr from reaction 1 [1–3]. Reaction 2 is schematic, in that $CaSiO_3$ is a generalized Ca-silicate mineral. In fact, the largest source of readily weatherable Ca silicates are arc-related rocks and are not particularly radiogenic. Thus, the assumption that radiogenic Sr should reflect reaction 2 and not reaction 1 is not generally valid. Weathering rocks with the greatest capacity for CO_2 consumption will tend to decrease the marine $^{87}Sr/^{86}Sr$ value, not increase it. Himalayan rivers are anomalous in their ability to affect the marine $^{87}Sr/^{86}Sr$ ratio, but are similar to other large catchments (Congo, Amazon) in the rate of CO_2 consumption by silicate weathering per square kilometer [4–6]. In contrast, rivers from Iceland and Reunion Island [7,8] show very high rates of CO_2 consumption but have a negative impact on seawater $^{87}Sr/^{86}Sr$.

Alkalinity Composition: A less widely considered but significant issue is that alkalinity generated in radiogenic silicate terranes is largely in the form of Na^+ and K^+ [4]. High $^{87}Sr/^{86}Sr$ rocks have high K/Ca almost by definition. In order for reaction 3 to remove CO_2, Na, or K, alkalinity must be converted to Ca or Mg. Ion exchange reactions allow some conversion, but a substantial fraction of the riverine K flux is removed by reverse weathering [9]. The budget for Na is less clear, because its very long oceanic residence time makes the assumption of steady state unrealistic. On a 10-m.y. timescale, longer than the timescale needed to affect CO_2 [10], changes in the Na alkalinity flux could simply result in increased $[Na^+]$ in the ocean. The composition of silicate-derived alkalinity is a critical control on the impact of weathering on the C cycle. At the moment, we have neither good estimates of the composition of silicate derived alkalinity globally, nor a solid understanding of the fate of Na and K alkalinity once delivered to the oceans. Without those constraints, Sr in the oceans cannot be a useful proxy of weathering fluxes through time.

References: [1] Quade J. et al. (1997) *Science, 276,* 1828–1831. [2] Blum J. D. et al. (1998) *Geology, 26,* 411–414. [3] Galy et al. (1999) *GCA,* in press. [4] France-Lanord C. and Derry L. A. (1997) *Nature, 390,* 65–67. [5] Gaillardet J. et al. (1995) *GCA, 59,* 3469–3485. [6] Gaillardet J.

et al. (1997) *Chem. Geol., 142,* 141–173. [7] Gislason S. R. et al. (1996) *Am. J. Sci., 296,* 837–907. [8] Louvat P. and Allègre C. J. (1997) *GCA, 61,* 3645–3669. [9] Michalopoulos P. and Aller R. C. (1997) *Science, 270,* 614–617. [10] Berner R. A. and Caldeira K. (1997) *Geology, 25,* 955–956.

NATURE OF FLUXES FROM SUBDUCTED SLAB TO MANTLE WEDGE IN THE LESSER ANTILLES ARC: ORIGIN OF M- AND C-SERIES BASALTS.

J. D. Devine[1], W. M. White[2], P. Copeland[3], and D. R. Gravatt[2], [1]Department of Geological Sciences, Brown University, Providence RI 02912, USA, [2]Department of Geological Sciences, Cornell University, Ithaca NY 14853, USA, [3]Department of Geosciences, University of Houston, Houston TX 77204-5503, USA.

Introduction: Two isotopically distinct basaltic magma series occur in the Lesser Antilles volcanic arc: the high-MgO, olivine-microphyric "M-series" and the high-Ca, augite-phyric "C-series" [1]. The existence of two types of parent magma suggests that there are two types of source region, which are separated in space or time, or both. The M-series magmas contain a strong subducted sediment component, but the C-series basalts are isotopically more MORB-like, and it has been suggested that their parent magmas contain a component derived from altered oceanic crust [1]. The magma types often occur together, suggesting that their respective source regions are not merely laterally separated. Either the source regions are vertically separated, or the magmas are derived from a single source region that changes with time.

Twenty-four basalts and basaltic andesites from Grenada have been dated by the $^{40}Ar/^{39}Ar$ method; the material dated was groundmass (20), amphibole (3), and whole rock (1). These results (while perhaps not entirely representative) suggest a reevaluation of the chronology of volcanism on the island. Most of the previously published ages from Grenada are K-Ar whole-rock analyses with a range in age from 0.94 to 21.2 Ma. We find no ages older than 6.0 Ma, but there has been sampling bias in favor of the youngest samples for the purpose of volcanic hazard assessment.

Evidence for Transport of Thorium (and Uranium) from Slab to Mantle-Wedge Source Regions by Aqueous Fluids: Bulk mixtures of potential endmember components involved in arc basalt genesis are conveniently represented in diagrams of elemental ratios normalized to Nb (Fig. 1). The end members are MORB sourcelike mantle, subducted sediments, subducted altered oceanic crust and a potential crustal sediment contaminant. Binary mixtures form straight lines on plots of ratios with a common denominator, and bulk mixtures of the four components listed above must lie within quadrangles defined by the end members. But the Th/Nb ratios of many M- and C-series basalts lie outside the quadrangle. The fractionation of Th from Nb cannot be explained by postulating that a Nb-bearing mineral like rutile is a residue of partial melting of the sediments. There is insufficient Ti to make enough rutile to account for the high Th/Nb ratios of arc basalts [2]. Rather than invoke some unspecified crystal/sediment-melt fractionation process [see 2], we conclude that aqueous fluid mobility of Th is a more likely explanation for the observed Th/Nb fractionation (D fluid/Cpx ~4 for Th; [3]). The occurence of both ^{230}Th and ^{238}U excesses in arcs is readily explained by variations in fluid compositions.

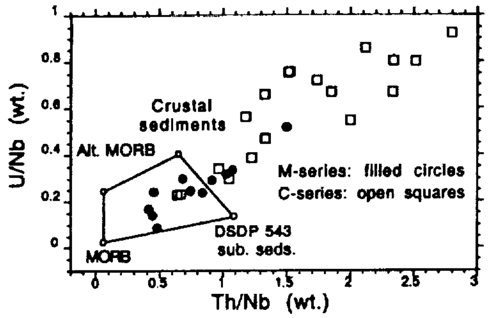

Fig. 1.

Evolving Mantle-Wedge Source Model: On the basis of U-series disequilibrium studies, Lundstrom et al. [4] concluded that the oceanic mantle consists of regions of depleted lherzolite interspersed with "chemically enriched mafic veins." The chemical and isotopic diversity of "off-ridge" ocean floor basalts was interpreted to reflect variable proportions of melts derived from the enriched veins (E-MORB) and the depleted lherzolite (N-MORB).

We propose a similar "marble cake" model for the sub-arc mantle wedge. Low-degree partial melting of down-dragged, *hydrated* peridotite produces melts that are dominated by trace-element fluxes from amphibole-bearing veins with a strong subducted sediment signature (due to previous release of aqueous fluids from dehydrating subducted sediments). At higher degrees of partial melting, the subducted sediment signature is diluted by melts from the depleted lherzolite. If aqueous fluids later released by breakdown of the altered oceanic crust subsequently invade volumes of mantle from which the veins were previously melted out, direct hydrous partial melting of depleted lherzolite may occur, producing C-series-like melts. This model predicts that C-series basalts should be younger than M-series basalts in a given area, a prediction that can be tested by $^{40}Ar/^{39}Ar$ dating of the respective basalts. Further dating will be required to document the migration of sites of active volcanism, the secular variations in basaltic magma geochemistry, and the evolution of mantle-wedge source regions.

References: [1] Thirlwall et al. (1996) *GCA, 60,* 4785–4810. [2] Elliott et al. (1997) *JGR, 102,* 14991–15019. [3] Keppler H. (1996) *Nature, 380,* 237–240. [4] Lundstrom C. C. et al. (1999) *Chem. Geol.,* in press.

CARBON-ISOTOPIC RECORDS AND EXTINCTION-TRIGGERED ECOLOGICAL COLLAPSE.

S. D'Hondt, Graduate School of Oceanography, University of Rhode Island, Narragansett RI 02882, USA (dhondt@gso.uri.edu).

Carbon-isotopic differences between the skeletons of planktic and benthic organisms catastrophically decreased at the Cretaceous-Tertiary (K/T) boundary and did not fully recover to preextinction levels for nearly 4 m.y. These reduced isotopic differences suggest that the flux of organic C from the ocean surface to the deep ocean was unusually low for nearly 4 m.y. The postextinction decrease in the downward flux of organic matter could have been caused by either the sinking to deep water of a slightly smaller fraction of total biological production [1] or a greatly decreased rate of biological production [2]. In either case, the decreased organic flux resulted from collapse of the open ocean ecosystem at the K/T boundary. Most physical and chemical consequences of large-body impacts are expected to disappear on timescales of a few months to a few centuries. Consequently, the long delay in recovery of the marine C cycle probably resulted from a long lag in final ecological recovery from the mass extinction, rather than from lingering physical effects of the K/T impact. A similar extinction-triggered ecological collapse may also have caused the C-isotopic anomaly that overlies the Permo-Triassic boundary in carbonate rocks throughout the Tethyan ocean [3]. If so, the early Triassic isotope anomaly may also have lingered for millions of years.

References: [1] D'Hondt S. et al. (1998) *Science, 282,* 276–279. [2] Hsü K. J. and McKenzie J. A. (1985) *AGU Geophys. Monogr. Ser., 32,* 251–269. [3] Baud A. et al. (1989) *Geologische Rundschau, 78,* 649–677.

THE NATURE OF INTRUSION AND MELT TRANSPORT IN THE LOWER OCEAN CRUST AT AN ULTRA-SLOW SPREADING RIDGE.

H. J. B. Dick,[1] J. H. Natland, J. Kinoshita, P. Robinson, C. MacLeod, A. J. Kvassnes, and the MODE '98 Leg IV, JR 31, and ODP Leg 176 Scientific Parties, [1]McLean Laboratory, Department of Geology and Geophysics, Woods Hole Oceanographic Institution, Woods Hole MA 02543-1539, USA.

Recent ocean drilling and mapping at Atlantis Bank in the Indian Ocean has provided a three-dimensional view of a large block of lower ocean crust in contact with the mantle. Atlantis Bank is an uplifted oceanic core complex unroofed and uplifted to sea level at the northern ridge-transform intersection of the Atlantis II F.Z. at 11 m.y. It has subsequently subsided some 700 m to its present depth. While the top of the bank and the more gentle slopes surrounding it largely expose the fault surface on which it was unroofed, the interior of the massif and its contact with the mantle are exposed where it is cut by the steep transform wall. Mapping of the seafloor around Atlantis Bank has shown that it lies not far from the distal end of the paleoridge segment, and the gabbros likely represent down-axis intrusion of moderately differentiated melts into the mantle near the transform. The crust-mantle boundary where it is exposed along the transform wall is marked by a quarter-kilometer-thick zone of sheared ferrogabbro mylonite, evidently due to tectonically driven melt migration of late-melt fractions into the crust-mantle boundary. The massif at its northern end consists of a thick section of gabbro comparable in composition and extent to those drilled in Hole 735B on the Atlantis Bank platform some 13 km to the southeast. This suggests the detachment fault on which the bank is exposed did not root down into the mantle, but lay within or immediately above the gabbro horizon for at least 1 m.y. Moreover, it also suggests that Hole 735B is representative of the lower crust in the near transform environment.

The principal igneous stratigraphy of Hole 735B is comprised of olivine gabbros crosscut by innumerable small bodies of ferrogabbro. The latter are volumetrically minor in the lower 500 m of the hole and increase in number and size upward in the upper kilometer. They are often associated with deformed intervals, and it is apparent that they represent local pooling of late melt within the olivine gabbros and migration into and along fault zones where it eventually solidified to form the ferrogabbros. This process left late-stage felsic veins, including tonalite, diorite, and trondhjemite, as the last differentiate of the migrating melts. Internally, the olivine gabbros contain five cycles of Fe enrichment. The individual units, as defined by these chemical trends, locally overlap, and each in turn appears to be a composite, composed of many smaller petrographically distinct intrusive intervals. Evidently each of these units represents some form of cyclic intrusion and *in situ* differentiation as melts worked their way upward through a specific intrusive horizon in the section. Despite lower overall olivine contents, the uppermost two olivine gabbro units have higher average Mg#s, lower TiO_2 and Na_2O, and are on average chemically more primitive than the lower three, suggesting different parental magmas. Detailed mineral profiles across the contact between the upper two units and the lower three appear to demonstrate that the lower were intrusive into the upper while it was still partially molten. Internal to the olivine gabbro units are fine to medium grained microgabbro dikes ranging from troctolite to oxide gabbronorite. These are interpreted as "protodikes" representing a further stage of melt transport through the section. Locally around these bodies there is evidence for solution channeling into the olivine gabbro, with the formation of anorthositic and pyroxenitic patches representing escape of late melts from the microgabbro into the olivine gabbro.

The internal stratigraphy of the 1.5-km Hole 735B section is exceedingly complex, representing intrusion and reintrusion at a wide variety of scales and modalities. This stratigraphy reflects a low but quasi-steady-state melt supply in an ultraslow spreading ridge environment that is quite distinct from that of the large single-stage magma chambers envisioned for some continental layered intrusions.

Acknowledgments: This abstract is co-authored with the MODE'98 Leg IV, JR31, and ODP Leg 176 scientific parties.

CARBON-ISOTOPIC BIOGEOCHEMISTRY OF AEROBIC BIODEGRADATION OF AROMATIC HYDROCARBONS.

E. J. M. Diegor[1], T. Abrajano[2], T. Patel[1], L. Stehmeier[3], and J. Gow[1], [1]Department of Earth Sciences and Department of Biology, Memorial University of Newfoundland, St. John's, NF A1B 3X5, Canada (x76ejmd@morgan.ucs.mun.ca), [2]Department of Earth and Environmental Sciences, Rensselaer Polytechnic Institute, Troy NY 12180-3590, USA (abrajt@rpi.edu), [3]Nova Chemicals, Ltd., Calgary AB, T2E 7K7, Canada.

Aromatic hydrocarbon contamination of soil and groundwater is a widespread environmental problem. Among the compounds of interest is a range of low molecular weight aromatic hydrocarbons that includes the so-called BTEX compounds (benzene, toluene, ethylebenzene, and xylenes). These compounds enter surface and groundwater environments through accidental spills and leakage of underground storage tanks, or through inadvertent releases during use, transport, or disposal.

Aerobic biodegradation by natural populations of microorganisms represents one of the primary mechanisms by which petroleum and other hydrocarbon pollutants are eliminated in the environment. Indicators that have been used to evaluate and monitor this process involve the measurement of changes over time of the concentration of hydrocarbon, number of bacteria, rate of bacterial activity, adaptation, metabolic byproducts, intermediary metabolites, growth-stimulating materials, and ratio of nondegradable to degradable compounds [1,2]. However, such measurements may be affected not only by biodegradation but also by other processes such as volatilization, dissolution, dilution, and migration off the site, sorption to the soil, or transformation via abiotic chemical reactions.

Previous works demonstrated the application of stable C-isotopic analysis in environmental studies, particularly in establishing sources of organic pollutants [3,4]. These studies showed that compounds have characteristic C-isotopic compositions that can be used to establish their origins. In the same manner, any process in which a compound is involved may impart significant isotopic fractionation [4]. Abiotic processes (volatilization, reductive halogenation) have been shown to affect the $^{13}C/^{12}C$ ratio [e.g., 4] but fractionation associated with biological transformation is known to produce the largest fractionation in natural systems [4–6].

The present paper focuses on the applicability of stable C-isotopic analysis to determine the magnitude and direction of transformation of stable C isotopes (^{12}C, ^{13}C) during microbial degradation of selected hydrocarbon compounds such as benzene, toluene, ethylbenzene, styrene, naphthalene, hexadecane, and methanol.

Microbial cultures were grown aerobically at room temperature in 250-mL sidearm flasks equipped with Teflon Mininert valves for ease of sampling. Each flask contains 35 mL of a hydrocarbon degrader medium (HDM) augmented with 2 µL of a particular hydrocarbon, inoculated with 5 mL of microbial culture, and intermittently shaken at about 150 rpm on a Gyratory shaker at room temperature (22° ± 1°C). To establish growth of microorganisms, optical density measurements of the bacterial cultures were taken. Optical density readings were made at 600 nm at the beginning of, at hourly intervals during, and at the end of the experiments. For hydrocarbon isotopic analysis, a 30-µL headspace periodically removed from the culture flasks is analyzed by gas chromatography continuous flow isotope ratio mass spectrometry (GC-IRMS). The GC is a Hewlett Packard HP5890 Series II. The column in the GC is a Restek RTX 502.2 (105 m length, 0.53-mm I.D.) with a 3-µm Crossband phenylmethyl polysiloxane film (Chromatographic Specialties, Inc.).

Biodegradation of benzene showed a decrease in benzene concentration, an increase in microbial culture absorbance as an indicator of microbial growth, and a steady increase in the $\delta^{13}C$. Similar results were obtained for styrene, where increasing microbial growth over a span of 8 h was indicated by increased optical density and corresponding increase in $\delta^{13}C$. Initial aerobic microbial degradation experiments were conducted on a toluene culture, where no C-isotopic fractionation seems to accompany microbial growth.

References: [1] NRC (1993) *In Situ Bioremediation: When Does it Work?*, National Research Council, National Academy. [2] Aggarwal P. K. and Hinchee R. E. (1991) *Environ. Sci. Technol.*, *25*, 1178–1180. [3] O'Malley V. P. et al. (1995) *Organic Geochem.*, *21*, 809–822. [4] Abrajano T. and Sherwood-Lollar B. (1999) *Organic Geochem.*, in press. [5] Galimov E. M. (1985) in *The Biological Fractionation of Isotopes*. [6] Stahl W. J. (1980) *GCA, 44*, 1903–1907.

DEVELOPMENT OF A HIGH-PRESSURE DIGESTION TECHNIQUE AND A DATA ACQUISITION AND REDUCTION PROCEDURE AND THEIR APPLICATION TO THE INDUCTIVELY COUPLED PLASMA MASS SPECTROMETRY ANALYSIS OF URBAN SEDIMENTS AND SOILS.

W. G. Diegor[1], H. P. Longerich[2], T. A. Abrajano[3], and I. Horn[4], [1]Environmental Science Programme, Memorial University of Newfoundland, St. John's NF, A1B 3X5, Canada, [2]Department of Earth Sciences, Memorial University of Newfoundland, St. John's NF, A1B 3X5, Canada, [3]Department of Earth and Environmental Sciences, Rensselaer Polytechnic Institute, Troy NY 12180-3590, USA, [4]Department of Earth and Planetary Sciences, Harvard University, Cambridge MA 02138, USA.

A high-pressure acid digestion technique and an inductively coupled plasma mass spectrometry (ICP-MS) data acquisition and reduction procedure were developed to determine transition metals and other trace elements in geological samples. The study was aimed at the problem of incompleteness of digestion of resistant mineral phases in geological materials, and at expanding the coverage of elements routinely analyzed on sediments with ICP-MS.

The high-pressure vessels were fabricated in-house from PTFE and were initially compared with an existing acid digest method, which uses screw cap teflon jars, in the analysis of several geochemical reference materials (GRMs) using the existing MUN ICP-MS trace-element package. Results for the marine sediment reference materials PACS-1, MESS-2, and BSK-1 demonstrated more complete digestion of resistant minerals (e.g., zircon grains) that were likely in high abundance in the sediments. This was indicated by higher Y, Zr, Nb, HREE, Hf, and U values when the pressure vessels were used.

The data acquisition and reduction procedure (environmental-exploration package) was developed for the measurement of 29 masses: ^{51}V, ^{52}Cr, ^{55}Mn, ^{59}Co, ^{60}Ni, ^{65}Cu, ^{66}Zn, ^{75}As, ^{77}Se, ^{79}Br, ^{98}Mo, ^{107}Ag, ^{111}Cd, ^{118}Sn, ^{121}Sb, ^{125}Te, ^{127}I, ^{139}La, ^{140}Ce, ^{141}Pr, ^{145}Nd, ^{167}Er, ^{169}Tm, ^{175}Lu, ^{183}W, ^{201}Hg, ^{208}Pb, ^{209}Bi, and ^{232}Th. Most important interferences were from ^{43}Ca^{16}O on ^{59}Co, ^{44}Ca^{16}O on ^{60}Ni, ^{49}Ti^{16}O on ^{65}Cu, and ^{50}Ti^{16}O on ^{66}Zn. Internal standards used were ^{45}Sc, ^{115}In, and ^{187}Re. Uranium-238 and ^{254}(UO) were measured to monitor polyatomic ion formation. Sensitivity of the elements was calculated from one of two external standards, except for three elements, which were calibrated through surrogate calibration (Sn using Sb, W using Lu, and Hg using Pb). Calibration was demonstrated to be successful for the pair Sn-Sb; though results were not as good for W-Lu, probably due to laboratory contamination. Mercury was most probably lost during sample digestion thus incorrect results were obtained for Hg in reference materials compared to literature values. Analysis of these reference materials using the new package showed excellent results for V, Co, Cr, Ni, Sn, Sb, Cu, Zn, Mo, Cd, and Pb compared with published values. Arsenic and Ag results were mostly near detection limits. Comparison with X-ray fluorescence (XRF) results indicated good agreement between the environmental-exploration package and the XRF. Compared with the MUN ICP-MS trace-element package, the new package was in good agreement for the elements Mo, La, Ce, Pr, Nd, Er, Tm, Lu, Pb, Bi, and Th.

Application of both digestion technique and analytical package to the analysis of urban stream sediment and soil samples from a limestone-underlain area in the Philippines showed good agreement for La, Ce, Pr, Nd, Er, Tm, Lu, Pb, Bi, and Th between the package and the MUN ICP-MS trace results. Nickel and As gave poor results because of the high concentrations in the calibration blanks for Ni and possibly because of volatility for As. Particle size may also have influenced the results for these two elements, because results for the reference materials indicated good agreement between the XRF and the environmental-exploration package. It was found that the GRMs are significantly finer grained than the stream sediment and soil samples (greater <53 μm fraction), suggesting that there may be a need to grind the stream sediment and soil samples to obtain better results.

Mapping of empirically derived geochemical classes showed that the spatial distribution of Cr, Ni, Cu, Zn, Pb, Sn, Sb, and Cd in the stream sediments corresponds to the large commercial zone in the southwest portion of the study area. Higher values of Cu and Zn point to an industrial zone to the east. The soil element data correspond to an industrial zone where manufacturing and use of metal parts abound. Arsenic was high in a relatively new land development that was formerly a site where storm drainage and airline night soil from a nearby air facility was collected. Except for Sb and Cd, the element concentrations in the stream sediments were high for a limestone terrain. The soil samples likewise indicated input from human activity. The derived geochemical landscape coincided with the known land use in the area.

INTERACTION OF SILICIC ACID WITH IRON OXIDES.

M. Dietzel, Geochemisches Institut der Universität Göttingen, D-37077 Göttingen, Germany (mdietze@gwdg.de).

Introduction: In sedimentary environments, the formation of iron ores is closely related to the precipitation of Fe-O-OH-phases from aqueous solutions at different chemical conditions. These solids have high specific surface areas and a high reactivity with respect to dissolved components, especially silicic acid. This affinity is documented for example by the relatively high silica content of many sedimentary iron oxide ores [1].

Methods: The interaction of silicic acid with iron oxides was studied via adsorption and precipitation experiments. The solids used for the adsorption experiments were goethite, akaganéite, feroxyhyte, lepidocrocite, hematite, magnetite, and ferrihydrite. In the following, only the experimental results for goethite are presented as a typical case. The surface density and the distribution of surface hydroxyl groups were analyzed via potentiometric titrations (goethite: 7.2 $\Sigma \equiv$ FeOH/nm^2). The precipitation experiments were carried out by oxidation of Fe^{2+} in solutions containing chloride at constant pH and $O_{2(aq)}$ concentrations.

Kinetics of Silica Adsorption: In all experiments the concentration of silicic acid decreased continuously as a function of reaction time via adsorption at the surface of the solid, following a first order law. Three stages may be distinguished. The first stage is finished within some minutes, the second one within hours, and the third one within about 15 days. The values of the reaction rate constants (second stage: $k_2 = 0.20\ h^{-1}$) are similar for all the above iron oxides.

Surface Complexation of Silica: The adsorption equilibrium may be described by the interaction of silicic acid with surface hydroxyl groups and the formation of specific surface complexes [e.g., 2]. In a simple approach, three different kinds of surface hydroxyl groups may be distinguished according to the reactions

$$\equiv FeOH_2^+ = \equiv FeOH^0 + H^+ ,\ K_1^{int} \quad (1)$$

$$\equiv FeOH^0 = \equiv FeO^- + H^+ ,\ K_2^{int} \quad (2)$$

The measurements yielded $K_1^{int} = 6.56$ and $K_2^{int} = 9.94$ for the present goethite (68 m^2/g). Following this approach the adsorption of silicic acid onto the surface of iron oxides may be described by a surface complex-ation according to the reactions

$$Si(OH)_4 + \equiv FeOH^0 = \equiv FeOSi(OH)_3^0 + H_2O ,\ K_{S1}^{int} \quad (3)$$

$$Si(OH)_4 + \equiv FeOH^0 = \equiv FeOSiO(OH)_2^- + H_2O + H^+ ,\ K_{S2}^{int} \quad (4)$$

The calculated concentration of the surface complexes of silica agree well with the experimental data, yielding $pK_{S1}^{int} = -2.6$ and $pK_{S2}^{int} = 4.6$. For calculation a correction with respect to the electrostatic behavior of the solid surface was considered [3].

Incorporation of Silica by Iron Oxides: In the experiments the precipitation of iron oxides was monitored by the decrease of Fe^{2+} concentration in the solution with and without silicic acid. For both types of experiments the kinetics of precipitation may be described by a first order law. The results show that the specific values of the reaction rate constant decrease significantly by the addition of silicic acid. Further, the solids contain appreciable amounts of silica. The incorporation of silica into the solids, essentially ferrihydrite, results in Si/Fe ratios of the iron oxides of about 0.13.

Implications for Natural Systems: It is shown that silicic acid forms specific surface complexes within a rather short time, as compared to timescales of natural processes. Most probably this complexation causes a decrease of the precipitation rates of iron oxides. As a matter of fact, the molar ratio of total concentrations of the silica surface complexes and of the hydroxyl groups is about 0.2 at a pH between 5 and 8. This ratio corresponds to the molar ratio of Si/Fe of the iron oxides obtained in the present precipitation experiments and is similar to that of recent sedimentary iron oxides

(0.16). It may be concluded that the silica content of sedimentary iron oxide ores is directly related to the adsorption of silicic acid onto the primary precipitates via the formation of the above surface complexes.

References: [1] James H. L. (1966) *U.S. Geological Survey Prof. Paper,* 60 pp. [2] Sigg L. and Stumm W. (1981) *Colloids and Surfaces, 2,* 101–117. [3] Dzombak D. A. and Morel F. M. M. (1990) in *Surface Complexation Modeling. Hydrous Ferric Oxide,* Wiley-Interscience, 393 pp.

GEOCHEMICAL AND RARE-EARTH-ELEMENT CHARACTERISTICS OF FERRUGINOUS SILICEOUS ROCKS OF BIOKOU GROUP, QINLING, CHINA: IMPLICATIONS FOR ANCIENT SEAFLOOR HYDROTHERMAL FLUID PROCESSES.

Z. J. Ding[1,2], C. Q. Liu[1], H. Y. Li[1], and Z. S. Yang[1], [1]Institute of Geochemistry, Chinese Academy of Sciences, Guiyang 550002, China (zjding@ms.gyig.ac.cn), [2]China University of Geosciences, Wuhan, 430074, China.

Ferruginous siliceous rocks are located on the top of volcanic rock series and paralleled to them in the Bikou group of south Qinling, which is a famous orogenic belt separating Chinese continent into two parts: North China and Yangtze plates. The Bikou group volcanic rocks are formed in the Proterozoic era and petrochemically are divided into tholeiite and calc-alkaline dacite, respectively, showing characteristics of bimodal volcanic rock clearly and a lack of typical intermediate rocks. The results [1,2] suggest that the volcanic rocks of Bikou group were generated in a rift tectonics setting. The ferruginous siliceous rocks are considered to be of hydrothermal origin on the ancient seafloor.

Major-Element Compositions: Ferruginous siliceous rocks are marked by extremely high Fe contents (total Fe_2O_3 = 40–30 wt%) and low Al contents (Al_2O_3 = 0.02–0.24 wt%), Al_2O_3/Fe_2O_3 ratios from 0.0004 to 0.01, sharing a general characteristic of hydrothermal sedimentary rocks. So the ferruginous siliceous rocks are thought to have precipitated from hydrothermal solutions on the ancient seafloor.

Rare-Earth-Element Compositions: The ferruginous siliceous rocks show two types of distribution patterns when normalized to PAAS: (1) Similar seawater in whole except Eu, which are characterized by LREE depletions (La/Sm_N = 0.1296–0.489), and HREE enrichments (Gd/Yb_N = 0.454–0.970). (2) More like to the high-temperature hydrothermal fluids of modern seafloor, which are characterized by both LREE and HREE depletions (La/Sm_N = 0.102–0.69, Gd/Yb_N = 1–3.03). There are variable positive Eu anomalies Eu/Eu* = 1.23–2.598, 1.05–9.29 and Ce anomalies Ce/Ce* = 0.463–1.02, 0.7034–1.223 respectively matching to former and latter in above-mentioned ferruginous siliceous rocks. Except a few samples with a positive Ce anomaly, all others possess varying magnitude of negative Ce and positive Eu anomalies. In general, appearances of negative Ce anomaly represent seawater contamination, while positive Eu anomalies indicate participation of high- temperature hydrothermal fluid components. So existences of the positive Eu and negative Ce anomalies in a sample may indicate that hydrothermal fluids mixed with seawater before the ferruginous siliceous rock deposit on ancient seafloor. The change in magnitudes of Ce and Eu anomaly more likely indicate mixture proportion differences of hydrothermal and seawater components [3]. Moreover, In Eu/Sm vs. La/Ce diagram samples are between different curvature mixture line of pure seawater and hydrothermal fluid end members (γ = 0.1–0.001), maybe reflecting physical-chemical differences resulting in siliceous rock precipitation while two fluids met on seafloor. So the mixture can explain the reason of samples distribution. If hydrothermal fluids mixed with seawater bearing some contents of terrigenous components, then the scattered sample can be well explained. So the ancient ocean of Proterozoic era in south Qinlin is not wide enough, or, in other words, is a limited oceanic basin.

References: [1] Zhang G. et al. (1996) *Science in China (series D), 26,* 193–200. [2] Xia L. et al. (1996) *Science in China (series D), 26,* 237–243. [3] Barrett T. J. et al. (1990) *Geology, 18,* 583–586.

PARTIAL MOLAR VOLUMES OF SIDEROPHILE ELEMENTS IN MELTS: IMPLICATIONS FOR THE PRESSURE-DEPENDENCE OF METAL-SILICATE PARTITIONING.

D. B. Dingwell [1], P. Courtial[1], C. Holzapfel[1,2], J. Gottsmann[1], A. Holzheid[3], and H. Palme[2], [1]Bayerisches Geoinstitut, University of Bayreuth, D95440 Bayreuth, Germany, [2]Mineralogie/Geochemie Abteilung, Universitat Köln, D50674 Köln, Germany, [3]Department of Earth, Atmospheric and Planetary Sciences, Massachussetts Institute of Technology, Cambridge MA 02139-4307, USA.

The abundances of moderately siderophile elements in the Earth's mantle place important constraints on the early history of the Earth. They are believed to have been strongly fractionated from the mantle into the core of the Earth such that their abundances in the residual mantle may constrain the core formation process. In fact, it is generally accepted that the depletion of siderophile elements results from their partitioning. However, as pointed out earlier [1], their abundances in the Earth's upper mantle are far too high to have been produced by a simple equilibration of core-forming metal with mantle-forming silicate.

Analysis of their partitioning behavior at high pressures and temperatures can place strong constraints on the nature and efficiency of processes operative in both the early and modern Earth. Whether the direct determination of partition coefficients for such elements at high pressures and temperatures under well-constrained conditions is feasible remains open. Thus we have proposed that such efforts might be well-complemented by high-pressure extrapolations from existing low-pressure partitioning data together with volumetric properties. Toward this end, we undertook the determination of the partial molar volumes of moderately siderophile elements in silicate liquids. The partial molar volumes of NiO and CoO liquids have been determined for Ni- and Co-containing Na-disilicate liquid over a wide range of temperatures by combining high-temperature measurements using the Pt-based double-bob Archimedean method and low-temperature measurements using the method described by Webb et al. [2].

The change in the partition behavior of elements between coexisting metal and silicate phases as function of pressure at constant temperature can be calculated based on the following equation:

$$D_{M\text{-}Fe}{}^{met\text{-}sil}{}_{T,P} = D_{M\text{-}Fe}{}^{met\text{-}sil}{}_{T,1bar}\, e^{-[(P \times VM\text{-}Fe/(RT)]}$$

where $D_{M\text{-}Fe}{}^{met\text{-}sil}{}_{T,1bar}$ and $D_{M\text{-}Fe}{}^{met\text{-}sil}{}_{T,P}$ are the metal-silicate partition coefficients of element M at temperature T and 1 bar and at temperature T and pressure P, respectively and $\Delta V_{M\text{-}Fe}$ the total volume change. In such an equation, the change of the partition coefficients as a function of pressure depends only on the $\Delta V_{M\text{-}Fe}$ term. Possible pressure dependence of the molar volume of MO (i.e., $\partial V/\partial P)_{MO}$ in the silicate liquid is ignored for simplicity [see also 2].

The molar volumes of pure MO liquids (i.e., NiO and CoO) and pure FeO liquids have been determined using their partial molar volumes and given by [3] respectively. Assuming that the partial molar volumes of NiO, CoO, and FeO liquids are not too different from the molar volumes of their pure liquids, the molar volume of NiO liquid is smaller than the one of FeO liquid at lower temperatures, but larger at higher temperatures. Within the entire temperature range, the molar volume of CoO liquid will be larger than the one of FeO liquid.

The present study shows that the metal-silicate exchange partition coefficient of both Ni and Co decreases with increasing pressure within the entire temperature range considered in this study (i.e., 800–3000 K). In several studies, the pressure dependence of NiO and CoO solubilities in FeO-containing silicate melts were recently investigated [e.g., 4–14]. All of these experimentally determined Ni-Fe and Co-Fe metal-silicate exchange partition coefficients show a decrease with increasing pressure at constant temperature, and this is independent of silicate and metal compositions. This is in good agreement with the qualitatively predicted pressure dependencies of $K_{DNi\text{-}Fe}{}^{met\text{-}sil}$ and $K_{DCo\text{-}Fe}{}^{met\text{-}sil}$, which is based on the partial molar volumes of NiO and CoO in silicate melts. Furthermore, the experimentally derived $K_{DCo\text{-}Fe}$ values recalculated to 2273 K from the high-pressure studies where Ni-, Co-, and Fe-containing metal alloys and silicate melts were present in the experimental charge [e.g., 10–12] show, at constant temperature, the same pressure dependence of $K_{DCo\text{-}Fe}{}^{met\text{-}sil}$ between 1 bar and high-pressure values.

Quantitatively, it has been found that $K_{DCo\text{-}Fe}{}^{met\text{-}sil}$ will decrease at the same temperature conditions relative to the one bar values by a factor of 0.39 and 0.24, at 10 and 15 GPa respectively, whereas $K_{DNi\text{-}Fe}{}^{met\text{-}sil}$ will decrease by a factor of 0.81 and 0.73 at 10 and 15 GPa respectively. Using least-square fits through the literature data of experimentally derived partition coefficients at 2373 K [i.e., 10–12], a decrease by a factor of 0.53 and 0.40 is observed for $K_{DCo\text{-}Fe}{}^{met\text{-}sil}$ and by a factor of 0.48 and 0.34 for $K_{DNi\text{-}Fe}{}^{met\text{-}sil}$ at 10 and 15 GPa respectively. This quantitative disagreement is likely due to the assumptions we made. As aforementioned, the pressure dependence on the molar volume, which was ignored as a first approximation, may greatly contribute to this disagreement. In addition, the assumption that the partial molar volume of NiO, CoO, and FeO liquids is the same as their respective molar volumes may also not occur. Analysis of data for Ga_2O_3 and GeO_2 in Na-silicate and anorthite-diopside melts is in progress.

References: [1] Ringwood (1966). [2] Webb et al. (1992). [3] O'Neill et al. (1998). [4] Lange and Carmichael (1987). [5] Urakawa (1991). [6] Suzuki et al. (1992). [7] Ohtani et al. (1992). [8] Ohtani et al. (1997). [9] Peach and Mathez (1993). [10] Walker et al. (1993). [11] Thibault and Walter (1995). [12] Holzheid et al. (1995). [13] Li and Agee (1996). [14] Ohtani an Yurimoto (1996). [15] Ito et al. (1998).

THE GEOCHEMISTRY AND PETROLOGY OF AN URBAN CANAL BED MUD.

J. S. Dodd[1], A. E. Milodowski[2], D. J. Large[1], N. J. Fortey[2], and S. J. Kemp[2], [1]School of Chemical, Environmental and Mining Engineering, University of Nottingham, Nottingham NG7 2RD, UK (enxjsd@nottingham.ac.uk), [2]Mineralogy and Petrology Group, British Geological Survey, UK.

Urban canal bed mud is highly contaminated and provides an ideal opportunity for investigating the geochemistry of a system dominated by anthropogenic inputs. This study investigates the relationship between porewater geochemistry and the petrology of Fe, S, and P in the canal mud. In order to build up a picture of canal bed mud, geochemistry cores of canal sediment, 25 cm in depth, were collected from an urban canal in Birmingham, a major industrial city in the UK, and their sediments and porewaters analyzed. In addition, the petrology of the sediment has been studied by a new cryogenic scanning electron microscope (cryoSEM) technique. CryoSEM analysis of sediment enables samples to be viewed directly without alteration of their chemistry or texture; energy-dispersive X-ray (EDX) analysis can then be used to determine mineral composition. Analysis of canal mud has revealed the most abundant authigenic mineral phases in order of decreasing abundance to be the Fe^{2+}-phosphate vivianite ($Fe_3(PO_4)_2$ $8H_2O$), mixed Fe, Zn, Cu sulphides, a variety of Fe sulphide minerals, and calcite.

Sulfate concentrations in the porewaters decline from ~200 ppm in the overlying water to <0.1 ppm at a depth of 3 cm in the sediment. A small peak in Fe porewater concentration of ~2 ppm occurs at the sediment-water interface, implying that Fe oxides are reduced at the sediment surface. This is supported by a drop in Eh from 0.4 V to –0.1 V across the sediment-water interface. Iron sulfide minerals were observed by cryoSEM in samples taken from the sediment water interface, suggesting that Fe^{2+} released by the reduction of easily reducible Fe-oxides is reacting with S^{2-} produced by SO_4^{2-} reduction. Sinks for Fe and sulfide include a complex mixture of biofilm coatings, mineralized organic matter, and framboidal structures that ranged in composition from FeS to FeS_2. In addition to the iron sulfides, authigenic Zn-Fe sulfides and Cu-Fe-sulfides are also common components of the sediment.

Phosphate concentration in the porewaters peaks at ~30 ppm, at a depth of 3–5 cm. This peak occurs below the near-surface peaks in Fe^{2+} and SO_4^{2-}. Phosphate is released to the sediment by organic matter degradation, and the rate of degradation should be highest at the sediment-water interface. The low concentrations of PO_4^{3-} above 3 cm are interpreted as resulting from high rates of Fe reduction that are greatly in excess of the supply of reduced S. This interpretation of excess Fe is partly supported by the high concentrations of Fe available in the sediment (~7% Fe). The excess supply of Fe^{2+} results in the precipitation of vivianite that was observed at the sediment-water interface. This is also supported by calculations that show that vivianite is oversaturated in the sediment porewater. The peak in PO_4^{3-} at 3 cm may result from the depletion of easily reducible Fe-oxides and a consequent reduced rate of Fe reduction relative to the rate of organic matter degradation.

Petrographic evidence of etched vivianite grains below 7 cm is interpreted as indicating that vivianite is dissolving. This etching becomes more pronounced with depth. A steady increase of Fe^{2+} concentration in the porewater at depths below 7 cm appears to support this evidence; however, PO_4^{3-} concentrations are highly variable and show no interpretable trend. Consideration of the Eh/pH stability of vivianite indicates that the dissolution of vivianite could be due to a decrease in pH. Petrographic evidence of vivianite dissolution is at odds with solubility calculations that indicate that the porewaters are supersaturated with respect to vivianite throughout the profile, suggesting the precipitation of vivianite should be favored over its dissolution. One possible explanation for this is that vivianite is being affected by localized variations in PO_4^{3-} demand by microorganisms in discrete microenvironments. Some evidence for the role of microenvironments may be the presence of both relatively unetched and highly etched vivianite grains in the same depth interval. Alternatively, there may be gaps in our understanding of P speciation in highly reducing organic-rich sediments.

SOME COMPARATIVE GEOCHEMISTRY OF OCEANIC AND CONTINENTAL IGNEOUS ROCKS.

B. R. Doe, 5508 Heming Avenue, Springfield VA 22151-3220, USA.

Previously, Doe [1] found mid-ocean ridge basalts (MORB), oceanic island basalts (OIB), and oceanic arc volcanics (OAV) to be distinguishable in a plot of Ce/Yb vs. Ba/Ce where OIB trends to high ratios in Ce/Yb and OAV to high ratios of Ba/Ce compared to MORB. Averages for MORB are Ce/Yb <10, Ba/Ce 2–4; OIB Ce/Yb >10, Ba/Ce 2.5–7; and OAV Ce/Yb <20, Ba/Ce >4. Averages are preferred to individual samples because Ba is somewhat mobile but usually does not move far. Although averages do not overlap, individual samples may (e.g., Juan de Fuca Rise for MORB and New Britain for primitive OAV). Hotspot-related continental rift volcanics (e.g., those of Marie Byrd Land and Ross Sea in Victoria Land, Antarctica) fall comfortably in the OIB field. The continental hotspot volcanics of the Yellowstone volcanic field, Wyoming, plot in the OAV field along with continental arc volcanics sites (e.g., the Cascade Mountains, Oregon, and Washington). Hildreth [2] concluded that all the basalts at Yellowstone may be crustally contaminated; however, he identified the Swan Lake Flat basalt as most likely the least affected because of its high ε_{Nd} (–2.4). Previously Doe et al. [3] identified the top flow of the basalt of The Narrows as possibly being an uncontaminated asthenosphere representative because of the lowest values of both $^{207}Pb/^{204}Pb$ (15.294) and $^{87}Sr/^{86}Sr$ (0.70385). Hildreth [2] subsequently found the ε_{Nd} of this flow to be –3.1. These two basalts have the lowest values of Ba/Ce and project into the lower part of the OIB field though still in the OAV field, supporting Hildreth's conclusion of possible crustal contamination in all Yellowstone basalts.

The value of V/Zn was found to be essentially constant in MORB [1], thus representing the ratio in the source magma. This ratio is also useful in distinguishing igneous environments. Using molar plots of Zn/Zr_M vs. V/Zr_M, most samples from N-MORB localities (e.g., So. EPR and Kane FZ, MAR) are in the range for Zn/Zr_M of 0.8–1.5, with only the Juan de Fuca Rise data being somewhat higher by 0.1–0.2 and in the range 4.0–7.5 for V/Zr_M. Indian Ocean ridges can be somewhat different from Pacific and Atlantic Ocean ridges. The Southwest Indian Ridge can have values of V/Zr_M down to 2.0, and the northwest Indian Ridge can have ratios >8.0. Data for hotspots (e.g., Hawai'i, and Tristan da Cunha) are lower, normally <4.0 for V/Zr_M with only Loihi Seamount tholeiites, Hawai'i, being in the MORB range. Samples from primitive OAV (e.g., New Britain and the Mariana Islands) tend to have values of Zn/Zr_M greater than for N-MORB for a given value of V/Zr_M (extreme in the case of the Tonga Islands) with large ranges in V/Zr_M that extend beyond 12 and can be <4 for the Mariana Islands. Mature OAV also have large ranges in these ratios and can have data overlapping with OIB (e.g., Indonesia), but Taupo, New Zealand, basalts have ratios much like the Juan de Fuca Rise. On continents, the Cascade Mountains volcanics are like some OAV whereas the Antarctic rift volcanics are much like OIB volcanics. Columbia River flood basalts have some samples similar to N-MORB, but many samples have values of V/Zr_M <4 like OIB, suggestive of mixtures of hotspot and depleted mantle or lithospheric magmas.

References: [1] Doe (1997). [2] Hildreth (1991). [3] Doe et al. (1982).

ZINC ADSORPTION ON IRON(II)/IRON(III) SUBSTRATES PRODUCED BY MICROBIAL REDUCTION OF HIGH-SURFACE-AREA GOETHITE.

R. J. Donahoe, K. D. Kirk, and E. Y. Graham, Department of Geosciences, University of Alabama, Tuscaloosa AL 35487-0338, USA (rdonahoe@wgs.geo.ua.edu).

Introduction: Reductive dissolution of ferric iron oxyhydroxide phases has been demonstrated to occur primarily through microbially catalyzed reactions for a variety of natural systems. These reactions impact the global cycling of Fe and C, and can potentially result in the mobilization of heavy metal elements bound to the surface of Fe(III) phases.

Experimental work performed by several investigators has shown that under most conditions only a minor fraction of the Fe(II) produced by microbial reductive dissolution of Fe(III) oxyhydroxide phases remains in the aqueous phase [1–3]. In addition, it was recently demonstrated that adsorbed or coprecipitated Zn is not mobilized by microbial reduction of HSA goethite [4]. These results have important implications for the mobility of heavy metal elements in anaerobic subsurface environments.

This study was performed to experimentally determine the adsorption capacity of Fe(II)/Fe(III) substrates produced by microbial reduction of HSA goethite for Zn under conditions appropriate to natural systems.

Methods and Materials: High-surface-area goethite (HSA-Gt; BET surface area = 220 m^2/g) was synthesized via FeCl$_2$ oxidation [5]. After thorough washing, the HSA-Gt was freeze-dried and passed through a 100-µm screen.

Shewanella alga (strain BrY) [6] is a gram-negative facultative anaerobe capable of dissimilatory reduction of amorphous and crystalline Fe(III) oxyhydroxides. *S. alga* was grown under anaerobic conditions at circumneutral pH and used in all incubation experiments.

Anaerobic artificial groundwater (AGW) incubation media having 50 mM Fe as HSA-Gt, 5 mM Lactate, 10 mM HCO$_3^-$, and either 0 mM or 10 mM HEPES buffer was prepared in 400-mL batches, distributed equally between 100-mL serum bottles, and inoculated with washed BrY cells. The bottles were incubated at ambient temperature and sampled periodically to determine the extent of Fe(III) reduction. Bottles were sacrificed after different time intervals to provide substrate having various reduction states for use in Zn-adsorption experiments. The substrates were separated from the incubation media by centrifugation and washed three times in anaerobic AGW. Anaerobic adsorption experiments were set up using partially reduced HSA-Gt substrate in the AGW + 10 mM HCO$_3^-$ matrix described above, 0–3.88 mg/L (0–59.35 µM) Zn, and having pH = 6.8.

Results and Discussion: Zinc sorption isotherms have been determined for 0–46% reduced HSA-Gt in the solution matrix described above, and for 0–37% reduced HSA-Gt in AGW + 10 mM HCO$_3^-$ + 10 mM HEPES buffer. In general, the percent sorption of Zn is fairly uniform (between 70% and 80%) over the range of Zn concentrations and HSA-Gt reduction states examined. Although the percent sorption of Zn on the reduced substrate is approximately 10–15% lower than that for unreduced HSA-Gt at pH = 6.8, the adsorption capacity is much greater than can be explained by the presence of residual, unreduced HSA-Gt. This, plus the observed slight overall trend of increasing percent sorption of Zn with increasing percent reduction, suggests that the partially reduced substrate possesses significant adsorption capacity for Zn. Possible sorption mechanisms include Zn adsorption on Fe(II) phases and/or biologic substrates, or incorporation/coprecipitation of Zn into the structure of a solid phase.

Data for Zn sorption on HSA-Gt reduced in the presence of HEPES buffer suggest that the presence of HEPES may increase the sorption capacity of the reduced substrate somewhat, particularly for higher percent reduction levels and lower Zn concentrations.

Langmuir and Freundlich isotherm fitting parameters were calculated from the measured adsorption data. Comparison of the experimental data to predicted isotherms showed that adsorption of Zn by partially reduced HSA-Gt is best modeled by Freundlich isotherms. Langmuir models underpredict Zn adsorption.

Iron(II) speciation is being examined by chemical modeling and X-ray diffraction (XRD), scanning electron microscopy (SEM), and Auger Microprobe analyses to attempt to characterize the reduced substrate phase(s) and determine the sorption mechanism(s) for Zn on this material.

Summary: The results of this study have shown that Zn adsorption by solid phases formed through the partial reduction of HSA-Gt by *Shewanella alga*, while lower than that for unreduced HSA-Gt, is still substantial. These results indicate that metals originally adsorbed to Fe(III) oxyhydroxide phases in soils, sediments, and aquifer materials will remain largely immobile even after reductive dissolution of the Fe(III) phases by anaerobic bacteria.

Acknowledgments: This work is funded by DOE/NABIR grant #DE-FG02-97ER62482. We are grateful for help provided by F. Picardal and D.C. Cooper at Indiana University, and E. Roden, M. Urrutia, and V. Keith at the University of Alabama.

References: [1] Urrutia M. M. et al. (1998) *Geomicrobiol., 15,* 269–291. [2] Fredrickson J. K. et al. (1999) *GCA, 62,* 3239–3257. [3] Chapelle F. H. (1993) *Ground-Water Microbiology & Geochemistry,* Wiley. [4] Cooper D. C. et al. (1999) *Geomicrobiol.,* submitted. [5] Goodman B. A. and Lewis D. G. (1981) *J. Soil Sci., 32,* 351–363. [6] Rosello-Mora R. A. et al. (1994) *System. Appl. Microbiol., 17,* 569–573.

NITROGEN-ISOTOPIC VALUES AS A PROXY FOR LAND-USE PATTERNS IN THE CONNECTICUT RIVER WATERSHED.

T. A. Douglas, C. P. Chamberlain, and R. R. Harrington, Department of Earth Sciences, Dartmouth College, Hanover NH 03755, USA.

Introduction: Recently, N-isotopic studies have been employed to quantify the extent of nonpoint source N contamination in natural waters [1,2]. Major nitrate sources include atmospheric deposition, nitrification of soils and snow, fertilizers and animal waste. Variations in δ^{15}N have been successful in defining these sources in waters [3]. We present here results from an ongoing study of the effect of land use on the chemistry of the Connecticut River watershed, USA. Nitrate concentrations and N-isotopic ratios suggest nitrate in the watershed is directly related to land-use practices.

Study Site: The Connecticut River watershed encompasses 15,750 square miles, stretching 383 miles from its source at the U.S.-Canada border south to Long Island Sound. Approximately 4.5 million people live within the river's drainage, with most concentrated in the lower third of the watershed. The Connecticut River begins in remote lakes surrounded by pristine hardwood forests. In southern New Hampshire and Vermont, the river travels through agricultural communities that rely on intensive use of fertilizers to produce corn and hay during the short growing season. The Connecticut River is ideally suited for a N-isotopic investigation because of these longitudinal differences.

Sampling and Land-Use Quantification: The entire Connecticut River watershed was sampled at 41 sites in August and December, 1998, and April, 1999. These three time periods constitute the major seasonal changes in the study area: summer to fall, fall to winter, and winter to summer. The Connecticut River was sampled above and below 11 major tributaries, which were selected for their representation of geology, land use, drainage population, and areal extent. Tributaries were sampled in an attempt to quantify small-scale changes in land use within the Connecticut River watershed. Maps from 1991 to 1993 LANDSAT thematic mapper images at 1:24,000 scale were checked with GIS land-use cover data. Mapping classified the sample sites into four distinct land use patterns, which are, from north to south, forest, mixed forest and agriculture, intense agriculture, and dense population.

Results and Discussion: Nitrate-N was measured at each site using a LaMotte colorimeter [4]. Nitrate-N concentrations in the 11 tributaries are related to their land-use classification (Fig. 1). The highest nitrate concentrations are in waters from tributaries draining heavily populated watersheds. δ^{15}N values of waters were measured using methods adapted from [5]. Results

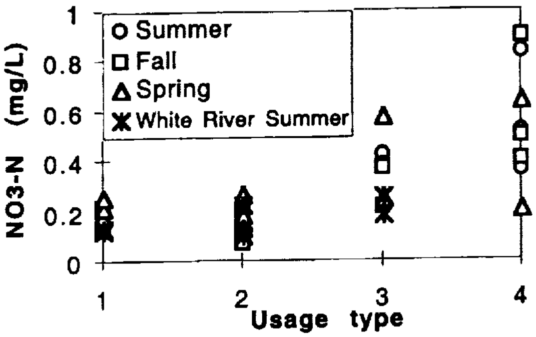

Fig. 1. Nitrate-N concentrations (mg/L) vs. land-use type for 11 catchments along the Connecticut River and six samples from the White River. 1 = forest, 2 = forest and agriculture, 3 = agriculture, and 4 = dense population. White River samples from [2].

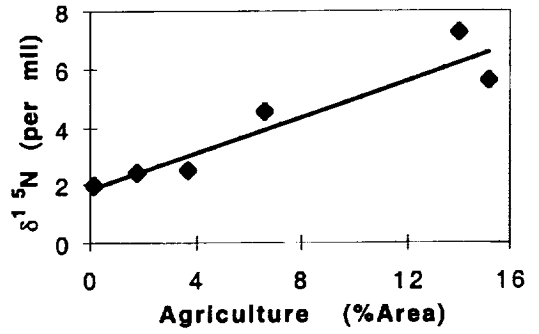

Fig. 2. Average δ^{15}N values of nitrate in stream water from the White River, Vermont. From [2].

δ^{15}N-isotopic values from the White River in Vermont (Fig. 2) suggest a linear correlation with the percent of agriculture. δ^{15}N values increase from 2‰ in the forested catchments to 7‰ in catchments draining lands categorized as 14% agriculture. Results from the N-isotopic analyses indicate this study should be extended to tributaries in the Connecticut River that drain densely populated areas to further quantify the relationship between land-use and nonpoint sources of nitrate.

References: [1] Ostrom N. E. et al. (1998) *Chem. Geol., 146,* 219–227. [2] Harrington R. R. et al. (1998) *Chem. Geol., 147,* 281–294. [3] Exner M. E. and Spalding R. F. (1994) *Appl. Geochem., 9,* 73–81. [4] American Public Health Association (1989) *Standard Methods for the Examinination of Water and Wastewater,* 17th ed. [5] Kendall C. et al. (1995) *International Association of Hydrological Sciences Publication 228,* pp. 339–347.

NATURE AND ORIGIN OF THE LOWER CRUST OF CRATONIC EUROPE: XENOLITH SUITES FROM THE BALTIC SHIELD AND EAST EUROPEAN PLATFORM.

H. Downes[1], A. J. W. Markwick[1], and P. D. Kempton[2], [1]Birkbeck/UCL Research School of Geological and Geophysical Sciences, Birkbeck College, Malet Street, London WC1E 7HX, UK (h.downes@ucl.ac.uk), [2]Isotope Geosciences Laboratory, National Environmental Research Council, Kingsley Dunham Centre, Keyworth NG12 5GG, UK (p.kempton@nigl.nerc.ac.uk).

Introduction: A crucial question of crustal evolution is whether processes that formed the lower continental crust in Archean/Proterozoic times were similar to those that have operated during the Phanerozoic. Direct sampling of the lower crust as xenoliths entrained in mafic alkaline magmas can yield information about its mineralogy, chemical composition, and origin. The European continent shows strong contrasts in crustal thickness, heat flow, and lithospheric structure between its Archean/Proterozoic cratonic areas and its Phanerozoic mobile belts [1]. These differences are reflected in the mineralogy, chemical composition, and metamorphic facies of lower crustal xenoliths in different parts of the continent [2]. The Baltic Shield and East European Platform is a region of thick (>40 km) Archean/Proterozoic cratonic crust with a high-velocity lower crust. Alkaline magmas (including lamprophyres, kimberlites, melilitites, and carbonatites) were intruded across the region in Devonian times, in some cases entraining lower crustal xenoliths. We have studied three garnet granulite xenolith suites from the Archean/Proterozoic cratonic areas of Europe (Kola Peninsula [3], Arkhangelsk [4], and Belarus [5]) and consider that the xenoliths represent metamorphosed Proterozoic mafic underplates.

Mineralogy, P-T Estimates, Seismic Velocity, and Density: The xenoliths grade from plagioclase-rich mafic garnet granulites to plagioclase-poor eclogitic granulites with <5% plagioclase. All are rutile-bearing. Less common xenoliths include metasomatized granulites and rare felsic (migmatised) granulites. The high pressure mineralogy contrasts strongly with the lower pressure granulite xenoliths of western Europe [2]. PT estimates yield pressures (12–15 kbar) similar to those anticipated for the geophysically imaged thick lower crust in the region, but temperatures are higher than the current estimates of lower crustal temperatures in the area, so we interpret the PT data as frozen equilibria. Estimates of the average density and seismic velocity of the Kola xenoliths are 3.2 Mg/m3 and 7.1 km/s, respectively.

Isotopic Compositions: Present-day Sr-isotopic compositions of the mafic granulite xenoliths from beneath the European craton are relatively low (0.7052–0.7122). Felsic xenoliths have Sr-isotopic ratios up to 0.725 and strongly metasomatized samples have the highest Sr-isotopic ratios (0.9), reflecting the presence of ancient metasomatic phlogopite. Neodymium-isotopic ratios in the xenoliths are also generally low (0.51124–0.51230 garnet granulites from Arkhangelsk differ from those of Kola and Belarus in defining a mixing hyperbola between depleted mantle and more enriched crustal compositions and may represent a younger addition to the crust in this region. Processes that can be inferred to have occurred in the lower crust of the Baltic Shield/East European Platform include (1) intrusion (underplating) of mafic magmas, (2) metamorphism/migmatization, and (3) metasomatism. Crustal assimilation may have occurred to an unknown but probably small extent.

The Sr- and Nd-isotopic array for granulite xenoliths worldwide shows that there are three main components that have contributed to the isotopic variability of the lower crust. One component has low ^{87}Sr/^{86}Sr and low ^{143}Nd/^{144}Nd ratios and is found only in the regions of ancient crust. The Baltic Shield/ East European Platform xenoliths represent this component and therefore contrast strongly with the majority of mafic lower crustal xenoliths from beneath Phanerozoic terranes. The mineralogy and isotope geochemistry of the xenolith suites from the Baltic Shield/ East European Platform are very similar to the rutile-bearing garnet granulites with eclogitic affinities from Lesotho, Greenland, West Africa, Kaapvaal, southern Australia, northern Canada, and Montana. Thus, these high-pressure granulites seem to be common in the lower crust beneath regions of ancient continental crust and/or Archean cratons. This indicates that there is a commonality of processes that have formed and modified the Earth's ancient lower continental crust.

References: [1] Blundell D. et al. (1992) *The European Geotraverse: A Continent Revealed,* Cambridge Univ. [2] Downes H. (1993) *Phys. Earth Planet. Int., 79,* 195–218. [3] Kempton P. D. et al. (1995) *Lithos., 36,* 157–184. [4] Markwick A. J. W. and Downes H. (1999) *Lithos.,* submitted. [5] Markwick A. J. W. et al. (1999) *Tectonophys.,* in press.

PRESIDENTIAL ADDRESS: FORMATION AND PRIMORDIAL DIFFERENTIATION OF THE EARTH.

M. J. Drake, Lunar and Planetary Laboratory, University of Arizona, Tucson AZ 85721-0092, USA.

The formation of metallic cores, the crystallization of magma oceans, the formation of early crusts, and the outgassing of planetary atmospheres is a natural consequence of planetary accretion. For a generation, the concept of heterogeneous accretion of the planets held sway. Now the idea has emerged that the siderophile element signatures in the mantles of the Earth, Moon, Mars, and Vesta result from equilibration of metal destined for planetary cores with silicate in magma ocean environments [1].

Righter and Drake [2] were able to account for even the abundance of the highly siderophile element Re by metal/silicate equilibrium in a magma ocean environment, but the chondritic (to within 4%) Re/Os ratio in the Earth's mantle inferred from Os-isotopic work may point to a hybrid model: the moderately siderophile element abundances were set by metal/silicate equilibrium in a magma ocean environment, while the highly siderophile elements may well have been delivered as a late veneer and mixed very efficiently into a by now metal-free (the metal had segregated into the planetary core) magma ocean.

A terrestrial magma ocean was almost certainly hydrous, a conclusion that derives both from modeling [2] and D/H observations of comets [3]. This conclusion raises the question of whether H is dissolved in planetary cores.

Magma oceans also offer the possibility that radioactive heat-producing elements such as K may dissolve in planetary cores. Chabot and Drake [4] find that K is more soluble in S-bearing metallic liquids than pure Fe metallic liquid and C-bearing metallic liquid, but is approximately 2 orders of magnitude under abundant in metallic liquid to be a significant contributor to the energy budget of Earth's core.

Fractionation of crystallizing silicate and oxide minerals from a deep magma ocean should result in fractionated ratios of refractory lithophile elements such as Sc/Sm in the primitive silicate Earth mantle, fractionations that are not observed. This observation suggests that Earth's magma ocean had fluid dynamical properties more akin to a dusty atmosphere than a sludgy silicate liquid, with the exception of density.

The preservation of reservoirs of different ^{129}Xe/^{132}Xe ratios in Earth and Mars indicates that their atmospheres were outgassed very early in solar system history. Water released from cooling magma oceans is an effective vehicle for fractionating I from Xe to create these reservoirs.

References: [1] Righter and Drake (1996) *Icarus, 124,* 513. [2] Righter and Drake (1997) *EPSL, 146,* 541. [3] Deloule et al. (1999) *GCA, 62,* 3367. [4] Chabot and Drake (1999) *EPSL,* submitted.

ON THE EARLY DIFFERENTIATION OF MARS.

G. Dreibus, Max-Planck-Institut für Chemie, P.O. Box 3060, D-55020 Mainz, Germany (dreibus@mpch-mainz.mpg.de).

The high-Cl concentrations of the Pathfinder rocks of ~0.25% after the correction of Cl from the adhering soil were taken as further evidence of an early enrichment of the volatile elements in the martian crust.

Using element correlations observed in SNC meteorites, postulated as martian rocks, and general cosmochemical constraints the bulk composition of Mars was estimated [1]. In this model the mean abundance values for moderately volatile elements Na, P, K, F, and Rb and most of the volatile elements like Cl, Br, and I in the martian mantle exceed the terrestrial values by about a factor of two. The striking depletion of all elements with chalcophile character (Cu, Co, Ni, etc.) indicates that the silicate phase of Mars, contrary to the Earth, was equilibrated with a S-rich core. Consequently Mars accreted homogeneously from 40% CI material (component B) and 60% of a volatile depleted highly reduced matter (component A). During the accretion and core formation the initially large water inventory from component B was lost due to the reaction of water with metallic iron from component A to H, which has subsequently escaped.

The high abundance of volatile-rich component B, which supplied large amounts of S, was responsible for an FeS-rich core extracting all chalcophile elements from the silicate phase according to their sulfide-silicate partition coefficients. Core formation must have occurred concurrently with the rapid accretion of Mars, which is inferred from excess ^{182}W in martian meteorites [2].

The Pathfinder mission yielded the first *in situ* analysis of the chemical composition of martian crustal rocks with the APX spectrometer [3]. The rocks embedded in the soil at the Pathfinder site turn out to be rather similar to each other but very different from compared to the soil. In contrast to the mafic character of the SNC meteorites, they are felsic rocks, rich in SiO_2 and K and low in Mg. Furthermore it became evident that rocks with no adhering soil show enhanced Cl concentrations of about 0.25%. Sulfur and Cl both dominate in the soil and were interpreted as an interaction of volcanic gases with the surface material [4]. However, the correlation of Cl vs. S for Pathfinder rocks and soils show that these two elements are slightly decoupled from each other. Not all Cl in these samples derived from a gas-solid reaction. The Cl concentration of ~0.25% in the rocks must be intrinsic. Chlorine as an incompatible and volatile element is enriched in these highly differentiated crustal rocks. A sedimentary origin or an infiltration from an early northern ocean [5] in the crustal rocks also cannot be excluded.

Such high-Cl concentrations in crustal material are outside the range observed in SNC meteorites and most terrestrial igneous rocks. Like the other halogens, Cl is easily extracted from heated rock samples in the presence of H_2O. Hence, it might be that under accretion conditions on Mars, Cl was removed from the interior of the planet very efficiently and was incorporated into the crustal rocks at that time. The observed higher ^{129}Xe/^{132}Xe ratio in the martian atmosphere compared to the interior of Mars [6,7] points to a very early extraction of I in the crust because of the short ^{129}I half-life of 16 m.y.

The absence or at most very limited plate tectonic activity on early Mars excludes an crustal recycling back to the mantle and preserves the isotope systems derived from the early crustal differentiation. The ^{129}I-^{129}Xe ($T_{1/2}$ 16 m.y.) and the ^{146}Sm-^{142}Nd ($T_{1/2}$ 103 m.y.) isotope systems indicate a rapid accretion and a very early formation of the crust with its enrichment of volatile and high incompatible lithophile elements. As no recycling to these elements reservoirs is possible the 4.5 Ga recorded by the martian meteorites Rb-Sr whole-rock isochron and by the old Pb-Pb model ages of the individual shergottites [8] might reflect the early time of crust-mantle separation. The recently observed correlation of radiogenic ^{182}W with radiogenic ^{142}Nd by [2] points also to a close relationship between core formation and mantle melting in the first ~30 m.y. of martian accretion.

References: [1] Wänke H. and Dreibus D. (1988) *Phil. Trans. R. Soc. Lond., A325,* 545–557. [2] Lee D.-C. and Halliday A. N. (1997) *Nature, 38,* 854–857. [3] Rieder R. et al. (1997) *Science, 278,* 1771. [4] Clark B. C. (1993) *GCA, 57,* 4575. [5] Head J. W. III et al. (1998) *GRL, 25,* 4401. [6] Swindle T. D. et al. (1986) *GCA, 50,* 1001. [7] Ott U. and Begemann F. (1985) *Nature, 317,* 509. [8] Jagoutz E. (1991) *Space Sci. Rev., 56,* 13–22.

RARE EARTH ELEMENTS IN OCEANIC PHILLIPSITES.

A. V. Dubinin, P. P. Shirshov Institute of Oceanology of Russian Academy of Sciences, Nahimovskiy Prospekt, 36, Moscow 117851, Russia (geochem@geo.sio.rssi.ru).

In order to investigate rare-earth-element (REE) distribution between authigenous minerals in pelagic sediments the phillipsite aggregates were analyzed. Phillipsites were hand picked using binoculars from size fraction >50 µm of four horizons of pelagic clays (37–40, 105–110, 165–175, and 189–190 cm), station 35 (29°36'S, 149°58'W). No chemical cleaning was applied prior analysis. REE in phillipsites were analyzed by inductively coupled plasma mass spectrometry (ICP-MS) [1]. For analysis of separate grains or aggregates, the electron and ion microprobe methods were used [2].

The comparison of phillipsite composition from four horizons has shown that they are quite close and may be presented as $Na_{1.4-2.1}K_{1.6-1.9}Ca_{0.1-0.3}Sr_{0.2}[Al_{4.1-4.3}Si_{10.5-11.2}O_{32}] \times 6H_2O$. REE contents measured by ICP-MS for phillipsite fractions strongly correlate with Fe and P. These two elements do not be entered in the phillipsite structure and were accumulated as dissipated Fe oxyhydroxides on phillipsite grain surfaces and inside the crystal as inclusions. REE patterns of phillipsite fractions are shown in Fig. 1. Negative Ce anomaly (Ce an = 2 × $Ce/Ce^{shale}/(La/La^{shale} + Nd/Nd^{shale})$) increases (1.07 → 0.70 → 0.26 → 0.23) with sediment depth that is connected

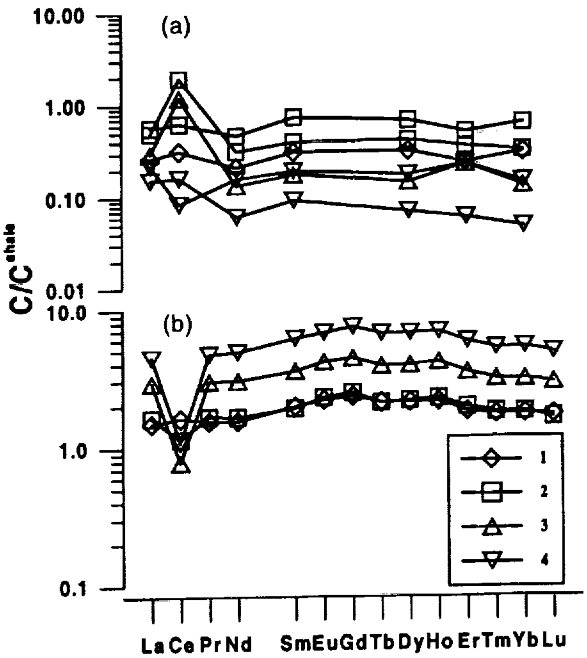

Fig. 1. Shale-normalized concentrations of REE in oceanic phillipsites. (a) Ion microprobe analysis of separate phillipsite grains. (b) ICP MS analysis of phillipsite fraction (>50 µm) of sediments, station 35. 1 = horizon 37–40 cm, 2 = horizon 105–110 cm, 3 = horizon 165–175 cm, 4 = horizon 189–190 cm.

with the increase of Fe, P, and trivalent REE in phillipsite composition. The increase of Fe in phillipsites coincides with increase of Fe contents in associated sediments with depth and may reflect the influence of hydrothermal material.

REE composition of phillipsite fraction is contaminated by REE from inclusions of Fe oxyhydroxide, biogenic apatite, and Fe-Ca hydroxophosphate. To avoid this contamination the REE contents of some grains were determined by ion microprobe method. The results of separate grain analysis are shown in Fig. 1. The shale-normalized concentrations of REE in separate grains of phillipsites do not exhibit negative Ce anomaly except one sample from horizon 189–190 cm. Two neighboring grains of phillipsites from horizon 105–110 cm have different Ce anomaly (4.7 and 1.2). REE contents determined by ion microprobe method are much smaller than those analyzed by ICP-MS. The reason of these differences are in the influence of dissipated Fe oxyhydroxides and Fe-Ca hydroxyphosphates, which preferably accumulate REE. Positive Ce anomaly in REE composition is a result of heterogeneity in phillipsite aggregates due to inclusions of Fe oxyhydroxides. Cesium is accumulated on Fe oxyhydroxides.

It is known from [3,4] that phillipsites of the oceanic sediments accumulate REE with pattern similar to that of seawater. From this study it is clear that high concentrations of REE in phillipsites and negative Ce anomaly may be a result of Fe oxyhydroxide influence. The oceanic phillipsites do not accumulate REE and inherit REE composition of seawater.

References: [1] Dubinin A. V. (1993) *Geokhimia, 11,* 1605–1619. [2] Sobolev A. V. (1996) *Petrologia, 4,* 228–239. [3] Piper D. Z. (1974) *GCA, 38,* 1007–1022. [4] Bernat M. (1975) *Cah. ORSTOM, Ser. Geol., VII,* 65–83.

KINETICS AND SURFACE MICROSTRUCTURAL EVOLUTION OF MICROBIALLY MEDIATED SULFIDE DISSOLUTION: IMPLICATIONS FOR MODELING ACID MINE DRAINAGE GENERATION.

K. J. Edwards[1], M. M. McGuire[2], R. J. Hamers[2], and J. F. Banfield[1], [1]Department of Geology and Geophysics, University of Wisconsin–Madison, 1215 W. Dayton Street, Madison WI 53706, USA, [2]Department of Chemistry, 1101 University Avenue, University of Wisconsin–Madison, Madison WI 53706, USA.

Introduction: Dissolution and surface morphology evolution of pyrite, marcasite, and arsenopyrite have been monitored during 22 d of reaction with mixed enrichment cultures, an Fe oxidizing isolate (*Ferriplasma acidarmanus*), a S-oxidizing isolate (*Thiobacillus caldus*), and abiotic controls. Results show that dissolution in the presence of *T. caldus* caused a reduction of Fe released to solution by ~18% in marcasite, and 30% in arsenopyrite relative to controls. Inhibition of pyrite dissolution in the presence of *T. caldus* was negligible. Inhibition of marcasite and arsenopyrite may in part be due to cell coverage and precipitation of iron oxides on surfaces of cells attached to minerals. Scanning electron microscopy (SEM) found that the surfaces reacted with *T. caldus* were depleted, though not completely absent of S deposits relative to controls. The conversion of S^0 to SO_4^{2-} in experiments with *T. caldus* consumes O, and this may suppress the inorganic rate at which the ferric iron surface oxidant is regenerated, lowering the sulfide dissolution rate.

The microbial contribution to dissolution rates of pyrite, marcasite, and arsenopyrite in enrichment cultures of Fe- and S-oxidizing organisms was ~1.5–6× greater than in cultures of the Fe-oxidizing archaea *F. acidarmanus*. Cell-normalized dissolution rates in experiments containing Fe-oxidizing microorganisms, calculated based on the average number of Fe-oxidizing cells present, ranged from 6×10^{-7} to 2×10^{-8} µMol Fe cell^{-1} d^{-1}. These rates are in close agreement with the only previously reported cell-normalized Fe oxidation rate estimate (4×10^{-7} µMol Fe cell^{-1} d^{-1} [1]). Variability in cell-normalized rates is partially attributed to changes in surface area that occurred during reaction, and to differences in microbial metabolic efficiencies.

Results indicate that the microbial contribution to acid generation is highly dependent on the cell density and surface area available. When surface area available for reactions is low and cell numbers are high, the microbial contribution to dissolution is high; when surface area is high and cell numbers are low, similar to many acid mine drainage (AMD) environments, the microbial contribution decreases relative to chemical oxidation. Cell-normalized rates were used to predict the microbial contribution to sulfide dissolution at an AMD site, Iron Mountain, California. Calculations suggest that the microbial contribution to AMD production may be approximately equal to abiological dissolution at this site.

References: [1] Edwards K. J. et al. (1998) *Am. Mineral., 83,* 1444–1453.

OXYGEN-ISOTOPIC EVIDENCE ON THE ORIGIN OF CHEMICAL VARIATION IN THE SOURCES OF NORMAL MID-OCEAN-RIDGE BASALTS.

J. M Eiler[1], P. Schiano[1,2], N. Kitchen[1], and E. M. Stolper[1], [1]Division of Geological and Planetary Sciences, California Institute of Technology, Pasadena CA 91125, USA (eiler@gps.caltech.edu), [2]Laboratoire Geochimie-Cosmochimie, IPG Paris, 4 Place Jussieu 75252, Paris Cedex 05, France.

Introduction: Mid-ocean-ridge basalts (MORBs) are the most abundant terrestrial magmas and are believed to be derived from partial melting of a globally extensive reservoir of ultramafic rocks in the upper mantle. The sources of MORBs vary significantly in the abundances of incompatible minor and trace elements and in several radiogenic isotopic ratios. A variety of mechanisms has been proposed for generating these variations by intramantle differentiation; alternatively, they could reflect refertilization of the sources of MORB with subducted crust. Relative to typical mantle peridotites, crustal rocks are commonly enriched or depleted in $^{18}O/^{16}O$ due to interaction with the hydrosphere; therefore the O-isotopic compositions of MORBs can provide a test of the importance of crustal recycling as the cause of chemical variations in their sources. Previous studies of the O-isotopic variability of MORBs report that values of $\delta^{18}O$ vary by ~1–2‰ (between 5.35‰ and 7.30‰ [1,2]; the high end of the range decreases to 6.22‰ if the results of [3] are excluded) and are not significantly correlated with other variables (geochemical or otherwise) believed to be important to understanding the mantle sources of MORBs.

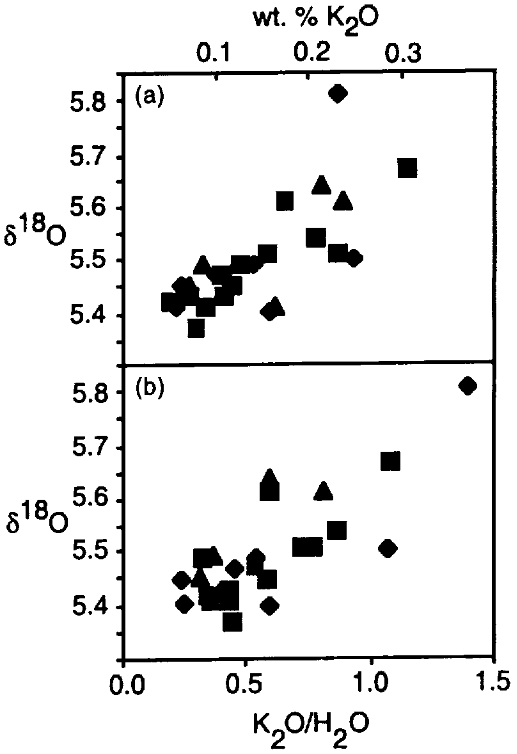

Fig. 1. Relationship between $\delta^{18}O$ and weight percent K_2O (a) and K_2O/H_2O (b) in N-MORB glass.

Methods: We have analyzed δ^{18}O values of 28 well-characterized N-MORB glasses from the East Pacific Rise, Mid-Atlantic Ridge, and Indian Ocean (described in [4]). Our measurements were made by laser fluorination of glass separates. The reproducibility of the measurements (based on multiple analyses of standards and unknowns) averages ±0.03‰ (1σ), and the average uncertainty in the mean for each sample is ±0.02‰ (1σ).

Results and Discussion: We find a range in δ^{18}O for N-MORB glass of 5.37–5.81‰. Values of δ^{18}O observed in this study are positively correlated with several chemical indices associated with "enrichment" in the mantle sources of MORB, including the concentration of K_2O (Fig. 1a) and the K_2O/TiO_2, K_2O/H_2O (Fig. 1b), La/Sm, Ba/Ta, and K/U ratios. Neither δ^{18}O values nor any of the other parameters are correlated with Mg#. Values of δ^{18}O are also uncorrelated with $Na_2O_{(8.0)}$ or the abundances of other incompatible elements that are principally sensitive to extents of melting but not usually considered to reflect enriched geochemical signatures in MORB (e.g., Ti, Ta). Values of δ^{18}O are also uncorrelated with H_2O and are therefore inconsistent with assimilation of water-rich, altered, upper-crustal rocks or sediments in the current oceanic crust or with ^{18}O-enrichment during subsolidus hydration. Moreover, calculated trends of fractional crystallization of a single parental magma or variable extents of melting of a single source are inconsistent with observed correlations between δ^{18}O and incompatible-element concentrations or ratios. We conclude that the small but significant variations in δ^{18}O in MORB that we have observed principally reflect variations in the δ^{18}O of their sources, and that such source variations cannot be produced readily by high-temperature differentiation of initially homogeneous mantle. Given the association of increasing δ^{18}O with enrichments in elements that are concentrated in high-δ^{18}O crustal rocks and sediments (e.g., K), observed trends (e.g., Fig. 1) could reflect the presence of subducted crustal materials into the MORB source.

References: [1] Harmon and Hoefs (1995) *CMP, 120,* 95–114. [2] Ito et al. (1987) *Chem. Geol., 62,* 157–176. [3] Taylor (1968) *CMP, 19,* 1–71. [4] Schiano et. al. (1997) *EPSL, 150,* 363–379.

URANIUM-THORIUM-PROTACTINIUM CONSTRAINTS ON MELTING BENEATH THE MARIANA ARC.

T. Elliott and G. Koetsier, Vrije Universiteit, Faculty of Earth Sciences, De Boelelaan 1085, 1081 HV Amsterdam, The Netherlands (ellt@geo.vu.nl; koet@geo.vu.nl).

We have measured ^{231}Pa disequilibrium to combine with an existing comprehensive geochemical dataset on historic lavas from the central island province of the Mariana arc. Variations in the chemistry of the lavas is inferred to represent variable sediment melt input to their sub-arc sources together with a near constant flux of "fluid" from the down-going altered oceanic crust. The fluid signature is seen most clearly in the most depleted samples, i.e., where least sediment has been added. Fluid addition is thought to contribute significantly to the Ba, Pb, Sr, and U budgets of the arc lavas, and to produce the striking ^{238}U excesses in the lavas, (^{238}U/^{230}Th) ~1.6 in Guguan lavas. In the lavas with greater sediment contribution, the fluid addition signature is masked. For example, some Uracas lavas show modest ^{230}Th excesses rather than ^{238}U excesses. The wide range in ^{238}U excesses, brought about by fluid addition to variably sediment enriched sources, notably correlate with (^{230}Th/^{232}Th), resulting in a pseudo-isochron of 30 ka for the bulk of Mariana samples. The two samples available from the island of Alamagan define an older isochron of 110 ka that nevertheless intersects the equiline at a similar initial ^{230}Th/^{232}Th to the main array. These "ages" are most simply inferred to represent the time between fluid addition and eruption of the melts. Since the fluid may itself trigger melting, then the age may perhaps reflect magma migration times.

The ^{235}U-^{231}Pa and ^{238}U-^{230}Th systematics are strikingly different despite being effectively linked by a common parent. All samples show ^{231}Pa excesses, with (^{231}Pa/^{235}U) ranging from 1.19–1.43, with little correlation with indices of sediment enrichment. It is notable, however, that a sample from Alamagan has the lowest (^{231}Pa/^{235}U). Mid-ocean ridge basalt (^{231}Pa/^{235}U) ratios are commonly ~2 and much greater than (^{230}Th/^{238}U) ratios ~1.2. It has thus been inferred that Pa is more incompatible than Th and this, coupled with its shorter half-life, result in the melting process generating much greater Pa excesses than Th excesses. In the arc environment, the (^{231}Pa/^{235}U) ratios might also be more strongly affected by the melting process than ^{230}Th-^{238}U disequilibrium. ^{231}Pa-^{235}U measurements may thus "see through" much of the additions of the slab component that more strongly influence the ^{230}Th-^{238}U measurements.

We have modeled the Marianas data starting from a set of sub-arc sources with variable U excesses, resulting from slab additions. In-growth melting models can readily reconcile the Pa excesses combined with ^{238}U excesses in melts derived from sources that initially have U excesses for both systems. For simplicity we have done these initial calculations using a "dynamic" (near fractional) model. In order to generate the significant Pa excesses, however, low porosities and melting rates are required. It also appears necessary to start melting within the garnet stability field (>80 km). Under these conditions, however, the melting process will also affect the ^{238}U-^{230}Th systematics. Modeling suggests the apparent isochrons defined by arc lavas on the equiline may reflect more the melting rates in the mantle wedge than melt transport time. This, however, should provide valuable information in comparing the melting process beneath arcs and at simpler tectonic environments such as mid-ocean ridges and plumes.

FUNDAMENTAL STUDIES OF PYRITE OXIDATION IN GASEOUS AND AQUEOUS ENVIRONMENTS.

A. R. Elsetinow[1], D. R. Strongin[1], and M. A. A. Schoonen[2], [1]Department of Chemistry, 1901 North 13th Street, Temple University, Philadelphia PA 19122, USA, [2]Department of Geosciences, State University of New York–Stony Brook, Stony Brook NY 11794-2100, USA.

The oxidation-induced degradation of pyrite in certain scenarios is of significant interest. This phenomenon, for example, in mine tailing piles has received significant attention, since the resulting production of sulfuric acid has a severe detrimental impact on the surrounding environment. Much of the information concerning the pyrite oxidation mechanism has been inferred from macroscopic observations in aqueous studies. Research in our laboratory, using modern surface science techniques, is helping to shed light on the microscopic properties of the pyrite surface that control its reactivity in oxic environments.

Electron spectroscopies and thermal desorption techniques carried out on {100} planes of pyrite under well-controlled conditions in ultra-high vacuum (UHV) have shown that relatively simple adsorbates, such as CH_3OH, H_2O, and H_2S bind preferentially to defect sites. These defects, at least in part, are thought to be S anion vacancy sites on the pyrite surface.

Using a combined high-pressure/ultra-high vacuum (UHV) apparatus pyrite surfaces were also reacted at environmentally relevant pressures. The reacted samples were then studied with electron spectroscopies, including X-ray photoelectron spectroscopy (XPS). Our studies showed that in the pure H_2O environment, oxidation of {100} planes was spatially limited to non-stoichiometric or S-deficient surface sites. Oxidation of the disulfide group of pyrite occurred if O_2 was present along with H_2O. Results have suggested that O_2 adsorption on the stoichiometric region of pyrite resulted in the formation of Fe^{3+} sites that facilitated the dissociation of H_2O and the oxidation of the disulfide group.

Additional studies have investigated the effect of phosphate on the oxidation behavior of pyrite. Experimental results suggest that phosphate binds strongly to surface Fe^{3+} in the oxide product that forms during the oxidation of S-deficient sites. The binding of phosphate to these sites, which populate only a minority fraction of the total pyrite surface, is found to significantly decrease the oxidation rate under our experimental conditions. It is suspected that the mechanism of oxidation inhibition exhibited by the small amount of phosphate is to block specific sites that would otherwise facilitate the oxidation process through electron transfer to O_2.

CRYSTALLIZATION, REPLACEMENT, ASSIMILATION, MELTING, AND INFILTRATION PROCESSES THAT FORM THE PLUTONIC FOUNDATION OF THE OCEANIC CRUST.

D. Elthon, Falls Church VA 22046, USA (delthon@nsf.gov).

Numerous studies of plutonic rocks from oceanic and ophiolitic regions have shown that the processes forming these rocks are very complicated and not well understood. Many fundamental uncertainties remain because of limited sampling and the complicated nature of the samples. Several important processes have been identified, or at least proposed, but the relative importance of each of these processes is not widely accepted.

At first glance, oceanic plutonic rocks are relatively simple and appear to have been formed by crystallization from mid-ocean ridge basalt (MORB) liquids. In support of this perspective, the most abundant minerals in oceanic plutonic rocks are olivine, plagioclase, and clinopyroxene, which are broadly similar in composition to the phenocrysts and megacrysts in MORBs. These similarities and the close association between MORBs and plutonic rocks clearly indicate that oceanic plutonic rocks are linked to MORBs by magma fractionation processes in subaxial magma chambers.

Studies of oceanic (and ophiolitic) plutonic rocks by several research groups have shown, however, that the processes that form plutonic rocks in the oceanic crust are very complicated. Systematic studies have shown that oceanic cumulates typically have mineral compositions that would not form from the low-pressure (~1 kbar) crystallization of MORB liquids. Some of the more common features are the presence of anomalously magnesian orthopyroxene and clinopyroxene, the common presence of ilmenite in magnesian cumulates, and unusual minor-element and trace-element abundances. There is no widely accepted explanation for these anomalous chemical characteristics in oceanic cumulates.

[Seismic imaging of the upper part of subaxial magma chambers has led to the general acceptance that such magma chambers are common in fast-spreading centers, but are probably very small and ephemeral along slow-spreading centers. The geometry and nature of the floor of oceanic subaxial magma chambers, and deeper parts of the crust (or crystal mush zone) are virtually unknown in terms of any systematic study, although significant information has been derived from the study of ophiolites, some oceanic plutonic rocks, and MORBs themselves. There is general agreement that a significant crystal mush zone exists beneath subaxial magma chambers, but the details of processes that occur in this crystal mush zone are poorly constrained.]

Petrologic study of erupted MORBs demonstrates that high-temperature basaltic liquids are routinely delivered into deep portions of the oceanic crust; these magmas are substantially out of thermal and chemical equilibrium with the surrounding rocks (or crystal mush) and certainly result in significant melting/assimilation of lower crustal materials. In fact, evidence of melting of cumulates is abundant in ophiolites and is supported by some studies of halogen/volatile species in MORBS.

It is also clear from studies of oceanic and ophiolitic cumulate suites that infiltration of early-formed cumulates by subsequent magmatic liquids (silicic to basaltic) is common at a variety of scales. Some of these forms of infiltration are easily observed (dikes and veins), but subtle and cryptic forms of infiltration are inferred from petrographic examination or geochemical trends.

In addition to infiltration processes, a growing body of evidence indicates that replacement phenomena frequently occur, particularly at deeper levels of the oceanic crust and in the upper mantle. Although the magnitude of these replacement processes is hard to constrain, its petrological importance in producing dunites, and maybe pyroxenites, is clear.

The impact that crustal-level melting of cumulates has on the compositions of erupted MORBs could be substantial, although not currently recognized.

THE SEARCH FOR THE PROTOSTOME-DEUTEROSOME ANCESTOR: CONFLICT BETWEEN PALEONTOLOGICAL AND MOLECULAR DATA.

D. H. Erwin, Department of Paleobiology, MRC-121, National Museum of Natural History, Washington DC 20560, USA (erwin.doug@nmnh.si.edu).

Analysis of molecular (DNA) sequences via a molecular clock suggests the divergence between the major higher-animal clades occurred well before the Cambrian radiation (dates range from 1500 to 630 Ma depending on the genes involved and the methods of analysis). Yet the fossil record shows no evidence of metazoans prior to 580 Ma, and no evidence of higher clades until 550 Ma. This striking dichotomy between paleontologic and molecular estimates of the age of a critical node in animal evolution has important implications for understanding the Cambrian radiation rates of molecular sequence evolution and developmental evolution.

Recent phylogenies of animal relationships have demonstrated that animals more complex than cnidarians are clustered into three large clades: the deuterostomes (including echinoderms and chordates) and two groups of protostomes (ecdysozoans, including arthropods, and lophotrochozoans, including molluscs, annelids and brachiopods). The common ancestor of these three clades (the protostome-deuterostome ancestor or PDA) occurred in the Neoproterozoic. The age and complexity of this animal is currently disputed. If it occurred well before 600 Ma, the divergence of these animal clades is necessarily decoupled from the ecological and environmental events of the Cambrian radiation. If the animal was younger, lineage divergence itself may have played a larger role. Since flies and vertebrates, both well studied by developmental biologists, are maximally separated in recent animal phylogenies, genes found in both groups are decended from genes in the PDA. Developmental studies reveal a large suite of such genes, but raise questions about their role in the PDA. Resolution of this conflict may require biogeochemical studies capable of recognizing early bilaterians and higher metazoan lineages, either through biomarker studies or other analyses.

SOME ABYSSAL PERIDOTITES ARE OLD!

S. Esperança[1], S. E. Sichel[2], M. F. Horan[3], R. J. Walker[1], T. Juteau[4], and R. Hekinian[5], [1]Isotope Geochemistry Laboratory, Department of Geology, University of Maryland, College Park MD 20742, USA, [2]LAGEMAR-UFF, Niterói, RJ, Brazil, [3]Department of Terrestrial Magnetism, Carnegie Institution of Washington, 5241 Broad Branch Road NW, Washington DC, USA, [4]Dépt. Sciences de la Terre, UBO, Brest, France, [5]Institut Français de Recherche pour l'Exploration de la MER, Center de Brest, DRO/GM, Plouzané, France.

Introduction: Studies of abyssal peridotites have been central to understanding processes of oceanic lithosphere formation at ridges and subsequent modification, for instance, at transform faults. A program of deep diving using the submersible Nautile was undertaken by a group of French and Brazilian scientists, with the purpose of better understanding the complexities of the St. Paul's Fracture Zone (SPFZ) in the Equatorial Atlantic. Previously, it was observed that the lithosphere surrounding the SPFZ is typically cooler than other areas in the Atlantic Ocean. Additionally, significant tectonic movement has exposed abundant abyssal peridotites, some of them on the islets of St. Pierre and St. Paul. Preliminary results of a Re-Pt-Os study of abyssal peridotite samples collected from the SPFZ are presented here.

Methods: Eleven samples were selected from hand specimens that showed minimum serpentinization, veining, etc. An attempt was made to examine samples that were geographically distributed between northern and southern portions of the Fracture Zone. Samples were dissolved in quartz Carrius tubes and spiked for Pt, Re, and Os. Rhenium and Os were analyzed by NTIMS at the University of Maryland, and Pt was analyzed by multiple collector inductively coupled plasma mass spectrometry (MC-ICP-MS) at the Carnegie Instititution of Washington.

Results: The range of Os-isotopic compositions obtained for this suite of rocks is large (^{187}Os/^{188}Os varies from 0.11986 to 0.1496) but the majority of the samples have γ_{Os} that are equal or below the chondritic average.

Surprisingly, Os-isotopic compositions show a positive correlation with Pt/Os ratios (Fig. 1), as has also been observed for drill-core samples obtained from a discrete block of abyssal peridotite from the Kane Transform Fault of the North Atlantic [1].

Discussion: The mechanisms by which the Pt/Os ratios of peridotites can be changed are yet unresolved. Because of the differential compatibility of Pt and Os in mantle assemblages, melt addition or depletion is likely to change the Pt/Os of mantle materials. It is yet unknown if Pt and Os can be stripped by seawater alteration, although it is unlikely that this process would be capable of producing the reasonably well-defined linear correlations between Os-isotopic composition and Pt/Os ratios observed in this study and that of Brandon et al. [1]. The depleted Os-isotopic compositions obtained for this suite cannot result from interaction between lherzolitic or harzburgitic mantle isolated during the opening of the Atlantic Ocean and melts with an average MORB-type isotopic composition. Unlike the two samples with radiogenic compositions, the depleted ones cannot be attributed to alteration of young oceanic mantle with seawater and sediments during periods of

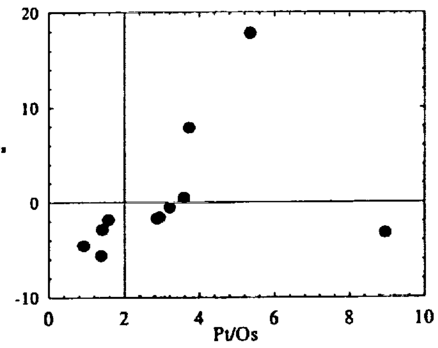

Fig. 1. Plot of γ_{Os} vs. Pt/Os for abyssal peridotite samples from the St. Paul's Fracture Zone. The vertical line is an average Pt/Os for chondrites. The horizontal line represents the average Os-isotopic composition of chondrites (modern day $^{187}Os/^{188}Os = 0.1270$).

exhumation or tectonic movement. Instead, the most depleted samples indicate Re depletion from typical upper mantle Os-isotopic evolution >1 Ga ago. The presence of older depleted lithosphere entrained in shallow zones of the oceanic mantle has been recognized previously in the Izu-Bonin-Mariana forearc [2] and in the Kerguelen Plateau [3]. The sources of older materials are most likely the mantle lithosphere once underlying continental crust. Rhenium-depleted model ages ranging from 0.6 to 1.0 Ga for four of the samples indicate that the lithosphere entrained in this part of the oceanic mantle could have formed in the Pan-African-Brasiliano orogeny. The increasing evidence for incorporation of old lithosphere into young oceanic lithosphere during continental breakup adds a new dimension to the definition of mantle reservoirs and mantle recycling.

References: [1] Brandon A. D. et al., this volume. [2] Parkinson I. J. et al. (1998) *Science, 281,* 2011–2013. [3] Hassler D. R. and Shimizu N. (1998) *Science, 280,* 418–421.

EXPERIMENTAL METHODS FOR DETERMINING THE RATES OF CONTAMINANT RELEASE FROM SPOIL MATERIAL AND DEEP MINES.

K. A. Evans[1] and S. A. Banwart[2], [1]Department of Civil Engineering, Sir Frederick Mappin Building, Mappin Street, Sheffield S1 3JD, UK (k.evans@sheffield.ac.uk), [2]Department of Civil Engineering, Sir Frederick Mappin Building, Mappin Street, Sheffield S1 3JD, UK (s.a.banwart@sheffield.ac.uk).

Details of unsaturated column weathering simulations of both spoil material and complete mine rock are presented. These simulations, which incorporate multilevel sampling, allow reaction progress to be determined as a function of column depth and time. This facilitates the separation of kinetic, advective and diffusive influences on reaction within the column.

Preliminary results from the columns are compared with field-based weathering rates at two sites. The first, a large, partly vegetated, coal-mine-derived spoil heap (10^6 m^3, average pyrite content 8.5%), is leaching high Fe (5–20 mg/L), Al (up to 53 mg/L), and low pH solutions as a result of unsaturated flow of rainwater through the pile. The second, an abandoned South Wales coal mine, is discharging 10^9 L/yr of very high Fe (20–450 mg/L), low Al (<0.6 mg/L), circumneutral waters from flooded workings.

Comparison of the two sets of results allows the importance of a number of different scaling parameters to be evaluated on the chosen sites. Differences in weathering rates determined in batch experiments [1], column experiments, [2], field observations, [3], and modeling, [4], have been accounted for using an integrated approach, [5], that considers: (1) relatively immobile water [6], which prevents weathering products being transported with site drainage; (2) the existence of large zones of nonreactive mine waste with neglible pyrite content; (3) particle-size effects where large amounts of rock mass is hosted within large particles and rock fragments that do not contribute to the weathering flux due to negligible reactive surface area; and (4) slower weathering rates resulting from activation energy effects and lower average temperature under field conditions.

References: [1] Stromberg B. and Banwart S. (1999) *J. Contaminant Hydrol.,* in press. [2] Stromberg B. and Banwart S. (1999) *App. Geochem., 14,* 1–16. [3] Stromberg B. and Banwart S. (1994) *App. Geochem., 9,* 583–595. [4] Ericksson N. and Destouni G. (1997) *Wat. Resour. Res., 35,* 471–483. [5] Banwart S. et al. (1998) in *Groundwater Quality: Remediation and Protection* (M. Herbert and K. Kovar, eds.), pp. 307–311, Publication No. 250, International Association of Hydrological Sciences, Wallingford, UK. [6] Eriksson N. et al. (1997) *J. Hydrol., 194,* 143–163.

HYDROTHERMAL SOURCE OF RADIOGENIC STRONTIUM TO HIMALAYAN RIVERS.

M. J. Evans[1], L. A. Derry[1], and S. P. Anderson[2], [1]Department of Geological Sciences, Cornell University, Ithaca NY 14853, USA (evans@geology.cornell.edu), [2]Institute of Tectonics, Department of Earth Sciences, University of California, Santa Cruz, Santa Cruz CA 95064, USA.

Introduction: Himalayan rivers have high $^{87}Sr/^{86}Sr$ relative to their Sr concentration compared to other world rivers [1]. However, the source of this radiogenic Sr signature and the extent to which it reflects silicate weathering remains unclear. Weathering of silicate rocks, radiogenic feldspars, biotites, and radiogenic carbonates have all been proposed as sources for the radiogenic Sr flux in Himalayan rivers [1–4]. Our new results from the Marsyandi River indicate that geothermal springs may be an important source of radiogenic Sr.

Setting: The Marsyandi River originates in the Annapurna range at ~3.5-km elevation and it empties into the Trisuli River at about 0.7 km. It drains an area of about 4500 km^2. The Marsyandi passes from the rain shadow behind the Annapurnas to the monsoon-soaked southern flank of the Himalaya. It is an ideal river to study as it flows over the three main lithologic units in Nepal as well as the two main shear zones that separate them. From its headwaters in the Tibetan Sedimentary Series (TSS), it flows across the South Tibetan detachment system [5] and into the High Himalayan Crystalline rocks (HHC). The Marsyandi next crosses the Main Central Thrust (MCT) and passes into Lesser Himalaya sequence (LH). Each of these lithologic units have distinct Sr characteristics that are reflected in tributary streams from monolithologic catchments. TSS streams have high Sr concentrations (4.5 µM) and low $^{87}Sr/^{86}Sr$ near 0.72 while LH streams have very high $^{87}Sr/^{86}Sr$ values (0.785) but concentrations of only 0.3 µM. Streams from HHC catchments lie between those of the LH and TSS with Sr concentrations around 0.6 µM and $^{87}Sr/^{86}Sr$ values of 0.74.

Riverine Strontium: Both main stem and tributary waters from a ~130-km stretch of the Marsyandi River have been analyzed for major ions as well as Sr concentration and isotopic ratios. In the high reaches of the Marsyandi the river has high [Sr] = 3–4 µM but low $^{87}Sr/^{86}Sr = 0.719$, reflecting carbonate weathering in the TSS. Across the detachment system, the $^{87}Sr/^{86}Sr$ of the main stem of the Marsyandi increases from 0.719 to 0.728, with a significant increase above the MCT, although (Sr) falls slightly (Fig. 1).

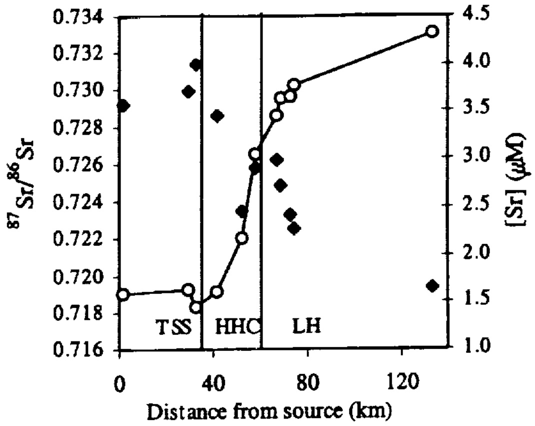

Fig. 1. Strontium-87/strontium-86 (circles) and [Sr] (diamonds) vs. downstream distance (kilometers).

The change in Marsyandi Sr cannot be accounted for with the observed tributary fluxes, because they are too diluted or insufficiently radiogenic (or both) to shift the main stem substantially in ^{87}Sr/^{86}Sr while maintaining [Sr] $\geq$2.5 μM. This increase in ^{87}Sr/^{86}Sr values is associated with spikes in the concentration of Na^+, K^+, Ca^{++}, Mg^{++}, and Cl^-. Geothermal springs are abundant along the MCT shear zone, and are evident along this stretch of the Marsyandi. Samples of hot spring waters above the MCT have [Sr] up to 115 μM and radiogenic ^{87}Sr/^{86}Sr up to 0.77. Addition of small amounts (<0.5%) of geothermal water to the stream can drive the observed shift in Marsyandi main stem Sr chemistry.

Addition of tributary waters from the predominantly silicate LH and HHC could raise the ^{87}Sr/^{86}Sr in the main stem but would result in very diluted (Sr). In contrast, hot spring waters contribute high ^{87}Sr/^{86}Sr while maintaining high (Sr). Hot spring fluids are a newly identified source of radiogenic Sr at high concentrations, but the relationship of this Sr to weathering-generated alkalinity is unclear. It does appear however that active geothermal zones can significantly affect river chemistry and isotopic signals in Himalayan rivers. The origin of the Sr in the hot springs is difficult to determine. Meteoric waters may enter along MCT shear zone, and react with LH to obtain radiogenic Sr. Geochemical anomalies associated with geothermal activity may permit improved estimates of hydrothermal heat loss along the major Himalayan shear zones.

References: [1] Edmond J. M. (1992) *Science, 258,* 1594–1597. [2] Krishnaswami S. et al. (1992) *EPSL, 109,* 243–253. [3] Blum J. D. et al. (1998) *Geology, 26,* 411–413. [4] Derry L. A. and France-Lanord C. (1996) *EPSL, 142,* 59–74. [5] Hodges K. V. et al. (1996) *Tectonics, 15,* 1264–1291.

HYDROGEN-ISOTOPIC FRACTIONATION BETWEEN AMORPHOUS SILICA AND WATER, AND ITS IMPLICATION IN THE FORMATION OF EPITHERMAL QUARTZ.

K. Faure[1,*] and Y. Matsuhisa[2], [1]Geological Survey of Japan, 1-1-3 Higashi, Tsukuba, 305-8567, Japan (*present address: Institute of Geological & Nuclear Sciences, 30 Gracefield Road, Lower Hutt, New Zealand; k.faure@gns.cri.nz), [2]Geological Survey of Japan, 1-1-3 Higashi, Tsukuba, 305-8567, Japan (mats@gsj.go.jp).

Introduction: Fine-grained crystalline quartz in epithermal veins of the Hishikari Au-Ag deposits, southern Japan, contains a large quantity of water, up to 1 wt%, despite the paucity of visible fluid inclusion [1]. We have attempted to determine the source of the mineralizing fluid by analyzing the H-isotopic ratios (D/H ratios) of the water contained in the quartz, because of a paucity of other suitable hydrous minerals at the stage of mineralization. The results indicate that the water in the quartz has a δΔ value of about –75‰, which is highly depleted in D compared to the present-day local meteoric water (~–50‰), and that the quartz crystallized from amorphous silica which was initially deposited from thermal water. The water in quartz is probably within microinclusions, invisible under the optical microscope, and may be remnant water expelled from amorphous silica when it crystallized to quartz. Water dissolved in amorphous silica is loosely bound to the silicate structure, and the H could have isotopically fractionated with the surrounding free water. Therefore, it is necessary to determine the magnitude of isotopic fractionation between hydrous amorphous silica and free water for estimating the original isotopic composition and the origin of the mineralizing fluid. In the present study, we collected amorphous silica and coexisting thermal waters at known temperatures from natural hot springs and geothermal power plants, and measured the temperature dependence of H- isotopic fractionation between waters in the two phases. Nine pairs of samples were collected from six localities in Japan and New Zealand with a temperature range of 85°–155°C. Some of the localities are associated with Au deposition, and the amorphous silica, which contains about 6 wt% water, could correspond to the precursor of Au-bearing epithermal quartz.

Results and Discussion: The pulverized and air-dried amorphous silica samples were thermally dehydrated in a vacuum line by first removing adsorbed water at 120°C for 4 h, and then slowly heated (30°C/min) up to 1200°C. Results show that the amorphous silica dehydrates over a large temperature range, probably being dependent on the bonding energy of water with the silicate structure. A good reproducibility of H-isotopic analysis (<±3‰) was obtained by analyzing total water recovered in the temperature range of 120°–1200°C.

Hydrogen-isotopic fractionation does occur between hydrous amorphous silica and free water. The temperature dependence of the fractionation factor (a) is approximated by the following equation:

$$1000 \ln \alpha = -22.1 \times 10^6 T^{-2} + 104$$

where α = (D/H) water in hydrous amorphous silica/(D/H) free water. At temperatures near 200°C, the fractionation is minimal, but with decreasing temperature, D is preferentially partitioned into the free water phase. The temperature of quartz formation in the Hishikari epithermal veins is estimated to be in the range of 195°–250°C [2,3], on the basis of O-isotopic fractionation between minerals and homogenization temperatures of fluid inclusions. The low D/H ratios (–75‰) measured for water in the quartz indicate that (1) precursor amorphous silica precipitated at temperatures lower than 200°C, or (2) the silica did precipitated at ~200°C, but the mineralizing water had a lower D/H ratio than the present-day meteoric water (–50‰), or (3) D-depletion of remaining water occurred when amorphous silica, which precipitated at about 200°C, dehydrated during crystallization to quartz.

References: [1] Faure K. et al. (1998) in *Water-Rock Interaction* (Arehart and Hulston, eds.), pp. 537–540, Balkem, Rotterdam. [2] Matsuhisa Y. and Aoki M. (1994) *Econ. Geol., 89,* 1608–1613. [3] Izawa E. et al. (1990) *J. Geochem. Expl., 36,* 1–56.

THE IODINE-129 SYSTEM AND ITS POTENTIAL FOR DATING ORGANIC MATERIAL.

U. Fehn, Department of Earth and Environmental Sciences, University of Rochester, Rochester NY 14627, USA.

Iodine is a strongly biophilic element and is therefore commonly found in association with organic material. It has one stable isotope, ^{127}I, and one long-lived radioisotope, ^{129}I, a member of the group called cosmogenic isotopes because of the production of these isotopes as a result of interaction of cosmic rays with atoms in the atmosphere. The relatively long half-life of ^{129}I, 15.7 Ma, make it potentially useful as a dating system for an age-range of up to 80 Ma. Although the concentration of ^{129}I in nature is very low, it is now possible to determine isotopic ratios, ^{129}I/I, even at natural levels using accelerator mass spectrometry (AMS). The pre-anthropogenic ratio in marine sediments has been determined to be 1.5×10^{-12}, which is two orders of magnitude above the current detection limit (1×10^{-14}) of AMS.

The characteristics of the ^{129}I system suggest applications for the dating and tracing of organic material, including potentially also black carbon. Potential and limitations of this system will be discussed based on results from three studies where the ^{129}I system was used for the dating of organic material. The first one was a study of the origin of hydrocarbons in oil fields from the Gulf Coast which indicated that hydrocarbons in this area are generally older than 50 Ma, largely independent of the reservoir formations they were found in. The second study is from a number of shallow marine sediment cores taken close to shore along the Pacific and Atlantic coast of North and South America. Although the sediments were not older than 50 ka, results in several of the cores demonstrated the presence of I with ages up to 30 Ma. We interpreted these results as evidence for the presence of fossil organic material derived from terrestrial sources. Finally, I will report the first results from an attempt to date I in pore fluids collected together with gas hydrates from a core drilled at the Blake Ridge (ODP 997). The pore fluids were extracted from sediments with ages ranging from late Miocene to early Pliocene, but the ^{129}I/I ratios are at or below 200×10^{-15}, indicating minimum ages of 45 Ma and older. These results strongly suggest that the pore fluids and, in association, the gas hydrates were formed at depth and have migrated upward to their present position. The results of these studies indicate that the ^{129}I system might be a helpful tool for the characterization of origin and history of organic material.

ISOTOPIC EXCHANGE ENERGETICS AND MECHANISMS OF SILICA IN WATER FROM AB INITIO CALCULATIONS.

M. A. Felipe[1], J. D. Kubicki[2], and D. M. Rye[1], [1]Kline Geology Laboratory, Yale University, Box 208109, New Haven CT 06520-8109, USA (mihali.felipe@yale.edu), [2]Department of Geosciences, Pennsylvania State University, University Park PA 16802, USA.

Introduction: Stable isotopes have been used by geochemists for decades to solve various problems involving Earth processes. Although the methods for solving problems have developed considerably, little is actually known about the mechanisms of isotopic exchange in heterogeneous systems. Knowledge of the mechanisms involves a detailed understanding of the energetics of these reactions.

Isotopic-exchange reactions are ultimately quantum mechanical (QM) in origin. Despite the success of recent numerical quantum mechanical methods in elucidating and predicting chemical properties, thermodynamics, and kinetics of systems, there is little geochemical research that utilizes these methods to understand and quantitatively predict the magnitude of isotopic exchange in heterogeneous reactions. There are some exceptions [1–3], but even these papers are more qualitative rather than quantitative in value. In this study, we used a numerical QM method to determine the rates at which silica exchanges O and H isotopes with water. In particular, the reactions we investigated are of the form

$$\mathrm{nH_2O + H^*O\text{-}Si\text{-}(OH)_x\ (O\text{-}Si\text{-}(OH)_3)_{3-x}} \leftrightarrow$$

$$\mathrm{(n-1)H_2O + H^*O\ H + HO\text{-}Si\text{-}(OH)_x\ (O\text{-}Si\text{-}(OH)_3)_{3-x}}$$

where n = 1, 2, ..., and x = 0, 2, 3. These were chosen to represent H-D and ^{16}O-^{18}O-isotopic exchange reactions of aqueous orthosilicic acid monomers and dimers (x = 3 and 2) as well as isotopic exchange on silicate surfaces (x = 0).

Theory and Methodology: Density functional theory (DFT) was used to trace the reaction coordinate on the potential energy surfaces of the systems of interest. Density functional theory considers electron correlation as well as exchange. Electron correlation can be a significant component of the potential energy surface near the transition state. Thus, DFT is superior to Hartree-Fock theory (which does not include electron correlation) for predicting reaction coordinates and activation energies.

The first step in modeling isotopic exchange is to determine the reaction path. Energy-minimized configurations for the reactant clusters were computed and used as starting geometries. Reaction pathways were generated by stepwise energy minimizations with one degree of freedom constrained. For example, in the cluster H_4SiO_4-H_2O, the distance between the H in the water molecule and the O in the SiOH group was shortened in steps of 0.04 Å until a "reaction" occurred. The result is a plot of potential energy along a reaction path. An automated procedure was developed to perform these calculations in conjunction with GAUSSIAN 94 [4].

The second step in modeling isotopic exchange is the computation of rate coefficient ratios between heavy and light isotope systems, k^*/k. Frequency calculations were carried out on the reactant and product configurations for each molecular cluster with different isotopic compositions at key sites. These calculations provide results that can be used to evaluate the kinetic isotope effects using an expansion of the partition functions [5].

Discussion: Our results reveal that, for a given silica-water cluster, a number of possible ground-state reaction paths for the same stoichiometric reaction may be traced on the potential energy surface. This was expected because numerous minima exist on the potential energy surface in agreement with the findings of other workers [e.g., 6]. The existence of several possible reactions makes necessary the detailed examination of the energetics to determine favored paths.

The families of possible reactions all involve two stages: the interaction of H and O atoms between the water molecules and the cluster-terminating hydroxides leading to proton transfer, and the subsequent exchange of O atoms. This implies that for any meaningful simulation of the isotope effects of the silica-water system, the terminating hydroxides have to be put into consideration.

We present the isotopic-exchange reaction paths and energetics of systems having varying cluster sizes and degrees of hydration. Furthermore, we show the improvement of our data over previous results and their comparison with empirical data.

References: [1] Lasaga A. C. and Gibbs G. V. (1990) *Am. J. Sci., 1,* 234. [2] Casey W. H. and Lasaga A. C. (1990) *GCA, 54,* 3369–3378. [3] Xiao Y. and Lasaga A. C. (1994) *GCA, 90,* 1151–1154. [4] Frisch M. J. et al. (1995) *Gaussian 94: Revision E.2.* [5] Van Hook W. A. (1970) *Isotope Effects in Chemical Reactions, ACS Monograph 167, I,* 1–89. [6] Hodges M. P. and Stone A. J. (1999) *J. Chem. Phys., 110,* 6766–6772.

PROBING THE ELECTRICAL DOUBLE-LAYER STRUCTURE AT THE RUTILE-WATER INTERFACE WITH X-RAY STANDING WAVES.

P. Fenter[1], L. Cheng[2], S. Rihs[1], M. Machesky[3], P. Geissbühler[4], M. J. Bedzyk[1,2], and N. C. Sturchio[1], [1]Argonne National Laboratory, Argonne IL 60439, USA, [2]Northwestern University, Evanston IL 60208, USA, [3]Illinois State Water Survey, Champaign IL 61820, USA, [4]University of Washington, Seattle WA 98195, USA.

Introduction: Knowledge of the distribution of ions at the solid-liquid interface is fundamentally important for understanding its properties. The continuing interest in the distribution of ionic species near an interface, generally referred to as the electrical double-layer (EDL), has led to the development of numerous models that use constraints such as electro-neutrality and electrostatics to explain and predict behavior of these systems. However, relatively little is directly known about the structure of the EDL, particularly through *in situ* studies at the mineral-aqueous interface. The current consensus concerning the EDL structure is that the distribution of a particular ion species consists of both a condensed ("Stern") and a diffuse layer. Such a distribution is expected to be found for both anions and cations.

A particularly challenging aspect of studying the EDL is to measure the relationship between ions in the condensed and diffuse layers. In addition to the normal difficulty of identifying techniques which have the sensitivity to probe structures at the solid-liquid interface, there is the additional challenge of probing the relationship between the localized and delocalized structures corresponding to the condensed and diffuse layers. It is generally assumed that the fraction of ions in the condensed layer will increase as the Debye length decreases. This partitioning of ions between the condensed and diffuse layers is likely to be sensitive to the strength and nature of the ion-substrate interactions. It will undoubtedly influence the reactivity of the solid surface, and therefore will be of fundamental importance in understanding environmental interfaces [1].

Of the many surface-sensitive techniques available, X-ray based techniques are promising as a means to elucidate the structure of the EDL. The weakly interacting nature of hard X-rays makes it possible to directly probe the liquid-solid interface under the conditions of interest. The measurements are truly quantitative since the interaction of X-rays with matter is well understood. The length scales over which X-ray scattering techniques naturally probe (from ~1 Å to ~10^4 Å) is also well matched to the length scales present in double layer structure. Surface X-ray diffraction and X-ray standing wave measurements have previously delineated the structure of condensed layers at the electrified metal-aqueous interface, and X-ray standing waves have been used to probe the Debye length associated with the diffuse layer [2].

Results and Discussion: We use the (110) surface of the TiO_2 polymorph rutile for this study since it has been extensively studied and is known to be chemically stable over a broad range of pH [3]. The structure of the rutile (110) surface has been measured [4], and exhibits only minor structural relaxations. Finally, the surface charging behavior of rutile has been extensively studied and reveals the pH of zero surface charge, $pH_{pzc} = 5.4$–5.7 [3,5]. Together these previous studies provide a significant database from which the present results can be interpreted.

Here we demonstrate that X-ray standing waves can provide direct insight into the partitioning of ions between the condensed and diffuse components of the EDL. Through both *in situ* and *ex situ* experiments, we have been able to measure the partitioning of these ions between the condensed and diffuse layers as well as the height of the cation in the condensed layer with respect to the rutile surface plane. By comparing the behavior of Sr^{++} and Rb^+ ions we have also been able to reveal the microscopic differences associated with alkali and alkaline-earth cations that had been previously inferred based upon potentiometric titration data of Ca^{++} and Na^+ ions at the rutile-water interface [6].

Acknowledgments: These experiments were performed at beamline 12-ID-D (BESSRC-CAT) at the Advanced Photon Source at Argonne National Laboratory. The work was supported by the Geosciences Research Program, Office of Basic Energy Sciences, U.S. Department of Energy. Use of the Advanced Photon Source was supported by the Office of Basic Energy Sciences, Office of Science, U.S. Department of Energy, under contract W-31-109-ENG-38 at Argonne National Laboratory.

References: [1] Brown G. E. Jr. et al. (1999) *Chem. Rev., 99,* 77–174. [2] Bedzyk M. J. et al. (1990) *Science, 248,* 52. [3] Machesky M. L. et al. (1998) *J. Coll. Int. Science, 200,* 298–309. [4]. Charlton G. et al. (1997) *Phys. Rev. Lett., 78,* 495–498. [5] Machesky M. L. et al. (1994) *GCA, 58,* 5627–5632. [6] Ridley M. K. et al. (1999) *GCA,* in press.

A NEW APPROACH OF DETERMINING THE $Fe^{3+}/\Sigma Fe$ IN MINERALS AND GLASSES WITH THE ELECTRON MICROPROBE.

M. Fialin[1] and C. Wagner[2], [1]Centre de Microanalyse CAMPARIS, Université Paris 6, 4 Place Jussieu, 75952 Paris Cedex 05, France (fialin@ccr.jussieu.fr), [2]Laboratoire de Pétrologie, European Space Agency 7058-Centre National de la Recherche Scientifique, Université Paris 6, 4 Place Jussieu, 75952 Paris Cedex 05, France (cw@ccr.jussieu.fr).

Introduction: The determination of Fe^{2+} and Fe^{3+} contents is crucial to many petrogenetic and thermodynamic parameters. Two methods are commonly used, wet chemistry and Mössbauer spectroscopy which both require relatively large amounts of materials. However, the knowledge of $Fe^{3+}/\Sigma Fe$ at the micrometer scale has revealed to be of great interest [1]. Microbeam spectroscopic techniques have been recently developed, which give a good accuracy in $Fe^{3+}/\Sigma Fe$ but have some disadvantages: e.g., destructive sample preparation (Electron Energy Loss Spectroscopy), a low accessibility synchrotron source (X-Ray absorption Near-Edge Spectroscopy), limited spatial resolution and long-time exposure (Mössbauer milliprobe). Another way is to explore the possibility of using the electron microprobe (EMP), a widespread microanalytical instrument, to determine directly $Fe^{3+}/\Sigma Fe$.

Principle of the Electron Microprobe $Fe^{3+}/\Sigma Fe$ Determination: The basic principle is that the X-Ray L emission spectra of transition metals shift with the oxidation state, both in the Lα, β peak position and in the Lα/Lβ intensity ratio [2]. The spectral distortions are caused by different self absorption coefficients (μ/ρ) on either sides of the LIII edges that are in close proximity of the Lα peak intensity maxima. In computer programs for EMP analyses the μ/ρ coefficients for the soft Lα peaks are deduced from polynomial fits of theoritical and experimental data collected in regions below the metal LIII edge. The latter data are generally erroneous. Quantitative μ/ρ can be given by EMP determination of the Fe concentration at varying beam energies. These experiments tend to show that μ/ρ is higher for Fe^{2+} than for Fe^{3+}. For instance the following experimental μ/ρ are found for FeO and Fe_2O_3: 3400 cm^3/g [3] and 2750 cm^2/g (this work) respectively. The μ/ρ deviations are reflected as increased spectral distortions for Fe^{2+}Lα compared to Fe^{3+}Lα.

Actually, three ways have been investigated to process Lα, β spectra: (1) measurement of the Lα peak shifts, (2) measurement of the change in Lβ/Lα intensity ratios, and (3) a hybrid method between (1) and (2) [4]. For either methods, $Fe^{3+}/\Sigma Fe$ is determined using calibration curves constructed from proper measurements on reference materials. The general criticism against these methods is that the set of standards should be as similar as possible (chemically and structurally) with the unknowns.

In this study we propose a reduced number of calibration curves constructed after the above method (1) and applicable to most silicates and glasses for which the total Fe content and the coordination number of both Fe^{2+} and Fe^{3+} have been previously established.

Results: The measurements were carried out with a CAMECA SX50 electron microprobe using a TAP monochromator and a beam energy of 15 kV, a common beam energy used in geological applications.

Iron Lα peak shift in silicate. In order to evaluate the contribution of Fe abundance on self absorption effects, the Fe Lα peak shift was plotted as a function of the Fe wt% concentration. The continuous peak shift observed towards longer wavelengths for Fe^{2+} is consistent with increasing self absorption as Fe wt% increases. The few data collected for Fe^{3+} show similar trend but the Fe^{3+} peak is shifted toward shorter wavelengths compared to Fe^{2+}: for example, at 10 wt% Fe the Fe^{2+}-Fe^{3+} peak distance is as large as 100 steps (one step corresponds to 2×10^{-5} Bragg sin angle).

Calibration curves for iron in octahedral environment. Calibration curves were constructed by adjusments to plots giving the peak positions relatives to the Fe^{2+}-Fe^{3+} curves defined in the previous paragraph, as a function of the nominal $Fe^{3+}/\Sigma Fe$ (calculated by stoichiometry and charge compensation) for a series of reference silicates: three clinopyroxenes and three garnets covering the ranges 5–23 wt% Fe and 4–94 $Fe^{3+}/\Sigma Fe$. These curves may be used for a precise determination of $Fe^{3+}/\Sigma Fe$ in unknown silicates.

Limitations: (1) The method is not applicable for samples with less than 3.5 wt% Fe, for which the very small Fe^{2+}-Fe^{3+} peak distance leads to large imprecision. (2) The self-absorption distorsions of Fe Lα emission also depend on the absorption of other components of the matrix and its mean atomic number (Z). Any phases with total μ/ρ and/or Z outside the common range encountered in most silicates or glasses, i.e., 10,000-15,000 cm^2/g and 10–15 respectively cannot be processed by the proposed calibration curves. (3) Finally, the effects of eventual beam damage have to be considered.

References: [1] Canil D. and O'Neill H. St. C. (1996) *J. Petrol., 37,* 609–635. [2] Fischer D. W. (1965) *J. Appl. Phys., 36,* 2048–2053. [3] Pouchou J.-L. and Pichoir F. M. A. (1988) *Microbeam Anal.,* 319–324. [4] Höfer H. E. et al. (1994) *Eur. J. Mineral., 6,* 407–418.

STRATABOUND COPPER OCCURRENCES AT THE BASE OF THE MIOCENE IN NORTHWEST SARDINIA, ITALY.

M. Fiori, Centro Studi Geominerari e Mineralurgici del Consiglio Nazionale delle Ricerche, Piazza d'Armi, 09123 Cagliari, Italy.

Studies concerning Tertiary metallogeny related to the calk-alkali volcanism during the Oligo-Miocene in Sardinia have produced evidence of stratabound deposits containing prevalently Cu and to a lesser extent Pb [1] associated with the bottom sediments of the marine transgression during the Miocene (west Sardinia).

Prospecting studies in the Logudoro region (northwest Sardinia) [2] have led to the discovery of a number of areas of interest for their mineralized formations.

The Logudoro region forms the northern part of the tectonic trough that extends from north to south Sardinia. This trough can be linked with the process that initiated during the Oligocene and resulted in the detachment of the Sard-Corse microplate and its rotational-translation shift eastward [3]. Within the graben thus formed intense volcanic activity took place, with products having calk-alkali affinity, typical of plate convergence zones. The ingression during the Miocene then contributed to its infilling. The terrigenous sediments show textural and compositional immaturity and contain a clastic component derived from the abundant volcanic rocks (lava and pyroclasts). They are usually have *lenticular bedding* and sometimes exhibit sedimentary structures such as laminations, indicative of low-energy depositional environments.

The mineralized formation occurs at the passage from pyroclasts to sediments and is hosted in the above detrital lithofacies, overlain by organogenic marine deposits again of the Miocene. The mineral assemblage consists of azurite, malachite, chalcopyrite, tennantite, enargite, covellite, pyrite, and digenite. The presence of mineralogical phases containing sulfides and oxidates of apparently primary origin suggests fluctuation between oxidizing and reducing depositional environments.

Fields observations and laboratory analysis indicated that the mineral deposit is always associated with the horizon, of a transitional-littoral nature, forming the bottom of the Miocene transgression. Thus a paleogeographic control exists, recognizable not only at the local but also at a regional scale. They also indicated that the morphology of the layer beneath the mineralized horizon suggests the presence of emerged paleoreliefs, composed of the volcanites, at the margins of which are located the mineralized areas.

The presence in the study area of calk-alkali volcanic rocks and of low sulfidation epithermal Au deposits associated there to, whose mineral assemblage contains various metals including Cu and As, suggests that the introduction of metals and the clasts making up the mineralized layers can be associated with the volcanic rocks themselves.

Suitable climatic conditions [4] may have resulted in the preconcentration of some metals and the leaching of others contained in the volcanic rocks.

References: [1] Fadda S. et al. (1998) *Ore Geol. Rev., 12,* 355–377. [2] Orrù D. (1997) Ph.D. thesis. [3] Beccaluva L. et al. (1985) *Rend. Soc. Ital. Mineral. Petrol., 40,* 57–72. [4] Samama J. C. (1973) *Ores Sed.,* pp. 247–265, Springer.

PRAGENETIC ASSEMBLAGE OF HIGH SULFIDATION EPITHERMAL GOLD DEPOSIT OF FURTEI, SARDINIA, ITALY.

M. Fiori[1] and S. M. Grillo[2], [1]Centro Studi Geominerari e Mineralurgici del Consiglio Nazionale Ricerche, Cagliari, Italy, [2]Dipartimento di Geoingegneria e Tecnologie Ambientali, Università di Cagliari, Italy.

The Oligocene-Miocene calkaline volcanic cycle in Sardinia was accompanied by intense hydrothermal phenomena, whose importance has come to light over the last 10 years. This hydrothermalism produces extensive alteration zones and deposition of ore, mostly of precious metals. In the study area, situated in the southern part of the island, a roughly concentric array of

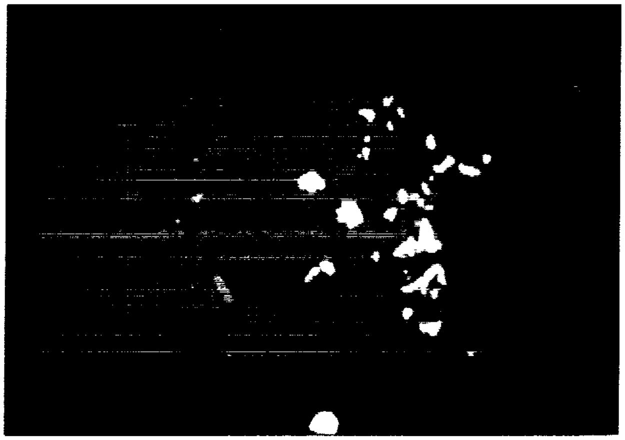

Fig. 1. Native Au (white) in enargite-luzonite. Polished section, 320×.

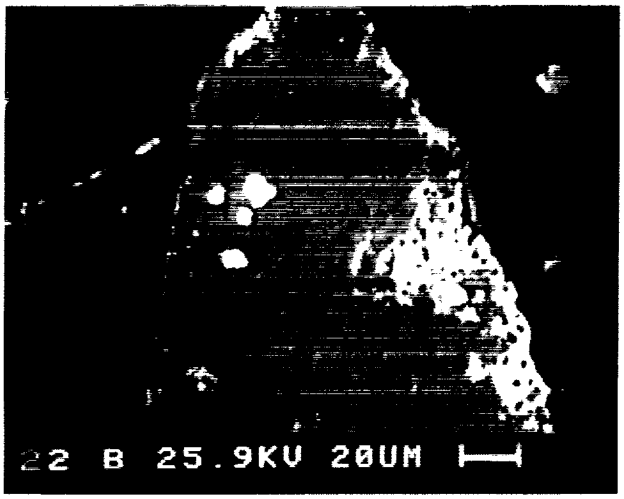

Fig. 2. Oxidation zone: high-fineness secondary Au, sometimes almost euhedral (white), in jarosite (light grey). BSE image.

alteration facies is observed. It presents an aureole of propylitic alteration and, inward, intermediate argillic and advanced argillic with intense silicification, including vuggy silica, and pyritization in the central part. Quartz calcedony and ore minerals occur in the latter zone, as networks of veinlets and a few vein-shaped bodies.

The Furtei mine is at present the only Au mine in Italy, and the first in Sardinia [1,2]. It started operating in 1997. The bodies explored so far are pipelike with vertical extension 200–300 m. The mineralization is of high-sulfidation type and is dominated by an assemblage including copper sulfosalts (enargite-luzonite and minor tetrahedrite-tennantite) (Fig. 1).

Minor base metal sulfides occur scattered, and Te-rich minerals (including Te-tetrhedrite, various tellurides, and native Te) appear to characterize the deeper parts of ore bodies. Gold occurs mostly as a high-fineness native metal and in some tellurides.

The upper parts of the known bodies are oxidized and contain at least 3 t of readily recoverable Au. The underlying reserves of unoxidized ore are much larger. Their Au grade is higher, and Cu is also contained in recoverable grades.

References: [1] Fiori M. and Grillo S. M. (1993) *L'Insustria Mineraria, 1,* 10–16. [2] Fiori M. et al. (1996) *Third Ethiopan Geosciences and Minerals Engineering Congress,* 1–13.

ISOTOPIC EVIDENCE OF HISTORIC AND CHRONIC INPUTS OF CONTAMINANT LEAD IN SAN FRANCISCO BAY. A. R. Flegal, D. J. Steding, and C. E. Dunlap, Earth Sciences and Environmental Toxicology, WIGS, University of California at Santa Cruz, Santa Cruz CA 95064, USA.

Stable Pb-isotopic composition analyses chronicle both historic and contemporary inputs of industrial Pb into the San Francisco Bay estuarine system. The former have recently been illustrated in analyses of a series of dated sediments cores extending back past the California Gold Rush, when hydraulic mining altered natural weathering processes and associated stable Pb-isotopic composition of sedimentation in the Bay [1]. The latter are now being illustrated in analyses of surface waters collected over the past decade, when the isotopic composition of surface sediments in the Bay continue to reflect anthropogenic emissions of leaded gasoline during the preceding decades. Together, these data chronicle the pervasive and chronic contamination of the Bay that extends over the last 150 yr and is projected to continue well into the next century.

The current and projected predominance of contaminant Pb in the Bay contrasts with numerous reports of dramatic, orders-of-magnitude reductions in environmental Pb contamination over the past two decades, which have been correlated with global reductions in industrial Pb emissions. These include marked reductions in Pb concentrations, and associated changes in Pb-isotopic composition, in the atmosphere, polar snow and ice, oceanic surface waters, rivers, lacustrine sediments, terrestrial soils, ombrotrophic bogs, other vegetation, and human blood. While those recent changes contrast with the relative constancy of both Pb concentrations and isotopic compositions in San Francisco Bay over the same period, that constancy is concordant with models of the biogeochemical cycling of unsupported ^{210}Pb, which has served as a model of the fate of metals in estuaries and the oceans for the past two decades [2]. Therefore, the apparently disparate behavior of the four stable Pb isotopes (^{204}Pb, ^{206}Pb, ^{207}Pb, and ^{208}Pb) in San Francisco Bay follows that of one of their radioactive parents (^{210}Pb).

References: [1] Ritson P. I. et al. (1999) *Mar. Chem., 64,* 71–83. [2] Turekian K K. (1977) *GCA, 41,* 1139–1144.

MOLECULAR-SCALE STUDIES OF ARSENIC AND SELENIUM SORPTION ON HYDROUS MANGANESE OXIDES. A. L. Foster[1,*], G. E. Brown Jr.[1,2], and G. A. Parks[1], [1]Geological and Environmental Sciences, Stanford University, Stanford CA 94305-2115, USA (*present address: U.S. Geological Survey, Menlo Park CA 94025, USA), [2]Stanford Synchrotron Radiation Laboratory, Stanford Linear Accelerator Center, P.O. Box 4349, Stanford CA 94309, USA.

Introduction: Sorption and heterogeneous oxidation reactions of hydrous manganese oxides and arsenic (As) and selenium (Se) oxoanions are important in determining the mobility of these toxic elements. X-ray absorption fine-structure spectroscopy (XAFS) at the As, Se, and Mn K-edges was used to determine the composition and infer the mode of As(V) and Se(IV) sorption on synthetic K-birnessite and synthetic vernadite (δ-MnO_2), two members of the group of hydrous manganese oxide (HMO) minerals.

Experimental: Sorption samples were prepared with 30–300 µM Se(IV) or As(V) solutions and 2–5 g/L sorbent. Under these conditions, equilibrium thermodynamic calculations predict subsaturation with respect to anhydrous $Mn_3(AsO_4)_2$ ($pK_{sp} = 28.72$) [1] and anhydrous $MnSeO_3$ ($pK_{sp} = 7.27$) [2] at pH 5. Oxidation of Se(IV) to Se(VI) by Mn(IV) was observed in only one low-coverage sample ($\Gamma = 0.09$ µmol/m^2, birnessite).

Arsenic Sorption Complexes: Arsenic(V) complexes on HMOs are bidentate and mononuclear with a characteristic As-Mn distance of ~3.16 Å. Manganese- and As-XAFS analysis of a $Mn(II)_x(AsO_4)_y \times zH_2O$ precipitate [with similar structure to $Mn_5(H_2O)_8(AsO_3OH)_2(AsO_4)_2 \times 2H_2O$] demonstrates that the local As structure in this compound is considerably different than that of the average sorption complex. The precipitate has a longer characteristic As-Mn distance of ~3.45 Å.

Selenium Sorption Complexes: The Se-Mn interatomic distances and coordination numbers indicate the formation of a novel surface-associated species indicated by a short refined Se-Mn interatomic distance (~3.08 Å). Manganese(II) or Mn(III) is the most likely backscatterer, and not Mn(IV),

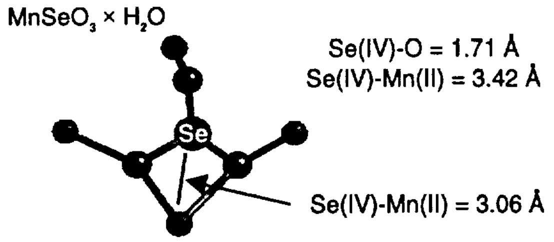

Fig. 1. Local structure of Se in MnSeO$_3$ × H$_2$O. The coordination geometry in this compound was used as a model for the type of Se(IV) surface complexes that could form on HMO surfaces.

because calculated Se-Mn(IV) interatomic distances for several possible sorption complexes are either much shorter or much longer than 3.08 Å. These and additional data lead to the conclusion that Se(IV) forms one of two types of surface-associated species on HMOs: (1) preferential adsorption of Se(IV) to surface-associated Mn(II) (produced by reductive dissolution of the solids or present in the structure due to incomplete oxidation of Mn(II) during synthesis) via edge-sharing, bidentate complexes and monodentate complexes with Mn(IV), Mn(III), or Mn(II); (2) formation of a Mn(II) precipitate having a structure similar to MnSeO$_3$ × H$_2$O, whose primary structural unit is an edge-sharing Se(IV)-Mn(II) complex (Fig. 1). The same local coordination is found in a crystalline Mn$_x$(SeO3)$_y$ × zH$_2$O precipitate synthesized in our laboratory. However, the Se(IV)-HMO sorption samples lack low-amplitude multiple-scattering (MS) paths that are present in the Mn$_x$(SeO$_3$)$_y$ × zH$_2$O precipitate, and that indicate a high degree of positional order. Mn-EXAFS of reacted d-MnO$_2$ and birnessite do not indicate significant changes in the local coordination of Mn after reaction with Se(IV), but changes in surface speciation could be masked by this bulk technique.

Using a bond valence model developed by Brown and Altermatt [3] and first applied to surface complexes by Bargar et al. [4], we have predicted the relative stability of As(III), As(V), Se(IV), and Se(VI) sorption complexes on ideal and Mn(II,III)-substituted HMO surfaces. The model predicts that these anions can only bind to [Mn-OH] or [Mn-OH$_2$] surface functional groups on HMOs, where the Mn valence is 2, 3, or 4. These predictions are consistent with the proposed bidentate, binuclear and edge-sharing, binuclear complexes. Adsorbed Mn(II) and/or Mn(III) may stabilize higher adsorption densities of As(III), As(V) and Se(IV) on HMOs by enabling the formation of additional types of complexes.

References: [1] Sillén L. G. and Martell A. E. (1964) *Stability Constants of Metal-Ion Complexes*, The Chemical Society, London. [2] Sharmasarkar S. et al. (1996) *Chem. Geol., 132,* 135–141. [3] Brown I. D. and Altermatt D. (1985) *Acta Cryst., B41,* 244–247. [4] Bargar J. R. et al. (1997) *GCA, 61,* 2617–2637.

THE PERMIAN-TRIASSIC BOUNDARY IN AUSTRALIA: ORGANIC CARBON-ISOTOPIC ANOMALIES RELATE TO ORGANOFACIES, NOT A BIOGEOCHEMICAL "EVENT."

C. B. Foster, G. A. Logan, and R. E. Summons, Australian Geological Survey Organisation, P.O. Box 378, Canberra ACT 2601, Australia.

Introduction: Placement of the Permian-Triassic boundary in Australia, and Gondwana in general, is hampered by the rarity of marine index fossils, particularly conodonts, that restrict correlation with the marine standard sections of northern hemisphere deposits. In eastern Australia's predominantly terrestrial sequences, the boundary has been taken as roughly coincident with the change from coal measures (Permian) to non-coaly sediments, principally redbeds (Triassic). Paleontological studies have focused on the demise of the *Glossopteris* flora as a marker for the upper boundary of the Permian System. More recently, palynological data have enabled broad links to the Pakistan Salt Range section and show that the close of coal measure sedimentation took place in the early Changhsingian. SHRIMP dating from Australian samples and zircons from the type Meishan section has confirmed these broad links but still does not provide an unambiguous boundary solution. Accordingly, we examined the detail of C-isotopic variations that may provide a facies-independent datum to mark the boundary in both terrestrial and marine sections.

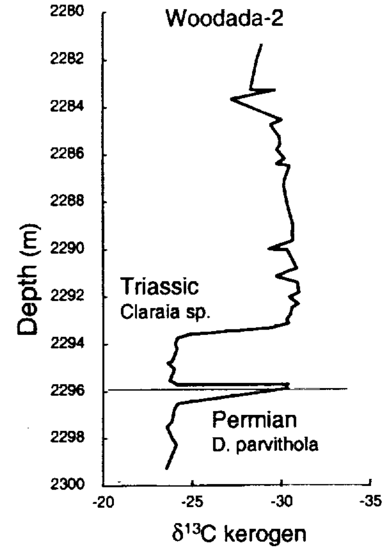

Fig. 1. δ^{13}C of bulk organic C at the Permian-Triassic contact in a marine section in Woodada-2 in the Perth Basin, Western Australia.

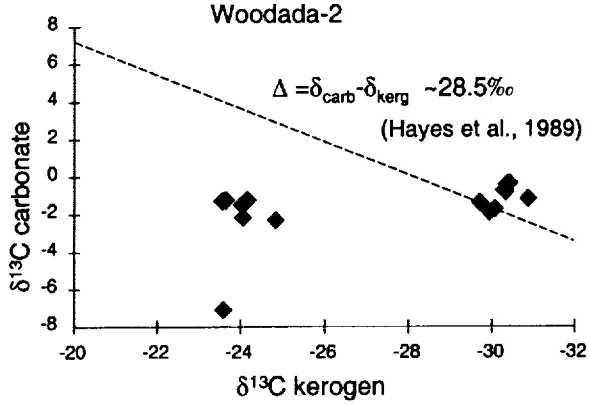

Fig. 2. Carbon-isotopic cross-plot showing fundamentally different organic C sources contribute to a lithologically uniform P-T contact in Woodada-2.

Results and Discussion: Carbon-isotopic analysis of carbonate and organic matter at the contact between Permian and Triassic marine sediments in the Woodada-2 borehole [1] revealed a signal similar to that reported in other Australian sections that were earlier proposed as a boundary proxy [2]. Although there was no systematic shift in the δ^{13}Ccarb, organic C showed an apparent shift of –8‰ across the contact (Fig. 1).

Detailed geochemical and palynological analysis of the samples showed that the "anomaly" was clearly not due to biogeochemical changes related to a boundary "event" but associated with a predominance of isotopically heavy and reworked woody material in the Permian section and an isotopically light acritarch-rich kerogen in the earliest Triassic. A cross-plot of the inorganic and organic C-isotopic data shows that the organic matter types are from fundamentally different sources (Fig. 2). Similar results were obtained from the equivalent age section in the Tern-3 well in the Bonaparte Basin in northwestern Australia, so the observation is not an isolated phenomenon.

We conclude that trends or anomalies in C isotopes of bulk organic matter do not provide a reliable chemostratigraphic tool for identifying the Permian-Triassic boundary [3]. Any use of bulk organic C-isotopic shifts to study global biogeochemical changes in the oceans that accompanied the Permian-Triassic extinction event must be done with great care.

References: [1] Foster C. B. et al. (1997) *Austr. Pet. Explor. Assoc. J., 37,* 472–488. [2] Morante R. et al. (1994) *Austr. Pet. Explor. Assoc. J., 34,* 330-336. [3] Foster C. B. et al. (1999) *Proc. Roy. Soc. Vic., 110,* 247–266.

THE TIMING OF PROGRADE METAMORPHISM IN THE HIMALAYA.

G. L. Foster[1], D. Vance[1], C. I. Prince[1], P. Kinny[2], and N. B. W. Harris[1], [1]Department of Earth Sciences, The Open University, Walton Hall, Milton Keynes MK7 6AA, UK, [2]School of Applied Geology, Curtin University of Technology, Perth, Western Australia.

Introduction: Much of what we understand about the thermal and mechanical properties of the continental crust comes from integrated studies of orogenic zones. The Himalaya, a spectacular example of collisional orogenesis, constitute a natural laboratory for such studies. Two decades of intensive research in the Himalaya, has resulted in a greater understanding of the later tectonic history of the belt — notably the late phase of crustal anatexis and the period of rapid exhumation and cooling that occurred around 20–25 Ma. The mechanisms for melting at this time are, however, still a subject of some debate. This debate largely centres around the heat source for the melting given that thermal models of the collisional process indicate that the crust should have cooled beneath melting temperatures by this time. Popular models to overcome this problem vary from decompression melting [1] to shear heating on major thrust faults [2]. The major cause of this uncertainty is a lack of understanding of the pre-exhumation thermal structure and evolution of the crust. Before we can fully understand the causes of this major phase of Miocene crustal anatexis, the prograde thermal history of the Himalaya must be established. With the advent of reliable and precise chronometers that can be linked to thermal information, such as the garnet Sm-Nd system and the *in situ* U-Th-Pb dating of monazite inclusions, we are now in a position to investigate the early tectonic history of the Himalaya. In this contribution we present prograde thermal information from several areas of the Himalaya, draw conclusions concerning the variations in the time scale of prograde metamorphism and gain insights into the potential heat sources available for granite genesis.

Results: In order to gain an insight into the style of prograde metamorphism within the Himalaya, we have combined a Sm-Nd garnet study, the *in situ* secondary ion mass spectrometry (SIMS) U-Th-Pb dating of monazite microinclusions within porphyroblast phases and detailed petrogenetic and thermobarometric studies. Following this approach we have established that prograde garnet growth occurred at high structural levels in the Pakistan Himalaya, synchronously with a minor phase of anatexis [3], at 44–46 Ma. At slightly deeper structural levels, garnet growth began ~40 Ma and continued until ~36 Ma. In both cases garnet growth occurred during burial and heating. Data from lower structural levels and ~150 km further east in northwest India indicate garnet grade metamorphic conditions were not reached until ~35 Ma, but continued during burial and heating until ~25 Ma. Garnet-grade conditions were reached slightly earlier further east in the northern Garhwal Himalaya (north India) at ~40 Ma, and were again accompanied by minor wet melting. At lower structural levels in Garhwal, garnet growth occurred at <36 Ma, while elevated temperatures sufficient to reset the U-Th-Pb systematics of monazite and the Sm-Nd systematics of garnet were maintained even further south until ~22 Ma. In all cases, despite temporal and geographic differences, garnet growth occurred during burial and heating and was terminated by rapid exhumation and cooling.

These data establish that continuous high-temperature conditions in the Himalaya lasted from 44 to 22 Ma and suggest that thermal models implying that cooling had set in by 25–30 Ma are erroneous. The data also suggest that the timing of prograde metamorphism propogated southwards and structurally downwards throughout this time period. One possible reason for this discrepancy between the models and reality, therefore, is that the system of southward-propagating thrusts that dominate the tectonics of the Himalaya simply resulted in a prolongation of high-temperature conditions in the orogen. In any case, these data suggest that no external heat source is necessary to account for the Miocene crustal anatexis in the Himalaya.

References: [1] Harris N. B. W. and Massey (1994) *Tectonics, 13,* 1537–1546. [2] Harrison T. M. et al. (1998) *JGR, 103,* 27017–27032. [3] Smith H. A. et al., *J. Geol., 102,* 493–508.

COPPER BIOMINERALIZATION: TOWARD QUANTIFYING THE EFFECTS OF BACTERIA ON PRECIPITATION.

D. A. Fowle[1], J. B. Fein[1], K. M. Kemner[2], B. A. Bunker[3], S. Kelly[2], and M. Boyanov[3], [1]Department of Civil Engineering and Geological Sciences, University of Notre Dame, Notre Dame IN 46556, USA (fowle.1@nd.edu), [2]Environmental Research Division, Argonne National Laboratory, Argonne IL 60439, USA, [3]Department of Physics, University of Notre Dame, Notre Dame IN 46556, USA.

Introduction: Bacterial cell walls have a high affinity for binding metal cations, and the interface between bacterial cell walls and aqueous solutions can potentially control the distribution of metal cations in geologic systems. Two processes may occur at this interface that influence metal distributions: surface adsorption and surface-induced mineral precipitation. Reversible adsorption of metal cations onto bacterial surfaces is well documented [1], and previous work by our group demonstrates that surface complexation modeling can accurately account for the metal adsorption [1–5]. To date there have been no systematic studies of the effects of bacteria on the extent of mineral precipitation. Several studies have demonstrated that bacteria can influence the composition and morphology of the precipitates [6–7] as well as the rate of precipitation from oversaturated solutions [8]. However, these studies do not unequivocally demonstrate that bacteria enhance the extent of precipitation or cause precipitation at otherwise undersaturated conditions.

In order to define and quantify the role of bacteria in the formation of metal (hydr)oxides, we measured Cu adsorption and precipitation onto the surface of *Bacillus subtilis* as a function of pH, aqueous Cu activity, and time. To differentiate between the sorption processes, X-ray absorption fine structure (XAFS) spectroscopy was used to probe the changes in the coordination sphere of Cu as a function of changing solution chemistry.

Experimental Methods: We conducted batch adsorption/precipitation experiments involving the gram-positive soil bacterium *B. subtilis*. In each experiment, a Cu-bearing aqueous solution was mixed with a known concentration of bacteria, the pH was adjusted and the system was allowed to equilibrate. After filtration, the Cu concentration of the solution was determined by flame atomic absorption spectrometry (AAS) or inductively coupled plasma atomic emission spectrometry (ICP-AES). Three types of adsorption/precipitation experiments were performed at constant ionic strength, with and without bacteria: (1) as a function of aqueous Cu activity at a constant pH, (2) as a function of pH, and (3) a kinetics study of Cu precipitation. Bulk chemical evidence for surface precipitation of Cu on *B. subtilis* was provided by plots of log Γ_{Cu} (sorbed amount of Cu) vs. log [Cu] (molal aqueous Cu), which indicate a continuum between adsorption and precipitation. The XAFS experiments that were conducted mirrored the laboratory experiments by examining the average local chemical environment of Cu in the filtered biomass as a function of pH and aqueous Cu activity.

Results and Discussion: Bulk chemistry results of the adsorption/precipitation experiments conducted as a function of pH indicate a significant amount of precipitation of a Cu phase at pH values lower than the abiotic controls. Furthermore, experiments conducted as a function of aqueous Cu activity at a constant pH display a surface precipitation behavior similar to mineral surfaces as evidenced by the log Γ_{Cu} vs. log [Cu] plots. At low aqueous Cu activities, Langmuir-type removal (adsorption) of Cu from solution is observed. At higher aqueous Cu concentrations, an adsorption plateau is attained where the maximum adsorptive capacity is reached. However, Cu is removed from solution at even higher Cu concentrations than those that correspond to the adsorption plateau, indicating significant Cu-phase precipitation. This phenomenon occurs at lower Cu activities in the presence of bacteria than in the abiotic controls. Preliminary XAFS results compare well with the bulk chemistry experiments and indicate a change in the coordination sphere of Cu with changing solution conditions. This phenomenon has been observed previously, caused by mineral surfaces, but our study is the first to demonstrate quantitatively that bacterial cell walls effectively increase the extent of metal precipitation by decreasing the solubility of metal (hydr)oxide mineral phases. The results of this study imply that bacteria, biofilms and cell wall fragments in near-surface water-rock systems are likely to have a profound effect on the mobility of metal cations by altering the stability of metal-bearing mineral precipitates.

References: [1] Fowle D. A. and Fein J. B. (1999) *Chem. Geol.*, submitted. [2] Fein et al. (1997) *GCA, 61*, 3319–3328. [3] Daughney C. J. and Fein J. B. (1998) *J. Coll. Inter. Sci., 198*, 53–77. [4] Daughney C. J. et al. (1998) *Chem. Geol., 144*, 161–176. [5] Fowle D. A. and Fein J. B. (1999) *GCA*, in press. [6] Fortin D. and Ferris F. G. (1998) *Geomicrobiol., 15*, 309–324. [7] Urrutia M. M. and Beveridge T. J. (1994) *Chem. Geol., 116*, 261–280. [8] Warren L. A. and Ferris F. G. (1998) *Chem. Geol., 32*, 2331–2337.

HOW THE HIMALAYAN-TIBET UPLIFT AFFECTS THE CARBON CYCLE.

C. France-Lanord[1], A. Galy[1], and L. A. Derry[2], [1]Centre de Recherche Pétrographique et Géochimiques–Centre National de la Recherche Scientifique, BP 20, 54501 Vandoeuvre-lès-Nancy, France (cfl@crpg.cnrs-nancy.fr), [2]Cornell University, Snee Hall, Ithaca NY 14850, USA.

Introduction: The Himalayan-Tibet uplift generates since Miocene a major erosion system. It potentially affects the C cycle throughout weathering processes, organic C (Corg) erosion/burial and, metamorphic CO_2 degassing. In addition, climate-tectonic interactions affect the erosion regime and may have triggered large environmental changes since 20 Ma. Several hypotheses have been proposed for "tectonic forcing" of the C cycle by the Himalayan uplift and erosion. Global geochemical proxies such as seawater isotopic composition of C, Sr, or Os have been proposed to document the fluxes of erosion; however, their relationship with the effective uptake of atmospheric CO_2 is far from straightforward [1,2]. The study of both the modern and past erosional fluxes via the river system and the synorogenic sedimentary record allows building relative and absolute estimates of CO_2 uptake by the different processes active during the erosion. This study is based on the results obtained on the Ganga-Brahmaputra-Bengal Fan system.

On the modern river system, a detailed study of the riverine chemistry and weathering mechanism in Himalayan watersheds and the delta of Ganga and Brahmaputra (G-B) allows us to evaluate how the flux of alkalinity of these rivers is related to silicate and carbonate weathering [3]. The flux of silicate alkalinity is around 2.7×10^{11} mol/yr. It is mostly related to Na silicate alteration, which tends to reduce the efficiency of silicate weathering in term of CO_2 uptake. In addition, 10–15% of the cation is balanced by sulfate which are derived from sulfide oxidation. The long-term CO_2 uptake is estimated to be lower than 1×10^{11} mol/yr. The particulate Corg flux to the ocean is around 4.2×10^{11} mol/yr based on an average [Corg] of 0.5 wt% in the monsooonal suspended load. The rate of preservation is unknown but is likely very high because Corg content in recent sediments of the Bengal fan is very similar. Metamorphic CO_2 release is more difficult to quantify. It is observed in several thermal springs in Himalaya and it produced high $\delta^{13}C$ alkalinity in certain rivers. Based on this type of signal, metamorphic CO_2 represents <5% of the total alkalinity flux of G-B.

The sedimentary records does not allow to reconstruct past fluxes because sedimentary volumes and accumulation are not sufficiently well established. However, the geochemical difference between the buried sediments and the Himalayan source rock allows to compare the uptake of CO_2 by silicate weathering and Corg burial. As in the modern system, uptake of CO_2 from the net Corg burial is 2–3× that resulting from silicate weathering.

The Himalayan uplift and erosion consumes C over the long term essentially via the burial of Corg rather than silicate weathering. This is largely the result of the combination of tectonic and climatic factors. Erosion generates a considerable increase of surface area which should enhance silicate weathering. However, chemical erosion of silicates for the whole G-B is ~10 t/km²/yr, similar to that of flat shield under tropical climate (e.g., Orinoco). It is because transport processes are remarkably rapid that alteration of eroded particles is limited. On the other hand, the considerable flux of physical erosion, which represent 5–15% of the global riverine input to the ocean, trigger a major flux of continental organic matter to the sedimentary reservoir. Finally, high-accumulation rates in the Bengal fan is also a key factor to preserve organic matter from degradation prior sedimentary burial. The comparison between modern river sediments in Bangladesh and Holocene Bengal Fan sediments suggests that the preservation of continental organic matter is certainly >50%.

References: [1] Derry L. A. and France-Lanord C. (1996) *Paleoceanography, 11*, 267–275. [2] Galy A. et al. (1999) *GCA*, in press. [3] Galy A. and France-Lanord C. (1999) *Chem. Geol., 159*, 31–60.

A MORE CHONDRITIC ARCHEAN MANTLE?

D. Francis, Department of Earth and Planetary Sciences, McGill University, 3450 University Street, Montréal, Québec H3A 2A7, Canada (donf@eps.mcgill.ca).

A resolution to the enigma of the origin of the orthopyroxene-rich mantle roots beneath some Archean cratons may be being hindered by current models for the composition of the Earth's primitive mantle. Most Pyrolite models for fertile primitive mantle (*P*, Figs. 1 and 2) are based on mantle xenoliths from alkaline basalts that are distinctly nonchondritic in terms of their high Mg/Si, and thus high olivine/pyroxene ratios. Any attempt to relate high-Mg Archean magmas to such pyrolitic mantle sources that involves a restite equivalent to the orthopyroxene-rich harzburgites of the Kaapvaal Craton is doomed to violate mass balance constraints [1] (Figs. 1 and 2).

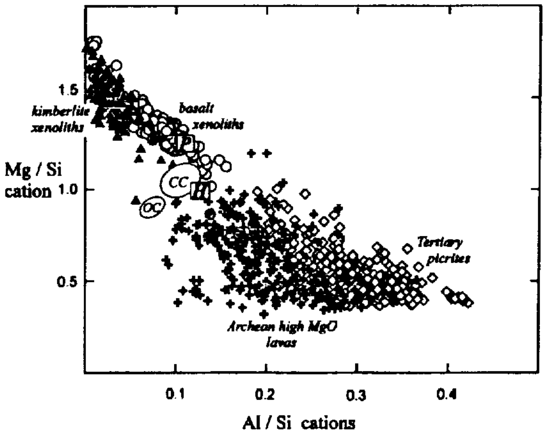

Fig. 1. Magnesium/silicon vs. Al/Si. P = pyrolitic mantle, H = HK-66, CC = carbonaceous chondrites, OC = ordinary chondrites.

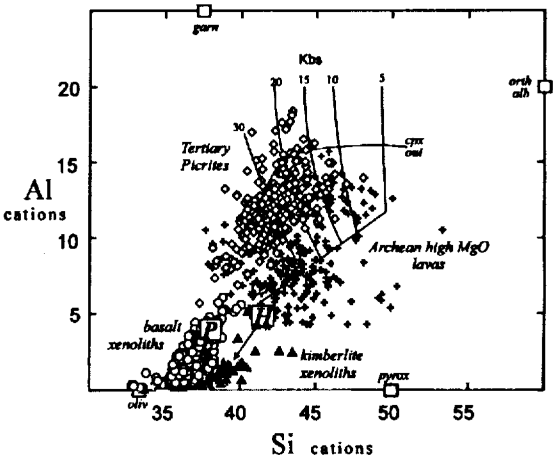

Fig. 2. Aluminum vs. Si. Grid indicates the pressure dependence of melt compositions derived from peridotitic sources. Other symbols as in Fig. 1.

A recent comparison of Tertiary picritic lavas to komatiites and other high-Mg Archean lavas [2] indicates that Archean high-Mg magmas are systematically higher in Fe, but have lower Al/Ti and Al/Si ratios than their Tertiary equivalents. These differences are such that no refractory mantle xenoliths exist that could represent the restite of the extraction of Archean high-Mg lavas from a pyrolitic mantle source. Furthermore, recent high-pressure melting experiments [3] on a pyrolitic mantle composition cannot be reconciled with the trace-element signatures and the Al systematics of komatiites, unless lower Al/Ti ratios and higher Si are assumed for their Archean mantle sources.

In a plot of Mg/Si vs. Al/Si (Fig. 1), fertile Pyrolitic mantle (P), Tertiary picrites, and basaltic mantle xenoliths define a well constrained array consistent with a source = melt + restite relationship. Archean high-Mg lavas, however, are shifted to systematically lower Mg/Si and Al/Si ratios compared to Tertiary picritic lavas, and may define an equivalent Archean array with a mantle source having a Mg/Si ratio similar to that of chondritic meteorites, and a restite equivalent to the orthopyroxene-rich harzburgites preserved in cratonic mantle roots. Figure 2 illustrates the proposed relationship between a more pyroxene-rich mantle source, such as xenolith HK-66 (*H*), and cratonic orthopyroxene-rich harzburgites.

All the mantle xenoliths that have been studied from alkaline basalt suites give Proterozoic Re/Os model ages [4]. This suggests that the current MORB-pyrolitic upper mantle system developed during the Proterozoic. The only remnants of the more chondritic Archean upper mantle are now preserved as the cold mantle roots beneath Archean cratons.

References: [1] Herzberg C. (1993) *EPSL, 120,* 13–29. [2] Francis D. et al. (1999) *EPSL, 167,* 197–213. [3] Walter M. J. (1998) *J. Petrol., 39,* 29–60. [4] Peslier A. et al. (1999) *Chem. Geol.,* submitted.

LEAD- AND NEODYMIUM-ISOTOPIC EVOLUTION OF WATER MASSES AT THE INDONESIAN SEAWAY DURING THE LAST 35 MILLION YEARS.

M. Frank[1,*] and R. K. O'Nions[2], [1]Department of Earth Sciences, University of Oxford, Parks Road, Oxford OX1 3PR, UK (martinf@earth.ox.ac.uk) (*present address: Eidgenössische Technische Hochshule Zürich, Institute for Isotope Geology and Mineral Resources, NO C 61, Sonneggstrasse 5, 8092 Zürich, Switzerland), [2]Department of Earth Sciences, University of Oxford, Parks Road, Oxford OX1 3PR, UK (keitho@earth.ox.ac.uk).

Introduction: At the present day, water-mass exchange between the Pacific and Indian Oceans through the Indonesian Archipelago is restricted to surface and thermocline water masses due to the existence of a number of shallow sills. Pacific water masses are intensely mixed and acquire new hydrographic characteristics on their way through the archipelagic straits. This is also mirrored by the Nd-isotopic composition of these water masses arriving in the eastern Indian Ocean (ε_{Nd} = –2 to –4), which reflects contributions from weathering of Indonesian Island Arc rocks [1].

Prior to about 30 Ma, the exchange of deep water masses between the Pacific and Indian Oceans was unrestricted [2]. After 30 Ma the rifting and northward movement of Australia away from Antarctica and the evolution of the Indonesian Island Arcs narrowed and shallowed the Indonesian Seaway: Deep-water exchange stopped in the mid-Miocene. After a period of possibly complete closure from 10 Ma onward, the present pattern of water mass flow started to develop ~4 Ma.

In this study we evaluate the effects of the history of the Indonesian Seaway and the evolution of the Indonesian Island Arcs on the Pb- and Nd-isotopic composition of water masses on the Scott Plateau, off the northwestern Australian continental margin using isotope time series of ferromanganese crust VA16 13 KD1 (water depth 2000 m).

Results: The crust was dated using a profile of $^{10}Be/^{9}Be$ ratios determined by secondary ion mass spectrometry (SIMS). The ε_{Nd} values display a continuous increase from about –7 at about 35 Ma ago to about –5 at the surface, which is in good agreement with present day measurements of seawater at the same location [1]. The Pb isotopes do not show strong variations but became continuously more radiogenic between ~30 and 5 Ma ago when these trends reversed.

Discussion: The time series of both isotope systems show no clear shifts related to the closing of the Indonesian Seaway in the mid-Miocene

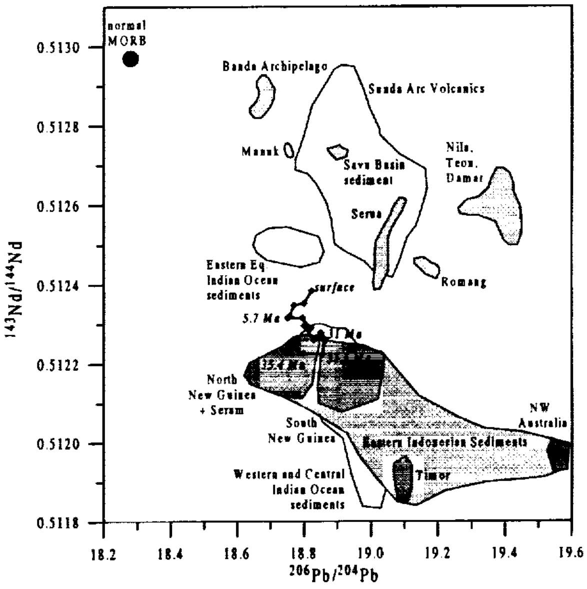

Fig. 1. Isotopic data from [4] and compiled in [5].

In order to evaluate the importance of changes in Nd- and Pb-provenance over time we compare the data of crust VA16 in Pb-Pb- and Pb-Nd-isotopic space. In Pb-Pb isotope space a complex set of binary mixing lines is resolved, which has been possible through the high-precision multiple collector inductively coupled plasma mass spectrometry (MC-ICP-MS) Pb-isotopic measurements using a Nu Instruments mass spectrometer [3]. The results suggest the influence of a variety of different local sources, probably dominated by New Guinea, over the period from 35 to ~3 Ma ago. After 3 Ma the Pb isotopes indicate a switch towards a different source, most probably the Sunda Arc volcanics. The comparison of the data in Pb-Nd-isotopic space appears to be a better diagnostic tool to evaluate the provenance changes because of the large and distinct isotopic differences within the Indonesian Island Arcs in ε_{Nd}. The data for the period between 35 and ~10 Ma also suggest that sources in New Guinea have been important until the data also shift towards the Sunda Arc array (Fig. 1), which shows that the present day Nd-isotopic composition at the site of VA16 is also influenced by weathering of the Sunda Arc or its shelf sediments. Although ε_{Nd} was shown to be a quasi-conservative water mass tracer in the Indonesian Seas [1] it appears that the changes of Nd- and and also Pb-isotopic composition of the water masses on Scott Plateau over time were dominated by changes of continental input sources rather than ocean circulation.

References: [1] Jeandel C. et al. (1998) *GCA, 62,* 2597–2607. [2] Kennett J. (1977) *JGR, 82,* 3843–3860. [3] Belshaw N. et al. (1998) *Int. J. Mass. Spectrom., 181,* 51–58. [4] Stolz A. J. et al. (1990) *Contrib. Mineral. Petrol., 105,* 585–601. [5] Vroon P. Z. et al. (1995) *GCA, 59,* 2573–2598.

SOUTHERN OCEAN RESPONSE TO LEAD- AND NEODYMIUM-ISOTOPIC CHANGES IN THE NORTHWEST ATLANTIC DURING THE LAST 10 MILLION YEARS.

M. Frank[1,*] and R. K. O'Nions[2], [1]Department of Earth Sciences, University of Oxford, Parks Road, Oxford OX1 3PR, UK (martinf@earth.ox.ac.uk) (*present address: Eidgenössische Technische Hochshule Zürich, Institute for Isotope Geology and Mineral Resources, NO C 61, Sonneggstrasse 5, 8092 Zürich, Switzerland), [2]Department of Earth Sciences, University of Oxford, Parks Road, Oxford OX1 3PR, UK (keitho@earth.ox.ac.uk).

Introduction: Drastic shifts towards more radiogenic Pb- and unradiogenic Nd-isotopic compositions of North Atlantic Deep Water (NADW) in the northwest Atlantic starting between 2 and 3 Ma have been recorded in ferromanganese crusts [1,2]. The reason for this is supposedly an increased glacial input of weathered material from the old continental crust of Greenland and the Canadian Shield [3]. At least for Nd, but probably also for Pb, the oceanic residence times are long enough to allow for the advection of such a signal to the southern Atlantic and Southern Ocean. The response of the Southern Ocean to this input signal should thus provide important information on the history of circulation within the Atlantic basin over the last 10 Ma. We present new Nd- (TIMS) and high-resolution and high-precision Pb-isotopic time series (measured by MC-ICPMS [4]) from a ferromanganese crust (109D-C from the Madagascar Basin [2]) and a Mn-nodule (6854-6 from the Cape Basin [5]).

Results: The crust and nodule were dated using profiles of $^{10}Be/^{9}Be$ ratios determined by SIMS. Other than the records from the northwest Atlantic the Southern Ocean and southern Atlantic records display a small increase in ε_{Nd} and a clearly resolved trend toward more radiogenic Pb-isotopic composition starting at about 4 Ma (Fig. 1). Prior to 4 Ma the isotopic records varied little. The pattern of the isotopic records in nodule 6854-6 is very similar to that of crust 109D-C but it is offset by about 1.5 ε_{Nd} units toward more unradiogenic values and slightly offset towards more radiogenic Pb-isotopic composition, which may be explainable by a stronger contribution of NADW to the location of the nodule in the Cape Basin.

Discussion: The fact that two isotopic profiles of nodule 6854-6 from the sediment-facing bottom side and the water-facing top side are indistinguishable from each other and in addition resemble the patterns observed in crust 109D-C suggests that Mn nodules are as reliable as crusts in recording the deep water isotopic characteristics of particle reactive elements such as Pb and Nd over time. The opposite trends in the isotopic profiles compared to the northwest Atlantic apparently shows that the signal has not been advected into the Southern Ocean and may therefore be a consequence of local provenance changes.

While such a local control is possible, there may also be other explanations for the apparent dicrepancy between the records from the northwest and south Atlantic Ocean. From the available water column Nd-isotopic data it was shown that the surfaces of the crusts and nodules reproduce the Nd-isotopic composition of ambient sea water within 1 ε_{Nd} unit [6]. The only major exception to this is in the western Atlantic sector of the Southern Ocean where the records of the crusts and nodules are systematically more radiogenic in their Nd-isotopic composition than the ambient deep water. It was suggested that the samples of the crusts which integrate over several glacial/interglacial periods may have recorded a diminished glacial NADW import into the Southern Ocean [6]. A comparison of the isotopic time series of this study in Pb-Pb-isotopic space shows that the slope for the last 3.5 m.y. is exactly the same as for the northwest Atlantic crusts and thus may support such an integrated effect of diminished glacial NADW supply. In addition, the timing of the start of the trends in the isotopic records agrees resonably well with the onset of northern hemisphere glaciation that has been the start of pronounced glacial/interglacial climatic contrasts.

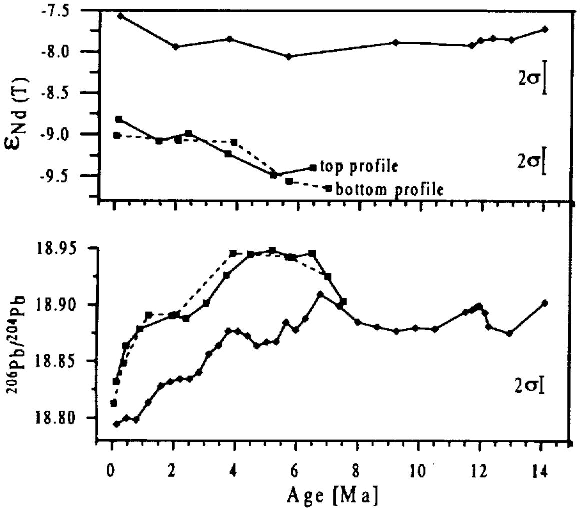

Fig. 1. Isotopic time series for crust 109D-C (diamonds) and Mn-nodule 6854-6 (open squares).

References: [1] Burton K. W. et al. (1997) *Nature, 386,* 382–85. [2] O'Nions R. K. et al. (1998) *EPSL, 155,* 15–2. [3] von Blanckenburg F. and O'Nions R. K. (1999) *EPSL, 167,* 175–182. [4] Belshaw N. et al. (1998) *Int. J. Mass. Spectrom., 181,* 51–58. [5] Rogers J. (1987) *Mar. Geol., 78,* 57–76. [6] Albarède et al. (1997) *GCA, 61,* 1277–1291.

UNRAVELING THE TECTONO-METAMORPHIC HISTORY IN THE ISUA SUPRACRUSTALS (WEST GREENLAND): MINERAL LEAD STEPWISE LEACHING EVIDENCE FOR EARLY- AND LATE ARCHEAN METASOMATIC-METAMORPHIC EVENTS.

R. Frei[1,2], M. T. Rosing[3,2], E. J. Krogstad[2], M. Storey[2], and F. Albarède[4], [1]Geological Institute, University of Copenhagen, Øster Voldgade 10, DK-1350 Copenhagen K, Denmark (robertf@geo.geol.ku.dk), [2]Danish Lithosphere Centre, Øster Voldgade 10, DK-1350 Copenhagen K, Denmark, [3]Geological Museum, Denmark, [4]Ecole Normale Supérieure de Lyon, France.

Introduction: The supracrustal rocks from Isua (ISB, West Greenland) have been extensively used to constrain the early Earth's crust-mantle differentiation history and were examined for evidence of crustal components older than ~3.8 Ga. Numerous isotopic studies, especially those focusing on presumably immobile elements (e.g., REE), have revealed inconsistent and in cases dubious results. These point to later "open system behavior" of the respective isotopic systems (e.g., Sm-Nd, Lu-Hf, U-Pb) in the Isua supracrustals [e.g., 1,2]. Although recognized long ago [3–6, and others] the effects of later tectono-metamorphic and hydrothermal overprints have however not adequately been accounted for by the interpretation of apparently "spurious" whole-rock geochemical data.

New mineral and whole-rock Pb-isotopic data from the supracrustals undoubtedly point to the existence (and thereby reinforce results from previous studies) of least 2–3 superimposed tectono-metamorphic events that were accompanied by hydrothermal-metasomatic fluids.

Results: PbSL data on a metasomatic garnet from within the contact zone between a meta-basaltic sequence and an intrusive gneiss sheet yields an isochron age of 3.74 ± 0.02 Ga (Fig. 1).

This date is compatible with a 3.74 ± 0.04 Ga PbSL isochron age obtained for tourmaline from within an undeformed, mixed-sulfide bearing quartz veinlet crosscutting a strongly deformed section of the same meta-basaltic package [7]. Both results, supported by congruous initial Pb-isotopic components, constrain a first metasomatic-hydrothermal event to a period during which earlier phases of the protoliths of Amîtsoq gneisses (>3.7 Ga) intruded the sequence. A second metasomatic event, characterized by slightly more evolved initial Pb-isotopic signatures, can be related to the younger (~3.65 Ga) Amîtsoq intrusions. Metasomatic fluids were characterized by high Th-REE bearing fluids, which today mimic apparent REE disturbances and

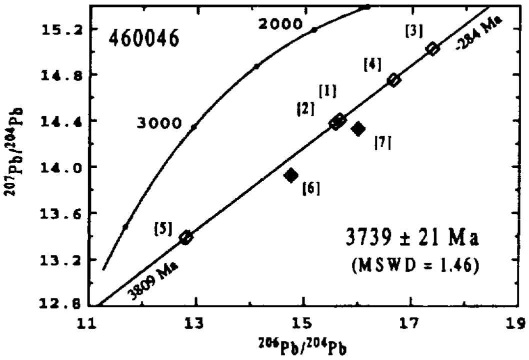

Fig. 1.

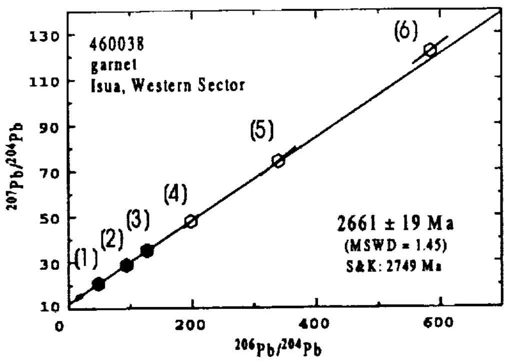

Fig. 2.

may account for the observed initial Nd and Hf heterogeneity in the different supracrustals. A late Archean tectono-thermal overprint, expressed in reactivation of earlier shear zones and in partial thermal resetting of mineral (or their inclusions) and whole-rock isotopic systematics, is now being demonstrated to be more widely distributed than initially thought (Fig. 2).

The extent to which late Archean fluids (related to the intrusion of Nuuk and Ikkattoq-type gneiss protoliths?) percolated through the piles remains still an open question.

Conclusions: At least two to three metasomatic-hydrothermal episodes, accompanied by metamorphic events, are superimposed on some of the ISB sequences. Because of their disturbing effects on the isotopic systematics, the recognition of these early and late Archean overprints are essential when applying isotopic data to addressing questions of early Earth's crustal evolution.

References: [1] Blichert-Toft J. et al. (1999) *GCA*, in press. [2] Frei et al. (1999) *GCA*, in press. [3] Rosing M. T. et al. (1996) *Geology, 24*, 43–46. [4] Nutman A. P. (1986) *Rapp. Grønlands Geol. Unders., 154*, 80 pp. [5] Shimizu H. et al. (1990) *GCA, 54*, 1147–1154. [6] Gruau G. et al. (1996) *Chem. Geol., 133*, 225–240. [7] Frei R. et al. (1998) *Eos Trans. AGU, 79*, F932.

SUSTAINABLE DEVELOPMENT: THE ROLE OF GEOCHEMISTRY.

W. S. Fyfe, Department of Earth Sciences, University of Western Ontario, London, Ontario N6A 5B7, Canada (mmcmahon@julian.uwo.ca).

Introduction: The science of the twentieth century has given us our incredible powers of observation and analysis. We can observe all elements and isotopes in all materials, in fluids and on surfaces. In June 1999, ICSU, UNESCO, are holding their world conference on Science, "Science for the twenty-first century a new commitment" in Budapest. But it must be noted that the Earth sciences are hardly mentioned.

The great future sustainable life-support systems that require urgent change include those for clean energy, clean water and water storage, soil remediation, clean mining, intelligent waste management including nuclear wastes, quality control of materials, and providing the new ultrapure materials for new technologies as with photovoltaics, photo dissociation of water to produce H and O, etc. *The Economist* recently reported that there is a world shortage of high-purity Si and now pure Ti is in increasing demand. If one examines most of those problems, all involve the Earth sciences with a major component from geochemistry. Examples include combustion gas disposal underground, clean coal and we now know that coals can be rich in a host of elements including the halogens, U, As, even Au. It is interesting to note that a few decades ago we knew more about the chemistry of the Moon's surface than coal.

For agriculture our knowledge of the geochemistry of fertilizer resources is often inadequate and this is true for many ore materials. Soil remediation requires knowledge of all the bio-essential elements (≅50) and the need for clean, often slow release, additives. The new knowledge of the deep biosphere, geomicrobiology, leads to a host of possibilities for clean mining, water purification, as with the global As, F problems.

We increasingly recognize that to solve many of the global problems and the development of truly sustainable systems requires the integration of knowledge from all sciences and in almost all cases geochemistry is a fundamental component.

THE EFFECT OF A WATER-RICH SUBDUCTION COMPONENT ON MELT PRODUCTION IN MANTLE PERIDOTITE.

G. A Gaetani[1,2] and T. L. Grove[1], [1]Department of Earth, Atmospheric and Planetary Sciences, Massachusetts Institute of Technology, Cambridge MA 02139, USA, [2]Department of Earth and Environmental Sciences, Rensselaer Polytechnic Institute, Troy NY 12180, USA.

Quantitative knowledge of the influence of a H_2O-rich subduction component on peridotite partial melting has the potential to place new constraints on models of convergent margin magmatism. Although melting of anhydrous mantle peridotite is thought to be a polybaric, near-fractional process [1,2], isobaric batch melting of hydrous mantle peridotite provides basic insights into melt generation processes at subduction zones. Here we investigate the effects of H_2O, K_2O, and Na_2O on the temperature at which hydrous batch melts coexist with mantle peridotite at 1.5 GPa, on isobaric melt production rates, and on the extent to which peridotite partially melts at a given pressure and temperature.

Liquidus temperatures were calculated for partial melts of an anhydrous peridotite, of a peridotite containing 0.15 wt% H_2O, and of a peridotite containing 0.32 wt% of an H_2O-Na_2O-K_2O subduction component (SC). Anhydrous liquidus temperatures were calculated using the model of [3], while the liquidus temperature depression caused by dissolved H_2O was calculated from olivine-melt thermometry [4]. The peridotite composition used in the calculations is the depleted MORB source of [3], and the SC composition was derived from the H_2O-rich Mariana component of [5] by normalizing the concentrations of H_2O, Na_2O, and K_2O to 100%.

The liquidus temperatures of the anhydrous partial melts increase from 1330°C at 2% partial melting to 1400°C at 20%. The temperature vs. melt fraction (T-F) curve is concave-downward. In contrast with the anhydrous case, a temperature increase of 120°C only increases the extent of partial melting of the H_2O-bearing peridotite from 2% to 5%. A temperature increase of 200°C is necessary to increase the extent of melting of the SC-bearing peridotite by the same amount. Increasing the partial melting from 5% to 20% for the H_2O-bearing peridotite requires that the temperature be raised by ~90°C and that of the SC-bearing peridotite be raised by ~130°C.

The large temperature increases required to partially melt H_2O- and SC-bearing peridotite under isobaric conditions are a reflection of their relative isobaric melt production rates, or the change in melt fraction for a given change in temperature at constant pressure. For the anhydrous peridotite, the isobaric melt production rate is 0.05%/°C at 2% melting and increases continuously with increasing extent of melting to 0.8%/°C at 20% partial melting. The H_2O-bearing peridotite has an isobaric melt production rate at 2% partial melting (0.01%/°C) that is a factor of 5 lower than the anhydrous case, while the melt production rate for the SC-bearing peridotite (0.007%/°C) is lower by a factor of 7. The melt production rates for both the H_2O- and SC-bearing peridotites increase faster as a function of F than the anhydrous case, so that at 20% partial melting they differ from the anhydrous isobaric melt production rate by approximately a factor of 2. If isobaric melt production rates are considered as a function of temperature, the H_2O- and SC-bearing peridotites have higher melt productivities than the anhydrous peridotite at a given temperature. This is due to the increase in isobaric melt production rate with increasing F, and reflects the increased extent of melting for the H_2O- and SC-bearing peridotites at a given temperature relative to the anhydrous peridotite.

The increase in melt fraction produced by raising the concentration of H_2O in the peridotite at a given temperature and pressure increases at progressively higher temperatures. For example, the addition of 0.25 wt% H_2O to a peridotite at 1200°C increases the extent of melting from 0.5% to 3%, while at 1350°C the melt fraction increases from 3% to 12%. In spite of this temperature dependence, the increase in melt fraction produced by raising the concentration of H_2O in the peridotite is significantly lower than the value inferred by [5] from a suite of basaltic glasses from the Mariana Trough. In the Mariana case the addition of 0.25 wt% H_2O to the peridotite increases the extent of melting by ~15%.

In order to reconcile our calculations with the observations of [5], we investigated the influence of refertilization of the peridotite on extent of melting. At 1330°C, the addition of any of the major constituents of the Mariana SC (H_2O, K_2O, and Na_2O) is not by itself sufficient to explain the observed increase in extent of melting. The addition of H_2O has the strongest effect on melt fraction, while the addition of K_2O produces a smaller melt fraction increase, and Na_2O has least effect on extent of melting. If, however, an H_2O-K_2O-Na_2O SC is added to the peridotite, the match between our calculated increase in extent of melting and that inferred for the Mariana glasses by [5] is very good. Although these calculations do not place rigorous constraints on the conditions of melt generation beneath the Mariana back arc, they do indicate that the melt fraction variation represented by the Mariana basalts can be explained by equilibration with mantle peridotite at nearly identical pressure-temperature conditions. The combined effects of H_2O and alkalis can account for the inferred melting extents without a systematic temperature increase.

References: [1] Klein E. M. and Langmuir C. H. (1987) *JGR, 92,* 8089–8115. [2] Johnson K. T. M. et al. (1990) *JGR, 95,* 2661–2678. [3] Kinzler R. J. (1997) *JGR, 102,* 853–874. [4] Gaetani G. A. and Grove T. L. (1998) *Contrib. Mineral. Petrol., 131,* 323–346. [5] Stolper E. M. and Newman S. (1994) *EPSL, 121,* 293–325.

OLIVINE-HOSTED MELT INCLUSIONS REMEMBER THE MAGMA CHAMBER, NOT THE MANTLE.

G. A. Gaetani and E. B. Watson, Department of Earth and Environmental Sciences, Rensselaer Polytechnic Institute, Troy NY 12180, USA.

Olivine-hosted melt inclusions represent an important source of information about the processes involved in partial melting of mantle peridotite. Trace-element studies of such inclusions have contributed significantly to our understanding of partial melting and melt extraction processes beneath mid-ocean ridges [1]. Isotopic studies have demonstrated local mantle heterogeneity on a scale not indicated by analyses of host lavas [2]. The utility of studying olivine-hosted melt inclusions derives from the strong incompatibility of most trace elements in the olivine. Understanding the major-element compositions of these inclusions is more complicated, however, because crystallization of olivine on the walls of the inclusion produces significant changes in the major-element composition of the melt during cooling.

Although it is commonly assumed that the compositional effects of post-entrapment crystallization can be accounted for through olivine addition calculations or heating experiments, the rapid diffusivities of FeO and MgO in olivine at magmatic temperatures allow communication between the inclusion and the magma containing the host olivine [3]. Therefore, it is likely that melt inclusions remain in Fe-Mg equilibrium with the magma outside the olivine host, and that information about the original melt inclusion composition is irretrievably lost during cooling. In order to investigate this scenario, we developed a finite-difference code to model crystallization and diffusion during cooling (and reheating) of spherical melt inclusions hosted by concentric spherical olivines. Equilibrium partitioning of FeO and MgO was maintained at the interface between the inclusion and the host olivine as a function of temperature and melt composition using expressions calibrated on the basis of 247 experiments from the literature.

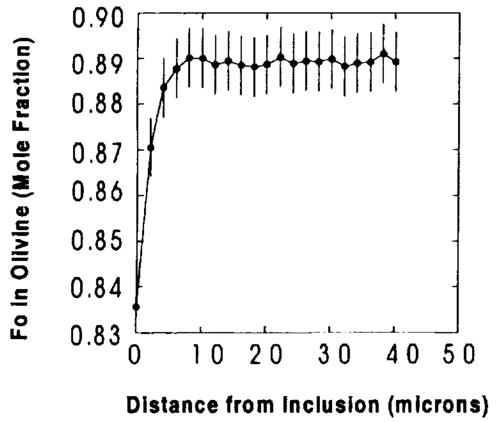

Fig. 1. Plot of distance from melt inclusion vs. forsterite content of olivine showing data for melt inclusion from Western Reykjanes Peninsula, Iceland. Error bars are 1σ based on counting statistics.

Simulations indicate that, even for relatively large host olivines, equilibrium is maintained between the melt inclusion and the host magma. For example, if a 100-µm-diameter melt inclusion hosted in a 2-mm-diameter olivine is cooled from 1215° to 1115°C in 10 yr, no measurable compositional gradient will develop in the olivine. The only potential information that could be gained from determining the major-element compositions of coexisting olivine and melt inclusion would be the temperature of final equilibration in the magma chamber.

This result is apparently at odds with studies of natural melt inclusions and host olivines, which record varying extents of disequilibrium [4]. Our modeling results can be reconciled with observations of natural melt inclusions, however, if the observed disequilibrium developed as the result of rapid cooling, such as during eruption of the host lava. Simulations indicate that at cooling rates of 100° to 200°C/h no meaningful diffusion occurs in the olivine. At these conditions compositional gradients are restricted to an ~5–10-µm-wide zone surrounding the inclusion.

In order to test the hypothesis that what is commonly thought of as "post-entrapment" crystallization is, in actuality, syn-eruptive crystallization, we examined olivine-hosted melt inclusions in picritic lavas from the Western Reykjanes Peninsula, Iceland [5]. Electron microprobe analyses of olivine surrounding ~100-µm-diameter melt inclusions show compositional gradients adjacent to the inclusions that are 5–10 µm wide. In some cases the forsterite content of the olivine changes by as much as 6 mol% over this distance (Fig. 1). We conclude, therefore, that while the trace-element compositions of olivine-hosted melt inclusions provide reliable information about mantle processes, major elements remember the magma chamber.

References: [1] Sobolev A. V. and Shimizu N. (1993) *Nature, 363,* 151–154. [2] Saal A. E. et al. (1998) *Science, 282,* 1481–1484. [3] Gaetani G. A. and Watson E. B. (1999) *Eos Trans. AGU, 80,* 373–374. [4] Shimizu N. (1998) *Phys. Earth Planet. Int., 107,* 183–201. [5] Jakobsson S. P. et al. (1978) *J. Pet., 19,* 669–705.

COSMOCHEMICAL DETERMINISM IN THE FORMATION OF HABITABLE PLANETS.

E. J. Gaidos, Mail Code 170-25, California Institute of Technology, Pasadena CA 91125, USA (gaidos@gps.caltech.edu).

The detection of circumstellar disks resembling one thought to have prefaced the formation of the solar system [1,2], and the discovery of giant planets around solar-type stars [3,4] have invited speculation on the existence of other Earth-like planets that support life. Previous researchers have proposed various criteria for hospitable planets, including a semimajor axis within the range of a continously habitable zone [5,6] stellar companions, a planetary mass sufficient to maintain volcanism and plate tectonics, the existence of giant planets [7], ultraviolet radiation from the parent star, and rotation. It has also been argued that the pace of stellar nucleosynthesis of heavy elements, especially C, regulated the appearance of life and intelligence [8]. While a minimum complement of heavy elements is certainly necessary, this is not the complete picture since these must exist in condensible form and be incorporated into planet-forming materials before the removal of the gaseous circumstellar disk. This process is controlled by nebular chemistry, particularly by its oxidation state.

Here, I propose that the oxidation state of a circumstellar disk is a fundamental cosmochemical parameter that controls two aspects of planet formation bearing on the appearance of Earth-like biospheres: (1) the formation of giant planets; and (2) the inventories of water, C, and N accreted by small rocky planets. The oxidation state is in turn tied to the initial ratio of C and O in the progenitor nebula. Carbon monoxide is the most stable form of C and O in the low-density environments of molecular clouds where it is readily detected at millimeter wavelengths. Its formation is overwhelmingly favored during the collapse of a molecular cloud core and the reduction of CO to CH_4 at the higher pressures in a disk is kinetically inhibited. As a result, the oxidation state of the disk is sensitive to whether C or O is in relative abundance. Oxidating systems with $C/O < 1$ will have plentiful water but could be depleted of reduced N and hydrocarbons: The converse is true for reducing systems with $C/O > 1$. Our solar system formed from a nebula of a globally oxidizing nature ($C/O \sim 0.5$). I argue that larger or smaller values of C/O would produce planetary systems with markedly different physical or chemical properties not necessarily compatible with the existence of Earth-like life. In principle, the relative abundance of C and O can be determined by spectroscopy of the parent star. A measurement of C/O, together with metal abundance, spectral type, and duplicity, will be particularly valuable in assessing the likelihood that a particular hosts planets hospitable to life.

References: [1] Smith and Terrile (1985) *Science, 226,* 1421. [2] Koerner et al. (1998) *Astrophys. J. Lett., 503,* L83. [3] Mayor and Queloz (1995) *Nature, 378,* 355. [4] Cochran et al. (1997) *Astrophys. J., 483,* 457. [5] Hart (1979) *Icarus, 31,* 351. [6] Kasting et al. (1993) *Icarus, 101,* 108. [7] Wetherill (1994) *Astrophys. Space Sci., 212,* 23. [8] Livio (1998) *Astrophys. J., 511,* 429.

CLIMATE AND GEOCHEMICAL MODELING OF PROTEROZOIC GLACIATIONS.

E. J. Gaidos[1] and J. L. Kirschvink, [1]Mail Code 107-25, California Institute of Technology, Pasadena CA 91125, USA (gaidos@gps.caltech.edu).

We describe preliminary models of the climate, atmospheric and ocean chemistry of the Paleoproterozoic and Neoproterozoic low-latitude glaciation events. The goal of these models is to suggest paleogeochemical tests for the theory that the glaciation became oceanically global, i.e., the "Snowball Earth" scenario, and to evaluate the potentially devastating impact of such an event on life. We examine the behavior of ocean pH, and redox balance throughout the glacial advance, during the snowball, and in the post-snowball aftermath. We pay particular attention to the behavior of dissolved CO_2, its acids, and the precipitation and dissolution of carbonate, including the budgets and distribution of Mg and Ca coprecipitated with the last. We look at the behavior of greenhouse gases in the atmosphere given certain assumptions about volcanic outgassing, biologically-derived O (or lack thereof), and soluble gases that may be involved in acid-mediated weathering of continental debris (sulfur dioxide, nitric oxide). A simple model of the evolution of the hydrological cycle is described and the initial growth and terminal destruction of continental glaciers are inferred. We are particularly interested in the sublimative redistribution of sea ice and glaciers during the snowball event itself, since this may have enormous consequences for the niches available to photosynthetic and chemosynthetic organisms. We also examine the interesting but hypothetical case of a large impact during a snowball event. We briefly touch on implications for the persistence and evolution of life on a snowball Earth, including an assessment of energy sources, especially sunlight reaching liquid water, adaptation to geochemical trauma, massive extinction, and subsequent post-snowball radiations.

MOLECULAR INFERENCES OF THE ORIGIN AND EVOLUTION OF OXIDANT-ASSOCIATED ENZYMES.

E. J. Gaidos[1], K. H. Nealson, P. Jayakumar, and J. L. Kirschvink, [1]Mail Code 107-25, California Institute of Technology, Pasadena CA 91125, USA (gaidos@gps.caltech.edu).

We present results of molecular phylogeny studies of enzymes involved in the use or mediation of common inorganic oxidants. The objective of these studies is to correlate the origin and major evolutionary steps of these enzymes (inferred from phylogenetic studies) with the geological and geochemical record on the Earth and the apparent change in the global oxidation state from an early reducing state to the present highly oxidized one. We present results from a study of portions of 214 sequences of the Fe-Mn superoxide dismutase enzyme (SOD) which is found in bacteria, archaea, and the mitochondria of eukaryotes. This enzyme protects organisms from the destructive chemistry associated with the production of OH radicals from O_{2-} and their interaction with DNA. We confirm the deep divergences between the Fe- and Mn-cofactor forms of the enzyme in the Archaea and Bacteria found by previous coauthors. Kirschvink et al. [1] have proposed that this divergence is associated with an "oxidation event" in the Paleoproterozoic recorded by large scale deposition of oxidized manganese in a marginal setting and associated with evidence of low-latitude glaciation. We present studies of the three families of nitrate reductase enzymes, one found in the mitochondria of eukaryotes, and the other two found with the bacteria and archaea. Phylogenetic analysis of the molybdopterin-binding portions of these enzymes suggest divergences from molybdoenzyme relative such as sulfite oxidates, formate dehydrogenase, and DMSO reductase suggest an origin at ~2 Ga. This would be consistent with the appearance of ubiquitous nitrates along with O and the enhancement of soluble oxidized forms of molybdenum in the oceans.

References: [1] Kirschvink et al. (1999).

NEW THORIUM-230 DATA FROM BARBADOS FOSSIL CORALS: THE BEGINNING AND END OF STAGE 5e AND THE TIMING AND AMPLITUDE OF EVENT 6.5.

C. D. Gallup[1], H. Cheng[2], R. Speed[3], and R. L. Edwards[2], [1]Department of Geology, University of Maryland, College Park MD 20742, USA, [2]Department of Geology and Geophysics, University of Minnesota, Minneapolis MN 55455, USA, [3]Department of Geological Sciences, Northwestern University, Evanston IL, USA.

Introduction: Constraints on the timing of the last interglacial (stage 5e) have come largely from the range of ^{230}Th ages exhibited by samples that grew during the high sea stand of the last interglacial (LI). Equally important, but harder to find, are samples that grew during the periods of sea level change that occurred just before and after the high sea level stand and thus delimit its duration. On Barbados, the area with the highest uplift rate, and thus the best place to look for such samples, is the Clermont-Mount Hillaby Anticline [1]. Here, the University of the West Indies campus is built upon the LI terrace at an elevation of 61 m. In 1994 [2] we reported two samples from this exposure: (1) sample UWI-2 from 30 m below the crest with an age of 129.4 ± 0.8 ka and an initial δ^{234}U value of 152.7 ± 2.1; and (2) sample UWI-16, part of a cobble deposit 20 m below the crest, with an age of 117.4 ± 1.0 ka and an initial of 153.4 ± 1.8. Note that these data have been recalculated using new half-lives for ^{234}U and ^{230}Th based on our recent work [3]. Because these were single dates and the deposits had not been well characterized, there was insufficient information to determine whether UWI-2 represents the sea-level rise and UWI-16 the sea-level fall before and after stage 5e.

New Data: We report here the results of a study in progress to use detailed stratigraphy and systematic U-Th-Pa analyses (using the new half-lives) of these and other Barbados deposits to further investigate the timing of sea-level change before and after the LI. In looking more carefully at the UWI-2 location, we were surprised to find not only LI samples, but also stage 6 samples. The UWI-2 deposit contains evidence for two stages of coral growth, both in place, separated by an unconformity. Samples below the unconformity give ages of 173.3 ± 1.1, 179.7 ± 1.5, and 189.9 ± 2.4 ka with initials of 159 ± 2, 164 ± 2, and 204 ± 3. The 179.7-ka sample has a concordant ^{231}Pa age. Samples above the unconformity include sample UWI-2 and a second with an age of 129.7 ± 0.8 and an initial of 149 ± 3. These samples suggest an age of 180 ka for the lower deposit and indicate an age of 129.7 ka for the upper deposit (this meets the criterion [2] for a ^{230}Th age accurate to ±2 ka). These suggest an initial sea level of –50 m (relative to present) at 180 ka and of –24 m at 129.7 ka. The stage 6 event likely correlates with event 6.5 [4]. The upper deposit likely records the rise in sea level leading to the LI.

At another location along the LI terrace, a construction site involved a pit dug near the base of the LI terrace. A sample from this pit, 25 m below the LI terrace crest, gives an age of 118.7 ± 1.0 ka and an initial of 162 ± 2. Though this sample does not meet the criterion, its age and elevation are consistent with sea level having dropped from its LI maximum by 20 m by 117 ka, as implied by sample UWI-16.

In addition, samples from terraces below the LI terrace provide new dates for stages 5c and 5a. They are as follows: stage 5c, 98.8 ± 0.4 ka with an initial of 148 ± 2 and stage 5a, 76.5 ± 0.4 ka with an initial of 143 ± 2. The corresponding initial sea levels are –17 and –29, respectively. Thus, the latter sample likely documents falling sea level at the end of stage 5a. These samples have been incorporated into the sea level interpretations of [5] and constrain the rate of sea level fall between stages 5a and 4 as well as between 5c and 5b.

Comparison with Other Data: Data from New Guinea corals include a 116.2 ± 1.8-ka sample [5], with concordant ^{230}Th and ^{231}Pa ages; also dated by Stein et al. [6] that records a sea level of –20 m and several samples with an average age of 130 ± 2 ka [7] that record a sea level of –90 m. Our data are consistent with the New Guinea data if it is possible to have a sea-level rise of 66 m in 2 ka. Our data are not consistent with samples from Hawai'i that suggest maximum LI sea-level lasting until 114.1 ± 1.8 ka [8].

The δ^{18}O value for event 6.5 in the stacked benthic record [4] would correspond to a lower sea level than –50 m if the benthic δ^{18}O record is purely a function of ice volume. Thus, it appears that deep ocean temperatures were cooler during event 6.5 than during interglacial periods, similar to the relationship observed for the last glacial cycle [e.g., 5,9].

References: [1] Taylor F. W. and Mann P. (1991) *Geology, 19,* 103–106. [2] Gallup C. D. et al. (1994) *Science, 263,* 796–800. [3] Cheng et al. (in review) *Chem. Geol.* [4] Martinson D. G. et al. (1987) *Quat. Res., 271,* 1–29. [5] Cutler et al., this volume. [6] Stein et al. (1993) *GCA, 57,* 2541–2554. [7] Esat et al. (1999) *Science, 283,* 197–201. [8] Szabo et al. (1994) *Science, 266,* 93–96. [9] Chappell and Shackleton (1986) *Nature, 324,* 137–140; Fairbanks R. G. and Matthews R. K. (1978) *Quat. Res., 10,* 181–196.

HIGH-PRECISION MAGNESIUM-ISOTOPIC RATIO MEASUREMENT BY MULTIPLE COLLECTOR INDUCTIVELY COUPLED MASS SPECTROMETRY: A NEW TOOL IN COSMOCHEMISTRY AND GEOCHEMISTRY.

A. Galy[1], L. Halicz[1,2], N. S. Belshaw[1], E. D. Young[1], and R. K. O'Nions[1], [1]Department of Earth Sciences, University of Oxford, Parks Road, OX1 3PR, UK (albertg@earth.ox.ac.uk), [2]Geological Survey of Israel, 30 Malkhe Street, Jerusalem 95501, Israel.

Introduction: Natural variations of the isotopic composition of Mg may arise through (1) incorporation of presolar grains into meteorites [1,2]; (2) the decay of ^{26}Al to ^{26}Mg [2–6]; (3) isotopic fractionation through volatilization/condensation reactions [7,8]; (4) isotopic fractionation during low-temperature fluid/rock interactions; and (5) kinetic and thermodynamic isotopic effects accompanying biological incorporation and rejection. The last 3 processes are characterized by a mass-dependent fractionation similar to the instrumental fractionation (α_{inst}).

Previous methods [thermal ionization mass spectrometry (TIMS) or secondary ion mass spectrometry (SIMS)] applied to the search for Mg-isotopic variations have an uncertainty of 1‰ on α_{inst} [2–6,9–10]. Because of this technical limitation to the accurate measurement of α_{inst} of Mg, relatively few investigations have been made of mass-dependent fractionation in terrestrial samples. Original investigations concluded that terrestrial variations of Mg-isotopic ratio are restricted to a few per mil [2,9–10]. The aim of this study is to use multiple collector inductively coupled mass spectrometry (MC-ICP-MS) for the measurement of Mg-isotopic ratios and to define a more accurate method, suitable for the study of terrestrial and extraterrestrial samples.

Methods and Results: Magnesium solutions are introduced through a Cetac MCN-6000 nebulizer into the MC-ICP-MS (Nu Instruments) [11]. This instrument allows simultaneous measurement of the three isotopes of Mg and a careful control of peak shapes. The α_{inst} has been determined on the international Mg-isotopic standard SRM980 [10] and is around 1.077/amu. The α_{inst} is sensitive to instrumental conditions, including both the nebulizer as well as ion formation, extraction, and focusing. Results are expressed in δ units relative to SRM 980 standard :

$$\delta^{25}\text{Mg} = \{(^{25}\text{Mg}/^{24}\text{Mg})_{\text{Sample}}/(^{25}\text{Mg}/^{24}\text{Mg})_{\text{SRM}} - 1\} \times 1000$$

$$\delta^{26}\text{Mg} = \{(^{26}\text{Mg}/^{24}\text{Mg})_{\text{Sample}}/(^{26}\text{Mg}/^{24}\text{Mg})_{\text{SRM}} - 1\} \times 1000$$

The reproducibility of the standard over a day is variable and ranges between 3‰ and 6‰. In order to reduce the effects of drift we adopted a standard-sample bracketing technique. In this protocol, standard and sample isotopic values are measured six and eight times, respectively, for 200 s each. The ionization efficiency and flow rate of our instrument allows the routine measurement of 500 ng of Mg.

The uncertainty in sample isotopic ratio measurement is between 0.02‰ and 0.33‰/amu (2σ) and includes counting statistics for the sample and the standard and the drift for the standard between two measurements of the sample. The external precision determined from standard-standard measurements is 0.08‰ (2σ, n = 15). Other Mg solutions have been measured and the external precision is 0.12‰/amu (2σ, n = 29). A range of more than 2‰ on δ^{25}Mg has been found for Mg metal and magnesite samples. δ^{26}Mg and δ^{25}Mg define a linear relation with a slope of 0.517, corresponding to mass-dependent fractionation.

Conclusion: The MC-ICP-MS allows the measurement of small variations of Mg-isotopic composition as small as 0.2‰/amu and provides a powerful tool in geochemistry and cosmochemistry.

Preliminary results suggest a terrestrial range in δ^{25}Mg at least of 2‰.

References: [1] Clayton R. N. et al. (1984) *GCA, 48,* 535–548. [2] Wasserburg G. J. et al. (1977) *GRL, 4,* 299–302. [3] Schramm D. N. et al. (1970) *EPSL, 10,* 44–59. [4] Lee T. et al. (1976) *GRL, 3,* 109–112. [5] Macdougall J. D. and Phinney D. (1979) *GRL, 6,* 215–218. [6] Russel S. S. et al. (1996) *Science, 273,* 757–762. [7] Clayton R. N. et al. (1974) *Proc. LSC 5th,* 1801–1809. [8] Molini-Velsko C. et al. (1984) *Meteoritics, 19,* 273–274. [9] Catanzaro E. J. and Murphy T. J. (1966) *JGR, 71,* 1271–1274. [10] Catanzaro E. J. et al. (1966) *J. Natl. Bur. Stand., 70A,* 453–458. [11] Belshaw N. S. et al. (1998) *Int. J. Mass Spectrom., 181,* 51–58.

COMPLEXATION OF METALS WITH AQUEOUS SULFIDE IN AN ANAEROBIC TREATMENT WETLANDS, BUTTE, MONTANA.

C. H. Gammons, Department of Geological Engineering, Montana Tech of the University of Montana, Butte MT 59701, USA (cgammons@mtech.edu).

Introduction: Anaerobic wetlands remove heavy metals from waste streams by creating a reducing environment in which aqueous sulfate is bacterially reduced to H_2S. The latter combines with dissolved metals to form insoluble metal sulfide precipitates, as shown by the following general reaction:

$$\text{Me}^{2+} + \text{H}_2\text{S} = \text{MeS(s)} + 2\text{H}^+ \qquad (1)$$

where Me^{2+} = any divalent metal. Based on published solubility products, the mobility of most metals of concern in the presence of measurable quantities of H_2S is exceedingly low (often less than the analytical detection limit). However, H_2S also forms aqueous complexes with these metals, which can lead to elevated solubility, as shown by the following example reactions:

$$\text{MeS(s)} + \text{H}_2\text{S} = \text{Me(HS)}_2\text{(aq)} \qquad (2)$$

$$0.5\text{Cu}_2\text{S(s)} + 1.5\text{H}_2\text{S} = \text{Cu(HS)}_2^- + \text{H}^+ \qquad (3)$$

$$0.5\text{As}_2\text{S}_3\text{(s)} + 0.5\text{H}_2\text{S} = \text{AsS}_2^- + \text{H}^+ \qquad (4)$$

These relationships are illustrated using field data collected from an anaerobic treatment wetlands in Butte, Montana, that operated between May 1996 and December 1998. The water being treated at this facility was near-neutral, but contained elevated levels of Zn, Mn, Cd, Cu, and other metals. The high-metal-content is chronic to surface and groundwaters in the vicinity of Butte and is a result of over a century of mining, processing, and smelting of hydrothermal mineral deposits on "The Richest Hill On Earth."

Methods: For approximately three years, students and staff at Montana Tech monitored the chemical and physical parameters at the constructed wetlands site. Most of the heavy metal attenuation occurred in four subsurface-flow anaerobic cells in which decay of organic matter promoted bacterial sulfate reduction and metal sulfide precipitation in the wetlands substrates. Influent and effluent water samples for each cell were taken every month, and analyzed for a complete set of metals (ICP-AES), anions (IC), H_2S (chromatography), and organic/inorganic C. Internal piezometers were also analyzed quarterly, which provided data on the change in fluid chemistry with depth and flow path within the cells. All metals data were collected using both filtered (0.45 μm) and unfiltered/acidified samples. A suite of solid precipitate samples has also been collected, and is in the process of being analyzed via SEM/EDX and XRD methods.

Results: The concentration of H_2S in effluent waters leaving the anaerobic cells varied widely from month to month and from cell to cell, from levels below detection (~0.01 mg/L) to as high as 50 mg/L. Throughout the cells, pH remains circumneutral (pH = 7 ± 0.5) for most of the year. Water temperature varied from ~20°C in the summer to ~1°C in the winter months. A positive correlation was noted between H_2S levels and temperature. In addition, freezing of the top few feet of substrate in the winter months resulted in a decrease in hydraulic residence time, which adversely effected bacterial H_2S production.

The dissolved concentrations of Cu, Cd, Fe, and Zn initially decreased rapidly with increase in $\{H_2S\}$, but then appeared to level off. In the presence of mg/L levels of H_2S, the threshold concentrations of Cu, Fe, and Zn, were ~2 μg/L, ~100 μg/L, and ~20 μg/L, respectively. In contrast, Mn levels were not effected by H_2S. Dissolved As levels often increased in the anaerobic cells to levels as high as 50 μg/L, indicating mobilization of As out of the wetlands substrate.

Thermodynamic modeling indicates that the majority of the dissolved metal leaving the anaerobic cells was present as aqueous sulfide complexes. In most cases, the observed concentrations are close to the computed theoretical solubilities for amorphous or poorly crystalline sulfides. However, the generally poor agreement in published low temperature studies of sulfide mineral solubility precludes a precise determination of reaction stoichiometries. In addition, modeling predicts that metal concentrations should go through a solubility minimum and then begin to increase with increase in H_2S concentration, as shown by the stoichiometry of reactions (2) through (4). With the possible exception of As, none of the metals monitored in our study displayed this type of U-shaped solubility relationship in the field. In the case of As, it appears that the measured concentrations are too low to be saturated with amorphous As_2S_3, although some other solid, such as As-rich pyrite or another Fe-sulfide phase, may be exerting a solubility control on this metal.

Analysis of data from the treatment wetlands in Butte offers a unique chance to see how well published experimental data on the stability of metal sulfide complexes at low temperature compares with our observed metal concentrations. Data interpretation is still in progress, and SEM/XRD characterization of sulfide precipitates may yield additional insight as to the precise minerals formed in this artificial wetlands environment.

ARE OCEANIC NITROGEN AND PHOSPHORUS CYCLES LINKED BY DENITRIFICATION AND PHOSPHOGENESIS IN UPWELLING MARGINS?

R. S. Ganeshram[1], T. F. Pedersen[2], and S. E. Calvert[2], [1]Department of Marine Chemistry and Geochemistry, Woods Hole Oceanographic Institution, Woods Hole MA 02543, USA (rganeshram@whoi.edu), [2]Department of Earth and Ocean Sciences, University of British Columbia, Vancouver V6T 1Z4, Canada (pedersen@eos.ubc.ca; calvert@eos.ubc.ca).

Water column denitrification and the burial of authigenic carbonate fluorapatite (CFA) are significant sinks for biologically available N and P in the modern ocean. Both processes occur at globally significant rates on upwelling continental margins bordering the Eastern Tropical North Pacific (ETNP), the Eastern Tropical South Pacific, the Arabian Sea, and the Eastern South Atlantic. We have investigated the spatial and temporal variations of these two processes in modern and Late Quaternary sediments off northwest Mexico (ETNP) using N-isotopic and formaninferal $\delta^{18}O$ measurements, AMS ^{14}C chronology, and solid-phase chemical measurements (Corg, opal, total P, Fe, and Al) in box and piston cores.

In the most recent sediments of the upper slope off northwest Mexico, CFA formation (phosphogenesis) and water column denitrification occur in close spatial proximity. The large flux of organic material and its degradation in the O minimum fuel globally significant rates of denitrification in the water column between 150 to 800 m. Authigenic CFA precipitation occurs in laminated organic-rich sediments that are in contact with O and nitrate-deficient waters. CFA occurs both as unconsolidated layers less than 1 cm thick, often visible in X-radiographs as dense layers containing up to 3 wt% P, and as disseminated grains. Thus, upwelling-induced productivity exerts a common mechanistic control on CFA formation and denitrification. On this margin, the large fluxes of organic matter fostering intense O deficiency and denitrification in the water column, also leads to the accumulation of organic-rich sediments with large quantities of remineralizable organic P. Suboxic diagenesis in organic-rich sediments bathed in bottom waters with near-zero O contents promotes phosphogenesis by elevating P concentrations in the interstitial waters.

Coherent glacial-interglacial variations in phosphogenesis and denitrification are also evident in a 10-m-long piston core raised from the upper slope off northwest Mexico. CFA layers as a rule are confined to laminated interglacial sediments rich in organic C and opal (isotope stages 1, 3, and 5) and are absent in organic C-poor bioturbated interglacial sections. The $\delta^{15}N_{total}$ record shows cyclic variations, heavier values (>8‰) indicating denitrification being largely confined to laminated interglacials and lighter values (6‰) being confined to glacials. Collectively, these results suggest that well oxygenated conditions prevailed in the O minimum and in the upper slope sediments off northwest Mexico during the glacial periods resulting in substantial reductions in denitrification and CFA precipitation. This diminishment is attributed to lower upwelling-induced productivity off northwest Mexico inferred from margin-wide decreases in the accumulation of Corg, opal and biogenic Ba in glacial sediments.

Available evidence indicates that the Late Quaternary history of phosphogenesis and denitrification off Peru and on the Arabian Sea margins may have been similar to that on the Mexican margin. The implications of these results for glacial-interglacial variations in oceanic nutrient contents, Redfield ratios, productivity and atmospheric pCO_2 will be discussed.

PHOSPHATE AND ARSENATE COMPLEXATION AT THE SURFACE OF GOETHITE IN 0.7 M SODIUM CHLORIDE SOLUTION.

Y. Gao and A. Mucci, Department of Earth and Planetary Sciences, McGill University, 3450 University Street, Montréal, Quebec, Canada (ygao@eps.mcgill.ca).

Laboratory experiments and freshwater studies have demonstrated that iron oxyhydroxides are strong sorbents for phosphate, arsenate, and they appear to dominate the chemical behavior of Group V elements in natural environments [1]. For example, it is believed that phosphate and arsenate are scavenged from the water column by settling particles during the mixing of freshwater and seawater in estuarine systems [2,5]. In sediments, phosphate and arsenate porewater concentrations and their flux to/from the overlying waters are limited by their strong affinity to authigenic iron oxyhydroxides that accumulate in oxic sediments [3,4].

Goethite, a crystalline iron oxyhydroxide (α-FeOOH), is the most widespread iron oxide in natural systems and has been used extensively in various adsorption studies including phosphate. Adsorption studies of arsenate onto the goethite surface have not been carried out and the nature of phosphate and arsenate interaction, as well as their competitive adsorption on the goethite surface in strong and complex electrolyte solutions like seawater, is unknown.

Potentiometric titrations of the goethite-water interface were carried out at 298.2 K in 0.1, 0.3, and 0.7 M NaCl solutions. The acid/base properties of goethite in 0.7 M NaCl solution can be described using two intrinsic surface acidity constants:

$$>FeOH + H^+ = >FeOH_2^+ \qquad \log K_1 = 7.45 \pm 0.06$$
$$>FeOH = >FeO^- + H^+ \qquad \log K_2 = -9.60 \pm 0.13$$

These experimental data as well as the results of phosphate and arsenate surface complexation studies were treated using a constant capacitance model and the computer program FITEQL. The specific capacitance of the goethite surface in a 0.7 M NaCl solution was determined to be 1.86 F m^{-2}.

Phosphate and arsenate complexation at the surface of goethite was studied by batch adsorption experiments. The experiments were conducted in 0.7 M NaCl solutions at 298.2 K in the pH range of 3.0 to 10.0. Phosphate shows a strong affinity for the goethite surface and the amount of phosphate adsorbed decreases with increasing pH. Phosphate complexation is described using a model consisting of three surface intrinsic constants.

$$>FeOH + H_2PO_4^- = >FePO_4^{2-} + H^+ + H_2O \qquad \log K_1 = 0.70 \pm 0.46$$
$$>FeOH + H_2PO_4^- = >FePO_4H^- + H_2O \qquad \log K_2 = 7.83 \pm 0.06$$
$$>FeOH + H_2PO_4^- + H^+ = >FePO_4H_2^0 + H_2O \qquad \log K_3 = 12.47 \pm 0.20$$

Arsenate shows a similar adsorption pattern on goethite but a higher affinity than phosphate. A model including three surface complexation constants also describes the arsenate adsorption.

$>FeOH + H_2AsO_4^- = >FeAsO_4^{2-} + H^+ + H_2O \quad \log K_1 = 1.24 \pm 0.23$
$>FeOH + H_2AsO_4^- = >FeAsO_4H^- + H_2O \quad \log K_2 = 8.24 \pm 0.10$
$>FeOH + H_2AsO_4^- + H^+ = >FeAsO_4H_2^0 + H_2O \quad \log K_3 = 12.75 \pm 0.14$

The experimental investigation of phosphate and arsenate competitive adsorption in 0.7 M NaCl was performed at $[PO_4]/[As]$ ratios of 1:1, 2.5:1, and 5:1. The complexation of both phosphate and arsenate decreases in competitive adsorption experiments. The equilibrium model derived from the binary subsystems (phosphate-goethite, arsenate-goethite) predicts the phosphate adsorption behavior but fails to reproduce the arsenate adsorption data. In competitive adsorption experiments, arsenate adsorption is lower than the model prediction and the discrepancy increases with increasing pH.

References: [1] Millward G. E. et al. (1985) in *Oceanic Process in Marine Pollution* (T. P. O'Conner et al., eds.), pp. 133–143. [2] Froelich P. N. et al. (1982) *Am. J. Sci., 33,* 649–668. [3] Sullivan K. A. and Aller R. C. (1996) *GCA, 60,* 1465–1477. [4] Sundby B. et al. (1992) *Limnol. Oceanogr., 37,* 1129–1145. [5] Tremblay G. H. and Gobeil C. (1990) *Mar. Poll. Bull., 21,* 465–469.

EVIDENCED REDOX DISEQUILIBRIUM FROM IRON AND ARSENIC BEHAVIOR IN TAILING LECHEATE (CHENI SITE, FRANCE).

O. L. Gaskova[1,2], M. Azaroual[2], F. Bodenan[2], and E. Gaucher[2], [1]UIGGM SB Russian Academy of Sciences, 630090 Novosibirsk, Russia (kolon@uiggm.nsc.ru), [2]BRGM, 45060 Orleans cedex2, France.

Introduction: The comparison of field-measured and computed from Fe^{3+}/Fe^{2+} and $H_2AsO_3^-/H_2AsO_4^-$ redox couples Eh values have been done. Problems associated with the concept of oxidation-reduction potential are discussed in connection with the possible internal disequilibrium in groundwater [1]. Because the ratio of all redox sensitive elements depends on their speciation in aqueous solution and solid phases, an extensive literature search to compile and critically evaluate the available thermodynamic data for arsenic species (at ambient conditions) was conducted [2]. Consistent data for metal-arsenate complexes and arsenate minerals were introduced in the database of EQ3NR [3] and used for modeling the thermodynamic state of a leachate, issued from meteoric weathering of old French arsenopyrite mine tailings.

Sampling and Speciation Calculations: Cheni's tailings are the result of gold ore mining from sulfide-quartz veins. Water from a saturated zone was sampled in five piezometers located in the heap (pz1), in 3 basins separated by dams (pz2, 5, 3), and near the river behind second dam (pz4). Measurements performed in the field include temperature, pH, Eh, total alkalinity, and dissolved reduced species of Fe (Fe^{2+}) and As (As^{3+}). Concentrations of other dissolved components (Na, K, Ca, etc.) where determined in BRGM laboratory using standard techniques. A comparative As and Fe total concentrations is presented in Fig.1. Only leachate of pz2 (points 5–8) shows acid pH (3.6–3.7), other fluids have near-neutral pH values (6–7).

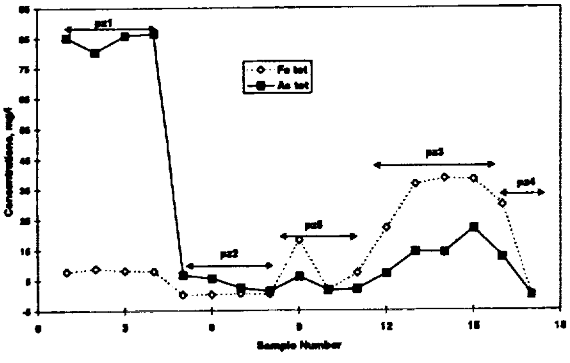

Fig. 1. Correlation between Fe and As concentrations in tailing leachates.

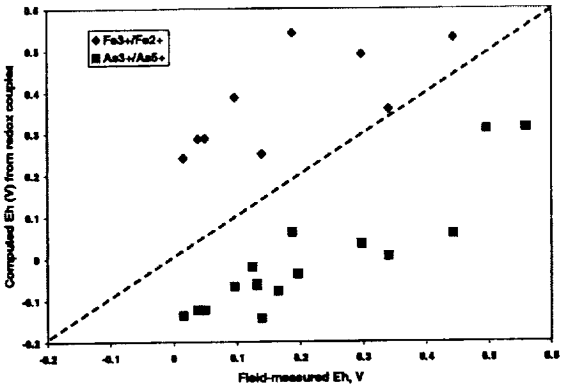

Fig. 2. Nernstian Eh values vs. field-measured Eh.

The EQ3NR speciation calculation is constrained by introduction of arsenate and arsenite, Fe(II) and Fe(III) concentrations separately into the input file. Consequently, the possible redox disequilibrium presented by these redox couples can be assessed. Results of these computations showed that the most important complexes of As are: $H_3AsO_3^0$ for As^{3+}, $FeAsO_4^0$, and $H_2AsO_4^-$ in acid conditions, and $Fe(AsO_4)_2^{3-}$ in near-neutral solutions for As^{5+}. For Fe, the main aqueous species are: Fe^{2+} and hydroxocomplexes for Fe^{3+} when $FeAsO_4^0$ is an important Fe-species only at low pH.

Redox Disequilibrium Conditions in Tailing Leachate: Figure 2 shows the results of computed Nerstian Eh data vs. field-measured Eh values. The dashed line presents the expected location of points if computed redox couples were at internal equilibrium.

One can see a wide range of computed Eh values, and the disequilbrium is clearly demonstrated. The negative deviation is for As couple (mean 0.22 V) and due to the low concentrations of Fe^{2+} in oxidizing conditions the deviation is positive for Fe^{3+}/Fe^{2+} (mean 0.18 V). The Eh measurement uncertainties being ±0.05 V. Consequently, the classical approach of redox equilibrium adopted in aqueous speciation calculations using Eh field measured values is not appropriate. Moreover, it is known that arsenate adsorption rate (the order of hours) is much more faster than the arsenite oxidation rate (the order of months). The combination of precise field measurements (i.e., specific electrodes, etc.) with more advanced geochemical models as in [4] allows a better understanding of pollutant transfer mechanisms in hydrogeochemical systems.

Acknowledgments: This work has been carried out with the financial support of the French "Région Centre" and BRGM.

References: [1] Lindberg R. D. and Runnells D. D. (1984) *Science, 225,* 925–927. [2] Gaskova O. and Azaroual M. (1999) *BRGM Report,* R 99-XX. [3] Wolery T. J. (1992) *EQ3NR, Theoretical Manual, User's Guide,* 246 pp. [4] McNab W. W. and Narasimhan T. N. (1994) *Water Res. Research, 30,* 2619–2635.

SUBCONTINENTAL MANTLE BELOW EIFEL, GERMANY: CONSTRAINTS BY NOBLE GASES.

C. Gautheron[1], M. Moreira[2], J. Kunz[1], J. L. Joron[3], M. Kurz[2], and C. J. Allègre[1], [1]Laboratoire de Géochimie et Cosmochimie, 4 place Jussieu, 75252 Paris Cedex 05, France (gauthero@ipgp.jussieu.fr), [2]Department of Marine Chemistry and Geochemistry, Woods Hole Oceanographic Institution, Woods Hole MA 02543-1541, USA (mmoreira@whoi.edu), [3]Laboratoire Pierre Süe CE/Saclay, 91191 Gif-sur-Yvette, France (joron@nimitz.cea.fr).

Introduction: We have analyzed the noble gases in mantle xenoliths from Eifel (Germany) to characterize the effects of metasomatism on the European subcontinental mantle. An extensive rift system has been developed in the early Cenozoic within western and central Europe. The main phases of volcanic activity occurred in the Neogene. The rocks are generally alkali basalts that contain crustal and mantle xenoliths [1]. The xenoliths used in this study are harzburgites and lherzolites, subdivided into hydrated and dry xenoliths [2]. The first group is characterized by the presence of amphibole

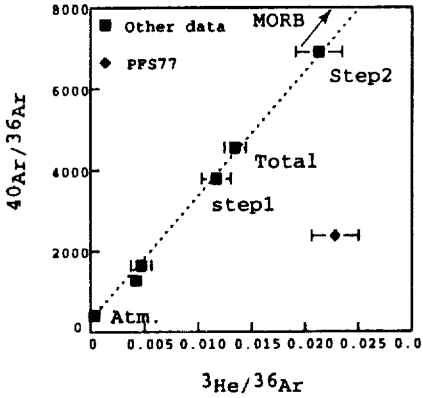

Fig. 1. Argon-40/argon-36 vs. $^3He/^{36}Ar$ showing a binary mixing. (The two step-crushings are indicated.)

and phlogopite. Pyroxene geothermometry yields equilibration temperatures of ≈1150°C for the anhydrous and ≈950°C for the hydrated xenoliths [2–3].

Results: We have analyzed noble gases in olivines, since they usually show a more pristine signature due to their low U and K contents. All the samples were crushed in vacuum in order to measure the compositions of He, Ne, and Ar trapped in the inclusions. The noble gas measurements were performed in Paris with ARESIBO II, and at the Woods Hole Oceanographic Institution (low-level He samples). The U and Th concentrations were obtained by instrumental neutron activation analysis (INAA) in Saclay.

Typical concentrations were: (2–90) × 10^{-9}, (1–100) × 10^{-13}, (4–270) × 10^{-12} ccSTP/g for ^4He, ^{22}Ne, and ^{36}Ar respectively. The He-isotopic ratios are very homogenous R/Ra = 5.5–6.7 (where R is the $^3He/^4He$ ratio and Ra the atmospheric ratio of 1.384 × 10^{-6}) but more radiogenic than the mean MORB ratio of 8 ± 1. These results are comparable to the results obtained on OPX and CPX from similar xenoliths [4].

The $^{20}Ne/^{22}Ne$ and $^{21}Ne/^{22}Ne$ ratios of our samples are distinct from air and the dots fall on the MORB line defined by [4]. The $^{38}Ar/^{36}Ar$ ratios are atmospheric, and the $^{40}Ar/^{36}Ar$ vary from atmospheric values (295.5) to more than 6900 (Fig. 1). They correlate also with the Ne-isotopic ratios.

Discussion: The results show a mixing between an airlike component and a mantle component. The mantle component is certainly the subcontinental mantle as indicated by the He-isotopic signature [5]. For the air component, two sources are possible: a contamination by atmospheric-like fluids near the surface (or after eruption), or fluids coming from dehydratation of subducted material. Several studies on fluid inclusions and pyroxenes from hydrated xenoliths from Eifel have shown that they have equilibrated at mantle temperatures, hence they must come from a minimum depth of 50 km [2–3,6]. The noble gases we analyzed come from these fluid inclusions. This implies that an atmospheric component could be present in the local subcontinental mantle [7]. The atmospheric fluids are attributed to recycling of altered oceanic lithosphere or sediments into the mantle via subduction, as suggested in [8]. However, we cannot totally preclude a shallow-level contamination.

Moreover, we did not find any evidence for a mantle plume coming from the lower mantle as a source of magmatism in the Eifel.

References: [1] Wison M. and Downes H. (1991) *J. Petrol., 32,* 811–849. [2] Stosch H.-G. and Seck H. A. (1980) *GCA, 44,* 457–470. [3] Stosch H.-G. and Lugmair (1986) *EPSL, 80,* 281–298. [4] Dunaï T. J. and Baur H. (1995) *GCA, 59,* 2767–2783. [5] Sarda P. et al. (1988) *EPSL, 91,* 73–88. [6] Seck H. A. and Wedepohl K. H. (1983) *Plateau Uplift,* pp. 343–349, Springer-Verlag. [7] Kempton et al. (1988) *EPSL, 89,* 273–287. [8] Bach W. and Nidermann S. (1998) *EPSL, 160,* 297–309.

ICELANDIC MANTLE STRUCTURE OR BASALT SEASONALITY?

M. A. M. Gee[1], M. F. Thirlwall[1], R. N. Taylor[2], and B. J. Murton[2], [1]Department of Geology, Royal Holloway, University of London, Egham, Surrey TW20 OEX, UK (m.gee@rhbnc.ac.uk), [2]Southampton Oceanography Centre, Empress Dock, European Way, Southampton SO14 3ZH, UK.

Introduction: We present chemical and isotopic data from Icelandic and associated Reykjanes Ridge lavas that show a spatial variation in the contribution to those lavas from isotopically distinct mantle sources. Three of these source components are isotopically defined here based on the characteristics of the most representative Icelandic lavas. Strontium-87/strontium-86, $^{143}Nd/^{144}Nd$, and $^{206}Pb/^{204}Pb$ of these lavas are: enriched (E): 0.7035, 0.51295, 19.3; depleted (D) 0.70287, 0.51315, 17.9; and odd (O) 0.7034, 0.513025, 18.00. Icelandic lavas tend to have a higher contribution from the E-source in the area closest to the proposed plume center, peripheral areas show increased contribution from D- and O- sources, while the Reykjanes Ridge lavas predominantly reflect the D-source. Reykjanes Peninsula lavas that define the D- and O- sources have MgO >10 wt%, are incompatible element depleted (Zr/Nb >20) and of a similar age, being erupted shortly after the end of the last glacial period [1]. Conversely, lavas with E-source characteristics are relatively incompatible element enriched (Zr/Nb <7), but also include high-MgO samples.

Discussion: Lanthanum/yttrium vs. Zr/Nb (Fig. 1) define a tight array. Depleted lavas, Zr/Nb >20, are fitted by variable pooled fractional melts from depleted mantle in spinel-facies. Samples with Zr/Nb <20 require an addition of melt from garnet-facies mantle. Those samples best fitted by a spinel-only melting trajectory also have higher SiO_2 and lower Fe_2O_3 for a given MgO than those lavas requiring contribution from garnet-facies. Consequently, major and trace elements indicate that the parental melts for these picritic lavas come from above the garnet to spinel transition zone (<60 km). Conversely, lavas with E-source characteristics require some input of garnet-facies melts from a chemically less-depleted source. The majority of the lavas erupted on the Reykjanes Peninsula however, arise from mixtures of varying degrees of melt from both garnet- and spinel-facies mantle. Lavas that reflect various aggregates of fractional melts from isotopically distinct mantle sources are closely related in space and time. Depleted flows are bracketed within 2–3 ka by lavas produced by lower degrees of melting, some of which took place in garnet facies and with a contribution from the E-source. Only the shallow lavas erupted at the end of the last glacial period define the D- and O-sources on the Reykjanes Peninsula. Lavas erupted in the past 7 ka are mixtures of melts from different depths, sources, and degrees of melting.

Shallow melts can evidently be extracted from the mantle without mixing with deeper garnet-facies melts. It follows that while shallow melts can be used to constrain very shallow mantle composition and structure this need

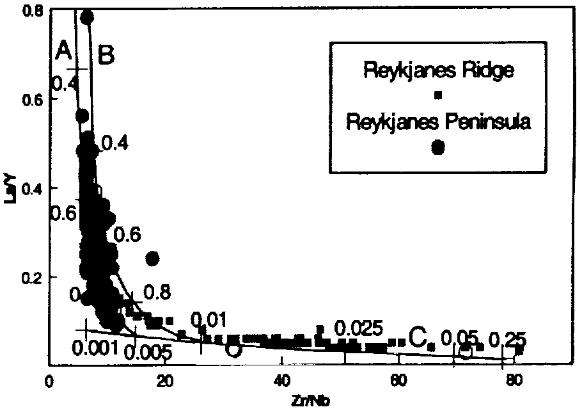

Fig. 1. Reykjanes Peninsula data: hollow circles ID-TIMS or ICP-MS, filled circles XRF (La >2.2 ppm). Reykjanes Ridge data ICP-MS. Point-average fractional melting trajectory in spinel-facies (C) for a depleted source with La/Y = 0.0138 and Zr/Nb = 78 labeled with percent melting. Mixing curves between 0.0001% and 0.005% garnet-facies MORB-source melts and 0.005% and 0.01% melts from the depleted mantle described above (A and B respectively), the percentage of spinel-facies melt in the mixture is labeled.

not be related to deeper mantle structure and composition. The structure of deeper mantle is less clear in that all mantle contributing to the melt must become increasingly chemically depleted as melting continues, reducing the chemical (and isotopic) domination of mixtures by melts from relatively enriched mantle. Residual melt will also provide further opportunities for chemical and isotopic "smoothing," thus disguising the scale of mantle heterogeneity.

References: [1] Gee M. A. M. et al. (1998) *EPSL, 148,* 1–8.

MINERAL FORMATION AND REDOX-SENSITIVE TRACE ELEMENTS IN A NEAR-SURFACE HYDROTHERMAL ALTERATION SYSTEM.

A. U. Gehring[1], P. M. Schosseler[2], and P. G. Weidler[3], [1]Eidgenössische Technische Hochschule Zentrum, 8092 Zürich, Switzerland (gehring@sl.ethz.ch), [2]Laboratorium für Physikalische Chemie, Eidgenössische Technische Hochschule Zürich, 8092 Zürich, Switzerland, [3]Institut für Terrestrische Ökologie, Eidgenössische Technische Hochschule Zürich, 8952 Schlieren, Switzerland (weidler@ito.umnw.ethz.ch).

A recent hydrothermal mudpool at the southwestern slope of the Rincón de la Vieja volcano in northwest Costa Rica exhibits an argillic alteration system formed by intense interaction of sulfuric acidic fluids with wall rock materials. Detailed mineralogical analysis revealed an assemblage with kaolinite, alunite, and opal-C as the major mineral phases. Electron paramagnetic spectroscopy (EPR) showed three different redox-sensitive cations associated with the mineral phases. Cu$^+$ is structure-bound in opal-C, whereas VO^{2+} and Fe^{3+} are located in the kaolinite structure. The location of the redox-sensitive cations in different minerals of the assemblage is indicative of different chemical conditions. The formation of the alteration products can be described schematically as a two-step process. In a first step alunite and opal-C were precipitated in a fluid with slightly reducing conditions and a low chloride availability. The second step is characterized by a decrease in K$^+$ activity and subsequent formation of kaolinite under weakly oxidizing to oxidizing redox conditions as indicated by structure-bound VO^{2+} and Fe^{3+}.

The detection of paramagnetic trace elements structure-bound in mineral phases by EPR provide direct information about the prevailing redox conditions during alteration and can, therefore, be used as additional insight into the genesis of the hydrothermal, near-surface system.

HYPERTHERMOPHILIC MICROORGANISMS IN ARSENIC-RICH HOT SPRINGS.

T. M. Gihring, G. K. Druschel, and J. F. Banfield, Department of Geology and Geophysics, University of Wisconsin–Madison, 1215 W. Dayton Street, Madison WI 53706, USA (tgihring@students.wisc.edu).

Introduction: Mineral and water samples from As-rich geothermal environments were characterized. Hyperthermophilic microorganisms were found living at the vents of Growler Hot Spring and Morgan Hot Springs at temperatures in excess of 90°C and As(III) concentrations up to 13.4 ppm. Mineral samples from the Morgan Hot Springs were found to contain the arsenic-sulfide mineral Realgar (AsS).

A previous study performed by Sorey et al. [1] describes a loss of As as waters flow downstream from the Growler and Morgan Hot Springs. The removal of As from solutions has been attributed to chemical oxidation and subsequent absorption to streambed sediments. Biological activity may also play an important role in As removal in these environments through either microbial As oxidation resulting in absorption and/or sulfate reduction leading to arsenic-sulfide precipitation [2].

Growler Hot Spring and Morgan Hot Springs are located south of Lassen Volcanic National Park in northern California. The geothermal waters discharging at these springs are slightly alkaline with high Na and chloride concentrations [1,3]. Mineral and water samples were collected from the outflow of the main vent at Growler Hot Spring and at approximately 90 cm and 180 cm downstream from the vent. Slime streamers approximately 240 cm downstream were also collected. Additional samples were collected from the main vents of two unnamed springs at Morgan Hot Springs designated as A and B.

Temperature, pH, conductivity, and dissolved O were measured in the main vents of the hot springs using portable meters and electrodes. Growler Hot Spring measured 94.1°C and pH 7.48, while conductivity and dissolved O were 6.66 mS/cm and 0.16 ppm respectively. The temperature of Morgan Hot Spring A was 93.2°C with a pH of 7.48, conductivity of 6.84 mS/cm, and dissolved O concentration of 0.21 ppm. The temperature, pH, conductivity, and dissolved O measurements at Morgan Hot Spring B were 91.1°C, 7.49, 6.92 mS/cm, and 0.48 ppm respectively. Temperatures reported were the maximum readings.

Samples for biological assays were transferred directly to fixative on site and transported to the lab on ice. Microbial cells were visualized and counted using an epifluorescence microscope and the DNA stain 4', 6 diamidino-2-phenylindole (DAPI). Fluorescence *in situ* hybridizations were performed to quantify cells belonging to the domains Bacteria, Archaea, and Eukarya.

Microorganisms of two distinctly different morphologies are present at all three hot springs sampled. Cells occur as either long, segmented filaments or as cocci. By fluorescence *in situ* hybridizations it was determined that both cell types are Archaea.

Cell numbers at the Growler Hot Spring were estimated to be ~2 × 10^9 cells/mL of saturated sand-sized minerals with >99% cocci at the vent outflow, 75% cocci and 25% filaments at 90 cm, and 40% cocci and 60% filaments at 180 cm downstream. Slime streamers 240 cm downstream from the vent were >99% filaments.

Morgan Hot Spring A was estimated to have approximately 5.0 × 10^8 cells/mL with 52% cocci and 48% filaments. Morgan Hot Spring B was estimated to have ~3.0 × 10^8 cells/mL with 70% cocci and 30% filaments.

Arsenic concentrations (determined using HPLC) at the Growler, Morgan A, and Morgan B vents were measured to be 9.0 ppm As(III), 13.4 ppm As(III), and 10.0 ppm As(III) respectively. Arsenic(V) was not detected at any of the hot-spring vents. X-ray diffraction was used to identify realgar present in mineral samples from Morgan A and B hot springs.

References: [1] Sorey M. L. et al. (1994) *USGS Water Resources Investigations Report 94-4180-B.* [2] Rittle K. A. et al. (1995) *Geomicrobiology Journal, 13,* 1–11. [3] Thompson J. M. (1985) *Journal of Volcanology and Geothermal Energy, 25,* 81–104.

THE EFFECT OF pH AND OXYGEN FUGACITY ON METAL MOBILITY BY METAL-CARBOXYLATE COMPLEXES.

T. H. Giordano, Department of Geological Sciences, New Mexico State University, Las Cruces NM 88003, USA (tgiordan@nmsu.edu).

Introduction: Metals commonly found in ore, gangue, and host-rock minerals have aqueous mobilties that are controlled by the complexation capacity, pH, and oxidation state of the fluid. Organic ligands are common constituents in many low to moderate temperature (<200°C) aqueous fluids in supergene and diagenetic ore-forming environments as well as supergene environments responsible for secondary dispersion of ore constituents. Humic and fulvic acids and carboxylic acid anions (acetate, propionate, oxalate, malonate, succinate, and glutarate) are the dominant dissolved organic ligands in surface/shallow subsurface environments and deep sedimentary basins respectively.

Carboxylate Ligands: It is well documented through the use of speciation models that common rock- and ore-forming metals are mobilized by metal-carboxylate complexes in deep sedimentary basins [1]. However, a more useful way to investigate the significance of these complexes as transport agents is to construct solubility contours for these complexes in log f_{O_2}-pH space for deep diagentic fluids with specified bulk compositions and temperature/pressure conditions [2]. These diagrams provide a means to evaluate rapidly, for a wide range of diagenetic and ore-forming conditions, mechanisms of metal transport and deposition involving metal-carboxylate complexes. Log f_{O_2}-pH/solubility relationships show that metal-carboxylate complexing can significantly influence metal transport in fluids characterized by pHs in the range of 5–8, oxidation states above the sulfate-sulfide boundary, and average to high concentrations of carboxylate ligands.

References: [1] Giordano T. H. and Kharaka Y. K. (1994) *Geol. Soc. Spec. Pub., 78,* 175–202. [2] Wood S. A. (1998) *Rev. Econ. Geol., 10,* 81–96.

BLACK CARBON IN TERRA PRETA SOILS OF THE BRAZILIAN AMAZON REGION.

B. Glaser[1], G. Guggenberger[1], L. Haumaier[1], and W. Zech[1], [1]Institute of Soil Science and Soil Geography, University of Bayreuth, D-95440 Bayreuth, Germany (bruno.glaser@uni-bayreuth.de).

Abstract: In the Brazilian Amazon region, patches of highly fertile anthropogenic soils, known as Terra Preta occur within the Oxisol and Ultisol landscape. Terra Preta soils are characterized by a large and stable soil organic matter (SOM) pool. Frequent charcoal findings provided evidence that black carbon is decisive for the SOM stability in these soils.

Black carbon was analyzed in the fine-earth, in particle-size and density fractions of Terra Preta and surrounding Oxisols with a novel technique using benzenecarboxylic acids (BCA) as specific markers for black carbon [1]. The analytical procedure includes acid digestion, oxidation, sample cleanup, derivatization, and gas chromatography.

The SOM of Terra Preta consists up to 30% of black carbon, which remains as residue after incomplete burning of biomass. Terra Preta (16–122 Mg ha^{-1} m^{-1}) contains up to 35× more black carbon than adjacent Oxisols (3–13 Mg ha^{-1} m^{-1}). More than 50% of black carbon is located in the silt and clay fraction indicating organo-mineral complexation. An increase of the black carbon content in the clay fraction with increasing soil depth makes leaching probable. Density fractionation, however, shows that the highest concentrations and absolute amounts of black carbon are located in the fraction <2.0 g cm^{-3}, even in 40-cm soil depth. This SOM fraction is assumed to be of particulate nature and corroborates the chemical and biological inertness of black carbon and favors the theory of transport by turbation into deeper soil horizons. On the other hand, black carbon is involved into organo-mineral complexation. This could be the reason for the high cation exchange capacities of Terra Preta. A small part of black carbon is embedded within plaques on the surface of minerals, isolated with the heavy fraction.

Our investigations show that the major part of black carbon in Terra Preta soils is of particulate nature and therefore chemically and microbiologically inert. A part of black carbon is involved in organo-mineral complexation and physical embedding.

References: [1] Glaser B. et al. (1998) *Organic Geochemistry, 29,* 811–819.

MUONG NONG-TYPE AUSTRALASIAN TEKTITES: IMPLICATIONS REGARDING THE PARENT MATERIAL AND SOURCE AREA.

B. P. Glass, Geology Department, University of Delaware, Newark DE 19716, USA (Billy.Glass@mvs.udel.edu).

Introduction: In 1963, I took a course in geochemistry from Brian Mason in which he had all the students write a term paper on tektites. Shortly thereafter I was studying deep-sea cores taken south of Australia and I kept finding small glass beads that I was calling "cosmic spherules (?)." Another graduate student, Dave Folger, who had also taken Brian's course, suggested that they might be tektites. It made sense. I realized that the glass beads only occurred on or adjacent to the Brunhes/Matuyama geomagnetic reversal boundary, indicating that their stratigraphic age was they same as the radiometric age of the australite tektites. I eventually published a paper announcing the discovery of microtektites [1]. This led to an interest in tektites, and then to impact cratering, shock metamorphism, and distal impact ejecta, subjects that I have spent most of my professional life studying. After graduation, I had to spend two years active duty in the U.S. Army and through the help of John A. O'Keefe was assigned to Goddard Space Flight Center. It was there that I heard of a faculty position at the University of Delaware for which I applied and where I have been ever since. So you could say that Brian Mason is responsible for my entire professional career. Ironically, Brian remains somewhat skeptical about the genetic relationship between microtektites and tektites [2]. Thus, this abstract deals with Muong Nong-type Australasian tektites rather than microtektites.

When I first started studying tektites, the origin was not agreed upon. Today, most researchers agree that tektites are the products of terrestrial impacts [3,4]. Source craters have been found for three out of the four known tektite strewnfields; however, the source crater for the Australasian strewnfield remains elusive. Muong Nong-type tektites may hold the answer to this problem.

Muong Nong-type Tektites: Muong Nong-type (MN) tektites are large, blocky, layered tektites found almost exclusively in the Indochina part of the Australasian strewnfield. MN tektites are compositionally and petrographically similar to the splash form and ablated tektites, but there are some important differences. They are compositionally more heterogeneous on a millimeter scale, and they have higher water and ^{10}Be contents [4], and unlike the splash form and ablated tektites, many MN tektites contain mineral inclusions.

Mineral Inclusions: Barnes [5] first reported detrital mineral gains (probably quartz) in MN tektites and Walter [6] was the first to report coesite. For several years we have been recovering mineral inclusions from MN tektites by crushing, sieving, and heavy-liquid separation [7]. In addition to quartz and coesite, we have recovered zircon, rutile, chromite, monazite, and a corundum-bearing phase. Quartz, zircon, rutile, chromite, and monazite appear to be relict grains, i.e., mineral grains that were present in the parent material that was melted to produce the tektite glass. On the other hand, coesite and the corundum-bearing phase are shock-produced phases. Coesite is a high-pressure phase produced from quartz. The corundum-bearing grains have an Al_2SiO_5 composition and appear to have formed by the breakdown of an Al_2SiO_5 mineral to corundum plus SiO_2 glass. Inclusion concentration (number per unit sample weight) varies from zero to over 2000 per 10 gm of tektite sample. The mineral inclusions generally range between ~20 and 200 µm and are size sorted according to density. The mineral inclusions show evidence of shock metamorphism including fragmentation, X-ray asterism, partial melting (especially rutile), and thermal decomposition (some of the zircons have partially decomposed to baddeleyite).

Discussion and Conclusion: The size, shape, sorting, and mineral assemblage of the inclusions recovered from MN tektites indicates that the parent material was a fine-grained, well-sorted sedimentary deposit [7]. A more recent study of the geographic variations in the concentration of mineral inclusions indicates that the highest concentration occurs in MN tektites from central Laos and adjacent eastern Thailand [8]. MN tektites from this region are also more likely to contain relict phases with lower melting temperatures, such as quartz and rutile, in addition to the phases with higher melting temperatures. Assuming that the degree of shock metamorphism increases away from the source crater, geographic variations in the concentration and kinds of mineral inclusions suggest that the source crater should be in the central Laos-eastern Thailand region. This study is continuing.

References: [1] Glass B. P. (1967) *Nature, 214,* 372–374. [2] Mason B. (1996) *Meteorite!, 2,* 11–15. [3] Taylor R. S. (1973) *Earth Sci. Rev., 9,* 101–123. [4] Koeberl C. (1994) *GSA Spec. Papers, 293,* 133–151. [5] Barnes V. E. (1964) *GCA, 28,* 1267–1271. [6] Walter L. S. (1965) *Science, 147,* 1029–1032. [7] Glass B. P. and Barlow R. A. (1979) *Meteoritics, 14,* 55–67. [8] Dass J. D. and Glass B. P. (1999) *LPS XXX,* 1081.

HOW DID THE GROWTH OF CONTINENTS INFLUENCE THE CHEMICAL AND ISOTOPIC EVOLUTION OF PRECAMBRIAN OCEANS?

Y. Goddéris[1], J. Veizer[2,3], and L. M. François[1], [1]LPAP-University of Liège, 5, Avenue de Cointe, 4000 Liège, Belgium (godderis@astro.ulg.ac.be; francois@astro.ulg.ac.be), [2]Department of Earth Sciences, University of Ottawa, Ottawa K1N6N5, Canada, [3]Institut für Geologie, Ruhr Universität, 44780 Bochum, Germany (veizer@geol.uottawa.ca).

A numerical model that couples C-S-Sr and atmospheric O cycles is used here to explore the impact of continental growth on the long term ($\geq 10^8$ yr) evolution of the isotopic composition of seawater [1]. Three growth scenarios are tested: "big bang" generation of continents shortly after the accretion of the Earth [2], and two more gradual scenarios, with a major growth episode around the Archean-Proterozoic boundary [3,4]. The corresponding ^{87}Sr/^{86}Sr, δ^{34}S and δ^{13}C of seawater, and the sizes of the respective crustal sedimentary reservoirs, are calculated for each scenario, and compared to the available data. The gradual continental growth scenarios yield a better fit to the existing ^{87}Sr/^{86}Sr and δ^{34}S-isotopic data for ancient seawater than does the "big bang" model. These scenarios also generate a progressive oxygenation of the ocean/atmosphere system, with a large pO_2 rise coincident with (and due to) the major continental growth event around the Archean-Proterozoic transition, in accord with the geologic record that indicates a major oxidation event in the early Proterozoic. The advancing oxygenation of the planetary exogenic system may therefore be a consequence of tectonic evolution, rather than of biological innovations, such as the photosystem 2. The latter may have predated considerably the impact of oxygenation visible in the geologic record. The model also generates a strong climatic cooling around the Archean-Proterozoic transition, coincident with the first glaciation of global extent in the early Proterozoic.

Seawater $\delta^{13}C$: The model also calculates the evolution of seawater $\delta^{13}C$. We show that a critical factor of the ocean-atmosphere-sedimentary ^{13}C cycle is the opening of this cycle to the mantle through the mid-oceanic ridge degassing over all the Earth history. Under the post-Early Proterozoic oxygenated conditions, only carbonates in close equilibrium with seawater return to the mantle at subduction zones, since there is only negligible accumulation of organic light C on the pelagic seafloor. This pushes the $\delta^{13}C$ of seawater towards equilibrium with mantle value (~–5‰) in a few hundred million years. This discrepancy with data can be solved if the MOR degassing became negligible after Archean times, but this is not in agreement with estimates of present day MOR degassing. We illustrate this problem with various model simulations. There is a strong need for a process able to remove or isolate light organic C from the ocean-atmosphere-sedimentary system.

Seawater $\delta^{18}O$: The calculated seawater $\delta^{18}O$ shows little fluctuations over the Earth history, in disagreement with the experimental record, at least for the Phanerozoic [5]. This inhibition is due to the links existing between ^{18}O and the C-alkalinity cycles [1], rather than to possible steady-state of the present-day ^{18}O cycle [6]. Focusing now only on the Phanerozoic (where reliable data exist [5]), we explore the possible range of fluctuations of the $\delta^{18}O$ compatible with a realistic C-alkalinity cycle in the ocean-atmosphere-sediments system. We show that fluctuations of ~2–3‰ are conceivable over the Paleozoic times, and compatible, at least qualitatively, with the simultaneous increase in observed seawater $\delta^{13}C$.

References: [1] Goddéris Y. and Veizer J. (1999) submitted. [2] Sylvester P. J. et al. (1997) *Science, 275,* 521–523. [3] Veizer J. and Jansen S. L. (1979) *J. Geol., 93,* 624–643. [4] Taylor S. R and Mc Lennan S. M. (1995) *Rev. Geophys., 33,* 241–265. [5] Veizer J. et al. (1999) *Chem. Geol.,* in press. [6] Muehlenbachs K. (1998) *Chem. Geol., 145,* 263–273.

EVIDENCE FOR RADIUM-BARIUM FRACTIONATION IN MID-OCEAN-RIDGE BASALT PLAGIOCLASE: IMPLICATIONS FOR GEOCHRONOLOGY AND MANTLE MELTING.

S. J. Goldstein[1], K. W. W. Sims[2], K. M. Cooper[3], M. T. Murrell[1], and A. J. Nunn[1], [1]Los Alamos National Laboratory, CST Division, MS K484, Los Alamos NM 87545, USA (sgoldstein@lanl.gov), [2]Department of Geology and Geophysics, Woods Hole Oceanographic Institution, Woods Hole MA 02543, USA, [3]Department of Earth and Space Sciences, University of California, Los Angeles, 595 Charles Young Drive East, Los Angeles CA 90095, USA.

Introduction: Radium-226 (half-life = 1600 yr) is widely utilized in geochemistry as both a tracer and chronometer of a variety of processes occurring on timescales of 10,000 yr or less. In most geochronological and mantle melting studies involving this isotope, it is commonly assumed that Ba acts as a stable analog for Ra. Hence ^{226}Ra-^{230}Th-Ba isochrons are commonly used to date young igneous rocks, and Ra partitioning during melting and crystallization is usually assumed to be equivalent to that for Ba.

The occurrence and subsequent sampling of an eruption event at the Northern Gorda Ridge in 1996 has allowed us to evaluate Th, Ra, and Pa systematics for both plagioclase and whole rock fractions of a truly "zero-age" sample of mid-ocean ridge basalt (MORB). These results permit us to evaluate ^{226}Ra-^{230}Th-Ba internal isochrons for dating ocean basalts and potentially quantify any Ra/Ba fractionation.

Geochronology: Measurements of Ra in small amounts of separated plagioclase were very challenging (0.6 fg ^{226}Ra analyzed), leading to relatively large uncertainties (10–20% 2σ). However, the results for a ^{226}Ra-^{230}Th-Ba isochron based on plagioclase, glass, and bulk samples clearly define a slope that is greater than 1, resulting in an undefined age. The most straightforward explanation of this result is that Ra and Ba were fractionated during plagioclase crystallization, which means that in this case Ba is an inappropriate normalizing element. Assuming a negligible magma storage age for this mafic lava and therefore a zero-age isochron, the ratio of Ra/Ba partitioning in plagioclase relative to the glass is ~0.4. Although there are no experimental measurements of Ra partitioning in plagioclase for comparison, similar fractionation of Ra/Ba in plagioclase (factor of 0.2) can be calculated based on theoretical models of trace-element substitution involving the size and elasticity of the crystal lattice sites [1]. These results along with the theoretical models support the notion that Ba-normalized ^{226}Ra-^{230}Th isochrons involving plagioclase and probably other minerals may require significant correction for Ra/Ba fractionation. Similar Ra/Ba fractionation is also suggested from our dating of Hawai'ian basalts. However, all of these observations and models need to be verified with actual experimental measurements of Ra partitioning in plagioclase and other minerals.

Mantle Melting: These results may also have implications for use and interpretation of $^{226}Ra/^{230}Th$ data in mantle melting and transport models. Radium partitioning during mantle melting of garnet peridotite or spinel is most likely controlled by clinopyroxene, with lesser partitioning in olivine, orthopyroxene, and garnet [2,3]. Since the partition coefficient for Ra in clinopyroxene has not been experimentally determined under any conditions, it is commonly assumed to behave like Ba, for which experimental measurements are available [2,3]. However, when the theoretical model for Ra/Ba partitioning is extended to clinopyroxene under mantle melting conditions, a relatively large fractionation (factor of 0.04) is calculated. Hence for mantle melting of garnet peridotite, D_{Ra} (~5×10^{-7}) may be much smaller than D_{Ba} (~2×10^{-5}).

The effect of a lower value of D_{Ra} in mantle melting and transport can be evaluated for a variety of situations including batch and ingrowth models for production of the large (>100%) ^{226}Ra excesses in MORB. Using a typical value of D_{Th} for garnet peridotite of 0.0014 [e.g., 3,4] and $D_{Ra} = 5 \times 10^{-7}$, the batch melting limit (melt fraction near zero) for Ra/Th fractionation is ~2800, as opposed to a value of ~70 based on Ba partitioning. This leads to significantly larger Ra/Th fractionation for a given melt fraction than would be predicted based on Ba partitioning. For ingrowth models which take into account the dynamics of mantle upwelling (e.g., dynamic melting and chromatographic melting), the length of time that Th spends in the melt column also influences the $^{226}Ra/^{230}Th$ activity ratio of the melt. Therefore, for ingrowth models where the melting or solid mantle upwelling rates are high and the ^{226}Ra excess is dominated by the initial Ra/Th fractionation, lower Ra partition coefficients would result in higher porosities for the melt column. However, as the melting rates decrease, ingrowth of ^{226}Ra during melting becomes important, and lower Ra partition coefficients have less influence on the calculated melt zone porosities.

References: [1] Blundy J. and Wood B. (1994) *Nature, 372,* 452–454. [2] Beattie P. (1993) *EPSL, 117,* 379–391. [3] Lundstrom C. C. et al. (1994) *EPSL, 128,* 407–423. [4] LaTourrette T. Z. and Burnett D. S. (1992) *EPSL, 110,* 227–244.

STRONTIUM ISOTOPES IN SOUTH ATLANTIC DETRITUS: A SURFACE CURRENT PROXY AND TRACER OF AGULHAS LEAKAGE.

S. L. Goldstein[1,2], S. R. Hemming[1,2], S. Kish[1,3], and R. Rutberg[1], [1,2]Lamont-Doherty Earth Observatory, Columbia University, Palisades NY 10964, USA, [2]Department of Earth and Environmental Sciences, Columbia University, Palisades NY 10964, USA, [3]Indiana University of Pennsylvania, Indiana PA 15705, USA.

Terrigenous clastic sediments are brought to the ocean from continents via rivers, ice and wind, and distributed by surface and deep currents. Due to variations in the age, history, and geochemistry of the continental sources, Nd-Sr-Pb isotopes in terrigenous detritus can trace the sources, and the transport processes leading to their deposition in marine sediments.

We report the first high-resolution record of detrital $^{87}Sr/^{86}Sr$ in a deep-sea core. RC11-83 (41.07°S–9.72°E, 4718 m), from the Cape Basin, southeast Atlantic, with a high sedimentation rate (~25 cm/k.y.) and high resolution stable isotopic record extending to the stage 4–5 transition [1,2].

Results display a striking periodicity coinciding with climatic stages (Fig. 1). Strontium-87/strontium-86 ratios are distinct in warm (~0.723) vs. cold (~0.717) intervals. Notable features of the pattern are (1) the sharpness of the interstadial Sr-isotopic shifts and coincidence with Stage boundaries, (2) small $^{87}Sr/^{86}Sr$ variations within stages relative to the interstadial differences, and (3) equivalence of $^{87}Sr/^{86}Sr$ ratios in warm stages 1,3,5. Throughout the core the Sr-isotopic shifts are remarkably coincident with shifts in

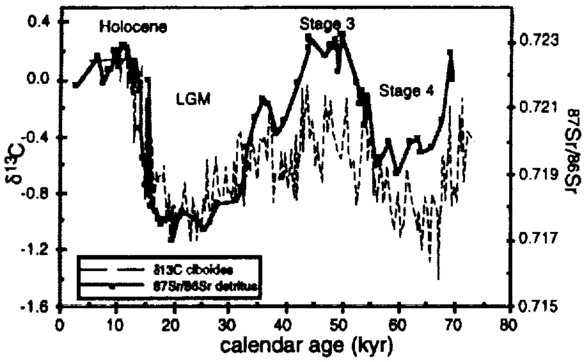

Fig. 1. Detrital $^{87}Sr/^{86}Sr$ and benthic $\delta^{13}C$ vs. age in RC11-83, south Atlantic, showing the linkage between the variations of the two proxies.

benthic foraminiferal $\delta^{13}C$. The mix of detritus thus alternated between distinct warm vs. cold climatic modes.

What controls the pattern of detrital Sr-isotopic variations? Possibilities include (1) local shifts in Cape Basin bottom current sediment transport; (2) changes in the deep southward flux of NADW, which has been suggested to explain the benthic $\delta^{13}C$ pattern of RC11-83 [1,2] and the clay mineral distribution in the south Atlantic [3]; (3) changes in the Antarctic Circumpolar Current; and (4) changes in surface currents. The few literature data from the southeast Atlantic [4] show $^{87}Sr/^{86}Sr$ ratios that are too low to explain the Holocene values of RC11-83.

Our new survey of detrital $^{87}Sr/^{86}Sr$ ratios in Holocene age core tops (Fig. 2) shows that high Sr-isotopic ratios are derived from sediment transported southward along the east coast of Africa. The transport path follows the Agulhas Current, indicating the high $^{87}Sr/^{86}Sr$ detritus is carried at shallow to intermediate depths. The Cape Basin is far to the west of the Agulhas Retroflection, where the bulk of Agulhas Current enters the ACC. However, a portion of the Agulhas Current leaks into the Atlantic, where it is swept northward in the Benguela Current to the Equatorial and North Atlantic. Comparison with the clay mineral distributions in the south Atlantic [3] indicates the general pattern may be controlled by surface currents.

Variations in intensity and direction of ocean currents have been among the most elusive paleoclimatic signals to track down. The Agulhas Leakage is an important means for return of heat and salt to the North Atlantic and an important positive feedback for the "great ocean conveyor" during warm climatic cycles [5]. The relationships observed suggest that this approach affords a means to address the glacial-interglacial history of the Agulhas Leakage and variations in South Atlantic surface current configurations.

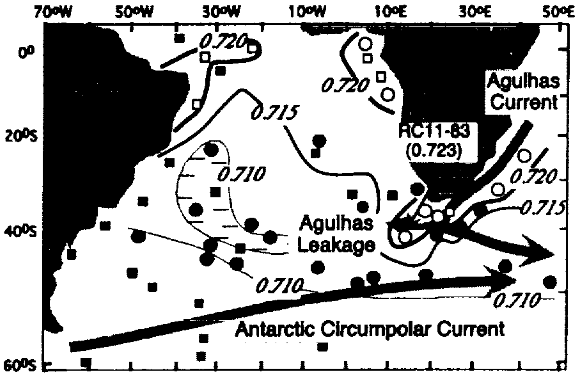

Fig. 2. Strontium-87/strontium-86 of Holocene detritus. The only regional source with the high Holocene values of RC11-83 is the east coast of Africa, indicating sediment transported by the Agulhas Current. Symbols: squares = data from [3]; circles = this study. Strontium-87/strontium-86 values: open symbols = >0.72; gray symbols = >0.715; black symbols = <0.715. Isolines are shown for 0.72, 0.715, and 0.710.

References: [1] Charles and Fairbanks (1992) *Nature, 355,* 416. [2] Charles et al. (1996) *EPSL, 142,* 19. [3] Petschick et al. (1996) *Mar. Geol., 130,* 223. [4] Dasch (1969) *GCA, 33,* 1521. [5] Gordon (1986) *JGR, 91,* 5037; Gordon et al. (1992) *JGR, 97,* 7223.

FROM A HOT SPOT TO A COLD SPOT: SPATIAL CORRELOGRAM ANALYSIS OF HELIUM-ISOTOPIC VARIATIONS ALONG THE SOUTHEAST INDIAN RIDGE.

D. W. Graham[1], F. J. Spera[2], J. E. Lupton[3], and D. M. Christie[1], [1]College of Oceanic and Atmospheric Sciences, Oregon State University, Corvallis OR 97331, USA, [2]Department of Geological Sciences, University of California, Santa Barbara CA 93106, USA, [3]Pacific Marine Environmental Laboratory/National Oceanic and Atmospheric Administration, Hatfield Marine Science Center, Newport OR 97365, USA.

Introduction: Relations between isotopic heterogeneity and convection in the Earth's mantle are central to geodynamics, and He isotopes have been especially important in this regard. High $^3He/^4He$ ratios at many ocean island hotspots (up to ~35 R_A, where R_A is the atmospheric ratio of 1.39×10^{-6}), along with relatively uniform values (7–9 R_A) in mid-ocean ridge basalts (MORB), are generally accepted to reflect a well-mixed upper mantle source for MORB and a deeper, less-degassed mantle source for ocean island basalts [1]. There is also considerable fine structure in $^3He/^4He$ along mid-ocean ridges away from hotspots, due to underlying mantle heterogeneity and the style of convection [2–7]. Here we present new He-isotopic results for MORB glasses along >5800 km of the Southeast Indian Ridge (SEIR). A long wavelength eastward decrease in $^3He/^4He$, from near the Amsterdam-St. Paul plateau to the Australian-Antarctic Discordance, coincides with sub-ridge mantle flow down a temperature gradient. Spatial correlogram analysis of the He-isotopic variations reveals a high degree of correlation (R >0.90) at length scales of ~400 km.

Background: The studied length of the SEIR stretches from the Rodrigues Triple Junction (25.6°S, 70.1°E) to an area east of the Australian Antarctic Discordance (AAD). The AAD is a region of deep axial bathymetry between 120°–128°E associated with relatively cold mantle and low melt production [8]. Between 76°–78°E, the SEIR crosses the Amsterdam-St. Paul (ASP) plateau, a shallow swell associated with hot mantle upwelling beneath Amsterdam and St. Paul islands. From 88°E to 120°E there is a large decrease in mantle temperature along axis, on the order of 150°C, marked by an increase in axial depth from 2400 m to >4000 m [8]. Given the nearly constant full spreading rate of 69–75 mm/yr and the absence of large transform offsets and nearby island hotspots, this portion of the SEIR provides a unique opportunity to study the geochemical effects of along-axis variations in upper mantle temperature.

Results: MORB glasses from 115 localities along the SEIR have been analyzed for $^3He/^4He$ by crushing in vacuum. Near the Amsterdam-St. Paul plateau, values range up to 14 R_A due to the influence of the nearby ASP mantle plume [7]. A long wavelength (2000 km) gradient in bathymetry, Fe_8 and $^3He/^4He$ stretches eastward, from 88°E to 120°E, resulting in $^3He/^4He$ ratios as low as 6.2 R_A in the AAD. Superimposed on the long-wavelength gradients there are nearly symmetric peaks in $^3He/^4He$ and Fe_8, ranging between 200 and 500 km in length including their tails. These $^3He/^4He$ peaks are most prominent near 88°E, 97°E, and 113°E longitude, and they diminish in amplitude toward the AAD. The covariation of $^3He/^4He$ and Fe_8 suggests that higher $^3He/^4He$ is associated with a higher mean pressure of melting in the underlying mantle. The peak structures cut across ridge segment boundaries such as transform faults, indicating that upwelling magma is poorly focused within the mantle along-strike of the ridge, and that melt redistribution within the crust of an individual ridge segment is minor. Spatial variation in the basalt He-isotopic compositions therefore tracks the length scale of variation in the underlying mantle.

We developed a computational algorithm to perform a spatial correlogram analysis of the He-isotopic variations. The correlation coefficient R is calculated between every pair of points at separation distance r. For each point pair, R(r) is given by the product of the deviations in $^3He/^4He$ from the population mean, normalized to the population variance [10]. The total number of point pairs (N) for n samples is given by N = n(n − 1)/2, which for our 115 sample localities gives 6555 sample pairs. The correlogram (R(r) vs. r) for all ^{3}He/^{4}He data (n = 115) shows the expected decrease in R(r) with separation distance, and has R(r) = 0 at r = 2000 km. A significant peak in R(r) (>0.90) occurs at r ~400 km. When MORB influenced by the ASP hotspot are excluded (n = 83), the correlogram is generally similar to that for the full data set, but R(r) is reduced (0.65) at r ~400 km, and R(r) = 0 at r = 1200 km.

Our correlogram results suggest the presence of convective mantle "cells" aligned orthogonally to the along-axis flow direction. For an aspect ratio of 1, these rolls would be ~200 km in diameter. They may be a feature induced by the wake of the Kerguelen plume [11], or they may be intrinsic to upper mantle convection in this region [12].

References: [1] Kurz M. et al. (1982) *Nature, 297,* 43–46. [2] Kurz M. et al. (1982) *EPSL, 58,* 1–14. [3] Mahoney J. et al. (1989) *JGR, 94,* 4033–4052. [4] Graham D. et al. (1992) *EPSL, 110,* 133–147. [5] Lupton J. et al. (1993) *GRL, 20,* 1851–1854. [6] Graham D. et al. (1996) *EPSL, 144,* 491–503. [7] Graham D. et al. (1999) *EPSL, 167,* 297–310. [8] Sempéré J.-C. et al. (1997) *JGR, 102,* 15489–15505. [9] Klein E. et al. (1991) *JGR, 96,* 2089–2107. [10] Danckwerts P. (1952) *App. Sci. Res., 3,* 279–296. [11] van Keken P. and Gable C. (1995) *JGR, 100,* 20291–20302. [12] Richter F. and Ribe N. (1979) *EPSL, 43,* 212–222.

ENVIRONMENTAL APPLICATIONS OF MULTIPLE COLLECTOR INDUCTIVELY COUPLED PLASMA MASS SPECTROMETRY: MEASUREMENT OF LEAD-ISOTOPIC RATIOS IN PRECIPITATION SAMPLES FROM THE GREAT LAKES AND EVERGLADES REGIONS.

J. R. Graney[1], J. N. Christensen[2], G. J. Keeler[3], A. N. Halliday[4], M. S. Landis[3], and J. T. Dvonch[3], [1]Department of Geological Sciences and Environmental Studies, State University of New York–Binghamton, P.O. Box 6000, Binghamton NY 13902-6000, USA (jgraney@binghamton.edu), [2]Department of Geological Sciences, University of Michigan, Ann Arbor MI 48109-1063, USA, [3]Air Quality Laboratory, University of Michigan, Ann Arbor MI 48109-2029, USA, [4]Institute for Isotope Geology and Mineral Resources, Eidgenössische Technische Hochschule Zentrum, NO C61 CH-8092, Zürich, Switzerland.

The measurement of Pb-isotopic ratios coupled with other trace-element determinations on a spatial and temporal basis has been used to differentiate between, and trace, the local and regional movement of aerosols from different sources of pollution [e.g., 1,2]. In most early studies, thermal ionization mass spectrometry (TIMS) was used to measure the Pb-isotopic ratios in aerosols, while less precise inductively coupled plasma mass spectrometry (ICP-MS) techniques are now in common use to trace transboundary pollutant sources [3,4].

The measurement of Pb-isotopic ratios in precipitation [5] has been less common than in aerosols. However, wet deposition processes often dominate pollutant transfer of heavy metals from the atmosphere, and the incorporation of Pb from aerosols into precipitation has the potential to be traced using Pb-isotopic ratios. Small sample amounts, low-Pb concentrations, and high labor/costs to obtain the high-precision Pb-isotopic ratios needed for source apportionment are reasons why this tracer approach has found scant use in precipitation studies. The development of multiple collector inductively coupled plasma mass spectrometry (MC-ICP-MS) techniques [6,7] has the potential to make precise Pb-isotopic ratio measurements from precipitation samples more routine.

To test and contrast the capabilities of MC-ICP-MS and conventional ICP-MS for pollutant tracing, Pb-isotopic ratios were measured from samples of precipitation previously collected to study Hg and trace-element transport and deposition in the south Florida/Everglades and Great Lakes regions. In south Florida, event precipitation samples were collected from locations proximal to several distinct point sources (oil-fired power plants and municipal incinerators) as well as from background sites (offshore) and downwind in the Everglades [8]. In the Great Lakes area, event precipitation samples were collected from five sites including a "background" site in central Illinois, an urban site in Chicago, and three rural sites surrounding Lake Michigan.

Precise measurements of Pb-isotopic ratios have been obtained from samples of precipitation containing 0.50–3.00 ppb concentrations of Pb using a Plasma54 MC-ICP-MS *without* Pb preconcentration (average ^{207}Pb/^{206}Pb and ^{208}Pb/^{206}Pb two σ precision of 0.060 and 0.057%, respectively, was obtained with sample consumption of <1 mL). Average two σ precision of ^{207}Pb/^{206}Pb and ^{208}Pb/^{206}Pb ratios obtained using conventional ICP-MS on the same samples was 0.58 and 0.95% respectively.

A simple, single-step IC Pb separation and preconcentration using Eichrom PbSpec® resin was also developed and tested to determine if improvements in precision on precipitation samples initially containing <1 ppb Pb concentrations could be achieved. The IC preconcentration technique resulted in ten-fold increases in Pb concentrations, negligible blank contributions, and an average ^{207}Pb/^{206}Pb and ^{208}Pb/^{206}Pb two σ precision of 0.027 and 0.032% respectively, on solutions containing, on average, 7.0 ppb Pb.

In the Great Lakes area, the ^{207}Pb/^{206}Pb and ^{208}Pb/^{206}Pb ratios in precipitation range from 0.780–0.880 and 1.93–2.09 respectively. Low ^{207}Pb/^{206}Pb and ^{208}Pb/^{206}Pb ratios are indicative of large contributions of Pb from smelter emissions in Missouri, whereas high ^{207}Pb/^{206}Pb and ^{208}Pb/^{206}Pb ratios indicate large contributions from Canadian sources. However, 70% of the ^{207}Pb/^{206}Pb and ^{208}Pb/^{206}Pb ratios cluster within ranges of 0.820–0.840 and 2.01–2.05 and indicate homogenized "urban" U.S. Pb sources.

In south Florida, 90% of the ^{207}Pb/^{206}Pb and ^{208}Pb/^{206}Pb ratios cluster within ranges of 0.820–0.840 and 2.01–2.05. Based on mass-balance constraints and deposition modeling, essentially all of the Pb in precipitation is of local origin; little originates from global scale transport of Saharan dust. The precision of Pb-isotopic ratios using conventional ICP-MS was not adequate to pinpoint local sources of pollutants; use of MC-ICP-MS was needed for source apportionment purposes.

References: [1] Settle D. M. and Patterson C. C. (1982) *JGR, 87,* 8857–8869. [2] Veron A. J. et al. (1994) *GCA, 58,* 3199–3206. [3] Sturges W. T. and Barrie L. A. (1987) *Nature, 329,* 144–146. [4] Sturges W. T. and Barrie L. A. (1989) *Atmos. Env., 23,* 1645–1657. [5] Church T. M. et al. (1990) *Global Biogeochem. Cycles, 4,* 431–443. [6] Walder A. J. and Freedman P. A. (1992) *J. Anal. At. Spect., 7,* 571. [7] Halliday A. N. et al. (1995) *Intl. J. Mass Spectrom. Ion Processes, 146/147,* 21. [8] Dvonch J. T. et al. (1998) *Sci. Tot. Env., 213,* 95–108.

MEASUREMENTS OF SULFUR-32,33,34 IN ALLAN HILLS 84001 AND NAKHLA SULFIDES BY MULTICOLLECTOR SECONDARY ION MASS SPECTROMETRY: IMPLICATIONS FOR CRUSTAL-ATMOSPHERIC EXCHANGE AND BIOGENIC ACTIVITY ON MARS.

J. P. Greenwood[1], S. J. Mojzsis[2], C. D. Coath[2], and J. T. Wasson[1,2,3], [1]Department of Chemistry and Biochemistry, 3845 Slichter Hall, University of California, Los Angeles, Los Angeles CA 90095-1567, USA, [2]Department of Earth and Space Sciences, 3845 Slichter Hall, University of California, Los Angeles, Los Angeles CA 90095-1567, USA, [3]Institute of Geophysics and Planetary Physics, 3845 Slichter Hall, University of California, Los Angeles, Los Angeles CA 90095-1567, USA.

Introduction: Previous ion microprobe studies of S isotopes (^{32}S, ^{34}S) in ALH 84001 [1–3] and Nakhla sulfides found no evidence for biogenic activity, but did find evidence for exchange between mantle S and the martian regolith via hydrothermal fluids [4]. Recent measurements of positive Δ^{17}O anomalies in carbonates from ALH 84001 [5], Nakhla, and Lafayette [6] have likewise been interpreted as evidence for exchange between the atmosphere and martian regolith. Negative Δ^{33}S (Δ^{33}S = δ^{33}S − 0.515 δ^{34}S) anomalies reported for S from Nakhla were also interpreted as evidence for crust-atmosphere exchange [6]. Here we report measurements of ^{32}S, ^{33}S, and ^{34}S from individual sulfide grains in ALH 84001 and Nakhla thin-sections by multicollector secondary ion mass spectrometry (SIMS) using the UCLA Cameca 1270 ion microprobe. We use these data to further evaluate evidence for putative biogenic activity and atmospheric contributions to martian hydrothermal systems.

Method: Detailed methods of multicollector-SIMS for S isotopes are reported in [7].

Results: *Nakhla.* The range of δ^{34}S values in this study (δ^{34}S: −4.5 to +1.4 ± 0.2‰) overlaps the previously determined range (δ^{34}S: −2.1 to +4.9‰). The six sulfide grains analyzed do not show a resolvable δ^{33}S anomaly.

ALH 84001. The $\delta^{34}S$ values measured here (–9.7 to 4.2 ± 0.1‰) extend the previously determined range (2.0 to 8.0‰) to much lighter values. Two sulfides show a significant negative $\delta^{33}S$ anomaly ($\delta^{33}S$: –0.7 ± 0.2 and –0.5 ± 0.2). Two other sulfides (not those with a negative $\delta^{33}S$ anomaly) with the isotopically lightest $\delta^{34}S$ yet reported from a meteorite (–9.7 ± 0.1‰; –9.4 ± 0.2‰) are distinguished from the other ALH 84001 sulfides in that they are both in a carbonate-rich region.

Discussion: *Nakhla.* The lack of a measurable $\delta^{33}S$ anomaly suggests either (1) the sulfides were only partially altered by a hydrothermal fluid with an atmospheric signature, (2) they were unaltered by later hydrothermal fluids, or (3) the atmospheric contribution to hydrothermal fluids was minimal. We favor (1) that is consistent with the results of [4]. The lack of a $\delta^{33}S$ anomaly in Nakhla sulfides can be easily understood if the anomalous S component measured by [6] is volumetrically minor with a large negative anomaly, and is mainly associated with the trace carbonates and iddingsite, rather than the magmatic sulfides.

ALH 84001. The negative $\delta^{33}S$ anomaly found in two individual sulfide grains is consistent with sulfide precipitation (and by association, the carbonates) from fluids that have isotopically exchanged with the martian atmosphere [5,6]. This exchange appears to have occurred to a greater extent than the fluids that modified the nakhlites [4].

The range of published $\delta^{34}S$ values for sulfides in ALH 84001 is now –9.7‰ to +8.0‰ [1–3]. This >16‰ spread about zero is similar to the range found for the early Proterozoic Michipicoten ($\delta^{34}S$: –10.5‰ to +10.1‰) and Woman River ($\delta^{34}S$: –6.8‰ to +8.2‰) banded iron formations (BIF) [8]. These BIFs are the type examples for the emergence of sulfate-reducing bacteria on Earth in the late Archean [8–10]. Unfortunately, the differences between an ion microprobe study of a twice-shocked orthopyroxenite meteorite and a conventional mass spectrometric study of a BIF make it difficult to draw parallels between the two studies. While inorganic processes above 200°C can also produce this type of variation [e.g., 4,11–13], the magnitude of this variation can be considered consistent with biological activity. We caution that ion microprobe studies of BIF sulfides, as well as further study of ALH 84001 sulfides, are needed to properly assess the validity of the S-isotopic biomarker as applied to ancient terrestrial rocks and martian samples.

References: [1] Greenwood J. P. et al. (1997) *GCA, 61,* 4449. [2] Shearer C. K. et al. (1996) *GCA, 60,* 2921. [3] Boctor N. Z. et al. (1998) *LPS XXIX,* Abstract #1787. [4] Greenwood J. P. et al. (1999) *GCA.* [5] Farquhar et al. (1998) *Science, 280,* 1580. [6] Farquhar et al., *LPS XXX.* [7] Mojzsis S. J. et al., this volume. [8] Goodwin A. M. et al. (1976) *Econ. Geol.,* 870. [9] Schidlowski M. et al. (1983) in *Earth's Earliest Biosphere: Its Origin and Evolution* (J. W. Schopf, ed.), p. 163. [10] Hayes et al. (1993) in *The Proterozoic Biosphere* (J. W. Schopf and C. Klein, eds.), p. 129. [11] Ohmoto H. and Goldhaber M. B. (1997) in *Geochemistry of Hydrothermal Deposits* (H. L. Barnes, ed.), p. 517. [12] Ohmoto H. and Lasaga A. C. (1982) *GCA, 46,* 1727. [13] Cameron E. M. and Hattori K. (1987) *Chem. Geol., 65,* 341.

MAPPING THE SUBCONTINENTAL LITHOSPHERE WITH GARNET POPULATIONS.

W. L. Griffin[1,2], S. Y. O'Reilly[1], N. I. Fisher[1,3], J. Friedman[1,4], C. G. Ryan[1,2], and E. van Achterbergh[1], [1]Key Centre for Geochemical Evolution and Metallogeny of Continents, Macquarie University, Sydney, NSW 2109, Australia (bill.griffin@mq.edu.au), [2]Commonwealth Scientific and Industrial Research Organisation, Exploration and Mining, North Ryde, NSW 2113, Australia, [3]Commonwealth Scientific and Industrial Research Organisation, Mathematical and Information Sciences, Locked Bag 17, North Ryde, NSW 1670, Australia, [4]Department of Statistics, Stanford University, Stanford CA 91045, USA.

A statistical analysis of >12,000 analyses of garnet xenocrysts has revealed significant differences related to the tectonothermal age of the crust penetrated by the host volcanic rock [1]. To explore these differences, we are developing new statistical approaches to define natural populations in the garnet database. Some preliminary results are presented here to show the power of the method. Cluster analysis by recursive partitioning (CARP) compares the real data with a "null" Monte Carlo set containing only clusters based on concentrations in each variable, to define clusters in the real data. We have identified 12 populations, accounting for 75% of the data (Table 1). Comparison with xenolith data suggests that these populations represent consistent combinations of features produced by both primary depletion and later metasomatic modification. The correlation of some populations with xenolith types is shown below, with examples of their distribution in SCLM sections. Each garnet grain has been assigned to a CARP population, and placed in depth context by reference of a Ni-based equilibration temperature (T_{Ni}) to the local geotherm.

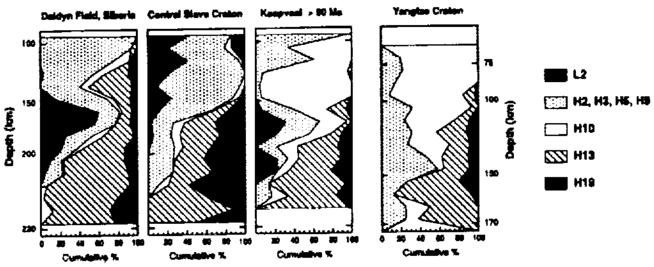

Fig. 1.

TABLE 1.

Class	Fo	Depleted Xenolith Types
L2	93.5	Subcalcic harzburgites,
H2	91	Mg-rich pyroxenites, low-Cr lherzolites
H3	92	Depleted granular lherzolites.
H5	92.5	Depleted granular lherzolites ± phlogopite
H19	92.5	Depleted granular and sheared lherzolites
H21	92.5	Refractory lherzolites, cryptic metsom.
Class	**Fo**	**Fertile Xenolith Types**
H9	89.5	Fe-rich coarse lherzolites (rare)
H10A	92	Phlogopite gran. lherzolites ± phlogopite
H10B	89.5	Very fertile granular lherzolites
H13	90.5	Fertile lherzolites, mostly sheared
H15	91.5	Mildly depleted granular lherzolites
H27	88.5	High-T sheared lherzolites

Archean SCLM sections tend to be strongly stratified, and the degree of depletion decreases downward. The Slave craton is an extreme example of this type, with a highly depleted upper part separated from a more lherzolitic lower part by a boundary zone <10 km thick; this structure has been mapped across >12,000 km^2 [2]. The Kaapvaal craton SCLM is less depleted but still markedly layered; granular phlogopite-bearing lherzolite (H10A population), which is a minor rock type in the Dalydn and Slave sections, is abundant at shallow depth, while deformed and metasomatised lherzolites (H13 garnet population) increase with depth. Proterozoic sections such as the Yangtze craton show a smaller range of rock types; harzburgites are rare, and stratigraphic layering is less pronounced. Typical Phanerozoic SCLM (not shown) is dominated by fertile spinel lherzolites, most of which have undergone <10% melt extraction; 90% of the garnet peridotites in these sections (typically near the base, due to high geotherms) classify as H10B, and are even less depleted than the spinel lherzolites.

THE HAFNIUM-ISOTOPIC COMPOSITION OF CRATONIC MANTLE: LASER ABLATION MICROPROBE MULTIPLE COLLECTOR INDUCTIVELY COUPLED PLASMA MASS SPECTROMETRY ANALYSIS OF ZIRCON MEGACRYSTS IN KIMBERLITES.

W. L. Griffin[1,2], N. J. Pearson[1], E. Belousova[1], S. E. Jackson[1], E. van Achterbergh[1], S. Y. O'Reilly[1], and S. R. Shee[3], [1]Key Centre for Geochemical Evolution and Metallogeny of Continents, Macquarie University, Sydney NSW 2109, Australia (bill.griffin@mq.edu.au), [2]Commonwealth Scientific and Industrial Research Organisation, Exploration and Mining, North Ryde, NSW 2113, Australia, [3]Stockdale Prospecting Ltd., P.O. Box 126, South Yarra, VIC 3141, Australia.

Introduction: Zircon is a widespread member of the low-Cr megacryst

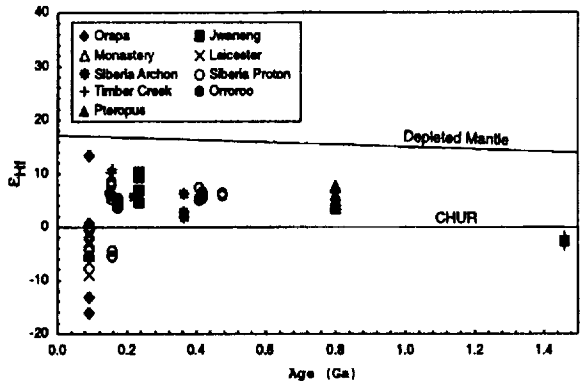

Fig. 1. ε_{Hf} vs. age for analyzed zircons.

suite that occurs in kimberlites worldwide, and the isotopic composition of Hf in this mineral carries information on lithospheric processes. Here we combine analyses of Hf isotopes in zircon megacrysts with data on the Lu and Hf contents of other mantle minerals to speculate on the Hf-isotopic budget of the lithospheric mantle.

Methods: The isotopic composition of Hf was measured *in situ* in 122 mantle-derived zircon megacrysts from African, Siberian, and Australian kimberlites using a Merchantek EO LUV (266 nm Nd:YAG) laser-ablation microprobe and a Nu Plasma multiple collector inductively coupled plasma mass spectrometer (MC-ICP-MS). Analyses were done with a beam diameter of ~80 μm, a 10-Hz repetition rate, and energies of 0.6–1.3 mJ/pulse. This gave total Hf signals of 1–6 × 10^{-11} A for Hf contents ranging from 0.5–1.5%. Typical ablation times were 80–120 s, resulting in flat-bottomed pits 40–60 μm deep. The total amount of Hf consumed in a typical single analysis was ~50 ng. Interference of ^{176}Lu and ^{176}Yb on ^{176}Hf was corrected using measured intensities of ^{175}Lu and ^{172}Yb. Internal precision on ^{176}Hf/^{177}Hf is typically ±0.000020 (2sd). Accuracy was established by 40 analyses of the 91500 zircon standard: ^{176}Hf/^{177}Hf = 0.282286 ± 44 (2sd); TIMS value [1] = 0.282290 ± 37. These values are relative to our ^{176}Hf/^{177}Hf = 0.282158 ± 40 for the JMC475 Hf and 0.282167 ± 20 for the same standard spiked to ^{176}Yb/^{177}Hf = 0.055 [3].

Results: The analyzed zircons range in age from 90 to 1460 Ma, as determined either directly by U-Pb dating or from kimberlite eruption age, and allow indirect analysis of mantle-derived Hf over a long time span and wide geographic area. Most values of ε_{Hf} fall between 0 and 10, but zircon suites from the Orapa (Botswana) Leicester (South Africa) and Ruslovaya (NE Siberia) kimberlites range down to $\varepsilon_{Hf} = -16$ (Fig. 1).

Discussion: Combined with published Nd data on the silicate members of the low-Cr megacryst suite [2], these data indicate derivation from magmas with $\Delta\varepsilon_{Hf}$ as low as –20. LAM-ICP-MS analyses of garnets and clinopyroxenes from mantle-derived peridotite xenoliths show that cratonic mantle has high Hf contents (0.4–1 ppm) and Hf/Nd (0.3–0.5) greater than estimated Bulk Silicate Earth. Depleted harzburgites, which are common in Archean lithospheric mantle, have Lu/Hf ratios low enough (<0.1) to account for the lowest ε_{Hf} observed in the zircons, over time spans of 1–3.5 Ga. We therefore suggest that the magmas from which the zircon megacrysts crystallized were derived from Depleted Mantle or OIB sources, and developed negative $\Delta\varepsilon_{Hf}$ through reaction with the subcontinental lithospheric mantle. This type of mantle has ε_{Hf}, ε_{Nd}, and Hf/Nd values appropriate to the "missing reservoir" required by global Hf/Nd systematics.

References: [1] Weidenbeck M. et al. (1995) *Geostandards Newsletter, 19,* 1–24. [2] Jones R. A. (1987) in *Mantle Xenoliths* (P. H. Nixon, ed.), pp. 711–724, Wiley. [3] Griffin W. L. et al. (1999) *GCA,* submitted.

HAFNIUM, LEAD, AND STRONTIUM ISOTOPES IN LIMA FROM THE JAGERSFONTEIN KIMBERLITE: *IN SITU* ANALYSIS BY LASER ABLATION MICROPROBE MULTIPLE COLLECTOR INDUCTIVELY COUPLED PLASMA MASS SPECTROMETRY.

W. L. Griffin[1,2], N. J. Pearson[1], S. E. Jackson[1], M. Zhang[1], S. Y. O'Reilly[1], and Z. Wang[3], [1]Key Centre for Geochemical Evolution and Metallogeny of Continents, Macquarie University, Sydney NSW 2109, Australia (bill.griffin@mq.edu.au), [2]Commonwealth Scientific and Industrial Research Organisation, Exploration and Mining, North Ryde NSW 2113, Australia, [3]Geologisk Inst., University of Uppsala, Sweden.

Introduction: Barium-potassium-zirconium-chromium titanates of the lindsleyite-mathiasite (LIMA) group occur in heavy-mineral concentrates and as metasomatic phases in mantle-derived peridotite xenoliths in the 86-Ma Jagersfontein kimberlite, South Africa [1]. Laser ablation microprobe inductively coupled plasma mass spectrometry (LAM-ICP-MS) analyses of mathiasite show high concentrations of Sr (5000 ppm), Hf (1000 ppm), Nd (250 ppm), Pb (100 ppm), U (550 ppm) and Th (60 ppm).

Methods: We have analyzed Hf, Sr, and Pb isotopes *in situ* in 2–3-mm grains of mathiasite, using a Merchantek EO UV (266 nm) Nd:YAG LAM and a Nu Plasma multicollector ICP-MS, to constrain the origin of the fluids from which the LIMA minerals grew. Data were collected in static mode using time-resolved analysis. Two to six spots per grain were analyzed for each system; quoted uncertainties are 2sd. Hafnium-isotopic measurements were carried out in a single cycle and corrected for Lu and Yb overlap as in [2]. With ablation pits ~150 μm in diameter, total Hf signals were 1–2 V (10^{11}-Ω resistor). Data collected for 1–2 min give typical internal precision of ±0.00002. Strontium-isotopic measurements used a 250-μm spot and gave total Sr signals of 1–2 V; Rb corrections are trivial (Rb ≈10 ppm). Typical precision (1–2-min runs) is ±0.00006. During Pb analysis, Tl vapor was bled into the transport line to provide an internal mass-bias correction; the isotopic composition of the Tl (205/203 = 2.3875) was fixed by analysis against the SRM981 Pb standard. Lead analyses were done in two static cycles; in cycle 1 (2-s integration) all Pb isotopes, ^{203}Tl, ^{205}Tl, and ^{202}Hg were measured in Faraday cups, and in cycle 2 (1-s integration) ^{238}U, ^{232}Th, and ^{208}Pb were measured. Using 150-μm ablation pits, Pb signals were 0.2–0.4 V; typical precision (1–2-min runs) is ±0.3% on 206/204, 207/204, and 208/204, and 0.08% on 207/206.

Results: The ^{176}Hf/^{177}Hf of each grain is homogeneous within analytical uncertainty, and six grains are identical at 0.28278 ± 2, (ε_{Hf} = 2.5 at 86 Ma or ε_{Hf} = 3.2 at 120 Ma.). One grain gives 0.28284 ± 2, (ε_{Hf} = 4.6 at 86 Ma or ε_{Hf} = 5.4 at 120 Ma). Strontium-87/strontium-86 is homogeneous in some grains (e.g., 0.70411 ± 4, n = 4), but varies across others. The largest range observed in a single grain is 0.7037–0.7054; the total range for eight grains is from 0.70564 ± 8 to 0.70353 ± 8 and the mean is 0.7043 ± 4. The isotopic composition of Pb is homogeneous within analytical uncertainty in some grains, but varies in others; the largest intragrain variation in 206/204 is from 23.15 ± 5 to 24.36 ± 6 and intragrain variation is larger. The mean (n = 5) is 206/204 = 21.1 ± 1.1, 207/204 = 15.63 ± 0.09, 208/204 = 39.1 ± 0.4. ^{206}Pb/^{204}Pb and ^{87}Sr/^{86}Sr are inversely correlated.

Discussion: Recalculated to 90 Ma, the Pb data define a trend lying below the NHRL in plots of 207/204 and 208/204 vs. 206/204. At 175 Ma, the time of the main Karroo magmatism, this array is linear (r = 0.93) and extends between the HIMU and EMI end members in Fig. 1, but the 208/204 of the low-206/204 end member is >38. The trend corresponds to a 1.0-Ga isochron, but is regarded as a mixing line. We suggest that the fluids that

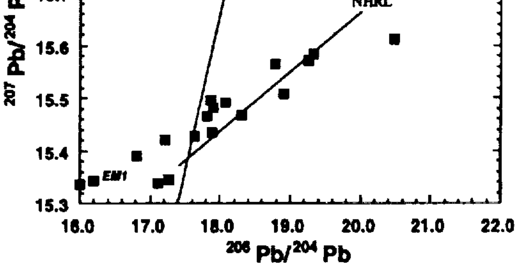

Fig. 1. LIMA Pb data recalculated to 175 Ma.

deposited the LIMA resulted from interaction between magmas derived from a HIMU-type plume source with ^{87}Sr/^{86}Sr $\leq$ 0.7035 and $\varepsilon_{Hf} \geq 5$, and an EMI-type lithospheric mantle with ^{87}Sr/^{86}Sr $\geq$ 0.705, high Th/U and $\varepsilon_{Hf} < 2$, and that these fluids were related to the Karroo plume.

References: [1] Haggerty S. E. et al. (1983) *Am. Mineral., 68,* 494–505. [2] Griffin W. L. et al. (1999) *GCA,* submitted.

ESTIMATION OF SORPTION OF TRACE METALS TO NATURAL SEDIMENTS.

J. Griffioen[1,2] and P. Venema[2], [1]Institute of Earth Sciences, University Utrecht, Budapestlaan 4, 3508 TA Utrecht, The Netherlands (griff@geo.uu.nl), [2]Netherlands Institute of Applied Geoscience TNO, P.O. Box 6012, 2600 J Delft, The Netherlands (p.venema@nitg.tno.nl).

Introduction: Natural sediments are heterogeneous consisting of different sorbents each having their own chemical characteristics. In order to be able to describe sorption processes to such natural sediments, advanced surface complexation models are increasingly applied. These models are limited in their practical use, however, because they need many parameters and they are not easy to incorporate in transport models and decision support systems. Another disadvantage of surface complexation models is that they suggest unrealistically high accuracy to nonspecialists. Because of these disadvantages, we developed a general methodology in which simple Freundlich isotherms are deduced for a limited range of conditions. These conditions are representative for porous media with fresh pore water.

Model Approach: Sorption of Cd, Ni, Zn, and Cu to clay minerals, ferrihydrite, and humic acid was characterized for fresh water in the pH range 4.0–7.0. The types of freshwater range from unpolluted groundwater in a nonreactive sandy sediment to agriculturally polluted groundwater. Calcium was the major cation and Al is important at low pH. Chloride and NO$_3$ were the major anions. The partial pressure of dissolved CO$_2$ is fixed to 0.01 atm, and HCO$_3$ is increasingly important with increasing pH. The concentrations considered for the four trace metals ranged from one tenth to ten times the Dutch drinking water limit. PHREEQC [1] and ECOSAT [2] were used for speciation calculations. Process parameters for cation-exchange to clay minerals and surface complexation to ferrihydrite and humic acid were based on literature data.

Results and Discussion: The modeling results for the individual sorbents unsurprisingly show that sorption of trace-metal increases with increasing pH at fixed trace-metal aqueous activity. However, the increase in sorbed amount, expressed as the fractional occupancy of the sorption type, varies considerably between clay minerals on the one hand and ferrihydrite and humic acid on the other hand. The results also show that sorption of trace metals is linear at pH is 4 to 5 and increasingly nonlinear with increasing pH for ferrihydrite and humic acid. Sorption is almost invariant to type of pore water for these two sorbents, whereas sorption to clay minerals strongly depends on the Ca and Al activity, i.e., pore water type. The absence or presence of Cu strongly influenced the intensity of sorption of the other trace metals for ferrihydrite and humic acid.

A two-step approach was deduced that satisfactorily described sorption of trace metals to clay minerals. First, the occupancy of the exchanger with all divalent cations is calculated depending on the sum of activities of all divalent cations and that of Al^{3+}. Second, the occupancy of an individual divalent cation is calculated from its activity relative to that of the other divalent cations together with the calculated occupancy with divalent cations. Sorption of trace metal to either ferrihydrite or humic acid is described by a Freundlich isotherm, where the two process parameters of the Freundlich function are described as third order polynomial functions of the pH. These polynomial functions were obtained by curve fitting of the function to a set of data points of one of the two parameters versus pH; the data points were calculated from the sorption isotherms obtained at the various pH considered in the speciation modeling.

References: [1] Parkhurst D. L. (1995) *U.S. Geol. Surv. Water Res. Inv. 95-4227,* 143 pp. [2] Keizer M. G and Van Riemsdijk W. H., Agricultural University Wageningen, The Netherlands.

SUBAQUEOUS SULFUR ERUPTIONS AT WAIOTAPU, NEW ZEALAND.

S. T. Grimes[1], D. Rickard[1], P. Browne[2], and S. Simmons[2], [1]Department of Earth Sciences, University of Wales, Cardiff, CF1 3YE, Wales, UK (grimesst@cardiff.ac.uk), [2]Geothermal Institute and Geology Department, University of Auckland, Private Bag 92019, Auckland, New Zealand.

Introduction: At the Waiotapu geothermal system, New Zealand, relict S mounds occur within a drained valley once connected to Lake Whangioterangi (Fig. 1a). These mounds (Fig. 1b) are similar in appearance to the subaerial S volcanos at Volcán Poás, Costa Rica [1,2]. In addition, black S globules (Fig. 1c), similar to those reported floating on the surface of Cinder Pool, Yellowstone [3], ascend within a 2-m-diameter area of bubbling water in Lake Whangioterangi.

Sulfur Mounds: There are four large S mounds in the valley, all >1 m high, and situated within depressions. All are composed of broken, yellow globules, within a fine grained yellow and gray powdered matrix. The glob-

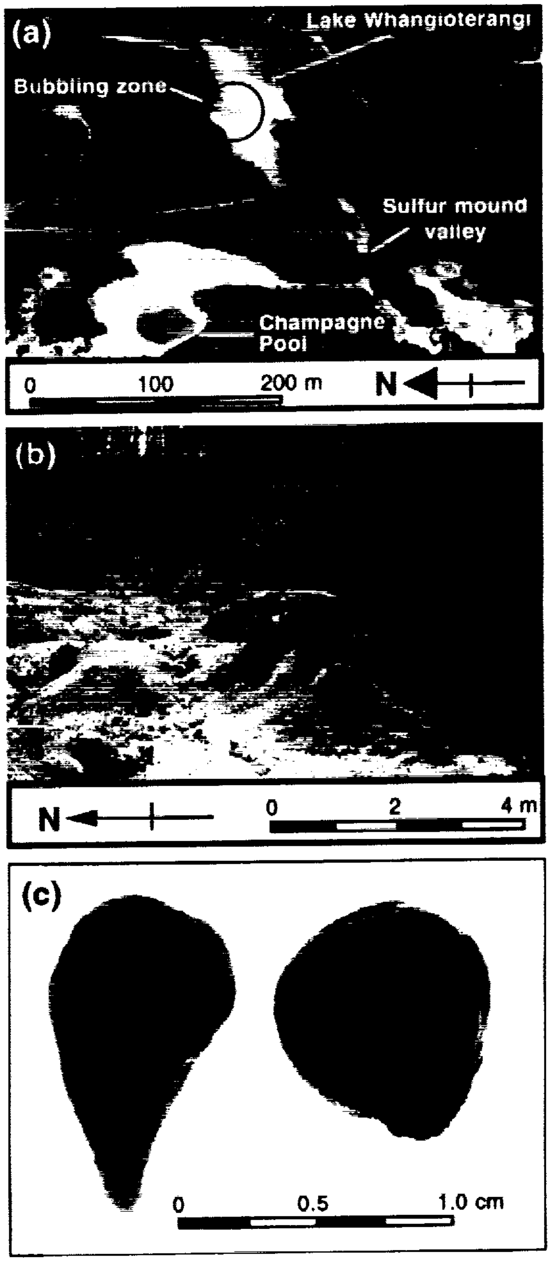

Fig. 1.

ules appear to have been hollow once, but are now filled with matrix material, and have one of three different morphologies: tear drop, spheroid, or elongate. There is no evidence of size sorting of the globules. The matrix is fine grained (<0.1 mm), yellow/gray and contains fragments of globules, a variety of plant axes, and an assemblage of diatoms. Carbon-14 dating of the burnt plant axes give an uncalibrated age of 820 ± 80 yr BP. Overlying one mound is a gray/white cap rock, 1.5 m long × 75 cm wide × 10 cm thick. Its base has a structure similar to that of the S mounds, with a 1-cm-thick top gravel layer devoid of globules.

Lake Whangioterangi: A 2-m-diameter bubbling zone is located on the lake surface (Fig. 1a). An ambient water temperature and the smell of H_2S indicates gas emission, rather than boiling. Within the zone, black S globules ascend to the surface and float outwards, where they either remain on the surface, or sink. The globules have two main morphologies, tear drop and spheroid (Fig. 1c), with hollow centers and <0.5-mm-thick brittle shells. A lead weight, lowered into the bubbling zone was coated in a black material, similar in appearance to the black globules. This indicates the presence of a molten S pool on the lake floor through which gas is discharging and generating the S globules.

Formation of the Sulfur Mounds: The S mounds were formed a maximum of 820 ± 80 yr ago as a result of the rapid subaqueous deposition of S globules, produced by fumarolic gases discharging through molten S pools. The pools were formed during the remobilization of older S deposits, possibly triggered by either the Okaro or the Ngahewa hydrothermal eruption events, ~900 yr ago [4]. A rapid cessation in activity occurred, probably due to the redirection of fumarolic gases away from the S pools.

References: [1] Grimes S. et al. (1999) *Geothermics*, in press. [2] Oppenheimer C. (1992) *J. Volcanol. Geotherm. Res.*, *49*, 1–21. [3] White D. E. et al. (1988) *U.S. Geological Survey Prof. Paper 1456*, 42–44. [4] Lloyd E. F. (1959) *NZ J. Geol. Geophys.*, *2*, 141–176.

EXPERIMENTAL PYRITIZATION OF PLANT CELLS.

S. T. Grimes, D. Rickard, D. Edwards, A. Oldroyd, L. Axe, and K. Davies, Department of Earth Sciences, Cardiff University, CF1 3YE Wales, UK (grimesst@cardiff.ac.uk).

Introduction: Our knowledge of plant evolution depends largely on the interpretation of fossilized plant remains. Fossilization through pyritization is an important process that is not well understood. Two possible pathways are conventionally mooted: (1) replacement, in which the original plant microstructure is preserved to molecular dimensions, and (2) infilling, where internal casts of the structure are preserved. In order to test the relative importance of these processes in pyritization, we carried out an experimental simulation of the process [1], based on the oxidation of Fe(II) monosulfide (FeS) by H_2S [2].

Methodology: The celery petiole (leaf stalk) was chosen as the reactant plant material because it contains a range of tissues with cell walls of varying composition (cellulose and lignin). The celery was sectioned into ~1-cm long chunks, and blanched in boiling deionized water for ~30 s. Iron(II) monosulfide was first precipitated by saturating the celery for 1 week each in 100 mL of 0.1 M, $(NH_4)_2Fe(SO_4)_2$ $6H_2O$ and 0.2 M, Na_2S $9H_2O$. Oxidation of the Fe(II) monosulfide was achieved with 0.01 M H_2S at 40°C in a reaction vessel also containing a pH buffer solution and a Eh poise (pH = 6, Eh = −250 mv, 0.01 M H_2S generated from Na_2S $9H_2O$ by the addition of ~2 mL 50% H_2SO_4).

Results: The initial Fe(II) monosulfide precipitates mainly within the water conducting vessels of the vascular bundles. There is little evidence for migration of FeS into the surrounding parenchyma cells. In contrast, octohedral pyrite crystals, up to 2 μm in diameter, are associated with parenchyma cells adjacent to near-empty tracheids. The octohedral pyrite crystals are located within the parenchyma cells (Fig. 1a), within the intercellular space (Fig. 1b), and within the cell-wall cellulose (Fig. 1c). There is no evidence for the direct replacement of any organic material.

Discussion/Conclusions: Replacement of organic matter by iron sulfides is a difficult process to envisage, because of the lack of a common ion. Our original hypothesis was that pyrite fossilization was a two-stage process: pyrite initially precipitated within the cells (infilling) and subsequently replaced organic components as they decayed [3] through microbial activity (replacement). The results from this study indicate that this may not be the case and that the whole process may be a simple single-stage process of infilling at both macroscopic and microscopic scales. In this process, apparent replacement is represented by infilling of interstial spaces in the plant microarchitecture at microscopic dimensions. The process suggests that pyrite formation in this system results from a reaction with aqueous rather than solid FeS [cf. 4], and that plant material may catalyze pyrite nucleation [cf. 5].

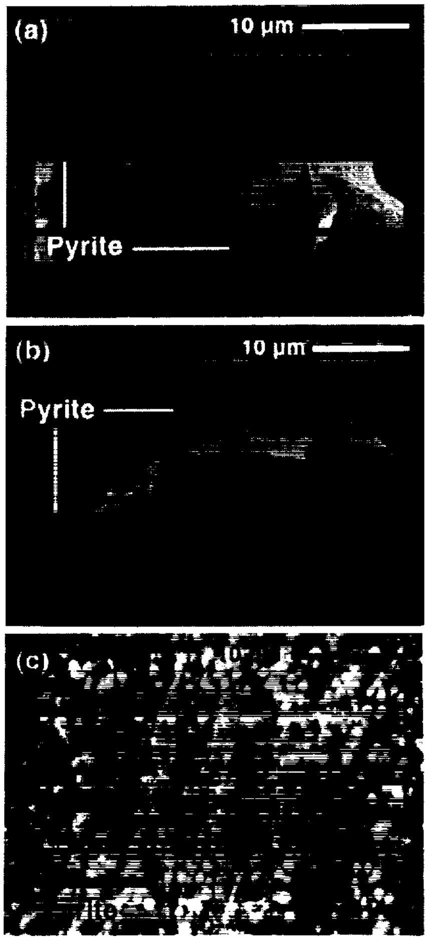

Fig. 1.

References: [1] Rickard D. et al., in preparation. [2] Rickard D. (1997) *GCA*, *63*, 115–134. [3] Kenrick P. and Edwards D. (1988) *Bot. J. Linn. Soc.*, *98*, 97–115. [4] Rickard D. and Luther G. III (1997) *GCA*, *63*, 135–147. [5] Schoonen M. A. A. and Barnes H. L. (1991) *GCA*, *55*, 1505–1514.

STRONTIUM-ISOTOPIC DISTRIBUTION IN THE BROADLANDS-OHAAKI GEOTHERMAL SYSTEM, NEW ZEALAND.

S. T. Grimes[1], D. Rickard[1], C. Hawkesworth[2], P. van Calsteren[2], and P. Browne[3], [1]Department of Earth Sciences, University of Wales, Cardiff, CF1 3YE Wales, UK (grimesst@cardiff.ac.uk), [2]Department of Earth Sciences, The Open University, Milton Keynes MK7 6AA,UK, [3]Geothermal Institute and Geology Department, University of Auckland, Private Bag 92019, Auckland, NZ.

Introduction: Broadlands-Ohaaki is situated on the eastern margin of the Taupo Volcanic Zone, New Zealand. Well BrO-29 penetrates a mixed volcanic/sedimentary rock sequence whose $^{87}Sr/^{86}Sr$ ratios display linear distributions when plotted against 1/Sr values (Fig. 1a,c). These linear distributions do not indicate binary mixing between unaltered lithological units and a single fluid end member [1].

Volcanics/Pyroclastics: All the samples display smectite-style alteration with plagioclase laths being either leached or altered to an assemblage of quartz and smectite. Whole-rock Sr concentrations range from 28 to 253 ppm with $^{87}Sr/^{86}Sr$ ratios ranging from 0.70635 to 0.70785. Based upon petrographic evidence of the degree of hydrothermal alteration and relative permeability of the units [2], we conclude that the linear distribution is not a natural variation in their unaltered equivalents, but is related to the following: (1) the permeability of the host rocks, (2) the degree of leaching of ^{86}Sr-rich primary plagioclase laths, and (3) the secondary crystallization of the groundmass by a recharge fluid represented by modified Taupo rainwater (Fig. 1b).

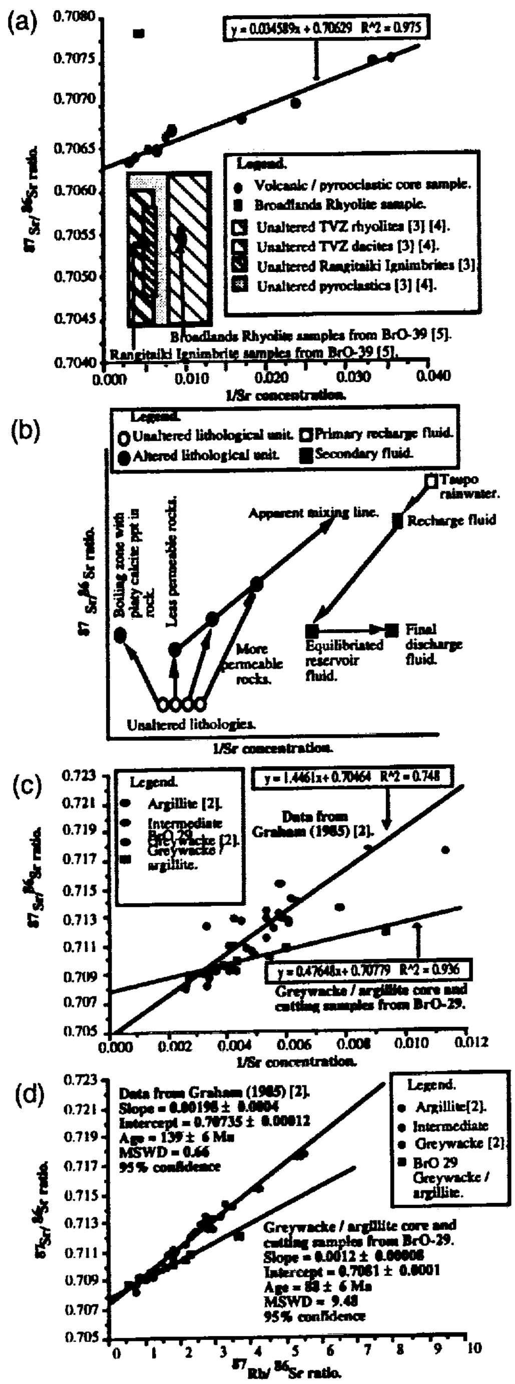

Fig. 1.

Greywackes/Argillites: The argillite fraction increases with depth, with mica being altered to chlorite and pyrite. Whole-rock Sr concentrations range from 108 to 370 ppm, Rb from 79 to 126 ppm, and $^{87}Sr/^{86}Sr$ ratios from 0.70876 to 0.71198. Separate linear isotopic trends occur when their $^{87}Sr/^{86}Sr$ ratios are plotted against 1/Sr values (Fig. 1c), in addition to yielding a Rb/Sr errorchron age of 88 ± 6 Ma (Fig. 1d). Based upon petrographic observations, the isotopic trends in the greywackes/argillites are believed to be an inherited metamorphic feature, from the Rangitata Orogeny (141 ± 3 Ma) [3], which has been modified by geothermal fluids preferentially leaching ^{87}Sr and ^{87}Rb from primary micas.

References: [1] Grimes S. G. et al. (1999) *Chem. Geol.*, in press. [2] Lonker S. W. et al. (1990) *Am. J. Sci.*, *290*, 995–1068. [3] Graham I. J. (1985) *Chem. Geol.*, *52*, 317–331. [4] Ewart A. and Stipp J. J. (1968) *GCA*, *32*, 699–736. [5] Graham I. J. et al. (1995) *J. Volcanol. Geotherm. Res.*, *68*, 59–87. [6] Grimes S. T. (1998) unpublished Ph.D. thesis, Univ. of Wales, Cardiff.

DENITRIFICATION DURING THE TOARCIAN OCEANIC ANOXIC EVENT AS RECORDED BY NITROGEN-ISOTOPIC RATIOS OF BULK MARINE ORGANIC MATTER.

D. R. Gröcke and H. C. Jenkyns, Department of Earth Sciences, University of Oxford, Parks Road, Oxford OX1 3PR, UK (darreng@earth.ox.ac.uk; hughj@earth.ox.ac.uk).

Introduction: Nitrogen-isotopic ($\delta^{15}N$) ratios in modern oceanographic studies have received a great deal of attention over the past decade [1]. However, the utility of N-isotopic ratios as a paleoceanographic tool in the study of Mesozoic sediments has been little tested [2]. Organic matter in black shales of the Jet Rock (Mulgrave Shale Member of the Whitby Mudstone, Lower Toarcian, northeast Yorkshire) and the Llanbedr (Mochras Farm) Borehole (Toarcian, Gwynedd, north Wales) has been analyzed for $\delta^{15}N$, $\delta^{13}C$ and total organic C (TOC) in order to investigate paleoproductivity changes during the early Toarcian Oceanic Anoxic Event. Both sequences are well dated by ammonite biostratigraphy [3,4].

Results: The Jet Rock, northeast Yorkshire, is characterized by a negative $\delta^{13}C_{org}$ excursion in the lower exaratum subzone, followed by a positive shift in the upper exaratum subzone [5]. This positive shift is also registered in $\delta^{13}C_{carb}$ (belemnites) from the Jet Rock where values exceed 6‰. Maximum values of TOC occur with relatively low $\delta^{13}C_{org}$ and high $\delta^{15}N_{org}$ values in the lower exaratum subzone (Fig. 1).

Although the sample resolution is not as detailed as for the Jet Rock, the same relative pattern is registered in the Mochras Borehole, north Wales. The sequence is also characterized by a negative excursion in $\delta^{13}C_{org}$ in the lower exaratum subzone and a positive shift in the upper exaratum subzone; $\delta^{15}N_{org}$ shows a positive and negative shift respectively over the same interval (Fig. 2).

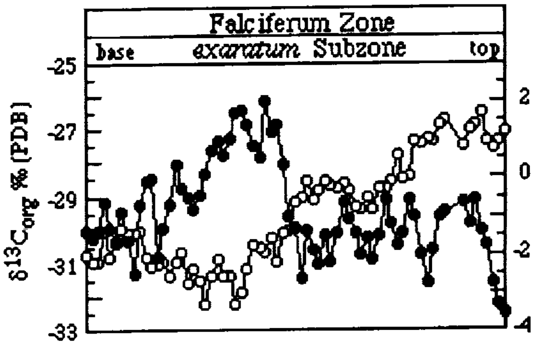

Fig. 1. $\delta^{13}C_{org}$ and $\delta^{15}N_{org}$ evolution for the exaratum subzone from the Jet Rock, northeast Yorkshire. Open circles = C, closed circles = N.

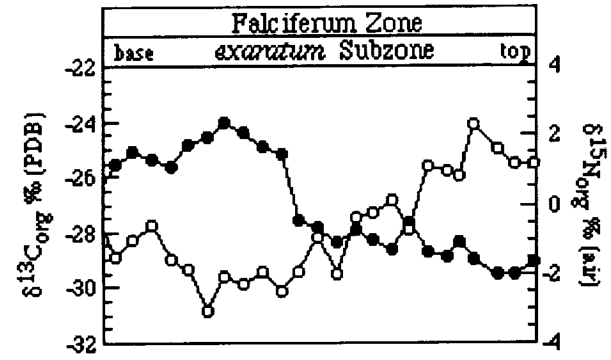

Fig. 2. $\delta^{13}C_{org}$ and $\delta^{15}N_{org}$ evolution for the exaratum subzone from the Mochras Borehole, north Wales. Open circles = C, closed circles = N.

Discussion: In modern oceans, relatively high $\delta^{15}N$ values are characteristic of water masses where nitrate utilization is high due to enhanced biological uptake and/or where denitrification has taken place. An increase in productivity alone would deplete near-surface waters in ^{12}C and ^{14}N, leading to higher values of $\delta^{13}C$ and $\delta^{15}N$. This is not the pattern seen in the excursion in the lower exaratum subzone, where $\delta^{13}C_{org}$ values fall. However, the correlation between more positive $\delta^{15}N_{org}$, more negative $\delta^{13}C_{org}$ values, and higher TOC values can be related to intense upwelling of poorly oxygenated waters, where much organic C had been oxidized and denitrification had taken place. It is hypothesized that upwelling returned ^{13}C-poor and ^{15}N-rich waters to the photic zone, where they could be directly utilized by phytoplankton, hence increasing the flux of organic matter to the seafloor. Such a mechanism would explain the isotopic records from the lower exaratum subzone of the Jet Rock and Mochras Borehole.

The main $\delta^{13}C_{org}$ and $\delta^{13}C_{carb}$ positive excursion is registered, wherever it is accurately dated in the UK, in the upper exaratum subzone, whereas in southern Europe it is dated simply as falciferum zone. In all investigated localities, however, this excursion occurs higher in the succession than the most C-rich sediments. This presents something of a paradox, as positive $\delta^{13}C$ excursions are conventionally interpreted [6] as reflecting an increase in the size of the global reduced C reservoir, most typically by an increase in productivity and rate of burial of organic matter in the world ocean. If this model is correct, the global deposition rate of organic C must have been at its maximum during the late exaratum subzone, and the major sinks for this material may lie outside Europe.

References: [1] Wu J. et al. (1997) *Deep-Sea Res., 44,* 287–314. [2] Rau G. H. et al. (1987) *EPSL, 82,* 269–279. [3] Howarth M. K. (1992) *Mono. Palaeon. Soc., 145,* 1–106. [4] Ivimey-Cook H. C. (1982) *Rep. Inst. Geol. Sci., 71,* 87–92. [5] Jenkyns H. C. and Clayton C. J. (1996) *Sedimentology, 44,* 687–706. [6] Scholle P. A. and Arthur M. A. (1980) *Bull. Am. Assoc. Petrol. Geol., 64,* 67–87.

STABLE ISOTOPIC AND CARBON/NITROGEN RATIOS OF FOSSIL WOOD FROM THE MESOZOIC: INSIGHTS INTO OCEAN-ATMOSPHERE LINKS.

D. R. Gröcke[1], S. P. Hesselbo[1], H. C. Jenkyns[1], G. Taylor[2], S. A. Robinson[1], and H.-J. Schöffel[1], Department of Earth Sciences, University of Oxford, Parks Road, Oxford OX1 3PR, UK (darreng@earth.ox.ac.uk; stephess@earth.ox.ac.uk; hughj@earth.ox.ac.uk; stuartr@earth.ox.ac.uk; hanss@earth.ox.ac.uk), [2]University of Southampton, Plants and Environment Laboratory, School of Biological Sciences, Bassett Crescent East, Southampton SO16 7PX, UK (g.taylor@soton.ac.uk).

Introduction: Fossil wood fragments were collected through a biostratigraphically well-constrained Aptian (Early Cretaceous) shallow-marine siliciclastic succession on the Isle of Wight, southern Britain, to determine paleoenvironmental changes with time. Fossil wood was analyzed for N-isotopic ($\delta^{15}N$) and C/N ratios. The C-isotopic data have been presented elsewhere [1].

Results and Discussion: *The carbon/nitrogen and $\delta^{15}N$ record.* One of the effects of increasing CO_2 on modern plant tissues is to increase the C/N ratio [2]. Since the assimilation of C is greater at elevated CO_2 levels, the amount of N being synthesized is reduced, possibly causing isotopic fractionation. Preliminary data from modern poplar plants grown in chambers with elevated CO_2 levels show that $\delta^{13}C_{wood}$ values and C/N ratios decrease and $\delta^{15}N_{wood}$ values increase. This relationship is surprising, as modern studies suggest that C/N ratios are higher in plants experiencing elevated CO_2 levels [2].

The Aptian was a time period that experienced elevated CO_2 levels [3] up to ~1450 ppm and, thus, on the basis of our modern poplar data, we would expect lower C/N ratios and higher $\delta^{15}N_{wood}$ values for Lower Cretaceous wood from the Isle of Wight. Figure 1 shows that this is the case. However, more modern plant C/N and $\delta^{15}N_{wood}$ data are required to confirm this model. We are currently in the process of analyzing both gymnosperm and angiosperm wood that has been grown in chambers with elevated CO_2 levels.

Cyclicity in carbon/nitrogen ratios. The uppermost Wealden group [upper Barremian, including magnetochron zero reversal (M0r) exhibits low C/N ratios (~30–70)], whereas after M0r, the Lower Greensand group (lower and upper Aptian) C/N ratios are generally high (~80–110). C/N ratios in the Lower Greensand group also display a cyclic pattern. We analyzed the power density spectrum of the C/N dataset. Due to the variation in sample spacing we first linear-interpolated the data before applying a Hann filter prior to the Fourier transformation.

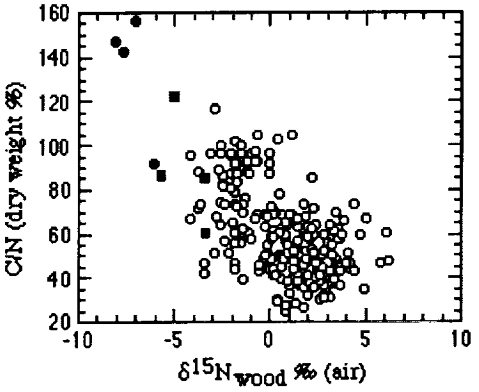

Fig. 1. Carbon/nitrogen and $\delta^{15}N_{wood}$ relationship in fossil wood (open circles) and modern poplar wood (filled circles ~350 ppm CO_2; filled squares ~700 ppm CO_2).

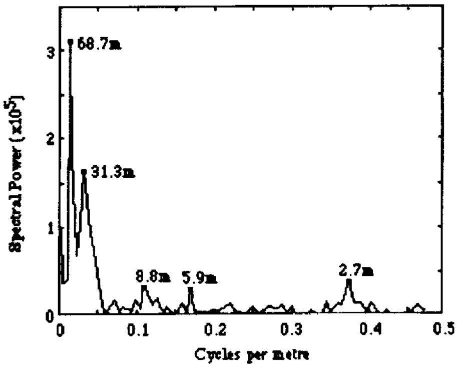

Fig. 2. Power spectrum of fossil wood C/N ratios from the lower- to middle Lower Greensand group.

Since we know, from sedimentology and biostratigraphy, that there are at least three stratigraphic gaps in the Lower Greensand group, the periodicity of C/N ratios from the Fourier transformation is a maximum estimate. On this basis and the timescale of Gradstein et al. [4], the periodicity of the C/N cycle falls into the Milankovitch band (<1 Ma). Assuming that the C/N ratios reflect paleo-pCO_2 levels, considerable variation in the atmospheric concentration of this greenhouse gas was characteristic of the Aptian.

References: [1] Gröcke D. R. et al. (1999) *Geology, 27,* 155–158. [2] Cotrufo M. F. et al. (1998) *Global Change Biol., 4,* 43–54. [3] Berner R. A. (1994) *Am. J. Sci., 294,* 56–91. [4] Gradstein F. M. et al. (1995) *SEPM Spec. Publ., 54,* 95–128.

STRONTIUM-ISOTOPIC CALIBRATION OF AMMONITE SUBZONES IN THE JURASSIC AND EARLY CRETACEOUS.

D. R. Gröcke[1], S. P. Hesselbo[1], J. Mutterlose[2], H. C. Jenkyns[1], R. L. Hall[3], and S. M. Robinson[3], [1]Department of Earth Sciences, University of Oxford, Parks Road, Oxford OX1 3PR, UK (darreng@earth.ox.ac.uk; stephess@earth.ox.ac.uk; hughj@earth.ox.ac.uk), [2]Institut für Geologie, Ruhr-Universität Bochum, Universitätsstrasse 150, 44801 Bochum, Germany (joerg.mutterlose@rz.ruhr-uni-bochum.de), [3]Department of Geology and Geophysics, University of Calgary, 2500 University Drive, NW Calgary, AB T2N 1N4, Canada (rhall@geo.ucalgary.ca; srobinso@ucalgary.ca).

Introduction: Strontium-isotopic ($^{87}Sr/^{86}Sr$) stratigraphy is based on three principles: (1) the $^{87}Sr/^{86}Sr$ ratio in seawater has always been homogenous throughout the oceans, as it is today; (2) the $^{87}Sr/^{86}Sr$ ratio of oceans has varied systematically through geological time; and (3) the $^{87}Sr/^{86}Sr$ ratio is accurately recorded in Ca-bearing minerals precipitated directly from seawater. The application of Sr-isotopic stratigraphy has been used as a global correlation tool extensively in the Tertiary [e.g., 2] and upper Cretaceous [e.g., 3]. Previous research on $^{87}Sr/^{86}Sr$ ratios in fossil belemnites and oysters conducted at the Age & Isotope Laboratory, University of Oxford, has provided a detailed curve for most of the Jurassic and a less-detailed curve for the Early Cretaceous [4,5]. This $^{87}Sr/^{86}Sr$ curve is calibrated against the northwest European standard faunal scheme. However the application of Sr-isotopic ratios from well-preserved belemnites and oysters has not been rigorously tested on other continents and/or against other ammonite zonal schemes (e.g., Boreal, Austral) for the Jurassic and Early Cretaceous. To address this problem, belemnites have been collected stratigraphically from localities in Germany, Portugal, Scotland, and Canada.

Screening for Diagenesis: Using the chemical procedure outlined by Jones et al. [4], belemnites have been screened for diagenetic alteration. The best method for screening belemnites for diagenetic alteration is analysis of the trace-element abundance of Fe and Mn. Belemnites with ≥150 ppm Fe and ≥75 ppm Mn have been excluded from the $^{87}Sr/^{86}Sr$ curve. In addition to trace-element abundance, cathodoluminescence was also employed, with high luminescent samples being rejected from the dataset. In all cases, the cathodoluminescent technique picked out samples with high levels of Mn.

Procedures of Normalization: To facilitate the comparison of $^{87}Sr/^{86}Sr$ ratios obtained from different laboratories, a normalization procedure should be incorporated. The most common standard used at present is NBS987. Since 1994, the Age & Isotope Laboratory has completed 178 analyses of the NBS987 standard and an average $^{87}Sr/^{86}Sr$ value of 0.710256 (std.dev., 1.4e-5) has been recorded. All belemnite and oyster $^{87}Sr/^{86}Sr$ values used in this discussion have been normalized to a NBS987 value of 0.710250.

Results and Discussion: The lower Jurassic is excellent for comparing different faunal schemes as the $^{87}Sr/^{86}Sr$ curve decreases systematically from the basal Sinemurian to the Pleinsbachian-Toarcian boundary, where it then increases. Belemnites collected from Peniche (Portugal) and the B27 Roadcut (southern Germany) record $^{87}Sr/^{86}Sr$ values within measurement error of English belemnites [6]. However, the $^{87}Sr/^{86}Sr$ ratios of belemnites from Peniche are somewhat offset compared to England and Germany. This possibly relates to uncertainty in definition of ammonite subzones in the Peniche succession. The $^{87}Sr/^{86}Sr$ ratios can be used to constrain the chrono-subzone boundaries at Peniche, especially where ammonite faunas are incomplete or absent altogether.

The Aalenian-Bajocian succession is characterized by relative stable $^{87}Sr/^{86}Sr$ ratios in the Aalenian followed by a gradual decrease in the Bajocian. It is extremely difficult to compare independently the Aalenian ammonite faunas of different regions due to the flatness of the $^{87}Sr/^{86}Sr$ curve. The Capo Mondego section in Portugal is defined as the global stratotype for the Aalenian/Bajocian boundary and, thus, an ideal locality for comparison with English $^{87}Sr/^{86}Sr$ data. $^{87}Sr/^{86}Sr$ data from Capo Mondego support the scattered data of Jones et al. [4] and confirm the gradual decrease in $^{87}Sr/^{86}Sr$ through the Bajocian.

Preliminary data from Alberta, Canada, suggest that $^{87}Sr/^{86}Sr$ ratios are extremely useful for correlating a succession with incomplete faunal presence to the northwest European standard faunal scheme. However, the diagenetic screening procedure of Jones et al. [4] may need to be adjusted for the Canadian sections to a level of ≥200 ppm Fe and ≥100 ppm Mn. Most of the samples have elevated Fe and Mn, which are possibly related to either the tectonic history of the region (i.e., hydrothermal fluids) and/or the migration and entrapment of postdepositional fluids such as oil. Despite this $^{87}Sr/^{86}Sr$ ratios for the sections investigated covering the lower and middle Jurassic were in good agreement with European $^{87}Sr/^{86}Sr$ data.

References: [1] Burke W. H. et al. (1982) *Geology, 10,* 515–519. [2] Hess J. et al. (1986) *Science, 231,* 979–984. [3] Bralower T. J. et al. (1997) *Bull. Geol. Soc. Am., 109,* 1421–1442. [4] Jones C. E. et al. (1994) *GCA, 58,* 1285–1301. [5] Jones C. E. et al. (1994) *GCA, 58,* 3061–3074. [6] Parkinson D. N. (1994) unpublished Ph.D. thesis, University of Oxford, UK.

NOVEL COPPER OXIDE REACTION PRODUCTS OF THERMALLY ALTERED *PINUS RESINOSA* WOOD.

J. A. Gudeman[1], J. Baldock[2], and J. I. Hedges[1], [1]School of Oceanography, University of Washington, Box 357940, Seattle WA 98195, USA (jgudeman@ocean.washington.edu; jihedges@u.washington.edu), [2]Commonwealth Scientific and Industrial Research Organisation Land and Water, PMB#2, Glen Osmond, SA 5064, Australia (jeff.baldock@adl.clw.csiro.au).

Alkaline CuO oxidation of charred wood samples was carried out in an attempt to identify reaction products indicative of sample thermal history. *Pinus resinosa* (Red Pine) sapwood was collected from the bole of living trees, ground and dried to constant mass at 70°C. Samples of the dried wood were heated to constant mass at temperatures of 150°, 200°, 250°, 300°, and 350°C. The wood samples were subsequently oxidized via alkaline CuO oxidation to release lignin-derived phenolic "monomers" and other oxidation products. The chemical structures of these products were confirmed using gas chromatography/mass spectroscopy. Compounds thus identified were quantified using authentic standards via gas chromatography/flame ionization detection.

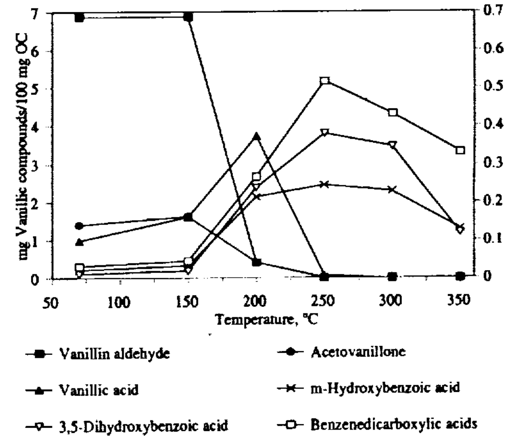

Fig. 1. Organic C-normalized yields of selective CuO oxidation products from thermally altered *Pinus resinosa* (Red Pine) sapwood. Benzoic acid compounds include m-Hydroxybenzoic acid, 3,5-dihydroxybenzoic acid and an extended suite of five benzenedicarboxylic acids.

Our results (Fig. 1) indicate the following three trends: (1) a decrease in the organic C-normalized yields of vanillin aldehyde and acetovanillone over the temperature range 70°–200°C; (2) an increase and subsequent decrease in the organic C-normalized yield of vanillic acid, peaking at 200°C before dropping to zero by 250°C; and (3) the appearance of an extended suite of benzenedicarboxylic acids, hydroxylated benzenedicarboxylic acids, and hydroxybenzoic acids (including 3,5-dihydroxybenzoic acid), with the organic C-normalized yields of these compounds increasing at temperatures above 150°C and decreasing at temperatures >300°C.

Preliminary results suggest that the observed benzenedicarboxylic acids, hydroxylated benzenedicarboxylic acids, and hydroxybenzoic acids (i.e., benzoic compounds), may be useful as molecular tracers of charred wood in the environment. Additional tests will be performed to confirm lignin rather than polysaccharide precursors as the source of the benzoic compounds. In addition, surface soil samples will be analyzed in an attempt to assess the usefulness of these compounds as tracers of charred wood in soils. Results of these analyses will be presented.

ADVANCES IN LEAD ISOTOPES IN THE HEALTH FIELD.

B. L. Gulson, Graduate School of the Environment, Macquarie University, Sydney NSW 2109, Australia (bgulson@gse.mq.edu.au), Commonwealth Scientific and Industrial Research Organisation Exploration and Mining, Sydney, Australia.

Introduction: Since the pioneering studies of Manton [1] and Rabinowitz and Wetherill [2] in the early 1970s, limited use has been made of Pb isotopes in the health field until recent years. Most investigations have focused on source apportionment of Pb in blood, with varying degrees of success depending on the complexity of sources and concentration of Pb in blood. In adult humans, >90% of the body burden of Pb is stored in the bones. There is concern that during times of physiological stress such as pregnancy and lactation, when the bones undergo resorption and accretion, Pb is released and transferred to the fetus at a critical time of the development of the central nervous system. Over the past decade, this hypothesis has been verified in two major studies supported by the U.S. National Institute of Environmental Health Sciences, one on lower primates in Ottawa [3] and the other on humans in Australia [4–6]. Only the results of the human study will be given here.

Methods: Subjects (n = 15) were from other countries (CIS, former Yugoslavia, Bulgaria, Poland, Albania, China) whose skeletal Pb-isotopic composition (i.c.) was different to that currently prevailing in Australia. They were compared with a control group (n = 8) of multigenerational Australian subjects. Samples analyzed with thermal ionization mass spectrometry (TIMS) for Pb i.c. (208/206, 207/206, and 206/204) and concentration (202 spike) included blood, urine, breast milk, food, gasoline, air particulates, water, and household dust.

Results: Blood Pb concentrations in 14 of the 15 immigrant subjects and for all Australian controls were < 5 µg/dL. Predicted changes in isotopic composition are shown in Fig. 1. Minimal changes in isotopic composition were observed for the Australian controls. The mean change for each individual in skeletal Pb contribution to blood Pb based on the isotopic composition during the second and third trimesters ranged from ~50% to 91%. During the first six months of the postpregnancy period, the mean increases for each individual in skeletal contribution to blood Pb based on the isotopic composition ranged from ~40% to 99%. As the pregnancy progressed, the contribution of skeletal Pb showed an approximately linear increase. During the postpregnancy period, the elevated percentage of skeletal Pb mobilized, reflected by the Pb isotopes, remained essentially constant for up to 6 months in spite of variations in length of breastfeeding ranging from <1 week to >6 months. Consistent, clear-cut changes in blood Pb concentration during pregnancy and the postpregnancy period were not identified for individuals. Environmental factors, especially diet, were not the major determinants of blood Pb because of the low $^{206}Pb/^{204}Pb$ ratios in household dust, air, water, and gasoline [4–6]. Only two subjects consumed dietary supplements for Ca, and mobilization of skeletal Pb to blood Pb was the lowest of all the subjects.

Conclusion: Endogenous sources of Pb, especially from the maternal skeleton, can be mobilized during pregnancy and even more so during the post-pregnancy period. Increased mobilization is consistent with increased bone resorption and may be associated with an inadequate Ca intake observed in quarterly 6-d duplicate diets. Calcium supplementation may be an important means of limiting fetal exposure to Pb.

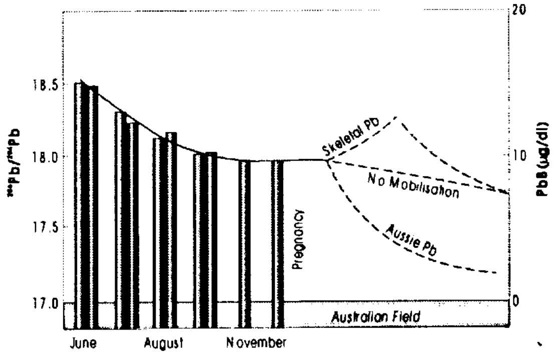

Fig. 1. Prediction of potential changes in isotopic composition ($^{206}Pb/^{204}Pb$) during pregnancy for an Eastern European subject. The data shown in bar form are those obtained during a pilot study; the left column at each time is for "spot" urine, the right column is for blood. The ratio decreases exponentially after arrival in Australia, related to clearance of Pb from the blood compartment, and then an equilibrium is reached between skeletal Pb and Australian environmental Pb. Predicted trends for mobilization of Pb from the skeleton, no mobilization, and rapid exchange of skeletal Pb with Australian Pb (Aussie Pb) are shown as dashed lines.

References: [1] Manton W. I. (1977) *Arch. Environ. Health, 32,* 149–157. [2] Rabinowitz et al. (1976) *J. Clin. Invest., 58,* 260–270. [3] Franklin et al. (1997) *Fund. Appl. Tox., 39,* 109–119. [4] Gulson et al. (1995) *J. Lab. Clin. Med., 125,* 703–712. [5] Gulson et al. (1997) *J. Lab. Clin. Med., 130,* 51–62. [6] Gulson et al. (1998) *J. Lab. Clin. Med., 131,* 324–329.

EXPERIMENTAL MEASUREMENTS OF ACID-BASE BUFFERING PROPERTIES AND METAL SORPTION BY LICHENS.

J. R. Haas, Department of Geography and Earth Sciences, University of North Carolina at Charlotte, Charlotte NC 28223, USA (jrhaas@email.uncc.edu).

Introduction: Lichens are widely used as natural biomonitors of environmental pollution. These lower plants are formed by the symbiosis of a fungal and one or more photosynthesizing microbial partners, and are ubiquitous in all terrestrial ecosystems, including severe polar and hot desert settings. Lichens are useful as pollution biomonitors because their biomass can strongly concentrate heavy metals, pollutant gases, and radionuclides from aerosol fallout, precipitation, or runoff. Under natural conditions, uptake of soluble metal species by lichen biomass can lead to long-term storage through the formation of biominerals [1] and trophic cycling of trace elements via lichen herbivory [2]. Lichens lack roots, a vascular system, or a protective waxy cuticle, and thus nutrient uptake is accomplished primarily through passive accumulation of incident chemical species from dry or wet deposition, or directly from the growth substrate.

Despite strong interest in lichens for environmental monitoring and biogeochemical cycling studies, the chemical properties and mechanisms governing metal uptake and sequestration by these organisms remain unclear. Although previous studies [3,4] have shown that adsorption mechanisms predominantly govern metal uptake by lichens and free-living fungi, experimental measurements quantifying interactions between dissolved cations and lichen surfaces remain generally unavailable in the literature. Data that exist are largely anecdotal [5] and cannot be generalized to conditions significantly different from those of the experiments. To address this problem, a series of experiments was carried out to measure the surface amphoteric properties and Cd, Cu, Pb, La, Nd, and Yb adsorption behavior of lichen biomass. Experimental data were used to develop an equilibrium thermodynamic model of lichen-aqueous interactions.

Experimental: Lichens representing genera that are globally distributed were chosen for this study, including *Cladina sp.* ("reindeer moss"), *Umbilicaria sp.* ("rock tripe"), and *Usnea sp.* ("old man's beard"). Surface amphoteric properties of biomass were measured through acid-base titrations of untreated natural lichen biomass in 0.01 mol/L $NaNO_3$ electrolyte solutions. Immersion pH for lichen samples, approximating the pH of a net-neutral surface buffering pH through proton exchange, was ~3.8–5.6. Titrations demonstrated that the lichens exhibit strong buffering capacities at pH values of ~3 to above 9.

Adsorption of Cd, Cu, Pb, La, Nd, and Yb by lichen biomass was measured as a function of pH and time in a dilute (0.01 M) $NaNO_3$ electrolyte. Uptake of cations by all lichens was initially rapid (~80% of equilibrium uptake within 2 h) but required 6–24 h for attainment of equilibrium. Rapid initial uptake followed by slower sorption indicates the presence of significant microporosity on the biomass surface, through which fluid-mass transfer is slow. Sorption experiments were allowed to incubate for 24 h. Reversed sorption-desorption trials were performed to investigate the reversibility of cation uptake: sorption was found to be 100% reversible within the time intervals studied. Metal uptake as a function of pH shows strong sorption-edge behavior similar to that of metals adsorbing onto mineral surfaces.

Theoretical: Titration data were modeled using FITEQL 2.0 to constrain surface properties in terms of reversible proton-exchange equilibria, using both a "humic acid" model (i.e., that the lichen surface behaves like a dissolved organic acid) and the constant capacitance (CC) model for the electrical double layer [6]. Specific surface area, required for the CC model, was measured using a methylene blue-adsorption technique [7]. Modeling results demonstrate that a multiple-site model best fits the experimental titration data, although this approach cannot distinguish the compositions of active surface functional groups. For example, the surface of the lichen *U. mammulata* is best approximated using a three-site model, for which preliminary optimal acid-dissociation constants (pKa) were ~6.5 (0.04 sites/nm^2 for this functional group population), ~7.6 (0.06 sites/nm^2), and ~9.9 (1.2 sites/nm^2). Similar results were obtained using both the "humic acid" and CC models.

Adsorption data were used in conjunction with modeled surface properties to regress properties of metal sorption reactions. Adsorption of cations was best described through complexation reactions involving negatively charged surface functional groups. A one-site model (that having the smallest pKa) best described metal uptake. Preliminary values for Cd, Cu, Pb, and Nd adsorption onto *U. mammulata* were 7.1, 7.4, 8.3, and 8.1 respectively. These values may be used to estimate the metal-uptake capacities of differing lichens under a wide range of field conditions using an equilibrium thermodynamics approach.

References: [1] Purvis O. W. (1996) *Lichenologist, 28,* 571–601. [2] Rissanen K. and Rahola T. (1990) *Rangifer, 3,* 55–61. [3] Richardson D. H. S. (1995) *Symbiosis, 18,* 119–127. [4] Brown D. H. (1991) *Symbiosis, 11,* 207–223. [5] Brady J. M. and Tobin J. M. (1994) *Enzyme and Microbial Technol., 16,* 671–675. [6] Stumm W. and Morgan J. J. (1996) *Aquatic Chemistry,* Wiley. [7] Pham T. H. and Brindely G. W. (1970) *Clays and Clay Mineral., 18,* 203–212.

TWO-STEP LASER MASS SPECTROMETRY: A TOOL FOR CHEMICAL CHARACTERIZATION AND SOURCE ASSIGNMENT OF BLACK CARBON.

O. P. Haefliger[1], R. Zenobi[1], and T. D. Bucheli[1,2], [1]Analytical Chemistry Group, Organic Chemistry, Eidgenössische Technische Hochschule, Universitätsstrasse 16, 8092 Zürich, Switzerland (haefliger@org.chem.ethz.ch), [2]Institute of Applied Environmental Research, Stockholm University, 10691 Stockholm, Sweden (thomas.bucheli@itm.su.se).

Black carbon (BC) is a strong sorbent especially for hydrophobic organic substances, such as polycyclic aromatic hydrocarbons (PAHs). When released into the environment as a result of incomplete combustion, BC inevitably carries such compounds, the composition of which is largely emission-source specific. The assignment of the main sources of BC is crucial to the understanding of its fate and behavior in the environment. Moreover, a significant

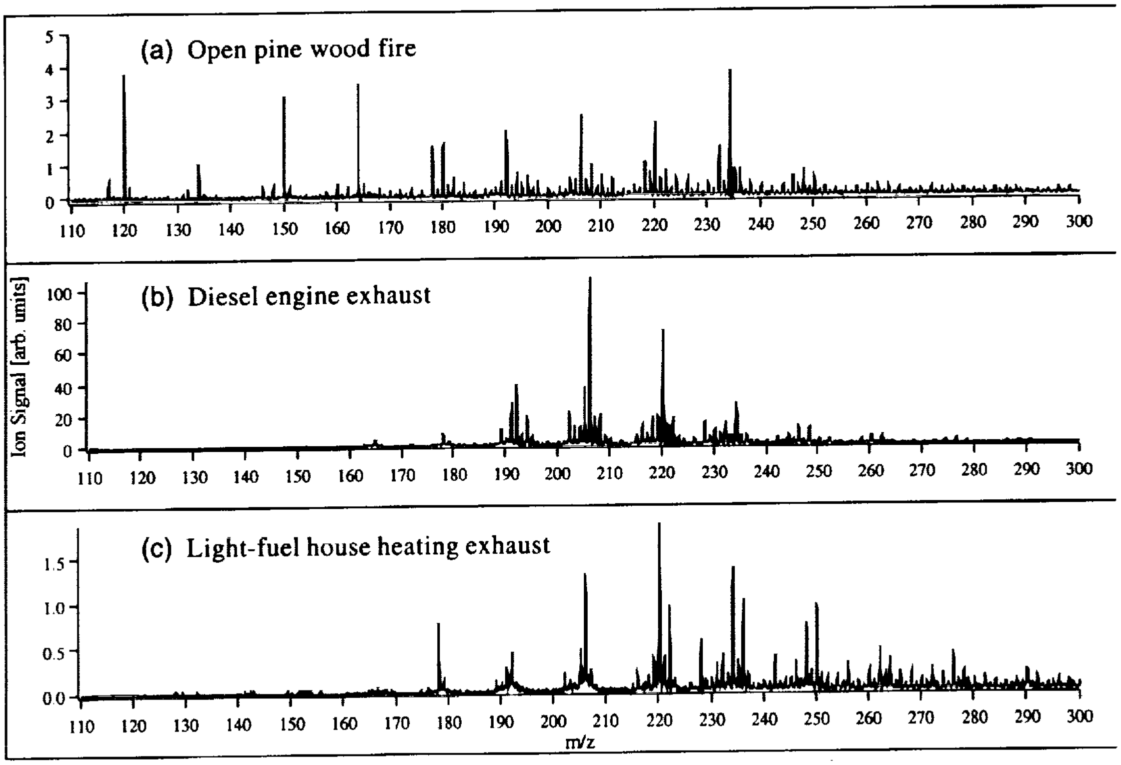

Fig. 1. Depicts L2MS spectra of different black carbon emission sources, such as (a) heating and natural wood-fire smoke, (b) gasoline and diesel engine exhaust, and (c) light-fuel house heating exhaust. The variations in the mass-spectral patterns of the different emission types are clearly evident.

part of the BCs ecotoxicological risk is attributed to its carcinogenic and mutagenic adsorbates. Therefore, the chemical characterization of BC is important.

Two-step laser mass spectrometry (L2MS) offers unique advantages over conventional trace-analytical methods for the determination of BC-bound PAHs, such as little or no sample preparation, short sampling and analysis time, small sample volumes, little matrix effects, and high sensitivity.

Sampling of airborne BC was performed on quartz-fiber filters. From there, an infrared laser pulse desorbs intact neutral analytes. Thereafter, an ultraviolet laser pulse (250-nm wavelength) is used for the resonance-enhanced two-photon ionization (1 + 1 REMPI) of the desorbed species. Mass analysis is then performed in a reflectron time-of-flight mass spectrometer. The mass spectra are dominated by intact parent ions of those compounds that strongly adsorb the selected ultraviolet laser wavelength.

Further, atmospheric particulate matter <10 µm (PM10) was collected at different locations (close to major motorways, at urban background sites, and in remote areas), and with varying temporal resolution (15 min for periods of 24 h, and 24 h over a whole year, respectively), and analyzed with L2MS. Multivariate statistics of the resulting mass spectra are used for the allocation of the major contributors to PM10 (Fig. 1).

HIGH-PRECISION CALCIUM-ISOTOPIC RATIO MEASUREMENT BY MULTIPLE COLLECTOR INDUCTIVELY COUPLED MASS SPECTROMETRY: PRELIMINARY DATA OF CALCIUM-ISOTOPIC RATIOS IN CARBONATES.

L. Halicz[1,2], A. Galy[1], N. S. Belshaw[1], and R. K. O'Nions[1], [1]Department of Earth Sciences, University of Oxford, Parks Road, OX1 3PR, UK, [2]Geological Survey of Israel, 30 Malkhey Israel Street, 95501 Jerusalem, Israel (ludwik@mail.gsi.gov.il).

Introduction: Calcium is an important element in animal and plant tissue. Biological incorporation of Ca affects its geological cycle, but its quantification remains difficult. One way is to use isotopic tracers such as stable isotopic rations of Ca. Few studies have been done on biological fractionation of Ca isotopes but already show an enrichment in light isotopes that can be as high as 0.8‰/amu in biomolecules and biomineralizations [1–4].

Multiple collector inductively coupled plasma mass spectrometry (MC-ICP-MS) is now an established technique for rapid measurement of isotope ratio to high precision. The MC-ICP-MS provided by Nu Instruments and described by Belshaw et al. [5] has previously been evaluated for lead and transition metals [5,6]. We present here a technique for the precise measurement of Ca isotopes by MC-ICP-MS.

Methods and Results: While accurate measurement of ^{40}Ca is made difficult by the presence of ^{40}Ar, the abundance of ^{44}Ca, ^{43}Ca, and ^{42}Ca is easily measured given the very low background arising from scattered ions of ^{40}Ar and ^{40}Ca. Molecular interferences in the Ca mass region observed in other ICP-MS work are insignificant when using the microconcentric nebulizer Cetac MCN-6000. However, it is important to monitor Sr^{2+} content, and this is carried out for $^{87}Sr^{2+}$ at mass 43.5. Simultaneous measurement of Ca isotopes and potential interferences was made possible by the 12-channel Faraday collectors array and the variable-dispersion geometry of the Nu Instrument mass spectrometer.

The method used to determine analytical repeatability is the "standard-sample bracketing" technique where Ca-isotopic ratios of samples are bracketed by measurement of the Ca standard. The internal precision for single 5-min analysis (5 repetitions) of ^{44}Ca/^{42}Ca and ^{43}Ca/^{42}Ca was 0.03 and 0.07‰ RSD respectively. The stability of uncorrected ratios of ^{44}Ca/^{42}Ca and ^{43}Ca/^{42}Ca during extended runs of 6 h was 0.10 and 0.15‰ RSD, respectively, and corrected to our standard 0.06 and 0.1‰ RSD, respectively.

The measured Ca-isotopic ratio was found to be insensitive over a solution concentration in the range of 2–45 ppm and was unaffected by Mg present in concentrations of up to twice that of Ca.

Conclusion: The performance of the MC-ICP-MS for Ca-isotopic ratios measurement is at least of the same level of precision and accuracy as the best results obtained by thermal ionization mass spectrometry (TIMS) [1–4].

The preliminary results of a few carbonate samples (calcretes, speleotherms, and corals) from different locations give interesting results and correlations. It is now necessary to investigate systematically the biological and geochemical control of Ca-isotopic ratios in the global Ca cycle.

References: [1] Price R. I. et al. (1990) *Biomed. Envir. Mass Spectrom., 19,* 353–359. [2] Platzner I. and Degani N. (1990) *Biomedical Envir. Mass Spectrom., 19,* 822–824. [3] Skulan J. et al. (1997) *GCA, 12,* 2505–2510. [4] Zhu P. and MacDougall J. D. (1998) *GCA, 62,* 1691–1698. [5] Belshaw N. S. et al. (1998) *Intl. J. Mass Spectrom., 181,* 51–58. [6] Zhu X. K. et al. (1999) *Chem. Geol.,* in press.

URANIUM IN KARST RIVER WATER IN THE GUIZHOU PROVINCE, CHINA.

G. L. Han and C. Q. Liu, The State Key Laboratory of Environmental Geochemistry, Institute of Geochemistry, Chinese Academy of Sciences, Guiyang 550002, China.

A number of scholars [1,2] have conducted research on the U geochemistry in river water to find the variation of input of U from rivers to oceans, and to get a better understanding of the geochemistry of U series in marine geochemistry. Moreover, the presence of uraninite in sediments has been proposed as an indicator of atmospheric oxidation and reduction levels [3]. This paper is focused on the variations of U in river water in carbonate regions (Wujiang River) drainage system, in order to learn the water chemistry of elements, understand the chemistry weathering of rock/soil in carbonate areas, and evaluate the impact on the environment by human activities.

The Wujiang River rises in the Wumeng Ranges on the Yunnan-Guizhou Plateau, and it is the largest tributary of the Changjiang River in the upper reaches and also the largest river in the Guizhou Province. The Wujiang River drainage system is located in karst areas of the Guizhou Province. The catchment represents many different and complicated lithologies, including Permian and Triassic limestones, dolomitic limestones, dolomites, and coal-bearing formations, as well as shales, sand shales, and siltstones.

Thirty-seven river water samples were collected January 7–27, 1999. Water temperature, pH, and conductivity were measured at sampling sites with a portable pH and SC (salt conductivity) meter. HCO_3^- was titrated by HCl on the spot. The river water samples were collected by placing an acid-cleaned linear polyethylene bottle in a plastic holder. Immediately after collection, all the samples were filtered through 0.22-µm membrane filters (Millipore) and acidified with ultra-purified hydrochloric acid (pH <2). Major cations (K, Na, Ca, Mg) were determined by atomic absorption spectrometry (AAS). Anions (Cl^-, SO_4^{2-}, NO_3^-) were measured by anion chromatography. The concentrations of dissolved trace elements were measured by inductively coupled plasma mass spectrometry (ICP-MS).

Except for sample 14 (U concentrations = 17.96 nmol/L), which had been polluted by waste discharged from factories, the U concentrations in the Wujiang River water vary from 0.78 to 7.25 nmol/L, with a mean value of 3.10 nmol/L, which is higher than the average value of global rivers (1.3 nmol/L [3]). On this basis, we calculated the flux of U to be 1656×10^3 mol/a.

There is a good correlation between U and total anion concentrations, and an inverse correlation between U and Si/total anion concentration, indicating that U in the river water from these large drainage basins is largely derived from nonsilicate weathering. The sample data of our research fall near the limestone weathering line, so it follows that the Wujiang River drainage system is located in a typical karst areas, and U in the Wujiang River water is derived from carbonate weathering. An additional source of U may be related to anthropogenic activities in agricultural production, as phosphate fertilizers are high in concentrations of U. The concentrations of PO_4^{3-} are very low (<0.01 mg/L). Furthermore, there is no correlation between PO_4^{3-} and U concentrations in the samples here. So we think that intensive agricultural activities would not necessarily lead to high river U levels.

The correlation between U and Sr shows the U/Sr (mol/mol) ratios are far smaller than the equivalent values of the upper crust, and in most river water samples, the ratios are far lower than the equivalent ones in limestones. As compared with limestones, there may be two factors that led to the depletion of U relative to Sr in the water body. One is the low solubility of U in the water body, and the other is the relative enrichment of U in residuals formed during the process of weathering of limestones. Uranium/strontium ratios are far greater than those of the upper continental crust, so the authors consider that in the process of weathering of limestones, Sr is more preferentially incorporated into the water body than U. So U is highly concentrated during the process of weathering.

References: [1] Shiller A. M. and Royle E. (1985) *Nature, 317,* 49–52. [2] Klinkhammer G. P. and Palmer M. R. (1991) *GCA, 55,* 1799–1806. [3] Palmer M. R. and Edmond J. M. (1993) *GCA, 576,* 4947–4955.

OSMIUM-, NEODYMIUM-, AND STRONTIUM-ISOTOPIC SYSTEMATICS IN YOUNG, FERTILE, AND WEAKLY METASOMATIZED SPINEL PERIDOTITE XENOLITHS FROM NORTHERN QUEENSLAND, AUSTRALIA.

M. R. Handler[1] and V. C. Bennett[2], [1]Department of Terrestrial Magnetism, Carnegie Institution of Washington, 5241 Broad Branch Road NW, Washington DC 20015, USA, [2]Research School of Earth Sciences, Australian National University, Canberra, ACT 0200, Australia.

Introduction: A suite of 13 peridotite xenoliths from the <3-Ma Atherton Tableland basalt province of northern Queensland, a region cratonized in the Paleozoic [1], comprise fertile samples of the upper mantle that have undergone only minimal metasomatic enrichment. As such they provide a relatively simple suite with which to investigate the evolution of young lithospheric mantle. We present Sr-, Nd-, and Os-isotopic data for the xenoliths, combined with major- and trace-element data, to constrain both the age of the samples and the Os-isotopic composition of the upper mantle from which they were derived.

The xenoliths are exclusively spinel-bearing lherzolites and are free from secondary volatile-bearing phases. They have limited major-element compositions, e.g., 2.6–3.4 wt% Al_2O_3 and 38.7–40.9 wt% MgO, with only the most incompatible trace elements showing indication of metasomatic enrichment, e.g., 0.11–1.49 (La/Yb)N, 0.12–0.45 (Sm/Yb)N. In particular, the middle rare earth elements are strongly fractionated, reflecting partial melt extraction in the presence of garnet. Measured Sm-Nd ratios therefore reflect melting processes rather than later metasomatic enrichment. This provides the opportunity to combine both the Sm-Nd- and Re-Os-isotopic systems for constraining the timing of melt extraction and lithosphere formation.

Isotopic Data and Discussion: Preliminary Sr- and Nd-isotopic data for four samples indicate derivation from a depleted mantle source. Strontium isotopes have a range from $^{87}Sr/^{88}Sr = 0.7029$ to 0.7047, while Nd isotopes range from $\varepsilon_{Nd} = 7$ to very radiogenic values of 19, supported by high Sm/Nd ratios ($^{147}Sm/^{144}Nd = 0.207–0.484$). The Sr- and Nd-isotopic data are consistent with the trace-element data, indicating that these samples have undergone melt extraction with no evidence for significant metasomatic enrichment in their history.

Measured Os-isotopic compositions for 12 samples range from $^{187}Os/^{188}Os = 0.1258$ to 0.1292, with one sample (MQ12) having a significantly less radiogenic composition of $^{187}Os/^{188}Os = 0.1228$. Most of the samples therefore have isotopic compositions that overlap with the range of estimates of modern mantle ($^{187}Os/^{188}Os = 0.1270–0.1290$ [e.g., 2,3]), so that any Os model ages calculated will vary widely depending on the model parameters chosen. However, the Os-isotopic composition of sample MQ12 is significantly lower than all the model estimates, and has a Re-depletion (TRD: a minimum model age based on the assumption that all Re was removed during melt extraction) age of ~800 Ma, consistent with speculation that Precambrian crust may underlie parts of the region [e.g., 4].

As the xenoliths have a limited range in fertility, the wide range in measured Os-isotopic compositions (even excluding sample MQ12) cannot be fully attributed to the samples evolving from a single event with significantly different Re/Os ratios. This indicates that either the samples span a range of ages or their upper mantle source was isotopically heterogeneous, or both.

Neodymium-depleted mantle model ages (TDM) offer a potential means of distinguishing between these possibilities, and thus constraining the Os composition of the source, as they can be used to estimate the time each sample segregated from the asthenospheric, or depleted upper mantle (DM). The TDM ages of three of the four samples analyzed (MQ12 excluded) have TDM ages of 220–270 Ma, which overlap with the timing of Permian magmatism and granite emplacement in the overlying Hodgkinson Province, but are younger than the oldest exposed crust (Silurian-Devonian sediments). This suggests these samples represent young, underplated lithospheric mantle. Furthermore, if all the samples (excepting MQ12) formed at this time, this would indicate a heterogeneous upper mantle source with a range in Os-isotopic composition that overlapped with both the more radiogenic measured abyssal peridotites (with average and maximum measured $^{187}Os/^{188}Os$ of 0.1246 and 0.127 respectively) [3], and the proposed primitive upper mantle (PUM) composition of Meisel et al. ($^{187}Os/^{188}Os = 0.129$) [2]. However, the age of the overlying crust and, in particular, the Os TRD age of MQ12 suggest melt extraction may extend back to the late Proterozoic. Samarium-neodymium analyses of the remaining samples are therefore needed before further constraints can be made.

Regardless of the age of the samples, however, the suite provides an example of relatively pristine subcontinental mantle that includes high, near-chondritic Os compositions.

References: [1] Bain J. H. C. and Draper J. J., eds. (1997) *North Queensland Geol.* [2] Meisel T. et al. (1996) *Nature, 383,* 517–520. [3] Snow J. E. and Reisberg L. (1995) *EPSL, 136,* 723–733. [4] Henderson R. A. (1980) in *The Geology and Geophysics of Northeastern Australia* (R. A. Henderson and P. J. Stephenson, eds.), pp. 1–26.

BLACK SHALE WEATHERING AND THE MOBILITY OF OSMIUM ISOTOPES, RHENIUM, AND PLATINUM GROUP ELEMENTS.

R. E. Hannigan[1] and B. Peucker-Ehrenbrink[2], [1]Department of Chemistry and Biochemistry, Old Dominion University, Norfolk VA 23539, USA (rhanniga@odu.edu), [2]Marine Chemistry and Geochemistry Department, Woods Hole Oceanographic Institution, Woods Hole MA 02543, USA (behrenbrink@whoi.edu).

Introduction: The Neogene marine Os budget has been dominated by input of radiogenic Os from the continents. The various sources of radiogenic Os to the oceans include Precambrian shield areas, Re-rich sulfides such as molybdenite, and sediments enriched in organic matter. Organic-rich sediments, black shales, and schists (hereafter simply referred to as black shales) are enriched by orders of magnitude in Re (10–2000 fold) and Os (5–80 fold), compared to average upper continental crust [1–3,5,6 and unpublished data]. Due to their high $^{187}Re/^{188}Os$ (up to ~1,400 [2]), they develop radiogenic Os-isotopic signatures with time. They are thus potentially important source rocks for mobile, radiogenic Os to the oceans [1–4]. Despite their ease of weathering, evidence for radiogenic runoff from terrains dominated by black shales is limited. In this study we investigate the mobility of Re and PGE by comparing the PGE and Re budget as well as the integrity of the Re-Os isotopic system of time-correlative pairs of fresh and weathered black shales samples.

Weathering and Platinum-Group-Element Mobility: Four time-correlative pairs of fresh (drill-core) and weathered (outcrop) black shales of upper Ordovician age (Utica Shale of Québec) were analyzed for Re and PGE concentrations and Os-isotopic compositions. Results indicate that surficial weathering dramatically alters the Re-Os isochron relationship as well as the PGE budget of black shales. More than 95% of the initial Re budget and between 46% and 90% of the Os budget are lost within <13,000 yr, the maximum age of exposure of the sections along the Jaques Cartier River and Dona Cona Creek. Iridium (40–82%), Ru (78–80%), Pt (50–78%), and Pd (26–61%) losses are also substantial. Whereas drill-core samples define an isochron age of 451 ± 5.7 m.y., which is, within uncertainty, identical to the biostratigraphic age, outcrop samples do not define an isochron (Fig. 1). The mobile Os fraction, calculated as the difference between unweathered and weathered samples, is significantly more radiogenic than the bulk shale. Our results show that black shales are indeed, as previously suggested, important sources of radiogenic Os to fresh and seawater.

Conclusions: Ravizza and Peucker-Ehrenbrink [7] estimate that only ~4% of the crustal Os budget is associated with organic-rich sediments. Only a small fraction of organic-rich sediments are black shales containing more than 15 wt% C_{org}, such as the USM samples. Thus, although black shales such as the ones analyzed in this study make up <1% of the upper crust, our analyses indicate that such rocks contribute disproportionately to the crustal inventory of mobile Os. Comparing the fraction of mobile Os in black shales with that of granitoid rocks can show this relationship. Peucker-Ehrenbrink and Blum [8] suggest that the mobile Os fraction in granitoid upper-crustal rocks accounts for only ~1% (~0.3 pg/g). In contrast, the results from this study indicate that 46–90% of the bulk black shale Os (0.2–0.85 ng/g),

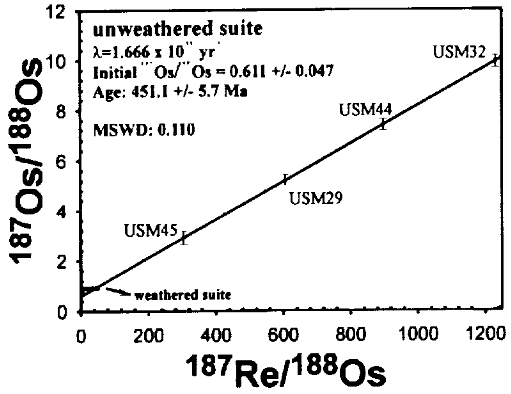

Fig. 1. Rhenium-osmium isochron for the unweathered USM samples. Note that the isochron age is approximately the same as the biostratigraphic age (451 Ma). All weathered samples plot in the box labeled "weathered suite."

~0.3 ng/g on average, is lost during surficial weathering of black shales. The mobile Os fraction associated with black shales is thus a factor of 10^3 larger than that associated with granitoid upper-crustal rocks. Even if not all of the mobile black shale Os is lost in dissolved form, this simple mass balance calculation indicates that weathering of black shales constitutes a significant source of radiogenic Os to river and seawater.

References: [1] Ravizza G. and Turekian K. K. (1989) *GCA, 53,* 3257–3262. [2] Ravizza G. et al. (1991) *GCA, 55,* 3741–3752. [3] Ravizza G. and Turekian K. K (1992) *EPSL, 110,* 1–6. [4] Pegram W. J. et al. (1992) *EPSL, 113,* 569–576. [5] Vine J. D. and Tourtelot E. B. (1970) *Econ. Geol., 65,* 253–272. [6] Ravizza G. and Esser B. K. (1993) *Chem. Geol., 107,* 255–258. [7] Ravizza G. and Peucker-Ehrenbrink B., in preparation. [8] Peucker-Ehrenbrink B. and Blum J. D. (1998) *GCA, 62,* 3193–3203.

SPECIATION AND BIOAVAILABILITY OF IRON IN LAKE KINNERET.

Y. Hareli[1], Y. Erel[1], C. Rosin[2], and A. Sukenik[2], [1]Institute of Earth Sciences, The Hebrew University, Israel, [2]The Kinneret Limnology Laboratory, Israel Limnology and Oceanography Research, Israel.

The chemical speciation of Fe with respect to its bioavailability was studied in Lake Kinneret (Sea of Galilee), a mesotrophic lake in the Jordan River Rift Valley.

This research is intriguing in light of the recent findings that Fe influences the productivity and species composition in coastal regions where Fe levels are much higher than in the open ocean. Fresh-water ecosystems of analogous Fe concentrations were barely studied as to the epilimnionic Fe speciation and its interactions with phytoplankton.

Lake Kinneret epiliminionic water samples were collected 6–12 times around the year from depths 0, 0.5, 1, 2, 4, 6, 8, 10, and 20 m (as an hypolimnion sample). We determined total digested Fe (Fe_{td}), Fe released by acidifying unfiltered lake water to pH 1 (Fe_{pH1}), Fe(II), Fe in 0.2-μm-filtered lake water (biota-free, $Fe_{0.2}$), Fe in 0.025-μm-filtered lake water (Fe_{diss}), labile Fe (8-hydroxyquinoline-Fe, Fe_{8qil}), and extracellular vs. intracellular Fe. Our study utilizes chemical (major ions and nutrients), physical (light, Secki depth, temperature), and biological (chlorophyll, biomass, primary productivity, species composition) parameters measured simultaneously by the Kinneret laboratory. In addition, we measured pH, dissolved O_2, dissolved organic matter, and total dissolved P.

In general, Fe concentrations in the epilimnion are highest (0.2–0.5 μM) in the winter and early spring, and they decrease in the spring and remain low (0.05–0.1 μM) throughout the summer and fall. Most of the Fe is added to the epilimnion by the winter and early spring runoffs and by up-welling from the anoxic hypolimnion when the lake is mixed. It is suggested that most of the epilimnionic Fe is scavenged by the Peridinim gastunese during its spring bloom. Thermal stratification of the lake and lack of summer runoffs maintain the low concentrations of Fe in the epilimnion.

In the spring and early summer we have observed significant differences between Fe_{td} and Fe_{pH1}, mainly in the maximum chlorophyll depths. These difference and the good correlation between Fe_{td} and chlorophyll suggest that most of the Fe is associated with biota. Whereas the lake total Fe is highly variable, "biota-free Fe" ($Fe_{0.2}$) is relatively stable throughout the year. In a few profiles there is a mirror image between "biota-free Fe" ($Fe_{0.2}$) and chlorophyll concentrations, suggesting a nutrient-like behavior of Fe.

In addition to field measurements we have established an experimental setup and have determined the reduction rates of Fe by several assemblages of microorganisms in the lake water. We found that the reduction rates of Fe are highly variable and species-dependent. Our results so far demonstrate the close link between Fe speciation in the lake and its role as a micronutrient.

THE RELEASE OF LEAD AND RARE EARTH ELEMENTS DURING GRANITOID DISSOLUTION.

Y. Harlavan[1,2] and Y. Erel[1], [1]Institute of Earth Sciences, The Hebrew University of Jerusalem, 91904 Jerusalem, Israel, [2]Geological Survey of Israel, 30 Malkhei Israel Street, 95501 Jerusalem, Israel.

A sequential leaching experiment was conducted on a granitic rock (El Capitan Granite, Sierra Nevada, California) in order to investigate the release of Pb and rare earth elements during granitoid weathering. Two aliquots of the rock sample were leached several times using a 0.6-M HCl solution. The amount of Si released by the first and final acid leaches was estimated to be equivalent to the release of Si after ~80 and 520 k.y. of weathering, respectively. The concentrations of the major elements decrease systematically with each successive leach and exhibit a preferential release of Mg, Fe, K, and Na over Si. During the early stages of granitoid weathering, as simulated by the first acid-leach fractions, Pb and REE are preferentially released due to the dissolution of accessory phases such as allanite. This results in higher $^{208}Pb/^{207}Pb$ ratios and different REE patterns in the acid-leach fractions relative to the whole-rock values. Allanite dissolution dominates the first 170 h of leaching, which are equal to ~260 k.y. In these early stages of weathering there is an increase of $^{208}Pb/^{207}Pb$, Ce/Pb, and chondrite-normalized Ce/Yb ratios toward allanite values. In addition, there is an enrichment of LREE compared with later leaching stages. The isotopic ratios of Pb and the chondrite-normalized Sm/Eu ratio indicate that in the following stages a significant dissolution of apatite and sphene is taking place. In the six final acid leaches, the isotopic ratios of Pb and the normalized REE patterns reflect the depletion of the accessory phases, and the increase in the contribution of feldspars.

Using the isotopic ratios of Pb, elemental compositions, and the REE concentrations, we were able to establish the following order of the relative weathering rates of accessory phases: allanite > apatite > sphene. In addition, biotite was found to be half as resistant to weathering as hornblende and probably dissolves completely after ~500 k.y. of weathering. These findings have relevance to soil-nutrient availability, soil development processes, Pb and REE concentrations in the soil and in groundwater, and the isotopic composition of Pb in marine sediments and ferromanganese crusts.

VARIATIONS IN HELIUM-3/HELIUM-4 (R/R$_a$) RATIOS IN AN ACTIVE RIFT ZONE: HENGILL COMPLEX, ICELAND.

D. Harrison[1], P. Burnard[2], and G. Turner[1], [1]Department of Earth Sciences, University of Manchester, M13 9PL, UK (dharrison@fs1.ge.man.ac.uk; gturner@fs1.ge.man.ac.uk), [2]Division of Geological and Planetary Sciences, California Institute of Technology, Pasadena CA 91125, USA (peteb@gps.caltech.edu).

Introduction: The neovolcanic zones of Iceland are unique in allowing access to subaerial sections of the mid-Atlantic Ridge spreading system. The geochemical influence of the Iceland plume on the ridge has produced elevated $^3He/^4He$ (R/R_a) ratios along the Peninsula. Published $^3He/^4He$ (R/R_a) values for the Peninsula vary between ≈13 and 24 [1–3] and appear to show a broad spatial provinciality. Small-scale variations in $^3He/^4He$ (R/R_a) have previously been attributed to both small-scale mantle heterogeneities [1] or the local addition of crustally derived radiogenic ^4He [2].

As part of an ongoing research project, this study will discuss variations in $^3He/^4He$ (R/R_a) measured in a suite of samples collected from a single fissure complex, the Hengill/Midfell Volcanic system.

Geology: The Hengill Complex is the surface manifestation of a ridge-transform triple junction. The area is structurally complex with ridge/fissure extension oblique to spreading. All lavas analyzed in this study were subglacially erupted between 20 and 40 ka [5].

Results and Discussion: A suite of picrite glasses and xenocrysts from the Hengill area have been analyzed by stepwise crushing for their trapped He and Ar (Figs. 1 and 2).

Initial modeling suggests that undegassed, early eruptions had a $^3He/^4He$ (R/R_a) ~17 and a $^{40}Ar^*/^4He$ ~0.5 (equivalent to the mantle production ratio), as found in the Dagmalafell/Midfell samples. This magma then degassed to various degrees, effectively decreasing the $^{40}Ar^*/^4He$ ratio due to different He and Ar solubilities. This resulted in the "degassing" trend shown in Fig. 2. A hiatus in eruption and subsequent crustal storage of the magma increased assimilation of lower crustal xenoliths. This resulted in a reduction of $^3He/^4He$ and an increase in $^{40}Ar^*/^4He$ as crustal ^{40}Ar and ^4He was added to the magma ("contamination trend" in Fig. 2). The starting composition for mixing with crustal contaminants is likely to be similar to the data with the lowest (i.e., most fractionated) $^{40}Ar^*/^4He$ values (Arnarfell). Analyses of xenocryst/glass pairs show the xenocrysts to have consistently lower $^3He/^4He$ (R/R_a) ratios [6], and a crustal xenolith from Husafell, southwest Reykjanes Peninsula has a $^3He/^4He$ (R/R_a) ~7.0, consistent with ingrowth of radiogenic He in the Reykjanes crust.

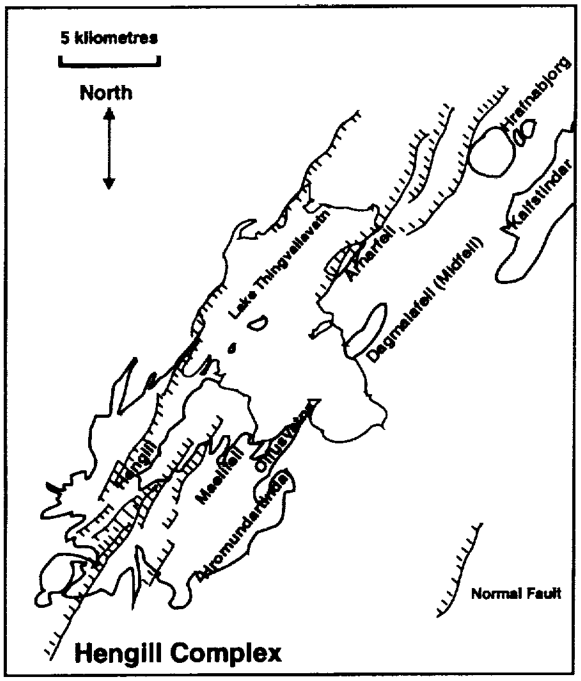

Fig. 1. The Hengill Volcanic Complex. Adapted from the Geological Map of Iceland [4].

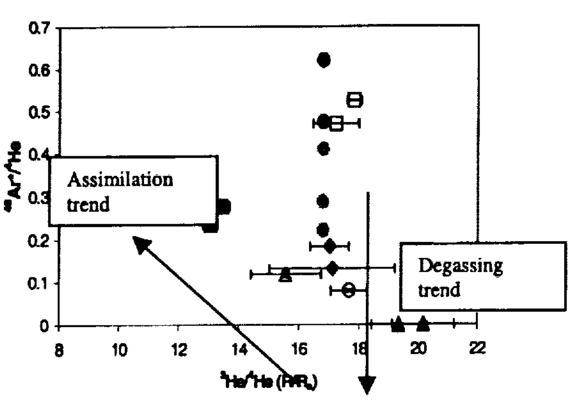

Fig. 2. Helium-3/helium-4 (R/R_a) vs. $^{40}Ar^*/^4He$. All data shown are from glasses. Maelifell (solid squares), Olfusvatns (open triangle), Hromundartindar (open circle), Arnarfell (solid triangles), Kalfstindar and Hrafnabjorg (solid diamonds), Dagmalafell (open squares). Analyses shown in solid circles are from Midfell (Dagmalafell) and Maelifell [6].

References: [1] Kurz et al. (1985) *EPSL.* [2] Condomines et al. (1983) *EPSL.* [3] Harrison et al. (1999) *EPSL,* in press. [4] Saemundsson et al. (1980). [5] Hansteen (1991) *Contrib. Mineral. Petrol.* [6] Burnard et al. (1994) *JGR.*

A HELIUM-ISOTOPIC TEST FOR THE ORIGIN OF PLUME MANTLE UNDER THE NORTHERN EAST SCOTIA RIDGE.

D. Harrison[1], P. T. Leat[2], and G. Turner[1], [1]Department of Earth Sciences, University of Manchester, M13 9PL, UK (dharrison@fs1.ge.man.ac.uk; gturner@fs1.ge.man.ac.uk), [2]British Antarctic Survey, Cambridge CB3 0ET, UK (p.leat@bas.ac.uk).

The East Scotia Ridge, situated in the South Atlantic, is the back-arc spreading center to the intra-oceanic Sandwich arc. New collections of samples from the ridge show a wide diversity in erupted magma compositions. Segment E2, in the northern part of the ridge, has an axial topographic high that contrasts with the riftlike topography common to most of the ridge. Lava compositions in the segment have been modeled by mixing of magmas derived from N-MORB-like mantle, a mantle plume component, and mantle modified by addition of fluids from the slab [1]. The mantle plume component is thought to have moved into the back-arc around the northern edge of the subducting slab. The "Bouvet-like" plume signature has higher $^3He/^4He(R/R_a)$, $^{87}Sr/^{86}Sr$, $^{206}Pb/^{204}Pb$, Nb/Yb, and lower $^{143}Nd/^{144}Nd$ than the local ambient mantle. This component can be traced from Bouvet Island to segment E2, via the South America-Antarctica Ridge, which connects the Bouvet triple junction to the Sandwich subduction system. As part of an ongoing investigation, four dredged samples from segment E2 have yielded $^3He/^4He$ (R/R_a) ratios of 8.0 ± 0.2, 8.1 ± 0.2, 8.4 ± 0.2, and 8.5 ± 0.1. These ratios compare with previously reported R/R_a ratios of 6.7–9.0 for the South American-Antarctic Ridge and 12.4 for Bouvet Island [2]. The MORB-like

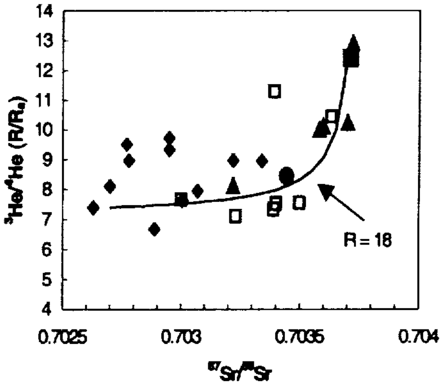

Fig. 1. Helium-3/helium-4 (R/R_a) vs. $^{87}Sr/^{86}Sr$. A comparison of data from Bouvet Island (filled square) [2], Bouvet Island Ridge (triangles) [2], America-Antarctic Ridge (diamonds) [2], southern mid-Atlantic Ridge (open squares) [2], and the E2 segment (circle). Mixing line is defined as $(He/Sr)_A/(He/Sr)_B$ and suggests that the E2 data can be explained by mixing between upper mantle and a degassed Bouvet plume source.

signature in the E2 segment contrasts with the plumelike signature recorded by other petrogenetic tracers. This is interpreted to be due to remelting of degassed plume material incorporated into the E2 mantle (Fig. 1). Degassing of the plume component is likely to have occurred beneath Bouvet Island, the Bouvet triple junction and the America-Antarctic Ridge. In consequence, He in magmas generated by mixing in segment E2 will be characterized by ambient upper mantle values, whereas Sr, Pb, etc. will be more influenced by the plume component.

References: [1] Leat P. T. et al. (1999) *J. Petrol.*, submitted. [2] Kurz M. D. et al. (1998) *GCA, 62,* 841–852.

INTRACRUSTAL PROCESSING OF VOLCANIC ARCS AS SHOWN BY OSMIUM-NEODYMIUM-STRONTIUM-ISOTOPIC VARIATIONS IN THE SOUTHERN CASCADE RANGE.

G. L. Hart[1], C. M. Johnson[1], S. B. Shirey[2], M. A. Clynne[3], C. R. Bacon[3], and R. L. Christiansen[3], [1]Department of Geology and Geophysics, University of Wisconsin–Madison, Madison WI 53706, USA, [2]Department of Terrestrial Magnetism, Carnegie Institution of Washington, Washington DC 20015, USA, [3]U.S. Geological Survey, Menlo Park CA 94025, USA.

Radiogenic isotopes have been very effective at detecting interaction between mantle-derived magmas and crust where the crustal component is old, as has been well demonstrated for Cordilleran batholiths that have been emplaced within Precambrian terranes [1]. The commonly used Sr-, Nd-, and Pb-isotopic systems will not evolve distinct isotopic compositions for the young crust that underlies many orogenic arcs, and therefore cannot address intra-crustal recycling of young mafic crust in such terranes.

The Re-Os-isotopic system, however, readily lends itself to detecting magma interaction with young mafic crustal material. Rhenium-osmium are siderophile elements and Os is compatible in the mantle, which yields high Re/Os in mafic- to intermediate-composition magmas. The exceedingly high Re/Os ratios of mafic lower crustal materials will rapidly produce very radiogenic Os-isotopic compositions within a few to tens of millions of years. Interaction of magmas with such radiogenic crust should be detectable in evolved volcanic rocks, especially those with low Os content.

The Cascade Range in the northwestern United States and southern British Columbia is a volcanic arc complex that was constructed on young mafic continental material. The arc has been active for the past 38 m.y., peaking between 35 and 17 Ma, and large volumes of mafic magma were produced and emplaced in the lower crust during this time. Such crust would likely be very radiogenic in Os-isotopic compositions, and yet would remain mantle-like in its Sr-, Nd-, and Pb-isotopic compositions.

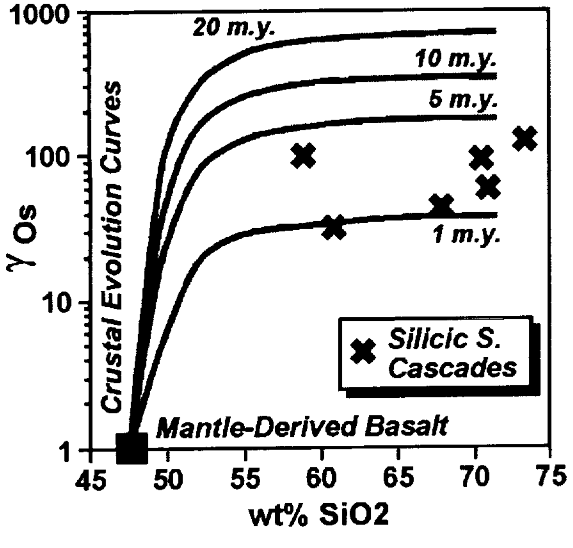

Fig. 1.

This study focuses on three volcanic centers of the southern Cascade Range: Lassen Peak, Mt. Shasta, and Crater Lake. Rhenium- and Os-isotopic compositions and abundances have been determined on magnetite separates (~1 g) for intermediate- to silicic-composition rocks from these three volcanic centers. The Os-isotopic data for these three centers show a substantial radiogenic Os component (γ_{Os} from 30 to 125) compared to what is expected from the mantle (γ_{Os} between –10 and 20), which could reflect mantle inhomogeneity, intracrustal recycling, or crustal contamination. The Os concentrations in these moderately evolved arc rocks are all very low (estimated at <3 ppt for whole rocks). However, magnetite has significantly elevated Os concentrations (up to 50 ppt) such that reasonably precise isotopic compositions may be determined.

An Os-isotopic evolution model for young crust suggests that the γ_{Os} of young mafic- to intermediate-composition lower crustal material can become highly radiogenic (γ_{Os} >500) over periods of 5–20 m.y., and subsequent partial melting or assimilation of this radiogenic source can explain the measured γ_{Os} compositions. Contamination of the magmas with old crust (Mesozoic or older) can be ruled out because this process would produce much less radiogenic Nd and more radiogenic Sr-isotopic compositions than are observed in the rocks.

Interpretation of continental crustal growth rates at convergent plate boundaries depends on the relative contribution of magma from the mantle vs. recycling of previously formed crustal material. The new Os-isotopic data suggest there is a component of recycled material in the eruptive rocks of the southern Cascade Range that is not easily seen in existing Sr-, Nd-, and Pb-isotopic data.

References: [1] DePaolo D. J. (1981) *JGR, 86,* 10470–10488.

PARTITIONING OF PYROGENIC AND PETROGENIC POLYCYCLIC AROMATIC HYDROCARBONS IN NARRAGANSETT BAY SEDIMENTS.

P. C. Hartmann and J. G. Quinn, University of Rhode Island, Narragansett RI 02882, USA (hartmann@gsosun1.gso.uri.edu; jgquinn@gsosun1.gso.uri.edu).

Polycyclic aromatic hydrocarbons (PAHs) are environmental contaminants that are found in most estuarine sediments, including those of Narragansett Bay, Rhode Island. There are two primary sources of PAHs to estuaries: pyrogenic PAHs derived from combustion sources and petrogenic PAHs derived from petroleum inputs. PAHs are an important class of environmental contaminants to study because some of these compounds are carcinogenic and/or mutagenic to mammals; in addition, they have both acute toxicity and sublethal effects on some aquatic organisms. PAHs may also bioaccumulate in edible shellfish, which gives them a pathway to humans. The EPA sediment quality criteria (SQC), based on current models of the sediment bioavailability of PAHs, use a partitioning coefficient between PAHs in pore water and on the total organic C in the sediments. However, recent work suggests that this partitioning in marine sediments does not agree with current models, and that small soot particles in the sediment may be responsible for some pyrogenically derived PAHs being less available to partition into porewater than petrogenic PAHs [1]. This is important because only the dissolved PAHs in porewater are considered bioavailable; conversely, the soot PAHs are strongly associated with solid phases and may be less susceptible to degradation in the sediments, thereby lasting for longer periods of time.

The objectives of our research project are to assess the contribution of pyrogenic and petrogenic PAHs to the sediments of Narragansett Bay and to evaluate the biogeochemical fate of these compounds with respect to soot carbon and organic carbon. We looked at 45 individual PAH compounds, including alkyl homologs, in over 40 surface sediment samples collected throughout Narragansett Bay. Previous studies at other sites have found a stronger relationship between selected PAHs and soot carbon than with organic carbon [2]. Our analysis did not find this relationship for bulk PAHs or the PAHs used in these other studies. We then turned to principal component analysis (PCA) to try and categorize sediment PAHs as pyrogenically or petrogenically dominated. Several materials were included in the analysis to help distinguish the sources of the PAHs. These included urban dust (SRM1649a), marine sediment (SRM1941a), #6 fuel oil, coal tar (SRM1597), #2 fuel oil, used crankcase oil, airplane soot, and fireplace soot. Pyrogenically-dominated sediments, as determined from PCA, showed a stronger correlation of PAHs with soot carbon than organic C, supporting the hypothesis that many of these PAHs are associated with soot particles. Petrogenically dominated sediments had a poor correlation of PAHs with both soot and organic C, possibly because they contain weakly associated PAHs that are strongly influenced by sediment diagenesis.

References: [1] McGroddy S. E. and Farrington J. W. (1995) *Environ. Sci. Tech., 29,* 1542–1550. [2] Gustafsson Ö. and Gschwend P. M. (1997) in *Molecular Markers in Environmental Geochemistry* (R. P. Eganhouse, ed.), pp. 365–380, American Chemical Society, Washington DC.

REACTIVITY OF BULK ORGANIC MATTER IN AQUIFER SEDIMENTS.

N. Hartog and J. Griffioen, Utrecht University, P.O. Box 80021, 3508 TA Utrecht, The Netherlands (nhartog@geo.uu.nl).

Introduction: Knowledge on the natural reduction capacity of aquifers has become increasingly important over the last decades, because of the excessive input of oxidants in groundwater systems, mainly by agricultural activities. The degradation of bulk organic matter (BOM) in aquifers contributes to the potential of sandy aquifers to reduce oxidants as O, nitrate, and sulfate. A previous study indicated the usefulness of the Micro-Oxymax™ respirometer to study the degradation of BOM in sandy aquifer sediments [1]. The degradation kinetics of BOM are primarily controlled by its reduction activity [2]. Therefore, the present study focused on the differences in BOM reactivity in various aquifer sands in different particle size fractions and tried to link the differences with the organic chemistry of the BOM determined with a pyrolysis-gas chromotography-mass spectrometry investigation.

References: [1] Hartog N. et al. (1998) *Mineral. Mag., 62A,* 579–580. [2] Bradley P. M. et al. (1992) *Environ. Sci. Technol., 26,* 2377–2381.

NITROGEN- AND CARBON-ISOTOPIC SYSTEMATICS WITHIN SIBERIAN DIAMONDS: CONSTRAINTS FROM SECONDARY ION MASS SPECTROMETRY AND FOURIER TRANSFORM INFRARED STUDIES.

E. Hauri[1], D. G. Pearson[2], G. Bulanova[2], and H. J. Milledge[3], [1]Department of Terrestrial Magnetism, Carnegie Institution of Washington, 5241 Broad Branch Road NW, Washington DC 20015, USA, [2]Department of Geological Sciences, Durham University, South Road, Durham, DH1 3LE, UK, [3]Department of Geological Sciences, University College London, Gower Street, London WC1E 6BT, UK.

Introduction: Studies of the isotopic characteristics of C ($\delta^{13}C$) and N ($\delta^{15}N$) in diamonds from kimberlites have revealed a wide range of isotopic signatures, the ultimate origins of which remain elusive. Diamonds containing peridotite-suite mineral inclusions (so-called P-type) and the rims of coated diamonds have been used to constrain the isotopic composition of their mantle-derived fluid source, which is broadly characterized by $\delta^{13}C$ and $\delta^{15}N$ values of –5‰ and 0‰ respectively [1–6]. This has been suggested to be the signature of primordial upper-mantle fluids. Diamonds containing eclogite-suite mineral inclusions (E-type) overlap the range of C and N isotopic ratios displayed by P-type diamonds, but also extend to much lower $\delta^{13}C$ and higher $\delta^{15}N$. In general, conventional bulk analyses of individual diamonds show no significant relationships between N aggregation, N isotopes, C isotopes, and inclusion paragenesis. Furthermore, the relationship between diamond stable isotope variations and recycling is unclear.

Results and Discussion: We have developed *in situ* techniques for the measurement of N abundance and C- and N-isotopic ratios in diamonds via secondary ion mass spectrometry (SIMS) using a Cameca IMS6f ion microprobe. Reproducibility (2σ) and accuracy are ±0.5‰ for $\delta^{13}C$, ±1.5‰ for $\delta^{15}N$ (>100 ppm N), and ±5% for N abundance. Reproducibility of $\delta^{15}N$ in areas with <100 ppm N ranges from 2–14‰ correlated with N abundance, and is limited by counting statistics on ^{15}N.

Carbon and N isotope ranges within individual diamonds vary widely, and at this early stage does not appear to be correlated with crystal habit, inclusion paragenesis, or extent of N aggregation. This is exemplified by two diamonds from Mir of different paragenesis (#1013 E-type, #1525 P-type), both of which display complex, irregularly zoned cores containing fully aggregated IaB N, surrounded by zones of octahedral growth with less aggregated N. The E-type specimen (#1013) has highly variable $\delta^{15}N$ and $\delta^{13}C$ (–8.8‰ to +1.7‰) in the core, with homogenous $\delta^{13}C$ (–4.5‰) and $\delta^{15}N$ (–2.4‰) in the surrounding octahedral growth. The P-type specimen (#1525), which displays only a 1.6‰ total variation in $\delta^{13}C$, has homogenous $\delta^{15}N$ of –2.4‰ in the core and variable $\delta^{15}N$ (–3.9‰ to +9.0‰) in the surrounding octahedral growth.

Within the dataset (and also within single diamonds), both $\delta^{13}C$ and $\delta^{15}N$ tend to increase as N abundance decreases. Possible origins for these correlations include (1) reservior effects during equilibrium diamond growth from a limited fluid reservoir, (2) changes in fluid speciation and C-N isotopic fractionation factors during equilibrium diamond growth, (3) fluctuations in the C-N-isotopic signatures of the fluid in an open system, and (4) kinetic isotope fractionations during disequilibrium growth. Constraints and possible tests of these hypotheses will be presented at the meeting.

References: [1] Cartingny P. et al., *Terra Nova, 9,* 175–179. [2] Boyd S. R. et al. (1992) *EPSL, 109,* 633–644. [3] Cartingny P. et al. (1998) *Science.* [4] Deines and Harris (1995) *GCA, 59,* 3173–3188. [5] Javoy et al. (1984) *EPSL, 68,* 399–412. [6] Javoy et al. (1986) *Chem. Geol., 57,* 41–62. [7] Bulanova G. P. (1995) *J. Geochem. Explor., 53,* 1–23. [8] Taylor W. R. et al. (1995) *Ext. Abstr. 6th Intl. Kimberlites Conf.,* 608–610. [9] Griffin B. J. et al. (1995) *Ext. Abstr. 6th Intl. Kimberlites Conf.,* 191–193. [10] Deines P. et al. (1989) *GCA, 53,* 1367–1378.

CRUSTAL RECYCLING OR CORE-MANTLE INTERACTION? STABLE ISOTOPIC SIGNATURES OF HAWAI'IAN BASALTS.

E. Hauri[1], P. Tomascak[2], and J. Lassiter[3], [1]Department of Terrestrial Magnetism, Carnegie Institution of Washington, 5241 Broad Branch Road NW, Washington DC 20015, USA, [2]Lamont-Doherty Earth Observatory, Columbia University, Palisades NY, USA, [3]Max-Planck-Institut für Chemie, Mainz, Germany.

Introduction: Recent geochemical studies of Hawai'ian basalts have revealed important correlations among major elements, trace elements, and various isotope ratios in tholeiitic lavas from the shield-building phase of many Hawai'ian volcanos. With recent data, new hypotheses advanced to explain the origin of these signatures include crustal assimilation, recycling of ancient subducted crust, and core-mantle interaction. Invariably, the debate among these hypotheses focuses on the volcanic end members that define the extremes in the geochemical data, namely the Loihi, Mauna Kea, and Koolau shields. In order to further constrain the origin of the heterogeneous Hawai'ian mantle, we present preliminary data from an ongoing stable isotope study of Hawai'ian lavas.

Results and Discussion: Lithium-isotopic data for whole rocks from Kilauea, Mauna Loa, and Koolau, measured by multiple collector inductively coupled plasma mass spectrometry (MC-ICP-MS), span a range of δ^7Li from 3.0‰ to 5.7‰, with the highest ratios measured in Koolau lavas. This signature is consistent with incorporation of material altered by seawater at low temperatures, concordant with the elevated O isotopes in olivines from these same Koolau lavas. Experiments are underway to perfect Li-isotopic measurements on olivine separates, thereby making possible a more direct comparison with the O-isotopic data.

We have also performed measurements of volatile abundances, D/H and $^{11}B/^{10}B$ ratios in individual Hawai'ian melt inclusions by secondary ion mass spectrometry (SIMS). Boron isotopes show elevated ratios ($\delta^{11}B$ up to 2.3‰) in melt inclusions containing the highest abundances of water and Cl. This is true even when examining melt inclusions from a single sample, suggesting the presence of a Cl-rich crustal brine contaminant similar to that proposed for Loihi by Kent et al. [1]. However, a Loihi melt inclusion with 1.39 wt% Cl and 20 ppm B has a $\delta^{11}B$ of only 0‰, suggesting a mixture of magmatic and seawater components in this brine. Melt inclusions display $\delta^{11}B$ as low as –16‰ from Koolau and –15‰ at Loihi, but neither the lowest nor highest values correlate with data for other radiogenic and stable isotopes. Koolau melt inclusions are also characterized by very low H_2O and Cl concentrations (down to 0.07 wt% and 8 ppm, respectively), and low D/H ratios (–120‰ to –165‰). Low-Cl melt inclusions from Koolau generally have the lowest δΔ, and average D/H ratios of each volcano (from melt inclusions and submarine glasses) correlate with Os, Sr, Nd, and Pb isotope averages.

In general, the stable isotope data are consistent with the Koolau end member containing a substantial fraction of recycled crustal material that has interacted with liquid water near the Earth's surface. The low H_2O and δΔ values of this component indicate it has been extensively dehydrated. Subduction dehydration will result in very low D/H and $\delta^{11}B$ with concurrently low $\delta^{7}Li$; the observation that Koolau has elevated $\delta^{7}Li$ may be due to the ease of substitution of Li into Mg sites in most minerals, perhaps making it more resistant to removal during dehydration. When considering together all the Hawai'ian geochemical data, it is difficult to find support for the core-mantle interaction hypothesis for the high-^{187}Os Koolau component, as advocated by Brandon et al. [2]. In addition, specific consequences of the addition of core material to this and other Hawai'ian mantle components, such as elevated Os and Re contents, buffered iron-wustite f_{O_2}, and decoupling of Os from other isotopes, are not indicated by the increasingly extensive geochemical database for Hawai'ian basalts.

References: [1] Kent et al. (1999). [2] Brandon et al. (1998).

A HISTORY OF OCEAN SALINITY DURING THE PHANEROZOIC, BASED ON SEDIMENTARY CYCLING.

W. W. Hay[1], S. Floegel[1], and C. N. Wold[2], [1]GEOMAR, Christian-Albrechts-University, Wischhofstrasse 1-3, D-24148 Kiel, Germany (whay@geomar.de; sfloegel@geomar.de), [2]Platte River Associates, 2790 Valmont Road, Boulder CO 80304, USA (chris@platte.com).

Introduction: The salinity of the ocean in the past can be reconstructed by using knowledge of existing evaporite deposits on land and offshore. The DSDP showed that evaporites can occur in the early deposits of an opening ocean basin. The salt deposits documented by DSDP and ODP are very large compared to those found on land. Holser et al. [1] suggested that during the Mesozoic and Cenozoic there have been significant declines from a higher level of ocean salinity in the Paleozoic.

Reconstructing Ancient Ocean Salinity: We assume that during the Phanerozoic the major sources of salt have been erosion of evaporite deposits and release of saline sedimentary pore waters. We assume that the masses of sediments that existed in the past can be estimated from the cycling rates determined from masses still in existence today [2,3]. We also assume that evaporites and saline pore waters on land follow the same rates of sedimentary cycling as other sedimentary materials; this allows reconstruction of both the original masses of evaporites deposited and the time-varying flux of salt to the sea. In contrast to other sedimentary materials, salt can be stored in the ocean until conditions appropriate for deposition occur. We assume that salt removals into the deep offshore, continental margin and marginal sea deposits, are not yet part of the recycling system. The conclusion is that during most of the Cenozoic and during all of the earlier Phanerozoic, ocean salinities have been higher than they are today. During the breakup of Pangaea, each of the major salt extractions into the developing young ocean basins caused a rapid decrease of oceanic salinity by a few per mil. In the Paleozoic and Triassic, ocean salinities were in the low 50s to high 40s. From the mid-Jurassic to mid-Cretaceous they declined to 43 and then 36. The late Miocene extractions (Mediterranean) lowered salinities to modern levels.

Effects of Lowering Salinity: Today, deep-water formation almost always involves density increase via a phase transformation involving large amounts of latent heat: salinization through evaporation or sea-ice formation. This is because at the modern mean salinity (34.7) temperature change has only a small effect on density near the freezing point. At higher salinities the density change with temperature near the freezing point becomes much larger, causing the ocean to behave differently [4]. The higher salinities indicated for the Paleozoic would have ensured that deep-water formation was via simple cooling, implying a climate system very different from that of today. The lowering of salinity induced by the Late Miocene extractions has made it easier to form sea ice around Antarctica, and may have been a factor in Neogene climate change.

The history of ocean plankton seems to be closely related to mean salinity. Hystrichospheres and acritarchs were the characteristic plankton of the earlier Paleozoic. The high salinities of the late Paleozoic coincided with the "plankton blackout." It was during the Mesozoic decline that very large quantities of petroleum-forming organic matter were buried, and only afterward did the calcareous plankton spread into the open ocean.

References: [1] Holser W. T. et al. (1980) *GSA Abstr. with Prog.*, 448. [2] Wold C. N. and Hay W. W. (1990) *Am. J. Sci., 290*, 1069–1089. [3] Wold C. N. and Hay W. W. (1993) *Geoinformatics, 4*, 137–144. [4] Hay W. W. et al. (1998) *Zentralblatt Geol. u. Pal. 1996 (11/12)*, 1445–1454.

DOES SURFACE STRUCTURE INFLUENCE H^+ and OH^- ADSORPTION ON SILICATES IN AN AQUEOUS MEDIUM? AN EXAMPLE BASED ON ALBITE AND ALBITE GLASS.

R. Hellmann, Crustal Fluids Group, Laboratoire de Géophysique Interne et Tectonophysique–Centre National de la Recherche Scientifique-Université de Grenoble I, 38041 Grenoble Cedex 9, France (hellmann@obs.ujf-grenoble.fr).

Introduction: It is well known that surface chemistry and structure affect the reactivity of solids. The surface chemistry/speciation of solids in contact with fluids is influenced by the adsorption of aqueous species at the fluid/solid interface. One of the most important reactions at fluid/metal oxide interfaces is the adsorption of proton and hydroxyl ions at surface sites. Studies of the adsorption behavior of protons on oxide surfaces have shown the importance of these reactions with respect to the overall pH-dependency of the dissolution rate of minerals [e.g., 1,2].

The purpose of this study is to determine the effect that surface structure exercises on the adsorption behavior of silicates having the same chemical composition. Albite and albite glass were chosen since their structures and dissolution behavior have been extensively studied. The main difference in their respective structures is their ring configurations: albite is composed of four-membered tetrahedral rings, whereas albite glass is characterized by six-membered tetrahedral rings [3].

Methods: Surface titrations are a commonly used technique for determining surface adsorption behavior of solids immersed in an aqueous medium. The technique relies on the incremental addition of acid or base to an aqueous suspension of powder. The resultant adsorption isotherms are based on data from the continuous titration of the same suspension over a wide pH range. In this study, a "mini-titration" technique was used. This modified titration technique is based on the addition of powder to an aliquot of fluid at a fixed initial pH; the pH rapidly changes over the course of less than 5 min. The concentration of adsorbed H^+ and OH^- is a function of ΔpH. After the pH equilibrates, the leachate is filtered and the concentrations of released elements due to dissolution (Na, Al, Si) are measured. This procedure is repeated with individual titrations of fresh powder over a wide range of pH (1–13); the resultant adsorption isotherms are therefore based on a series of independent mini-titrations. There are several important advantages to this technique: (1) the use of fresh powder for each experimental data point ensures that the titration measures H^+ and OH^- adsorption on unaltered material (i.e., changes in surface chemistry that can occur during a continuous titration are not a problem); (2) the concentrations of elements released into solution due to dissolution can be measured at the end of each mini-titration; this is not the case in a continuous titration; (3) the adsorption isotherm is based on titrations using a constant solid-to-fluid ratio; it does not change, as is the case in a continuous titration (especially over a large pH range); and (4) the kinetics of adsorption at any specific pH can be recorded.

Results: Preliminary results indicate that the adsorption behavior of albite and albite glass at 25°C is very similar. The adsorption of H^+ on both albite and albite glass surfaces consists of interstitial Na^+ sites (due to ion exchange), as well as adsorption at >Si-OH, >Al-OH, and >Si-Obr -Al< sites (Obr denotes a bridging O site). Adsorption of OH^- presumably occurs at the same types of sites, with the exception of the interstitial Na^+ sites (i.e., ion exchange is pH-dependent). The concentrations of adsorbed H^+ and OH^- for both materials is at a minimum in the pH range of 7–9; this corresponds to the minima determined in other feldspar titration studies [e.g., 4,5]. In order to calculate the concentration of H^+ adsorbed exclusively at >Si-OH, >Al-OH, and >Si-Obr-Al< surface sites, ion exchange of H^+ with Na^+ must be subtracted from the overall H^+ adsorption measurement. This correction has a dramatic effect on the H^+ adsorption isotherm; it is shifted to much lower pH values, such that for both albite and albite glass, the ion exchange-corrected concentrations of H^+ adsorbed at the surface are ~0 at pH 3.5–4.0. This can be compared to a theoretical estimate of pH 5.2 for the zero-point-of-charge of low albite [6]. Over the pH range 4–10, the exact determination of the net surface charge due to adsorption at >Si-OH, >Al-OH, and >Si-Obr-Al< surface sites is not possible, due to difficulty in deconvoluting the overall adsorption signal (i.e., correction of $[H^+]$ and $[OH^-]$ in solution due to speciation changes of aqueous Al and Si released by dissolution of the powder). In any case, the quantification of the surface charge over the pH range 4–10 is not important since this corresponds to the region of minimum surface charge. Adsorption isotherms (log surface $[H^+]$ and $[OH^-]$ as a function of pH) allow for linear regressions of the H^+ and OH^- adsorption data. The albite and albite glass isotherms reveal similar slopes: −0.5 to −0.6 in the acid pH range, and 0.9 in the basic pH range. The slopes in the acid pH range compare closely to those of albite determined in a previous study [4], whereas the slopes in the basic pH range are significantly higher.

References: [1] Zinder B. et al. (1986) *GCA, 50,* 1861–1869. [2] Stumm W. and Furrer G. (1987) in *Aquatic Surface Chemistry* (W. Stumm, ed.), pp. 197–219. [3] Taylor M. and Brown G. E. Jr. (1979) *GCA, 43,* 61–75. [4] Blum A. E. and Lasaga A. C (1991) *GCA, 55,* 2193–2201. [5] Stillings L. et al. (1995) *GCA, 59,* 1473–1482. [6] Sverjensky D. A. (1994) *GCA, 58,* 3123–3129.

MOLYBDENUM(VI) SPECIATION AND KINETICS IN SULFIDIC WATERS.

G. R. Helz and B. E. Erickson, Department of Chemistry and Biochemistry and Water Resources Research Center, University of Maryland, College Park MD, USA (ghl7@umail.umd.edu; b_erickson@acs.org).

Molybdenum in sediments and sedimentary rocks is a potential indicator of paleoenvironmental conditions. This application demands better knowledge of Mo deposition mechanisms and in turn requires improved understanding of Mo speciation in anaerobic natural waters. In sulfidic water, molybdate undergoes sulfidation in four steps, leading finally to tetrathio-molybdate:

$$MoO_xS_{4-x}{}^{2-} + H_2S(aq) \rightarrow MoO_{x-1}S_{5-x}{}^{2-} + H_2O(l)$$

where ($1 \leq x \leq 4$). Equilibrium constants ($K_{(4-x)(5-x)}$) and rate constants ($k_{(4-x)(5-x)}$) for these reactions have been measured by UV-visible spectroscopy. At 25°C, over a wide range of ionic strength, $\log K_{01} = 5.19 \pm 0.03$, $\log K_{12} = 4.80 \pm 0.12$, $\log K_{23} = 5.00 \pm 0.13$, and $\log K_{34} = 4.88 \pm 0.28$. The intermediates have negligible stability fields. Therefore, provided the rate of increase in $H_2S(aq)$ is slow enough to maintain near-equilibrium conditions, increasing $H_2S(aq)$ causes a sharp transition from $MoO_4{}^{2-}$ to $MoS_4{}^{2-}$ at ~11 μM $H_2S(aq)$ (the action point of a geochemical switch) [1]. The resulting transformation of the predominant Mo anion from a hard to a soft base changes profoundly the geochemical properties of this element.

On the other hand, because the rate of each successive sulfidation reaction is approximately one order of magnitude slower than the previous one, di → tri and tri → tetrathiomolybdate equilibria may not be achieved in seasonally or intermittently sulfidic water columns. In such environments, unstable mixtures of intermediate thiomolybdates may predominate. The sulfidation reactions are acid catalyzed; environments such as sediment pores, which are enriched in Brønsted acids ($NH_4{}^+$, $H_2CO_3{}^0$, R-COOH, protonated mineral surface sites), will therefore promote equilibration. This may explain previous observations that Mo fixation in sedimentary environments occurs primarily by diagenetic processes rather than water-column scavenging.

This paper calls attention to the potential for kinetic controls in trace-element speciation. Thermodynamics predicts that Mo will occur only as $MoO_4{}^{2-}$, or $MoS_4{}^{2-}$; kinetics predicts that intermediates such as $MoO_2S_2{}^{2-}$, will predominate in dynamic, seasonally variable systems. Thermodynamics predicts that $MoO_4{}^{2-}$ will be the only form in O_2-bearing (low HS^-) waters whereas $MoS_4{}^{2-}$ is in fact capable of persisting metastably in such waters for weeks (possibly accounting for some of the fixed sulfide observed in low HS^- marine surface waters).

References: [1] Helz G. R. et al. (1996) *GCA, 60,* 3631–3642.

OSMIUM-ISOTOPIC ANALYSIS BY DYNAMIC MULTIPLE COLLECTOR INDUCTIVELY COUPLED PLASMA MASS SPECTROMETRY USING IRIDIUM-191 SIGNAL NORMALIZATION.

N. G. Hemming[1], S. L. Goldstein[1,2], and R. G. Fairbanks[1,2], [1]Lamont-Doherty Earth Observatory, Columbia University, Palisades NY 10964, USA, [2]Department of Earth and Environmental Sciences, Columbia University, USA (hemming@ldeo.columbia.edu; steveg@ldeo.columbia.edu; fairbank@ldeo.columbia.edu).

Introduction: Early studies [1,2] of Os-isotopic geochemistry (i.e., ion probe and surface ionization mass spectrometry work) set the stage for the application of this relatively new geochemical tool. However, widespread use of this system was not seen until the advent of negative thermal ionization mass spectrometry techniques (NTIMS) [3,4] that dramatically simplified Os analysis, both increasing precision while reducing sample size. Since that time, the increase in publications using the Re-Os system is dramatic. We present a technique for obtaining $^{187}Os/^{188}Os$ using a multiple collector inductively coupled plasma mass spectrometer (MC-ICP-MS). The precision and amount of Os necessary for this technique is comparable to recently published NTIMS work. The sample preparation and analysis time, however, is greatly improved.

Technique: Our technique was developed on a VG Plasma-54 multi-collector 90° sector double-focusing mass spectrometer equipped with nine Faraday collectors, a Daly ion counting system, and an inductively coupled plasma (ICP) source. Sample introduction was by a CETAC MCN 6000 desolvating nebulizing system. Osmium standard solutions ranging from 85 to 500 ppt were introduced into the nebulizer by self-aspiration at a rate of ~40 μL/min. Total sample volume necessary for analysis is <2 mL. The analysis consisted of five blocks of ten scans on relevant peaks. Each analysis took about 1 h and thus was a significant improvement over the time necessary for NTIMS analysis.

An important addition to the sample solutions is dilute hydroxylamine hydrochloride to facilitate washout of the Os from the MCN [5]. Without that addition, significant Os signals were observed even hours after a sample was analyzed, while complete washout was seen after only 3 min when the hydroxylamine hydrochloride was used. This addition keeps the Os reduced as it passes through the desolvating apparatus.

Results and Discussion: The Os isotopes analyzed are shown in Table 1. Table 1 shows the Faraday cup configuration and the sequence of the mass scan. The ratios $^{186}Os/^{191}Ir$, $^{187}Os/^{191}Ir$, $^{188}Os/^{191}Ir$, and $^{189}Os/^{191}Ir$ are all measured with the Os isotope in the multiplier and the ^{191}Ir in the high-mass Faraday cups 4, 3, 2, and 1, respectively.

The Ir concentration in the sample solutions is about 200 ppb, resulting in a 1-V signal on ^{191}Ir. The $^{186}Os/^{188}Os$ is calculated by dividing the $^{186}Os/^{191}Ir$ by the $^{189}Os/^{191}Ir$, and the $^{187}Os/^{188}Os$ ratios is calculated by dividing

TABLE 1. Collector configuration for Os-isotopic analysis.

Cycle	Low 2	Low 1	Daly	High 1	High 2	High 3	High 4
1	**181**	184	**185**	187	188	189	190
2	182	185	**186**	188	189	190	**191**
3	183	186	**187**	189	190	**191**	192
4	184	187	**188**	190	**191**	192	193
5	185	188	**189**	**191**	192	193	194
6	178	**181**	**182**	184	185	186	187

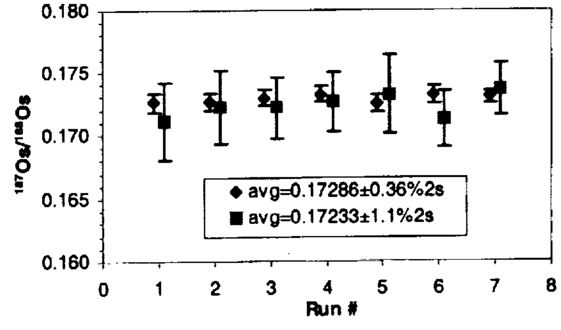

Fig. 1. Osmium-187/osmium-186 with (diamonds) and without (squares) ^{191}Ir signal-normalization. Error bars show 2σ in-run precision.

the ^{187}Os/^{191}Ir by the ^{189}Os/^{191}Ir. This approach normalizes out much of the signal noise inherent to MC-ICP-MS analysis. Comparing analyses with and without the ^{191}Ir shows the dramatic improvement that the normalization achieves (Fig. 1). A mass fractionation correction is applied using the measured ^{191}Ir-signal normalized ^{189}Os/^{188}Os ratio, normalized to a value of 1.21968. The average of these analyses are 0.17286 ± 0.37% 2σ for the signal-normalized values and 0.17233 ± 1.1% 2σ for the unnormalized. Note that data for both the signal-normalized and unnormalized were collected simultaneously.

In order to make a correction for the ^{187}Re interference on ^{187}Os, ^{185}Re is also measured. As the ^{191}Ir mass cannot be monitored during this scan, ^{181}Ta was also added to the sample solutions. In addition, ^{186}W was monitored using ^{182}W. However, due to a significant W contamination (up to 20% of the mass 186 signal), this correction is unreliable and thus the ^{186}Os/^{188}Os ratios have very poor reproducibility. This source of contamination must be removed if this method is to prove useful for Pt-Os work.

This technique opens up the use of MC-ICP-MS for Os analysis of small geologic samples, and can be extrapolated to other isotope systems. The time savings realized by the simple sample introduction over that necessary for NTIMS is significant, while for normal size samples the precision is comparable to NTIMS.

References: [1] Luck J.-M. and Allègre C. J. (1983) *Nature, 380,* 130–132. [2] Walker R. J. and Fassett J. D. (1986) *Anal. Chem., 58,* 2923–2927. [3] Heumann K. G. et al. (1988) in *Inorganic Mass Spectrometry,* pp. 301–376, Wiley and Sons. [4] Creaser R. A. et al. (1991) *GCA, 55,* 397–401. [5] Fleisher M., personal communication.

NEODYMIUM-ISOTOPIC CONSTRAINTS ON DEEP OCEAN CIRCULATION DURING THE LATE QUATERNARY.

S. R. Hemming and S. L. Goldstein, Department of Earth and Environmental Sciences and Lamont-Doherty Earth Observatory, Columbia University, Route 9W, Palisades NY 10964, USA (sidney@ldeo.columbia.edu).

The formation of North Atlantic Deep Water (NADW) is acknowledged to be of fundamental importance in thermohaline circulation, and thus in global climate change. Broecker and Denton [1] proposed that major glacial-interglacial reorganizations, possibly a complete shutdown of NADW formation, triggered or enhanced dramatic changes in the global climate. Studies of paleocirculation proxies in South Atlantic sediment cores have yielded conflicting interpretations about the glacial mode of thermohaline circulation. The importance of deep circulation in modulating the global climate warrants the use of additional proxies to resolve these conflicts.

Published data for seawater deeper than 2000 m from the Atlantic Ocean show that the Nd-isotopic composition is remarkably correlated with the silica content of deep ocean water [2–4]. The endmember compositions for North Atlantic, Pacific, and Antarctic deep water are 10 μmol silica and ε_{Nd} of −13.5, 180 μmol silica and ε_{Nd} of −3, and 130 μmol silica and ε_{Nd} of −8 respectively [2–5]. Neodymium-isotopic variations within deep waters of the ocean represent mixing of these end members. Accordingly, they imply that Nd could be a powerful tracer of paleowater mass changes.

Data from the outermost layer of Mn crusts indicate a strong coherence between the Nd-isotopic compositions of deep waters and these precipitates [6]. However, there is a notable exception in the mismatch between ferromanganese crusts and nearby seawater values from the southern ocean. It has been suggested that the bias is due to the slow growth rate of crusts (millimeters per million years), combined with changes in mixing proportions of deepwater components on glacial to interglacial timescales [6–8]. The outermost layers of crusts from the central Pacific Ocean and from the North Atlantic have values very close to local bottom water, consistent with little difference in the isotope composition of the end members during glacial times.

We have been employing a method to selectively leach the ferromanganese precipitates from marine sediments, with the goal of evaluating glacial to interglacial variations in the Nd-isotopic composition of deep water [9]. As a first-order test of the method, we made a core-top survey from the Atlantic Ocean. When the Nd-isotopic compositions are plotted with silica estimates taken from the Levitus database [10], the samples lie on the trend established with water measurements. The successful results from these core-top data further emphasize the likelihood that ferromanganese precipitates from marine sediments may be a robust proxy for past variations in deepwater composition. An additional test is the Sr-isotopic composition of the ferromanganese leach. In the case that the leach matches the Sr composition of seawater, it can be reasonably assumed that the Nd-isotopic composition is also faithfully recording the seawater value. Our success rate from this test is high, but there are samples that have Sr compositions that deviate substantially from seawater. In southern ocean sediments, this problem appears to be a diagenetic effect but in North Atlantic samples, it may be simply detrital contamination.

Rutberg et al. [11] found a systematic glacial to interglacial variation in the Nd-isotopic composition of bottom waters from two cores in the southeastern Atlantic Ocean that follows shifts in the C-isotopic composition. A core from the southern Pacific Ocean also shows the shift toward higher glacial ε_{Nd}. All of these samples have Sr-isotopic ratios equal to that of seawater. These results corroborate the interpretation based on Mn crusts and highlight the potential application of this method as a proxy for deepwater circulation changes. Another consideration in the application of this proxy is whether the end members remained constant. So far the results confirm a constant Pacific end member as well as the existence of a strong glacial-interglacial shift in southern ocean sediments. North Atlantic samples have low ferromanganese contents, and hence low Nd concentrations, and we are working to minimize detrital contamination in these samples. Because NADW is a mixture of several sources of deepwater with distinct Nd-isotopic compositions, and because incursion of southern ocean water appears to have been important in the glacial, it will require a relatively large set of samples to quantify this end member.

References: [1] Broecker and Denton. [2] Piepgras D. J. (1982) *Science, 217,* 207–214. [3] Piepgras D. J. and Wasserburg G. J. (1987) *GCA, 51,* 1257–1271. [4] Jeandel C. (1993) *EPSL, 117,* 581–591. [5] Piepgras D. J. and Jacobsen S. B. (1988) *GCA, 52,* 1373–1381. [6] Albarède F. and Goldstein S. L. (1992) *Geology, 20,* 761–763. [7] Abouchami W. and Goldstein S. L. (1995) *GCA, 59,* 1809–1820. [8] Abouchami W. et al. (1997) *GCA, 61,* 3957–3974. [9] Rutberg R. et al. (1997) *AGU, 78,* F376. [10] Levitus S. et al. (1994) *World Ocean Atlas.* [11] Rutberg R. et al. (1998) *Mineral. Mag., 62A,* 1304–1305.

LEAD-ISOTOPIC MEASUREMENTS OF SANIDINE MONITOR STANDARDS: IMPLICATIONS FOR PROVENANCE ANALYSIS AND TEPHROCHRONOLOGY.

S. R. Hemming[1] and E. T. Rasbury[2], [1]Department of Earth and Environmental Sciences and Lamont-Doherty Earth Observatory, Columbia University, Route 9W, Palisades NY 10964, USA (sidney@ldeo.columbia.edu), [2]Department of Geosciences, State University of New York–Stony Brook, Stony Brook NY 11794-2100, USA (troy@pbisotopes.ess.sunysb.edu).

Introduction: The Pb-isotopic system in feldspar is a powerful fingerprint, recording near-initial isotope ratios due to the very low ratios of U and Th to Pb in this mineral group, especially in K-feldspar. This same mineral group also has demonstrated applicability for ^{40}Ar/^{39}Ar geochronology. Procedures that allow multiple proxies to be obtained on the same samples have a great deal of value, and the combination of age and initial Pb-isotopic composition of feldspar has wide potential application in studies of volcanic stratigraphy as well as sedimentary provenance.

The Pb-isotopic system in detrital feldspar is a sensitive provenance tool, and in many cases it is possible to analyze individual grains. The value of making analyses on individual grains is clear in provenance studies where it cannot be assumed that any two grains came from the same source. However, despite relatively high concentration of Pb in K-feldspar, on average ~50 ppm [1], it is not possible to obtain high-quality Pb-isotopic measurements routinely on grains between 150 and 250 μm, although feldspar in this size range is very common in sandy deposits. In studies of sediment provenance, the ^{40}Ar/^{39}Ar age of a feldspar sample may also provide important constraints on sources. In cases where the Pb abundance is not adequate for individual grain analysis, the combination of these two systems would allow combining several grains with similar ^{40}Ar/^{39}Ar ages.

Provenance of volcanic rocks may also be constrained by the isotope composition of mineral constituents. Argon-40/argon-39 geochronology of volcanic sanidine is a highly successful and accepted method of dating ash layers, but limits on attainable precision leave open the question of correlation in noncontiguous sections. In favorable cases radiogenic isotope measurements could be made on the same crystals that are used to constrain the age, and this additional information would settle questions of whether samples are coeval.

Testing the Method: The value of multiple proxies derived from the same individual components is clear, but in order to apply the combination of $^{40}Ar/^{39}Ar$ dating and Pb-isotopic composition, it must be first established that the irradiation and fusion of feldspar for $^{40}Ar/^{39}Ar$ geochronology does not compromise the Pb-isotopic system. This paper is a report of a pilot project where we undertook to compare the Pb-isotopic composition of untreated sanidine monitor standards to those that have been irradiated and fused for dating. Samples were irradiated for various amounts of time and fused in either stainless steel or Cu disks.

Sanidine from the Fish Canyon Tuff is a popular monitor standard with an reported age of ~28 Ma [2,3]. The Cobb Mountain sanidine monitor standard is from the Alder Creek rhyolite and has a reported age of 1.18 Ma [3,4]. Both are popular monitor standards for $^{40}Ar/^{39}Ar$ geochronology.

Samples of Fish Canyon and Cobb Mountain sanidine monitor standards were co-irradiated for 1 h with unknown samples for $^{40}Ar/^{39}Ar$ geochronology in the Cd-lined, in-core facility (CLICIT) at the Oregon State University reactor. Single-step laser fusion data were collected at Lamont-Doherty Earth Observatory. Samples of several grains each, weighing from 1.3 to 3.8 mg, were analyzed for their Pb-isotopic composition and Pb concentration. The Pb-isotopic composition and concentration of Pb were unchanged by irradiation to produce ^{39}Ar from ^{39}K and fusion with a CO_2 laser using 7 W. This means that the way is open to apply combined $^{40}Ar/^{39}Ar$ and Pb isotope ratios to geological questions such as tracing volcanic ash layers for tephrochronology or tracing the sources of sedimentary grains.

Summary: Samples of Fish Canyon and Cobb Mountain sanidine monitor standards that were irradiated and fused with a CO_2 laser for $^{40}Ar/^{39}Ar$ geochronology analysis give Pb-isotopic composition and Pb concentrations that are indistinguishable from unprocessed aliquots of the same monitors. The lack of Pb loss means that Pb volatility is not a substantial concern during the laser fusion process. The lack of change in Pb-isotopic composition means it should be possible to measure the Pb-isotopic composition of feldspar grains that have been previously analyzed for their $^{40}Ar/^{39}Ar$ ages. Therefore, it should be possible to fingerprint datable volcanic ash layers for purposes of correlating noncontiguous layers with similar ages. This combined technique should also improve the sensitivity of provenance analysis.

References: [1] Patterson and Tatsumoto (1964) *GCA, 28,* 1–22. [2] Cebula G. T. et al. (1986) *ICOG6,* 139. [3] Renne P. R. et al. (1998) *Chem. Geol., 145,* 117–152. [4] Turrin B. D. (1994) *Geology, 22,* 251–254.

THE FOUNDATION SEAMOUNTS (SOUTH PACIFIC): GEOCHEMICAL EVIDENCE OF PAST AND PRESENT RIDGE-HOTSPOT INTERACTIONS?

C. Hémond[1], C. W. Devey[2], and M. Maia[1], [1]Unité Mixte de Recherche, 6538 Domaines Océaniques, IUEM, Place N. Copernic, F-29280 Plouzané, France (chhemond@sdt.univ-brest.fr), [2]Fachbereich 5 Geowissenschaften, Universität Bremen, Postfach 330440, D-28334 Bremen, Germany.

The existence of interaction processes between mid-oceanic ridges and hotspots was first suggested by Morgan [1]. The Foundation hotspot appears to be a good example of this. The magmatic expression of the Foundation hot-spot that represents activity is located in the vicinity of the Pacific-Antarctic ridge (PAR) that resulted in a volcanic chain (32°S,127°W–38°S,111°W). The age regression from west to east [2] leaves no doubt about the hotspot origin of this chain. We can divide it into three areas on the basis of the morphology of the edifices. The westernmost section of the volcanic chain is made of elongated, deformed, and not well aligned seamounts. It is suggested [3] that the magmatic expression was controlled by the structure of the litho-sphere: magmatism was led through preexisting weak zones. The central part of the volcanic chain (33°S,125°W–36°S,115°W) consists of large and well individualized elevated volcanos sometimes grouped in clusters of two or three edifices. The easternmost section begins 350 km before the PAR. The morphology switches to two lines of seamounts organized in elongated ridges obliquely to the main trend of the chain. One hundred forty kilometers away from the PAR, this double line breaks into several small ridges with very subdued topography until the PAR at 38°S.

Trace element concentrations have shown that the chain can also be divided into three parts: (1) the westernmost part, made of transitional lavas [$0.8 \leq (La/Sm)N \leq 1.2$]; (2) the central part, consisting of alkali basalts, which are likely to be the chemical expression of the plume where $(La/Sm)N \geq 2$; and (3) the easternmost part which consists of elongated ridges connecting the last typical intraplate seamounts of the chain and the spreading axis with highly variable (La/Sm)N but always <2. Extended trace-element patterns confirm this classification. The patterns obtained for the alkali basalts of the central part have the highest normalized concentrations for Nb and Ta and show a depletion of the most incompatible elements (Rb, Ba, Th, and U) relative to these two. This is characteristic of a source that contains some HIMU component.

Strontium, Nd, and Pb isotopes have been determined on more than 60 samples. Their isotopic message is consistent with the one delivered by the the trace elements. The westernmost part of the chain has rather unradiogenic $^{87}Sr/^{86}Sr$ (0.7027) and $^{206}Pb/^{204}Pb$ (18.5) ratio and rather radiogenic $^{143}Nd/^{144}Nd$ compositions (0.51305), whereas the central section exhibits slightly more elevated $^{87}Sr/^{86}Sr$ (0.7030), lower $^{143}Nd/^{144}Nd$ (0.51288), and much higher $^{206}Pb/^{204}Pb$ (up to 20.2). The $^{206}Pb/^{204}Pb$ reaches such high value only in seamount lavas and is significant of a large contribution of a HIMU component in the plume. This seamount is the last well individualized seamount of the chain at its Eastern end just before deformation in the shape of the following seamounts appears. Moreover, there is on average a rather continuous increase of the $^{206}Pb/^{204}Pb$ within the central section of the chain from west to east and it peaks at this seamount. Eastward, reaching the first elongated seamount of the eastern part, Sr- and Pb-isotopic compositions drop and then scatter between values sligtly less radiogenic than the last enriched seamount and more Pacific MORB-like values and this continues until it hits the PAR. The spreading axis samples remain intermediate isotopically and do not exhibit the most "depleted" values. Modeling a mixing of two magmatic liquids whose compositions are chosen to be the most extreme analyzed samples leads to an assumption of a contribution of the plume to the spreading axis of ~50%.

It is also worth noting that the most unradiogenic Sr and Pb and radiogenic Nd compositions do not appear in samples from the spreading axis but in rocks dredged on the oblique ridges. This could be produced by a contribution of isotopically depleted melts coming from a depleted component of the plume. Alternatively, melts produced from the upper mantle underneath the spreading axis may have been deviated toward the oblique ridges, which may be the locus of active interaction and mixing of melts from both origins.

References: [1] Morgan W. J. (1978) *JGR, 83,* 5355–5360. [2] O'Connor J. M. et al. (1998) *EPSL, 164,* 41–59. [3] Maia et al., in preparation.

STABILITY OF ALLANITE TO HIGH PRESSURE-TEMPERATURE: IMPLICATIONS FOR LIGHT RARE-EARTH-ELEMENT BUDGET IN SUBDUCTED CRUST.

J. Hermann, Research School of Earth Sciences, Australian National University, Canberra 0200, Australia (joerg.hermann@anu.edu.au).

Introduction: Dehydration and partial melting of subducted crustal material is an important process for mass transfer from the slab to the mantle wedge. This metasomatism of the mantle wedge initiates partial melting and is a key factor in the understanding of subduction zone magmatism. The element transfer is controlled by three main factors: (1) the stability of hydrous phases in subduction zones, (2) the partitioning between stable phases and fluid/melt, and (3) the mobility of the elements. We present new experimental and petrographic data on the stability of allanite that permits insight into the light rare-earth-element (LREE) budget of subducted crustal material.

Experiments: Synthesis piston cylinder experiments in the KCMASH system were carried out in the range 700°–1150°C and 2.0–4.5 GPa. Rubidium, Sr, Ba, Y, Zr, La, Ce, Nd, Sm, Eu, Gd, and Yb were added at a 100–300-ppm level. The addition of trace elements led to the stabilization of allanite as an accessory mineral well above the determined stability of clinozoisite (Fig. 1). Allanite was stable at 4.5 GPa, 1000°C together with

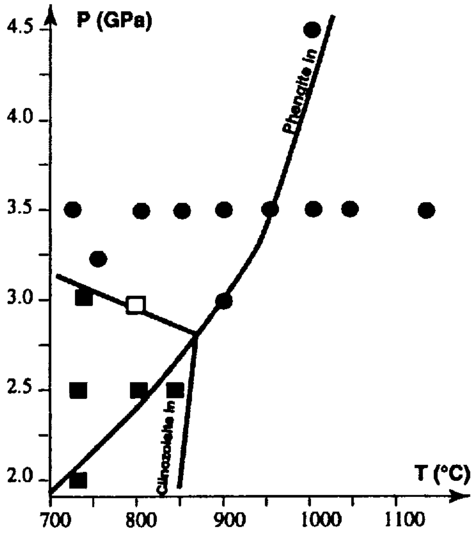

Fig. 1. Runs with allanite present (dots) and clinozoisite stable (squares). White square indicates a run with only minor clinozoisite. The determined stability of phengite and clinozoisite are shown.

clinopyroxene, garnet, coesite, kyanite, and phengite. Even above the fluid-absent melting due to phengite breakdown, allanite is present up to temperatures of 1150°C (Fig. 1). However, the abundance of allanite decreases with increasing temperature parallel to an increase in melt volume.

Allanite is an epidote group mineral that can incorporate significant amounts of LREE. The measured allanites contain up to 4.9 wt% La_2O_3, 6.2% Ce_2O_3, 2.2% Nd_2O_3, 0.5% Sm_2O_3 and 1.2% Gd_2O_3 resulting in ~0.5 cations REE (p.f.u). All allanites contained 3–6 wt% MgO, indicating that the LREE are most probably incorporated in allanite by the composite exchange Ca + Al = LREE + Mg. The partitioning of LREE between allanite and melt is in the order of D(allanite/melt) = 200 demonstrating that the LREE are highly compatible in allanite.

Petrographic Data: Allanite has been found in several rock types of the Dora-Maira massif (Alps) which were metamorphosed at ~750°C and 3.8 GPa. Allanite coexists with garnet, omphacite, phengite, quartz (excoesite), and rutile in eclogites and with and garnet, kyanite, phengite, quartz (excoesite), and rutile in metasediments in agreement to parageneses produced in the experiments. This indicates that at a depth of ~130 km, allanite is still stable in rocks of crustal composition.

Discussion: The stability of allanite to unexpectedly high temperature and high pressure has important consequences for the composition of fluids/melts generated in the presence of allanite because allanite buffers the LREE contents of these melts. Already an abundance of 0.5% of allanite can increase the bulk rock/melt partition coefficient of an eclogite by about a factor of ~20. Tribuzio [2] have shown that the LREE budget in eclogites is dominated by accessory allanite and apatite without significant contribution of omphacite. Allanite is stable at higher temperatures than the dehydration of phengite (Fig. 1) which is an important water reservoir in subducted oceanic crust [1]. The transfer of LREE from the subducted slab to the overlaying mantle wedge by melts/fluids originating from dehydration of subducted crust is thus restricted as long as allanite is stable.

Lawsonite has been considered as one of the most important carriers of LREE to great depth [3]. LREE liberated by lawsonite breakdown (700°–750°C at 3–5 GPa; [2]) might be incorporated in allanite which has a much higher thermal stability. Although the breakdown of allanite has not yet been determined, it is suggested that allanite may play an important role in LREE recycling to the mantle by subducted crust.

References: [1] Schmidt M. W. (1996) *Science, 272,* 1927–1931. [2] Tribuzio R. et al. (1996) *Geology, 24,* 711–714. [3] Poli S. and Schmidt M. W. (1995) *JGR, 100,* 22299–23314.

EXPERIMENTAL CONSTRAINTS ON CONTINENTAL ROCKS IN ULTRA-HIGH-PRESSURE METAMORPHISM.

J. Hermann and D. H. Green, Research School of Earth Sciences, Australian National University, Canberra 0200, Australia (joerg.hermann@anu.edu.au).

Introduction: Exhumed ultra-high-pressure (UHP) metamorphosed rocks permit insights in the dynamics of subduction zones and are crucial for the understanding of convergent plate boundaries. Piston cylinder experiments in the range 700°–1100°C and 2.0–3.5 GPa using gneissic to pelitic compositions were carried out in order to understand better the phase and melting relations in deeply subducted continental crust. The paragenesis coesite + kyanite + garnet + clinopyroxene + phengite is stable at UHP conditions in various rock types of the continental crust. The simplest chemical system to produce this paragenesis consists of K_2O-CaO-MgO-Al_2O_3-SiO_2-H_2O (KCMASH). The proportion of the oxides (SiO_2 = 61%; Al_2O_3 = 21%; MgO = 8%; CaO = 6%; K_2O = 3 wt%) was chosen in order to get saturation of kyanite and quartz/coesite. Synthesis experiments with run duration of 50–650 h were carried out with 2–10% water added as H_2O or as OH in phengite, talc, and $Al(OH)_3$. Results are compared to rocks from the Dora Maira massif (Alps) and from the Kokchetav massif (Kazakhstan), which represent continental crust subducted to more than 100 km depth.

Results: Generally, five phases plus fluid/melt were present in the experiments, which is in agreement with the phase rule indicating the absence of metastable phases. Minerals were generally unzoned; however, they occasionally showed a chemical variation from grain to grain. Chemical compositions of phases changed systematically with P and T. These observations suggest that equilibrium was approached in the experiments. In the range 20–30 kbar and 700°–900°C, the paragenesis changed in small P-T intervals and is thus an excellent indicator for metamorphic conditions. A common feature in all parageneses is the absence of feldspars, which may be used to define HP-metamorphism in gneissic to pelitic rocks. At pressure above 32 kbar, T <900°–1000°C, the divariant parageneses coesite + kyanite + garnet + clinopyroxene + phengite is stable over a significant P-T range. Composition of garnet and phengite is fixed at every P-T point by the equilibria (1) 2 Gro + 1 Py + 3 Cel = 6 Di + 3 Mu; (2) 3 Di + 2 Ky = Py + Gro + 2 Coe; (3) 4 Ky + 3 Cel = Py + 3 Mu + 4 Coe; and (4) Gro + 2 Ky + 3 Cel = 3 Di + 3 Mu + 2 Coe, indicating the potential of this paragenesis for UHP thermobarometers.

Phengite, biotite, clinopyroxene, and garnet display a systematic change in composition with P and T. The Si content (pfu) of phengite changes from 3.3 at 740°C, 2.5 GPa to 3.55 at 720°C, 3.5 GPa to 3.35 at 950°C, 3.5 GPa. The Si content of biotite is also a pressure sensor and changes from 2.9 at 900°C, 2.0 GPa to 3.22 at 800°C, 3.5 GPa. The Al_2O_3 content of pyroxenes is mainly temperature dependent and increases from 1.5 wt% at 720°C to 11 wt% at 1150°C, 3.5 GPa. The grossular content in garnet increases with pressure at T = 1000°C from 17% (2.0 GPa) to 31% (4.5 GPa) and with temperature at P = 3.5 GPa from 18% (900°C) to 29% (1150°C).

The stability of hydrous phases is very important because their breakdown liberates fluids or melts that might be responsible for mass transfer from the slab to the mantle wedge. Amphibole was stable at T <750°C, P <3.0 GPa and clinozoisite at T <850°C, P <3.0 GPa. Below 3.0 GPa biotite has the highest thermal stability up to temperatures of about 900°–950°C. At higher pressures, biotite reacts to phengite, which was stable at 950°C, 3.5 GPa, and 1000°C, 4.5 GPa. Talc was observed at 720°C, 3.5 GPa. Melts resulting from the breakdown of the hydrous phases were granitic in composition.

Dora Maira: White schists at Dora Maira consist of quartz (excoesite), kyanite, garnet, phengite, and minor talc. The breakdown of talc to kyanite and garnet occurs at ~750°C above 35 kbar in the experiments. The measured Si content of 3.6 (pfu) in phengite indicates a pressure of about 38–40 kbar for the white schist formation.

Kokchetav: Metamorphic microdiamonds occur in UHP gneisses and metacarbonates in the Kokchetav massiv [1]. In UHP gneisses garnets contain diamond and often biotite inclusions. The experiments clearly show that biotite has a limited pressure stability that never overlaps with the diamond stability field. Thus, garnet most probably grew during retrograde metamorphic conditions although diamond is present. The metamorphic diamonds from the Kokchetav rocks display a fibrous texture and contain water-rich inclusions, indicating that fluid/melt has to be involved in their formation [2]. Based on the experimentally determined stability of hydrous phases in gneissic rocks, it is evident that only the breakdown of phengite can provide the H_2O for partial melting and diamond formation. In fact, at the estimated conditions of diamond formation (1000°C, 4.5 GPa [1]) phengite was still stable in the experiments. It is suggested that fluid-absent melting of phengite and interaction of these melts with neighboring carbonates might be an important process triggering metamorphic diamond formation in deeply subducted continental crust.

References: [1] Shatsky V. S. et al. (1995) in *Ultrahigh Pressure Metamorphism* (R. G. Coleman and X. Wang, eds.), pp. 427–455, Cambridge University Press. [2] De Corte K. et al. (1998) *GCA, 62,* 3765–3773.

CUMULATE PROCESSES AND GEOCHEMICAL DIFFERENTIATION WITHIN OCEANIC LAYER 3.

J. Hertogen, Fysico-Chemische Geologie, University of Leuven, Celestijnenlaan 200C, B-3001 Leuven, Belgium (jan.hertogen@geo.kuleuven.ac.be).

Oceanic Layer 3 has been drilled at two slow spreading ridge segments: Ocean Drilling Program (ODP) Hole 735B on the southwest Indian Ridge (Legs 118 and 176 [1,2]) and Sites 921, 922, and 923 on the western wall of the mid-Atlantic Rift Valley south of the Kane Transform (MARK area) (ODP Leg 153 [3]). Some 220 samples have been analyzed for major and trace elements with a view of better understanding geochemical fractionation processes operating during plutonic differentiation.

The recovered sections at these drill sites do not represent segments of a continuously evolving large magma chamber. Rather, the cores represent oceanic layer 3 that accreted by episodic injection of 100–500-m-thick magma sheets or dikes. At the two localities the gabbros formed from moderately depleted MORB magma. Neither the trace-element data nor the isotopic ratios [4,5] indicate any substantial change in the composition of the parental magma among the successive magmatic pulses.

In the two cases the trace-element abundances, in particular of the rare earth elements (REE), exhibit large first-order variation as a result of changes in modal cumulate mineralogy (ranging from primitive troctolites to highly evolved Fe-Ti-oxide-rich gabbros) and of variations in the amount of trapped intercumulus liquid. The trace-element trends within several units of the 1805-m-deep Hole 735B can be reproduced satisfactorily with a fractional crystallization model, allowing for adcumulus growth with simultaneous compaction and residual melt expulsion. In almost all the H735B units, this resulted in a gradual chemical change from bottom (more primitive) to top (more evolved).

However, the trace-element characteristics of many gabbro samples do not fit into such a regular model. The bimodal suite of samples from Site 922 (MARK) is a good example. Evolved oxide-rich gabbros have high REE contents and negative Eu anomalies. They apparently crystallized from pods of highly evolved residual liquids. The oxide-rich gabbros occur together with primitive troctolitic gabbro having remarkably high REE abundances and high-REE/Sc ratios, characteristics normally associated with evolved compositions. These troctolites can be modeled as mixtures between barren troctolites and strongly enriched residual liquids.

Plagiogranitic and granitic veins are rather common in the H735B cores. They are indeed strongly enriched in REE and show prominent negative Eu anomalies. Throughout the whole H735B drill core, there is ample petrographic and geochemical evidence for migration of and impregnation with Fe-Ti-REE-rich residual melts. Enrichment of residual liquid in sheared zones indicate that plutonic differentiation has been modulated by ductile and brittle deformation processes. Moreover, samples from several highly altered veins and veined zones turned out to be very enriched in REE. This is evidence that fluid-rich residual liquids rather than hydrothermal fluids were the main agents of metasomatic alteration in these particular sections of the core.

The geochemical data for the Hole 735B and Site 922 gabbros raise a number of questions regarding (1) the ultimate fate of residual liquid generated in oceanic layer 3, and (2) the trace-element mass balance of the oceanic crust. There is the geochemically interesting possibility that residual liquids are swept out by a new batch of magma, part of which erupts as a lava flow. The swept-out liquids could then impart geochemical heterogeneity to ocean floor magmas that could be mistakenly interpreted as mantle source heterogeneity.

References: [1] Von Herzen R. P. et al. (1991) *Proc. ODP, Sci. Results, 118.* [2] Dick H. J. B. et al. (1999) *Proc. ODP, Init. Rpt., 176,* in press. [3] Karson J. A. et al. (1997) *Proc. ODP, Sci. Results, 153.* [4] Kempton P. D. et al. (1991) *Proc. ODP, Sci. Results, 118,* 127–144. [5] Barling J. et al. (1997) *Proc. ODP, Sci. Results, 153,* 351–362.

EXTRATERRESTRIAL HELIUM-3 FLUX RECORDED IN MARINE SEDIMENTS IN THE NORTH PACIFIC AT ODP SITES 885/886 OVER THE PAST 4 MILLION YEARS.

S. M. Higgins[1], R. F. Anderson[1], F. Marcantonio[2], M. Stute[1,3], and P. Schlosser[1], [1]Lamont-Doherty Earth Observatory, Columbia University, Route 9W, Palisades NY 10964, USA (sean@ldeo.columbia.edu), [2]Tulane University, New Orleans LA, USA, [3]Barnard College, New York NY, USA.

Introduction: Estimates of the flux of interplanetary dust particles (IDPs) determined from measurement of ^{3}He in marine sediment records are in general agreement with each other over the past several hundred thousand years [1–6]. These estimates range from ~0.5 to 1 pccSTP ^{3}He/cm^2/k.y.). Prior to ~0.5 Ma, the estimates of ^{3}He flux vary from an average of <0.5 to >1 pccSTP/cm^2/k.y. The interest in developing detailed records of IDP flux changes is that such records can constrain astrophysical models of dust/meteorite production [7–9], provide timing of asteroid/comet impacts in the sedimentary record [3,10], and potentially be used to evaluate sediment accumulation rates as a relatively "constant flux" tool on long timescales [2]. In addition, a proposed 100-k.y. cyclicity of this IDP flux [8,11,12] has been suggested as a way to explain the frequency of Late Quaternary ice ages. This 100-k.y. cyclicity has not been observed in all marine sediment records [1,2,5] but has been suggested by other studies [4,13].

Long-term Helium-3 Flux Estimates: There are only three published estimates of the long-term ^{3}He flux. The longest record comes from core LL44-GPC3, located in the central North Pacific, which covers the entire Cenozoic [3]. Two other estimates from KH 68-4-18 and ODP Site 806 are both from the western equatorial Pacific and cover primarily the last 2–3 m.y. [4,6]. All three of these records agree that the ^{3}He flux over the last 700 k.y. is about ~1 pccSTP/cm^2/k.y. Prior to 700 k.y., the ODP 806 record drops to a level of ~0.5 pcc back to 1.9 m.y., the LL44-GPC3 record continues at ~1 pcc and drops off to a lower level at 1.5 m.y., and the KH 68-4-18 record remains at ~1 pcc for its entire length (~3 m.y.). The ODP 806 record is by far the most detailed of the three while the other records are limited in resolution (KH 68-4-18) and by poor geochronologic control and resolution (LL44-GPC3). This timing discrepancy and variability has important implications for the use of ^{3}He fluxes for sediment studies and a proposed climatic link for the late Quaternary. In order to evaluate this discrepancy, we are developing a new record at ODP Sites 885/886 (5700-m water depth) located at 45°N, 168°E in the North Pacific. This record is similar in environment to LL44-GPC3 but with a much more resolved geochronology, better mass accumulation rate information, and higher sedimentation rates over the last 10 m.y. [14].

Results: To date, we have extended the ^{3}He flux record at ODP 885/886 back to 4 Ma at approximately 100-k.y. resolution. Estimated ^{3}He fluxes average 1.03 (±0.35) pcc/cm^2/k.y. over the last 3.6 m.y. Very abruptly at 3.6 Ma, our initial results show a decrease to values of 0.4 pcc/cm^2/k.y. between 3.6 to 4 m.y. This period of reduced flux ends with the onset of eolian dust accumulation in the North Pacific at 3.6 Ma and marks a sharp lithologic break between diatom ooze (3.6–4 Ma) and the clay-dominated sediments in the younger section. This sharp decrease in ^{3}He fluxes also occurs in LL44-GPC3 record at ~1.5 Ma, but it appears that may be the result of poor temporal resolution in ^{3}He measurements and geochronologic control over that interval. Mass accumulation rate (MAR) data for LL44-GPC3 show that lithologic change between increasing eolian-dominated sediments also begins around 3–3.5 Ma [15,16]. Our new record at ODP 885/886 is in good agreement with the long-term average flux of ~1.5 (±1.0) pccSTP/cm^2/k.y. at the site of KH 68-4-18 over the last 3 m.y. The record from KH 68-4-18 has relatively constant MAR and is not complicated by large inputs of eolian detritus. Existing ^{10}Be data for LL44-GPC3 and KH 68-4-18 also allow us to normalize ^{3}He data at these sites [17,18]. The results of this ^{3}He/^{10}Be normalization also support the relative constancy of ^{3}He flux over the past 3.5 m.y. The detailed ^{3}He flux record for the last 1.9 m.y. at ODP 806 remains at ~0.5 pccSTP/cm^2/k.y. from 0.7 to 1.9 m.y. and is at odds with all other values. We have no good explanation as of yet for why that record should be so different from others in the same region. However, the strong sensitivity of all of these long-term estimates to MAR calculations highlights the importance of understanding sedimentary environments at each of these locations and may be the cause of the observed differences.

References: [1] Marcantonio F. et al. (1996) *Nature, 383,* 705–707. [2] Marcantonio F. et al. (1995) *EPSL, 133,* 549–555. [3] Farley K. A. (1995) *Nature, 376,* 153–156. [4] Patterson D. B. and Farley K. A. (1998) *GCA, 62,* 3669–3682. [5] Higgins S. M. et al. (1998) *Eos Trans. AGU, 79.* [6] Takayanagi M. and Ozima M. (1987) *JGR, 92,* 12531–12538. [7] Dermott S. F. et al. (1996) *ASPC, 104,* 143–153. [8] Kortenkamp S. J. and Dermott S. F. (1998) *Science, 280,* 874–876. [9] Love S. G. and Brownlee D. E., *Science, 262,* 874–876. [10] Farley K. A. et al. (1998) *Science, 280,* 1250–1253. [11] Muller R. A. and MacDonald G. J. (1995) *Nature, 377,* 107–108. [12] Muller R. A. and MacDonald G. J. (1997) *Science, 277,* 215–218. [13] Farley K. A. and Patterson D. B. (1995) *Nature, 378,* 600–603. [14] Rea et al. (1998) *Paleoceanogr., 13,* 215–224. [15] Kyte F. T. et al. (1993) *GCA, 57,* 1719–1740. [16] Janicek T. R. and Rea D. K. (1983) *GSA Bull., 94,* 730–738. [17] Mangini et al (1984) *Nuc. Inst. Meth., B29,* 326–333. [18] Inoue T. and Tanaka S. (1979) *Nature, 277,* 209–210.

HELIUM-ISOTOPIC INVESTIGATIONS OF SOURCE MIXING IN THE ICELANDIC MANTLE.

D. R. Hilton[1], K. Gronvold[2], C. G. Macpherson[1,*], and P. R. Castillo[1], [1]Geosciences Research Division, Scripps Institute of Oceanography, La Jolla CA 92093-0244, USA (drhilton@ucsd.edu; pcastillo@ucsd.edu), (*present address: Department of Geology, Royal Holloway University London, Egham, Surrey, UK; c.macpherson@gl.rhbnc.ac.uk), [2]Nordic Volcanological Institute, Reykjavik, Iceland (karl@norvol.hi.is).

Introduction: There is abundant geochemical and isotopic evidence for the involvement of distinct mantle components in the genesis of Icelandic lavas: these include a deep-seated mantle plume component, enriched in incompatible elements and possessing relatively radiogenic Sr-isotopic compositions [1], and a "more depleted" component that shows certain similarities to N-MORB [e.g., 2]. Crustal processes have also been advocated to account for various features of the geochemical and isotopic systematics of Iceland [3].

Helium-isotopic studies in Iceland [4–9] have provided a complementary picture of different mantle source components and the possible superimposed effects of crustal interaction: reports of ^{3}He/^{4}He ratios in geothermal fluids and recent lavas span the range of terrestrial values — from "high-^{3}He" hotspot highs of 30R_A (where R_A= air ^{3}He/^{4}He) through the MORB range (8 ± 1R_A) to predominantly crustal values ($\leq 4R_A$). To elucidate further: (1) the diagnostic ^{3}He/^{4}He signature of Icelandic mantle source components, (2) mixing relationships between these source components, and (3) possible crustal contamination effects, we report new He-isotopic data from two areas that have been key in establishing the range of ^{3}He/^{4}He ratios on Iceland.

Vestfirdir (Northwest Iceland): Vestfirdir, the oldest region of the Icelandic crust (up to ~15 Ma), is the location of the highest geothermal ^{3}He/^{4}He ratios observed to date for Iceland (30 R_A) [9]. New data for the region, obtained by crushing olivine phenocrysts *in vacuo,* show a consistent pattern of He release with a ^{3}He/^{4}He ratio of 37 R_A — significantly greater than the previously reported maximum value. Melting of resultant powders shows typically radiogenic He values excluding the presence of a spallation component. Such high values record the He-isotopic signature of the Iceland plume ca. 14 Ma, soon after rift relocation to the Snaefellsnes rift zone [10]. The radiogenic isotope systematics of the high ^{3}He/^{4}He sample (^{87}Sr/^{86}Sr = 0.70347, ^{143}Nd/^{144}Nd = 0.51297, ^{206}Pb/^{204}Pb = 18.653) place it in the FOZO region in the mantle tetrahedron [11]. In this case, the Vestfirdir sample would define the purest expression of the FOZO component available to date, given He-isotopic evidence of minimal dilution with other (lower ^{3}He/^{4}He) mantle components.

Central Iceland: Hyloclastic glasses and phenocryst-bearing lavas were collected from the region of the hypothesized center of the Icelandic plume in central Iceland [12]. The highest values observed were ~34 R_A — significantly higher than ratios reported to date for rift-zone volcanics. Although there is considerable scatter in measured values, probably reflecting source mixing with lower ^{3}He/^{4}He (MORB?) mantle, there are some samples where radiogenic He (and crustal contamination) predominates. However, the broad picture is one of a sharp discontinuity (over a ~100-km-length-scale) between high (hotspot) ^{3}He/^{4}He ratios of the western rift zone and MORB-like ^{3}He/^{4}He values (~8 R_A) characteristic of the northern rift zone.

Discussion: High and variable ^{3}He/^{4}He ratios throughout Iceland are consistent with the presence of two distinct mantle components: a high ^{3}He/^{4}He plume component and a MORB-like component. A detailed picture of mantle mixing between these components (± magma aging and crustal contamination) emerges when the new results from Vestfirdir and central Iceland are combined with those from previous studies [e.g., 4–9]. The pertinent features of this "mantle mixing map" of Iceland will be discussed, taking into account recent seismic studies of the Icelandic plume [13–14], and emphasizing regions such as (1) central Iceland, where mixing appears to be inhibited, (2) Vestfirdir, which records a temporal record of the plume component, and (3) other areas where crustal interaction appears enhanced.

References: [1] Schilling J.-G. (1973) *Nature, 242,* 565–571. [2] Fitton J. G. (1997) *EPSL, 153,* 197–208. [3] Oskarsson N. et al. (1985) *JGR, 90,* 10011–10025. [4] Polak B. G. et al. (1976) *Intl. Assoc. Hydrol. Sci., 119,* 17–33. [5] Condomines et al. (1983) *EPSL, 66,* 125–136. [6] Kurz M. D. et al. (1985) *EPSL, 74,* 291–305. [7] Hilton D. R. et al. (1990) *Chem. Geol., 88,* 53–67. [8] Poreda R. J. et al. (1992) *GCA, 56,* 4221–4228. [9] Hilton D. R. et al. (1998) *Chem. Geol., 149,* 173–187. [10] Hardarson et al. (1997) *EPSL, 153,* 181–196. [11] Hart et al. (1992) *Science, 256,* 517–520. [12] Einarsson P. (1997) *Eos Trans. AGU, 78,* 369–375. [13] Wolfe et al. (1997) *Nature, 385,* 245–247. [14] Shen et al. (1998) *Nature, 395,* 62–65.

ACETATE AND C1 COMPOUNDS ARE LARGELY IGNORED BY METHANOGENS IN NORTHERN WETLANDS.

M. E. Hines[1], K. N. Duddleston[1], R. B. Reich[1], and R. P. Kiene[2], [1]Department of Biological Sciences, University of Alaska–Anchorage, Anchorage AK 99508, USA (afmeh@uaa.alaska.edu), [2]University of South Alabama, Mobile AL 36688, USA.

Introduction: Typical methanogenic decomposition pathways include near-terminal C intermediates that turn over rapidly with small pool sizes. The most important of these is acetate, which occupies a pivotal position between fermenting and acetogenic processes and methanogenesis. Other molecules that are utilized directly by methanogens, such as C1 compounds [e.g., methanol and dimethylsulfide (DMS)], behave similarly in that they are often present in small pools that cycle quickly. Some of these latter materials, such as methanol, can also be important intermediates in the anaerobic C cycle. Our investigations revealed that incubations of peat from oligotrophic wetlands like bogs display linear increases in DMS with no consumption [1]. Here we report that the accumulation of DMS is due to the lack of consumption by methanogens at low pH and low temperature. Further studies revealed that under these conditions other C1 compounds and acetate are also not utilized.

Experimental: Peat samples from a poor fen in New Hampshire and several wetlands in Alaska were used for incubation studies for examining the turnover of several compounds. Results were compared to those from sediment samples from lakes and creeks. Anaerobic slurry incubations were amended with various electron acceptors and inhibitors, and concentrations of CH_4, CO_2, DMS, and acetate determined by GC or IC techniques. Turnover rates of acetate, methanol, trimethylamine, and methylmercury were determined using radiotracers. A seasonal study of pore-water chemistry and microbial rates is being conducted in an Alaskan bog.

Results: *Sphagnum*-dominated wetlands did not consume acetate or any of the C1 compounds when the natural pH was below 4.6 or the temperature was below 15°C. In some instances, we were unable to detect any turnover using ^{14}C substrates with incubations of several hours to days. Higher-pH wetlands in Alaska did not consume these compounds either. However, temperate minerotrophic fens and freshwater sediments readily consumed all compounds tested. Alaskan peats that were held at 22°C for several weeks began to consume the intermediates, albeit slowly. The lack of consumption of intermediates occurred only when methanogenesis was the terminal process. However, under these conditions methane production continued actively. Introduction of O_2 into slurries, in which acetate had previously accumulated anaerobically, resulted in a steady decrease in acetate levels. Acetate production appeared to be predominantly fermentative rather than autotrophic via acetogenesis, and rates of production were significant (up to 0.5 mM L^{-1} d^{-1}). Pore-water acetate concentrations reached 1.0 mM.

Discussion: It is generally thought that C1 compounds like DMS and important intermediates like acetate are rapidly cycled in anaerobic environments [2,3]. However, in wetland soils typical of northern latitudes and in more southerly habitats that are oligotrophic, these compounds are not utilized methanogenically. This differs from the instance where acetate levels are high during the spring prior to the commencement of rapid acetoclastic methanogenesis [4]. In the wetlands we are studying, acetate can accumulate in all seasons despite the occurrence of rapid methane production. It also appears to differ from situations where homoacetogenesis occurs in lieu of methanogenesis.

The lack of consumption of compounds, particularly acetate, greatly affects how we envisage terminal degradation processes in methanogenic northern wetlands. First, methanogenesis is restricted primarily to H_2 metabolism. Second, under methanogenic conditions, acetate production represents a terminal process and is a sink for a significant portion of metabolized C. The ultimate fate of this acetate is aerobic oxidation to CO_2 after diffusion into surficial peats. Hence, C destined for CH_4 is bypassed to CO_2 via O_2 respiration, and does not contribute to atmospheric CH_4. Global warming may reverse this trend by enhancing the methanogenic degradation of acetate.

References: [1] Kiene R. P. and Hines M. E. (1995) *AEM, 61,* 2720–2726. [2] Lomans B. P. et al. (1999) *AEM, 65,* 2116–2121. [3] Fenchel T. et al. (1998) *Bacterial Biogeochem.*, Academic. [4] Shannon R. D. and White J. R. (1996) *L&O, 41,* 434–443.

A NEW APPROACH TO THE STUDY OF ANAEROBIC METHANE-OXIDIZING CONSORTIA IN MARINE SEDIMENTS: BIOMARKER AND PHYLOGENETIC EVIDENCE.

K.-U. Hinrichs[1], E. F. DeLong[2], and J. M. Hayes[1], [1]Mail Stop 4, Woods Hole Oceanographic Institution, Woods Hole MA 02543, USA (khinrichs@whoi.edu), [2]Monterey Bay Aquarium Research Institute, Moss Landing CA 95039, USA.

Background: Several geochemical studies have demonstrated the importance of anaerobic oxidation of methane in marine sediments [1]. Of the 85 Tg of methane that is produced annually in marine sediments, however, all but 10 Tg is consumed before it can reach the atmosphere, mostly anaerobically [2]. The most plausible mechanism involves a consortium of methanogenic and sulfate-reducing bacteria, with the methanogens working in a reversed mode and sulfate-reducers utilizing products of methane oxidation [3]. However, all attempts to reproduce natural conditions in laboratory experiments and to identify the responsible organism have failed.

Results and Discussion: We studied marine sediments taken from cold methane seeps along the continental margin off northern California, searching for molecular signals related to anaerobic oxidation of methane. We will present molecular-isotopic and phylogenetic evidence that novel archaea, related to known methanogenic bacteria, oxidize methane and use it as substrate for growth [4]. Our interpretation is based on the extreme depletion in ^{13}C ($\delta^{13}C$ <–100‰) of archaea-specific biomarkers, which is consistent with a utilization of isotopically light methane as a C source for biosynthesis. These biomarkers are the bisphytanylglycerolether, or archaeol, and the highly source-specific sn-2-hydroxyarchaeol, with the latter compound being indicative for the methanogenic order *Methanosarcinales*.

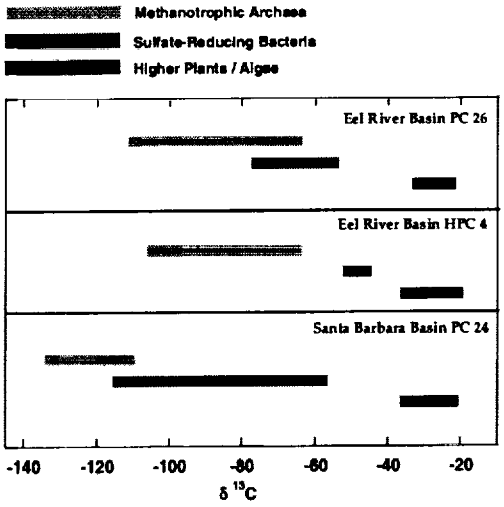

Fig. 1. Range of C-isotopic compositions of individual compounds that are assigned to the methane-oxidizing microbial community and to sedimentary organic matter derived from marine algae and terrestrial plants.

Parallel 16S rRNA gene surveys indicate the predominance of a novel archaeal group peripherally related to the methanogenic orders *Methanomicrobiales* and *Methanosarcinales*. In accordance with the consortium hypothesis by Hoehler et al. [3], the presence of other members of the methane-oxidizing microbial community is indicated by lipids that are interpreted to be derived from sulfate-reducing bacteria (e.g., highly ^{13}C-depleted nonbranched and branched fatty acids). These compounds commonly are less depleted in ^{13}C than lipids derived from methane-oxidizing archaea (Fig. 1).

Archaeol and sn-2-hydroxyarchaeol were found at all active seeps at different sedimentary environments along the California margin, reaching maximum ^{13}C depletions in the Santa Barbara Basin (–136‰). These two compounds appear to characterize a crucial member of the archaeal community, whereas site-specific distributions of other archaeal compounds appear to be linked to environmental factors. Similarly, differences in C-isotopic composition are interpreted to be related to methane flux and $\delta^{13}C$ of methane.

References: [1] Hoehler T. M. and Alperin M. J. (1996) in *Microbial Growth on C_1 compounds* (M. E. Lidstrom and F. R. Tabita, eds.), pp. 326–333, Kluwer Academic Publishers, Dordrecht. [2] Reeburgh W. S. (1996) in *Microbial Growth on C_1 compounds* (M. E. Lidstrom and F. R. Tabita, eds.), pp. 334–342, Kluwer Academic Publishers, Dordrecht. [3] Hoehler T. M. et al. (1994) *Global Biogeochem. Cycles, 8,* 451–463. [4] Hinrichs K. et al. (1999) *Nature, 398,* 802–805.

EXPERIMENTAL STUDY OF PARTIAL MELTS OF CLINOPYROXENITE AND THE ORIGIN OF ULTRACALCIC MELT INCLUSIONS.

M. M. Hirschmann[1] and P. Schiano[2], [1]Department of Geology and Geophysics, University of Minnesota, Minneapolis MN 55455, USA (marc.m.hirschmann-1@umn.edu), [2]Laboratoire Geochimie-Cosmochimie, Université Paris VII, 4 place Jussieu, 75252, Paris Cedex 05, France.

Recent studies of melt inclusions in olivine from ridges and arcs have documented primitive mafic glasses that are enriched in CaO with high CaO/Al_2O_3 relative to MORB or IAB. Homogenized ultracalcic inclusions from MORB have up to 14.9 wt% CaO and CaO/Al_2O_3 as high as 1.16 [1,2] and those from arcs contain up to 18.7 wt% CaO, with CaO/Al_2O_3 up to 1.38 [3]. Partial melting experiments on anhydrous peridotite produce liquids with <14 wt% CaO and CaO/Al_2O_3 <0.9 [4]. The CaO and CaO/Al_2O_3 enrichments in the inclusions are difficult to explain by fractionation, and therefore suggest an exotic lithology or component in the glass's source regions. Based on major and trace elements, Kamenetsky et al. [1] and Sours-Page et al. [2] inferred derivation of ultracalcic glasses from MORB from a cpx-rich component. Partial melts generated from experiments on garnet pyroxenite and eclogite compositions between 1 and 3 GPa are not ultracalcic [5], but partial melts of clinopyroxenites, which have more CaO than these other lithologies, could be. Here we present partial melting experiments on a clinopyroxenite in order to evaluate its possible role in generation of ultracalcic liquids.

A series of partial melting experiments have been conducted on a synthetic composition (Table 1) at 1 GPa between 1325° and 1400°C in a piston-cylinder apparatus. Vitreous C spheres were used to isolate glasses from quench effects. Observed phases over this temperature interval include only cpx and glass. Mass balance calculations indicate melt fractions ranging from 21% up to 69%. Glasses at 1325° and 1350°C are mildly alkalic mafic liquids (alkali olivine basalt to basanite) and are not ultracalcic (Table 1). At 1400°C, the glass is ultracalcic. We have also performed preliminary experiments at 2.5 GPa and 1450° and 1500°C, where we also observe cpx coexisting with glass. There are indications of disequilibrium at this pressure, as the C spheres devitrify under these conditions and communication between melt and minerals may be lost. Although the 2.5 GPa results must be interpreted with caution, glasses contain ~14 wt% CaO, suggesting that partial

TABLE 1. Composition of starting material and glasses from 1-GPa experiments.

	Bulk Composition	Temperature and Time 1400°C 23 h	 1350°C 45 h	 1325°C 24 h
SiO_2	51.2	49.7(4)	47.5(2)	46.2(3)
TiO_2	0.5	0.76(5)	1.21(3)	1.29(6)
Al_2O_3	6.1	8.47(8)	13.60(7)	13.1(2)
FeO*	7.1	8.9(2)	11.7(1)	13.7(3)
MnO	0.1	0.12(3)	0.09(5)	0.12(4)
MgO	16.4	14.7(2)	11.0(1)	10.4(3)
CaO	17.7	16.6(2)	12.4(1)	12.2(3)
Na_2O	1	1.28(5)	2.43(7)	2.84(2)
K_2O	0	NA	0.06(2)	0.06(1)
Total	100.1	100.46	100.00*	100.00*
F (% melt)	69	30	21	

* Normalized analyses. Probe totals are low on thin glass rims around vitreous carbon spheres.

melts of clinopyroxenite do not become markedly more calcic with increased pressure.

Ultracalcic glasses from arcs are unlike the experimentally produced CaO-rich liquid, as the former are strongly undersaturated (<45 wt% SiO2, >10% ne) while the latter is only weakly so (1% ne). Put another way, partial melts of clinopyroxenite approach cpx stoichiometry, but CaO-rich glass inclusions have less SiO_2 than a stoichiometric cpx. MORB-related ultracalcic glasses are hy-normative but have some similarities to experimental glasses. CaO contents of interpolated compositions intermediate between the 1400° and 1350°C experiments (14.5 wt%) are similar to the average homogenized composition (14.2 wt%) from Kamenetsky et al. [1] and are similar in most other respects except that the natural glasses have more Al_2O_3 (14.3 vs. 11 wt%) and have less FeO* (6.3 vs. 10.3 wt%). Given the arbitary composition of the experimental starting material, which was chosen for its similarity to arc ultracalcic liquids, these differences may not be significant. On projected ternary diagrams (Wo-En-Al_2O_3 [Ol] and Ol-Q-CaTs [Wo]), the natural glasses plot between the experimental glasses and MORB, so they may result from mixing of clinopyroxenite partial melts and MORB. However the temperature required to generate appropriate liquid endmember compositions (~1375°C) is higher than that of likely MORB parent liquids at 1 GPa. Thus, it is unlikely that partial melting of clinopyroxenite veins accounts for the ultracalcic inclusions in MORB. Melting of a more complex cpx-rich lithology (wehrlite or websterite) or melt-rock reaction between peridotite partial melts and clinopyroxene-rich domains may be required to generate ultracalcic liquids beneath ridges at reasonable temperatures.

References: [1] Kamenetsky et al., *EPSL, 160,* 115–132. [2] Sours-Page et al., *CMP, 134,* 342–363. [3] Sisson and Bronto, *Nature, 391,* 883–886; Schiano et al., this volume. [4] Baker and Stolper (1994) *GCA, 58,* 2811–2827; Wasylenki et al. (1996) *Eos Trans. AGU, 77,* 847. [5] Ito and Kennedy (1974) *82,* 383–392; Yasuda et al. (1994) *JGR, 99,* 9401–9414; Hirschmann et al. (1995) *76,* 696; Pertermann and Hirschmann, unpublished data.

THERMODYNAMICS OF MOLECULAR HYDROGEN IN ANAEROBIC MICROBIAL ECOSYSTEMS.

T. M. Hoehler, M. J. Alperin, D. B. Albert, and C. S. Martens.

Molecular H is produced or consumed by an extremely broad variety of bacterially mediated redox reactions, making it a nearly universal carrier of electrons in anoxic ecosystems. In relatively oligotrophic systems, competition for H_2 among bacteria can maintain its concentration at extremely low levels that correspond to a minimum biologically useful energy. In such situations, variations in H concentrations become strongly dependent on the bioenergetics of the H_2-consuming bacteria and the response of H_2 to variations in environmental parameters (e.g., temperature, terminal electron acceptor, sulfate concentration, pH) can be related to simple thermodynamic predictions. Similarly, H concentrations exert thermodynamic control on a range of bacterial processes, causing inhibition, alteration of products, or even complete reversal. A thorough understanding of H_2 thermodynamics thus provides a novel and semiquantitative framework in which to relate variations in environmental factors to the overall function and emergent properties of anaerobic bacterial ecosystems as a whole.

TROPICAL CARBONATE $\delta^{13}C$ RECORD OF A NEOPROTEROZOIC SNOWBALL EARTH.

P. F. Hoffman[1], G. P. Halverson[1], D. P. Schrag[1], G. Soffer[1], and A. J. Kaufman[2], [1]Department of Earth and Planetary Sciences, Harvard University, Cambridge MA 02138, USA, [2]Department of Geology, University of Maryland, College Park MD 20742, USA.

A worldwide distribution of glacial deposits and paleomagetic evidence for ice lines at sea level close to the equator point to three or more runaway ice-albedo catastrophes between ~755 and 575 Ma. In order to reverse the high albedo of a snowball Earth, atmospheric CO_2 levels must have risen ~350× to >0.12 bar, consequent to millions of years of normal volcanic outgassing in the absence of sinks for C (no silicate weathering or organic fixation). Accordingly, Neoproterozoic ice ages were long-lived (millions to tens of millions of years) and they terminated under ultra-greenhouse conditions. Calculated global-average sea-ice thickness at thermal equilibrium with geothermal input was reduced from ~1.4 to 0.4 km as atmospheric CO_2 rose. Once the tropical ocean began to open, deglaciation proceeded violently as the hydrologic cycle was renewed, with attendant water vapor greenhouse feedback. Intense silicate weathering, driven by high temperatures, strong hydrologic cycle, and extreme surface area of unaltered rock flour and debris, consumed the excess CO_2 and led to rapid inorganic precipitation of post-glacial cap carbonates widely observed. Paleomagnetic data from elsewhere on the Congo craton imply that the younger Ghaub glaciation on the Otavi carbonate platform and its southern foreslope in northern Namibia occurred at low southerly latitudes, and we assume a carbonate accumulation rate of ~50 m/m.y. based on a thermal subsidence model of the platform. Inorganic $\delta^{13}C$ records from before and after the glaciation show the following widely-developed secular pattern: (1) *Preglacial stage:* $\delta^{13}C$ values (VPDB) of 5–8‰ were sustained for >8 m.y., indicating high fractional rates of organic C burial accompanying a breakup phase of the Rodinia supercontinent. (2) *Incipient glacial stage:* A steep monotonic decline from +8‰ to –6‰ signaled a dramatic decline in fractional organic burial during the last 0.5 m.y. prior to glaciation. This unique (~14‰) shift in inorganic $\delta^{13}C$ is unaccompanied by any systematic shift in $\delta^{18}O$ and is variably truncated by the subglacial erosion surface, making a diagenetic origin unlikely. (3) *Snowball stage:* Sea level fell, exposing the platform and shedding debris basinward. The platform subsided tectonically for >6 m.y. to ~100 m below normal (postglacial) sea level and was enveloped in sea ice frozen onto the bed. Primary carbonates are absent and hence there is no direct record of the isotopic composition of the full glacial ocean. (4) *Greenhouse aftermath stage:* After cap carbonate deposition began, $\delta^{13}C$ values fell rapidly from –2‰ to –6‰, while $\delta^{18}O$ values fell ~6‰. Values for DIC in the surface ocean were initially raised, compared with the end of the incipient glacial stage, by isotopic fractionation accompanying the hydration of CO_2, then lowered as the atmospheric reservoir was driven downward through Rayleigh distillation. (5) *Postglacial stage:* High rates of inorganic cap-carbonate accumulation (>10 cm/yr on the platform and ~1 cm/yr on the slope), including reeflike buildups of crystalline aragonite pseudomorphs on the raised rim of the platform, kept $\delta^{13}C$ values low despite presumed recovery of biological activity. After accumulation of ~300 m of cap carbonate, the platform had been raised to sea level and $\delta^{13}C$ values rose toward 0‰, reflecting a return to more normal fractional rates of organic C burial.

TRACING WATER FLOWPATHS DURING A STORM EVENT USING STRONTIUM-87/STRONTIUM-86 RATIOS.

J. F. Hogan[1] and J. D. Blum[1,2], [1]Department of Earth Sciences, Dartmouth College, Hanover NH 03755, USA (jhogan@dartmouth.edu), [2]Department of Geological Sciences, University of Michigan, Ann Arbor MI 48109, USA.

Introduction: Oxygen-isotopic studies have shown that stormflow in small catchments consists mainly of water already present in the subsurface ("old water") and not precipitation ("new water") [1]. Oxygen isotopes, however, provide no information about the flowpath of this water. Strontium-87/strontium-86 ratios provide an additional tracer that is useful for separat-

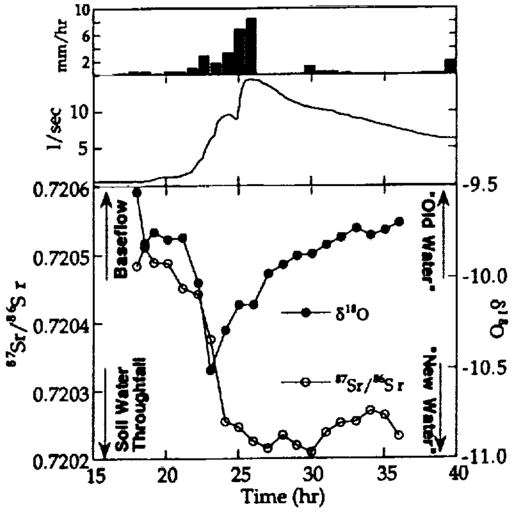

Fig. 1. Storm event of November 1–2, 1997. Time is from midnight on November 1.

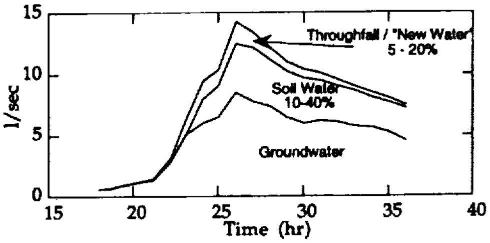

Fig. 2. Hydrograph separation using ^{87}Sr/^{86}Sr and δ^{18}O variation.

ing water by flowpath [2]. This is possible in many watersheds because the ^{87}Sr/^{86}Sr ratio of exchangeable Sr in the soil profile is a mixture of two Sr sources, atmospheric inputs (^{87}Sr/^{86}Sr ~0.710 [2]) and bedrock weathering. This difference in ^{87}Sr/^{86}Sr ratios allows for the tracing of water flowpaths during stormflow. Deeper flow will be closer to the weathering value whereas shallow flow will be similar to the soil value.

Methods: We sampled four storm events and one snowmelt event at Watershed 1, an 11-ha first-order catchment located in the Hubbard Brook Experimental Forest of New Hampshire. The ^{87}Sr/^{86}Sr ratio from chemical weathering is ~0.725 [3] providing a strong contrast to that of atmospheric Sr. During storm events, stream samples, precipitation, and throughfall were collected hourly. Streamflow and rainfall were continuously recorded by the U.S. Forest Service. Lysimeter water samples were collected monthly. Samples were analyzed for elemental concentrations and O and Sr isotopic composition.

Results: Figure 1 shows the results from a storm event on November 1–2, 1997. δ^{18}O values show a shift toward lighter values with the addition of new water (rain: −14.5 ± 0.8‰) to the stream during rainfall, but quickly returns to values similar to the start of the storm even though discharge remains high. Strontium-isotopic ratios shift to lower values with the lowest values occurring at peak discharge. Unlike δ^{18}O, the ^{87}Sr/^{86}Sr ratio remains low on the falling limb of the hydrograph. Other storms studied show similar patterns.

Soil water from eight nested lysimeters located along the length of the stream had an average ^{87}Sr/^{86}Sr ratio of 0.7198; however a large range of values was observed (0.7186–0.7205). The ^{87}Sr/^{86}Sr ratios of soil water at various depths for each location is relatively constant and showed no seasonal changes. Precipitation is low in Sr (~0.5 ppb) but throughfall is significantly higher (~6 ppb) due to leaching of biomass. Throughfall measured at one location near the base of the watershed had ^{87}Sr/^{86}Sr ratio of 0.7188. It is likely that there is also isotopic heterogeneity in throughfall similar to that observed in soil waters.

Discussion: Stormflow can be separated into "new water" and "old water" using δ^{18}O variation and a two-component mixing model. The end member for "old water" is assumed to be the value of baseflow (δ^{18}O = −9.5‰) whereas "new water" is taken as the weighted average for rainfall (δ^{18}O = −14.5‰). Stormflow can be separated using ^{87}Sr/^{86}Sr ratios into deep and shallow flowpaths. The end member for deep flow is assumed to be the baseflow value of 0.7025, whereas the end member for shallow flowpaths is based on the average soil water value of 0.7198. We assume that throughfall has the same ^{87}Sr/^{86}Sr ratio as soil water and combine the two into shallow flowpaths. Strontium concentrations measured for all endmember waters is ~6 ppb, so there is no need to account for changes in concentration in our mixing equations. Figure 2 shows the results of these calculations. New water is a small component of stormflow. The majority of stormflow is derived from increased deep flow and the flushing of old water through shallow flowpaths.

References: [1] Genereux D. P. and Hooper R. P. (1998) *Isotope Tracers in Catchment Hydrology,* 319–346. [2] Bullen T. D. and Kendall C. (1998) *Isotope Tracers in Catchment Hydrology,* 610–646. [3] Bailey et al. (1996) *WRR, 32,* 707–719.

IN SITU HAFNIUM-, URANIUM/LEAD-, AND LEAD/LEAD-ISOTOPIC ANALYSES OF ZIRCONS AND BADDELEYITE BY LASER ABLATION MULTIPLE COLLECTOR INDUCTIVELY COUPLED PLASMA MASS SPECTROMETRY.

I. Horn[1], W. F. McDonough[1], and R. L. Rudnick[1], [1]Department of Earth and Planetary Sciences, Harvard University, 20 Oxford Street, Cambridge MA 02138, USA (horn@eps.harvard.edu).

Introduction: It has been demonstrated that quadrupole-based ICP-MS coupled to a laser ablation (LA) system is capable of determining Pb/Pb and U/Pb ages with precision of better than ±2% (2σ) on Paleozoic zircons and baddeleyite [1]. By comparison, multiple collector inductively coupled plasma mass spectrometry (MC-ICP-MS) eliminates signal noise produced by plasma flicker and should therefore produce isotopic ratios with ~200× higher precision compared to quadrupole based ICP-MS. This should allow precise determination of the ^{176}Hf/^{177}Hf in phases enriched in Hf (and relatively depleted in Lu) such as zircon and baddeleyite. These data can then be used to determine the Hf model age of the phase (assuming crystallization from a chondritic Earth), or, using U-Pb and Pb-Pb ages, the Hf data can be used to determine the precise initial Hf-isotopic composition of the rock.

Here, we use laser ablation inductively coupled plasma mass spectrometry (LA-ICP-MS) to obtain *in situ* Hf-isotopic compositions of the 91500 Harvard standard zircon (Hf = 6000 ppm) [2] and Phalaborwa baddeleyite using MC-ICP-MS.

Analytical Techniques: A series of preliminary Hf-isotopic analyses were conducted on a micromass isoprobe multiple collector ICP-MS at the Harvard University Laser Ablation lab. The mass spectrometer is coupled to an in-house-built laser ablation system using a Lambda Phsyik (Göttingen, Germany) Compex 110 excimer laser operating in the deep UV at 193 nm. Spot sizes ranged between 40 and 70 µm. Ablation duration varied between specimens, but ranged from 60 to 100 s. Mass bias correction using an exponential law was done with respect to ^{178}Hf/^{177}Hf = 1.46714. Masses 173 and 175 were monitored in order to correct for Yb and Lu interferences on mass 176.

Results and Discussion: Preliminary results for two spot analyses on the 91500 zircon, which has a ^{238}U/^{206}Pb age of 1065 ± 0.6 Ma, yield ^{176}Hf/^{177}Hf values of 0.282224 (21) and 0.282268 (68), and yield Hf model ages of 858 and 928 Ma respectively. These data compare favorably with existing TIMS data, i.e., 0.282284 [3] and 812 Ma determined on six separate dissolutions [2].

The average of five spots on a Phalaborwa baddeleyite yielded a mean ^{176}Hf/^{177}Hf ratio of 0.281105 (27) for ablation times of 80 s per spot. The total ion beam obtained for a 70-µm spot reached 25 V, allowing us to obtain good results using spot sizes of 40 µm or less.

The external precision of better than 0.01% RSD (2σ) is well below that required for dating minerals using the Hf-isotopic system. An advantage of the laser ablation technique is that the time-resolved acquisition protocol allows delineation of different growth zones in single crystals from metamorphic rocks since any mineral overgrowths will be visible during data acquisition.

References: [1] Horn I. et al. (1999) *Chem. Geol.*, in review. [2] Wiedenbeck M. et al. (1995) *Geostandards Newslett., 19*, 1–23. [3] Reischmann T. (1995) *S. Afr. J. Geol., 98*, 1–4.

MULTINUCLEAR MAGNETIC RESONANCE INVESTIGATION OF THE STRUCTURE AND DYNAMICS OF SURFACE AND INTERLAYER SPECIES OF HYDROTALCITE-LIKE COMPOUNDS.

X. Hou and R. J. Kirkpatrick, Department of Geology, University of Illinois, Urbana IL 61801, USA (xhou@uiuc.edu, kirkpat@uiuc.edu).

Hydrotalcite-like Compounds (HTs) and Nuclear Magnetic Resonance: Hydrotalcite-like compounds are layer-structured hydroxides with positive permanent charge due to isomorphous substitution and have significant anion-exchange capacity [1]. They are widely used as catalysts or catalyst precursors and also have potential applications in waste management [2,3]. Understanding the molecular-scale structure and dynamics of interlayer species in HTs is essential to fundamental prediction and analysis of the behavior and technological application of these materials and to comprehensive understanding of the behavior of intercalated species in layer-structure materials. Nuclear magnetic resonance (NMR) spectroscopy has shown remarkable capacity in studying the local structure and dynamics of surface and interlayer anions on and in HTs [3–6]. NMR-resolvable surface-absorbed and interlayer anions have been observed for HTs intercalated with $^{35}Cl^-$ (HT-Cl), $^{15}NO_3^-$ (HT-NO_3), $^{77}SeO_3^{2-}$ (HT-SeO_3), $^{77}SeO_4^{2-}$ (HT-SeO_4), and $^{13}CO_3^{2-}$ (HT-CO_3). Anions on surface and interlayer sites show dramatically different dynamical characteristics. The dynamics and structural environments of the surface anions are markedly dependent on the relative humidities (RH) and temperature. Reorientational frequencies and activation energy can be extracted from the analysis of the temperature and RH dependences of the NMR peak width. In contrast, the structure and dynamics of most interlayer anions are less dependent on RH and temperature.

Examples: For example, in HT-NO_3, interlayer nitrate retains its characteristic uniaxial chemical shift anisotropy (CSA) pattern even at 80°C and full hydration, indicating that it undergoes no significant reorientational motion. In contrast, surface nitrate undergoes isotropic reorientational motion at room temperature at frequencies from ~0 Hz at RH = 0%, to 4.2×10^4 Hz at RH = 11%, and to 6×10^5 Hz at RH = 100%. Its apparent activation energy is 12.6 kJ/mol^{-1}, somewhat greater than for water on kaolinite [7], probably due to the combined effects of H-bonding and electrostatic attraction to the hydroxide layer. The mobility of interlayer nitrate in HT is intermediate between that of carbonate and chloride. The ^{13}C NMR spectra of Van der Pol et al. [6] indicate that carbonate is rigidly held. They proposed that it is H bonded to the OH groups of the main layer and that the C_2 symmetry axes of water and the C_3 axes of carbonate are perpendicular to the layer. We believe that this is also true for nitrate HTs, although the nitrate may be undergoing rapid three-fold rotation. Chlorine-35 NMR spectra for hydrotalcite show that interlayer Cl^- is mobile, with an increasing reorientational frequency with increasing temperature at temperatures above −80°C [3]. This motion averages the local electric field gradient and thus decreases the apparent quadrupole coupling constant. In contrast, isotropic reorientation of interlayer nitrate is not observed. This is probably a steric effect due to the nonspherical shape of the nitrate, but greater H bonding to the three oxygens may contribute.

For HT-SeO_4, RH and temperature affect the dynamics of both interlayer and surface $^{77}SeO_4^{2-}$. Unexpected uniaxial CSA patterns and a small isotropic component are observed for samples at RHs from 11% to 100% at room temperature. The CSA tensor values vary in a complicated pattern with hydration state. At RH = 100%, variable temperature ^{77}Se NMR data show that with increasing temperature from −90°C to 90°C, the $^{77}SeO_4^{2-}$ CSA peak is averaged to a narrow, symmetric peak, indicating isotropic reorientational motion at frequencies $>2 \times 10^4$ Hz. The minor isotropic component is interpreted as surface $^{77}SeO_4^{2-}$ and the CSA component as interlayer $^{77}SeO_4^{2-}$. The unexpected uniaxial CSA pattern of $^{77}SeO_4^{2-}$ must be due to the effects of bonding to the octahedral layers. The observed $^{77}SeO_4^{2-}$ NMR behavior is consistent with X-ray diffraction (XRD) observations, which show that the basal d-spacing for HT-SeO_4 varies with RH. In contrast, the basal d-spacing of HT-NO_3 and HT-CO_3 are the same at room humidity and at 100% RH, and these species do not undergo reorientational motion in the observed temperature range.

Conclusions: This study has shown that the structure and dynamics of the surface and interlayer chargebalancing anions in HTs vary with their charge, size, polarity and steric configuration as well as the crystallinity of HTs. No single parameter such as charge/radius ratio is adequate to fully explain the observations.

References: [1] Bellotto M. et al. (1996) *J. Phys. Chem., 100*, 8527–8534. [2] Moini A. and Pinnavaia T. J. (1988) *Solid State Ionics, 26*, 119–123. [3] Kirkpatrick R. J. et al. (1999) *Am. Mineral.*, submitted. [4] Dupuis J. et al. (1990) *Solid State Ionics, 42*, 251–255. [5] Marcelin G. et al. (1989) *J. Phys. Chem., 93*, 4646–4650. [6] van der Pol A. et al. (1994) *J. Phys. Chem., 98*, 4050–4054. [7] Jonas J. and Brown D. (1982) *J. Colloid. Interface Sci., 89*, 374–378.

OXYGEN-ISOTOPIC FRACTIONATION IN THE SYSTEM OF QUARTZ-NaCl-CaCl$_2$-WATER AT HIGH PRESSURE AND HIGH TEMPERATURE.

G. Hu[1] and R. N. Clayton[1,2], [1]Department of the Geophysical Sciences, University of Chicago, Chicago IL 60637, USA, [2]Enrico Fermi Institute and Department of Chemistry, University of Chicago, Chicago IL 60637, USA.

Introduction: Aqueous fluids with various amount of salts are widespread at the surface and in the upper lithosphere and play important roles in a variety of geological processes. Compared to our knowledge of the temperature dependence on isotopic fractionation, our knowledge of the effect of pressure and fluid composition on isotopic fractionation is very limited. Some early studies on the isotope salt effect either show complex dependence on temperature or no salt effect [1–3]. A series of studies on isotope salt effect in a liquid-vapor system by Horita et al. [4–7] indicates that the isotope salt effect at relatively low temperature and pressure is by no means negligible. The isotope salt effect in mineral-water systems at high pressure and high temperature may have profound geochemical implications.

Experimental: Oxygen-isotopic exchange between quartz and salt solutions was carried out in piston-cylinder apparatus as described by Clayton et al. [8]. The isotope salt effect was obtained by

$$\Delta_{\text{salt-effect}} = \Delta_{\text{mineral-saline solution}} - \Delta_{\text{mineral-pure water}}$$

Results and Discussion: Figure 1 shows the salt effect of NaCl on O-isotopic fractionation between quartz and water. The concentration of NaCl

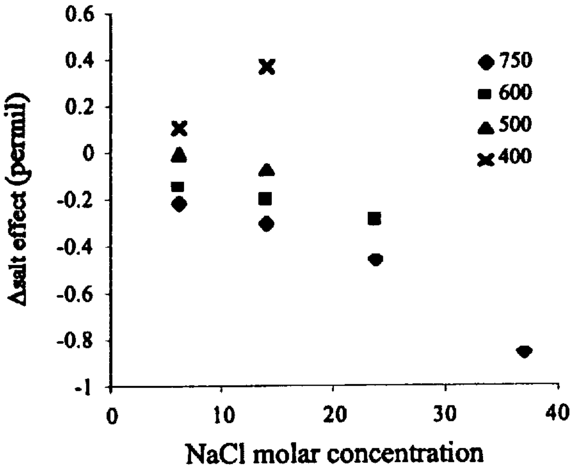

Fig. 1. Salt effect of NaCl on O-isotopic fractionation between quartz and water under 15 kbar (temperature in Centigrade).

ranged from 0 to saturation at a given temperature and pressure [9]. At 600° and 750°C, the salt effect of NaCl on O-isotopic fractionation is negative. The magnitude increases linearly with NaCl concentration and with temperature. At 500°C the salt effect is slight and is almost negligible within analytical uncertainty. In contrast to the salt effect of NaCl above 500°C, a positive trend of salt effect has been observed at 400°C and 15 kbar.

The magnitude of the salt effect of NaCl on O-isotopic fractionation is much smaller than that derived from the results on liquid-vapor experiments [7]. However, it should be pointed out that the investigation of isotope salt effect in liquid-vapor system was conducted at pressure lower than 221 bar while our experiments were carried out at 15 kbar. The smaller isotope salt effect and change of NaCl effect from negative to positive could be produced by high pressure.

Oxygen-isotopic fractionation between quartz and 6.2 M $CaCl_2$ solution has been carried out at 600°C and 750°C and 15 kbar. The salt effect of 6.2 M $CaCl_2$ at 750°C is −0.61‰ and at 600°C is −0.69‰. Compared to NaCl with the same molar concentration, $CaCl_2$ has a larger salt effect and the magnitude increases with decreasing temperature.

References: [1] Truesdell A. H. (1974) *EPSL, 23,* 387–396. [2] Poulson S. R. et al. (1994) *Chem. Geol., 116,* 305–315. [3] Zhang L. et al. (1989) *Econ. Geol., 84,* 1643–1650. [4] Horita J. et al. (1993a) *GCA, 57,* 2797–2817. [5] Horita J. et al. (1993b) *GCA, 57,* 4703–4711. [6] Horita J. et al. (1994) *GCA, 58,* 3425–3437. [7] Horita J. et al. (1995) *GCA, 59,* 1139–1151. [8] Clayton R. N. et al. (1975) *GCA, 39,* 197–1201. [9] Aranovich et al. (1996) *Contrib. Mineral. Petrol., 125,* 200–212.

NONREACTIVE SOLUTE DISPERSION IN TRIASSIC SANDSTONE: LABORATORY SIMULATION AND AN APPLICATION TO THE FIELD.

W. Huang and D. N. Lerner, Department of Civil and Structural Engineering, University of Sheffield, Mappin Street, Sheffield S1 3JD, UK (cip98wh@sheffield.ac.uk; d.n.lerner@sheffield.ac.uk).

Introduction: Groundwater is often polluted by organic chemicals that are extremely expensive to remove. In some cases, there is a substantial travel distance and time between the pollution source and the receptor (e.g., a drinking water borehole). Natural attenuation (mostly biodegradation) may reduce contaminant concentration significantly without any treatment. However, the rate of biodegradation depends on the rate of supply of electron acceptors. One of the important problems for modeling natural attenuation is the rate at which the oxidant mixes into a pollution plume, driven by mechanical mixing (dispersion) and diffusion. Better prediction of mixing will give greater confidence in use of monitored natural attenuation as a cost-effective option for some polluted sites. Before establishing a biodegradation model, a nonreactive model should be developed.

Nonreactive solute dispersion in a Triassic sandstone aquifer in the UK was studied by simulating conservative chemical (chloride and fluoride) plumes transport in the subsurface. A two-dimensional, nonreactive solute transport model was developed in the laboratory and a suitable mathematical model was used to simulate the transport. A new noninvasive imaging technique was developed to investigate plume transport in porous media in the laboratory. Sintered glass (particle size 53–106 μm) was used to simulate the Triassic sandstone and a dye (fluorescein sodium salt) was selected as a conservative tracer. The dye in sintered glass was excited by UV light and emitted visible light. A CCD camera was installed to record tracer transport process and the images of tracer distribution in two-dimensional sintered glass sheet. The brightness of images was processed and transferred to tracer concentration distribution. The size of sintered glass sheet is 140 mm long, 87 mm wide, and the width of the continuous line source (tracer) is 3 mm. The results show that the tracer distribution can be described by a mathematical model of two-dimensional continuous line source. Experiments show that dispersivity of the sintered glass sheet is 0.00056 m. The range of 50-percentile diameter (median) of particles at field site is 150–200 μm and groundwater velocity is ~10 m/yr. Field data from two monitoring boleholes which are respectively 130 m and 350 m from the source along the multilevel plume flow path were simulated by the laboratory confirmed model. The edges of the conservative chemical plumes are simulated on the assumption that the edge plume is not disturbed by the middle. The distributions of chloride and fluoride remain unchanged with time, and these plumes were regarded as continuous sources. The simulation shows that the vertical dispersivity of the field site is 0.0038 m and the same simulation parameters can predict the transport of different conservative chemicals in two boleholes. It also shows that the edges of different plumes (chloride, fluoride, and sulfate) went down the same depth (13 m) in the subsurface between the two boreholes. All of these results may support the assumption of an undisturbed plume edge. As for the low dispersion coefficient (1.2×10^{-9} m^2/s) of the field site, it may show that molecular diffusion is a significant factor account for vertical dispersion.

BIOREMEDIATION OF PETROCHEMICAL CONTAMINANTS IN UNSATURATED SOIL.

W. Huang[1], D. N. Lerner[1], and G. Li[2], [1]Department of Civil and Structural Engineering, University of Sheffield, Mappin Street, Sheffield, S1 3JD, UK (cip98wh@sheffield.ac.uk), [2]Department of Environmental Science and Engineering, Tsinghua University, Beijing 100084, China.

Introduction: Soil at a site near Zibo City, China, is polluted with petroleum hydrocarbons at concentrations up to 200 g kg^{-1} dry soil. Sample analysis indicates that the contaminants are mainly composed of heavy oil and PAHs. The soil contained 10^7 microbial cells g^{-1} dry soil, and aerobic-degradation bacteria concentrations of 10^6–10^7 cells g^{-1} dry soil in different layers of the soil. In laboratory investigations, aerobic-degradation bacteria from the soil show an obvious affinity for liquid paraffin and an ability to emulsify the liquid paraffin. Nearly all bacteria remain on the surface of the oil droplets, with few bacteria separately growing in the pure water phase. The bacteria therefore tend to colonize the boundary between the oil droplet and water. An effective and rapid method to measure the aerobic degradation rate by measuring the respiration of the bacteria in the polluted soil is presented. The most active specie aerobic heterotrophic bacteria (*Xanthomonas, Bacillus,* and *Hyphomicrobium*) were screened and isolated. The factors that can influence biodegradation rate were studied. The field investigation of the polluted soil shows that pH is close to neutral, and N and P contents are typically 0.1% and are sufficient to sustain the natural and enhanced biodegradation. The laboratory experimental results show that under these conditions soil O content, temperature, moisture content as well as the activity and number of aerobic degradation bacteria are the dominant factors that influence biodegradation rates. A biological activated C (BAC) system was established to enrich indigenous microbes to enhance biodegradation rates in the laboratory. In this BAC system, C source was restricted to specific target petroleum hydrocarbons. The system was inoculated with bacteria from the polluted soil. The porous surface offers a large area for mixing of bacteria and media and results in the enrichment of bacteria that degrade the target petroleum hydrocarbons. Bacteria released from the activated C have lower viscosity and pass more easily through the soil. The feasibility of feeding enriched indigenous bacteria to the polluted soils has been studied. Three methods for enhancing biodegradation rate were investigated in the laboratory. The methods are (1) adding enriched bacteria, (2) tilling and keeping moisture content of the soils constant, and (3) combining treatment to the polluted soil by adding enriched bacteria, keeping moisture (60% W/W) content constant, and tilling the soils. The three methods gave rise to 15, 57, and 70% decrease of petroleum hydrocarbons respectively, and a control sample showed 0.8% degradation over the same period of 72 d. This may suggest that tilling could elevate the O content in the polluted soil, accelerate biodegradation to product low molecular weight hydrocarbons and increase valorization of these hydrocarbons. In the unsaturated soil, maintaining suitable moisture content in the polluted soil is also important, because bacteria that contribute to biodegradation tend to grow the boundary between the petroleum hydrocarbons and water. However, too much high moisture content may inhibit the aerobic respiration and decelerate the biodegradation rate in the soil.

EL NIÑO DURING THE LAST INTERGLACIAL PERIOD RECORDED BY A FOSSIL CORAL FROM INDONESIA.

K. A. Hughen[1], D. P. Schrag[1], S. B. Jacobsen[1], and W. Hantoro[2], [1]Department of Earth and Planetary Sciences, Harvard University, 20 Oxford Street, Cambridge MA 02138, USA, [2]Research and Development Center for Geotechnology, Indonesian Institute of Sciences (LIPI), JL Sangkuriaug Bandung, Indonesia.

Oxygen isotopes ($\delta^{18}O$) and elemental ratios (Sr/Ca) in coral skeletons from Indonesia reflect changes in sea-surface temperature (SST) and salinity, and can be used to reconstruct El Niño-Southern Oscillation (ENSO) variability from the past. Sulawesi Island, in central Indonesia, is located in the center of the negative precipitation anomaly (drought) caused by El Niño. Modern corals from Bunaken Island, North Sulawesi, record the seasonal climate cycle and respond sensitively to even slight perturbations in rainfall from both El Niño and La Niña events. Uranium/thorium disequilibrium dating showed that a fossil coral from Bunaken Island grew ~123 k.y. ago, during the last interglacial period, Marine Isotope Stage (MIS) 5e. Sixty-five-year-long $\delta^{18}O$ and Sr/Ca records from the fossil coral show slightly warmer SSTs and a seasonal cycle much stronger than today, consistent with an increased southeast Asian monsoon during MIS 5e. Analyses across a distinct mineralogical boundary from aragonite to calcite were used to quantify the effects of diagenesis on coral geochemistry and demonstrate that diagenetic alteration has not affected the paleoclimate records. The $\delta^{18}O$ record shows distinct interannual variability from El Niño and La Niña events, indicating that ENSO was robust during a time of slightly warmer global climate. Time series analysis reveals that the power spectral estimates for the coral and early instrumental (1856–1976) ENSO records are strikingly similar, but distinct from the most recent period (1960–1998). The fossil record reveals ENSO behavior during a period prior to anthropogenic influence on climate, and together with the pre-1976 modern record comprises a view of the natural variability of the ENSO climate system, suggesting that, during interglacials, ENSO may be more stable than previously believed. Changes in ENSO magnitude and frequency after 1976 appear anomalous with respect to the earlier periods and support the hypothesis that recent ENSO behavior lies outside the range of natural variability.

LITHIUM AND ITS ISOTOPES IN RIVER WATER AND SUSPENDED MATERIAL.

Y. Huh[1], L.-H. Chan[2], and J. M. Edmond[1], [1]Mail Stop E34-166, Department of Earth, Atmospheric and Planetary Sciences, Massachusetts Institute of Technology, Cambridge MA 02139, USA (yhuh@mit.edu; jedmond@mit.edu), [2]Department of Geology and Geophysics, Louisiana State University, Baton Rouge LA 70803, USA (lchan@geol.lsu.edu).

Introduction: Lithium isotopes have the potential to be an effective tracer of weathering processes due to their large relative mass difference and therefore fractionation. Previous reconnaissance study of the dissolved load of major world rivers showed a large range from –6 to –32‰ [1]. However, there was no clear relationship to any other chemical parameter. One of the gaps in knowledge was the amount and isotopic ratio of Li carried as suspended material and its interaction with the dissolved load. We have analyzed additional samples of both the dissolved and suspended load to address this issue.

Mafic Terrains: Two river water samples were analyzed to determine the value for basaltic terrains. The Mayn, a tributary of the Anadyr, drains arc basalts of the Mesozoic collision zone between the Kolyma and Siberian cratons. The $^{87}Sr/^{86}Sr$ ratio shows a characteristic basaltic value of 0.70488, Mg/Ca = 0.8 mole ratio, and a high Si value of 193 µM. The Li/Mg ratio is 0.66×10^{-3} and δ^6Li is –28.7‰. The Baghicha, a tributary of the Indus, drains the ophiolitic belt. It has unradiogenic $^{87}Sr/^{86}Sr$ of 0.70451, Mg/Ca of 0.4, and Si of 98 µM. The Li/Mg ratio is 0.49×10^{-3} and δ^6Li is –22.2‰.

Lithium Mass Balance within the Orinoco Watershed: A crude mass-balance study was carried out to determine if within-channel storage and adsorption/desorption or ion exchange reactions played a significant part. The Orinoco basin was chosen because it flows along the boundary between two markedly different terrains, the Precambrian Guayana Shield on the right and the Andes on the left, and has well-known hydrology and water chemistry.

Dissolved load. We have accounted for 60% of the discharge, and the Li concentrations and isotopic ratios balance within this uncertainty. Conspicuous in this is the clear divide in the isotopic ratios between the Andean tributaries and those draining the Shield. The Upper Orinoco, Ventuari, Caura, and Caroni, all draining the Shield, have Li concentrations 27–77 nM with δ^6Li of –13‰ to –22‰. The Guaviare, Meta and Apure draining the Andes and its foreland basin have 39–127 nM and –30‰ to –36‰. The Meta (–36.1‰) provides the bulk of the dissolved Li and so the Orinoco at its mouth has ratios close to that (–32.2‰).

Suspended load. The suspended load of the Orinoco River is predominantly derived from the Andes. In addition, the suspended Li concentration is ~7× higher in the Andean rivers (38.3–71.3 ppm) than those from the Shield (5.2–19.1 ppm). Thus, the overwhelming proportion of suspended Li is from the combined areas of the Andes and its wide alluvial plain, the Llanos. However, the isotopic composition is indistinguishable between the two regions: –5.4 to 0.9 in the Shield rivers vs. –6.4 to –0.8 in Andean rivers.

δ^6Li of Suspended Material vs. Dissolved: The differences in δ^6Li between suspended and dissolved Li are much larger in the Andean rivers (~30‰) than in the Shield rivers (~15‰).

Conclusion: The Li-isotopic ratios are much lighter in the suspended material. Apparently, ^6Li is preferentially partitioned into clays during weathering. This is in contrast with other reactive isotopes, e.g., C and O, where the heavier isotopes prefer solid phases. To a first approximation, during superficial weathering in high-relief, tectonically active terrains, ^7Li is preferentially leached and in large amounts, whereas in stable shield regions the weathering is intensive so that the concentrations are low and the ratios in the water becomes lighter with increasing degree of weathering. The heavier isotopic composition of the Andean Rivers may also reflect dominant weathering of carbonate and evaporites, as well as adsorption as water percolates through clay-rich weathering profiles. The latter process is not significant in tropical shields where silicates are completely transformed to gibbsite.

References: [1] Huh Y. et al. (1998) *GCA, 62,* 2039–2051.

A NICKEL CARBONATE ELEGY.

W. Hummel, Waste Management Laboratory, Paul Scherrer Institute, CH-5232 Villigen PSI, Switzerland (hummel@psi.ch).

Introduction: Any geochemical model aimed at a reliable description of the behavior of contaminants in groundwater has to consider, at a minimum, the influence of hydroxide and carbonate on the speciation of trace metals. The influence of hydroxide complexation is the scope of the comprehensive monograph *The Hydrolysis of Cations* [1]. No comparable work has been published yet about the influence of carbonate complexation on trace-metal speciation. Regarding the ubiquity of carbonate in groundwater systems, this lack of a suitable monograph is somewhat astonishing. In the case of Ni, a fair number of complexation constants can be found in the literature, and it seemed to be an easy task to evaluate the most reliable ones.

A Pretended Experimental Study: In [2], numbers can be found for the complexes $NiCO_3(aq)$ and $NiHCO_3^+$, apparently measured at 25°C in an ionic medium of 0.7 M.

Only one reference [3] is given in [2] as source of these stability constants. The authors of [3] somewhat cryptically state that they determined their numbers by the "Garrels method." The reference in [3] for this method is a Russian translation of the popular textbook by Garrels and Christ [4]. A patient search in the 450 pages of the original textbook finally revealed the meaning of the "Garrels method": The numbers in [3] are just estimates derived from a plot of complexation constants vs. electronegativity on page 98 in [4]. Subsequently, the estimated values were extrapolated from zero ionic strength to 0.7 M NaCl [3].

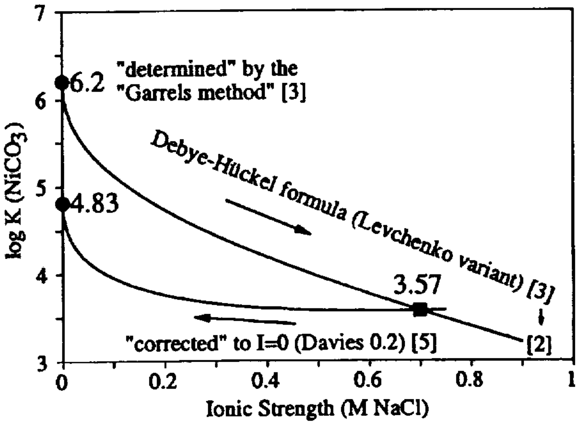

Fig. 1. An example of a data diagenesis process.

These estimated and extrapolated numbers were mistaken by [2] as experimental data and included in their collection of recommended stability constants.

Ironically, this is not the end of our story. The authors of a "Critical Reevaluation of Stability Constants" [5] were also deceived to take these numbers as experimental data, but they added a further twist to this anecdote. They report "selected values" that have been "corrected to I = 0 from [3]" by using a different method for ionic strength correction than [3].

A graphical representation of the entire multistep process of data diagenesis is shown in Fig. 1. Note that not only the "precision" of the estimated number increased by extrapolating back and forth in ionic strength using different formulae, but also that the final value dropped by more than one order of magnitude compared with the original value "determined" by the "Garrels method."

More Guesswork: These are not the only numbers concerning nickel carbonate complexation floating around in thermodynamic data collections. A literature review revealed an entire series of numbers, derived by various estimation procedures, but none of them had actually been measured. Nonetheless, the estimated numbers usually are presented with an apparent "precision" of two digits in logarithmic units. On the other hand, the estimated values published so far vary over more than four orders of magnitude. A very detailed inspection of the individual estimation procedures revealed that the estimated values are based on shaky grounds, to say the least. It proved necessary to reevaluate the most promising estimation methods but with the sobering result that, despite of all efforts, the range of uncertainty remains large.

The End of the Story: Summarizing the results of my detailed review of estimation procedures, I expect stability constants within the following ranges

$$Ni^{2+} + CO_3^{2-} \Leftrightarrow NiCO_3(aq) \qquad 4 < \log K_1 < 5.5$$

$$NiCO_3(aq) + CO_3^{2-} \Leftrightarrow Ni(CO_3)_2^{2-} \qquad \log K_2 < \log K_1 - 2$$

$$Ni^{2+} + HCO_3^- \Leftrightarrow NiHCO_3^+ \qquad 1 < \log {}_HK^0 < 2$$

References: [1] Baes C. F. and Mesmer R. E. (1976) *The Hydrolysis of Cations*, Krieger Publishing Company, Malabar, FL. [2] Smith R. M. and Martell A. E. (1989) *Critical Stability Constants. Vol. 6: Second Supplement*, Plenum Press, NY. [3] Zhorov V. A. et al. (1976) *Oceanology, 16*, 463–466. [4] Garrels R. M. and Christ C. L. (1965) *Solutions, Minerals, and Equilibria*, Harper & Row, NY. [5] Fouillac C. and Criaud A. (1984) *Geochem. J., 18*, 297–303.

TIMESCALE OF AQUEOUS ACTIVITY IN THE EARLY SOLAR SYSTEM.

I. D. Hutcheon[1], L. Browning[2], K. Keil[3], A. N. Krot[3], D. L. Phinney[1], M. Prinz[4], and M. K. Weisberg[4], [1]Lawrence Livermore National Laboratory, Livermore CA 94551, USA (hutcheon1@llnl.gov), [2]Southwest Research Institute, San Antonio TX 78238, USA, [3]University of Hawai'i, Honolulu HI 96822, USA, [4]American Museum of Natural History, New York NY 10024, USA.

Although they are among the most chemically primitive solar system materials, the carbonaceous chondrites are not pristine relics from the earliest epoch of solar system history but have been extensively modified within their parent bodies [1]. Aqueous alteration, in particular, has played an important role in the petrogenesis of the C chondrites, generating a complex array of secondary minerals, including oxides, hydroxides, carbonates, and sulfates, and hydrous and anhydrous silicates. The extent of alteration varies widely, from completely hydrated CM-like clasts, to nearly anhydrous CV material, and it is unlikely that all secondary minerals are coeval but formed over an extended period, in a variety of locales. Many secondary minerals have high Mn/Cr, and we have applied the ^{53}Mn-^{53}Cr chronometer ($\tau_{1/2}$ = 3.7 Ma) to investigate the timescales of aqueous activity in the early solar system.

Secondary mineral phases have been investigated in 4 C-chondrite classes: carbonates in CI, CM, and CR chondrites and fayalite in CV chondrites. Carbonates — ferroan magnesite and dolomite in CIs, dolomite in CMs, and calcite and dolomite in CRs — occur primarily as isolated matrix grains exhibiting no common association with other phases; some CI carbonates contain included magnetite [2]. Fayalite in CV chondrites occurs in type I (Mg-rich) chondrules associated with magnetite, sulfide, and Fe-rich pyroxene [3]. Carbonate and fayalite have extremely low Cr content (≪1 ppm) with $^{55}Mn/^{52}Cr$ of up to ~100,000.

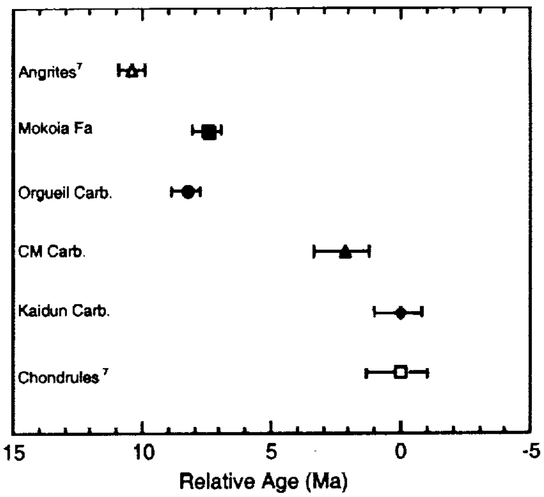

Fig. 1. Manganese-53–chromium-53 chronology.

Carbonate and fayalite in all four classes of C chondrites contain large excesses of ^{53}Cr, ranging up to ~1300‰, correlated with the respective Mn/Cr. The linear correlation between the magnitudes of the ^{53}Cr excesses and Mn/Cr is characteristic of the *in situ* decay of ^{53}Mn and demonstrates unequivocally that these secondary minerals formed while short-lived ^{53}Mn was still extant. The data do not plot along a single correlation line on a ^{53}Mn-^{53}Cr evolution diagram but define groups, each characterized by a distinct $^{53}Mn/^{55}Mn$ associated with the host lithology. Orgueil (CI) carbonates and Mokoia (CV) fayalites have similar $^{53}Mn/^{55}Mn$ of $(1.96 \pm 0.25) \times 10^{-6}$ and $(2.32 \pm 0.18) \times 10^{-6}$ respectively [4,5], while Nogoya and Y 791198 (CM) carbonates have $^{53}Mn/^{55}Mn$ of $(6.4 \pm 1.2) \times 10^{-6}$ and Kaidun (CR-like) carbonates have $^{53}Mn/^{55}Mn$ of $(9.4 \pm 1.6) \times 10^{-6}$ [6].

Assuming a uniform initial $^{53}Mn/^{55}Mn$ in the region of the nebula where chondrites formed, we use these data to construct a relative chronology of aqueous activity (Fig. 1). The $^{53}Mn/^{55}Mn$ ratio for the Kaidun carbonates is among the highest ever measured and comparable to the value measured in Bishunpur and Chainpur chondrules [7]. The Kaidun carbonates appear contemporaneous with chondrules, suggesting aqueous activity began on some chondrite parent bodies when nebular temperatures remained hot enough for chondrule formation. The time interval relative to CAI formation is uncertain but cannot exceed 6 m.y. The CM carbonates appear to have formed ~2 m.y. after Kaidun carbonates. The scatter of individual analyses about the best-fit CM line raises the possibility of variations in age among coexisting CM carbonates and suggests aqueous activity on the CM parent planet was episodic. Fayalite in Mokoia and carbonate in Orgueil have the lowest initial $^{53}Mn/^{55}Mn$, suggesting formation ~8 m.y. after Kaidun carbonates. The onset of aqueous activity on the CI and CV parent bodies may have postdated that on the CR and CM parent planets or fayalite and ferroan magnesite may represent mineralization in the final stages of an extended epoch of aqueous alteration. Liquid water must have begun to flow on parent bodies very early in solar system history and persisted for at least 8 m.y. The evidence for ^{53}Mn in secondary minerals requires the formation of small planetesimals and heating to melt ice within a few million years of CAI formation.

References: [1] Richardson S. M. (1978) *Meteoritics, 13*, 141–159. [2] Johnson C. A. and Prinz M. (1993) *GCA, 57*, 2843–2852. [3] Hua X. and Buseck P. R. (1995) *GCA, 59*, 563–579. [4] Endress M. et al. (1996) *Nature, 379*, 701–703. [5] Hutcheon I. D. et al. (1998) *Science, 282*, 1865–1867. [6] Hutcheon I. D. et al. (1999) *LPS XXX*, Abstract #1722. [7] Nyquist L. E. et al. (1997) *LPS XXVIII*, 1033–1034.

EXPERIMENTAL VERIFICATION OF STRATIFICATION FORMATION IN SOLIDIFYING MEDIUM UNDER THE ACTION OF STANDING WAVE.

V. L. Il'chenko, Geological Institute of the Kola Science Centre, Russian Academy of Sciences, Apatity, Fersman Street 14, 184200, Russia.

Explaining the origin of horizontal stratification in the upper crust and the formation of layered intrusions, which commonly concentrate ore minerals (PGM, for example), is an important problem. The solution of this problem will increase the efficiency of geological and geophysical prospecting. Geophysical and direct observations show that different wave effects play a significant role in all natural processes. A peculiarity of standing waves is the formation of stable sections along the ray in the medium. These sections are called nodes, if the oscillation is almost absent and antinodes if the oscillation is maximum. The basis for our experiment is the idea that stratification originates under the action of the standing wave on the viscous solidifying medium. A mixture of epoxy and silica sand was used as the medium. The mixture was placed into a container with conditions favorable for the appearance of a standing wave: a source of supersonic P-waves was at the base of the container and a hard reflective plate on its top. The experiment was carried out until the mixture solidified completely. After that, the cubic sample was made from this material, and it was analyzed by means of the acoustopolariscopic method. It has been found that the medium obtained has a plane-type anisotropy common for textured and layered rocks. Because the sample anisotropy plane is normal to the wave spreading direction, it is evident that the influence of the standing wave formed by pulsation of a hypothetic deep source and reflection from the hard surface of the Earth crust is one of possible reasons of the stratification in the solidifying solution (igneous melt together with processes, caused by gravity).

THE SYSTEMATIC EVOLUTION OF THE LANTHANIDE TETRAD EFFECT IN PERALUMINOUS GRANITE SUITES.

W. Irber, Lehrstuhl für Angewandte Mineralogie und Geochemie der Technischen Universität München, Lichtenbergstrasse 4, D-85747 Garching, Germany (wolfgang.irber@geo.tum.de).

Introduction: Chondrite-normalized REE patterns showing the lanthanide tetrad effect are observed at more highly evolved Hercynian peraluminous granites from mideast Germany (Central Erzgebirge, Western Erzgebirge, Fichtelgebirge, and Northern Oberpfalz, Fig. 1).

Method: In order to examine when and why the tetrad effect occurs in REE patterns of granite samples, the degree of the tetrad effect ($TE_{1,3}$) is estimated by a simple formula [1]. The resulting values for each sample are plotted vs. K/Rb, Sr/Eu, Eu/Eu*, Y/Ho, and Zr/Hf. Those element pairs are known to be sensitive to granite differentiation and the late-stage influence of aqueous phases during the final stage of granite crystallization [2].

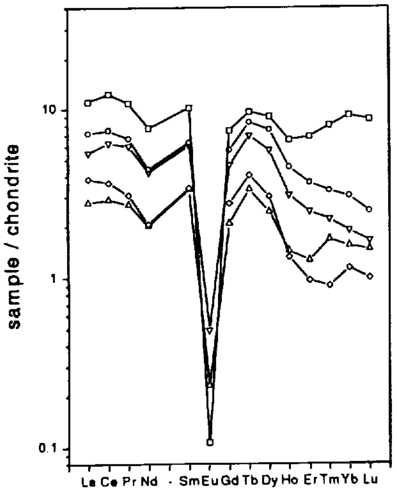

Fig. 1. Rare-earth-element patterns with marked tetrad effect from highly evolved pera-luminous granites of mideast Germany.

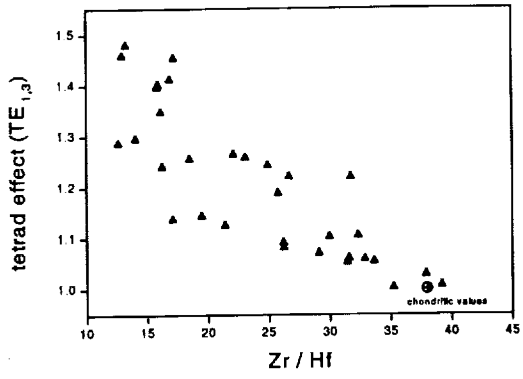

Fig. 2. The degree of the tetrad effect vs. Zr/Hf of differently evolved granite samples from massifs in mideast Germany. The cross marks the chondritic values.

Results: The diagrams reveal that the tetrad effect develops parallel to granite evolution. Marked tetrad effects are limited to highly differentiated rock samples. The tetrad effect ($TE_{1,3}$) correlates positively with Y/Ho and Sr/Eu and negatively with K/Rb, Eu/Eu*, and Zr/Hf (Fig. 2).

Discussion: Mineral fractionation as a cause for generating the tetrad effect is not supported by a calculated Rayleigh fractionation. The calculation also failed to explain the fractionation trends of Sr/Eu and Eu/Eu*. The strong decrease of Eu concentrations in highly evolved rocks suggests that Eu fractionates between the residual melt and a coexisting aqueous high-temperature fluid. Mineral fractionation as a reason for the tetrad effect is even more unlikely, as REE patterns of accessory minerals display similar tetrad effects as the respective host rocks. The accessory minerals inherit the REE signature of the melt and do not contribute to the bulk-rock tetrad effect via mineral fractionation.

Conclusion: The results point to significant changes of element fractionation behavior in highly evolved granitic melts: ionic radius and charge, which commonly control the element distribution between mineral and melt, are no longer the exclusive control [2]. The distinct trace-element behavior and the common features of magmatic-hydrothermal alteration in the studied rocks suggest the increasing importance of an aqueous-like fluid system during the final stage of granite crystallization. The positive correlation of $TE_{1,3}$ with bulk-rock F contents indicates a REE complexation with F in generating the tetrad effect. As the evolution of a REE pattern with tetrad effect (M-type) implies the removal of a respective mirroring REE pattern (W-type), the tetrad effect identifies open-system conditions during granite crystallization.

References: [1] Irber W. (1999) *GCA*, in press. [2] Bau M. (1997) *Contrib. Mineral. Petrol., 128,* 409–412.

GEOCHRONOLOGY OF HIGH-GRADE METAMORPHISM IN NEW ZEALAND.

T. R. Ireland, Department of Geological and Environmental Sciences, Stanford University, Stanford CA 94305-2115, USA.

Introduction: New Zealand lies on the boundary between the Indo-Australian and Pacific plates. This position results in a tectonically active region responsible for the uplift of high-grade metamorphic rocks. Two structural levels are exposed: higher levels in Westland and deeper levels in Fiordland, but the geology and geochronology can be linked between these regions [1]. In Westland, gneisses grading up to upper amphibolite facies are exposed [e.g., 2], while in Fiordland up to granulite-facies rocks are found. Zircon and monazite have been separated from these gneisses and analyzed by ion microprobe.

Geochronology: Zircon ages in paragneisses indicate a predominant source from turbidites of the Greenland Group. This detrital pattern is a characteristic of the Cambrian-Ordovician Gondwana margin and represents material being shed off the continent at that time. The dominant contribution is 500–650 Ma, with a secondary peak at 1000–1200 Ma, an indistinct group at 1700 Ma, and scattered ages out to the Archean. Upper-amphibolite-grade metamorphism of the peilites has produced metamorphic monazite. U-Pb analysis indicates a Devonian metamorphism, coincident with the emplacement of Karamea Suite granites (~370 Ma). Monazite ages indicate orthogneisses in the region are largely Cretaceous and are related to the emplacement of Separation Point Suite and Rahu Suite granites (~120–110 Ma) and the formation of metamorphic core complexes fram extension prior to the opening of the Tasman Sea.

In Fiordland, deeper levels of crust are exposed, but the geology is similar. The core of Fiordland is the Western Fiordland Orthogneiss (WFO), and it is surrounded by high-grade metamorphic rocks including orthogneisses and metapelites. All of these rocks have been subjected to pressures of ~10 kbar. The emplacement of WFO at 126–119 Ma has largely masked many geological and geochronological relationships. The WFO represents the roots of the Separation Point suite rocks in northwest Nelson and in most cases, heating associated with its emplacement has reset, or at least disturbed, the U-Pb-isotopic system in both zircon and monazite. The oldest units in Fiordland are Cambrian-Ordvician granites, similar in age to those in Nelson at 500–490 Ma. Widespread granite emplacement also occurred during the Devonian-Carboniferous (~370–340 Ma).

Metapelites from central Fiordland are variably metamorphosed to sillimanite grade (M1) and kyanite grade (M2). Kyanite-grade metapelites largely surround the WFO, and it has been suggested that the high-pressure metamorphism experienced by these rocks is due to magmatic loading of the crust following the emplacement of WFO. In this case the kyanite metamorphism should have a Cretaceous age. The metapelites from central Fiordland are again sourced from Cambrian-Ordovician turbidites of similar chronologic parantage to the lower-grade metapelites in Westland. The age of metamorphism has been determined by analyzing monazite. Two ages of metamorphism are evident in Fiordland: M1 sillimanite grade at ~360 Ma and M2 kyanite grade at 340–330 Ma. The age of M1 metamorphism is again similar to that of Karamea-suite granite emplacement, while the M2 event is close in age to granites from southwestern Fiordland such as the Kakapo Granite. The monazites also preserve complicated inheritance patterns of detrital monazite in an M1 metapsammite, and M1 metamorphic monazite preserved in an M2 metapelite. These systematics clearly indicate monazite can survive high-grade metamorphism under apposite conditions

The close spatial association of kyanite-grade metapelites around the WFO has suggested a causal link with kyanite-grade metamorphism following emplacement of WFO. However, the monazite geochronology indicates that M2 is Paleozoic and is not related to the emplacement of the WFO.

References: [1] Ireland T. R. and Gibson G. M. (1998) *J. Metam. Geol., 16,* 149–168. [2] Mason B. and Taylor S. R. (1987) *J. Roy. Soc. New Zealand, 17,* 115–138.

AGE OF THE LITHOSPHERIC MANTLE BENEATH AND AROUND THE SLAVE CRATON: A RHENIUM-OSMIUM-ISOTOPIC STUDY OF PERIDOTITE XENOLITHS FROM THE JERICHO AND SOMERSET ISLAND KIMBERLITES.

G. J. Irvine[1], M. G. Kopylova[3], R. W. Carlson[2], D. G. Pearson[1], S. B. Shirey[2], and B. A. Kjarsgaard[4], [1]Department of Geological Sciences, Durham University, South Road, Durham DH1 3LE, UK, [2]Department of Terrestrial Magnetism, Carnegie Institution of Washington, 5241 Broad Branch Road NW, Washington DC 20015, USA, [3]Department of Earth and Ocean Science, University of British Columbia, Vancouver BC, V6T 1Z4, Canada, [4]Geological Survey of Canada, 601 Booth Street, Ottawa ON, K1A 0E8, Canada.

Introduction: The discovery of kimberlites in the Slave Craton over the last decade [1] has provided an opportunity to assess the areal and depth extent of the Archaean Craton via entrained mantle xenoliths. We have applied the Re-Os-isotopic system to a suite of xenoliths, sampling a range of depths, from the Jericho and Somerset Island kimberlites in order to constrain the age and evolution of the lithosphere underlying the Slave Craton and surrounding areas.

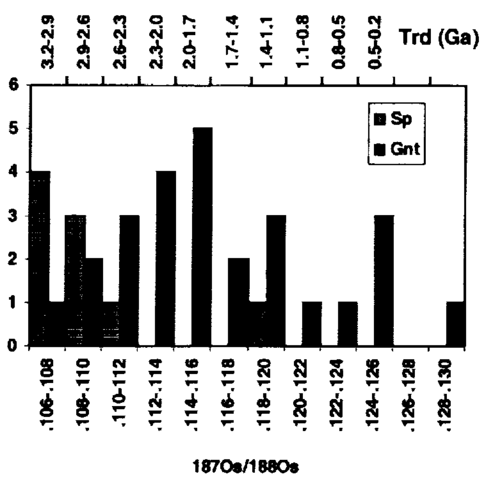

Fig. 1.

Geology: The Slave Craton is dominated by late Archaean supracrustal and plutonic rocks (2.6–2.7 Ga) [2], but also contains blocks of older gneisses (2.8–4.0 Ga) [3]. New studies suggest central Slave basement is much more significant in areal extent than previously thought [4]. The Jericho kimberlite is located 400 km northeast of Yellowknife in the Northwest Territories and intrudes Archaean granitoids and supracrustal rocks [5]. Somerset Island lies to the northeast of the Slave Craton and is intruded by several kimberlites. Precambrian basement ages vary from 2.48 to 1.71 Ga with Nd model ages of 3.0 to 2.2 Ga, suggesting the presence of juvenile Proterozoic crust plus reworked Archaean material [6].

Results: *Jericho.* Thirty-five whole-rock samples from Jericho were analyzed, comprising various peridotites and two wehrlites. Peridotite Os concentrations ranged from 21 to 0.31 ppb (mean = 4.47 ppb, n = 35) with Re 0.27–0.013 ppb (mean = 0.098 ppb, n = 9). The overall range in ^{187}Os/^{188}Os is 0.1066–0.1305 (Fig. 1). Although this range is large, good systematics exist for individual lithologies. Osmium-187/osmium-188 for spinel facies peridotite range from 0.1066 to 0.1189. This range equates to T_{RD} model ages of 3.1–1.3 Ga. Eight out of nine samples have T_{RD} ages >2.5 Ga and three samples have T_{RD} = 3.1 Ga. Osmium-187/osmium-188 for garnet facies peridotites range from 0.1074 to 0.1305. The range in ^{187}Os/^{188}Os in garnet peridotites corresponds to T_{RD} ages between 0.5 and 3.0 Ga. For samples where Re has been measured, some show considerably older T_{MA} ages, whereas for others T_{RD} ages are within 200 m.y. of the T_{MA} ages. One garnet peridotite and two wehrlites give T_{MA} ages ~500 Ma.

Somerset Island. Nine whole-rock samples from Somerset were analyzed. The overall range in ^{187}Os/^{188}Os is 0.1094–0.1146. Samples appear to fall within three distinct groups: two samples ~0.1095, three samples ~0.111, and four samples ~0.114. T_{RD} ages range from 2.7 to 2.0 Ga. T_{MA} model ages of up to 2.9 Ga were obtained.

Discussion: The lithospheric mantle beneath Jericho has a wide age range compared to the Kaapvaal and Siberian cratons. [7] On the basis of mineral chemical data, it has been suggested that the mantle beneath Jericho is Proterozoic [8]. The T_{RD} ages of spinel facies peridotites and some garnet facies peridotites from Jericho are clearly Archaean. Many of the garnet facies peridotites, however, could either be Proterozoic, or reworked Archaean, altered by numerous magmatic events (including the Mackenzie plume event). T_{MA} ages of wehrlites and some peridotites indicate a magmatic "event" at ~450 Ma. The oldest T_{RD} ages for Somerset peridotites are late Archaean suggesting the existence of some cratonic lithospheric material beneath this region.

References: [1] Pell J. A. (1997) *Geosci. Canada, 24,* 77–91. [2] Padgham W. A and Fyson W. K. (1992) *Can. J. Earth Sci., 29,* 2072–2086. [3] Percival J. A. (1996) *Geological Survey Canada Open-File 3228,* 161–

169. [4] Bleeker and Davis. (1999) *Can. J. Earth Sci.*, in press. [5] Kopylova M. G. et al. (1999) *J. Petrol.*, *40*, 79–104. [6] Kjarsgaard B. A. (1996) *Geological Survey Canada Open-File 3228*, 61–66. [7] Carlson R. W. et al. (1999) *Proc. 7th Intl. Kimberlites Conf.*, in press. [8] Griffin W. L. et al. (1998) *Ext. Abstr. 7th Intl. Kimberlites Conf.*, 271–273.

QUANTITATIVE LASER ABLATION MICROPROBE INDUCTIVELY COUPLED PLASMA MASS SPECTROMETRY ANALYSIS OF TRACE ELEMENTS IN DIAMONDS.

S. E. Jackson[1], R. M. Davies[1], W. L. Griffin[1,2], S. Y. O'Reilly[1], and B. Doyle[3], [1]Key Centre for Geochemical Evolution and Metallogeny of Continents, Macquarie University, Sydney, NSW 2109, Australia (sijackso@laurel.ocs.mq.edu.au), [2]Commonwealth Scientific and Industrial Research Organisation Exploration and Mining, North Ryde, NSW 2113, Australia, [3]Kennecott Canada Inc., 200 Granville Street, Vancouver BC, V6C 1S4, Canada.

Natural diamonds erupted by kimberlites and lamproites are unmodified samples of the deepest upper mantle. Trace-element analysis of their impurities provides information on the composition of their source environment. Questions to be addressed through the trace-element study of diamonds include the following: (1) Do diamonds of different parageneses crystallize from different fluids? (2) What are the origins of these fluids? (3) Are diamond-forming processes similar worldwide or depend on mantle age and composition? and (4) Can we "fingerprint" diamonds from a particular locality?

A laser ablation microprobe inductively coupled plasma mass spectrometry (LAM-ICP-MS) technique, developed for trace-element analysis of carbonaceous substances [2], has been used to analyze trace elements in fibrous and nonfibrous diamonds. The custom-built LAM employed in this work uses a Continuum Surelite I-20, Q-switched Nd:YAG laser frequency quadrupled to 266-nm wavelength and operated at a frequency of 10 Hz. The ICP-MS is a Perkin-Elmer Sciex ELAN 6000. Calibration was performed by direct ablation of a certified oil reference material (S-21, 50 ppm; Conostan) contained in a capillary tube. A bitumen standard reference material (SRM1632b; NIST) was used to extend the list of elements calibrated and to crosscheck the data. Carbon was used as an internal standard to correct for differing ablation yields. Laser pulse energy used was 0.15 mJ/pulse for the oil and bitumen standards, and 2.0–2.2 mJ/pulse for diamond. For each sample, optimal background (~60 replicates counted on the Ar carrier gas) and ablation (~120 replicates) regions were selected from the time-resolved spectra and integrated to determine the net count rates and concentrations for each element [2]. Two to four analyses were averaged for each diamond. Relative deviations for replicate analyses of fibrous diamond samples ranged between 2 and 81% for different elements (median 20%), indicating significant heterogeneity from spot to spot.

TABLE 1. Comparative data on trace-element abundances in diamond Jwn110 from LAM-ICP-MS, PIXE and EMP + NAA analyses. Values are in parts per million.

	LAM	PIXE	EMP, NAA
mg#	33		45
Na	5		6.0
Mg	11		
Al	12		
Si	211		
K	58	69	61.3
Ca	96	53	
Ti	8	7	
V	<3		
Cr	1	0	0.16
Mn	0.3		
Fe	24	35	31.20
Ni	0.5	0.9	0.54
Cu	0.3	1.7	
Zn	<3	1.2	0.17
Ge	n.d.		
Br	<15	0.2	0.15
Rb	0.2	0.2	0.22
Sr	0.9	1.7	1.47
Y	0.04		
Zr	n.d.	2.1	1.12
Sn	3.8		
Ba	1.6		1.70
Ce	0.2		0.19
Tb	n.d.		0.02
Yb	n.d.		0.01
Pb	0.02	0.5	

To test the accuracy of the results, we have analyzed fibrous diamonds from the Jwaneng kimberlite (Jwn 110 and Jwn 115) previously analyzed by NAA [5], EMP [4], and PIXE [6]. Good agreement was found between the methods, considering sample heterogeneity and the different volumes sampled by the different analytical methods (Table 1). The results demonstrate that the LAM-ICP-MS can rapidly and accurately measure a wide suite of trace elements with high spatial resolution. Several improvements are being made to the technique. They include development of a frequency quintupled laser wavelength option (λ = 213 nm) to improve ablation efficiency of the diamonds, and development of a synthetic aqueous standard(s) to extend the list of elements that can be quantified (halogens, S, etc.).

To compare diamonds of different paragenesis, we are analyzing nonfibrous diamonds from the DO27 kimberlite, Slave Craton, whose parageneses (peridotitic, eclogitic, and superdeep or ferropericlase-bearing) were defined from mineral-inclusion studies [1]. Preliminary results show that diamonds from the three parageneses are significantly different. Relative to peridotitic diamonds, Na, Mg, Al, K, Rb, Sr, Y, Sn, and Ce are high in eclogitic stones and low in superdeep ones. The differences suggest that meaningful trace-element "fingerprinting" to identify a diamond as being from a single locality is unlikely to be successful.

References: [1] Davies R. M. et al. (1999) *Proc. 7th Intl. Kimberlites Conf.*, in press. [2] Longerich H. P. et al., *JAAS, 11*, 899–904. [3] Mossman D. J. et al. (1999) *Econ. Geol.*, submitted. [4] Schrauder M. and Navon O. (1994) *GCA, 58*, 761–771. [5] Schrauder M. et al. (1996) *GCA, 60*, 4711–4724. [6] Griffin W. L. and Ryan C. G., unpublished data.

DETERMINATION OF HIGH-PRECISION ISOTOPIC RATIOS BY LASER ABLATION MULTIPLE COLLECTOR INDUCTIVELY COUPLED PLASMA MASS SPECTROMETRY.

S. E. Jackson[1], W. L. Griffin[1,2], and N. J. Pearson[1], [1]Key Centre for Geochemical Evolution and Metallogeny of Continents, Department of Earth and Planetary Sciences, Macquarie University, Sydney NSW 2109, Australia (sijackso@laurel.ocs.mq.edu.au), [2]Commonwealth Scientific and Industrial Research Organisation Exploration and Mining, NSW 2113, Australia.

Introduction: The multiple collector inductively coupled plasma mass spectrometer (MC-ICP-MS) makes determination of high-precision isotopic ratios of wide range of elements routinely possible. Furthermore, the lack of time-dependent differential ionization of elements allows elemental spikes to be used for mass bias correction and isobaric overlap corrections to be made, allowing for the effective use of laser ablation (LA) sampling for *in situ* determination of high-precision isotopic ratios.

Instrumentation: The instrumentation used was a Merchantek LUV266 Nd:YAG laser ablation sampler operating at a wavelength of 266 nm. This was coupled to a Nu Plasma MC-ICP-MS featuring an ICP coupled to a double-focusing electrostatic/magnetic mass analyzer. Novel variable dispersion ion optics focus the ions into a fixed collector array con-sisting of 12 faraday cups and 3 ion counting detectors. Both instruments were installed at Macquarie University in November 1998.

Methodology: Mass bias correction was effected using two procedures: (1) calculation of mass bias using a stable isotopic ratio of the element of interest, where present (e.g., Sr, Hf); (2) where no fixed stable isotopic ratio was available (e.g., Cu, Pb, etc.), mass bias was determined from another element, which was introduced via a T-junction into the sample carrier gas stream as a "dry" aerosol generated using a CETAC MCN6000 desolvating nebulization system. For laser analyses, data were acquired using a time resolved analysis acquisition protocol that reports signals 10 times/s, thereby allowing assessment of isotopic ratios as a function of ablation time. Here we report several critical observations on isotopic fractionation during laser ablation sampling.

Hafnium isotopes. Hafnium isotopes were measured on several zircons [1] and LIMA minerals [2]. Mass-bias correction was achieved using the stable isotopic ratio^{179}Hf/^{177}Hf. Significant changes were observed during each ablation analysis in the uncorrected ^{179}Hf/^{177}Hf ratios that correlated inversely with total Hf signal intensity. However, corrected ^{176}Hf/^{177}Hf showed no relationship with ablation time. Multiple analyses of two zircon standards gave highly precise ^{176}Hf/^{177}Hf ratios that were in agreement with thermal ionization mass spectrometry (TIMS) data.

Strontium isotopes. Strontium-isotopic analyses of several LIMA minerals [3] were made using the stable ^{88}Sr/^{86}Sr ratio for mass-bias correction. As with Hf isotopes, the stable isotopic ratio generally showed an inverse relationship with total signal intensity during ablation.

Antimony isotopes. Antimony-isotopic measurements were made on Sb-bearing native Ag and sulfide minerals using Sn introduced via the MCN6000 for mass-bias correction. Strong within-run variation (up to 0.4%) in ^{123}Sb/^{121}Sb ratios, showing a positive correlation with total Sb signal, were typical while ^{124}Sn/^{122}Sn ratios showed minimal or no correlation with signal intensity.

Copper isotopes. Copper-isotopic ratios were measured on chalcopyrite and Cu metal using Zn introduced via the MCN6000 for mass-bias correction. Strong within-run variation (up to 0.2%) in uncorrected ^{65}Cu/^{63}Cu ratios were typical, which, like Sb, showed a positive correlation with total signal, while ^{64}Zn/^{62}Zn ratios showed minimal or no correlation with signal intensity. Laser ablation analyses of chalcopyrite and Cu metal gave ^{65}Cu/^{63}Cu ratios that were significantly lower than analyses of the same samples digested and analyzed by solution introduction

Discussion: Both lithophile (Hf and Sr) and chalcophile (Sb and Cu) elements showed within-run isotopic variations during laser-ablation sampling. For the lithophile elements, the heavy/light ratios showed a negative correlation with total signal intensity, whereas, for the chalcophile elements, the heavy/light ratios showed a positive correlation. Elements introduced via the MCN6000 showed minimal within-run isotopic variations. The different isotopic behavior of elements derived by laser ablation and the MCN 6000 suggests that observed fractionations cannot be attributed to the MC-ICP-MS and that the laser sampling/transport process can fractionate isotopes to a very significant degree. The isotopically light Cu-isotopic ratios produced by laser ablation are in accord with a fractionation mechanism involving differential volatilization and condensation processes during laser sampling/transport.

The relationships between the observed isotopic fractionation patterns and ablation conditions are not yet understood. However, strong elemental fractionation of lithophile and chalcophile elements can occur during laser sampling, suggesting that their ablation mechanisms may be fundamentally different.

Highly precise and accurate Hf-isotopic data indicate that mass bias correction using a stable isotopic ratio of the element of interest adequately corrects laser sampling-related fractionation. However, when mass bias is corrected using an introduced element, laser sampling-related fractionations are detrimental to the precision and accuracy of the technique. Experiments using alternative transport gases and laser cell designs are under way to further investigate and deal with the problem.

References: [1] Griffin W. L. et al. (1999) *GCA*, submitted. [2] Griffin W. L. et al., this volume.

ISOTOPES AND METHODS FOR MODELING OF GEOCHEMICAL CYCLES.

S. B. Jacobsen, Department of Earth and Planetary Sciences, Harvard University, 20 Oxford Street, Cambridge MA 02138, USA (jacobsen@neodymium.harvard.edu).

Introduction: The concept of geochemical cycles dates back to Goldschmidt [1], with his early version of the C cycle. He realized that man already had made a significant perturbation of this cycle due to fossil-fuel burning. Barth [2] introduced the concept of residence time in a discussion of some of Goldschmidt's earlier work on geochemical cycles. Mason's textbook [3] included a general chapter on geochemical cycles. The fundamental equations for the kinetics of evolving systems of reservoirs was discussed by Lotka [4] with applications to problems in biology. Lasaga [5] used such techniques for quantitative evaluation of geochemical cycles. The critical step is calculating the eigenvalues and eigenvectors of the geochemical cycle matrix (K).

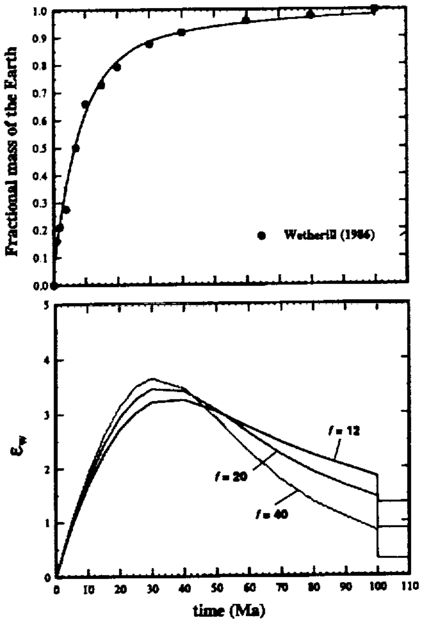

Fig. 1.

Geochemical Cycle Models Based on Isotopes: Elemental cycles are usually modeled using a linear cycles approach with a K matrix that is independent of time. The geochemical cycle matrix K is, however, in general a function of time, and better constraints on the dynamic evolution of the Earth can be obtained from radiogenic and stable isotopic evolution of Earth reservoirs. For long-lived radionuclides, the isotopic effects (ε) can be directly related to the mean age of the reservoir [6]. The radiogenic-isotopic evolution equations ($d\varepsilon/dt = Qf + K\varepsilon$; Q is a bulk Earth factor, and f is the chemical fractionation of the parent/daughter ratio) can be used to constrain the K matrix and thus the mass fluxes between all the reservoirs [7]. Examples of the application to stable isotopic ratios (in particular δ^{13}C) for constraining the C cycle will also be given [8].

Accretion of the Earth: The extinct nuclide system ^{182}Hf-^{182}W can be used to constrain the rate of accretion and core formation using these principles. The upper part of Fig. 1 [from 9] shows the results of Wetherill's [10] accretion calculations (97.5% of the Earth is made before 100 Ma and the last 2.5% is assumed to be added at 100 Ma). This model yields a mean time of formation of 16 Ma for the Earth. The resulting isotopic evolution of W (ε_W) in the silicate portion of the Earth is shown for $f^{Hf/W}$ ratios of 12, 20, and 40 using a magma ocean differentiation model. In all cases the ε_W values show a peak at ~30 Ma. Subsequent to that time the ε_W value decays more rapidly for higher values of $f^{Hf/W}$. The last 2.5% of accretion is sufficient to reduce the effect in the Earth to 1 ε_W unit or less. A variety of such models have the following features in common: (1) They can produce a large early ε_W anomaly in the silicate Earth provided the initial growth stage of the Earth is rapid (more than 50% formed in the first 20 m.y.); (2) if substantial (>20%) growth of the Earth occurs subsequent to 20–30 Ma, then the ε_W anomaly is almost always reduced to <1 ε_W unit by 100 Ma; and (3) late giant impacts result in a ε_W anomaly of <0.5 ε_W units. It is necessary to have the Moon form by an early (~25-Ma) giant impact, while the Earth still had a substantial ε_W anomaly. At least 20% of the Earth must have accreted subsequent to the formation of the Moon to effectively erase the ε_W anomaly in the silicate Earth. A scenario in which the Earth's core is formed after 60 Ma and the Moon simultaneously by giant impact is implausible.

References: [1] Goldschmidt V. M. (1934) *Geol. Fören. Förh., 56,* 416. [2] Barth T. F. W. (1952) *Theoretical Petrology,* Wiley, 416 pp. [3] Mason

B. (1966) *Principles of Geochemistry,* Wiley, 329 pp. [4] Lotka A. J. (1924) *Elements of Physical Biology,* Williams & Wilkins, 465 pp. [5] Lasaga A. C. (1980) *GCA, 44,* 815–828. [6] Jacobsen S. B. and Wasserburg G. J. (1979) *JGR, 84,* 7411–7427. [7] Jacobsen S. B. (1988) *GCA, 52,* 1341–1350. [8] Jacobsen S. B. and Kaufman A. J. (1999) *Chem. Geol.,* in press. [9] Jacobsen S. B. (1999) *LPS XXX,* Abstract #1978. [10] Wetherill G. W. (1986) in *Origin of the Moon* (W. K. Hartmann et al., eds), pp. 519–550, LPI.

TOWARD A CONSISTENT EARLY SOLAR SYSTEM CHRONOLOGY.

S. B. Jacobsen, Department of Earth and Planetary Sciences, Harvard University, 20 Oxford Street, Cambridge MA 02138, USA (jacobsen@neodymium.harvard.edu).

Introduction: Long-lived chronometers (e.g., U-Pb, Sm-Nd, Rb-Sr, Lu-Hf, and Re-Os) provide some broad constraints on the chronology and differentiation processes in the early solar system. However, the isotopic record of extinct radionuclides may potentially yield more reliable constraints on the rates of accretion, core formation, and the evolution of the mantle and crust at very early times in planetesimals and planets.

Early Solar System Chronology: The upper panel in Fig. 1 shows the U-Pb age vs. time with the Angrite LEW defined as time = 0. This meteorite has a well-determined U-Pb age of 4557.8 ± 0.5 [1]. This is clearly younger than the U-Pb age for CAIs of 4566 ± 2 [2]. However, [3] preferred a slightly older CAI age on the U-Pb scale of 4568.3 ± 0.7. These are the two solid points in the upper panel in Fig. 1. The ages or relative formation times of all the other objects are inferred from the Mn-Cr and Pd-Ag systems shown below. Manganese-chromium [3] on LEW, pallasite Omolon, and an HED whole-rock isochron yield their relative ages. The chondrule point [4] indicates that CAIs and chondrules are almost of the same age. Considering uncertainties, they could be different by up to 1–2 m.y. Using Pd-Ag for pallasites from the summary of [5] we obtain relative ages of mesosiderites, group I, II, and III iron meteorites (all mostly very similar) but with IVA irons being somewhat older. We use the group I, II, and III iron meteorites to obtain a consistent chronology for the Hf-W system [6,8]. An obvious problem is the Hf-W eucrite data of [7]. They yield ^{182}Hf/^{180}Hf = 1.3 × 10^{-4} consistent with the age of LEW rather than HED! Also, metal from chondrites yields ^{182}Hf/^{180}Hf values similar to those of group I, II, and III iron meteorites [8] suggesting no time difference between metal formation in chondrites and core formation in the parent bodies of group I, II, and III iron meteorites. A preliminary result for the Tc-Mo system is also shown (data from this lab). The ^{146}Sm/^{144}Sm determined for the LEW angrite of 0.0071 ± 17 [1]. This value should only be 0.0005 lower than the initial value for CAIs. Even so, higher values have been suggested for mesosiderites and the IA iron meteorite Caddo [9]. Note that the primary constraints comes from the chronometers U-Pb, Pd-Ag, and Mn-Cr that are all affected by multiple processes. It is not clear what processes the ages refer to. These chronologies need to be tested and compared to results from additional systems that are more uniquely fractionated by a single planetary differentiation process (Hf-W, Tc-Mo, and Sm-Nd). Such constraints are clearly useful in the evaluation of models of the origin of the planets. This method of approach provides a means to better constrain the conditions and timescales associated with planetary coagulation and differentiation.

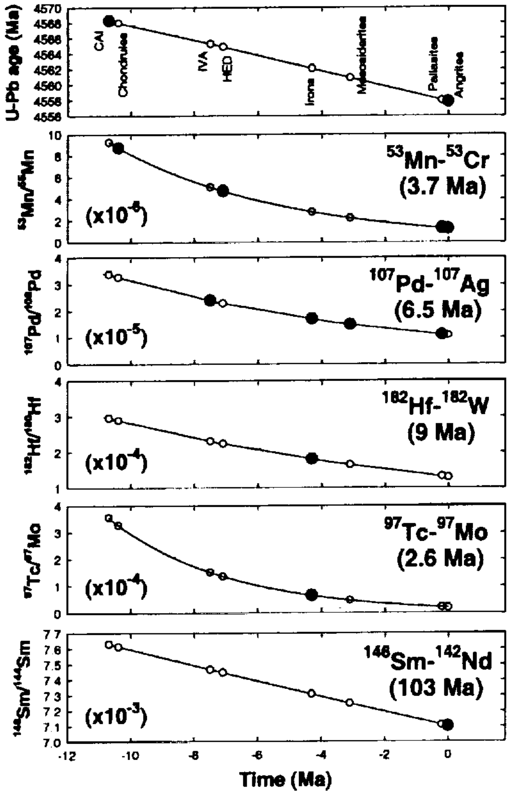

Fig. 1. Uranium-lead and five extinct nuclide chronologies (half-lives given in parenthesis). Solid symbols represent data discussed in the text. Open symbols represent points calculated to obtain a consistent chronology for the objects labeled in the top panel.

References: [1] Lugmair G. W. and Galer S. J. G. (1992) *GCA, 56,* 1673–1694. [2] Göpel C. et al. (1991) *Meteoritics, 26,* 338. [3] Lugmair G. W. and Shukolyukov A. (1998) *GCA, 62,* 2863–2886. [4] Nyquist L. E. et al. (1997) *LPS XXVIII,* 1033–1034. [5] Chen J. H. and Wasserburg G. J. (1996) *Geophys. Monogr., 95,* 1–20. [6] Horan M. F. et al. (1998) *GCA, 62,* 545–554. [7] Lee D. C. and Halliday A. N. (1997) *Nature, 388,* 854–857. [8] Jacobsen S. B. and Yin Q. Z. (1998) *LPS XXIX,* Abstract #1852. [9] Stewart B. et al. (1996) *EPSL, 143,* 1–12.

STRONTIUM-, CARBON-, AND OXYGEN-ISOTOPIC VARIATIONS OF NEOPROTEROZOIC SEAWATER.

S. B. Jacobsen[1] and A. J. Kaufman[2], [1]Department of Earth and Planetary Sciences, Harvard University, Cambridge MA 02138, USA (jacobsen@neodymium.harvard.edu), [2]Department of Geology, University of Maryland, College Park MD 20742, USA (kaufman@geology.umd.edu).

We present a relatively detailed first-order record of isotopic variation (^{87}Sr/^{86}Sr, δ^{13}C, and δ^{18}O) in seawater through the late Neoproterozoic Era, during which several discrete global ice ages (snowball glaciations) occurred (V1, V2, S1, and S2) and the first macroscopic animals evolved. The data was obtained on well-preserved marine limestone from Siberia, Namibia, Canada, Svalbard, and East Greenland.

During this time, the lowest ^{87}Sr/^{86}Sr-values (~0.7056) characterize the interval between ~750–800 Ma and have been interpreted to reflect a major

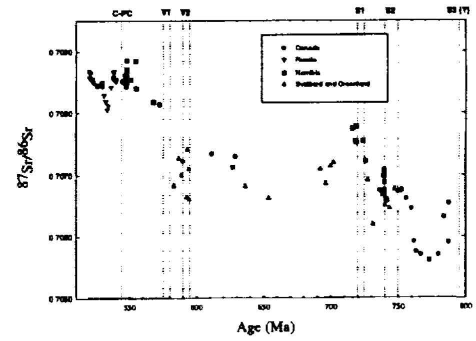

Fig. 1.

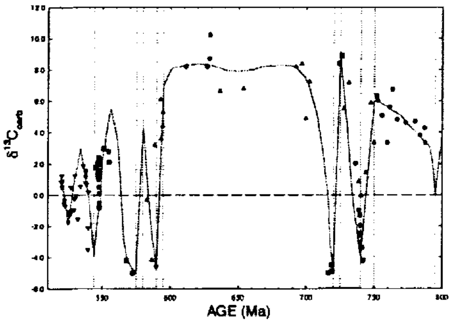

Fig. 2.

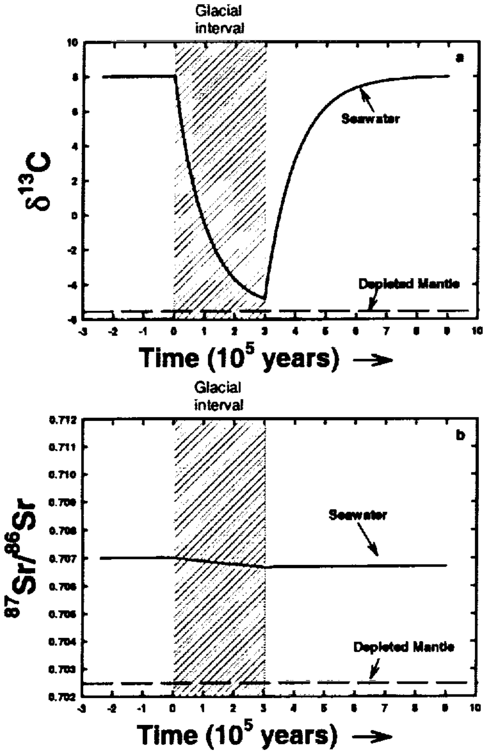

Fig. 3.

hydrothermal event. From 750 to 600 Ma the $^{87}Sr/^{86}Sr$ isotope values vary between 0.7063 and 0.7074. Between 600 Ma and the Early Cambrian (~535 Ma), $^{87}Sr/^{86}Sr$ values rise sharply from 0.7063 to 0.7087. This rise is thought to reflect enhanced continental input to the oceans associated with a pan-African continental collision.

The $\delta^{13}C$-curve rises from values close to 0 prior to 800 Ma to ~6 at 750 Ma and ~8 for the time between 600 and 730 Ma. During the time between 600 and 542 Ma, the highest values are ~4 (higher values in each interval are preserved in little-altered dolomites). Strong positive-to-negative excursions to values of -5 are associated with both Vendian glaciations estimated at ~575 and 590 Ma and with Sturtian glaciations estimated at ~720 and 740 Ma. In strong contrast, there are no distinct changes in $^{87}Sr/^{86}Sr$ across Neoproterozoic glacial intervals.

The duration of these global refrigeration events is a subject of considerable debate. Figure 3 shows the response of $^{87}Sr/^{86}Sr$ and $\delta^{13}C$ to a glacial event that is 3× the C residence time in seawater. This calculation assumes that the maximal organic C burial flux, interpreted from $\delta^{13}C$ value (~8) of preglacial carbonate, stops and starts instantaneously at t = 0 and t = 3 × 10^5 yr, respectively. Over this interval, $^{87}Sr/^{86}Sr$ of seawater would experience little change due the much longer residence time of this element.

In contrast, for a ~10-m.y. glacial interval, the $^{87}Sr/^{86}Sr$ value would drop from 0.707 to below 0.703 assuming total cessation of continental inputs. Including a diagenetic flux of Sr similar to today (1×), then $^{87}Sr/^{86}Sr$ would drop to ~0.7038 after 10 Ma. Unless it can be shown that diagenetic fluxes were an order of magnitude greater during snowball glaciations, we conclude that the Neoproterozoic glaciations lasted less than ~1 m.y. each and that any model to explain these glaciations needs to account for this constraint. The relationship between $\delta^{13}C$ and $^{87}Sr/^{86}Sr$ variations suggests that these negative C-isotopic excursions would have lasted at least 350,000 yr and no more than ~1 m.y., assuming modern diagenetic fluxes of Sr to the oceans and total absence of continental fluxes.

ON THE SEARCH FOR NEODYMIUM-142 IN TERRESTRIAL ROCKS.

E. Jagoutz and R. Jotter, Max-Planck-Institut für Chemie, Postfach 3060, D-55020, Mainz, Germany (jagoutz@mpch-mainz.mpg.de).

Neodymium-142 is a decay product of ^{146}Sm (half-life of 103 m.y.). Samarium-146 is a so-called extinct radioisotope [1]. It existed at 4.56 Ga (0.008 ± 0.001 $^{146}Sm/^{144}Sm$ [2]) but was essentially extinct after 300 m.y. There is a indirect sign of ^{146}Sm existence by observation of ^{142}Nd variations in meteorites [1]. The first finding of ^{142}Nd in terrestrial rocks was reported from a single sample of the Isua supercrustal [3]. Several groups challenged this finding. However, those anomalous rocks from Isua were remeasured by [4].

A ^{142}Nd anomaly is created by an early Sm/Nd fractionation. In a reservoir with a high Sm/Nd ratio, radiogenic ^{142}Nd will be generated, while in a low Sm/Nd ratio reservoir, a deficit of ^{142}Nd will remain. After decay of ^{146}Sm, those reservoirs will keep their ^{142}Nd anomalies as long as these two reservoirs are not remixed again. A later differentiation within such a reservoir will not affect the anomaly. First attempts to find a ^{142}Nd anomaly on Earth were simply guided by measuring old rocks and hoping that some of the Isua rocks were derived from an early differentiated reservoir.

We found reason to believe that some of the cratonic lithosphere might actually be a remnant of a primary differentiation. The first indication in this direction was the finding that the cratonic ultramafic in South Africa are having a higher modal abundance of orthopyroxene [5] than the primitive mantle. Later, the higher modal orthopyroxene contained was also demonstrated for the Siberian Craton [6]. Herzberg actually proposed that this might be caused by a primary differentiation on Earth [7]. We found that, besides other geochemical peculiarities, a depletion of Al is evident in such cratonic ultramafics. A geochemical parallelism is found in SNC meteorites and Urelites. In SNC meteorites, a variation of ^{142}Nd is evident [8], indicating that the Al deficit was caused by a very early differentiation. A similar style of primary differentiation could have produced the cratonic lithosphere. This made us search for a ^{142}Nd anomaly in cratonic ultramafics. In one of our samples, we found a 30 ± 10-ppm deviation from the standard ^{142}Nd. However, this needs further confirmation by additional measurements. We are willing to distribute splits of such samples to groups interested after our measurements are finished.

Realizing the need for better ^{142}Nd data, especially on meteorites, we systematically improved the precision of our ^{142}Nd measurements. This has involved updating the hardware and software of our mass spectrometer, including installing a relational database that saves all parameters from each scan measured on the machine. The latter not only makes data reduction easier, but also provides a powerful "diagnostic tool" for identifying critical parameters during the analysis. Our amplifier bias is constant with or without a beam entering the cup, but the bias does exhibit small temperature dependence. All data handling (e.g., time interpolation, bias subtraction) is performed using database functions. A considerable effort was made to minimize the error contribution by data handling. The time interpolation is especially crucial and therefore we optimized this routine for ^{142}Nd measurements. A second-order fractionation correction was applied to the data to further improve analytical precision. We reproduced the standard ^{142}Nd within a 10-ppm error. However, we realized that the sample Nd must be very clean, since chemical impurities influence the results on this extreme level of precision.

References: [1] Lugmair and Marti (1977) *EPSL, 35,* 273–284. [2] Lugmair and Galer (1992) *GCA, 56,* 1673–1694. [3] Harper and Jacobsen (1992) *Nature, 360,* 728–732. [4] Sharma et al. (1996) *GCA, 60,* 2037–2047. [5] Boyd F. R. (1989) *EPSL, 96,* 15–26. [6] Boyd F. R. et al. (1997) *Contrib. Mineral. Petrol., 128,* 228–246. [7] Herzberg C. T. (1993) *EPSL, 120,* 13–29. [8] Harper et al. (1995) *Science, 267,* 213–217.

TEMPERATURE, PRESSURE, AND RHENIUM-OSMIUM AGE SYSTEMATICS OF OFF-CRATON PERIDOTITE XENOLITHS FROM THE NAMAQUA-NATAL BELT, WESTERN SOUTH AFRICA.

P. E. Janney[1], R. W. Carlson[1], S. B. Shirey[1], D. R. Bell[2], and A. P. le Roex[2], [1]Department of Terrestrial Magnetism, Carnegie Institution of Washington, 5241 Broad Branch Road NW, Washington DC 20015, USA (pjanney@dtm.ciw.edu), [2]Department of Geological Sciences, University of Cape Town, Private Bag, Rondebosch 7700, South Africa.

Introduction: Proterozoic mobile-belt lithosphere constitutes approximately half of the southern African continent, yet its age and formation history are poorly known compared to the Archean cratons of the region, particularly the well-studied Kaapvaal craton. We have collected a suite of garnet and spinel-bearing peridotite xenoliths from six kimberlite and melilitite pipes in the Namaqua-Natal mobile belt of western South Africa. Five of the localities are in the central Karoo region, located between 50 and 175 km southwest of the Kaapvaal craton boundary (Fig. 1). The sixth locality is located in northern Namaqualand (just south of Namibia), ~300 km west of the Kaapvaal craton.

Thermobarometry: Estimates of pressure and temperature based on mineral compositions using the Brey and Köhler [1] thermobarometer for the garnet peridotites (lherzolite and websterite) yield pressures and temperatures of 25–50 kbar and 800°–1200°C respectively. Most P-T data form a linear array that is displaced 75°–150°C above the cratonic geotherm, possibly reflecting higher heat flow in the thin mobile-belt lithosphere [2]. There appears to be a weak anticorrelation between the maximum equilibration pressure of peridotites and their distance from the craton, but additional data are needed to make any firm conclusions.

TABLE. 1.

Locality	Distance from Craton	Age Range (T_{RD})
Uintjesberg	75 km	0.86–2.34 Ga
Hebron	100 km	1.80–2.15 Ga
Gansfontein	175 km	1.14–1.20 Ga
Hoedkop	300 km	1.37 Ga

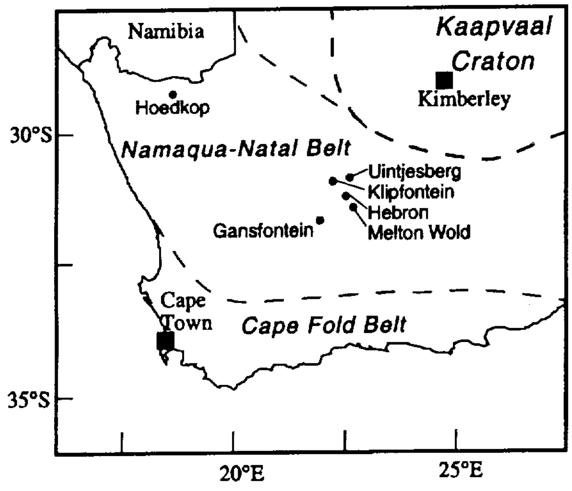

Fig. 1. Off-craton peridotite xenolith localities investigated in this study.

Rhenium-Osmium Ages and Discussion: Rhenium-Osmium isotopic data are being obtained on the xenolith suite in order to date the accretion/stabilization of the terranes constituting the Namaqua-Natal Belt. The ^{187}Os/^{188}Os isotopic ratios, corrected to the age of the host kimberlite, vary between 0.1119 and 0.1226. In general, the maximum Re-depletion ages (T_{RD}; minimum model age calculated by assuming that all Re in the peridotite was added at the time of host kimberlite eruption) from each locality decreases with increasing distance from the craton. The large spread of ages at Uintjesberg most likely indicates a complex history with multiple stages of melt extraction and addition.

The oldest T_{RD} ages determined on the peridotites (1.8–2.34 Ga) are essentially identical to the oldest Nd and Pb-Pb Namaqua-Natal crustal model ages (1.9–2.3 Ga) [3,4], supporting the hypothesis that crust formation and stabilization of lithospheric mantle occurred simultaneously, as in the Kaapvaal craton [e.g., 5]. The younger T_{RD} ages (1.14–1.37 Ga) may also correspond to widespread crustal generation/metamorphism events at 1.5–1.3 and 1.1 Ga recorded by the Namaqua gneisses of western South Africa [4,6]. It is possible that the younger T_{RD} and crustal ages at Hoedkop and Gansfontein indicate the presence of a younger terrane accreted or stabilized (by large-degree melt extraction) at this time.

One exceptional attribute of this sample set is that most localities lie within the region covered by the Kaapvaal Seismic Experiment seismometer network. This will allow us to correlate the seismic velocity structure of the lithosphere southwest of the Kaapvaal craton with age, composition, and pressure-temperature data obtained from the peridotites.

References: [1] Brey G. P. and Köhler T. (1990) *J. Petrol., 31,* 1353–1378. [2] Nyblade A. A. and Robinson S. W. (1994) *GRL, 21,* 765–768. [3] Harris N. B. W. et al. (1987) *EPSL, 83,* 85–93. [4] Reid D. L. et al. (1997) *S. Afr. J. Geol., 100,* 11–22. [5] Pearson D. G. et al. (1995) *EPSL, 134,* 341–357. [6] Cornell D. H. et al. (1986) *S. Afr. J. Geol., 89,* 17–28.

A NOVEL REACTOR TO DETERMINE THE RATE OF PYRITE OXIDATION IN AIR.

J. K. Jerz and J. D. Rimstidt, Virginia Polytechnic Institute and State University, 4044 Derring Hall, Blacksburg VA 24061, USA (jejerz@vt.edu; jdr02@vt.edu).

Introduction: Pyrite exposed by mining operations oxidizes to create acidic solutions by the multistep, multipath reaction that can be summarized as follows:

$$FeS_2 + 7/2\ O_2 + H_2O \rightarrow Fe^{3+} + 2\ SO_4^{2-} + 2\ H^+ \qquad (1)$$

The acid and metals released by this process have severe implications for the environment and aquatic life. U.S. Water Reports estimated the cost of dealing with this pollution at $71 billion [1]. In order to effectively control AMD, the reaction-path that generates acid most quickly must be identified. To this end, researchers have studied extensively the oxidation of pyrite in aqueous solution. However, much pyrite is contained in above ground waste piles and is not submerged in water. Our initial data indicate that pyrite oxidation occurs significantly faster in air than in solution (Fig. 1).

Because it seems that oxidation of pyrite in air is possibly the fastest acid-producing reaction, we are quantifying the rate of pyrite oxidation as a function of O partial pressure (P_{O_2}) and relative humidity (RH). A reactor was built that was capable of determining this rate in a short time interval using a small amount of sample.

Reactor Design: Oxygen was chosen as the rate monitoring parameter of the pyrite oxidation reaction (reaction 1). A reactor system was designed to measure very small amounts of O consumption under conditions of fixed relative humidity (RH), gas composition, and temperature (Fig. 2). The experiment consists of two chambers, one for pyrite and one as a control, linked by a manometer. In both chambers, RH is controlled by the equilibrium between salt solutions and the atmosphere. The temperature of the

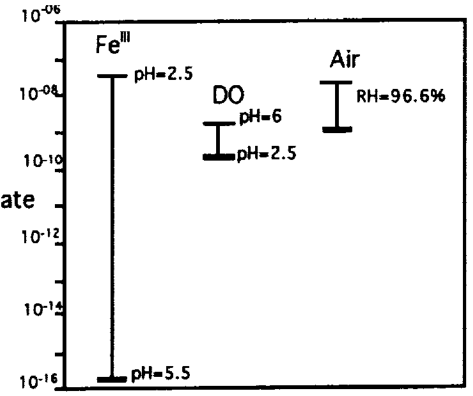

Fig. 1. Relative rates (mol/m^{2}s) of pyrite oxidation. Rates for ferric iron and dissolved O are from Williamson and Rimstidt [2] assuming equilibrium with amorphous iron hydroxide for Fe^{III} and 9 mg/kg O_2 for DO. The air oxidation rates were determined in this study.

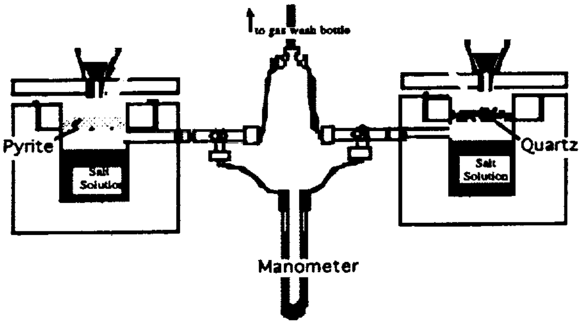

Fig. 2. Differential manometer system used to determine the rate of pyrite oxidation in air.

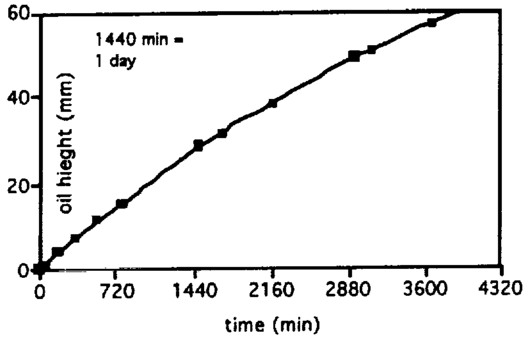

Fig. 3. Data from initial experiments.

system is controlled by a constant temperature bath. The O partial pressure can be varied using O_2-N_2 mixtures. The manometer is filled with a special low-density fluid with a low vapor pressure that can measure as little 0.0000001 mol of O consumption. The control chamber is used as a reference for the pyrite chamber. This allows for the manometer readings to be independent of variations in atmospheric temperature and pressure. Quartz is present in the control chamber to ensure that the internal volumes of the two chambers are equal.

Results: Several experiments have been performed at ~25°C, 96–99% RH, and $P_{O_2} = 0.21$ bar (Fig. 3). The rates of pyrite oxidation calculated from these data using the initial rate method were on the order of 10^{-8} mol(pyrite)/m^{2}s. Additional experiments will be carried out over a range of O_2 partial pressures and relative humidities. The rate of pyrite oxidation rates in air appears to be as fast or faster than aqueous oxidation rates under most conditions (Fig. 1).

References: [1] *US Water News* (Oct. 1993), 10. [2] Williamson M. A. and Rimstidt J. D. (1994) *GCA, 58,* 5443–5454.

ELEMENTAL GEOCHEMISTRY OF DOLOMITITE WEATHERING PROFILE AND ITS IMPLICATION FOR COMPOSITION OF THE UPPER CONTINENTAL CRUST.

H. B. Ji, S. J. Wang, Z. Y. Ouyang, and D. Q. Zhou, The State Key Laboratory of Environmental Geochemistry, Insistute of Geochemistry, Chinese Academy of Sciences, Guiyang 550002, China (hdh@public1.gy.gz.cn).

It has been one of fast developing fields in geochemical researches that sedimentary materials are used to trace the nature of source areas, find the composition of continental crust and study the evolution of the crust. The amount and nature of the information included in sedimentary materials that are derived from chemical weathering is determined, at least in part, by the degree of weathering to which the primary minerals in weathering profile have been subjected [1]. In this article, the Xinpu weathering profile that was developed on the bedrock Cambrian dolomitite and morphologically located in upland in karst terrain in the Northern Guizhou, P. R. China and proved to be *in situ* dolomitite weathering product [2], was selected as research object. Our aim was to make a thorough inquiry of elemental geochemistry behavior and profile evolution feature to soluble rocks in chemical weathering processes, evaluate weathering probably effect on the average upper continental crust and recover the composition of upper continental crust in regional dimensions in karst terrain.

In the A-CN-K and A-CNK-FM triangular plots [3], the soil samples were concentrated in the relatively more weathered region in those two diagrams and between the terminal A and the terminal K in the A-CN-K diagram. It was obvious to divide the dolomitite chemical weathering trend into two stages in these two diagrams: the first stage for dolomitite dissolution residue accumulation to form soil and the second stage for chemical weathering of the residuum, which is similar to the weathering process of the other rocks. From the lower to upper part of the Xinpu profile the chemical index of alteration (CIA) values of the soil samples increased from 57 to 92, indicating positive weathering succession of the profile.

Element mobility in the Xinpu weathering profile was characterized by the mass-transfer coefficient τ_j, which was computed from the mass ratio in terms of a conservative component Al_2O_3 [4]. Sodium, Ca, and Mg were totally depleted at the soil-bedrock interface. Approximately 10% of Ti, Mn, and Fe^{2+}, and 30% of Si and K were retained in residual soil. The contents of Fe^{3+} and P increased in the upper and the intermediate zone. Concentrations of trace elements for samples were also normalized to Al_2O_3 to evaluate the loss or gain during the weathering processes. Compared to the parent rock, the concentrations of three groups of trace elements for soil samples decreased in the order of Y, Rb, Ba, Ga, Th, and U, V, Zn, Co, Sr, Pb, and Hf, Zr, Nb, Ta at least. However, the contents of Li, Cs increased and those of Ni, Cr, Mo, W, and Ti were unchanged in soil. Elemental losses and gains in the residual soil were not essentially constant and varied with depth of the profile, indicating that the chemical weathering occurred not only at the rock-soil interface, but also during the evolution of residual soil in the profile. The geochemical behavior of rare earth elements (REEs) in dolomitite weathering profile was similar to those observed in weathering profiles of the other rocks, such as granodiorite and sediments. There existed REEs fractionation with at least change in Ce and the largest change in Gd for samples during chemical weathering process. Two REE and other elements (e.g., P, Hf, Zr, Nb, Ta)-rich beds had also been observed in the research profile, and were postulated to come from the environmental changes in the evolution of the profile.

Based on the above results, the concentration of trace elements in the uppermost part and the lowermost part of the profile that had undergone strong chemical weathering are suggested to represent mobile elements and immobile elements of the composition of upper continental crust in karst area respectively. The acid-insoluble residuum in the carbonate rocks, like loess and glacial clay deposits, could be considered as the average chemical composition of upper continental crust in karst area.

References: [1] Nesbitt H. W. and Markovics G. (1997) *GCA, 61,* 1653–1670. [2] Wang S. J. et al., this volume. [3] Nesbitt H. W. and Young G. M. (1989) *J. Geol., 97,* 129–147. [4] White A. F. (1995) *Rev. Mineral., 31,* 407–461.

ISOTOPIC SIGNATURES ACROSS THE FRASNIAN-FAMENNIAN BOUNDARY: EVIDENCE FOR ENHANCED PRODUCTIVITY, WATER COLUMN ANOXIA, AND VARIATIONS IN SEAWATER TEMPERATURE.

M. M. Joachimski, Institute of Geology, University of Erlangen, Schlossgarten 5, 91054 Erlangen, Germany (joachimski@geol.uni-erlangen.de).

Introduction: The Late Devonian extinction event represents one of the "Big Five" mass extinctions in Earth history. The biotic event records severe changes at various trophic levels. Most important, the low-latitude stromatoporoid-coral reef ecosystem vanished during the late Frasnian. The causes of the mass extinction are discussed controversially. A bolide impact was proposed [1] as the ultimate cause. However, no compelling geochemical evidence for a cometary strike was presented up to today. The data presented in this paper argue for Earth-derived causes of the mass extinction.

Results: The investigation of the trace-element and organic geochemistry of a basinal Frasnian-Famennian boundary section at Kowala (Holy Cross Mountains/Poland) shows that the lower water column was O-deficient during Late Frasnian and Early Famennian times. The abundance and C-isotopic composition of isorenieratane, a biomarker indicative for green S bacteria, proves that euxinic waters reached into the photic zone, at least episodically. TOC contents show a maximum that is time-equivalent to the Upper Kellwasser horizon that marks the Frasnian-Famennian boundary. Enhanced TOC concentrations in the basinal Kowala section are explained by a higher primary productivity presumably as consequence of an enhanced nutrient supply from the continent. This interpretation is supported by a concomitant increase in the $^{87}Sr/^{86}Sr$ ratio measured on well-preserved brachiopod calcite [2]. The enhanced burial of ^{12}C-enriched organic C is indicated by a 3‰ excursion measured for TOC as well as for individual n-alkanes and isoprenoids. $\delta^{13}C$ of total organic C and individual biomarkers representative for primary organic C parallel the global $\delta^{13}C$ record of inorganic C [3]. The positive excursions in $\delta^{13}C_{carb}$ and $\delta^{13}C_{org}$ are explained by a 10% increase in the organic C burial fraction on total C burial. The burial of large amounts of organic C is expected to result in a decrease in pCO_2, in climatic changes and variations in sea-surface temperature. Indeed, preliminary high-resolution $\delta^{18}O$ data on condont and fish teeth apatite suggest variations in sea-surface temperature across the Frasnian-Famennian boundary. In addition, a decrease in pCO_2 is expected to affect the photosynthetic C-isotopic fractionation (ε_p). The fact that the $\delta^{13}C$ records of biomarkers representative for primary producers and of inorganic C parallel each other suggests that ε_p was most probably at maximum values as a consequence of high atmospheric and oceanic-dissolved CO_2 concentrations during the Devonian.

The S-isotopic composition of pyritic and organically-bound S show a 27‰ excursion across the boundary. The significant positive $\delta^{34}S_{pyrite}$ excursion may be interpreted either as a regional signal due to an enhanced sulfate reduction rate as a consequence of a higher supply of metabolizable organic C or as a global signal. In the latter case, seawater sulfate $\delta^{34}S$ is expected to increase parallel to the observed shift in $\delta^{34}S_{pyrite}$. A 25‰ excursion in $\delta^{34}S_{sulfate}$ of barite [4] measured in sediments from the Selwyn Basin (Yukon/Canada) was assumed to be of middle Frasnian age. But, since biostratigraphic control in the nonbioturbated euxinic sediments is poor [5], it is not certain whether the excursion in $\delta^{34}S_{sulfate}$ is or is not time-equivalent to the Late Frasnian pyrite $\delta^{34}S$ excursion.

Conclusions: Carbon-, O-, and S-isotopic signatures show prominent changes across the Frasnian-Famennian boundary. These variations are interpreted to point to severe changes in the global C cycle, in the climatic conditions as well as in the oceanic ventilation and circulation pattern. It is assumed that the subtropical to tropical shallow-water ecosystem suffered dramatically from these changes.

References: [1] McLaren D. (1970) *J. Paleontol., 48,* 801–805. [2] Veizer J. et al (1997) *Palaeogeogr., Palaeoclimatol., Palaeoecol., 132,* 65–77. [3] Joachimski M. M. and Buggisch W. (1993) *Geology, 21,* 675–678. [4] Goodfellow W. and Jonasson I. R. (1984) *Geology, 12,* 583–586. [5] Geldsetzer H. J. et al. (1987) *Geology, 15,* 393–396.

LATE QUATERNARY PALEOENVIRONMENTS AND THE EXTINCTION OF THE AUSTRALIAN MEGAFAUNA.

B. J. Johnson[1], G. H. Miller[2], M. L. Fogel[3], and J. W. Magee[4], [1]School of Oceanography, University Washington, Seattle WA 98195-7940, USA (bjohnson@ocean.washington.edu), [2]INSTAAR, University of Colorado, Boulder CO 80309-0450, USA, [3]Geophysical Laboratory, Carnegie Institution of Washington, 5251 Broad Branch Road NW, Washington DC 20015-1305, USA, [4]Department of Geology, Australian National University, Canberra ACT 0200, Australia.

Approximately 85% of Australia's large land animals went extinct in the late Quaternary [1]. *Genyornis newtoni,* a large flightless bird and element of the Australian megafauna disappeared from the Australian interior ~50 ka ago, during a period of moderate climate change [2] and roughly coincident with the arrival of the first human immigrants ~60 ka ago [3].

We use stable C isotopes ($\delta^{13}C$) in fossil eggshell carbonate laid by the extinct *Genyornis newtoni* and the extant *Dromaius novaehollandiae* (emu) from Lake Eyre, South Australia, to better understand the paleoecology and dietary preferences of both birds. Between 50 and 65 ka, *Genyornis* was primarily a C_3 feeder, and relied heavily on the presence of C_3 trees and shrubs, whereas *Dromaius* had a much broader dietary range including a significant component of C_4 grasses. We speculate that after 60 ka, a decrease in shrub and tree cover resulted from an increase in fire frequency brought about by the arrival of the first human immigrants, and contributed to the ultimate demise of *Genyornis* [3].

The $\delta^{13}C$ of *Dromaius* eggshell provides the first continuous paleovegetation record from the Australian interior that extends through the last 65 ka [4]. Because the Australian monsoon controls summer precipitation over Lake Eyre, changes in the relative abundance of C_4 grasses serves as an indirect proxy for the effectiveness of the Australian monsoon. The monsoon was most effective when C_4 grass abundance was highest (between 45 and 65 ka), and least effective when C_4 grass abundance was lowest (between 15 and 28 ka). The Holocene had intermediate levels of C_4 grasses, and a moderately effective summer monsoon.

Our isotopic results are consistent with a human overprint on natural climate change. The effectiveness of the summer monsoon at Lake Eyre decreased significantly at approximately the same time as the megafauna extinction and never fully recovered despite an invigorated planetary monsoon during the early Holocene [5]. Furthermore, a change in vegetation type across northern Australia may have reduced the southward penetration of the Australian monsoon by decreasing the amount of moisture transfer to the atmosphere. Continued investigations of vegetation and fire histories are currently under way.

References: [1] Flannery T. (1994) *The Future Eaters,* Reed Books, Melbourne. [2] Miller G. H. et al. (1999) *Science, 283,* 205. [3] Roberts R. G. et al. (1994) *Quat. Geochronol., 13,* 575. [4] Johnson B. J. et al. (1999) *Science,* in press. [5] Xiao J. L. et al. (1999) *Quat. Sci. Rev., 18,* 147.

FATE OF CYANIDE USED IN PROCESSING OF GOLD ORES: NEW EVIDENCE FROM ISOTOPIC MEASUREMENTS.

C. A. Johnson[1], D. J. Grimes[2], and R. O. Rye[1], [1]Mail Stop 963, U.S. Geological Survey, Box 25046, Denver CO 80225, USA, [2]Mail Stop 973, U.S. Geological Survey, Box 25046, Denver CO 80225, USA.

Introduction: Solutions of cyanide (CN^-) are used at mines worldwide to recover gold from ores. Consumption of cyanide can be considerable; the estimate for ore processing operations within Nevada alone is 64,000 metric tons CN^-/yr. Cyanide releases during or after mining are an environmental concern because of the documented toxicity of cyanide to wildlife. Here we describe the processes controlling cyanide degradation, loss, or persistence at active and inactive mineral processing operations in the southwestern U.S. The ultimate objective of the work is to provide a complete mass-balance accounting for cyanide at representative operations. New in our work is the application of stable isotopic ($^{15}N/^{14}N$, $^{13}C/^{12}C$) tools [1].

Results of Case Studies and Experiments: In active heap leach circuits, cyanide can be lost from process solutions via three general pathways [2]: (1) offgassing of HCN to the atmosphere; (2) microbial or abiotic oxidation to form dissolved inorganic C and N species; and (3) retention in the ore heaps as precipitated, coprecipitated, or adsorbed species. In case studies at three circuits in Nevada [3], we have found that cyanide in barren process solutions contains C that is isotopically very light (–51‰ to –33‰ relative to PDB) and N that is slightly light (–5‰ to –2‰ relative to air). The isotopic compositions reflect the compositions of the natural gas and air N_2 that are commonly used in the manufacturing process. After passage of the solutions through ore heaps the cyanide can show decreases of up to 4‰ in $\delta^{13}C$ and up to 7‰ in $\delta^{15}N$. Isotopic shifts are greatest in solutions that are most depleted in cyanide. The decrease in δ-values of dissolved cyanide resembles the behavior found in laboratory experiments where cyanide was precipitated as a cyanometallic compound, but is the reverse of the kinetically controlled behavior found in experiments where HCN was offgassed. The isotopic data suggest that significant amounts of cyanide may be retained in the heaps as precipitates, and that offgassing may be less important than has been proposed by other workers [e.g., 2].

Isotopic analyses of dissolved nitrate, nitrite, and ammonium at active operations show $\delta^{15}N$ values of 1–15‰, systematically higher than the negative $\delta^{15}N$ values found for cyanide. The highest values (13–15‰) are found where process solutions are stored in ponds. Such large ^{15}N enrichments are strong evidence that $\delta^{15}N$ of noncyanide N species is affected by bacterially-mediated denitrification reactions. Total oxidized C was extracted from pond samples (the method used recovers C from CO_3^{2-}, HCO_3^-, H_2CO_3, and CNO^-) and was found to have low, cyanide-like $\delta^{13}C$ values. This indicates that significant amounts of cyanide are destroyed by oxidation. It is clear that process solution nitrate is produced by cyanide oxidation, but the degree to which other nitrate sources are important (e.g., explosive residues) is difficult to determine from isotopic or chemical data.

Where we have studied spent ore heaps that are being rinsed to lower their final cyanide content, or groundwaters that have been contaminated by process solutions leaks, cyanide mobility is controlled by strong Co and Fe cyanocomplexes. The strong complexes are known to break down when solutions are exposed to UV light or sunlight. However, whether they are susceptible to microbial or abiotic oxidation, or to retention as solids in the subsurface, are questions that need further investigation. Isotopic analyses of nitrate N and bicarbonate C give no obvious indication of cyanocomplex oxidation, but the large isotopic effects of nitrate denitrification and microbial respiration, and the lack of information on isotopic fractionation during cyanide oxidation, preclude a firm conclusion.

Conclusions: At active heap leach circuits studied to date, stable isotopic data provide evidence of cyanide loss by retention as solids within the ore heaps, and by oxidation. Cyanide offgassing must also occur at these operations, but it does not appear to be the dominant cyanide loss mechanism. Thus the flux of cyanide gas to the atmosphere from mineral processing operations is substantially lower than the total cyanide consumption. On the other hand, spent ore heaps may be larger cyanide reservoirs than previously thought. The chemical form and mobility of retained cyanide are in need of further investigation.

References: [1] Johnson C. A. (1996) *Anal. Chem., 68,* 1429–1431. [2] Smith A. and Mudder T. (1991) *The Chemistry and Treatment of Cyanidation Wastes,* Mining Journal Books Ltd., London, 345 pp. [3] Johnson C. A. et al. (1998) *U.S. Geological Survey Open-File Rept., 98-753,* 7 pp.

DEVELOPMENT OF SELENIUM STABLE ISOTOPES FOR ENVIRONMENTAL APPLICATIONS.

T. M. Johnson[1], M. J. Herbel[1,2], and T. D. Bullen[2], [1]Mail Code 102, Geology Department, University of Illinois, Urbana IL 61820, USA (tmjohnsn@uiuc.edu), [2]Mail Stop 420, Water Resources Division, U.S. Geological Survey, 345 Middlefield Road, Menlo Park CA 94025, USA.

Selenium in the Environment: Selenium is potentially toxic to wildlife at levels as low as 3 μg/L in water. This problem is compounded by agricultural mobilization of selenate from seleniferous soils developed on black shales, and Se accumulation in wetlands of the western U.S. that are critical to migration and reproduction of birds and waterfowl. Fly ash and other coal combustion byproducts, mining waste and backfill materials, and industrial wastewater also contain potentially harmful levels of Se. The complexity of Se biogeochemistry complicates predictions of Se transport and bioavailability. Selenate, ($SeO_4^=$), is soluble and mobile. Selenite, ($SeO_3^=$), is soluble but prone to sorption. Elemental Se, Se^0, is readily precipitated, immobile, and resistant to reoxidation. Selenide is reactive and often found in soluble or volatile organic compounds. It is common for selenate to be removed from solution by reduction to elemental Se, a process which is probably mediated by microbes. Nitrogen and S isotopes are useful indicators of denitrification, sulfate reduction, and sulfate/nitrate sources; Se isotopes should be similarly useful as indicators of selenate and selenite reduction, and Se sources.

TABLE 1. Selenium-isotopic fractionation (as $^{80}Se/^{76}Se$).

Study	Reaction	e* (‰)
[4]	$SeO_4^=$ to $SeO_3^=$ abiotic	–12
This study	$SeO_4^=$ to $SeO_3^=$ bacteria	–0.9 to –4.5
[1,3–5]	$SeO_3^=$ to Se^0 abiotic	–7 to –13
[2]	$SeO_3^=$ to Se^0 Microbes	–3 to –27
This study	$SeO_3^=$ to Se^0 bacteria	–7.3 to –8.2
This study	Soil-Se oxidation	<0.5
This study	$SeO_3^=$ adsorption	<0.5
This study	Se volatilization by algae	<1.1
This study	Se volatilization by soil microbes	<0.6

*Some values are converted to $^{80}Se/^{76}Se$ from $^{82}Se/^{76}Se$.

Selenium Isotope Measurements: Several studies, starting with work by Krouse and Thode in 1962 [1–5], showed that selenate and selenite reduction induced isotopic fractionation of up to 40‰ in $^{82}Se/^{76}Se$. The SeF_6 gas-source technique used in these studies required large quantities of Se, and thus analysis of all but the most contaminated waters and sediments was extremely difficult. Negative thermal ion mass spectrometry (NTIMS) methods developed by K. Heumann's group [6] brought the sample requirement down to submicrogram levels, but precision suffered from uncontrollable discrimination during heating of the unavoidably volatile Se. We developed a double-spike NTIMS technique (spike ^{74}Se and ^{82}Se, measure $^{80}Se/^{76}Se$) that corrects for fractionation during sample preparation and mass spectrometry, yielding an overall reproducibility of ±0.2‰. A major advantage of this approach is the ability to use reductive H_2Se generation, which is well developed for Se concentration analyses, as a purification method.

Selenium-isotopic Fractionation: We have conducted several laboratory experiments to measure Se-isotopic fractionation during biogeochemical transformations. The results, combined with those from earlier studies, provide a nearly complete reconnaissance of Se-isotopic systematics (Table 1). Selenate and selenite reduction, both microbial and abiotic, are the major isotopic fractionating mechanisms, whereas other transformations cause little or no isotopic fractionation. The microbial fractionations are variable, because of metabolic effects, as is observed with sulfate and nitrate reduction. In summary, Se-isotopic fractionation should be a good indicator of selenate and selenite reduction in environmental studies, but the laboratory results do not predict the size of the fractionation in a given natural setting.

Field Studies: Reconnaissance field studies are in progress. Samples from the San Francisco estuary, California, showed little contrast between elemental Se in sediments and the estuary waters; this corroborates independent evidence that Se is transported into the mud flats and marshes as particulate, and selenate/selenite reduction is a less important process in these relatively oxidized sediments. However, further research into Se-isotopic fractionations in natural settings is necessary to support such studies.

References: [1] Krouse and Thode (1962) *Can. J. Chem., 40,* 367–375. [2] Rashid et al. (1978) in *Short Papers of the Fourth International Conference, Geochronology, Cosmochronology, Isotope Geology* (Zartman, ed.), USGS Open-File Rept. 78-701. [3] Rashid and Krouse (1985) *Can. J. Chem., 63,* 3195–3199. [4] Rees and Thode (1966) *Can. J. Chem., 44,* 419–427. [5] Webster (1972) Ph.D. dissertation, Colorado State Univ. [6] Wachsmann and Heumann (1992) *Int. J. Mass Spectrom. Ion Proc., 114,* 209–220.

COMPARATIVE MAGMA OCEANOGRAPHY.

J. H. Jones, Mail Code SN2, NASA Johnson Space Center, Houston TX 77058, USA (jjones2@ems.jsc.nasa.gov).

The question of whether the Earth ever passed through a magma ocean stage is of considerable interest. Geochemical evidence strongly suggests that the Moon had a magma ocean and the evidence is mounting that the same was true for Mars. Analyses of martian (SNC) meteorites have yielded insights into the differentiation history of Mars, and consequently, it is interesting to compare that planet to the Earth. Three primary features of Mars contrast strongly to those of the Earth: (1) the extremely ancient ages of the martian core, mantle, and crust (~4.55 Ga); (2) the highly depleted nature of the martian mantle; and (3) the extreme ranges of Nd-isotopic compositions that arise within the crust and depleted mantle.

The easiest way to explain the ages and diverse isotopic compositions of martian basalts is to postulate that Mars had an early magma ocean. Cumulates of this magma ocean were later remelted to form the SNC meteorite suite and some of these melts assimilated crustal materials enriched in incompatible elements. The REE pattern of the crust assimilated by these SNC magmas was LREE enriched. If this pattern is typical of the crust as a whole, the martian crust is probably similar in composition to melts generated by small degrees of partial melting (~5%) of a primitive source. Higher degrees of partial melting would cause the crustal LREE pattern to be essentially flat. In the context of a magma ocean model, where large degrees of partial melting presumably prevailed, the crust would have to be dominated by late-stage, LREE-enriched residual liquids. Regardless of the exact physical setting, Nd- and W-isotopic evidence indicates that martian geochemical reservoirs must have formed early and that they have not been efficiently remixed since. The important point is that in both the Moon and Mars we see evidence of a magma ocean phase and that we recognize it as such.

Several lines of theoretical inference point to an early Earth that was also hot and, perhaps, mostly molten. The giant impact hypothesis for the origin of the Moon offers a tremendous input of thermal energy and the same could be true for core formation. And current solar system models favor the formation of a limited number of large (~1000 km) planetesimals that, upon accreting to Earth, would cause great heating, being lesser versions of the Giant Impact.

Several lines of geochemical evidence do not favor this hot early Earth scenario: (1) Terrestrial mantle xenoliths are sometimes nearly chondritic in their major element compositions, suggesting that these rocks have never been much molten. Large degrees of partial melting probably promote differentiation rather than homogenization. (2) Unlike the case of Mars, the continental crust probably did not form as a highly fractionated residual liquid from a magma ocean (~99% crystallization), but, rather, formed in multiple steps. [The simplest model for the formation of continental crust is complicated: (1) ~10% melting of a primitive mantle, making basalt; (2) hydrothermal alteration of that basalt, converting it to greenstone; and (3) 10% partial melting of that greenstone, producing tonalite.] This model is reinforced by the recent observation from old (~4.1 Ga) zircons that the early crust formed from an undepleted mantle having a chondritic Lu/Hf ratio. (3) If the mantle were once differentiated by a magma ocean, the mantle xenolith suite requires that it subsequently be homogenized. The Os-isotopic compositions of fertile spinel lherzolites place constraints on the timing of that homogenization. The Os-isotopic composition of spinel lherzolites approaches that of chondrites and correlates with elements such as Lu and Al. As Lu and Al concentrations approach those of the primitive mantle, Os-isotopic compositions approach chondritic. The Re and Os in these xenoliths were probably added as a late veneer. Thus, the mantle that received the late veneer must have been nearly chondritic in terms of its major elements (excluding Fe). If the mantle that the veneer was mixed into was not already homogenized, then Os isotopes should not correlate with incompatible elements such as Al. Consequently, either early differentiation of the mantle did not occur or the homogenization of this differentiation must have occurred before the late veneer was added. The timing of the late veneer is itself uncertain but presumably postdated core formation at ~4.45 Ga and did not postdate the 3.8–3.9-Ga late bombardment of the Moon. This timing based on siderophile elements is consistent with the Hf-isotopic evidence cited above.

If the Earth, Moon, and Mars had magma oceans, the Earth subsequently rehomogenized whereas the Moon and Mars did not. The simplest solution to this observation is that homogenization of igneous differentiates was never necessary on Earth, either because the hypothetical magma ocean never occurred or because this event did not produce mantle differentiation.

THE EARLIEST KNOWN OCCURRENCES OF CHARCOAL IN THE FOSSIL RECORD.

T. P. Jones[1] and N. P. Rowe[2], [1]School of Biosciences, Cardiff University, Museum Avenue, Cardiff, CF1 3US, Wales, UK (jonestp@cardiff.ac.uk), [2]Laboratoire de Paleobotanique, Place E. Bataillion, Université de Montpellier II, 34059 Montpellier, France (rowe@isem.univ-montp2.fr).

Introduction: There is an established fossil charcoal record, from the Lower Carboniferous to the present. Pre-Carboniferous "charcoal-like" plant fossils exist, but their modes of preservation are problematic and subject to debate. In the literature there are "anecdotal" references to Devonian charcoal; but it has never been satisfactorily demonstrated. It is important to distinguish between charcoal, the end product of a process, i.e., fire; and fusain, a fossil material defined by physicochemical characteristics. A fossil record of charcoal has important implications for limiting atmospheric O levels, palaeoenvironmental reconstructions, plant evolution, and long- and short-term global C budgeting. Fossil charcoal is recognized by: plant three-dimensional anatomical preservation, black color, silky or fibrous texture, friable nature, the homogenization of previously-stratified plant cell walls, and its general appearance — overall similarity in size and shape to modern charcoal.

Problematic Pre-Carboniferous "Charcoal": *Prototaxites* a "plant" fossil of uncertain affinity is preserved as "fusain," and is possibly the world's oldest charcoal [1–3]. Plant fragments have been found in Devonian gneiss, but the metamorphic conditions have eradicated any clues to the fossil's

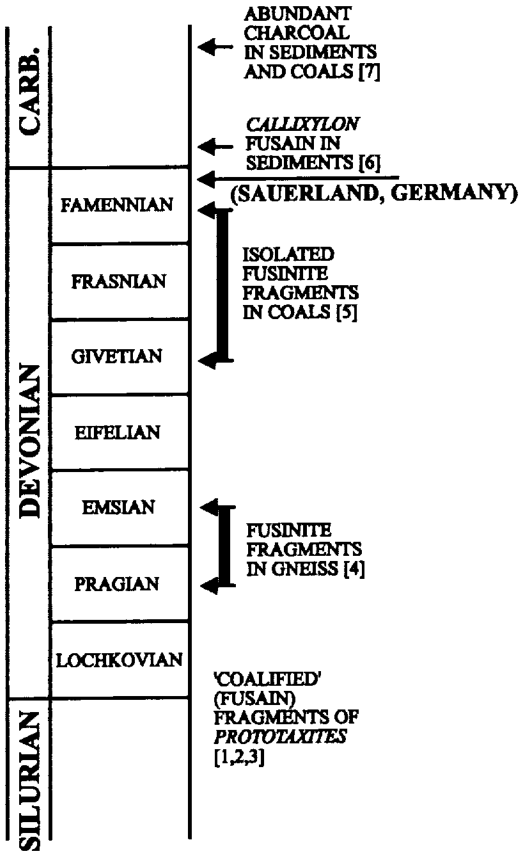
CARB.
DEVONIAN
SILURIAN
FAMENNIAN
FRASNIAN
GIVETIAN
EIFELIAN
EMSIAN
PRAGIAN
LOCHKOVIAN
ABUNDANT CHARCOAL IN SEDIMENTS AND COALS [7]
CALLIXYLON FUSAIN IN SEDIMENTS [6]
(SAUERLAND, GERMANY)
ISOLATED FUSINITE FRAGMENTS IN COALS [5]
FUSINITE FRAGMENTS IN GNEISS [4]
'COALIFIED' (FUSAIN) FRAGMENTS OF *PROTOTAXITES* [1,2,3]

Fig. 1. The earliest record of charcoal.

taphonomy [4]. Fusinite has been recorded in Devonian coals, however, in small amounts, and off unknown taphonomy [5]. Fusain has been recovered from Mississippian clastic sediments, but a non-fire microbial taphonomy has been proposed [6]. Fossils confidently identified as charcoal are abundant from the late Tournasian onwards, with an extensive literature from 1847 [7] to the present day [8].

Devonian Charcoal: Charcoal has been recovered from sediments in Sauerland in Central Germany, a couple of meters below the D-C boundary, in the LN miospore zone, at the very top of the Famennian. This section is famous for containing early winged seed fossils [9]. The fossils were macerated from sediments by HCl and HF, followed by HNO_3 to remove any non-inert organic component. Under a scanning electron microscope (SEM) can be seen exceptional three-dimensional preservation of very delicate anatomical features. Furthermore the cell walls are homogenized. The charcoal is found in association with coalified and petrified plants; thus, clearly there were two distinct and very different mechanisms of plant preservation. Not enough material was available to undertake reflected light studies. Despite the latter, it meets all other requirements to be confidently identified as the earliest unambiguous fossil charcoal; the end product of an ancient wildfire.

References: [1] Robinson J. M. et al. (1997) *NATO ASI Series 1, 51,* 253–270. [2] Edwards D. et al. (1995) *Bot. J. Lin. Soc., 117,* 233–254. [3] Cope M. J. (1984) Ph.D. thesis, University of London, UK. [4] Pflug H. D. and Prössel K. F. (1991) *Scientific Drilling, 2,* 13–33. [5] Goodarzi F. et al. (1989) *Cont. Can. Coal Geosci.,* 120–130. [6] Beck C. B. et al. (1982) *Am. J. Bot., 69,* 54–76. [7] Lyell C. (1847) *Quart. J. Geol. Soc., 47,* 261–280. [8] Jones T. P. and Rowe N. P. (1999) *Fossil Plants and Spores: Modern Techniques,* Geological Society of London. [9] Rowe N. P. (1997) *Palaeontology, 40,* 575–595.

THE ROLE OF LOWER CRUSTAL DELAMINATION IN THE GENESIS OF CONTINENTAL CRUST.

M. Jull and P. B. Kelemen, Woods Hole Oceanographic Institution, Woods Hole MA 02543, USA (jull@whoi.edu; pkelemen@whoi.edu).

The average composition of the upper, lower, and bulk continental crust lies along a calc-alkaline magmatic trend and can be characterized as high Mg# andesite (i.e., wt% Mg# >0.3 and <10 wt% MgO; see [1] and references therein). High Mg# andesite (HMA) lavas with compositions similar to the continental crust are found in many contemporary arcs, suggesting that continental crust formed as a result of arc magmatism [e.g., 2]. Despite decades of effort, melting experiments have not confirmed the hypothesis that HMA is produced from a fractionated basaltic parent magma. However, mixing of the endmember compositions from a fractionation trend (e.g., "basalt" and "granite") can produce the HMA composition of the bulk crust [1].

For a mixing mechanism to generate continental crust, some process is required to remove the cumulates and residues formed during generation of the highly silicic "granitic" end member. Kay and Kay [3] proposed that mafic lower crust, if it is thickened sufficiently, will convert to high-density mineral assemblages, leading to a gravitationally unstable configuration in which the lower crust can delaminate and sink into the lower density mantle. Similarly, Arndt and Goldstein [4] pointed out that ultramafic cumulates are always denser than residual upper mantle peridotites, and proposed that they may undergo delamination.

We consider the possibility of lower crustal delamination as a means by which to remove a mafic and ultramafic residue generated in the process of HMA formation. Though there is an extensive body of work on delamination [e.g., 5], most of this has focused on the density instability generated by the conductive cooling of the mantle lithosphere. Controversy exists as to whether the density inversion created by conductive cooling of the lithosphere is counter balanced by the positive compositional buoyancy of the lithosphere by the extraction of melt (the isopycnic hypothesis of Jordan [6]).

In any case, high-density phase transformations of a mafic to ultramafic lower crust are likely to create density inversions that can drive lower crustal delamination events. However, high-mantle viscosity at low temperatures may impede this process,

In this study, delamination of the lower crust is evaluated using a finite element model developed by Houseman and Molnar [5], which allows us to calculate growth rates for finite deformation of gravitationally unstable (i.e., Rayleigh Taylor instability) layered configurations. We consider a range of rheologies and density structures to represent the lower crust and underlying mantle. Rheologies for the lower crust are assumed to be that of clinopyroxenite and jadeite, while that of the upper mantle and lithosphere is assumed to be dry olivine.

Results of the modeling show that high temperatures are necessary for delamination to occur on geologically significant timescales. Using a range of lower crustal and lithospheric mantle bulk compositions, ranging from ultramafic cumulates to basaltic compositions, we calculated the subsolidus phase assemblage and resulting density using the programs of Asimow and Ghiorso [7] and Connolly [8]. These calculations allowed us to determine the density of the lower crust as a function of temperature and pressure and to calculate the growth rates of instabilities under a variety of conditions. The results show that lower crustal delamination is a viable mechanism for the removal of mafic and ultramafic layers from the lower crust on geologically relevant time scales. Specifically, no geologically likely density contrast can go unstable in less than 100 m.y. if the mantle temperature is less than ~900°C. Thus, delamination is highly improbable within stable cratons and during continent-continent collisions.

While negative buoyancy of basaltic and gabbroic compositions requires growth of garnet, and is thus pressure dependent and kinetically unfavorable during slow cooling under H_2O-free conditions, negative buoyancy of ultramafic cumulates is due mainly to composition, and not phase transformations. Formation of ultramafic cumulates at the base of the crust creates a dense layer, which is always unstable and likely to delaminate in <10 m.y. at virtually any pressure, provided the underlying mantle temperature is >~1000°C.

References: [1] Kelemen P. B. (1995) *Contrib. Mineral. Petrol., 120,* 1–19. [2] Taylor S. R. (1985) *Tectonophys., 4,* 17–34. [3] Kay R. W. and Kay S. M. (1994) *The Geology of North America, Vol. 1,* 687–722. [4] Arndt N. T. and Goldstein S. L. (1987) *Tectonophys., 161,* 201–212. [5] Houseman G. A. and Molnar P. (1997) *Geophys. J. Int., 128,* 125–150. [6] Jordan T. H. (1988) *J. Petrol.,* 11–37. [7] Asimow P. D. and Ghiorso M. S. (1998) *Am. Mineral., 83,* 1127–1132. [8] Connolly J. A. D. (1990) *Am. J. Sci., 290,* 666–718.

MELT GENERATION AND TRANSPORT: CONSTRAINTS FROM THE DEGLACIATION OF ICELAND.

M. Jull[1], D. McKenzie[2], J. Maclennan[2], L. Slater[2], and K. Gronvold[3], [1]Woods Hole Oceanographic Institution, Woods Hole MA 02543, USA, [2]Bullard Laboratories, University of Cambridge, Cambridge CB3 0EZ, UK, [3]Nordic Volcanological Institute, University of Iceland, Reykjavik, Iceland.

The generation and transport of melt through the mantle is the center of much controversy and debate. Constraints from both the chemistry of erupted magmas and physical models of melt transport have led to two endmember theories. One of these considers melt transport as a "dynamic" process in which melt is chemically isolated from the solid matrix and transported to the surface as soon as a critical threshold porosity is attained [1]. The other considers melt transport to be a reactive process in which melt percolates through a porous matrix resulting in chemical exchange, leading to the formation of high-porosity conduits [2]. Both models are constrained by the chemical signature of melt erupted at the surface. In particular, their ability to account for the disequilibrium of U-series elements observed in erupted magmas is cited as one of the key pieces of evidence that validates these models. However, both melting models interpret the U-series disequilibria as the result of different processes. In the dynamic model, U-series disequilibria is generated near the solidus and fast melt transport through conduits or channels is required to maintain the observed disequilibrium. The reactive porous flow model requires that U-series disequilibria is initiated at the solidus and is then maintained by chromatographic effects as melt migrates via porous flow through a melt column in which there is continuous chemical interaction with the surrounding matrix [3].

Despite the ability of both these models to explain the U-series disequilibria, there are some problems. For example, the reactive porous flow model requires that U-series disequilibria be initiated at the solidus and then maintained by chromatographic melt flow. This theory is challenged by observations from Hawai'i that show that elements with different compatibilities have strong temporal correlations [4,5], indicating that chromatographic separation of elements has had little effect on the melt as it has migrated through the mantle. Though such observations have yet to be made at mid ocean ridges, where melting extends over a greater depth range than that of Hawai'i, the results from Hawai'i raise some questions of doubt. Dynamic melt transport, on the other hand, is challenged by an apparently negative correlation between ($^{226}Ra/^{230}Th$) and ($^{230}Th/^{238}U$) observed at mid-ocean ridges [2]. If excesses of both ^{226}Ra and ^{230}Th are produced at the solidus, as proposed in the dynamic model, it is unclear why the observed excesses appear to be negatively correlated.

Since both melt transport models can, to a certain extent, account for the observed U-series disequilibria, other independent criteria are needed to constrain mantle melting and transport through the mantle. One such constraint is provided by the deglaciation of Iceland. In response to the rapid unloading of ice ~11 ka, melt production in Iceland increased by a factor of 20–30 and trace-element concentrations decreased in response to enhanced decompression melting [6–9]. This perturbation to the melting state of the mantle gives us an opportunity to observe changes in melt chemistry and volume as the melting region departs from steady state. The timing between deglaciation and the surge in postglacial magmatic activity gives an independent constraint on melt transport, with a rate of ~50 m/yr, and is consistent with the dynamic melting model, where ^{226}Ra excesses are generated near the solidus.

The change in composition of melt in response to deglaciation also allows us to constrain the melt distribution in the mantle. Inverse modeling of REE concentrations to calculate melt distributions in the mantle [10] have been criticized for the implicit *a priori* assumption of a starting source composition. The change in chemistry from deglaciation allows us to avoid this assumption because it provides an opportunity to invert for the melt distribution by comparing the change in chemistry between glacial and postglacial magmas. Our results show that the melt distribution calculated from the inversion of REE concentrations of glacial and postglacial magmas has a productivity that continuously increases with decreasing depth, which is consistent with the results of recent thermodynamic calculations [11].

References: [1] McKenzie D. (1985) *EPSL, 72,* 149–157. [2] Kelemen P. B. et al. (1997) *Phil. Trans. R. Soc. Lond., 355,* 283–318. [3] Spiegelman M. and Elliot T. (1993) *EPSL, 118,* 1–20. [4] Cohen A. S. et al. (1996) *EPSL, 143,* 111–124. [5] Hauri E. H. et al. (1996) *JGR, 101,* 11793–11806. [6] Hardarson and Fitton (1991) *Nature, 353,* 62–64. [7] Jull M. and McKenzie D. (1996) *JGR, 101,* 21815–21828. [8] Slater L. et al. (1998) *EPSL, 164,* 151–164. [9] Maclennan J. et al., in preparation. [10] McKenzie D. and O'Nions K. (1991) *J. Petrol., 32,* 1021–1091. [11] Asimow P. et al. (1995) *GCA, 59,* 4489–4506.

THE EFFECT OF HYDROGEN BONDING ON THE STRUCTURE AND PROPERTIES OF AQUEOUS HYDROTHERMAL FLUIDS: COMPUTER SIMULATION STUDIES.

A. G. Kalinichev[1,2], [1]Department of Geology, University of Illinois, Urbana IL 61801, USA (andreyk@hercules.geology.uiuc.edu), [2]Institute of Experimental Mineralogy, Russian Academy of Sciences, Chernogolovka, Moscow Region, 142432, Russia.

Introduction: Accurate thermodynamic modeling of hydrothermal fluids is complicated by the presence of specific H bonding interactions between water molecules. The question of the ranges of temperature and pressure (density) where these specific interactions can significantly influence the observable properties of water is very important for the construction of realistic thermodynamic and structural models of hydrothermal fluids. Several experimental sources suggest that some degree of H bonding persists well into the supercritical region of water [1]. However, such evidences are often indirect and inconclusive. On the other hand, numerous Monte Carlo (MC) and molecular dynamics (MD) computer simulation studies of supercritical water have been performed over the last decade [2]. The advantage of computer "experiments" is in their ability to generate and analyze in detail spatial and energetic environments of every individual molecule or multimolecular configuration, thus providing extremely useful microthermodynamic and microstructural information on the molecular level, not available from any real physical measurement.

Computer Simulations: Monte Carlo and molecular dynamics simulations of water using several realistic intermolecular potential functions were carried out at more then 50 states covering a very wide range of thermodynamic conditions typical for many hydrothermal and metamorphic processes: $273 \leq T \leq 1273$ K; $0.02 \leq \rho \leq 1.67$ g/cm^3; $0.1 \leq P \leq 10000$ MPa [2,3]. Simulated PVT-properties, as well as enthalpy, internal energy, heat capacity, isothermal compressibility, thermal expansion and self-diffusion coefficients agree surprisingly well with available experimental data, if one correctly accounts for some differences in the critical parameters between the models and real water. The simulated structure of supercritical water also agrees well with X-ray and neutron diffraction data, and is consistent with several other computer simulations using inherently different intermolecular potentials. This qualitatively and quantitatively correct behavior of many simulated properties over very wide ranges of thermodynamic conditions allows us to analyze with reasonable confidence the detailed temperature- and density dependencies of local spatial and energetic arrangements of water molecules leading to H bonding.

Hydrogen Bonding under Hydrothermal Conditions: Quantitative analysis of H bonding in supercritical water was performed on the basis of hybrid distance-energy criterion of H bond formation [4]. With increasing temperature, the average number of H bonds per a water molecule, $\langle n_{HB} \rangle$, decreases with the same slope for both liquid-like (~1.0 g/cm^3) as well as vapor-like (~0.2 g/cm^3) supercritical water. This result agrees well with all available estimates based on experimental data from various sources. Over the whole supercritical region, except for the most high-density states, $\langle n_{HB} \rangle$ is always below the percolation threshold (~1.6) indicating that the continuous percolating network of H bonds is broken. Nevertheless, up to 40% of H-bonds present in liquid water at room temperature can still be preserved under supercritical conditions. For a typical hydrothermal thermodynamic state ($T = 673$ K; $P = 80$ MPa; $\rho = 0.66$ g/cm^3), average H bonds are almost 10% weaker energetically, 5% longer, and ~8° more bent, compared to those in normal liquid water.

Clusterization in Supercritical Water: Although the infinite percolating network of H bonds largely breaks apart under hydrothermal conditions, individual water molecules for significant amount of time still remain bonded together in smaller molecular aggregates, or clusters [2]. Quantitative understanding of the size and structure of such clusters is important for many fundamental and practical reasons. For example, large pressure effects on the isotopic fractionation between hydrothermal solutions and minerals can be explained by taking into account the degree of clusterization in water vapor [5].

Present simulation results demonstrate that even low-density hydrothermal fluid (ρ <0.2 g/cm3) can contain relatively large H bonded clusters, consisting of up to 10 water molecules. We observed no significant density dependence of relative abundances for topologically different water clusters, and chain-like clusters are found predominant. In contrast to the results of quantum chemical calculations for isolated water clusters, which identify ring-like clusters as the most stable energetically, such clusters are only rarely formed under hydrothermal conditions [6]. The fraction of pentamers topologically organized as complete tetrahedra is also insignificant under these conditions.

References: [1] Gorbaty Y. E. and Kalinichev A. G. (1995) *J. Phys. Chem., 99,* 5336–5340. [2] Kalinichev A. G. and Bass J. D. (1997) *J. Phys. Chem. A, 101,* 9720–9727. [3] Kalinichev A. G. and Heinzinger K. (1995) *GCA, 59,* 641–650. [4] Kalinichev A. G. and Bass J. D. (1994) *Chem. Phys. Lett., 231,* 301–307. [5] Driesner T. (1997) *Science, 277,* 791–793. [6] Kalinichev A. G. and Churakov S. V. (1999) *Chem. Phys. Lett., 302,* 411–417.

COMPUTER SIMULATIONS OF THE INTERLAYER STRUCTURE AND DYNAMICS OF MIXED-METAL LAYERED HYDROXIDES.

A. G. Kalinichev[1], R. J. Kirkpatrick[1], and R. T. Cygan[2], [1]Department of Geology, University of Illinois at Urbana-Champaign, Urbana IL 61801, USA (kalinich@uiuc.edu), [2]Geochemistry Department, Sandia National Laboratories, Albuquerque NM 87185-0750, USA.

Introduction: Mixed-metal layered hydroxides (MMLHs) are among the few oxide-based materials with permanent anion exchange capacity developed through isomorphous substitution. They occur in many natural environments, are readily synthesized, and are receiving rapidly increasing attention from a wide variety of applications as materials for catalysis, environmental remediation, etc. [1–2]. MMLHs have a layered structure based on that of $Mg(OH)_2$ or $Ca(OH)_2$. Substitution of +3 cations (often Al) for the +2 cations (often Mg or Ca) leads to a permanent positive layer charge. Anions and associated water molecules occur in the interlayer space and on the particle surfaces. The Ca-MMLHs are unique in having an ordered Ca,Al distribution and a highly ordered interlayer space due to coordination of the interlayer H_2O molecules to Ca in the hydroxide layer, resulting in 7-coordinate Ca.

Molecular Dynamics Simulations: We modeled and analyzed the dynamical behavior of the anions and water molecules in the interlayer of MMLHs over a range of temperatures using molecular dynamics (MD) computer simulation technique. A modified consistent valence force field was used to model all ion-ion and ion-water interactions [3]. For water, a flexible version of the "simple point charge" model [4] was employed. The electronic structure of the simulated materials was determined using periodic density functional theory [5]. Mulliken analysis of the electron population was performed in order to estimate partial charges of the atoms.

In MD simulations of layered materials, the atoms in the main oxide layers are often constrained to be immovable. This approach is computationally very effective, but it prevents the momentum exchange between the interlayer/surface species and the rigid lattice. Thus, realistic modeling of the dynamics of H bonding to the surface, adsorption, and surface complexation is limited by the momentum and energy conservation laws. This can result in the overestimation of surface diffusion rates and can influence the calculated structure of the interfacial water layers.

In our MD simulations, all atoms were treated as movable. Moreover, the size and shape of the simulation cell were unconstrained. The isothermal-isobaric simulations were performed for bulk crystals, dehydrated crystals at high temperature, and for the interface of MMLH phases with bulk water.

Interlayer Structure and Dynamics: For the particular case of $[Ca_2Al(OH)_6]Cl \times 2H_2O$ (Friedel's salt) structure, the resulting crystal lattice parameters and density are all reproduced within ~1% of their measured room temperature values [6]. A minimum of the lattice parameter *a* around 0°C is found, which closely corresponds to the phase transition observed for this material in NMR experiments at ~6°C [7].

In contrast to the highly ordered arrangement of interlayer water molecules presumed from the X-ray diffraction measurements [6], MD simulations reveal significant orientational disorder which is preserved even at temperatures as low as –100°C [8]. Nevertheless, each Cl^- ion is still H bonded on average to four interlayer H_2O molecules and additionally coordinated by six OH groups from two adjacent hydroxide layers, thus forming an axially symmetric arrangement. This H bonding environment effectively keeps anions immobile within the structure even at high temperatures.

Power spectra of translational, librational, and vibrational motions of interlayer anions and water molecules were calculated as Fourier transforms of the velocity autocorrelation functions for each species. The spectrum of the interlayer Cl^- and H_2O hindered translations consists of tree distinct frequency bands centered around 50, 90, and 140 cm^{-1}. The 50 cm^{-1} band corresponds to O···O···O flexing motions of the intermolecular H-bonds in bulk liquid water (e.g., [9]).

Strong electrostatic attraction between interlayer water molecules and corresponding Ca atoms in the hydroxide layer results in very low interlayer diffusion rates and makes the Ca···O bond direction the most preferable axis for H_2O librations (hindered rotations). This is in sharp contrast to the molecular librations in bulk liquid water where, on average, four equally strong H bonds acting on every water molecule create almost isotropic librational environment resulting in much broader spectral peaks of these hindered rotations [9]. To some extent, this is also true for H_2O molecules adsorbed on the crystal/water interface.

References: [1] Cavani F. et al. (1991) *Catalysis Today, 11,* 173–301. [2] Ulibarri M. A. et al. (1995) *Appl. Clay Sci., 10,* 131–145. [3] Molecular Simulations Inc. (1998) *Cerius² User Guide.* [4] Berendsen H. J. C. et al. (1981) in *Intermolecular Forces* (Pullman B., ed.), pp. 331–342, Riedel, Dordrecht. [5] Delley B. (1990) *J. Chem. Phys., 92,* 508–517. [6] Terzip A. et al. (1987) *Z. Kristallogr., 181,* 29–34. [7] Kirkpatrick R. J. et al. (1999) *Am. Mineral.,* in press. [8] Kalinichev A. G. et al. (1999) *Am. Mineral.,* in preparation. [9] Kalinichev A. G. and Heinzinger K. (1992) *Adv. Phys. Geochem., 10,* 1–59.

MECHANISMS OF PYRITE OXIDATION REVEALED FROM *IN SITU* MEASUREMENTS OF DISSOLVED OXYGEN, Eh, AND pH OF SOLUTIONS IN A CLOSED SYSTEM.

G. Kamei[1] and H. Ohmoto[2], [1]Japan Nuclear Cycle Development Institute, Tokai-mura, Ibaraki 319-1194, Japan (kamei@tokai.jnc.go.jp), [2]Astrobiology Research Center and Department of Geosciences, Pennsylvania State University, University Park PA 16802, USA (ohmoto@geosc.psu.edu).

Previous experimental studies on the kinetics of pyrite oxidation were all carried out in systems open to O_2. In order to test if the rate law derived from open-system experiments is applicable to groundwater problems, we have conducted a series of pyrite oxidation experiments in a system closed to dissolved O (DO). Distilled and de-ionized water was first saturated with the air, and sealed in a 1.4-L-volume batch reactor (Pyrex glass) together with 1–3 g of crushed and cleaned pyrite grains; the ratios of surface area of pyrite to volume of water (S/V) were 0.037 to 0.112 m²/L. The reactions were carried out at 25°C and 37°C for periods lasting ~30 h to ~160 h. The values of DO, Eh, and pH of the experimental solutions were continuously monitored, *in situ,* during reactions. The SO_4^{2-} content was analyzed for the solutions periodically withdrawn from the experimental reactor; the Fe^{2+} content was calculated from mass and charge balance equations.

The changes with time in DO, Eh, pH, SO_4^{2-}, and Fe^{2+} values followed complicated paths, but the paths can be discussed in terms of three stages of reactions. During the first stage, which typically lasted for less than ~5 h, Eh decreased rapidly by ~100 to ~200 mV, pH rose from ~5.6 to ~6, and SO_4^{2-} and Fe^{2+} increased to ~0.005 mM, but DO did not change. During the second stage, which typically lasted for ~3 to ~25 h after the first stage, Eh and DO slowly decreased, SO_4^{2-} and Fe^{2+} slowly increased, but pH remained essentially constant. During the third stage (t >~3 to ~25 h), Eh, DO, and pH decreased very slowly, but SO_4^{2-} and Fe^{2+} remained essentially constant. The above trends with time in the chemical composition of experimental solutions suggest the following series of dominant reactions.

Consumption of H^+ from the dissolved H_2CO_3 (i.e., the dissolved atmospheric CO_2) by pyrite:

$$H^+ + FeS_2 \Rightarrow Fe^{2+} + HS_2^- \qquad (1)$$

Oxidation of HS_2^- by the surface electrons of pyrite:

$$3(e^-)_{pyrite} + HS_2^- + 8H_2O \Rightarrow 2SO_4^{2-} + 8H_2 + H^+ \qquad (2)$$

Oxidation of H_2 by O_2:

$$H_2 + 1/2O_2 \Rightarrow H_2O \qquad (3)$$

Oxidation of Fe^{2+} by O_2:

$$Fe^{2+} + 1/4\ O_2 + 5/2\ H_2O \Rightarrow Fe(OH)_3 + 2H^+ \qquad (4)$$

Reactions (1) and (2) are important in stage 1. Reactions (3) and (4) start to become important in stages 2 and 3 respectively. Reaction (2) appears to slow down once the pyrite surface is coated with the ferric hydroxides produced by reaction (4).

The rates of pyrite oxidation during the first two stages are several orders of magnitude higher than those in the third stage. The rates of pyrite oxidation during the second and third stages appear to follow the first-order rate law with respect to DO as first suggested by Manaka [1]: $-d[py]/dt = -k(S/V)[DO]$ where k is the rate constant. The k values were determined to be (6.76 ± 2.02 × 10^{-7} L/m²s at 25°C and (2.02 ± 1.03) × 10^{-6} L/m²s at 37°C. These values give the activation energy of 47–80 kJ/mol for pyrite oxidation by dissolved O.

References: [1] Manaka M. (1997) Ph.D. thesis, Tohoku Univ.

THE GENESIS OF SIDERITE IN ARCHEAN AND PALEOPROTEROZOIC OCEANS.

A. J. Kaufman, Department of Geology, University of Maryland, College Park MD 20742, USA (kaufman@geol.umd.edu).

The genesis and the exodus of Archean and Paleoproterozoic banded iron-formations (BIFs) is generally considered to be the logical result of the biological production of O. In this view, the origin of these enigmatic marine deposits is related to the immobilization of soluble iron by fixation with O_2 produced during oxygenic photosynthesis, and deposition of BIF ceased when the deep oceans became pervasively oxidized ca. 1.8 Ga. The Sr- and Nd-isotopic records indicate that Archean and early Paleoproterozoic oceans were dominated by hydrothermal fluids [1–3], and were therefore anoxic, acidic, and rich in soluble ferrous iron; isolated plumes of iron-poor, oxygenated water spread out from stromatolitic platforms. Eventually these plumes spread, coalesced, and deepened. In their wake iron was swept from the oceans. However, rather than being driven by biological sources from above, the primary control of the oxidation state of the deep ocean appears to be exerted by tectonic forces controlling the flux of reduced ions from below. Based on modern studies in volcanic lakes [4], as well as petrographic and C-isotopic analyses [5–7] of BIF siderite microbands, the primary control on the deposition iron-bearing BIF minerals appears to be related to changes in pH and iron availability across the transition from anoxic to oxygenated waters.

The current model suggests an abiological process for the primary precipitation of siderite in the Archean and Paleoproterozoic oceans [cf. 8, 9]. Soluble ferrous iron as well as CO_2-rich and sulfide-poor solutions were upwelled from deep hydrothermal sources to shallow shelves. At a chemocline these acidic solutions were neutralized by the dissolution of calcium carbonate raining down from the surface or swept off from shallow water subtidal and peritidal environments. Dissolution would result in a noticable increase in alkalinity; because siderite is 100-fold less soluble than calcite [10] and ferrous iron was readily available in the ascending water column, siderite would precipitate. The rain of siderite down from the chemocline would accumulate at the sediment-water interface. This iron-bearing mineral would have persisted to a depth where the acidity of ascending waters neutralized the less soluble carbonate. The Archean and Paleoproterozoic oceans may thus have been characterized by having both calcite and siderite compensation depths.

References: [1] Veizer J. and Compston W. (1976) *GCA, 40,* 905–914. [2] Jacobsen S. B. and Pimentel-Klose M. R. (1988) *EPSL, 87,* 29–44. [3] Jacobsen S. B. and Kaufman A. J. (1999) *Chem. Geol.,* in press. [4] Bahrig B. (1988) *Palaeogeogr. Palaeoclimatol. Palaeoecol., 70,* 139–151. [5] Kaufman A. J. et al. (1990) *GCA, 54,* 3461–3473. [6] Kaufman A. J. (1996) *Precambrian Res., 79,* 171–193. [7] Winter B. L. and Knauth L. P. (1992) *Precambrian Res., 59,* 283–313. [8] Klein C. and Beukes N. J. (1989) *Econ. Geol., 84,* 1733–1774. [9] Beukes N. J. et al. (1990) *Econ. Geol., 85,* 663–690. [10] Eugster H. P. and Chou I-M. (1973) *Econ. Geol., 68,* 1144–1168.

LANTHANIDE TETRAD EFFECTS IN RARE-EARTH-ELEMENT FRACTIONATION AMONG PARTICULATE, COLLOIDAL, AND SOLUTION FORMS IN RIVER WATER.

I. Kawabe[1], I. Ohnishi, T. Sakakibara, and K. Yamamoto, [1]Department of Earth and Planetary Sciences, Graduate School of Science, Nagoya University, Chikusa, Nagoya 464-8602, Japan (kawabe@eps.nagoya-u.ac.jp).

Introduction: Rare earth elements in river water comprise "particulate," "colloidal," and "solution" forms [1–3]. The particulate REEs are obtained by filtration using 0.45–0.2-µm-pore-sized filters. The filtrate includes the colloidal and the solution REEs. The colloidal REEs can be identified by filtration using progressively finer pore-sized filters [2,3]. Suspended and colloidal particles have shale-like REE compositions, but the solution REEs are highly enriched in heavy REEs relative to the suspended and colloidal particles or the average shale [1–3]. The fractionated REEs of solution form relative to average crustal ones are comparable with those of coastal seawater samples [1,3]. We will focus on whether lanthanide tetrad effects are associated with the REE fractionation among the three forms in river water. The seawater REE patterns normalized by chondrite or average shale show concave tetrad effects [4–6]. The previous data for REEs in river water have been obtained by isotope dilution-thermal ionization mass spectrometry (ID-TIMS), but they lack the analytical data for mono-isotopic REEs (Pr, Tb, Ho, and Tm) and Y. It is difficult to examine tetrad effects in REE data by ID-TIMS. However, the preconcentration of REE and Y in seawater [7] and inductively coupled plasma mass spectrometry (ICP-MS) made it possible to determine all REE and Y in filtered water samples. Our ICP-MS data of REE and Y for suspended particles and filtrates of water samples from Kiso River, central Japan, reveal tetrad effects in REE fractionation among the particulate, colloidal, and solution forms in river water.

Sample and Experimental: Water samples have been collected at two locations (A and B) of Kiso River, 25 km east of Nagoya, central Japan on 28 October, 1998. The samples at A are normal river water (S = 0.0‰), but the samples at B are slightly saline water (S = 1.5‰) in the estuarine zone. Two 20-L samples for REE and Y analysis and one 500-mL sample for chemical analysis of major constituents have been collected at each site. Two filtrates (A1 and A2) were obtained by filtering samples from A with Nuclepore filter (0.40 µm) and PTFE filter (0.50 µm) respectively. The suspended particles on the Nuclepore filter (SP-A1) were also recovered. Four filtrates were obtained from the water samples at B: B1 by the paper filter [Toyo No. 5A], B2 by Nuclepore filter (0.40 µm), B3 by the paper filter and PTFE filter (0.50 µm), and B4 by the paper filter and cellulose nitrate membrane filter (0.2 µm). Two suspended particle samples (SP-B1 and SP-B2) were collected on the paper filter and Nuclepore filter (0.40 µm), respectively. REE and Y in all filtrates were concentrated by the method of [7], and their ICP-MS determinations were made as well as for the suspended particle samples.

Results and Discussion: There is no systematic REE fractionation among the three suspended particle samples (SP-A1, SP-B1, and SP-B2). The suspended particle samples show almost the same tetrad effects in their shale-normalized REE patterns, but their tetrad effects when normalized by NASC and PAAS are different. The PAAS-normalized REE patterns for suspended particles show typical Gd breaks due to the octad effect. This means that the tetrad and octad effect features are different among the suspended particles of Kiso River and the average shales. The REE concentrations in the water filtered the more thoroughly become the lower, and show the larger fractionation between light and heavy REEs. These features are in accordance with the previous results by ID-TIMS [2,3]. Observed large variations in REE concentrations in the four filtrates (B1–B4) can be explained by a simple model that REE concentrations in the respective filtrates are sums of colloidal and solution REEs both compositions of which are common among the filtrates but their colloidal particle concentrations are different. The REE fractionation patterns between colloidal and suspended particles are not totally smooth. Small tetrad and octad effects are recognized in the REE patterns. The REE patterns for the solution form relative to the colloidal one show concave tetrad effects in light to middle REEs that resemble the seawater tetrad effect. The seawater tetrad effect begins with the fractionated solution REE feature in slightly estuarine river water. However, there still remain significant differences in REE and Y features concerning heavy REEs (Er-Lu) and the Y/Ho ratio between the slightly estuarine water and coastal seawater.

References: [1] Elderfield H. et al. (1990) *GCA, 54,* 971–991. [2] Sholkovitz E. R. (1992) *EPSL, 114,* 77–84. [3] Sholkovitz E. R. (1995) *Aquat. Chem., 1,* 1–34. [4] Masuda A. and Ikeuchi Y. (1979) *Geochem. J., 13,* 19–22. [5] Akagi T. et al. (1993) *GCA, 57,* 2899–2905. [6] Kawabe I. et al. (1998) *Geochem. J., 32,* 213–229. [7] Shabani M. B. et al. (1992) *Anal. Chem., 64,* 737–743.

CREATION, MODIFICATION, AND DESTRUCTION OF CONTINENTAL LITHOSPHERE IN THE NEOGENE CENTRAL ANDES.

S. M. Kay and R. W. Kay, Department of Geological Sciences, Snee Hall, Cornell University, Ithaca NY 14853, USA (smk16@cornell.edu; rwk6@cornell.edu).

Introduction: The Neogene Central Andes is a major site of creation, modification and destruction of the post-Archean continental lithosphere. Arc magmatism is the major process of new addition whereas loss occurs by delamination of thickened crust, tectonic forearc erosion, and loss of the base of the arc and backarc lithosphere above nearly horizontal segments of the subducting Nazca plate. Modification is severest as magmatism ceases over a shallowing slab, as the arc front migrates, or as magmatism re-initiates over a steepening slab. Three east-west transects are discussed below as examples of along strike lithospheric modification and loss as the dip of the slab varies in time and space. In each transect, evolving magmatic patterns carry robust keys to rapid changes in crustal and mantle lithospheric conditions and loss. These examples are more than a local story as substantial amounts of continental lithosphere has passed through Andean arclike crucibles.

Lithospheric Processes: Miocene shallowing of the subducting slab initiated an important episode of continental lithospheric loss beneath the modern nonvolcanic Chilean flatslab region (28°–33°S). Estimates of loss since 18 Ma for a 400-km-long east-west transect east of the Early Miocene arc front near 30°–31°S are up to 69% [1,2]. The mechanism must be more mechanical than thermal as loss occurred with a shallowing slab, a thinning asthenosphere, and a thickening crust. Estimates of crustal thickening from 18 Ma to 6 Ma under the arc region are ~25 km. The principal driving force is inferred to be westward wedging of mid to lower crust from beneath the thrust belt to the east into the hot magma-injected arc crust. Lithospheric changes beneath the arc are recorded by temporal variations in isotopic and trace-element signatures that reflect a cooling mantle, a changing crustal basement, and an increasingly higher pressure residual mineral assemblage in equilibrium with erupted magmas [2]. Isotopic and trace-element signatures of subduction-related magmas erupted up to 700 km from the trench have components removed from the base of the lithosphere further west [see 1,2].

Contemporaneous steepening of the subducting slab to the north (~22°–25°S) [1] precipitated major lithospheric modifications that are reflected by giant Miocene/Pliocene ignimbrites in the central part of the high Andean plateau. These dacitic ignimbrites reflect massive melting of thick crust and thin hydrated lithosphere developed over a formerly shallow subduction zone. Their chemical and isotopic signatures reflect these sources as well as mid-crustal storage before being erupted in response to horizontal compressional collapse and thickening of the hot magma-injected crust. The volcanic zone narrowed to the west as the lithosphere thickened in response to underthrusting of the Brazilian shield and lithospheric cooling above the steepening slab.

The most dramatic lithospheric change occurred to the north of the Chilean flatslab (25°–28°S) where the slab retained an intermediate dip and the arc front migrated ~50 km to the east from ~7 to 3 Ma. The presence of 7 Ma arc lavas ~80 km above the modern seismic zone signals the magnitude of this change. Some of the highest La/Ta and La/Yb ratios known in post Archean rocks occur in mafic andesitic to rhyolitic flows erupted in the zone of the migrating arc. High La/Ta ratios (to 100) suggest retention of Ti group elements in oxide phases stabilized by especially oxidizing/hydrous conditions above the adjusting slab. Lanthanum/ytterbium ratios up to 60 in mafic andesites suggest some mantle magmas equilibrated with garnet peridotite above this slab. High La/Yb ratios in silicic flows (to 100) reflect mixing of arc magmas with thickened garnet granulite to eclogitic crust or with tectonically removed forearc crust subducted into the mantle. Isotopic signatures of mantle-derived Pleistocene arc magmas ($^{87}Sr/^{86}Sr = 0.7058$, $\varepsilon_{Nd} = -2$) erupted east of the sediment barren trench are consistent with mixing of tectonically removed crust into the mantle. Arc migration ended with widespread dacitic ignimbrites erupted before the typical modern central Andean volcanic arc centers became established. Other changes occurred in the backarc where delamination of over-thickened eclogitic crust and the underlying mantle lithosphere can explain the distribution of <~6 Ma intraplate, calc-alkaline and shoshonitic lavas, and the voluminous Cerro Galan ignimbrite [3]. The intraplate lavas and crustal melting that produced the ignimbrite reflect asthenospheric mantle inflow into the gap left by the delaminated lithosphere. Evidence for melting of eclogitic crust comes from glassy dacitic flows with high La/Yb ratios (to 100) and radiogenic isotopes ($^{87}Sr/^{86}Sr = 0.7098$, $\varepsilon_{Nd} = -6.6$) that erupted along faults generated by stress re-orientation above the delaminated lithosphere.

References: [1] Kay S. M. et al. (1999) *Soc. Econ. Geol. Spec. Pub. 7*, in press. [2] Kay S. M. and Abbruzzi J. (1996) *Tectonophys., 259,* 15–28. [3] Kay S. M. et al. (1994) *JGR, 99,* 24323–24339.

COMPARISON OF CHEMICAL VARIATION IN GABBROS FROM OPHIOLITES, OCEANIC CRUST, AND CONTINENTAL, IGNEOUS LAYERED INTRUSIONS.

P. B. Kelemen, Woods Hole Oceanographic Institution, Woods Hole MA 02543, USA (peterk@whoi.edu).

A compilation of data on variation of mineral compositions with height, or "cryptic variation" reveals a first order difference between oceanic and continental layered gabbros. Studies of cryptic variation in modally layered gabbros from the Oman ophiolite [1], and in gabbroic drill core from the southwest Indian Ocean (ODP Site 735), Pacific (Hess Deep, ODP Site 894), and Atlantic (MARK, ODP Sites 921, 922 and 923) show that olivine and clinopyroxene molar Mg/(Mg + Fe), or Mg#, vary by more than 10%, and plagioclase molar Ca/(Ca + Na), or An, varies by 10–20%, over vertical intervals of tens to hundreds of meters. By contrast, variation in compiled data for the Stillwater, Bushveld, Kiglapait, and Duluth gabbroic intrusions is much more subdued, with Mg# and An varying by less than 5% over hundreds of meters. Even the Skaergaard intrusion, with its well known Fe-enrichment trend, does not show large variations in mineral composition on vertical scales of tens of meters. The Troodos ophiolite CY-4 drill core also has subdued variation with height, more like the continental layered intrusions than like other "oceanic" sample suites.

Kelemen et al. [2] and Korenaga and Kelemen [3] argued that preservation of large cryptic variations over short vertical intervals in Oman lower crustal gabbros, coupled with well-correlated chemical variation in different minerals, precludes large volumes of diffuse, reactive porous flow of melt through the gabbros after the chemical layering was formed, and requires that most of the melt that formed upper crustal dikes and lava flows must have followed conduits of focused flow, perhaps in hydrofractures. In a simple model [4] porous flow in a conductive geotherm leads to cooling of melt, crystallization in pore space, formation of permeability barriers underlain by overpressured melt lenses, visco-elastic failure of the barrier, and melt extraction by flow in cracks.

Substantial variation of composition with height may never have formed in continental intrusions. Alternatively, vertical variation in continental intrusions may have formed and then become damped as a result of diffuse, reactive porous flow of melt. Evidence for reactive flow processes in layered intrusions has been documented in many studies by McBirney, Irvine, Boudreau and a host of others. Most continental intrusions may contain larger instantaneous melt volumes than individual intrusions beneath oceanic spreading ridges. If so, compaction in the lower "half" of continental intrusions would drive melt upward into hotter rock at lower pressure. This would take the liquid (on its own composition) away from its saturation surface. In reactive porous flow, this would lead to partial dissolution of preexisting crystals and an up-section increase in porosity and permeability. Dissolution reactions in the adiabatically upwelling mantle, combined with viscous compaction, may lead to formation of localized conduits of focused melt flow [5–7]. However, in large layered intrusions the upward increase in permeability may be so marked, and the viscous response so slow, that focused flow is rarely developed. Instead diffuse, reactive porous flow may be the dominant mode of melt transport.

References: [1] Browning P., thesis, Open Univ. [2] Kelemen et al. (1997) *EPSL.* [3] Korenaga and Kelemen (1997) *JGR;* (1998) *EPSL.* [4] Kelemen and Aharonov (1998) AGU Monograph. [5] Kelemen et al. (1995) *JGR.* [6] Aharonov et al. (1995,1997) *JGR.* [7] Spiegelman et al. (1999) *JGR,* submitted.

SPECULATION ON CONSEQUENCES OF DELAMINATION OF ULTRAMAFIC PLUTONIC ROCKS FROM THE LOWER CRUST AND IMPLICATIONS FOR THE GENESIS OF THE CONTINENTAL CRUST.

P. B. Kelemen and M. Jull, Woods Hole Oceanographic Institution, Woods Hole MA 02543, USA (peterk@whoi.edu).

At this meeting, Jull and Kelemen report calculations bearing on "delamination" of ultramafic plutonic rocks previously formed at the base of igneous crust. Ultramafic plutonic rocks, formed by partial crystallization of mafic magmas, have lower molar Mg/(Mg + Fe), or Mg#, than underlying mantle, and therefore will be denser than underlying mantle when the mantle is as hot or hotter than the plutonic rocks. As suggested by Arndt and Goldstein [1] this creates an unstable density inversion. We calculate that, for ultramafic layers 1–10-km-thick, with mantle at 900°–1200°C, this will lead to delamination in <10 m.y. At <900°C, mantle viscosity is too high for delamination to occur on geologic timescales. Thus, lower crustal delamination due to formation of dense eclogite from basaltic lower crust at <900°C [e.g., 2,3] seems comparatively unlikely.

The most likely setting for formation and subsequent delamination of ultramafic plutonic rocks is the base of the crust beneath subduction-related volcanic arcs, where the combination of high-magmatic H_2O and pressures >1 GPa combine to suppress plagioclase stability relative to olivine and pyroxenes. Formation of ultramafic cumulates is known from arc crustal sections and plutonic xenoliths in arc lavas [e.g., 4–6]. Upper-mantle temperatures in arcs are likely >1000°C, based on heat flow and seismic observations [e.g., 7,8]. Thus, the base of the crust beneath active arcs may be characterized by continuous formation of ultramafic plutonic rocks via crystal fractionation from hydrous magmas, and periodic delamination of these plutonic rocks. Ultramafic plutonic rocks in xenolith suites and arc sections may be remnants of a larger mass, of which much has been delaminated.

Other scenarios in which ultramafic plutonic rocks may form include: (1) at the base of thick crust beneath rifting continental margins, where high pressure may supress plagioclase crystallization; and (2) beneath intraplate hotspot volcanos, such as Hawai'i, where ultramafic cumulates are known to form in the crust and in the upper mantle [e.g., 9,10]. Reheating of mantle beneath an ancient, ultramafic layer at the base of continental crust could also lead to delamination.

A consequence of this process is that igneous crust, after delamination, will be more SiO_2-rich, and MgO- and FeO-poor, than melts in equilibrium with the upper mantle. This may account, in part, for the relatively SiO_2-rich nature of continental crust. Delamination of eclogite derived from plagioclase-rich gabbroic rocks should produce relative depletion of Sr and Eu in remaining crust. Such depletions are not observed [e.g., 11], suggesting that delamination of gabbroic compositions was not important in continental genesis. In contrast, delamination of ultramafic plutonic rocks would not result in Sr and Eu depletion.

Where upper mantle temperatures are above their solidus temperature, delaminating plutonic rocks may undergo anatexis [3], and because buoyant melt moves much faster than surrounding solids, anatectic melts could rise into the overlying crust. The composition of melts of ultramafic plutonic rocks could vary widely, depending on the solid phase assemblage, temperature, and pressure. There is a need for more experimental data. Small degree melts may be SiO_2-rich, varying from quartz-normative where melting occurs at 1–2 GPa and where olivine is not a part of the melting assemblage, to alkaline where melting occurs at higher pressure and where olivine is a part of the melting assemblage. Also of interest will be the presence or absence of residual garnet and rutile during melting, because the presence of these residual phases seems essential in understanding the light REE enriched, Nb and Ta depleted nature of the continental crust [e.g., 12,13].

Evidence that delamination and anatexis of ultramafic cumulates does occur, producing alkali-rich, SiO_2-rich melts and high Mg# andesites may be found in (1) the southern Sierra Nevada, where seismic data and evidence from xenoliths suggests that a layer of pyroxenite and eclogite was removed from the base of the crust [14,15]; (2) Baja California, where eruption of high-Mg# andesite magmas after cessation of subduction [16,17] suggests partial melting of a "trapped slab" or of delaminating lower crustal rocks combined with melt/rock reaction with surrounding mantle [e.g., 18]; (3) a similar situation in Chile where delamination is interpreted to be more likely than melting of subducted material [3]; and (4) in suites of alkali-rich granites and syenites along the Atlantic margins of North America and Greenland during and after rifting.

References: [1] Arndt N. T. and Goldstein S. L. (1989) *Tectonophys., 161,* 201–212. [2] Kay R. W. and Kay S. M. (1991) *Geol. Rundsch., 80,* 259–278. [3] Kay R. W. and Kay S. M. (1993) *Tectonophys., 219,* 177–189. [4] Conrad W. K. and Kay R. W. (1984) *J. Petrol., 25,* 88–125. [5] DeBari S. M. and Coleman R. G. (1989) *JGR, 94,* 4373–4391. [6] Jan M. Q. and Howie R. A. (1981) *J. Petrol., 22,* 85–126. [7] Blackwell D. D. et al. (1982) *JGR, 87,* 8735–8754. [8] Zhao D. et al. (1992) *JGR, 97,* 19909–19928. [9] Sen G. and Jones R. E. (1990) *Science, 249,* 1154–1157. [10] Sen G. and Presnall D. C. (1986) *J. Petrol., 27,* 197–217. [11] Rudnick R. L. (1995) *Nature, 378,* 571–577. [12] Ryerson F. J. and Watson E. B. (1987) *EPSL, 86,* 225–239. [13] Kelemen P. B. et al. (1993) *EPSL, 120,* 111–134. [14] Ducea M. N. and Saleeby J. B. (1996) *JGR, 101,* 8229–8244. [15] Wernicke B. et al. (1996) *Science, 271,* 190–193. [16] Rogers G. et al. (1985) *Nature, 315,* 389–392. [17] Saunders A. D. et al. (1987) *JVGR, 32,* 223–245. [18] Kay R. W. (1978) *JVGR, 4,* 117–132.

UPDATED REVIEW OF MELT-EXTRACTION PROCESSES IN THE UPPER MANTLE BENEATH OCEANIC SPREADING RIDGES AND INTRAPLATE VOLCANIC CENTERS.

P. B. Kelemen[1], G. Hirth[1] and M. Spiegelman[2], [1]Woods Hole Oceanographic Institution, Woods Hole MA 02543, USA (peterk@whoi.edu; ghirth@whoi.edu), [2]Lamont-Doherty Earth Observatory, Columbia University, Palisades NY 10964, USA (mspieg@ldeo.columbia.edu).

We will provide an updated review of melt transport mechanisms beneath mid-ocean ridges, following from the 1997 review of Kelemen et al. [1] with a comparison to related data from intraplate volcanic centers. First, we concentrate on the adiabatically upwelling region, emphasizing the following points.

1. New literature data on U series disequilibrium in MORB continue to support the hypothesis that melt migration beneath ridges occurs in a two-porosity network, in which most melt migrates through the upper 30 or 40 km of the mantle in chemically isolated conduits, but some melt migrates by reactive porous flow through highly depleted residual peridotite, resulting in high ^{226}Ra excess in the most light REE depleted melts. This is in contrast to U-series data from Hawai'i, in which ^{226}Ra excess is correlated with incompatible trace element abundance [2], probably because reactive porous flow is a less important process beneath Hawai'i, and the depletion of residues is smaller.

2. A review of melt migration mechanisms proposed to date [3–10], together with seismic evidence from the East Pacific Rise [11,12], shows that only porous melt transport mechanisms can explain the observation that igneous crustal accretion beneath spreading ridges is concentrated within a few kilometers of the ridge axis. Combinations of different porous flow processes are likely, and might enhance focusing of melt toward the ridge. As emphasized in our earlier review, if hydrofractures do occur in the adiabatically upwelling region, they probably form within preexisting, high porosity conduits [1]. Cracks might also propogate within porous conduits that coalesce toward the ridge axis.

3. Size/frequency and spatial distribution statistics on the distribution of dunite veins in ophiolites [13,14] record the presence of a coalescing network of porous melt conduits that chemically isolate ascending melt from surrounding, residual mantle peridotite [15].

We also review mechanisms of melt migration as melt passes into the conductive thermal boundary layer at the base of a plate. There, competition between the rate of crystallization (filling pore space) and viscous decompaction (preserving pore space) can lead to two distinct results [16].

1. Intergranular pores become clogged with new crystals, leading to ponding of melt at increasing pressure beneath a permeability barrier. This, in turn, will lead to hydrofracture and rapid melt transport in cracks through the permeability barrier [17]. This may explain the presence of primitive "cumulate" plutonic rocks formed near the base of the crust in ophiolites [18], and observed as high-pressure xenoliths that crystallized at ~3 GPa near the base of the thermal boundary layer beneath Hawai'i [19]. Such a process could be the general explanation for the transition from continuous porous flow in the mantle to periodic emplacement of dikes and lava flows in the upper crust at ridges and in other magmatic settings [17].

2. Alternatively, where crystallization in pore space is slow compared to decompaction, melts may continue to ascend into the conductive boundary layer. Diffuse porous flow coupled with crystallization is inherently diffuse [10,20], leading to pervasive melt/rock reaction at low melt/rock ratios. In these circumstances, combined crystal fractionation and melt/rock reaction can lead to extreme enrichment of incompatible elements in small amounts of migrating melt at high, nearly constant Mg# [1,21]. Consequences of these processes may include some kinds of mantle metasomatism, production of immiscible carbonatite liquids, crystallization of trace-element-rich minor phases such as apatite and rutile from evolved silicate or carbonatite liquids, and ultimately hydrofracture and explosive eruption of vapor-saturated melts. Although it is evident that this type of combined fractional crystallization and melt/rock reaction may be important in intraplate settings where melt flux is small and the rate of change of temperature with height is small, this process may operate beneath mid-ocean ridges as well [1]. This may explain formation of "over-enriched" melts — with high incompatible element abundances at a given Mg# — which are observed in melt inclusions and rare lavas from ridges [e.g., 22].

References: [1] Kelemen et al. P. B. (1997) *Phil. Trans. Roy. Soc. London, A355,* 283–318. [2] Sims K. W. W. et al. (1995) *Science, 267,* 508–512. [3] Nicolas A. (1986) *J. Petrol., 27,* 999–1022. [4] Phipps Morgan J. (1987) *GRL, 14,* 1238–1241. [5] Spiegelman M. and McKenzie D. (1987) *EPSL, 83,* 137–152. [6] Sleep N. H. (1988) *JGR, 93,* 10255–10272. [7] Nicolas A. (1990) in *Magma Transport and Storage* (M. P. Ryan, ed.), pp. 159–173. [8] Sparks D. W. and Parmentier E. M. (1991) *EPSL, 105,* 368–377. [9] Kelemen P. B. and Dick H. J. B. (1995) *JGR, 100,* 423–438. [10] Kelemen P. B. et al. (1995) *JGR, 100,* 475–496. [11] Forsyth D. W. et al. (1998) *Science, 280,* 1215–1218. [12] Forsyth D. W. et al. (1998) *Science, 280,* 1235–1238. [13] Kelemen P. B. et al. (1998) *Eos Trans. AGU, 79,* S225. [14] Kelemen P. et al. (1999) *Eos Trans. AGU, 80,* in press. [15] Kelemen P. B. et al. (1995) *Nature, 375,* 747–753. [16] Korenaga J.

and Kelemen P. B. (1997) *JGR, 102,* 27729–27749. [17] Kelemen P. B. and Aharonov E. (1998) *Geophys. Monogr., 106,* 267–289. [18] Kelemen P. B. et al. (1997) *EPSL, 146,* 475–488. [19] Sen G. and Jones R. E. (1990) *Science, 249,* 1154–1157. [20] E. Aharonov et al. (1997) *JGR, 102,* 14821–14833. [21] Kelemen P. B. (1986) *J. Geol., 94,* 829–843. [22] Sours-Page R. et al. (1996) *Eos Trans. AGU, 77,* 842.

MANTLE FLOW AND GEOCHEMICAL HETEROGENEITY.

J. B. Kellogg and R. J. O'Connell, Department of Earth and Planetary Sciences, Harvard University, 20 Oxford Street, Cambridge MA 02138, USA (kellogg@geophysics.harvard.edu; oconnell@geophysics.harvard.edu).

The reconciliation of geochemical and geophysical datasets remains among the most challenging problems of earth science. The most vexing geochemical datasets involve the noble gases, which seem inescapably to indicate relatively undegassed regions in the mantle. If one envisions perfect mixing within the proposed upper and lower mantle reservoirs, then this observation is directly at odds with recent tomographic studies showing that subducting slabs continue into the lower mantle, resulting in a high-mass flux between the reservoirs. However, if mixing is incomplete or significantly more sluggish in the lower mantle, then it may be possible to preserve undegassed material in a fully convecting mantle with large mass flux between the upper and lower layers.

While two-dimensional numerical investigations of mixing are numerous, few studies exist in the literature that take into account the full three-dimensionality of the problem. We revisit the problem, focusing specifically on the effects of viscous layering and rigid plates. We present results dynamical calculations in a Cartesian geometry as well as ongoing work in a spherical geometry incorporating realistic plate configurations. The latter suite of calculations include flow driven by plates and density anomalies drawn from tomographic results.

The presence of lateral plates gives rise to a uniquely three-dimensional flow feature: toroidal motion. We find that this effect enhances mixing in the upper mantle versus the lower, but conclude that this mechanism is not sufficient to explain the inferred differences between the MORB and OIB source regions; the high-mass flux across the upper-lower mantle boundary cycles virtually all the material through the high-strain rate upper mantle. In fact, toroidal motion serves to break up convection cells, reducing bias between the layers.

We conclude that if the geochemical data is taken at face value there must be regions of the mantle which exhibit fundamentally different mechanical and dynamical behavior, either through higher density or higher viscosity. We address the latter possibility in a separate talk in which we find that geochemically primitive or enriched, highly viscous blobs may persist over geologically long periods. Such blobs would be subject to sampling by upwelling plumes, but not by MORs, thereby explaining the observed systematic differences between the two.

GARNET GRANULITE XENOLITHS FROM THE NORTHERN BALTIC SHIELD: THE LOWER CRUST OF A PALEOPROTEROZOIC LIP.

P. D. Kempton[1], H. Downes[2], L. Neymark[3], E. V. Sharkov[4], R. Zartman[5], and J. Wartho[6], [1]Isotope Geosciences Laboratory, National Environmental Research Council, Kingsley Dunham Centre, Keyworth, NG12 5GG, UK (p.kempton@nigl.nerc.ac.uk), [2]Birkbeck/UCL Research School of Geological and Geophysical Sciences, Birkbeck College, Malet Street, London WC1E 7HX, UK (h.downes@ucl.ac.uk), [3]U.S. Geological Survey, Denver, CO, USA (lneymark@usgs.gov), [4]Institute of Ore Deposits, Geology, Petrology, Mineralogy, and Geochemistry, Staromonetny per 35, Moscow, 109017, Russia (sharkov@igem.msk.su), [5]Department of Geological Sciences, University of Cape Town, Rondebosch 7700, South Africa (rzart@geology.uct.ac.za), [6]Department of Earth Sciences, The Open University, Milton Keynes MK7 6AA, UK (j.wartho@open.ac.uk).

Introduction: It is generally believed that growth of continental crust has occurred through either or both of two mechanisms — i.e., volcanic arc accretion [1] and oceanic plateau accretion [2–4] — but have the relative contributions of these two mechanisms varied with time? Although the former is a model of long standing, the latter may be able to explain periods of rapid continental growth better than the volcanic arc accretion model. In order to improve our understanding of the processes involved in the formation and evolution of continental crust in Archean/Proterozoic time, we have undertaken a geochemical and isotopic study of a suite of Proterozoic lower crustal xenoliths from the northern Baltic Shield [5].

The Kola Xenoliths: The Kola xenoliths were brought to the surface by a Devonian ultramafic lamprophyre diatreme on Elovy island (Kola Peninsula). The xenolith suite includes mafic granulite (gar + cpx + rutile ± plag ± opx ± phlog ± amph), felsic granulite (gar + cpx + plag + rutile ± qtz ± Kspar ± phlg ± amph), and pyroxenite (± phlog ± amph), but "eclogitic" plagioclase-poor granulites predominate. Although some samples are restites, there is no evidence for a predominance of magmatic cumulates, as is common for Phanerozoic lower crustal xenolith suites. Instead, most of the protoliths of the granulites were mafic, LREE-enriched norites to gabbronorites.

Major-element, trace-element, and isotopic evidence indicates that the Kola xenoliths are the high-grade metamorphic equivalents of continental flood tholeiites, emplaced into the Baltic Shield lower crust in early Proterozoic time (~2.4–2.6 Ga). Similarities in major- and trace-element systematics suggest that they formed in response to the same plume-driven magmatic event that created the widespread Paleoproterozoic igneous province in the area at 2.4–2.5 Ga. Thus, the mafic protoliths may have formed in a manner analogous to Phanerozoic lower crustal rocks (i.e., basaltic underplating), but in this case the underplating was the result of an actively upwelling plume rather than passive upwelling asthenosphere beneath an extending region. The Kola xenoliths, therefore, represent the first lower crust of a Paleoproterozoic LIP to be studied in petrological detail.

The granulites exhibit a wide range in isotopic values that can be related to primary lithology and the presence or absence of secondary hydrous phases. Present-day Sr-isotopic values range from 0.7052 to 0.9564; Nd isotopes range from 0.5112 to 0.5123. Lead isotopes exhibit an extreme range of values: 6/4Pb = 17.39–22.47, 7/4Pb = 15.42–16.03, and 8/4Pb = 37.46–54.83. The unusual radiogenic Pb-isotopic compositions of the xenoliths are the product of an ancient metasomatic event and not a function of initial protolith composition, such as might be the case for ancient metasediments. Indeed, amphibole and/or phlogopite occur commonly in xenoliths of all types, and are interpreted to be metasomatic in origin. Ar-Ar dating of a phlogopite separate from one strongly metasomatized xenolith indicates that introduction of K-rich fluids occurred sometime ~2 Ga; this event resulted in substantial enrichment in Rb, K, LREE/HREE, Th/U, Th/Pb, and, to a lesser extent, Nb and Ti. The fluids responsible for this metasomatism were probably alkalic volatile-rich melts generated from enriched lithospheric mantle above an incubating plume head that arrived beneath the region at ~2.0 Ga. These data indicate that the lower crust has not been uniformly depleted in U-Th-Pb since ancient times, but locally may have had extreme Th/Pb, Th/U, and U/Pb ratios for ~2 b.y.

Evidence for partial melting of mafic crust exists in the presence of migmatitic granulites. The timing of migmatization overlaps that of metasomatism, and it is suggested that migmatization was faciliated by the metasomatism. The metamorphism, metasomatism and migmatization recorded in the Kola granulite xenoliths may be representative of the processes responsible for converting Archean LIP-generated protocontinents into continental crust.

References: [1] Taylor S. R. (1967) *Tectonophys., 4,* 17. [2] Stein M. and Hofmann A. W. (1994) *Nature, 372,* 63–68. [3] Stein M. and Goldstein S. (1996) *Nature, 382,* 773–778. [4] Abbott D. and Mooney W. (1995) *Rev. Geophys., 33,* 231–242. [5] Kempton P. D. et al. (1999) *J. Petrol.,* submitted.

THE DEPLETED COMPONENTS OF MANTLE PLUMES: A STRONTIUM-NEODYMIUM-LEAD-HAFNIUM STUDY OF THE NORTH ATLANTIC RIFTED MARGIN.

P. D. Kempton[1], J. G. Fitton[2], A. D. Saunders[3], G. M. Nowell[1], R. Taylor[4], and B. S. Hardarson[2], [1]Isotope Geosciences Laboratory, National Environmental Research Council, Kingsley Dunham Centre, Keyworth NG12 5GG, UK (p.kempton@nigl.nerc.ac.uk), [2]Grant Institute, University of Edinburgh, Edinburgh EH9 3JW, UK (gfitton@glg.ed.ac.uk), [3]Department of Geology, Leicester University, Leicester LE1 7RH, UK (ads@leicester.ac.uk), [4]Southampton Oceanography Centre, Southampton SO14 3ZH, UK (rex@soc.soton.ac.uk).

Introduction: Numerous studies have demonstrated that most mantle plumes are enriched in incompatible trace elements relative to MORB. However, the character of this enrichment varies from plume to plume, leading to the identification of various enriched mantle components (e.g., EM1, EM2, HIMU) [1,2]. More recently, the question has been asked whether mantle plumes also contain a depleted component that is distinct from MORB-source mantle [3–6]. In an effort to address this question, we have undertaken a geochemical and isotopic study of basalts from the North Atlantic Igneous Province (NAIP). We will show that, in combination with Nd isotopes and Zr-Nb-Y trace-element systematics, Hf isotopes provide a robust means by which to discriminate the various mantle components. This in turn allows us to speculate on the origin and structure of the Iceland plume.

Results: New Sr-Nd-Pb-Hf data require the existence of at least four mantle components in the genesis of basalts from the NAIP: (1) one (or more likely a small range of) enriched component(s) within the Iceland plume, (2) a depleted component within the Iceland plume, (3) a depleted sheath surrounding the plume, and (4) shallow N-MORB source mantle. These components have been available since the major phase of igneous activity associated with plume head impact during Paleogene times.

In ε_{Nd} vs. ε_{Hf}, samples from Iceland, DSDP Leg 49, ODP Legs 152 and 163 (southeast Greenland margin), the Reykjanes Ridge, Kolbeinsey Ridge, and DSDP Leg 38 (Site 348) define fields that are oblique to the main ocean island basalt array and extend toward a component with higher ^{176}Hf/^{177}Hf than the N-MORB source available prior to plume impact, as indicated by the compositions of Cretaceous basalts from the Goban Spur (~95 Ma). Aside from Goban Spur, only basalts from Hatton Bank (DSDP Leg 81) lie consistently within the field of N-MORB, which indicates that the compositional influence of the plume did not reach this far south and east ~55 Ma. (Note that two very high ^{176}Hf/^{177}Hf values previously reported for Iceland basalts [5] are now known to be in error because of inadequate correction for REE interferences on ^{176}Hf during mass spectrometry. This indicates that in contrast to the results of [7], our first two column stages do not adequately separate ^{176}Yb and ^{176}Lu from ^{176}Hf in all cases, particularly for samples that have high Yb/Hf ratios, e.g., some depleted rocks from Iceland and mid-ocean ridges. We now use a third column pass to purify these samples.)

Thus, Hf-Nd-isotopic systematics are consistent with previous studies that indicate that shallow MORB mantle does not represent the depleted component within the Iceland plume [4,8,9]. They also indicate that the depleted component is a long-lived and intrinsic feature of the Iceland plume, generated during an ancient melting event in which a mineral (such as garnet) with a high Lu/Hf was a residual phase.

Conclusions: Collectively, our data suggest a model for the Iceland plume in which a heterogeneous core, derived from the lower mantle, consists of "enriched" streaks or blobs dispersed in a more depleted matrix. A distinguishing feature of both the enriched and the depleted components is high Nb/Y for a given Zr/Y (i.e., positive ΔNb), but the enriched component has higher Sr- and Pb-isotopic ratios, combined with lower ε_{Nd} and ε_{Hf}. This heterogeneous core is surrounded by a relatively broad sheath of depleted material, similar to the depleted component of the Iceland plume in its ε_{Nd} and ε_{Hf}, but with lower ^{87}Sr/^{86}Sr, ^{208}Pb/^{204}Pb and *negative* ΔNb; this material was probably entrained from near the 670-km discontinuity when the plume stalled at the boundary between the upper and lower mantle. The plume sheath displaced more normal MORB asthenosphere (distinguished by its lower ε_{Hf} for a given ε_{Nd} or Zr/Nb ratio), which existed in the North Atlantic prior to plume impact.

Preliminary data on MORBs from near the Azores plume suggest that much of the North Atlantic may be "polluted" by material similar to the Iceland plume sheath. If correct, this may provide a general explanation for some of the compositional diversity and variations in inferred depth of melting [9] along the MAR in the North Atlantic.

References: [1] Zindler and Hart (1986) *Annu. Rev. Earth Planet. Sci., 14,* 493–571. [2] Hart et al. (1992) *Science, 256,* 517. [3] Kerr et al. (1995) *Geology, 23,* 843–846. [4] Fitton et al. (1997) *EPSL, 153,* 197–208. [5] Kempton et al. (1998) *Mineral. Mag., 62A,* 759–760. [6] Nowell et al. (1998) *Chem. Geol., 149,* 211–233. [7] Blichert-Toft and Albarède (1997) *EPSL, 148,* 243–258. [8] Thirlwall (1995) *J. Geol. Soc. London, 152,* 991–996. [9] Hards et al. (1995) *J. Geol. Soc. London, 152,* 1003–1009.

HALOGEN AND NOBLE GAS EVIDENCE FOR THE AGE AND ORIGIN OF MINERALIZING FLUIDS IN COPPER-PORPHRY DEPOSITS.

M. Kendrick, R. Burgess, R. Pattrick, and G. Turner, Department of Earth Sciences, University of Manchester, Oxford Road, Manchester M13 9PL, UK.

Introduction: Noble gases and halogens are proving to be an excellent aid to understanding the sources and interactions of ore-forming fluids and the timing of mineralization [1–3]. This approach utilizes the ability of noble gases to distinguish in a quantitative way the contribution of crust, mantle, and hydrosphere to these hydrothermal fluids. Because the halogens may be strongly fractionated by processes such as evaporation and organic activity, I/Cl and Br/Cl ratios can provide a fingerprint of the sources of fluids and mixing processes in the Earth's crust.

Methods: We have analyzed fluid inclusion-bearing quartz samples from Laramide copper porphyries (75–55 Ma) in southern Arizona (Silverbell, Ray, Mission, Pinto Valley, and Globe Miami) and the Bingham Canyon deposit (39 Ma) in Utah. Crushing, UV laser probe, and stepped-heating gas extraction techniques have been used for simultaneous determination of neutron-produced noble gas isotopes formed from Cl, Br, I, and K, and natural isotopes of Ar, Kr, and Xe.

Halogens: Data obtained from fluid inclusion-bearing quartz from Bingham Canyon illustrate the complimentary nature of the different extraction techniques (Fig. 1). During crushing and stepped heating there is a progressive change in Br/Cl and I/Cl toward the bulk value (arrows in Fig. 1a), which we believe reflects preferential release from fluid during crushing and from solid (halite crystals) during stepped heating. The difference in halogen ratios is explained by the low partition coefficient of the large halide ions, Br and I, in halite crystals, which leads to their enrichment in the fluid. Laser extraction of fluid inclusions, however, analyzes fluid and solid phases together, and these results provide evidence of fluids having a range in Br/Cl between 0.60 and 1.51 × 10^{-3} molar (M) (Fig. 1b, dotted lines). With the exception of Silverbell, bulk Br/Cl values for the deposits are between 0.6 and 1.4 × 10^{-3} (Silverbell 1.3–1.7 × 10^{-3} M), and I/Cl are 0.1–0.4 × 10^{-5} M (Silverbell 0.8–1.2 × 10^{-5} M).

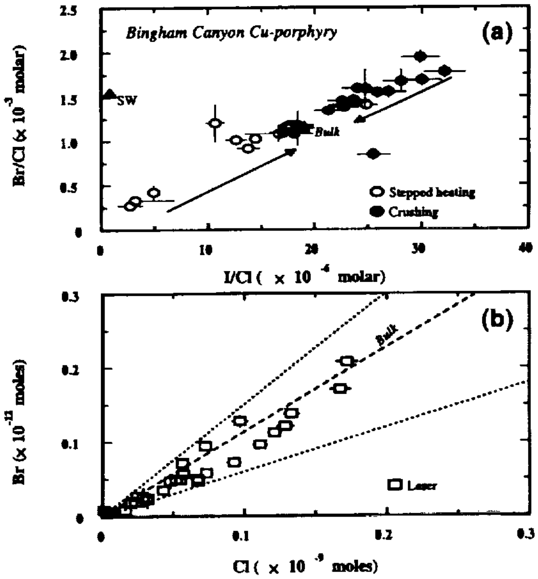

Fig. 1. Halogens in fluid inclusion-bearing quartz from Bingham Canyon. **(a)** Crushing and stepped heating, and **(b)** laser microprobe extraction of fluid inclusions.

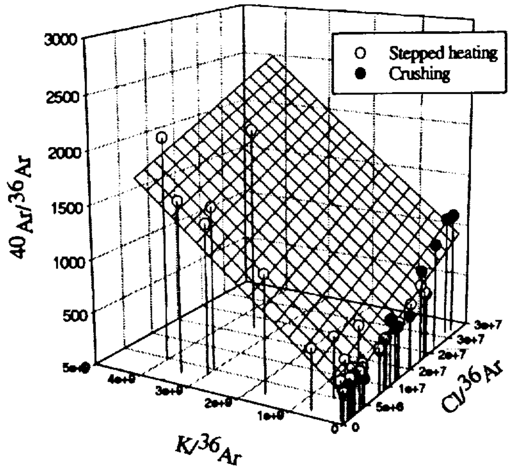

Fig. 2. Argon-potassium-chlorine diagram for stepped heating and crushing fluid includsion-bearing quartz from Silverbell.

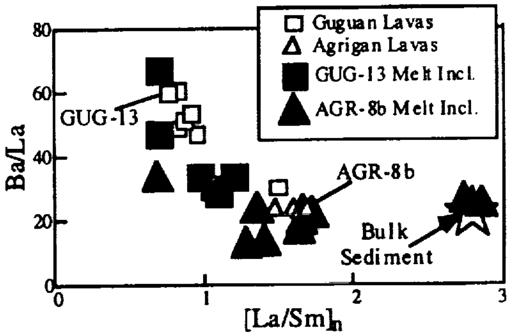

Fig. 1. Barium/lanthanum vs. [La/Sm]$_n$ for lavas from Agrigan and Guguan and olivine-hosted melt inclusions from sample AGR-8b (Agrigan) and GUG-13 (Guguan). Although melt inclusions show a large range in composition compared to the bulk lavas, the general characteristics of the host lavas are apparent in the melt inclusion populations (e.g., high [La/Sm]$_n$ and low Ba/La for Agrigan and low [La/Sm]$_n$ and high Ba/La for Guguan). Data for lava samples and bulk subducted sediment are from [7].

Age Constraints: Dating of mineralization suffers from the problem of excess ^{40}Ar, but this can be overcome using correlations with ^{36}Ar, K, and Cl, and by taking advantage of the selective nature of the extraction techniques. Using data from Silverbell as an example (Fig. 2), it can be seen that during crushing excess ^{40}Ar is released, which correlates with Cl (fluid). In contrast, ^{40}Ar liberated during stepped heating is dominantly radiogenic and correlates with the release of K from a solid phase. A plane fit to the data in Fig. 2 gives an age of 56 ± 2 Ma for Silverbell. Other deposit ages are Ray 65 ± 2 Ma; Globe Miami 62 ± 3 Ma, and Pinto Valley 63 ± 8 Ma.

References: [1] Kelley S. P. et al. (1986) *EPSL, 79,* 303–318. [2] Bohlke J. K. and Irwin J. J. (1992) *GCA, 56,* 203–225. [3] Turner G. and Bannon M. P. (1992) *GCA, 56,* 227–243.

MELT INCLUSIONS IN SUBDUCTION-RELATED BASALTS: AN EXAMPLE FROM THE MARIANA ARC.

A. J. R. Kent[1] and T. Elliot[2], [1]Mail Code L-202, Lawrence Livermore National Laboratory, Livermore CA 94551, USA (kent5@llnl.gov), [2]Faculteit der Aardwetenschappen, Vrie Universiteit, Amsterdam, The Netherlands (ellt@mailhost.geo.vu.nl).

Introduction: In this abstract we will discuss the results of a study of melt inclusions hosted within olivine and clinopyroxene phenocrysts from recent lavas from the Mariana arc.

Melt inclusions in basaltic rocks offer a unique means to investigate the formation and origin of mantle-derived melts [1–6]. In many environments melt inclusions from phenocrysts preserve a wide range of magmatic compositions, many of which are not represented in the suites of lavas or intrusive rocks that comprise the end-products of magmatic activity. Melt inclusions provide information about a number of different magmatic processes; in MORB compositional variations between melt inclusions provide insight into melting processes and interactions between ascending melts and the surrounding mantle [1,2]. In OIB and other plume-related rocks, melt inclusions may provide information on the diversity of chemical and isotopic compositions present within a given magmatic source region [3,4].

Studies of melt inclusions are also useful in investigating mantle-derived rocks from convergent margins [5,6]. In particular the ability of melt inclusions to preserve the diversity of chemical components present in a magmatic source region provides a means to enhance identification and characterization of components from the depleted mantle and slab-derived melts and fluids that contribute to magmatism in a given arc system.

Homogenized melt inclusions from olivine and clinopyroxene phenocrysts from lava samples from Agrigan and Guguan islands in the Mariana arc were analyzed by electron microprobe for major elements and Cl, and by ion microprobe for a range of trace elements. Lavas from these islands represent two compositional end members [7]. Agrigan lavas contain a significant subducted sediment component, apparent as unradiogenic ^{143}Nd/^{144}Nd, high [La/Sm]$_n$ ratios (Fig. 1) and negative Ce anomalies, while Guguan lavas have excess ^{238}U/^{230}Th and high Ba/La and Ba/Nb ratios (Fig. 1), thought to represent addition of an aqueous fluid derived from the down-going slab.

Results and Discussion: The compositions of melt inclusions from single samples from Agrigan and Guguan show substantially more compositional variation than that evident between lavas from these islands. This is evident in both major- and trace-element concentrations and in the ratios of incompatible elements. However, inclusions from Agrigan and Guguan also exhibit features typical of lavas from these islands. For example, inclusions from AGR-8b have large Nb depletions, marked negative Ce anomalies, low Ba/Nb and Ba/La, and high [La/Sm]$_n$ (Fig. 1), whereas those from GUG-13 have negligible Ce anomalies, high Ba/Nb and Ba/La, and lower [La/Sm]$_n$ (Fig. 1).

The compositions of melt inclusions also provide insight into the variety of magmatic sources for Agrigan and Guguan lavas. On the plot of Ba/La vs. [La/Sm]$_n$ given in Fig. 1, inclusions from Agrigan form an array between the bulk sediment value and lower [La/Sm]$_n$, suggesting that the inclusions represent melts that contain variable degrees of a subducted sediment component. In contrast, inclusions from Guguan form an array between high Ba/Nb, and lower Ba/Nb and higher [La/Sm]$_n$. High Ba/Nb is considered to be a signature of a slab-derived fluid component [7], suggesting that Guguan inclusions represent melts that contain variable degrees of a slab-derived fluid.

Acknowledgments: Work performed under the auspices of DOE contract W-7405-Eng.

References: [1] Sobolev A. V. and Shimizu N. (1993) *Nature, 363,* 151–154. [2] Shimizu N. (1998) *Phys. Earth Planet. Sci, 107,* 183–201. [3] Kent A. J. R. et al. (1998) *Mineral. Mag., 62A,* 765–766. [4] Saal A. et al. (1998) *Science, 282,* 481–484. [5] Sisson T. W. and Bronto S. (1998) *Nature, 391,* 883–886. [6] Kamenetsky D. et. al. (1998) *EPSL, 151,* 205–223. [7] Elliot T. et al. (1997) *JGR, 102,* 14991–15019.

MERCURY SORPTION TO IRON- AND ALUMINUM-(HYDR)OXIDES AND SPECIATION IN NATURAL SAMPLES.

C. S. Kim[1], G. E. Brown Jr.[1], and J. J. Rytuba[2], [1]Department of Geological and Environmental Sciences, Building 320, Room 118, Stanford University, Stanford CA 94305-2115, USA (chriskim@pangea.stanford.edu), [2]Mail Stop 901, U.S. Geological Survey, 345 Middlefield Road, Menlo Park CA 94025, USA.

Introduction: Mercury ore deposits are located extensively throughout the California Coast Range, occurring either as near-surface hot-spring deposits or coincident with silica-carbonate alteration rock [1]. Weathering of

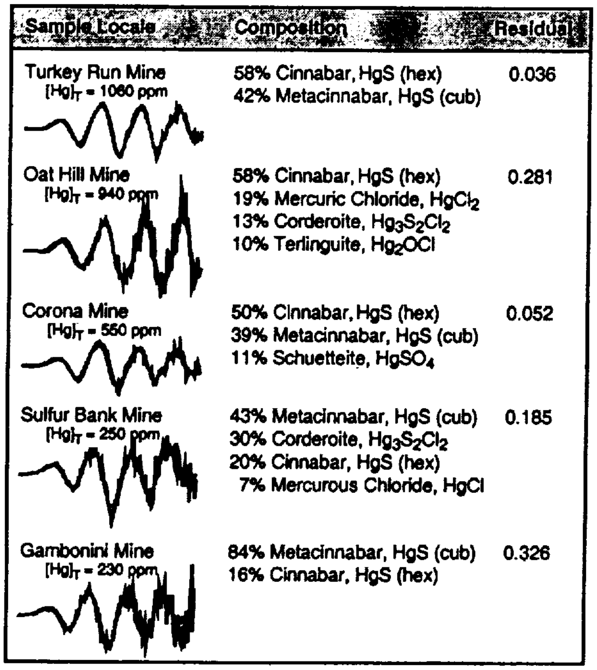

Sample Locale	Composition	Residual
Turkey Run Mine $[Hg]_T$ = 1060 ppm	58% Cinnabar, HgS (hex) 42% Metacinnabar, HgS (cub)	0.036
Oat Hill Mine $[Hg]_T$ = 940 ppm	58% Cinnabar, HgS (hex) 19% Mercuric Chloride, $HgCl_2$ 13% Corderoite, $Hg_3S_2Cl_2$ 10% Terlinguite, Hg_2OCl	0.281
Corona Mine $[Hg]_T$ = 550 ppm	50% Cinnabar, HgS (hex) 39% Metacinnabar, HgS (cub) 11% Schuetteite, $HgSO_4$	0.052
Sulfur Bank Mine $[Hg]_T$ = 250 ppm	43% Metacinnabar, HgS (cub) 30% Corderoite, $Hg_3S_2Cl_2$ 20% Cinnabar, HgS (hex) 7% Mercurous Chloride, HgCl	0.185
Gambonini Mine $[Hg]_T$ = 230 ppm	84% Metacinnabar, HgS (cub) 16% Cinnabar, HgS (hex)	0.326

Fig. 1. Results of linear combination fitting of the contaminated calcines, compositional results, and residual values corresponding to the quality of the fit.

waste piles generated from past mining of the Hg ore in these areas can result in the release of Hg to surface-water supplies. As Hg travels downstream, it may become associated with streambed sediments either through sorption to solid particles or by incorporation into precipitates, effectively sequestering Hg back into a solid phase. Both processes have direct implications for the mobility of Hg in the environment and therefore its potential toxicity to living organisms. The objectives of this study are (1) to demonstrate the feasibility of extended X-ray absorption fine structure (EXAFS) spectroscopy in directly characterizing the speciation of Hg in calcine piles, and (2) to investigate the sorption processes occurring between Hg and various synthetic and natural substrates.

Results/Discussion: The speciation of Hg in various calcines was achieved by generating linear least-square fits that matched EXAFS spectra collected from the calcines against a database of EXAFS spectra from known Hg minerals (Fig. 1). The results indicate that most Hg is present in the sulfide form but that secondary, more soluble Hg phases are also present and may represent a significant source of soluble Hg. EXAFS analysis also indicates the presence of Hg-Cl phases in "hot-spring" calcines, where chloride levels are known to be elevated [2], but not in "silica-carbonate" calcines. Such direct knowledge of the speciation in Hg-bearing wastes can aid in the prioritization of contaminated sites that are in most immediate need of remediation.

Mercury(II) was found to sorb strongly to a synthetic goethite (α-FeOOH) substrate as reported in [3] and to an amorphous Fe precipitate from the Knoxville Mine, California. EXAFS analysis of the sorption products (Fig. 2) indicates the formation of bidentate innersphere complexes in both cases. In contrast, uptake measurements as a function of pH indicate weak sorption of Hg(II) on synthetic γ-Al_2O_3. However, the presence of second-neighbor features in the Fourier transform of the EXAFS spectrum (not shown) suggests the formation of a precipitate, perhaps a mixed Al/Hg coprecipitate. Such mixed-metal coprecipitates have been observed in other systems [4,5]. The sorption and precipitation of Hg(II) in natural systems may be significant processes by which Hg is removed from the aqueous phase and concentrated into sediments, thus reducing its potential bioavailability in the environment.

References: [1] Rytuba J. J. (1996) *Geology and Ore Deposits of the American Cordillera Symposium Proceedings*, Geological Society of Nevada. [2] Rytuba J. J. (1986) *USGS Bull. 1693*, 178–179. [3] Barrow N. J. and Cox V. C. (1992) *J. Soil Sci., 43*, 295–304. [4] Towle S. N. et al. (1997) *J. Coll. Intl. Sci., 187*, 62–82. [5] Scheidegger A. M. et al. (1997) *J. Coll. Intl. Sci., 186*, 118–128.

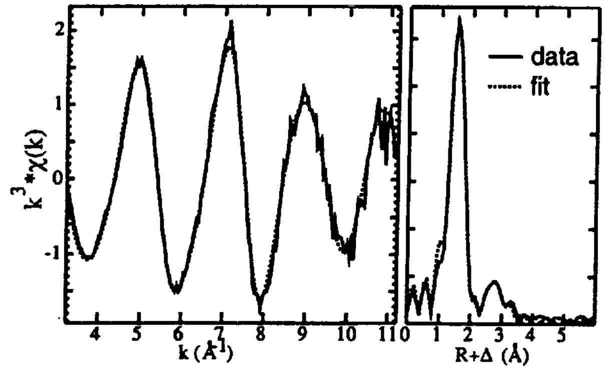

Fig. 2. EXAFS spectrum and Fourier transform of Hg sorbed to goethite. The fit indicates that the second shell consists of Fe atoms, consistent with innersphere Hg adsorption.

MAJOR- AND TRACE-ELEMENT GEOCHEMISTRY OF SILICEOUS SHALE, MIDDLE MIOCENE ONNAGAWA FORMATION (6–13 Ma), JAPAN: CAUSES FOR VARIATIONS IN PRIMARY PRODUCTIVITY AND REDOX.

S. Kimura and N. Shikazono, Department of Applied Chemistry, Keio University, 3-14-1, Hiyoshi, Kouhoku-ku, Yokohama 223-0061, Japan (sikazono@applc.keio.ac.jp).

Middle Miocene organic C-rich siliceous shale are common in northeast Japan. These sediments, known as potential source rock for oil and natural gas in northern Honshu, might have been formed related to the combination of local as well as global geologic and climate changes thorough the middle Miocene age. To elucidate the paleoceanographical conditions of the Sea of Japan in the middle Miocene, particularly the primary productivity and redox state, and causes for their variations, we examined mineralogical and geochemical studies on 37 rock samples, collected from early Miocene to Pliocene sedimentary rock units, Oga peninsula, northeast Japan.

The studied sedimentary rocks are Nishikurosawa (Early Miocene, massive dark greenish shale, 12 samples), Onnagawa (middle to late Miocene, banded black colored siliceous shale, 20 samples) and Funakawa Formation (Pliocene, massive light grayish shale, 7 samples) in ascending order.

The siliceous shale is mainly composed of quartz; minor amounts of feldspar, pyrite, illite, smectite, and kaolinite are found. In the siliceous shale, illite is dominant among clay minerals, compared to the shale of Nishikurosawa and Funakawa Formation. The clay minerals in these sediments are thought to be mainly detritus in origin (not diagenetic in origin). Mineralogical study of Quaternaly Sea of Japan sediments shows that most illite is not back-arc in origin. The difference in clay minerals suggests that detritus material in the siliceous shale was probably derived mostly from the continent of China.

Barium/aluminum (proxy for primary productivity), Mo/Al, Ni/Al, and U/Al (proxy for redox state) ratios and organic C contents of the siliceous shale are generally higher than those of the shale of Nishikurosawa and Funakawa Formation. These ratios of the siliceous shale are variable in their stratigraphic positions. Siliceous shale in the (1) lower (~12.5 Ma), (2) middle (~10–11 Ma), and (3) upper (~7–8 Ma) horizon has high Ba/Al, P/Al, Mo/Al, Ni/Al, and U/Al ratios. Magnetic susceptibility value and illite contents (detritus contents) are also high in (2) and (3) horizons. These geochemical variations imply that high primary productivity and reducing conditions of the Sea of Japan in (2) and (3) horizons were caused by upwelling of deep seawater, influenced by strong wind or increase of river flux from China. They are related to sudden uplift of Tibet-Himalaya.

STRUCTURE AND DYNAMICS OF SURFACE AND INTERLAYER SPECIES: A COMBINED NUCLEAR MAGNETIC RESONANCE AND MOLECULAR MODELING PERSPECTIVE.

R. J. Kirkpatrick[1], P. Yu[2], X. Hou[1], A. Kalinichev[1], and R. T. Cygan[3], [1]Department of Geology, University of Illinois at Urbana-Champaign, Urbana IL 61801, USA (kirkpat@uiuc.edu), [2]Department of Materials Science and Engineering, University of Illinois at Urbana-Champaign, Urbana IL 61801, USA, [3]Geochemistry Department, Sandia National Laboratories, Albuquerque NM 87185-0750, USA.

Introduction: The combination of nuclear magnetic resonance (NMR) spectroscopy and molecular modeling methods allows for the determination of a wide variety of structural and dynamical characteristics of geochemically significant cationic and anionic surface and interlayer species in and on a wide variety of minerals. Such surface and interlayer species are difficult to observe, because the underlying particles are often small, the local structures are disordered and nonrepetitive, and the dynamics often occur at quite low frequencies. Understanding these processes is essential to a comprehensive understanding of sorption and exchange, surface precipitation, aqueous solute transport in rocks, impurity incorporation in growing crystals, and the mechanisms of mineral growth and dissolution.

Nuclear Magnetic Resonance Spectroscopy: NMR is the only direct, simultaneous probe of local, molecular-scale structure and dynamical information in the 1-10^8-Hz frequency range. Structural information can be derived from the chemical shift, chemical shift anisotropy and quadrupole coupling constant and asymmetry parameter. Dynamical information in the ~1-10^5-Hz range comes from the T_2 relaxation rate and lineshape analysis, and in the 10^7–10^8-Hz range from the T_1 relaxation rate. Many processes relevant to chemical reactions occur at these frequencies, and thus NMR often provides unique and significant information about them.

Although the concentrations of the surface and exchanged species are often quite low, the sensitivity of modern high-field NMR spectrometers is high enough to allow not only for the acquisition of single room-temperature spectra but also variable temperature T_1 and T_2 values. Nuclides that can be readily investigated and that commonly occur in sorbed or exchanged species include ^{1}H, ^{2}H, ^{6,7}Li, ^{11}B, ^{13}C, ^{15}N, ^{17}O, ^{19}F, ^{23}Na, ^{27}Al, ^{29}Si, ^{35}Cl, ^{31}P, ^{77}Se, and ^{133}Cs. Many others remain to be more thoroughly investigated. The instrumentation needed for this work is a standard solid-state NMR spectrometer, although variable temperature capabilities are often needed because of the temperature-dependent surface and interlayer dynamics.

Molecular Modeling: Molecular modeling methods including energy minimization and molecular dynamics calculations provide significant insight into the structural interpretations based on NMR and other spectroscopic techniques, and can substantially improve molecular scale understanding of the dynamical information obtained via NMR. This is true even though the characteristic timescales of the experiments and calculations are different. Proper incorporation of water and the dynamics of the underlying crystal structure are key to these calculations and have been a focus of our research. These calculations also provide important connections to vibrational spectroscopy and to the details of high-frequency processes.

Examples: Successful examples of combining NMR and molecular modeling methods include the use of ^{23}Na and ^{133}Cs NMR and energy minimization and sorption map calculations to understand Na and Cs sorption on illite, and the use of ^{35}Cl NMR and molecular-dynamics calculations to understand surface and interlayer Cl^- in mixed-metal layered hydroxides. For surface Na and Cs on illite, the NMR results suggest that Cs occurs as both innersphere and outersphere complexes and Na as outersphere complexes, and that the illite surface prefers Cs to Na. Energy calculations and three-dimensional sorption-energy maps confirm these interpretations and indicate that sorption on broken edges is greatly preferred to sorption on the basal surfaces. The lowest energy sorption sites occur at the level of the interlayer space associated with tetrahedral sites containing Al, providing a clear explanation for the origin of the variation in ^{133}Cs NMR chemical shift with decreasing extent of surface exchange. For Cl in mixed-metal layered hydroxides, NMR shows a dynamical order-disorder phase transition associated with thermally induced motion of the interlayer species. At the transition, the interlayer Cl^- becomes mobile and its symmetry changes from triaxial to uniaxial. With increasing temperature above the transition, site hopping decreases the time-averaged ^{35}Cl electric field gradient. Molecular-dynamics simulations show the significance of H-bonding in controlling the Cl^- structural environment and demonstrate how the orientational disorder and high-frequency librational dynamics of the interlayer water molecules lead to the time-averaged uniaxial Cl^- symmetry, even though the instantaneous symmetry is triaxial.

CONTINENTAL GROWTH AND ENVIRONMENTS OF ARCHEAN CONTINENTAL CRUST: AN EXAMPLE OF THE COASTAL PILBARA TERRAIN, WESTERN AUSTRALIA.

S. Kiyokawa[1], A. Taira[2], T. Byrne[3], and Y. Sano[4], [1]Department of Geology, National Science Museum, 3-23-1 Hyakuninn-cho, Shinjyuku-ku Tokyo 169-0073, Japan (kiyokawa@kahaku.go.jp), [2]ORI University of Tokyo, 1-15-1 Minamidai Nakano-ku, Tokyo 164-0014, Japan (ataira@ori.u-tokyo.ac.jp), [3]Department of Geology and Geophysics, University of Connecticut 354 Mansfield Road, Storrs CT 06269, USA (byrne@geol.uconn.edu), Department of Earth Science, Hiroshima University, 1-2-1 Kagamiyama Higashihiroshima 739-8512, Japan.

Introduction: The Archean continental growth mechanism is very important in determining the Earth crustal evolution. Late Archean, continental evolution has been changed to Wilson cycle system that is identified as the formation of supercontinent and its fragmented environment. Many people have noted that the early and middle Archean microcontinent formed a piece of a jigsaw puzzle, which is the basic crustal material of continents [e.g., 1,2].

Kiyokawa and Taira [3] suggested that the coastal Pilbara terrane originated as an immature oceanic island arc setting. The tectonic evolution of the Pilbara Craton, especially at middle Archean, is not well recognized. Here we provide detailed structural analysis and reconstruct the tectonic history of the 3.2-Ga greenstone-granite terrane, the coastal Pilbara terrane. We considered that this area provides the most appropriate tectonic mechanism for the evolution of middle Archean granitoid-greenstone terranes.

Regional Geology: The Pilbara Craton of Western Australia is one of the best preserved Archean greenstone-granite terrains in the world. Three lithologic parts are identified as follows: greenstone terrane, which contains the volcani-sedimentary sequence, granite batholith, and strike-slip sedimentary basin [4]. Recent U-Pb zircon age dating suggests, the greenstone-granite terrane of the Pilbara craton grows from east to west and ranges from 3.5 to 3.0 Ga [5]. The coastal Pilbara terrane, which is westernmost of the Pilbara craton, is preserved the early continental growth evidence to recognized its growth tectonics at 3.0–3.2 Ga.

Lithology: The coastal Pilbara terrane is composed of two lithotectonic units: the Karratha and Cleaverville-Roebourne Supercomplexes. The Karratha supercomplex, which lies tectonically beneath the Cleaverville-Roebourne supercomplex, consists of 3265-Ma granitic batholiths and metamorphosed terrigenous sediments, which is quite similar to continental shelf facies. The Cleaverville-Roebourne Supercomplex consists of an imbricated ophiolite-like crustal section that includes a 3200-Ma felsic bimodal volcanic-chemical sedimentary sequence, metabasite, low-K granitic gneiss and a peridotite [3]. The cyclic bimodal volcano sedimentary sequence suggests that the greenstone complex identified as the island arc setting environment. The 3020-Ma felsic porphyry and granite intrude this terrane.

Structural Evidence: Detailed structural analyses suggest that the Cleaverville-Roebourne Supercomplex records at least three deformation events (Fig. 1). D_1 is characterized by a top-to-the northwest thrusting occurred sometime during 3020–3200 Ma. After 3020-Ma felsic magmatism, D_2 is characterized by regional-scale left-lateral strike-slip faulting (~2950–3020 Ma). D_2 appears to have affected the entire Pilbara Craton and is interpreted to be related to craton-scale deformation. D_3 is represented by localized right-lateral Sholl shear zone which truncates both D_1 and D_2 structures.

Tectonic Environment: We propose that the coastal Pilbara terrane evolved collision between an immature island arc - an old Pilbara continent. The 3020-Ma granite intrusion might be related the postcollision volcanism.

After the D_1 collision event, D_2 represents intraplate crustal scale deformation of the stabilizing Pilbara Craton. Regional strike-slip deformations have been reported elsewhere in the Pilbara terrane; Mulgandinnah shear zone [6], the Lalla Rookh, and the Whim Creek belts [7]. These regional-scale, strike-slip events resulted in the formation of oblong terranes 50–100 km wide

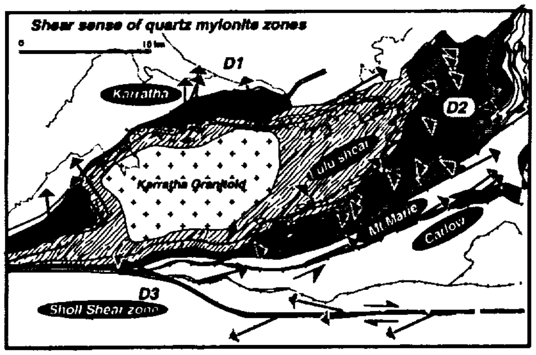

Fig. 1.

and more than 500 km long. The size of these terranes might be related to the strength or thickness of the Archean craton.

Finally, D_3 is more localized strike-slip deformation than that of the regional-scale D_2. This change of deformation characteristics from regional deformation to localized deformation within a terrane might suggest a change in strength of the continent. The change from D_2 to D_3 may therefore suggest a timing of continental stabilization (2.8–2.9 Ga)

In this way, the coastal Pilbara terrane has been recognized three tectonic stages: (1) arc-continent collision, (2) regional crustal scale strike-slip deformation, and (3) final localized strike-slip stages. After these tectonic series, the Mt. Bruce Supergroup unconformably overlay this craton at 2.77 Ga. The three relationships are one example of a crustal formation and stabilization at middle Archean Craton.

References: [1] de Wit M. J. et al. (1992) *Nature, 357,* 553–562. [2] M. J. de Wit and L. D. Ashwal, eds. (1997) *Greenstone Belt.* [3] Kiyokawa S. and Taira A. (1998) *Precambrian Res., 88,* 109–142. [4] Krapez B. and Barley M. E. (1987) *Geol. Mag., 124,* 555–567. [5] Nelson D. R. (1998) *GSWA, Record 1998/2,* 242. [6] Kusky T. M. and Vearncombe J. R. (1997) in *Greenstone Belt* (M. J. de Wit and L. D. Ashwal, eds.), pp. 91–124. [7] Zegers T. E. et al. (1998) *Precambrian Res., 88,* 233–247. [8] Krapez B. (1993) *Precambrian Res., 60,* 1–45.

HORIZONTAL DISTRIBUTIONS OF INORGANIC AND ORGANIC SULFUR IN ESTUARINE SURFACE SEDIMENTS FROM TOYAMA BAY, JAPAN.

Y. Kiyosu, I. Yamaguchi, and K. Katsuyama, Department of Environmental Biology and Chemistry, Toyama University, Toyama 930-8555, Japan (kiyosu@sci.toyama-u.ac.jp).

Recent data from surface sediments indicate that reaction rates for formation of organic S species are slower than those of inorganic S such as pyrite [e.g., 1,2]. Furthermore, delayed organic S species are suggested by enriched ^{34}S of humic and fulvic acid-S relative to coexisting pyrite. However, very few data of S species have been reported in estuarine sediments [2,3]. In this study, data are presented for the horizontal abundance and isotopic ratio of dissolved sulfate and sulfide, inorganic, and organic S from Zinzu and Oyabe estuarine surface sediments in Toyama Bay, Japan.

Results and Discussion: The concentration of Zinzu dissolved sulfate showing a near than that of seawater sulfate (28 mM) is horizonatally constant, whereas the value of Oyabe, being lower than that of seawater sulfate, increases toward its estuary. In Zinzu samples, δ^{34}S values of porewater sulfate show a slight enrichment in ^{34}S relative to seawater sulfate whereas the isotopic ratio of Oyabe samples ranges from 25‰ to 40‰, indicating that the rate of sulfate reduction and the removal of S from porewater are fast. The contents of acid-volatile S (AVS) in Zinzu and Oyabe sediment samples are lower than those of pyrite S in Oyabe.

The inorganic S (AVS, pyrite) content in Zinzu is lower than that in Oyabe. The δ^{34}S values of pyrite range from –21‰ to –7.7‰ in Zinzu and –18.7‰ to +2.0‰ in Oyabe respectively, and decrease with increasing pyrite content, indicating the proceeding process of sulfate reduction in sediments. The abundance of fulvic-acid S slightly exceeds that of AVS, and increases at upriver and estuarine points, although its fraction is smaller than that of pyrite. The values of δ^{34}S for fulvic-acid S are –19.2‰ to –9.4‰ in Zinzu and –12.3‰ to +0.5‰ in Oyabe respectively, and higher than those of pyrite S. The content of humic-acid S represents only a small fraction of total S. The kinetic isotopic effects during sulfate reduction obtained from the δ^{34}S values of pyrite are ~40‰ in Zinzu and ~30‰ in Oyabe. Since industrial contamination is strongest in Oyabe, active sulfate reduction occurred in enriched organic matter in river. Thus, it would be expected that isotopic fractionation during sulfate reduction is small.

References: [1] Kohnen M. E. T. et al. (1990) *ASC Symp. Ser., 429,* 444–485. [2] Brüchert V. and Pratt L. M. (1996) *GCA, 60,* 2325–2332. [3] Brüchert V. (1998) *GCA, 62,* 1567–1586.

OXYGEN-ISOTOPIC ANALYSES OF DIAGENETIC CHERTS AND THE CLIMATIC TEMPERATURE HISTORY OF THE EARTH.

L. P. Knauth, Department of Geology, Box 871404, Arizona State University, Tempe AZ 85287-1404, USA (knauth@asu.edu).

Figure 1 gives δ^{18}O analyses of over 1000 early diagenetic cherts over geologic time. Most of the samples are replacement cherts that display field and/or petrographic evidence of precompaction silicification and/or lithification within meters of the sediment/water interface. Exceptions are several Tertiary and Devonian bedded chert suites that include postcompaction conversion of preexisting opaline phases to quartz.

At any given geologic time, δ^{18}O of these cherts varies over a range of ~6–10‰. For bedded cherts, this variation is related to depth of burial; cherts that form at deeper burial temperatures have lower δ^{18}O. For the more common replacement cherts, the variation is related primarily to the amount of low-^{18}O meteoric water involved in the silicification process. These cherts form in hydrodynamically active coastal groundwaters that are a mixture of meteoric and marine pore fluids [1]. Cherts with lower δ^{18}O values formed in fluids that were primarily meteoric. Silicification usually occurs during initial stabilization of carbonate when aragonite and high-Mg calcite are replaced with low-Mg calcite and dolomite. Silicification is less well understood in Precambrian carbonates, but field and petrographic evidence suggests little difference in the timing and sedimentologic setting of silicification. Cherts in Archean strata are even more problematic, but nearly all are examples of precompaction replacement of carbonates, volcaniclastics, and possibly evaporites. Initial silicification for the overwhelming majority of the samples in Fig. 1 thus occurred during shallow burial at temperatures equal to that of any overlying water mass or at the ambient climatic temperature.

The 6–10‰ range of δ^{18}O values for early diagenetic cherts is similar at any given time, but the range shifts to dramatically lower values going back in time. Archean cherts are ~10‰ lower in δ^{18}O relative to their Phanerozoic counterparts. The change with time is a huge isotope effect and must be related either to higher past climatic temperatures, lower δ^{18}O of the early hydrosphere, wholesale lowering of δ^{18}O by alteration of the record during late diagenesis and/or metamorphism, or change in style of silicification in which all Archean and low ^{18}O cherts are hydrothermal deposits.

δ^{18}O of the oceans appears to be held within ±2‰ of the present value by interaction with mid-ocean ridge basalts [2,3] and is now the least likely explanation for the secular variation. δ^{18}O does not correlate at all with metamorphic grade of the host rocks, and no metamorphic event could reasonably produce the 6–12‰ values observed for some microfossil-bearing late Archean examples. While metamorphism may locally lower δ^{18}O by several per mil, this is not a satisfactory explanation for the general secular trend. Some coarse-grained cherts cross-cutting Archean volcanic rocks are clearly hydrothermal and have δ^{18}O values in the range 12–15. Hydrothermal fluids can produce the low ^{18}O values observed in the Archean, but most of the samples in the figure are from microcrystalline stratiform cherts displaying no field evidence that they formed around hydrothermal vents. Archean strata are silicified on a scale unknown since. The sea floor today is not massively silicified around vents and spreading centers. Suggestions that widespread Archean silicification is related to hydrothermal circulation near intrusions is not supported by modern analogs or the geologic setting of most examples.

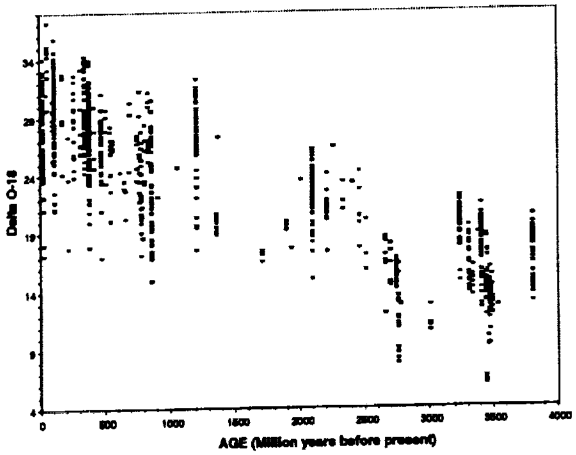

Fig. 1.

The data are most easily explained in terms of climatic temperatures that were ~40°–50°C warmer in the Archean and declined to modern values over geologic time. The smaller isotopic fractionation between quartz and water at higher temperatures can readily account for the data shown. In essence, waters on the early Earth constituted an open hydrothermal system in which sediments were readily silicified yielding $\delta^{18}O$ values as shown. The extremely low ^{18}O values for the upper Archean examples are for microfossil-rich cherts that probably formed in nonmarine environments, consistent with sedimentologic interpretations. Cherts that demonstrably formed during the narrow time intervals of the Precambrian glaciations are not known, but analyses of any such samples could provide a useful test of the climatic temperature interpretation.

An intriguing possibility is that the inferred temperature decline with time is related to a gradual draw-down of atmospheric CO_2. If so, the interpretation suggests that the recent spate of ice ages is a result of an Earth that has cooled down so much that glaciation is more likely and that the Earth is in danger of freezing over for good. Burning of fossil fuels could be the saving grace.

References: [1] Knauth L. P. (1994) *Rev. Mineral., 29,* 233–258. [2] Muehlenbachs K. and Clayton R. N. (1976) *JGR, 81,* 4365–4469. [3] Holmden C. and Muehlenbachs K. (1993) *Science, 259,* 1733–1736.

SALINITY HISTORY OF SEAWATER.

L. P. Knauth, Department of Geology, Box 871404, Arizona State University, Tempe AZ 85287-1404, USA (knauth@asu.edu).

Chlorine is a volatile element that probably outgassed as HCl along with H_2O early in Earth's history. Sodium was leached from rocks to make an initial ocean rich in dissolved NaCl. Precipitation of halite is the only known mechanism for removing large amounts of NaCl from the oceans. Until large-scale evaporite deposition began, the oceans would have been at their maximum salinity [1–2]. This salinity could have been twice the modern value (or even more) depending upon poorly constrained estimates of the amount of halite and basinal brine (evapoconcentrated seawater and/or dissolved halite) subsequently removed from seawater and stored in sedimentary basins [3].

Evaporite deposits are easily recycled and any salinity draw-down of the oceans requires extensive sequestration of large salt deposits within epicratonic sedimentary sequences. The salinity draw-down of the earliest oceans thus depends upon when continents formed and the rate at which giant salt deposits and brine masses accumulated. Salt deposits are widely preserved in the Phanerozoic, but the abundance falls off dramatically in successively older Precambrian strata [4]. The degree to which this decrease is due strictly to dissolution of salt with time is unknown. Over half the known salt was deposited within 100 m.y. in the upper Paleozoic. Salt deposition is clearly episodic. Precambrian "source" rocks from which huge thicknesses of salt were removed have not yet been identified. It is possible that the improbable tectonic, geographic, and climatic conditions necessary for the formation of "saline giants" did not develop until late in the Precambrian.

The issue of when long-lived cratons developed upon which salt and brine could be sequestered is continually confused with the question of the growth rate of tonalitic continental crust. Even if tonalite were completely separated from the mantle prior to 3.5 Ga, the issue is still whether large assembled cratons were present and accumulating saline giants and saline formation waters. The lack of evidence of such deposits plus the question of whether cratons could sequester saline giants during the late bombardment raises the real possibility that ocean salinity was in fact high throughout the Archean and possibly well into the mid-upper Proterozoic.

Resolution of this issue requires a better inventory of NaCl in evaporites and continental brines, a better understanding of the development and history of cratons, and more fluid inclusion measurements in possible seafloor phases. Existing fluid-inclusion data [5] can be interpreted as indicating an ocean salinity 1.7× the modern value [3], in accordance with reasonable guesses regarding the salt/brine inventory and growth rates of long-lived cratons. Such high values carry significant implications for the early evolution of life, the geochemical character of Precambrian sediments, and the relationship between dissolved O and atmospheric O levels in the Precambrian.

References: [1] Walker J. C. G. (1983) *Nature, 302,* 518–520. [2] Holland H. D. (1984) *The Chemical Evolution of the Atmosphere and Oceans,* Princeton Univ. [3] Knauth L. P. (1998) *Nature, 395,* 554–555. [4] Holser W. T. et al. (1980) *GSA Abstr. with Prog., 12,* 449. [5] DeRonde C. E. J. et al. (1997) *GCA, 61,* 4025–4042.

FRACTIONATED CRUST OF MARS AS AN ADEQUATE RESPONSE TO ITS BODY WAVE WARPING.

G. G. Kochemasov, Institute of Ore Deposits, Geology, Petrology, Mineralogy, and Geochemistry, Russian Academy of Sciences, 35 Staromonetny, Moscow 109017, Russia.

A significant compositional difference between martian lowlands and highlands was predicted two years before the Pathfinder landing [1] and then two months before this event [2]. Our confidence was based on regularities of wave planetology [3 et al.] indicating that with increasing solar distance (orbital periods) planetary bodies become tectonically "coarser grained," less spherical, and more disrupted (relief range increases), and hence must acquire higher density (compositional) differences between highland and lowland lithologies. All these regularities are consequences of elongated elliptical orbits of celestial bodies (much more pronounced in the geological past when much of body shaping occurred). They imply periodically changing orbital curvatures and body accelerations leading to standing inertia-gravity waves warping rotating bodies in four ortho- and diagonal directions. Interference of these waves leads to formation of uplifting /+/, subsiding /–/ and neutral /0, alternation of + and –/ segments, sectors and other polygonal blocks, constructing surfaces and deeper spheres of any cosmic body.

The following theorems of planetary tectonics proved by laws of wave interference are formulated: (1) Celestial bodies are dichotomic, (2) celestial bodies are sectoral, (3) celestial bodies are granular, and (4) angular momenta of different level blocks tend to be equal.

The first theorem reflects interference of fundamental waves long $2\pi R$, where R is a body radius. The second one reflects interference of the first obertone waves long πR and subsequent harmonics. The third one concerns interference of wave lengths that are proportional to orbital periods: the characteristic size formed by rounded (polygonal in details) blocks-supergranulas is, e.g., for Mercury $\pi R/16$, Venus $\pi R/6$, Earth $\pi R/4$, Mars $\pi R/2$, and asteroids $\pi R/1$. The fourth theorem demands equilibration of angular momenta of hypsometrically (tectonically) different level blocks comprising one rotating body to keep its integrity.

Angular-momenta equilibration requires light (not dense) martian continents standing high over lowlands. In the sequence Venus-Earth-Mars with *in situ* studied compositions of lowlands (Mg-basalts, tholeiites, Fe-basalts) and partially highlands [alkali basalts, andesites (on an average)?] the highest range between densities and hence compositions is expected for Mars having the highest relief range. Discovered by the alpha-proton X-ray (APX) spectrometer of the Sojourner rover andesite rocks [4] characterize the contact zone between the northern lowlands and southern highlands. Otherwise, more acidic (less dense) rocks have to be expected in the highlands themselves. Somewhat elevated K content in the Pathfinder soils, otherwise similar to the Viking soils, is due to contamination by the near continent (not an analitical error as suggested by H. Wänke, oral communication). On the whole, elevated Cl content in the martian soils is possibly due to widespread eolian contamination by wind (sand)-eroded material of highlands. Preferentially eroded soft Cl minerals, such as halite and sodalite, cannot be excluded from acid highland lithologies (syenites, granites, albitites, etc.).

References: [1] Kochemasov G. G. (1995) *LPI Tech. Rpt. 95-01,* Part 1, LPI, Houston, 63 pp. [2] Kochemasov G. G. (1997) *Annales Geophysicae, Suppl. III,* 767. [3] Kochemasov G. G. (1992) *16th Russian-American (Vernadsky-Brown) Microsymposium on Planetology,* Vernadsky Inst. (GEOKHI), 36–37. [4] Wänke H. et al. (1997) *26th Russian-American (Vernadsky-Brown) Microsymposium on Comparative Planetology,* Vernadsky Inst. (GEOKHI), 131–132.

INTRUSION STRATIFICATION AS A RESPONSE TO CHANGES IN THE EARTH'S ROTATION RATE WITH VARIOUS PERIODS.

G. G. Kochemasov, Institute of Ore Deposits, Geology, Petrology, Mineralogy, and Geochemistry, Russian Academy of Sciences, 35 Staromonetny, Moscow 109017, Russia.

Liquation, crystal differentiation, volatile action, and other mechanisms alone normally cannot adequately explain observed patterns of stratification of known layered intrusions. More or less pronounced layering is an intrinsic feature of large numbers of intrusive bodies of various compositions (and practically in all basic intrusions) and ages (from AR to Mz-Cz). A layering pattern often repeats itself in the same body in various scales (periodicity of various scales). Researchers usually referring to a gravity settling nevertheless pay main attention to the chemistry and PT conditions of various mineral phases, not to their densities. But in a rotating body as Earth, density of mineral phases composing rocks are much more important than their chemistry, as density (mass) is one of the members in the angular momentum formula (rate of rotation and radius-vector being the remaining two). Physics plays the first determinant role, and chemistry follows it. Now one could consider periodical sequences of layers in stratiform intrusions as an alternation of differing densities layers called to compensate oscillation of rotation rates with various periods and amplitudes. Certain rotation rates require formation of layers with certain densities at certain depths. Mechanisms of their formation including partial melting and magma ascent can vary, depending on local conditions.

Important density variations one observes in nature: Dufek massif — anorthosites and magnetitites; Bushveld — anorthosites and chromitites, and platiniferous reefs; Noril'sk — anorthosites and Ni-Cu-sulfides layers; Lovozero massif (Kola Peninsula) — urtites and loparite malignites, aegirinites. Layers in massifs are discrete and can have transitions between them as well as rotation rates change abruptly and more smoothly. During cooling of an intrusive a few kilometers thick (say, tens of thousands to 1 m.y.) rotation rates oscillated considerably and, combined with changing radius-vector, specially in orogens, must have influenced distribution of densities in a cooling column. These determinant factors existed during the whole geological history of Earth and are imprinted in structures of layered intrusions of various ages and compositions.

Rotation of celestial bodies is connected to their convexo-concave shape or tectonic dichotomy [1]. Body warping is a consequence of interference of standing inertia-gravity waves proceeding in four ortho- and diagonal directions. They appear in bodies in response to their movement in elliptical orbits, much more pronounced in the geological past. This implies periodically changing orbit curvatures and accelerations leading to inertia forces and producing inertia-gravity warping waves. Their interference gives uplifted, subsided and neutral segments, sectors, and other polygonal blocks composing surfaces and deeper spheres of any cosmic body. The following theorems of planetary wave tectonics are formulated [2]: (1) Celestial bodies are dichotomic, (2) celestial bodies are sectoral, (3) celestial bodies are granular, and (4) angular momenta of different level blocks tend to be equal. The first theorem reflects interference of fundamental waves long 2πR, where R is a body radius. The second one reflects interference of the first obertone waves long πR and subsequent harmonics. The third one concerns interference of wave lengths that are proportional to orbital periods: the characteristic size formed by these rounded (polygonal in details) blocks-supergranulas is for Mercury πR/16, Venus πR/6, Earth πR/4, Mars πR/2, and asteroids πR/1. The fourth theorem demands equilibration of angular momenta of hypsometrically (tectonically) differing level blocks composing one rotating body to keep its integrity. Intrusion density layering is to be considered in relation to angular momentum leveling processes.

References: [1] Kochemasov G. G. (1998) *Annales Geophysicae, Suppl. III to Vol. 16, Pt. III,* C987. [2] Kochemasov G. G. (1999) *Geophys. Res. Abstr., Vol. 1, N3,* 700.

CONSTRAINTS ON DIAGENETIC AGE DISTURBANCE: COMBINED URANIUM-PROTACTINIUM AND URANIUM-THORIUM AGES OF THE KEY LARGO FORMATION, FLORIDA KEYS, USA.

G. Koetsier, T. Elliott, and C. Fruijtier, Vrije Universiteit, Faculty of Earth Sciences, De Boelelaan 1085, 1081 HV Amsterdam, The Netherlands. (koet@geo.vu.nl; ellt@geo.vu.nl).

Reconstructing the timing of sea-level change around the last interglacial provides key constraints in determining the response of the Earth to changing solar insolation and in testing Milankovitch theory. Uranium-238-uranium-234-thorium-230 measurements provide a potentially high-resolution dating tool for this period, but unfortunately diagenesis severely impairs the accuracy of such dates for many last-interglacial samples. Moreover, diagenesis is frequently inferred for U-series nuclides in samples that otherwise appear pristine (e.g., >99% aragonite). Samples may be screened for "reliability" using initial ^{234}U/^{238}U activity ratios, (^{234}U/^{238}U)^{T}, which appear to be readily perturbed by diagenesis from closed system, seawater values of 1.15. Such a test, however, does not necessarily guarantee closed-system behavior, and more importantly, very few last-interglacial corals would pass a strigent (^{234}U/^{238}U)^{T} test. It is thus important to better understand the process of diagenesis and assess if any of the many nonclosed system samples might nevertheless provide accurate ages. An ultimate goal would be to predict the inaccuracies of perturbed samples.

With this aim in mind, we investigated ^{235}U-^{231}Pa disequilibrium in combination with ^{238}U-^{234}U-^{230}Th measurements. Closed-system samples should provide concordant ^{235}U-^{231}Pa and ^{234}U-^{230}Th [2,3]. Since the two chronometers have a somewhat different half-life (i.e., t1/2 ^{230}Th ~75 ka, t1/2 ^{231}Pa ~32 ka), but are both headed by U, the systematics of discordant samples should hopefully provide a constraint on the timing and magnitude of age perturbation in a similar manner to U-Pb zircon chronology [3]. The low concentration of Pa in corals, which is on the order of 10–1000 fg/g, however, poses an analytical challenge to determine ^{231}Pa concentrations to sufficient precision. We have developed a new method for the chemical extraction and measurement of a few hundred femtograms Pa by thermal ionization mass spectrometry (TIMS).

We have analyzed a set of last interglacial samples from the Florida Keys that are all marked by (^{234}U/^{238}U)^{T} well in excess of seawater values, 1.163–1.176 [1], and therefore show clear evidence of open-system U-series behavior. Uranium-thorium ages from the petrographically freshest samples range from 125 to 138 ka. Here we present mass spectrometric ^{231}Pa-^{235}U ages on the same samples. Five out of seven samples are discordant with ^{231}Pa-^{235}U ages ranging from 121 to 195 ka. The discordant samples show significantly older ^{231}Pa-^{235}U ages relative to ^{234}U-^{230}Th ages, i.e., samples lie above the concordia. This can be explained by recent ^{235}U loss or ^{231}Pa addition. Clearly ^{235}U loss should be mirrored by a pattern of ^{238}U loss evident in the ^{238}U-^{234}U-^{230}Th systematics. This does not appear to be the case. For example, samples with the oldest U-Th ages do not give the oldest ^{231}Pa-^{235}U ages, in the same way that samples with the most perturbed ^{234}U/^{238}U ratios do not yield the oldest Th-U ages. This implies independent addition of all three daughter nuclides, ^{234}U, ^{230}Th, and ^{231}Pa. This, sadly, greatly diminishes the potential of combined ^{238}U-^{234}U-^{230}Th and ^{235}U-^{231}Pa measurements in unraveling the alteration history of corals. The important constraint that alteration must have been recent, however, does explain why samples as old as 80 ka still appear to remain closed system, as at present they are beneath sea level and so protected from the recent phase of meteoric alteration suffered by the ~120-ka samples.

References: [1] Fruijtier C. et al. (1999) *GSA*, in press. [2] Edwards R. L. et al. (1997) *Science, 276*, 782–786. [3] Cheng H. et al. (1998) *GCA, 62*, 3437–3452.

REDISTRIBUTION OF TRACE ELEMENTS DURING GARNET TO SPINEL PERIDOTITE FACIES TRANSFORMATIONS.

K. T. Koga, N. Shimizu, and T. L. Grove, Mail Stop 23, Woods Hole Oceanographic Institution, Woods Hole MA 02543, USA (ktkoga@mit.edu).

Introduction: Primitive mantle-normalized La/Yb ratio of mid-ocean-ridge basalt is often used for determining "garnet signature," that is evidence for equilibrium partial melts from garnet peridotite. If garnet peridotite is stable at pressures higher than 2.7 GPa, partial melting starting from the depth to the surface results in surplus of melt compared to the quantity determined from thickness of ocean crust formed at mid-ocean ridges. This so-called "garnet paradox" can be explained if melting of spinel peridotite produces the trace-element characteristics accounted for garnet signature.

Our observation of trace-element "inheritance" in pyroxenes (cpx and opx) as the result of garnet breakdown reaction suggests a possible contribution for reconciling the "garnet paradox." Melting of zoned pyroxenes produced by subsolidus garnet breakdown reaction favors a production of garnet signature from spinel peridotite. However, determination of exact condition to produce garnet signature requires a forward model including diffusion and melting rate of mantle phases.

Observation of Disequilibrium Distribution: Trace elements are redistributed to product pyroxenes during the breakdown reaction of garnet caused by decompression of mantle. Observations are made for experimental and natural samples showing the consequence of the reaction. For some timescale of reaction, trace-element diffusion is slower than growth of pyroxenes, and results in pyroxenes to "inheriting" trace-element abundances from reactant garnet. Figure 1 shows the composition of pyroxenes and garnet. Rare-earth-element (REE) abundances in pyroxenes are indistinguishable and almost the same as reactant garnet [1]. A similar conclusion has been drawn for peridotite form Lashaine [2]. It has been shown that REE abundances of pyroxenes and garnet are similar and REE "inheritance" is evident.

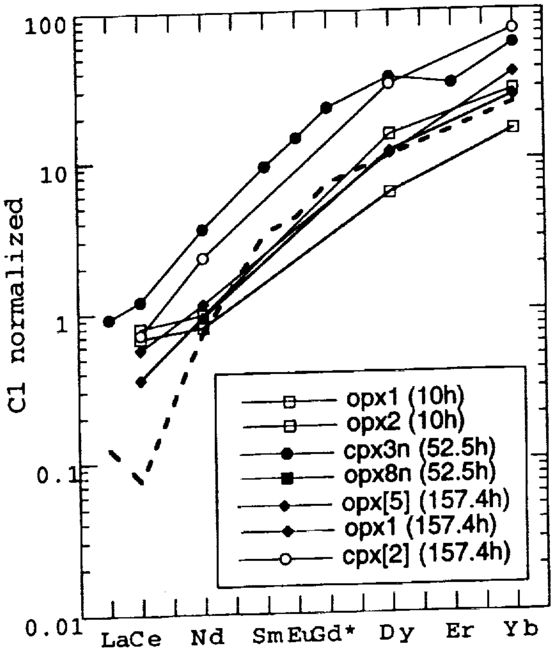

Fig. 1. Rare-earth-element mineral composition in garnet breakdown experiments.

Estimates from experiments predict that the transformation from garnet to spinel peridotite facies is instantaneous in geological timescale [1]. Diffusion experiments demonstrated that major-element diffusion in cpx is faster than trace-element diffusion [e.g., 3]. Considering these experimental results, it is likely that phase transformation in mantle results in disequilibrium distribution of trace elements, because transformation and major-element equilibration are fast enough that trace elements cannot equilibrate through diffusion.

Element Distribution During Melting: The pyroxenes "inherited" trace-element abundance of garnet may contribute "garnet signature" at the time of melting. Only possible circumstance is melting of zoned pyroxene in peridotite. The rim is newly grown garnetlike pyroxene and the core composition is cpx composition equilibrated to protolith garnet peridotite. In this case, the core of cpx has higher LREE abundances than the rim, and HREE are more abundandant toward the rim. Progress of melting increases the flux of LREE in melt while decreasing HREE flux, favoring the production of a high La/Yb ratio. It is important to note that if melting is equilibrium, "inherited" trace-element abundance reequilibrates with the rest of peridotite and there is no significance of melting pyroxenes that are not equilibrium. In contrast, trace-element diffusion data show that equilibration of trace element is limited by diffusion for LREE [3]. Qualitatively, LREE diffusion is slow and has stronger tendency for disequilibrium. Effective D(cpx/melt) is therefore closer to unity than experimentally determined D. HREE is closer to equilibrium; effective D is the same as experimentally determined D. However, melting starting with homogeneous garnetlike pyroxenes cannot produce La/Yb more than one, since D difference between La and Yb is not large enough [3].

References: [1] Koga K. T. et al. (1998) *Ext. Abstr. 7th Intl. Kimberlites Conf.*, 443–445. [2] Koga K. T. et al. (1999) *Eos Trans. AGU, 80*, S361. [3] Van Orman J. A. et al. (1998) *Eos Trans. AGU, 79*, S371.

STABILITY OF HYDROSULFIDE COMPLEX $AuHS^0$ IN GOLD-BEARING SOLUTIONS.

G. R. Kolonin, G. A. Pal'yanova, and G. P. Shironosova, Institute of Mineralogy and Petrography of Siberian Branch, Russian Academy of Sciences, Novosibirsk, Russia.

According to [1], "additional experimental work is warranted to determine the stability of $AuHS^0$ at high temperatures." The main goal of this study is to obtain new experimental data for this complex as well as to estimate its parameters for the revised HKF equations of state. As the first step, a set of Gibbs free energy of $AuHS^0$ was developed on the base of experimental data [2–5] together with the results of [6] recalculated in terms of this form as an alternative of $HAu(HS)_2{}^0$ protonated complex, dominated probably in more concentrated sulfide solutions. As the second step, the code UT-HEL as a part of the Hch computer program [7] was used to treat these data and to obtain parameters for HKF equations together with the standard $AuHS^0$ thermodynamic values. Finally, their additional adjustment was realized through "HELGESON" code [8]. The assumption that Born's coefficient for $AuHS^0$ is taken to be –0.038 by analogy with neutral $AgOH^0$, $AgCl^0$, and $AuCl^0$ complexes is a fundamental part of the performed calculations. Table 1 demonstrates the obtained parameters of HKF equations for species $AuHS^0$ and $AgHS^0$ (obtained the same way as for $AuHS^0$ along with the standard thermodynamic characteristics at 25°C and 1 bar).

The experiments on solubility of Au-Ag alloys of various compositions in chloride-sulfide solutions in the presence of the quartz-muscovite-K-feldspar and pyrite-pyrrhotite-magnetite mineral buffers at 350°C and 0.5 kbar were carried out to check additionally the obtained values. The Au-Ag alloys were used not only as the initial soluble matters, but as the inner universal indicators of redox [9] and activity S conditions. Gold and Ag concentrations in solutions were determined by atomic absorbtion method, with the previous concentration of the metals by organic extracting agents (analyst: V. Zimbalist, Analytical Centrum, UIGGM). The initial composition of the Au-Ag alloys in the experiments was in the interval from 0.2 to 0.7 mol. fraction of Ag (N_{Ag}). Its variation after the experiments was controlled by the use of microprobe analysis. A solution 1.0 m KCl + 0.1 m HCl was used as initial. The duration of experiments was 30 d.

TABLE 1. Standard thermodynamic characteristics and HKF parameters for $AuHS^0$ and $AgHS^0$, obtained in the present work.

Species	$AuHS^0$	$AgHS^0$
$\Delta_f G^0_{298}$ kal/mol	6117	−680
S^0_{298} kal/(mol × K)	43.23	18.06
$C_{P,298}$ kal/(mol × K)	−15.76	−4.14
V_{298} cm^3/mol	19.28	11.674
$a_1 \times 10$ kal/(mol × bar)	4.3888	3.3482
$a_2 \times 10^{-2}$ kal/mol	2.9350	0.3938
a_3 kal × K/(mol × bar)	4.5961	5.595
$a_4 \times 10^{-4}$ kal × K/mol	−2.9003	−2.7953
c_1 kal/(mol × K)	−3.4159	3.3941
$c_2 \times 10^{-4}$ kal × K/mol	−6.2449	−3.8779
$\omega \times 10^{-5}$ kal/mol	−0.038	−0.038

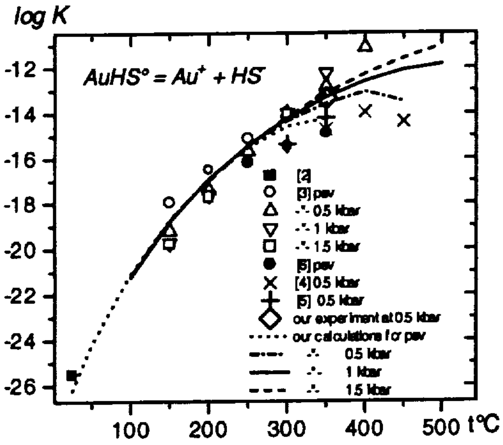

Fig. 1. Comparison of log K dissociation of AuHS complex on [2–6] data with the experimental and calculated results.

In acid solutions the experimental data can be represented by the reaction

$$Au_{alloy} + H_2S(aq) = AuHS^0 + 0.5H_2(aq)$$

Its constant −5.74 ± 0.22 was calculated with the help of equation

$$\log K = \log m_{Au} + 0.5 \log m_{H_2} - \log m_{H_2S} - \log a_{Au(alloy)}$$

by the following recalculation in terms of the $AuHS^0$ dissociation constant ($\log K_{dis.} = -13.35 \pm 0.25$). As it is seen on Fig.1, the latter within the limits of experimental errors coincided with $\log K_{dis} = -13.58$ of $AuHS^0$ at 350°C and 0.5 kbar, which was calculated on the base of data of Table 1 as well as with the data of [3] for the pressures of saturated vapor and 0.5 kbar. At the same time the log Kdis is about one order higher than those calculated using the data from [5] and [6].

Acknowledgments: This research is supported by Russian Foundation on Base Researches (grant no. 97-05-65252).

References: [1] Shenberger D. M. and Barnes H. L. (1989) *GCA, 53,* 269–278. [2] Renders P. J. and Seward T. M. (1989) *GCA, 53,* 245–253. [3] Bening L. G. and Seward T. M. (1996) *GCA, 60,* 1849–1872. [4] Gibert F. et al. (1993) *Proceed. of the 4th ISHR. Nancy,* 65–68. [5] Baranova N. N. and Zotov A. V. (1998) *Mineral. Mag., 62,* 116–117. [6] Hayashi K. and Ohmoto H. (1991) *GCA, 55,* 2111–2126. [7] Shvarov Yu. V. (1999) *Geochimia, 6,* in press (in Russian). [8] Akinfiev N. N. (1995) Ph.D. thesis, The Vernadsky Institute, Moscow. [9] Gammons and Williams-Jones (1995) *GCA, 59,* 3453–3468.

MICROBIAL-SILICA INTERACTIONS IN MODERN HOT SPRING SINTER.

K. O. Konhauser[1], V. R. Phoenix[1], and D. G. Adams[2], [1]School of Earth Sciences, University of Leeds, Leeds, LS2 9JT, UK (k.konhauser@earth.leeds.ac.uk), [2]Department of Microbiology, University of Leeds, Leeds, LS2 9JT, UK.

Intimately layered microcrystalline siliceous sediments, associated with biogenic deposits such as stromatolites, occur throughout the geological record but are a striking feature of the Archean. Stromatolites and their recognizable microfossils represent some of the earliest records of life on Earth [1]. Analogous silicified deposits occur in present hot-spring environments, but the mechanisms of silicification (and crucially the role of microorganisms) are still largely unresolved.

Recent studies using electron microscopy have shown that microorganisms (viable and lysed) actually provide favorable nucleation sites for amorphous silica precipitation [2–5]. The mineralization consists of spheroidal grains (hundreds of nanometers in diameter), formed epicellularly on the sheaths of living cells, and intracellularly, within the cytoplasm, presumably after the cells had lysed. Often, the silica particles coalesced such that individual precipitates were no longer distinguishable; entire colonies became cemented together in a siliceous matrix several micrometers thick. Eventually, only the sheath and cell wall of the original organic framework, or some remnants of cytoplasm, remained recognizable. In terms of the sinter's overall structure, nearly half the thickness is attributed to silicified microorganisms, and it now seems indisputable that sinter formation is intimately linked to microbial activity [4].

The above observations indicate that silicification begins when the microorganisms are living and continues for some time after their death. The bacteria appear to facilitate silicification by providing reactive interfaces for silica adsorption, thereby reducing activation energy barriers to nucleation and allowing surface chemical interactions that sorb more silica from solution to take place. In this way, the bacterium functions as a reactive interface, or template, for heterogeneous nucleation. Because a sufficient supply of silica is generally available in hot-spring effluent (in excess of mineral solubility), continued adsorption results in the surface sites becoming saturated, with particle nucleation taking place. After bacteria initiate silica precipitation, continued growth presumably occurs autocatalytically and abiogenically due to the increased surface area generated by the small silica phases.

A certain degree of periodicity in silicification must also be occurring at hot springs, because these mineralized structures are frequently laminated. In both the Geysir and Krisuvik hot springs, Iceland, two very distinct lamina types consistently form throughout the sinter, a "porous" layer in which viable and preferentially aligned microorganisms (growing upward toward sinter-water interface) are associated with silica, while a finely laminated silica layer appears to be completely inorganic in composition. In all cases, the "porous" layers have a sharply defined base, overlying the finely laminated silica, and a gradational upper surface into the finely laminated silica. The gradational top surface suggests that silica precipitation must have at some point exceeded the bacteria's ability to compensate (i.e., grow upward); this possibly reflects their natural slow/death phase during the dark winter months of Iceland. In turn, the defined base suggests rapid recolonization of the inorganic precipitate surface by free-living bacteria in the effluent, once conditions for surface attachment became favorable (i.e., in the spring). Thus, the laminations might reflect seasonal variations in microbe-silica interactions.

The siliceous sinters are reminiscent of silicified Archean stromatolites in terms of their morphology and microbial component [1], suggesting that we may be witnessing contemporaneous biomineralization processes and growth patterns to those on the early Earth. Experiments on the silicification of cyanobacteria have already shown that the silica coatings serve as effective UV shields, possibly having afforded Archean microbes with the opportunity to colonize shallow-water environments [6]. Furthermore, the findings that phototrophic bacteria are still viable several millimeters beneath the sinter surface (and there is no evidence of upward burrowing by the cells) suggests that these microbes receive adequate light at depth [4]. Thus, cell motility is not critical to their survival, precluding previously held beliefs that Archean microbes (growing as stromatolites) needed to move upward, through overlying sediment, faster than rates of accretion.

References: [1] Awramik S. M. (1992) *Photo. Res., 33,* 75–89. [2] Schultze-Lam S. et al. (1995) *Can. J. Earth Sci., 32,* 2021–2026. [3] Konhauser K. O. and Ferris F. G. (1996) *Geology, 24,* 323–326. [4] Konhauser K. O et al. (1999) *Geology,* in review. [5] Phoenix V. R. et al. (1999) *Chem. Geol.,* in review. [6] Phoenix V. R. et al. (1999) *Geology,* in review.

THE ISOTOPIC COMPOSITION OF CONODONTS AND BRACHIOPODS AS PROXIES FOR EVOLUTION OF TRIASSIC SEAWATER.

C. Korte[1], J. Veizer[1,2], and H. Kozur[3], [1]Institut für Geologie, Ruhr-Universität, 44801 Bochum, Germany (christoph.korte@ruhr-uni-bochum.de), [2]Ottawa-Carleton Geoscience Center, University of Ottawa, Ontario K1N 6N5, Canada (veizer@geol.uottawa.ca), [3]Rézsü u. 83, H-1029 Budapest, Hungary, (kozurh@helka.iif.hu).

Introduction: The ^{87}Sr/^{86}Sr, δ^{18}O, and δ^{13}C of stratigraphically well-defined conodonts and brachiopods reflect the isotopic evolution of past seawater [1]. The precondition is that the samples are not diageneticaly altered [2,3], and in order to evaluate the state of preservation, the fossils were studied by optical microscopy, scanning electron microscopy (SEM), inductively coupled plasma atomic emission spectrometry (ICP-AES), and particle-induced X-ray emission (PIXE). Only conodont samples with a CAI index of 1–1.5, and brachiopod samples with Mn content <250 ppm and Sr content >400 ppm, complemented by well-preserved textures under SEM, were considered in this study.

Results and Discussion: PIXE studies of Triassic conodonts [4,5] show, in contrast to their Cambrian counterparts [5,6] a homogeneous distribution of Sr and Nd. The "crown material" as well as the "basal bodies" of the Triassic conodonts yielded concordant ^{87}Sr/^{86}Sr values regardless of the duration of leaching by acetic acid.

The ^{87}Sr/^{86}Sr values of conodonts and brachiopods rise abruptly from 0.7074 to 0.7082 in the lower Triassic, fall to 0.7075 during the middle Triassic, and rise to 0.7082 at the end of this interval, followed by a decline to 0.7077 in the Rhaetian. The δ^{13}C values of brachiopods are ~0.5–0.8‰ PDB in the middle Triassic, rise abruptly by 2‰ at the Ladinian/Carnian boundary to 3‰ in the upper Carnian, and subsequently fall to 2‰ in the Rhaetian.

The shape of the δ^{13}C curve may possibly reflect the intensity of coeval coal formation, since the 2‰ Ladinian/Carnian jump correlates with the renewed global phase of coal deposition [7]. The oscillations of δ^{13}C in the upper Triassic appear to correlate with the declining sea level stand.

The Sr-isotopic data apparently reflect tectonic events, with high ^{87}Sr/^{86}Sr ratios in the lower Triassic coincident with the uplift of the Appalachians and in the upper Triassic with those of the Cimmerides, Gondwanides, and Indosinians.

References: [1] Veizer J. et al., *Chem. Geol.* [2] Veizer J. (1983) *SEPM short course, 10,* 1–100. [3] Veizer J. (1983) *Rev. Min., 11,* 265–299. [4] Bruhn F. et al. (1997) *Nucl. Inst. and Meth. B, 130,* 636–640. [5] Korte C. (1999) Thesis, Ruhr-Universität Bochum, Germany. [6] Holmden C. et al. (1996) *EPSL, 142,* 425–437. [7] Retallack G. J. et al. (1996) *Bull. GSA, 108,* 195–207.

ISOTOPIC STRUCTURE AND CRUST-FORMING EVENTS OF CENTRAL ASIA: EVIDENCE FOR EXTENSIVE CONTINENTAL CRUST GROWTH IN THE PHANEROZOIC.

V. P. Kovach[2], V. I. Kovalenko[1], V. V. Yarmolyuk[1], A. B. Kotov[2], I. K. Kozakov[2], and E. B. Salnikova[2], [1]Institute of Geology of Ore Deposits, Petrography, Mineralogy and Geochemistry, Russian Academy of Sciences, Staromonetny, 35, Moscow 109017, Russia (aprel@igem.ru), [2]Institute of Precambrian Geology and Geochronology, Russian Academy of Sciences, Makarova emb., 2, St. Petersburg 199034, Russia (kotov@ad.iggp.rus.spb.ru).

Central Asia Orogenic Belt (CAOB) — "the granite crown of Asia" — separates the Siberian and Sino-Korean-Tarim Cratons of northern Eurasia and stretches for ~5000 km at 1000–2000 km width. The architecture of the CAOB is defined by the mosaic combination of Phanerozoic mobile belts extended for hundreds and thousands kilometers and microcontinents with presumably Precambrian basement and Vendian-Early Palaeozoic sedimentary cover.

The following isotopic provinces have been recognized on the basis of Nd-isotopic investigations of intrusive granitoids of different ages (120–2645 Ma) and tectonic setting: "Archaean" (T_{Nd}(DM) = 2.9–3.3 Ga) (Baidarik block of the Dzabkhanian microcontinent) and "Paleoproterozoic" (T_{Nd}(DM) = 1.9–2.6 Ga) (Baikal-Patom and Barguzin-Vitim terrains, Baidarik block) which appear to represent fragments of the old cratons; "Neoproterozoic" (T_{Nd}(DM) = 1.15–1.65 Ga) in the crystalline basement of microcontinents (e.g., Tuvino-Mongolian); "Caledonian" (T_{Nd}(DM) = 0.7–0.95 Ga); and "Hercynian" (T_{Nd}(DM) = 0.55–0.75 Ma) that coincide with coeval tectonic zones.

Phanerozoic (120–530-Ma) granitoids of the "Precambrian" isotopic provinces display wide variations in ε_{Nd}(T) values (–12.9–4.6) whereas granitoids of the "Caledonian" and "Hercynian" isotopic provinces are characterized by positive ε_{Nd}(T) values (predominantly from 0.7 to 5.8 and 3.5 to 6.2 respectively). Neodymium-isotopic compositions of granitoids of these provinces exhibit narrow linear trends with insignificant variations in their ε_{Nd}(T) values (~2 ε units) for rocks of similar age. These data provide evidence for the isotopic homogeneity of the continental crust in the Caledonian and Hercynian tectonic structures and vertical heterogeneity of continental crust of "Precambrian" provinces that expressed in underlying of Precambrian continental crust by "juvenile" Caledonian crust.

Available geological, geochronological, and isotopic data indicate that considerable volumes of continental crust in Central Asia were formed from juvenile sources with contribution of old crustal material in the island arcs or Andean type of active continental margin environments during Early Caledonian and Hercynian orogenesis. The sources for melts for young granites formed after collision of Caledonian, Hercynian, and Precambrian structures were the continental crusts of these structures. By this means crustal growth in central Asia had episodic character and important crust-forming events took place in the Phanerozoic.

Acknowledgments: Financial support for this study was provided by the Russian Foundation for Basic Research, projects 97-05-64384, 99-05-65647, 99-05-65645, and 99-05-65687.

EFFECT OF DESFERRIOXAMINE-B AND DFOMTA ON THE ADSORPTION OF LEAD AND EUROPIUM ON THE GOETHITE SURFACE.

S. M. Kraemer[1] J. Xu[2], K. N. Raymond[2], and G. Sposito[1], [1]Ecosystem Sciences Division, University of California, Berkeley CA 94720-3110, USA (skraemer@nature.berkeley.edu), [2]Department of Chemistry, University of California, Berkeley CA 94720-1460, USA.

Introduction: Siderophores are organic ligands released by microorganisms to solubilize and assimilate Fe. They form Fe complexes of exceptional stability and specificity. Desferrioxamine B (DFO-B) is an example of a trihydroxamate siderophore that is produced by a soil microorganism, *Streptomyces pilosus,* under Fe-deficient conditions [1]. With a 1:1 stability constant of $10^{30.6}$, DFO-B has a higher affinity for Fe than for other major dissolved ions in soil solutions. However, it also forms strong complexes with a range of metal ions. A few trace metal-DFO-B complexes actually approach or exceed the stability of the Fe complex, e.g., Th(IV) and Pu(IV) complexes with 1:1 stability constants of $10^{26.6}$ and $10^{30.8}$ respectively [2]. The microbial release of DFO-B in soils could therefore have an important effect on the transport of trace metals, such as actinides, in the environment.

Pollution of soils with actinides is a major environmental problem and health concern. Actinide-specific DFO derivatives have been developed for their potential for decontamination procedures [2,3]. DFOMTA is an example of an actinide-specific DFO derivative that complexes Pu(IV) in octadentate coordination with 1:1 stability constants of $10^{38.6}$ [2].

This study focuses on the effect of DFO-B and DFOMTA on the adsorption of Pb and Eu on the goethite surface. Lead(II) has been chosen for its relevance as soil trace pollutant, and Eu(III) as a model for actinide ions.

Materials and Methods: DFO-B was produced by Ciba-Geigy and received as a gift from the Salutar Corporation. The concentration of DFO-B was measured spectrophotometrically at 463.2 nm as the Fe-siderophore complex in the presence of excess Fe at pH 1.5. Lead and Eu were measured using inductively coupled plasma atomic emission spectrometry (ICP-AES).

All adsorption experiments were performed using a batch method at an ionic strength of 0.01 M $NaClO_4$. Lead and Eu adsorption measurements were conducted at a goethite concentration of 0.5 g/L between pH 3 and 9 in the presence of 240 µM (DFO-B) or 150 µM (DFOMTA). A higher solids concentration of 13 g/L was needed for DFO-B measurements.

Results: *Adsorption of DFO-B.* The adsorption envelopes of DFO-B on goethite showed cationlike behavior. The adsorption isotherm at pH 6.6 showed a low maximum surface concentration of 1.5 µmol/g. This is far lower then the maximum observed surface concentration (30 µmol/g) of acetohydroxamic acid, a monohydroxamate ligand [4].

Effect of DFO-B on lead and europium adsorption. In the absence of an organic ligand, Pb and Eu adsorb strongly to goethite with increasing pH. We observed a $pH_{50} \approx 5.5$ and 6.3 for Pb and Eu, respectively. The siderophores had a significant effect on metal ion adsorption. Less than 70% of the initial Pb concentration and less then 20% of the initial Eu were adsorbed between pH 3 and 9 in the presence of 240 µM DFO-B.

Effect of DFOMTA on lead adsorption. DFOMTA had a stronger effect on Pb adsorption as compared to DFO-B. Less than 50% of the initial Pb concentration was adsorbed between pH 3 and 9 in the presence of 150 µM DFOMTA. However, Pb sorption increased by up to 30% relative to adsorption in the absence of a ligand at pH <5.5.

Conclusions: DFO-B and DFOMTA have a significant effect on the adsorption of Pb(II) and Eu(III) by goethite. This indicates that natural and synthetic siderophores can substantially influence the mobility of trace metals in soils and sediments.

Acknowledgments: The authors thank Dr. Sing-Foong Cheah, Rita Zapf, and Claudio Coccoza for discussions and assistance. Support was from DOE grant DE-FG03-96ER14667.

References: [1] Bickel H. et al. (1960) *Helv. Chim. Acta, 43,* 2118–2128. [2] Whisenhunt D. W. et al. (1996) *Inorg. Chem., 35,* 4128–4136. [3] Hou Z. et al. (1994) *J. Am. Chem. Soc., 116,* 840–846. [4] Holmén B. A. and Casey W. H. (1996) *GCA, 60,* 4403–4416.

THE INFLUENCE OF SOIL-RESPIRED CARBON DIOXIDE ON MINERAL WEATHERING AND SOIL WATER GEOCHEMISTRY: RESULTS FROM NATURAL AND EXPERIMENTAL (ELEVATED CARBON DIOXIDE) TEMPERATE FOREST ECOSYSTEMS.

T. C. W. Ku[1], L. M. Walter[1], J. M. Budai[1], G. W. Kling[2], D. R. Zak[3], and E. L. Williams[1], [1]Department of Geological Sciences, University of Michigan, Ann Arbor MI 48109, USA, [2]Department of Biology, University of Michigan, Ann Arbor MI 48109, USA, [3]School of Natural Resources and Environment, University of Michigan, Ann Arbor MI 48109, USA.

Introduction: The rapid rise in atmospheric CO_2 concentrations is altering the biogeochemical cycling of C at Earth's surface. Previous experiments demonstrated that plants grown under elevated CO_2 conditions had increased levels of photosynthesis, root production, respiration, and belowground biomass [1]. Associated increases in soil-respired CO_2 may enhance chemical weathering of associated minerals and sequester C in regional groundwater systems. The soil-water and gas-chemical compositions of two natural temperate forested ecosystems (aspen and sugar maple) in the Cheboygan watershed, northern Michigan, are compared with soil-water and gas analyses from nearby open-top chamber experiments. Here, aspen and sugar maple trees are grown in different treatments of atmospheric CO_2 (ambient and twice-ambient) and soil N availability (low and high). Importantly, these forests grow on thick Pleistocene glacial deposits containing abundant, highly reactive carbonate minerals. The combination of rapid biologic C cycling and availability of reactive minerals provides an ideal opportunity to assess the effects of elevated CO_2 conditions on near-surface environments.

Discussion: The principal mechanisms of CO_2 production in forest soils are root respiration, microbial respiration, and oxidation of organic matter. The accumulation of CO_2 in the vadose zone is influenced by the production rates and several environmental factors such as temperature, soil moisture, and porosity. Since soil gas quickly equilibrates with changes in atmospheric pressure, the mass transport of CO_2 via advection is negligible. Therefore, the partial pressure of CO_2 in the vadose zone is controlled by soil respiration and diffusion. In temperate forest soils, increased biologic activity in the summer elevates the production of soil CO_2, creating a seasonal progression of CO_2-depth profiles.

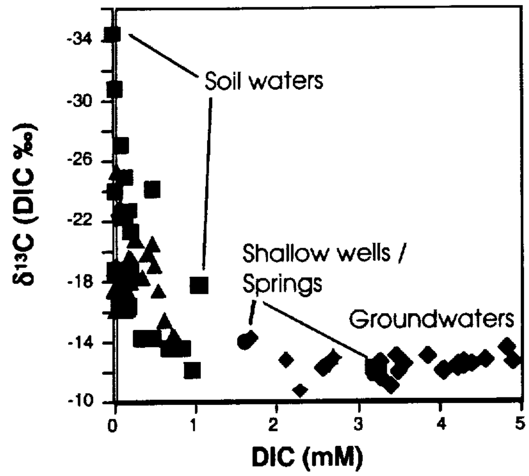

Fig. 1. $\delta^{13}C_{DIC}$ vs. DIC. Carbon-isotopic evolution from soil waters to groundwaters.

In the aspen and sugar-maple soils, CO_2 concentrations increased with depth and reached maximum values (~7000 ppmv) in August. The dissolution of carbonate minerals is regulated by organic and inorganic acids, and by pCO_2 with higher pCO_2 values resulting in greater amounts of carbonate dissolution. In addition, carbonate dissolution proceeding under "open-system" conditions with an unlimited supply of soil CO_2 will dissolve greater amounts of carbonate compared to "closed-system" conditions where dissolution is limited by a fixed amount of soil CO_2 [2]. Based on a physicochemical model and our measured carbonate parameters (pH, DIC, Ca^{+2}, Mg^{+2}, $\delta^{13}C_{DIC}$), we determined that carbonate dissolution in the glacial drift is occurring under "open-system" conditions.

The soil-water evolution is tracked by the C-isotopic composition of DIC. $\delta^{13}C$ analyses of soil gas CO_2 were ~–22‰ VPBD, indicative of a mainly C_3 organic source. In shallow soil waters, soil-respired CO_2 is the dominant inorganic C source, resulting in $\delta^{13}C_{DIC}$ values near –22‰. In addition, the low pH of most shallow soil waters increase the H_2CO_3 proportion of DIC, resulting in lower $\delta^{13}C_{DIC}$ values due to the $H_2CO_3(aq)$-$CO_2(g)$ fractionation factor of –1.1‰. As the water migrates downward through the vadose zone, progressive weathering of Paleozoic carbonates (–0‰ VPDB) shift the $\delta^{13}C_{DIC}$ to –12‰, the typical value of regional groundwater (Fig. 1).

Experimental trees grown under ambient CO_2 conditions and low N availability had the lowest range of soil-gas concentrations, indicating that both elevated CO_2 and high nutrient treatments increased soil respiration rates. In contrast to natural forest sites, the experimental chambers had relatively high Ca^{+2}-Mg^{+2}-DIC concentrations. This is in part due to sediment reworking and increased exposure of reactive carbonate minerals. While the carbonate weathering differed from the natural sites, the extent of silicate dissolution was realized immediately at shallow depths. Also, elevated NO_3^- concentrations were observed in the initial phases of the experiment and were correlated with Ca^{+2} and Mg^{+2} concentrations. The high NO_3^- concentrations were tracked moving downward through the soil and diminished with time.

References: [1] Zak et al. (1993) *Plant Soil, 151,* 105–117. [2] Deines et al. (1974) *GCA, 88,* 1147–1164.

MOLECULAR MODELING OF SOOT AND INTERACTIONS WITH POLYCYCLIC AROMATIC HYDROCARBONS.

J. D. Kubicki[1], [1]Department of Geosciences, Pennsylvania State University, University Park PA 16802, USA (kubicki@geosc.psu.edu).

Introduction: Partition coefficients of polycyclic aromatic hydrocarbons (PAHs) between soot and water can be extraordinarily high [1]. PAHs are common pollutants that reach the environment through a variety of processes including combustion and leakage of petroleum products. Association of PAHs with soot particles can be the result of either co-formation during combustion or partitioning from the aqueous phase. In either case, sorption of PAHs into the soot matrix can decrease the bioavailability and increase the lifetime of PAHs in the environment.

Although the PAH-soot association is clear [2], the molecular-level chemistry of bonding between PAHs and soot is not well understood. Molecular modeling techniques can be useful in this regard [3]. Using experimentally determined models for soot [4] and the known structures of PAHs, molecular structures and bonding energetics between these two types of compounds can be predicted with a variety of techniques.

Computational Methods: PAH-soot interactions may occur on a range of length scales. For this reason, model simulations were carried out with three types of methods that address different aspects of the problem. The three methods employed were molecular mechanics, semiempirical quantum mechanics and density functional theory (DFT) calculations. Molecular mechanics simplifies bonding interactions into analytical terms such as bond stretching and angle bending. Ignoring computation of the molecular electron density allows model systems on the order of hundreds of atoms to be simulated. Energy minimizations and molecular dynamics (MD) simulations with molecular mechanics potentials can then be used to predict long-range structures and dynamics for PAHs and soot. The simplification of molecular bonding into analytical terms can lead to errors in calculating H or van der Waal's bonding. Semiempirical quantum mechanical calculations can be used to improve the model predictions of these types of interactions. However, computer limitations require that smaller model systems on the order of tens of atoms be used for this type of calculation. Semiempirical calculations also make several approximations for atomic interactions that may lead to significant errors [5]. Hence, DFT calculations can be used to determine the magnitude of these errors. DFT calculations with large basis sets to describe the electron density can result in a highly accurate picture of molecular bonding. In this case, only small molecules can be used within practical computational constraints. However, the use of these three methods in combination can provide an accurate and realistic description of molecular bonding between PAHs and soot.

Results: Molecular mechanics energy minimizations of a model soot molecule [4] consisting of 683 atoms ($C_{489}H_{160}O_{34}$) predicted a relatively open, planar structure. Hydrogen bonding between large molecules was strong enough to keep molecular fragments associated. Molecular dynamics simulations of the same system conducted at 300 K undergo structural rearrangements from the minimum energy structure, however. Hydrogen bonding switches from a phenol-ketone association as suggested in [4] to a phenol-carboxylic anhydride association. Furthermore, the soot structure becomes more crenulated in the MD simulations as distortions from the potential energy minimum structure were sampled.

Semiempirical energy minimizations of a $C_{127}H_{48}O_{14}$ fragment of the original soot model including four benzene molecules were also conducted. Original benzene positions presented the possibilities of H-H, H-O, H-π, and π-π type interactions between the benzene molecules and soot substrate. Optimized structures suggested that the H-O and π-π interactions were not significant and that the dominant bonding mechanisms were H-H van der Waal's bonding and H-π bonding.

Molecular orbital calculations were carried out on smaller molecular clusters to test the results of the molecular mechanics and semiempirical simulations. Hydrogen-bonding interactions between phenol and a cyclic ketone as well as a cyclic carboxylic anhydride were modeled with a 6-31G* basis set and Møller-Plesset second order perturbation theory (MP2). Intermolecular bonding energetics are much more accurate at this level than in molecular mechanics so these results will be used to assess the validity of the larger scale simulations. To test the accuracy of the molecular mechanics and semiempirical calculations with regard to π-π interactions, DFT calculations employing the Becke exchange functional [6] and Lee-Yang-Parr correlation functional [7] were performed on naphthalene associated with various soot fragments.

References: [1] Chin Y-P. and Gschwend P. M. (1992) *ES&T, 26,* 1621. [2] Gustafsson O. et al. (1997) *ES&T, 31,* 203. [3] Kubicki J. D. and Apitz S. E. (1999) *Org. Geochem.*, in press. [4] Akhter M. S. et al. (1985) *Appl. Spect., 39,* 143. [5] Stewart J. J. P. (1989) *J. Comp. Chem., 10,* 209. [6] Becke A. D. (1988) *Phys. Rev. A, 38,* 3098. [7] Lee C. et al. (1988) *Phys. Rev. B., 37,* 785.

ISOTOPIC AGE OF MAIN GEOLOGICAL EVENTS OF THE ARCHEAN KOLMOZERO-VORONJA GREENSTONE BELT, KOLA PENINSULA, RUSSIA.

N. M. Kudryashov, Geological Institute of the Kola Science Centre of the Russian Academy of Sciences, Apatity, Russia.

Greenstone belt Kolmozero-Voronja is one of the most ancient geological structures of Kola Peninsula having kept basic features and pecularities of Archean endogenic processesPrezently apart from obtaining new geochronological data one should correct available dating on some geological objects of the belt.

The Kolmozero-Voronja greenstone belt is located between Murmansk, Central Kola and Keivy terrains of Upper Archean. It is stretched in a northwest-southeast direction being more than 150 km long and ~10–12 km wide. Four suites are distinguished in the greenstone belt: Ljavozerskya (lower terrigenous formation), Polmostundrovskya (komatiite-tholeiite), Voronjatundrovskya (basalt-andesite-dacite), and Chervurtskya (an upper terrigenous formation). All rocks are metamorphosed in amfibolitic facies in late Archean (andalusite-staurolitic subfacies) and early Karelian (kyanite-staurolitic subfacies) time, display complicated isoclinal faults, and intruded with granodiorites, plagiomicrocline and tourmaline granites and pegmatitic veins. Uranium-lead zircon dating of quartz porphyries and granodiorites, U-Pb titanite dating of ovoid plagioamphibolites and Pb-Pb dating of tourmaline from tourmaline granites were carried out.

Quartz porphyries are found in the northwest part of the complex. They cross the rocks of the Polmostundrovskya formation and occur as subconcordant bodies in the upper part of the Voronjatundrovskya suite. They are considered to be intrusive vein analogs of acid volcanites. Quartz porphyry is a fine-grained pale-grey rock with quartz and plagioclase impregnants (up to 5 mm). Zircon in the quartz porphyry consists of long prismatic and short prismatic crystals with an oscillatory zoning that is characteristic of magmatic crystallization. Eight fractions of these zircons yield a discordant U-Pb age of 2828 ± 8 Ma, which we interpret as an age of intrusive emplacement of quartz porphyry that at the final stage of the belt development.

Small bodies (10–15 m in thickness) of ovoid plagioamphibolites are present among shistosed plagioamphibolites of the Polmostundrovsky suite. The ovoid plagioamphibolites are dark green rocks with large rounded aggregates of plagioclase (40–50 mm in diameter).

Titanite in the ovoid plagioamphibolites consists of pale-yellow crystals of irregular crystallographic forms. Dating of three fractions of sphene yielded an U-Pb age of 2595 ± 20 Ma that is probably connected with the closure of the U-Pb isotopic system during the regional andalusite-sillimanite facies metamorphism.

Porosozero granodioritic complex is located in the southeast part of the belt between granites of Murmansk terrain, migmatites and gneisses of Central Kola terrain and Keivy alkaline granites. It is intruded into rhythmically layered plagioamfibolites and biotite gneisses forming intersecting veins in them. The granodiorites are medium-grained, even-grained rock with grain size ~1–2 mm. They are composed of plagioclase (30–35%), microcline (5–10%), quartz (20–25%), amphibole (15–20%), biotite (5–10%), and epidote (2–5%). Zircon sample is presented by bipyramidal prismatic crystals of brownish color. In immersion, thin oscillatory inner zoning is clearly visible that implies magmatic genesis of the zircon. Uranium-lead age obtained for the zircon 2733 ± 6 Ma is interpreted as an age of emplacement of the complex.

Tourmaline granites are found all over Kolmozero-Voronya belt occurring among volcanogenic-sedimentary rocks. The granites differ distinctly from other granitoids of the region. They are characterized by big content of muscovite and contain tourmaline, apatite, and garnet inclusions easy perceptible by an eye. The rocks have light-gray color with big, up to 5 cm black tourmaline crystals and gneiss texture. Fine- and medium-grained, sometimes coarse-grained and pegmatoid varieties can be extracted. Tourmaline granites are compounded by 15–20% microcline, 20–25% plagioclase, 30–45% quartz, 5–15% muscovite, 0–5% biotite, 3–7% tourmaline, and 1–5% garnet.

Lead-lead dating of tourmaline extracted from tourmaline-muscovite granites was carried out using the differential dissolving method [1]. It yielded good linear correlation of 2520 ± 70 Ma. This age appears to denote the time when Pb-Pb system had been closed due to tourmaline crystallization at post-magmatic stage of the complex formation.

The studied rocks of greenstone belt Kolmozero-Voronja are of Late Archean age the geochronological data obtained imply long and complicated evolution of the belt.

References: [1] Frei (1995).

BLACK CARBON AND THE GLOBAL CARBON AND OXYGEN CYCLE.

T. A. J. Kuhlbusch, University of Duisburg, FB9/AMT, Bismarckstrasse 81, 47057 Duisburg, Germany (tky@uni-duisburg.de).

Introduction: Black carbon is ubiquitously distributed in the Earth's environment. It can be found in soils, sediments, water bodies, polar ice, and the atmosphere. The presence of black carbon throughout our environment has various implication due to its unique physical and chemical properties. One of its properties is its refractoriness concerning degradation. Thus conversion of plant organic matter to black carbon (here defined as the refractory C fraction of fire residues and emissions) represents sequestration of C from the short-term bioatmospheric C cycle to the long-term geological C cycle.

Black Carbon Formation: Black carbon (BC) formation in dependence of the volatilization of the fire-exposed C (VC/CE) was investigated for grass fires in the field and experimental fires in a container [1,2].

In Fig. 1 we generally see a rise of the BC/CE ratio with increasing C volatilization (VC) by the fire. The curves seem to be reasonable giving low conversion factors (BC/CE) for low- and high-VC values with a maximum in between. If the burning efficiency is low, not all biomass is exposed to thermal degradation. Thus only little BC is produced resulting in a low conversion factor. This factor increases up to a maximum (84–89% VC) where BC formation is in equilibrium with the thermal degradation of BC. Then the conversion factor decreases up to the point where all C was volatilized and thus no BC remains in the residue.

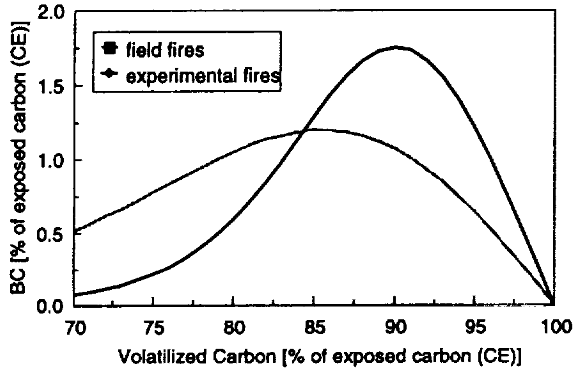

Fig. 1. Black carbon formation in dependence of the volatilization.

TABLE 1. Global estimate of black carbon (BC) formation in residues.

Source	Carbon Exposed [5] Tg C yr^{-1}	Conversion Factor BC/CE (%)	BC in Residues Tg C yr^{-1}
Shift. agricult.	1000–2000	1.5–3.0	15–60
Perm. deforest.	500–1400	1.5–3.0	8–42
Savanna fires	400–2000	1.0–2.0	4–40
Fuel wood	300–600	2.5–3.5	8–21
Agricultural waste	500–800	1.0–2.0	5–16
Total	2700–6800		40–179

The maximum conversion factors determined for the experimental and field fires was 1.8 ± 0.2% and 1.3 ± 0.4% respectively. Comparisons of these conversion factors with emission factors for BC emitted with the fire plumes [3] show that more than 80% of BC produced by vegetation fires remains on site in the residues.

Global Estimate: These conversion factors as well as some based on data by Fearnside et al. [4] were used to estimate the annual global formation rate of BC [2].

Another estimate based on the BC/CO_2 ratio gave an annual BC formation rate of 76–241 Tg (10^{12} g) C yr^{-1}. These ranges of BC in residues together with the BC emitted with the smoke (6.4–28 Tg C yr^{-1} [5]) leads to an annual formation of 50–270 Tg BC yr^{-1}.

Conclusions: BC formation by, e.g., savanna fires represents a net sink of atmospheric CO_2 since these kinds of vegetation fires are no net source (C load per area unit before a fire is reached again 1–2 yr after the fire). BC formation by e.g., deforestation fires just reduce the net atmospheric CO_2 source. Overall, the rate of BC formation estimated above reduces net CO_2 emissions by deforestation by 2–25% and may constitute a significant fraction of the "missing C" in the anthropogenically disturbed C balance.

The formation of BC from plant matter also releases O (1 mol plant C = >1 mol BC + 1.9 mole O). An estimate of O release based on the oldest record of charcoal (340 m.y. ago) and assuming an average BC formation of 10% of that of today gives 8× more O_2 than the current atmospheric O_2 content. An estimate of O_2 release by the burial of organic C in oceanic sediments gives ~25× the present atmospheric O_2 content.

References: [1] Kuhlbusch T. A. J. et al. (1996) *JGR, 101,* 23651–23665. [2] Kuhlbusch T. A. J. and Crutzen P. J. (1995) *GBC, 9,* 491–501. [3] Cachier et al. (1996) in *Biomass Burning and Global Change Vol. 1,* pp. 428–440, MIT. [4] Fearnside P. M. et al. (1993) *JGR, 98,* 16733–16743. [5] Crutzen P. J. and Andreae M. O. (1990) *Science, 250,* 1669–1678.

AN ANALYTICAL METHOD FOR THE DETERMINATION OF DIFFERENT CARBON FRACTIONS IN SOILS.

T. A. J. Kuhlbusch[1,2], R. G. Zepp[1], and S. E. Trumbore[3], [1]Environmental Protection Agency, Ecosystem Assessment Branch, Athens GA, USA [2]NRC Associate, University of Duisburg, FB9/AMT, Bismarckstrasse 81, 47057 Duisburg, Germany (tky@uni-duisburg.de), [3]Earth System Science, University of California, Irvine CA 92697-3100, USA (setrumbo@uci.edu).

Introduction: Carbon in terrestrial vegetation and soils worldwide outweighs the amount found in the atmosphere and the ocean surface layers. This terrestrial C pool, especially in the northern hemisphere, is currently thought to be a sink for atmospheric CO_2, but how this pool will change in view of global climate change is still highly uncertain and the subject of widespread debate. Turnover times are only a rough estimate of the speed with which C cycles through the soil. Some soil C compounds are retained for only days while others remain in soils for thousands of years (e.g., some humic substances and black carbon). Thus there is a need for a method to fractionate soil C constituents by degradability in order to estimate the different soil C pools (labile/refractory) and to study processes influencing the pools.

Method: The analytical method developed to determine the different C fractions in soils is based on the method by Kuhlbusch [1] for vegetation fire residues and divides soil C into 7 fractions; total inorganic C (TIC), solvent extractable organic C (OC1, light and dense fraction), thermally extractable organic C (OC2, light and dense fraction), and refractory organic C (RC, light and dense). The general scheme is also shown in Fig. 1.

A sample of the bulk soil sample was analyzed for C and the associated H by an elemental analysis before and after decarbonization to determine the total organic and inorganic C content. A Na polytungstate solution (density 1.6 g cm^{-3}) was used to divide the soil C into a light and dense fraction [2]. Then the same analysis scheme was used for the light and dense fraction: First step: 10 ml different solvents in following order: 2 × NaOH, 1 × HNO_3, 4 ×

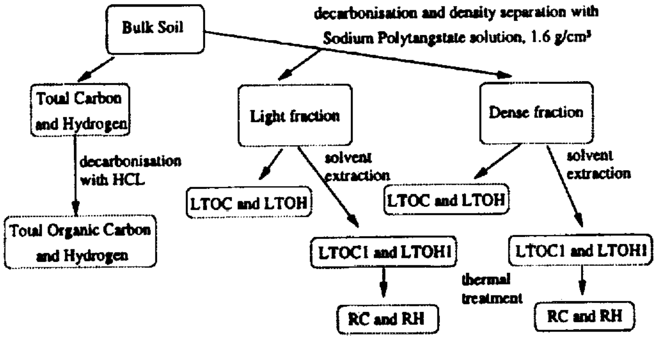

LTOC: Total organic carbon, light fraction; LTOC1: Organic carbon content after solvent extraction, light fraction; LRC: Refractory Carbon, light fraction, carbon content after solvent and thermal extraction; LOC1: solvent extracted carbon, light fraction, calculated: LTOC-LTOC1; LOC2: thermally extracted carbon, light fraction, calculated: LTOC1-RC; LRC: directly measured; Parallel scheme for the dense fraction; H: same for hydrogen.

Fig. 1. Soil C analysis scheme.

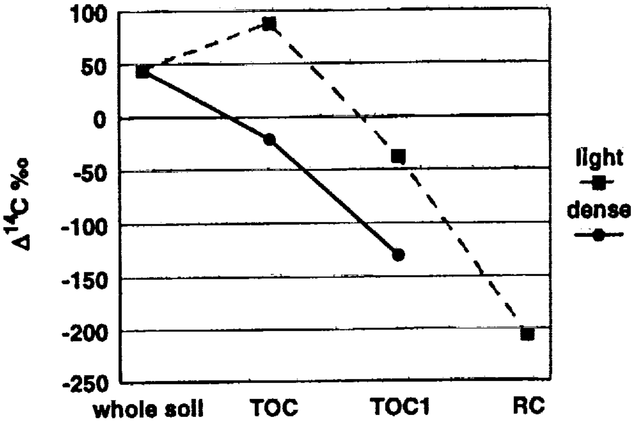

Fig. 2. Δ^{14}C values after the different treatment steps.

NaOH, 1 × HCl, 2 × H_2O, 1 × HF, and H_2O. A thermal treatment (2 h, 340°C, pure O_2) followed as the second step. All samples and subsamples were analyzed for C and H to derive the contents of the various fractions. The ^{14}C analysis was conducted as described in [2].

Results: Figure 2 gives the results of the ^{14}C analysis of the different C fractions for a humus/clay layer from Thompson, Manitoba, Canada.

It can be seen that the dense fraction has an older apparent ^{14}C age than the light fraction, and that the apparent ^{14}C age increases with each treatment step. Similar results were obtained for a humus layer and a prairie soil as well.

Conclusions: Δ^{14}C values of the different C fractions show that the presented soil fractionation scheme is capable of separating soil C constituents by their degradability. This scheme enables studies of physical and chemical protection [3] by the separation of light and dense material, and the breaking of the inorganic matrix by the HF-treatment (solvent extraction). The results of this analysis also provide useful constraints for models of soil C dynamics by allowing the determination of different C pools in soils. An upper limit of the input of black carbon (combustion derived recalcitrant C fraction in, e.g., charcoals) to soils can be derived from the RC-fraction.

References: [1] Kuhlbusch T. A. J. (1995) *ES&T, 29,* 2695–2702. [2] Trumbore S. E. (1993) *GBC, 7,* 275–290. [3] Oades J. M. (1995) *Dahlem Workshop Rpt., Environ. Sci., 16,* 293–303.

RARE GASES CONSTRAIN MANTLE MIXING IN THE RÉUNION HOT SPOT.

J. Kunz and C. J. Allègre, Institut de Physique du Globe de Paris, Laboratoire de Géochimie et Cosmochimie, 4 place Jussieu, 75252 Paris Cedex 05, France (kunz@ipgp.jussieu.fr).

Introduction: The island of La Réunion in the Indian ocean is the most recent manifestation of a mantle plume, which has been active during the last ~70 m.y. Geothermal spring waters and fluid inclusions in mantle xenoliths bear a primitive He signature with ^{4}He/^{3}He = ~54,000 [1 and references therein]; which is R = ^{3}He/^{4}He = ~13 Ra (Ra = atmospheric ^{3}He/^{4}He = 1.38×10^{-6}). This ratio is in between typical MORB values of ~90,000 (R/Ra = 8) and values of ~20,000 (R/Ra = 35) observed at Loihi seamount (Hawai'i), the most pristine hot spot concerning primordial He [2–4 and references therein]. This may result from some kind of mixing of pristine, Loihi-type He with a more radiogenic (e.g., MORB-type) component. Surprisingly, this isotopic signature of the Réunion hot spot has been quite constant since end of Cretaceous. This indicates that the He-isotopic ratios are likely to represents the signature of the plume source itself and that this source must be relatively gas-rich [5]. Otherwise, radiogenic increase in the source or a more or less erratic contamination during the rise of the plume, the residence in a magma chamber or during eruption should have destroyed the constancy.

Neon, Ar, and Xe isotopes could give important information about the Réunion plume source. However, their composition is less well known, because only few samples revealed significant isotopic anomalies compared to air. It is the aim of this study to establish the isotopic signature of all rare gases in the source of the Réunion hot spot and to constrain the possible mixing of mantle reservoirs therein.

Experimental: We select xenoliths (dunites) that have been analyzed previously [1]. Samples are either xenolith "whole rocks" or olivine separates. We apply step-heating or step-crushing techniques for gas extraction and measure all isotopes on ARESIBO I with a single-ion-counting facility (except ^{4}He and ^{40}Ar with a Faraday cup). Analyses are still in progress.

Preliminary Results: Typical concentrations in cm^3STPg^{-1} (in parts per billion) are 5×10^{-7} (9×10^{-2}), 1×10^{-11} (1×10^{-5}), 1×10^{-10} (2×10^{-4}), 5×10^{-12} (2×10^{-5}), and 5×10^{-14} (3×10^{-7}) for ^{4}He, ^{22}Ne, ^{36}Ar, ^{84}Kr, and ^{130}Xe respectively. The He-isotopic ratios are quite homogeneous (^{4}He/^{3}He = ~53,500 ± 1900, 1σ deviation) and agree well with previous measurements. We observe Ne anomalies up to ^{20}Ne/^{22}Ne = 12.3 (air: 9.80) that correlate closely with elevated ^{21}Ne/^{22}Ne ratios up to 0.039 (air: 0.029). The Ne mixing line for the Réunion hot spot has a slightly smaller slope than the Kilauea-Loihi mixing line [2,3], but it is considerably steeper than the MORB trend [4]. Argon-40/argon-36 ratios vary between ~500 and ~8000 (air: 295.5) and show a close correlation with elevated ^{20}Ne/^{22}Ne ratios. Correction for air contamination by extrapolating toward ^{20}Ne/^{22}Ne = 13.8 (solar Ne composition) gives ^{40}Ar/^{36}Ar = ~14,000 for the plume source, which is in between best estimates for uncontaminated Loihi source (2000–6000) [3] and MORB mantle (44,000) [4]. ^{38}Ar/^{36}Ar ratios scatter around the atmospheric value (0.188) and show no correlation with Ne or ^{40}Ar/^{36}Ar anomalies. Therefore, the presence of a solarlike Ar component (~0.175) is unlikely [6,7]. Krypton isotopes yield atmospheric ratios, too. Xenon shows some isotopic anomalies up to ^{129}Xe/^{130}Xe = ~6.9 (air: 6.496) and ^{136}Xe/^{130}Xe = ~2.3 (air: 2.176). Despite rather large error bars because of the quite low concentrations, we can observe a correlation between radiogenic ^{129}Xe- and fissiogenic ^{136}Xe-excesses that is quite similar to the MORB trend [8]. The correlation between Xe and Ne anomalies is even less well constrained. Thus, a correction for atmospheric contamination of the Xe is quite uncertain. However, it may indicate, that the plume source has an ^{129}Xe/^{130}Xe = ~7, significantly below the best estimate for uncontaminated MORB mantle (~8.2) [4].

Discussion: Neon, Ar, and Xe systematics confirm the He result that the source of the Réunion hot-shot rare gases is likely to be a mixture of different mantle reservoirs. The most simple approach is to assume a binary mixing between a Loihi-type component and the MORB mantle. This mixture is well homogenized (and apparently quite constant for the last ~70 m.y.!), before probably magma chamber processes and/or the eruption cause the variable degrees of atmospheric contamination. The inferred MORB:Loihi mixing ratios are ~1:1 for He and ~1:5 for Ne and Ar. The difference in the mixing ratios may be due a locally more radiogenic MORB signature for He. Local MORB mantle may be influenced by the DUPAL anomaly [9], which could significantly change the He-isotopic ratios with only minor effects on Ne and Ar.

Application of this simple mixing model for the Xe systematics indicates that the Loihi-type source should have only small (or no) Xe anomalies, in agreement with the proposed less-degassed state of the this mantle reservoir.

References: [1] Staudacher T. et al. (1990) *Chem. Geol., 89,* 1–17. [2] Honda et al. (1991) *Nature, 349,* 149–151. [3] Valbracht et al. (1997) *EPSL, 150,* 399–411. [4] Moreira M. et al. (1998) *Science, 279,* 1178–1181. [5] Staudacher T. et al. (1997) *Terra Nova Abstract Suppl., 9,* 52. [6] Pepin R. O. (1998) *Nature, 394,* 664–667. [7] Kunz J. (1999) *Nature,* in press. [8] Kunz J. et al. (1998) *Science, 280,* 877–880. [9] Dupré B. and Allègre C. J. (1983) *Nature, 303,* 142–146.

TRACE-ELEMENT REDISTRIBUTION AND ASIAN DUST ACCUMULATION IN A HAWAI'IAN SOIL CHRONOSEQUENCE.

A. C. Kurtz[1], L. A. Derry[1], and O. A. Chadwick[2], [1]Department of Geological Sciences, Cornell University, Ithaca NY, USA (kurtz@geology.cornell.edu), [2]Department of Geography, University of California, Santa Barbara CA, USA.

Introduction: Soils are complex open systems with material losses from weathering, and addition of new material from atmospheric pathways. A well-characterized chronosequence of Hawai'ian soils provides an opportunity to quantify elemental fluxes to, from, and within the soil system. Important processes include: residual enrichment of relatively insoluble trace elements during weathering; leaching and reprecipitation of these elements within the soil column; partial loss of all but the most insoluble elements; addition of trace elements to the soil by inputs of Asian dust; weathering and loss of the dust itself. Although the dust flux to Hawai'i is relatively low, dust is both geochemically and ecologically significant in older soils.

Hawai'i Long Substrate Age Gradient: The soil chronosequence is developed on basalt substrates ranging in age from 0.3 ka to 4.1 Ma [1]. All sites are located near 1200-m elevation, receive ~250 cm/yr rainfall, and are dominated by the same tree species. Parent material at the four older sites (>20 ka) is inferred to be hawai'ite. Degree of soil development differs substantially across the age gradient. Secondary mineralogy of intermediate aged soils (20–150 ka) is dominated by noncrystalline aluminosilicate "gels." Kaolin and crystalline sesquioxide minerals dominate soils older than 1 Ma. Dust-derived quartz and mica are important in ≥20 ka soils.

Trace-element Distributions: We sampled the 20 ka to 4.1 Ma sites over the top ~1 m of soil, and measured a group of relatively insoluble elements (Zr, Hf, Nb, Ta, Th, U, and REE) on Li-metaborate fusions by inductively coupled plasma mass spectrometry (ICP-MS). This dataset allows us to evaluate the behavior of these elements over 20 ka to 4 Ma timescales in intensely weathered soils. Niobium and Ta appear to be the least mobile elements. Tantalum/niobium ratios are not fractionated in even the oldest soils, while other elements, including Th and Zr are depleted relative to Nb at the surface and enriched at depth. Thorium enrichments in the deep soils cannot be balanced by Th lost from the upper part of the soil column. This "excess Th" is easily accounted for by mobilization of dust derived Th.

Rare Earth Elements: REEs are strongly leached from the surface horizons, and in some cases reprecipitated deeper in the soil column. LREEs appear to be preferentially leached, resulting in parent-normalized LREE depletion in the leached zone, and LREE enrichment in the zone of accumulation. There are no significant Ce anomalies in these soils. Intense leaching in surface horizons results in low basaltic REE concentrations, amplifying the influence of Asian dust on REE budgets. Individual horizons at these sites have ε_{Nd} as low at −6.9, indicating that >75% of this ε_{Nd} is dust-derived.

Dust Accumulation and Weathering: We calculate minimum long-term dust additions to these soils by integrating the mass of quartz present in the soil, and normalizing to the quartz content of dust. We find ~6 g of dust per square centimeter of soil at the 20-ka site, and ~14–18 g/cm^2 in the three older sites. There is no increase in quartz content in soils >150 k.y. old, suggesting that the rate of quartz loss by weathering is balanced by the input rate on long timescales. Dust-derived mica weathers more rapidly than quartz, especially in the oldest soils.

We calculate a dust addition rate ≈300 mg/cm^2/ky to the Hawai'i chronosequence sites, based on quartz addition to the 20-ka site. This estimate is about a factor of 5 higher than the background deposition rate in the Pacific Ocean near Hawai'i [2], likely reflecting orographic effects on precipitation. Still, the flux is 1–3 orders of magnitude lower than dust fluxes to continental soils. Dust supplies ~2 mg/cm^2/yr of phosphorus to the soils. Phosphorus release rate should be approximately equal to deposition rate in the older soils where dust is readily weathered. Weathering of dust becomes a biogeochemically relevant source of P in old Hawai'ian soils where P availability can limit forest growth [3].

References: [1] Chadwick O. A. et al. (1997) *GSA Today, 7,* 1–8. [2] Rea D. K. (1994) *Rev. Geophys., 32,* 159–195. [3] Chadwick O. A. et al. (1999) *Nature, 397,* 491–497.

DYNAMICS OF THE GALAPAGOS HOTSPOT FROM HELIUM-ISOTOPIC GEOCHEMISTRY.

M. D. Kurz[1], J. M. Curtice[1], A. E. Saal[1], and D. Geist[2], [1]Mail Stop 25, Woods Hole Oceanographic Institution, Woods Hole MA 02543, USA (mkurz@whoi.edu), [2]Department of Geology, University of Idaho, Moscow ID 83843, USA.

In order to utilize He as a tracer of the plume contribution to oceanic island volcanism, we have obtained isotopic (He, Sr, Nd, and Pb), major-element, trace-element, and exposure-age data from recent lava flows throughout the Galapagos archipelago, with an emphasis on the island of Fernandina. The measured $^3He/^4He$ ratios range from 8.6 to 31× atmospheric (Ra), with the highest values found at Fernandina, suggesting that it is the center of the hotspot/mantle plume. The only other oceanic island with such high $^3He/^4He$ ratios is Loihi Seamount (Hawai'i). Fernandina's location at the western edge of the archipelago, at the leading edge with respect to plate motion, and that it is the most active volcano, are consistent with it being the center of the hotspot. In addition, the $^3He/^4He$ ratios decrease systematically in all directions from Fernandina. This spatial variability is assumed to reflect the relative contributions of the plume component, and shows that He is one of the most sensitive indicators of plume influence. The isotopic data are consistent with earlier radiogenic isotopic studies, confirming extensive contribution of MORB or lithospheric mantle sources, especially to the central islands. Correlations are observed between $^3He/^4He$ and other isotopes (particularly Nd), trace elements (e.g., Nb/La, Sm/Yb), and major elements showing that the spatial variations are a combination of melting effects and source heterogeneity. Because the climate is so arid, Galapagos lava flows are extremely well preserved, and it was possible to obtain surface exposure dates for most of the samples using cosmic-ray-produced ^3He in the olivines. The predominantly young ages found in the western Galapagos (all <61 Ka) show that these volcanos have been erupting distinct compositions simultaneously for the last ~10 ka. The Fernandina lava flows are all younger than ~4 ka, and the data demonstrates that the ^3He surface exposure age dating method can be used to date lava flows as young as several hundred years. Combining the exposure ages with eruptive volumes calculated by Rowland [1] shows that Fernandina is growing at rates similar to Kilauea, making it one of the most active in the world. Significant (systematic) isotopic variation is found at Fernandina, with older lavas having higher $^3He/^4He$ ratios. These new data suggest that the extremely high $^3He/^4He$ ratios found in the Galapagos, and at some other oceanic islands, are derived from deep mantle sources.

References: [1] Rowland (1996).

INFLUENCE OF PRESSURE ON THE DIFFUSIVITY OF CARBON AND OXYGEN IN CALCITE.

T. C. Labotka,[1] D. R. Cole,[2] and L. R. Riciputi[2], [1]Department of Geological Sciences, University of Tennessee, Knoxville TN 37996-1410, USA (tlabotka@utk.edu), [2]Chemical and Analytical Sciences Division, Oak Ridge National Laboratory, Oak Ridge TN 37831-6110, USA.

The self-diffusion coefficients for C and O in calcite were determined in hydrothermal cold-seal vessels in the temperature range 600°–800°C at a pressure of 100 MPa. Single calcite crystals were encapsulated with pure, isotopically labeled $^{13}C^{18}O_2$ in Pt capsules to eliminate the catalytic effects of H_2O on diffusion. The resulting diffusion coefficients are $D_O = 7.5 \times 10^{-3}$ exp $(-29108/T)$ and $D_C = 7.8 \times 10^{-9}$ exp $(-19966/T)$. These values, although

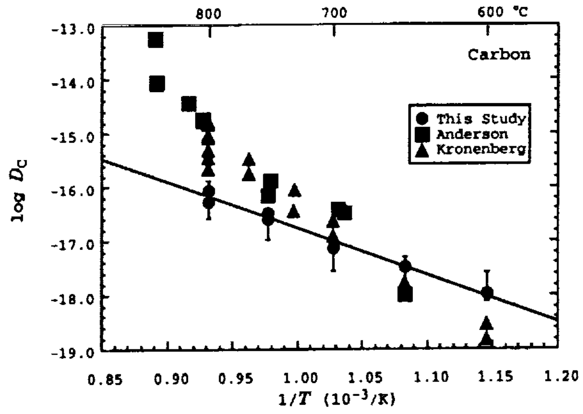

Fig. 1.

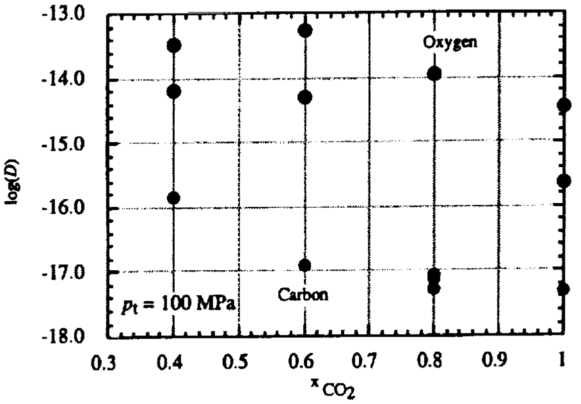

Fig. 2.

similar in magnitude, indicate significantly different activation energies from those determined by Anderson [1] and Kronenberg et al. [2], who measured the diffusivities at ~1 atm. A comparison between our 100 MPa data and their low-pressure data for C is shown in the Fig. 1. The activation energies measured by Anderson and Kronenberg are E_A/R = 44022 (mol K)$^{-1}$, more than twice that measured by us.

The regression for the low-pressure data intersects our line at ~700°C. The difference appears to result from the difference in pressure of the experiments, even though the experimental design of Anderson is much different from ours.

We are conducting a series of experiments to determine the influence of pressure on the diffusivities. The first series consists of single crystals of calcite in pure CO_2 heated to temperatures between 600° and 800°C at pressures ranging from ~0.2 to 200 Mpa. The low-pressure experiments are conducted in platinum capsules with a calcite crystal and ~0.1 Mpa CO_2, and the capsules are heated in a muffle furnace. The total pressure results from the heating of the encapsulated gas. The first results for the low-pressure diffusion of C indicate a slightly higher diffusivity at 700°C, which is consistent with Anderson's results.

The second series consists of experiments conducted at 700°C and a total pressure of 100 Mpa but the gas phase consists of a mixture of the labeled CO_2 and N_2. The N_2 is introduced to the capsule as Cu_3N, which readily decomposes at low temperature to Cu and N_2. The mole fraction of CO_2 ranges from 1.0 to 0.2. The experiment is designed to determine whether the partial pressure of CO_2 rather than the total pressure on the crystal has an effect on the diffusion of C and O in calcite. The results for O are ambiguous but indicate little or no effect on the diffusion coefficient (see Fig. 2). The values of D for C are much more precisely determined than for O, despite the lower diffusivity of C.

The diffusivity of C appears to increase with decreasing p_{CO_2}, although the effect is highly determined by the value at x_{CO_2} = 0.4. Preliminary results indicate that the activation energy and the diffusivity decreases with increasing pressure. These suggest a change in the mechanism of diffusion with pressure and a positive ΔV of activation.

References: [1] Anderson T. F (1969) *JGR, 74,* 3918–3932. [2] Kronenberg A. K. et al. (1984) *Phys. Chem. Mineral., 11,* 101–112.

OSMIUM-ISOTOPIC AND ABUNDANCE VARIATIONS IN MEXICAN ARC LAVAS: CONSTRAINTS ON THE PARTITIONING OF OSMIUM IN ARC AND NON-ARC SETTINGS.

J. C. Lassiter[1] and J. F. Luhr[2], [1]Max-Planck Institut für Chemie, 55020 Mainz, Germany (lassiter@mpch-mainz.mpg.de), [2]Department of Mineral Sciences, Smithsonian Institution, NBH 119, Washington D.C. 20560, USA.

Introduction: Compared with other isotopic tracers such as Sr or Nd, the geochemical behavior of Os during melt generation and evolution is poorly understood. There is considerable debate concerning the relative importance of silicates and sulfides in controlling Os abundances in basaltic melts, and several recent studies have suggested that Os abundances are controlled not by equilibrium partitioning of Os between melts and residual phases but instead by disequilibrium melting processes such as partial dissolution of mantle sulfides by ascending S-undersaturated magmas [1]. The potential for Os to be transported from subducting slabs via aqueous fluids is also poorly constrained, although elevated $^{187}Os/^{188}Os$ values in some arc-derived mantle xenoliths suggest that such transport does occur [2]. We have examined Os-isotope and abundance variations in a suite of arc lavas from the Western Mexican Volcanic Belt in order to address two basic questions. (1) Is the geochemical behavior of Os qualitatively different in highly oxidized arc lavas than in less oxidized MORBs or OIBs, as would be expected if Os contents were primarily controlled by sulfide partitioning or dissolution? (2) Do Os-isotope variations in arc lavas primarily result from radiogenic Os input from subducted crust and sediments [3], or from shallow-level crust/melt interaction?

Results and Discussion: Osmium isotopes and abundances vary greatly in the Mexican lavas, with $^{187}Os/^{188}Os$ ranging from 0.128 to 0.207 and [Os] from 10 to 400 ppt. Both Os abundance and isotopic composition are strongly correlated with MgO and Ni content, with more evolved samples having lower Os abundances and higher $^{187}Os/^{188}Os$. The Ni-Os and MgO-Os trends are consistent with bulk D_{Os}/D_{Ni} ≈ 1–2 during fractional crystallization. Lavas with Ni content consistent with near-primary mantle melts (Ni ≈ 200–400 ppm) for the most part have Os concentrations between 30 and 100 ppt. Samples with higher Ni and Os concentrations have experienced olivine accumulation or contain xenocrystic olivines from disaggregated mantle xenoliths.

Numerous oceanic basalt suites display similar correlations between Os, Ni, and MgO abundance. Nickel-osmium trends in low-Ni lavas that have experienced olivine fractionation (<200 ppm Ni) are consistent with D_{Os}/D_{Ni} ≈ 1–5 during fractional crystallization in most basaltic suites. The vast majority of MORB, OIBs, and arc lavas that have undergone minimal olivine fractionation or accumulation contain between 30 and 300 ppt Os. No systematic differences in Os contents of near-primary melts are observed with respect to tectonic setting, oxidation state, or degree of partial melting. Using an average mantle composition with ~2000 ppm Ni and ~3000 ppt Os, this concentration range is consistent with bulk D_{Os}/D_{Ni} ≈ 2–15 for moderate degrees of partial melting, or ~2–3× the bulk D_{Os}/D_{Ni} values observed during fractional crystallization.

Sulfur solubility in basaltic magmas increases with increasing f_{O_2}, and S speciation progressively switches from primarily sulfide at low f_{O_2} (ΔNNO <~1) to primarily sulfate at high f_{O_2} (ΔNNO >1) [4]. The similarity of MgO-Ni-Os trends in high f_{O_2} arc lavas (ΔNNO up to 6) with less oxidized oceanic basalts (ΔNNO ≈ -3 to 1) suggests that disequilibrium melting of sulfides [1] cannot account for the Os abundances in primary mantle melts. Instead, equilibrium partitioning of Os between melt and silicate and sulfide phases can reproduce the observed Ni and Os concentrations in primitive magmas and the observed fractionation trends provided that sulfide/melt K_D is <~2 × 10^5, which is an order of magnitude lower that the estimate of Hart and Ravizza [1].

The correlations between Os isotopes and Os content and indicators of fractional crystallization indicate that most if not all of the isotopic variability observed in the Mexican arc lavas reflects crustal assimilation rather than Os flux from the downgoing slab. Similar $1/[Os] - {}^{187}Os/{}^{188}Os$ correlations are observed in numerous other suites of evolved magmas, including MORBs [5] and arc lavas from Java [3]. Given the high compatibility of Os during fractional crystallization, such correlations cannot reflect primary mixing of mantle-derived components, because the Os concentrations in evolved lavas bare little relation to primary Os concentrations. Therefore, $1/[Os] - {}^{187}Os/{}^{188}Os$ correlations in evolved melts must reflect late-stage contamination by crustal- or seawater-derived Os.

References: [1] Hart S. R. and Ravizza G. E. (1996) *AGU Geophys. Monogr., 95,* 123–134. [2] Brandon A. D. et al. (1996) *Science, 272,* 861–864. [3] Alves S. et al. (1999) *EPSL, 168,* 65–77. [4] Wallace P. and Carmichael I. S. E. (1992) *GCA, 56,* 1863–1874. [5] Schiano P. et al. (1997) *EPSL, 150,* 363–379.

TRACE-ELEMENT ANALYSIS OF SULFIDE AND SILICATE PHASES WITH HIGH-RESOLUTION SECONDARY ION MASS SPECTROMETRY.

G. D. Layne and N. Shimizu, Mail Stop 23, Woods Hole Oceanographic Institution, Woods Hole MA 02543-1541, USA (glayne@whoi.edu; nshimizu@whoi.edu).

Introduction: Large-format, high-resolution, high-transmission ion microprobes, such as the Cameca IMS 1270, allow a new approach to secondary ion mass spectrometry (SIMS) analysis of trace elements in geologically important mineral phases. Essentially, elemental analysis can now be accomplished through explicit peak resolution, rather than the more traditional means of energy filtering commonly used on smaller format SIMS instruments. Mass resolving powers (MRP) as high as 10,000 have been used stably in magnetic peak switching mode to accomplish accurate multi-element analysis of REE and other trace elements (TE) while retaining detection limits of <1–100 ppb, depending on the element of interest.

The high-transmission characteristic of the instrument means that low primary beam currents may be utilized. Consequently, lateral spatial resolutions of <5–10 µm may be maintained where necessary. This makes the technique readily applicable to problems involving the analysis of experimental charges or very finely textured or zoned natural samples.

Sulfide Analysis: The IMS 1270 is now being utilized for the analysis of low level TEs in pyrite, chalcopyrite and other simple sulfide phases. To date we have demonstrated the practicability of simultaneous quantitative determination of Co, As, Ag, Se, Pb, and Bi. MRP of 8500 is more than sufficient to resolve all substantial isobaric interferences (e.g., $^{58}FeH^+$ on $^{59}Co^+$, $^{75}As^{34}S^+$ and FeO_3^+ on $^{109}Ag^+$), while retaining sufficient signal and peak flatness to produce precise analyses. These same parameters also show promise for the determination of Mo, Th, and U.

This technique is currently being applied to the study of TE distributions in pyrite and chalcopyrite from seafloor massive sulfide deposits, as a key to evolving physicochemical parameters and the mass transfer of metals within these systems.

Silicate Analysis: Smaller format ion microprobes, such as the Cameca IMS3/4/5/6f series, have long been used productively for the measurement of REE in silicate glasses and minerals. In many applications, isobaric interferences resulting from BaO_x^+ and $(LREE)O_x^+$ may be effectively eliminated by the technique of energy filtering. In this manner, a useful subset of REE (usually La, Ce, Nd, Sm, Eu, Dy, Er, and Yb) can be determined in many silicate matrices, with detection limits in the range of 1–5 ppb [1]. However, for LREE-enriched phases, such as plagioclase, it becomes necessary to empirically peak strip these same isobars from the signals for the HREE — increasing practical detection limits to 20–30 ppb for these elements [2].

Using the IMS 1270, procedures for the quantitative determination of ten REE (La, Ce, Nd, Sm, Eu, Gd, Dy, Er, Yb, and Lu) in silicate minerals and glasses have been developed using MRP of 9500. Using this technique, oxide interferences — such as $^{158}GdO^+$, $^{158}DyO^+$, $^{142}NdO_2^+$ and $^{142}CeO_2^+$ on $^{174}Yb^+$ — are completely resolved. As a check on the accuracy of these measurements, the natural isotope ratios of Nd, Sm, Eu, Gd, Dy, Er, and Yb were replicated with accuracies within the expected counting error (better than 2%).

Using primary beam currents of 15 nA (with a consequent lateral spatial resolution of <15 µm) and a typical run time of 25 min, analyses of clinopyroxene, orthopyroxene, and olivine have been performed with detection limits ranging from 0.07 ppb for La to 9 ppb for Yb. Measurements of reference materials with known REE concentrations show that considerable matrix effects remain with respect to major-element concentration, but that accurate analyses can be accomplished by using an appropriate reference material for each phase of interest.

References: [1] Jones R. H. and Layne G. D. (1997) *Am. Mineral., 82,* 534–545. [2] Pun A. et al. (1997) *GCA, 61,* 5089–5097.

DELAMINATION OF CONTINENTAL LITHOSPHERE BENEATH AN ACTIVE MARGIN? THERMOBAROMETRIC AND RHENIUM-OSMIUM-ISOTOPIC CONSTRAINTS FROM SIERRA NEVADAN XENOLITHS.

C.-T. Lee[1], Q. Z. Yin[1], J. T. Chesley[2], R. L. Rudnick[1], W. F. McDonough[1], G. H. Brimhall Jr.[3], and S. B. Jacobsen[1], [1]Department of Earth and Planetary Sciences, Harvard University, 20 Oxford Street, Cambridge MA 02138, USA (ctlee@fas.harvard.edu), [2]Department of Geosciences, University of Arizona, Tucson AZ 85712-0077, USA, [3]Department of Geology and Geophysics, University of California, Berkeley CA 94720, USA.

Introduction: Delamination of the lithosphere, defined as any detachment of the lithospheric mantle or lower crust into the asthenosphere, has been proposed as a mechanism for recycling continental material back into the convecting mantle and as an integral process in the geodynamic development of orogenic zones. However, it is still unclear how and where delamination occurs. Western North America is one region where circumstantial evidence suggests recent delamination based on decreased sub-Moho seismic velocities and increased heat flow, magmatism, and uplift. These phenomena are especially apparent in the Sierra Nevada, California, located on the western edge of the Precambrian Laurentian craton. In particular, Ducea and Saleeby [1] report that mid-Miocene alkali basalts erupted through the axis of the Sierra Nevada have abundant garnet-bearing lower crustal rocks, while Pliocene basalts, erupted through the same region, are devoid of garnet-bearing lithologies, suggesting removal of the lower crust and lithospheric mantle between late Miocene to Pliocene.

While the evidence for delamination is compelling, there is also evidence to the contrary. Basalts erupted through the eastern Sierra Nevada and western Basin and Range have enriched Sr- and Nd-isotopic signatures that have been interpreted to derive from ancient, incompatible-element-enriched, subcontinental lithospheric mantle, which must persist beneath much of western North America [2]. In addition, radiogenic $^3He/^4He$ ratios in some of these basalts have been interpreted to represent radiogenic ingrowth of He in enriched lithospheric mantle [3].

Here, we attempt to reconcile this controversy by studying peridotitic xenoliths from mid-Miocene and Pliocene alkali basalts erupted through the Sierra Nevada. We use the Re-Os-isotopic system to test whether any of these xenoliths represent ancient lithospheric mantle or renewed asthenospheric mantle. The former would be characterized by subchondritic $^{187}Os/^{188}Os$ (0.11–0.12) while the latter would be characterized by asthenospheric ratios (0.125–0.129, based on abyssal peridotite compositions).

Mid-Miocene Xenolith Suites: In these basalts, there are rare refractory garnet-bearing spinel peridotite xenoliths (Fo 90–91), which record unambiguous evidence for cooling: pervasive exsolution of garnet from pyroxenes, formation of garnet at the expense of spinel, and high Ca and Al cores of orthopyroxenes. The high Ca orthopyroxene cores require initial temperatures to be near-solidus (~1400°C) while garnet-pyroxene thermometry on exsolved lamallae suggest that these rocks cooled to temperatures of ~750°C; within the range of temperatures inferred from garnet-clinopyroxenites [1,3]. Equilibration pressures are between 2–3 GPa, placing these peridotites near the geotherm inferred from low surface heat flow measurements. These cooling textures suggest intrusion of the peridotites into cooler lithosphere and cooling to the ambient geotherm sometime prior to the Miocene. Preliminary results show these peridotites to have asthenospheric (0.125–0.126) and more radiogenic Os-isotopic compositions (0.140). We thus interpret these peridotites to be samples of hot, asthenospheric mantle upwellings that rose into cold lithosphere and subsequently "froze" in place.

Late Pliocene Xenolith Suites: These xenoliths are characterized by more fertile compositions (<Fo 90), general lack of chemical disequilibrium,

and higher equilibration temperatures (~1000°–1100°C). Based on the absence of garnet, these peridotites come from shallower depths than peridotites in the mid-Miocene basalts. Preliminary data reveal Os-isotopic compositions of 0.126, consistent with these being asthenospheric mantle rather than ancient lithopsheric mantle.

Discussion: Our limited data show that the Os-isotopic values between Miocene and Pliocene upper mantle xenoliths are indistinguishable and similar to modern asthenosphere. We have not yet found evidence for Proterozoic mantle lithosphere beneath the Sierra Nevada. If these findings are born out by additional measurements currently underway, they suggest loss of the Proterozoic mantle lithosphere prior to the Miocene. These results would further suggest that the differences in mafic xenolith abundances between Miocene and Pliocene pipes may be ascribed to incomplete sampling of the lithosphere by the host magmas and do not require post-Miocene delamination of this material. We are currently measuring the Os-isotopic compositions of the "cold" peridotites in the Miocene host, which may represent the best chance of finding ancient lithosphere.

References: [1] Ducea M. N. and Saleeby J. B. (1996) *JGR, 101,* 8229–8241. [2] Ormerod D. S. (1988) *Nature, 333,* 349–353. [3] Dodson A. et al. (1998) *GCA, 62,* 3775–3787.

METASEDIMENTS IN THE LOWER CRUST: TECTONIC ORIGIN INFERRED FROM *IN SITU* HAFNIUM-ISOTOPIC ANALYSES OF ZIRCONS IN A METASEDIMENTARY XENOLITH.

C.-T. Lee, Q. Z. Yin, I. Horn, R. L. Rudnick, and W. F. McDonough, Department of Earth and Planetary Sciences, Harvard University, 20 Oxford Street, Cambridge MA 02138, USA (ctlee@fas.harvard.edu).

Introduction: It is generally believed that the lower crust is mafic in composition, being formed primarily by mafic underplating or by partial melting of thickened crust that leaves behind a mafic residue. However, metasedimentary xenoliths are a rare but ubiquitous component of lower crustal xenolith suites [1]. It is thus important to document these suprcrustal lithologies to understand how and when they were emplaced in the lower crust.

Rare metasedimentary xenoliths occur in a Miocene diatreme erupted through the Sierra Nevada batholith, a remnant of a Mesozoic arc. The xenoliths are garnet-bearing metaquartzites, containing abundant rutile, apatite, graphite and zircon as accessory minerals. The goal of this study is to constrain the provenance, timing of deposition, and timing of emplacement of these metasediments.

Here, we use laser ablation inductively coupled plasma mass spectrometry (LA-ICP-MS) to obtain *in situ* Hf-isotopic compositions of these zircons. Zircons are ideally suited for determining initial Hf-isotopic compositions because they have abundant Hf and very low Lu/Hf ratios and they are generally resistant to Lu/Hf disturbance. For these reasons, *in situ* analysis of zircons may be a rapid reconnaissance tool in provenance studies.

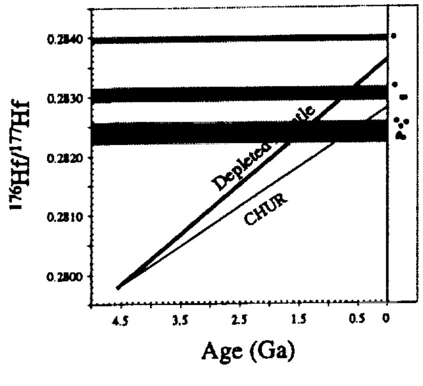

Fig. 1. Hafnium-isotopic ratios plotted with depleted mantle evolution curve. 2σ mean <6ε. Model ages estimated by assuming Lu/Hf ~0.

Lutetium-depletion Model Ages: When combined with the fact that the crust has low Lu/Hf, the Hf-isotopic composition of a zircon always provides a minimum, but reasonable, estimate of the age of juvenile crust formation, i.e., the model age is calculated assuming Lu/Hf ~0. This approach closely parallels the use of the Re-Os-isotopic system for dating mantle differentiation: the residual mantle has very low Re/Os so that a minimum estimate of the age of differentiation can be estimated by assuming Re/Os = 0.

Analytical Techniques: Hafnium-isotopic analyses were conducted on a Micromass Isoprobe multiple collector ICP-MS at the Harvard University Laser Ablation facility. Spot analyses ranged between 25 and 50 µm. Ratios were normalized to ^{178}Hf/^{177}Hf = 1.46714, using an exponential law. Interference free masses ^{173}Yb and ^{175}Lu were monitored in order to correct for Yb and Lu interferences on mass 176. Signal sizes were <1 V, giving internal precision for ^{176}Hf/^{177}Hf between 0.5–6ε ($2\sigma_m$), depending on signal size. Accuracy was monitored using standard 91500 zircons [2], yielding reproducibility to within 2ε (^{176}Hf/^{177}Hf = 0.282284). Lutetium-176/hafnium-177 in zircons ranged between 0.0005–0.001.

Results and Discussion: Using the depleted mantle evolution curve taken from the array of oceanic basalts [3], two age populations were discovered, 1.25–1.70 Ga and 0.6–0.8 Ga (Fig. 1). One zircon gave an unusually radiogenic isotopic ratio of 0.2840 ± 0.0001, significantly higher than depleted mantle.

The mid-Proterozoic ages are consistent with the age of juvenile crust and crustal reworking in southwestern North America [4]. The lack of Archean ages suggests that the sediment provenance was local basement rather than distal Archean basement to the north. Alternatively, these ages may be associated with sediments derived from Grenvillian basement (Sm-Nd model ages of 1.0–1.6 Ga) remobilized during the Caledonian-Appalachian orogeny [5].

The late Proterozoic to Cambrian ages are enigmatic because no major juvenile crust formation exists during this period of time. This curious distribution of ages mirrors that found in Triassic sediments of the Golconda terrane in central Nevada [6] and may thus correspond to a distinct allochthonous terrane, or in our opinion, to zircons associated with volcanism during Precambrian rifting of the western edge of Laurentia. As such, these sediments could have been emplaced during Mesozoic subduction.

References: [1] Rudnick and Fountain (1995) *Rev. Geophys., 33,* 267–309. [2] Wiedenbeck M. et al. (1995) *Geostandards Newslett., 19,* 1–23. [3] Patchett P. J. et al. (1981) *Contrib. Mineral. Petrol., 78,* 279–297. [4] Wooden J. L. and Miller D. M. (1990) *JGR, 95,* 20133–20146. [5] Patchett P. J. et al. (1999) *Science, 283,* 671–673. [6] Gehrels G. E. (1995) *Geology, 23,* 831–834.

NATROCARBONATITE PETROGENESIS: LIMESTONE-TRONA (EVAPORITE) VOLATILE-FLUXING AND SYNTECTIC REACTIONS REVISITED.

D. R. Lentz, Department of Geology, University of New Brunswick, Fredericton, New Brunswick E3B 5A3, Canada (dlentz@unb.ca).

Introduction: Brogger and Daly's simple limestone melting and silicate magma-limestone syntectic relations were the first magmatic hypotheses for carbonatite genesis [1,2]. Since the early 1960s, however, mantle-related hypotheses gained momentum because of the enrichments in F, P, Nb, U, Th, REE, etc., and preliminary stable and radiogenic isotopic signatures were unlike sedimentary limestones [4]. Also, syntectic relations involving limestone were deemed problematic [5–7]. However, volatile-fluxing of calcareous rocks during contact metasomatism has theoretically been shown to generate carbonate melts [8,9]. Therefore, earlier objections to syntectic hypotheses are no longer as problematic (see below), if water-rich, limestone-derived carbonate (or trona-derived natrocarbonatite) melts are involved [10].

Oldoinyo Lengai Petrogenesis: This unique, active natrocarbonatite and related hyperperalkalic volcanic system are presently postulated as originating from the mantle either as liquid immiscibility phenomena [11–14] or from extremely peralkalic magmas [15,16]. However, Milton [17,18] suggested these lavas formed via interaction between a silicate magma and troniferous (evaporitic) lacustrine sediments (Lake Magadi-type) that underlie the area. He postulated that peri-eutectic (partial) melting in the $CaCO_3$-$NaCO_3$ system, as experimentally determined by Niggli [19], was pertinent to partial melting then syntectic reaction evolving into immiscible separation of relatively buoyant natrocarbonate magma.

Volatile-Fluxing and Syntectic Relations: Using Wyllie and Tuttle's classic study [20], the possible role of volatiles in exocontact limestone melting was recognized [9,10,21]. Considering the role of mixed volatiles (H_2O-CO_2) in melting [20], it is evident they should also depress the volatile-saturated $CaCO_3$-$NaCO_3$-K_2CO_3 liquidi/solidus [22] from >750°C to <600°C. This is consistent with measured eruptive temperatures (575°–600°C) [23] and gas compositions [24]. If intruding A-type magmas were responsible for volatile-fluxed sediments, then syntectic reaction of these derivative (natro)carbonate melts with the silicate magma could generated these comagmatic systems analogous to the earlier thermochemical predictions [25,26]. Syntectic chemical interaction would involve elemental exchange between evolving immiscible, volatile-fluxed trona melts (natrocarbonatite) and hyperfractionating peralkalic silicate magma. Hyperfractionation results from complex syntectic processes (coupled desilication of the A-type magma and sial silication of the carbonatitic melt coexisting immiscibly). The derivative Ca-Mg hypersolidus endoskarn-like syntectic products are reminiscent of mantle assemblages, although are typical high-T endoskarn phases (e.g., Wo, Fo, Di, Mtc, Mel, Ttn, And). Differential degassing of a shallow-level syntectically evolving system and the high-T of A-type magmas make earlier objections to syntexis untenable and, in fact, complimentary to existing experimental evidence on the solubility of $CaCO_3$ [6,7,27,28] and $NaCO_3$ [29–31] in some silicate magmas.

Elemental partitioning/exchange reactions between immiscible "secondary" natrocarbonatite and A-type magmas during dynamic interaction is analogous to known partitioning equilibria (31,32). A combination of Rayleigh decarbonation processes and elemental partitioning between coexisting melts would result in isotopically heterogeneous (natro)carbonatite and (hyper)peralkalic melts with "crustally contaminated" mantle-like signatures, based on mass-balance considerations. Therefore, traditional studies cannot readily distinguish between Daly-Brogger syntectic and mantle-derived genetic models, including those for Oldoinyo Lengai.

References: [1] Heinrich E. W. (1966) in *The Geology of Carbonatites,* Rand McNally, NY. [2] Daly R. A. (1933) in *Igneous Rocks and the Depths of the Earth,* McGraw-Hill, NY. [3] Tuttle O. F. and Gittins J. (1966) in *Carbonatites,* pp. xi–xiv, Wiley, NY. [4] Watkinson D. H. and Wyllie P. J. (1964) *Nature, 204,* 1053–1054. [5] Watkinson D. H. and Wyllie P. J. (1969) *GSA Bull., 80,* 1565–1576. [6] Wyllie P. J. and Watkinson D. H. (1970) *Can. Mineral., 10,* 362–374. [7] Wyllie P. J. (1974) in *The Alkaline Rocks,* pp. 459–474, Wiley, NY. [8] Lentz D. R. (1999) *Geology, 27,* 335–338. [9] Lentz D. R (1998) in *Mineralized Intrusion-Related Skarn Systems. Min. Assoc. Can. Short Course, 26,* 519–657. [10] Lentz D. R. (1999) *GAC/MAC Abstr., 24,* in press. [11] Peterson T. D. (1990) *Contrib. Mineral. Petrol., 105,* 143–155. [12] Peterson T. D. and Kjarsgaard B. A. (1995) in *Carbonatite Volcanism: Oldoinyo Lengai and the Petrogenesis of Natrocarbonatites, IAVCEI Proc. Volc., 4,* pp. 148–162, Springer-Verlag, NY. [13] Kjarsgaard B. A. et al. (1995) in *Carbonatite Volcanism: Oldoinyo Lengai and the Petrogenesis of Natrocarbonatites, IAVCEI Proc. in Volc. 4,* pp. 163–190, Springer-Verlag, NY. [14] Dawson J. B. et al. (1996) *J. Geol., 104,* 41–54. [15] Gittins J. (1989) in *Carbonatites: Genesis and Evolution,* pp. 580–600, Unwin-Hyman, London. [16] Bell K. and Dawson J. B. (1995) in *Carbonatite Volcanism: Oldoinyo Lengai and the Petrogenesis of Natrocarbonatites, IAVCEI Proc. Volc. 4,* pp. 137–147, Springer-Verlag, NY. [17] Milton C. (1968) *GSA Prog. Abstr.,* 202. [18] Milton C. (1989) *28th Intl. Geol. Cong.,* Washington, 2–4. [19] Niggli P. (1916) *Z. Anorg. Allg. Chem., 98,* 241–326. [20] Wyllie P. J. and Tuttle O. F. (1960) *J. Petrol., 1,* 1–46. [21] Schuiling R. D. (1961) *Nature, 192,* 1280. [22] Cooper A. F. et al. (1975) *Am. J. Sci., 275,* 534–560. [23] Dawson J. B. et al. (1990) *Geology, 18,* 260–263. [24] Javoy M. et al. (1989) *Terra Abstr., 1,* 324. [25] Schuiling R. D. (1964) *Nature, 201,* 1115–1116. [26] Schuiling R. D. (1964) *Nature, 204,* 1054–1055. [27] Watkinson D. H. and Wyllie P. J. (1971) *J. Petrol., 12,* 357–378. [28] Woh-Jer Lee and Wyllie P. J. (1994) *Intl. Geol. Rev., 36,* 797–819. [29] Koster van Groos A. F. and Wyllie P. J. (1966) *Am. J. Sci., 264,* 234–255. [30] Koster van Groos A. F. and Wyllie P. J. (1968) *Am. J. Sci., 266,* 932–967. [31] Koster van Groos A. F. and Wyllie P. J. (1973) *Am. J. Sci., 273,* 465–487. [32] Hamilton D. L. et al. (1989) in *Carbonatites: Genesis and Evolution,* pp. 405–427, Unwin-Hyman, London. [33] Jones J. H. et al. (1995) *GCA, 59,* 1307–1320.

CHLORINE-ISOTOPIC FRACTIONATION IN A SEQUENCE OF BLACK SHALES.

S. M. Lev and R. D. Vocke Jr., Mail Stop 8391, National Institute of Standards and Technology, Advanced Chemical Sciences Laboratory, 100 Bureau Drive, Gaithersburg MD 20899-8391, USA.

Introduction: Clay mineral formation, alteration, dehydration, and transformation as well as ion filtration have been identified as potentially important mechanisms for fractionating Cl isotopes in sedimentary systems [1–3]. To date, Cl-isotopic variations in sedimentary sequences that have interacted with diagenetic pore fluids have not been systematically quantified.

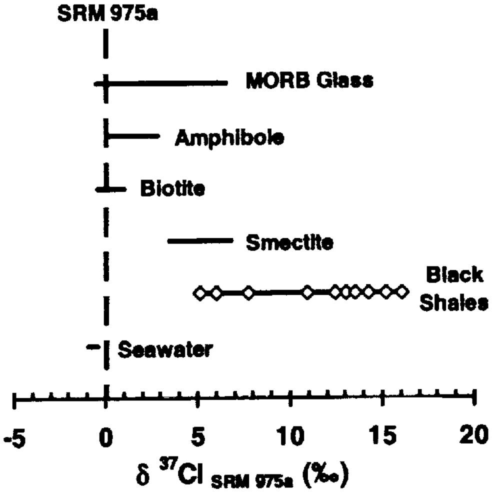

Fig. 1. $\delta^{37}Cl_{SRM\ 975a}$ (‰) for the Welsh black shales from this study compared with literature values for a variety of silicate phases. The width of the dashed line at 0 represents a ±0.15‰ uncertainty.

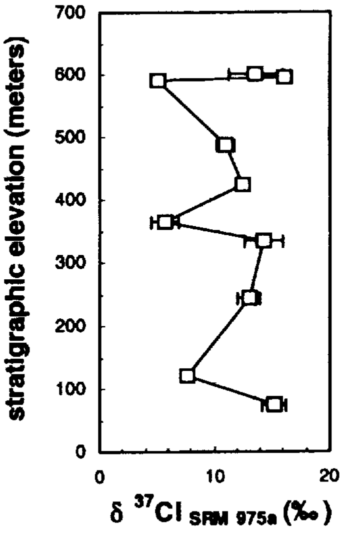

Fig. 2. The range in $\delta^{37}Cl_{SRM\ 975a}$ displayed by the Welsh Basin black shales relative to their stratigraphic position.

This study reports the Cl-isotopic signatures of a sequence of diagenetically altered Mid-Ordovician black shales deposited in the Welsh Basin, UK [4,5]. The total range in $\delta^{37}Cl_{SRM\,975a}$ (‰) values is between 5‰ and 16‰ (Fig. 1). These measurements considerably expand the previously measured range in Cl-isotopic fractionation observed in silicates.

Methods: Chlorine was extracted from shale samples using a modified pyrohydrolysis technique [6,7]. The extracted Cl was purified and converted to Cs_2Cl^+ [8]. All samples were run by positive-ion thermal ionization mass spectrometry. NIST isotopic reference material 975a was run in parallel to monitor external reproducibility, which was ~0.15‰ at a 95% confidence interval. The use of SRM 975a as a normalizing standard over SMOC allows for correction of ratio data to an absolute value. It also facilitates a more precise normalization and consequent inter-laboratory comparisons by providing a homogeneous isotopic artifact that is readily available.

Discussion: The shales examined in this study span ~700 m of section and have had extensive interaction with early and late diagenetic fluids [4,5]. The range in chlorine isotopic composition displayed by these rocks doubtless reflects this complicated diagenetic history (Fig. 2) and probably requires a kinetic rather than a chemical or biologic fractionation mechanism due to the observed range of values and the conservative behavior of chlorine in natural systems.

References: [1] Ransom et al. (1995) *Geology, 23,* 715–718. [2] Phillips F. M. and Bentley H. W. (1987) *GCA, 51,* 683–695. [3] Loomis J. L. et al. (1998) *Mineralogical Mag., 62A,* 901–902. [4] Lev S. M. et al. (1998) *JSR, 68,* 970–980. [5] Lev S. M. et al. (1999) *JSR, Part A,* in press. [6] Dreibus et al. (1977) in *Origin and Distribution of the Elements,* pp. 33–38, Permagon, Oxford. [7] Mangenheim et al. (1994) *GCA, 58,* 3117–3121. [8] Xiao Y.-K. and Zhang C.-G. (1992) *Intl. J. Mass Spectrom. Ion Proc., 116,* 183–192.

GEOCHEMISTRY OF THE SHUIQUANGOU GOLD-BEARING ALKALINE METASOMATIC COMPLEX IN NORTHWEST HEBEI, CHINA.

H. Y. Li, Z. S. Yang, Z. M. Gao, Z. J. Ding, and T. Y. Luo, Institute of Geochemistry, Chinese Academy of Sciences, Guiyang 550002, China (zjding@ms.gyig.ac.cn).

A unique Au-bearing alkaline metasomatic complex is well developed in the Au-Ag-polymetallic enriched area in northwest Hebei [1]. The complex extends over 400 km^2. It consists of alkaline metasomatic rocks including K metasomatic syenites, Na metasomatic monzonites and acid metasomatic granites, and Au deposits that include potassic altered rock-type (Dongping) and quartz vein-type (Xiaoyingpan). From its center to periphery, it is characterized by the alkaline metasomatism from intensive to weak, dimensional to fracture-filled, fractures from ductile to brittle-ductile and to brittle, Au mineralization from the potassic altered rock-type to the quartz vein-type, Sm-Nd isochron ages from 251.3 to 157.8 Ma [2]. The separations of K from Na, acid from alkaline and ore from alkaline occurred orderly in the system as the alkaline metasomatic hydrothermal system evolved from closed to partially opened and to fully opened. Sodic, potassic, siliceous and ore constituents are characterized by complex horizontal and vertical zonalities [3].

The extensive dimensional alkaline metasomatism could account for the widespread occurrence of the K-metasomatic syenites, Na-metasomatic monzonites and acid metasomatic granites. This early stage metasomatism not only formed largely the complex, but provided some Au elements for mineralization and made the Au elements in the Sanggan group (with an average Au content of 8 ppb) around the complex mobilize, migrate and move into it, which resulted in a primary Au concentration in its endomorphic zone (with an average Au content of 12.5 ppb), a Au depletion in the metamorphic rocks of the Sanggan Group (with an average Au content of 4 ppb) near the complex. The majority of the alkaline feldspar-quartz veins, potassic-siliceous altered lodes, milklike white quartz veins, and Au-bearing quartz lodes (quartz vein-type Au deposits), were formed during late-stage fracture-filled type alkaline metasomatism [2].

The most notable chemical changes from the unaltered original rocks were the introduction of K_2O, Na_2O, and SiO_2, and the loss of CaO, MgO, FeO, and TiO_2 during the alkaline metasomatism. K_2O contents (average) increase from 1.81% in the unaltered original rocks to 6.05% in the K-metasomatic syenites and up to 13.5% in the Au-bearing potassic altered rocks. Na_2O contents (average) add from 2.74% in the unaltered rocks to 5.59% in the K-metasomatic syenites and up to 7.52% in the Na-metasomatic monzonites. SiO_2 contents (average) change from 55.15% in the unaltered rocks to 66.50% in the Na-metasomatic monzonites and up to 90% in the quartz veins. The low content of Na_2O (0.3% average) in the Au-bearing potassic altered rocks reflects the separation of K from Na. The Au-bearing quartz veins are low in K_2O (0.07% average) and Na_2O (1.38% average), suggesting the separations of alkaline from acid and ore from alkaline [2].

FeO/MgO ratios from the alkaline metasomatic rocks fall within the restricted range of 1.73–2.18.With significant depletion of Cr, Ni, Co, and V, the K metasomatic syenites and Na metasomatic monzonites have lower REE between 18.65 to 62.38 ppm, $Sr_{initial}$ values between 0.701 to 0.706, $^{143}Nd/^{144}Nd$ ratios between 0.512708 to 0.512765 $\delta^{18}O$ values between 7.06‰ to 10.02‰. The $\delta^{34}S$ values for pyrites in the Au deposits range from –3.8‰ to +4.5‰. These evidences show that the formation of the complex was effected by fluids of mantle source or mixed mantle-crust source.

References: [1] Li H. Y et al. (1996) *Mineral Deposits, 15,* 249–256 (in Chinese). [2] Li H. Y. et al. (1994) *Gold, 15,* 1–6 (in Chinese). [3] Du L. T. (1983) *Mineral Deposits, 2,* 33–41 (in Chinese).

HYDROXYL BEHAVIOR IN OXYHYDROXIDE PHASES (MOOH, M = Al, Fe, Mn) BASED ON PERIODIC MOLECULAR ORBITAL CALCULATIONS.

J-J. Liang and R. T. Cygan, Geochemistry Department, Sandia National Laboratories, Albuquerque NM 87185-0750, USA (jliang@sandia.gov; rtcygan@sandia.gov).

The oxyhydroxides (MOOH) comprise a class of crystalline materials that have important members, such as AlOOH, FeOOH, and MnOOH, that are closely associated with industrial applications [1,2] and with geochemical processes involving adsorption of chemical and radioactive wastes [3]. A molecular-level understanding of the bulk crystal structure of these phases will provide a fundamental basis for the evaluation of mineral reactivity and surface properties that are central to the environmental and industrial applications. The extremely fine-grained nature of these compounds has hindered any conclusive structural determination of the orthorhombic phases that are of the boehmite (γ-AlOOH) structure type.

In our present study, we used periodic nonlocal density functional theory (DFT) to examine the structural details, particularly the orientation and energetics of the hydroxyl groups in the oxyhydroxides. Two periodic DFT programs, $DMOL^3$ [4] and CASTEP [5], were used in the calculation. The plane wave pseudopotential-based CASTEP was used to relax the unit cell dimensions, while $DMOL^3$ was used for the more accurate all-electron calculation. In CASTEP calculations, all atom species are represented by a set of ultrasoft potentials. In the $DMOL^3$ calculations, a nonlocal DFT method

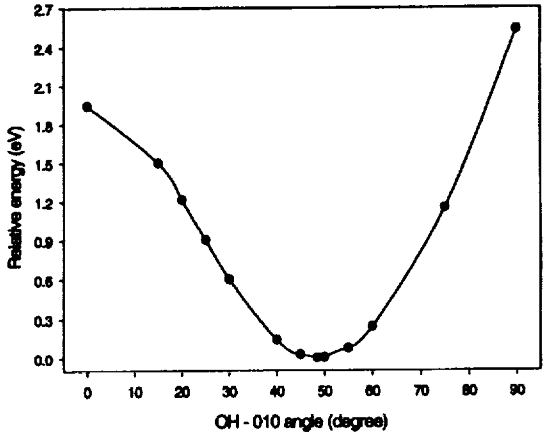

Fig. 1. Variation of energy of the boehmite structure ($Cmc2_1$) as a function of the angle between OH vector and the 010 plane.

was used based on a DNP (double numeric functions together with polarization functions) basis set for all atom species. Boehmite structure type was studied in detail, and the experimentally-determined boehmite structure [6] was used as starting model for all compositions. Unit-cell dimensions for known phases (γ-AlOOH and γ-FeOOH) were reproduced to within 3% of the observed values, and non-H atom positions to within 0.1 Å. Structure energies of the boehmite structure in space group $Cmc2_1$ were calculated as a function of OH orientation (Fig. 1). When the OH bond orientation vector is ~48° to the (010) plane, the structure energy obtains a value at a well-defined minimum (Fig. 1). This result agrees with the neutron structure refinement in space group $Cmc2_1$. In order to detect lower symmetry due to H atom disordering, a unit cell with H atoms distributed such that the cell assumes $Pmc2_1$ symmetry was constructed. A single-point energy calculation using $DMOL^3$ showed that this configuration is 0.77 eV less stable than the configuration assuming $Cmc2_1$ symmetry. An energy optimization without symmetry constraints (all atoms in the unit cell freely movable independent of each other) with an initial $Pmc2_1$ symmetry resulted in a configuration that is identical to that assuming $Cmc2_1$ symmetry. Therefore, an entropic stabilization of at least 0.77 eV is needed for the structure to assume a disordered configuration with $Pmc2_1$ symmetry as suggested by spectroscopic studies [7,8]. Similar calculations for the FeOOH phase gave opposite results, with the hydroxyl configuration assuming $Pmc2_1$ symmetry 3.28 eV more favorable than that assuming the $Cmc2_1$ symmetry.

An energetically stable structure was found for MnOOH assuming the boehmite structure that has not been reported previously, with unit cell dimensions (in ångstroms) of a = 2.8558, b = 12.5628, and c = 4.0343 respectively.

Acknowledgments: This research was supported by the U. S. Department of Energy, Office of Basic Energy Sciences, Geosciences Research, under contract DE-AC04-94AL85000 with Sandia National Laboratories.

References: [1] Morooka S. and Kusakabe K. (1999) *MRS Bull., 24,* 25–29. [2] Blesa M. A. et al. (1994) in *Chemical Dissolution of Metal Oxides,* CRC Press. [3] Rai D. and Zachara J. M. (1988) *Tech. Rpt. EPRI-EA-5741,* Electric Power Research Institute. [4] Delley B. (1990) *J. Chem. Phys., 92,* 508–517. [5] Payne M. C. et al. (1992) *Rev. Mod. Phys., 64,* 1045–1097. [6] Christensen A. N. et al. (1982) *Acta Chemica Scandinavica, 36A,* 303–308. [7] Farmer V. C. (1980) *Spectrochimica Acta, 36A,* 585–586. [8] Slade R. C. T. and Halstead T. K. (1980) *J. Solid State Chem., 32,* 119–122.

URANIUM-THORIUM-RADIUM-BARIUM SYSTEMATIC OF BALTIC FERROMANGANESE CONCRETIONS.

V. Liebetrau[1], A. Eisenhauer[2], N. Gussone[1], G. Wörner[1], and B. T. Hansen[3], [1]Geochemisches Institut, Universität Göttingen, Goldschmidtstrasse 1, D-37077 Göttingen, Germany (vliebet@ugcvax.dnet.gwdg.de), [2]GEOMAR, Abteilung für Marine Umweltgeologie, Wischofstrasse 1-3, D-24148 Kiel, Germany (aeisenhauer@geomar.de), [3]IGDL, Universität Göttingen, Goldschmidtstrasse 3, D-37077 Göttingen, Germany.

Although no precise geochronological information is available for Baltic Sea Fe-Mn-crusts at the present, these are considered to be geochemical archives for the last hundreds to thousands of years. However, precise geochronological data of the past are necessary for monitoring perturbations of the geochemical cycles in the Baltic induced by mankind before and since the industrial revolution [1].

The U-Th-Ra-Ba systematic is a potential geochronometer to date Baltic Fe-Mn-crusts. In particular this is because the ^{226}Ra half-life is in the range of the age of these concretions. However, before robust age information can be gained from the U-Th-Ra-Ba systematic its geochemical behavior in the marine environment of the Baltic and in the Mn/Fe-crusts has to be studied in detail.

Samples: Baltic ferromanganese concretions can be divided into three main types based on their abundance, morphology, composition and mode of formation; those from the Gulfs of Bothnia, Finland and Riga, from the Baltic Proper and from the western Belt Sea [2]. For this study we selected two concretions from the "Lübeck-Mecklenburg Bay" (type: western Belt Sea), which grew in shallow water depths of 20–28 m at the boundary between sands and mud in zones of active bottom currents. At this sampling site ("Blinkerhügel") the occurrence of concretions is restricted to limited areas where glacial till is exposed through mud [2]. The recent growth conditions give indication for seasonal influences on the growth zonation. The investigated discoidal concretions have different growth directions. The predominant growth is parallel to the sediment/water interface (investigated on sample I) and the minor one is vertically oriented (possible to be investigated on sample II, because in both directions 2.5× larger than sample I). The texture along the horizontal growth direction is relative constant. However, the vertical growth direction shows indications of partial dissolution under reducing conditions at the sediment/concretion interface.

Methods: Following a newly developed chemical procedure the samples were chemically prepared for thermal ionization mass spectrometry (TIMS) measurements of U, Th, and Ra isotopes. Barium was measured with inductively coupled plasma optical emission spectrometry (ICP-OES).

Results: In profile I (sample I, horizontal) the ^{226}Ra concentration inclines from 1.7×10^{-12} g/g (0–0.2 cm) to $\sim 2.6 \times 10^{-12}$ g/g (2–2.2 cm) as a function of depth. In profile II the ^{226}Ra concentrations declines from 40×10^{-12} g/g (0–0.2 cm) to 15×10^{-12} g/g (0.9–1.1 cm) as a function of depth. Nevertheless, in both profiles the ^{226}Ra/Ba ratios are declining with depth. Uranium-238 concentrations varies between 4 ppm and 13 ppm. The ^{234}U/^{238}U activity ratios is relatively constant around 1.16 and close to the open ocean U-activity ratio of ~1.144. The ^{230}Th concentrations varies in the range between 20 to 8 ppt. Neither the Th/U nor the Ra/Th activity ratios are in secular equilibrium.

From the downward trend of the ^{226}Ra/Ba ratios in profile I (sample I, horizontal) an apparent growth rate of ~0.02 mm/yr can be calculated which corresponds to an age for the entire concretion of ~1000 yr. From profile II (sample II, vertical) a lower growth rate of 0.003 mm/yr can be calculated corresponding to ~3000 yr for the entire concretion. The difference in estimated ages corresponds to the differences in size of the two samples. The horizontal growth rate of profile I is in general accord with other independent growth rate determinations of Baltic Fe-Mn-crusts [1,3], in which the predominant growth direction was investigated. However, we consider our results to be preliminary pending more geochemical studies in the future.

References: [1] Hlawatsch S. (1999) *GEOMAR Report,* in press. [2] Glasby G. P. et al. (1997) *Geol. Soc. Spec. Publ., 119,* 213–237. [3] Heuser S. (1988) *Berichte Reports Geol. Paläont. Inst. Univ. Kiel, 26.*

AN ISOTOPIC STUDY OF GROUNDWATER IN GRANITIC TERRAINS (NORTHWEST PORTUGAL).

A. S. Lima[1], M. O. Silva[2], P. M. Carreira[3], and D. Nunes[3], [1]Departamento de Ciências da Terra, Universidade do Minho, 4700-320 Braga, Portugal (aslima@dct.uminho.pt), [2]Departamento de Geologia, Faculdade de Ciências, Universidade de Lisboa, 1700 Lisboa, Portugal (mosilva@fc.ul.pt), [3]Departamento de Química, Instituto Tecnológico e Nuclear, 2686 Sacavém Codex, Portugal (carreira@itn1.itn.pt).

Introduction: Several mineral and thermal springs used for both bottling and hydrotherapy in health spas can be found in northwestern Portugal. These springs occur in granitic terrains and their water temperatures range from 15.7°C to 61.0°C. In this paper we present stable isotopic composition ($\delta^{18}O$ and δ^2H) of rainwater and groundwater from this region. A thermal spring (72.6°C) in Lovios (Spain), near Gerês (Portugal), was too considered in this study, because it is probably related to the Gerês major fault.

Sampling and analytical methods: Six samples of precipitation were collected from seaside to high-elevation areas (1500 m a. s. l.) inland. Groundwater samples were obtained from two sources: (1) springs discharging shallow aquifers and (2) springs and wells related with deep flow paths. Isotopic values are expressed in relation to Vienna Standard Mean Ocean Water (VSMOW). Precision is ±0.1‰ for the $\delta^{18}O$ and ±1‰ for the δ^2H analyses.

Results and Discussion: $\delta^{18}O$ and δ^2H values of precipitation range from −6.98‰ to −4.09‰ and from −37.0‰ to −15.3‰, respectively. The δ^2H-$\delta^{18}O$ relationship in rainwater is shown (Fig. 1) by the least-squares regression line, according to the equation $\delta^2H = 6.15\ \delta^{18}O + 8.56$, defining the local meteoric waterline, which is different from both the global meteoric waterline [1] and the meteoric waterline of Oporto [2]. To determine relationships between isotopic composition of precipitation and geographic variables (altitude and distance inland), a multivariate least squares regression yields the equation, $\delta^{18}O = (-0.0013{*}\text{altitude}) + (-0.01531{*}\text{distance}$

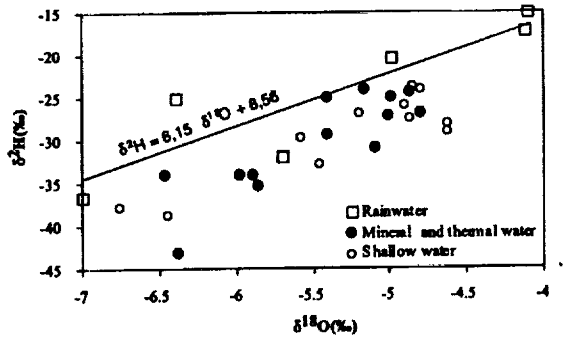

Fig. 1. δ^2H vs. δ^{18}O plot of rainwater, mineral-thermal water and shallow water samples from Northwest Portugal and Lovios (Spain).

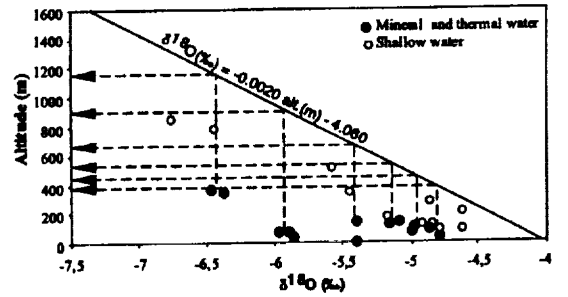

Fig. 2. Estimation of mean recharge altitudes from δ^{18}O contents.

inland) + (–4.03). This equation shows a mean δ^{18}O value of –4.03‰ for coastal precipitation.

In groundwater samples, the isotopic contents lie between –6.76‰ and –4.63‰ for ^{18}O and –43.2‰ and –23.8‰ for D. Groundwater isotopic compositions is plotted below the local meteoric waterline, defining a trend that follows this line (Fig. 1). For mineral and thermal groundwater there is a greater scattering of values of isotopic ratios than for shallow groundwater. These differences suggest distinct pathways of mineral and thermal water and shallow water. Nevertheless, meteoric origin for both sorts of water seems to be confirmed.

Based on the relationship between isotopic composition of precipitation and altitude, areas of recharge were estimated (Fig. 2). Shallow-water samples are plotted close to the meteoric regional isotopic gradient. These samples show a difference of altitude between recharge and discharge areas ranging from 85 m to 490 m. For deep waters this difference ranges from 320 m to 890 m. Furthermore, for mineral and thermal waters, δ^{18}O contents are affected by isotopic exchange between water and host rock and, therefore, mean recharge altitudes are probably higher. Mean elevation difference between recharge and discharge areas is ~300 m for shallow groundwater. Mineral and thermal water gradient is divergent relatively to the regional one, from low to high altitudes.

Conclusions: Regardless of their pathways, both mineral-thermal and shallow groundwater seem to have a meteoric origin. Stable isotopic ratio differences should be related with the flow paths and with the magnitude of rock-water interaction reactions. Comparing isotopic composition of groundwater with regional isotopic gradient of rainwater, one can distinguish deep flow paths from shallow ones.

References: [1] Clark I. and Fritz P. (1997) *Environmental Isotopes in Hydrogeology.* [2] GNIP Database (1998) IAEA/WMO, http://www.iaea.org/programs/ri/gnip/gnipmain/htm.

TRACE-ELEMENT CHEMISTRY AND PETROGENESIS OF PERIDOTITE AND PYROXENITE XENOLITHS FROM PLIOCENE BASANITES OF THE DZHILINDA RIVER, VITIM VOLCANIC FIELD.

K. D. Litasov[1], Yu. D. Litasov[1], A. S. Mekhonoshin[2], and V. G. Mal'kovets[1], [1]United Institute of Geology, Geophysics and Mineralogy, Russian Academy of Sciences, Koptyuga Ave. 3, Novosibirsk 630090, Russia (kostik@uiggm.nsc.ru), [2]Institute of Geochemistry, Russian Academy of Sciences, Favorskogo Street 1a, Irkutsk 664033, Russia.

Three series of peridotite xenoliths from Pliocene basanites of the Dzhilinda river were determined: (1) high-T gar and sp lherzolites, (2) low-T sp lherzolites and harzburgites, (3) low-T titaniferous sp lherzolites. Pyroxenites are divided into: (4) Cr-diopside gar and sp websterites, including Al-poor sub-series; (5) Al-augite sp websterites; (6) skarn-like clinopyroxenites. Megacryst assemblage (7) is presented by clinopyroxene, garnet, and ilmenite.

1. Protogranular peridotites of the series 1 represent primitive or slightly depleted mantle from depths 60–80 km at T = 1100°–1250°C. Trace-element patterns in clinopyroxenes are indicative of low degree partial melting of the primitive mantle. Rare poikiloblastic harzburgites composed of low-Mg minerals (Mg = 84–85) occur at the gar lherzolite facies depth. Their relic clinopyroxenes are characterized by convex-upward REE patterns, of which a formation is interpreted as a significant modification of peridotites reacting with percolating porous melt [1].

2. Peridotites of the series 2 correspond to the depths 40–50 km at T = 800°–900°C. They were divided into 2a-coarse-grained protogranular and 2b-fine-grained tabular equigranular. 2a-peridotites are often depleted in modal composition and contain LREE-rich, HFSE-poor clinopyroxene: $(La/Yb)_n$ = 1.2–3.5 and $(Ti/Eu)_n$ = 0.2–0.4. Such patterns may be formed due to a melt percolation through peridotite matrix with reaction "lherzolite-dunite" [2]. Peridotites of the series 2b are often observed in contact with Al-poor pyroxenites. They contain clinopyroxenes with slightly convex-upward REE patterns and low HFSE, Sr contents.

3. Titaniferous peridotites enriched in pyroxenes and spinel were newly detected. They have a mosaic equigranular texture and are interpreted as a rare type of melt/mantle interaction. T-estimations within 750°–850°C allow extrapolations to the uppermost mantle section (40–50 km depth). Minerals of these peridotites have a specific chemistry. Clinopyroxene (Mg# = 92–93) contain 2–2.2% TiO_2. Olivine (Mg# = 91–92) contain 0.7% NiO. Spinel (Mg# = 77, Cr# = 16–17) contain 0.6–0.7% NiO and 0.9–1.0% ZnO. High Ti content (TiO_2 = 0.55% in bulk rock) may characterize a metasomatizing melt originated from ilmenite- and/or phlogopite-bearing source. Very high contents of Cr, Ni, Zn, V, Ga, and Ge allow to suggest an initial rock type as a dunite or harzburgite. Clinopyroxene REE patterns $(La/Yb)_n$ = 0.01–0.08) reveal an evidence for MORB-like composition of coexisting melt. This interaction has been found nowhere before.

4. By the mineral composition, the Cr-diopside pyroxenites as well as peridotites form high-T (1050°–1230°C) and low-T (860°–1000°C) subseries. They are considered as products of interaction between basaltic melts and primitive wall peridotites at two depth levels: 60–80 km and ~50 km. Clinopyroxene REE patterns vary from primitive with $(La/Yb)_n$ = 0.3 to fractionated with $(La/Yb)_n$ = 5.1.

The Al-poor pyroxenites are characterized by low contents of Al_2O_3 = 3–4%, Na_2O = 0.2–0.5%. Regarding to mineral composition, these are close to low-temperature peridotites of the series 2b. Clinopyroxene has convex-upward REE patterns. The Al-poor pyroxenites are interpreted as products of interaction between basaltic melts and depleted wall peridotites (harzburgites to dunites).

5. Aluminum-augite pyroxenites are represented by two series of sp websterites. The first contain dark-green clinopyroxene and have transitional varieties to lower-T Cr-diopside pyroxenites. REE patterns of their clinopyroxene are similar to that from Cr-diopside pyroxenites. However, the second contains brownish clinopyroxene with higher Mg#, REE, Ti. Aluminum-augite pyroxenites are formed near the Moho boundary due to a segregation of melt in magma chambers.

6. Aluminum-poor (0.5–1.5% Al_2O_3) skarn-like clinopyroxenites may be formed in the lower-middle crust due to an interaction with fluid or volatile-rich melt. Their REE patterns have inflections near Sm and strong LREE enrichment. Probably, these rocks were modified from clinopyroxenite or gabbro having MORB characteristics.

7. The megacryst clinopyroxenes reveal certain trends of compositional variations, such as an increasing in TiO_2, Al_2O_3, REE, and decreasing in Cr_2O_3, while Mg-number decreases. These features are an evidence for their formation by fractional crystallization of alkaline basaltic or picrobasaltic melt similar to those reported for megacryst assemblage from Miocene picrobasalts [3].

Acknowledgments: This work is supported by RFBR gr. #97-05-65309.

References: [1] Xu Y.-G. et al. (1998) *Contrib. Mineral. Petrol., 132,* 65–84. [2] Bedini R. M. et al. (1997) *EPSL, 153,* 67–83. [3] Ashchepkov I. V. et al. (1995) *Ext. Abstr. 6th Int. Kimb. Conf.,* Novosibirsk, 17–19.

MELT POCKETS IN MANTLE XENOLITHS FROM ALKALI BASALTS OF VITIM AND UDOKAN VOLCANIC FIELDS, EAST SIBERIA.

K. D. Litasov, V. V. Sharygin, Yu. D. Litasov, and S. Z. Smirnov, United Institute of Geology, Geophysics and Mineralogy, Russian Academy of Sciences, Koptyuga Avenue 3, Novosibirsk 630090, Russia, (kostik@uiggm.nsc.ru).

Melt pockets are often found in mantle xenoliths from the Late Cenozoic basaltic rocks of the Baikal Rift system volcanic fields. We studied major- and trace-element chemistry of primary minerals and glasses from melt pockets in three spinel peridotite xenoliths. Host rocks are represented by picrobasalt (16 Ma, Vitim field) with Mg# = 69–72, TiO_2 = 1.9–2.1%, K_2O = 1.0–1.4%, Cr = 495 ppm, and melanephelinites (14 Ma, Udokan field) with Mg# = 67–70, TiO_2 = 2.7–3.5%, K_2O = 2.2–3.2%, and Cr = 320–410 ppm [1].

Melt pockets in amphibole-bearing spinel lherzolite from the Vitim picrobasalt were found around spongy-rimmed amphibole grains and consist of glass, olivine, spinel microphenocrysts and rare ilmenite needles in glass. Primary amphibole has Mg# = 86.2 and contain TiO_2 = 2.4–2.8%, Cr_2O_3 = 0.9%, K_2O = 2.1–2.6%. Glass contain SiO_2 = 54–59%, TiO_2 = 2.0–2.5%, K_2O = 2.0–3.2%, Cr = 14 ppm. Trace-element patterns of glass and melt coexisting with primary amphibole are very similar: $(La/Yb)_n$ = 5.7 and 8.5, $(Nb/La)_n$ = 3.2 and 3.0, $(Zr/Sm)_n$ = 0.7 and 0.8 respectively. Olivine microphenocrysts have composition similar to primary lherzolitic olivine with Mg# = 89.5–90.0 and CaO = 0.08–0.1%. Spinel in melt pockets contain 15–16% Cr_2O_3. Primary spinel in lherzolite contain 7–8% Cr_2O_3. Trace-element characteristics of melt coexisting with primary clinopyroxene are different from those for amphibole and glass: $(La/Yb)_n$ = 16, $(Nb/La)_n$ = 0.5, $(Zr/Sm)_n$ = 0.4.

Melt pockets in phlogopite-bearing spinel lherzolite from the Vitim picrobasalt were found around resorbed phlogopite grains. They consist of olivine microphenocrysts and glass with ilmenite inclusions. Phlogopite has Mg# = 92 and contains TiO_2 = 3–4%, Cr_2O_3 = 0.41%, BaO = 0.4%. Glass contains SiO_2 = 63–66%, TiO_2 = 1.7–2.6%, K_2O = 7–10%, Cr_2O_3 = 0.2%. Trace-element patterns of glass and melt coexisting with phlogopite are also similar: $(La/Yb)_n$ = 8.5 and 9.6, $(Nb/La)_n$ = 18 and 22, $(Zr/Sm)_n$ = 0.52 and 0.75 respectively. Olivine in melt pockets has Mg# = 88.7 and contains CaO = 0.13%. Primary olivine has Mg# = 86.5 and CaO = 0.01%.

Melt pockets in "dry" spinel lherzolite from Udokan melahephelinites fill interstices between primary minerals. Melt pockets include olivine, clinopyroxene, felsic glass, minor chromite, sanidine, and Fe-Ni-Cu-sulfide blebs. Lherzolitic clinopyroxene has Mg# = 92 and contains TiO_2 = 0.7%, Cr_2O_3 = 0.7%, Al_2O_3 = 7.3%. Clinopyroxene in melt pockets has Mg# = 85–92 and contains TiO_2 = 0.1–0.7%, Cr_2O_3 = 0.7–1.3%, and Al_2O_3 = 0.3–0.6%. Chromite from melt pockets contains Cr_2O_3 = 61–62%, while primary spinel is less rich in Cr_2O_3 (7.7–8%). Olivine in melt pockets has Mg# = 83–90 and contains CaO = 0.15–0.3% and NiO = 0.2–0.3%. Primary olivine has Mg# = 89 and contains less CaO = 0.02–0.1% and more NiO = 0.35–0.4%. Glasses were divided into two types. The first contains SiO_2 = 62–65%, Al_2O_3 = 20–23%, TiO_2 = 0.7–1.0%, and K_2O = 4–7% being similar to glassy inclusions from phenocrysts in the host volcanics. The second has SiO_2 = 70–74%, lower Al_2O_3 = 13–17% and same TiO_2, K_2O. Trace-element patterns of felsic glass and melt coexisting with primary clinopyroxene is quite different. Glass has $(La/Yb)_n$ = 24, Yb_n = 1.5, $(Nb/La)_n$ = 1.1. Melt coexisting with clinopyroxene has $(La/Yb)_n$ = 4.6 Yb_n = 12.7, $(Nb/La)_n$ = 0.5.

Origin of the glasses in Vitim nodules is connected with partial melting of hydrous peridotite minerals, what comes to be obvious from a similarity in major- and trace-element compositions of glass and melting phases. Glass in the Udokan nodule was formed by reaction between peridotite minerals and basaltic melt before or during xenoliths entrainment to the surface. Origin of such Si-rich glasses in mantle xenoliths is still under discussion. Shaw et al. [2] suggested them to be formed due to low-pressure orthopyroxene dissolution. Studied heated (SiO_2 = 50–64%) and unheated (SiO_2 = 65–76%) melt inclusions in clinopyroxene from Vitim clinopyroxenites [3] show that Si-rich glass can be produced during a deep fractionation in close system and reaction with host peridotite minerals. We suggest the same mechanism for the studied glasses in the Udokan nodules.

Acknowledgments: Work is supported by RFBR grants 97-05-65309 and 97-05-65331. Used partition coefficients are after [4–5], and primitive mantle normalization is after [6].

References: [1] Rasskazov S. V. et al. (1997) *Petrology, 5,* 115–136. [2] Shaw C. S. J. et al. (1998) *Contrib. Mineral. Petrol., 133,* 354–370. [3] Litasov K. D. et al. (1997) *Abstr. of ECROFI XIV,* 186–187. [4] Halliday A. H. et al. (1995) *EPSL, 133,* 379–395. [5] Hart S. R. and Dunn T. (1993) *Contrib. Mineral. Petrol., 113,* 1–8. [6] McDonough W. F. and Sun S. S. (1995) *Chem. Geol., 120,* 223–253.

VARIATIONS IN CONCENTRATIONS OF DISSOLVED TRACE ELEMENTS IN RIVER WATER OF GUIZHOU, CHINA.

C. Q. Liu and G. L. Han, The State Key Laboratory of Environmental Geochemistry, Institute of Geochemistry, Chinese Academy of Sciences, Guiyang 550002, China.

Geochemical studies of trace elements, especially heavy metals in river water, can provide grounds for the assessment of the influence of human activities on the environment [1–3]. The authors have carried out systematic studies on the variations in concentration of dissolved trace elements and their controlling factors, while some systematic studies are under way on the major compositions of river water in the Wujiang drainage system in Guizhou Province, a typical karst area in China. This paper is concerned mainly with the trace-element composition of river water and characteristics of geochemical environment with an attempt to evaluate the effects of human activities on the Wujiang River Valley.

The comparison of dissolved trace elements in river water with trace elements in the upper continental crust demonstrates that Mn and Sr are strongly concentrated relative to other elements in river water, while Rb, Pb, Zn, and Ni are relatively depleted, indicating that the process of chemical weathering has led to the differentiation of different elements between water body and weathered crust. The concentrations of U in the Wujiang River Valley are within the range of 1.78–7.25 nmol/L, far higher than the average value of global rivers (1.3 nmol/L [3]). Uranium is mainly derived from dissolution of limestones. Our work shows that U is enriched in river water relative to Pb, so the variation of U/Pb ratio can be used to discuss the capability of particles to adsorb heavy metals. The U/Pb ratios tend to increase from the upper to the lower reaches. For this there may be two explanations. One is that the Wujiang River flows through a Pb-Zn mining district in its upper reaches, so the concentrations of Pb are relatively high in river water (~2.67–10.04 nmol/L), but those of U are of little variation. That is why the U/Pb ratios are relatively low. This appears to be the result of weathering of carbonates or industrial pollution caused by mining activities in the drainage area. The other explanation is that Pb in ocean water is readily adsorbed on particles (particle action), and therefore it can also be readily adsorbed on particles in river water. On the contrary, U usually exists in a dissolved state in river water. So U tends to be concentrated whereas Pb will be adsorbed on particles from the upper to the lower reaches.

Lead is often closely coexistent with Zn in sulfide ore deposits. In ore deposits, Zn usually occurs as sphalerite. The process of oxidation of sphalerite $ZnSO_4$ has such a high solubility as to be easily transported into river water. It can be transported over a long distance in neutral, acidic, and weakly alkaline solutions. The concentrations of dissolved Zn in the Wujiang River water are far higher than those of Pb, which vary over a range of 12.02–54.31 nmol/L, far higher than the average value of global rivers (3 nmol/L [3]).

Manganese is highly enriched in the Wujiang River water. That is because Mn is present in the form of carbonate ($MnCO_3$) or bicarbonate [$Mn(HCO_3)_2$] in karst areas and can be readily dissolved in water. But in the limestone areas, Fe^{2+} is often oxidized into $Fe(OH)_3$ before precipitation. Therefore, as compared with the upper crust, the Wujiang River water is enriched in Mn and depleted in Fe.

Zhang and Haung [4] considered that the concentrations of dissolved trace elements in the Yellow River are controlled mainly by weathering and erosion in the drainage area. Dupre et al. [5] considered that the concentrations of U, Rb, Ba, and Sr in the Congo River are controlled mainly by rock types in the drainage area. According to the authors, the dissolution of limestone and dolomite would exert obvious constraints on the distribution of U, Mn, Sr, and Ba in river water. However, the distribution of other heavy metallic elements seems to be controlled by the chemical composition of river water, (e.g., the influence of particle adsorption). High concentrations of dissolved trace elements in the Wujiang River water are probably related to the chemical behavior of the complex HCO_3^- in the river water. On the other hand, under high pH conditions, the dissolved trace elements are easily adsorbed on particles. So the authors hold that under high pH conditions the high concentrations of dissolved trace elements in river water provide evidence that the mechanism of controlling the concentrations of dissolved trace elements is very complicated, which may be a controlling mechanism of adsorption/desorption and precipitation/dissolution equilibrium.

References: [1] Hu M. H. et al. (1982) *Nature, 298,* 550–553. [2] Shiller A. M. and Royle E. (1985) *Nature, 317,* 49–52. [3] Palmer M. R. and Edmond J. M. (1993) *GCA, 576,* 4947–4955. [4] Zhang J. and Huang W. W. (1993) *WR, 27,* 1–8. [5] Dupré B. et al. (1996) *GCA, 60,* 1301–1321.

THE CONTINENTAL EXHALATION OF COPPER DEPOSITS FROM RED CLASTIC FORMATION IN THE LANPING-SIMAO BASIN, WESTERN YUNNAN, CHINA.

J. Liu, C. Liu, C. Li, J. Pan, and T. Zhang, OLODG, Institute of Geochemistry, Chinese Academy of Sciences, Guiyang 550002, China.

The Cu deposits occurring in the Lanping-Simao basin of western Yunnan are the new type of Cu deposits closely associated with continental exhalation and showing many unique features. The Cu deposits exist in the Mesozonic and Cenzonic clastic rock formation composed of sandstone, siltite and argillite. The Cu orebodies mostly occur in the hosted rocks with not only vein and network forms but also bedded-quasibedded and lenslike forms. The ores have very simple mineral assemblages. Over 20 mineral species have been identified at present. Besides ordinary sulfides of Cu minerals such as chalcopyrite, tetrahedrite, bornite, and chalcocite, there are also other minerals of pyrite, galena, sphalerite, azurite, stibnite, quartz, calcite, ferroan dolomite, and barite. The ore fabrics are characterized by vein, network, brecciated mainly and bedded, laminated, disseminated partially. The wall rock alterations are mostly silication, calcitization, and baritzation.

Based on the systematical studies on the trace elements and their characteristic ratios, the rare earth element distribution patterns, the fluid inclusions, the physical-chemical conditions, and the isotopic compositions of S, Pb, C, Si, O, and H in the Cu ores in the Lanping-Simao Basin, the author concludes that the formation of the Cu deposits progressed through two mineralization stages, i.e., the stage of sedimention and diagenesis and the stage of continental exhalation. The former stage is marked by the formation of banded and laminated structures of chalcopyrite, etc., showing initial and/or locally concentrated ore substances. The latter brought about remobilization and reconcentration of ore substances, thus leading to the formation of mineral deposits of commercial value.

Because they occur in the red clastic formation, the Cu deposits are comparable with typical sandstone and/or shale-type deposits [1,2]. However, there are obvious differences between the typical sandstone and/or shale-type Cu deposits and the present type, both in Cu occurrence forms, mineral paragenesis, and metallogenetic mechanism. Therefore, the deposits belong to a new type of Cu deposit associated with continental exhalation. It is worthy to mention that the research on the continental exhalation type of Cu deposit is just at the initial episode. Further systematical study and exploration of this type of deposit will surely improve greatly both the theoretical development concerning Cu mineralization and the exploitation of Cu resources in China.

Acknowledgments: This project is supported by a CAS-Yunnan Province cooperation and by the "Hundred People Program" Foundation of Chinese Academy of Sciences.

References: [1] He M. et al. (1998) *Yunnan. Geol. Pros., 34,* 13–15. [2] Jue M. et al. (1998) *The Copper Deposits of Lanping and Simao Basins,* Geological Publishing House, Beijing, 109 pp.

THE CHARACTERISTICS OF ORE-BEARING CHERT FROM CAMBRIAN GOLD DEPOSITS AND THEIR SEDIMENTARY ENVIRONMENTAL IMPLICATIONS IN THE WESTERN QINLING MOUNTAINS, CHINA.

J. Liu[1], C. Liu[1], J. Liu[2], and T. Gu[1], [1]OLODG, Institute of Geochemistry, Chinese Academy of Sciences, Guiyang 550002, China, [2]The Research Center of Mineral Resources Exploration, Chinese Academy of Sciences, Beijing 100101, China.

The ore-bearing chert serves as the source strata of Cambrian Au deposits in the western Qinling Mountains, China. The presence of the typical chert offers important evidence to evaluate the possible submarine exhalative system and its role over the formation of the source strata and Au deposits [1].

The ore-bearing chert occurs as layered black rocks, containing more or less clays and organic matter. It is characterized by bedded, striped, laminated, massive hold, and pseudobrecciated structures that change regularly in space. The thickness of a chert bed generally varies from 30 to 200 m. Host elements are simple and concentrated in the chert. Besides SiO_2 (95.30% on average), only FeO, Fe_2O_3, and organic C reach or exceed 1.0%. The ratios of Al/(Al + Fe + Mn) in all chert samples are lower than 0.3 (0.153 on average). In the Fe/Ti vs. Al/(Al + Fe + Mn) diagram and the Al-Fe-Mn triangle diagram, the chert samples fall into the hydrothermal field. However, the chert is enriched in most trace elements, characterized by not only the basic and ultrabasic elements group (e.g., Au, Ag, Pt, Pd, Cu, and Cr) but also the acid elements group (e.g., W, Mo, U). REE are characterized by a low total content (ranging between 3.29×10^{-6} and 100×10^{-6}), negative Ce anomal, and a gradually increasing NASC-normalized value with increasing atomic number of REE. The $\delta^{18}O$ values of chert mainly vary from 17.60‰ to 23.24‰ (19.17‰ on average), suggesting that the temperature for deposition was from 70.9° to 118.1°C. The $\delta^{30}Si$ values of the chert in the area range mainly from 0.4‰ to 0.8‰.

Both the geological and geochemical characteristics show that the chert is the product of hydrothermal sedimentation. In the early Paleozoic periods, there were several syngenetic faults transecting the crust of this area (Bailongjiang basin) and providing conduits for the hydrothermal activity. Crustal extension along these faults resulted in the formation of a series of basins and uplifts inserted among the basin. It may have formed in this sedimentary environment. The characteristics of the P_2O_5 and MgO contents, the δCe values, and the $\delta^{30}Si$ values manifest that the chert deposited in the deep and half-deep sea environment.

Acknowledgments: This project is supported by the National Natural Science Foundation of China (No. 49773197) and by the "Hundred People Program" Foundation of Chinese Academy of Sciences.

References: [1] Liu J. et al. (1998) *Chinese Sci. Bull., 43,* 85–86.

CHARACTERISTICS OF MANTLE METASOMATISM AND GEOCHEMICAL MECHANISM OF PETROGENESIS AND MINERALIZATION OF ALKALI-RICH PORPHYRIES.

X. Liu, Z. Gao, J. Liu, X. Zhan, C. Li, and W. Su, Institute of Geochemistry, Chinese Academy of Sciences, Guiyang 550002, China.

The Ailaoshan-Jinshajiang (Ailao Mountains-Jinsha River) alkali-rich intrusive rock belt is a large-scale northwest-trending Cenozoic alkali-rich potassic magmatic rock belt in southwest China. As an essential component of the belt, the alkali-rich porphyry is closely related to the polymetallic mineral resources in the region. On the basis of comprehensive investigations, the geochemistry and dynamic mechanism for the petrogenesis and mineralization of alkali-rich porphyries can be briefly described as following:

During geological history, the energy and subtance equilibrium in deep mantle was destroyed by large-scale tectonic movements and plate subductions, and it resulted in the origination of mantle metasomatism and alkali-rich magma and accompanied accumulation of ore-forming materials and mineralizers. At the beginning of the Cenozoic, a new cycle of strong tectonic movements stimulated the upward transferring of alkali-rich magma and Si-rich fluids, which have been formed in deep mantle, with upper mantle xenoliths and along large-scale deep faults across the crust/mantle boundary. A part of alkali-rich magma with Si-rich fluids might directly enter upper crust trap structures, and mineralization could result from the auto-metasomatism of fluids accompanied by crystallization and petrogenesis of alkali-rich magma. Another part, predominated by fluids, might be mixed with formation water from various sources during migration, then be activated and extracted from ore-forming materials and mineralizers and from crust/mantle mixing ore-forming hydrothermal fluids. Furthermore, these fluids may enter upper-crust trap structures along ore-conducting fractures, and superimpose on the mineralization caused by the fluid metasomatism and alteration accompanied with the crystalization and petrogenesis of alkali-rich magma. It is obvious that the former mineralization may be on a rather small scale, while the latter could result in the formation of large or even superlarge deposits if the fluid could move through preliminarily enriched source beds with various ore-forming materials and the superimposed mineralization of multisources materials happened. Thus, it can be seen that the well combination of deep-seated geological process and large-scale deep faults should be an essential condition for wide-spread mineralization in this region, and an unitized intrinsic constraint. And the coupling of deep and shallow geological processes and the resulted superimposition of deep- and shallow-source ore-forming materials and mineralizers must be a sufficient condition for the formation of large or superlarge deposits in this region in Cenozoic. The complicated and various ore-forming phenomena of Cenozoic era in the region reflected the separation or combination of the above-mentioned two kinds of geological processes or ore-forming materials to varying extent.

XENOLITH EVIDENCE FOR TECTONIC UNDERPLATING OF SEDIMENTARY ROCKS AND LAYERED COMPOSITIONS OF THE LOWER CRUST AT THE NORTHERN MARGIN OF THE NORTH CHINA CRATON.

Y. S. Liu[1] and S. Gao[1,2], [1]Faculty of Earth Sciences, China University of Geosciences, Wuhan, 430074, China (yshliu@cug.edu.cn), [2]Department of Geology, Northwest University, Xi'an, 710069, China (gaoshan@cug.edu.cn).

Granulite-facies lower crustal xenoliths in the Neogene Hannuoba alkaline basalt at the northern margin of the North China craton are unique in their diversity of lithology, abundance, freshness, and size (up to 50 cm in diameter). They provide a rare opportunity to study the nature, formation and evolution of the deep crust in this area. The xenoliths occur mostly in two localities of Damaping and Zhouba, and they show contrasting lithology, age, and depth of derivation. Those from Damaping are dominantly mafic with less important intermediate (plagioclase + clinopyroxene ± orthopyroxene ± K-feldspar) and felsic (quartz + plagioclase ± K-feldspar ± clinopyroxenew ± orthopyroxene) members. They were equilibrated at 800°–950° based on the two-pyroxene geothermometer [1]. Their Nd-isotopic compositions are largely homogenized at the mineral scale. The whole-rock samples give an imprecise Sm-Nd isochron age of 145 Ma, which is not at great variance with the single zircon U-Pb age (120–140 Ma) [2]. The age is interpreted to represent the age of basaltic underplating followed by granulite-facies metamorphism. Petrological evidence and geochemical and Nd-isotopic studies suggest that the Damaping mafic to felsic granulite xenoliths were products of fractional crystallization of pyroxene and plagioclase from a basaltic magma chamber underplating at the base of the crust.

In contrast, granulite xenoliths from Zhouba are exclusively felsic and some contain graphite and sillimanite, indicating a sedimentary protolith. Mineral assemblage and incomplete kelyphitization of garnet suggest that they were derived from shallower depth compared to the Damaping xenoliths. Whole-rock, garnet and plagioclase separates from one Zhouba graphite-sillimanite bearing felsic granulite yield a Sm-Nd isochron age of 424 ± 10 Ma, which is interpreted to represent the age of granulite-facies metamorphism unrelated to the Cretaceous event. The characteristic significant positive Eu anomalies for many samples of the Zhouba xenoliths and their early Paleozoic age of granulite-facies metamorphism readily distinguish from clastic metasedimentary rocks of khondolite character in the nearby Archean granulite terrains of the North China craton, which possess post-Archean-like negative Eu anomalies [3]. Detrital zircon dating by the evaporation method for the Zhouba metasedimentary xenolith produces an age range of 727–1551 Ma, which constrains the maximum age of deposition. The evidence documents that the Zhouba xenoliths were not from the Archean terrains. Instead, they are interpreted to be the product of tectonic underplating of Neoproterozoic to early Paleozoic sedimentary rocks from the Mongolian orogenic belt north of the North China craton. The tectonic underplating is considered to be related to the Caledonian closure and subduction of the early Paleozoic Mongolian oceanic crust beneath the North China craton. Our conclusions are based on the observation that the interior of the North China craton lacks deposition of late Ordovician to Devonian strata and tectonic and magmatic activities in the Paleozoic, whereas early Paleozoic granitoid intrusions are abundant along the northern margin of the North China craton and were related to the subduction of the Mongolian oceanic crust.

Seismic refractions reveal a rather homogenous crustal structure throughout the entire North China craton, including the Hannuoba area [4]. It shows a four-layered structure consisting of the upper, the middle, the upper-lower, and the lowermost crust. The upper-lower crust varies from 3 to 17 km and the lowermost crust from 1 to 9 km in thickness. P-wave velocities of upper and lowermost crustal layers show limited lateral variations from 6.5 to 6.7 km s^{-1} and from 6.8 to 7.2 km s^{-1} for the upper-lower crust and lowermost crust respectively.

The above evidence, along with correlation of measured and calculated P-wave velocities of the xenoliths with results from seismic refractions, indicates two layers of lower crust composition of contrasting origins at the northern margin of the North China craton. The lowermost crust is represented by the Damaping xenoliths and is mafic, young, and formed by basaltic underplating, while the upper lower crust is represented by the Zhouba xenoliths and is felsic, older, and formed by tectonic underplating.

References: [1] Chen S. H. et al. (1998) *Acta Petrol. Sinica, 14,* 366–380 (in Chinese). [2] Fan Q. C. et al. (1998) *Sci. Bull., 43,* 133–137 (in Chinese). [3] Gao S. and Wedepohl K. H. (1995) *EPSL, 133,* 81–94. [4] Gao S. et al. (1998) *EPSL, 161,* 101–117.

OSMIUM-ISOTOPIC COMPOSITIONS OF HOROMAN ULTRAMAFIC COMPLEX IN HOKKAIDO, JAPAN.

Y. Z. Liu and T. Tanaka, Department of Earth and Planetary Sciences, Nagoya University, Chikusa, Nagoya 464-8602, Japan (liu-yz@turnip.eps.nagoya-u.ac.jp).

Introduction: Island arcs like Japanese islands are considered to be tectonic composites of various crustal blocks that accreted from various parts of the Earth's surface at different periods. Isotopic characteristics of the surface crustal materials have been examined extensively in the past few decades to clarify their source region or hinterland. Some areas in Japan strongly show Precambrian continental affinities while others show mantle-derived oceanic. Even in the Quaternary volcanics, isotopic ratios show areal variations from the Pacific side to the Sea of Japan side. This indicates certain heterogeneities in the source mantle. Present and past materials that underlie the island arcs are expected to have extensive variations in their chemical and isotopic features.

This work reports some results of Os-isotopic study of the Horoman ultramfic complex. It is known that Re-Os system can provide a unique perspective on the understanding of the origin and evolution of mantle, because, unlike other daughter elements, Os did not strongly partition into partial melts of the mantle. The high Os concentrations of Horoman ultramafic rocks could result in resistance to the metasomatic disturbance, and this allows Os systematics to be used to determine the partial melting history of the massif. We also aimed in this work to find the evidence of processes using Re-Os system, which other systems such as Rb-Sr and Sm-Nd obviously cannot offer.

Geologic Setting: The Horoman ultramafic complex is one of the largest samples of mantle-derived peridotites (~8 × 10-km area and >3-km thickness) in Japan. It situates at the southwestern end of the Hidaka metamorphic belt in Hokkaido, Japan, and was regarded the representative of an alpine-type peridotite intrusion [1]. The rocks of the Horoman ultramafic complex are fresh and have well-developed layering and good exposures. These characteristics make it very suitable for the petrological and geochemical studies on Horoman massif origin and mode of emplacement.

The Horoman ultramafic complex is composed of three peridotite suites with distinct petrographic characteristics. The main harzburgite-lherzolite (MHL) suite consists of harzburgite, spinel lherzolite, and plagioclase lherzolite and occupies the largest part of the complex at more than 94 vol%.

The banded dunite (BDH) suite consists of layered dunite, harzburgite, and olivine orthopyroxenite. The spinel-rich dunite-wehrlite (SDW) suite consists of dunite containing abundant large oblate chromian spinel grains [2].

Analytical Methods: Osmium was preconcentrated using fire assay technique, in which sample powder, borax, sodium carbonate, S powder, and Ni powder were well mixed and then placed in oven at 1100°C for 1 h. The recovery of Os for fire assay technique is ~75–95% based on the weight of NiS bead. Osmium was separated by distillation method using chromium oxide as the oxidant in 6N H_2SO_4 after the filtration of the digested NiS bead in 6N HCl. A microdistillation method using a closed Teflon vial put directly on a hot plate was applied for further Os purification. The employed negative themal ionization mass spectrometry (N-TIMS) was VG Sector 54 for Os measurement.

Results and Discussion: The Os-isotopic ratios of 10 samples of the Horoman ultramafic complex, which is composed of four ultramafic rock types as dunite, harzburgite, lherzolite, and plagioclase lherzolite, were examined. The result of ^{187}Os/^{186}Os ratio ranges from 0.994 to 1.12. This is similar to the range of the ^{187}Os/^{186}Os ratio for abyssal peridotites and orogenic peridotites between 0.98 and 1.12. The Os concentrations of these samples range from 2.3 to 6.0 ppb, and are also in accordance with the range of Os concentrations found in mantle peridotite nodules from 1.1 to 6.9 ppb [3]. The lower ^{187}Os/^{186}Os ratios measured here correspond to the higher Os concentrations, reflecting the Re depletion related to the melt extraction event. It is observed that the peridotite with high content of clinopyroxene shows a relatively high ^{187}Os/^{186}Os ratio. This result supports the idea of oceanic mantle origin for Horoman MHL suite peridotites [4,5]. In addition, the lower ^{187}Os/^{186}Os ratio and higher Os concentration, up to the limits of 0.994 and 3 ppb respectively for MHL suite peridotites, might support another conclusion that MHL suite peridotite represents a residual peridotite after a slight to moderate degree of partial melting [2].

References: [1] Niida K. (1984) *J. Fac. Sci., 21,* 197–250. [2] Takahashi N. (1991) *J. Mineral. Petrol. Econ. Geol., 86,* 199–215. [3] Walker R. J. et al. (1989) *GCA, 53,* 1583–1595. [4] Dick H. J. B. et al. (1984) *EPSL, 69,* 88–106. [5] Komatsu M. et al. (1986) *Petrol. Tectonics, 1,* 21–22 (in Japanese).

TERMINAL PROTEROZOIC BENTHIC MICROBIAL MATS AND THEIR ENVIRONMENTAL SIGNIFICANCE.

G. A. Logan[1], C. R. Calver[2], P. Gorjan[3], R. E. Summons[1], J. M. Hayes[4], and M. R. Walter[3], [1]Australian Geological Survey Organisation, P.O. Box 378, Canberra, ACT 2601, Australia, [2]Tasmanian Geological Survey, P.O. Box 56, Rosny Park, Tasmania 7018, Australia, [3]School of Earth Sciences, Macquarie University, Sydney, NSW 2109, Australia, [4]Mail Stop 8, Woods Hole Oceanographic Institution, Woods Hole MA 02543, USA.

A combined sedimentological and biogeochemical study was conducted on several Terminal Proterozoic mid-shelf microbial mat facies samples from the Centralian super basin. Isotopic and organic geochemical analysis of the bitumen and kerogen indicated that two sources of organic matter from "planktonic" and "benthic microbial-mat" populations contributed to the sediment. The "planktonic" source provided a suite of n-alkanes with $<C_{20}$ predominance and the odd n-alkanes $>C_{20}$, whereas the "benthic" source contributed an overlay of n-alkanes $>C_{20}$, with a strong even preference accompanied by an unusual suite of midchain methyl alkanes (Fig. 1).

Kerogen and biomarkers derived from the microbial mat were depleted in ^{13}C relative to planktonic material. Pyrite in the microbial mats was also found to be depleted in ^{34}S compared to the surrounding sediment. The combination of these observations suggested that the mats may have been at least partly composed of sulfide-oxidizing bacteria. These organisms have specific environmental tolerances that set limits on paleoenvironment. Their requirement for O indicates that the water column above the mid-shelf could not have been continuously anoxic. Accordingly, from these results and age determinations, it would appear that mid-shelf environments of the Centralian super basin of Australia were seeing significant levels of O through the Ediacarian [1].

Recent analyses [2] of hydrocarbons extracted from sediment samples within a middle Proterozoic Pb-Zn deposit in northern Australia show an interesting correlation with the Wallara-1 mat samples (Fig. 2).

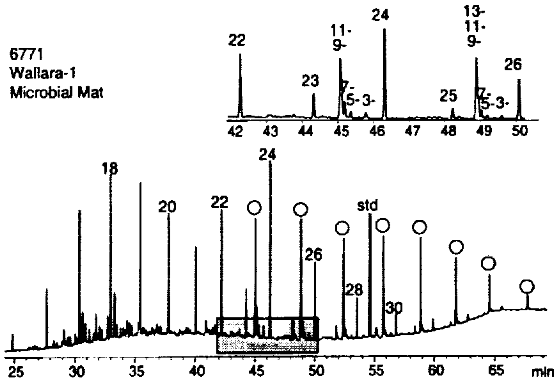

Fig. 1. Unusual hydrocarbon pattern in an extract from the Wallara-1 microbial mat facies.

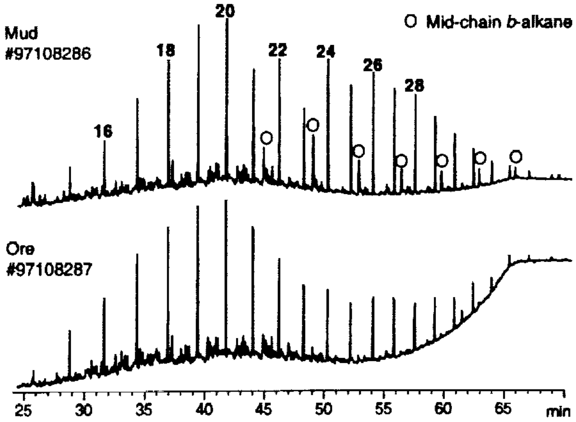

Fig. 2. A comparison of hydrocarbon distributions in a Pb-Zn sulfide ore and adjacent poorly mineralized turbiditic muds.

Samples derived from sulfide ore and adjacent poorly mineralized turbitic mud show two distinct hydrocarbon patterns. Within the muds, a similar but more subtle distribution of even C number compounds occurs compared to the Wallara mats, coupled with a population of large filamentous microfossils. It is thought that H_2S and CO_2 were provided by the subsurface mineralization processes and that mixing of the water column during turbidite deposition provided O_2 for populations of sulfide-oxidizing bacteria to flourish on the surfaces of the turbiditic muds.

References: [1] Logan G. A. et al. (1999) *GCA, 63,* in press. [2] Logan G. A. et al. (1999) *GCA,* submitted.

EVALUATING SECULAR CHANGES IN SEAWATER CHEMISTRY.

T. K. Lowenstein[1], M. N. Timofeeff[1], L. A. Hardie[2], and S. T. Brennan[1], [1]Department of Geology and Environmental Studies, State University of New York at Binghamton, Binghamton NY 13902, USA (lowenst@binghamton.edu; bf21297@binghamton.edu; bg20824@binghamton.edu), [2]Department of Earth and Planetary Sciences, Johns Hopkins University, Baltimore MD 21218, USA (hardie@gibbs.eps.jhu.edu).

Fluid inclusions from marine halite deposits may be used to test the hypothesis that secular changes in seawater chemistry have occurred in the Phanerozoic Eon [1]. To assess the chemistry of ancient seawater, the following are required: (1) an accurate technique for the chemical analysis of individual fluid inclusions, (2) criteria for establishing that the fluid inclusions contain seawater, and (3) methods for back-calculating seawater from the chemical composition of brines in fluid inclusions that have undergone evaporative concentration.

Fluid inclusions in halite can form from surface waters other than seawater and may be trapped at any time during diagenetic cementation and recrystallization. Criteria are therefore required to establish that the fluid inclusions contain evaporated seawater. Halites from ancient evaporites may contain well-preserved sedimentary textures and fabrics, including the well known chevron crystal growth fabrics and settle-out cumulate textures, which are identical to features observed in modern environments where halite precipitates from surface brines [2]. These "primary" halite crystals commonly contain abundant fluid inclusions along bands parallel to crystal-growth faces. Halite formed during later cementation or burial recrystallization lacks the growth textures and fluid-inclusion banding that develop during precipitation from open surface waters.

Halite from the marginal marine saline pan of Salina Omotepec, Baja California, Mexico [2,3], was examined to verify that primary fluid inclusions in chevron halite from a modern setting contain unmistakable samples of evaporated seawater. Twenty-four fluid inclusions were analyzed using the ESEM-EDS technique. The environmental scanning electron microscope (ESEM) with an attached X-ray energy-dispersive system (EDS) is capable of producing accurate major-element chemical analyses of individual fluid inclusions in halite greater than ~30 µm in size. The chemical analyses of the major ions Na, Mg, K, Cl, and SO_4 show distinctive linear trends when plotted against one another that closely track the evaporation path of seawater as it evolved during the crystallization of halite. Fluid inclusions in halite from Baja California contain uncontaminated evaporated seawater, despite the fact that nonmarine inflow and syndepositional recycling of previously deposited salts have occurred in this setting.

How do we know fluid inclusions in ancient halites contain evaporated seawater? The best way to detect a seawater signal in ancient halites is to plot fluid-inclusion chemistries from several basins of about the same age, which we have done for deposits of Permian age (San Andres Formation, Salado salts, and Zechstein I halites) and Cretaceous age (Aptian of Congo Basin and the Sergipe Basin, coastal Brazil; Khorat Plateau, Thailand and Laos). For example, if Permian halites each have fluid-inclusion chemistries that fall along a distinctive evaporation path, and if the paths for the three geographically separated basins of about the same age overlap one another, the implication is that the parent water was "global" seawater of common chemical composition. In addition, the effects of nonmarine inflow and syndepositional recycling were not strong enough to greatly modify the overlapping evaporation paths.

How can we back-calculate the chemistry of seawater from fluid inclusions in halite that have undergone evaporative concentration? Once an evaporation path is established from fluid inclusions in geographically separate deposits of about the same age, the final step is to calculate the chemical composition of the original seawater. This can be done with the Harvie-Moller-Weare [4] computer program, which can simulate evaporative concentration of parent seawaters that best fit the evaporation pathways of the major elements defined by fluid-inclusion chemistries.

Our results show that Permian seawater was enriched in K (~50%) and depleted in Mg (15–20%) and SO_4 relative to modern seawater. Cretaceous seawater was probably substantially different from modern seawater because the concentration of Ca was greater than SO_4. Assuming the Cl concentration to be the same as in modern seawater, Cretaceous seawater was enriched in K and Ca and depleted in Mg (~40%) and Na. Our results for Permian and Cretaceous seawater generally match predictions of the major-element chemical composition of seawater [1] and strongly support the Hardie hypothesis that secular changes in seawater chemistry have occurred as a result of changes in the flux of mid-ocean ridge hydrothermal brines.

References: [1] Hardie L. A. (1996) *Geology, 24,* 279–283. [2] Lowenstein T. K. and Hardie L. A. (1985) *Sedimentology, 32,* 627–644. [3] Shearman D. J. (1970) *Trans. Inst. Mineral. Metall. B., 79,* 155–162. [4] Harvie C. E. et al. (1984) *GCA, 48,* 723–751.

ASSESSMENT OF HUMAN IMPACT ON A COASTAL EMBAYMENT, CEBU, PHILIPPINES: ANALYSIS OF BAY WATER AND SEDIMENTS.

A. R. Lucero Jr., M. E. S. Lupo, and P. C. Momongan, Department of Environment and Natural Resources, Mines and Geosciences Bureau, Region 7, Mandaue City, Philippines 6014 (mgb7cebu@mozcom.com; pcmomongan@hotmail.com).

The rapid industrialization that is currently taking place on the island of Cebu in central Philippines has resulted in the degradation of its natural environment. Some of the most conspicuous problem areas involve the pollution of coastal embayments including the Cansaga Bay, which was previously ringed by natural wetlands. With a surface extent of ~850 ha, the bay is located between heavily industrializing towns along the northeast coastline of the island. Among the residual patches of mangrove vegetation proliferates a host of human activities such as ship building, land reclamation, fishpond construction, and housing projects. This paper describes a study relating the effects of these encroachments on the natural environment of the embayed area.

Water and bottom-sediment samples from the bay area were collected for analysis, while information about the existing coastal land use was updated. The sediments were taken from the inner portion of the bay as well as from its outer fringes near the main shoreline. The sampling was done during a cycle of wet-dry-wet seasons in 1997–1998 to determine seasonal variations in the chemical characteristics of the sampling media. Appropriate sampling methods and handling were employed to reduce the risk of contamination. Proper protocols for storage and chain of custody were also followed. Water samples were analyzed using standard procedures for water and wastewater analysis. Determined parameters were acidity, alkalinity, CO_2, Cl, NaCl, total solids, Ca, Mg, Fe, turbidity, color units, pH, and SO_4. Sediment samples were analyzed for the majors: SiO_2, Al_2O_3, Fe_2O_3, CaO, and MgO. Atomic absorption spectrometry was used to determine Na, Al, Ca, Ti, Cr, Mn, Fe, Co, Ni, Cu, Zn, Mo, Cd, Sn, and Pb in the water and sediment samples.

The terrane enclosing the bay area is underlain chiefly by a Pliocene-Pleistocene coralline limestone unit. However, this young limestone formation flanks the older core of rocks in the island, which consists of Cretaceous to Tertiary volcanic and sedimentary sequences.

Results of chemical analysis showed that the inner sediments of the bay tend to have higher silica and alumina, and lower lime content, while the outer-bay sediments have lower silica and alumina and higher lime content. Lithology of the terrane along the coast seems to be the major factor controlling the spatial distribution of the majors in the bottom sediments. The inner-bay sediments indicate a strong influence from clastic dispersion from older terrigenous sources. The outer-bay sediments reflect sourcing from the younger limestone formation, and also possibly from the limestone-filling materials being used for reclamation of a portion of the bay. Sediments near the ship-building industry showed a high concentration of Cu, Pb, Zn, Mn, Fe, Mo, Ni, and Cr.

Seawater samples showed Cu, Zn, Cd, Cr, Ni, and Sn concentrations above acceptable levels. Chloride and sulfate tend to be higher in the inner bay due to weaker water circulation imposed by developments in the area. Total solids, chloride, and sulfate in the seawater samples were generally low during the rainy season due to dilution by increased runoff and rainwater. There is an increase in Ca in freshwater samples during the rainy season, brought about most likely by the increased interaction of the groundwater with the limestone aquifer.

ZINC AND COPPER ISOTOPES AS TRACERS OF METAL ORIGIN IN THE DISSOLVED AND PARTICULATE LOADS OF RAIN.

J. M. Luck[1], D. Ben Othman[1], F. Albarède[2], and P. Telouk[2], [1]Unité Mixte de Recherche, 5569 Hydrosciences (cc 057), Université Montpellier 2, 34095 Montpellier, France (jmluck@dstu.univ-montp2.fr), [2]Géologie, Ecole Normale Supérieure de Lyon, 69364 Lyon, France.

For the first time, Cu- and Zn-isotopic compositions (expressed as $\delta^{65}Cu$ and $\delta^{66}Zn$) are reported for dissolved and particulate loads of rains, and also for weak acid leaches and HF/HNO_3 dissolution on the particulates and aerosols from the northwestern Mediterranean. Both continental and marine rains have been sampled. Additional data on regional natural and anthropic (rocks, fertilizers, chemicals, urban effluents, industrial emissions, and coal ashes) end members are also presented (characterized in trace elements and Pb isotopes in [1]). Values that we obtained on loesses from Europe and Asia

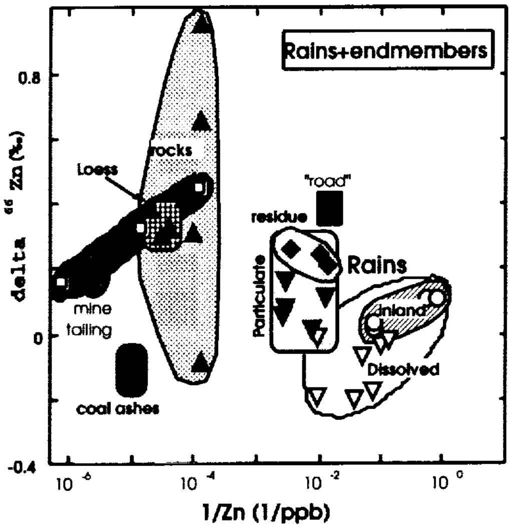

Fig. 1. Isotopic composition of Zn (expressed as δ^{66}Zn vs. ^{64}Zn, in per mil) vs. inverse of concentration in rains and in various natural and anthropogenic end members.

are used to constrain the Zn-isotopic signature of mean natural aerosol component.

As isotopic variations for transition metals have recently been reported in ores, sediments etc. [2], our data are aimed to establish Cu and Zn as new possible isotopic tracers in surface processes and to better understand the origins and proportions — natural and anthropic — of these metals in rains and rivers.

A new chemical separation procedure was developed for separating metals on anion-exchange and macroporous resins, and includes the procedure developped by Marechal for Cu [2]. The whole procedure was checked for possible isotopic effects. Isotopic compositions were measured on the VG Plasma 54 at ENS Lyon. Combined precision and reproducibility is ±0.02‰.

Zinc data for 11 rains are presented in Fig. 1. Zinc-isotopic data show that (1) inland rain has generally heavier values (higher δ^{66}Zn) in the dissolved load than coastal rain; (2) on the whole, particulate loads show also heavier (higher δ^{66}Zn) Zn-isotopic values than dissolved loads; (3) loess samples have clustered values around δ^{66}Zn = 0.3–0.4‰, similar to sediment values reported elsewhere; and (4) HF-dissolved residues from particulates show Zn values similar to loess.

The detailed investigation on a three-part sequential rain indicates that the Zn (and Pb: see companion abstract by Ben Othman et al., this volume) adsorbed on the surface of particulates exhibits lower δ^{66}Zn-isotopic values than those measured on the corresponding HF-dissolved residue. Coal ashes samples are characterized by quite low values, presumably linked to biological fractionation. Although an end member with a low δ^{66}Zn has yet to be found, these observations open up the possibility of using Zn and Cu isotopes for better determining the proportions of natural vs. anthropic metals in the atmosphere.

References: [1] Luck J. M. and Ben Othman D. (1998) *Chem. Geol., 150,* 263–282. [2] Maréchal C. et al. (1999) *Chem. Geol., 156,* 251–273.

HOW WELL CAN WE REALLY DO TIMESCALE GEOCHRONOLOGY WITH ZIRCON URANIUM-LEAD?

K. R. Ludwig[1], R. Mundil[1], and P. R. Renne[1], [1]Berkeley Geochronology Center, 2455 Ridge Road, Berkeley CA 94709, USA (kludwig@bgc.org; rmundil@bgc.org; prenne@gbc.org).

The U/Pb method has several impressive advantages over any other technique for timescale geochronology: it is the only method with really precisely measured decay constants, a plethora of high-accuracy isotopic standards exist for spike calibration, and the unique mathematical power of two coupled decay schemes yields a delightful intellectual garden of methods for assessing (and, in favorable circumstances, correcting) open-system behavior. Taking advantage of these and other circumstances, many laboratories can now routinely determine the U-Pb age of typical single zircon crystals from volcanics of Phanerozoic age to a precision of a few per mil. Further, the highest-quality crystals can be preselected (using both normal and cathodoluminescence microscopy) to be as free as possible of obvious defects, high U content, or older cores, thus minimizing the possibilities of both Pb loss and inheritance. One might hope, therefore, that because of the absence of evidence for thermal or hydrothermal events in most timescale sections, and because of the easy detection (through internal U-Pb discordance) of much-older inherited zircons, routine and reliable timescale zircon geochronology at accuracies approaching a fraction of the single-crystal analytical precision should be possible. Pooling of ^{206}Pb/^{238}U ages (or, even better, "Concordia" ages) rather than ^{207}Pb/^{206}Pb ages for this purpose is especially attractive, because the former avoids the ~5-m.y. accuracy limitation (from decay-constant errors) of the latter, as well as reliance on the inherent but seldom objectively justifiable assumption that any Pb loss must have occurred only very late in the zircon's history.

Unfortunately, there seem to be few cases (with adequate numbers of replicate analyses) that permit such a straightforward approach. As examples, we will show several instances of small (0.5–2%) but clearly resolvable amounts of apparent-age dispersion in multiply-replicated analyses of carefully selected and prepared zircon crystals, involving tuffs ranging from Cretaceous to late Precambrian age. In cases where both subtle Pb loss and also slightly older xenocrysts coexist in a zircon population, and where geochemical/crystallographic criteria to distinguish xenocrysts are absent, it may be impossible to objectively deconvolute the resulting age pattern — especially for Mesozoic or younger rocks, where internal concordance is maintained in spite of significant Pb loss. Even when slightly older xenocrysts are identifiable (from morphological or geochemical criteria) or absent, so that the oldest clump of Pb/U apparent ages must be the best approximation of true age, it is possible that the best-estimate age remains biased by a small but pervasive amount of Pb loss, perhaps averaged over the nontrivial volume of zircon crystal.

The solution to this dilemma is not clear, although we argue that mathematical deconvolution of such datasets is not the answer. More extensive evaluation of vigorous sample pretreatment, either for identification of imperfect crystals (à la Krogh's NaOH pretreatment; [1]) or removal of damaged zones (à la Krogh's or Mattinson's HF leaching [1,2]) seems to be one of the few promising avenues.

References: [1] Krogh T. E. (1990) *U.S. Geological Survey Circ., 1107,* 180. [2] McLelland W. C. and Mattinson J. M. (1990) *U.S. Geological Survey Circ., 1107,* 209.

HOW ALKALI BASALTS ASCENDING IN MELT CONDUITS CAN AFFECT MELTING IN ADJACENT PERIDOTITE.

C. C. Lundstrom, Department of Geology, University of Illinois, 245 Natural History Building, Urbana IL 61801, USA.

Introduction: Mantle melting is generally accepted to be a polybaric process whereby melts are generated over a range of depths followed by aggregation prior to eruption. However, the extent to which magmas formed at greater depths interact with mantle solids at shallower depths during ascent is controversial. Melt transport beneath mid-ocean ridges has been proposed to reflect channelized flow through dunites [1], since incompatible element contents of abyssal peridotites [2] require isolation from typical MORB magmas. If melts are channeled into a melt conduit through the upper portions of a melting column, are there important interactions between melts equilibrated deeper in the melting column now in the conduit and the adjacent peridotite?

Experimental: Piston-cylinder experiments examining the interaction between basanite and peridotite were performed at 1 GPa in Mo/Pt-sealed graphite capsules at 1200°–1300°C. The starting materials were a primitive basanite (43% SiO_2) from the Canary Islands (representative of a melt in equilibrium with peridotite at greater depths) and either a fertile spinel facies peridotite (KLB-1) or a harzburgite. Separate capsules of each material were first synthesized at 1 GPa and the desired run temperature forming (1) basaltic glass + olivine ± cpx and (2) peridotite with interstitial melt. Following synthesis, one basanite capsule and one peridotite capsule were each polished on an end, juxtaposed and pressurized with the basanite on top of the peridotite, and ramped quickly (500°C/min) to run temperature. Experiments at 1250°C and 1300°C using KLB-1 were held at run temperature for 10 min before rapid quenching. Experiments at 1200°C (KLB-1) and 1300°C (harzburgite) were held at temperature for 30 min.

Results: In all experiments, Na_2O diffuses from the basanite into the melt within the peridotite forming a pronounced peak in concentration ~200 μm from the interface. In the 1250° and 1300°C experiments, Na_2O rapidly infiltrates the peridotite due to the large melt porosities in the original KLB-1 starting materiel (5 and 10% melt respectively) being higher than its original concentration for >1 mm from the interface. In the harzburgite and 1200°C KLB-1 experiments (with <1% melt originally present), a high concentration Na_2O peak is found close to the interface, but the lack of melt farther from the interface precluded assessing the extent of Na_2O infiltration. SiO_2 shows a peak in concentration exactly coinciding with the Na_2O peak in all experiments reaching values as high as 58%; however, this high concentration is not explicable by diffusion. Mineral modes change with distance to the basanite-lherzolite interface. In the 1300°C experiment, the orthopyroxene mode decreases from 18% in the starting material down to ~6% near the interface. The melt mode correspondingly increases from 8 to 22% as the interface is approached. Based on TiO_2 contents, this cannot reflect the basanite melt infiltrating the peridotite; instead, increased melt reflects the effect of Na_2O addition alone by diffusion on the peridotite phase relations. Spinel and clinopyroxene compositions also systematically changed with distance to the interface.

To gain further insight into this interaction process, basanite-tholeiite melt diffusion couples were executed at 1450°C in order to quantify elemental diffusion rates. Most elements have binary diffusion profiles with D (diffusion coefficient) $\sim 1 \times 10^{-6} cm^2/s$. Notably, Na diffusion is strongly coupled to gradients in SiO_2 with $D_{Na} \sim 5 \times 10^{-5} cm^2/s$. K has $D_K \sim 5 \times 10^{-6} cm^2/s$ and Li (ion probe) has $D_{Li} \sim 2 \times 10^{-5} cm^2/s$.

Discussion: The rapid diffusion of alkalis into the peridotite is consistent with the strong preference of alkali cations for more polymerized, higher silica melts [3]. The effect of addition of alkalis to melts in equilibrium with peridotite is to increase SiO_2 contents [4]. Therefore, diffusive infiltration of Na_2O favors the production of high silica melts through the preferential melting of orthopyroxene and will occur any time higher-pressure melts pass through shallow peridotite that contains melt. The diffusive infiltration process documented by these experiments could play a critical role in altering how spinel lherzolite melts relative to that expected based on peridotite melting experiments. Namely, this process could provide an explanation for the high olivine/orthopyroxene mode ratios observed in abyssal peridotites [5]. Using the diffusion coefficient obtained above, melting in peridotite as far as 230 m from a dunite melt conduit might be affected by this process. In addition, this process may provide a means for producing the high-alkali, high-SiO_2 glasses found ubiquitously in mantle xenoliths.

References: [1] Kelemen P. et al. (1997) *Phil. Trans. Royal Soc., 355,* 283–318. [2] Johnson K. T. M. et al. (1990) *JGR, 95,* 2661–2678. [3] Watson E. B. (1982) *Contrib. Mineral. Petrol., 80,* 73–87. [4] Hirschmann M. M. et al. (1998) *GCA, 62,* 883–902. [5] Y. Niu et al. (1997) *EPSL, 152,* 251–265.

ELECTROCHEMISTRY AND STRUCTURE OF YTTRIA-STABILIZED ZIRCONIA MEMBRANES FOR POTENTIOMETRIC MEASUREMENTS IN HYDROTHERMAL SYSTEMS.

S. N. Lvov[1,2], G. C. Ulmer[4], X. Y. Zhou[2], S. M. Ulyanov[2], L. G. Benning[3], D. E. Grandstaff[4], M. Manna[4], E. Vicenzi[5], and H. L. Barnes[3], [1]Department of Energy and Geo-Environmental Engineering, Pennsylvania State University, University Park PA 16802, USA, [2]The Energy Institute, Pennsylvania State University, University Park PA 16802, USA, [3]Department of Geosciences, Pennsylvania State University, University Park PA 16802, USA, [4]Department of Geology, Temple University, Philadelphia PA 19122, USA, [5]Princeton Materials Institute, Princeton University, Princeton NJ 08540, USA.

The electrochemical and structural properties of yttria-stabilized zirconia (YSZ) membranes were investigated for use in high-temperature potentiometric and pH measurements. These membranes were incorporated into a new electrochemical cell designed and constructed for use with different electrochemical probes up to ~450°C.

Commercial ZrO_2 membranes were employed having 8 mol% Y_2O_3 (solid-solution-stabilizing the cubic phase) and an impedance of $<10^{12}$ Ω in the temperature range of study. A new flow-through YSZ pH sensor design has been developed and tested at temperatures >300°C. The potentiometric response of the flow-through YSZ pH sensor was found to be identical to that of a flow-through H (Pt) electrode also developed in this research. Both probes are being evaluated as accurate direct-reading high-temperature pH sensors.

Analyses of the available commercial YSZ membranes revealed that the cells are both texturally and compositionally less than ideal. The cells contain ~5 vol% of Ca-Al-Silicate glass ($1.5 < Si/Al < 1.6$, $1.27 < Al/Ca < 1.40$, and $1.78 < Si/Ca < 1.85$, molar ratios). Texturally, nearly all of the grain boundaries intersect at dihedral angles and are decorated with this glass phase. In the present use of the YSZ, the data obtained suggest that the impedance contribution of this glass is not seriously interfering with measurement of pH. However, this glass reduces the long-term (10^2–10^3 h) chemical durability of the cell, resulting in premature disaggregation of the cells in acidic solutions (as dilute as 0.001 mol kg^{-1} HCl), even at moderate temperatures (200°C). In spite of the lack of durability of the commercial membranes in our new electrode systems, we found the rate of pH response to be fast, apparently limited by the rate of mixing of solutions pumped into the cell. A resolution of ~±5 mV was measured with a corresponding uncertainty of ±0.05 pH unit.

Other commercially fabricated YSZ membranes have also been investigated. Almost all contain grain-boundary phases that have been accidentally or purposely added to the YSZ. Identified phases included glass, diopside, and wollastonite. Impedance spectroscopy reveals that these grain-boundary phases may change the bulk impedance by orders of magnitude. In some cells, yttria is not homogeneously distributed, leading to incomplete stabilization of the cubic phase, and abrupt bulk impedance variations with changes in temperature. Such changes affect Nernstian response. Some minor impurities, such as TiO_2, are desirable because they increase thermal shock resistance, whereas others, like HfO_2, are undesirable because they increase susceptibility to neutron activation of sensors to be used in nuclear reactor environments.

Acknowledgments: Under this collaborative research, sponsored by NSF (EAR 9725191 and EAR 9727118), we are therefore fabricating high-purity isostatically hot-pressed YSZ membranes for further evaluation.

SULFUR GEOCHEMISTRY OF THE MESOPROTEROZOIC BYLOT SUPERGROUP, NORTHERN BAFFIN AND BYLOT ISLANDS, CANADA: LOCAL AND GLOBAL IMPLICATIONS.

T. W. Lyons and L. C. Kah, Department of Geological Sciences, University of Missouri, Columbia MO 65211, USA (lyonst@missouri.edu).

The Bylot supergroup is a thick succession (~6000 m) of nearly undeformed siliciclastic and carbonate rocks, along with minor evaporite and volcanic lithologies, exposed within fault-bounded basins of northernmost Baffin and Bylot islands. Paleomagnetic and biostratigraphic constraints suggest that deposition of the Bylot supergroup occurred between ~1270 and 1000 Ma, which is supported by a recent Pb-Pb age of 1204 ± 22 Ma for carbonates of the Society Cliffs and Victor Bay Formations within the Bylot supergroup. From a geochemical standpoint, this represents a critical episode in the development/evolution of the oxygenated ocean-atmosphere system but is an interval for which very little elemental and isotopic data are available.

In order to test and constrain the general hypothesis of increased biospheric oxidation in the Mesoproterozoic, we have undertaken a detailed characterization of the S geochemistry of the Bylot supergroup within the context of a broader geochemical study. The focus is threefold: (1) iron sulfide and complementary trace-element data for centimeter-scale black shaley intercalations within the carbonate/evaporite sequence, as well as from over- and underlying red and black shales; (2) carbonate-associated trace sulfate [CAS] thought to be incorporated within the lattice of calcite and dolomite; and (3) the geochemistry of bedded gypsum. Regarding the latter, highly evaporative sections on Bylot Island contain well-preserved bedded gypsum (10–15% of the lowermost 300 m; beds up to 2 m in thickness) interbedded with carbonate and black shaley lithologies.

Analysis of 33 gypsum samples from the Society Cliffs Formation has revealed a striking monotonic up-section increase in $\delta^{34}S$ values from 24 to 32‰, which spans ~300 m and likely records seawater compositions variably influenced by local reservoir conditions. Elemental data from the bedded sulfates, as well as compositional data from interbedded shaley and carbonate units, are helping to constrain the local environmental factors that may have influenced the preserved geochemical records. In particular, trace-element relationships and Sr-isotopic data speak to the records of local reservoir effects (e.g., variations in the quantity and character of local fluvial inputs) vs. short-term variation in the global S-isotopic composition of seawater sulfate. The latter will assist in strengthening our understanding of the secular S-isotopic trend for Mesoproterozoic seawater and thus, when viewed in light of complementary C-isotopic results, help constrain the balance in fluxes between reservoirs of reduced and oxidized S and associated effects on levels of atmospheric O.

Carbonate-associated trace sulfate as a constraint on the amount and isotopic composition of sulfate in the ocean is receiving wide attention within the geochemical community. Unlike gypsum deposits, the carbonate rocks that yield these data abound in the Precambrian record, and because the deposition of the carbonate rocks reflects marine conditions less restricted than those of the gypsum deposition, they can provide a less ambiguous record of marine sulfate if sufficiently deficient in organic matter. Organic matter has the potential to drive microbial sulfate reduction within the pore waters that could mask the primary signal of the overlying water. The sedimentological uniqueness of the undeformed Mesoproterozoic interbedded carbonate-evaporite succession of the Bylot supergroup provides a rigorous test for the generation and interpretation of combined gypsum/CAS analyses using bulk sample analysis, particularly given the large and systematic stratigraphic variation within the gypsum $\delta^{34}S$ record. Finally, the presence of iron sulfides within the black shales provides a mechanism for evaluating the net isotopic fractionation between sulfides and essentially coeval sulfate. Temporal trends in the magnitude of this fractionation have been linked to shifts in the redox state of the ocean-atmosphere system and corresponding responses in the Precambrian microbial ecosystem [1,2].

References: [1] Canfield D. E. and Teske A. (1996) *Nature, 382,* 127–132. [2] Canfield D. E. (1998) *Nature, 396,* 450–453.

MINERALOGY AND GEOCHEMISTRY OF THE LATERITIC PROFILES IN SOUTH JIANGXI, CHINA: IMPLICATIONS FOR SOURCE-AREA WEATHERING AND PROVENANCE.

Y. J. Ma and C. Q. Liu, Institute of Geochemistry, Chinese Academy of Sciences, Guiyang 550002, China (yjma@ms.gyig.ac.cn).

Introduction: The mineralogical and trace-element compositions of fine-grained detrital sediments are widely used to trace provenance, the evolution of the crust, paleoclimates, and tectonic activity [1–3], but there are few detailed studies documenting the effects of chemical weathering on the compositions of sediments [4]. Lateritic profiles are widespread in southern China, where an ideal chance is provided to test the premise that the characteristics of a provenance area can be inferred from a study of siliciclastic sediments. This study is to investigate the mineralogical, major-element, and trace-element changes in the lateritic profiles, and evaluate the effects of chemical weathering and erosion on the compositions of siliciclastic sediments.

Results and Discussion: The lateritic profiles studied are developed respectively on granite and acid volcanic rocks in South Jiangxi, China, which have different maturity controlled by the balance between erosion and chemical weathering. With the increase of chemical weathering intensity, quartz content increases, plagioclase is rapidly converted to halloysite and kaolinite, and biotite is rapidly altered to clay minerals. K-feldspar:plagioclase ratios increase and the residual plagioclase becomes more albitic than that in the parent rocks. Generally speaking, the intensity of chemical weathering plays an important role in determining the mineralogy of the weathering profiles, and continued chemical weathering, erosion, and hydraulic sorting would probably result in the separation of aluminous clay mineral-rich muds from sands with abundant quartz, feldspar, and higher K-feldspar:plagioclase ratios than those of the parent rocks. So the mineralogy of sediments more closely reflects those of weathering profiles than bedrocks from which they are derived.

In these lateritic profiles, Fe(T)/Ti, Al/Ti, Zr/Ti, and Th/Ti ratios almost stay constant regardless of the weathering intensity, implying the homogeneity of parent rocks and immobility of these elements. With the increase of chemical-weathering intensity, alkalis and alkaline earths (e.g., Na, K, Rb, Cs, Ca, Sr, Ba) are rapidly leached away, resulting in the rapid decrease of element/Ti ratios from the bottom to top of the profiles. Transition metal/Ti ratios (e.g., Sc/Ti, Zn/Ti, V/Ti, Co/Ti, and Ni/Ti) and high field strength element/Ti ratios (e.g., Hf/Ti, Nb/Ti, Ta/Ti) display minimal changes relative to those of parent rocks, suggesting similar behaviors of these elements to Ti.

In high weathered mature profiles subjected to minimal erosion, LREEs are extremely enriched in the intermediate zones of the profiles, which implies that LREEs are leached from the top zones of profiles and transported by soil solution to the intermediate zones to deposit. However, Eu and HREEs are depleted in the top zones and their element/Ti ratios gradually decrease from the bottom to top of the profiles, indicating that HREEs are more mobile than LREEs during chemical-weathering. LREE/HREE ratios obviously increase with the increase of chemical weathering intensity. Chondrite-normalized REE patterns of weathering samples are similar to parent rock, but with the increase of chemical weathering intensity, LREEs become more enriched and the negative Ce anomaly (in bedrocks) gradually turns into a positive one (in top soil zones). On the contrary, in immature profiles subjected to rapid erosion, the uppermost REE-leached zones are eroded away and the element accumulation zones are exposed in the top of the profiles. From the bottom to top of the profiles, REE/Ti ratios and Ce/Ce* increase, while LREE/HREE decreases.

It is obvious that element distribution trends in weathering profiles are controlled by the change of relative rates of chemical weathering and erosion, and the trace-element characteristics of derived siliciclastic sediments vary depending on the weathering zones eroded. When the REE-depleted zones of high weathered profiles are eroded, the REE contents in sediments will be less than that in source rocks and REE patterns will also have some difference. When the immature weathering zones, extremely enriched in REEs, are eroded, REEs in derived sediments should be more abundant than in source rock. Tectonism and climate generally determine the relative rates of erosion and chemical weathering [1,2].

With the exception of Th/Sc, Sm/Nd, Zr/Hf, and Nb/Ta, none of the trace-element ratios can be transferred with minimal changes from bedrock to weathering profiles and then to sediments. So caution needs to be exercised when using trace-element ratios in fine-grained detrital sediments to trace-sediment provenance.

References: [1] Taylor S. R. and McLennan S. M. (1985) *The Continental Crust: Its Composition and Evolution,* Blackwell. [2] McLennan S. M. and Taylor S. R. (1991) *J. Geol., 99,* 1–21. [3] Condie K. C. (1993) *Chem. Geol., 104,* 1–37. [4] Nesbitt H. W. et al. (1996) *J. Geol., 104,* 525–542.

SEASONAL MIGRATION OF REDOX BOUNDARY AND ITS INFLUENCE ON WATER QUALITY IN LAKE LUGU, YUNNAN, CHINA.

Y. J. Ma and C. Q. Liu, The State Key Laboratory of Environmental Geochemistry, Institute of Geochemistry, Chinese Academy of Sciences, Guiyang 550002, China (yjma@ms.gyig.ac.cn).

Introduction: Lake sediments are a major repository for heavy metals, both of anthropogenic and natural origin. However, these metal pollutants can be released to the overlying water column from the sediments when environmental conditions (e.g., redox regime, degradation of organic matter, pH, and bioturbation) change [1,2]. Studies indicate that to a large extent the early diagenetic behavior of heavy metals depends on the redox conditions in the sediments [1–4]. The redox cycling of Fe and Mn is a major geochemical process near the sediment-water interface of the lake [1,2]. The aim of this investigation is to study the seasonal migration of the redox boundary and quantify the diffusive fluxes of heavy metals at the sediment-water interface, meanwhile estimating the influence of heavy-metal diffusion on the overlying water quality in Lake Lugu, Yunnan, China.

Methods: From November 1991 to July 1994, the water columns and sediment cores were collected in the shallow and deep part of Lake Lugu, where the Mosuo nationality lives in an isolated matriarchal community and there is little anthropogenic impact on the lake environment. Sediment cores were cut into 0.5–1-cm-thick sections and pore water was obtained by *in situ* centrifugation. All water samples were filtered through a 0.45-μm cellulose acetate membrane and analyzed for Fe, Mn, Cu, Ni, Cr, Co, Cd, and Pb by GFAAS. The temperature, pH, and dissolved O (DO) were measured *in situ*. Nitrate and sulfate were analyzed by ionic chromatography.

Results and Discussion: In winter, DO, NO_3^-, and SO_4^{2-} concentrations are constant along the lake water column respectively at 5.20, 1.10, and 0.76 mg/L, but these oxidizers rapidly decrease at the interface and are completely consumed within the upper 5 mm of sediments. In summer, DO and NO_3^- concentrations are close to 0 both at the interface and in the pore water, implying that the redox conditions become anoxic.

With the seasonal change of redox regime, the concentration profiles of dissolved heavy metals also show typical seasonal variations. In the pore water of the topmost sediment layer, the heavy-metal concentrations are mostly higher than in the bottom water, and always reach a maximum within 10 cm depth of the sediments, implying that release of heavy metals is likely to occur. The positions of heavy metal-peaks in the porewater profiles are always higher in summer than in winter, and the form of peaks usually becomes sharper in summer. The heavy-metal concentrations in the bottom water are also higher in summer than in winter.

The Mn and Fe data, in conjunction with pH, DO, NO_3^-, and SO_4^{2-}, were used to establish the redox zonation in this lake. In winter, the oxic-anoxic boundary coincides with the sediment-water interface, under which Mn shows a broad peak in the Mn reduction zone, heavy metals are significantly enriched in the topmost sediments, and little diffusion out of the sediments occurs. However, in summer, the oxic-anoxic boundary moves upward into the bottom water, and the heavy metals in the topmost sediments are significantly released into overlying water, leading to the near-surface depletion of heavy metals in anoxic sediments. In fact, the releasing rates and patterns of different metals are different due to the formation of metal sulfides [1–4].

If the heavy metal distributions in the sediments are assumed to be controlled by a one-dimensional vertical transport process, the diffusive fluxes of heavy metals across the sediment-water interface (J_{diff}) can be calculated according to Fick's first law. Meanwhile, we quantified the influence of heavy-metal diffusion on the lakewater quality. The results show that the diffusive fluxes of heavy metals are significantly higher in summer than in winter, at deeper stations (more anoxic) than at shallower ones. The diffusion at the interface significantly affects the concentrations of heavy metals in overlying water, and can even lead to a 35× increase of Mn concentration in the bottom water. Generally, the diffusion across the sediment-water interface is an important process to control the water quality of lakes, especially of those with less water depth, longer residence time of water and lower heavy-metal concentrations in water.

References: [1] Davison W. (1993) *Earth Sci. Rev., 34,* 119–163. [2] Chen Z. et al. (1996) *Chinese Sci. Bull., 41,* 1359–1363. [3] Shaw T. J. et al. (1990) *GCA, 54,* 1233–1246. [4] Lapp B. and Balzer W. (1993) *GCA, 57,* 4639–4652.

VARIABILITY OF MERCURY AND PHOSPHORUS IN EVERGLADES PEAT CORES: IMPLICATIONS FOR MERCURY MOBILITY.

A. W. Macfarlane[1] and C. Arfstrom[2], [1]Department of Geology, Florida International University, Miami FL 33199, USA (macfarla@fiu.edu), [2]CH2M Hill, Tampa FL, USA.

The Everglades are presently used only for recreation, flood control, and water supply, with intensive sugar farming in their northern reaches. When up to 3 ppm Hg were discovered in Everglades fish in the late 1980s [1], the high Hg levels were initially surprising. Subsequent research has sought to identify the source of the anomalous Hg and the mechanism by which it is incorporated into animal life. Proposed Hg sources include agricultural runoff, contamination from industrial plants and incinerators, and enhanced methylation of resident soil Hg.

Analyses of Hg in peat cores in particular have been used to estimate the rates of Hg accumulation in Everglades soils through time, assuming that the Hg remains immobile in the peat after deposition. Studies based on this methodology have concluded that Hg deposition in Everglades peat since 1985 (23–141 μg/m²*yr) has been ~5× as rapid as at the turn of the century [2]; however, recent direct measurements of atmospheric Hg deposition (19–28 μg/m²*yr) [3] do not support the elevated rates proposed from studies of peat cores. We analyzed Hg and P in surface and core samples to look for areal patterns that could indicate contamination from local Hg sources such as canals or incinerators, to evaluate possible correlations between soil P and Hg, and to examine soil Hg and P variations with depth. Southern WCA-3A is centrally located and probably represents average conditions in the Everglades Trough.

Mercury contents of 64 surface samples collected on a 1-mile grid over a 500-km² area average 28.7 ng/cc (209 ppb dry sediment), which is typical of organic-rich soils. High Hg contents in Everglades fish are therefore not simply caused by anomalous soil Hg. Phosphorus contents of surface samples (350–850 ppm dry sediment) are typical of previous data from the interior regions of WCAs away from canals bearing agricultural wastewater. Mercury and P contents do not show systematic gradients from north to south or with distance from canals. Spatially homogenous sources are suggested for both elements, rather than point sources such as local dumps or incinerators or overflow from the canals. The most likely such source is dispersed atmospheric deposition.

Ores from nine sites contain more Hg and P at or near the surface than at 20–30 cm depth. Maximum Hg and P concentrations in several cores lie 4–8 cm below the surface. Mercury and P contents of individual cores correlate well and define statistically separate background and anomalous populations. The Everglades are naturally nutrient-poor, and subsurface P distributions are probably determined by the uptake of P by sawgrass and other plants. The correlation between P and Hg suggests that Hg may also be remobilized during uptake by plants, causing both elements to become concentrated near the surface in the zone of accumulation and decay of the plant matter. Although atmospheric Hg deposition has undoubtedly increased in recent decades, remobilization of Hg by plants would accentuate the near-surface Hg enrichment seen in the cores, and violate the assumption of immobility of Hg in peat used in earlier studies. Mercury deposition rates estimated from peat cores therefore may have been large overestimates.

A simple model is presented to evaluate the assumption of Hg immobility in peat, using data from our cores and assuming homogenous deposition of Hg from the atmosphere. The model indicates that Hg cannot have been immobile in the peat after deposition unless surface deposition was very heterogenous.

References: [1] Ware F. et al., *Proc. Am. Conf. SEAFWA, 44,* 5–12. [2] Rood B. E. et al., *Water, Air and Soil Poll., 80,* 981–990. [3] Guentzel J. L. et al., *Water, Air and Soil Poll., 80,* 393–402.

SEASONAL CHANGES IN LAKE MICHIGAN SEDIMENT MICROBIAL ACTIVITY: A MODEL FOR "TOP-DOWN" CONTROL OF CARBON CONVERSION.

B. J. MacGregor[1], M. Maurer[1], B. Baker[2], D. P. Moser[2,3], K. H. Nealson[2,4], and D. A. Stahl[1], [1]Civil Engineering Department, Northwestern University, 2145 Sheridan Road, Evanston IL 60208, USA (bmacgreg@anton.civil.nwu.edu), [2]Great Lakes Water Research Institute, University of Wisconsin-Milwaukee, 600 E. Greenfield Avenue, Milwaukee WI 53204, USA, [3]Department of Geosciences, Princeton University, Princeton NJ 08544, USA, [4]Mail Stop 183-501, Jet Propulsion Laboratory, California Institute of Technology, 4800 Oak Grove Drive, Pasadena CA 91109, USA.

We have been using molecular biological methods to study the distribution of microbial populations in offshore Lake Michigan sediments, in relation to electron acceptor availability [1]. Our study site (Fox Point) is at ~100-m depth, with year-round water temperatures of 1°–4°C. The sediments are fine silt, deposited at ~0.25 cm yr^{-1}, and are considered mesotrophic to oligotrophic.

Sediment was collected with a 30-cm² box core. Three-inch-diameter subcores were then squeezed to extract porewater for chemical determinations or sectioned at 0.5-cm intervals under a N atmosphere for nucleic acid (RNA and DNA) extractions. Extracted RNA was hybridized to nylon membranes and probed with radiolabeled oligonucleotides complementary to small-subunit ribosomal RNA (SSU rRNA). Ribosomes are intracellular protein-RNA complexes responsible for the translation of messenger RNA into protein. Because their production is growth-rate regulated, SSU rRNA levels are a sensitive indicator of metabolic activity.

Sediment cores collected over a one-year period (Fig. 1) had relatively constant O, sulfate, and dissolved Fe and Mn profiles, while nitrate concentrations and SSU rRNA concentrations changed seasonally. Surficial April

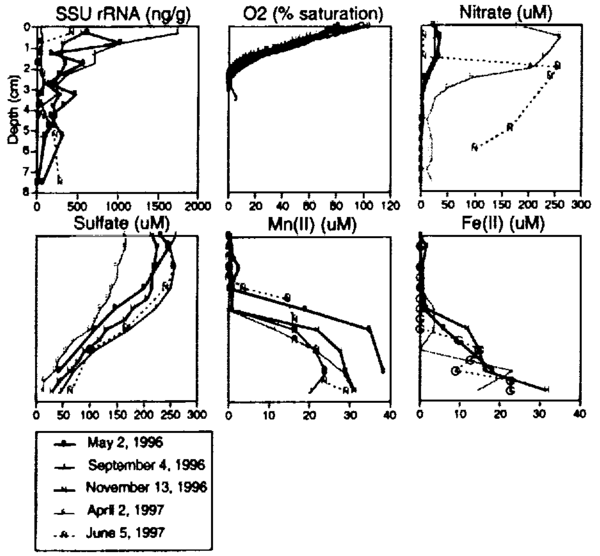

Fig. 1. Small-subunit rRNA recovery and chemical profiles.

sediments had the highest near-surface nitrate concentration (~200 vs. <50 µm) and the lowest SSU rRNA concentration (<100 vs. 400–1800 ng/g sediment). We hypothesize that a subpopulation of autotrophic nitrifying bacteria may be active in the spring before nitrate-utilizing heterotrophs, allowing for nitrate buildup. Preliminary SSU rDNA sequence data suggest that nitrifiers related to *Nitrosomonas* spp. are active in Fox Point sediments.

We further suggest that eukaryotic grazers such as *Mysis relicta* and *Pontoporeia hoyi*, abundant in profundal Lake Michigan, may drive this seasonal pattern. Easily degraded C from the spring diatom bloom may be rapidly utilized by grazers, which excrete ammonia that is converted to ammonia by nitrifying bacteria, while heterotroph activity increases only as more recalcitrant C compounds are hydrolyzed.

To test the feasability of this hypothesis, we have designed a model that describes the behavior of the sediment with respect to the flow of electron acceptors and donors. It assumes that within the sediment, molecular diffusion is responsible for the transport of soluble species, and that they are converted by biologically mediated processes only. The dynamic character of the model allows us to simulate temporally variable seston deposition.

The following processes are used to describe the observed concentration profiles: (1) Aerobic conversion of fresh seston by higher organisms into detritus; (2) hydrolysis of detritus by extracellular enzymes into soluble, microbially accessible compounds; (3) aerobic and anoxic growth of heterotrophic organisms; (4) nitrification; (5) anaerobic production of reduced species (sulfide and methane) in deeper regions of the sediment; and (6) aerobic conversion of reduced species.

A sensitivity analysis shows that the amount of C removed by eukaryotic grazers (as CO_2 or biomass) and the rate of aerobic and anaerobic hydrolysis have the biggest influence on the concentration profiles. Nitrification rates, half-saturation coefficients for electron acceptors, and mechanical mixing by the grazers play only a minor role.

The model is able to explain quantitatively the measured concentration profiles for the different seasons. The results indicate that higher organisms play a significant role in the dynamics of C conversion and that they have a significant influence on microbial activity in the sediment. As a first test of this model, we propose using oligonucleotide probes to follow the seasonal activity of nitrifying and total bacteria in relation to the rate of spring bloom C and N deposition.

References: [1] MacGregor B. J. et al. (1997) *Appl. and Environ. Microbiol., 63,* 1178–1181.

MAGMA TRANSPORT AND STORAGE IN THE MELT LENS AND UNDERLYING CRYSTAL MUSH AT FAST-SPREADING RIDGES: CONSTRAINTS FROM THE OMAN OPHIOLITE.

C. J. MacLeod[1], G. Yaouancq[1], R. M. Thomas[1], L. A. Coogan[1], and M. J. O'Hara[1], [1]Department of Earth Sciences, Cardiff University, P.O. Box 914, Cardiff CF1 3YE, Wales, UK (macleod@cardiff.ac.uk).

Introduction: From seismic evidence we know that a small body of magma is present at mid-crustal levels beneath most fast-spreading ridges, and that this small sill or melt lens overlies a much broader area of hot but largely solid material (a "crystal mush") that constitutes the lower ocean crust. Beyond this, however, we have little direct knowledge of the the physical and chemical processes that operate in and below the melt lens, nor of the mechanisms by which magma is transported through the lower crust to the melt lens and thence the surface. We here attempt to constrain the mechanisms of magma transport and residence in the middle crust by carrying out a structural and geochemical study through the crustal section of the Oman ophiolite, concentrating on the upper plutonic sequence and transition into sheeted dikes.

Architecture of the Lower Crust in the Oman Ophiolite: The lower two-thirds of the Oman plutonic section is composed of modally layered gabbros, intruded in some places by later wehrlite bodies. The layering in the gabbros is parallel to the petrological Moho. Penetrative l–s shape fabrics, with foliations parallel to the layering and consistent lineation directions, indicate that the gabbroic lower crust has been transposed by simple shear magmatic flow. In the upper third of the lower crustal section, compositional variation in the gabbros dies away, and the magmatic foliation becomes steep and lineation subvertical. Texturally, these foliated gabbros are less well equilibrated than the layered gabbros, suggesting faster cooling rates. Plagioclase crystals exhibit pronounced zoning, in constrast to the layered gabbros, in which plagioclase is rarely, if ever, zoned. The foliated gabbros pass up into a very heterogeneous "varitextured" gabbro horizon typically 100–150-m thick. Foliated gabbros, with steep magmatic fabrics parallel to those beneath, pass laterally and vertically over a few meters into isotropic gabbros with variable grain size and abundant oxide-rich pegmatitic segregations. Silica-rich "plagiogranite" segregations are common in some sections but absent in many others. Grain size within the isotropic gabbros decreases toward the top of the varitextured gabbro horizon and the proportion of pegmatite diminishes. Asymmetric doleritic chills are observed and can be traced upward into a sheeted dike complex.

Geochemistry of the Lower Crustal Section: Whole-rock analyses of both the layered and foliated gabbros show very high Mg#s (typically 80–85), very low abundances of incompatible elements, and positive Eu anomalies, consistent with their intepretation as "cumulates," i.e., crystal residues left after the partial crystallization of a magma and subsequent removal of the remaining liquid. Simple geochemical modeling indicates that the proportion of trapped interstitial liquid or "residual melt porosity" is uniformly very low, and that the mineral phases crystallized from liquids that span the range of compositions of the overlying sheeted dikes and lavas. No systematic variation with stratigraphic height is observed through the layered and foliated gabbros; instead, almost the entire range of variability is observed at any one stratigraphic level.

The varitextured gabbros, in marked contrast, are very heterogeneous in composition. The foliated gabbro remnants are identical in composition to the layered and foliated gabbros below, but the isotropic gabbros (Mg#s of 53–78) are either of basaltic composition or represent mixtures of this basaltic liquid and a variable proportion of cumulus crystals. The oxide-bearing pegmatites are ferrobasaltic, containing up to 16 wt% $Fe_2O_3^{tot}$ and 4.5 wt% TiO_2. The calculated bulk composition of this horizon is basaltic, with an Mg# of 60 and TiO_2 of 1.5 wt%.

Interpretation: We interpret the varitextured gabbro horizon as a fossilized melt lens, filled with pooled liquids of basaltic composition evicted from the crystal mush pile below. The ferrogabbro pegmatites represent late-stage fractionates of this liquid that formed *in situ* at the cooler edges of the melt lens.

We can place some constraints on the scale and nature of melt transport in the submelt lens crystal mush. Field relationships preclude the steep fabrics in these rocks, having formed by "gabbro glacier" subsidence of originally horizontal layers [e.g., 1]; instead, we suggest the fabrics record the ascent of crystallizing magma batches, frozen in the transport direction at the transition from suspension to grain-supported flow. It has been suggested [2] that the layered gabbros are a sill complex and, on the basis of cryptic variations in mineral compositions, that melt is extracted from the lower crust through melt-filled cracks rather than by diffuse porous flow. Noting the prominent mineral zoning in the foliated gabbros and absence in the layered gabbros, we suggest that porous flow may, however, be an important melt transport mechanism in the immediate submelt lens region, and/or that the crystal mush directly below the melt lens is typified, at least episodically, by much greater proportions of melt. The low residual melt porosity preserved in the Oman-foliated gabbros implies that final removal of the interstitial melt upward into the melt lens was extremely efficient.

References: [1] Quick J. Denlinger R. (1993) *JGR, 98,* 14015–14027. [2] Korenaga J. and Kelemen P. (1997) *JGR, 102,* 27729–27749.

TIMING OF MAMMAL-LIKE REPTILE EXTINCTIONS AND THE USE OF CARBON ISOTOPES IN THE STUDY OF THE PERMIAN/TRIASSIC BOUNDARY.

K. G. MacLeod[1], P. L. Koch[2], R. H. M. Smith[3], M. J. de Wit[4], and N. A. Rakotosolofo[5], [1]Department of Geological Sciences, University of Missouri, Columbia MO 65211, USA (macleodk@missouri.edu), [2]Earth Sciences Department, University of California, Santa Cruz CA 95064, USA, [3]South African Museum, P.O. Box 61, 8000 Cape Town, South Africa, [4,5]Department of Geological Sciences, University of Cape Town, Private Bag, Rondebosch 7701, South Africa.

The Permian/Triassic (P/T) extinction event is the largest of the Phanerozoic, and many possible causal mechanisms have been proposed. Different mechanisms predict different global-scale spatial and temporal patterns of change, but correlation with adequate resolution is difficult to achieve. Many areas lack independently dated material, and litho- and biostratigraphic techniques are often inappropriate due to the physical and environmental separation between sections. Carbon-isotopic stratigraphy is one of the few means of consistently providing global chronostratigraphic control. The surface ocean mixes on timescales of 10^4 yr and, because its C-isotopic composition is in dynamic equilibrium with the atmosphere (which mixes on much shorter timescales), global δ^{13}C excursions should be geologically simultaneous in continental and shallow marine environments [1].

We have found a large δ^{13}C excursion (Fig. 1) that coincides with the P/T boundary in a section from the interior of Pangea. A similar δ^{13}C excursion has been described at the P/T boundary from a number of globally distributed marine and coastal nonmarine sections in both organic and inorganic samples. Thus, the P/T boundary event was synchronous across environments ranging from the marine realm to (super)continental interiors.

Our δ^{13}C data are not as useful for determining the nature or tempo of change. We argue that the nodule results ($\sim$10‰ shift) are more robust than the tusk results (3–4‰ shift), but other studies have reported an excursion ranging from 3 to $>$10‰. Further, stratigraphic gaps between occurrences of Bethulie nodules compromise our ability to directly access the rate of δ^{13}C change or to resolve any possible higher-order features of the δ^{13}C curve. Our ongoing efforts to confirm the Bethulie curve at other sections and in different C-bearing phases have so far had limited success. The data suggest no long-term δ^{13}C changes through hundreds of meters of section at the end of the Permian and underscore the need to rigorously test for diagenetic artifacts, but they do not refine the δ^{13}C curve across the boundary.

To estimate the rate of change at Bethulie, we cite sedimentological and biostratigraphic observations. Within the resolution of sampling, the lowest δ^{13}C values coincide with a 15-m-thick overlap zone between Permian and Triassic taxa. The stratigraphic co-occurrence of these taxa cannot be attributed to taphonomic mixing of temporally distinct faunas, and the overlap zone contains several paleosol horizons that would have each required $>10^3$ yr to form. Recent radiometric dates from Chinese marine sections have placed a maximum duration of $\sim10^6$ yr for changes across the P/T boundary [2]. Our data show that, although the event was geologically rapid, it was not geologically instantaneous.

Existing δ^{13}C data do not point to a unique cause for the P/T event, but viable extinction scenarios must explain a large, rapid, negative δ^{13}C excursion. Better control on P/T δ^{13}C curves could provide additional constraints and would help avoid the potential circularity of using δ^{13}C data both for correlation and interpretation.

References: [1] Koch P. L. et al. (1992) *Nature, 358,* 319–322. [2] Bowring S. A. et al. (1998) *Science, 280,* 1039–1045. [3] Smith R. M. H. (1995) *Palaeogeogr. Palaeoclimatol. Palaeoecol., 117,* 81–104.

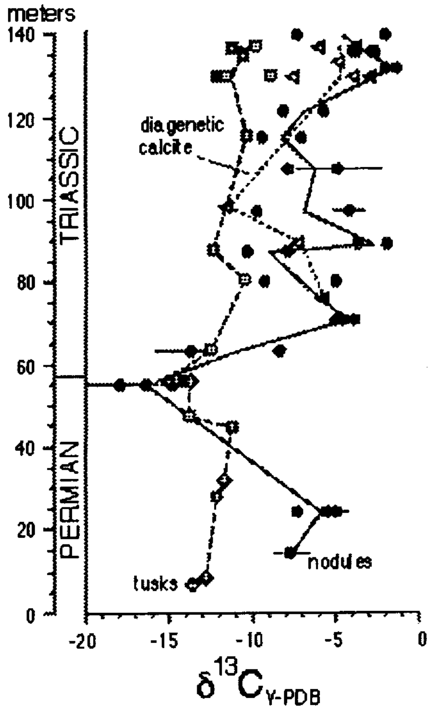

Fig. 1. Stratigraphic pattern of δ^{13}C in pedogenic nodules, dicynodont tusks, and diagenetic calcite at Bethulie (South Africa). The P/T boundary is placed at the last occurrence of *Dicynodon,* which, in this section, is 15 m above the first occurrence of *Lystrosaurus* [3].

CALCIUM-ALUMINUM-RICH INCLUSIONS IN CHONDRITE METEORITES: THE CASE FOR LOCAL PRODUCTION IN THE SOLAR NEBULA.

G. J. MacPherson, Department of Mineral Sciences, U.S. National Museum of Natural History, Smithsonian Institution, Washington DC 20560-0119, USA (glenn@glennm.si.edu).

Chondrite meteorites are 4.5-Ga aggregates containing diverse kinds of preplanetary grains and dust, and retain direct physical clues to high- and low-temperature processes in the preplanetary solar nebula as well as accretionary and alteration processes on early asteroidal bodies. The relative abundances of nonvolatile elements in chondrite bulk compositions approximate those in the solar photosphere [1]. The properties of chondrites and their components anchor models of the earliest solar system.

Chondrules (igneous olivine- and low-Ca pyroxene-rich spherules) and the less-abundant Ca-Al-rich inclusions (CAIs) are varieties of chondritic grains that occur in most (except CI) subtypes of chondrites. Both formed by very high-temperature processes in the solar nebula. The submillimeter- to centimeter-sized CAIs hold special importance in understanding the earliest solar system: they are the oldest objects formed in the solar system, and they partially preserve isotopic signatures of the presolar dust from which they formed. They are the principal carriers of evidence for the short-lived radionuclide ($t_{1/2}$ ~0.7 Ma) ^{26}Al in the solar nebula, a possible heat source for early planetary melting. They are also unusually enriched in ^{16}O. Until the fall of the large Allende carbonaceous chondrite in 1969, few people had ever heard of CAIs and fewer still had studied them. Brian Mason, to whom this paper is respectfully dedicated, was one of the first, publishing a series of papers [e.g., 2–4] on the geochemistry of the large and abundant Allende CAIs that helped establish their importance to solar nebula models.

Calcium-aluminum-rich inclusions were originally interpreted to be the products of gas-solid (equilibrium) condensation from a nebula that was uniformly hot at least out to the asteroid belt [e.g., 5]. But the preservation of presolar dust and the existence of widespread isotopic heterogeneity among the constituent grains of chondrites (including CAIs) make a uniformly hot nebula unlikely. Yet CAIs undeniably formed at high temperatures, so where and how did they originate? New O-isotopic evidence suggests an intriguing possibility. Carbonaceous, ordinary, and enstatite chondrites differ from one another in their bulk O-isotopic compositions, and these compositions cannot be related to one another by processes that result in simple mass-dependent isotopic fractionation. Multiple isotope reservoirs are required. Chondrules have O-isotopic compositions that reflect those of their host chondrites but, until recently only CAIs from carbonaceous chondrites had been analyzed for O isotopes (mainly because only those from Allende and similar chondrites were large enough to analyze by conventional techniques). Recent advances in ion microprobe techniques allowed *in situ* analyses of individual mineral grains within small (<500 μm) CAIs in thin sections of ordinary chondrites. The data show that these CAIs are similar to CAIs in carbonaceous chondrites in terms of O-isotopic composition [6], even though the chondrules from the two chondrite types lie on different mixing lines. These early results appear inconsistent with nebula-wide production of CAIs, because of the voluminous meteoritic data showing that the asteroid belt (and by implication the nebula) was isotopically quite heterogeneous in terms of O [7]. The data may be more consistent a new model [8] in which all CAIs formed in a restricted and isotopically homogeneous region of the solar nebula, near the infant Sun, then were later distributed more globally via bipolar outflow to the different chondrite accretion regions. Supporting evidence comes from CAIs in enstatite chondrites, whose mineralogy suggests they did not form in the enstatite chondrite formation region of the nebula [9]. One consequence of the local CAI production model is that CAIs and chondrules may have formed in different places by different mechanisms. The model of [8] also proposes local production of ^{26}Al as a way of explaining the ≥5× higher initial ratio of ^{26}Al/^{27}Al in CAIs relative to chondrules. An anomalously ^{26}Al-enriched CAI formation region would mean the CAI/chondrule isotopic difference cannot be interpreted as resulting from a 2–3-m.y. age difference [10]. However, correlations of ^{26}Al with ^{41}Ca [11] in CAI imply ^{26}Al was not locally produced. A chronologic interpretation of the Al-Mg-isotopic data remains plausible if controversial.

References: [1] Anders E. and Grevasse N. (1989) *GCA, 53,* 197–214. [2] Martin P. M. and Mason B. (1974) *Nature, 249,* 333–334. [3] Mason B. and Martin P. M. (1974) *EPSL, 22,* 141–144. [4] Mason B. and Taylor S. R. (1982) *Smithsonian Contrib. Earth Sci., 25,* 30 pp. [5] Grossman L. (1972) *GCA, 36,* 597–619. [6] McKeegan K. D. et al. (1998) *Science, 280,* 414–418. [7] Clayton R. N. (1993) *Ann. Rev. Earth Sci., 21,* 115–149. [8] Shu F. H. et al. (1996) *Science, 271,* 1545–1552. [9] Guan Y. et al. (1999) *LPS XXX.* [10] MacPherson G. J. et al. (1995) *Meteoritics, 30,* 365–386. [11] Sahijpal S. et al. (1998) *Nature, 391,* 559.

CONTAMINATION OF THE BUSHVELD COMPLEX THROUGH PROGRESSIVE PARTIAL MELTING OF CRUSTAL WALL ROCKS.

W. Maier[1], N. Arndt[2], E. Curl[3], and M. Ohnenstetter[4], [1]Department of Geology, University of Pretoria, Pretoria 0002, South Africa, [2]LGCA, Université Joseph Fourrier, 38031 Grenoble Cédex, France, [3]Department of Earth Sciences, Monash University, Clayton, Vic 3168, Australia, [4]Centre National de la Recherche Scientifique-Centre de Recherche Pétrographiques et Géochimiques, B.P. 230, 54501 Vandoeuvre-les-Nancy, France.

The Bushveld Complex is a large layered mafic ultramafic intrusion emplaced 2.06 Ga in the Kaapvaal craton in South Africa. The lower part consists mainly of opx and olivine cumulates (the lower and critical zones); the upper part of plag and pyroxene cumulates (main and upper zones). The Merensky Reef, one of the world's largest deposits of Pt metals, occurs at the top of the critical zone.

Trace-element and isotopic compositions vary widely in the complex. The lower ultramafic parts have highly fractionated trace elements (high Th/La and La/Sm) combined with relatively low initial Sr-isotopic compositions [(^{87}Sr/^{86}Sr)i = 0.7045–0.706] (Fig.1). The parental liquids, whose compositions are estimated from compositions of the cumulates or associated sills, had high trace-element concentrations. The upper gabbroic to anorthositic parts have less fractionated trace elements (lower Th/La and La/Sm) but higher (^{87}Sr/^{86}Sr)i = (0.707–0.709). Inferred parental liquids have lower trace-element contents. Newly obtained Nd-isotopic data are consistent with the published Sr data: the lower zone has ε_{Nd}(T = 2.06) between −5 and −6; the upper critical and main zones have ε_{Nd} between −6.5 and −7.5.

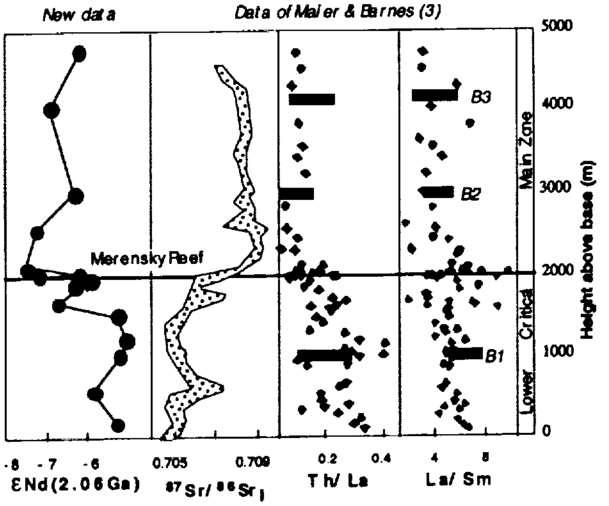

Fig. 1. Isotopic and trace-element variations in the Bushveld Complex. The bars labeled B1 to B3 indicate the compositions of associated sill.

To explain the decoupling between trace elements and isotopes, we call on a model proposed by Sharpe et al. [1] and Hatton [2]. These authors suggested that the contrasting magma types in the complex resulted from assimilation of a crustal component whose composition changed progressively during emplacement of the complex. The contamination took place in a staging chamber below the complex. This chamber was fed by picritic magmas hot enough to partially melt the crustal wall rocks. Early magmas contaminated by low-temperature partial melts migrated into the overlying chamber where they crystallized to form the lower part of the complex. The crustal melt was strongly enriched in incompatible elements such that a relatively small proportion (we calculate ~20%) radically changed the trace-element pattern of the hybrid magma. The effect on the isotopic composition, however, was relatively small. The refractory residue left in the crust after extraction of the low-melting fraction was depleted in incompatible elements, with low Th and LREE and a flatter REE pattern, but high Sr because of abundant residual plagioclase. Continued contamination formed a hybrid magma with the trace-element composition of the upper part of the complex.

The Merensky Reef is enriched not only in siderophile/chalcophile elements such as Pt, Ni, and Cu, but also in incompatible lithophile elements. Its trace-element pattern resembles that of lower-zone cumulates and contrasts with patterns in critical-zone norites. We propose that the reef formed when pockets of siliceous, hydrous, trace-element-rich granite or pegmatite was encountered during assimilation of the refractory margin of the lower magma chamber. The resultant hybrid magma mixed with magma in the main chamber, causing precipitation of the usual mineral assemblage of the reef.

The Bushveld Complex is a medium-sized igneous province (MIP) petrologically and geochemically similar to continental flood basalts. The processes that operated during formation of the complex parallel those that control the compositions of flood basalts.

References: [1] Sharpe M. R. et al. (1986) *Geocongress,* Univ. Witwatersrand, 621–624. [2] Hatton C. J. (1995) *Communs. Geol. Surv. Namibia, 10,* 93–98. [3] Maier W. D. and Barnes S.-J. (1998) *Chem. Geol., 150,* 85–103.

EXPERIMENTAL STUDY OF PYRITE OXIDATION BY DISSOLVED OXYGEN: OXIDATION MODEL BASED ON SURFACE OBSERVATIONS.

M. Manaka[1] and H. Ohmoto[2], [1]Japan Nuclear Cycle Development Institute, Tokai Works, 4-33 Muramatsu, Tokai-mura, Ibaraki-ken, 319-1194, Japan (manaka@tokai.jnc.go.jp), [2]Astrobiology Research Center and Department of Geosciences, Pennsylvania State University, University Park PA 16802, USA (ohmoto@geosc.psu.edu).

In order to understand the detailed mechanisms of oxidation of pyrite by dissolved O (DO) at near neutral pH, three different pyrite grains were reacted with air-saturated distilled water at 65°C for 31 d. The changes in various properties of pyrite surfaces were investigated using reflected-light microscopy, scanning electron microprobe (SEM), energy dispersive X-ray spectroscopy (EDS), X-ray photoelectron spectroscopy (XPS), and auger electron spectroscopy (AES).

Oxidation proceeded from the central to the marginal parts of grain surfaces. The surfaces after oxidation were rough and contained corrosion pits. A variety of S-, Fe-, and O-bearing species was observed on the surfaces. The most abundant S species was iron-monosulfide, while the second most abundant surface species was iron-polysulfide. The presence of thiosulfate and sulfate on the reacted surfaces was not confirmed. Iron-hydroxide and iron-oxide precipitates also formed on the reacted pyrite surfaces. From the changes with time in the properties of various reaction products on the oxidized pyrite surfaces, we propose a three-step reaction mechanism for oxidative dissolution of pyrite. The first step is a decomposition reaction from pyrite to iron-monosulfide and iron-polysulfide caused by DO. The second step is the oxidation of iron-monosulfide and iron-polysulfides by DO to form aqueous Fe^{2+} and SO_4^{2-}. The third step is the oxidation of Fe^{2+} by DO to form $Fe(OH)_3$(am) precipitates.

WHAT DO WE LEARN FROM PEAKS OF URANIUM AND MANGANESE IN DEEP SEA SEDIMENTS?

A. Mangini, Heidelberger Akademie der Wissenschaften, INF 229 D-69120 Heidelberg, Germany (mg@uphys1.uphys.uni-heidelberg.de).

Introduction: Uranium and Mn are two redox-sensitive trace elements with complementary behavior. Under anoxic conditions U is immobile, while reduced Mn is dissolved in porewater of sediments. Uranium thus diffuses from seawater into reducing sediments and is enriched there [1,2]. The depth of the redoxcline and the sediment accumulation rate determine the enrichment of authigenic U. On the contrary, Mn diffuses from the reduced sediment sections and forms peaks of Mn-oxide just above the redoxcline [3]. The depth of the subsurface peak of Mn, corresponds to the last event of shoaling of the redoxcline. Thus, both Mn and authigenic U record the depth of the redoxcline during periods of O limitation in the sediments.

Results: Estimates of the depth of the redoxcline during the last glacial were derived for several cores at localitites in the Atlantic and Southern Oceans. Modeling of the redoxcline as a function of the O content of the water column and of the flux of organic matter to the sediments constrains these values during periods of extreme shallow redoxcline depths.

Burn down of organic matter and deepening of the redoxcline during the Holocene may have altered significantly the glacial organic matter and U signals in the sediments. At present-day conditions, sediments accumulating at rates smaller than 2 cm/ka may have lost these signals [4]. The lack of peaks of U in slowly accumulating sediments cannot be used as an argument against conditions of suboxic diagenesis of Ba [5]. Peaks of Mn are then the only record for a less ventilated sediment column in the past [6].

References: [1] Gariepy C. et al. (1994) *Can. J. Earth Sci., 31,* 28–37. [2] Shaw T. J. et al. (1994) *GCA, 58,* 2985–2995. [3] Froelich P. N. et al. (1979) *GCA, 43,* 1075–1090. [4] Jung M. et al. (1997) *Mar. Geol., 141,* 51–60. [5] McManus J. et al. (1999) *GCA, 62,* 3453–3474. [6] Mangini A. et al. (1990) *Paleoceanography, 5,* 811–821.

ACCESSORY MINERALS AND TRACE-ELEMENT FRACTIONATION IN GRANITES.

J. Mareels, M. Verhaeren, and J. Hertogen, Fysicochemische Geologie, University of Leuven, Celestijnenlaan 200C, B-3001 Leuven, Belgium (joyce.mareels@geo.kuleuven.ac.be; jan.hertogen@geo.kuleuven.ac.be).

The accessory minerals zircon, apatite, sphene, monazite, xenotime, allanite, rutile, etc., are the main host phases (up to 95%) of incompatible trace elements in granitic (s.l.) rocks, in spite of the low combined modal abundance (<1%) [1,2]. There is however much uncertainty about the role that the accessory minerals play in the trace-element fractionation attending differentiation during intrusion and solidification of granitic crystal/melt mushes. In order to control trace-element fractionation, an accessory mineral must be a liquidus phase during the main stages of melt/solid segregation. While this may reasonably hold for zircon and apatite, it is a contentious assumption for even rarer accessory minerals [3].

In situ microanalysis of the trace-element content of accessory minerals in their natural textural environment is able to provide the appropriate data base to assess the control of accessories on trace-element fractionation. Laser ablation inductively coupled plasma mass spectrometry (LA-ICP-MS) holds much promise [4]. The technique has lower spatial resolution than ion microprobe or electron microprobe analysis, but is becoming much more widely available than the former and has superior sensitivity than the latter.

Results are presented of a case study of the Variscan leucogranites of Natzwiller and Kagenfels, Northern Vosges, France. Whole-rock samples have been analyzed for major-element composition and for trace elements (by INAA and XRF). The distribution of accessory minerals is studied by optical and backscattered electron microscopy. Judging from the major-element (Ca, Fe, and Ti) variation the different units of the evolved Kagenfels granite span a substantial range of differentiation. Several textural types ("rhyolitic," granophyric, symplectitic, medium-grained, and porphyritic) are distinguished. The Natzwiller granite is less evolved and shows less variation. There is no indication for the presence of restite material. The accessory minerals of the muscovite-bearing Kagenfels granite are zircon, apatite, monazite, and lesser amounts of rutile, sphene, and ilmenite. The biotite-bearing Natzwiller granite contains zircon, apatite, ilmenite, and allanite; monazite is very rare. In both units, the accessory minerals dominantly occur in polymineralic clusters, although zircon and apatite are occasionally present as isolated grains. Results will be reported of work in progresss using a 266-nm ultraviolet LA-ICP-MS probe, which allows microanalysis of individual grains down to a grain size of 10 μm. Standardization of probe response is still the major analytical difficulty at present. An additional problem is the recasting of results of microanalysis of a closed microsystem into realistic partition coefficient values.

The clustering of accessory minerals could indicate that they precipitated from patches of highly evolved trapped residual liquids, remaining after crystallization of major minerals quartz and feldspars. If that is the case, the role of accessory minerals on the trace-element variation trends of granites becomes ambiguous. Observations made on rock samples might reflect conditions during the final stages of solidification, but may not be entirely relevant to conditions pertaining during the actual differentiation processes.

Nonetheless, the rare earth element (REE) variation with differentiation within the Kagenfels suite, is difficult to explain without invoking the control of a light REE-enriched phase, such as monazite. The prominent decline of light and middle REE with differentiation cannot be attributed to crystallization of only apatite and zircon. One can argue that a prominent role in the trace-element fractionation must be attributed to residual liquids escaped from largely solidified parts of the rising granitic crystal/melt mush.

References: [1] Gromet L. P. and Silver L. T. (1983) *GCA, 47,* 925–939. [2] Wark D. A. and Miller C. F. (1993) *Chem. Geol., 110,* 49–67. [3] Evans O. C. and Hanson G. N. (1993) *Chem. Geol., 110,* 69–93. [4] Jackson S. E. et al. (1992) *Can. Mineral., 30,* 1049–1064.

SILL STACK MUSH COLUMN MAGMATISM.

B. D. Marsh, Morton K. Blaustein Department of Earth and Planetary Sciences, Johns Hopkins University, Baltimore MD 21218, USA (bmarsh@jhu.edu).

A vertically extensive, intricately integrated stack of ephemeral sills forming an interactive magmatic mush column is emerging as a common theme of magmatism. The local scales of the sill reservoirs and the interconnecting necks produce a wide spectrum of crystallization environments. Extensive horizontal and vertical mushy walls provide conditions conducive to specific processes of differentiation from solidification front instability to sidewall porous flow. Coupled with the size and strength of the system, these processes define the fundamental compositional diversity of the mush column. Entrainment, transport, and sorting of cumulate crystals also contributes to compositional diversity and local layered intrusive complexes. The large scale of these systems is well defined by the seismicity of Hawai'i and the detailed dynamics are well exemplified by ophiolites and the Ferrar dolerite system of the Dry Valleys of Antarctica. The Ferrar-DV system contains $\sim 10^4$ km^3 of dolerite distributed throughout a fir-tree like stack of 4 or 5 areally extensive 300–750-m-thick sills. The lowest sill contains a vast tongue of orthopyroxene (opx) cumulates emplaced with the sill itself. The bulk sill composition varies from 20% MgO in the tongue center to 7% in the leading tip and margins of the sill, which itself defines the compositional spectrum of the whole complex and is remarkably similar to that of Hawai'i. Relative sorting of large (1–50 mm) opx and small (1–3 mm) plagioclase due to kinetic sieving in the tongue produces pervasive anorthosite stringers. This has culminated in the formation of a small, well formed layered intrusion (the Dais Intrusion) consisting of alternating layers of orthopyroxenite and anorthosite, complete with apparent ripples, and channel (4 x 20 m) fills. Cryptic layering is also evident, which is also found within the vast opx tongue. The opx composition varies systematically from Fe-rich (En_{45}) at the tongue top to Mg-rich (En_{75}) at the bottom. Upwards in the system the sills become progressively depleted in MgO and temporally and spatially contiguous lavas are 7% MgO tholeiites with no sign of opx cumulates. Entrained cumulates thus become systematically depleted upward in the system. The size, extent, and number of sills suggests emplacement with a time progression similar to that of volcanic episodes and the internal structure of individual sills suggests a rhythm of injection similar to volcanic eruptions themselves. The continued horizontal stretching of a system of this type would lead to processes as recorded by ophiolites. On the other hand, repeated injection into a single reservoir would undoubtedly lead to a massive layered intrusion.

THE POLYCYCLIC AROMATIC HYDROCARBONS AND BIOMARKERS IN CARBONACEOUS MATTER OF KIMBERLITE PIPE "MIR" AND HOSTED SEDIMENTARY ROCKS.

D. Kh. Martikhaeva, E. A. Razvozzhaeva, A. G. Polozov, and A. E. Vorontsov, Institute of Geochemistry, Siberian Branch of Russian Academy of Sciences, P.O. Box 4019, Irkutsk 664033, Russia (poloz@igc.irk.ru).

Introduction: The study of molecules — markers (PAHs and biomarkers) of carbonaceous matter (CM) of rocks — allows the recognition of its sources and revealing a degree of transformation.

The carbonaceous matters from open pit mine of diamond bearing pipe "Mir" and hosted, brecciated and hydrothermally altered sedimentary rocks (dolostone) of the Siberian platform was examined. Using the modern methods of organic geochemistry, CM was extracted by chloroform at room temperature, and divided into a fraction with using HPLC method. The structure of molecules of markers identified by gas chromatography with mass spectrometry (GC-MS).

Results and Discussions: The CM from "Mir" pipe is poor in terms of heteroatoms. The basic reductants are hydrocarbons, ethanol-benzol gum and asphaltene. In CM from hosted, brecciated and hydrothermally altered rocks, the share of asphaltogene acids is decreases and the contents of hydrocarbons increase.

On the infrared spectrum of CM from the "Mir" pipe absorption bands of aromatic patterns (1610 ± 30 cm^{-1}), methyl and methylene patterns of paraffines (1310, 1380, and 1460 cm^{-1}), naphthene (970, 2920, and 2970 cm^{-1}), and also oxychemicals such as aromatic acids, aethers and ketones (1720 cm^{-1}) are clearly expressed. The infrared spectra of bitumen from the host rocks testify a presence of S containing groups (1000–1140 cm^{-1}), oxygenated functional groups (1700 cm^{-1}), aliphatic unsaturated groups (1600 cm^{-1} and 1640 cm^{-1}) and aromatic patterns (1615–1690 cm^{-1}).

The carbonaceous matter from the "Mir" pipe refers to a biogenic matter by isotope data, and the distribution of $\delta^{13}C$ isotopes in fractions corresponds to a isotope-fractional curve, characteristic of a humus type matter. As a result of weak thermal effect on sedimentary rocks a heavy isotope ^{13}C (up to 4.4‰ concerning other fractions) enriched a benzene fraction.

TABLE 1. Identification of hydrocarbons (HCs) from hexane fraction of bitumen from "Mir" pipe.

Peaks No.	Percent of HCs total	M.W.	Composition	Compound
8	5.9	384	$C_{28}C_{48}$	C_{28} – triterpane
9	36.1	202	$C_{16}C_{10}$	Pyrene
11	40.0	228	$C_{18}C_{12}$	Chrysene
12	6.2	370	$C_{27}C_{46}$	C_{27} – triterpane
14	0.4	470	$C_{34}C_{60}$	C_{34} – hopane

TABLE 2. Identification of hydrocarbons (HCs) from hexane fraction of bitumen from hosted rocks.

Peaks No.	Percent of HCs total	M.W.	Composition	Compound
Sample I, well 90, depth 289 m				
12	10.9	254	$C_{18}H_{38}$	n-alkane
16	5.2	302	$C_{24}H_{26}$	Benzpyrene
18	6.1	276	$C_{22}H_{12}$	Anthanthrene
19	9.7	300	$C_{24}H_{12}$	Coronene
26	0.5	370	$C_{27}H_{46}$	C_{27} – hopane
30	0.7	486	$C_{35}H_{66}$	C_{35} – hopane
Sample 2, well 90, depth 847 m				
5	0.9	296	$C_{21}H_{44}$	n-alkane
7	17.3	252	$C_{20}H_{12}$	Perylene
8	19.8	276	$C_{22}H_{12}$	Anthanthrene
9	19.4	300	$C_{24}H_{12}$	Coronene
10	18.9	426	$C_{31}H_{54}$	Homohopane
11	17.8	370	$C_{27}H_{46}$	C_{27} – triterpane
12	0.9	412	$C_{30}H_{52}$	C_{30} – hopane

The results obtained by us on study of CM from hosted rocks coincide with those published earlier.

The PAHs chrysene and pyrene were identified on mass fragmentogram of sample (Table 1). They are peculiar to associations, which generate in reduction conditions at high concentration of carbonaceous compounds. Detected hopanes C_{27}, C_{28}, and C_{34} confirm availability of the contribution of CM of procariot-bacterias and single-celled algaes in total mass.

PAHs of the CM from the hosted sedimentary rocks are presented (Table 2) by coronene, benzpyrene, perylene, and anthanthrene, which is interpreted as the presence of hydrothermal and petroleum associations of PAH. The presence of alkanes C_{18}, C_{19}, C_{20}, and C_{23} in sample 1 is generically related, probably, to marine algae, and the alkane C_{33} is the sign of contribution of land plants. The naphthenic HCs are significant and result from microbiological transformation of CM. The detecting instrument of microbe activity of disintegrating of vegetation remnants are hopanoids C_{27}, C_{29}, C_{31}, C_{33}, and C_{35}. PAH and hopanoids are detected in sample 2 while alkanes and naphthene are not available. The CM of this sample is identical to the same ones from open pit mine of "Mir" pipe by chromatogram patterns and quantitative characteristics of hydrocarbons.

PALEOGEOGRAPHIC RECONSTRUCTION OF A PALEOCENE CARBONIFEROUS BASIN (LOS CUERVOS FORMATION, TÁCHIRA STATE, VENEZUELA) BY USING TRACE-ELEMENT CONTENT AND GEOSTATISTICAL ANALYSIS OF COALS.

M. Martínez, M. Escobar, and C. López, Centro de Geoquimica, Instituto de Ciências de la Tierra, Facultad de Ciências, Universidad Central de Venezuela, Caracas 1010 A, Venezuela.

The carboniferous basin of the Táchira State, at the Venezuelan Andes, contains coalfields with different levels of maturity, belonging to two stratigraphic units: Los Cuervos formation and Carbonera formation, from Paleocene and Late Eocene respectively.

Four litostratigraphic columns from the Los Cuervos formation, in different localities of the basin were described and sampled. Collected coals were analyzed for 30 minor and trace elements (Mo, Cu, Pb, Zn, B, Ti, Al, P, Ni, V, La, Na, K, Ca, Sr, Mg, Bi, Au, W, S, As, Sb, Cr, Mn, Fe, Co, Th, U, Ag, and Cd) as well as moisture, volatile matter, fixed C, ash content, and vitrinite reflectance. The purpose of this work is to characterize the coals, and to obtain an integrated geochemical model of the studied unit in the basin.

Four statistical associations were found by using factor analysis on the matrix data. These factors (Ag-Cd-Mo, La-V-Th, Fe-S-As, and Ca-Mg-Sr) reflect four geochemical sources in the basin. Analyzing their variation and distribution, it was possible to establish the source rock, trace-element anomalies, input vectors, and variations in the sedimentary dynamics of the basin during the accumulation time.

The obtained results allowed establishing the areas of the basin with the higher marine influence, as well as vertical changes in the sedimentary unit provided by marine incursions. The results show at least three sources of clastic sediments (granitic, volcano-clastics, and calcareous). It was also determined the approximate direction of each sedimentary source, the subsidence history, and posterior lifting of the basin.

IDENTIFICATION OF MICROBIAL METHANE DEPOSITS VIA CORE ANALYSIS.

A. M. Martini[1], L. M. Walter[2], J. C. McIntosh[2], and J. M. Budai[2], [1]Department of Geology, Amherst College, P.O. Box 5000, Amherst MA 01002, USA (ammartini@amherst.edu), [2]Department of Geological Sciences, University of Michigan, Ann Arbor MI 48109, USA.

Introduction: Organic-rich shales and coal beds are increasingly being developed as a source for natural gas. In many of these deposits, a significant proportion of the methane is microbially generated and, subsequently, possesses a distinct compositional and isotopic signature [1]. Natural gas (methane, ethane, propane, and higher chain hydrocarbons) is stored in these reservoirs by adsorption onto the organic matter within the matrix of the rocks. Compositional and isotopic values of gas generated from crushed core samples permit determination of the origin of the gas.

New Albany Shale, Illinois Basin: The New Albany shale, a Devonian-aged black shale located in the Illinois basin, has recently undergone exploration as a potential source for natural gas. Coupled water and gas analyses from New Albany shale producing wells have allowed a delineation of thermogenic and bacterial gas zones based primarily on (1) concentration and $\delta^{13}C$ values for DIC in the reservoir, (2) δD values for methane and water coproduced from the reservoir, and (3) concentrations of the various gas fractions [1].

Core samples from zones of thermogenic and mixed microbial/thermogenic gas production were analyzed via gas chromatography combustion mass spectrometry (GC/C/MS) to verify the association between produced gas and water and gas stored within the rock.

Relative concentrations of hydrocarbons and CO_2 for both zones are indicative of the genesis of the gas. In Fig. 1a, high (20%) concentrations by volume of ethane and propane, absent CO_2, and mole volume percent of all species that are invariant with respect to depth (Fig. 1a) suggests a thermogenic origin for this gas. In contrast, the core data from a zone of mixed microbial/thermogenic gas has significant concentrations (up to 10% by volume) of CO_2, a byproduct of bacterial methanogenesis. In addition, the relative concentrations of gaseous components are variable with methane and CO_2 increasing near the top of the reservoir while the mole volume percent of higher chain hydrocarbons are reduced, most likely by microbial oxidation.

The variations in $\delta^{13}C_{C_2}$ vs. ethane concentration (Fig. 2a, open triangles) strongly indicate that microbial oxidation is occurring in the core representing a "mixed" gas origin. This process accounts for both the decrease in the amount of ethane and the isotopic shift as microbes metabolize ethane with low $\delta^{13}C$ values first. Ethane concentrations from the thermogenic zone (solid triangles) are invariant with values typical of immature thermogenic natural gases. The presence of microbial gas in the mixed zone core is clearly demonstrated by the plot of $\delta^{13}C_{CO_2}$ vs. total gas content (Fig. 2b). High $\delta^{13}C_{CO_2}$ values, linked to microbial methanogenesis [1], and increases in the amount of gas stored may be related, suggesting that the addition of microbial gas to this reservoir is of economic significance.

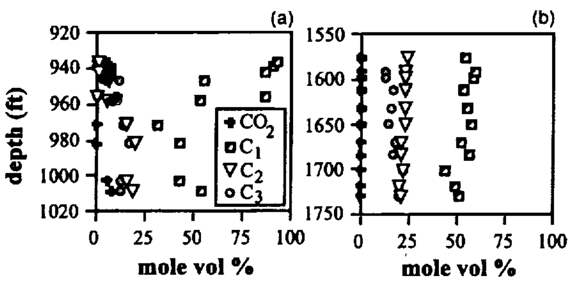

Fig. 1. (a) Methane, ethane, propane, and CO_2 gas compositions from two cores, one located in a known thermogenic zone, and (b) one from a mixed microbial/thermogenic source.

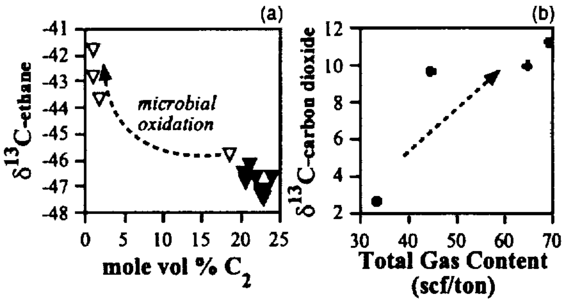

Fig. 2. (a) Carbon-isotopic values vs. ethane concentrations from a thermogenic zone (solid triangles) and a microbial/thermogenic zone (open triangles). (b) Carbon-isotopic values for CO_2 vs. total gas content in the mixed microbial/thermogenic zone.

Implications: Preliminary results suggest that microbial processes, both methane generation and hydrocarbon oxidation, can be identified using core analysis. It may be possible to "prospect" for these microbial gas deposits using previously collected core material due to the slow desorption rates for certain gaseous components.

References: [1] Martini A. M. et al. (1998) *GCA, 62,* 1699–1720.

GOLDSCHMIDT'S LEGACY: BRIAN MASON'S CONTRIBUTIONS TO GEOCHEMISTRY AND METEORITICS.

U. B. Marvin, Harvard-Smithsonian Center for Astrophysics, 60 Garden Street, Cambridge MA 02138, USA (marvin@cfa.harvard.edu).

Introduction: On March 17, 1937, V. M. Goldschmidt presented a lecture to the Chemical Society of London entitled, *The Principles of Distribution of the Chemical Elements in Minerals and Rocks.* Subsequently, the Society's journal carried a copy of his talk to far-off New Zealand where it caught the eye of B. Mason, a fourth-year student at Canterbury College in Christchurch. For Mason, Goldschmidt's demonstration that analyses of meteorites are the key to the absolute abundances of the elements opened up an exciting new field that never had been mentioned in any of his courses in chemistry or geology. Two years later, when he received a Graduate Fellowship for study abroad, Mason wrote to Goldschmidt asking if he might come to his institute in Oslo. Goldschmidt replied that he never had had a student from the Antipodes and Mason would be very welcome.

Interrupted Research in Oslo: Mason arrived in Oslo in January, 1940, four months after World War II was declared. At Goldschmidt's suggestion, Mason began research on the geochemistry of Te, but, on April 9, 1940, the Germans invaded Norway and Mason rode out of Oslo two hours ahead of Hitler's troops. In Stockholm, Mason enrolled in the university and took up research on mineralogy. In December, 1942, Goldschmidt, who had been interned in a concentration camp in Norway, suddenly appeared in Stockholm, where he had been spirited by the Norwegian underground. Soon afterward, the British flew Goldschmidt to England. Mason received his doctorate in May 1943, and left Stockholm for England where he spent several months X-raying minerals, by the hour, at the British Museum. He managed to meet with Goldschmidt only once. After the war, Goldschmidt returned to Oslo hoping to resume his research, but his health was failing and he died on March 20, 1947. Their association had been brief, but Goldschmidt's insights had been decisive in shaping Mason's interest in geochemistry.

Mason's Career Moves and *Geochemistry*: In 1944, Mason returned to New Zealand, where he taught mineralogy and geochemistry until 1947 and then moved to Indiana University. While there, he served as thesis advisor to S. R. Taylor, a former student from Christchurch. Mason's book, *Principles of Geochemistry,* appeared in 1952. As the first textbook of geochemistry in English, it opened this new interdisciplinary science to legions of students in geology, chemistry, and contingent fields. In 1953, Mason accepted a curatorial position at the American Museum of Natural History in New York, with an adjunct professorship at Columbia University. His lectures were attended by E. Anders in 1953 and B. P. Glass in 1960, each of whom would pioneer new lines of research. At the museum, Mason reorganized the meteorite collection and collaborated with the Finnish chemist, B. Wiik, on a new classification of carbonaceous chondrites. He also mastered the technique of rapidly classifying ordinary chondrites by the γ-indices of refraction of their olivines — a skill that proved invaluable in later years when he assumed responsibility for classifying the large influx of meteorites collected by U.S. teams in Antarctica.

The Space Age and *Meteorites*: After the orbiting of Sputnik IV in 1957, Mason redoubled his research on meteorites and supplied critically important samples to an ever increasing number of scientists. In 1961, he presented a seminar on meteorites at the University of Tokyo and expanded his lectures into his book, *Meteorites*, which appeared in 1962. Once again, Mason authored the first textbook in English on a subject of key importance. In 1965, Mason made his final career move to the Smithsonian Institution, where he conducted research on meteorites and lunar samples. Brian Mason contributed significantly to the opening of a new era in geochemistry, cosmochemistry, and the planetary sciences.

BLACK CARBON (CARBON-14) IN THE SANTA MONICA BASIN: RIVERINE DELIVERY AND SEDIMENTARY ACCUMULATION.

C. A. Masiello, E. R. M. Druffel, and S. Griffin, Mail Code 3100, Department of Earth System Science, University of California, Irvine CA 92697-3100, USA (masiello@essgrad.ps.uci.edu; edruffel@uci.edu).

Although numerous studies have shown black carbon to be a significant component of deep-ocean sedimentary organic carbon [1–3], very little data is available on black carbon budgets for coastal margins. This is a significant data gap, because coastal margins and river deltas account for more than 95% of Holocene organic carbon accumulation [4]. Additionally, mass-balance studies [5] and measurements of the age of black carbon in deep-ocean sediments [2] suggest that rivers may be a significant source for the ocean's sedimentary black carbon pool.

We present mass and radiocarbon results for a coastal sediment core taken in the Santa Monica Basin. The Santa Monica Basin is located off the coast of Southern California and has been anoxic and laminated since approximately 1600 A.D. The sedimentation rate at this site is high enough that we can observe (1) the overall enrichment in surface organic C ^{14}C due to the testing of thermonuclear weapons in the 1960s, and (2) the decrease in the ^{14}C of sedimentary black carbon due to either human combustion of fossil fuels or human increases in the California soil erosion rate. We also document changes in black carbon concentration and radiocarbon age through the oxic/anoxic boundary at this site, providing a glimpse of the effects of O exposure on black carbon sedimentary preservation.

In addition to measurements of black carbon in the Santa Monica Basin, we also present black carbon mass flux and radiocarbon measurements made during the winter of 1997–1998 in the Santa Clara River, the main source of terrestrial C to California Borderland sediments. The radiocarbon age of black carbon in the Santa Clara River is highly variable (–570 ± 180‰) and strongly correlated with the bulk organic C age, suggesting that the black carbon age is not due to inclusion of fossil fuel C. In this presentation we will compare the mass and isotopic signatures of black carbon river sources and sedimentary sinks, with the goal of understanding more about black carbon transport and storage processes.

References: [1] Smith D. M. et al. (1973) *Nature, 241,* 268–271. [2] Verardo D. J. and Ruddiman W. F. (1996) *Geology, 24,* 855–857. [3] Masiello C. A. and Druffel E. R. M. (1998) *Science, 208,* 1911–1913. [4] Hedges J. I. and Keil R. G. (1995) *Mar. Chem., 49,* 81–115. [5] Suman D. O. (1983) Ph.D. thesis, Univ. California, San Diego.

A NEW METHOD FOR *IN SITU* HIGH-PRECISION SULFUR-ISOTOPIC RATIO MEASUREMENTS BY LASER ABLATION MULTIPLE COLLECTOR INDUCTIVELY COUPLED PLASMA MASS SPECTROMETRY.

P. R. D. Mason[1], C-J. de Hoog[1], and S. Meffan-Main[2], [1]Faculty of Earth Sciences, University of Utrecht, Budapestlaan 4, 3584 CD Utrecht, The Netherlands (mason@geo.uu.nl), [2]Micromass UK Limited, Floats Road, Wythenshawe, Manchester M23 9LZ, U.K.

Introduction: A new method utilizing Xe gas in a hexapole reaction cell and Cl isotopes for internal mass bias correction enables the accurate and precise measurement of S isotopes by multiple collector inductively coupled plasma mass spectrometry (MC-ICP-MS). The technique, when coupled to a laser ablation sample introduction system, allows isotopic ratios to be measured directly within solid samples on a scale down to 100 μm. Preliminary data obtained by the new technique can reproduce the levels of accuracy and precision possible by other techniques [1–3].

Experimental: Pressed powder pellets and sulfide minerals were ablated to varying degrees of spatial resolution using a commercially available 266-nm ultraviolet laser ablation system. A solution of 20% HCl was nebulized at low flow rates (100 μL min^{-1}) and mixed with the ablated vapor. A hexapole ion-focussing device containing a mixture of He and Xe was used to focus S$^+$ and remove O$_2$$^+$ ions [4]. The interfering O$_2$$^+$ background at ^{32}S was eliminated or reduced to insignificant levels. The combined signal from simultaneous laser ablation and solution nebulization was measured statically using the MC-ICP-MS.

Results and Discussion: Internal precision when ablating sulfides, sulfates, native S, and pressed powder pellets was often excellent, approaching levels not easily achievable by other *in situ* analytical techniques (≤0.1‰ s.e.). In contrast a major problem during analysis was poor external precision due to mass-dependent instrumental drift (Fig. 1a). To account for medium term response fluctuations in the S-isotopic ratios the ^{37}Cl/^{35}Cl ratio was measured simultaneously during each run. The internal variation for Cl isotopes was insignificant compared to the intrasample/standard S variation and any Cl component in the samples was negligible compared to the Cl introduced by the solution nebulization system. Significant improvement in ^{34}S/^{32}S external reproducibility was seen after Cl-normalization (Fig. 1b). Improvements

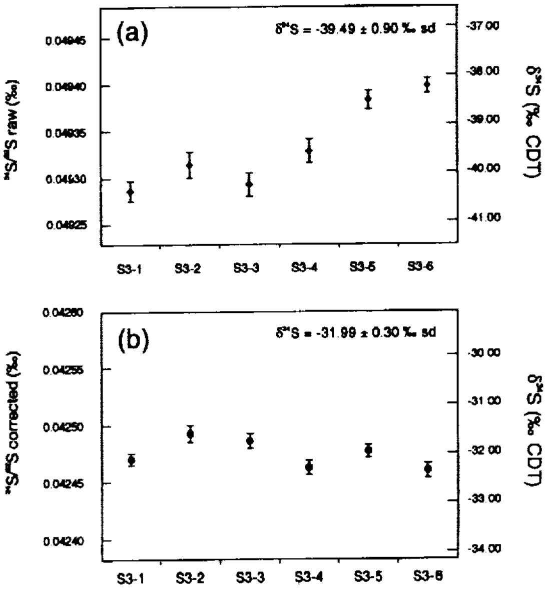

Fig. 1. Sulfur-34/sulfur-32 and δ^{34}S values of six repeats on IAEA-S3 standard (FeS$_2$; cert. –32.1‰). **(a)** Uncorrected values; **(b)** Cl-corrected values. δ^{34}S is corrected for mass bias relative to IAEA-S1 standard (FeS$_2$; –0.3‰). Internal precision is reported as 2 s.e.

in internal precision were also observed. The majority of the instrumental mass bias was corrected using the Cl normalization so that the Cl-corrected ^{32}S/^{34}S ratio approached the value expected assuming zero instrumental mass bias.

δ^{34}S accuracy when calibrating sulfide standards against one another was good (±1‰). However matrix effects, probably linked to space charge effects in the ion beam extracted from the plasma, were observed between sulfides, elemental S and sulfate. Five pyrite samples [independently analyzed by gas source mass spectrometry (GSMS)] were ablated and when calibrated against one another showed good accuracy and reproducibility.

MC-ICP-MS offers an alternative technique for the investigation of S-isotopic ratios. With further optimization of the technique it may be possible to extrapolate the performance of the system to smaller ablated spot sizes and down to percent levels of S that takes it beyond the capabilities of current techniques. Chlorine internal standardization proved to be very effective and similar procedures may be beneficial for the investigation of other light isotopic systems by ICP-MS.

References: [1] Kelley S. P. and Fallick A. E. (1990) *GCA, 54,* 883–888. [2] Crowe D. E. et al. (1990) *GCA, 54,* 2075–2092. [3] Kakegawa et al. (1998) *GCA, 62,* 3205–3220. [4] Mason P. R. D. et al. (1999) *J. Atom. Anal. Spectrom.*, in press.

THE ‘LOMAGUNDI’ CARBON-ISOTOPIC ANOMALY REVISITED: EXTREMELY HIGH δ^{13}C EXCURSION IN CONTINENTAL AND MARINE CARBONATE ROCKS OF THE CIRCA 2.1-Ga MAGONDI SUPERGROUP, ZIMBABWE.

S. Master[1], B. Th. Verhagen[2], and J. D. Kramers[3], [1]Department of Geology, University of the Witwatersrand, Private Bag 3, Wits 2050, Johannesburg, South Africa (065sha@cosmos.wits.ac.za). [2]Schonland Research Centre for Nuclear Sciences, University of the Witwatersrand, Private Bag 3, Wits 2050, Johannesburg, South Africa, [3]Isotope Geology Group, Mineralogy and Petrology Institute, University of Bern, Erlachstrasse 9a, 3012, Bern, Switzerland.

Introduction: The Paleoproterozoic Lomagundi dolomite in the Magondi supergroup of Zimbabwe is well known as the first rock sequence in which the ~2-Ga positive δ^{13}C excursion in marine carbonates was identified [1]. Schidlowski et al. [1] reported an average δ^{13}C value of the Lomagundi dolomite of 8.2‰ PDB, n = 67, but this was based on analyses of samples collected over a wide area with no stratigraphic control. In 1993, a 20-km-diameter meteorite impact structure was found in the Magondi belt [2], over an area that was sampled by Schidlowski [1] for C isotopes. The carbonate rocks within the impact structure have been highly deformed and shock metamorphosed, and many rocks there previously mapped as Lomagundi group have been reassigned to the underlying Deweras group [2]. Some of Schidlowski's samples [1] were from the contact zones of mafic dykes, or from areas of amphibolite-grade regional metamorphism. We report here the results of the first detailed stratigraphically controlled C- and O-isotopic profile through the lower dolomite of the Mcheka formation, Lomagundi group, in an area of low metamorphism (greenschist facies) well away from the impact structure. We also report on C and O isotopes in evaporitic lacustrine carbonates from the continental Deweras group that underlies the Lomagundi group.

Lomagundi Group: The Lomagundi group has a minimum age of 1.97 ± 0.07 Ga, based on K-Ar dating of phyllites. Its depositional age is ~2.1 Ga, based on model Pb ages of galena from the facies-equivalent Piriwiri group. In the Lomagundi group section sampled, the lower dolomite is 5.5 m thick, and consists of fine-grained massive white dolomite, with a few thin interbeds of pink dolomite and dolomitic shale. There are four beds, between 10 and 30 cm thick, in which there are centimeter-sized oval nodules of sparry calcite. The results of very tight sampling at an average spacing of 20 cm (n = 30), show that although most of the samples are extremely enriched in ^{13}C, and have high positive δ^{13}C values, there is a marked control on C- and O-isotopic values by sedimentary facies. The gray shale and pink dolomite interbeds have δ^{13}C values lighter by up to 2–3‰ compared to the massive fine-grained white dolomites, which show little variation from a mean δ^{13}C value of around 10.8‰. The sparry calcite nodules have similar δ^{13}C values to the host dolomite, to within 0.5‰, but with one value going down to 3.4‰ in a sample showing a fan structure. Such negative shifts in δ^{13}C have been reported from carbonates replacing sulfate evaporites, and it is possible that some of the carbonate "fans" may be of similar origin. The O isotopes are also fairly constant, but with variations in δ^{18}O up to 1‰ from a mean value around –8‰ PDB, and show an antipathetic trend to the variations in C isotopes. The δ^{18}O values of the calcite nodules are 1.5–2.5‰ lighter than the host dolomite, possibly reflecting meteoric water influx during diagenesis. Strontium-isotopic data on Lomagundi dolomites indicate values of ^{87}Sr/^{86}Sr (calculated for 2.06 Ga) ranging from 0.703 to 0.708 [4].

Deweras Group: The Deweras group, which unconformably underlies the Lomagundi group, consists of continental red beds comprising arkoses, conglomerates, siltstones and anhydrite-bearing evaporitic dolostones, and subalkaline basalts and pyroclastics that have been metamorphosed to greenschist facies. The rocks were deposited in continental rift-related alluvial fan, eolian dune, playa flat, and playa lake environments [3]. Age constraints on the Deweras group are as follows: mafic lavas dated at 2060 ± 100 Ma (W.R. Rb-Sr); Pb model age of ~2.1 Ga on galena from metamorphic veins [3], and a ^{207}Pb/^{206}Pb age on dolomites and anhydrites of ~2 Ga [4]. Carbon-isotopic data on the Deweras group playa flat carbonates show that they are also extremely enriched in ^{13}C [5]. Their δ^{13}C values range from 5.74‰ to 16.19‰ PDB, with an average of 11.15‰ PDB (n = 23). The δ^{18}O of these carbonates range from –13.35‰ to –20.01‰ PDB, with an average δ^{18}O of –16.59‰ PDB (n = 23). The presence of the "Lomagundi" C-isotopic anomaly in continental carbonates of the Deweras group indicates that the anomaly is due to a global perturbation in the entire C cycle, involving the ocean-atmosphere-continent systems, and is not just the result of special restricted environments in the marine sequences that have been studied up to now.

References: [1] Schidlowski M. et al. (1976) *GCA, 40,* 449–455. [2] Master S. et al. (1995) *LPS XXVI,* 903–904. [3] Master S. (1991) Ph.D. thesis, Univ. Witwatersrand. [4] J. D. K., unpublished data. [5] Master S. et al. (1990) *Geocongress '90, 23rd Earth Sci. Congr. Geol. Soc. S. Afr.*, Cape Town, 346–348.

COMPARISON OF DEPTH PROFILES FOR LIGHT RARE-EARTH-ELEMENT TETRAD EFFECT IN REPRESENTATIVE OCEANS.

A. Masuda[1] and J. Shimoda[2], Department of Chemistry, University of Tokyo, Hongo, Tokyo 113-0033, Japan (masfield@green.ocn.ne.jp), [2]Department of Chemistry, University of Electro-Communications, Chofu, Tokyo, Japan.

Introduction: Quantification of tetrad effect is of essential significance. For this purpose, four parabolic curves are drawn, each spanning the "tetrad" [1]. The degree of the LREE tetrad effect is defined as AEL (or ABEXEL) value [2]. Its utility has been proved [3] for the water column of the Cariaco Trench [4]. Evaluation of AEL has been made based on the data published in papers [5–9,11].

Characteristics for Representative Oceans: The depth profiles for LREE tetrad effect in the Pacific, Indian, and Atlantic Oceans are shown in Figs. 1 and 2. It is seen that the depth profile for west north Pacific are flat (not strictly vertical). In particular, the profile for 271-1 [5] is very flat except the upper layer. The profiles for west Indian Ocean [6] near Madagascar are also flat, but show somewhat larger range of variation than the Pacific Ocean.

Unlike the Pacific and Indian Oceans, the Atlantic Ocean seawaters show the notably large range of variation of AEL value, with areal characteristics. At station 10404 located at the outlet of Mediterranean outflow [7], the absolute value of AEL decreases smoothly from the top toward a discontinuity at 700 m, which may be related with salt fingering. Depth profile at Sargasso Sea [8] exhibits the largest range of variation of AEL. A dip of AEL value to –0.263 around 700 m and a sudden rise to –0.034 ~ –0.006 are interpreted to reflect an especially developed pycnocline and the related peculiarity in stratification and in distributional state of specified lanthanides. Depth profile at GEOSECS 115 [9] is considered to represent that for the rather "ordinary" site in Atlantic Ocean. Even this profile exhibits much larger extent of AEL variation than those for Indian and Pacific Oceans. The depth for maximum absolute value of negative AEL is located around 2140 m. The depth profile for Indian Ocean at site 1502 [6] has "miniaturized" features qualitatively similar to GEOSECS 115. Depth profile [10] for the Southern

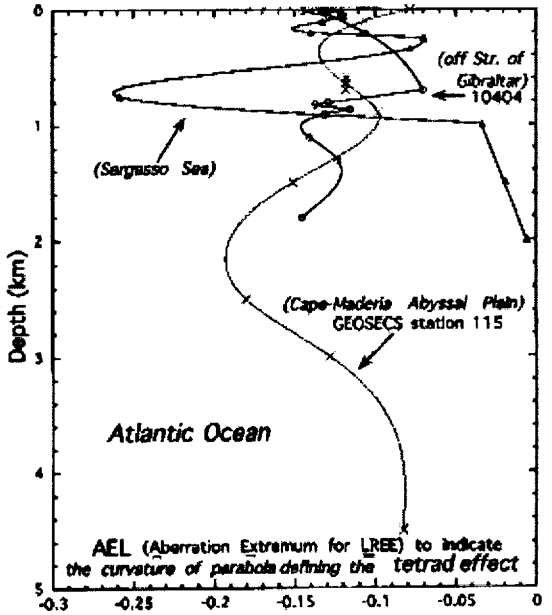

Fig. 1. Depth profile of LREE tetrad effect in Pacific and Indian Oceans.

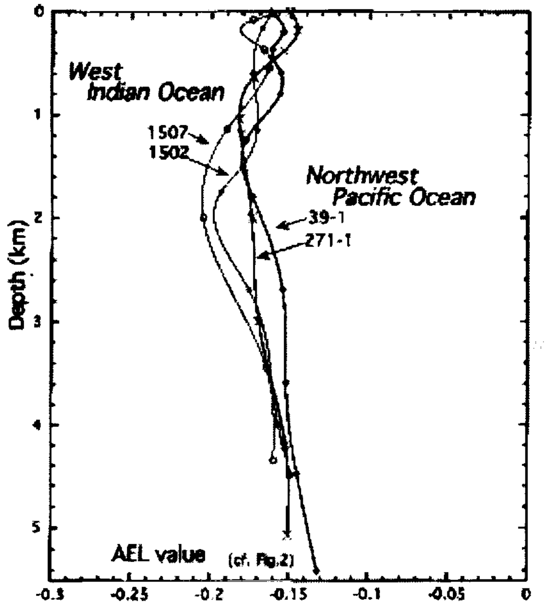

Fig. 2. Depth profiles of LREE tetrad effect in the Atlantic Ocean.

Ocean [11] shows unique features different from those for any of other oceans displayed in Figs. 1 and 2.

References: [1] Masuda A. et al. (1994) *Proc. Japan Acad., 70B,* 169–174. [2] Masuda A. and Shimoda J. (1996) *Proc. Japan Acad., 72B,* 202–207. [3] Masuda A. et al. (1998) *Geochem. J., 32,* 275–280. [4] De Baar H. J. W. et al. (1988) *GCA, 52,* 1203–1219. [5] Piepgras D. J. and Jacobsen S. B. (1992) *GCA, 56,* 1851–1862. [6] Bertram C. J. and Elderfield H. (1993) *GCA, 57,* 1957–1986. [7] Greaves M. J. et al. (1991) *EPSL, 103,* 169–181. [8] Sholkovitz E. R. et al. (1994) *GCA, 58,* 1567–1579. [9] Elderfield H. and Greaves M. J. (1982) *Nature, 296,* 214–219. [10] Masuda A. and Shimoda J. (1997) *Proc. Japan Acad., 73B,* 195–200. [11] German C. R. et al. (1995) *GCA, 59,* 1551–1558.

RHENIUM-OSMIUM EVIDENCE FOR CRUSTAL INFLUENCES ON PORPHYRY COPPER SULFIDES AND DURATION OF MINERALIZATION.

R. Mathur[1], J. Ruiz[1], and F. Munizaga[2], [1]Department of Geosciences, University of Arizona, Tucson AZ 85721, USA, [2] Departamento de Geología, Universidad de Chile, Casilla 13518 Correo 21, Santiago, Chile.

Two outstanding questions in studies of metallogenesis are the source of the ore-forming metals and the duration of mineralization. Rhenium-osmium isotopes can constrain the answers to these questions because these elements are chalcophile and found in the sulfides. Thus it is possible to get information directly from the sulfides rather than solely from associated alteration silicates. We report new Re-Os-isotopic data from pyrites, chalcopyrites from six porphyry copper deposits (five from the Andean Cordillera and one from the South Pacific).

Sulfides from the deposits have Re concentrations ranging from 0.8 to 300 ppb. Osmium concentrations range from 0.004 to 0.2 ppb. Initial $^{187}Os/^{188}Os$ ratios for the sulfides range from 0.25 to 9. There is no difference seen between porphyry deposits occurring in a continental arc, such as the Andes or a less mature arc such as Panguna in the South Pacific. The calculated initial isotopic ratios for the sulfides contain too much radiogenic Os to be derived solely from the mantle that should have an $^{187}Os/^{188}Os$ ratio close to 0.13. There are several possible sources for the radiogenic Os. These include the subducted slab, metalliferous or organic-rich subducted sediments, or lower continental crust. Trace-element, Pb, and Nd isotopes, suggest that subducted sediments could be the source for some of the Os, but the lower crust is a more likely source for the radiogenic Os because of the relatively low concentrations of Os.

The Os-isotopic data yield sulfide isochrons with ages that agree with U-Pb ages on zircons from the productive intrusions. The sulfide ages, however, can be much older than $^{40}Ar/^{39}Ar$ ages obtained from potassic and quartz-sericitic alteration thought to be associated with the mineralization. The Re-Os data indicate that the large base metal porphyry deposits are probably the result of a complex series of magmatic-hydrothermal events that occurred over a period of ~4 Ma. Thermal modeling shows that the mineralizing events cannot be the result of a single cooling intrusive and points to a complex magmatic history that must include multiple intrusions and cooling episodes.

HAFNIUM-ISOTOPIC CONSTRAINTS ON THE SOURCE OF KERGUELEN ARCHIPELAGO LAVAS.

N. Mattielli[1], J. Blichert-Toft[2], D. Weis[1], D. Damasceno[1], J. S. Scoates[1], F. A. Frey[3], F. Albarède[2], and A. Giret[4], [1]Département des Sciences de la Terre et de l'Environnement, Université Libre de Bruxelles, CP 160/02, ULB, B-1050 Brussels, Belgium (nmattiel@ulb.ac.be), [2]Ecole Normale Supérieure de Lyon, 69364 Lyon Cedex 7, France, [3]Department of Earth, Atmospheric, and Planetary Sciences, Massachusetts Institute of Technology, Cambridge MA 02139, USA, [4]Université Jean Monnet, 42023 St. Etienne Cedex 2, France.

One of the strongest constraints on Earth differentiation is provided by the combined variations in Hf- and Nd-isotopic compositions. As one end member of the OIB array, the Kerguelen basalts are key oceanic lavas for delimiting the total range of Nd-Hf-isotopic correlation in OIB. We report an extensive new data set of Hf-isotopic compositions for Kerguelen Archipelago lavas. Our primary goals are to determine the Hf-Nd-isotopic variability and to better characterize the source-components of the Kerguelen lavas. We selected over 30 samples, mostly from basaltic stratigraphic sections that span the complete range of chemical compositions (transitional to highly alkaline), Sr-Nd-Pb-isotopic compositions [1], and ages (0.1–29 Ma [2]) of the archipelago lavas.

Hafnium-isotopic analyses were carried out by plasma-source mass spectrometry (Plasma 54). The age corrections for Hf-isotopic ratios are small, a maximum of 10 ppm for the oldest lavas (29 Ma). The slightly less radiogenic age-corrected $^{176}Hf/^{177}Hf$ do not modify the overall isotopic data distribution or the interpretation of the results.

Hafnium-isotopic compositions for the Kerguelen lavas show a large range of values, covering 13 $\varepsilon_{Hf(T)}$ units. Variations in $^{176}Hf/^{177}Hf$ (0.28307–0.28283) and $^{143}Nd/^{144}Nd$ (0.51288–0.51258) show an extremely good positive correlation ($\varepsilon_{Hf} \sim 1.6 * \varepsilon_{Nd} + 2.8$). The large spread of the Hf-Nd-isotopic field for the Kerguelen lavas defines the low Hf-Nd end of the OIB array and largely determines the shape of the EMI-EMII endmember field.

The dominant isotopic signature defined by more than 100 samples in Sr-Nd-Pb-isotopic space and now mirrored in Hf-isotopic space, reflects the Kerguelen plume signature. A few lavas from three volcanic sections, older than 25 Ma, which represent as a whole <10% of the sample population, show relatively low $^{87}Sr/^{86}Sr$ and high $^{143}Nd/^{144}Nd$ and $^{176}Hf/^{177}Hf$. These lavas were called group D (for depleted samples) [3]. The Sr-Nd- and Pb-Pb-isotopic trends for these lavas imply the contribution of oceanic crust as a source-component added to the Kerguelen Plume; our Hf-isotopic data for the group D lavas are consistent with this interpretation. The youngest archipelago lavas, including those from Mt Ross (2–0.1 Ma), have lower $^{206}Pb/^{204}Pb$ for given Nd- and Sr-isotopic compositions [4] and also have lower $^{176}Hf/^{177}Hf$. As for the other isotope systems, the temporal trend of the archipelago lavas towards less radiogenic Hf-isotopic compositions with decreasing eruption age reflects changes in the relative proportions of different components entrained by or incorporated into the Kerguelen Plume.

The broad positive correlation between Hf and Nd isotopes for the Kerguelen Archipelago lavas also holds within each volcanic section (corresponding to time intervals from ~300 to 900 k.y.), as observed for the Mauna Loa and Mauna Kea drilled lava flows [5]. The Hf-Nd-isotopic correlation is usually attributed to the presence of garnet as a residual phase during basalt extraction. The importance of residual garnet is indicated by Kerguelen lavas with similar $^{87}Sr/^{86}Sr$, $^{143}Nd/^{144}Nd$, and $^{176}Hf/^{177}Hf$ and variable (more than a factor of two) La/Yb [6]. In addition, the entire ε_{Hf} range of Kerguelen lavas indicates source components with different Lu/Hf ratios.

The large variability in Hf-isotopic compositions, in conjunction with variations in Sr, Nd, and Pb isotopes in Kerguelen Archipelago lavas, reflects the dominant role of the Kerguelen Plume, together with the influence of other components in their genesis: a depleted component well expressed in the group D lavas [3], and a minor low $^{206}Pb/^{204}Pb$ component, possibly continental material, in the youngest and also most differentiated lavas (<10 Ma). A contribution of continental lithosphere is present in some Kerguelen mantle xenoliths [7]; however it is not expressed in >95% of the archipelago lavas. Nevertheless for the youngest, most differentiated lavas, the lower $^{206}Pb/^{204}Pb$ and Hf ratios for comparable Sr- and Nd-isotopic ratios, characteristic of the Kerguelen Plume, may reflect the same process of continental incorporation. Ongoing studies on Kerguelen Archipelago lavas and lavas from the recently drilled ODP Leg 183 should allow the continental component to be identified.

References: [1] Weis D. et al. (1998) *Mineral. Mag., 62A,* 1643–1644. [2] Nicolaysen K. et al. (1996) *Eos Trans. AGU, 77,* F824. [3] Yang et al. (1998) *J. Petrol., 39,* 771–748. [4] Weis et al. (1993) *EPSL, 118,* 101–119; Weis et al. (1998) *J. Petrol., 39,* 973–994. [5] Blichert-Toft J. and Albarède F. (1999) *GRL, 26,* 935–938. [6] Frey et al. (1999) *Chem. Geol.*, in press. [7] Hassler and Shimizu (1998) *Science, 480,* 218–221; Mattielli N. et al. (1999) *J. Petrol.*, in press.

DISSOLUTION OF ALUMINUM-SUBSTITUTED GOETHITES BY AN AEROBIC *PSEUDOMONAS MENDOCINA VAR.* BACTERIA.

P. A. Maurice[1], Y.-J. Lee[1], and L. E. Hersman[2], [1]Department of Geology, Kent State University, Kent OH 44242, USA, [2]Life Sciences Division, Los Alamos National Laboratory, Los Alamos NM 87545, USA.

In soil environments, goethite particles often contain Al^{3+} substituted for Fe^{3+} in octahedrally coordinated sites. Aluminum substitution has been shown to result in a variety of microtopographic, micromorphologic, and crystal structure changes as well as changes in abiotic dissolution rates and mineral stability. This study focused on the effects of Al substitution (to 8.8 mol%) on goethite dissolution by an aerobic *Pseudomonas mendocina var.* bacteria. In contrast to dissimilatory iron-reducing bacteria (DIRB), this bacteria is not capable of using Fe as a terminal electron acceptor for oxidative phosphorylation. Because the aerobic *P. mendocina var.* bacteria do not utilize Fe as a terminal electron acceptor, they require only micromole quantites of Fe, compared to the micromole concentrations used by DIRB.

Pure, and Al-substituted goethites were synthesized and analyzed by BET (surface area by gas adsorption), X-ray diffraction (XRD), atomic force microscopy (AFM), scanning electron microscopy (SEM), and X-ray photoelectron spectroscopy (XPS). Growth experiments conducted in aerobic conditions, in the dark at 22°C, showed that maximum microbial growth did not correlate with particle specific surface area. However, microbial growth was observed to increase with increasing Al content of the goethites, as well as decreasing particle size, decreasing multidomainicity, and decreasing particle aspect ratio. Due to the formation of dense biofilms, we were unable to observe dissolution features by AFM. The heterogeneous nature of the biofilms suggested that mineral aggregate structure may be important in determining microbial attachment and dissolution rates. Although the mechanistic reasons behind the observed microbial growth/mineral dissolution trends remain unknown, it is clear that the microorganisms are well adapted to utilizing Al substituted goethites, as are commonly found in aerobic soils.

THE SULFIDE CAPACITIES OF HAPLOBASALTIC AND BASALTIC SILICATE MELTS AT 1400°C AND 1 BAR.

J. A. Mavrogenes and H. St. C. O'Neill, Research School of Earth Sciences, Australian National University, Canberra ACT 0200, Australia (john.mavrogenes@anu.edu.au; hugh.oneill@anu.edu.au).

Fincham and Richardson [1] showed that S dissolves in silicate melts at low f_{O_2} (f_{O_2} <QFM) as S^{2-}, and does so by replacing O^{2-} on the anion sublattice, as described by the reaction

$$O^{2-} + 1/2\ S_2 = S^{2-} + 1/2\ S_2$$

This suggests the relationship

$$[S] = C_S\ (f_{S_2}/f_{O_2})^{0.5}$$

where [S] is the S content of the melt (e.g., in parts per million) and C_S is the "sulfide capacity" of the melt, which is a function of melt composition as well as temperature and pressure. Fincham and Richardson [1] experimentally verified the $(f_{S_2}/f_{O_2})^{0.5}$ relationship for simplified metallurgical slag compositions in the system CAS by varying f_{S_2} and f_{O_2} independently at 1 atm. Subsequent work has repeatedly confirmed the validity of the Fincham and Richardson model for other simple metallurgical slag compositions, but there is only limited information on the solubility of S in silicate melts relevant to geology.

Obviously C_S has meaning only if the $(f_{S_2}/f_{O_2})^{0.5}$ dependence is obeyed. While this relationship has been validated for an Hawai'ian tholeiite [2], other studies [3–5] have exhibited disturbing deviations from the relationship, which, if real, would demand a fundamental rethinking of the sulfide solubility theory as developed by the metallurgists. Moreover, there are apparent inconsistencies in the geological studies that presently preclude the development of a quantitative model relating sulfide solubility to melt composition.

Accordingly we have embarked on an experimental program to study S solubilities in silicate melts under controlled f_{O_2} and f_{S_2}, to test the $(f_{S_2}/f_{O_2})^{0.5}$ relationship over a wide range of silicate melt compositions, and, if the relationship is confirmed, to determine the compositional dependence of C_S. Initially, experiments have been undertaken at the relatively high temperature of 1400°C to access as wide a range of melt compositions as possible.

Experiments were conducted in a conventional vertical tube furnace equipped for gas mixing, using CO_2-CO-SO_2 mixtures to impose f_{O_2} and f_{S_2}. The major experimental problem was condensation of solid S on the cool parts at the top of the furnace, which, if allowed to build up, may then fall off into the hot part of the furnace, greatly increasing f_{S_2} over that calculated from the gas mixture.

Four strategies for varying melt composition were used. First, we selected seven near-eutectic compositions in the CMAS system, plus compositions along the anorthite-diopside join. Second, starting with anorthite-diopside eutectic as the base composition, we added the following components: SiO_2,

$MgSiO_3$, $CaSiO_3$, Mg_2SiO_4, FeO, Fe_2SiO_4, TiO_2, and $NaAlSi_3O_8$. Third, we studied an assortment of natural melt compositions spanning a range of FeO contents. Fourth, we attempted to replicate some measurements on compositions studied by previous investigators.

Samples were hung on Pt wire loops (or Re or Fe-Ir loops for some Fe-bearing compositions), and run generally six at a time. Quenching was by dropping into water. Samples were analyzed by electron microprobe using WDS with a troilite standard for S. Energy dispersive X-ray spectrometry (EDS) was used to confirm major-element compositions. As expected, loss of alkalis by volatilization and Fe loss into Pt loops were pervasive problems.

The results were fitted by a global nonlinear least squares regression to an expression of the form

$$[S] = (f_{S_2}/f_{O_2})^{0.5}\ \Sigma A_M[MO_x]$$

where $[MO_x]$ are the oxide components of the melt in weight percent, and the coefficients A_M are used to describe the compositional dependence of C_S. The fit to the data shows that the $(f_{S_2}/f_{O_2})^{0.5}$ relationship is followed by all compositions. We find $A_{Fe} > A_{Ca} \gg A_{Mg} > A_{Ti}$, with the coefficients for other oxide components (SiO_2, Al_2O_3, Na_2O) being effectively zero. The magnitude of A_M correlates roughly with the magnitude of the free energies for the reactions

$$MO_x + 1/2x\ S_2 = MS_x + 1/2x\ S_2$$

for M = Fe, Ca, Mg, Ti, Al, and Si, but this relationship breaks down for alkalis, for which it would predict A_{Na} to be large, rather than negligible as observed.

Our results are not in good agreement with the previous work [3–5], although allowance needs to be made for the different temperature (1200°C) of the latter study [5]. Importantly, we find a much higher value of A_{Fe}, indicating that FeO has a stronger influence on C_S than hitherto thought. Our high value of A_{Fe} helps explain the observation [6] that the S content at sulfide saturation (SCSS) of natural basaltic melts increases with increasing [FeO] in the melt, despite the simple prediction from the law of mass action for the reaction

$$FeO_{(melt)} + S^{2-}{}_{(melt)} = FeS_{(sulfide)} + O^{2-}{}_{(melt)}$$

that increasing [FeO] in the melt should correlate with lower, not higher, values of $S^{2-}{}_{(melt)}$, i.e., SCSS. C_S in complex melt compositions is poorly predicted by generalized melt descriptions such as NBO/T or optical basicity.

References: [1] Fincham C. J. B. and Richardson F. D. (1954) *Proc. Roy. Soc. London, 223A,* 40–61. [2] Katsura T. and Nagashima S. (1974) *GCA, 38,* 517–531. [3] Buchanan D. L. and Nolan J. (1979) *Can. Mineral., 17,* 483–494. [4] Buchanan D. L. et al. (1983) *Spec. Pub. Geol. Soc. S. Afr., 7,* 83–391. [5] Haughton D. et al. (1974) *Econ. Geol., 69,* 451–467. [6] Mathez E. A. (1976) *J. Geophys., 81,* 4269–4275.

TRACING THE FATE OF ANTHROPOGENIC NITROGEN IN LARGE WATERSHEDS BY ISOTOPIC TECHNIQUES.

B. Mayer[1] and C. Heinzer[2], [1]Departments of Physics and Astronomy and Geology and Geophysics, University of Calgary, 2500 University Drive, Calgary, Alberta T2N 1N4, Canada (bernhard@earth.geo.ucalgary.ca), [2]Institut für Geologie, Ruhr-Universität Bochum, Universitätsstrasse 150, D-47780 Bochum, Germany (constanze.heinzer@ruhr-uni-bochum.de).

Introduction: Human activity has greatly altered the N cycle in terrestrial and aquatic ecosystems and increased the N flow in many rivers. Preliminary work of the International SCOPE Nitrogen Project indicates that only 20% of the human-controlled N inputs to large watersheds are exported to the oceans in riverine flows [1]. Therefore, ~80% of the anthropogenic N inputs are either stored or denitrified in the catchments.

Anthropogenic N can be retained in forests as a result of increased productivity or in agricultural soils and can potentially be stored in groundwater. These sinks are in all likelihood not large enough to account for the "missing" N. It is therefore assumed that the majority of the human-controlled N inputs to large watersheds is denitrified in soils, riparian zones, wetlands, lakes, and rivers.

Objective: In this study we performed isotopic analyses on riverine nitrate from 20 streams draining into the north Atlantic Ocean. Both $\delta^{15}N_{nitrate}$ and $\delta^{18}O_{nitrate}$ values were determined in order to identify the sources of the dissolved nitrate. A further objective was to test whether the isotopic composition of dissolved nitrate provides a measure for the extent to which denitrification occurs in the respective watersheds.

Results and Discussion: The isotopic composition of dissolved nitrate in all investigated rivers and streams revealed that atmospheric deposition and fertilizer input were generally not a significant primary source of riverine nitrate. For 15 watersheds in the northeastern United States, $\delta^{15}N_{nitrate}$ values between 4‰ and 7‰ and $\delta^{18}O_{nitrate}$ values varying from 10‰ to 15‰ indicated that most of the dissolved nitrate in surface runoff was derived from nitrification processes in soils. The obtained isotopic data provided no evidence for significant in-stream denitrification in these catchments.

In several German rivers, $\delta^{15}N_{nitrate}$ values as high as 30‰ and $\delta^{18}O_{nitrate}$ values of more than 25‰ were occasionally observed. This is evidence for intensive denitrification within the catchment areas, a process during which the heavier isotopes ^{15}N and ^{18}O are progressively enriched in the remaining dissolved nitrate. It appeared that point sources such as sewage treatment plants were the major contributor of dissolved nitrate with extraordinary high $\delta^{15}N$ and $\delta^{18}O$ values along some of the investigated German rivers.

Conclusions: The isotopic composition of dissolved nitrate appears to be a valuable tracer, which enables us to determine the sources of riverine nitrate. Elevated $\delta^{15}N$ and $\delta^{18}O$ values can provide additionally evidence for the occurrence of denitrification processes within watersheds. It is, however, difficult to assess isotopically, where and to which extent anthropogenic N inputs are denitrified in large watersheds.

References: [1] Howarth R. W. (1998).

SULFUR- AND RHENIUM-OSMIUM-ISOTOPIC SYSTEMATICS IN PRECAMBRIAN SEAFLOOR MASSIVE SULFIDES.

T. E. McCandless[1], R. D. Mathur[1], C. J. Eastoe[1], and A. Kontinen[2], [1]Center for Mineral Resources, University of Arizona, Tucson AZ 85721, USA (diamonds@geo.arizona.edu), [2]Geological Survey of Finland, P.O. Box 1237, 70211, Kuopio, Finland (asko.kontinen@gsf.fi).

Introduction: Sulfide deposits that form on the modern-day seafloor record an extensive interaction of mantle-derived Os and seawater Os, with ranges in $^{187}Os/^{188}Os$ from 0.16 to 1.04 [1]. This interaction is easily recognized because oceanic mantle has a $^{187}Os/^{188}Os$ ratio of ~0.1, whereas seawater Os is around 1.0. The mantle $^{187}Os/^{188}Os$ ratio varies only slightly from 0.1 over geologic time, whereas seawater values in the Precambrian are unknown but should be equal to or greater than the mantle. The $^{187}Os/^{188}Os$ ratios recorded in Precambrian seafloor massive sulfides therefore should record minimum estimates of the Os-isotopic compositions of the seawater involved in their formation. Sulfide samples were obtained from the deposits at Outokumpu, Finland, Jerome, Arizona, and Otjihase, Namibia, to evaluate this possibility. The Cu-Fe-Zn-Co sulfide deposits of the Outokumpu district occur in clastic metasedimentary sequences that are spatially associated with 2.0-Ga ophiolites in the Svecokarelides of Finland. The Jerome Cu-Fe-Zn deposit occurs in 1.7-Ga submarine felsic, intermediate, and mafic metavolcanic rocks that are metamorphosed to grennschist facies. Copper-iron-zinc sulfides at Otjihase are directly associated with the Matchless Belt, a 350-km linear belt of amphibolite that defines the 0.7-Ga rifting phase of the Damara Orogen.

Preparation: The samples were manually crushed and sulfides were physically concentrated with three splits taken from each sample. The first split is examined by microprobe and back scattered electron (BSE) imaging to evaluate the sulfide separates, as primary and secondary textural, mineralogical, and chemical features can be identified and mapped out in detail. For example, BSE examination of sulfides from the smoker structures at Jerome revealed that their textures were identical to textures observed in modern-day smoker sulfides from the Juan de Fuca Ridge, suggesting that very little deformation or alteration of the smoker sulfides had taken place since their formation 1700 m.y. ago.

Sulfur Isotopes: The second split from each sample was analyzed for S isotopes, as S isotopes can help to characterize the type of seafloor setting in which each deposit formed. For example, sphalerite and pyrite separates from Jerome have a $\delta^{34}S$ range of –0.5‰ to +0.9‰, which is within the range for sulfides from the Guaymas Basin (–3 to 5) [2], the best modern-day analog for Jerome. Sulfides and their host amphibolites at Otjihase form a narrow belt with the Kuiseb Formation, a schist representing voluminous clastic metasediments. Pyrite and chalcopyrite from Otjihase have $\delta^{34}S$ values from 0.5‰ to 7.7‰, similar to modern-day sulfides from the sediment-filled Escanaba Trough (1–13‰) [2].

Rhenium-Osmium Isotopes: Rhenium and Os were separated and purified from the third split using a Carius tube dissolution, followed by distillation and anion resin column exchange techniques. Rhenium and Os concentrations are from 0.07 to 3.07 and 00.08 to 3.00 ppb, respectively, and these ranges are similar to modern-day sulfides (0.005–4.0 ppb Os [1]). Preliminary data for sulfides from the Jerome deposits give an errorchron with an age of 1.45 ± 0.30 Ga and an initial $^{187}Os/^{188}Os$ of 0.898, within the range of modern seafloor sulfides. The elevated initial $^{187}Os/^{188}Os$ ratio suggests that seawater may have been very radiogenic during some periods of time in the Precambrian.

References: [1] Ravizza et al. (1996) *EPSL, 138,* 105–119. [2] Shanks et al. (1995) *AGU Monogr., 91,* 194–221.

NEW DEVELOPMENTS IN *IN SITU* ANALYSES: HARVARD UNIVERSITY'S LASER ABLATION INDUCTIVELY COUPLED PLASMA MASS SPECTROMETRY (QUAD AND MULTICOLLECTOR) LABORATORY.

W. F. McDonough, R. L. Rudnick, and I. Horn, Department of Earth and Planetary Sciences, Harvard University, 20 Oxford Street, Cambridge MA 02138, USA (mcdonough@eps.harvard.edu).

Introduction: Recent advances in laser and inductively coupled plasma mass spectrometry (ICP-MS) technologies are providing unparalleled opportunities for *in situ* analyses at high spatial resolution. Both elemental and isotopic compositions of a wide spectrum of geological and meteoritical materials can now be determined [1]. Over the past two years we have developed a laser ablation laboratory at Harvard University (http://www-eps.harvard.edu/la-icp-ms.html) that employs an excimer laser in combination with both a quadrupole and a multiple collector ICP-MS. This presentation is an opportunity to share the latest results from our laboratory (including ones not yet available at the time of writing).

Laser: Our homemade laser ablation system [2] uses a Compex 110 excimer laser (Lambda Phsyik) operating in the deep UV at 193 nm. Pulse energy can be varied from <0.1 to ~10 mJ, as too can pulse repetition rates that vary from 1 to 100 Hz. Because the spot is an image of a blanking aperture in the beam path, spot shapes can be any geometry required (i.e., circles, rectangles, squares, even triangles). Diameters for circular spots (the most commonly used geometry) can be set at any size between 10 and 400 µm. Helium is used as the carrier gas in the sample cell that results in increased transmission over Ar carrier gas, yielding a factor of ~5 increase in sensitivity [3].

Quadrupole Inductively Coupled Plasma Mass Spectrometry: Our quadrupole ICP-MS is a PQ2+ (VG Elemental) with typical solution (Meinhard) sensitivity of 10^8 cps/ppm on ^{115}In. When coupled with the excimer laser we can achieve detection limits of 10–100 ppb for high mass (>85) and low 1st ip (<8eV) elements for a 20-µm spot, or 100–200 ppb for the PGE, many of which have higher ionization potentials. We have employed our quadrupole in a variety of *in situ* trace-element applications [e.g., 4,8]. In addition, through simultaneous solution nebulization and laser ablation, we have achieved ~2% precision (2σ) on Pb-Pb and U/Pb ages for Paleozoic zircons [2].

Multiple Collector Inductively Coupled Plasma Mass Spectrometry: Our newly acquired multiple collector ICP-MS, an Isoprobe (Micromass) (Fig. 1) is equipped with nine faraday cups and a wide flight tube for simultaneous collection of isotopes across a mass range of 15%. It has a hexpole filter before the laminated magnet that serves to narrow the ion energy spread to ~1 eV, and eliminate Ar interferences (when using Ar and H gases in the hexapole). It also includes two channeltrons at the low mass end and a moveable axial faraday that provides access to a WARP filter followed by a Daly detector. Abundance sensitivity is <10 ppm with the faradays, or 15 ppb using the WARP filter on the Daly. Our instrument has achieved a sensitivity of >3 × 10^{10} cps/ppm (i.e., 500 V/ppm) on U using a CETAC MCN6000. Internal run precision for $^{87}Sr/^{86}Sr$ and $^{143}Nd/^{144}Nd$ ratios is 8 ppm, and external precision is 6–30 ppm, measured over several hours on 100 ppb standard solutions. Accuracy for $^{206}Pb/^{204}Pb$, $^{143}Nd/^{144}Nd$ and $^{87}Sr/^{86}Sr$ ratios on standard solutions is 70, 20, and 40 ppm respectively.

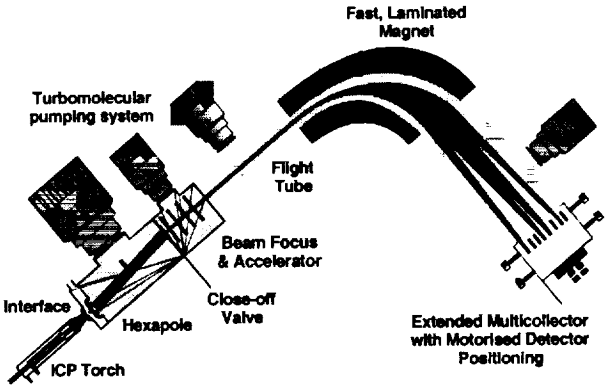

Fig. 1. Schematic of Isoprobe (Micromass).

When coupled to the excimer laser we have achieved ε level precision on Hf-isotopic ratios for samples with concentrations of hundreds to thousands of parts per million, depending on spot size and abundance level [5,6]. In a search for extinct ^{92}Nb, we achieved ±3 ε level precision on Zr isotopes in rutiles [7]. In addition, Paul Mason showed, using the Micromass demo machine (similarly equipped), that they could measure $\delta^{34}S$ in sulfides to a precision of ±0.2‰ [9]. New results gathered over the summer on these and other isotopic systems, applied to a spectrum of cosmological and geochemical problems, will be reported at the meeting.

References: [1] Eggins et al. (1997) *EPSL;* Christensen et al. (1994) *EPSL;* Hirata and Nesbitt (1998) *EPSL.* [2] Horn et al. (1999) *Chem. Geol.,* in review. [3] Eggins et al. (1998) *App. Sur. Sci.* [4] Rudnick et al., this volume. [5] Horn et al, this volume. [6] Lee C.-T. et al., this volume, [7] Yin Q. et al., this volume. [8] Barth et al., this volume. [9] Mason et al., this volume.

SURFACE CHEMISTRY OF SULFIDE MINERALS DURING OXIDATIVE DISSOLUTION.

M. M. McGuire[1], K. J. Edwards[2], J. F. Banfield[2], and R. J. Hamers[1], [1]Department of Chemistry, University of Wisconsin-Madison, 1101 University Avenue, Madison WI 53706, USA, [2]Department of Geology and Geophysics, University of Wisconsin–Madison, 1215 West Dayton Street, Madison WI 53706, USA.

The surface chemistry of sulfide minerals during oxidative dissolution at 37°C and pH 1.5 was examined. Samples of pyrite, marcasite, and arsenopyrite were exposed to an Fe-oxidizing microbial isolate (*Ferriplasma acidarmanus*), a S-oxidizing isolate (*Thiobacillus caldus*), and a mixed enrichment culture. Changes in chemical speciation of the mineral surface products were monitored by Raman spectroscopy. Results indicate that the most abundant surface product under abiotic conditions or in the presence of an Fe-oxidizing microbial species is elemental S. In the case of marcasite and arsenopyrite, calibration of the intensity of the Raman signal from S suggests that it forms in amounts on the order of thousands of atomic layers within days. Pyrite, however, exhibited a dissimilar surface chemistry, producing significantly less S than either marcasite or arsenopyrite.

Mineral surfaces in the presence of the S-oxidizing isolate reveal very little evidence of elemental S. Surprisingly, the removal of the surface S layer by the S-oxidizing species does not correlate with an increase in dissolution rate as compared with the abiotic control reactions. These findings suggest that the elemental S layer does not passivate the mineral surface from further reaction, but rather must form a porous structure that continues to allow the passage of oxidants to the surface.

CHEMICAL AND ISOTOPIC EVIDENCE FOR PLEISTOCENE RECHARGE TO SILURIAN-DEVONIAN AQUIFERS, ILLINOIS BASIN.

J. C. McIntosh[1], L. M. Walter[1], J. M. Budai[1], and A. M. Martini[2], [1]Department of Geological Sciences, University of Michigan, Ann Arbor, Michigan 48109-1063, USA (jmcintos@umich.edu), [2]Amherst College, Amherst MA 01002-5000, USA.

Introduction: The midcontinent region of the United States is characterized by a number of sag-type basins that have been influenced by repeated Pleistocene glaciations. Many of these basins have seen little tectonic disturbance and so have low topographic gradients. Thus, glaciation can significantly change fluid and rock stress regimes, especially near basin margins. This is evidenced by recharge of Pleistocene waters into various regional aquifer systems. For example, glacial meltwater recharge into the Cambrian-Ordovician aquifers of the northern Illinois basin has been established [1,2]. This recharge locus can also play a key role in generating unconventional biogenic gas deposits where organic rich shale units are in proximity to basin margin recharge. Martini et al. [3], for example, established a link between Pleistocene glaciation and shallow biogenic gas deposits in the Michigan basin.

New Developments in the Illinois Basin: Our current study targets the eastern part of the Illinois basin where Devonian black shales subcrop near the basin margin. Previous studies show that underlying Silurian-Devonian carbonate aquifers have significant salinity depletions [4] suggestive of freshwater recharge in this part of the basin. Recent exploration for shallow biogenic gas occurrences in these black shales has made a large number of new wells available in this hitherto unexplored margin of the Illinois basin. Of special significance is the association of biogenic gas production with high volumes of dilute formation water.

Formation water and gas samples from the New Albany and over- and underlying aquifer systems have been collected and analyzed for element and isotopic geochemistry. Salinity and isotopic variations in the New Albany shale and underlying Silurian-Devonian waters indicate selective recharge of glacial meltwater into Silurian-Devonian carbonates. This is compatible with the regional arc of the carbonate subcrop in the northern limb of the Illinois basin (Fig. 1). The chloride content of Silurian-Devonian formation waters is extremely variable. Dilute water, near-potable near the surface, penetrates to close to 2000-feet depth. At that point, salinities increase rapidly to values in excess of 3000 mM (Fig. 2). The overlying New Albany shale formation waters show a similar suppressed salinity pattern with depth. Stable isotopic constraints coupled with these depth/salinity relations demonstrate that glacial meltwater has recharged Silurian-Devonian aquifers and migrated upward through a regional fracture system established in the New Albany shale. Deuterium-isotopic values of the New Albany shale waters vary co-linearly with chloride from basinal brine values (−4‰) to values more depleted than modern rainfall in this area (−46‰ vs. −40‰ today). Oxygen-isotopic values follow a similar pattern: formation waters vary from basinal brine values (1.38‰) to values more depleted than modern Indiana groundwater (−7.5‰ vs. −6‰ today).

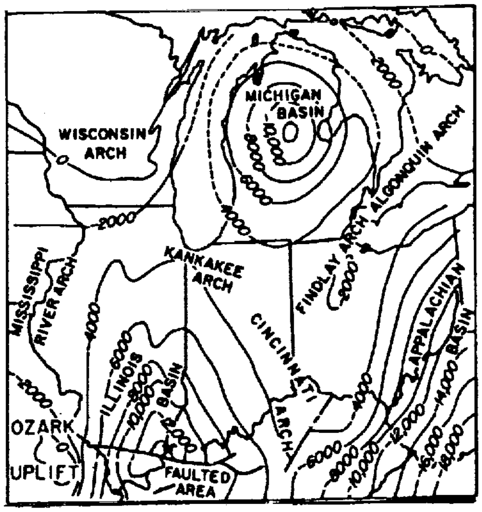

Fig. 1. Structural map of U.S. midcontinent region (adapted from [5]). The Silurian-Devonian aquifer system subcrops along the Kankakee and Cincinnati arches, overlying Cambrian-Ordovician strata.

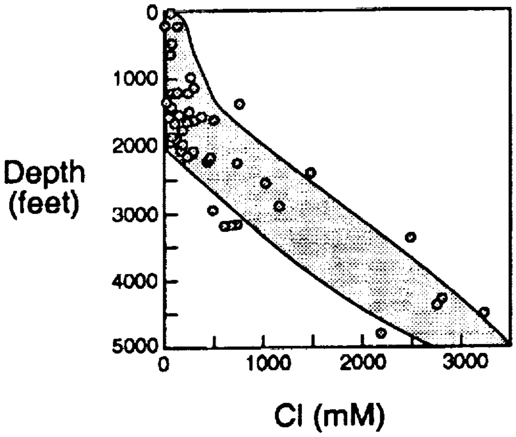

Fig. 2. Silurian-Devonian carbonate formation saters: Cl (mM) vs. depth.

Summary: The chemical and isotopic variations of Silurian-Devonian and New Albany shale waters, along with studies from other parts of the basin, confirm that Pleistocene waters have recharged Silurian-Devonian and Cambrian-Ordovician aquifers during major glaciations and that invasion of freshwater was regionally extensive. As with the Michigan basin, the invasion of dilute waters into the organic-rich New Albany shale formation induced the generation of biogenic gas along the basin margin.

References: [1] Siegel D. I. (1989) *U.S. Geological Survey Prof. Paper 1405-D,* 76. [2] Stueber A. M. and Walter L. M. (1994) *Bull. GSA, 106,* 1430–1439. [3] Martini A. M. et al. (1996) *Nature, 383,* 155–158. [4] Keller S. J. (1983) *GS Occasional Paper 41,* 30. [5] Droste J. B. and Shaver R. H. (1983) *GS Spec. Rpt. 32,* 2.

GEOCHEMICAL EVIDENCE FOR SEDIMENTARY SILICA ON MARS.

S. M. McLennan, Department of Geosciences, State University of New York at Stony Brook, Stony Brook NY 11794-2100, USA (scott.mclennan@sunysb.edu).

Introduction: There is abundant evidence from imaging, spectroscopy, magnetics, thermodynamic considerations, and chemical analyses that a variety of sedimentary processes have affected the martian surface. Among those processes that have been identified or proposed are conversion of basalt to palagonite and clays during low temperature alteration [1], oxidation of igneous minerals to form hematite and other iron-oxides [1,2] possibly including a magnetic iron oxide mineral [3], chemical evidence consistent with heavy mineral fractionation during sedimentary transport [4], and evidence for Mg (and possibly Fe) sulfates and chlorides in martian soils [2,4,5].

Analyses of SNC meteorites and martian rocks and soils also indicate that the martian surface is dominated by mafic to ultramafic rocks [6]. During weathering and low-temperature alteration of basalt on Earth, large amounts of SiO_2 may be liberated and under certain near-surface conditions silica is highly mobile. Accordingly, an important question is whether or not similar processes take place on Mars and if so, what role does sedimentary silica play?

A variety of workers have recognized that silica may play a role during alteration processes [e.g., 1,5] and Burns [1] alluded to "hydrous iron oxide-silica deposits" in the Argyre and Hellas basins. However, the possibility of extensive silica deposits at or near the martian surface has been inadequately explored.

Low-temperature Alteration of Terrestrial Basalt: Alteration of terrestrial basalt across a broad range of conditions from weathering to hydrothermal is commonly accompanied by loss of up to >50% of SiO_2 due to the dissolution of unstable mafic minerals and glass [e.g., 7,8]. Examples of idealized dissolution reactions for olivine and pyroxene include

Fayalite: $Fe_2SiO_4 + 4H^+ = 2Fe^{2+} + H_4SiO_4$
Forsterite: $Mg_2SiO_4 + 4H^+ = 2Mg^{2+} + H_4SiO_4$
Diopside: $CaMgSi_2O_6 + 4H^+ + 2H_2O = Mg^{2+} + Ca^{2+} + 2H_4SiO_4$

On Earth weathering processes often proceed under largely open system conditions and much of the silica is either transported to less altered portions of the weathering zone where it may be involved in other weathering reactions or is lost entirely from the weathering zone to streams and groundwater.

Evidence for Low-temperature Alteration of Martian Basalt: Among the most surprising results of the chemical analyses of martian soils and rocks are the high abundances of S and Cl [9,10]. At the Pathfinder site, only MgO (and possibly FeO_T) correlate positively with SO_3 and Cl, suggesting that a significant fraction, if not all, of the Mg in soils is present as sulfide and chloride minerals [4,5,11]. It is also generally agreed that much of the Fe in martian surficial deposits is present as secondary oxide minerals such as hematite [1,2]. Chemical data are also consistent with fractionation of Fe-rich phases (e.g., hematite, Fe-sulfate) in martian soils and rocks, likely during sedimentary transport [4].

The significance of these relationships is that much of the Mg and Fe derived from alteration of mafic minerals reacted to form nonsilicate minerals. Accordingly, there is a likelihood that substantial amounts of SiO_2, also derived from alteration reactions, would be available to form discrete sedimentary silica phases, including noncrystalline or crystalline opals, microcrystalline quartz (e.g., chacedony) or quartz.

Fate of Sedimentary Silica: The ultimate fate of silica is difficult to constrain because little is known about the nature of the martian hydrosphere over geological history. Near alteration zones, silicon may combine with Al (from plagioclase) and various cations to form palagonite and a variety of clays (e.g., saponite, nontronite, sepiolite, montmorillonite, etc.). However, silica that is lost to near-surface waters could be transported considerable distance and precipitated as a separate silica phase Thus silica could be found in a variety of geological settings, including sedimentary chert deposits (iron formations of Burns [1]?), veins, fracture fillings, mineral overgrowths, encrustations on rock surfaces, authigenic mineral grains, or dust coatings. The presence of abundant silica would have important implications for interpreting imaging, remote sensing, and chemical data that have been returned from Mars.

References: [1] Burns R. G. (1993) *GCA, 57,* 4555–4574. [2] Bell J. F. III (1996) *Geochem. Soc. Spec. Publ. 5,* 359–380. [3] Madsen M. B. (1999) *JGR, 104,* 8761–8779. [4] McLennan S. M. (1999) *LPS XXX,* Abstract #1700. [5] McSween H. Y. Jr. et al. (1999) *JGR, 104,* 8679–8715. [6] McSween H. Y. Jr. and Treiman A. H. (1998) *Rev. Mineral., 36,* 6/1–6/53. [7] Nesbitt H. W. and Wilson R. E. (1992) *Am. J. Sci., 292,* 740–777. [8] Daux V. et al. (1994) *GCA, 58,* 4941–4954. [9] Clark B. C. (1982) *JGR, 87,* 10059–10067. [10] Rieder R. et al. (1997) *Science, 278,* 1771–1774. [11] Clark B. C. (1993) *GCA, 57,* 4574–4581.

COPPER-CHLORIDE COMPLEXING IN HYDROTHERMAL BRINES.

D. C. McPhail[1], J. Brugger[1], W. Liu[1], L. Spiccia[2], and J. Black[1], [1]Department of Earth Sciences, Victorian Institute of Earth and Planetary Sciences, Monash University, Clayton, Victoria 3168, Australia (bear@mail.earth.monash.edu.au), [2]Department of Chemistry, Monash University, Clayton, Victoria 3168, Australia.

Introduction: The concentrations and transport of Cu in ore-forming and other environments is controlled in part by how Cu and chloride complex together in high-temperature brines. Despite the importance of Cu in many types of hydrothermal ore deposits (e.g., porphyry, epithermal, SEDEX), little is known about the complexes of Cu with chloride. Copper geochemistry is complicated because of the two important valence states of aqueous Cu [Cu(I) and Cu(II)]. We are studying the hydrothermal geochemistry of Cu(I,II)-chloride complexes using a combination of mineral solubility and UV-Vis-NIR spectrophotometric experiments and thermodynamic modeling.

Cuprite Solubility: The solubility of cuprite [Cu(I)] was measured in preliminary experiments using water bath (under N atmosphere) and evacuated silica-glass tubes at temperatures between 25°C and 250°C, vapor-saturated pressure and in acetic-acid and phosphate pH buffered waters with variable NaCl concentrations (0–2 mol). Copper oxidized or disproportionated in all experiments with less than ~0.1 mol NaCl concentrations and in most water bath experiments, even when vessels were closed and under a constant flow of purified N. Successful experiments have been run at 50° and 150°C using evacuated silica glass tubes, acetic-acid pH buffer (0.1 mol to 1.0 total acetate) and 0.01–2.0 mol NaCl. Aqueous Cu is greater than 95% Cu(I) based on measured absorbance spectra and quantitative measurements using the neocuproine analytical method. At 150°C and measured $pH_{25°C}$ ~4.7, measured log $mol_{Cu,total}$ increases linearly from –3 to –1 between log $mol_{Cl,total}$ of –2 and 0, with a reproducibility of better than 6%. The slope of the curve is one, indicating that CuCl(aq) predominated at the conditions of the experiment. Total acetate concentration was varied at a constant 0.1 mol NaCl, resulting in a small increase in measured Cu concentrations and indicating that some Cu(I)-acetate was present in the experiments.

Ultraviolet–Visible–Near-Infrared Spectrophotometry: Ultraviolet–Visible–Near-Infrared spectra of Cu(II)-chloride complexes have been measured successfully using conventional methods at 25°C, 60°C, and 90°C for acidified 30 ppm Cu (ultraviolet wavelengths) and 500 ppm Cu (visible wavelengths) solutions between 0 and 18 mol LiCl. Cu(II)-chloride system was chosen for three reasons: (1) to develop the necessary methodologies of running the experiments and interpreting the data, (2) extend the range of existing experimental data for Cu(II)-chloride species, and (3) understand the positions and shapes of the important absorbance spectra for Cu(II) species so that we can identify potential interferences with the absorbances of Cu(I) species. The UV spectra of Cu(II) complexes are easier to interpret than the visible spectra at all temperatures and indicate at least five species based on a principal component analysis. The most probable stoichiometries of species in these experiments were Cu^{2+}, $CuCl^+$, $CuCl_2(aq)$, $CuCl_4^{2-}$ and an unknown species. There appears to be an octahedral-tetrahedral transition with increasing LiCl concentration, based on a comparison with solid-phase spectra. The transition is apparent between 2 and 5 mol LiCl at all three temperatures. A preliminary interpretation of the spectra indicates the change in predominance of species with LiCl concentration (Fig. 1). UV-Vis-NIR spectra of Cu(I)-chloride complexes in LiCl solutions was measured at 25°C, but at higher temperature the Cu oxidized too quickly to measure reliable spectra.

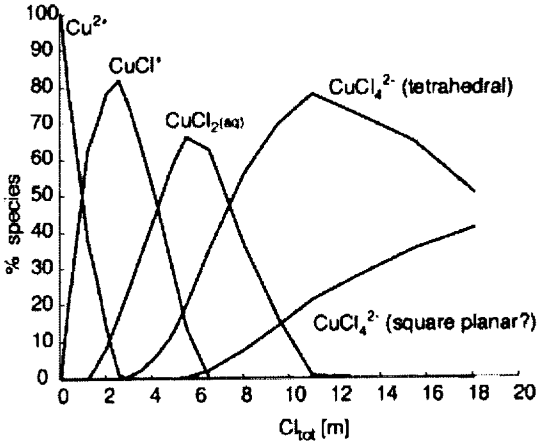

Fig. 1. Estimated percentages of Cu(II)-chloride species derived from UV absorbance data at 25°C.

High-temperature Ultraviolet–Visible–Near-Infrared Spectrophotometry: A newly designed Ti pressure cell with sapphire windows has been successfully tested to 300°C. The cell has four windows that allow both liquid and vapor spectra to be measured in the same experiment. We are currently using the cell to extend the temperature range for Cu(II)-chloride spectra, measure Cu(I)-chloride spectra, and detect liquid-vapor partitioning of Cu in chloride, bisulfide and ammine systems. Preliminary measurements of Cu(II)-chloride liquid-vapor up to 300°C do not show any Cu vapor species.

Thermodynamic Modeling: Modeling suggests that disproportionation is important at low temperatures and low salinities. Comparisons of our data with recently published thermodynamic properties show good agreement for Cu(II)-chloride species at low salinity; however, there is less agreement for Cu(II)-chloride species at high salinities and Cu(I)-chloride species.

THREE PALEOPROTEROZOIC POSITIVE ISOTOPIC EXCURSIONS OF CARBONATE CARBON-13/CARBON-12: STILL A PARADOX.

V. A. Melezhik[1] and A. E. Fallick[2], [1]Geological Survey of Norway, Leiv Erikssons vei 39, 7491, Trondheim, Norway (victor.melezhik@ngu.no), [2]Scottish Universities Research and Reactor Centre, East Kilbride G75 0QF, Scotland (t.fallick@surrc.gla.ac.uk).

Until recently a 2.06–2.33-Ga Paleoproterozoic positive excursion of $\delta^{13}C_{carb}$ has been considered as a single isotopic event lasting over 200 Ma [e.g., 1]. Since Buick et al. [2] reported a new ~2.40-Ga $^{13}C_{carb}$–rich occurrence this long-lasting single isotopic event may perhaps be better considered as three or four positive shifts of $\delta^{13}C_{carb}$ separated by returns to 0‰.

Although there is very little doubt that the 2.06–2.40-Ga positive excursions of $\delta^{13}C$ have a widespread character, the isotopic event is unique in terms of both duration (>300 Ma) and ^{13}C enrichment (up to 18‰). The mechanism responsible for one of the most significant C isotopic shifts in Earth history remains highly debatable. To date, $\delta^{13}C$ of 10–15‰ cannot be balanced by organic C burial as there is no geological evidence for an enhanced C_{org} accumulation prior to or synchronous with the excursion.

For the interval 2.06–2.4 Ga there is a paucity in $\delta^{13}C_{org}$ data at the time when the positive carbonate excursion developed. Consequently, neither Δ_c nor f_{org} can be established with meaningful precision. Surprisingly, the Paleoproterozoic isotopic event is followed by formation of a vast reservoir of ^{13}C-depleted organic material (down to −42‰ at Shunga) and by one of the earliest known oil-generation episodes at 2.0 Ga. The latter time is also marked by the first appearance, and then by the worldwide development, of diagenetic carbonate concretions marked by negative $\delta^{13}C_{carb}$ values. This may be the first reliable evidence that organic material was recycled during diagenesis under oxic conditions.

Predominantly highly oxidized "red beds" with evaporitic affinities are associated with ^{13}C-rich carbonates. Close association of ^{13}C-rich carbonates with abundant stromatolites is a further striking fact, perhaps as yet underestimated. The data available indicate that the global $\delta^{13}C$ values for the Paleoproterozoic excursions could, in fact, be at lower levels than often considered. The extreme enrichment in ^{13}C (above 5‰?) might well have been caused by local factors such as an intensive development of cyanobacteria, coupled with evaporation in restricted basins that were apparently not in full equilibrium with atmospheric CO_2.

However even if global $\delta^{13}C$ values for the Paleoproterozoic excursions were to be constrained at 5‰ there is not yet known any organic C reservoirs that can balance this value. Moreover none of the three positive excursions of $\delta^{13}C_{carb}$ are followed by negative isotopic shifts significantly below 0‰, as has always been observed in younger isotopic events reflecting an overturn of a major marine C reservoirs. Could the absence of such shifts in the Paleoproterozoic indicate that perhaps there were no such reservoirs (i.e., f_{org} was constant)? If so, it is necessary to investigate other options to explain the Paleoproterozoic positive excursion of $\delta^{13}C_{carb}$. Perhaps the traditional approach via f_{org} change is not applicable to 2.06–2.40 Ga. As this period of time was marked by transition from generally O-free to gradually oxygenated atmosphere, this might have influenced the mechanism involved in the production of organic C. Onset of intensive methane cycling [e.g., 3] resulting in Δ_c change is another possibility. We have to accept that a "cause-and-effect" relationship between the excursion and a series of related phenomena is still not fully understood.

References: [1] Karhu and Holland (1996). [2] Buick et al. (1998). [3] Hayes (1998).

ISOTOPIC COMPOSITION OF CONCRETIONARY SULFIDES FROM THE 2000-Ma NONEUXINIC BASIN, PECHENGA GREENSTONE BELT, NORTHWEST RUSSIA.

V. A. Melezhik[1], L. N. Grinenko[2], and A. E. Fallick[3], [1]Geological Survey of Norway, Leiv Erikssons vei 39, 7491 Trondheim, Norway (victor.melezhik@ngu.no), [2]Institute of Geochemistry and Analytical Chemistry, Russian Academy of Sciences, Moscow, Russia, [3]Scottish Universities Research and Reactor Centre, East Kilbride, Glasgow G75 0QF, Scotland, UK (t.fallick@surrc.gla.ac.uk).

Two hundred and fifty-nine sulfide samples from metamorphosed (greenschist facies) black shales of the 2000-Ma productive formation belonging to the Petsamo supergroup in the Kola region (northwest Russia) have been analyzed for their S isotope ratio. The sulfide-bearing black shales were formed in a non-euxinic basin within an oceanic rift environment. The black shales are marked by very high S/C_{org} ratios and a strong positive correlation between C_{org} and S (r = 0.70) with zero intercept on the S axis. Different generations of sulfide concretions have been distinguished by means of concretional analysis. Individual isotope study of synsedimentary sulfide layers and sulfides from early, mid- and late diagenetic-catagenetic sulfide concretions yields trends, which suggest bacterial sulfate reduction as the concretion-forming process. The overall spread of $\delta^{34}S$ from −8.3‰ to +24.9‰ indicates $\delta^{34}S_{sulfate-sulfide}$ between +29‰ and −4‰, given a seawater sulfate at around 21‰. The first-order trend is a progressive enrichment in ^{34}S with increase of burial. Two major populations of sulfides have been distinguished. The first (concretions and perhaps thin layers) formed in an open system with respect to seawater sulfate and has a limited $\delta^{34}S$ range of −2.7‰ to +3.8‰. This is coupled with extensive formation of diagenetic carbonate beds marked by $\delta^{13}C$ of −8.7‰ to −12.5‰. The second population (lenses, thin layers, concretions, and microconcretions in carbonate nodules) formed in a closed system and is characterized by a high Fe^{2+}/S^{2-} ratio and progressive development of a Rayleigh distillation process which drove $\delta^{34}S$ from −8.3‰ up to +24.9‰. The high Fe^{2+}/S^{2-} and possibly change in pH parameter resulted in pyrrhotite rather than in pyrite. Associated abundant carbonate nodules have $\delta^{13}C$ in the range −8.2‰ to −14.1‰. Overall low $\delta^{34}S_{sulfate-sulfide}$ and the high S/C_{org} ratio are consistent with one-stage bacterial sulfate reduction in a noneuxinic basin. The observed $\delta^{34}S_{sulfate-sulfide}$ of 29‰ (as maximum) is within the "pure sulfate-reducing bacteria" range of 4–46‰. Advanced isotopic modification involving the oxidative part of the S cycle has not been detected. Based on the data available one cannot exclude the presence of a third population of sulfides (thin massive layers with $\delta^{34}S$ from −2.5‰ to +0.3‰) that might have inorganic origin and formed from an exhalative source.

EVOLUTION OF MINERAL AND GLASS SURFACE ROUGHNESS WITH DISSOLUTION.

N. P. Mellott[1], S. L. Brantley[1], and C. G. Pantano[2], [1]Department of Geosciences, Pennsylvania State University, University Park PA 16802, USA, [2]Department of Materials Science and Engineering, Pennsylvania State University, University Park PA 16802, USA.

Introduction: Mineral surface area may be the least understood parameter in the standard equation of mineral dissolution rates. Recent investigations of mineral surface morphology and microtexture bring to light the need to understand how mineral surfaces change with dissolution [1–5]. In this study, the evolution of the surface roughness of laboratory-dissolved albite powders and plates is examined and quantified using BET adsorption and atomic force microscopy (AFM). Results from this study can be applied to help constrain assumptions made in the derivation and application of dissolution rate models.

Materials and Methods: Albite crystal and glass (prepared by melting crystalline albite) used in this study were prepared as powders and polished plates. Crystalline and glass albite were each ground in an agate mortar and pestle and sieved to collect powders of 75–150 µm. Powders were then

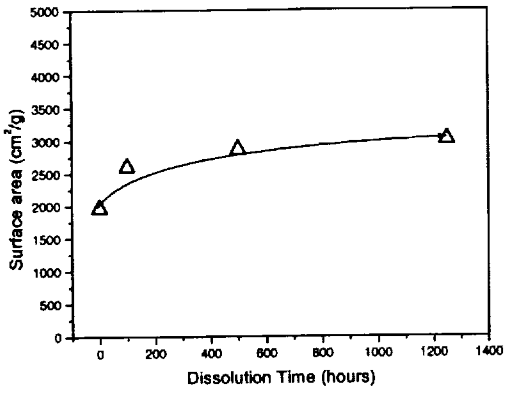

Fig. 1. Plot of specific surface area evolution of albite powders with time.

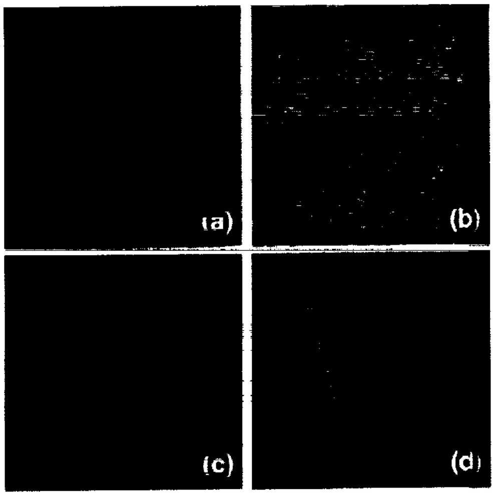

Fig. 2. (a) Representative AFM-height image of an unleached polished albite crystal plate. (b) Representative AFM-height image of an albite plate leached in a pH 2 solution for 5000 h. (c) Representative AFM-amplitude image of unleached powdered albite. (d) Representative AFM-amplitude image of powdered albite leached in a pH 2 solution for 1250 h. All figures have scales of 10 μm on the x-axis, y-axis scales of 10 μm, and z-axis scales of 50 nm.

dissolved in an HCl (pH 2) solution in batch reactors for various lengths of time. Solution chemistry was monitored throughout dissolution. Albite mineral and glass plates were cut and polished to 0.05 μm and dissolved in both static and flow reactors, at several values of pH for various lengths of time [6].

BET surface area was measured by adsorption of N gas with a Micromeritics ASAP 2000 surface area analyzer. Powdered and polished samples were imaged using a Digital Instrument Nanoscope IIIa Dimension 3100 AFM. Surface features were quantified by roughness, power spectral density, and fractal analyses.

Results: Surface area of powdered albite crystal increases by a factor of ~1.5 with dissolution in a pH 2 solution. Rate of increase in surface area is fast for the first 100 h, and then decreases with time (Fig. 1).

Similarly, the rate of increase in Si in solution is at first fast and then slows with time.

Atomic force microscopy imaging also reveals changing surface microtopography throughout dissolution on both polished and powder surfaces. Roughness, as imaged using AFM, increases rapidly from 0 to 1000 h, and then increases less rapidly between 1000 and 5000 h.

Discussion and Conclusions: Results from BET and AFM analysis suggest surface roughness and surface area increase over 5000 h for both albite glass and crystal. The rate of increase of surface topography decreases with time, similar to the rate of dissolution as measured by solution chemistry. These observations may imply that surface area does not reach a steady state, at least in most laboratory experiments. Changing surface area must presumably be taken into account when deriving a rate equation. If surface area does not obtain a steady state value, it may be incorrect to assume that dissolution reaches a true steady state.

References: [1] White A. F. and Peterson M. L. (1990) *ACS Symposium, 416,* 461–475. [2] Anbeek C. A. (1992) *GCA, 56,* 1461–1469. [3] Lee M. R. and Parsons I. (1995) *GCA, 59,* 4465–4488. [4] Hochella M. F. and Banfield J. F. (1995) *MSA Reviews, 31,* 353–401. [5] Brantley S. L. et al. (1999) *Surface Area,* in press. [6] Hamilton et al. (1999) *GCA,* submitted.

SOURCE DISCRIMINATION OF ATMOSPHERIC AEROSOLS AT ALERT, ARCTIC CANADA DURING 1994–1995 USING A YEAR-LONG RECORD OF LEAD-ISOTOPIC AND TRACE-ELEMENT DATA.

G. Mercier[1], C. Gariépy[1], L. A. Barrie[2], and A. Simonetti[1], [1]Centre de Recherche en Géochimie Isotopique et en Géochronologie, Université de Québec à Montréal, CP 8888 succ. Centreville, Montréal H3C 3P8, Canada, [2]Environment Canada, 4905 Dufferin Street, Toronto M3H 5T4, Canada.

The Alert meteorological station, located at ~82°N on Ellesmere Island, collects weekly samples of aerosols to provide information concerning the origin and atmospheric pathways of Arctic pollution. The latter is most pronounced during episodes of Arctic haze, which occur predominantly between December and April, when polluted air masses from Eurasia penetrate into the Arctic [1]. Samples of atmospheric aerosols from Alert, collected in 1983–1984, indeed yielded very uniform ^{206}Pb/^{207}Pb ratios for the period between November and May, averaging 1.160 ± 0.010 [2]. This signature is consistent with a model involving equal contributions of atmospheric constituents from Western Europe, Eastern Europe, and Asia [3].

Weekly samples (n = 51) were analyzed, covering the period from June 1994 to May 1995. Isotopic abundances of all stable Pb isotopes were determined by thermal ionization mass spectrometry (TIMS) after digestion (leaching) in 0.8 N HBr and conventional anion exchange chromatography. Complete digestion of residual materials (n = 3) yielded exactly the same Pb-isotopic compositions as the corresponding leachates. Elemental abundances were obtained on total samples using inductively coupled plasma mass spectrometry (ICP-MS) and instrumental neutron activation analysis (INAA).

On a seasonal basis, average aerosol Pb abundances are: summer $\ll$0.1 ng/m^3; fall ~0.5 ng/m^3; winter ~1.2 ng/m^3; and spring ~0.7 ng/m^3. The winter and spring Pb aerosol abundances are well correlated with concentrations of SO_4, Cu, and Zn [4], a feature characteristic of the Arctic haze phenomenon. However, this is not the case for samples collected in the fall.

Aerosol Al abundances, which is a proxy for the amount of natural (silicate) materials present in the atmosphere, are systematically low (typically 20–150 ng/m^3) with the following exception: half of the fall samples have Al contents >500 ng/m^3, and peaking to 2200 ng/m^3. These Al-rich samples have higher, but poorly correlated, levels of Pb, Cu, and Zn.

The summer aerosols have nearly identical isotopic compositions with ^{206}Pb/^{204}Pb, ^{208}Pb/^{204}Pb, and ^{206}Pb/^{207}Pb ratios averaging 18.17 ± 0.06, 38.09 ± 0.15, and 1.164 ± 0.003 respectively. The fall aerosols describe a well-defined positive correlation between their Al content and their Pb-isotopic ratios (r^2 >0.85). This can only represent mixing of an Al-poor (unradiogenic) end member and Al-rich component(s) with ^{206}Pb/^{204}Pb, ^{208}Pb/^{204}Pb, and ^{206}Pb/^{207}Pb ratios = 18.5, 38.5, and 1.19 respectively. The latter represent the minimum Pb-isotopic composition of the natural materials that are transported in the Arctic troposphere during the fall season.

The winter and spring aerosols display different relationships. Their isotopic ratios are negatively correlated with their Pb contents that represent mixing between two anthropogenic components. The most radiogenic end member (A) contains ^{206}Pb/^{204}Pb, ^{208}Pb/^{204}Pb, and ^{206}Pb/^{207}Pb ratios of ~18.1, ~38.1, and ~1.16 respectively. Component A is derived from sources in Asia and/or the former Soviet Union. At Barrow, Alaska, from February to March

1990, mean $^{206}Pb/^{207}Pb$ and $^{208}Pb/^{207}Pb$ values of 1.161 and 2.432 were reported [5], consistent with component A. The Pb-rich end member (B), has $^{206}Pb/^{204}Pb$, $^{208}Pb/^{204}Pb$, and $^{206}Pb/^{207}Pb$ ratios = 17.6, 37.5, and 1.14 respectively. This can only be attributed to atmospheric inputs from sources located in Western and/or Northwest Europe [3], where gasoline Pb additives have very unradiogenic signatures. Although uncertain, apportionment of Pb deposited at Alert is of the same order of magnitude from components A and B.

A weekly sample from early August 1994, with very low contents of both Al and heavy metals, yields a remarkably unradiogenic isotopic composition having $^{206}Pb/^{204}Pb$, $^{208}Pb/^{204}Pb$, and $^{206}Pb/^{207}Pb$ ratios of 16.94, 36.67, and 1.090 respectively. Back-trajectory calculations (925 mbar) for this period are consistent with these aerosols being mainly derived from anthropogenic sources located in the Siberian Plateau region [6]. The unradiogenic Pb-isotopic character suggests a Precambrian, nonferrous ore source.

Trace-element and Pb-isotopic data discriminate between three major sources of atmospheric aerosols reaching the Canadian high Arctic. These comprise: (1) A radiogenic "natural" end member that was preponderant during the month of September 1994; back-trajectory calculations suggest it originated from the Canadian Arctic Islands and the coastal areas of West Greenland. (2) Unradiogenic end member B originating from west and/or northwest Europe, well recognized in the late fall and winter samples. (3) Anthropogenic end member A, characterized by $^{206}Pb/^{207}Pb$ ratios of ~1.16 [2,5], originating from Asia and prominent during the late spring and early summer.

References: [1] Barrie (1986) *Atmos. Environ., 20,* 643–663. [2] Sturges and Barrie (1989) *Atmos. Environ., 23,* 2513–2519. [3] Hopper et al. (1991) *Tellus, 43B,* 45–60. [4] Sirois and Barrie (1999) *JGR, 104,* in press. [5] Sturges et al. (1993) *Atmos. Environ., 27a,* 2865–2871. [6] Hopper and Barrie (1988) *Tellus, 40B,* 446–462.

ANOMALOUS XENON IN THE PRECAMBRIAN NUCLEAR REACTOR IN OKELOBONDO (GABON): A POSSIBLE CONNECTION TO THE FISSION COMPONENT IN THE TERRESTRIAL ATMOSPHERE.

A. P. Meshik, K. Kehm, and C. M. Hohenberg, Campus Box 1105, McDonnell Center for the Space Sciences, Washington University, One Brookings Drive, Saint Louis MO 63130, USA (am@howdy.wustl.edu).

Introduction: Some chemically fractionated fission Xenon (CFF-Xe), whose isotopic composition is established by simultaneous decay and migration of radioactive fission products, is probably present in the Earth's lithosphere, a conclusion based on available Xe data from various crustal and mantle rocks [1]. Our recent isotopic analysis of Xe in alumophosphate from zone 13 of Okelobondo (southern extension of Oklo), along with the independent estimation of the isotopic composition of atmospheric fission Xe [2], supports the hypothesis that CFF-Xe was produced on a planetary scale.

Experimental: Using a microanalytical laser extraction technique [3], we measured Xe and Kr in various mineral phases in the 6 × 3 × 0.5-mm polished section of U ore from reactor Zone 13 in Okelobondo (southern extension of the Oklo deposit [4]). A Q-switched Nd-YAG laser focused through an optical microscope allowed us to locally degas some 8 ng of target material typically using 0.3-s bursts of 25 W at 500 Hz. Spatial resolution under these conditions was ~10 μm. Before Xe analysis the polished section was examined by scanning electron microscopy-energy dispersive X-ray spectrometry (SEM-EDX) to determine mineral composition.

Results: The isotopic composition of Xe in all U-rich phases was close ^{235}U neutron fission, as expected from a natural nuclear chain reaction. However, Xe with the CFF-isotopic pattern — enrichments in ^{132}Xe, ^{131}Xe, ^{129}Xe — was found in a U-free alumophosphate adjacent to the host U-phase. The average isotopic composition among nine individual alumophosphate inclusions corrected for air contamination (assuming no radiogenic ^{128}Xe) is the following: $^{136}Xe/^{134}Xe/^{132}Xe/^{131}Xe/^{130}Xe/^{129}Xe/^{128}Xe = 1/1.25/1.73/0.89/0.0045/0.274/0$. The concentration of CFF-Xe was determined to be on the order of 10^{-2} cm^3 STP/g, the highest Xe concentration ever measured in natural material. These results indicate that the alumophosphate is a carrier for CFF-Xe in the Okelobondo.

Implication: The theoretical fission Xe component in the Earth's atmosphere was estimated using multivariate correlation analysis applied to existing data on carbonaceous meteorites [2]. This inferred fission Xe composition is in good agreement with the earlier estimate [5]. Despite the large error bars on the inferred composition, the match with either ^{238}U, or ^{244}Pu is unsatisfactory, although the latter seems to be a better candidate (Fig. 1). Meanwhile CFF-Xe, as found in the Okelobondo alumophosphates, looks isotopically identical to the estimated atmospheric fission Xe composition [2,5] (Fig. 1).

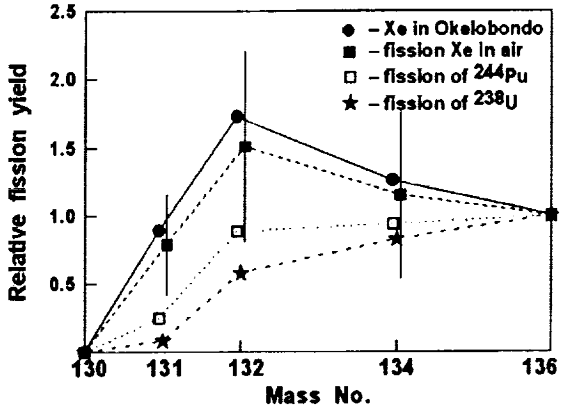

Fig. 1. The inferred isotopic composition of fission Xe in the Earth's atmosphere [2] is more similar to CFF-Xe [this work] than ^{238}U or ^{244}Pu.

To supply the total inventory of fission Xe in the Earth's atmosphere (8 × 10^{14} cm^3 STP), some 5 × 10^{10} tons of the Okelobondo alumophosphate has to be degassed. This requires that less than a thousandth of the total crustal U must have gone through a Precambrian reactor stage followed by the selective release of evolved CFF-Xe.

Conclusion: Mineral specific laser excavation of Xe from Okelobondo ore revealed that alumophosphate is a carrier of CFF-Xe. Its isotopic pattern suggests that it is present in the Earth's atmosphere. If indeed so, natural nuclear reactors must have been common during the Precambrian when the conditions for starting fission chain reaction were the most favorable.

Acknowledgments: This work was supported by NASA grant NAG5-4173.

References: [1] Meshik A. P. et al. (1997) *LPS XXVIII,* 943–944. [2] Igarashi G. (1995) *AIP Conf. Proc., 341,* 70–80. [3] Nichols R. H. Jr. et al. (1995) *Adv. Anal. Geochem., 2,* 119–140. [4] Sample provided by Dr. M. Pagel, CREGU, France. [5] Takaoka N. (1972) *Mass spectrometry, 20(4),* 287–302.

H_2O CHARACTERISTICS OF MANTLE END MEMBERS: EVIDENCE FROM MID-OCEAN-RIDGE BASALTS AND OCEAN ISLAND BASALTS.

P. J. Michael, Department of Geosciences, University of Tulsa, 600 S. College Avenue, Tulsa OK 74104, USA (pjm@utulsa.edu).

Introduction: The identification and characterization of chemical mantle components has contributed a great deal to the understanding of Earth history and dynamics. HIMU, EMI, EMII, and DMM are components that have been defined on the basis of isotopes [1] and trace elements [2] in ocean island basalts (OIB), and mid-ocean-ridge basalts (MORB). Other components, e.g., "C" [3] are internal to the isotopic array defined by the others. The origin of these mantle components has been attributed to processes such as depletion through crustal generation (DMM); subduction and recycling into the mantle of oceanic crust (HIMU), sometimes with pelagic sediments (EMII) or terrigenous sediments (EMI) [1]; the delamination and recycling of subcontinental lithosphere (EMI) [4] and mantle metasomatism by small degree melts [5]. The concentration of H_2O in enriched mantle components provides further evidence about their origins. To factor out effects of partial melting and fractional crystallization, the ratio of H_2O to incompatible elements is

TABLE 1.

Sample Suite	Component	H_2O/Ce
Ocean island basalts		
Galapagos platform	HIMU or C	180
Loihi [6]	plume	170
Loihi [6]	lithospheric	220
Loihi [6]	Koolau	160
Mid-ocean ridge basalts		
Northeast Pacific [8]	No-EM	170
MAR 33°S [8]	HIMU + EM	200
MAR 35°–39°S (Tristan)	Strong EM	200
Easter [8,9]	HIMU or no-EM	210

examined. In MORB, H_2O/Ce ratios are most constant, so this ratio is discussed below.

Samples: Submarine tholeiitic glasses from the Galapagos platform (this study) and from Loihi [6] preserve their magmatic H_2O contents and can be used to describe enriched mantle sources. But most of the OIB glasses we analyzed have lost H_2O by degassing and do not preserve information about their mantle sources. This includes the deeply erupted submarine basalts from Tristan da Cunha, Pitcairn Island (EMI), Society Islands (EMII) and Easter Island (HIMU). The best evidence for EM plumes therefore comes from EMORB that are associated with these hotspots, and whose isotopic and trace-element compositions form mixing arrays toward those distinctive mantle components. Additional insights are provided by E-MORB from the northeast Pacific that fall on the "No-EM array" [7].

Results: The most important finding is that there are not large differences in H_2O/Ce between diverse mantle enriched components. There are no correlations between H_2O/Ce and indicators such as Ba/Nb or $^{87}Sr/^{86}Sr$.

Discussion: The lack of significant correlation between H_2O/Ce and ratios that characterize the EM components suggests that whatever material that carries the EM-isotopic and trace-element signature either has such a small volume that it does not influence the H_2O/Ce ratios, or that it has the same H_2O/Ce as the other mantle components such as HIMU and no-EM.

Crustal recycling. The observations are consistent with proposals based on isotopes and incompatible elements in which HIMU is related to subducted oceanic crust, while the EM signature is created by subducted oceanic crust plus a few percent sediments [10]. In this case, the quantity of sediments is not sufficient to strongly influence H_2O content of recycled material and suggests that sediments play only a minor role compared to altered oceanic crust in any return flux of H_2O to the deep mantle.

Variations in H_2O/Ce associated with different mantle components are smaller than regional variations. H_2O/Ce is ~260 in E-MORB from the MAR north of 35°N [8]. If crustal recycling accounts the trace element and isotopic characteristics of OIBs, then regionally high H_2O/Ce may be associated with rapidly subducted materials in which hydrous phases were preserved. No correlations have been found between H_2O and other trace element and isotopic parameters because H_2O is controlled by the altered oceanic crust while most other distinctive ratios (e.g., Ba/Nb) are related to sediment subduction. High H_2O/Ce may also be associated with plume heads, as they are found at Ontong Java plateau [11].

Mantle metasomatism. It has also been proposed that OIB sources are created by mantle metasomatism and the creation of small degree partial melts in equilibrium with trace residual phases [5]. In this case, the limited range of H_2O/Ce ratios might reflect the nature and stability of these trace phases during small extents of melting.

References: [1] Zindler A. and Hart S. R. (1986) *Annu. Rev. Earth Planet. Sci., 14,* 493–571. [2] Weaver B. L. (1991) *Geology, 19,* 123–126. [3] Hanan B. B. and Graham D. W. (1996) *Science, 272,* 991–995. [4] McKenzie D. and O'Nions R. K. (1983) *Nature, 301,* 229–231. [5] Halliday A. N. et al. (1995) *EPSL, 133,* 379–395. [6] Dixon J. E. and Clague D. A. (1998) *Eos Trans. AGU, 79,* F939. [7] Hart S. R. (1988) *EPSL, 90,* 273–296. [8] Michael P. J. (1995) *EPSL, 131,* 301–320. [9] Dixon J. E. et al. (1998) *Eos Trans. AGU, 78,* F688. [10] Chauvel C. et al. (1992) *EPSL, 110,* 99–119. [11] Michael (1999) *EPSL,* in preparation.

EXPERIMENTAL STUDY OF CASSITERITE SOLUBILITY IN HYDROGEN-CHLORIDE-BEARING WATER VAPOR.

A. A. Migdisov and A. E. Williams-Jones, Department of Earth and Planetary Sciences, McGill University, Montréal, Québec H3A 2A7, Canada (artas@eps.mcgill.ca).

Introduction: Boiling is a common feature of hydrothermal systems, and is an important factor in the formation of metallic mineral deposits due to preferential fractionation of components between liquid and vapor. Most researchers have assumed that the metals are concentrated primarily in the liquid phase and that the role of boiling is to saturate this phase with ore minerals by removing volatile components. However, a number of studies have suggested that the vapor phase may dissolve appreciable concentrations of metals. Our particular interest is Sn for which concentrations as high as 2.5 ppm were reported by Gemmel [1] and Ouisefit et al. [2] from analyses of condensates collected from Momotombo volcano, Nicaragua. In particular, we would like to understand the factors controlling the solubility of Sn in the vapor phase. Given that cassiterite is the main ore mineral of Sn, it is reasonable to expect that its properties will determine tin speciation and solubility in the vapor phase. Based on theoretical considerations, we can predict that cassiterite will dissolve mainly as chloride and hydroxy/oxide species. The goal of this study was to obtain thermodynamic information on soluble stannous chloride and hydroxy/oxide species in water vapor at temperatures up to 360°C and pressures up to 200 bar.

Experimental Method: Experiments were carried out at temperatures between 300° and 360°C. The vertical temperature gradient in the furnace during a run was typically in the range 1.0°–2.5°C/m. Temperature during runs was measured with two chromel-alumel thermocouples, located at the top and bottom of the furnace.

The experiments were performed in Ti autoclaves, and involved measuring the solubility of synthetic cassiterite in HCl-bearing water vapor. Autoclaves were loaded with preweighed quartz ampoules containing single crystals of SnO_2. The ampoule was suspended near the top of the autoclave using a quartz needle. A known mass of HCl solution was placed in the bottom of the autoclave in order to prevent contact of solid SnO_2 with liquid H_2O. The HCl was added in quantities that yielded solutions with pH values of 1.5–4.0. Care was taken to ensure that the mass of water introduced into the autoclavedid not saturate the system with liquid at the experimental conditions, and that SnO_2 dissolution was restricted to the vapor. The total pressure in a run was assumed to that of pure water vapor. The redox potential of the system was buffered by a MoO_2/MoO_3 oxides mixture. After a run, the autoclave was air-cooled down to room temperature, and the condensates was sampled. SnO_2 condensed on the walls of the autoclave was dissolved using 5–7 mL of HCl (pH = 0.5). The concentrations of dissolved Sn in the condensates and washing solutions were determined by inductively coupled plasma mass spectrometry (ICP-MS).

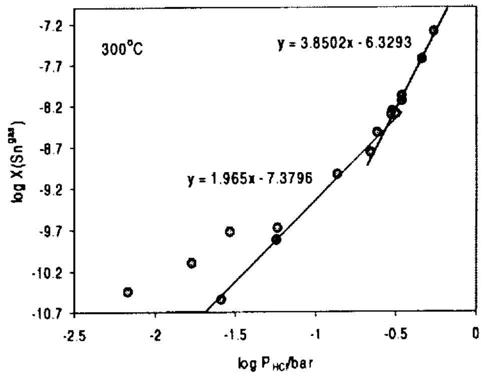

Fig. 1.

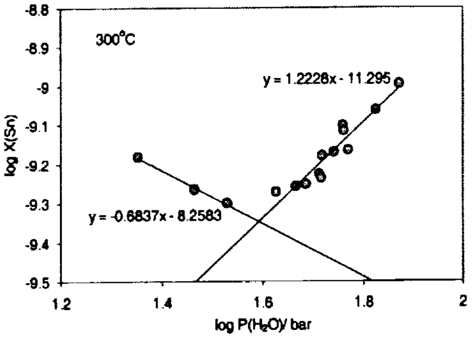

Fig. 2.

Preliminary Results: The concentration of Sn in water vapor varied with the partial pressure of HCl at 300°C and constant $P(H_2O)$ as illustrated in Fig. 1. Figure 2 shows the dependence of Sn solubility with $P(H_2O)$ at constant P(HCl) and 300°C.

Based on these preliminary data we conclude that Sn occurs in two main gaseous forms, $SnCl_2$ and $SnCl_4$. The calculated partial pressures of stannous chloride are several orders of magnitude higher, than those for the water-free system. We propose that stannous chlorides dissolve in water vapor in the form of the hydrated species $SnCl_2(H_2O)_4$ and $SnCl_4(H_2O)_2$.

References: [1] Gemmel B. J. (1987) *J. Volcanol. Geotherm. Res., 33,* 161–181. [2] Quisefit J. P. et al. (1989) *GCA, 53,* 2591–2608. [3] Menyailov I. A. and Nikitina L. P. (1980) *Bull. Volcanol., 43(1),* 197–205.

THE MASS-DEPENDENT OXYGEN-ISOTOPIC FRACTIONATION LINE: NEW MEASUREMENTS AND THE NEED FOR A REPORTING CONSENSUS.

M. F. Miller, I. A. Franchi, and C. T. Pillinger, Planetary Sciences Research Institute, The Open University, Walton Hall, Milton Keynes MK7 6AA, UK (m.f.miller@open.ac.uk).

Introduction: With notable exceptions in the fields of meteoritics and stratospheric chemistry, $^{17}O/^{16}O$ and $^{18}O/^{16}O$ fractionation factors generally follow a mass-dependent relationship given by

$$({}^{17}R_s/{}^{17}R_r) = ({}^{18}R_s/{}^{18}R_r)^{\lambda}$$

where ${}^{x}R$ is ${}^{x}O/{}^{16}O$, s and r represent sample and reference, respectively, and λ ~0.5 [1,2]. In terms of the δ notation

$$\ln(1 + 10^{-3}\ \delta^{17}O) = \lambda\ \ln(1 + 10^{-3}\ \delta^{18}O)$$

where the respective δ values are not large, and using the fact that $\ln(1 + x) \approx x$ for $x \ll 1$, this expression is usually approximated to

$$\delta^{17}O = \lambda'\delta^{18}O$$

Here we distinguish the proportionality constant λ' from the exponent λ, although much of the literature overlooks this distinction. Theoretical considerations suggest that the value of λ varies for different compounds and processes, ranging from 0.50 to ~0.53 [3,4]. An early empirical measurement of λ' [3], involving 35 terrestrial samples (various waters and rocks) gave a value of 0.5164 ± 0.0033 (standard error). This result, rounded to two decimal places, has since provided the baseline for quantifying O-isotopic heterogeneities preserved in primitive meteorites [5–7]. Departures from the mass-dependent fractionation line are thence recorded as $\Delta^{17}O$, defined as $\delta^{17}O - 0.52\ \delta^{17}O$ [8]. More recent measurements [9], comparing λ' as determined from Precambrian and modern cherts, together with mantle-derived lavas, suggested that, by 3.5 Ga, the Earth was essentially homogenous with regard to O isotopes. A major objective of the present work was to investigate whether, with significantly improved $\delta^{17}O$ measurement precision compared to earlier studies, it was possible to further reduce the scatter in the terrestrial fractionation line and thus obtain a better definition of the $\delta^{17}O$-$\delta^{18}O$ relationship.

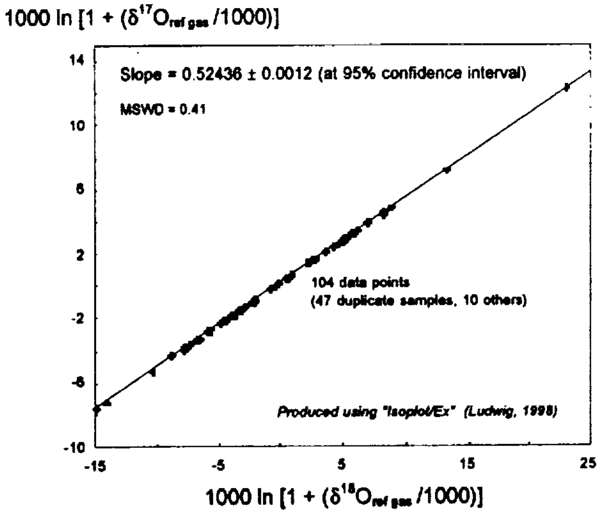

Fig. 1. Mass-dependent fractionation line, based on the "exact" relationship between $\delta^{17}O$ and $\delta^{18}O$.

Experimental: $\delta^{17}O$ and $\delta^{18}O$ measurements were made of 57 well-characterized whole-rock and mineral specimens (mostly in duplicate), spanning a $\delta^{18}O_{SMOW}$ range of 37.8‰. Basalts, mantle xenoliths, metamorphosed igneous rocks, and metasediments were included in the study and spanned an age range of ~2.5 Ga. Infrared laser-assisted fluorination using BrF_5 was used to release the O_2, with isotopic data provided by high-resolution isotope ratio mass spectrometry (IRMS). Respective 1σ precisions of individual $\delta^{17}O$ and $\delta^{18}O$ measurements for the complete analytical procedure were typically 0.08 and 0.04‰; full details are given in [10].

Results and Discussion: Data regression by the York algorithm [11], using the "exact" $\delta^{17}O$-$\delta^{18}O$ relationship, is shown in Fig. 1; Isoplot/Ex [12] was used for this purpose. The precision significantly exceeds those reported in earlier, comparable investigations and supports the view that a single reference line adequately describes the relationship between $\delta^{17}O$ and $\delta^{18}O$ in terrestrial silicate rocks, regardless of age or composition. Surprisingly good agreement was obtained between λ and λ' values; the latter was 0.52457 ± 0.0012 (95% confidence level). However, our experience shows that this is not always the case. Furthermore, unlike λ, λ' is not invariant to the isotopic composition of the reference gas. For consistency, we endorse the recommendation [13] that the "exact" expression for the fractionation line be adopted for reporting in future.

References: [1] Craig H. (1954) *J. Geol., 62,* 115–118. [2] Craig H. (1957) *GCA, 12,* 133–149. [3] Matsuhisa Y. et al. (1978) *GCA, 42,* 173–182. [4] Thiemens M. H. (1999) *Science, 283,* 341–345. [5] Clayton R. N. et al. (1973) *Science, 182,* 485–488. [6] Clayton R. N. (1993) *Annu. Rev. Earth Planet. Sci., 21,* 115–149. [7] Clayton R. N. and Mayeda T. K. (1993) *GCA, 60,* 1999–2017. [8] Clayton R. N. and Mayeda T. K. (1988) *GCA, 52,* 1313–1318. [9] Robert F. et al. (1992) *EPSL, 108,* 1–9. [10] Miller M. F. et al. (1999) *Rapid. Comm. Mass. Spectrom.,* in press. [11] York D. (1969) *EPSL, 108,* 1–9. [12] Ludwig K. R. (1998) *Berkeley Geochron. Center Spec. Publ. 1.* [13] Meijer H. A. J. and Li W. J. (1998) *Isotopes Environ. Health Stud., 34,* 349–369.

THE RIVERINE DISCHARGE OF BLACK CARBON INTO COASTAL SEDIMENTS OF THE GULF OF MEXICO.

S. Mitra[1], T. S. Bianchi[1], and B. A. McKee[2], [1]Institute for Earth and Ecosystem Sciences, Department of Ecology, Evolution, and Organismal Biology, 310 Dinwiddie Hall, Tulane University, New Orleans LA 70118, USA (smitra@

mailhost.tcs.tulane.edu; tbianch@mailhost.tcs.tulane.edu), [2]Institute for Earth and Ecosystem Sciences, Department of Ecology, Evolution, and Organismal Biology, 310 Dinwiddie Hall, Tulane University, New Orleans LA 70118, USA, [2]Institute for Earth and Ecosystem Sciences, Department of Geology, 120 Dinwiddie Hall, Tulane University, New Orleans LA 70118, USA.

Black carbon (BC) concentrations in water column particulates (>0.7 μm) and sediments were quantified in the Mississippi River and Gulf of Mexico (GOM) using the recently verified 375° thermal oxidation method. Concentrations of BC for a select set of samples from surface and bottom waters of the Mississippi River indicated higher concentrations of BC in bottom water particulates relative to surface water particulates. Black carbon concentrations in suspended particles in the river ranged from ~0.03 to 1 mg BC/L. This represented ~0.5–35% of the total organic carbon (TOC) for riverine water column particles. Similarly, concentrations of BC in surface and bottom water suspended particles from the GOM inner shelf ranged from 0 to 0.1 mg BC/L representing as much as 60% of the TOC in particulates from the inner shelf. Surface sediment concentrations of BC throughout the deposition zones in the lower Mississippi River and GOM in our samples ranged from 3% to 20% of the sedimentary TOC; generally lower in BC/TOC relative to bottom water particulates. Taken together, these preliminary results indicate that BC aerosols are likely associated with the operationally defined "dissolved" phase in surface waters and possibly through aggregation, represent a greater fraction of particulate C at depth. Following deposition into the seabed, this refractory pool of C is then diluted with other pools ("old" and "new") of C.

RARE-EARTH-ELEMENT AND STRONTIUM-ISOTOPIC STUDY OF THE MIDDLE PERMIAN LIMESTONE-DOLOSTONE SEQUENCE IN KUZUU AREA, CENTRAL JAPAN.

N. Miura[1], Y. Asahara, and I. Kawabe, [1]Department of Earth and Planetary Sciences, Graduate School of Science, Nagoya University, Chikusa, Nagoya 464-8602, Japan (miura@gcl.eps.nagoya-u.ac.jp).

Introduction: The Kuzuu limestone-dolostone complex, in central Japan, is a remnant of a middle Permian carbonate succession [1,2] formed on a basaltic seamount in an open-sea realm without inputs of terrigenous materials. Hence they are geologically similar to the Tertiary to Holocene atoll carbonate sequences in the Pacific, not to the continental platform-type carbonate sequences. Their rare-earth-element (REE) and Sr-isotopic data are clues to understanding the diagenetic process of biogenic carbonates to crystalline carbonate minerals. We will focus our attention on how seawater REE and Sr-isotopic signatures in middle Permian are retained in the carbonate rocks and how REE and Sr-isotopic features are different between the limestones and dolostones.

Samples and Analytical Methods: The carbonate rocks of Nabeyama Formation were sampled in the Yoshizawa Mine in Kuzuu. This formation consists of the lower Limestone, the middle Dolostone and the upper Limestone members [1]. Three samples are from the lower Limestone, five samples from the Middle Dolostone and four samples from the upper Limestone.

All REEs including Y, major and minor elements of those samples have been determined for HCl-soluble parts. Rare-earth-elements and Y were separated from matrix elements by the method of coprecipitation with Fe hydroxide and cation-exchange chromatography, and measured by inductively coupled plasma atomic emission spectrometry (ICP-AES).

For determining ^{87}Sr/^{86} isotopic ratio of each bulk sample, HCl-soluble part of Sr was purified by a cation-exchange resin column, and determined their Sr-isotopic ratios by thermal ionization mass spectrometry (TIMS). In order to determine the Sr-isotopic ratios of calcite and dolomite in each dolostone sample, it was leached with acetic acid. The Sr fractions in leachate and residue represent those of calcite and dolomite, respectively, for each dolostone sample.

Results and Discussion: The ^{87}Sr/^{86}Sr ratios of bulk carbonate samples are 0.7073–0.7076, and their Sr-isotopic stratigraphic age (260 ± 5 Ma) coincides with their fusulinid fossil age (263 ± 8 Ma).

The carbonate rocks have much higher REE/Ca ratios than modern biogenic carbonates [3] by factors of 10^2–10^4. The chondrite-normalized REE patterns for the Kuzuu samples show large negative Ce anomalies, together with seawater-like tetrad effects and high Y/Ho ratios. Their Ce anomalies are comparable to those of present-day ocean waters at depths of 600–800 m, except for the bottom part samples polluted with Fe(III) oxyhydroxide possibly by fluids derived from underlying basaltic volcanics. Their REE patterns normalized by shallow Pacific water [4] exhibit smooth light REE enrichment trends similar to the experimental partitioning coefficients of REE between calcite-overgrowths and seawater solutions [5]. There is no significant difference in REE and Y features between limestones and dolostones.

The original biogenic carbonates deposited on a basaltic seamount in shallow water environment, but subsequently they were subsided to the water depths suggested by their Ce anomalies. At the water depths, the biogenic carbonates were recrystallized to calcite under a condition of sufficient supply of the seawater, and the seawater REE and Y were incorporated into calcite.

The ^{87}Sr/^{86}Sr ratios of dolomite, however, are slightly lower than those of coexistent calcite by 0.0002, which is a time interval of ~2 Ma by the seawater ^{87}Sr/^{86}Sr curve [6] for Middle to Late Permian. The dolomitization therefore occurred almost immediately after the recrystallization of biogenic carbonate to calcite in a relatively deep water, and did not alter the REE and Y features of limestone precursors. This is consistent with the recent diagenetic model for the carbonate sequences of Neogene atolls in the Pacific [7] emphasizing the role of thermal convection of moderately deep water.

References: [1] Matsuda H. and Iijima A. (1989) *J. Fac. Sci. Univ. Tokyo Section, 22,* 89–119. [2] Kobayashi F. (1979) *J. Geol. Soc. Japan, 85,* 627–642. [3] Sholkovitz E. and Shen G. T. (1995) *GCA, 59,* 2749–2756. [4] Piepgras D. and Jacobsen S. B. (1992) *GCA, 56,* 1851–1862. [5] Zhong S. and Mucci A. (1995) *GCA, 59,* 443–453. [6] Denison R. E. et al. (1994) *Chem. J., 112,* 145–167. [7] Aharon P. et al. (1987) *Geology, 95,* 187–203.

GEOCHRONOLOGICAL STUDIES OF THE OLDEST KNOWN MARINE SEDIMENTS.

S. J. Mojzsis[1] and T. M. Harrison[1,2], [1]Department of Earth and Space Sciences, Institute for Geophysics and Planetary Physics, Center for Astrobiology, University of California, Los Angeles, Los Angeles CA 90095-1567, USA, [2]Institute for Geophysics and Planetary Physics, University of California, Los Angeles, Los Angeles CA 90095-1567, USA (sjm@argon.ess.ucla.edu).

Introduction: The oldest known marine sediment [1], which also contains the oldest evidence of biological processes active during time of deposition [1,2], is a 5-m-thick layer of banded iron formation (BIF) with thin layers of Fe-rich silicates and magnetite contained within a body of metamorphosed mafic and komatiitic rocks. The BIF is found on the southern tip of the Akilia Island, southern West Greenland. An intrusive sheet of granodioritic orthogneiss that cross-cuts the supracrustal package containing the BIF yields U-Pb zircon ages that are interpreted as indicating an age of crystallization of the magmatic protolith at 3850 Ma [2]. If this interpretation is correct, then the BIF is at least as old as 3850 Ma, or several tens of millions of years older than the oldest dated rocks in the Isua supracrustal belt (ISB), some 150 km to the northeast [3].

Age of Banded Iron Formations: Direct information regarding the depositional ages of the BIFs and other metamorphosed sedimentary rocks (e.g., quartzites, metapelites) can perhaps be established by searching for zircons incorporated in the accumulating sediments from nearby volcanism, and/or detrital zircons from weathering subaerial landmasses. Some units of the BIF and quartzite of the ~3700–3800-Ma ISB are found to contain rare ~3710-Ma zircons associated with both intermediate and felsic volcanogenic sediments with ages determined separately as 3708 ± 3 Ma [2,3]. The eastern ISB contains abundant BIF and quartzites that contain rare zircons with an age range of 3690–3700 Ma (A. Nutman, pers. comm.). Such zircons may represent low-level contamination from volcanic inputs, which would establish the time of deposition of these sediments at ~3700 Ma. Previous mineral separation work done on ~2 kg of BIF from Akilia island [2] yielded rare zircons with ^{207}Pb/^{206}Pb ages between ~2700 and 2590 Ma. It was proposed that these zircons formed during one or more episodes of late Archean high-grade metamorphism. However, earlier metamorphic events of similar intensity such as at ~3650 Ma [2–4] should have likewise resulted in the formation of metamorphic zircons. Zircons from earlier stages of growth might be ex-

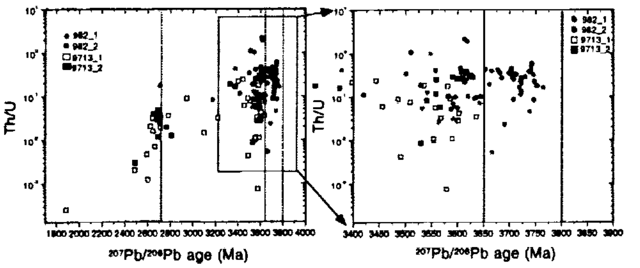

Fig. 1. [Thorium/uranium] of orthogneiss zircons 98/2 and BIF 97/13 multiple measurements and their relationship to the metamorphic history of the Akilia district.

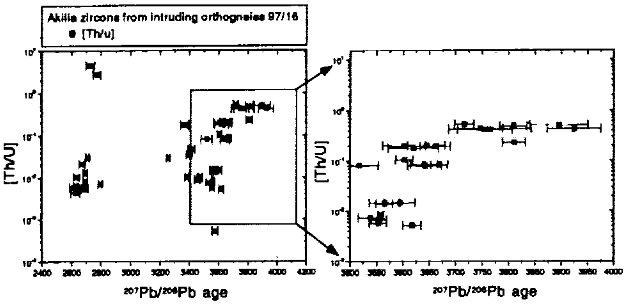

Fig. 2. [Thorium/uranium] relationships of orthogneiss zircons 97/16 and their relationship to the metamorphic hisotry of the Akilia district.

pected to survive later overprinting and serve as nuclei for further metamorphic zircon growth.

To test this hypothesis, we have separated zircon from sample 97/13 BIF from Akilia Island and performed U-Pb geochronology (Fig. 1) to establish the sequences of events that would have led to their formation. The chemical compositions of these BIF zircons are different from the igneous cores of older grains found in geochronological studies we have undertaken of the crosscutting orthogneiss 97/16 (see Fig. 2) but do follow the pattern of decreasing Th/U ratios with later growth stages in all samples.

Discussion: Suggestions that the >3650-Ma zircons reflect xenocryst contamination are challenged by (1) the lack of a recognized source of such ancient material, and (2) the highly zircon undersaturated nature of the granodioritic melts that produced the protolith of orthogneisses. Nonetheless, we recognize the possibility that zircon contamination occurring late in the crystallization history might be preserved. To assess this scenario, we are investigating the relationship between zircon age and petrologic context by *in situ* high-resolution ion microprobe U-Pb measurements of zircons identified in thin sections. We are performing full characterization using cathodoluminescence imagery of mineral structures, relict cores, and overgrowths in zircon. Zircons included in early crystallization phases from granodiorites are expected to be reliable indicators of formational age. We suggest that these studies could be used to resolve the origin of the very old grains as either primary magmatic "survivors," inherited "hitchhikers," or metamorphic "parasites."

References: [1] Mojzsis S. J. et al. (1996) *Nature, 384,* 55–59. [2] Nutman et al. (1997) *GCA, 16,* 2475–2484. [3] Nutman et al. (1996) *Precambrian Res., 78,* 1–39. [4] Kambe S. A. and Moorbath S. (1998) *Chem. Geol., 150,* 19–41.

GEOCHEMISTRY OF THE THERMAL WATERS AND ASSOCIATED TRACE ELEMENTS IN FALCON STATE, VENEZUELA.

R. L. Montero[1], M. Martínez, W. G. Meléndez, and G. Garbán, [1]Centro de Geoqu Mica, Instituto de Ciencias de la Tierra, Facultad de Ciencias, Universidad Central de Venezuela, Caracas 1010A, DF AP3895, Venezuela.

The Venezuelan thermal manifestations are wide, mainly associated with fault zones. Within the manifestations, the most spectacular are found on the Falcón basin. This area is geologically characterized by formations derived from marine environments, whose deposits are of Eocene until Quaternary Age, with a complex structural and tectonic history. These structures promote the percolation of the spring thermal waters. The most widely utilization of these waters in our country, it has been directed related with medicinal purposes. However, it does not exist relevant geochemical information, allowing to deduce processes involved during the water-local rocks. This work is a contribution at the knowledge and comprehension of this process in the Falcón basin.

Thermal waters from eight Falcón localities were sampled. Simultaneously, the parameters pH, conductivity and temperature were measured. At the laboratory, water samples were analyzed for major, and minor chemical species: Na^+, K^+, Ca^{2+}, Mg^{2+}, Sr^{2+}, F^-, Cl^-, SO_4^{2-}, HCO_3^-, and SiO_2; and the trace elements Al, Ba, Fe, Mn, Ni, Cu, and Zn.

The temperature in the collected waters oscillate among 30° and 36°C, while the conductivity shows values between 1239 and 7730 µS/cm; pH varies among 6.84 and 8.23. The major is Na^+, with concentration values oscillating between 164.0 and 1964.4 mg/L; followed by Ca^{2+}, between 2.3 and 175.2 mg/L Mg^{2+} content in studied waters show a range of 0.6–22.2 mg/L; and the K^+ is between 2.7 and 21.8 mg/L. On the other hand, the predominant anion is HCO_3^-, whose values varies between 436 and 4527 mg/L; followed by $SO_4^=$, oscillating between 1 and 101 mg/L; the Cl^- varies from 4.0 until 940.0 mg/L; and the F^- is among 1.1 and 6.6 mg/L, while SiO_2 content show concentration values between 15.7 and 29.8 mg/L.

The obtained results indicate that of eight thermal water samples, seven are of the type HCO_3^--Na^+ and one is $SO_4^=$-Na^+-Ca^{2+}. The results strongly suggest that the calcite, gypsum, pyrite, and dolomite dissolution, including some ferruginous sections, derived from a few geological beds, leached by such waters govern the chemical composition of these waters. In this way, the ferruginous and calcareous sections are controlling the presence of the Sr, Al, Ba, Fe, Mn, Ni, Cu, and Zn. Other processes controlling the chemical composition of these waters are the ionic exchange, and the precipitation of calcite and alunite in some thermal springs. It is suggested a contribution of mixed meteoric and connate marine origin, for the thermal waters studied.

NOBLE GAS CONSTRAINTS ON DEGASSING PROCESSES.

M. M. Moreira[1] and P. Sarda[2], [1]Woods Hole Oceanographic Institution, Woods Hole MA 02543, USA (mmoreira@whoi.edu), [2]Groupe de Géochimie des Gaz Rares, Departement Sciences de la Terre et U.M.R., Orsayterre, Université Paris 11-Sud, 91405 Orsay Cedex, France.

The upper-mantle source of mid-ocean-ridge basalts (MORB) is relatively degassed and its He-isotopic signature results from the radiogenic production of ^4He in a high (U + Th)/^3He material. The "primordial" He-isotopic signatures of some OIBs are interpreted as due to the existence of a less degassed reservoir, probably located in the lower mantle. In this simple model of mantle structure, there are two problems: why the plume samples have much lower He concentration than the MORB samples (a factor 100)? What is the Xe-isotopic composition of this plume source mantle? This last question is very important to understand terrestrial degassing history and the flux from the lower mantle to the upper mantle. In order to constain these problems, we have compared the rare gas elemental ratios in glass samples of MORB and primitive plumes to model estimates of the same ratios for upper and lower mantle reservoirs. The combined use of He, Ne, and Ar elemental systematics allows differentiation between the degassing process at mantle plumes, which appears to be controlled by distillation, and at normal mid-oceanic ridges, where vesiculation occurs at equilibrium, followed by degassing of the magma chamber (Fig. 1).

The consequences for plume elemental and isotopic composition of noble gases of such a distillation process are as follows: (1) The He is not very degassed by such a process (<10%); and (2) the Xe is completely lost, even if only 5% of the He is lost. This explains why Xe-isotopic anomalies are not observed in plume basalts. The question of the He content of plume source still exists. We propose that the He is diluted in degassed magma chambers to explain the relatively low He content of plumes.

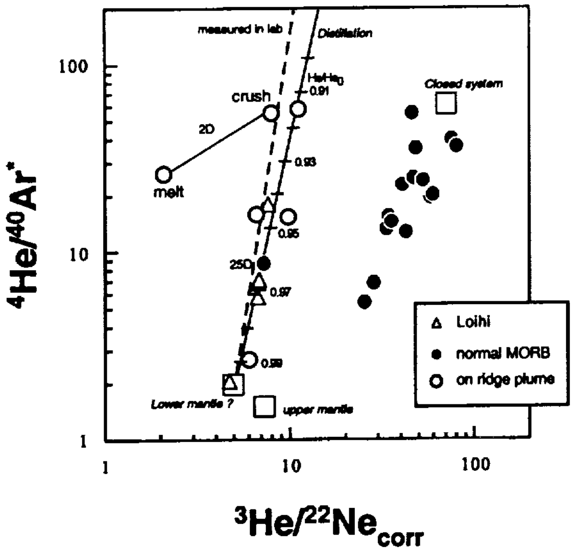

Fig. 1. Helium-4/argon-40* vs. $^3He/^{22}Ne$ corrected for atmospheric contamination, using a solar $^{20}Ne/^{22}Ne$. This diagram shows that the vesiculation at plume context is in open system degassing whereas the vesiculation at ridges is in closed system vesiculation.

The physical process responsible for the distillation occurring in the plume context is actually not clear. It can be due to melt-gas separation during magma percolation through the lithosphere or the crust, due to the high surface tension of the bubbles.

These results show that Xe anomalies should not be found in plume basalts and that He is not lost during the distillation process due to its high solubility in magma.

KINETICS OF ^{40}Ar, H_2O, H_2 RELEASE DURING GLAUCONITE HYDROTHERMAL TRANSFORMATION.

I. M. Morozova, A. V. Maslenikov, and L. K. Levskiy, Institute of Precambrian Geology and Geochronology, Russian Academy of Sciences, Makarova emb., 2, 199034, St. Petersburg, Russia (lev@ad.iggp.ras.spb.ru).

Excess radiogenic Ar was found in the products of glauconite hydrothermal alterations at P_{H_2O} = 1–2 kbar, T = 400°–600°C, run duration 3–14 d. The newly formed minerals were biotite and potassic feldspar. Isotopic analysis of run products proved that the excess Ar was not captured from the fluid but directly inherited by newly phases from the original mineral during solid-state to potactic transformation without complete dissolution in fluid. The resultant inheritance shows variations in radiogenic Ar ranging up to 70% of its content in starting sample and is independent on bulk composition, Al-content in the octahedral layer and phase relations of run products.

Kinetics of ^{40}Ar, H_2O, and H_2 release have revealed some factors favor the Ar inheritance. The low temperature of transformation and simultaneity the processes of dehydroxylization and transformation restrict Ar diffusive loss and explains the greater inheritance in Fe-bearing glauconites. But the main factor determining the inheritance is the rate of Fe^{+3} to Fe^{+2} reduction in autoclave. The emergence of H in the volatile at the expense of Fe^{+2} to Fe^{+3} in the octahedral layer of newly formed biotite is a tracer of reduction intensity. In the case of reduction occurring prior to glauconite transformation the portion of inherited Ar is small (not more than 15%). This results from the fact that replacement of a larger newly formed ion Fe^{+2} into biotite transposition is being accompanied by the rapture of bonds in the anion framework thus removing radiogenic Ar. The inherited Ar content is maximum (70%) for the samples showing no H in pyrolise of run products under conditions of complete transformation of original glauconite.

Kinetics of Fe^{+3} reduction is defined by different energetic state of glauconite lattice. More precisely it depends on octahedral Fe-bearing layer perfection. The most reactive will be samples showing a disturbed anion framework that might have derived from a partial postcrystallization dehydration resulting in the decrease in Fe coordination relative O in the octahedral layer. Thus rate of Fe^{+3} reduction in glauconite is assumed to be a criterion of its lattice perfectness and hence of openness degree of isotope system. However, taken into account are to be reversibility of oxidization-reduction reaction and its possible repeated realization in the nature so that any reliable criteria are to be obtained only through investigation of radiogenic isotope migration pattern under different P-T-X-conditions, and this migrations known to be essentially irreversible process.

URANIUM-LEAD ZIRCON SYSTEM DURING THE ALKALINE METASOMATISM: NATURAL AND EXPERIMENTAL MODELING.

I. M. Morozova, N. G. Rizvanova, and L. K. Levskiy, Institute of Precambrian Geology and Geochronology, Russian Academy of Sciences, Makarova emb. 2, 199034 St. Petersburg, Russia (lev@ad.iggp.ras.spb.ru).

1. The behavior of U-Pb zircon system in the alkaline metasomatism zone (contact of "Ozernaya Varaka" alkaline-ultrabasic intrusion with Belomorian gneisses) is verified by reference to the result of experimental modeling of the process with 2M Na_2CO_3-solution at P = 1 and 5 kbar, T = 200°–800°C.

2. Naturally occurring processes and experimental data suggest that carbonate fluids result in considerable, however, varying influence on U-Pb zircon system mobility with migration of both Pb and U.

3. Experimental modeling of isotope migration is shown to be accompanied by zircon phase alteration to form Na-Zr-silicate and baddeleyite whose two stages are being fixed by radiographic and electron microscope techniques.

4. Optical study of metasomatic zircons derived from the phenitization zone shows them to be represented by dull brown-yellow varieties with transparent thin shale which corresponds by its optical and radiographic features to grains of unaltered zircons occurring far from the contact.

5. Direct impact of alkaline fluid on formation of altered grains is shown by composition of their volatiles (H_2O, CO_2, CH_4) identical to that of fluid accompanying intrusion and exhibiting different gas saturation.

6. Isotope analysis and radiography indicate to higher U abundance and maximal discordance of U-Pb system in the crystal center with the preservation of preexisting low-U shell. The revealed tendency of U-Pb system disturbance is consistent with experimental modeling data which exhibit modifications appearing first in more defected fragments, occurring even in the crystal center at the gain of fluid.

7. Different behavior of U-Pb zircon system in the nature and experiment may be the result of differency in temperature, fluid content, and its movement in the open natural system.

Acknowledgments: This work is supported by Grant RFFI (Project # 97-05-65483).

OXYGEN-SULFUR-ISOTOPIC MEASUREMENT IN CONTINUOUS FLOW MODE: APPLICATION TO THE ORIGIN OF DISSOLVED SULFATES IN HIMALAYAN RIVERS USING ELEMENTAL ANALYZER STABLE ISOTOPE RATIO MASS SPECTROMETRY.

J. Morrison[1], C. France-Lanord[2], and A. C. Pierson-Wickmann[2], [1]Micromass UK Ltd., Floats Road, Wythenshawe, Manchester M23 9LZ, UK (john.morrison@micromass.co.uk), [2]Centre de Recherches Pétrographiques et Géochimiques–Centre National de la Recherche Scientifique, BP 20-15 rue Notre Dame des Pauvres, 54501 Vandoeuvre-lès-Nancy, France (cfl@crpg.cnrs-nancy.fr; annecath@crpg.cnrs-nancy.fr).

The technique of interfacing an elemental analyzer to a stable isotope ratio mass spectrometer in continuous flow mode (CF-IRMS) has been successfully applied to the analysis of S and O isotopes. This technique provides the analyst with a routine, small sample, high throughput, $\delta^{34}S$ and $\delta^{18}O$ measurement capability for inorganic samples.

A Carlo Erba NC2500 elemental analyzer configured in combustion mode was interfaced via an open split to an Optima stable isotope ratio mass spectrometer and used to measure $\delta^{34}S$ in sulfate samples incorporating a suite of sulfate standards at sample sizes of 15–25 μg S. The elemental analyzer was then reconfigured for pyrolysis operation and used to measure $\delta^{18}O$ in the same set of samples again incorporating a suite standards at sample sizes of 10–15 μg O.

Rivers derived from the Himalayas have a very high content of dissolved sulfate. The sulfate can originate either from dissolution of marine evaporites from the sedimentary formation in Himalaya or from oxidation of sulfides. This last hypothesis is important with respect to (1) weathering budget in this system as sulfuric acid released by this reaction is a very important weathering agent, and (2) large sulfite alteration may be linked to the release of large amount of elements such as As or Os.

The presented data will show results from north to south, with sulfide oxidation being the likely source of dissolved sulfate in the north. On the south flank of the river, dissolved sulfates have higher $\delta^{34}S$ and $\delta^{18}O$ implying a different origin, possibly involving evaporitic sulfates.

A detailed description of the analytical techniques and a preliminary interpretation of the results will be presented.

SUBOXIC NITRIFICATION IN RECENT SEDIMENTS FROM A SCOTTISH SEA LOCH.

R. J. G. Mortimer[1], M. D. Krom[1], P. Hayes[2], and I. M. Davies[2], [1]School of Earth Sciences, University of Leeds, Leeds LS2 9JT, UK, [2]Fisheries Research Services, Marine Laboratory, Aberdeen AB11 9DB, UK.

Most of the chemical changes that take place during the early stages of diagenesis in marine sediments are redox mediated and controlled by a well defined succession of bacterial communities. The resulting biogeochemical zones that are recognized by a characteristic sequence of chemical changes in the sediment pore waters, are the classic framework within which recent sediment geochemistry is described (Table 1; [1]).

TABLE 1. Depth-related scheme of biogeochemical zones (BGZ).

Microbial Respiration Reaction	Code of Zone
Oxic respiration	Ox
Nitrate reduction	NR
Mn oxide reduction	MnR
Fe oxide reduction	FeR
Sulphate reduction	SR
Methane production	Me

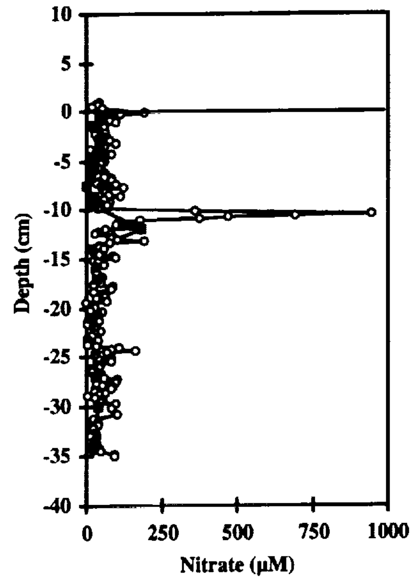

Fig. 1. Pore-water nitrate profile, Loch Duich, showing peak at the boundary between the FeR and SR zones (open circles = gel, black squares = core)

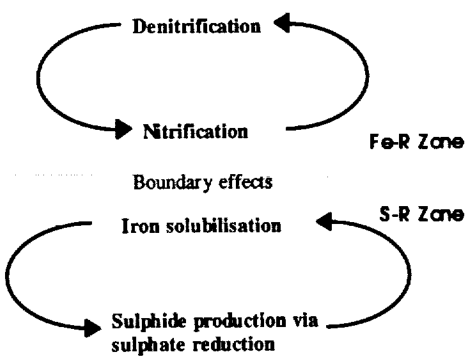

Fig. 2. New conceptual model of biogeochemical zones involving rapid microbial recycling within zones.

Deployment of our new technology of gel probes [2] in Loch Duich, Scotland, has revealed details of pore-water geochemistry that have not been seen previously. The high resolution pore-water profiles obtained provide direct evidence for a novel microbial process: suboxic nitrification. This was observed as a sharp peak at the boundary between the Fe and sulfate reduction zones (Fig. 1).

It is suggested that there is coupled nitrification-denitrification occurring throughout the Fe reduction zone. This peak has been interpreted as net nitrate production coupled with local suppression of denitrification, possibly by sulfide inhibition [3].

We also have evidence from Fe-DGT profiles [4] for rapid recycling of Fe and S in the sulfate reduction zone. Such complex recycling processes were not recognized within the classical framework, and they lead us to propose a new conceptual model for subsurface microbial processes (Fig. 2). This model states that the chemical changes that have been used to define the classical scheme of biogeochemcal zones (BGZ) are the net effects of more complex recycling processes within BGZ and non-steady-state effects at the boundaries. It is only now that we are able to measure pore-water chemistry at much higher resolution that we are beginning to see evidence for this more complex picture.

References: [1] Froelich P. N. et al. (1979) *GCA, 43,* 1075–1090. [2] Mortimer R. J. G. et al. (1998) *Marine Chem., 63,* 119–129. [3] Jørgensen B. B. (1983) in *The Major Biochemical Cycles and Their Interactions* (B. Bolin and R. B. Cook, eds.), pp. 477–515, Wiley, NY. [4] Zhang and Davison, unpublished data.

ISOTOPIC EVOLUTION OF KAUAI SHIELD-STAGE LAVAS.

S. Mukhopadhyay[1], J. C. Lassiter[2], S. W. Bogue[3], and K. A. Farley[1], [1]Mail Stop 170-25, Division of Geological and Planetary Sciences, California Institute of Technology, Pasadena CA 91125, USA, [2]Max-Planck-Institut für Chemie, Postfach 3060, 55020 Mainz, Germany, [3]Department of Geology, Occidental College, 1660 Campus Road, Los Angeles CA 90041, USA.

Introduction: Previous studies have shown that Hawai'ian lavas are characterized by high $^3He/^4He$ ratios (8–32 R_A) compared to MORB glasses (8–10 R_A), with Loihi Seamount having the highest ratios (~20–32 R_A) from any ocean island volcano. However, the temporal variations in He-isotopic compositions during the evolution of a shield volcano and the question of coupling of He to other nonvolatile tracers (like Sr, Nd, and Pb) are still subject to debate. To address the above issues, we have measured He-isotopic ratios in olivine separates from stratigraphically and paleomagnetically controlled lavas from Kauai, and analyzed Sr, Nd, Pb, and Os isotopes from a subset of the samples on which He measurements were made.

Results and Discussion: Helium-isotopic analyses were made from west Kauai (Polihale and Ohaiula ridge sections), central Kauai (Kahililoa section) and east Kauai (Anahola section). Helium-3/helium-4 ratios from the Kauai shield are generally >20 R_A. Samples from west Kauai have a range of $^3He/$

^{4}He ratios from 17.9 to 28.2 R_A (n = 18). Central Kauai ranges from 19.5 to 26.6 R_A (n = 6) while samples from east Kauai range from 19.7 to 27.4 R_A (n = 10). Step crushing and fusion analyses of crushed powders indicate little to no contribution from cosmogenic or radiogenic sources, and we conclude that the range in He-isotopic values reflects the composition of the mantle sources of these lavas.

The range of ^{3}He/^{4}He ratios measured from the Kauai shield is very similar to that reported from Loihi Seamount and is clearly distinct from the other Hawai'ian shield volcanos, which with the exception of a few flows have ^{3}He/^{4}He ratios ≤20 R_A. Our results from Kauai thus challenge the prevailing notion that high ^{3}He/^{4}He ratios are restricted to the preshield stage of Hawai'ian volcanism.

Helium-3/helium-4 ratios in the west, central, and east Kauai shield lavas vary erratically with stratigraphic position. Chronostratigraphic control from paleomagnetic data indicates very rapid changes in the ^{3}He/^{4}He ratios (up to 6 R_A units), in some cases probably on timescales of 10^2 yr. Such variations are extremely rapid, and must reflect the dynamics and timescales of mixing between the different mantle sources.

Strontium, Nd, Pb, and Os data suggest east and west Kauai to be isotopically distinct, in agreement with [1,2]. There are good correlations among the radiogenic isotopes, consistent with trends observed for other Hawai'ian lavas. West Kauai appears to be isotopically similar to the "Loihi end member" while east Kauai looks more "Koolau-like." Based on the Sr, Pb and Os data, we predict east Kauai to have anomalously heavy O-isotopic composition ($\delta^{18}O$ ~5.5‰).

In isotopic space (e.g., Sr vs. Pb, Sr vs. Os, Sr vs. Nd, or Os vs. Pb) east and west Kauai define the isotopic extremes in our dataset, with central Kauai lying in between, as shown with Sr and Nd by [2]. This is probably either due to a change in the mantle sources (from more "Loihi-like" to more "Koolau-like") through time as the locus of volcanism moved from west to east Kauai, or possibly west and east Kauai are in fact different shield volcanos [1].

One of the objectives of this study is to determine how the He-isotopic ratios relate to the radiogenic isotope compositions. Helium-strontium data suggest that west, central, and east Kauai share a common high ^{3}He/^{4}He end-member ("Loihi"), but while samples from west Kauai display a positive correlation, those from central and east Kauai seem to display a negative correlation, similar to that observed for Mauna Loa [3]. More work is under way to confirm the positive correlation seen in the west Kauai shield lavas. Our results also suggest a positive correlation between He-isotopic ratios and the thorogenic component of Pb (v2 vector, [4]) further confirming coupling of He and Pb during Hawai'ian magmatism.

The good stratigraphic control of the Kauai samples, the ^{3}He/^{4}He signature in the lavas, and the correlation between He, Sr, and Pb raises the possibility of better characterization of the high ^{3}He/^{4}He end member, and a better understanding of the relative importance of the different mantle sources during the evolution of Hawai'ian volcanos.

References: [1] Holcomb R. T. et al. (1997) *Geology, 25,* 811–814. [2] Reiners P. W. et al. (1999) *GSA Bull., 111,* 674–685. [3] Kurz M. D. and Kammer D. P. (1991) *EPSL, 103,* 257–269. [4] Eiler J. M. et al. (1998) *GCA, 62,* 1977–1984.

COMPARISON BETWEEN BLACK CARBON DISTRIBUTION IN ALPINE LACUSTRINE AND COASTAL MARINE SEDIMENTS.

G. Muri[1], B. Cermelj[2], J. Faganeli[2], and A. Brancelj[1], [1]National Institute of Biology, Vecna pot 111, POB 141, 1001 Ljubljana, Slovenia (gregor.muri@uni-lj.si), [2]Marine Biological Station, Fornace 41, 6330 Piran, Slovenia.

Black carbon (BC), organic carbon (OC), and total N (TN) concentrations were determined in recent sediments of three high-altitude alpine lakes in Slovenia, i.e., Lake Zgornje krisko jezero, Lake Jezero v Ledvicah, and Lake Jezero na Planini pri jezeru, in one eutrophic subalpine lake (Lake Bled) and at two different sites in coastal marine zone in the Gulf of Trieste (northern Adriatic).

In parallel, sedimentation rates were determined by measuring the excess ^{210}Pb activity, except for one coastal marine site, for which the $^{14}C_{org}$ measurement was used.

The BC content is the highest in alpine lakes, approaching the value of 10 mg/gdw (gram dry weight). The amount is lower in Lake Bled, averaging 5 mg/gdw and coastal marine sediments, amounting to 1.5 mg/gdw. Based on sedimentation rates, all maximum values were determined around the 1950s, when the pollution seemed to be the most intensive.

The OC distribution is similar. Again, the highest rates were measured in alpine lakes, with maximum value of 170 mg/gdw. At the other sites rates are much lower, reaching 55 mg/gdw in Lake Bled and 15 mg/gdw in Gulf of Trieste. In most cases the vertical profile shows exponential decrease of OC concentration.

The pattern of TN follows the OC distribution. Also, the highest values were measured in the alpine lakes and the lowest in coastal marine sediments.

Ratio BC/OC is the lowest in alpine area, with mean values of 5–8% and increases to 10% in subalpine area and to 10–17% in coastal marine zone. This clearly shows the difference between the remote and more polluted urban sites.

DIFFERENTIAL WEATHERING OF GRANITIC QUARRY SAMPLES AND MONUMENT STONES.

M. Nasraoui[1], N. Clauer[2], and M. I. Prudêncio[1], [1]Instituto Tecnologico e Nuclear, EN 10, 2686-953 Sacavém, Portugal, [2]Centre de Géochimie de la Surface, 1 rue Blessig, 67084 Strasbourg, France.

Abstract: Weathering of granitic wall stones of the Evora Cathedral (Portugal) was compared to the natural weathering of this rock lithology in a nearby quarry. The rock samples were subjected to a sequential leaching experiment involving H_2O, HAc, HCl, and HNO_3 leachings. Natural weathering induces mainly elemental removals during HNO_3 leaching that suggests interference of organic matter. When used as stones, these rocks lose systematically more elements during the experiments, the most being again by HNO_3 leaching (increase of the contents by a factor up to 5). More pervasive weathering of wall stones seems to be monitored mainly by organic matter. Differential weathering of granitic stones, relative to natural weathering in quarries, can also be identified by the REE patterns of the H_2O, HAc, HCl, and HNO_3 leachates. The overall concentrations of the wall stones are similar to those of the fresh rock, but the patterns of the HNO_3 leachates are systematically more fractionated, indicating preferential scavenging of the HREE by the occurring organic matter.

Results: A sequential leaching experiment was performed on three quarry samples representing a sequence from fresh to brownish most-weathered facies, and on three cathedral sones taken in the same vicinity on the wall near the small garden. The experience consisted in successive leachings with bi-distilled water, dilute acetic acid (1N), dilute hydrochloric acid (1N) and dilute nitric acid (1N). The purpose of this experiment was to remove successively the salts, the highly soluble mineral phases such as the carbonates and phosphates, the less-soluble mineral phases such as the oxides, and to oxidize the organic matter with HNO_3 and subsequently analyze the released elements. The residues were dissolved afterwards in a mixture of fluorhydric and nitric acids. Major (Si, Al, Mg, Ca, Fe, Mn, Ti, P, Na, and K) elements were determined by inductively coupled plasma atomic emission spectrometry (ICP-AES) with a precision of 10 x%, and the rare earth elements (REE) were determined by inductively coupled plasma mass spectrometry (ICP-MS) with a precision of 5%. The successive H_2O, HAc, HCl, and HNO_3 leachings of the fresh reference rock remove 1.2, 2.2, 1.6, and 2.3 mg elements pro g of rock respectively. The elements removed first by H_2O yield following sequence: Ca > Si > K > Na > Al. The sequence becomes Ca > Al > K > Si > P for the HAc leaching, Al > Ca > Si > K > Fe for the HCl leaching and Fe > Al > K > Ca > Na for the HNO_3 leaching. Compared to these reference values, the naturally weathered rock in the quarry lost successively 0.2, 2.9, 1.3, and 7.2 mg elements pro g of rock for the H_2O, HAc, HCl, and HNO_3 leaching, respectively. The elements removed first by H_2O are almost identical to those lost by the fresh rock, Mg replacing Al. The HAc leachate contains following sequence Al > Fe > Si > Ca > Mg, the HCl leachate yields the sequence Al > Fe > Si > K > Mg and the HNO_3 leachate yields the sequence Fe > Al > K > Mg > Ti. Among the three wall stones of the cathedral, the H_2O leachates contain 0.6, 1.1, and 55.8 mg elements pro g of rock, the HAc leachates contain 3.0, 3.4, and 6.2 mg elements pro g of rock, the HCl leachate contains 5.6, 3.3, and 6.2 mg elements pro g of rock and the HNO_3 leachates contain 33.3, 17.2, and 26.5 mg elements pro g of rock. The elemental sequences of the three wall stones are quite reproductible as follows: Na > Si > K > Ca > Mg for H_2O leaching, Ca > K > Fe > Al > P (Fe) for HAc leaching, Fe > Al > K > Si > Ca for HCl leaching, and Fe > K > Al > Mg > Ti for HNO_3 leaching. The fresh granitic rock of the quarry yields REE distribution patterns for the HAc, HCl, and HNO_3 leachates that are slightly enriched in the light REE (LREE) relative to the chondrite reference, and slightly depleted in the heavy REE (HREE). The HAc and HCl patterns exhibit a negative Eu anomaly, whereas the HNO_3 pattern yields a positive Eu anomaly. The REE pattern of the H_2O leachate shows a strong concentration depletion of a factor 1000 relative to the chondrite reference. The pattern suggests a slight increase of the HREE relative to the LREE. The REE patterns of the HAc, HCl, and HNO_3 leachates of the naturally weathered rock of the quarry are very similar: enriched by a factor 10 relative to the fresh rock, a significant fractionation and a similar negative Eu anomaly. The H_2O pattern is enriched by a factor 10 and is almost flat, relative to the chondrite reference. The different patterns of the leachates recovered from wall stones are very similar: they are slightly fractionated, the most being the HNO_3 leachates, and they yield pronounced negative Eu anomalies. The overall concentrations are similar to those of the fresh rock. On the other hand, the H_2O leachates yield similar concentrations than the same leachate from naturally weathered granitic sample. A slight fractionation in favor of the LREE is visible.

Discussion: Natural weathering, relative to the fresh-rock reference, induces mainly elemental removals during the HNO_3 leaching (increase of the contents by a factor of 3), involving oxidation of the organic matter present in the rock. The most affected elements are Fe, Al, and K. When used as stones, these rocks release systematically more elements during the HAc, HCl and HNO_3 leachings, the most efficient being again the latter (increase of the contents by a factor of 2 to 5). The elements mostly removed are again Fe, Al, and K, but also Ti. This differentiated leachings suggest that more pervasive weathering of wall stones is clearly related to the occurrence of organic matter. The differential weathering of granitic stones, relative to natural weathering in quarries, can also be identified by the REE patterns of sequential leachings, as the pattern of the HNO_3 leachates are systematically more fractionated, indicating preferential scavenging of the HREE by the occurring organic matter. Even the REE patterns of the H_2O leachates are depleted in the HREE.

DIFFERENTIATION BY DEFORMATION IN THE OCEAN CRUST.

J. H. Natland and H. J. B. Dick, Rosenstiel School of Marine and Atmospheric Science/Marine Geology and Geophysics, University of Miami, 4600 Rickenbacker Causeway, Miami FL 33149, USA (jnatland@rsmas.miami.edu).

In a paper now largely forgotten, N. L. Bowen (1920) postulated that crystallization differentiation could be driven not only by gravitational movement of crystals, but also by deformation of partially molten masses of igneous rock. Although differentiation by deformation has not proved to be important in the study of continental layered igneous intrusions, it now appears to be a fundamental process in the ocean crust.

Bowen predicted that crystallization during deformation would result in unusually efficient separation of melt from crystals, leading to monomineralic rocks, or as more generally termed today, adcumulates, of extreme purity. Such pure adcumulates might also form intrusives with sharp contacts but still would not represent liquid compositions. Rock masses that experienced such deformation might have cross-cutting lithologies that crystallized at different temperatures, including gabbros cut by complementary granophyric dikes and veins. This Bowen termed discontinuous crystallization. The deformed rocks could develop primary banding, or foliation, while still containing abundant melt. In this way they would resemble metamorphic rocks, although having been deformed under super- rather than subsolidus conditions. Finally, very late-stage differentiates might segregate into cavities formed by stretching or rupturing of a crystalline mesh, there to crystallize to coarse grain size.

The gabbroic rocks drilled at ODP Hole 735B, Atlantis II Fracture Zone, Southwest Indian Ridge, and dredged from other fracture zones in the Indian Ocean, exhibit all of these features. The rocks are cumulates, being aggregates of minerals separated from liquids, and most are adcumulates with very low residual melt porosities. Cumulate theory based on layered intrusions does not apply to these rocks. Instead, all gabbros, including the oxide gabbros, crystallized in a dense crystal mush in patterns dominated by fractures, channelized flow, and intergranular porous flow. Most gabbros are not layered; weak modal layering of uncertain origin is present in <2% of the rocks. Porosity reduction leading to formation of adcumulates at all stages was extremely efficient. This involved compaction under conditions of both lithostatic loading and shear, dissolution and reprecipitation of minerals along grain boundaries, and pressure solution, which was the final agent in porosity reduction.

The cores of Hole 735B comprise five main intervals or plutons, each ~250–450 m thick, consisting of troctolite, olivine gabbro, and olivine gabbro-norite showing similar trends in cryptic variation. Each appears to represent an episode of significant addition to the ocean crust. Each pluton in turn consists of hundreds of small crystallization intervals of contrasting lithology and grain size, and having sharp or sutured intrusive contacts. The five plutons are cut by hundreds of small oxide gabbros, many of them deformed, throughout the core. Over 200 of these are associated with felsic/granitic veinlets. These were derived by internal differentiation of individual crystallization intervals, each containing a solidification front, many of which were disrupted by deformation, leading to removal of buoyant differentiated melt along a developing fracture network. There is a large coalescence of oxide gabbro seams from 200–270 m deep in the section, perhaps representing aggregation of differentiated melts beneath a permeability cap. This zone was also an inclined active fault along which the two blocks of primitive gabbros were being juxtaposed at the time. Many of these rocks consequently have porphyroclastic, gneissic, and even mylonitic textures. Deformation and magmatic overpressure widened porosity structure in some of these rocks, leading to formation of magmatic breccias with up to 30% ilmenite and magnetite. The oxides form a cementing matrix for fragments of angular and irregular, highly-deformed porphyroclastic to mylonitic gabbro. These represent Bowen's stretching or rupturing of a crystalline mesh, and crystallization to coarse grain size. The process can be traced down to the scale of individual mineral grains, resulting in troctolites, for example, in rims of ilmenite on Cr-spinel and crack-fillings of ilmenite in forsteritic olivine. Intergranular mixing between primitive pore melts and injected differentiates resulted in complex mineralogical relations, including early precipitation of magnesian orthopyroxene and multiple late-stage liquid lines of descent.

ORIGIN OF DEEP-SEATED HYDROTHERMAL BRINES IN NORTHERN GERMANY: GEOCHEMISTRY OF GASES AND ISOTOPES.

D. Naumann[1], J. Erzinger[1], and E. Faber[2], [1]Geoforschungszentrum Potsdam, Telegrafenberg, Section 4.2, D-14473 Potsdam, Germany (dirk@gfz-potsdam.de), [2]Federal Institute for Geosciences and Natural Resources, Stilleweg 2, D-30655 Hannover, Germany.

We present geochemical results of sedimentary brines from northeast Germany that are used for geothermal energy production and brines derived from two newly drilled bore holes. The thermal waters are Na-Cl-dominated brines and originate from upper Triassic and lower Jurassic formations. Their salinity varies from 130 to 230 g/L depending on depth and temperature (55°–128°C). The total gas content of the investigated brines reaches values of 10 vol%. The gas phase is dominated by N_2, CO_2, and CH_4, the concentrations of the minor constituents He, H_2, Ar, and other hydrocarbons are <1 vol% each. With increasing depth, CO_2 and CH_4 increases.

The $\delta D/\delta^{18}O$-ratios of three of the investigated thermal waters are similar and plot close to the "meteoric water line" (MWL) [1]. Thus we assume that there was no isotopic exchange between fluids and rocks. The $\delta D/\delta^{18}O$-ratios of the two most saline brines plot further away from the MWL. These brines are possibly a mixture of old ("connate") seawater with meteoric water, which was infiltrated at a time when average atmospheric temperature was significantly higher than today.

$\delta^{11}B$-data of 24–36‰ show that most of the boron in the brines originated from marine evaporites and/or marine carbonates, which are abundant in this part of the N-German basin [2]. This is consistent with TDS/Br^--ratios (after [3]), which also show that the salt content of the waters may originate from evaporated seawater and/or the dissolution of marine evaporites.

N_2-Ar-He-ratios lead to the assumption that the brines were infiltrated from the surface, following which the radiogenic production of He and Ar altered the composition of the gas phase. This is consistent with the results of He- and Ar-isotopic analysis. Very low $^3He/^4He$-ratios of in average 1.4 × 10^{-8} ($^3He/^4He$-ratio of the atmosphere = 1.4 × 10^{-6}) indicate that most of He is unequivocally radiogenic and that there is no influence of a "mantle-He" component [4,5]. Argon-40/argon-36-ratios of up to 367.5 (atmosphere = 295.5) support the evolution of the brines from surface waters to crustal fluids.

Carbon-isotopic signatures of methane, ethane and propane ($\delta^{13}C_{1,2,3}$) from the brine of the geothermal heat plant Neustadt-Glewe indicate a thermogenic origin from a marine source rock. The $\delta^{13}C$-ratios correspond to a vitrinite reflectivity of the gas generating organic matter of ~1.2%. Therefore the methane seems to originate from organic matter near to and/or in the aquifer itself and did not migrate from deeper Carboniferous formations.

In addition, knowledge on the physico-chemical behavior of gases in brines is important for engineers to design heat plants. In particular, detailed information is necessary if there is a risk of degassing of flammable components.

References: [1] Craig H. (1961) *Science, 133,* 1702–1703. [2] Vengosh A. et al. (1992) *Geology, 20,* 799–802. [3] Rittenhouse G. (1967) *Am. Assoc. Pert. Geol. Bull., 51,* 2430–2440. [4] Hooker P. J. et al. (1985) *Nature, 318,* 273–275. [5] Mamyrin B. A. and Tolstikhin I. N. (1984) *Develop. Geochem., 3,* 273 pp.

ROLE OF WATER IN ENERGETICS OF ZEOLITES AND LAYERED MATERIALS.

A. Navrotsky, Department of Chemical Engineering and Materials Science, University of California at Davis, One Shields Avenue, Davis CA 95616, USA (anavrotsky@ucdavis.edu).

The University of California at Davis Thermochemistry Facility has been studying the enthalpies of formation of zeolites, octahedral molecular sieves, and layered materials by a combination of high-temperature reaction calorimetric techniques. We find several common trends. Dehydrated frameworks are metastable with respect to dense phases by 5–15 kJ/mol but hydrated frameworks are energetically stable by a similar amount (referred to liquid water and a 2-O framework formula unit). This energetic stabilization is counterbalanced by a negative entropy of hydration. The DH and ΔS terms scale with each other. Thus the localization of water within the cage or layer is a major driving force in the formation of both framework and layered materials. New thermochemical data for a variety of zeolites and manganese oxide based materials will be reviewed in the context of hydration energetics.

PROBING THE INTERIORS OF THE TERRESTRIAL PLANETS: DATA FROM THE MOON AND MARS.

C. R. Neal, J. C. Ely, and J. C. Jain, Department of Civil Engineering and Geological Sciences, University of Notre Dame, Notre Dame IN 46556, USA (neal.1@nd.edu).

Introduction: The Moon and Mars are the only other planetary bodies that we have samples from and can analyze. Using a combination of high field strength (HFS) and platinum group element (PGE) data for three martian meteorites (0.18-Ga basalt EETA 79001 lithology B; 1.3 Ga clinopyroxenite Nakhla; ~4-Ga orthopyroxenite ALH 84001), along with lunar basalts and pyroclastic glasses, different reservoirs are identified and can be placed in the context of planetary differentiation. Rarely is a full suite of trace elements determined on the same aliquot of extraterrestrial sample. X-ray fluorescense (XRF) and instrumental neutron activation analysis (INAA) cannot individually quantify all HFSEs and combining these data (obtained from different sample aliquots) produces large errors in HFSE ratios. While the abundances of the HFSEs in different aliquots may vary, their ratios should not; any differences between samples are source-related.

The Moon: Pyroclastic glasses are not petroegenetically related to the basalts [1] and experimental evidence [e.g., 2,3] suggests they originated from sources deeper than the crystalline basalts. Differences in Zr/Y ratios (Fig. 1) could be due to the presence of residual garnet in the source region of the glasses.

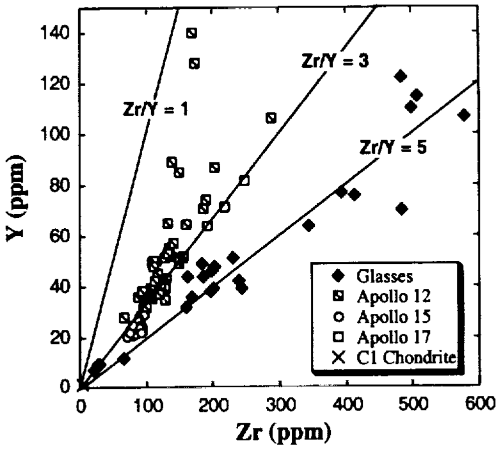

Fig. 1.

Platinum-group-element profiles from three Apollo 12 basalts, one each from the three groups present, are in Fig. 2. The subparallel profiles testify to the general PGE-depleted nature of the Moon. If the Moon originated from the Earth's (upper?) mantle after core segregation and underwent further core separation during lunar differentiation, then ratios between the low and high melting point PGEs should be affected and this is observed [4]. We suggest that the source region, for at least the Apollo 12 basalts, have experienced two PGE fractionation events. The first when the Earth's core differentiated and the second when the lunar core formed. The pyroclastic glasses maybe derived from a garnet-bearing region that did no melt during the lunar magma ocean (LMO) formation ("primitive Moon"); the crystalline basalts originated from the cumulate LMO mantle.

Mars: Our results show HFSE ratios approximate those of chondrites for the older two meteorites, but depart from chondritic values for EETA 79001. These ratios should not be affected by crystal fractionation so even though these three samples represent two pyroxenites and a basalt, they should be indicative of source region. Platinum-group-element ratios indicate that differentiation was active early in the history of Mars, but in comparison with the HFSEs, this was primarily the formation of a metallic core. The PGE profiles (Fig. 2) demonstrate that ALH 84001 is depleted and flatter than the

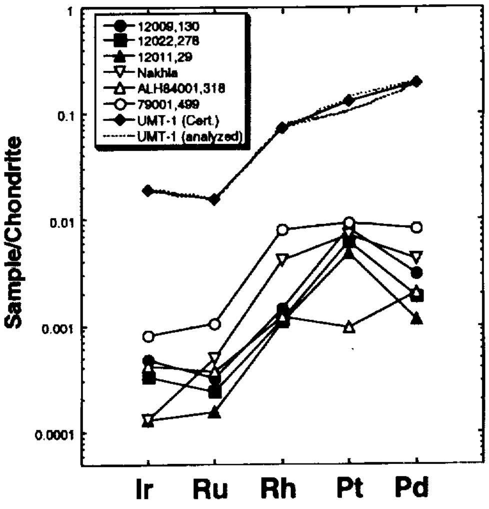

Fig. 2.

other two meteorites. There is a general increase in PGE abundance with *decreasing* age. These data support the hypothesis that ALH 84001 was formed before any late accretion (veneer) of siderophile element rich meteorites, but after the segregation of a metal-rich core [5]. However, the relative enrichment in the PGEs in the younger meteorites could be due to a change in volcanic productivity from shallow melting when Mars was young (and hotter) to deep-seated, plume volcanism as the planet cooled. The increase in PGEs in the younger meteorites could represent incorporation of a core component. The initial interpretation of the data presented here is that Mars underwent an early metal-rich core formation (consistent with [6]), but substantial silicate differentiation did not occur until much later (inconsistent with [7]).

References: [1] Delano (1986) *JGR, 91,* D201. [2] Longhi (1992) *GCA, 56,* 2235. [3] Longhi (1993) *LPS XXIV,* 895. [4] Neal et al. (1999) *LPS XXX,* Abstract #1003. [5] Warren and Kallemeyn (1996) *MAPS, 31,* 97. [6] Lee and Halliday (1997) *Nature, 388,* 854. [7] Harper et al. (1995) *Science, 267,* 213.

THE ONTONG JAVA PLATEAU: EVIDENCE OF A DEEP EARTH ORIGIN.

C. R. Neal[1], J. C. Ely[1], A. L. Birkhold[1], J. C. Jain[1], J. J. Mahoney[2], and R. A. Duncan[3], [1]Department of Civil Engineering and Geological Sciences, University of Notre Dame, Notre Dame IN 46556, USA (neal.1@nd.edu), [2]School of Ocean and Earth Science and Technology, University of Hawai'i, [3]College of Oceanic and Atmospheric Sciences, Oregon State University, Corvallis OR 97331-5503, USA.

Introduction: The Ontong Java Plateau (OJP) in the southwest Pacific represents the worlds largest "large igneous province (LIP)" [1,2] that has been postulated to have formed by plume volcanism and originate at the core-mantle boundary (CMB) [2]. The erupted basalts have been produced by large degrees of partial melting [3,4], consistent with decompression melting of a surfacing plume head [5].

Two isotopically distinct OJP basalt types [4,6] are found across the plateau. Elemental abundances/ratios and petrographic observations demonstrate that these basalts have experienced moderate to high degrees of fractional crystallization (20–30%) [4]. Generally, the basalts are slightly quartz normative, are cpx-plagioclase-phyric with only rare, corroded olivine phenocrysts seen in a few examples, and have MgO vales generally <10 wt%.

Core-Mantle Boundary Origin: Seismic evidence of a CMB origin for mantle plumes is now available [e.g., 7] and supports modeling [e.g., 2] experimental evidence for such an origin [e.g., 5,8] However, chemical evidence for such an origin is not as strong. Such evidence may be found in the siderophile elements using the assumption that an origin at the siderophile element-rich core-mantle boundary should enrich the upwelling mantle in these elements. Geophysical modeling suggests such chemical interactions across the CMB would be minor [e.g., 9] or <3–6% [10]. Walker et al. [11,12] used Re-Os isotopes, specifically an enrichment in ^{187}Os, to suggest that some plumes originated at the CMB and that the observed ^{187}Os enrichment was due to the influence of the core.

Ontong Java Plateau: The OJP basalts are not primary and fractional crystallization processes may obscure possible source compositions. Significant fractionation of olivine and spinel lowers the abundance of Os in the residual melt, negating Re-Os-isotopic determinations of the desired accuracy and precision. Therefore, Re-Os analyses of the OJP basalts have not been conducted.

Studies of the OJP include ODP drill legs [13] as well as fieldwork on the islands of Santa Isabel and Malaita, Solomon Islands [1,4,14] where outcrops of the OJP occur [4,15,16]. Recent studies of basaltic outcrops on the island of Makira demonstrated the presence of OJP basalts, and also OIB and MORB varieties that are stratigraphically intercalated [17]. Our preliminary interpretation is that the presence of MORBs on Makira is consistent with an on-ridge/near-ridge setting with MORB erupting during periods of plume quiescence. The OIB flows may represent the tail of the plume head that formed the OJP basalts.

The data presented are platinum-group-element (PGE) abundances for OJP basalts. We are using these as an indicator of a CMB origin. We have determined the abundances of Ru, Rh, Pd, Ir, and Pt in two OIBs island and two OJP basalts (Fig. 1). The OJP basalts represent the two groups defined on Malaita and from ODP drill cores [13]. The OIBs are from Makira.

Using the plume head/tail model, the tail should contain relatively more material from the source and it should have higher PGE abundances. This is the case. Melting models using spinel and garnet peridotites (±sulfide) demonstrate the PGE abundances in the OJP basalts cannot be generated from typical upper mantle. Large degree partial melting will dilute the silicate-incompatible PGEs. While fractional crystallization accounts for the relative depletion of Ir, Ru, and Rh [cf. 18,19], it cannot generate the observed abundances. We conclude that the PGE abundances support an origin at the CMB and formation via plume magmatism.

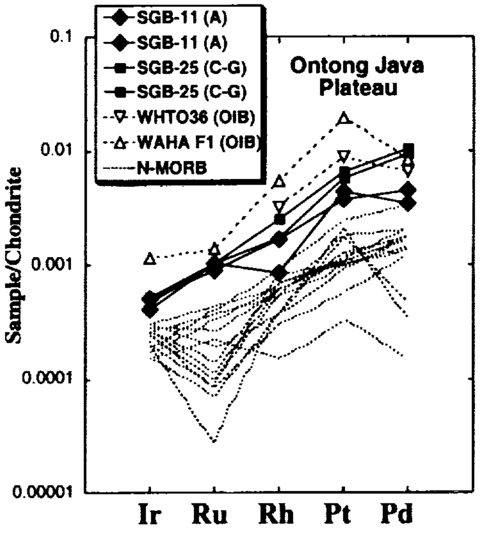

Fig. 1.

References: [1] Mahoney (1987) *Geophys. Monogr., 43,* 207–220. [2] Coffin and Eldholm (1993) *Geology, 21,* 515–518. [3] Mahoney and Spencer (1991) *EPSL, 104,* 196–210. [4] Neal C. R. et al. (1997) *Geophys. Monogr., 100,* 183–216. [5] Campbell and Griffiths (1990) *EPSL, 99,* 79–93. [6] Mahoney et al. (1993) *Geophys. Monogr., 77,* 233–262. [7] Bijwaard and Spakman (1999) *EPSL, 166,* 121–126. [8] Thompson and Tackley (1998) *GRL, 25,* 1999–2002. [9] Boehler et al. (1995) *Chem. Geol., 120,* 199–205. [10] Kellogg and King (1993) *GRL, 20,* 379–382. [11] Walker et al. (1995) *Science, 269,* 819–822. [12] Walker et al. (1997) *GCA, 61,* 3145–3160. [13] Mahoney et al. (1993). [14] Tejada et al. (1996) *J. Petrol., 37,* 361–394. [15] Coleman and Kroenke (1981) *Geo-Marine Lett., 1,* 129–134. [16] Petterson et al. (1998) *Tectnophys., 283,* 1–33. [17] Birkhold et al. (1997) *Eos Trans. AGU, 78,* 826. [18] Capobianco and Drake (1990) *GCA, 54,* 869–874. [19] Barnes et al. (1985) *Chem. Geol., 53,* 303–323.

GEOCHRONOLOGICAL CONSTRAINTS ON THE SOURCE OF CONTINENTAL ROCKS FROM THE KERGUELEN PLATEAU, ODP SITE 1137 ELAN BANK.

K. E. Nicolaysen[1], D. Weis[2], F. A. Frey[1], S. A. Bowring[1], M. F. Coffin[3], and the Leg 183 Shipboard Scientific Party, [1]Department of Earth, Atmospheric and Planetary Sciences, Massachusetts Institute of Technology, 77 Massachusetts Avenue, Cambridge MA 02139, USA (knic@mit.edu), [2]Département des Sciences de la Terre, Université Libre de Bruxelles, Brussels, Belgium.

Located in the southern Indian Ocean, the Kerguelen Plateau is part of a large igneous province (LIP) formed by volcanic activity of the Kerguelen plume during the last ~115 m.y. [1 and references therein]. Leg 183 of the Ocean Drilling Program sampled igneous basement in eight locations on the Kerguelen Plateau and its conjugate Broken Ridge. Isotopic heterogeneity in lavas from the Kerguelen LIP (~2 × 10^6 km^2) has, in part, been ascribed to contamination by continental material, either in the plume source or in the shallow lithosphere [2]. Elan Bank (~1.35 × 10^5 km^2) protrudes from the western margin of the central and southern Kerguelen Plateau (CKP and SKP respectively). Although gravity and bathymetry lows separate Elan Bank from the CKP and SKP, seismic reflection data show that no major normal or reverse faults at the boundaries; however, one or more relict spreading centers and fracture zones, possibly obscured by volcanic cover, may exist in the vicinity. Seismic velocities of 6.7–6.9 km/s had previously suggested the presence of continental crust in the lower crust of the ~20-km-thick Elan Bank [3]. Newly recovered drill core from the previously unsampled and undated Elan Bank includes garnet-biotite gneiss clasts contained within a ~26-m-thick conglomerate interbedded with basalt flows [1] which provides the first direct evidence of continental crust from the Kerguelen Plateau.

Drilling at Elan Bank, Site 1137 (56°50.0'S, 68°05.6'E), penetrated to a depth of 371 m below seafloor and recovered ten basement units. The ten units include seven basaltic lava flows, ~90 m total thickness, and three interbedded sedimentary units. The unit 5 sandstone and siltstone (4.4 m thick) consists of volcanic fragments and minor amounts of feldspar, biotite, and hornblende. Coarse sandy layers contain sparse detrital garnet and zircon. The underlying volcanic lithic conglomerate (unit 6, 31.1 m thick) contains evolved volcanic and metamorphic lithologies including clasts of feldspar-bearing trachyte, flow-banded rhyolite, actinolite-bearing gneiss, granitoid, and garnetiferous biotite gneiss. The Leg 183 Shipboard Scientific Party concluded that these sedimentary units were deposited in a fluvial environment.

Although the Kerguelen Plateau is currently hundreds to thousands of kilometers from circum-Indian Ocean continental margins, plate tectonic reconstructions [e.g., 4] place Elan Bank proximal to the eastern margin of India at ~100 Ma, well after the separation of India and Antarctica. Biostratigraphy of marine sediments above the basement units provides a Campanian age (~74 Ma) [3]. However the basal sedimentary sequence containing the Campanian microfossils thickens to the east of site 1137, so the biostratigraphy provides an extreme minimum age for the reworked continental material.

Whole-rock ^{87}Sr/^{86}Sr analyses provide preliminary isotopic constraints on the age of the garnet-biotite gneiss and the evolved volcanic clasts. The evolved trachyte and flow-banded rhyolite yield ^{87}Sr/^{86}Sr of 0.713042 ± 8 and 0.732206 ± 7 respectively. The quoted uncertainties are 2 σ errors in the last place digit. Shipboard XRF analyses of Rb and Sr concentrations yield ^{87}Rb/^{86}Sr of 1.93 and 16.2 respectively. The resulting two point whole rock isochron provides an age of 94.6 Ma with an initial ratio of 0.7104. The garnet-biotite gneiss gave an ^{87}Sr/^{86}Sr of 0.785608 ± 8 and an ^{87}Rb/^{86}Sr of 5.2. Assuming initial ^{87}Sr/^{86}Sr values of 0.702 and 0.705, the resulting model ages are 1.13 and 1.09 Ga respectively. The calculated model ages are not greatly affected by the picked values for the initial ratio. This preliminary ~1-Ga model age for the garnet-biotite gneiss correlates with Grenvillian ages of gneisses on the east Indian and east Antarctic margins [e.g., 5].

Uranium-lead geochronology and Sr-isotopic analysis of mineral separates will provide additional constraints on the potential sources of the conglomerate clasts. The occurrence of the garnet biotite gneiss and its age will revise our understanding of the evolution of the Kerguelen Plateau within the early Indian Ocean.

Acknowledgments: Members of the Leg 183 Scientific Party include M. Antretter, N. Arndt, J. Barling, F. Boehm, M. Borre, H. Coxall, D. Damasceno, J. Damuth, H. Delius, R. Duncan, H. Inokuchi, L. Keszthelyi, J. Mahoney, L. Moore, R. D. Müller, C. Neal, M. Pringle, D. Reusch, P. Saccocia, D. Teagle, V. Wahnert, P. Wallace, S. Wise, and X. Zhao

References: [1] Frey F. and Leg 183 Scientific Party (1999) *Science*, submitted. [2] Mahoney et al. (1995) *Chem. Geol., 120,* 315–345. [3] Charvis P. et al. (1997) *Eos Trans. AGU, 78,* F711. [4] Müller R. D. et al. (1998) in *The Sedimentary Basins of Western Australia 2, Proc. of the Western Austral. Basins Sympos.* (P. Purcell and R. Purcell, eds.), pp. 55–71. [5] Mezger K. and Cosca M. (1999) *Precambrian. Res., 94,* 251–271.

TRACE-ELEMENT VARIATIONS IN MANTLE WEDGE PERIDOTITES ABOVE MODERN SUBDUCTION ZONES.

Y. Niu[1], R. L. Fisher[2], and J. W. Hawkins[2], [1]Department of Earth Sciences, University of Queensland, Brisbane, Qld 4072, Australia (niu@earthsciences.uq.edu.au), [2]Scripps Institution of Oceanography, University of California, La Jolla CA 92093, USA (jhawkins@popmail.ucsd.edu).

Island arc volcanism is thought to result from slab-dehydration induced melting of peridotites in the mantle wedge overlying subduction zones. The mantle wedge peridotites, which are mostly highly depleted harzburgites, have been interpreted to be residues of hydrous melting beneath arcs. Whole-rock, trace-element studies of these residues should therefore provide complementary information that may not be available from studying arc basalts alone about melting and melt extraction processes beneath arcs, but such studies are scarce [1]. We report here the results of an inductively coupled plasma mass spectrometry (ICP-MS) trace-element (~40 elements) study of whole-rock mantle wedge harzburgites dredged from the landward slopes of the Tonga and Mariana trenches [2–4].

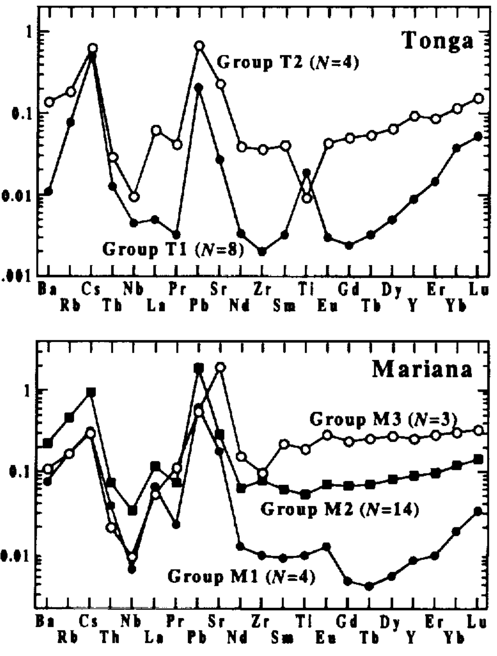

Fig. 1. Primitive mantle [5] normalized element abundances of average Tonga and Mariana harzburgites.

The samples studied include fresh (<~0.45% total volatiles) and variably serpentinized (9–14% total volatiles) harzburgites. These samples show huge variations in rare earth element (REE) abundances (from ~0.003 to ~1× chondritic values), and exhibit smooth yet variable chondrite-normalized REE patterns [i.e., variable (La/Sm)CN, (Sm/Dy)CN, and (Dy/Yb)CN ratios]. Nevertheless, the significant, though scattered, correlations of (Sm/Yb)CN with REE and other incompatible elements (e.g., Nb, Th, Zr, Ti, Y, Ba, Rb, and to a lesser extent Sr and Pb) suggest that, in addition to possible source compositional effect, varying extents of melting and post-melting refertilization are the primary processes responsible for the compositional differences in these harzburgites.

The Tonga harzburgites can be divided into T1 and T2 groups (Fig. 1). T1 group samples are unusually fresh, and have low-REE abundances with high (La/Sm)CN (~1.58) and low (Gd/Yb)CN (~0.05). While the REE patterns of T1 samples can be modeled as residues by 15–20% melting of a depleted lherzolite, the positive anomalies of Ti, Pb, Sr, Cs, Rb, and to a lesser extent, Nb, Th, and Ba (Fig. 1) are unexplained by this process using published partition coefficient data. Nor can such combined elemental anomalies be readily explained by volatile-rich melt metasomatism. The freshness, the lack of petrographic "anomalies" and the overall extremely melt-depleted mineral composition [4] of T1 group harzburgites suggest that they could be true melting residues beneath arcs. Positive Ti anomalies have been observed in depleted harzburgites [6,7], but a detailed trace-element study of the constituent minerals is needed to reveal the residence characteristics of Ti, Pb, Sr, Cs, Rb, Nb, Th, and Ba in unaltered, highly depleted harzburgites. The incompatible element abundances of T2 harzburgites (Fig. 1) can be produced, to a first order, from a T1 residue modified through "interactions" of an ascending "arc" melts (i.e., depleted in Nb and Ti). The Mariana harzburgites (M1, M2, and M3 groups; Fig. 1) show broad similarities to T2 harzburgites, and could be produced similarly. However, the actual residues here may differ from T1 group harzburgites, and the "interacting" melts may differ and vary in composition as well.

The fact that this interaction process does not affect the highly depleted composition of residual minerals [2–4] suggests that the melt-solid interaction is mostly passive (vs. reactive), as seen in abyssal peridotites formed beneath ocean ridges [8].

References: [1] Parkinson I. J. and Pearce J. A. (1998) *J. Petrol., 39,* 1577–1618. [2] Fisher R. L. and Engel C. G. (1969) *GSA Bull., 80,* 1373–1378. [3] Bloomer S. H. and Hawkins J. W. (1983) *AGU Monogr., 27,* 274–317. [4] Bloomer S. H. and Fisher R. L. (1987) *J. Geol., 95,* 469–495. [5] Sun S.-s. and McDonough W. F. (1989) *Geol. Soc. London Spec. Publ., 42,* 323–345. [6] Niu Y. and Hekinian R. (1997) *EPSL, 146,* 243–258. [7] McDonough W. F. et al. (1992) *CMP, 110,* 321–328. [8] Sevin L. et al. (1998) *Eos Trans. AGU, 79,* F990–F991.

PLATINUM-GROUP-ELEMENT AND RHENIUM ABUNDANCES IN HAWAI'IAN PICRITES: COMPOSITIONAL VARIATIONS IN THE MANTLE PLUME AND POSSIBLE SECONDARY MOBILITY.

M. D. Norman[1], V. C. Bennett[2], and M. O Garcia[3], [1]Centre for Ore Deposit Research, University of Tasmania, Hobart TAS 7001, Australia (marc.norman@utas.edu.au), [2]Research School of Earth Sciences, Australian National University, Canberra ACT 0200, Australia, [3]Center for Volcanology, School of Ocean and Earth Science and Technology, University of Hawai'i, Honolulu HI 96822, USA.

Introduction: The Hawai'ian plume is geochemically heterogeneous on scales of tens of kilometers times tens of years. The plume probably originates at considerable depth and it may sample material from sources as diverse as the transition zone, the lower mantle, and the core-mantle boundary. At least some geochemical components in the plume probably originated as recycled lithosphere. Osmium-187- and ^{186}Os-isotopic compositions of Hawai'ian tholeiites [1–3] show that the plume components record long term differences in relative abundances of siderophile and chalcophile elements, so these elements may provide useful tracers for the origins of mantle plume source regions. To provide additional information on the siderophile element characteristics of mantle plumes, we measured the concentrations of platinum group elements (PGEs) and Re in primitive tholeiitic picrites from the major Hawai'ian volcanic centers [4].

Results: Five picrites were analyzed for PGEs and another 10 for Re abundances by isotope dilution ICP-MS. One to two grams of aliquots were dissolved by carius tube and HF-HCl. PGE were preconcentrated by Te coprecipitation and Re by anion exchange.

Platinum-group-element abundances range from 0.04 to 0.3 × PM for Ir, 0.09 to 0.3 × PM for Ru, 0.3 to 0.8 × PM for Pt, and 0.3 to 1.6 × PM for Pd. Rhenium abundances range from 0.27 to 0.95 ppb. Picrites from Loihi and Kilauea generally have higher PGE and Re abundances than those from Mauna Loa and Hualalai. Koolau picrites have among the lowest PGE and Re abundances in this suite. The Kilauea 1840 picrite is exceptional in having low Re contents, more similar to picrites from Koolau than to the other picrites from Kilauea.

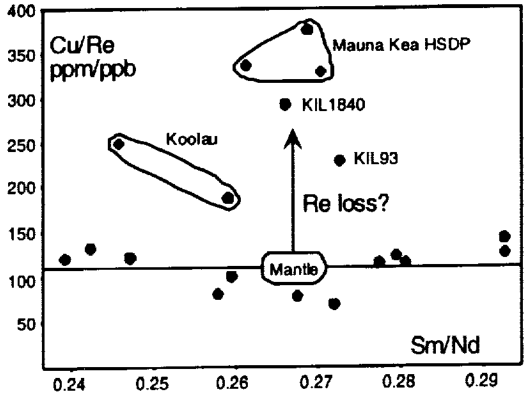

Fig. 1.

Discussion: Platinum-group-element and Re contents of primitive Hawai'ian tholeiites appear to be linked with other source characteristics of the mantle plume, as indicated by their good correlations with Os and Pb isotopic compositions and trace-element characteristics such as Zr/Nb [3,4]. Similar Os/Pb and incompatible trace-element compositions in the Hawai'ian plume components [1,3,4] imply generally similar PGE contents in these components, so the variable PGE and Re abundances of the picrites may reflect other differences in source characteristics during melting.

Platinum-group-element and Re abundances in the mantle are strongly influenced by sulfides, and their concentrations in these picrites can be modeled using variable amounts of residual sulfide during melting, with the higher concentrations of Re and the PGEs in the Loihi and Kilauea picrites implying less residual sulfide in the source of these lavas during melting.

Glass rims and melt inclusions in the Loihi and Kilauea picrites have high contents of reduced S (1200–1500 ppm) and small blebs of immiscible sulfides which show the melts were S saturated on eruption. Our limited data indicates generally lower S contents in submarine glasses from Mauna Loa and Koolau, and less-abundant sulfide compared to Loihi and Kilauea. Higher concentrations of PGEs, Re, and S in the Loihi and Kilauea picrites may reflect either greater solubility or mobility of mantle sulfides in the Loihi and Kilauea parental melts [7] or different D's for PGEs and Re in the residual sulfide during melting.

Secondary alteration also appears to have modified the Re and perhaps the PGE contents of some Hawai'ian lavas. For example, the low Re contents of the Koolau and Kilauea 1840 picrites may reflect alteration and partial loss of this element. Most of the picrites studied here have nearly constant Cu/Re ratios that are similar to the mantle value [5], indicated by the line in Fig. 1. In contrast, the Koolau picrites, the Kilauea 1840 picrite, and a 9% MgO tholeiite collected from Pu'u O'o (KIL93) all have low Re contents and high Cu/Re ratios. Subaerial tholeiites collected from Mauna Kea by HSDP also have high Cu/Re ratios and low Re contents (data from [1,6]). Rhenium depletion in these subaerial lavas may reflect partial loss during outgassing in shallow magma chambers, on eruption, or by weathering. These data raise the possibility that Re and perhaps the PGE contents of subaerial Hawai'ian tholeiites may have been modified during evolution and eruption of these lavas.

References: [1] Lassiter and Hauri (1998) *EPSL, 164,* 483 [2] Brandon et al. (1998) *Science, 280,* 1570 [3] Bennett et al. (1996) *Nature, 381,* 221 [4] Norman and Garcia (1999) *EPSL, 168,* 27. [5] McDonough and Sun (1995) *Chem. Geol., 120,* 223. [6] Albarède (1996) *JGR, 101,* 11841. [7] Gaetani and Grove (1999) *EPSL, 169,* 147.

HYDROCARBON SPECIATION IN CARBON-OXYGEN-HYDROGEN FLUIDS DURING SERPENTINIZATION.

C. Normand and A. E. Williams-Jones, Department of Earth and Planetary Sciences, McGill University, 3450 University Street, Montréal, Québec, Canada H3A 2A7 (charlesn@eps.mcgill.ca).

Several studies have documented the presence of CH_4 and hydrocarbons in fluids produced during serpentinization [1,2]. Although the origin of these fluids is controversial, several authors have suggested that they form as a result of Fischer-Tropsch synthesis involving a magnetite-catalyzed nonequilibrium reaction between CO_2 and H_2, the latter gas being the product of serpentinization reactions of the type FeO (silicate) + $0.5H_2O$ = $FeO_{1.5}$ (silicate, oxide) + $0.5H_2$.

In this paper we report the results of a study of hydrocarbon fluids trapped in rodingites hosted in serpentinites from the Jeffrey Mine, Asbestos, Québec. Gas chromatographic analyses of fluid inclusions contained in purple and green vesuvianite, and in wollastonite, reveal that CH_4 is the dominant carbonic species, followed by C_2H_6, C_3H_8, n-C_4H_{10}, and n-C_5H_{12}. In the case of the purple vesuvianite, the relative proportions of the gases describe a Schulz-Flory distribution ($\alpha = M_{n+1}/M_n$) with a value for α of 0.29 (Fig. 1). This distribution also describes the relative proportions of hydrocarbon gases produced during magnetite-catalyzed Fischer-Tropsch synthesis (α = 0.33; [3]). The distribution of hydrocarbons in green vesuvianite and wollastonite also displays a Schulz-Flory distribution. However, the values of α (0.01,

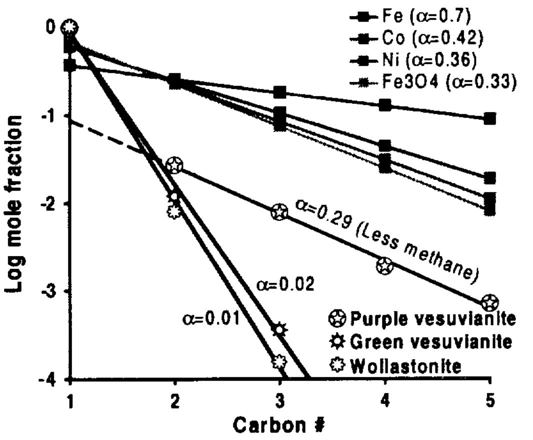

Fig. 1.

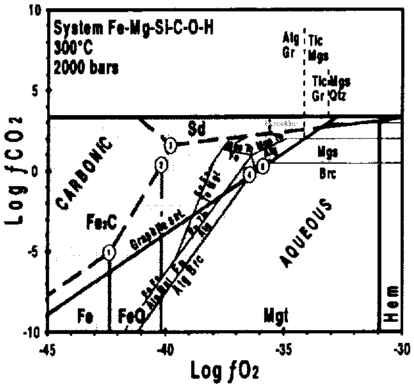

Fig. 2.

0.02) do not correspond to those predicted for any known Fischer-Tropsch catalyst.

An alternative explanation for the production of higher hydrocarbons during serpentinization is exsolution of a reduced carbonic phase from the hydrothermal fluid, and nonequilibrium reactions of this phase with Fe oxides, Fe-Ni alloys, and Fe-Ni carbide species. In Fig. 2, we present a f_{O_2}-f_{CO_2} phase diagram in the system Fe-Mg-Si-C-O-H at 300°C and 2000 bar among the phases cohenite (Fe_3C), siderite (Sd), iron (Fe), ferrous oxide (FeO), magnetite (Mgt), hematite (Hem), forsterite (Fo), fayalite (Fa), antigorite (Atg), brucite (Brc), talc (Tc), magnesite (Mgs), graphite (Gr), and quartz (Qtz). The shaded field corresponds to a system dominated by a carbonic fluid. Also shown on this figure are a series of pseudoinvariant conditions for which we have calculated a series of compositions in the system C-O-H. The distribution of n-alkanes in this system is shown in Fig. 3. Also shown on this figure are the distributions of hydrocarbons present in purple vesuvianite, green vesuvianite and wollastonite. The theoretical and measured distributions follow the Schulz-Flory rule. It is also evident that higher hydrocarbons in green vesuvianite and wollastonite have distributions greater than those calculated theoretically for conditions defined by invariant points 4 and 5 which represent maximum equilibrium values at the serpentinizing front, assuming graphite saturation, on the limbs of the solvus between a predominantly carbonic and a predominantly aqueous fluid. By contrast, the distribution of hydrocarbons in purple vesuvianite is similar to that for invariant point 2 representing equilibrium between Fe_3C-FeO-Mgt, i.e., conditions that are considerably more reducing and of higher f_{CO_2}.

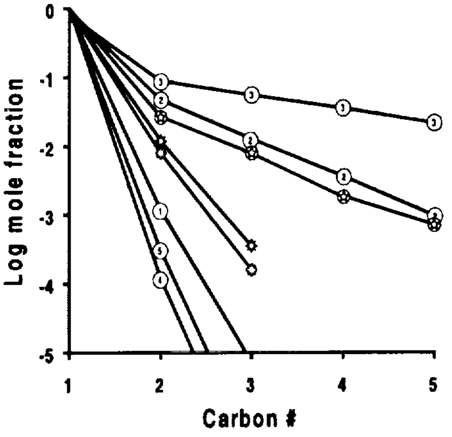

Fig. 3.

Based on the results of this study, we conclude that while Fischer-Tropsch processes may play a role in the production of hydrocarbons during serpentinization, the presence of these hydrocarbons is equally well explained by separation of a reduced carbonic fluid from the aqueous serpentinizing fluid and reaction with phases like awaruite (Ni_3Fe), cohenite and magnetite.

References: [1] Thayer T. P. (1966) *Am. Mineral., 51,* 685–710. [2] Aabrajano T. A. et al. (1988) *Chem. Geol., 71,* 211–222. [3] Berndt M. E. et al. (1996) *Geology, 24,* 351–354.

HAFNIUM-ISOTOPIC SYSTEMATICS OF KIMBERLITES, LAMPROITES, AND MEGACRYSTS: IMPLICATIONS FOR MANTLE RESERVOIRS AND THE COMPOSITION OF BULK SILICATE EARTH.

G. M. Nowell[1,2], D.G. Pearson[1], and P. D. Kempton[2], [1]Isotope Geosciences Laboratory, National Environmental Research Council, Kingsley Dunham Centre, Keyworth, Nottingham NG12 5GG, UK (gmn@wpo.nerc.ac.uk), [2]Department of Geological Sciences, Durham University, South Road, Durham DH1 3LE, UK.

Introduction: The isotopic composition of BSE is at present one of the central issues in Hf-Nd-isotopic geochemistry, as it has important implications for the evolution of the Earth [1–5]. Although several model Hf-isotopic compositions for BSE have been proposed recently [2,3], the Blichert-Toft and Albarède (BSE_{BTA}, [1]) model has been the catalyst for most discussion because it is displaced below the terrestrial array (TA; Fig. 1; [2])

The apparent discrepancy between terrestrial Hf-Nd isotopes and the BSE_{BTA} chondritic reference value could be resolved by any one of the following non-unique solutions: (1) the Earth is not chondritic in composition; (2) the present Hf-Nd chondritic values do not accurately represent BSE [2,3]; (3) a third, unsampled, major reservoir, with ε_{Hf}-ε_{Nd} values that place it below the TA, is "hidden" within the Earth [1].

Here we focus only on the latter solution and illustrate the significance of our Hf-Nd-isotopic data for lamproites, kimberlites and megacrysts to the existence of a "hidden" terrestrial Hf reservoir.

Results and Discussion: Lamproites and kimberlites (L&K) are unique amongst terrestrial magmas, as they clearly do not plot along the Hf-Nd array defined by all other terrestrial samples [4–5]. Although the slope of the L&K arrays are quite different, their common and most important feature is a trend toward, and convergence on, ε_{Hf}-ε_{Nd} values significantly below the TA (–ve $\Delta\varepsilon_{Hf}$; Fig 1, [4–5]). The Hf-Nd data presented in Fig. 1 therefore provide the clearest and most direct evidence yet for the existence of an additional "hidden" terrestrial component, i.e., one not previously observed. This component has at least the correct isotopic composition to potentially account for the displacement of BSE_{BTA} below the TA.

One question arising from Fig. 1 is the identity of this –ve $\Delta\varepsilon_{Hf}$ component [5]. Is it continental lithospheric mantle (CLM) or a much deeper mantle

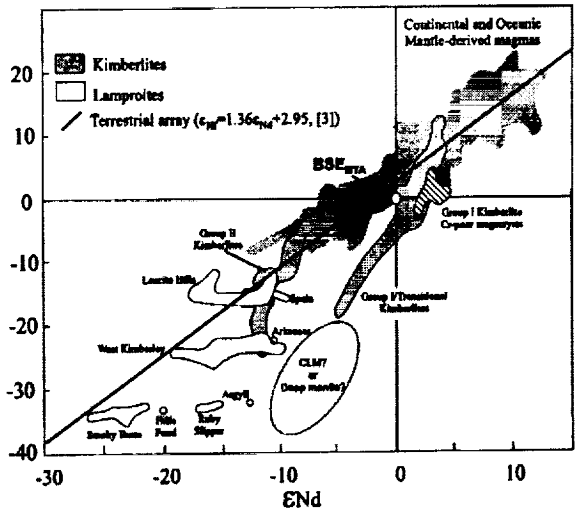

Fig. 1.

component? Such information is necessary to provide constraints on whether this component is likely to be volumetrically significant enough to account for the displacement of BSE_{BTA} alone.

As this –ve $\Delta\epsilon_{Hf}$ component contributes to L&Ks, it might be logical for it to be located within the CLM. If this is the case, because lamproites are believed to sample some of the most isotopically extreme CLM known, the –ve $\Delta\epsilon_{Hf}$ component may be no more isotopically extreme than the area outlined in Fig. 1. However, it is unlikely that a –ve $\Delta\epsilon_{Hf}$ component located in the CLM could account for the position of BSE_{BTA} below the TA alone. The CLM represents only 2–3% of the silicate Earth, and it is unlikely that the whole of this reservoir would be characterized by the composition shown in Fig. 1. If this –ve $\Delta\epsilon_{Hf}$ component resides in the CLM, our data would not appear to preclude those recent models that place BSE within the terrestrial array [2,3].

However, there are several arguments, including the displacement of megacrysts and HIMU toward this –ve $\Delta\epsilon_{Hf}$ component [4,5], that suggest that the –ve $\Delta\epsilon_{Hf}$ component might reside in the deeper sub-CLM mantle (>200 km; [4,5]). Such a component would nevertheless need to be located in a boundary layer reservoir, e.g., 670-km discontinuity or the core-mantle boundary, because of the necessity for long-term isolation from convection. A 200-km-thick D" region [6] would account for over 11% of the volume of the silicate mantle. If such a region had the composition outlined in Fig. 1, it could potentially account for the displacement of BSE_{BTA} below the TA alone

Our data clearly have important implications for the composition of BSE and lends support for the BSE_{BTA} model [1].

References: [1] Blichert-Toft J. and Albarède F. (1997) *EPSL, 148,* 243–258. [2] Salters V. J. and White W. M. (1998) *Chem. Geol., 145,* 447–460. [3] Vervoort J. D. et al. (1999) *EPSL, 168,* 79–99. [4] Nowell G. M. et al (1998) *EPSL,* submitted. [5] Nowell G. M. et al. (1998) *7th Intl. Kimberlites Conf. Ext. Abstr. Vol.,* 628–630. [6] Jeanloz R. and Williams Q. (1998) *Physics and Chemistry of the Earth's Deep Interior, 37,* 241–259.

HAFNIUM-ISOTOPIC ANALYSIS OF KIMBERLITE MEGACRYSTS BY LASER ABLATION AND SOLUTION MODE PLASMA IONIZATION MULTICOLLECTOR MASS SPECTROMETRY: EVIDENCE FOR A CONTRIBUTION FROM A DEEP MANTLE COMPONENT IN KIMBERLITES AND MEGACRYST MAGMAS?

G. M. Nowell[1], D. G. Pearson[2], P. D. Kempton[1], R. W. Carlson[3], D. Bell[4], and R. E. Zartmann[4], [1]Isotope Geosciences Laboratory, National Environmental Research Council, Kingsley Dunham Centre, Keyworth, Nottingham NG12 5GG, UK (gmn@wpo.nerc.ac.uk), [2]Department of Geological Sciences, University of Durham, South Road, Durham DH1 3LE, UK, [3]Carnegie Institution of Washington, 5241 Broad Branch Road NW, Washington DC 20015, USA, [4]Department of Geological Sciences, University of Cape Town, Rondebosch 7700, South Africa.

Introduction: Silicate and oxide minerals of the Cr-poor megacryst assemblage (CPMA) are characteristic of group I kimberlites worldwide. High P-T equilibrium conditions and trace-element compositions of megacrysts suggest they crystallized from an OIB-like parental magma at the base of the lithospheric mantle. The parental megacryst magma, sometimes referred to as a "protokimberlite," may eventually evolve toward kimberlitic compositions through the interaction and assimilation of enriched lithospheric mantle. Megacrysts therefore provide an important opportunity to determine the isotopic composition and evolution of precursor kimberlite magmas prior to lithospheric contamination. Previous isotopic studies on the CPMA have focussed on mainly Sr and Nd and were restricted in their coverage because only garnet and clinopyroxene had sufficient concentrations of these elements to permit isotopic analysis. Such restrictions do not apply to Hf, which is present in most megacryst mineral phases at concentrations sufficient for straightforward isotopic analysis of virtually the whole CPMA with the new generation plasma ionization multicollector mass spectrometers (PIMMS).

Results and Discussion: Previous Hf-isotopic studies of South African kimberlites reveal a unique source component that plots well below the mantle array conjectured to represent a deep Earth reservoir [1–3]. To further constrain the isotopic composition of the "protokimberlite" magma, we have determined the Hf-isotopic composition of a variety of CPMA mineral phases from the Monastery and other southern African kimberlites on a VG-Elemental P54. Analyses of ilmenite, garnet and clinopyroxene megacrysts were

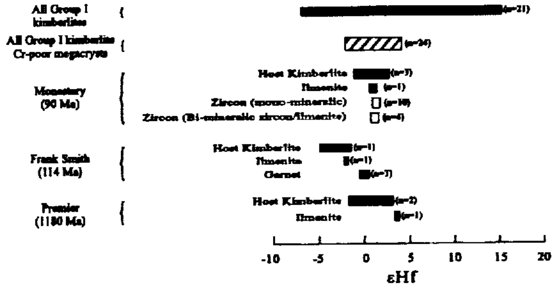

Fig. 1.

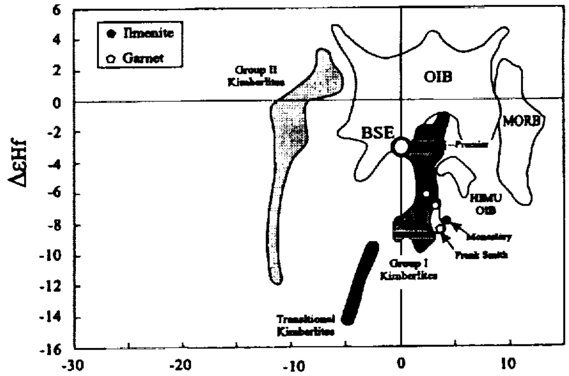

Fig. 2.

carried out by solution mode-PIMMS, while mono-mineralic zircons and zircon-ilmenite intergrowths were analyzed by both solution- and laser ablation-PIMMS. The first Nd-isotopic analyses of mantle ilmenites, obtained by thermal ionization mass spectrometry, will also be presented. The CPMA has a limited range in ε_{Hf}, –2.8 to 2.9 (Fig. 1). There is no clear systematic isotopic variation within the megacryst crystallization sequence. Furthermore, like their host kimberlites, the CPMA is characterized by some of the most extreme displacements of any terrestrial samples below the mantle array in $\Delta\varepsilon_{Hf}$-ε_{Nd} space (Fig.2; [2]).

Our Hf data give no indication for any significant isotopic evolution of the parental CPMA magma during crystallization of the CPMA due to lithospheric contamination. The CPMA therefore appear to give a true reflection of the isotopic composition of a magma, perhaps a "protokimberlite," which was derived from sublithospheric mantle depths. It is also clear that this "protokimberlite" magma was isotopically unlike any melt known to be derived from the convecting mantle. We argue that a distinct component, lying below the mantle array in ε_{Hf}-ε_{Nd} space, must exist within a deep mantle boundary layer, perhaps at the 650 km discontinuity or probably D" layer.

References: [1] Nowell G. M. et al. (1998) *7th Intl. Kimberlites Conf. Ext. Abstr. Vol.*, 634–636. [2] Nowell G. M. et al (1998) *EPSL*, submitted. [3] Nowell G. M. et al., *Proc 7th Intl. Kimberlites Conf. Cape Town.*

THE EFFECT OF GROWTH RATE, $(U/Ca)_{aq}$, AND Mg^{2+} ON URANYL ION COPRECIPITATION WITH CALCITE.

M. Nugent and R. J. Reeder, Department of Geosciences, State University of New York–Stony Brook, Stony Brook NY 11794-2100, USA (nugent@sbmp04.ess.sunysb.edu).

Aqueous U (VI) transport and immobilization in oxidizing waters is controlled, in part, by adsorption and precipitation processes. Calcite is a common aquifer and soil mineral that may provide a template for aqueous U removal from groundwater solutions via adsorption and coprecipitation. Low temperature uranyl incorporation into calcite is expected to be kinetically-controlled, based on reported results for other metal-calcite low-temperature systems [1]. However, to date, the quantity and mechanism of incorporation of the uranyl ion into calcite have not been documented for steady state coprecipitation. Therefore, the distribution coefficient for UO_2^{2+} in calcite was determined as a function of calcite growth rate, $(U/Ca)_{aq}$ ratio, and the presence/absence of Mg ion.

The distribution coefficient (K_d) for uranyl ion (UO_2^{2+}) in calcite can be defined by

$$K_d = \frac{(U/Ca)_{solid}}{(U/Ca)_{aq}}$$

where aqueous and solid concentrations are in moles/liter and moles, respectively. Steady-state growth onto calcite seed material was achieved via constant addition of growth nutrients (Ca and bicarbonate) at constant temperature and ionic strength (0.2 M NaCl). Mg-containing growth solutions contained 0.005 M Mg, and Mg-free growth solutions were prepared by filtering a preequilibrated calcite — 0.2 m NaCl solution, which had been equilibrated at atmospheric P_{CO_2}. Calcite growth rate varied over almost 2.5 orders of magnitude (from $10^{-2.7}$ to $10^{-5.0}$ $mol_{calcite}/m^2/hr$) and the U to Ca ratio in solution varied over more than 2.5 orders of magnitude (from 0.05 to 0.0001).

The distribution coefficient for uranyl ion in calcite is <1 in all cases, and, for Mg-free solutions, increases with increasing growth rate, in agreement with previously reported data for other trace metal-calcite systems with K_d <1 [1]. However, in the presence of Mg, we do not observe a growth rate effect on the K_d. At low calcite growth rates, the amount of U incorporated into calcite is significantly less when Mg is present than when Mg is absent (for example, at a calcite growth rate of $10^{-4.0}$ $mol_{calcite}/m^2/hr$ in Mg-free solutions, approximately half as much U is incorporated as for Mg-bearing solutions). Yet, at faster growth rates ($10^{-3.5}$ to $10^{-2.7}$ $mol_{calcite}/m^2/hr$), the K_d is indistinguishable for Mg-free and Mg-bearing solutions. Finally, as $(U/Ca)_{aq}$ decreases, the distribution coefficient increases, over the range in $(U/Ca)_{aq}$ studied. However, the amount of U incorporated into the solid does not increase significantly as the distribution coefficient increases.

Because our distribution coefficient is in all cases <1, coprecipitation with calcite may not serve as an effective immobilizing agent for aqueous uranyl ion. However, we expect that coprecipitation may become more effective for U immobilization in natural groundwaters and soils when there is low aqueous Mg^{2+} and high calcite precipitation rates, because of the strong growth-rate dependence for the K_d in Mg-free growth solutions.

References: [1] Mucci A. and Morse J. W. (1990) *Aqua. Sci., 3,* 217–254.

GEOLOGICAL CONSTRAINTS ON INTERPRETING EARLY ARCHEAN MINERAL AND WHOLE-ROCK ISOTOPIC DATA: CASE HISTORY FROM THE ITSAQ GNEISS COMPLEX, GREENLAND.

A. P. Nutman[1], V. C. Bennett[1], and C. R. L. Friend[2], [1]Research School of Earth Sciences, Australian National University, Canberra ACT, Australia, [2]Department of Geology, Oxford Brookes University, Headington, Oxford, UK.

Introduction to a Controversy: To what degree are the granitic (*sensu lato*) gneisses dominating the Itsaq Gneiss Complex of West Greenland the products of a single 3600–3650-Ma crust formation "superevent," or of several unrelated events between ~3850 Ma and 3560 Ma? Which of these age interpretations is correct has major implications regarding what the whole-rock radiogenic isotopic record (Pb-Pb, Sm/Nd, Lu/Hf, and Rb/Sr) reveals

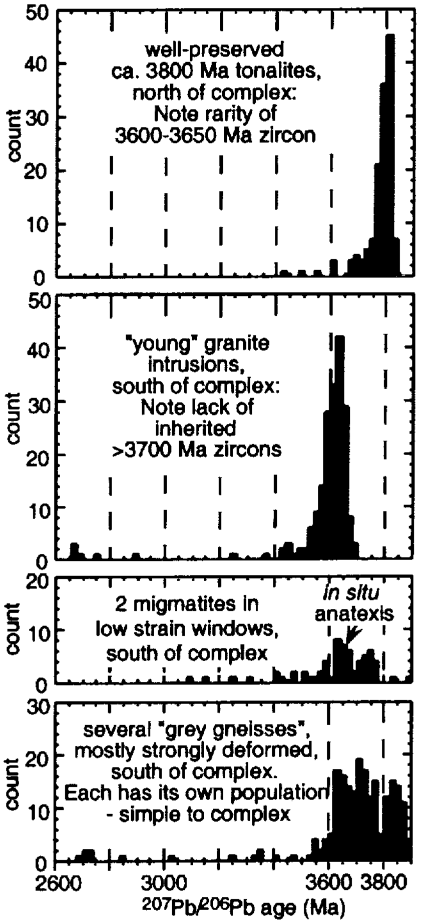

Fig. 1. Lead-207/lead-206 age (Ma) of zircons from orthogneisses and metagranitoids. (**a**) and (**b**) examples of rocks clearly different in age; (**c**) complex zircon populations in migmatites; (**d**) gray gneisses, including two with simple 3.85-Ga magmatic populations. Note: there are *no* single-phase granitoids with abundant inherited older zircon.

about continental crust formation and very early terrestrial differentiation. There is also debate if *some* West Greenland metasediments with C-isotopic evidence for life [1] are ≥3850 m.y. or only ≥3650 m.y. old, with implications for the origin of life.

Methods: Some workers [e.g., 2,3] have chosen to base their conclusions mostly on high MSWD Sm-Nd and Pb-Pb "isochrons" from regional collections of whole rocks and feldspars. The starting point of our studies are field observations and sampling from low strain zones, where the origin and nature of the rocks are best preserved and understood, closely integrated with U-Pb zircon geochronological data and cathodoluminescence imagery of the dated zircons.

Results and Implications: Our approach shows that most single-phase, well-preserved, granitoid samples have simple zircon populations dominated by grains formed when their host magmas crystallized. On the other hand, migmatites and some strongly deformed banded gneisses have much more complex zircon populations. These findings demonstrate that in the studied parts of the Itsaq Gneiss Complex: (1) exposed granitoids formed during multiple magmatic events between ~3850 and 3560 Ma and are *not* mostly 3650–3600-Ma rocks carrying abundant >3650 Ma inherited zircons; (2) abundant ≥3750-Ma granitoids are present; (3) some waterlain sediments containing C-isotopic evidence for life were deposited as early as 3850 Ma; (4) the combined field evidence and zircon geochronology demonstrate that the whole-rock Sm-Nd isochron technique fails to distinguish 3600 Ma from 3800-Ma rocks and reinforces previous indications for markedly depleted (≥2.5 ε_{Nd}) domains in the pre-3750-Ma mantle; (5) variation of initial zircon ε_{Hf} [4] between samples of a ~3630-Ma plutonic suite free of inherited zircons warns that even when the rocks are the same age, they may not meet criteria necessary to derive their age and initial ratio by the isochron method.

References: [1] Mojzsis S. et al. (1996) *Nature, 270,* 43–45. [2] Moorbath S. et al. (1997) *Chem. Geol., 135,* 213–231. [3] Kamber B. S. and Moorbath S. (1998) *Chem. Geol., 150,* 19–41. [4] Vervoort J. et al. (1996) *Nature, 279,* 624–627.

EVALUATION OF HUMAN IMPACT ON LACUSTRINE ENVIRONMENTS AND ECOSYSTEMS IN THE TWENTIETH CENTURY BY USING STABLE ISOTOPIC RATIOS OF FISH SPECIMENS.

N. O. Ogawa[1,2], H. Oda[3], T. Nakamura[3], N. Ohkouchi[2,4], N. S. Smirnova-Zalumi[5], V. V. Smirnov[6], N. G. Melnik[5], N. A. Bondarenko[5], T. Koitabashi[7], and E. Wada[7], [1]Graduate School of Environmental Earth Science, Hokkaido University, Sapporo, 060-0810, Japan (nanako@eea.hokudai.ac.jp), [2]Department of Marine Chemistry and Geochemistry, Woods Hole Oceanographic Institution, 360 Woods Hole Road, Woods Hole MA 02543, USA, [3]Dating and Materials Research Center, Nagoya University, Japan, [4]Institute of Low Temperature Science, Hokkaido University, Japan, [5]Limnological Institute, Russian Academy of Sciences, Moscow, Russia, [6]Baikal Museum, Russian Academy of Sciences, Moscow, Russia, [7]Center for Ecological Research, Kyoto University, Japan.

Anthropogenic perturbation has been evident both in global and regional environments such as the increase in the atmospheric CO_2 and lake eutrophication in these 100 yr. However, reconstruction of these perturbation has often been difficult, because of paucity of direct observational records. In this study, C- and N-isotopic ratios of fish specimens will be introduced as one of new approaches to precisely describe these perturbations and to understand the processes. To reconstruct the recent fluctuations of global and lacustrine environments in this century, we measured isotopic ratios of fish specimens which have been collected in the last several decades from Lake Baikal and Lake Biwa.

In Lake Baikal, isotopic ratios of scale specimens of Omul fish (Coregonus autumnalis migratorius) collected from 1947 to 1995 were measured. $\delta^{13}C$ of scale specimen showed around –21.4‰ in 1947, but they gradually decreased to –22.8‰ in 1995. The decreasing rate of the C-isotopic ratio is ~0.02‰/yr. The decrease of the C-isotopic ratio may reflect the variation of C-isotopic records of atmospheric CO_2, which is the ultimate source of C in fish scale. The reported isotope ratio of atmospheric CO_2 measured at Mauna Roa and in an ice core from the Antarctic showed same decreasing rate (0.02‰/yr.) during the last 40 yr, which is caused by an additional input of fossil fuel C to the atmosphere. In addition, $\delta^{13}C$ and $\delta^{15}N$ of fish scales showed oscillation with its period of ~20 yr. This cyclicity may be explained by some ecological effect, such as changes in phytoplankton biomass or foodweb structures in the lake might link to it.

In Lake Biwa, N-isotopic ratio was measured for Isaza fish (Chaenogobius isaza) in 1916, 1952, 1963–1995 and lake sediment. The $\delta^{15}N$ records in Isaza fish and sediments both showed a small change (<1‰) until 1963 but they rapidly increased more than 3‰ from 1965–1980. The total increase is up to 4‰ during the last 100 yr. These variations of N-isotopic ratio may be attributed to an eutrophication of Lake Biwa. A close relationship can be observed between the N-isotopic records of Isaza fish and nitrate concentration of lake water, which is one of the indicators of eutrophication. The eutrophication may have caused low O environments in the bottom water, which induce denitrification whose processes leave residual N larger in the isotopic ratio.

Fish specimens from many lakes in the world have been collected and stored in universities and museums over the 20th century when anthropogenic perturbation of the global and regional environments has become evident. Thus, these fish specimens are expected to provide us a novel materials for reconstructing and evaluating human impacts on the Earth's environments. In this poster presentation both usefulness and limitation of this technique will be discussed with presenting results from Lake Baikal and Lake Biwa.

ORGANIC CARBON AND NITROGEN ISOTOPES AS SOURCE INDICATORS OF ORGANIC MATTER PRESERVED IN SEDIMENTS OF THE GULF OF TRIESTE (NORTH ADRIATIC).

N. Ogrinc[1], G. Fontolan[2], J. Faganeli[3], and S. Covelli[2], [1]J. Stefan Institute, Department of Environmental Sciences, Jamova 39, 1000 Ljubljana, Slovenia, [2]Department of Geological, Environmental, and Marine Sciences, University of Trieste, Via E. Weiss 2, 34127 Trieste, Italy, [3]Marine Biological Station, Fornae 41, 6330 Piran, Slovenia.

Understanding the paleoenvironmental conditions in coastal marine areas is important for predicting of future changes of biogeochemical processes in these areas, including eutrophication. The combination of stable N and C isotopes was used to trace the historical evolution of the sources and deposition of organic matter in marine sediments of the Gulf of Trieste (northern Adriatic) and increased eutrophication in this marine basin.

Sediment samples from three long cores, two of them (~3 m long) taken at two locations in the central part in the Gulf of Trieste (cores GT1 and GT2) and another (~40 m long) in the salt marsh area along the southern shoreline (V6 core), were analyzed for organic C, total N, $\delta^{13}C_{org}$ and $\delta^{15}N$ values, and ^{14}C of sedimentary organic C ($^{14}C_{org}$). The downcore trend of $\delta^{13}C_{org}$ and $\delta^{15}N$ values shows the important influence of allochthonous organic input in the past. $\delta^{15}N$ decreased to 3‰, while $\delta^{13}C$ values decreased to lower than –26‰, which is typical for terrigenous plants. The conventional ^{14}C age of sedimentary organic C in the sediments from GT1 and GT2 cores ranges from 3370–9380 yr in the depth range of ~14 cm down to a depth of 200 cm. These spatial variations are thought to be influenced predominantly by inputs of older organic matter from lateral transport, mass wasting, or variable C sources. Using calculated mixing rates, an input of 50% of terrigenous N material and 35% of POC into the central part of the Gulf of Trieste is calculated for today.

SULFUR-ISOTOPIC RECORDS AROUND LIVELLO BONARELLI BLACK SHALE AT THE CENOMANIAN-TURONIAN BOUNDARY.

N. Ohkouchi[1], Y. Kajiwara[2], and A. Taira[3], [1]Department of Marine Chemistry and Geochemistry, Woods Hole Oceanographic Institution, 360 Woods Hole Road, Woods Hole MA 02543, USA (nohkouchi@whoi.edu), [2]Institute of Geoscience, University of Tsukuba, Tsukuba 305, Japan, [3]Ocean Research Institute, University of Tokyo, Nakano-ku Tokyo 164, Japan.

Among a number of Cretaceous black shales, one from the Cenomanian-Turonian (C-T) stage boundary at 93.5 Ma is locally characterized by extraordinarily high contents of organic C (more than 50%) and is often referred to as Oceanic Anoxic Event-2 (OAE-2) [1]. Evidence of OAE-2 is widespread throughout the Atlantic Ocean, Tethys Ocean, and some part of the Pacific Ocean [2]. In this study we report isotopic compositions of sulfate S in the rocks deposited around the OAE-2 shale that crops out at Gorgo Cerbara in the northern Apennines, Italy, and argue that the S cycle of the C-T ocean that should have varied sensitively with the redox conditions of the ocean [3].

Previous studies of infrared spectra and X-ray near-edge structure (XANES) analyses of sedimentary carbonates indicated that S in carbonate rocks is not in the form of gypsum or anhydrite inclusions, but rather sulfate substituting for carbonate [4]. Thus, isotopic composition of the carbonate-hosted sulfate presumably represents that of dissolved sulfate in seawater at the time of carbonate formation [5], although the detailed nature of sulfate incorporation in carbonate is not well known.

Pulverized rock samples were treated with NaOCl solution and benzene to remove organically bonded S and elemental S, respectively. The bleached residue was then treated with dilute HCl to decompose carbonate. Hydrogen sulfide that is evolved from certain acid-soluble sulfides was immediately eliminated by the N_2 stream, being trapped and collected in a zinc acetate solution. Acid-soluble sulfate hosted by carbonate is dissolved into the solution and collected as $BaSO_4$. The $BaSO_4$ was converted to Ag_2S by Kiba method, and then converted to SO_2 by means of a vacuum-distillation technique. Isotopic measurements were performed by a Finnigan MAT Delta-E. The analytical precision is ±0.2‰.

The S-isotopic ratios of sulfate ($\delta^{34}S_{SO_4}$) in the organic-poor carbonate and chert sequence are 16.5 ± 2.1‰ in the Cenomanian and 20.7 ± 2.2‰ in the Turonian. A remarkable increase of $\delta^{34}S_{SO_4}$ was observed across the Bonarelli horizon with the whole amplitude of 5–7‰. The positive shift of $\delta^{34}S_{SO_4}$ suggests that the burial rate of pyrite, which has lighter isotopic ratios, considerably increased during the black shale deposition. Because the period of C-T event lasted ~0.8 m.y., the rate of the $\delta^{34}S_{SO_4}$ shift at the C-T boundary is calculated to be 6–9‰/m.y. Model calculations suggest that the increase of pyrite burial during the OAE-2 results in a decrease of 9–27% in the oceanic reservoir of sulfate.

One of the most impressive phenomena associated with a large amount of pyrite burial is an elevation of O flux from the ocean to the atmosphere. The excess O_2 flux to the atmosphere during the OAE-2 is calculated as 9–27 × 10^{18} mol/m.y., which corresponds to 200–600% of average O_2 flux in the Phanerozoic [6]. Coupled with an effect of elevated burial rate of organic C, atmospheric O_2 concentration could have significantly increased during this event. Some feedback mechanisms that compensate for this additional flux of O_2 may be considered.

References: [1] Arthur M. A. and Schlanger S. O. (1979) *AAPG Bull., 63,* 870–885. [2] Arthur M. A. et al. (1988) *Nature, 335,* 714–717. [3] Ohkouchi N. et al. (1999) *Geology,* in press. [4] Pingitore N. E. et al. (1995) *GCA, 59,* 2477–2483. [5] Burdett J. W. et al. (1989) *EPSL, 94,* 189–198. [6] Kump L. R. and Garrels R. M. (1986) *Am. J. Sci., 286,* 337–360.

CARBON-ISOTOPIC RECORDS OF MARINE AND TERRESTRIAL BIOMARKERS IN THE SOUTHERN OCEAN SEDIMENTS.

N. Ohkouchi[1,2], K. Kawamura[2], N. Takemoto[2], M. Ikehara[2], and T. Nakatsuka[2], [1]Department of Marine Chemistry and Geochemistry, Woods Hole Oceanographic Institution, 360 Woods Hole Road, Woods Hole MA 02543, USA (nohkouchi@whoi.edu), [2]Institute of Low Temperature Science, Hokkaido University, N19W8 Kita-ku, Sapporo 060-0819, Japan.

We studied C-isotopic ratios of C_{31} n-alkane and C_{37} alkenes in the surface sediments collected from the Australian sector of the Southern Ocean (from 48° to 66°S). The C_{31} n-alkane is produced as one of the major components of epicuticular wax of higher plant leaf and is long-range transported through the atmosphere to open ocean [1]. On the other hand, C_{37} alkenes are produced by haptophyte algae such as *Emiliania huxleyi,* especially in low-temperature ocean [2]. The primary purpose of this study is to obtain the distribution of C-isotopic ratios for these source specific compounds in the pelagic surface sediments from the Southern Ocean. On the basis of these "core-top" records, we discuss the relationship between atmosphere/ocean environments and C-isotopic ratios of biomarkers deposited on the underlying sediments.

Nine surface sediments (0–1 cm) were collected with a multiple corer along a north-south transect in the Australian sector of the Southern Ocean during the KH94-4 *R/V Hakuho-Maru* cruise. Lipids were extracted from the sediments with methanol and CH_2Cl_2. The extracts were washed with 0.15 M HCl and saponified with 0.5 M KOH/methanol. Neutral lipids were obtained from the combined extracts by extraction with n-hexane/CH_2Cl_2. The neutral components were further separated into subfractions by silica gel column chromatography. Quantification of compounds was performed with a Carlo Erba 8000 GC/FID. Identification of compounds was performed with a Thermoquest Voyager GC/MS equipped with an electron impact mode. A fraction containing alkanes and alkenes was also analyzed using a Finnigan MAT Delta-Plus GC/C/irMS. Isotopic calibration was done with an internal standard (5α-cholestane) and standard mixture of C_{15}-C_{34} n-alkanes whose isotopic ratio had been independently determined by a conventional method. Analytical errors were determined on the basis of three or four injections of the sample.

The $\delta^{13}C$ of C_{31} alkane derived from higher plant wax shows little change along the latitude (avg. –28.7‰), whereas $\delta^{13}C$ of C_{37} alkenes derived from haptophyte algae decreases from –24.6 ± 0.7‰ at 47.6°S to –32.1 ± 1.2‰ at 63.9°S with an overall amplitude of ~7.5‰. Relatively heavy $\delta^{13}C$ of C_{31} alkane suggests a significant contribution of C4 plant waxes or conifer resin whose $\delta^{13}C$ of alkanes are significantly heavier than those of C3 plants. The $\delta^{13}C$ values of total organic C are around –20 to –21‰ from 47.6° to 60°S. However, they show a sharp decline from 60.0°S (–21.7‰) to 65.5°S (–26.0‰) with an overall amplitude of 5.3‰. It exhibits a latitudinal pattern similar to that of C_{37} alkenes, suggesting that organic C in the sediments is primarily of marine origin.

We will also present the $\delta^{13}C$ record of C_{31} n-alkane in a sediment core from Tasman Sea Plateau. Clear 2‰ increases were observed in the climatic transitions from stage 2–1 and from stage 6–5, which may reflect a dispersion of C3 plants in the southern hemisphere during these periods.

References: [1] Ohkouchi N. et al (1997) *GCA, 61,* 1911–1918. [2] Brassell S. C. (1993) in *Organic Geochem.,* pp. 699–738.

DOES SIDERITE CONSTRAIN THE pCO_2 AND pO_2 LEVELS OF THE ARCHEAN ATMOSPHERE?

H. Ohmoto, Astrobiology Research Center and Department of Geosciences, Pennsylvania State University, University Park PA 16802, USA (ohmoto@geosc.psu.edu).

The behavior of siderite in soils and sediments of Precambrian age has been used by some investigators to support a model of a reduced atmosphere prior to ~2.0 Ga. For example, based on the absence of siderite in paleosols >2.0 Ga, Rye et al. [1] argue that the atmospheric pCO_2 level was less than one-half of the level required from climatic models [2]. They suggest that the additional greenhouse gas was provided by methane. An implication of their model is $pO_2 \ll pCH_4$ in the Archean atmosphere; if not, most of the CH_4 would have been converted to CO_2 by photochemical reactions. Based on the presence of detrital grains of siderite in some sandstones and conglomerates of ~3.0 Ga, Rasmussen and Buick [3] conclude that the siderite grains, as well as pyrite and uraninite, survived during weathering and fluvial transportation because they believe siderite is stable under a reducing atmosphere but unstable under an oxic atmosphere. However, the arguments by these investigators neglect the fact that the solubility and dissolution kinetics of siderite are dependent on pH and pCO_2.

The pH of rainwater ~3.0 Ga would have been less than ~4.6, compared to ~5.6 today, if the pCO_2 was >100 PAL. However, because the pH-pCO_2 relationship of rainwater parallels that of siderite solubility, the siderite solubility in rainwater becomes essentially constant (~0.4 mol/1000 g H_2O at 25°C), regardless of the atmospheric pCO_2 level. The absence of siderite in the pre-2.0-Ga paleosols is, therefore, due to the very high solubility of siderite in rainwater, not because the atmospheric pCO_2 was below a certain level as suggested by Rye et al. [1]. The absence of siderite in paleosols does not constrain the atmospheric pCO_2 level.

In the presence of free O_2, chemical weathering of siderite proceeds through the following two steps:

$$FeCO_3 + 2\,H^+ \Rightarrow Fe^{2+} + H_2O + CO_2 \qquad (1)$$

and

$$Fe^{2+} + 1/4\,O_2 + 5/2\,H_2O \Rightarrow Fe(OH)_3 + 2\,H^+ \qquad (2)$$

Coating of siderite surfaces by insoluble ferric hydroxides formed by reaction 2 would slow down siderite dissolution (reaction 1). If there were no free O_2 in the Archean atmosphere, ferric hydroxides would not have formed to slow down siderite weathering. Furthermore, according to the available experimental data, the rate of reaction 2 decreases with decreasing pH [4], and that of reaction 1 increases with decreasing pH and increasing pCO_2 [5]. Then, the rate of chemical weathering of siderite under the Archean atmosphere must have been much faster than that of today. The *surviving* grains of "detrital" siderite must have been protected from chemical weathering; their presence in some Archean rocks, therefore, does not imply a reduced Archean atmosphere. It suggests that these "detrital" grains were liberated by fragmentation and abrasion of *unusual* host rocks (e.g., quartz veins, massive sulfide ores, siderite BIFs) while transported in streambeds during floods, and that they deposited in desert environments. Their exposure time to the surface water was probably much less than that of *normal* sediments.

In fact, the disappearance of *primary* grains of siderite, uraninite, and pyrite in paleosols and the absence of *detrital* grains of these minerals in *ordinary* sedimentary rocks of all geologic age [6] are more compatible with the models of an oxygenated Archean atmosphere [6–8] than with those of a reducing atmosphere [9].

References: [1] Rye R. et al. (1995) *Nature, 378,* 603–605. [2] Kasting J. F. (1993) *Science, 259,* 920–926. [3] Rasmussen B. and Buick R. (1999) *Geology, 27,* 115–118. [4] Stumm W. and Morgan J. J. (1996) *Aquatic Chemistry,* Wiley, 1022 pp. [5] Langmuir D. (1997) *Aqueous Environmental Chemistry,* Prentice Hall, 600 pp. [6] Dimroth E. and Kimberley M. M. (1976) *Can. J. Earth Sci., 13,* 1161–1185. [7] Towe K. M. (1981) *Precambrian Res., 16,* 1–10. [8] Ohmoto H. (1996) *Geology, 24,* 1135–1138. [9] Holland H. D. (1994) in *Early Life on Earth* (S. Bengtson, ed.), pp. 237–244, Columbia Univ.

EXPERIMENTAL STUDY OF DISTRIBUTION COEFFICIENTS OF RARE EARTH ELEMENTS BETWEEN IRON-MANGANESE DEPOSITS AND SEAWATER IN VIEW OF RARE-EARTH-ELEMENT(III)-CARBONATE COMPLEXATION CONSTANTS.

A. Ohta and I. Kawabe, Department of Earth and Planetary Sciences, Graduate School of Science, Nagoya University, Chikusa, Nagoya 464-8602, Japan (ohta@gcl.eps.nagoya-u.ac.jp).

Introduction: Rare earth elements (REEs) are highly enriched in marine Fe-Mn deposits. The REE removal by Fe-Mn oxyhydroxides from seawater into marine suspending particles and sediments is an important geochemical process. In seawater, dissolved REE species are mainly $REECO_3{}^+{}_{(aq)}$ and $REE(CO_3)_2{}^-{}_{(aq)}$ [1]. It is important to examine how REE(III)-carbonate complexation affects the REE partitioning process in seawater. Although REE(III)-carbonate complexation constants have been reported by Byrne et al. [2 and references therein], studies of REE incorporation or sorption into Fe and Mn oxyhydroxide are not as well understood [3–5]. We have determined REE partitioning coefficients, K_d(REE: ppt./sol.), between Fe oxyhydroxides and NaCl solutions with different carbonate ion concentrations. REE(III)-carbonate complexation constants have also been determined from our experimental data. We have examined whether our experimental results can reproduce apparent K_d(REE) values between Fe-Mn deposits and seawater.

Experimental Method: Rare earth elements were coprecipitated with Fe(III) oxyhydroxide precipitates in 0.5 M NaCl solutions with various amounts of $NaHCO_3$ (0.0–12.0 mM). The precipitates formed in solutions were gently stirred with magnetic stirrers in glass flasks places in a water bath at 25°C for 135–145 h. Fe(III) in the precipitate was separated from REEs by the cation-exchange column. Iron(III) and REE were determined by inductively coupled plasma atomic emission spectrometry (ICP-AES). Dissolved REEs in each NaCl solution were collected by Fe(III) coprecipitation method.

Results and Discussions: The REE distribution coefficients of log K_d(REE) in the systems without $NaHCO_3$ show heavy REE-enriched patterns, small positive Ce anomalies, $K_d(Y)/K_d(Ho)$ ratios smaller than unity, $K_d(Sc)$ values much larger than those of heavy REEs, and similar convex tetrad effects. With increasing $NaHCO_3$ concentration in NaCl solution from 0.0 mM to 12.0 mM, however, REE distribution coefficients show the following systematic variations: (1) the decrease of K_d(REE) is pronounced in heavy REE relative to light REE, (2) the convex tetrad effect becomes less obvious, (3) the $K_d(Y)/K_d(Ho)$ ratio becomes large, and (4) the decrease of $K_d(Sc)$ is much greater than those for heavy REE.

These variations with increasing $NaHCO_3$ concentration are caused by REE(III)-carbonate complexation. We have determined REE(III)-carbonate complexation constants from our experimental data of log K_d(REE) as a function of carbonate ion concentration. When our complexation constants are compared with the previously reported data by solvent-extraction method [2] at 25°C and infinite dilution, ours are higher than literature data by 1.0–1.5 in log unit. However, the increasing trend of REE(III)-carbonate complexation constants with atomic number of REE and convex tetrad effects in their series variations are quite similar between our results by Fe oxyhydroxide coprecipitation method and those of [2] by solvent-extraction method.

We have confirmed that experimental values of log K_d(REE) in the system with the carbonate ion concentration similar to seawater can reproduce the characteristics of apparent K_d(REE) between Fe-Mn deposit and deep water, except for a large positive Ce anomaly. However, the speciation calculation in seawater using our REE(III)-carbonate complexation constants is different from the result using those by solvent extraction. The speciation calculation using our complexation constants indicates that the dominant species is $REECO_3{}^+{}_{(aq)}$ except for heavy REE. In contrast, the calculation using the constants by solvent extraction shows that $REE(CO_3)_2{}^-{}_{(aq)}$ is the dominant species except for light REE [1–2]. Referring to field and experimental data as to K_d(REE) affected by REE(III)-carbonate complexation, we can examine which complexation constants are able to explain both natural and experimental systems simultaneously. Field and experimental K_d(REE) values were recalculated into log $\{m[REE(OH)_3]\ nH_2O\}/[REE(CO_3)_2{}^-,{}_{aq}]$ and log $\{m[REE(OH)_3]\ nH_2O\}/[REE(CO_3)^+,{}_{aq}]$ by using REE(III)-carbonate complexation constants. When we compared recalculated K_d(REE) values between field and experimental data, we have confirmed that our complexation constants are better to explain laboratory and field data simultaneously than those by solvent-extraction method.

References: [1] Byrne R. H. and Sholkovitz E. R. (1996) *Handbook of the Physics and Chemistry of Rare Earths, 23,* 497–593. [2] Liu X. and Byrne R. H. (1998) *J. Sol. Chem., 27,* 803–815. [3] Koeppenkastrop D. and De Carlo E. H. (1992) *Chem. Geol., 95,* 251–263. [4] Kawabe I. et al. (1999) *Geochem. J.,* in press. [5] Kawabe I. et al. (1999) *Geochem. J.,* in press.

A CHEMICAL WEATHERING STUDY OF A SMALL MOUNTAINOUS GRANITIC WATERSHED (ESTIBÈRE, FRANCE): WATER CHEMISTRY, SOIL AND ROCK MINERALOGY, AND STRONTIUM-87/STRONTIUM-86-ISOTOPIC COMPOSITION.

P. Oliva[1], B. Dupré[1], M. Remaury[2], T. Gauquelin[2], F. Martin[1], and J. Darrozes[1], [1]Laboratoire des Mécanismes de Transfert en Géologie, 38 rue des 36 ponts, 31400 Toulouse, France (oliva@lucid.ups-tlse.fr), [2]Laboratoire d'Ecologie, 39 allées Jules Guesdes, 31400 Toulouse, France.

This study is focused on the chemical and isotopic compositions of different element reservoirs (waters, soils, river sediments, and parent rock) of a small alpine granitic watershed in Estibère, Hautes Pyrénées, southwest France. This site offers a unique opportunity to identify and quantify weathering processes occurring in an alpine environment by coupling soil and water chemistry. Moreover, this work provide major insights within the framework of river geochemistry such as the estimation of present-day denudation rate in continental regions and its role on the controls of atmospheric CO_2.

The Estbère watershed is located in a protected natural reserve site in the Neouvielle massif in the Pyrénées. It has an area of approximated 6 km² at an elevation of 2000–2700 m. The watershed rests in an hercynian granitic basement (300 ± 20 Ma, [1]) and is mainly composed of biotite-rich monzogranites except at the watershed outlet, where hornblende-rich granodiorites are exposed. Mylonitic formations are also present in the northern side of the watershed. A small pedological cover rich in organic matter develops over these rock formations. Two types of soils could be described: (1) a ranker type soil, sometimes cryptopodzolic, and (2) a typical alpine type podzol. Numerous streams feed the Estibère main stream. Lakes and peat bogs develop in the natural depressions of the watershed. At this high altitude, the atmospheric contribution is important and is manifested by the snow chemistry during its accumulation in winter time. Vegetation is mainly composed by alpine grassland with *Pinus uncinata* and *Rododendron ferrugineum* groves.

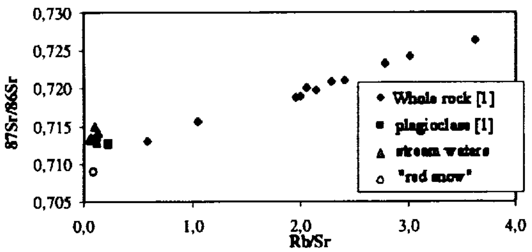

Fig. 1.

Dissolved concentrations of major ions (Cl, SO_4, NO_3, HCO_3, Ca, Na, Mg, and K) and trace elements (Al, Fe, Rb, and Sr) were determined by ion chromatography (HPLC) and by inductively coupled plasma mass spectrometry (ICP-MS) respectively. Aqueous silica concentrations were measured by standard colorimetry. Soil, sediment, and rock mineralogy were characterized by X-ray diffraction (XRD), infrared spectroscopy (IR), scanning electron microscopy (SEM), high-resolution transmission electron microscopy (HTEM), electron microprobe analysis (EMPA), and ICP-MS.

In the Estibère river stream, the dissolved fraction (i.e., <0.2 µm) is not influenced by any anthropic contributions but is only affected by atmospheric inputs and chemical weathering. Interestingly, Ca^{++} is the major cation (4–5 mg/L) in these waters, having a neutral pH 6.7–8. Although these waters are depleted in many dissolved elements, they are among the most concentrated relative to other waters draining granitic formations in the Pyrénées. The chemistry of atmospheric inputs is very heterogeneous. Indeed, Pyrénées mountains are strongly affected by snow bearing red dust coming from north Africa. This causes the snow to be very enriched in major cations and thus could be an important source for cations input in these stream waters [2]. Pedological and mineralogical characteristics on the podzol-type soil samples are of particular interest. The podzol is composed of five major horizons, from the bedrock to the surface: (1) a deep saprolithic horizon constituted mainly of quartz, weathered feldspath and biotite, chlorite, and kaolinite; (2) an unusual Al-rich dark BP_2 horizon, mainly composed of clays (e.g., kaolinite) and organic matter rich in humic acids; (3) an ocreous Fe-rich BP_1 horizon with organic matter rich in fulvic acids; (4) an ash-gray eluvial horizon; and (5) an organic-rich surface horizon composed of secondary phases such as illite, smectite, kaolinite, and amorphous aluminosilicates (e.g., imogolite, allophane). Strontium-isotopic analyses are used in this work to evaluate the contributions of each different reservoir to the stream chemistry (Fig. 1).

In conclusion, this study attempts to discuss the origin of the chemical signature of stream waters in this alpine environment. It's the result of their chemical interaction with soils and parent rock and the atmospheric inputs. Thus, Ca^{++} enrichments in these waters can be explained by the atmospheric contribution. On the other side, the Sr-isotopic compositions of the stream have signatures more similar to those of minerals from the rock basement.

References: [1] Alibert C. et al. (1988) *C. R. Acad. Sci. Paris, 306,* 49–54. [2] Avila A. et al. (1998) *Atmos. Environ., 32,* 179–191.

THE EFFECT OF MELT COMPOSITION ON THE ACTIVITY COEFFICIENTS OF SOME SIDEROPHILE ELEMENT COMPONENTS (FeO, NiO, CoO, MoO_2, MoO_3 and WO_2) IN MELTS IN THE CMAS SYSTEM.

H. St. C. O'Neill[1] and S. M. Eggins[2], [1]Research School of Earth Sciences, Australian National University, Canberra ACT 0200, Australia (hugh.oneill@anu.edu.au), [2]Department of Geology, Australian National University, Canberra ACT 0200, Australia (stephen.eggins@anu.edu.au).

The partitioning of trace elements between silicate melt and crystalline phases is one of the main tools used by geochemists to unravel the history of igneous rocks. There is, however, a complication: trace-element partition coefficients are not constants, but vary with the major-element composition of both the silicate melt and the crystalline phase, as well as temperature and pressure. Exactly which of these variables is of practical importance has been much debated. The subject has recently had a burst of attention due to the development of crystal site-strain theory [e.g., 1,2], which emphasizes the controlling influence of the crystalline phase, but other authors have considered the silicate melt composition to be a key variable [e.g., 3].

This issue has remained controversial for so long because in direct studies of crystal/melt partitioning, it is not possible to vary independently melt composition, crystal composition, temperature, or pressure so as to deconvolute the effects of each of these variables. Consequently, trace-element partitioning data can generally be fitted adequately (statistically speaking) to several alternative models, and so cannot be used to select which model is correct theoretically. However, for certain elements whose oxide components are easily reduced to the metal, it is possible to measure the effect of melt composition directly, while keeping all other variables constant, using redox reactions of the type

$$\underset{\text{metal}}{M} + x/4\ O_2 = \underset{\text{sil melt}}{MO_{x/2}}$$

We have used this approach to determine the effects of changing major-element melt composition on the activity coefficients ($\gamma_{MO_{x/2}}$) of FeO, NiO, CoO, WO_2, and MoO_2 and MoO_3 in simple system $CaO\text{-}MgO\text{-}Al_2O_3\text{-}SiO_2 \pm TiO_2$ silicate melts at 1400°C and 1 bar.

Nineteen silicate melt compositions were studied, four in the ternary CAS, two in the ternary MAS, twelve in the quaternary CMAS, and one in the system CMAS-TiO_2. Compositions were selected so as to be liquid at our chosen experimental temperature of 1400°C and to quench to glasses. This limits the compositional space available in the CAS and MAS systems to small areas near eutectics. For the CMAS system, we chose both near-eutectic compositions and also near-liquidus compositions that are close to saturation with SiO_2, Mg_2SiO_4, $MgSiO_3$, and $CaSiO_3$.

Beads of each composition were loaded onto wire loops made from the pure metal of interest, and hung, six or seven at a time, in a vertical-tube furnace equipped for gas mixing. Oxygen fugacity was imposed using CO-CO_2 gas mixtures. The f_{O_2} for each metal was selected from previous work [4,5] to produce concentrations near ~4000 ppm of W, Co, and Ni in most compositions, and ~3% of Fe. Since Mo occurs in two oxidation states at experimentally accessible f_{O_2} [4], this element was studied as a function of f_{O_2} over as wide a range of f_{O_2} as was experimentally feasible. Time series experiments showed that ~4 h was all that was needed for the samples to closely approach equilibrium, but most experiments were run for ~40 h. Samples were quenched by dropping into water.

The major-element compositions of all samples were checked by electron microprobe analysis in the energy-dispersive spectrometry (EDS) mode. Iron, Ni, Co, and, in a few runs, Mo, were also determined by electron microprobe using WDS and the pure metals as standards. Tungsten, Mo, Ni, and Co were determined by laser-ablation inductively coupled plasma mass spectrometry (LA-ICP-MS), a relatively new analytical technique that is ideally suited for this type of study. Analytical precision from either method is ~3% (1 s.d.)

In deriving values of $\gamma_{MO_{x/2}}$ from the measured element solubilities, the only other significant non-systematic uncertainty is that in f_{O_2}, which is estimated to be ±0.02 log-bar units (1 s.d.). However, for each set of samples hung in the furnace, any error in f_{O_2} is common to all samples and may therefore be ignored in comparing the effects of melt composition. Hence the relative accuracy of $\gamma_{MO_{x/2}}$ is ±3%.

For MoO_2, MoO_3, and WO_2, solubilities (hence $1/\gamma_{MO_{x/2}}$) at constant f_{O_2} vary with melt composition by nearly an order of magnitude; much of the variation may be explained by a strong positive correlation with [CaO] in the melt, suggesting the importance of $CaMoO_3$, $CaMoO_4$, and $CaWO_3$ as melt species. For FeO, CoO, and NiO, the variation with melt composition is much more limited, and, as a first approximation, γ_{FeO} could be represented by a single value for all CMAS compositions to within ±30%, and γ_{CoO} to within ±20%. Ternary CAS compositions tend to have lower solubilities (higher $\gamma_{MO_{x/2}}$) for all three elements, whereas MAS samples have high solubilities. For the quaternary CMAS samples, when the small variations are considered, there is almost no correlation between γ_{FeO} and γ_{CoO}, γ_{FeO} and γ_{NiO}, or γ_{NiO} and γ_{CoO}. This implies that attempts to parameterize values of γ_{MO} for these elements using simple global-melt descriptors such as NBO/T or melt basicity will not be successful.

References: [1] Blundy J. D. and Wood B. J. (1994) *Nature, 372,* 452–454. [2] Wood B. J. and Blundy J. D. (1997) *Contrib. Mineral. Petrol., 129,* 166–181. [3] Nielsen R. L. (1988) *GCA, 2,* 27–38. [4] Holzheid A. et al. (1994) *GCA, 58,* 1975–1981. [5] Ertel W. et al. (1996) *GCA, 60,* 1171–1180.

ATMOSPHERIC CO_2 LEVELS DURING THE LATE MIOCENE AND THE EXPANSION OF C_4 GRASSES.

M. Pagani, K. H. Freeman, and M. A. Arthur, Department of Earth Sciences, University of California, Santa Cruz CA 95064, USA (pagani@es.ucsc.edu).

Trends in C-isotopic compositions of soil carbonates and mammalian tooth enamel provide strong evidence for a global expansion of C_4 grasslands in the late Miocene [1,2]. This event has been attributed to a large-scale decrease in pCO_2, which would have favored C_4 over C_3 plant metabolism. This triggering mechanism is controversial, in part due to a lack of direct evidence for pCO_2 change and because other factors (such as growing-season temperature and precipitation) are also important in the favoring of plants with different metabolisms. This study reconstructs late Miocene pCO_2 from ε_p values based on C-isotopic analyses of diunsaturated alkenones and planktonic foraminifera. Alkenone-based pCO_2 estimates from Deep Sea Drilling Project Site 588 show no evidence for a major change in pCO_2 during the late Miocene (5–10 Ma). Instead, estimated pCO_2 steadily increased from ~14 to 9 Ma and stabilized at approximately pre-industrial values by 9 Ma. We propose that C_4 expansion was triggered by an episode of enhanced low-latitude aridity and/or changes in seasonal precipition patterns on a global scale associated with both existing low pCO_2 conditions and a late Miocene phase of Asian orogeny.

References: [1] Cerling T. E. et al. (1993) *Nature, 361,* 344–345. [2] Cerling T. E. et al. (1997) *Nature, 389,* 153–158.

NEW GEOCHEMICAL (MAJOR- AND TRACE-ELEMENT, INCLUDING RARE-EARTH-ELEMENT) DATA FROM PRONTO MINE AND VILLE MARIE WEATHERING PROFILES IN ONTARIO AND QUÉBEC, CANADA: ELEMENTAL MOBILITY DURING PALEOPROTEROZOIC WEATHERING OF ARCHEAN GRANITIC BASEMENT.

A. Panahi and G. M. Young, Department of Earth Sciences, University of Western Ontario, London ON, N6A 5B7, Canada.

New geochemical analyses were obtained from samples of the Pronto Mine and Ville Marie paleosols in Ontario and Québec using inductively coupled plasma mass spectrometry (ICP-MS). The Pronto Mine weathering profile formed on Archean calk-alkaline granite at ~2.4–2.5 Ga and is marked by the presence of a thin cap of sorted sediments. Both paleosol and associated sediments are overlain by basal pyritic, uraniferous quartz pebble conglomerates and sandstones of the Matinenda Formation in the Huronian supergroup. The Ville Marie weathering profile formed on Archean alkali granite between 2.4 and 2.2 Ga and is overlain by sandstones of the Lorrain Formation. Both weathering profiles are exceptionally well preserved.

Mass-balance calculations indicate that Na, Ca, P, and Sr were lost from the profiles, whereas K, Rb, and Ba were introduced. Iron and Mg were also added at Ville Marie. Titanium, Nb, Th, Zr, Hf, and Ta were essentially immobile. Rare earth elements (REE) were leached from the weathering samples of both paleosols.

Rare-earth-element/titanium ratios of the average bulk sample from Pronto Mine weathered profile are ~60% (LREE) to 20–40% (HREE) lower than that of the protolith. $(La/Yb)_N$, $(La/Sm)_N$, and La/Th ratios in samples from the Pronto paleosol are generally lower than those for the protolith. REE were leached from the primary minerals during weathering of the granite. The $(La/Yb)_N$ ratio for the average paleosol sample is 34.34. The ratio for the average paleosol-related sediments (59.69) closely resembles that of the protolith sample (54.09). LREEs were preferentially concentrated in the fine-fraction (sericitic) of the sediments. The paleosol-related sediments may have acted as a reservoir for REEs that were leached from the primary minerals. The Eu/Eu* for the parent sample is 0.78. All samples from the weathering profile and associated sediments have stronger negative Eu anomalies (Eu/Eu* = 0.44–0.66) than the protolith, suggesting that Eu was lost from the profile. Cerium/cerium* ratios remained relatively unchanged.

Up to 40% of the REEs were leached from the Ville Marie weathering profile relative to protolith and $(La/Yb)_N$ ratios for the weathered samples are generally lower than that of the protolith, reflecting preferential depletion of LREE relative to HREE. $(Gd/Yb)_N$, $(La/Sm)_N$, Zr/Hf, Th/U, and Th/Co ratios for the entire profile are generally the same as those of the protolith. Europium/europium* values for the samples of the Ville Marie weathering profile are in the range of that of the protolith and the ratio for the average paleosol (0.72) resembles that of the protolith (0.71). Europium/europium* values in the samples from the bottom part of the profile, however, are lower than that of the protolith, and Eu is positively correlated with Sr in these samples.

Previous studies indicate that negative Eu anomalies can be produced during chemical weathering. The negative Eu anomalies in the samples from Pronto Mine and Ville Marie were probably produced during chemical weathering as a result of the destruction of feldspars. The magnitude of the Eu anomalies may be controlled by Eh conditions.

MOLECULAR SIMULATION OF METHANE HYDRATE STRUCTURE AND DYNAMICS IN MONTMORILLONITE INTERLAYERS.

S.-H. Park[1] and G. Sposito[2], Geochemistry Department, Earth Sciences Division, Lawrence Berkeley National Laboratory, University of California, Berkeley CA 94720, USA (spark@nature.berkeley.edu; gsposito@nature.berkeley.edu).

Introduction: Methane hydrates became industrially important after their discovery in 1934 as blocking material in a gas pipeline [1]. Thirty years later they were reported as natural reserves of hydrocarbons in Siberian permafrost [2]. Methane hydrates (clathrates) are environmentally important inclusion compounds naturally occurring in deep ocean floors and in permafrost. They potentially serve as energy resources, as an atmospheric methane sink that may influence global climate, and as intercalates that affect the strength of oceanic sediments, leading to submarine landslides [3]. Computer simulation using the conventional Metropolis algorithm (Monte Carlo simulation) can be useful to study the equilibrium structure of methane hydrates in this experimentally hard-to-achieve environment [4]. Sloan and coworkers have studied the effect of bentonite (sodium montmorillonite) on methane hydrate formation [5,6]. Our computer simulations of methane hydrate formation for the first time include this clay type, which is a typical component of drilling fluids in the oil industry as well as of ocean sediments responsible for landslides.

Methods: We used Monte Carlo (MC) and molecular dynamics (MD) simulations to study methane hydrate structure and dynamics. Details about the use of this combination of two computational methods for the same Na-montmorillonite system (without methane hydrate) to study the structure and dynamics of water in clay interlayers can be found elsewhere [7]. MC simulations were carried out at 1, 10, 20, 30, 40, and 50 atm for different loadings of methane with three adsorbed layers of water within the montmorillonite pore space. The simulation cell we used contains 8 unit cells of Wyoming-type montmorillonite clay, $Na_6[Si_{62}Al_2](Al_{28}Mg_4)O_{160}(OH)_{32}$. MD simulations were carried out for P/T of 10 atm/300 K, 20 atm/300 K, and 30 atm/300 K for 4, 8, and 18 methane molecules per simulation cell, respectively.

Results: Our recent Monte Carlo simulations [8] show some aspects of the detailed structure of methane hydrates when in the presence of smectite clay minerals. The inherent hydrophobicity of the smectite siloxane surface, as well as the interaction between methane and water, led to a distorted 20-fold CH_4-O coordination (Fig. 1). Equilibrium physical properties in terms of equilibrium structure and coordination number were compared with previous experimental results and with theoretical results on synthetic methane hydrates.

We also carried out constant volume (NVT) molecular dynamics simulations after obtaining a possible subset of equilibrium structures from the constant-pressure (NPT) ensemble Monte Carlo simulations. A complete and detailed molecular picture using this time-dependent simulation provided us with valuable insight into the structure of methane clathrates and the behavior of water at an elevated pressure representing the sediment environments where methane hydrates are found.

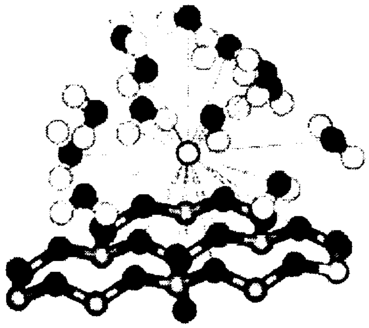

Fig. 1. Visualization of a methane molecule adsorbed in the interlayer region of the three-layer hydrate of Na-montmorillonite, based on MC simulation. The typical 20-fold coordination between CH_4 and O occurs, but with nearly half of the O being in the siloxane surface (at bottom).

Acknowledgments: The authors express gratitude to the National Energy Research Scientific Computing Center for allocations of time on its Cray supercomputers. This research was supported in part by the Director, Office of Energy Research, Office of Basic Energy Sciences, Geosciences Division of the U.S. Department of Energy under Contract DE-AC03-76SF00098.

References: [1] Hammerschmidt E. G. (1934) *Ind. Eng. Chem., 26,* 851. [2] Makogon Y. F. (1965) *Gazov. Promst., 5,* 14. [3] Kvenvolden K. A. (1999) *Proc. Natl. Acad. Sci. USA, 96,* 3420. [4] Sposito G. et al. (1999) *Clays Clay Mineral., 47,* 192. [5] Ouar H. et al., *Trans IchemE, 70,* 48. [6] Cha S. B. et al., *J. Phys. Chem., 92,* 6492. [7] Chang F.-R. et al., *Langmuir, 14,* 1201. [8] Sposito G. et al. (1999) *Proc. Natl. Acad. Sci. USA, 96,* 3358.

THE ROLE OF H_2O IN CONTROLLING THE COMPOSITION OF HIGH-DEGREE MANTLE MELTS.

S. W. Parman and T. L. Grove, Department of Earth, Atmospheric, and Planetary Sciences, Massachusetts Institute of Technology, Cambridge MA 02139, USA (parman@mit.edu; tlgrove@mit.edu).

Introduction: Many hydrous magmas are in equilibrium with residues of olivine and orthopyroxene at elevated pressures (e.g., high-Mg andesites, boninites, and Barberton komatiites). To understand the effect that H_2O has on the compositions of these magmas, we have performed experiments on a komatiite composition that is saturated with olivine and orthopyroxene over a range of P (0.001–22 kbar), T, and H_2O contents (0 and 6 wt%). H_2O loss was minimized by using capsules made of AuPd alloys. Capsules with more than 10 wt% Pd were presaturated with Fe to avoid Fe loss during the experiment.

Compositional Effects of H_2O: The primary effect of H_2O addition is to raise the SiO_2 content of the melt, but only when the melt is calculated on an anhydrous basis [1,2]. Gaetani and Grove [2] noted that when H_2O is included in the melt composition, the SiO_2 is diluted, and the hydrous melts actually have less SiO_2 than the anhydrous melts. The more fundamental effect of H_2O is to raise the SiO_2/MgO ratio of melts relative to anhydrous melts at the same pressure. This is true whether one includes H_2O in the melt composition or not.

Thermodynamic Controls on Composition: The compositional effects are primarily the result of lowering the temperature at which the phases coexist. This effect is best seen by considering the activities and activity coefficients for SiO_2 in the melts. These values were estimated by first calculating the equilibrium constant (K) for the reaction

$$Mg_2SiO_{4\ \mathrm{olivine}} + SiO_{2\ \mathrm{melt}} = MgSiO_{3\ \mathrm{pyroxene}}$$

using the thermodynamic data of [3]. Then, the activities of forsterite in the olivine (a_{ol}) and enstatite (a_{en}) in the pyroxene were calculated. The equation for the equilibrium constant

$$K = a_{en}/a_{SiO_2}a_{ol}$$

was then solved for activity of SiO_2 in the melt (a_{SiO_2}). The results show that the activity of SiO_2 decreases with temperature. Thus, the temperature lowering effect of H_2O causes increased SiO_2 activity. At the same time, SiO_2 concentrations are lower at lower temperature. This requires the activity coefficient to rise as temperature decreases. Magnesium oxide contents must decrease even more than SiO_2, because the SiO_2/MgO ratio increases with the addition of H_2O. Therefore, the effect of H_2O on the activity coefficient of MgO in the melt must be larger than its effect on the activity coefficient of SiO_2 in the melt. An alternative explanation of our data is that H_2O is the main control on SiO_2 activity coefficients and that temperature has a secondary effect [2]. The ambiguity between temperature and H_2O arises because the two are strongly correlated in our experimental data, and there is little overlap in the temperature of the hydrous and anhydrous experiments to help resolve their effects. Both interpretations are permissible at this point, though the temperature model fits our data better.

Effect of Pressure: Another feature of the experiments is that the hydrous and anhydrous ol-opx boundaries converge at higher pressure. This implies that the elevated SiO_2/MgO of hydrous magmas should be most extreme at low pressures and should decrease at higher pressure. This result is consistent with the composition of sampled hydrous magmas. Boninites are hydrous magmas produced at low P (<10 kbar) and show very high SiO_2 (54–60 wt% [4]) relative to anhydrous basalts (~50 wt%). High-Mg andesites are produced at higher P (10–20 kbar) and have moderately high SiO_2 (53–58 wt% [5]). Barberton komatiites are Archean hydrous magmas that were produced at pressures of ~22 kbar and have SiO_2 contents of ~49 wt% [6]. Though the SiO_2 contents of Barberton komatiites are low, they are higher than anhydrous melts at the same pressure and melt fraction.

References: [1] Kushiro I. (1969) *Am. J. Sci., 267-A,* 269–294. [2] Gaetani G. A. and Grove T. L. (1998) *CMP, 131,* 323–346. [3] Davidson P. M. and Lindsley D. H. (1989) *Am. Mineral., 74,* 18–30. [4] Crawford A. J. et al. (1989) in *Boninites,* pp. 2–44, Unwin Hymann. [5] Baker et al. (1994) *CMP, 118,* 111–129. [6] Parman S. W. et al. (1997) *EPSL, 150,* 303–323.

LASER ABLATION PLASMA IONIZATION MULTICOLLECTOR MASS SPECTROMETRY: A NEW METHOD FOR INTRACRYSTAL URANIUM-THORIUM-LEAD GEOCHRONOLOGY USING MICROSAMPLING TECHNIQUES.

R. Parrish[1,2], M. Horstwood[2,3], G. Nowell[2], S. Noble[2], H. Timmermann[2], P. Shaw[4], and I. Bowen[4], [1]Department of Geology, University of Leicester, University Road, Leicester, UK, [2]Isotope Geoscience Laboratory, National Environmental Research Council, British Geological Survey, Keyworth, Nottingham, NG12 5GG, UK, [3]Centre de Recherche en Géochimie Isotopique et en Géochronologie, Université de Québec à Montréal, C.P.8888, Succ. A, Montréal, Québec H3C 3P8, Canada, [4]VG Elemental, Ion Path, Road Three, Winsford, Cheshire CW7 3BX, UK.

A VG Elemental P54 plasma ionization multicollector mass spectrometer (PIMMS), equipped with multiple Faraday detectors and a VG Microprobe-II 266-nm UV laser, has been used to measure the full spectrum of U, Th, and Pb isotopes in the minerals monazite, xenotime, and zircon, including corrections for mass-bias using Tl with a natural isotopic composition.

Using two different standards of 55 Ma and 1876 Ma, a linear, zero-intercept calibration function relating measured to known ratios has been empirically verified using both the $^{208}Pb/^{232}Th$ and $^{206}Pb/^{238}U$ decay systems for monazite, and the $^{206}Pb/^{238}U$ decay system for xenotime and zircon (Fig. 1).

Repeated measurement of the standards over the course of a day's operation has produced uncertainties in the slope of the calibration line of 3–8% (1 s.d.), within sampled areas of ~30 µm across by 10–20 µm depth. The small variation in interelement ratios and the fact that the slope of the measured vs. actual ratios are within 10% of 1.0 imply limited and fairly constant differential ionization/volatilization in our procedure. Figure 2 displays these relatively constant U/Th-Pb ratios during a time-resolved analysis. This result is in contrast to many previous LA-ICP-(quadrupole)-MS

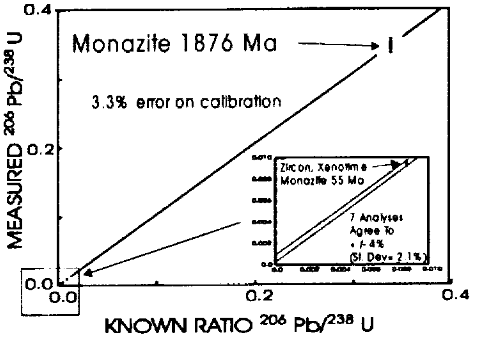

Fig. 1.

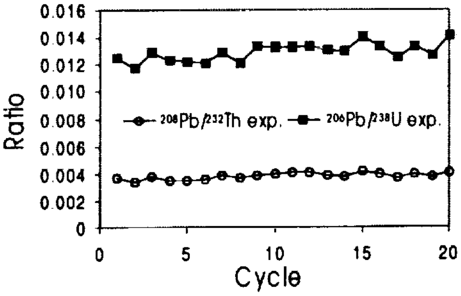

Fig. 2.

zircon analyses from a number of laboratories who have found it difficult to control the inter-element laser-induced fractionation to these levels of uncertainty using UV lasers [1,2].

In a separate experiment, ^{208}Pb/^{232}Th and/or ^{206}Pb/^{238}U were measured from zircon, xenotime, and monazite from the 55-Ma standard. The results showed that irrespective of the mineral analyzed, the measurements agree to within 4% (absolute variation, 2.1% 1 s.d.), proving that there is no significant "matrix" effect. By contrast, ion microprobe-based U-Pb geochronology (i.e., SHRIMP or CAMECA 1270) involves complex calibration functions as well as the necessity to match the matrices of sample and unknown [3]. Because of the linearity of the calibration, its zero intercept, and its nondependence on matrix, the method outlined here elegantly overcomes many of the problems inherent to ion microprobe isotopic micro-analysis for geochronology, and facilitates rapid sampling and isotopic measurement, simpler standardization procedures, and reduced cost. It is believed that this approach to *in situ* isotopic analysis will be an extremely promising method in future geochronological and isotopic research.

References: [1] Feng R. et al. (1993) *GCA, 57,* 3479–3486. [2] Hirata T. and Nesbitt R. W. (1995) *GCA, 59,* 2491–2500. [3] Compston W. et al. (1984) *JGR, 89,* B525–B534.

CRUSTAL GROWTH MECHANISMS: THE ROLE OF TRANSFORM CONTINENTAL MARGINS.

P. J. Patchett and C. G. Chase, Department of Geosciences, University of Arizona, Tucson AZ 85721, USA (patchett@geo.arizona.edu; chase@geo.arizona.edu)

Introduction: There has been much discussion of juvenile arc vs. oceanic plateau initiation for crustal growth. Both in the case of growth by creation and addition of arcs [e.g., 1,2], and by addition of plume-related plateau structures [e.g., 3–6], it is observed that most mid-upper crustal rocks eventually preserved in orogenic belts are subduction-related magmatic products or derived sediments. To first order, the rate of production of subduction-zone magmas from any protolith must be a function of subduction rate, but also of the water content of subducted rocks. Considering also factors that inhibited long-term stabilization of continents in the pre-3.5-Ga Earth, no close relationship between the heat budget and continent generation is expected.

Rates of Growth: Perceived need for plume-driven crust generation comes from apparent growth rates that locally exceed those of present-day arcs by large amounts [e.g., 7,8]. This problem can be partly explained away by the serial accretion of arc structures [1,9], but assemblages of crust such as northern hemisphere 1.7–1.9 Ga [1] and 0.6–0.9 Ga Arabia [9] still seem to require very large growth rates. It is assumed that an oceanic plateau, with a thick section of wetted basaltic protolith, whether obducted, accreted, or subducted, would provide a large amount of "fuel" for a major crust generation episode [e.g., 6].

Episodicity: Episodicity of crust generation in individual continents has long been known. Episodicity on a global scale is not expected [10], as corroborated by important generation periods showing up in lesser-known continents [e.g., 4], to fill the "gaps" seen in North America and Europe. Any apparent global episodicity that remains is probably an artifact of poorly known continents, and cannot be used, in our view, to constrain mechanisms [cf. 11].

Transform Continental Margins: Both the problems of high local growth rates and apparent episodicity are explained if mechanisms exist to pile up juvenile crust into one or more restricted zones of orogenic belts. This could be through serial arc accretion [e.g., 9,12], or by transform faulting along the continental margin [12]. All that is needed in Proterozoic time is more intense development of the accretion and transform faulting seen in the Canadian Cordillera [12]. Here, after subduction of the mid-ocean ridge, the Pacific margins of Canada and of California have become transform margins, with transport of accreted terranes to the north. Large strike faults are visible and in part active, but can become nondescript shear zones in ancient terranes [e.g., 13, and cf. 2].

Modeling of Transform Margins: We have constructed models of the development, frequency, and duration of transform margins to continents. The critical factor is a large continental margin re-entrant ("armpit") established either at time of rifting or by subsequent accretion patterns. If a large re-entrant exists, then one of its sides must become either a transform margin, or at least have a large component of transpressive convergence. The larger the continental re-entrant, and the longer-lived the ocean basin, the greater the pile-up of juvenile arc material into the re-entrant area. The Monte Carlo models compare successfully to paleogeography [14] for Phanerozoic time. Geographic comparisons are close to impossible in Precambrian time. Nevertheless, to qualitatively explain episodes like the 1.7–1.9-Ga crust or the Arabian-Nubian Shield, we show that major transform margins are expected whenever large ocean basins had a protracted history of convergence at their margins. Models indicate that a major transform margin has a high probability of existing somewhere on the globe at all times. A major transform margin is expected to continue to operate, continuously or intermittently, for the lifetime of the ocean basin, hence for 150–300 m.y. This explains apparent rapid growth and episodicity without resorting to extraordinary mechanisms.

References: [1] Patchett P. J. and Arndt N. T. (1986) *EPSL, 78,* 329–338. [2] Condie K. C. and Chomiak B. (1996) *Tectonophys., 265,* 101–126. [3] Vervoort J. D. et al. (1993) *Econ. Geol., 88,* 1598–1614. [4] Boher M. et al. (1992) *JGR, 97,* 345–369. [5] Stein M. and Hofmann A. W. (1994) *Nature, 372,* 63–67. [6] Stein M. and Goldstein S. L. (1996) *Nature, 382,* 773–778. [7] Reymer A. and Schubert G. (1984) *Tectonics, 3,* 63–77. [8] Reymer A. and Schubert G. (1986) *Geology, 14,* 299–302. [9] Pallister J. S. et al. (1990) *Geology, 18,* 35–39. [10] Gurnis M. and Davies G. F. (1986) *Geology, 14,* 396–399. [11] Albarède F. (1998) *Tectonophys., 296,* 1–14. [12] Samson S. D. and Patchett P. J. (1991) *Austr. J. Earth Sci., 38,* 595–611. [13] Karlstrom K. E. et al. (1987) *GSA Bull., 99,* 529–538. [14] Scotese C., Web site.

RADIOGENIC ISOTOPES AND CLASTIC SEDIMENTS.

P. J. Patchett[1], G. M. Ross[2], J. D. Vervoort[1], J. Blichert-Toft[3], and F. Albarède[3], [1]Department of Geosciences, University of Arizona, Tucson AZ 85721, USA (patchett@geo.arizona.edu) [2]Geological Survey of Canada, 3303 33rd Street NW, Calgary, Canada, [3]ENS de Lyon, 46 Allée d'Italie, 69364 Lyon, France.

The gross aspects of element partitioning between chemical elements in the weathering, soil, and sedimentary system were already evident in the early days of geochemistry, exemplified in Goldschmidt's posthumous book of 1954 [1] and in *Principles of Geochemistry* by Brian Mason (1952–1966) [2], as well as in the many references contained in those works.

Trace elements, particularly REE, proved important and useful in defining the general nature of sources, and in crustal evolution [e.g., 3]. Compared to all these approaches, radiogenic isotopes were slow to develop because dating of shales by Rb-Sr appeared tricky [e.g., 4]. As far as provenance and Sr were concerned, it was realized early on that the fractionations between Na, K, Rb, Ca, and Sr inherent in weathering and clay mineral and carbonate formation rendered the Rb-Sr system of doubtful value [e.g., 5].

The advent of Nd-isotopic studies [e.g., 6,7] provided a huge field of study, because of the known generally conservative behavior of REE in clastic sediments. Studies have generally been effective at large scales, because of long-distance transport of mud fractions in sedimentary systems. Applications have been pursued to regional tectonic evolution [e.g., 8,9], large-scale eolian transport [e.g., 10], and continent-scale dispersal from mountains [e.g., 11]. The presentation will review and preview research in our group on Nd isotopes and large-scale sediment dispersal, and its importance for topographic history of continents, in particular mantle-driven dynamic topography.

The multiple collector inductively coupled plasma mass spectrometer (MC-ICP-MS), which can measure Hf isotopes more than 100x better than thermal ionization mass spectrometry (TIMS) machines [12], has opened Hf isotopes to provenance studies. Hafnium-isotopic studies are now only <2x more difficult than Nd, instead of 50x more difficult. To date, results have shown the similarities to Nd isotopes in shales, and demonstrated variations on a generalized global basis for shales of all ages [13]. A fractionation due to slow weathering of zircon [14], thought to be very important for global crust-mantle recycling discussions, is now shown to be of minor significance over the whole globe and over large slices of geologic time [13,15]. The talk will overview these global Hf-Nd isotopic studies conducted in our group(s) [13], as well as older work on Lu-Hf fractionation and the use of U-Pb systematics from detrital zircons. Use of Hf isotopes in a manner comparable to Nd, for regional and continent-scale provenance studies, will certainly follow in the future.

References: [1] Goldschmidt V. M. (1954) *Geochemistry,* Clarendon, Oxford. [2] Mason B. (1966) *Principles of Geochemistry, 3rd ed.,* Wiley, New York. [3] Taylor S. R. and McLennan S. M. (1981) *Phil Trans. R. Soc., A301,* 381–399. [4] Clauer N. (1979) in *Lectures in Isotope Geology* (E. Jäger and J. C. Hunziker, eds.), pp. 30–51, Springer. [5] Goldstein S. L. (1988) *Nature, 336,* 733–738. [6] Allègre C. J. and Rousseau D. (1984) *EPSL, 67,* 19–34. [7] Miller R. G. and O'Nions R. K. (1984) *EPSL, 68,* 459–470. [8] Frost C. D. and Coombs C. (1989) *Am. J. Sci.,* 744–770. [9] Patchett P. J. and Gehrels G. E. (1998) *J. Geol., 106,* 269–280. [10] Jones C. E. et al. (1994) *EPSL, 127,* 55–66. [11] Patchett P. J. et al. (1999) *Science, 283,* 671–673. [12] Blichert-Toft et al. (1997) *CMP, 127,* 248–260. [13] Vervoort J. D. et al. (1999) *EPSL, 168,* 79–99. [14] Patchett P. J. et al. (1984) *EPSL, 69,* 365–378. [15] Plank T. and Langmuir C. H. (1998) *Chem. Geol., 145,* 325–394.

OPEN SYSTEM MODELS OF LEAD-ISOTOPIC EVOLUTION OF THE EARTH.

D. Paul and W. M. White, Department of Geological Sciences, Cornell University, Ithaca NY 14850, USA (dp55@cornell.edu).

Introduction: Suitable models of the isotopic composition of the Earth must reproduce not only the present-day radiogenic isotopic ratios in each terrestrial reservoir, but also the parent-daughter ratios in those reservoirs. The U-Th-Pb system provides a particularly powerful constraint on such models because three radioactive parents (^{235}U, ^{238}U, and ^{232}Th) decay to different isotopes of Pb (^{207}Pb, ^{206}Pb, and ^{208}Pb) with very different half-lives. Galer et al. [1] observed that ^{230}Th/^{232}Th ratios of mid-ocean-ridge basalts (MORB) imply a present ^{232}Th/^{238}U ratio (κ) in the depleted upper mantle (DUM) of <2.5, whereas ^{208}Pb*/^{206}Pb* ratios implied a much higher time-integrated κ of >3.7. Subsequently, White [2] concluded that while ^{206}Pb/^{204}Pb ratios in MORB implied a time-integrated ^{238}U/^{204}Pb (μ) ratio in the DUM of >8, the present μ in the DUM must be <6. A number of published mass-balance and isotopic evolution models of the Earth produce plausible distributions of ^{87}Sr/^{86}Sr and ε_{Nd} and their respective parent-daughter ratios between the crust and the upper and lower mantle [e.g., 3]. However, none of them adequately describe the distribution of isotopes of the U-Th-Pb system incorporating the constraints of Galer et al. [1] and White [2].

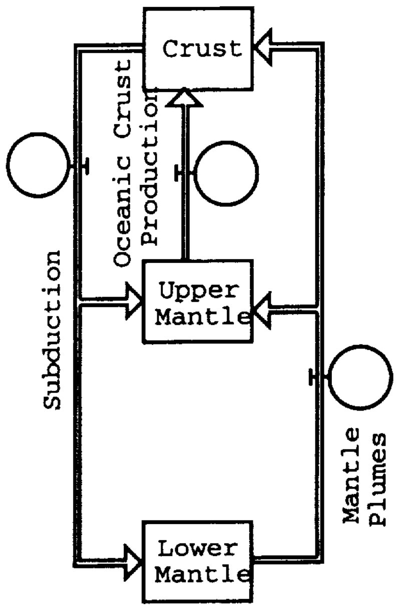

Fig. 1. Three-reservoir model of the Earth incorporating mantle plumes, subduction, and oceanic crust production.

Galer et al. [1] and White [2] argued that the contrast between low present κ and μ and high time-integrated κ and μ in the DUM reflected a short residence time (0–500 Ma) of Pb in the DUM. According to this view, the high time-integrated κ and μ reflects results not from *in situ* U and Th decay in the DUM, but is inherited from earlier residence of Pb in a reservoir with high κ and μ, presumably the lower mantle.

Here we present a simple three reservoir model of the U-Th-Pb system of the Earth. The model produces a plausible distribution of Pb isotopes and parent-daughter ratios in these reservoirs. In particular, our model reproduces the difference in present and time-integrated values of κ and μ in the DUM.

The Model: The essential features of the model are shown in Fig. 1. It consists of three reservoirs: crust, upper mantle, and lower mantle, with fluxes between them representing mantle plume, oceanic crust production, and subduction (at this point, we do not differentiate between upper and lower crust). Mantle plume and oceanic crust production vary with time in proportion to radiogenic heat production and are scaled to yield the observed present fluxes. These fluxes, together with subduction fluxes, are further constrained to produce the present-day mass of the crust. Relative sizes of the two mantle reservoirs and fractionation of U, Th, and Pb (representing partitioning during partial melting and subduction dehydration) are adjustable parameters of the model. Mathematically, the model is a series of differential equations representing changing reservoir compositions. These are solved over 4.55 Ga at 10-m.y. intervals using the Runge-Kutta method.

Results: One interesting aspect of the results is that reservoir compositions become nearly steady-state within 1–1.5 b.y. Using reasonable values for the adjustable parameters, we can approximately reproduce many features of Pb-isotopic geochemistry of the real Earth. For example, one model yields present values of μ and κ for the DUM: of 3.9 and 2.1 respectively, with corresponding time-integrated μ and κ of 7.9 and 2.1 respectively. This model also produces reasonable compositions for the crust and lower mantle that imitate features of the real Earth. For example, the DUM and crust have similar ^{206}Pb/^{204}Pb (17.4 and 17.9 respectively), but the crust has, in a relative sense, much higher ^{207}Pb/^{204}Pb (15.55 vs. 15.46). In this particular model, upper and lower mantle had similar masses and the residence time of Pb in the upper mantle was 750 m.y. We conclude that rapid cycling of Pb through the upper mantle is indeed responsible for many of the enigmatic features of terrestrial Pb-isotopic geochemistry.

References: [1] Galer S. J. G. and O'Nions R. K. (1985) *Nature, 316,* 778–782. [2] White W. M. (1993) *EPSL, 115,* 211–226. [3] Jacobsen S. B. (1988) *GCA, 52,* 1341–1350.

GREENHOUSE WARMING BY CH_4 IN THE ARCHEAN ATMOSPHERE.

A. A. Pavlov and J. F. Kasting, Department of Geosciences, Pennsylvania State University, University Park PA 16802, USA (pavlov@essc.psu.edu).

Earth appears to have been warm during its early history despite the faintness of the young Sun. Greenhouse warming by gaseous CO_2 and H_2O is in conflict with constraints on atmospheric CO_2 levels derived from paleosols for early Earth [1]. In the present work we explored the greenhouse warming by methane. We find that a CH_4 mixing ratio of 10^{-4} (100 ppmv) or more in Earth's early atmosphere would provide agreement with the paleosol data from 2.8 Ga. Such a CH_4 concentration could have been readily maintained by methanogenic bacteria, which are thought to have been an important component of the biota at that time.

Model is currently being updated to include the effect of stratospheric aerosols that may form as a result of methane photolysis. New results will be presented at the meeting.

References: [1] Rye R. (1995) *Nature, 378,* 603–605.

RADIOCARBON EVIDENCE FOR AUTOTROPHIC METABOLISM IN MARINE PLANKTONIC *ARCHAEA*.

A. Pearson, T. I. Eglinton, and J. M. Hayes, Woods Hole Oceanographic Institution, Woods Hole MA 02543, USA (apearson@whoi.edu).

Numerous recent studies document the presence of archaeoplankton in seawater and raise questions about their metabolic pathways, ecological niches, and impact on marine biogeochemistry. Unlike their relatives that live in regions of high temperature, salinity, acidity, or severe anoxia, these *Archaea* are non-extremophiles. Riobosomal RNA sequences show a widespread distribution of these organisms in the marine water column, and lipid biomarkers characteristic of *Archaea* have been found in both the water column and in marine sediments. The organisms themselves have not been isolated or cultured, and as a result, their metabolism remains unknown. Heavy stable C-isotopic ($\delta^{13}C$) values previously observed [1] for archaeal lipids could be interpreted as a result of either (1) heterotrophic uptake of isotopically-enriched algal carbohydrates and proteins, or (2) assimilation of dissolved bicarbonate during autotrophic growth. The two alternatives have fundamentally different implications for the utilization of nutrients and energy within the global ocean. In this work we exploit the gradient in $\Delta^{14}C$ of water-column dissolved inorganic C (DIC) to distinguish whether the archaeal lipids preserved in the sediments of Santa Monica and Santa Barbara Basins, California, are reflecting a ^{14}C-enriched, surface-water C source (currently 70‰) or whether they are ^{14}C-depleted.

The archaeal lipids analyzed were 40-C-atom (C_{40}) isoprenoid hydrocarbon sidechains of caldarchaeol, a dibiphytanyldiglycerol tetraether membrane lipid of thermophilic and non-thermophilic *Crenarchaeota*. These compounds were extracted from sedimentary horizons dating to both before and after significant uptake of "bomb-^{14}C" into the surface water DIC pool. In all cases, the $\Delta^{14}C$ values measured for archaeal lipids (–143‰ to –98‰) are not characteristic of either biomass production in surface waters or of heterotrophic uptake of sinking phytodetritus with a euphotic zone origin. These ^{14}C contents correspond, in both sites, to the isotopic composition of DIC near the water-column O minimum. Other lipids of heterotrophic bacteria, in contrast, clearly document the consumption of freshly degrading phytodetritus (C_{30} hopanol, 50‰; $C_{31,32}$ hopanols, 15‰). Accordingly, the compound-specific radiocarbon analyses provide compelling evidence for the growth of these organisms as autotrophs that fix inorganic C within the deep Santa Monica and Santa Barbara Basin environment.

References: [1] Hoefs M. J. L. et al. (1997) *Appl. Environ. Microbiol., 63,* 3090–3098.

ISOTOPE DILUTION INDUCTIVELY COUPLED PLASMA MASS SPECTROMETRY ANALYSES OF RHENIUM-OSMIUM ISOTOPES AND PLATINUM GROUP ELEMENTS VIA SOLVENT-EXTRACTION AND ANION-EXCHANGE PRECONCENTRATION AND A DESOLVATING NEBULIZER.

D. G. Pearson and S. J. Woodland, Department of Geological Sciences, Durham University, South Road, Durham DH1 3LE, UK (d.g.pearson@durham.ac.uk).

Introduction: The recent increase in interest in platinum group elements (PGEs) and their isotopes for tracing terrestrial fractionation events and possible core-mantle interaction, combined with the widespread use of inductively coupled plasma mass spectrometry (ICP-MS) instrumentation, has lead a drive to improve analytical techniques for these elements. Most available PGE analytical techniques for geological samples are not amenable to the analysis of both Re and Os (for isotopes if desired) and other PGEs from the same sample digestion. In addition, many of these techniques suffer from very variable total procedural blanks that are highly reagent dependent, and great effort has to be made to obtain pure reagents. Here we report a low-blank, isotope dilution Carius Tube digestion technique that allows solvent-extraction separation of Os, followed by anion-exchange separation of Ir, Pt, Ru, Re, and Pd from the same sample dissolution and analysis by ICP-MS [1].

Chemistry: Samples are spiked with ^{106}Pd, ^{99}Ru, ^{185}Re, ^{190}Os, ^{191}Ir, and ^{194}Pt. Following Carius Tube digestion [2], Os is separated by a triple solvent extraction method, using CCl_4 and HBr, based on Cohen and Waters [3]. The residual aqua regia is dried, treated with Hf-HNO_3, taken up in 1N HCl and chlorinated to oxidize Ir^{3+} to Ir^{4+}. This solution is loaded onto 1 mL of fresh AG1-X8 resin in chloride form, pretreated with Cl water, to maintain an oxidizing environment and prevent reduction of Ir IV to Ir III. A mixed 1N HF/HCl wash plus 0.8N HNO_3 is performed to remove excess Hf and Zr, which form interfering oxide ions and suppress ionization. Ir is reduced with sulfurous acid and eluted with 2N HCl. Platinum is then eluted with 6N HCl. Rhenium and Ru are eluted with 4N HNO_3. Palladium is eluted with warm (80°C) 12N HNO_3. Rhenium, Ru, and Pd can be eluted together as can Ir and Pt if desired. Solutions are dried and diluted to volume to run. Yields are ~70% except Ru, which is variable.

Blanks: Total procedural blanks are typically <5 pg for Os, Ir, and Re, <10 pg for Ru and Pd, and <25 pg for Pt. In common with Rehkamper et al. [4] we found considerable Pt in poorly cleaned borosilicate glass Carius Tubes. This was reduced to 30 pg or below by rigourous boiling in aqua regia. Such blanks are adequate for most geological samples and apart from Pt, scale with sample size.

Analysis: Solutions containing different PGE fractions were determined by quadrupole ICP-MS on a Perkin Elmer Elan 6000. Oxide intereferences are minimized using a CETAC Aridus desolvating nebulizer. Osmium concentrations are analyzed by ICP-MS using a CETAC direct injection nebulizer, which provides a low memory sample introduction system. Osmium can also be analyzed for isotope ratios and concentration by N-TIMS. Mass-bias and oxide corrections are made using standard solutions.

Results: The komatiite standard WITS-1 [5] initially was used to assess accuracy and precision. This standard has PGE concentrations within the range of many standard silicate rocks. Eighteen replicates were run as separate digestions for full PGE analyses. Nine Os samples run by N-TIMS gave 1.09 ± 0.08 (2 SD) ppb, while nine samples run by DIN-ICP-MS gave 1.07 ± 0.1 ppb. Osmium, Ir, and Ru reproducibility is 7.5–13% (2* RSD), and close to "accepted" values [5]. More mobile elements such as Re, Pt, and Pd appear much less reproducible (20–40% 2* RSD). Although our reproducibility is comparable to other methods using this standard (better for Os, Ir, and Ru) it is somewhat worse than expected and we suspect possible heterogeneity for the more mobile PGEs within the sample. Replicates on a suite of West Greenland picrites from the Vaigat Formation [6] show much better reproducibility than WITS-1, despite being of similar major-element chemistry and PGE concentration range. The following reproducibility was obtained (2* RSD): Os 2.5%; Ir 4%; Ru 5%; Pt 4%; Pd 3%; Re 6%. A suite of volcanic rocks from Grenada, Lesser Antilles arc [7], show progressively poorer reproducibility as PGE abundances decline to <100 ppt; however, the sense of the relative PGE fractionations is consistent for all replicates. It is evident that different geological samples show different levels of sample heterogeneity for PGEs and replicate analyses of particular sample types, rather than standard rocks, are probably the best way to assess reproducibility of data for a particular sample suite.

Summary: Our technique allows accurate and precise measurement of Re, Os, Ir, Ru, Pt, and Pd by ICP-MS, with the option of running Os by N-TIMS. Blanks are mostly controlled by reagents and so are easy to regulate.

Results for a variety of samples allow confidence to be placed in the reproducibility of interelement PGE abundances for geological samples in the parts-per-billion range, in order to search for evidence of primordial Earth PGE fractionation events.

References: [1] Pearson D. G. and Woodland S. J. (1999) *Chem. Geol.*, in press. [2] Shirey S. B. and Walker R. J. (1995) *Anal. Chem., 67,* 2136. [3] Cohen and Waters (1996) *A. Chim. Acta, 332,* 269. [4] Rehkamper M. et al. (1998) *Fress. J. A. Chem., 361,* 217. [5] Treadoux M. and McDonald I. (1996) *Geostandard Newslett., 20,* 267. [6] Pearson D. G. et al., this volume. [7] Woodland S. J. et al., this volume.

THE DEEP SOURCES OF PLUMES: RHENIUM-OSMIUM–PLATINUM-OSMIUM-ISOTOPIC AND PLATINUM-GROUP-ELEMENT SYSTEMATICS OF HIGH HELIUM-3/HELIUM-4 WEST GREENLAND PICRITES.

D. G. Pearson[1], L-M. Larsen[2], R. J. Walker[3], S. J. Woodland[1], A. K. Pedersen[4], R. W. Carlson[5], and S. B. Shirey[5], [1]Department of Geological Sciences, Durham University, South Road, Durham DH1 3LE, UK, [2]Geological Survey of Denmark and Greenland, Thoravej 8, DK-2400 Copenhagen NV, Denmark, [3]Department of Geology, University of Maryland, College Park MD 20742, USA, [4]Geological Museum, Øster Voldgade 5-7, DK-1350 Copenhagen K, Denmark, [5]Department of Terrestrial Magnetism, Carnegie Institution of Washington, 5241 Broad Branch Road NW, Washington DC 20015, USA.

Introduction: Combined Re-Os and Pt-Os isotopic systematics in mantle-derived rocks offer considerable promise in being able to discern possible interactions between the Earth's core and mantle-source regions of plume-derived magmas [1,2]. The discovery of very high ^{3}He/^{4}He ratios in picrites of the Vaigat Formation, West Greenland [3], suggests their derivation from a mantle plume sampling a deep, incompletely degassed reservoir such as the lower mantle or core-mantle boundary. We have applied the Re-Os- and Pt-Os-isotopic systems, plus platinum-group-element (PGE) analyses to investigate possible source components in a suite of Vaigat Formation picrites.

Geology: The Vaigat Formation is the earliest of the Tertiary volcanic rocks erupted in West Greenland, on Disko Island and the Nuussuaq Peninsula. The succession is dated at 60–61 Ma [4] and divided into three separate members: the Anaanaa Member, overlain by the Naujánguit, and the Ordlingassoq members. All three members contain an unusually high proportion of picrites [5] with inferred parental magma MgO contents of >19 wt%, indicating very high potential temperatures (1540°–1600°C) and large degree of melting. Strontium-neodymium-lead isotopic studies suggest contributions from both a MORB-like and an Icelandic mantle component, with the Ordlingassoq component containing the clearest signature of the ancestral Iceland plume [5,6]. Neodymium-isotopic compositions for picrites of the Ordlingassoq member are generally enriched relative to north Atlantic MORB (ε_{Ndi} 7.5–9.0, i.e., Icelandic values). Samples from Ordlingassoq and Naujánguit Members have ^{3}He/^{4}He (R/R_A) values ranging up to 30; one Anaanaa Mb sample has a value of 17.6 [3] The samples studied are uncontaminated with continental crust, as judged from their isotopic and trace-element compositions.

Results: *Platinum group elements.* PGEs were determined by ID-ICP-MS using Carius Tube digestion followed by solvent extraction and anion-exchange separation [7]. Oxide intereferences are minimized using a CETAC Aridus desolvating nebulizer. Picrites from all three members of the Vaigat Formation have relatively unfractionated PGE patterns (Pd/Ir 5.8–8.0), and high levels of I-PGEs (0.8–1.9 ppb Ir), consistent with their derivation as large melt fractions undersaturated in S. P-PGEs show good inverse correlations with La/Sm for all members.

Rhenium-osmium-isotopic systematics. Rhenium/osmium values are low (most <0.25). γ_{Osi} values for the Anaanaa and Naujánguit Members are close to chondritic (–0.3 to 0.7) and define a correlation on an isochron diagram that is within error of eruption age. Ordlingassoq samples have higher γ_{Osi} values (1.7–3.9) and define a steeper correlation on an isochron diagram with a more radiogenic initial ^{187}Os/^{188}Os. There is no correlation between ^{187}Os/^{188}Os and ^{3}He/^{4}He based on the few He analyses. No systematic trends are apparent in these rocks to indicate that crustal contamination has a significant effect on Os-isotopic compositions. High Os contents (1.5–3.8 ppb) mean that more than 10% of Archean crust would be required to generate the most radiogenic ^{187}Os/^{188}Os values. For Ordlingassoq Mb samples, their steep correlation on the Re-Os isochron diagram could be interpreted as mixing with a high Re/Os, radiogenic Os component in the plume source.

Platinum-osmium-isotopic systematics. Variations in ^{186}Os/^{188}Os for high-Os rocks such as the Vaigat picrites are extremely insensitive to contamination by crust. Four picrites have been analyzed for ^{186}Os/^{188}Os at UMD-CP. Three Ordlingassoq samples have chondritic to suprachondritic ^{186}Os/^{188}Os that lie on the lower part of the trend defined by Hawai'ian picrites analyzed by Brandon et al. [1]. The most straightforward interpretation of this data, combined with the Re-Os isotopic mixing correlation, is that it reveals incorporation of a small component (<<1%) with time-integrated high Re/Os and Pt/Os such as the outer core. This interpretation would be consistent with the very high ^{3}He/^{4}He ratios in these rocks. One Naujánguit sample with relatively unradiogenic ^{187}Os/^{188}Os (γ_{Osi} 0.2) shows enrichment in ^{186}Os relative to chondrites. This observation is more difficult to explain with a two-component mixing model. The sample also has very high ^{3}He/^{4}He (R/R_A ~30). If ^{186}Os enrichment does track the deep-plume signature in these magmas, then Pt-Os systematics appear more sensitive than trace-element discriminants that indicate that the Naujánguit Member is dominated by a MORB-like source.

References: [1] Walker R. J. et al. (1997) *GCA, 61,* 4799. [2] Brandon A. D. et al. (1998) *Science, 280,* 1344. [3] Graham D. W. et al. (1998) *EPSL, 160,* 241. [4] Storey M. et al. (1998) *EPSL, 160,* 569. [5] Larsen L. M. and Pedersen A. K. (1996) *J. Conf. Abstr., 1,* 349. [6] Holm P. M. et al. (1993) *EPSL, 115,* 227. [7] Pearson D. G. and Woodland S. J. (1999) *Chem. Geol.*, in press.

MAGMATIC PROCESSES OPERATING IN THE LOWERMOST OCEANIC CRUST: EXAMPLES FROM THE LEKA OPHIOLITE COMPLEX (NORWAY).

R. B. Pedersen[1] and B. Tikoff[2], [1]Department of Geology, University of Bergen, Allégaten 41, 5007 Bergen, Norway (rolf.pedersen@geol.uib.no), [2]Department of Geology and Geophysics, University of Wisconsin, Madison WI 53706, USA (basil@geology.wisc.edu).

Introduction: Because of the lack of penetration of the lowermost units of the ocean crust by deep-sea drilling, studies of the layered series of ophiolite complexes remain the main source of information on the tectono-magmatic processes that operate close to the crust/mantle interface. A several-hundred-meter-thick sequence of layered ultramafic cumulate is exposed above mantle tectonites within the Caledonian Leka Ophiolite Complex. The ultramafic sequence is exceptionally well exposed and meter-thick layers may be followed laterally for several kilometers. Two-dimensional cryptic variations have been studied in parts of the layered ultramafic sequence in order to clarify lower crustal magmatic processes.

Nature and Significance of Layering: The layered sequence shows layering on three different scales: small-scale (decimeters), medium-scale (10 m), and large-scale (100 m). The small-scale layering is defined by modal variations in amounts of olivine, cpx, opx, chromite, and sulfides, and individual layers are typically <50 cm. The medium-scale layering is defined by the repetition of units, each ~10 m thick, made up of successions of dunite, wehrlite, and websterite, which are regularly repeated stratigraphically, and this layering may be compared with the macrorhythmic units of layered intrusions. The macrorhythmic units show lateral continuity for at least several kilometers. The large-scale layering is defined by 50–200-m-thick subzones of dunite that are interlayered with other subzones dominated by peridotite and pyroxenite. The subzones are typically each composed of several successive macrorhythmic units that show similar degree of completeness. The subzones show a substantial lateral continuity and some have been mapped for almost 7 km. The three scales of layering may be explained by that the rate of extraction of melts from the mantle to the crust oscillated on at least three different wavelengths.

Rapid reversals in olivine compositions (from Fo_{86} to Fo_{93} over less than a meter) are present at the base of some macrorhythmic units, suggesting that the inflowing magma did not mix with more evolved magmas when it entered the lowermost crust. The inflowing magma seems therefore occasionally either to have pooled in bottom layers or to have formed new intrusions. Systematic upward Fe-enrichment trends are present in some macrorhythmic units, while other units exhibit no significant variations in olivine compositions for several tens of meters. The lack of upward Fe-enrichment in parts of the sequence suggests that inflow of magma was continuous during long periods of time.

Some dunite-chromite layers show features suggesting that they represent tonguelike phenocryst deposits. The parental melt appears therefore occasionally to have been loaded with crystal when it entered the lowermost crust. The apparent transport of phenocryst across the crust-mantle interface implies that the transition from porous to channeled flow took place within the mantle. The magma flow velocity must at least have been on the order of 1 m/h during influx events when chromite phenocrysts became transported, and this would have required channels that were at least 1 cm across.

Lateral Gradients: Lateral gradients in forsterite contents on the order of 1%/1000 m are present in the cumulates. The lateral gradients disappear and reappear through the sequence, and the polarity of the gradients changes several times. The change in the polarity of the lateral gradients may possibly be explained by a stratified magma column above a floor that changed slope with time. We favor, however, a model where the changing gradients are explained by variations in the velocity and direction of the flow of a crystallizing magma through an interconnected system of sills that acted as a conduit for the transfer of melt from the mantle to the upper crust.

Extraction of Interstitial Melts: The steep gradients in olivine compositions present at the bases of several macrorhythmic units are incompatible with extensive upward porous flow of interstitial melts — demonstrating that these lower crustal rocks could not have formed from a crystal mush zone. Interstitial melts appear to have segregated into pods of pyroxenite that are present as elongated, layer-parallel bodies that locally show a sigmoidal shape. Structural analyses of these bodies suggest that they represent "P-shear" tensional bridges that formed low-pressure domains toward which interstitial melts streamed by porous flow. Interconnected networks of pods and veins are present, and we suggest that the interstitial melts were transported out of the cumulate pile through such networks. The study indicates therefore that tectonic processes play a fundamental role in segregating and transporting interstitial melts in the lowermost oceanic crust.

DISSOLUTION AND GROWTH OF THE ALUMINA MINERALS GIBBSITE, DIASPORE, AND BOEHMITE STUDIED USING ATOMIC FORCE MICROSCOPY.

C. D. Peskleway[1], G. S. Henderson[1], and F. J. Wicks[2], [1]Department of Geology, University of Toronto, 22 Russell Street, Toronto, ON, M5S 3B1, Canada (claytonp@rom.on.ca), [2]Department of Earth Sciences, Royal Ontario Museum, Toronto, ON, M5S 2C6, Canada.

We are studying the dissolution and growth of $Al(OH)_3$ and AlOOH minerals *in situ* using fluid-cell atomic force microscopy (AFM) in both contact and tapping modes. The AFM allows high-resolution observations of surface processes in real time, while fluid compositions are varied.

The dissolution of natural gibbsite in nitric acid was followed on the (001) face. The surfaces had complex topography, consisting of terraces with wide variations in step heights and densities, with 0.5-nm-high steps observed. Dissolution was strongly dependent on crystallographic direction, and steps either formed at angles corresponding to the forms {110} and {100}, or existing ledges corresponding to these crystallographic orientations retreated. With increasing dissolution, the ledges became straighter and more uniform in height and spacing.

Preliminary *in situ* gibbsite growth experiments using natural gibbsite surfaces as a substrate were carried out in the presence of NaOH solutions supersaturated with respect to $Al(OH)_3$. Growth occurred by the formation of equant polygonal islands with diameters of <5–50 nm. The island edges appeared to conform to crystallographic orientations corresponding to the forms {100} and {110}.

The microtopography of the (010) face of natural diaspore was observed during dissolution under both acidic and basic conditions. In NaOH solutions, ~5-nm-deep dissolution pits formed and grew. The etch pits had polygonal outlines conforming to crystallographic orientations corresponding to the {100}, {110}, and {210} forms. However, the rate of dissolution was affected by the presence of the AFM tip, which also influenced pit geometry. Etch pits were more regular in shape with respect to crystallographic direction when the AFM tip was not being rastered across the surface. The rate of dissolution of diaspore in nitric acid as measured by step retreat was 2–3× lower than that of gibbsite at the same pH. In some cases etch pits formed having ledges with angles corresponding to the form {100}, and existing ledges with these orientations retreated. In other cases, the surface consisted of superimposed equant polygonal terraces, 20–80 nm in diameter and 1–2-nm high. Like gibbsite above, the edges of the steps conformed to the crystallographic orientations (in this case the {100}, {110}, and {210} forms) and retreated with increasing dissolution. No effect from the AFM tip was observed. The observations of gibbsite and diaspore dissolution noted above are fully consistent with previous proposed dissolution mechanisms. The results are in agreement with models in which dissolution occurs along planes of crystal defects that exist parallel to crystallographic directions.

PLATINUM-GROUP-ELEMENT CONCENTRATIONS AND OSMIUM-ISOTOPIC RATIOS IN LOESS: A PROXY FOR THE ERODING UPPER CONTINENTAL CRUST?

B. Peucker-Ehrenbrink[1] and B. M. Jahn[2], [1]Mail Stop 25, Woods Hole Oceanographic Institution, Woodshole MA 02541-1541, USA (behrenbrink@whoi.edu), [2]Department of Geosciences, University of Rennes, 35042 Rennes, France (jahn@univ-rennes1.fr).

Introduction: The geochemistry of loess deposits has been used extensively to infer the average chemical composition of the eroding upper continental crust (UCC) [e.g., 1]. In this study we test the applicability of this concept for the platinum group elements (PGE) and Os-isotopic compositions. Due to the chalcophile and siderophile behavior of Re and PGE it is not (*a priori*) clear if sedimentary deposits such as loess are valid proxies for eroding UCC in general. The applicability of loess as a proxy for the PGE concentrations and Os-isotopic composition of UCC depends on the extent of fractionation of PGE-bearing mineral phases during erosion/weathering of source rocks, eolian transport, and *in situ* weathering of loess deposits.

Samples: We use a well-characterized suite of 16 loesses and paleosols from China, France, Belgium, United Kingdom, Argentina, and Spitzbergen. All samples previously have been analyzed for major- and trace-element concentration as well as Sr- and Nd-isotopic compositions [2,3]. Strontium- and Nd-isotopic compositions are inversely correlated and range from 0.70633–0.73025 and 0.51197–0.51256, respectively, thus covering a wide range in Sr-Nd-isotopic space.

Weathering: The geochemistry of loess samples analyzed differs in several important ways from estimates for UCC. On average, loess samples are enriched in silica by ~5 wt%. Enrichment in quartz and/or loss/enrichment due to weathering causes the concentration of Na, K, Al, and Mg to fall below the average for UCC. The chemical index of alteration (CIA) for our samples ranges from 55 to 66 and is thus higher than estimates for UCC (CIA of 48–54). However, in comparison to other sedimentary proxies for the chemical composition of UCC such as shales (PAAS, NASC) that are characterized by even higher CIA values of 68–77, loess samples used in this study deviate less from average UCC. Higher CIA values of loess relative to UCC may reflect disproportionately large contributions from shales as source rocks to loess and/or weathering of source material during erosion, transport, and deposition. Depletion of trace elements such as Sr, Rb, Ba, and Ni as well as enrichments in Zr and Ta also indicate chemical modification relative to UCC, either caused by enrichment of quartz and zircon, loss during weathering (Rb,Sr), and, potentially, fractionation of trace phases such as sulfides and oxides during weathering and transport (e.g., low-Ni, high-Ta).

Osmium-isotopic Composition: The $^{187}Os/^{188}Os$ of the eroding UCC previously has been estimated at 1.26 (1.90 for average UCC), based on analyses of two loess samples from North America as well as Mississippi River and delta sediments [4]. The average (median) $^{187}Os/^{188}Os$ of loess samples analyzed in this study of 1.022 ± 0.23 (1 s.d.) (1.016) is less radiogenic than Esser and Turekian's estimate [4] of eroding UCC. Osmium-187/osmium-188 values do not correlate with $^{87}Sr/^{86}Sr$ and $^{143}Nd/^{144}Nd$. The Os-isotopic composition of loess most likely places a lower limit on the Os-isotopic composition of eroding UCC because several studies have indicated that the most labile fraction of Os during weathering of granitoid rocks [5] and black shales [6] is significantly more radiogenic than bulk rocks. A radiogenic fraction of Os thus may have been lost in the early stages of weathering of source rock. The fact that present-day seawater $^{187}Os/^{188}Os$ of 1.06–1.07 [7,8] is slightly more radiogenic than average loess indicates that

(1) the average isotopic composition of continental runoff is more radiogenic than eroding UCC [e.g., 5,9–11], and/or (2) that volumetrically less important radiogenic lithologies enriched in Re and Os relative to UCC, such as black shales, control the evolution of the marine Os-isotopic record [6,12].

Platinum-Group-Element and Rhenium Concentrations: Estimates of the Re, Os, Ir, and Pt concentrations in UCC range from 0.4 to 0.5, 0.03 to 0.05, 0.03 to 0.05, and 1 to 1.5 ng/g, respectively [4,13,14]. Average (median) values for Re, Os, Ir, and Pt concentrations in our loess samples are 379 (133), 35 (28), 26 (30), and 477 (359) pg/g, respectively. Ruthenium and Pd analyses are still in progress. The large discrepancy between average and median Re (and Os) concentrations is due to a Holocene loess sample from Spitzbergen with high Re (3.59 ng/g) and Os (155 pg/g) concentrations. These results indicate that the average (median) ^{187}Re/^{188}Os of 40.5 (25.1) is slightly lower and the average ^{190}Pt/^{188}Os of 0.016 (0.012) is significantly lower than previous estimates for UCC.

References: [1] Taylor S. R. et al. (1983) *GCA, 47,* 1897–1905. [2] Gallet S. et al. (1998) *EPSL, 156,* 157–172. [3] Gallet S. et al. (1999) *JGR,* submitted. [4] Esser B. K. and Turekian K. K. (1993) *GCA, 57,* 3093–3104. [5] Peucker-Ehrenbrink B. and Blum J. D. (1998) *GCA, 60,* 3193–3203. [6] Hannigan R. E. and Peucker-Ehrenbrink B. (1998) *Eos Trans. AGU, 79,* 427. [7] Levasseur S. et al. (1998) *Science, 282,* 272–274. [8] Woodhouse O. B. et al. (1999) *EPSL,* submitted. [9] Pegram W. J. et al. (1994) *EPSL, 128,* 591–599. [10] Peucker-Ehrenbrink B. and Ravizza G. (1996) *Geology, 24,* 327–330. [11] Levasseur S. et al. (1999) *J. Conf. Abstr., 4,* 231. [12] Ravizza G. et al. (1998) *Eos Trans. AGU, 79,* 427. [13] Schmidt G. et al. (1997) *Yearbook Inst. Nuclear Chem.,* p.15, Mainz, Germany. [14] Taylor S. R. and McLennan S. M. (1995) *Rev. Geophys., 33,* 241–265.

PHOTOSYNTHESIS INFLUENCES SILICA BIOMINERALIZATION?

V. R. Phoenix[1], K. O. Konhauser[1], and D. G. Adams[2], [1]School of Earth Sciences, University of Leeds, Leeds LS2 9JT, UK (vernon@earth.leeds.ac.uk), [2]Department of Microbiology, University of Leeds, Leeds LS2 9JT, UK.

Introduction: Several studies suggest that bacterial photosynthesis can control biomineralization by mediating the pH of the surrounding microenvironment. It is believed that the production of hydroxyl ions during photosynthesis creates an alkali environment around the microbe [1,2], which may result in the precipitation of epicellular carbonates [3]. In addition to this, the sheath of some cyanobacteria may act as a partial diffusion barrier, causing very high alkalinity levels to build up within the sheath matrix. This has been proposed to result in the formation of calcite sphericules inside this extracellular polysaccharide [2]. In this study we consider how such processes may influence bacterial silicification.

Bacterial silicification is abundant at many hot-spring sites, where the microorganisms are often found encrusted in layers of silica several micrometers thick [4,5]. These crusts appear to form from colloids [4,5]; colloidal silica probably being a dominant component of these supersaturated waters. A recent study has demonstrated that these microbes may still function with such a mineral coating [6], and it thus follows that they may photosynthetically influence the silicification process.

Methods: We tested how photosynthesis may control bacterial silicification by mineralizing the cyanobacteria *Calothrix* in a laboratory setting. This microorganism was mineralized by culturing on agar using BG11 N+ as nutrients, and then placing in beakers containing 1 L of 300-ppm silica solution. The solution was replaced every 2–3 d to ensure continual supply of silica. Bacterial samples were also collected for electron microscopy. Furthermore, polycationized Ferritin (PCF), and iron-cored protein 11 nm in diameter, was used both to label electronegative sites upon the sheath and to determine the sheaths impermeability to particles of similar size, such as colloidal silica.

Results and Discussion: After 20 d, many filaments had become mineralized in a siliceous crust several micrometers thick. These crusts were dominantly restricted to the outer surface of the sheath, and mineralization was very rarely observed within the sheath matrix. The crusts also appeared to form from the merger of silica colloids ~20 nm in diameter.

The PCF adhered to the outer surface of the sheath, indicating its strong anionic characteristic and hence suitability as a mineral nucleation site. The PCF failed, however, to penetrate the sheath matrix, suggesting the sheath had acted as a filter and was impermeable to particles of this size (i.e., ≥11 nm).

The silicification model. Based upon our observations and the previously described models for bacterial calcification, we tentatively suggest that silicification is restricted to the outer surface of the sheath by photosynthetic controls on pH, which in turn control silica-solution chemistry. The model is described as follows:

The microenvironment surrounding the bacteria can be separated into two domains. In the outer domain, outside the sheath, the production of hydroxyl ions during photosynthesis results in moderately alkali conditions (pH 7–9). Under these conditions, silica saturated with respect to amorphous silica occurs dominantly as colloids [7], which are bound electrostatically to the surface of the sheath. These colloids are unable to penetrate the sheath, due to its degree of impermeability, and hence silica only accumulates on the sheath's outer surface. Inside the sheath matrix (the inner zone), the partial diffusion barrier created by the sheath creates a very high alkalinity with pH values ≥10. Under these conditions, silica exhibits higher solubility and is dominantly monomeric, a form that is unable to bind to organic surfaces [8]. Thus silicification does not occur within the sheath matrix. Once cell lysis occurs there is no photosynthetically induced alkalinization, and hence silicification occurs within the sheath matrix and ultimately upon the cell wall and cytoplasm.

References: [1] Miller A. G. and Coleman B. (1980) *Plant Physiol., 2,* 397–402. [2] Verrecchia E. P. et al. (1995) *J. Sed. Res., A65,* 690–700. [3] Thompson J. B. and Ferris F. G. (1990) *Geology, 18,* 995–998. [4] Konhauser K. O. and Ferris F. G. (1996) *Geology, 24,* 323–326. [5] Schultze-Lam S. et al. (1995) *Can. J. Earth. Sci., 32,* 2021–2026. [6] Phoenix V. R. et al. (1999) *Geology,* in review. [7] Shimada K. and Tarutani T. (1979) *J. Chromatography, 168,* 401–406. [8] Heaney P. J. and Yates D. M. (1998) *GSA Abstr. with Prog.*

THE OSMIUM BUDGET OF HIMALAYAN RIVER SEDIMENTS AND SOILS: IMPORTANCE OF BLACK SHALE EROSION.

A.-C. Pierson-Wickmann[1], L. Reisberg[1], and C. France-Lanord[1] [1]Centre de Recherches Pétrographiques et Géochimiques–Centre National de la Recherche Scientifique, B.P 20, 54501 Vandoeuvre-les-Nancy Cedex, France (annecath@crpg.cnrs-nancy.fr; reisberg@crpg.cnrs-nancy.fr; cfl@crpg.cnrs-nancy.fr).

The marked increase of the ^{187}Os/^{188}Os ratio of seawater during the last 15 m.y. is often thought to be due to Himalayan uplift and associated weathering [1], in analogy with proposed explanations for changes in the marine Sr-isotopic record. In order to test this hypothesis, we have characterized the Os-isotopic compositions of river bedloads from Central Nepal and Bangladesh, as well as potential source rocks in the main Himalayan formations. We have also determined the Os compositions of several soil profiles. Our goals are (1) to identify the sources of radiogenic Os, (2) to investigate the behavior of Os during erosion, and (3) to evaluate the importance of Himalayan weathering on the marine Os budget.

The Himalayan Range is composed of three main formations, from north to south: (1) The Tethyan Sedimantary Series (TSS), composed of Phanerozoic sediments, is characterized by nonradiogenic bedrocks and bedloads with ^{187}Os/^{188}Os = 0.6–1.9 and (Os) = 20–200 ppt. (2) The High Himalayan Crystallines (HHC), highly metamorphosed paragneisses and leucogranites, are the principal source of eroded material of the range. Bedrocks have ^{187}Os/^{188}Os = 0.8–1.6, while bedload ratios = 1.1–1.8. (3) The LH formation consists of metasediments with ε_{Nd} values indicative of long crustal residence. ^{187}Os/^{188}Os = 0.7–3.0 in the bedloads and 0.9–8.5 in the bedrocks. The Os concentration also varies widely, from 7 to 530 ppt. The highest Os-isotopic ratios are associated with the highest [Os], and are derived from black shales containing 6–10 wt% black carbon.

Thus, with the exception of the LH black shales, the Himalayan formations generally have Os-isotopic ratios close to that of average eroded continental crust [2] (^{187}Os/^{188}Os = 1–1.3). In contrast, the Os-isotopic ratios of river bedloads sampled near the outflow of the range are very radiogenic, as high as 3.8. Thus a very minor lithology, the black shales, that represent <3%

of the volume of the LH formation controls the Os-isotopic composition of the sediments delivered from the Himalayan chain.

Results from three soil profiles confirm the conclusions deduced from the river sediment data. Soils developed on the HHC and LH formations display the same Os signature as the HHC and LH bedloads uninfluenced by black shales, though the Os concentrations are somewhat higher (18–50 ppt). The $^{187}Os/^{188}Os$ ratio of a soil profile taken from the HHC is constant with depth (~1.3), except for a single layer with a ratio of 2.0. The $^{187}Os/^{188}Os$ ratio (~1.1) of a LH profile also does not vary notably with depth. Interestingly, this profile overlies a saprolith with $^{187}Os/^{188}Os$ = 1.95 and (Os) = 320 ppt. A third soil profile, developed on alluvium in the floodplain at the outflow of the range, has a strikingly high $^{187}Os/^{188}Os$ ratio (>4), which again is roughly constant with depth. This ratio, comparable to those of nearby bedloads, again shows the great influence of rare LH black shales on the Os budget.

Mass-balance calculations, based solely on Os concentrations and assuming erosion at steady state, indicate that HHC and non-black shale LH rocks do not contain enough Os to explain the total Os flux (bedload, suspended and dissolved [4] loads) of the Ganga River. Thus Os concentrations alone require the presence of an Os-rich component. Taking into account the Os-isotopic ratios, it can be shown that the addition of ~4% of black shales similar to those found in Central Nepal can explain the Os characteristics of the bedloads at the outflow of the range. This proportion is much too high, both because black shales represent only a minor lithology at the scale of the basin (<1%) and because the bedload C contents are too low to be consistent with such a high input from organic-rich rocks. Black shales with higher Os could be proposed as the mixing end member. However black shales with the required characteristics are quite rare (1 out of the 33, given in [3]). Thus simple mixing does not adequately explain the data. Instead chemical erosion, perhaps involving preferential removal of radiogenic Os from black shales [5] and interaction between dissolved and sediment loads must be considered. Ganga river water [4] has an Os ratio similar to those of the bedloads, suggesting that some equilibration has occurred between the dissolved and solid phases. Finally, the fact that the dissolved fraction represents ~30% of the total Ganga Os flux underscores the importance of chemical erosional processes.

The highly radiogenic nature of the dissolved [4] and bedloads of the Ganga River suggest that Himalyan derived Os may play an important role in the rapid rise in the seawater Os ratio during the last 15 m.y. This radiogenic signature is derived from a very minor lithology, black shale. These data suggest that black shale, rather than silicate, erosion largely influences the marine Os record.

References: [1] Pegram et al. (1992) *EPSL, 113,* 569–576. [2] Esser (1991) thesis, Yale Univ. [3] Singh et al. (1999) *EPSL,* in press. [4] Levasseur et al. (1999) *Terra Abstr., 11,* 231. [5] Peucker-Ehrenbrink and Hannigan (1999) *Terra Abstr., 11,* 231.

MICROBIAL COMMUNITIES IN CHARCOAL FROM WILFIRE AND THE UNDERLYING HUMUS.

J. Pietikainen, O. Kiikkila, and H. Fritze, Finnish Forest Research Institute, P.O. Box 18, FIN-01301 Vantaa, Finland (janna.pietikainen@metla.fi).

Introduction: Forest fires or prescribed burning produce a layer of black charcoal, which originates from the charred remnants of vegetation, litter and logging slash. This charcoal has been shown to have adsorbing capacity resembling that of activated C, and it has an active role in forest regeneration since it adsorbs allelopathic compounds, e.g., phenolics [1]. Since the charcoal layer is capable of adsorbing phenolics, we presumed that it can also adsorb other organic compounds from the percolating soil water. On top of the charcoal layer formed during a fire, a layer of new litter starts to accumulate originating from the newly formed vegetation. This pioneer vegetation produces litter that is rich in water-soluble compounds [2]. The water-soluble compounds include, e.g., carbohydrates, amino acids, and phenolics [3]. These substances serve as an energy-rich C source for microbes.

After a fire, a more or less heated humus can be found under the charcoal layer. The microbial biomass in the underlying humus has been shown to decrease after fire [4], and the recovery to preburn levels takes ~10 yr [5]. We hypothesized that (1) the charcoal has a capacity to adsorb organic compounds and thus form a new habitat for microbes utilizing these substrates, and (2) the charcoal may negatively affect the microbial community of the underlying humus by capturing otherwise available substrates from soil water.

Material and Methods: We produced charcoal (at 450°C) from dried and sieved forest humus (HuCh) and crowberry *Empetrum nigrum* (EmpCh), which is a common dwarf shrub. Using these two types of charcoal and activated C (ActC) and nonadsorbing pumice (Pum) as controls, we prepared microcosms with 25 g fresh, untreated humus in the bottom, and 25 g of one of the adsorbents on top. The microcosms were incubated at 20°C, moistened regularly with birch leaf litter extract, and after one month both the overlying adsorbent and the humus was destructively sampled. From adsorbents and humus we measured the total microbial biomass by substrate-induced respiration, basal respiration, microbial phospholipid fatty acid (PLFA) pattern [6], substrate utilization pattern [7], and bacterial growth rate as ^{3}H-thymidine incorporation [8].

Results and Discussion: The potential adsorbing capacity of the adsorbents was tested prior to the incubation, and it increased in the order Pum < HuCh < EmpCh < ActC. After the incubation, all the adsorbents harbored microbial biomass. The amount of microbial biomass C was lowest in Pum (0.3 mg g^{-1}), and highest in EmpCh (1.5 mg g^{-1}). On average, the amount of microbial biomass in the adsorbents was 16% of that in the humus. Basal respiration got low values in Pum and ActC, while the level in both charcoals (EmpCh and HuCh) was 3–4× the value measured in Pum and ActC. A similar response pattern was also seen for thymidine incorporation rate, with EmpCh and HuCh showing the highest bacterial growth rates. The specific growth rate per bacterial cell was one magnitude higher in the adsorbents than in the humus. Thus, the substrates of the birch-leaf litter extract supported a small but highly active microbial community in the adsorbents.

In addition to the size of the microbial biomass, its structure was also dependent on the properties of the adsorbent. As revealed by both PLFA and substrate utilization patterns, totally different kinds of microbial communities were formed in the four adsorbents. When the community structure data were subjected to principal component analysis, and the scores of the first principal component were tested with one-way ANOVA, it was seen that the microbial community of Pum differed significantly from ActC + EmpCh (by PLFA profiling). These results show that charcoal from forest fire or prescribed burning can form a new habitat for microbes, which confirms our first hypothesis.

The microbial biomass in the underlying humus did not differ between adsorbents. If the adsorbents had captured substrates from the litter extract, the microbial biomass should have been higher under Pum than under, e.g., ActC. Since this was not confirmed by our results, we rejected our second hypothesis. However, the microbial communities were affected by the overlying adsorbents, with the communities under Pum and EmpCh being most dissimilar.

Conditions similar to those in our microcosms can be found in the field a few years after burning. According to our results, a microbial population can be expected to live in the charcoal layer, the porous structure of which obviously offers shelter for the microbes against faunal predators [1]. However, the charcoal is not responsible for the commonly observed reduction in microbial biomass in the underlying humus.

References: [1] Zackrisson O. et al. (1996) *Oikos, 77,* 10–19. [2] Johansson M.-B. (1995) *Forestry, 68,* 49–62. [3] Palm C. A. and Rowland A. P. (1997) in *Driven by Nature* (G. Cadisch and K. E. Giller, eds.), pp. 379–392, CAB International, Wallingford, UK. [4] Pietikainen J. and Fritze H. (1995) *Soil Biol. Biochem., 27,* 101–109. [5] Fritze H. et al. (1993) *Can J. For. Res., 23,* 1286–1290. [6] Frostegård Å. et al. (1993) *Soil. Biol. Biochem., 25,* 723–730. [7] Pennanen T. et al. (1998) *FEMS Microbiol. Ecol., 27,* 291–300. [8] Bååth E. (1992) *Soil. Biol. Biochem., 24,* 1157–1165.

URANIUM-238–THORIUM-230–RADIUM-226 DISEQUILIBRIA IN HISTORICAL KILAUEA VOLCANO LAVAS: MANTLE MELTING WITHIN THE HAWAI'IAN PLUME.

A. J. Pietruszka[1,*], K. H. Rubin[1], and M. O. Garcia[1], [1]Deptartment of Geology and Geophysics, University of Hawai'i, Honolulu HI 96822, USA (*present address: Department of Terrestrial Magnetism, Carnegie Institution of Washington, Washington DC 20015, USA).

Introduction: A fundamental goal of geochemical research at ocean-island volcanos and mid-ocean ridges is to infer the process of basaltic melt generation and transport. The U-series isotopic abundances of lavas, in conjunction with other high-resolution geochemical tracers, are particularly well suited for this purpose because they can be used to quantify the timescales of magmatic processes (such as the melting rate). We conducted a detailed study of the U-series isotope geochemistry of a suite of historical Kilauea Volcano lavas (1790–1998) using high-precision mass spectrometric techniques to evaluate the melting process within the Hawai'ian mantle plume. Our results show that the $(^{230}\mathrm{Th}/^{238}\mathrm{U})$ and $(^{226}\mathrm{Ra}/^{230}\mathrm{Th})$ ratios of Kilauea's historical lavas, 1.01–1.04 and 1.08–1.15, respectively, have remained small and constant over the last 200 yr, despite large (factor of ~2) variations in the degree of partial melting (inferred from the melting-related changes in ratios of incompatible trace elements such as La/Yb or Nb/Y). In this study, we reconcile these observations using the two endmember "ingrowth" models for producing U-series disequilibria during mantle melting (dynamic melting [1] and equilibrium percolation melting [2]) and then estimate the melting parameters for Kilauea lavas.

The Effect of Melt Fraction: Previous workers have suggested that the $^{226}\mathrm{Ra}$-$^{230}\mathrm{Th}$-$^{238}\mathrm{U}$ disequilibria of lavas from ocean-island volcanos should correlate with melt fraction [3,4]. Given the evidence for relatively large variations in the degree of partial melting from the incompatible trace-element ratios of Kilauea's historical lavas, a correlation between the inferred melt fraction and the U-series disequilibria might be expected. However, no obvious correlation exists. Our U-series model results resolve this problem because the calculated $^{230}\mathrm{Th}$ and $^{226}\mathrm{Ra}$ disequilibria (at a given melting rate and melt-zone porosity) are insensitive to $[(^{230}\mathrm{Th}/^{238}\mathrm{U})$ ratios] or unaffected by $[(^{226}\mathrm{Ra}/^{230}\mathrm{Th})$ ratios] changes in melt fraction from 5–20%, which is the range expected for Hawai'ian shield lavas [5].

Physical Constraints on the Melting Process: The large $^{226}\mathrm{Ra}$-$^{230}\mathrm{Th}$-$^{238}\mathrm{U}$ disequilibria observed in young mid-ocean-ridge basalts (MORB) require very low melting rates and melt-zone porosities [2,6]. Based on the relatively small $^{226}\mathrm{Ra}$-$^{230}\mathrm{Th}$-$^{238}\mathrm{U}$ disequilibria of Kilauea and Mauna Loa lavas, previous workers have suggested that Hawai'ian tholeiitic basalts are produced at higher melting rates and melt-zone porosities compared to MORB and have calculated moderate melting rates of >0.0005 kg m^{-3} yr^{-1} and porosities of <0.1–1% [3,7]. However, we found that the melting rates and melt-zone porosities calculated from the ingrowth models were strongly dependent (by an order of magnitude or more) on the choice of the partition coefficients (D). Given the range of published D values for Ra, Th, and U (which likely vary as a function of composition and pressure), the melting parameters (for either MORB or ocean-island lavas) cannot be estimated simply from U-series disequilibria alone. Instead, physical constraints are required.

The geochemical differences between adjacent, active Hawai'ian volcanos, such as Kilauea, Mauna Loa, and Loihi, place strong physical constraints on the melting process. These intershield geochemical differences require that the mantle sources, melting regions, and magma pathways between these volcanos be physically distinct on the 25–50-km-length scale of the distance between the volcanos [8]. The "instantaneous" mantle source volumes needed to sustain Kilauea's average magma supply rate (0.06 km^3/yr) can be calculated using the melting rates from our U-series modeling results. The radii of these source volumes (assuming a cylindrical 55-km-long melting column [5]; Fig. 1) are generally much wider than permitted by the intershield geochemical differences. The smallest acceptable source volumes (and radii) are obtained for those parameterizations of the equilibrium percolation model (only) that give the highest average melting rates (0.003–0.007 kg m^{-3} yr^{-1}) and melt-zone porosities (0.4–2%). These may be the most reliable estimates so far of these melting parameters for tholeiitic basalt production within the Hawai'ian plume.

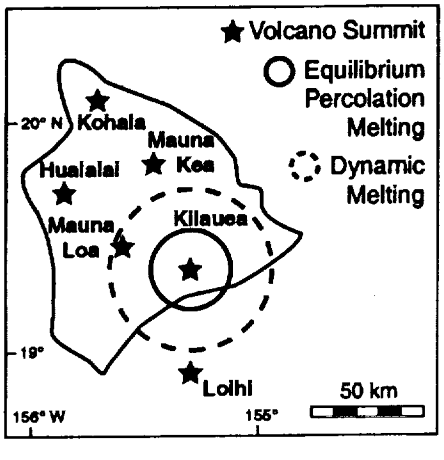

Fig. 1. The calculated radii of the source volumes should be ≤1/2 the intershield distance.

References: [1] McKenzie D. (1985) *EPSL, 72,* 149–157. [2] Spiegelman M. and Elliott T. (1993) *EPSL, 118,* 1–20. [3] Hémond C. et al. (1994) *Chem. Geol., 116,* 163–180. [4] Chabaux F. and Allègre C. J. (1994) *EPSL, 126,* 61–74. [5] Watson S. and McKenzie D. (1991) *J. Petrol., 32,* 501–537. [6] Williams R. W. and Gill J. B. (1989) *GCA, 53,* 1607–1619. [7] Cohen A. S. and O'Nions R. K. (1993) *EPSL, 120,* 169–175. [8] Frey F. A. and Rhodes J. M. (1993) *Phil. Trans. R. Soc. Lond. A, 342,* 121–136.

A HAFNIUM-ISOTOPIC COMPOSITION RECORD OF THE CENTRAL INDIAN OCEAN FROM FERROMANGANESE CRUSTS.

A. M. Piotrowski[1], D-C. Lee[1], A. N. Halliday[1,2], J. N. Christensen[1], and J. R. Hein[3], [1]Department of Geological Sciences, University of Michigan, Ann Arbor MI 48109-1063, USA (ampiotro@umich.edu), [2]Institute für Isotopengeologie und Mineralische Rohstoffe, Department für Erdwissenschafeten, Eidgenössische Technische Hochschule-Zentrum, NO, CH-9092, Zürich, Switzerland, [3]U.S. Geological Survey, Menlo Park CA 94025-3591, USA.

Although variable, the present-day Hf- and Nd-isotopic compositions of the Indian Ocean are intermediate between the relatively radiogenic Pacific Ocean and unradiogenic Atlantic Ocean. The processes that directly control the global distribution of Hf and Nd in deep ocean water include weathering from proximal land masses and large-scale water mass mixing between ocean basins. In the case of the Indian Ocean, the uplift of the Himalayas over the last 20 m.y. could have affected the Hf- and Nd-isotopic composition of the Indian Ocean. However, the Indian Ocean may also have been affected by a number of paleoceanographic changes, including the increasing global influence of North Atlantic deepwater (NADW) via circum-Antarctic deepwater, and the closure of the Indonesian gateway. Recently published Nd-isotopic profiles of Indian Ocean Fe-Mn crusts show little variation, and do not show the shift to nonradiogenic values expected to accompany proximal weathering of continental material accompanying Himalayan uplift [1]. The Hf in seawater is expected to be more variable than Nd because of the larger variation in Hf relative to Nd in weathered materials capable of entering the deep ocean [2]. Hafnium may also provide a record of MOR hydrothermal activity, since unlike Nd, it is not believed to be effectively scavenged in vent plumes. Here we present the first high-resolution Hf-isotopic profiles of two central Indian Ocean Fe-Mn crusts, 109D and SS663, in an attempt to better constrain the evolution history of Hf in the central Indian Ocean and its implications to paleoceanographic changes.

The Hf-isotopic composition of the southern crust 109D remains 4 ± 1 ε_{Hf} throughout the entire 20-m.y. growth history. The northern crust SS663, which is more proximal to the Himalayan erosional source, records a Hf-isotopic composition of is 6 ± 1 ε_{Hf} prior to 5 Ma. Between 5 and 3 Ma there is an abrupt nonradiogenic shift, after which the Hf composition remains 4 ± 1 ε_{Hf}. The nonradiogenic shift observed in SS663, but not in the more southern 109D, suggests a change in either Himalayan erosion rates or Indian Ocean paleocirculation ~5 Ma.

The circum-Antarctic current plays a major role in interocean deepwater mixing and in controlling the global elemental abundance distribution of seawater chemistry. The present-day Nd- and Pb-isotopic composition of circum-Antarctic water has been shown to be influenced in part by the incorporation of modified NADW [3]. The strengthening of NADW during the last 5 m.y. [4], accompanied by northern hemisphere glaciation, would have indirectly affected the composition Indian Ocean deepwater. Thus, the Hf-isotopic records displayed by these two Indian Ocean crusts could suggest that NADW modified circum-Antarctic water of nonradiogenic composition started to affect the Indian Ocean at 5 Ma. It is worth noting that our Hf-isotopic composition for the Atlantic shows a radiogenic peak centered at 2 Ma, with less radiogenic values both before and after this time. Though speculative, it is conceivable that some of the variability observed in the high-resolution records of Indian Ocean Hf-isotopic composition over the last 2 m.y. may have been caused by pulses of less radiogenic NADW into circum-Antarctic deepwater. Other possible causes for the shift in Hf-isotopic composition at 5 Ma include a change in deepwater flux from the Pacific Ocean through the Indonesian gateway and changes in hydrothermal activity.

The question as to whether weathering from proximal landmasses or large-scale mixing between ocean basins is the more dominant factor in controlling Hf-isotopic composition is still open. The case of the Indian Ocean, as well as some observations from the North Atlantic, seem to indicate that both sample location and depth in relation to major water masses must be taken into account in order to interpret the isotopic record preserved by ferromanganese crusts. Complete profiles of Nd- and Hf-isotopic composition with depth through the present-day Indian Ocean may help deciphering the pathway of Himalayan erosional flux.

References: [1] O'Nions R. K. et al. (1998) *EPSL, 155,* 15–28. [2] Lee D-C. et al. (1999) *Science,* in press. [3] Goldstein and Abouchami (1997) *GCA, 61,* 3957–3974. [4] Burton K. W. et al. (1997) *Nature, 386,* 382–385.

CONSTRAINTS FROM THORIUM/LANTHANUM ON THE EVOLUTION OF THE CONTINENTS.

T. Plank[1,2], [1]Department of Earth Sciences, Boston University, 685 Commonwealth Avenue, Boston MA 02215, USA (tplank@bu.edu), [2]Department of Geology, University of Kansas, 120 Lindley Hall, Lawrence KS 66045, USA (tplank@kuhub.cc.ukans.ed).

Continental growth involves formation of juvenile continental material at convergent margins, and this process may explain similar trace-element ratios in volcanic arcs and the continental crust, such as low Ce/Pb, high Th/Nb, and high Th/La. An alternative explanation for the common traits, however, is that arc volcanics inherit continental ratios from subducted sediment. How much of the continental signature in arc basalts is created in subduction zones, and how much is inherited from subducted sediment? To evaluate this question, we consider the fractionation of Th/La in subduction zones.

Thorium/lanthanum is low (<0.12) in the mantle but enriched (>0.3) in the continents, and varies in arc basalts from 0.09 to 0.34. Thorium/lanthanum fractionation in the subduction zone can be evaluated simply because both Th and La enrichments derive predominantly from subducted sediment, with little contribution from subducted oceanic crust. Thorium/lanthanum varies in marine sediments from <0.1 in metalliferous and red clays, to ~0.15 in volcaniclastics and 0.3–0.4 in terrigenous turbidites. The bulk Th/La of different sedimentary columns subducting at trenches strongly affects the Th/La of the related volcanic arc. For high-sediment flux margins, sediment and arc Th/La correlate well and form a trend with a slope of 1. This reflects a direct inheritance of the sediment ratio by the arc with little new fractionation in the subduction zone.

Thus the high Th/La ratio of the continents is not created in modern subduction zones. A small part of the fractionation between the continents and mantle took place in the Archean (Th/La in Archean continents was ~0.17), but upper crustal compositions show a large secular increase in Th/La during the last 2 b.y. One mechanism for increasing Th/La in the bulk continental crust is intracrustal fractionation and lower crustal foundering. As the continent differentiates into a granitic upper crust and restitic lower crust, Th/La fractionates from >0.5 in some granites to <0.15 in lower crustal granulites, possibly due to the partitioning of La over Th in restitic apatite. Periodic foundering of the lower crust into the mantle will continually enrich the continents in Th/La. Therefore, although the continents form in part at subduction zones, other crustal recycling processes, such as lower crustal foundering, are needed for the continental crust to reach its present chemical composition.

AN EARTH-SYSTEM SCIENCE APPROACH TO UNDERSTANDING, PREDICTING, MITIGATING, AND REMEDIATING METAL MOBILITY FROM MINES AND UNMINED MINERAL DEPOSITS.

G. S. Plumlee[1] and M. J. Logsdon[2], [1]Mail Stop 964, U.S. Geological Survey, Federal Center, Denver CO 80225, USA (gplumlee@usgs.gov), [2]Geochimica, Inc., Suite M, 206 N. Signal, Ojai CA 93023, USA (mark.logsdon@worldnet.att.net).

Introduction: Environmental issues have become important, if not critical, factors in the success of proposed mining projects worldwide. The Earth, engineering, and life sciences (which we group here under the term "Earth-system sciences," or ESS for short) provide an ample toolkit that can be drawn upon to better understand, anticipate, prevent, and remediate the environmental effects of mining and mineral processing [1].

Controls on Metal Mobility from Mining and Mineral Processing Sites and Unmined Mineral Deposits: The natural weathering and erosion of a mineral deposit at the Earth's surface disperses its constituents into the waters, soils, and sediments of its surrounding environment. There, the constituents may be taken up by plants and/or organisms. The potential environmental effects of unmined mineral deposits are a complex function of the geologic characteristics of the deposits and their surrounding watersheds, the climatic setting of the deposits and their watersheds, and geochemical, biogeochemical, and hydrologic processes (such as sulfide oxidation, acid generation, evaporation, sorption, and dilution).

Modern mining and mineral processing activities employ a wide variety of methods to prevent or minimize adverse environmental impacts. However, if not carried out with appropriate mitigation and prevention practices (as was common in most historical mining), or as a result of accidental releases, mining and mineral processing can disperse potentially deleterious metals, other deposit constituents, and mineral processing chemicals or byproducts into the environment. The environmental effects of mining and mineral processing are controlled by the same factors as those of unmined mineral deposits, as well as the mining or mineral processing methods used and the preventive/mitigative processes followed.

Tools in the Toolkit: A large number of techniques developed for Earth-system science investigations are also directly applicable to mineral-environmental issues. As with any toolkit, it is the professional's responsibility to choose the tool(s) best suited to a specific job, based on their professional judgment. Examples of tools in the toolkit include include geologic characterization studies (geologic mapping, mineralogic characterization, structural analysis); mineral deposit models and geoenvironmental models of mineral deposits; mineral resource, mineral-environmental, ecosystem, and abandoned mine lands assessments; geochemical characterization of waters, soils, sediments, plants, mine wastes, mineral processing wastes, and other media; other geochemical studies (laboratory simulation experiments, geochemical modeling, stable and radiogenic isotopes, and age dating); geophysical characterization (including a variety of field methods such as resistivity, ground-penetrating radar, and seismic tomography surveys, and remote methods such as aeromagnetic and airborne electromagnetic surveys); remote-sensing surveys; biological, toxicological, and ecological characterization and testing; and geospatial databases and geographic information systems (GIS) analysis of the data in the databases.

Interdisciplinary studies that integrate tools in the ESS toolkit provide truly powerful insights into the environmental impacts of mineral deposits, mining, and mineral processing. In general, these studies, as well as mineral-environmental characterization, prediction, mitigation, and remediation, are best carried out within a watershed context. For example, the downstream environmental effects of acid drainage from a particular mine site or unmined deposit are a function of the contributions of acid and metals from the site relative to those from other sources in the watershed. They are also a function of the proportions and compositions of the site waters relative to those of the surface waters or ground waters with which the site waters mix.

References: [1] Plumlee G. S. and Logsdon M. J. (1999) *Soc. Econ. Geol. Rev. in Econ. Geol., 6A,* 1–27.

RHENIUM-OSMIUM-ISOTOPIC SYSTEMATICS OF SEVERAL DECCAN ALKALINE COMPLEXES.

A. Poirier[1], L. Reisberg[2], A. Simonetti[1], C. Gariépy[1], and S. L. Goldstein[3], [1]Centre de Recherche en Géochimie Isotopique et en Géochronologie, Université du Québec à Montréal, CP 8888 succursale Centre-ville, Montréal H3C 3P8, Canada,

[2]Centre de Recherches Pétrographiques et Géochimiques–Centre National de la Recherche Scientifique, 15 rue Notre-dame des Pauvres, BP 20, 54501 Vandoeuvre-lès-Nancy Cedex, France, [3]Lamont-Doherty Earth Observatory, Columbia University, Palisades NY 10964, USA.

The Deccan igneous province consists of a volumetrically large succession of predominantly tholeiitic lava flows, which mark the first surface expression of the Réunion hotspot on the Indian subcontinent [1]. Potassium-argon and $^{39}Ar/^{40}Ar$ geochronological data, studies of paleomagnetism, and paleontological evidence all suggest that ~2,000,000 km^3 of basalt within the Deccan igneous province erupted ~65 Ma, within a time interval of <l m.y. [2]. Moreover, alkaline complexes consisting predominantly of Si-undersaturated (nephelinite, melilitite ± carbonatite) rocks occur within the northwestern region of the Deccan province. Recent $^{39}Ar/^{40}Ar$ dates from several of these complexes revealed that alkaline magmatic activity may have been slightly older in the northern part of the province (~68.5 Ma) than in the south (~65 Ma [3]). Several of these complexes, namely Barmer, Bhuj, Mundwara, and Amba Dongar, were the focus of a recent Nd-Pb-Sr-isotopic investigation [4]. These isotopic data suggest that Réunion mantle played a more prominent role during the early stages of Deccan volcanism involving small-degree melting of plume-modified (metasomatized) lithosphere. As time progressed, the isotope systematics of both alkaline and tholeiitic magmatism recorded a larger lithospheric imprint.

Previous studies, focused on the trace-element chemistry and Nd-Pb-Sr-isotopic systematics of Deccan basalts, indicate a large degree of heterogeneity, which has been attributed either to crustal contamination of the magmas or to interaction with a metasomatized mantle source. In contrast, a recent study of the Re-Os-isotopic systematics of Deccan basalts collected over several hundreds of kilometers within the igneous province [5] provides a well-defined isochron corresponding to an age of 65.6 ± 0.3 Ma, which is in excellent agreement with the existing K-Ar and Ar-Ar dates. The basalts yield an initial $^{187}Os/^{188}Os$ that is typically chondritic (~0.128), and indicate that crustal contamination and metasomatic activity played a very small role in the Re-Os budget during formation of the Deccan basaltic province.

We present here preliminary Re-Os data for samples with known Sr-, Nd-, and Pb-isotopic compositions from the Barmer, Bhuj, Mundwara, and Amba Dongar complexes [4]. This study is among the first to report Os-isotopic data from alkaline, Si-undersaturated rocks (± carbonatite). The main objective is to use the Os-isotopic data to evaluate plume-lithosphere interactions and the role of metasomatic processes that were involved in the generation of Deccan alkaline magmatism.

The results obtained to date are as follows: Samples of ijolite, tephrite, and nephelinite from the Mundwara complex (~68.5 Ma) yield initial $^{187}Os/^{188}Os$ values of 0.136, 0.148, and 0.169, respectively, with Os contents of 42–103 ppt. From the region of Bhuj (~66 Ma), four basanites yield initial $^{187}Os/^{188}Os$ values from 0.141 to 0.170, with Os concentrations from 19 to 64 ppt. Overall, Os contents and initial ratios are roughly anticorrelated, suggesting mixing between a mantle component and a more radiogenic end member. If the latter is represented by average continental crust (i.e., $^{187}Os/^{188}Os$ ~1.2 [7]), simple calculations require ~3–4% of crustallike Os in those samples with 20–30 ppt total Os. On the other hand, a basanite from Amba Dongar (~61 Ma) with a lower Os content of 15 ppt yields a chondritic initial $^{187}Os/^{188}Os$ of 0.125, which is indicative of essentially no crustal contamination. A carbonatite dike from the Barmer complex (68.6 Ma) containing 6 ppt Os yields a very radiogenic initial $^{187}Os/^{188}Os$ of 2.28. Finally, a pyroxenite dike from the Mundwara complex with 3 ppt Os yields an even higer initial ratio of 3.70. While these latter two results could result from contamination by unusually radiogenic crustal rocks, they may alternatively indicate derivation from ancient pyroxenite veins.

Based on available Sr-, Nd-, and Pb-isotopic data, the origin of the Deccan alkaline complexes are best explained by the involvement of at least three mantle end members: Réunion plume, MORB-like asthenosphere, and metasomatized subcontinental lithosphere. The Os budget of some samples from the Mundwara and Bhuj complexes may be marginally affected by crustal Os. However, it remains that a pyroxenite dike and a carbonatite have initial ratios higher than those of most crustal rocks, which may indicate derivation from ancient pyroxenite veins in the subcontinental lithosphere. Finally, the very low Os concentration of the Barmer carbonatite supports the notion that CO_2-related metasomatism does not play an important role in the mantle Os budget.

References: [1] Vandamme D. et al. (1991) *Rev. Geophys., 29,* 159–190. [2] Courtillot V. et al. (1986) *EPSL, 80,* 361–374. [3] Basu A. R. et al. (1993) *Science, 261,* 902–906. [4] Simonetti A. et al. (1998) *J. Petrol., 39,* 1847–1864. [5] Allègre C. J. et al. (1999) *EPSL,* in press. [6] Pegram W. J. and Allègre C. J. (1992) *EPSL, 111,* 59–68. [7] Esser B. K. and Turekian K. K. (1993) *GCA, 52,* 1383–1388.

CHEMICAL STRUCTURE OF THE REFRACTORY ORGANIC FRACTION ISOLATED FROM A FOREST SOIL (LACADÉE, SOUTHWEST FRANCE): BLACK CARBON CONTRIBUTION AND ANALYTICAL BIAS.

N. Poirier[1,2], C. Largeau[2], J.-N. Rouzaud[3], S. Derenne[2], A. Mariotti[1], and J. Balesdent[4], [1]Biogéochimie Isotopique, Institut National de la Recherche Agronomique/Centre National de la Recherche Scientifique/Université Pierre et Marie Curie, Paris, France, [2]Chimie Bioorganique et Organique Physique, Centre National de la Recherche Scientifique/L'École Nationale Supérieure de Chimie de Paris, Paris, France, [3]CRM-Centre National de la Recherche Scientifique, Orléans, France, [4]Commissariat à l'Energie Atomique, Saint-Paul les Durance, France.

Soil organic matter (SOM) is comprised of several pools with different turnover rates, including a stable pool with mean residence times up to millenia. Information on the nature and fate upon changes in land use of the latter pool is important, since variations in its abundance would generate large CO_2 flows between atmosphere and soil. However, the mechanism that accounts for the stability of refractory SOM is still far from being completely elucidated [e.g., 1]. Protection by minerals is often considered, but intrinsic resistance of some SOM constituents, directly related to their chemical structure, might also be an important factor. Nevertheless, the chemical composition of the refractory fraction of SOM is still a matter of debate.

A number of studies, chiefly based on solid-state ^{13}C NMR observations, pointed to the occurrence of highly aliphatic recalcitrant structures in SOM, reviewed in [2]. In contrast with the above findings, it was also considered that aromatic carbon tends to accumulate as SOM decomposition proceeds. Indeed, recent studies showed that black carbon accounts for a substantial fraction of total organic carbon in various soils [1,3]. Accordingly, black carbon might be an important source for the refractory, aromatic, carbon pool in soils [1,4], as recently shown in the case of marine sediments [e.g., 5].

In a previous study [6] we observed that a substantial part (~25%) of total humin in a forest soil from Lacadée (southwest France) is composed of nonhydrolysable macromolecular material and preliminary studies, via solid-state ^{13}C NMR, and Curie point pyrolysis gas chromatography mass spectrometry (Py/GC/MS) pointed to a highly aliphatic structure for this refractory fraction [6].

In the present work, this refractory material was further examined via a combination of elemental analysis, Fourier transform infrared spectroscopy, quantitative pyrolysis, and transmission electron microscopy with electron diffraction and dark-field imaging. It thus appeared that (1) aliphatic moieties are only minor components in the refractory fraction of the Lacadée soil, and (2) this fraction is dominated by a mixture of black carbon and melanoidin-type macromolecules. The refractory fraction of the Lacadée soil thus exhibits a complex and heterogeneous composition. In addition, this study illustrates how the chemical structure inferred for such material can be highly biased when analytical methods such as solid-state ^{13}C NMR and Curie point Py/GC/MS are used, since black carbon contribution is highly underestimated by these methods.

References: [1] Skjemstad J. O. et al. (1996) *Aust. J. Soil Res., 34,* 251–271. [2] Preston C. M. (1996) *Soil Sci., 161,* 144–166. [3] Glaser B. et al. (1998) *Org. Geochem., 29,* 811–819. [4] Haumaier L. and Zech W. (1995) *Org. Geochem., 23,* 191–196. [5] Gustafsson Ö. and Gschwend P. M. (1998) *GCA, 62,* 465–472. [6] Augris N. et al. (1998) *Org. Geochem., 28,* 119–124.

BONINITE-LIKE VOLCANIC ROCKS IN THE 3.7–3.8-BILLION-YEAR-OLD ISUA GREENSTONE BELT (CENTRAL TECTONIC DOMAIN), SOUTHWEST GREENLAND.

A. Polat[1], A. W. Hofmann[1],

M. Rosing[2], and J. Myers[3], [1]Max-Planck-Institut für Chemie, Abteilung Geochemie, 55020 Mainz, Germany (polat@mpch-mainz-mpg.de; hofmann@mpch-mainz-mpg.de), [2]Geological Museum, University of Copenhagen, Oester Voldgade 5-7, Copenhagen 1350, Denmark, [3]Geological Survey of Western Australia, 77 Falls Road, Lesmurdie, Australia.

The 3.7–3.8-Ga Isua greenstone belt of southwest Greenland is characterized by metamorphosed, metasomatized, and deformed lithotectonic successions of volcanic and sedimentary rocks [1,2]. The volcanic rocks are composed of pillow basalts intercalated with ultramafic units. The sedimentary units consist mainly of banded iron formations, cherts, and siliciclastic turbidites. The belt is 35 km long and up to 4 km wide, occurring in 3.7–3.8-Ga Amitsoq gneisses.

The voluminous, intra-oceanic, mafic to ultramafic (MgO = 7–25 wt%, Ni = 60–827 ppm, Cr = 60–3450 ppm) metavolcanic rocks (garbenschiefer amphibolites) from the central tectonic domain [1] of the Isua greenstone belt have typically low TiO_2 (0.20–0.40 wt%) but high (Al_2O_3 = 13–20 wt%) contents, resulting in high Al_2O_3/TiO_2 = 45–90 ratios. They tend to have subchondritic Zr/Y = 1.2–2.3, Ti/Zr = 65–112, and Ti/V = 7–10 ratios. On a chondrite-normalized diagram they possess the following significant features: (1) low MREE/HREE ratios (Gd/Ybn = 0.40–0.60); and (2) highly depleted to enriched LREEs (La/Smn = 0.45–1.40), generating concave-upward REE patterns. In addition, they are characterized by depletion of Nb, but enrichment of Zr, Pb, and Sr with respect to neighboring REEs. Alteration and fractional crystallization can be ruled out as the cause of the distinct and coherent composition. The progressive depletion of highly incompatible to compatible elements (e.g., Th, LREE, Zr, Ti, Y, HREE) may have resulted from a previous melt extraction event from the mantle source, consistent with positive ε_{Nd} (1.5) values [3]. The concave-upward LREE patterns, combined with the systematic depletion of Nb, relative to Th and La, and the enrichment of Pb and Sr, with respect to Sm and Nd, may indicate subduction-zone influence on a previously depleted mantle source. Collectively, these geochemical characteristics of the garbenschiefer metavolcanic rocks are comparable to those of Phanerozoic low-Ti island arc volcanic series (e.g., boninites).

References: [1] Appel P. W. U. et al. (1998) *Terra Nova, 10,* 57–62. [2] Rosing M. T. et al. (1996) *Geology, 24,* 43–46. [3] Gruau G. et al. (1996) *Chem. Geol., 133,* 225–240.

GEOCHEMISTRY OF 3.7–3.8-BILLION-YEAR-OLD PILLOW BASALT CORES AND RIMS FROM THE ISUA GREENSTONE BELT (NORTHWESTERN TECTONIC DOMAIN), GREENLAND: IMPLICATIONS FOR GEODYNAMIC SETTINGS.

A. Polat[1], A. W. Hofmann[1], J. Myers[2], and P. W. U. Appel[3], [1]Max-Planck-Institut für Chemie, Abteilung Geochemie, 55020 Mainz, Germany (polat@mpch-mainz.mpg.de; hofmann@mpch-mainz.mpg.de), [2]Geological Survey of Western Australia, 77 Falls Road, Lesmurdie, Australia, [3]Geological Survey of Denmark and Greenland, 2400-Copenhagen, Denmark.

The Isua Greenstone Belt of West Greenland contains the world's oldest known, relatively well-preserved, metavolcanic and metasedimentary rocks, providing important information about the early history of the Earth. The rocks are all deformed, metasomatized, and metemorphosed up to amphibolite facies grade [1,2].

Pillow basalts with well-preserved rims and cores are exposed in the northwestern tectonic domain of the eastern part of the belt [1]. The rims, up to two centimeters thick, are characterized by fine-grained hornblende + biotite ± quartz ± carbonates. The pillow cores, with radial and concentric cooling fractures, contain hornblende + quartz + feldspar + biotite ± epidote ± carbonates (calcite). Compositionally, they are tholeiitic basalts and basaltic andesites. Both the rims and cores have comparable Al_2O_3 (11–13 wt%), TiO_2 (0.84–0.96 wt%), Cr (40–390 ppm), Ni (60–130 ppm), Sc (20–50 ppm), Zr (63–73 ppm), Th (0.40–0.60 ppm), and Y (12–24 ppm) contents, and Al_2O_3/TiO_2 (13–14), Zr/Y (2.4–3.8), and Ti/Zr (70–90) ratios. The rims are more enriched in Fe_2O_3 (17.5–20.4 vs. 9.6–18.8 wt%) compared to the cores. Large ion lithophile elements (LILE: Sr, Rb, Ba, K) have large variations both in the cores and rims, consistent with mobilization of these elements by secondary processes. In some rims, LREEs appear to have been lost during either seafloor hydrothermal alteration or subsequent amphibolite facies grade metamorphism, whereas HFSEs (Th, Nb, Zr, and Ti) have remained relatively unchanged. In contrast to the rims, most cores appear to have preserved their original REE and HFSE signatures. On a primitive mantle-normalized diagram, samples screened for minimum alteration have the following significant characteristics: (1) slightly to moderately enriched REE patterns, where La/Yb_n = 1.5–3.0; (2) depletion of Nb with respect to Th and La (Th/Nb_n = 1.13–1.94, La/Nb_n = 1.2–2.3); (3) depletion of Zr and Hf with respect to Sm and Nd (Zr/Sm_n = 0.86–1.0); (4) depletion of Ti relative to Sm and Gd (Ti/Sm_n = 0.58–0.70); and (5) minor negative Eu anomalies (Eu/Eu* = 0.85–1.0). Alteration, crustal contamination, and fractional crystallization can be ruled out as the cause of distinct and coherent trace-element patterns. The enrichment of LREE and depletion of HFSE in the Isua pillow basalts are comparable to those of Phanerozoic juvenile oceanic island arc basalts, suggesting that modern convergent marginlike tectonic settings existed as early as 3.7–3.8 Ga.

References: [1] Appel P. W. U. et al. (1998) *Terra Nova, 10,* 57–62. [2] Rosing M. T. et al. (1996) *Geology, 24,* 43–46.

A COMMERCIAL CELESTINE ORES IN IRON-ORE DEPOSITS OF THE SIBERIAN PLATFORM.

A. G. Polozov[1], T. N. Moroz[2], N. A. Palchik[2], L. V. Miroshnichenko[2], O. Yu. Belozerova[1], I. M. Romanenko[3], and P. F. Benedyuk[1], [1]Institute of Geochemistry, Siberian Branch of Russian Academy of Sciences, P.O. Box 4019, Irkutsk 664033, Russia (poloz@igc.irk.ru), [2]United Institute of Geology, Geophysics, and Mineralogy, Siberian Branch of Russian Academy of Sciences, Academy Koptug Avenue 3, Novosibirsk 630090, Russia (moroz@uiggm.nsc.ru), [3]Institute of Experimental Mineralogy of Russian Academy of Sciences, Chernogolovka, Moscow District 142432, Russia (igor@iem.ac.ru).

Introduction: The sulfate (Sr, Ba, and Ca) mineral assemblages are found in all iron-ore deposits of the Siberian platform. Within some of these deposits the commercial celestine ores have been discovered, but their compositions are not well examined. This situation is not favorable for the development of the model of genesis, and for the creation of processing scheme for the such ore types.

Geological Sketch: The iron-ore deposits of the so-called Angara-Ilim type are located in intricately built breccia-fissure zones, often of tubular (columnar) configuration, and occur within the Phanerozoic cover of the Siberian platform. The researchers proposed diverse genetic concepts (also those reciprocally excluding each other) available in the theory of ore formation, on the origin of structures, hosted rocks, and ores.

Sulfate mineral assemblages occur ubiquitously. Beyond columnar structures, in surrounding rocks, in the columnar structures proper and particularly within sedimentary deposits of cupholes, developed in the upper parts of deposits. Beyond columnar structures, the veins and rare nests in sedimentary rocks of different composition primarily represent these assemblages. In the columnar structures proper they occur through entire depth as nests and

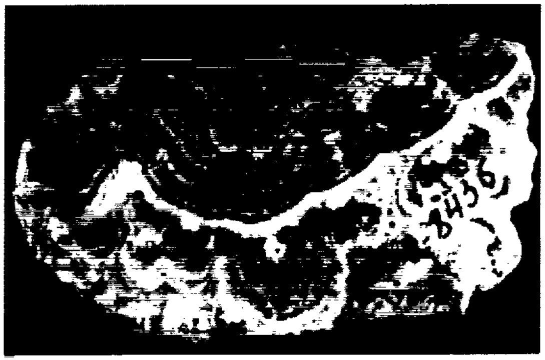

Fig. 1. A polished section of the celestine nodule.

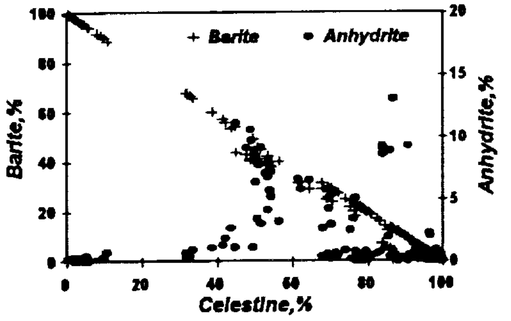

Fig. 2. A celestine-barite-anhydrite minal patterns of the celestine ores from iron-ore deposits.

veinlets in the silicate rocks of the basic composition, different metasomatic rocks and ores. In the cupholes the sulfate minerals are available across the whole section of deposits, but the main one is located at the bottom, in the domain of distribution of brecciated and more coarse-grained rock varieties where mineralization is represented as a thick, crescentlike deposit. In the center of depressions (up the cross-section) there are rocks enriched in the spots and veinlets primarily of Cu minerals. These horizons are described as bedded Cu ores. The near-surface parts contain widespread large nodules of celestine (Fig. 1), forming the lens and beds of commercial ores.

Mineral Composition: The mineral composition of commercial ores was investigated using electron microprobe analyzer and by means of X-ray powder diffraction method, Raman, and infrared spectroscopy.

Cationic and anionic isomorphous substitutions take place in the examined sulfate minerals. The Sr ion is replaced by Ba in the celestine lattice and vice versa in barite ones and intermediate compositions are found as well (Fig. 2).

The celestine of intermediate compositions (*celestinobarite*) forms the main part of commercial celestine ores. The Ca content in such celestine increases (up to 3.2% of CaO). The X-ray patterns and Raman spectroscopy indicate the gypsum and anhydrite impurities in some celestine samples. In the Raman spectrum the band due to v_1 mode of SO_4^{2-} is expected to be the most intense. A replacement of the SO_4^{2-} anions by CO_3^{2-} was observed on infrared spectra of *celestinobarite* crystals.

Summary: The Ca-content *celestinobarite* with substitution of SO_4^{2-} anions by CO_3^{2-} ones compose the main part of commercial celestine ores. These features should be accounted for to develop the model of genesis and ore processing scheme.

Acknowledgments: This work is supported by Russian Foundation for Basic Research grants No. 98-05-65204.

TRANSFORMATION OF BASALT ON CONTACT TO SALTS IN THE SIBERIAN PLATFORM SEDIMENTARY COVER.

A. B. Polozov, O. A. Proidakova, G. P. Sandimirova, and E. V. Smirnova, Institute of Geochemistry, Siberian Branch of Russian Academy of Sciences, P.O. Box 4019, Irkutsk 664033, Russia (poloz@igc.irk.ru).

Introduction: The basalt-salt interactions are interesting geochemical phenomena, not only for the waste-disposal modeling (natural analogs), but for the petrology and ore geology as well. The rare occurrence of similar natural experiments requires in each case a close, detailed, and therefore complex study.

Geologic Setting: The contacts steeply dipping of basalt dike disposed in salts of Nepa potash deposits of the Siberian platform sedimentary cover were studied. The lying side of dike is changed as much as possible, i.e., it becomes cavernous, and the caverns are filled in new formed minerals: silicates, sulfides, phosphates, oxides, sulfates, carbonates, and halite. The dike itself is broken by numerous fractures with visible zones of alterations and gangue minerals, e.g., silicates, sulfides, carbonates, and halite. As it was known earlier, the cavernous develop in the lying side of dikes and sills, at close contact, due to their impregnation into the water-saturated stratas under conditions of volatile mixing of underlying stratas and cooled magmatic body.

Experiment: The basalt sample was crushed up to a fraction 1–0.5 mm and then the fractions of unaltered ("fresh") basalt and altered ones were separated. Thereafter these two samples were analyzed chemically, and the residual was divided into three parts. One of the parts was not treated and two of the others were leached by a double distillate water within 48 h; one of them was powdered and the other was a fraction. After processing all three parts were dichotomized and half of samples were treated by 1.5 N hydrochloric acid during 15–30 min. The water and chloride extracts were analyzed, as was leached basalt.

Results and Discussion: On the REE chondrite normalized patterns, as shown in Fig. 1, a "standard" slope and position characterize the basalt from contact to salts. The altered basalt practically does not differ by REE pattern from the "fresh" ones. The basalt treated by hydrochloric acid has not a "basalt" slope of a normalized curve and demonstrates a sharp Ce minimum with conjugated Eu maximum.

The REE analysis of unaltered basalt fractions, treated by water, demonstrates a weak slope in the LREE part explained as migration with a water-soluble salts, though this phenomenon required further special investigations. The slope of a curve for samples treated by hydrochloric acid (fractions and powder) were rather essentially changed. It is explained by preferential LREE incorporation in carbonaceous phases.

Conjugate appearance of Ce minimum and Eu maximum in basalt, treated by hydrochloric acid (Figs. 1 and 2), and newly formed minerals range from caverns and basalt itself have allowed to offer the model of origin of such pattern on chondrite-normalized curves. Appearance of the sulfate-containing solutions on contacts of anhydrite stratas and cooled magmatic body

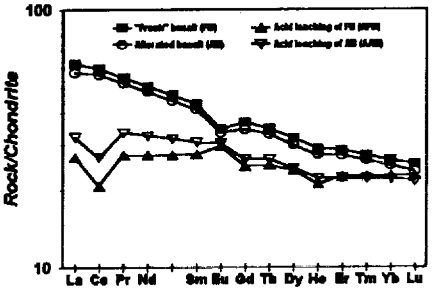

Fig. 1. The REE pattern of "fresh" and altered basalts and those treated by hydrochloric acid.

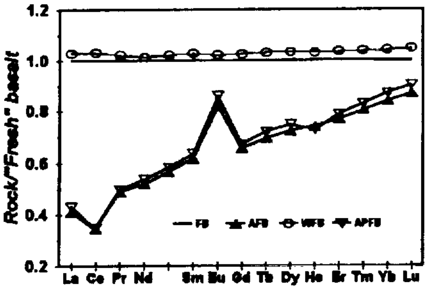

Fig. 2. The REE pattern of "fresh" basalt, treated by double distillate water and hydrochloric acid. FB = a "fresh" basalt, AFB = a basalt fraction treated by hydrochloric acid, WFB = a "fresh" basalt treated by water, APFB = a basalt powder treated by hydrochloric acid.

results in thermal sulfate reduction. Under redox conditions (during anhydrite decomposition) the S_2^- anions are formed, Eu becomes bivalent and separate from the other REE, and sulfide-anion forms the sulfide minerals, as observed in the basalt matrix. This phenomenon has a subjected role that depends from the many other conditions. The sulfate-containing solution oxidized the cerium up to Ce^{4+}, and this element as well as LREE incorporate into the calcite crystals formed in place of decomposed anhydrite and volatile originated from cooled magma and superheated sedimentary rocks. So the calcite and sulfides grains from such basalt are the scavengers of LREE and S_2^-.

Acknowledgments: This work is supported by the Russian Foundation for Basic Research grants No. 98-05-64245.

CHARRED ORGANIC MATTER IN BLACK SOILS OF SASKATCHEWAN.

E. V. Ponomarenko[1] and D. W. Anderson[2], [1]Canadian Museum of Civilization, 100 Laurier Street, P.O. Box 3100, Station B Hull, Québec J8X 4H2, Canada (led@cyberus.ca), [2]Department of Soil Science, University of Saskatchewan, Saskatoon, Saskatchewan, S7N 0W0, Canada (darwin_anderson@duke.usask.ca).

A combination of both conventional and novel techniques such as micromorphology, high-energy ultraviolet (UV) photo-oxidation, and scanning electron microscopy (SEM), has been applied to estimate the proportion of charred organic carbon (C) in the Black Chernozemic soils in Saskatchewan. The scheme of the UV oxidation-based experiment developed by Skjemstad (1993) was modified and complemented by detailed morphological and botanical analysis of char.

The following morphons and horizons have been investigated within both sand and loam soil profiles: (1) plough horizons in both erosional and accumulative positions, (2) humus horizons in the noncultivated profiles, (3) zoogenic AB horizons, and (4) buried humus horizon.

The investigation has been carried out on gravel, sand, silt, and clay fractions of the samples.

Gravel size fractions of most samples from both plough horizons and AB horizons included only arboreal charcoal. In other fractions char is represented by products of incomplete combustion of both arboreal and herbaceous vegetation, with the latter corresponding to incomplete combustion of sod in wet conditions such as spring or late autumn/winter fires.

Char pool in sand fractions reflects results from a series of fire events, which can be distinguished on the basis of particle shape, surface area, and type of fuel combusted. In sand fractions up to 25% of charred particles originate from herbaceous fuel (straw of grasses). Preservation of fragile herbaceous char in sand size fractions points to its recent origins, presumably due to manmade fires in agro-ecosystems.

The scanning electron microscopy (SEM) investigation of char in particle size fractions showed that the surface area significantly differs for charred particles associated with silt and clay fractions (separated by sedimentation).

Char in sand and clay fractions as well as those separated with heavy liquids has a well-pronounced anatomical structure and high porosity. Charred particles separated with NaI as a part of light fraction (LF) are never smaller than silt size. Distinctive char particles, sedimented with mineral particles of clay, are of silt size as well.

Char in silt fraction has low surface area with pores mostly in-filled by clay. Plant anatomical structure is not pronounced because of clay coatings. This has been interpreted as older age of char associated with silt fraction ("heavy" char).

In plough horizons of Black Chernozemic soils, the charred C, estimated as a UV-oxidation resistant part of a C pool (ORC), contributed up to 60% of total C content (TOC). The contribution is higher in accumulative elements of landscape than in erosional ones (60% vs. 45–50% for the same site).

The humus horizons of uncultivated soils have a noticeably higher percentage of char than the plough horizons of cultivated soils (difference is 10–30% for the same site).

In paleosols UV-oxidation-resistant C contributes up to 80% of TOC.

In AB horizons ORC contributes 30–60% of TOC, high variability of char content being characteristic.

The maximum percentage of UV-oxidation-resistant C from the TOC in the particle size fractions is in the sand fraction (up to 70% of TOC in the fraction); the char content in the clay fraction is generally the lowest (20–40%). The major amount of ORC is stored in sand size fraction for AB horizons, and clay fraction for paleosol.

Distribution of C among pools of particulated organic matter (POM), oxidizable C, and charred C has been estimated with reference to soil C pools of different lability. Comparison of oxidizable C content with the content of LF in the same samples showed that at least 50% of oxidizable C is represented by particulated organic matter.

This work demonstrates that further investigation, involving separation of both charred C and particulated organic matter, is required for accurate estimation of the role of soil humic substances in soil C pool of Black Soils.

References: [1] Skjemstad et al. (1993) *J. Soil. Sci., 44,* 485–499.

KINETICS OF THE ABIOTIC REDUCTION OF COLLOIDAL MnO_2 BY NITRITE.

J. I. Popp and G. W. Luther III, University of Delaware, 700 Pilottown Road, Lewes DE 19958, USA (jpopp@udel.edu).

Introduction: Manganese oxides are considered significant oxidants for organic matter (OM) decomposition in the environment. The oceanographic paradigm for OM decomposition has been designed to show a sequence of oxidants based on the oxidant yielding the most free energy. This model ranks the oxidants in the following order: O_2 reduction, NO_3^- reduction, MnO_2 reduction, Fe_2O_3 reduction, SO_4^{2-} reduction, and methanogensis. Manganese dioxide reduction occurs after nitrate reduction (denitrification); however, an overlap of these zones has been shown to a certain degree in pelagic sediments. Much of the research involving MnO_2 reduction has centered on solid phases; however, little has been done with soluble or polymeric forms. Soluble Mn(III, IV) compounds could be of extreme importance at the interfaces of oxic, suboxic, and anoxic zones and in low-salinity waters. In this study, a colloidal form of MnO_2 {MnO_2(c)} is used to determine the empirical rate law and the activation energy for the reduction of MnO_2(c) by nitrite to form nitrate. Nitrite is an intermediate species in denitrification as well as nitrification. In natural environments, the reduction of solid MnO_2 {MnO_2(s)} by nitrite has been shown. In this study, the rates of reduction of MnO_2(c) were measured as a function of pH (4.5–6) and temperature (11.5°–31.5°C). The stoichiometry of the reduction of MnO_2(c) by nitrite has been proved to follow the reaction

$$MnO_2(c) + 2H^+ + NO_2^- \rightarrow Mn(II) + NO_3^- + H_2O$$

The rates of reduction of MnO_2(c) by nitrite determined in this study were considerably faster than the rates determined for the same reaction using MnO_2(s) instead of MnO_2(c).

ORGANIC CARBON AND SULFIDE SULFUR-ISOTOPIC STUDIES FROM THE OXYGEN/SULFUR AND SULFER/DEUTERIUM BOUNDARY SEDIMENTS IN POLAND.

E. Porebska[1], Z. Sawlowicz[1], and H. Strauss[2], [1]Institute of Geological Sciences, Jagiellonian University, ul. Oleandry 2A, 30-638 Krakow, Poland (zbyszek@ing.uj.edu.pl), [2]Geologisch-Paläontologisches Institut, Westfälische Wilhelms-Universität Münster, 48149 Münster, Germany.

Introduction: Most of the presented isotopic data come from the well-studied Lower Palaeozoic deep-sea section in Zdanow. A few additional samples from the S/D transition in the East European Platform (EEP) shelf sediments were also studied. The Zdanow section represents a part of the basinal sequence of the Bardzkie Mountains (Sudetes, southwest Poland). The sequence, which includes the uppermost Ordovician to Lower Carboniferous sediments, belongs to an accretionary prism that is believed to be deposited to the north from the Gondwana-derived Armorica microcontinent, located in the high southern lattitude during early Silurian. The O/S boundary interval is characterized by a transition from the flysch-dominated Jodlownik Beds (upper Ashgill) into hemipelagic and pelagic Lower Graptolitic Shales (lower Llandovery) [1]. The S/D transition in the Bardzkie Moutains is developed as deep-water graptolitic black clayey and siliceous shales. The highest

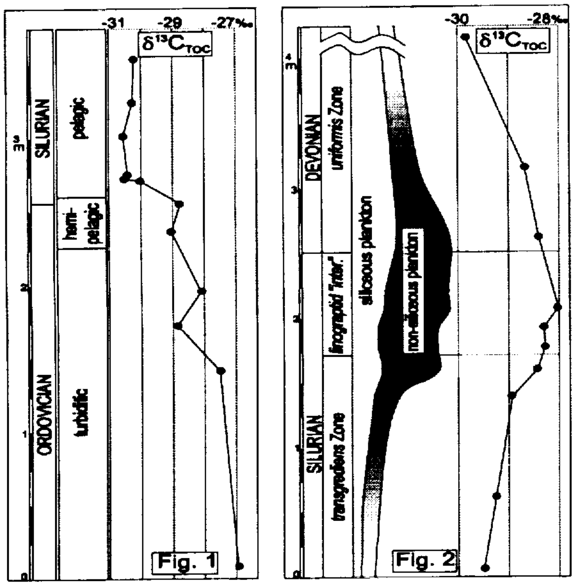

Fig. 1.

Silurian *transgrediens* zone and the first Devonian *uniformis* zone are separated by a thin (30-cm) interval of a linograptid "interregnum" [2]. EEP shelf sediments are represented by gray marls deposited in an oxic environment of high accumulation rate.

Geochemistry: Organic C-isotopic data (12 samples) vary according to the sedimentological and geochemical characteristics of the sediment around the O/S boundary (Fig. 1). Lower turbidite-dominated oxic sediments, which probably mark the end of Hirnantian glaciation, have $\delta^{13}C_{TOC}$ values around –27.5‰, hemipelagic transitional facies of anoxic shales have values around –28.5‰, and pelagic radiolarian black cherts have values around –30.3‰. A drastic change in redox conditions and in the style of deposition observed in the studied section may be related to a glacio-eustatic sea-level fluctuation, recognized around the O/S boundary in other regions where shift in $\delta^{13}C$ values is up to 5‰ [3]. Sulfur-isotopic data are limited. One sample of black shale has $\delta^{34}S$ value 15.8‰, whereas values for three samples of cherts changes from –15.1‰ to –7.9‰.

$\delta^{13}C_{TOC}$ values (11 samples) at the S/D transition change gradually from –29.5‰ in *transgrediens* zone to –28.0‰ in the linograptid "interregnum," and return to –29.8‰ in the *uniformis* zone. These values strongly coincide with estimated higher primary productivity and contribution of nonsiliceous plankton during the "interregnum" period (Fig. 2). Porebska and Sawlowicz [2] suggested that the linograptid burst, accompanied by changing sediment geochemistry across the S/D boundary, was attributed to short-term shallowing of the upwelling system, which introduced specific nutrient-rich waters into the mixed layer. $\delta^{34}S$ values in *transgrediens* zone change irregularly from –11.2‰ to –19.5‰, stabilize around –17.6‰ at the "interregnum" sediments, and decrease rapidly to values around –21.3‰ in the *uniformis* zone. No significant correlation is discernible between S-isotopic data and Fe, S, and TOC contents.

$\delta^{13}C_{TOC}$ values (four samples from two boreholes) from the S/D transition in EEP shelf sediments vary from –25.8‰ to –26.5‰ and are significantly heavier than values from the Zdanow section. This could be related to a higher contribution of land plants (*cooksonia* have been found here). $\delta^{34}S$ values from the EEP sediments vary from –14.2‰ to –2.4‰ in the uppermost Silurian to 6.7‰ in the lowermost Devonian.

References: [1] Sawlowicz Z. and Porebska E. (1998) *Mineral. Mag., 62A,* 1326–1327. [2] Porebska E. and Sawlowicz Z. (1997) *Palaeogeogr., Palaeoclimatol., Palaeoecol., 132,* 343–354. [3] Marshall J. D. et al. (1997) *Palaeogeogr., Palaeoclimatol., Palaeoecol., 132,* 195–210.

SPATIAL DISTRIBUTION OF CHROMIUM IN NORTHEAST ARABIAN SEA SEDIMENTS.

C. Prakash Babu[1], H.-J. Brumsack[2], and B. Schnetger[2], [1]National Institute of Oceanography, Dona Paula, Goa, 403 004, India (pbabu@csnio.ren.nic.in; pbabu@darya.nio.org), [2]Institute of Chemistry and Biology of the Marine Environment, Oldenburg University, P.O. Box 2503, D-26111 Oldenburg, Germany (brumsack@icbm.de; b.schnetger@icbm.de).

Along the western continental margin of India, Cr (normalized to Al) is relatively enriched in sediments overlain by the O minimum zone (OMZ, 150–1200 m; range 17–33 × 10^{-4}; mean 25 × 10^{-4}) when compared to deeper sediments (16–26 × 10^{-4}, mean 20 × 10^{-4}) when the samples with low terrigenous component are considered. Within the OMZ, Cr seems relatively less enriched in the southern Arabian Sea (southwest coast of India, maximum 26 × 10^{-4}) when compared to northern Arabian Sea sediments (maximum 31 × 10^{-4}) even though the mean concentrations are the same. Incidentally, the productivity and organic C content (TOC) are relatively high (>1 g C/m^2/d and 2–4%) in the south when compared to the northern Arabian Sea (0.50–1.0 g C/m^2/d and 1–2%). Chromium/aluminum show a positive correlation with TOC/Al, Se/Al, and P/Al in the north (0.88, 0.89, and 0.80) but not in the south (0.34, –0.26, and 0.44).

The poor correlation of Cr with TOC, Se, and P appears to suggest the derivation of Cr either from heavy and opaque minerals and/or partial release of biogenic Cr in southern Arabian Sea sediments, whereas Cr appears to be accumulated in the northern Arabian Sea. The release of biogenic Cr seems to indicate a relatively oxygenated sediment/seawater interface in the southern Arabian Sea, whereas the accumulation of Cr indicates the reduction of Cr^{+VI} to Cr^{+III}, which is particle reactive. It appears that Cr^{+III} is being adsorbed onto settling particles and accumulates in the sediments. Uranium, a redox-sensitive element, also shows a positive correlation with Cr/Al (r = 0.69, n = 17), supporting the idea of Cr reduction in the northern Arabian Sea.

The normalized river particulate enrichment factor (EF) for Cr in the study area is high even in comparison to anoxic basins, i.e., Framvaren fjord and Cariaco trench. It appears that the suboxic water column causes Cr reduction in the northern Arabian Sea, and the presence of a midwater turbid layer, as reported in earlier studies, augments the rapid accumulation of Cr.

Our study suggests the potential use of Cr as a proxy for paleoxygenation in northern Arabian Sea sediments, provided care is taken for Cr enrichment during early diagenesis and potential variation in Cr/Al ratios owing to provenance of terrigenous detrital matter.

BIOGEOCHEMISTRY OF THE CAUVERY FLOOD PLAIN SEDIMENTS, SOUTHERN INDIA: IMPLICATIONS TO THEIR ORIGIN AND FARMING.

G. K. Prasad and V. Rajamani, School of Environmental Sciences, Jawaharlal Nehru University, New Delhi 110 067, India.

Soil, an essential Earth resource for food production, is formed by the interaction of the physical, biological, and chemical forces of nature. Alluvial soils and flood plain sediments are known to be very fertile and rich in plant nutrients. The nutrient elements are derived from rocks in the catchment areas by complex weathering processes. Rock weathering, soil erosion, transportation, and deposition of these weathered materials has resulted in the formation of nutrient enriched, easily weatherable sediments. The alluvial sediments are home to billions of organisms, which utilize the bio-available nutrients, in turn accelerating the process of bioweathering by secreting various kinds of organic acids and complex chemical compounds into the sediments. Action of these compounds leads to further weathering and release of nutrients, thus making the area a highly fertile farmland. Understanding this complex biogeochemical process is very important for sustainable agriculture. Cauvery constitutes a major river system of southern India. It originates in the western ghats, in the Mysore plateau, flows eastward, and finally drains into the Bay of Bengal. Along the way it flows through granitic, gneissic, and charnockitic terranes that are subjected to repeated uplifts, and forms a vast and highly fertile flood plain in the down stream area. Sediment samples from the flood plain areas were collected from a depth of 0–20 cm, within 200 m on either side of the river channel. The dominant type of fungi present in the samples were isolated, cultured, and identified using techniques in microbiology. *Aspergillus niger, A. terreus var. terreus, Byssochlamys nive* (Westling), *Rhizomucor pusillus,* and *Fusarium solani* were the major fungi identified. All these organisms are known to secrete organic acids and hence may play an active role in bio-weathering. Humic acids (HA) and fulvic acids (FA) extracted from the sediment samples, were analyzed by inductively coupled plasma atomic emission spectrometry (ICP-AES) for various elements, and by X-ray diffraction (XRD) and infrared (IR) spectroscopy for mineralogy and organic characteristics. The analyses indicate that, possibly, the humus is fresh and not very complex in nature. Concentrations of all major oxides in bulk samples, including the calculated Chemical Index of Alteration (CIA), suggest little chemical weathering, of the samples as well as their sources. The samples are predominantly alkaline in nature, with low EC values indicating very little free ions. The organic C content is well below the average expected values (<1.5%) and constitutes nearly 80% of the total C in the soil samples. Nitrogen content is also at best low to average. Organic acid concentration is low and does not seem to have influenced the pH of sediments to any great extent. Neither the texture nor the composition of the sediments show any perceptible variation along the course of the river downstream, to suggest any further chemical weathering. Most of the nutrients are still trapped in the minerals of the sediments, perhaps because of their very recent origin.

IODINE-XENON DATING: SENSITIVE CHRONOMETER FOR REPROCESSING IN THE PRIMITIVE SOLAR SYSTEM.

O. V. Pravdivtseva and C. M. Hohenberg, Campus Box 1105, McDonnell Center for the Space Sciences, Washington University, One Brookings Drive, St. Louis MO 63130-4899, USA (am@howdy.wustl.edu).

Introduction: The I-Xe chronometer is based upon decay of ^{129}I to ^{129}Xe in the early solar system. Recent comparison of I-Xe system in individual mineral separates from 12 different meteorites [1] with independent Pb-Pb data [2] has demonstrated that I-Xe clock is a reliable sensitive chronometer when applied to a single mineral system. Since most I hosts are secondary minerals, the I-Xe clock generally records postformational processing, providing the information on early meteorite evolution. Absolute I-Xe ages can be found by normalization using the measured I-Xe and Pb-Pb ages of Acapulco phosphate (4.557 ± 0.002 Ga). Absolute ages for the I-Xe internal standards Shallowater and Bjurböle, 4.566 ± 0.002 Ga and 4.565 ± 0.003 Ga, respectively, provide absolute I-Xe ages for all other samples. The I-Xe age of bulk meteorite is meaningful and interpretable only when the carrier of primordial I is a major mineral phase (e.g., enstatite chondrites [3]). Using the "monomineral" approach, separated phases from the Richardton H5 chondrite provide a case history of postformational alteration in this object [4]. This work applies the I-Xe chronometer to determine the times of reprocessing of selected minerals in single meteorite types. A preliminary account of this work was recently reported [5].

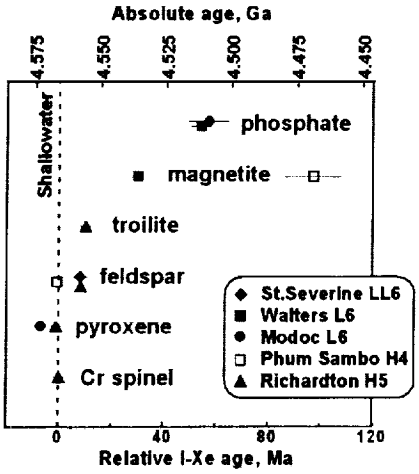

Fig. 1. Iodine-xenon ages relative to the Shallowater standard for separated mineral phases from L, LL, and H chondrites.

Results: Our recent measurements of I-Xe ages of L, LL, and H chondrites along with earlier results from our group [1] were combined together and shown on a single plot (Fig. 1). Minerals whose isotopic system expected to close first during metamorphism (Cr-spinel and pyroxene) have the oldest I-Xe ages, while phosphates and magnetites are among the youngest. Troilite and feldspar have intermediate ages. Although specific closure temperatures of different minerals may vary depending upon chemistry, solid-state reactions and thermodynamic properties, the observed trend is suggestive.

Conclusion: Iodine-xenon chronometer applied to a single mineral system shows different closure times for different mineral separates from the same meteorite class. This observation gives us encouragement that the I-Xe system can resolve mineral-specific meteorite evolution both with qualitative sequence and quantitative formation times.

Acknowledgments: This work is supported by NASA grant NAG5-4173.

References: [1] Brazzle et al. (1999) *GCA,* in press. [2] Göpel C. et al. (1994) *EPSL, 121,* 153–171. [3] Kehm K. et al. (1994) *LPS XXV,* 683–684. [4] Pravdivtseva O. V. et al. (1998) *MAPS, 33,* A126–A127. [5] Pravdivtseva O. V. and Hohenberg C. M. (1999) *LPS XXX,* Abstract #2047.

A FAST THERMAL METHOD FOR BLACK CARBON ANALYSIS OF NATURAL SAMPLES.

K. M. Prentice and J. I. Hedges, Box 357940, School of Oceanography, University of Washington, Seattle WA 98195-7940, USA (prentice@u.washington.edu; jihedges@u.washington.edu).

Introduction: With increasing concerns of anthropogenic effects on the natural environment and questions concerning paleoclimatology, many studies have been aimed at quantifying the amount of black carbon (BC) in the environment. These studies are characterized by numerous and occasionally opposing definitions of BC, difficulties in quantification, and often involve complex procedural steps. The goal of our study was to test a simple and rapid thermal oxidation method to measure black carbon (BC) in natural samples (including pollen, coal, wood, marine sediment, and soils). This method was then compared directly to photo-oxidation and dichromate methods of measurement [1,2].

Method: The thermal oxidation method described below is based on a method developed by Gustafsson et al. [3]. Natural samples were spiked with a known amount of carbon black-acetylene (Alfa) before treatment in order to utilize a standard addition method of quantification. Carbon black was also used as an internal standard to account for any loss of BC during thermal oxidation. Samples were weighed into pretared silver boats (5 × 3.5 mm, Microanalysis) and thermally oxidized for 24 h at 375°C. After cooling to room temperature, samples were exposed to HCl vapor for 24 h to remove carbonate [4]. Samples were then analyzed for weight percent BC in a CHN-Elemental Analyzer (Carlo Erba, Model 1106).

Results: The ratio of BC to organic C was very small in all natural samples, implying that BC may not be a large factor in C cycling. In comparison to other oxidation methods, thermal oxidation gives consistently lower BC concentrations for a given sample. These BC measurements result from the inability of the thermal oxidation method to measure char materials.

Acknowledgments: We would like to thank J. Baldock, C. Masiello, and J. Skjemstad for providing samples and valuable input. We would also like to thank the AOG group for all of their guidance.

References: [1] Skjemstad J. O. et al. (1999) in press. [2] Masiello C. A. and Druffel E. R. M. (1998) *Science, 280,* 1911–1913. [3] Gustafsson Ö. et al. (1997) *Environ. Sci. Technol., 31,* 203–209. [4] Hedges J. I. and J. H. Stern (1983) *Limnol. Oceanogr., 29,* 657–663.

PLATINUM GROUP ELEMENTS IN THE 2.8-GA KOSTOMUKSHA GREENSTONE BELT.

I. S. Puchtel and M. Humayun, Department of the Geophysical Sciences, University of Chicago, 5734 S. Ellis Avenue, Chicago IL 60637, USA (ipuchtel@geosci.uchicago.edu; hum8@midway.uchicago.edu).

Introduction: Platinum group elements (Ru, Rh, Pd, Os, Ir, and Pt) are present at higher levels in komatiites than in basalts making komatiites better probes of mantle PGE abundances. Abundances of PGEs in komatiites and basalts provide complementary information to that derived from mantle xenoliths. We are investigating Archaean mantle PGE abundances using komatiites, and associated basalts, from the Baltic Shield to better constrain the effects of partial melting and fractional crystallization on PGE abundances and to estimate source compositions. Here, we report precise PGE data for the 2.8-Ga Kostomuksha greenstone belt. Based on field relationships, trace-element, and Nd-Pb-Os-isotopic data, the submarine lava sequences of this greenstone belt have been proposed to be remnants of the upper crustal portion of an Archaean oceanic plateau [1]. Osmium isotopes indicate that the source of the Kostomuksha lavas had a superchondritic initial γ^{187}Os of 3.2 ± 0.9 [2]. These komatiites were thus derived from one of the earliest known plumes with a ^{187}Os-enriched isotopic composition [3].

Experimental: Samples analyzed were from pillow and massive basalts, and olivine spinifex-textured and cumulate komatiites, from a number of well-preserved lava flows, recovered from deep (up to 600 m) diamond drill holes. A Finnigan Element™, magnetic sector inductively coupled plasma mass spectrometer (ICP-MS), with a CETAC MCN6000 nebulizer, was used to measure the PGEs by isotope dilution. Samples were spiked with a mixed spike (^{99}Ru, ^{110}Pd, ^{190}Os, ^{191}Ir, and ^{198}Pt) and then fused with NiS. Group-separated PGEs were directly analyzed, and spectral interferences were corrected as follows: Mo and NiAr$^+$ on Ru, Cd on Pd, Pt on Os, and Hg on Pt. Procedural blanks were determined by analyzing four aliquots, 0.5–4.5 g in size, of a low PGE basalt and were (in pg): Ru 19, Pd 626, Os 12, Ir 14, and Pt 317. Blank corrections applied were <2% for komatiites and 5–20% for basalts.

Results and Discussion: Data are shown in Fig. 1, normalized to a mantle composition (PM) with CI-relative abundances [4] and Ir = 3.2 ppb [5].

Basalts. The basalts have MgO abundances ranging from 6.5% to 8.4%, and are characterized by having highly fractionated PGE patterns, $(\mathrm{Pt/Os})_N$ = 10 ± 4, and subchondritic $(\mathrm{Os/Ir})_N$ = 0.71 ± 0.16. The PGE abundances show a strong positive correlation with MgO, Ni, and Cr, and thus behave compatibly in the basalts.

Komatiites. The spinifex-textured (MgO = 25–28%) and cumulate (MgO = 34–37%) komatiites are moderately enriched in Pt and Pd relative to Os and Ir with $(\mathrm{Pt/Os})_N$ = 2.5 ± 0.4, and exhibit chondritic $(\mathrm{Os/Ir})_N$ = 0.98 ± 0.06 ratios. The PGE abundances in the eight analyzed spinifex-textured komatiites vary by 11–16% about the mean. The cumulate komatiites show a systematic decrease in Pt and Pd with increasing MgO. This is consistent with dilution of these melts by olivine. In contrast to the basalts, PGEs behave incompatibly in the early cumulate phase of these komatiites, probably due to sulfide undersaturation. Thus, the relative PGE abundances are representative of primary komatiite melts.

From mass-balance considerations we find that removal of average Kostomuksha komatiite from a chondritic mantle source produces depletions of Pd (up to 75% for 30% melting) in the residue, and enrichments of the compatible Os and Ir (25%), with minor effect on Ru and Pt abundances (<10%). A residue of this type may be represented by the Biu harzburgite [6]. With the exception of Pd, the PGEs appear to behave compatibly during komatiite extraction, implying little Pt/Os fractionation in the residual mantle.

Our calculations show that the Pt/Os enrichment combined with the Os abundance observed in these samples is still insufficient to account for radiogenic ^{186}Os/^{188}Os observed in some plumes [7] with reasonable assumptions regarding the amount of komatiite subducted and mixed into a chondritic mantle source. We conclude that the origin of the radiogenic ^{186}Os/^{188}Os signature requires a noncrustal source, supporting previous arguments [3,7,8].

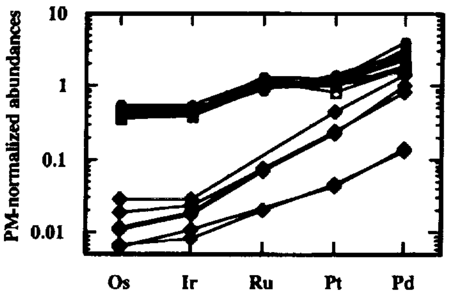

Fig. 1. Platinum-group-element abundances in komatiites (circles = spx; open squares = cumulate) and basalts (diamonds).

References: [1] Puchtel I. S. et al. (1998) *EPSL, 155*, 57–74. [2] Puchtel I. S. et al. (1998) *AGU Fall.* [3] Walker R. J. et al. (1995) *Science, 269*, 819–822. [4] Anders E. and Grevesse N. (1989) *GCA, 53*, 197–214. [5] Morgan J. W. (1986) *JGR, 91*, 12375–12387. [6] Rĕhkamper et al. (1997) *Science, 278*, 1595–1598. [7] Brandon A. D. et al. (1998) *Science, 280*, 1570–1573. [8] Walker R. J. et al. (1997) *GCA, 61*, 4799–4807.

CLAY CHARACTERIZATION WITH AN ELECTRON MICROPROBE: AN ARCHAEOLOGICAL EXAMPLE USING COARSE POTTERY FROM THE AZTEC CULTURAL HORIZON IN MORELOS, MEXICO.

G. Purcell[1], D. Wark[2], and S. Adhya[3], [1]Department of Anthropology, University at Albany, State University of New York, Albany NY 12222, USA (gp9420@cnsvax.albany.edu), [2]Director of the Microprobe Facility, Department of Geosciences, Rensselaer Polytechnic Institute, Troy NY 12180, USA (warkd@rpi.edu), [3]Department of Earth and Atmospheric Sciences, University at Albany, State University of New York, Albany NY 12222, USA (sa8438@csc.albany.edu).

Coarse pottery usually results from firing an intentional mixture of clay and nonclay minerals and rock fragments (clasts), although some naturally-occuring clays are suitable for pot-making without added "temper." In particular, clay chemical variability in coarse pottery may provide a set of signatures for particular pot-making recipes and/or natural sources of clay. Traditionally, neutron activation analysis (NAA) has been used to determine this chemical variability. While NAA can be used to characterize the clay chemistry of finewares, it has serious limitations when used to assay coarsewares, since it conflates in one analysis/assay what are essentially different populations (clay minerals, nonclay minerals, and clasts). Since these can covary unpredictably in coarse pottery in several ways, NAA is unlikely to produce a reliable assay of the clay chemistry of the any one discrete population within this material.

In this research, electron microprobe analysis (EMA) was used to assay the elemental composition of the clay in a set of well-documented pottery sherds from in and around the Valley of Yautepec, Morelos. Our goal was to assess the suitability of ema for such clay characterization, and to compare the results of NAA assays of precisely the same coarse pottery, using the same set of elements. The probe was set up to assay 14 elements: Si, Ti, Al, Fe, Mn, Mg, Ca, Na, K, Zn, Cr, Ba, V, and Ce. The result of the work suggests that EMA of the clay chemistry of coarse pottery represents an improvement over the traditional NAA method for the purposes of archaeological inference.

MECHANISM OF ADSORPTION OF CADMIUM ONTO GOETHITE AND HYDROUS FERRIC OXIDE IN THE PRESENCE OF SELENITE.

K. V. Ragnarsdottir[1,2], L. Spadini[2], and A. Manceau[2], [1]Department of Earth Sciences, University of Bristol, Bristol BS8 1RJ, UK (vala.ragnarsdottir@bris.ac.uk), [2]Laboratoire de Géophysique Interne et Tectonophysique/Centre National de la Recherche Scientifique, Observatoire de Grenoble, Universite de Joseph Fourier, 38041 Grenoble Cedex 9, France.

Introduction: The understanding of the sorption of cations and anions to mineral surfaces is fundamental for many processes in soil and environmental geochemistry and has thus received considerable interest in the past decades [1,2]. We now know that heavy metal cations such as Cd bind to mineral surfaces such as the iron(oxyhydr)oxides by the formation of innersphere complexes through hydroxyl groups on the mineral surface [3–5]. Oxyanions such as selenite ($\mathrm{SeO_3}^{2-}$) also form innersphere complexes by binding to hydroxyls at the surface in a similar manner [6–8]. However, the mechanism of cation sorption in the presence of a ligand such a selenite is not well understood. Workers in the field of mineral interface geochemistry have suggested three possibilities: Shift of sorption isotherm to lower pH by electrostatic interaction; formation of ternary cation-anion-surface complex; and formation of a surface precipitate [2,9]. In this study we report the results of extended X-ray absorption fine structure (EXAFS) spectroscopy for co-adsorption of Cd and selenite to goethite and hydrous ferric iron. We will demonstrate that the pH shift of the sorption isotherm is electrostatic and that no ternary surface complexes are formed.

Methods: Goethite (αFeOOH) was prepared from commercially available material (Bayer). Hydrous ferric oxide (HFO) was synthesized by hydrolyzing a ferric nitrate salt. The density of protonable surface sites as measured by potentiometric titrations was found to be 1.1×10^{-2} site per Fe atom for goethite (1.2 site nm^{-1}), and 1.15×10^{-1} site per Fe atom for HFO. 0.3 M $NaClO_4$ was used as a background electrolyte. The solids were reacted with solutions containing first dissolved Cd, then Se or vice versa. The solutions were monitored for pH and dissolved ions. The solids were separated from the solutions by centrifugation and dry solids were presented to the EXAFS beam. EXAFS measurements were undertaken at the Daresbury Laboratory, UK, for Cd and LURE, Orsay, for Se. Data reduction followed a classical procedure. Selenium-iron and Cd-Fe crystallographic distances were determined with theoretical phase shift functions.

Results: Preliminary data analysis indicates that the sorption mechanism for Cd to both goethite and HFO is independent of selenite presence. Fitting of the EXAFS spectra give ~6 O at a distance of 2.3 Å from the Cd central atom, ~1 Fe at a distance of 3.2–3.3 Å and ~1 Fe at 3.5 Å, indicating edge sharing and corner sharing binding mechanisms, respectively, for Cd as for Cd sorption in the absence of Se [4,10]. These sites correlate with the so-called high-affinity sites (edge sharing; termination of chains) and low-affinity (corner sharing) sites [4,11]. No Se is observed in the coordination sphere of Cd.

For selenite, which has the coordination of a pyramid, sorbed onto goethite or HFO 3 O are found at 1.7 Å, ~0.5 Fe at ~2.9 Å and ~2.0 Fe at 3.3 Å corresponding to edge and double corner sharing respectively. Similar sorption mechanism is observed for selenate [7], arsenate [8,12], and chromate [12]. No Cd is observed in the coordination sphere of Se.

Discussion: The data presented here indicate that selenite and Cd have a similar binding mechanism for goethite and HFO surfaces. No ternary complexing is observed in any of the spectra, whether Cd is adsorbed first and then selenite, or vice versa. This is in agreement with results for co-adsorption of Cd with phosphate and sulfate on goethite [13]. The absence of ternary complexes on these mineral surfaces will simplify future thermodynamic modeling of cations to iron(oxyhydr)oxides.

References: [1] Davis J. A. and Kent D. B. (1990) in *Mineral-water Interface Geochemistry* (Hochella M. F. and White A. F., eds.), pp. 177–260, Rev. Mineral. 23, Min. Soc. Amer. [2] Stumm W. (1993) *Chemistry of the Solid-water Interface,* Wiley. [3] Hiemstra et al. (1989) *J. Colloid Interf. Sci., 133,* 91–99. [4] Spadini et al. (1994) *J. Colloid Interf. Sci., 168,* 83–86. [5] Brown G. E. Jr. (1990) in *Mineral-water Interface Geochemistry* (Hochella M. F. and White A. F., eds.), pp. 309–364, Rev. Mineral. 23, Min. Soc. Amer. [6] Hayes et al. (1987) *Science, 238,* 783–786. [7] Manceau A. and Charlet L. (1994) *J. Colloid Interf. Sci., 168,* 87–93. [8] Manceau A. (1995) *GCA, 59,* 3647–3653. [9] Schindler P. (1990) in *Mineral-water Interface Geochemistry* (Hochella M. F. and White A. F., eds.), pp. 281–308, Rev. Mineral. 23, Min. Soc. Amer. [10] Randall et al. (1999) *GCA,* in press. [11] Dzombak D. A. and Morel F. M. M. (1990) *Surface Complexation Modeling: Hydrous Ferric Oxide,* Wiley. [12] Fendorf et al. (1997) *Environ. Sci. Technol., 31,* 315–320. [13] Collins et al. (1999) *GCA,* in press.

CHARACTERIZATION AND ORIGIN OF AN ULTRAPOTASSIC ALUMINOUS A-TYPE GRANITOID FROM SOUTHWESTERN INDIA.

H. M. Rajesh, Department of Geosciences, Faculty of Science, Osaka City University, Sugimoto 3-3-138, Sumiyoshi-ku, Osaka 558-8585, Japan (rajesh@sci.osaka-cu.ac.jp).

Introduction: The Proterozoic granulite facies terrain of the southwestern part of the Indian Peninsula is intruded by a suite of alkali granite and syenite plutons preserving evidence for a prominent pan-African felsic magmatic event [1,2]. These intrusives are considered to represent anorogenic or postorogenic A-type magmas generated in rift-related environments of high heat flow and abundant volatile activity, correlative with an extensional tectonic regime and probably including melts generated from both upper mantle and lower crustal sources. The Pan-African (~550 Ma) Peralimala (PM) alkali granite pluton (within northern Kerala) forms the largest granitic pluton in this suite and forms the focus of this study.

Field Setting, Petrography, and Conditions of Crystallization: The PM pluton is spatially associated with the Bavali lineament. The pluton was aligned nearly parallel to the northwest-southeast to east-west fault in the basement, consistent with magma ascent along preexisting deep-fault lineament in an extensional tectonic regime. The PM pluton shows compositional variation from quartz syenite to leucogranite to less dominant marginal syenite, but it is difficult to delineate the different facies within the pluton. Granitic dikes, having similar mineralogy with the PM granite, occur within the pluton as well as in the surrounding gneissic rock, and are probably offshoots of the main plutonic body. The granitic body exhibit sharp contacts (wherever exposures are available) with surrounding gneissic rock (hornblende gneiss, hornblende-biotite gneiss, and biotite hornblende gneiss) and opx (cpx ± hbl ± bt)-bearing quartzo-feldspathic charnockite. The pluton is characterized by the presence of Fe-rich hydrous mafic minerals, Fe-rich clinopyroxene, primary magnetite, f_{O_2} above the Ni-NiO buffer and high initial emplacement temperatures near 950°C. Significantly magnetite coexists with titanite and shows very low mole fraction of the ulvöspinel component and Ti content.

Major-, Trace-, Rare-Earth-Element, and Strontium-Isotopic Chemistry: The PM granite is a high-K (K_2O ~12 wt%) granite, belonging to the transitional group IV ultrapotassic rock classification of [3]. The rock composition significantly varies from slightly peralkaline to mostly metaluminous to slightly peraluminous. Features like high total alkalis, high total Fe, low CaO, and MgO, low mg-number, medium to high TiO_2/MgO, high concentration of HFSE and REE are typical of A-type granitoids. Al_2O_3 content ranges from ~14 to 19 wt%, designating the PM granite as aluminous. The REE abundances generally increase with increasing SiO_2 from syenitic to quartz syenitic to granitic facies within the pluton. In the various tectonic discrimination diagrams, the PM granite samples straddle between volcanic-arc granite and within-plate granite fields, while they belong to the A_2 subtype of [4]. The low initial $^{87}Sr/^{86}Sr$ ratio (0.7032) is in the range expected for rocks derived from lower crustal or upper mantle protoliths.

A Plausible Petrogenetic Model: Many of the petrogenetic problems posed by ultrapotassic rocks, like explanation of extreme incompatible element enrichments, etc., are similar to those of other alkaline rock types. Hypotheses previously suggested for the petrogenesis of ultrapotassic rocks (see [5] and [3] for a detailed review of petrogenetic models) seem not to explain the trends of the PM granite samples. The major-, trace-, and REE patterns imply that the PM pluton is not related to fractional crystallization process. Major element models that use observed phases are consistent with an origin by partial melting from a charnockitic parent. The overall characteristics of the trace and REE patterns of PM granite are similar to those of igneous charnockites (C-type) from northern Kerala. Trace-element and REE modeling give reliable fits when the igneous charnockitic source is used, but fails for other source rocks from northern Kerala. A petrogenetic model involving partial melting of a charnockitic mafic-intermediate lower crust is proposed for the PM granite. Fluid inclusion studies in the PM granite-quartz samples prompt for the notion of infiltrating CO_2-rich fluids enhancing the melting. The late crystallization of hydrous mafic minerals together with the presence of granitic dikes in the granite suggests an increase in f_{H_2O} toward the final stages of crystallization.

References: [1] Santosh M. and Drury S. A. (1988) *J. Geol., 96,* 275–284. [2] Rajesh H. M. et al. (1996) *J. Southeast Asi. Earth. Sci., 14,* 275–291. [3] Foley S. F. et al. (1987) *Earth Sci. Rev., 24,* 81–134. [4] Eby G. N. (1992) *Geology, 20,* 641–644. [5] Gupta A. K. and Yagi K. (1980) Springer-Verlag.

FATTY ACIDS IN PARTICULATES FROM CONCEPTION BAY, NEWFOUNDLAND: MOLECULAR AND CARBON-ISOTOPIC VARIATIONS ACROSS THE 1996 SPRING BLOOM.

C. S. Ramos[1,2], C. Parrish[3], T. Quibuyen[1], and T. Abrajano[2], [1]Institute of Chemistry, University of the Philippines, Diliman, Quezon City, Philippines 3008 (ramosc@rpi.edu), [2]Department of Earth and Environmental Sciences, Rensselaer Polytechnic Institute, Troy NY 12180-3590, USA (abrajt@rpi.edu), [3]Ocean Science Centre, Memorial University of Newfoundland, St. John's, NF A1B 3X5, Canada.

Molecular variations in the types of fatty acids incorporated by algae into lipids across the spring bloom will have a direct impact on subsequent utilization of this C and energy source for the pelagic and benthic food webs. Previous work has also shown that $\delta^{13}C$ of primary photosynthates is sensitive to the timing of biogenic production because of isotope effects associated with changes in temperature, DIC concentration, $\delta^{13}C_{DIC}$ and algal growth rate. In this work, we examined the molecular (lipid classes and fatty acid molecular distribution) and compound-specific $\delta^{13}C$ (individual fatty acids) variations across the spring bloom (tow nets and sediment traps) in Conception Bay, Newfoundland, to elucidate the transfer of primary photosynthate to benthic and hyperbenthic environments in the Bay.

Fluxes for total lipids and selected lipid classes were recorded separately for poisoned and nonpoisoned sediment traps. The higher "flux" of material in the poisoned traps (total lipids: >100 mg/m^2/d at peak of the bloom) compared to the nonpoisoned traps (total lipids: < 80 mg/m^2/d at peak of the bloom) suggests a significant contribution of material by zooplankton (swimmers) in poisoned traps. There is likewise a discrepancy between the fluxes at the 80 m (total lipids: 60–80 mg/m^2/d at peak of the bloom) and 220 m (total lipids: <40 mg/m^2/d at peak of the bloom) sediment traps signifying loss of organic material with increasing depth.

Temporal changes in molecular composition of fatty acids in particulates provides useful information on the sources and fate of settling organic material [1]. For example, ω-3 PUFAs are believed to be synthesized de novo only in phytoplankton [2]. PUFAs are major components of neutral and phospholipid photosynthetic cells but occur in very low levels in phospholipids of animals compared to the neutral lipid fraction [3]. In Conception Bay, the variation in Σ16:0/Σ18:0 and 16:4ω1 mimicked the temporal variation of total lipids noted above, indicating that the C16 fatty acids are primarily diatom-sourced.

Compound specific $\delta^{13}C$ values measured on fatty acids revealed overall isotopic patterns consistent with expected variations across the phytoplankton bloom. Among the saturated fatty acids, for example, 14:0 is mostly present in neutral lipid as metabolic energy reserve but is absent in phospholipid and this makes 14:0 a useful marker in the food web. Measured $\delta^{13}C_{14:0}$ values during the bloom are consistently 5–6‰ enriched in ^{13}C when compared to $\delta^{13}C_{14:0}$ values measured after the bloom. This shift could indicate either growth rate effects or DIC substrate limitations at the peak of the bloom [4]. Intermolecular $\delta^{13}C$ variation observed in phytoplankton tow nets range from 1–3‰, but larger variations were observed in sediment traps. Intermolecular $\delta^{13}C$ fatty acid variation of up to 8‰ was apparent in sediment traps, which approximates intermolecular variations also observed for benthic organisms [5]. In contrast to observations made on bulk organic $\delta^{13}C$, compound-specific $\delta^{13}C$ variations cannot be explained by changing "terrestrial input," although very depleted values for terrestrially-derived fatty acids were noted in the present work. Given the limited intermolecular $\delta^{13}C$ variations already noted for primary production, we suggest that the larger variations observed for sinking particulates may be related to heterotrophic utilization, a suggestion consistent with lipid loss recorded in our molecular data.

References: [1] Parrish C. C. (1998) *Organic Geochem., 29,* 1531–1545. [2] Fraser A. J. and Sargent J. R. (1989) *Marine Chem., 27,* 1–18. [3] Sargent J. R. and Whittle K. J. (1981) in *Analysis of Marine Ecosystems* (Longhurst, ed.), pp. 491–533, A. R. Academic Press, London. [4] Bieger T. et al. (1997) *Organic Geochem., 26,* 207–218. [5] Abrajano et al. (1994) *Organic Geochem., 21,* 611–617.

THE FATE OF SORBED ARSENIC AND CHROMIUM DURING EARLY DIAGENETIC TRANFORMATIONS OF IRON OXIDES: INSIGHTS FROM EXTENDED X-RAY ABSORPTION FINE STRUCTURE SPECTROSCOPY.

S. R. Randall, D. M. Sherman, and K. V. Ragnarsdottir, Department of Earth Sciences, University of Bristol, Bristol BS8 1RJ, UK (dave.sherman@bris.ac.uk).

Arsenic and Cr are significant contaminants in many soil and sediment systems around the world, largely as a consequence of anthropogenic activities. Fortunately, natural attenuation by sorption on sediment and soil components currently limits mobility and bioavailability of As and Cr. However, early diagenetic processes have the potential to liberate sorbed metals and turn many contaminated areas into persistent sources of pollution. This problem can only be mitigated by an understanding of the processes that will control the long-term mobility of As and Cr.

Chromium and Arsenic During Transformation of Ferrihydrite: Naturally occurring, poorly crystalline iron oxyhydroxides such as ferrihydrite are known to be very effective sorbents of As(V) [1–3] and Cr(III) [4]. Ferrihydrite is metastable and over time it ages into more crystalline phases such as goethite (α-FeOOH) and/or hematite (α-Fe_2O_3) [5]. We observe that neither As nor Fe are released to solution during the aging of As(V)-contaminated ferrihydrite. Increasing levels of As(V) favoured the formation of hematite over goethite and slowed the reaction to a point where it was arrested completely at As/(As + Fe) = 0.032. Extended X-ray absorption fine-structure spectroscopy (EXAFS) analysis showed that while As(V) remained as surface complexes throughout the aging process (i.e., it did not coprecipitate with and/or form a solid solution with Fe), the local coordination environment was different to that of As(V) adsorbed on pure goethite or hematite. Introducing As to the system prior to ferrihydrite nucleation did not alter the ultimate As coordination environment.

In contrast to the As(V)-ferrihydrite aging experiments, aging of Cr(III)-contaminated ferrihydrite resulted in a persistent release to solution of Cr(III), although there was no release of Fe. Increasing levels of Cr(III) did slow the aging process, but goethite was always the sole aging product. EXAFS analysis showed that Cr(III) persisted in a γ-MeOOH-type environment throughout. There was only limited evidence for Cr(III) in an α-MeOOH environment that would have indicated substitution for Fe(III) in α-FeOOH.

Oxidation of Green Rust. Green rust ($Fe_4(II)Fe_2(III)(OH)_{12}SO_4\ 3H_2O$) is a likely intermediate phase in the formation of iron (oxyhydr)oxides such as goethite, lepidocrocite, and magnetite, and current thinking is that it occurs in many soil and sediment systems. Green rust is of potentially great importance to trace-metal mobility because of its mixed valence. However, our EXAFS analysis has shown that As(V) is not reduced to the more mobile and toxic As(III) form following equilibrium with green rust for 24 h. It remains adsorbed in surface complexes throughout, even during the oxidation of green rust to lepidocrocite. The same result is obtained whether As(V) is added prior to or after green rust nucleation. In contrast, Cr(VI) undergoes instantaneous reduction to Cr(III) following interaction with green rust.

Sulfidization of Iron Oxides: Whereas iron oxyhydroxides generally limit the mobility of As(V) under oxic conditions, As mobility is limited by equilibrium with authigenic Fe and/or As sulfides under reducing, S-rich environments [8]. We observe that sulfidization of As(V)-contaminated goethite results in the formation of poorly crystalline mackinawite (FeS_{1-x}), and that As(V) is rapidly reduced to As(III). In association with mackinawite, dissolved As concentrations remain low, and EXAFS analysis shows that the first coordination shell around As(III) is identical to that in poorly crystalline orpiment (As_2S_3(am)) [9]. We find no evidence of arsenopyrite formation over the time scale of our experiments.

References: [1] Fuller C. C. and J. A. Davis (1989) *Nature, 340,* 52–54. [2] Waychunas G. A. et al. (1993) *GCA, 57,* 2251–2269. [3] Manceau A. (1995) *GCA, 59,* 3647–3653. [4] Charlet L. and Manceau A. A. (1992) *J. Coll. Int. Sci., 148,* 443–458. [5] Schwertmann U. and E. Murad (1983) *Clays Clay Mineral., 31,* 277–284. [6] Hansen et al. (1994) *GCA, 58,* 2599–2608. [7] Myneni S. C. B. et al. (1997) *Science, 278,* 1106–1109. [8] Moore et al. (1988) *Environ. Sci. Technol., 22,* 432–437. [9] Helz G. R. et al. (1995) *GCA, 59,* 4591–4604.

CHARACTERIZATION OF COLLOIDS OF ENVIRONMENTAL AND GEOCHEMICAL INTEREST USING FIELD-FLOW FRACTIONATION INDUCTIVELY COUPLED PLASMA MASS SPECTROMETRY.

J. F. Ranville[1], R. Beckett[2], and D. J. Chittleborough[3], [1]Department of Chemistry and Geochemistry, Colorado School of Mines, Golden CO 80401, USA (jranvill@mines.edu), [2]Water Studies Centre, Monash University, Clayton, VIC, Australia 3168, and [3]Department of Soil Science, Waite Agricultural Research Institute, University of Adelaide, Glen Osmond, SA, Australia 5064.

Introduction: Colloidal particles, which are generally described as being from 0.001–1.0 µm in size, are important components of aquatic, soil, and groundwater systems [1]. The importance of colloids arises from both their high specific surface areas, which facilitates reactions at the water-solid interface, and from their mobility in surface and ground waters [2,3]. Our current understanding of the role of natural colloids is somewhat limited by the lack of methods capable of unambiguously determining their physical and chemical characteristics. Colloid size is one important physical characteristic. Size in-part establishes specific surface area, influences mineralogy and

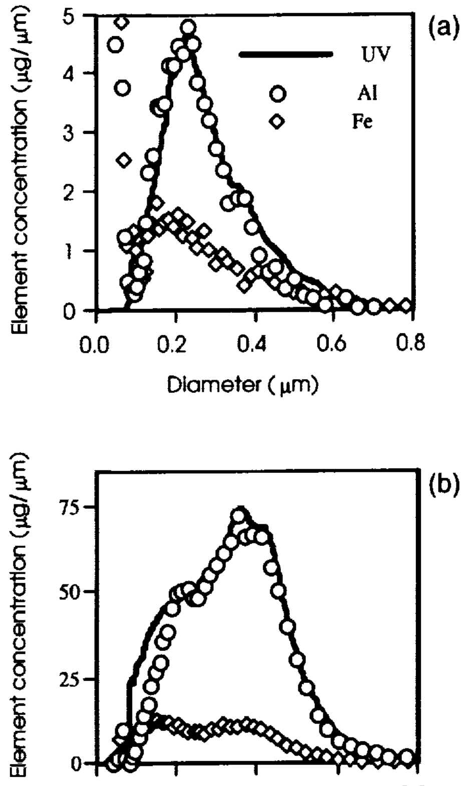

Fig. 1. (a) A2/B1 mobile colloids; (b) A2 soil matrix colloids.

chemical composition, and affects the transport of colloids [4]. Field-flow fractionation (FFF) is a relatively new, chromatography-like method that can be used to obtain high-resolution size distributions, and also to provide size-based separations of natural colloids, [5]. The separating ability of FFF allows collection of fractions, of narrow size range, which can then be further characterized. Coupling of FFF to inductively coupled plasma-mass spectrometry (ICP-MS), or to another atomic spectroscopic method [i.e., inductively coupled plasma atomic emission spectrometry (ICP-AES), and atomic absorption spectrometry (AAS)], provides a particularly powerful means of investigating the influence of colloid size on elemental composition [6]. Field-flow fractionation fractions are also commonly characterized by electron microscopy and X-ray diffraction (XRD).

Field-Flow Fractionation Methods: An FFF analysis is performed by injecting a small volume of particle suspension into the FFF channel. Particles are transported down the channel by a carrier liquid. Laminar flow establishes a parabolic distribution of flow velocities within the channel. The application of a force perpendicular to the flow direction causes the particles to migrate to one wall of the channel. In the case of submicron particles, the applied force is opposed by diffusion of the particles, which increases with decreasing particle size. As a result, smaller particles are able to interact with higher velocity flow lines, resulting in an earlier elution time than that for larger particles. Colloids are detected as the elute from the FFF channel by a UV detector. The resulting plot of detector response vs. time is termed a fractogram. Fractograms can be readily converted to particle size distributions using fundamental equations [5].

Field-Flow Fractionation Applications: Field-flow fractionation-inductively coupled plasma has been applied to a number of geochemical studies. One specific example, to be presented in the talk, includes the investigation of transport of mobile soil colloids through soil macropores. Comparison of the particle size distributions of mass (UV response), Al, and Fe for a mobile soil colloids vs. the soil matrix colloids in the A2 horizon of a soil are shown below. Through use of element ratio distributions, the role of soil mineralogy on colloid transport was investigated.

References: [1] Ranville J. F. and Schmiermund R. L. (1999) in *Reviews in Economic Geology, Vol. 6* (G. Plumblee, ed.), in press. [2] Ryan J. N. and Elimelech M. (1996) *Colloids and Surf. A, 107,* 1–56. [3] Buffle J. and Leppard G. G. (1995) *Environ. Sci Technol., 29,* 2169–2184. [4] Harvey R. W. et. al. (1989) *Environ. Sci. Technol., 23,* 51–56. [5] Beckett R. and Hart B. T., in *Environmental Particles* (J. Buffle and H. P. V. Leeuwen, eds.), pp. 165–205. [6] Ranville J. F. et. al. (1999) *Anal. Chim. Acta, 381,* 315–329.

NEW INSIGHTS INTO THE SEISMOTECTONICS OF DEEP-SEATED INTRUSIONS.

A. S. P. Rao, 12-13-483/10, Nagarjunanagar, Tarnaka, Hyderabad-5000 17, India (idcoucea@hdl.vsnl.net.in)

The author presents a new model for the origin of tectonic earthquakes that occur by the reactivation of variety of preexisting zones of weakness in response to the new stress field generated by the upward movement of the deep-seated plutons into the overlying lithospheric crust. According to this model, deep-seated (a few tens of kilometers) intrusions emplaced into the orogenic or nonorogenic regions are confined to enormous lithostatic pressures (~20–10 kbar) and are in a state of dynamic equilibrium with the thick crust overlying them. The author [1] presented evidences for the forceful and upward movement of deep-seated anorthositic plutons in solid state, subsequent to magmatic emplacement into the overlying crust. Spatial association between mafic (and ultramafic) plutons (hidden plutons inferred from local gravity highs) and local seismicity has been suggested [5]. Therefore it is reasonable to believe that tectonic earthquakes are caused by the upward movement of plutons into the lithospheric crust overlying them. Data from detailed observations of earthquakes suggest that direction of transmission of stress is from hypocenter locations to epicentral areas. The periodic (responsible for return period of earthquake) upward movement of an intrusion (depending on its size, shape, and depth) subjects the overlying lithospheric crust to enormous stresses and strains, produces foreshocks, changes in electrical resistivity, gravity anomalies, Earth's magnetic field, Vp/Vs ratios, water table level and sand boils, reduction of strength of rocks and friction between moving parts of rocks, tilt, subtle uplift of ground and creep besides geochemical and geothermal changes in soils and water and unusual behavior of animals, and ultimately leading to bending, breaking (when stresses exceed the strength of the rock) and causing displacement and/or extension of preexisting fault (reactivation of old faults on the surface) or generating faults at depth (blind faults) leading to stress relief. There is evidence that seismicity is relatively high along belts where alkaline igneous rocks were emplaced, although these are not always clearly related to the distribution of earthquakes [2]. For different types of earthquakes the precursory phenomena are different and are controlled by local geology, structural discontinuities, water table conditions, and their effect on the mechanical properties of crust and soils [3] above the pluton besides the size shape, depth, and composition of the pluton. Upward movements of deep-seated plutons in ductile (few hundred kilometers deep in the Circum Pacific belt, i.e., plutons in very deep subduction zones and in orogenic Mediterranean belts) cause earthquakes and are usually weakly felt while shallow plutons in brittle zones (few tens of kilometers, i.e, plutons in highly eroded Alpine-Himalayan belt and Andes young fold belts and plutons underlying thin continental crust riddled with faults, as in the state of California) can cause damaging earthquakes. The ancient shield areas (Peninsular India, etc.) are zones of mild seismic activity because plutons intruded into them had since already reached static equilibrium. However, ancient shield areas that had experienced locally, geologically young extrusive and intrusive activity (60-Ma Deccan Traps volcanic activity in Peninsular India) are zones of potential earthquakes (e.g., Lathur 1993 and Jabalpur 1997 earthquakes) and the New Madrid earthquake in USA was due to reactivation by alkali pluton of the rift A rising pluton will activate another pluton to cause earthquake. (The Kobe 1995 earthquake Japan was activated by two earthquakes that occurred in 1944 and 1946.) The Chamoli 1999 earthquake (India) activated another pluton (50 km away) that caused the earthquake between Rudranath and Gopeshwar. Seismic gaps represent potential zones underlain by plutons for future earthquakes while asperites represent areas where destressing has commenced on the hidden plutons. Plutonic complexes are the sites of frequent earthquakes.

Prediction of earthquake involves exact location by a suitable geological and geophysical technique (seismic tomography [4]) of an active pluton hidden beneath continental crust, or in deeply eroded young fold belt or in (rift its size, shape, and depth) and also from the precursory phenomena (microseismic activity). Foreshocks can be used in tracking its upward movement and assessing the resulting impact on the crust and soil above the pluton. Plutons intruded into crust at shallow depth (~10 km) are not very dangerous. But beware of plutons beneath thin continental crustal plates (wet) riddled with structural discontinuities (state of California), continental rifts filled with sediments (New Madrid area), and plutons in young orogenic belts experiencing rapid erosion (Himalayas, Andes, etc.) and failed rifts hosting plutons and also reservoirs built on areas underlain by dormant plutons.

References: [1] Rao A. S. P., this volume. [2] Sykes L. R. (1978) *Rev. Geophys. and Space Phys., 16,* 621–688. [3] Rao A. S. P. (1989) *28th I.G.C.* [4] Director's essay (1996) *CIW Yearbook,* 55–61. [5] McKeown F. A. (1978) *J. Res. USGS, 6,* 41–50.

NEW INSIGHTS INTO THE TECTONICS OF PROTEROZOIC ANORTHOSITES.

A. S. P. Rao, 12-13-483/10, Nagarjunanagar, Tarnaka, Hyderabad-5000 17, India (idcoucea@hd1.vsnl.net.in).

The authors presented a new tectonic and petrologic model for the origin of the Proterozoic anorthosites [1]. The author now presents field, tectonic geochemical, experimental and geochronological evidences that show that deep-seated anorthositic plutons, subsequent to magmatic intrusion into the crust in the Grenville Province and in the Rogaland complex, had dynamically forced their way upward, lubricated by noritic liquids (can't be residual liquids expelled from the diapir due to filter pressing) generated by frictional heat in P-T gradient as tectonic intrusions into the overlying crust and show signs of deformation at the margins while the anorthositic plutons emplaced at shallow depths of ~10 km (leuconorites and leucotroctolites) in the Labrador remained more or less static with signs of little or no deformation at their margins. The plutons in the Labrador could not rise upward tectonically into the overlying crust due to insufficient stress relief produced by the erosion of the thin crust (~10 km) overlying them. Therefore, the pristine, underformed and layered *in situ* plutons in the Labrador have anorthositic dikes in the surrounding country rocks, show chilled margins, high-temperature contact metamorphic effects and remobilized gneiss [2], and according to expectation they show (e.g., Kiglapait intrusion) concordant Sm-Nd (1416 ± 50 Ma) and Rb-Sr (1413 ± 54 Ma) internal ages [3]. In contrast, the deep-seated anorthosite plutons that were under enormous confining lithostatic pressure and were under dynamic equilibrium with the thick crust overlying them, now found in deeply eroded mid-to-late Proterozoic Grenville orogenic belt and in Sveconorwegian orogenic province, dynamically responded to destressing conditions (caused by easy erosion of deformed rocks of few tens of kilometers thick over a period of 200–500 m.y.) and moved upward. These plutons show variable degrees of deformation (severe protocalstic structure shown by Egersund-Ogna massif in Rogaland, Norway) at their margins due to variable upward movement, contamination effects at the margins of Marcy massif (Adirondacks) where, the marginal sample have high Rb content (up to 38 ppm) and I_{sr} (up to 0.705) compared to interior samples that typically have 5 ppm Rb and I_{sr} = 0.704 [4], and show osumilite at short distances from the contacts, but do not show high-temperature contact metamorphic effects, chilled margins and anorthostic dikes in the country rock as these feature were left behind at depth due to upliftment of the plutons. These evidences are consistent with the view that the massif anorthosites found in the Grenville Province and in the Sveconorwegian Province are not *in situ* massifs and indeed had moved upward into the overlying crust subsequent to their magmatic emplacement from very deep level. This view is further supported by the presence of anorthositic dikes within the diapiric pluton type 1 [5]. It is evident from the presence of anorthositic dike within the diapiric massif that during the uplift of the massif effective detachment and separation of the dike from the massif had taken place. Giant pyroxene megacrysts (highly aluminous) with exsolved plagioclase lamellae from the Marcy massif, Adirondacks and relatively primitive Mg/Mg + Fe up to 0.8 that are thought to have been products of crystallization at high pressures [6,7] show the highest Nd initial ratio (ε_{Nd} = 5) were not affected by crustal contamination [4], implying that the pluton moved upward to a higher level into the crust as a solid surrounded by thin layer of silicate liquid at the margin. The megacrysts of plagioclase and orthopyroxene from the center part of the Egersund-Ogna body and also rocks that retained their primary texture as well as mineralogy from the Marcy massif [4] plot along an "oder" isochrons (1500 ± 300 Ma) and (1288 ± 36 Ma) respectively while the recrystallized rocks formed from the remelting of marginal rocks of the massif show lower "ages" (i.e., 919 ± 12 Ma for the Marcy sample and 1200–1000 Ma for the leuconorite from the Egersund-Ogna body). Therefore geochronological evidence supports the view that massifs moved upward as solids without perterbing isotopic ratios. Some anorthosites and related Elsonian plutons were uplifted and eroded in a relatively short time following their emplacement [8]. Tectonic emplacement mechanism for the massif-type anorthosite, consistent with abundant mylonite at and near the anorthosite country rocks contact, was proposed [9]. There is evidence for isotopic exchange between anorthosites and circulating, hot meteoric waters [10], implying that isotopic exchange took place between anorthosite and circulating, hot meteoric water after the massif was tectonically transported to shallow depth (~10 km).

References: [1] Rao A. S. P. and Srinivas K. (1997) *LPI Contrib., 921,* 169–170. [2] Wiebe R. A. (1980) *Nature, 286,* 564–567. [3] Depaolo D. J. (1981) *GSA, 13,* 437. [4] Ashwal L. D. and Wooden J. L. (1983) *Nature, 306,* 679–680. [5] Wiebe R. A. (1992) in *Proterozoic Crustal Evolution* (K. C. Condie, ed.), pp. 215–261, Elsevier, Amsterdam. [6] Emslie R. F. (1975) *Candian Mineral., 13,* 138–145. [7] Longhi J. et al. (1993) *Am. Mineral., 78,* 1016–1030. [8] Emslie R. F. (1978) *Can. J. E. Sci., 15,* 431–453. [9] Ashwal L. D. et al. (1998) *C. M. P., 133,* 389–401. [10] Valley J. W. and O'Neil J. R. (1982) *Nature, 300,* 497–500.

MICROBIAL AND CHEMICAL REDOX REACTIONS OF IRON IN DEPTH PROFILES OF PADDY SOIL.

S. Ratering and S. Schnell, Max-Planck-Institute for Terrestrial Microbiology, Karl-von-Frisch-Strasse, D-35043 Marburg, Germany (ratering@mailer.uni-marburg.de; schnell@mailer.uni-marburg.de).

Rice soil is subjected to periodic changes of oxic and anoxic conditions. After flooding of the fields a major part of the soil becomes anoxic. Before the rice is harvested the fields are drained, and O is available for oxidation of reduced compounds like ammonium, Fe(II), and sulfide. Beside the seasonal reoxidation event a steady reoxidation of reduced copounds occurs during flooding. On the soil surface, dissolved O from the flooding water is consumed by chemical and microbial oxidation of reduced inganic compounds and aerobic degradation of organic matter. Oxygen is also available for oxidation processes in the close proximity of rice roots due to the diffusive transport via the aerenchym. In the present study, Fe-reducing and Fe-oxidizing activities were localized in rice soil by profile measurements of solid phase Fe(II) and Fe(III) determined after extraction with 0.5 M hydrochloric acid [1]. Dissolved Fe(II) was measured directly in the pore water.

The development of the Fe(II) and Fe(III) profiles at the surface of flooded rice soil was observed in microscale over a time period of 11 weeks (Fig. 1). After that time the profiles were stable and showed lowest concentrations of solid phase Fe(II) on the soil surface with increasing concentrations to a soil depth of 10 mm (100 μmol/cm^3). Porewater Fe(II) concentrations were 3 orders of magnitude lower than extracted Fe(II) that indicated that most of the Fe(II) was precipitated as siderite or vivianite or immobilized by adsorption to solid phases. Profiles of Fe(III) showed maximum concentrations at a depth of 2–4 mm (100–200 μmol/cm^3). In contrast to the Fe(III) profiles highest concentrations of the electron acceptors O, nitrate, and sulfate were determined at the soil surface. Dissolved O showed supersaturation at the soil surface due to phototrophic production and a depletion of O below 3 mm depth. Sulfate and nitrate concentrations in the porewater were highest directly in the upper 100 μm soil layer (40 μM sulfate and 10 μM nitrate) and decreased with soil depths. Methane production rates measured from soil layers incubated separately in closed vessels were zero at the soil surface and increased with soil depth.

Iron profiles of paddy soil planted with rice were determined from soil cores that were cut out between the rice plants growing in a distance of 60 mm to each other. The Fe(III) profile showed a narrow peak beneath the soil surface in a depth of 0.5 mm to 2.5 mm with Fe concentrations up to

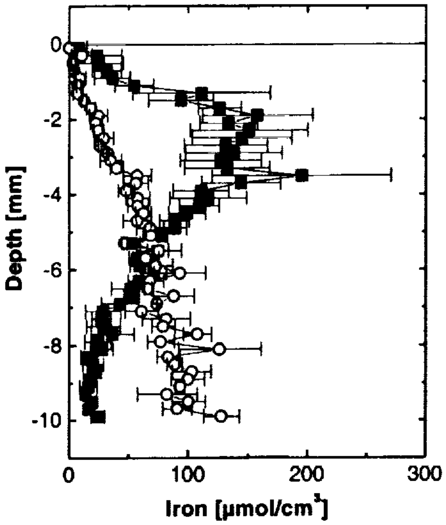

Fig. 1. Depth profile of solid phase Fe(II) (○) and Fe(III) (■) concentrations of unplanted rice soil cores incubated under flooding conditions for 11 weeks in the greenhouse.

390 µmol/cm³. Below 2.5 mm soil depth, the Fe(III) concentrations decreased to values of 15 µmol/cm³. The Fe(II) profile was similar to profiles of unplanted soil.

From all the profiles, various zones of different reactions of Fe were identified in flooded rice paddies. Directly at the soil surface solid-phase Fe(II) concentrations were low due to diffusive loss of porewater Fe(II) into the flooding water. High concentrations of organic acids in this soil layer complexed Fe(III) and enhanced diffusion thus preventing accumulation. The soil layer between 2 and 4 mm is characterized by Fe(III) accumulation resulting from diffusive transport of porewater Fe(II) from deeper soil layers and Fe(II) oxidation by O and nitrate. Iron-reducing activity was localized in a depth of 3–8 mm. Below this depth methanogenesis was the predominant process due to the lack of alternative electron acceptors. In planted rice paddies the O release of roots stimulated both Fe(II) oxidation and Fe(III) reduction.

References: [1] Schnell S. et al. (1998) *Environ. Sci. Technol., 32,* 1530–1537.

OSMIUM ISOTOPES AS TRACERS OF SEWAGE DISPERSAL IN THE MARINE ENVIRONMENT.

G. Ravizza[1], C. B. Tuit[1], and M. H. Bothner[2], [1]Woods Hole Oceanographic Institution, Woods Hole MA 02543, USA (gravizza@whoi.edu), [2]U.S. Geological Survey, Woods Hole MA 02543, USA.

Introduction: The Os concentration of sewage is enriched 10- to 100-fold relative to average crustal material, and the $^{187}Os/^{188}Os$ of sewage is distinctly lower than the $^{187}Os/^{188}Os$ in typical marine sediments. This elemental enrichment and isotopic contrast allows Os-isotopic variations in marine sediments to be used as a tracer of anthropogenic metals in the marine environment [1–3]. Low $^{187}Os/^{188}Os$ (0.15–0.33) in municipal sewage reflects the ultramafic affinities of the Pt group metal deposits from which Os is mined for industrial and medical uses. High $^{187}Os/^{188}Os$ in typical marine sediments (1.0–1.3) reflects the isotopic composition of Os in common continental rocks and seawater. The pathways by which anthropogenic Os is released to the marine environment are not fully understood; however, it is believed that disposal of Os-bearing solutions that are used as stains in medical electron microscopy laboratories is the primary reason municipal sewage is enriched in Os.

Here we report the results of two complementary studies designed to further assess the utility of Os isotopes as tracers of the dispersal sewage particles in the marine environment. In the first study we examine the influence of the cessation of sludge release on sediments from Boston Harbor. In the second study we examine the influence of sludge release on the Os-isotopic composition of sediments from a deep water dump site located off the coast of the eastern United States, far removed from other sources of contaminant input.

Boston Harbor Sediments: For several decades, the primary source of both suspended solids and metals to Boston Harbor was the discharge of sewage sludge and waste waters from municipal treatment facilities. All sludge release to the harbor stopped in December 1991. Surface sediments recovered from Boston Harbor in 1978, 1993, and 1996 show a clear trend toward lower Os concentration and higher $^{187}Os/^{188}Os$ in more recent samples. A surface sediment sample from 1978 is highly enriched in Os (852 ppt) relative to average crustal material (~50 ppt), and has a $^{187}Os/^{188}Os = 0.279$, slightly higher than measured in Boston sewage sludge (0.15–0.171 [2]). The very unradiogenic character of 1978 surface sediment indicates that in excess of 80% of the Os in this sample is derived from anthropogenic sources. By 1996, the Os concentration of Boston Harbor surface sediment decreased more than six-fold relative to the 1978 surface sample. Osmium-187/osmium-188 of 1996 surface sediment increased to 0.842, indicating ~25% of the Os in this sample is derived from anthropogenic sources. 1993 surface sediment is intermediate between the 1978 and 1996 samples in both $^{187}Os/^{188}Os$ and Os concentration. A down-core profile from a 1993 core records a similar shift toward greater anthropogenic influence with depth in the core, suggesting that down-core records of Os-isotopic variations may reflect the history of sludge release. The concentrations of Pb and Ag have decreased in Boston Harbor sediments over the same time interval [4]; however, the magnitude of the concentration decreases (<50%) is not as large as the shift in Os-isotopic composition.

Deep Ocean Dump Site 106: Between 1986 and 1992, ~36 million metric tons of wet sewage was dumped at a 270 km² site 196 km southeast of New York City in a water depth of roughly 2500 m. We have investigated the Os concentration and Os-isotopic composition of a 30 cm sediment core recovered using DSRV Alvin. The concentrations of Ag, Linear alkylbenzenes (LABs), and coprostanol in this core have already been reported [5], and allow a comparison of Os isotopes to other tracers of sewage in the marine environment. In general, down-core Os-isotopic variations mimic the other tracers of sewage input, with the strongest anthropogenic signature at the core top ($^{187}Os/^{188}Os = 0.605$), and decreasing to background values at depth. Os concentration enrichments in the 0–1-cm sample are 2–3× above background values, similar to Ag enrichments. In detail the distribution of the different contaminant tracers differs, with the Os-isotopic data suggesting the influence of sewage penetrates to 10 cm below the sediment-water interface. In contrast discernible Ag enrichments are confined to the upper 6 cm of the core. LABs and coprostanol persist to depth greater than 6 cm but only in trace amounts. The differing distribution of these sewage tracers in this core requires either differing source terms for the different tracers over the dumping period, or differential transport during sedimentation and diagenesis, or both. Thus while all tracers yield similar qualitative results, quantitative estimates of the magnitude of sewage influence differs among the different tracers. In the least impacted samples, these differences are most pronounced.

Summary: In both the Boston Harbor and Deep Water Dump Site studies Os isotopes were shown to be sensitive tracers of sewage impact on marine sediments. The Boston Harbor study indicates that Os isotopes have responded rapidly to the changes in sewage discharge patterns, reflecting diminished input of anthropogenic Os. The Deep Water Dump Site study demonstrates that the sensitivity of Os isotopes is similar to that of other sewage tracers.

References: [1] Esser and Turekian (1993) *ES&T, 27,* 2719–2724. [2] Ravizza and Bothner (1996) *GCA, 60,* 2753–2763. [3] Williams et al. (1997) *EPSL, 148,* 341–347. [4] Bothner et al. (1998) *M. Environ. Res., 45,* 127–155. [5] Bothner et al. (1994) *M. Environ. Res., 38,* 43–59.

CARBON-ISOTOPIC CHARACTERISTICS OF PYROGENIC POLYCYCLIC AROMATIC HYDROCARBONS AND BLACK CARBON IN AQUATIC SEDIMENTS: DEVELOPMENT OF METHODS.

C. M. Reddy and T. I. Eglinton, Woods Hole Oceanographic Institution, Woods Hole MA 02543, USA.

Introduction: Some sedimentary records of polycyclic aromatic hydrocarbons (PAHs) and black carbon (BC) show that these chemicals are well-

TABLE 1. Concentration and δ^{13}C of BC in sediments.

Sample ID	SC (mg g^{-1})	δ^{13}C (‰)
SL 0–2 cm (n = 2)	1.90 ± 0.12	–23.35 ± 0.04
SL 6–8 cm (n = 2)	**2.50 ± 0.03**	**–23.44 ± 0.10**
SL 10–12 cm (n = 2)	**2.79 ± 0.28**	**–23.62 ± 0.01**
SL 28–30 cm (n = 1)	2.13	–24.11

correlated and suggest similar sources [1,2]. As part of a project utilizing C isotopic compositions of PAHs to determine historical variations in the deposition of combustion-derived contaminants, we are developing a parallel method to measure the ^{13}C and ^{14}C content of BC. These results will aid in examining the extent to which these combustion products are coupled.

Sample Location: Sediment cores from Siskiwit Lake, Isle Royale, MI were collected. This site was chosen because the input of PAHs is mostly via atmospherically-transported particles and the fluxes and chronologies of PAHs inputs have been previously determined [3]. Four sediment horizons (0–2, 6–8, 10–12, and 28–30 cm) were initially analyzed that should represent contemporary inputs, post-bomb testing and high concentrations of PAHs (~1965), pre-bomb testing (~1945) and moderate concentrations of PAHs, and pre-industrial activity (~1800) and trace levels of PAHs respectively.

Method: We used a modified version of the Gustafsson et al. [1] method for measuring BC. This thermal method operationally defines BC in sediments as the fraction of C remaining after thermal oxidation at 375°C for 24 h (to remove labile organic C) and acidification (to remove inorganic carbonates).

Briefly, ~200 mg of sediment was placed into a precombusted 12-mm (I.D.) × 20-cm (length) quartz tube. The sediment was placed horizontally in a muffle oven and heated at 375°C for 24 h. The tubes were then removed, allowed to cool, and treated with HCl to remove carbonates. The aqueous phase was removed, and the tubes were then dried overnight at 70°C. Copper oxide and elemental Ag were added to each tube containing the treated sediment. Each tube was attached to a vacuum line, evacuated, flame sealed, and combusted at 850°C. After cooling, each tube was attached onto a vacuum line, and the CO_2 was purified and measured manometrically. The δ^{13}C of the CO_2 was measured by isotope ratio mass spectrometry. Splits of the CO_2 were reserved for ^{14}C analysis by accelerator mass spectrometry.

To compare the SC results, we will compare them to the ^{14}C and δ^{13}C of individual PAHs in similar sediments. Briefly, sediments are extracted with organic solvents, and the extracts are fractionated with silica-gel and high-pressure liquid chromatography. Individual PAH are then separated and collected by repeated injections on a preparative capillary gas chromatograph until 25–250 mg of each individual PAH are obtained [4]. Each PAH is then converted to graphite for ^{14}C analysis. The δ^{13}C of each PAH is measured on an isotope-ratio-monitoring gas chromatograph mass spectrometer (irmGC/MS).

Results: The initial results of the BC method are shown below in Table 1. The precision on duplicate analysis was good for both the concentration and the δ^{13}C of SC. The concentrations of SC are similar to values measured by Gustafsson et al. [1,5] for lacustrine, estuarine, and coastal sediments. The largest concentration of SC was in the 10–12 cm and may be due to a local forest fire in 1936. There was a clear trend in the δ^{13}C values from –24.11‰ at 28–30 cm and increased to –23.35 cm at 0–2 cm, which may be due to a slight but consistent change in the source of BC. Other published values for the δ^{13}C of sedimentary BC or elemental C range from –25‰ to –15.8‰ [6,7].

Summary: These initial results from this method are promising. Refinements are presently underway and are targeted at streamlining the procedure. We believe that the ^{14}C of the BC and the co-eval PAHs will prove particularly useful in distinguishing sources and processes. We also intend to compare this SC method to other methods, especially chemical [6,7].

References: [1] Gustafsson Ö. et al. (1997) *ES&T, 31,* 203–209. [2] Broman D. et al. (1990) *Chemosphere, 21,* 69–77. [3] McVeety B. and Hites R. (1988) *Atmos. Environ., 22,* 511–536. [4] Currie L. A. et al. (1997) *Nucl. Instr. and Meth., 123,* 475–486. [5] Gustafsson Ö. and Gschwend P. (1998) *GCA, 62,* 465–472. [6] Masiello C. A. and Druffel E. (1998) *Science, 280,* 1911–1913. [7] Bird M. I. and Cali J. A. (1998) *Nature, 394,* 767–769.

CHLORINE-ISOTOPIC RATIOS OF SEMIVOLATILE CHLORINATED ORGANIC COMPOUNDS.

C. M. Reddy[1], L. J. Heraty[2], B. D. Holt[2], N. C. Sturchio[2], T. I. Eglinton[1], K. A. Maruya[3], and J. L. Lake[4], [1]Woods Hole Oceanographic Institution, Falmouth MA 02543, USA, [2]Argonne National Laboratory, Argonne IL 60439, USA, [3]Skidaway Institute of Oceanography, Savannah GA 31411, USA, and [4]U.S. Environmental Protection Agency, Narragansett RI 02882, USA.

Introduction: To investigate the biogeochemistry of semi-volatile organic compounds in the environment, we have begun to investigate their stable Cl-isotopic ratios. There are two naturally occurring stable isotopes of Cl, ^{35}Cl, and ^{37}Cl. The relative abundance of each isotope is 76% and 24% respectively. This ratio of Cl is typically expressed as δ^{37}Cl (‰) = [($R_{sample}/R_{standard}$) – 1] × 1000, where R_{sample} is the ^{37}Cl/^{35}Cl of the sample and $R_{standard}$ is the ^{37}Cl/^{35}Cl of standard mean ocean chloride (SMOC). Due to kinetic and thermodynamic effects, there can be small, but measurable, differences in the ratio of these isotopes, which may be useful in apportioning sources and identifying and understanding processes that influence their fate. Here, we have measured the δ^{37}Cl in several mixtures of polychlorinated biphenyls (PCBs), chlordane, ppDDT, toxaphene, and PCBs that have been isolated from contaminated sediments.

Methods: Technical mixtures of chlorinated semivolatile organic compounds were purchased from several different suppliers and analyzed. They included Aroclors 1016, 1242, 1254, 1260, and 1268. (Aroclors are mixtures of PCBs. The last two digits are the mass percentage of Cl in these mixtures, except for 1016, which is 41% Cl.) Technical mixtures of chlordane, ppDDT, and toxaphene were also analyzed. Sediment samples were collected from the Turtle River estuary (GA) and New Bedford Harbor (MA). The Turtle River estuary is contaminated primarily with Aroclor 1268 and there is little evidence of any environmental weathering of these PCBs [1]. New Bedford Harbor is contaminated with mostly Aroclors 1242 and 1254 and perhaps some Aroclor 1016 from two nearby electrical capacitor plants. Some of these sediments show significant effects of PCB weathering, especially from reductive dehalogenation [2].

Polychlorinated biphenyls were extracted from the sediments and then isolated after treatment with sulfuric acid and silica gel chromatography. The δ^{37}Cl values of the commercial mixtures and the PCBs extracted from the sediments were determined by the method of Holt et al. [3]. Briefly, samples were added to pyrex tubes with CuO and evacuated on a vacuum line. The tubes are combusted to form copper chloride that is reacted with methyl iodide to form methyl chloride. The δ^{37}Cl is determined on the methyl chloride by isotope ratio mass spectrometry at a precision of ~0.12‰.

Results: The δ^{37}Cl values of the chlorinated mixtures were from –5.10‰ to +1.22‰ (Table 1) and within the ranges of values published for other chlorinated compounds, –6.8‰ to +4.4‰ [3–5]. For the Aroclors, there was no trend between the percent Cl and δ^{37}Cl, and there was some bias amongst the suppliers. Aroclors purchased from Chem Service were the most depleted and the ones purchased from Accustandard were the most enriched

TABLE 1. The δ^{37}Cl of chlorinated mixtures.

Mixture	Cl (%)	Supplier	δ^{37}Cl (‰)
Toxaphene	69	Ultra Scientific	–5.10
Toxaphene	69	Supelco	–4.21
ppDDT	50	Ultra Scientific	–3.49
Aroclor 1016	41	ChemService	–3.07
Aroclor 1016	41	AccuStandard	–2.60
Aroclor 1242	42	ChemService	–2.89
Aroclor 1242	42	Ultra Scientific	–2.20
Aroclor 1242	42	AccuStandard	–2.11
Aroclor 1254	54	ChemService	–3.38
Aroclor 1254	54	Ultra Scientific	–2.93
Aroclor 1254	54	AccuStandard	–2.68
Aroclor 1260	60	Ultra Scientific	–2.96
Aroclor 1268	68	ChemService	–3.22
Aroclor 1268	68	Ultra Scientific	–2.83
Aroclor 1268	68	AccuStandard	–2.44
Chlordane	69	Ultra Scientific	1.22

in ^{37}Cl. The δ^{37}Cl values of the total PCBs extracted from the Turtle River Estuary sediments ranged from −2.84‰ to −2.25‰ and were similar or slightly enriched when compared to the δ^{37}Cl from the three different suppliers of Aroclor 1268. For the New Bedford Harbor sediments, the δ^{37}Cl values of the total PCBs ranged from −4.54‰ to −2.53‰ and some were clearly depleted in ^{37}Cl relative to the Aroclor 1242, 1254, and 1016 mixtures that were analyzed. The sediments that were most dehalogenated and concentrated were also the most enriched in ^{37}Cl, and we are currently investigating possible explanations for these results.

References: [1] Kannan K. et al. (1997) *ES&T, 31,* 1483–1488. [2] Lake J. L. et al. (1992) *Marine Env. Res., 33,* 31–47. [3] Holt B. D. et al. (1997) *Anal. Chem., 69,* 2727–2733. [4] Tanaka N. and Rye D. M. (1991) *Nature, 353,* 707. [5] van Warmerdam S. K. et al. (1995) *Appl. Geochem., 10,* 547–552.

CARBON BLACK FROM AUTOMOBILE TIRES.

C. M. Reddy[1], H. Takada[2], and H. Kumata[3], [1]Woods Hole Oceanographic Institution, Woods Hole MA 02543, USA, [2]Tokyo University of Agriculture and Technology, Fuchu, Tokyo 183, Japan, [3]Tokyo University of Pharmacy and Life Sciences, Hachioji, Tokyo 192-0392, Japan.

Introduction: The major source of highly condensed carbonaceous residues, often referred as black carbon (BC), elemental C (EC), or soot carbon (SC), to the environment is the incomplete combustion of organic matter [1]. This is mainly from vegetation or biomass burning and the anthropogenic combustion of fossil fuels. Another source of carbonaceous residues is carbon black (CB). This industrial chemical is synthesized by the incomplete combustion of petroleum products and is used as a reinforcing agent in automobile tires, resistors in electrical circuits, and as a pigment for inks, paints and carbon paper [2]. Most of this highly produced chemical is used in automobile tires, where it comprises ~25% of the tire by mass [3].

Automobile tires physically degrade and produce small particles, which then enter the environment [4]. This amount is not accurately known but has been estimated to be 1.3 Tg/yr in the United States [5]. Hence, tires may release ~0.3 Tg of CB in the United States per year. While this amount is small compared to global vegetation burning of 50–270 Tg of BC per year [6], CB in tire particles may be an important reservoir because (1) it is encapsulated within a rubber matrix that may affect its transport and preservation, especially when compared to other inputs of BC, EC, or SC; (2) the majority of it is made from the incomplete combustion of petroleum [2], hence it should have little or no radiocarbon and possibly a wide range of stable C-isotopic ratios that may affect isotopic-based source apportionment techniques; and (3) it contains a high concentration of polycyclic aromatic hydrocarbons (PAHs). For example, CB can be as much as 0.2% PAHs by weight [7]. However, it is unclear how the CB within the rubber matrix of the tire affects the bioavailability of these PAHs. This point is important when considering the work of Gustafasson et al. [8], who has shown that SC is a strong sorbent of PAHs in aquatic sediments. To gauge the impact of tire-derived CB in the environment, we developed a method to estimate it in sediments and urban dust. Here, we briefly describe the method and results.

Background and Methods: Over the past decade, benzothiazoles have been used as molecular markers of tire particles [5,9–11]. These compounds are from the vulcanization accelerators and antioxidants added to rubber during manufacturing. By measuring the concentration of these compounds in environmental samples, the concentrations of tire particles in the samples has been estimated. For example in one study, Reddy and Quinn [5] estimated that tire particles composed 0–3.4% of urban runoff particles, 0.2–2.8% of urban aerosols, 0.03–0.1% of road dust, and 0.03–0.04% in sediments. This approach assumes that tire particles are the only source of benzothiazoles to sediments, the concentration of the benzothiazoles is the same for all automobile tires and, furthermore, that the concentration of benzothiazoles remains constant throughout the tire's lifetime. While the first assumption may be valid [5], the latter two assumptions are unlikely. Nevertheless, we used this approach to provide some estimate of tire-derived CB in sediments and urban dust, by also assuming that all tire particles are ~25% CB.

Results: Over 45 sediment samples were considered. They were collected at depths from 0 to 50 cm in several estuaries and ponds. The estimated amount of tire-derived CB ranged from 0.003 to 8 mg g^{-1} (corresponding to 0.001–3% tire particles by mass respectively), except for one sediment that was 38 mg g^{-1}. Most of the samples were less than 2 mg g^{-1} and tended to be highest near areas with high automobile traffic. These values are similar to SC values measured in estuarine and coastal sediments [8]. For two samples of urban dust prepared by the National Institute of Standards and Technology (NIST), SRM 1648 and 1649, the values were 1 and 2 g g^{-1}, respectively.

Summary: We have presented an approach for estimating tire-derived CB in environmental samples, which is not ideal and makes many assumptions. Nevertheless, it appears that in urban areas, where automobile activity is high, tire particles may substantially contribute to the inventory of carbonaceous residues and additional research is warranted.

References: [1] Goldberg E. (1985) *Black Carbon in the Environment,* Wiley, NY. [2] *Hawley's Condensed Chemical Dictionary* (1993) Van Norstrand, NY. [3] *Encyclopedia of Chemical Technology* (1985) Wiley, NY. [4] Dannis M. (1974) *Rubber Chem. and Tech., 47,* 1011–1037. [5] Reddy C. and Quinn J. (1997) *ES&T, 31,* 2847–2853. [6] Kuhlbusch T. and Crutzen P. (1995) *Global Biogeochemical Cycles, 9,* 491–501. [7] Lee M. and Hites R. (1976) *Anal. Chem., 48,* 1890–1893. [8] Gustafsson O. et al. (1997) *ES&T, 31,* 203–209. [9] Spies R. et al. (1987) *Nature, 327,* 697–699. [10] Rogge W. et al. (1993) *ES&T, 27,* 1892–1904. [11] Kumata H. et al. (1996) *Anal.Chem., 68,* 1976–1981.

X-RAY ABSORPTION FINE STRUCTURE STUDY OF THE INCORPORATION MODES OF URANYL SPECIES INTO CALCITE AND ARAGONITE.

R. J. Reeder[1], M. Nugent[1],and G. M. Lamble[2], [1]Department of Geosciences, State University of New York–Stony Brook, Stony Brook NY 11794-2100, USA (rjreeder@sunysb.edu), [2]Earth Sciences Division, Lawrence Berkeley National Laboratory, Berkeley CA 94720, USA.

X-ray absorption fine structure (XAFS) spectroscopy of U(VI)-containing calcite and aragonite was undertaken to resolve fundamental geochemical and environmental questions about the structural state of U in carbonate minerals. Calcite and aragonite were grown from room-temperature, supersaturated aqueous solutions doped with uranyl ion (UO_2^{2+}). Aqueous speciation calculations indicate the dominant uranyl species were bis- and triscarbonate monomers. Uranium concentrations were 700 and 1890 ppm in two calcites and 985 ppm in an aragonite. Absorption spectra were collected for the U L_3-edge at NSLS beamline X-11A using a 13-element Ge detector. Observed edge positions coincide exactly with that for U(VI) standards.

The XAFS spectrum for the aragonite sample is qualitatively similar to that for the aqueous uranyl triscarbonate monomer; differences are evident for the calcite spectra. Fitting using theoretical phases and amplitudes (and confirmed by comparison with reference compounds) shows a distinct difference in U coordination between the calcite and aragonite. Fourier transforms for both carbonates are dominated by a main peak attributed to the axial oxygens, characteristic of the linear uranyl moiety (O = U = O), and a slightly smaller peak due primarily to O coordination in the equatorial plane. For both calcite and aragonite, two axial oxygens occur at a distance of 1.80(1) Å. The difference in coordination between calcite and aragonite is found in the equatorial plane. Fits for aragonite show 6.4 ± 1 oxygens at 2.44(1) Å, with 2.3 ± 1 C atoms at 2.87(1) Å. These distances and coordination numbers are consistent with a bidentate coordination of three CO_3 groups in the equatorial plane of the O = U = O moiety, which is very similar to the coordination of the aqueous uranyl triscarbonate monomer species. In contrast, the equatorial coordination of the O = U = O moiety in calcite is 3.9 ± 1 oxygens at 2.33(1) Å and 3.5 ± 1 C atoms at 2.90(2) Å. The significantly shorter U-O_{eq} distance and smaller coordination number in the first equatorial shell indicate that CO_3 groups are not in bidentate coordination but probably monodentate. For both calcite and aragonite, there are weaker contributions, including one multiple-scattering contribution, at greater distances. We could not identify unambiguous evidence for backscattering by Ca, and we cannot rule out the possibility that either sample may have a minor contribution from more than one uranyl species.

Because growth solutions for aragonite and calcite differed only by the presence of Mg^{2+} in the aragonite system, the striking difference in equatorial coordination indicates that differences between the aragonite and calcite structure, or their growth surfaces, influence the local coordination of the coprecipitated uranyl species. The similarity of the uranyl coordination in aragonite with the triscarbonate monomer species suggests that the equatorial coordination remains largely intact during incorporation. In calcite, however, the equatorial coordination of the CO_3 groups apparently changes from bidentate to monodentate during incorporation. Because we cannot positively identify a Ca shell, the exact positions of the uranyl species within the different carbonate structures remain unclear. Nevertheless, the observed local configurations around the U(VI) atoms must give rise to significant local disruption of the structure. This contrasts with other recent XAFS work [1] showing that U(IV) substitutes in the Ca site of calcite with only minor structural disruption. Consequently, calcite (and aragonite) containing U(VI) may be significantly less stable than samples with comparable levels of other trace elements that cause less structural disruption. Because coprecipitation is an important mechanism of contaminant and trace metal uptake by carbonates, any enhanced solubility could make uranyl ion more susceptible to remobilization by dissolution.

References: [1] Sturchio N. C. et al. (1998) *Science, 281,* 971–973.

IN SITU URANIUM-LEAD AGES OF ZIRCONS FROM THE BISHOP TUFF: NO EVIDENCE FOR LONG CRYSTAL RESIDENCE TIMES.

M. R. Reid[1] and C. D. Coath, [1]Department of Earth and Space Sciences, University of California, Los Angeles, 595 Charles Young Drive East, Los Angeles CA 90095-1567, USA (reid@ess.ucla.edu).

Introduction: Cataclysmic eruption of >500 km^3 of rhyolite gave rise to the Bishop Tuff in the Long Valley area of California ~0.8 Ma. An emerging but controversial time-line for the differentiation, accumulation, and storage of the Bishop Tuff rhyolite suggests that appreciable portions of the magmatic system were multiply saturated by at least 1 Ma and potentially as early as 2 Ma. In particular, melt inclusion bearing quartz crystals in some of the first-erupted portions of the Bishop Tuff yield radiogenic Ar ages [1] and Sr model ages [2] of 2.0–2.3 Ma and 1.3–2.5 Ma respectively. Sr mineral and whole-rock isochrons for the pre-caldera Glass Mountain rhyolites seem to indicate a similar age for the onset of differentiation of the Bishop Tuff magmatic system [3].

Zircon crystallization and separation probably accompanied differentiation of much of the Bishop Tuff rhyolite. For the early lavas, temperatures inferred for zircon saturation are 735°–775°C, consistent with geothermometry obtained on the Fe-Ti oxides with which the zircons coexist. These conditions probably prevailed in the evolved upper portion of the magma chamber. Zircons present in these early lavas must therefore have crystallized at least in part from the time that such temperatures were attained. If, in addition, the efficacy of zircon separation from the magma was stochastic, a zircon population which more broadly reflects the down-temperature history of the evolving system would be expected; in this case, crystallization ages would yield a maximum age for attainment of magmatic $T <780°C$.

Results: Spot analyses were performed on ~150-μm polished zircon grains separated from the airfall pumice and lower cooling unit of the Bishop Tuff exposed in the lower Owens Gorge. Out of a total of 26 grains analyzed, two (one each from the airfall and ashflow deposits) give ages for which the weighted mean of 4 spot analyses is 211 ± 2 Ma. Comparable ages (~210 Ma) have been obtained on exposures of Sierra Nevada granitoids; notably they are only found in that portion of the batholith that is associated with Long Valley caldera. Evidently these zircons are xenocrysts of Triassic arc basement which experienced little or no isotopic reequilibration after they were incorporated into the Bishop Tuff magmatic system.

Most of the zircons separated from the Bishop Tuff yield $^{206}Pb^*/^{238}U$ of $0.6–1.4 \times 10^{-4}$. Initial $^{206}Pb/^{238}U$ ratios were extremely low in these zircons such that >90% of the ^{206}Pb is radiogenic in approximately half of the spots analyzed. If fractionation between the daughter nuclides of the U-series decay chain is neglected, the $^{206}Pb^*/^{238}U$ values obtained correspond to ages of 0.41–0.93 Ma. Considered together with $^{207}Pb^*$-^{235}U, the data define a relatively narrow band with respect to concordia that suggests that the apparent distribution of $^{206}Pb^*$-^{238}U ages is more likely the result of statistical uncertainties in the background and common Pb corrections than of variability in the true ages of the zircons. When regressed through concordia, the data arrays yield weighted mean ages of 0.74 ± 0.01 Ma (MSWD = 2.4) for the airfall and of 0.75 ± 0.02 Ma (MSWD = 1.8) for the ashflow tuff. These apparent ages are comparable to or somewhat younger than recent estimates for the eruption age of the Bishop Tuff (0.76–0.79 Ma).

Because they assume no fractionation of the intermediate daughters in the decay chain, the intercept ages must represent minimum ages for zircon growth. Of the ^{238}U-series decay daughters other than ^{234}U, ^{230}Th is the most abundant and, relative to U, is preferentially excluded during zircon crystallization. Using the observed magnitude of zircon U/Th fractionation to correct for initial ^{234}U-^{230}Th disequilibria in zircon, more realistic U-Pb ages of 0.83–0.84 Ma probably pertain to these zircons. While arguably older than the age of eruption of the Bishop Tuff, they are nonetheless younger than many other estimates for differentiation and crystallization of the magma reservoir.

Discussion: The striking results of our study are the young and remarkably narrow range of ages delimited by zircons from both the air-fall and ashflow deposits. Accordingly, either zircon growth occurred within <100 ka of eruption of the Bishop Tuff or zircons that precipitated earlier continued to partially equilibrate with the magma. The second possibility is difficult to rigorously evaluate because quantitative constraints on the diffusion of relevant chemical species at magmatic conditions are lacking; note, however, that highly open-system behavior would necessarily be required in order for zircon crystallization to have occurred on timescales consistent with those inferred from melt inclusion bearing quartz. We believe that there is other compelling evidence that such extensive equilibration between zircon and melt did not occur. It seems likely that the disaggregation of xenolithic material that was responsible for incorporation of Triassic zircons must have preceded extensive crystal growth, yet these zircons appear to have exchanged little with the rhyolitic magma. Further, the zircon U-Pb ages are comparable to estimates of 0.82–0.85 Ma for the average age of feldspar growth in the early and intermediate Bishop Tuff. The latter ages are unlikely to have been modified significantly by concurrent diffusional reequilibration with the magma. Considered together with the limited distribution of zircon ages, it appears that extensive crystal growth did not occur prior to ~0.85 Ma. It is possible, therefore, that most of the crystallization of the Bishop Tuff occurred <100 ka before eruption. By analogy to recent results obtained for the Bandelier tuff [4], it seems likely that the quartz crystals are not representative of the major evolution of the Bishop Tuff rhyolite. Therefore, the implication of ages obtained on these crystals for magmatic differentiation and storage remains uncertain.

References: [1] van den Bogaard P. and Schirnick C. (1995) *Geology, 23,* 759–762. [2] Christensen J. N. and Halliday A. N. (1996) *EPSL, 144,* 547–563. [3] Davies G. R. et al. (1994) *EPSL, 125,* 17–37. [4] Wolff et al. (1999) *Geology,* in press.

PROGRESS REPORT ON HIGH-RESOLUTION COMPARISON OF ARGON/ARGON AND URANIUM/LEAD SYSTEMS.

P. R. Renne[1,2], R. Mundil[1], K. Min[2], and K. R. Ludwig[1], [1]Berkeley Geochronology Center, 2455 Ridge Road, Berkeley CA 94709, USA, [2]Department of Geology and Geophysics, University of California, Berkeley CA 94720, USA.

The Ar/Ar and U-Pb methods are unequivocally the most important timescale chronometers for most of geologic time. Both systems have strengths and weaknesses, but the U-Pb system presently has much higher potential accuracy due to the high precision of the U decay constant determinations. In contrast, uncertainties in both electron capture and β decay constants for K, and in isotopic data for standards, presently limit the accuracy of Ar/Ar dating to ~2%, whereas the precision of this method is commonly better than 0.1%.

The K decay constants used by geologists since 1977 are based on summaries of α and γ counting data by Beckinsale and Gale [1], updated by Steiger and Jäger [2] to include new data (Garner et al., 1975) for the isotopic composition of K. Beckinsale and Gale [1] also included a hypothetical gamma-less electron capture decay that accounts for ~0.2% of the total K decay constant value they reported, but which has never been verified. Subsequent compilations of available data [e.g., 3] produce total decay constant values that differ from those of [2] by up to 2%. The summaries of Endt and Van der Leun [3] and subsequent compilations in the nuclear physics literature use a more appropriate statistical approach, yielding ~50% larger uncertainties.

Potassium-argon data for Ar/Ar standards are also large sources of systematic error in Ar/Ar ages. Although reported intralaboratory precision better than 1% for K and Ar concentration measurements, the interlaboratory range in K-Ar, exemplified by data from the Fish Canyon Tuff, is nearly 4%.

An ongoing comparison at BGC of Ar/Ar and U-Pb data for pre-Cenozoic volcanic rocks that should be free of differential closure histories due to slow cooling, and in which zircon residence time effects should be negligible, shows that a consistent bias exists between ages from the two systems when the decay constants recommended by [2], and the age of 28.02 Ma for Fish Canyon sanidine (for Ar/Ar ages), are used. Four silicic tuffs with Ar/Ar plateau ages of 130, 250, 449, and 1088 Ma, determined on alkali feldspars and biotite, yield U-Pb data from multiple single-grain zircon analyses that are consistently ~1% older.

The magnitude of this ~1% bias is within the scope of the relatively large systematic errors affecting Ar/Ar ages. With more pairs of Ar/Ar and U-Pb, it will be possible to constrain that source of systematic error (i.e., which of the two K decay constants, or the age of the standard) is most important as a contributor to the bias. It is particularly important for this purpose to resolve any variation in bias as a function of age, since younger ages are more sensitive to the electron capture than the beta decay constant for K. Ultimately, with sufficient data of high quality and freedom from non-analytical errors, it may be possible to recalculate all of these values relevant to the Ar/Ar system through normalization to the U-Pb system.

One of the most challenging difficulties in this approach is to avoid the relatively large effects of U decay constant uncertainties on ^{207}Pb/^{206}Pb ages by generating an overlapping cluster of concordant analyses, whose "Concordia age" or ^{206}Pb/^{238}U age is then regarded as the closest approximation of the crystallization age. To avoid the accuracy limitations of Pb/Pb or U-Pb concordia-intercept ages, it is essential to generate suites of statistically coherent analyses of single zircons unaffected by Pb loss or inheritance. However, as discussed in a companion abstract, producing U-Pb datasets of such quality is not always easy.

Difficulties with the U-Pb system, ironically, underscore the desirability of placing the Ar/Ar system on more solid footing in terms of accuracy: as a broadly utile, high-precision geochronometer, Ar/Ar is unsurpassed. However, if one wants to know the "absolute age" of a geologic event, this system presently gives a very fuzzy (i.e., worse than ±2%) answer.

References: [1] Beckinsale R. D. and Gale N. H. (1969) *EPSL, 6,* 289–294. [2] Steiger R. H. and Jäger E. (1977) *EPSL, 36,* 359–362. [3] Endt P. M. and Van der Leun C. (1973) *Nucl. Phys., A214,* 1–625.

CHRONOSTRATIGRAPHY OF THE SAGANTOLE FORMATION, AFAR, ETHIOPIA, AND THE AGE OF ARDIPITHECUS RAMIDUS.

P. R. Renne[1], G. WoldeGabriel, W. K. Hart, G. Heiken, and T. D. White, [1]Berkeley Geochronology Center, 2455 Ridge Road, Berkeley CA 94709, USA (prenne@bgc.org).

The Sagantole Formation comprises over 200 m of lacustrine, fluvial, alluvial, and volcaniclastic sediments, plus compositionally bimodal tephras and basaltic lavas, exposed in a domelike horst named the Central Awash Complex in the southwestern Afar Rift of Ethiopia. The Sagantole Formation is widely known for abundant vertebrate faunas, including the primitive hominid *Ardipithecus ramidus*. The Sagantole Formation has been recently subdivided into the Kuseralee, Gawto, Haradaso, Aramis, Beidareem, Adgantole, and Belohdelie members, in ascending order. The members are defined on the basis of lithologic differences and laterally continuous bounding tephras. *A. ramidus* is known from widely distributed locations at the base of the Aramis member.

Argon-40/argon-39 dating of 11 intercalated volcanic units firmly establishes the age of the Sagantole Formation to be 3.9–5.6 Ma, significantly older than previous proposals based on erroneous correlations. Most of the new dates are determined by laser-fusion analyses 23–107 individual grains per sample of plagioclase (5 samples) and sanidine (2 samples) phenocrysts from variably reworked tephras. Single grain analyses are critical for dating these units, as pervasive contamination by 23–24-Ma sanidine occurs in many tephras throughout the section. Sanidine phenocrysts from trachyte cobbles in intercalated conglomerates also yield 23–24 Ma ages, indicating that the contaminant population was ubiquitous in the fluvial environments of the Sagantole Formation. The provenance of the 23–24-Ma volcanics is uncertain, but they may be exposed by the Afar-bounding escarpment some 20 km to the west.

Additional dates were obtained by laser step-heating of basaltic glass lapilli that yield undisturbed spectra and reasonable plateau ages. Though shown in some cases elsewhere to be prone to open-system behavior, our data indicate that this is not always the case and in fact basaltic glass may be unduly stigmatized as a material for ^{40}Ar/^{39}Ar dating. All known ocurrences of *A. ramidus* are between a silicic tuff dated at 4.378 ± 0.008 Ma (sanidine) and an overlying basaltic tuff dated at 4.388 ± .053 Ma (glass), based on Fish Canyon sanidine at 27.84 Ma for comparison with previous work.

Magnetostratigraphic data reveal eight paleomagnetic polarity zones that can be correlated unambiguously with the Thvera, Sidufjall, Nunivak, and Cochiti subchrons of the Gilbert chron. The density of dated tephras permits reasonably precise ages to be calculated for the reversals, and the results are generally consistent with the astronomical timescale. By reference to the Cande and Kent (1995) geomagnetic polarity timescale, seven additional chronological datums can be placed in the Sagantole Formation. With a total of 18 such datum horizons, the age resolution anywhere in the Sagantole Formation is better than ±100 k.y., making this the best dated Mio-Pliocene succession in Africa.

NEODYMIUM AND LEAD ISOTOPES IN ATLANTIC IRON-MANGANESE CRUSTS: PANAMA GATEWAY AND INTENSIFICATION OF NORTHERN HEMISPHERE GLACIATION.

B. C. Reynolds, M. Frank, and R. K. O'Nions, Department of Earth Sciences, University of Oxford, Parks Road, Oxon OX1 3PR, UK (benr@earth.ox.ac.uk).

Introduction: Hydrogenous ferromanganese crusts from the western north Atlantic have recorded remarkable Nd- and Pb-isotopic variations over the last 5 Ma [1,2]. A decrease of ε_{Nd} values in crusts BM1969.05 and ALV539 from ~–11 to –13 over this period appear to correspond to shifts in Pb isotopes: ^{206}Pb/^{204}Pb increases from 18.9 to 19.2, while ^{207}Pb/^{206}Pb decreases from 0.825 to 0.815. The precise timing and cause of these shifts have been the subject of debate and have been considered to relate to oceanographic changes caused by the closure of the Panama Gateway in the early Pliocene. The closure of this Gateway has been suggested by some as the cause of northern hemisphere glaciation (NHG).

In order to address this debate, three crusts from the northwest Atlantic (BM1969.05, BM1963.897, and D-14) have been sampled for Nd isotopes and at high spatial resolution for Pb-isotopic analysis by multiple collector inductively coupled plasma mass spectrometry (MC-ICP-MS). These crusts have been dated using ^{10}Be/^{9}Be ratios.

Results: The Pb-isotopic variations in each crust over the last 6 Ma are virtually indistinguishable in their ^{206}Pb/^{204}Pb, ^{207}Pb/^{206}Pb, and ^{208}Pb/^{206}Pb ratios, indicating a common provenance for Pb. Isotopic shifts evident over the last 3 m.y. are most pronounced over the last 1.8 m.y., when ^{206}Pb/^{204}Pb, ^{207}Pb/^{206}Pb, and ^{208}Pb/^{206}Pb ratios have changed from 18.97, 0.825, and 2.053 to 19.24, 0.815, and 2.047 respectively.

Shifts in Nd- and Pb-isotopic composition in crust BM1963.897 from the Blake Plateau (~850-m depth) occur before 5 Ma, and have not been observed in other Atlantic crusts. These shifts indicate the presence of a different water mass on the Blake Plateau, which was most dominant at ~8 Ma when the crust recorded relatively high ε_{Nd} values of –7.5. In this crust the timing of Pb-isotopic variations, measured by MC-ICP-MS, roughly correspond to that of ε_{Nd}.

Discussion: The shift toward lower ε_{Nd} values and more radiogenic Pb-isotopic ratios in each of the northwest Atlantic crusts indicates increased contribution of Nd and Pb derived from older continental crust. This may have arisen through a relative increase in the input of older terrigenous material into the Atlantic or alternatively a change of Atlantic circulation that altered the provenance of water masses in the northwest Atlantic. The low ε_{Nd} value of present day North Atlantic Deep Water originates from continental material introduced from the Canadian Shield. This material also enters the Arctic Ocean so that changes in the input from this area should be observed in both the Arctic and northwest Atlantic Oceans. Neodymium and Pb isotopes in Fe-Mn micronodules recovered from Arctic Ocean sediment cores have recorded a progressive increase in the supply of material derived from older continental sources over the last 1.7 Ma [3] (Fig. 1). This coincides with an increase in dropstone occurrences in the sediment cores reflecting increased ice rafted detritus [3]. The correlation of isotopic records the northwest Atlantic and Arctic Oceans over the last ~1.8 Ma thus reflects an increased input of Pb and Nd from the Canadian Shield rather than any major paleoceanographic changes.

The relatively high ε_{Nd} values (–7.5) observed in BM1963.897 at 8 Ma are much higher than any other measurements from Atlantic samples, or present-day particulate material from the Mississippi and Hudson rivers (ε_{Nd} ~11 [4]). Together with the expected short advective length scale of Pb, this suggests that it was Pacific water, rather than Southern Ocean Water, which was the dominant influence at the location of BM1963.897 at ~8 Ma. The rapid decline in this component between 8 and 5 Ma most probably reflects a decrease in advection of water through the closing Panama Gateway, which is somewhat earlier than the time of a surface water salinity increase at 4.2 Ma in the Caribbean [5]. This salinity increase occurred as a consequence of a reduction of the flow of Atlantic surface water westward through the Gateway and may indicate that the recorded eastward currents from the Pacific were slowly cut off some 1 m.y. before the shallower westward-flowing surface currents.

Conclusions: Although the Northern Hemisphere glaciation became more intense between 3.1 and 2.5 Ma, it did apparently not affect the amount of Nd and Pb input into the northwest Atlantic and Arctic Oceans until ~1.8 Ma, when increased ice rafting occurred.

The inferred timing of closure of the Panama Gateway before 4 Ma is significantly earlier than the intensification of NHG and indicates that the closure of the Panama Gateway may only have been a precondition for the onset of major NHG rather than a direct cause.

References: [1] Burton K. W. et al. (1997) *Nature, 386,* 382–385. [2] O'Nions R. K. et al. (1998) *EPSL, 155,* 15–28. [3] Winter B. et. al. (1996) *GCA, 60,* 4957–4963. [4] Goldstein S. L. et. al. (1984) *EPSL, 70,* 221–236. [5] Keller G. et al. (1989) *J. S. Am. Earth Sci., 2,* 73–108.

THORIUM-230 AND CARBON-14 DATING OF SPELEOTHEMS FROM THE BAHAMAS: IMPLICATIONS FOR THE CALIBRATION OF THE RADIOCARBON TIMESCALE.

D. A. Richards[1], J. W. Beck[2], D. J. Donahue[2], P. L. Smart[1], and R. L. Edwards[3], [1]School of Geographical Sciences, University of Bristol, Bristol, UK (david.richards@bristol.ac.uk), [2]National Science Foundation American Meteorological Society Facility, Department of Physics, University of Arizona, Tucson AZ, USA, [3]Minnesota Isotope Laboratory, Department of Geology and Geophysics, University of Minnesota, Minneapolis MN, USA.

Introduction: It is well known that there have been shifts in the offset between ^{14}C ages and true calendar ages for the last 50 ka as a result of substantial variation in ^{14}C production rate and changes in the global C cycle. Calibration of the radiocarbon timescale prior to 11 ka is based on a relatively small number of coupled ^{230}Th and ^{14}C ages of corals and ^{14}C ages of annually laminated sediments. Here, we present thermal ionization mass spectrometry (TIMS) ^{230}Th-^{234}U-^{238}U, ^{231}Pa-^{235}U and accelerator mass spectrometry (AMS) ^{14}C ages for speleothems from submerged caves of Grand Bahama that offer considerable potential for an accurate and continuous calibration curve from 11 to 45 ka and provide valuable information about C cycling and geomagnetic intensity.

Sampling Strategy: Low-U concentrations in speleothems from the Bahamas (typically <500 ppb) demand that ^{14}C and U-series isotopic analyses are performed on subsamples of different mass (10–20 and 500–1000 mg respectively) and sampling interval (1–2 mm and 5–20 mm respectively) from the principal growth axis of the stalagmites (up to 620 mm). Growth rates (>10 mm ka^{-1}) were nonuniform and drip loci often moved during periods of continuous growth, causing variable stalagmite morphology. The sampling strategy is therefore critical, and implications for the "^{230}Th-age growth model" and estimates of the true calendar age will be discussed.

Initial Conditions: Accurate calibration of the radiocarbon timescale is dependent on a reasonable knowledge of the initial "dead C fraction" and ^{230}Th. Comparison of the offset between ^{230}Th and ^{14}C ages for Bahamas speleothems and coral/laminated-sediment records for the period 11–20 ka indicates that there is a relatively constant "dead C" effect from dissolution of ancient carbonates of 16% (see Fig. 1). Thorium-232 concentrations are generally low (<0.6 ppb); however, in a few subsamples, where ^{230}Th/^{232}Th atomic ratios were <1 × 10^{-3}, correction for initial Th conditions had a significant effect. Using isochron techniques, we have discovered a high initial ^{232}Th/^{232}Th activity of 16.5. We find no evidence for postdepositional mobility of the isotopes of interest, and are therefore confident that past activities of atmospheric ^{14}C can be estimated accurately.

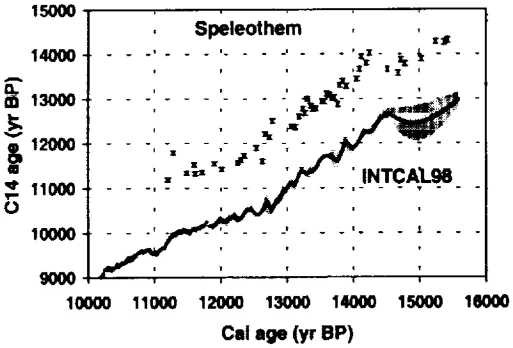

Fig. 1. Bahamas speleotherm and INTCAL98 (10–15 k.y. ago). Speleotherm ages uncorrected for initial dead C contribution, hence offset from INTCAL98 dataset by ~1400 yr.

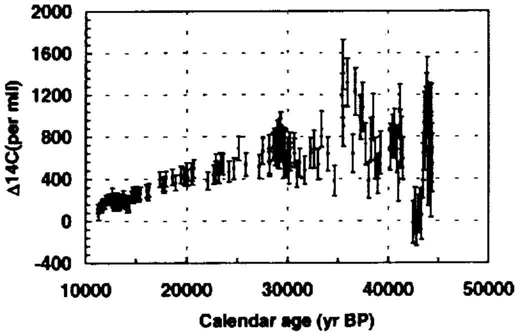

Fig. 2. Δ^{14}C record (45–11 ka).

Results and Discussion: Using the derived calendar-age model for stalagmite growth and initial-corrected AMS ^{14}C ages, close correspondence is found between existing records and the speleothem results for the period 11–16 ka. Substantial variation in past atmospheric ^{14}C is observed during the period 28–50 ka, with peaks of Δ^{14}C >800‰ (Fig. 2). Estimates of Δ^{14}C near the limit of ^{14}C dating are subject to large errors and we have paid careful consideration to the effects of variable growth rate, initial ^{230}Th, and dead-C contribution on their precisions. Similar, large and abrupt peaks have been observed in numerous independent records of cosmogenic nuclide production (e.g., ^{10}Be and ^{36}Cl in the polar ice cores) and inferred from records of geomagnetic intensity in volcanic and sedimentary rocks, yet there is no consensus on their timing, magnitude, or cause. The continuous and radiometrically dated record of ^{14}C activity presented here should help to resolve this.

OLD ZIRCON MEGACRYSTS FROM YOUNG NORTHWEST TERRITORIES KIMBERLITES.

S. H. Richardson[1], R. E. Zartman[1], and J. A. Carlson[2], [1]Department of Geological Sciences, University of Cape Town, Rondebosch 7701, South Africa, [2]BHP Diamonds Inc., #8 1699 Powick Road, Kelowna, British Columbia, Canada.

Uranium-thorium-lead ages have been obtained for two generations of megacrystic zircon with U contents of 14–40 ppm recovered from bulk samples of four diamondiferous kimberlites comprising the Ekati cluster [1], Slave craton, NWT, Canada. The first generation is late Archean in age and characterized by high Th/U (0.38–1.60) while the second is early Tertiary and characterized by lower Th/U (0.21). The latter value lies within the published range of Th/U (0.17–0.35) for young kimberlitic zircon from the Kaapvaal craton [2,3].

One young zircon from the Panda kimberlite gives a well-constrained ^{238}U-^{206}Pb age of 59.0 ± 0.4 Ma, which is marginally older than a macrocryst phlogopite Rb-Sr age of 53.2 ± 3.8 Ma [1]. However, both these values lie within the previously reported range of phlogopite Rb-Sr and perovskite U-Pb ages (47 to 84 Ma respectively) for central Slave craton kimberlites [1].

Six out of seven old and variably discordant zircon from the Koala, Fox, and Sable kimberlites give a concordia upper intercept age of 2549 ± 15 Ma (n = 8 including duplicates), although the seventh (from Fox) has a significantly younger $^{207}Pb/^{206}Pb$ age of 2250 Ma. A better defined upper intercept age of 2549 ± 7 Ma can be obtained using only six of the analyses that could be identifying a discrete crystallization event at ~2550 Ma. The corresponding lower intercept age of 128 ± 99 Ma is within error of the time of kimberlite emplacement and also is barely distinguishable from the present. The proportionality between U and Th concentration and degree of discordance is consistent with Pb loss being related to the amount of accumulated radiation damage. Given the young lower intercept age, Pb loss appears to have taken place at or after the time of zircon entrainment in the host kimberlite rather than continuously during continental mantle/crustal storage.

The age and Th/U distribution of the two generations of mantle zircon is reminiscent of that for the 240-Ma Jwaneng kimberlite [2,4], Kaapvaal Craton, Botswana. Existing data are thus consistent with a decreasing Th/U in the depleted upper mantle source of megacryst magmas on a billion-year timescale. Such a trend is predicted by crust-mantle evolution models (e.g., plumbotectonics [5]) whereby crustal U is preferentially recycled back into the upper mantle relative to Th.

References: [1] Carlson J. A. et al. (1998) *7th Intl. Kimb. Conf. Proc.*, in press. [2] Kinny P. D. et al. (1989) *4th Intl. Kimb. Conf. Proc.*, *14*, 833–842. [3] Zartman R. E. et al. (1998) *7th Intl. Kimb. Conf. Ext. Abstr.*, 989–991. [4] Valley J. W. et al. (1998) *CMP*, *133*, 1–11. [5] Zartman R. E. and Haines S. M. (1988) *GCA*, *52*, 1327–1339.

A PYRITE GRAND UNIFIED THEORY.

D. Rickard, Department of Earth Sciences, Cardiff University, Park Place, Cardiff CF1 3YE, Wales, UK (rickard@cardiff.ac.uk).

Introduction: As with many simple inorganic compounds, pyrite (FeS_2), can be synthesized by several recipes in the laboratory from aqueous solutions at temperatures below 100°C [1]. The abundance of pyrite in natural systems and its key role in several global biogeochemical cycles has led to some debate over which of these routes is followed in nature. This paper presents a grand unified theory (GUT) for pyrite formation that proposes a consistent explanation for the different synthetic processes in terms of a limited number of controlling factors.

Pyrite-forming Reactions: All present pyrite forming reactions involve precursor Fe(II) monosulfides [2]. Several authors have recently demonstrated that these are not necessarily solid phases (e.g., precipitated, amorphous FeS or mackinawite) but aqueous FeS species with similar K values to the solid phases [3–5]. Pyrite forms through the oxidation of the S in precursor FeS from S(-II) to S(-I), whereas Fe(II) is not oxidized. This contrasts with (a) greigite, Fe_3S_4, formation from FeS where Fe(II) is oxidized to Fe(III) and S(-II) is not oxidized. This reaction is a solid-state reaction [6]. In contrast, all kinetic and discriminatory observational evidence suggests that pyrite formation involves a dissolved stage [7]. This suggests that the Fe(II) → Fe(III) reaction (S(-II) constant) is a solid-state reaction and that S(-II) → S(-I) reaction (Fe(II) constant) is a solution reaction.

Nucleation Kinetics: It is clear that the reluctance of pyrite to nucleate has been a major barrier to reproducible experimental studies [8]. The nucleation energy barrier for pyrite may be overcome in the presence of surfaces with large numbers of active sites. Several such surfaces have been identified. The most obvious of these is amorphous, precipitated FeS or mackinawite, which is already in most experimental systems, because of the exceptionally high reactant concentrations used. Other surfaces where pyrite has nucleated include biological surfaces [9], S [10], and greigite [11]. It is possible that surfaces may be activated by reactions with other agents, such as O [12] and carbonyl groups [13]. It is probable that the catalysis of pyrite formation through the trace compounds such as these will prove to be a fruitful area of future investigation.

Oxidizing Agents: Several oxidizing agents have been implicated in the pyrite-forming reaction, including H_2S, S^0, S_n^{2-}, and O_2 [1,7]. These oxidizing agents are divided into two groups: (1) direct reactants (e.g., H_2S), and (2) indirect reactants (e.g., S^0, S_n^{2-}, and O_2). Experimentally, the presence of S^0, S_n^{2-}, and O_2 enhance the formation of pyrite. However, their involvement in the process is complex and variable, involving reaction intermediaries (S_n^{2-}) and nucleation catalysis (S^0 and O_2). The common factor in all the experimentation involving these compounds has been the presence of H_2S. The contribution of the H_2S reaction has not been deconvoluted from these mixed experimental systems.

The reluctance of pyrite to nucleate suggests that very high supersaturations are required for pyrite to form. This is consistent with observations on many sparingly soluble salts and is related to the size of the critical nucleus. The relative degree of supersaturation, Ω, is related to the equilibrium solubility of pyrite. Ω is a complex function of pe-pH-pS space and increases sharply toward the S(-II)/SO_4 boundary. The role of S^0, S_n^{2-}, and O_2 is to move the system closer towards this boundary, thereby increasing Ω and enhancing pyrite formation.

Conclusions: Pyrite forms in aqueous environments through the reaction of aqueous FeS with H_2S. Pyrite nucleation is catalyzed by the presence of active surfaces, such as amorphous, precipitated FeS, mackinawite, greigite, S, and biological materials. These may be activated by *in absentia* O_2 or carboxyl groups. Sulfur, polysulfides, and O_2 have the added role of moving the system closer to increased pyrite supersaturation

References: [1] Rickard D. et al. (1995) *ACS Symp. Series*, *612*, 168–193. [2] Morse J. W. et al. (1987) *Earth Sci Rev.*, *24*, 1–42. [3] Luther G. W. III and Ferdelman T. G. (1993) *Environ. Sci. Technol.*, *27*, 1154–1162. [4] Davison W. et al. (1998) *Anal. Chim. Acta*, *377*, 193–203 [5] Rickard D. et al. (1999) *Estuaries*, in press. [6] Pósfai M. et al. (1998) *Science*, *280*, 880–883. [7] Rickard D. and Luther G. W. III (1997) *GCA*, *61*, 135–147. [8] Schoonen M. A. A. and Barnes H. L. (1991) *GCA*, *55*, 1495–1504. [9] Rickard D. et al. (1999), in press. [10] Graham U. M. and Ohmoto H. (1994) *GCA*, *58*, 2187–2202. [11] Sweeney R. E. and Kaplan I. R. (1973) *Econ. Geol.*, *68*, 618–634. [12] Wilkin R. T. and Barnes H. L. (1996) *GCA*, *60*, 4167–4179. [13] Rickard D. et al., in preparation.

EXPERIMENTAL CONSTRAINTS ON THE BEHAVIOR OF RHENIUM AND OSMIUM DURING MANTLE MELTING AND MAGMATIC DIFFERENTIATION.

K. Righter, Lunar and Planetary Laboratory, University of Arizona, Tucson AZ 85721, USA (righter@lpl.arizona.edu).

Introduction: In order to better understand the Re-Os-isotopic system, and highly siderophile element (HSE) partitioning in general, experimental studies of crystal-melt partitioning have been undertaken. Previous experimental work has established that Re is compatible in garnet, but incompatible in orthopyroxene [1]. New results indicate that clinopyroxene-melt partitioning of Re is dependent upon f_{O_2}, Re is mildly incompatible in phlogopite and amphibole, and Re, Os, and other HSE oxides dissolve in magnesioferrite, a component of terrestrial cubic oxides.

Experimental: Two compositions were used to study clinopyroxene-melt equilibria: a composition in the CaO-MgO-Al_2O_3-SiO_2-TiO_2 (CMAST) system and an augite minette. The CMAST glass was welded into Pt tubing, together with a mixture of NiO, and NiRe metal alloy, and held in the hotspot of a vertical 1-atm furnace. The metal-oxide mixture acted as an f_{O_2} sensor, and also buffered the amount of ReO_2 dissolved in the glass. Oxygen fugacities in these experiments ranged from air to the nickel-nickel oxide (NNO) buffer. The augite minette, together with a Co-(CoO,MgO) f_{O_2} sensor, 10–20 μL of distilled water and 1 wt% ReO_2, was contained in a graphite-lined Pt capsule, and heated to 1120°–1150°C at 10 kbar in a piston cylinder apparatus. Most of the Re in the latter experiments stabilized as Re metal, but a small amount dissolved in the silicate melt. Oxygen fugacities were ~2–3 $\log f_{O_2}$ units below the NNO buffer. Finally, mixtures of HSEs (ReO_2, Os, Pt, IrO_2, RuO_2, and Rh_2O_3) and magnesioferrite ($MgFe_2O_4$) were welded into Pt tubing and allowed to equilibrate in a 1-atm furnace, for as long as 1 week.

Analytical: For the more oxidized runs, Re could be analyzed using an electron microprobe because Re is present at concentration levels greater than ~100 ppm. Operating conditions were 15 kV accelerating voltage, 200-nA sample current, and 60–360-s counting times on the ReMβ peak. For more reduced runs, Re was present at concentrations <100 ppm; glasses and crystals from these runs were analyzed using an ion microprobe, with analytical conditions similar to those used by [1].

Results and Discussion: Rhenium is incompatible in clinopyroxene in the most oxidized runs, with a D(cpx/melt) ~0.03, in agreement with previous work [2]. At more reduced conditions, Re becomes less incompatible, and at the most reduced conditions (NNO-3) it is compatible, with a D(cpx/melt) = ~5. In these experiments, phlogopite and amphibole (kaersutite) were also stable; D(Re) amphibole-melt and phlogopite-melt are both <0.1. Mantle metasomatic processes involving these phases are not likely to produce significant radiogenic Os over time as a result of this incompatibility. HSE oxides and magnesioferrite react under oxidized conditions (1 atm) to produce HSE-rich ferrites. HSEs readily dissolve into magnesioferrite at moderate temperatures (1100°–1200°C). In particular, as much as 16 wt% Re and 9 wt% Os can dissolve into magnesioferrite under these conditions. In addition, 13, 22, 9, and 13.5 wt% Pt, Rh, Ru, and Ir, respectively, can dissolve in magnesioferrite. Because there will be a small magnesioferrite component in terrestrial cubic oxides, these results show that a cubic oxide such as chromite or titanomagnetite can be important, not only in the distribution of Re and Os but also many other HSEs, during melting and fractionation. Compatibility of Ir, Os, and Ru in basic magmatic suites [e.g., 3] may be due to chromite as well as olivine, consistent with recent analyses of olivine and spinel separates from picrites [4]. Compatibility of Re and Os in cubic oxides suggests a 3+ valence; such a high valence is also consistent with results of solubility studies for Os [5].

Acknowledgments: This research is supported by NSF grant EAR-9706024.

References: [1] Righter K. and Hauri E. (1998) *Science, 280,* 1737–1741. [2] Watson E. B. et al. (1987) *Chem. Geol., 62,* 191–208. [3] Brügmann G. et al. (1987) *GCA, 51,* 2159–2169. [4] Walker R. J. et al. (1999) *GCA,* in press. [5] Borisov A. and Walker R. J. (1998) in *Origin of the Earth and Moon,* p. 2, LPI.

CORE FORMATION AND WET TERRESTRIAL ACCRETION.

K. Righter and M. J. Drake, Lunar and Planetary Laboratory, University of Arizona, Tucson AZ 85721, USA (righter@lpl.arizona.edu).

Introduction: There are several views on the origin of Earth's volatiles. The main astronomical paradigm is that the Earth accreted as an anhydrous body and volatiles were subsequently added through late cometary impact [e.g., 1]. Another view is that the terrestrial planets accreted in the presence of H gas of the solar nebula, and thus water was present in the earliest phase of accretion [e.g., 2]. The latter scenario is an environment that increasingly seems to accommodate our understanding of the early Earth. The critical evidence that allows discrimination between these viewpoints has been the relatively recent determinations of the D/H ratios of comets [3]. The D/H ratios in Comets P-Halley, P-Hyakutake, and P-Hale-Bopp fall within the range ~3.2×10^{-4}. The bulk Earth's D/H ratio is ~1.5×10^{-4}. If these three comets are broadly representative of all comets, a plausible but unproved assumption, then the post-accretion influx of water to the Earth from comets is limited to less than ~20%. Therefore, the Earth must have accreted at least in part from hydrated materials.

Such a scenario raises some questions about core formation that have not previously been addressed: What is the effect of water on reactions of the type $M + H_2O = MO + H_2$ (where M = Fe, Ni, Co, etc.)? Most previous studies of metal-silicate partitioning of these siderophile elements were done under dry conditions (with the exception of [4,5]). In order to better understand the impact of water on metal-silicate equilibria in the early Earth, we have undertaken a series of experiments designed to isolate the effect of dissolved water on the partitioning of siderophile elements between metal and silicate liquid.

Summary of Effect of Water on D(Met/sil): All experiments were performed in a 1/2" non-end-loaded piston cylinder apparatus at the University of Arizona [6], at 1300°C and 10 kbar with solid metal compositions of pure Fe or FeNiCo alloy. Silicate compositions used were a synthetic eucrite basalt (doped with W) and a natural hawaiite (doped with P), both with distilled water added. Metal-silicate partition coefficients are affected by changes in melt composition (X_{FeO}) and f_{O_2} caused by addition of water, but dissolved water has no special effect on the value of partition coefficients for Ni, Co, Mo, and W (in agreement with [5]) and only a minimal effect on those for P.

Discussion: Predictive expressions for metal-silicate partitioning of siderophile elements from our earlier studies have been revised and augmented with new metal-silicate partition coefficient data. The new form of the predictive expression is

$$\ln D(\mathrm{met/sil}) = a\ln f_{O_2} + b/T + cP/T + \Sigma d_iX_i + e\ln(1 - X_S) + f\ln(1 - X_C) + g$$

where X_i, X_S, and X_C are the mole fractions of an oxide component (i) in the silicate melt, S and C in the metallic liquid respectively. Earlier conclusions that terrestrial upper mantle abundances of Ni, Co, Mo, W, and P are consistent with metal-silicate equilibrium at the base of a deep hydrous magma ocean [6] remain robust with the addition of these new data. The terrestrial primitive upper mantle Ni, Co, Mo, W, and P depletions [7], can be best matched using partition coefficients calculated for conditions of 240 kbar, 2250 K (1977°C), ΔIW = –0.40, $X_S = 0.15$, and $X_C = 0.08$ for a hydrous fertile peridotite with 3 wt% water ($X_{H_2O} = 0.08$).

Implications: Because the partitioning of trace siderophile elements between metal and silicate melt is not affected by small amounts of dissolved water (but Fe is), accretion models in which metallic iron is oxidized by water may be entertained. Second, volatiles dissolved in an early magma ocean may be the source of Earth's current atmosphere and hydrosphere, and thus would obviate the need for a late chondritic veneer for Earth's volatile budget.

References: [1] Delsemme A. (1997) in *Comets and the Origin and Evolution of Life* (P. J. Thomas et al., eds.), Springer-Verlag, New York, 296 pp. [2] Hayashi C. et al. (1979) *EPSL, 43,* 22–28. [3] Meier R. et al. (1998) *Science, 279,* 1707. [4] Jana D. and Walker D. (1999) *GCA,* in press [5] Righter K. and Drake M. J. (1999) *EPSL,* submitted. [6] Righter K. et al. (1997) *PEPI, 100,* 115–129. [7] Newsom (1995) in *Global Earth Physics: A Handbook of Physical Constants* (T. J. Ahrens, ed.), pp. 159–189, American Geophysical Union, Washington.

MICROMETER SCALE VARIATIONS OF δ^{18}O IN CORALS.

C. Rollion-Bard, M. Chaussidon[1], C. France-Lanord[1], and E. Bard[2], [1]Centre de Recherche Pétrographiques et Géochimiques–Centre National de la Recherche Scientifique, 15 rue Notre Dame des Pauvres, BP 20, 54 501 Vandoeuvre-lès-Nancy Cédex, France (rollion@crpg.cnrs-nancy.fr), [2]Centre Européen de Recherche et d'Enseignement de Géosciences de l'Environnement, Europôle de l'Arbois, BP 80, 13 545 Aix-en-Provence Cédex 4, France.

Introduction: Millimeter scale variations in trace-element ratios (Mg/Ca and Sr/Ca) and in isotopic ratios (δ^{11}B, δ^{13}C, and δ^{18}O) in reef corals have been intensively used as indicators of changes in environmental variables like temperature, pH, and composition of the seawater. The isotopic measurements are classically carried out by mass spectrometry after phosphoric acid digestion. In this study we report the development of combined analysis in marine biogenic carbonates of B-, C-, and O-isotopic compositions and Mg/Ca and Sr/Ca ratios using a large radius ims 1270 ion microprobe. This technique offers the advantage of a small spatial resolution on the order of 20 μm and enables the measurement of the different proxies (trace-element and isotopic ratios) in a single spot. The technique has been first developed on a sample of modern coral species *Porites* from New Caledonia.

Ion Probe Analysis: The Mg/Ca and Sr/Ca ratios and B-isotopic measurements are made using an O^- primary beam by counting the secondary positive ^{10}B, ^{11}B, ^{24}Mg, ^{40}Ca, and ^{88}Sr ions. The C- and O-isotopic measurements are made with a Cs^+ primary beam, by analyzing secondary negative ions (^{12}C, ^{13}C, ^{16}O, and ^{18}O) at a mass resolution of 5000 (e.g., 1579 is needed to separate ^{18}O and $H_2{}^{16}O$ and 2916 to separate ^{13}C and ^{12}CH). For δ^{18}O, secondary ions are counted on a faraday cup for ^{16}O (1.3×10^8 cps) during 4 s and on an electron multiplier for ^{18}O (2.6×10^5 cps) during 5 s in monocollection, and during 3 s for the both ions in multicollection with

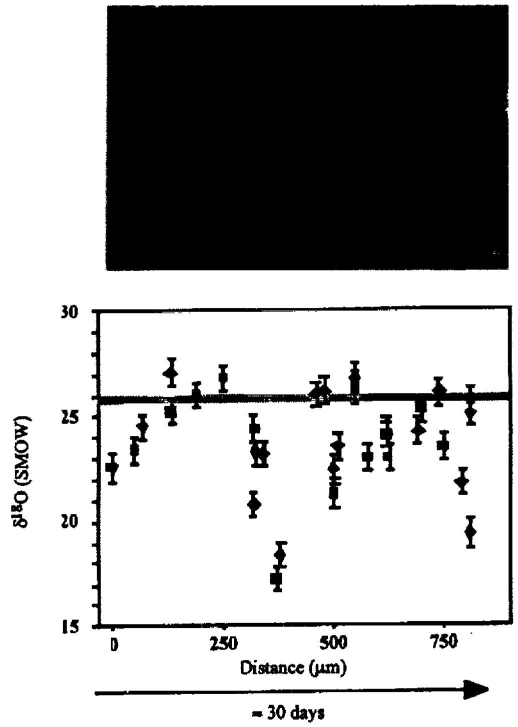

Fig. 1. Scanning electron microscopy picture of the fraction of the coral studied and graph of O-isotopic measurements vs. distance in micrometers. The blue and red curves correspond to two adjacent septa. The most ^{18}O-depleted values are observed on the synapticula linking the two septa. The gray section indicates the value obtained by conventional method.

~10^6 cps for ^{18}O. At present the measurement precision is on the order of ±0.4‰ in monocollection.

Results: Oxygen-isotopic measurements made by conventional method show variations of ~1‰. These variations correspond to 4°C variations of the temperature between 22° and 26°C using the equation of McConnaughey [1]. The first results in O with the ion probe show greater variations up to 10‰ over 100 μm (Fig. 1). These variations cannot be explained by variations in temperature (they correspond to an amplitude of 40°C). The data are depleted by 12.5‰ to 2.8‰ relative to inorganic aragonite in equilibrium with seawater at 24°C. Variations are linked to the structure with the more depleted values on the synapticula. So the bulk vital effect that is reported as 3.5‰ at 24°C for this species results from a highly heterogeneous distribution of $\delta^{18}O$ in the coral.

References: [1] McConnaughey T. (1989) *GCA, 53,* 151–162.

BORON-ISOTOPIC ANALYSIS IN SEDIMENTS BY ION MICROPROBE: IMPLICATIONS FOR WEATHERING AND THE OCEANIC BORON BUDGET.

E. F. Rose*, M. Chaussidon, and C. France-Lanord, Centre de Recherches Pétrographiques et Géochimiques–Centre National del la Recherche Scientifique, BP20, Vandoeuvre Cedex, France, (*present address: Mail Stop 23, Woods Hole Oceanographic Institution, Woods Hole MA 02543, USA; erose@whoi.edu).

Introduction: The B-isotopic system has been proposed to be a unique tracer of the paleo-pH of seawater because B speciation in water is very sensitive to pH variation [1]. One of the major B input to the ocean is by rivers. This study focuses on the different part of one of Earth most important erosion system: the Himalayan Range. The investigation of B-isotopic fractionation during continental weathering processes will provide new insights on B behavior during water/rock interactions and constraints the riverine B flux to the ocean. This is a major step in the understanding of what controls the geological record of $\delta^{11}B$ of the ocean [2].

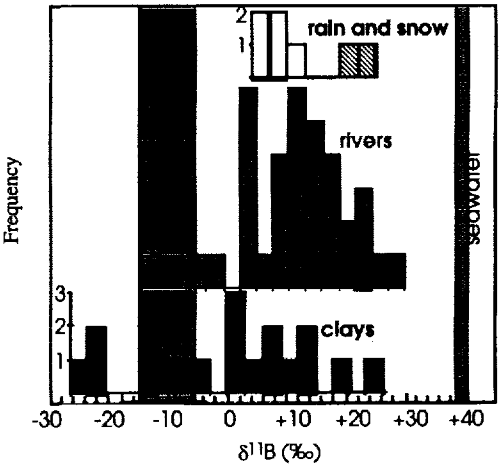

Fig. 1. Histogram displaying the B-isotopic variations of the Himalayan clay and river samples.

Method: Boron-11/boron-10 ratios were measured on river sediments (corresponding river samples were elsewhere [3]), and soil samples (clay fractions <0.1 μm and <2 μm) with the CRPG-CNRS ims3f ion microprobe that offers a high sensitivity for B analysis. A precision of ±1‰ on the $^{11}B/^{10}B$ ratio is demonstrated by repeated analyses of the B NBS951 standard and of seawater.

Results: $\delta^{11}B$ of Himalayan rivers range between –10‰ and +30‰ whereas $\delta^{11}B$ of weathering products (clays) range between –27‰ and +25‰ (Fig. 1). All samples are highly fractionated compared to the continental source rocks and most samples are shifted toward heavier $\delta^{11}B$.

The atmospheric B contribution to the rivers is negligible ($[B]_{average}$ = 0.15 μmol/L) as well as the "carbonate B" contribution (2 orders of magnitude less B in the river than what is predicted from carbonate dissolution). Therefore, after correction of the "evaporitic B," the dissolved B in rivers seems to be controlled by silicates alteration. A systematic enrichment in B concentration is noticed in silicate weathering products as compared to the source rock.

Discussion: The large variation of $\delta^{11}B$ in silicates can only be explained by changing conditions during the formation of the secondary minerals in soils. The B-isotopic system allows to discriminate between the conditions under which the clays form, either with variable water/rock ratios and/or variable pH. The lower $\delta^{11}B$ = –27‰ corresponding to the highest water/rock ratio of 50 (or to the lowest pH = 6.5), and the highest $\delta^{11}B$ = +24.3‰ corresponding to a water/rock = 4.5 (or to a pH = 7.7). Such variations are certainly favored by the particularly contrasted climate of the Nepalese region. Nevertheless a first observation of this B budget suffers from an obvious isotopic mass-balance problem that might be explained by what remains in soils during/after continental weathering processes.

The discharge of rivers to the ocean produces two antagonist effects on the $\delta^{11}B$ value of the ocean. It increases due to B adsorption on river particles [5] (particulate B) and decreases due to low $\delta^{11}B$ riverine input (dissolved B, Fig. 1). Because of their high particle load it seems that Himalayan rivers are the only rivers where these two processes balance. Taking into account a global average river discharge to the ocean [6], the effect of the dissolved B input overtakes the effect of particulate B input and the $\delta^{11}B$ value of the ocean is predicted to decrease over time to its modern value of 40‰. Therefore, we reach a situation where it needs to be understood what maintains the $\delta^{11}B$ of the ocean constant through geological time [2,4].

References: [1] Sanyal A. et al. (1996) *Paleoceanography, 11,* 513–517. [2] Palmer M. R. et al. (1998) *Science, 282,* 1468–1471. [3] Rose E. F. et al. (1999) *GCA,* in press. [4] Spivack A. J. et al. (1987) *GCA, 51,* 1939–1949. [5] Schwarcz H. P. et al. (1969) *EPSL, 6,* 1–5. [6] Lemarchand D. et al. (1999) *EUG X Conf. Abs.,* 579.

DEPOSITION AND STORAGE OF SPHEROIDAL CARBONACEOUS PARTICLES IN EUROPEAN MOUNTAIN LAKES AND THEIR CATCHMENTS.

N. L. Rose[1], E. Shilland[1], H. Yang[1], P. G. Appleby[2], T. Berg[3], L. Camarero[4], M. Gabathuler[5], K. Hanselmann[6], R. Harriman[7], K. Koinig[8], L. Lien[9], U. Nickus[10], B. Steiner Trad[11], E. Stuchlík[12], H. Thies[7], and M. Ventura[4], [1]Environmental Change Research Centre, University College London, 26 Bedford Way, London WC1H 0AP, UK, [2]Department of Mathematical Sciences, University of Liverpool, P.O. Box 147, Liverpool L69 3BX, UK, [3]Norwegian Institute for Air Research, P.O. Box 100, Instituttveien 18, N-2007 Kjeller, Norway, [4]Departament d'Ecologia, Fac. Biologia, Universitat de Barcelona, Diagonal 645, Barcelona 08028, Spain, [5]Atmosphärenphysik, HPP L 3.2, Eidgenössische Technische Hochschule Hönggerberg, CH-8093 Zürich, Switzerland, [6]Institute of Plant Biology/Microbiology, University of Zürich, Zollikerstrasse 107, CH-8008 Zurich, Switzerland, [7]Freshwater Fisheries Laboratory, SOAFD, Faskally, Pitlochry, Perthshire, Scotland, UK, [8]Institut für Zoologie and Limnologie, Leopold Franzens Universität Innsbruck, Technikerstrasse 25, A-6020 Innsbruck, Austria, [9]Norwegian Institute for Water Research, P.O. Box 173, Kjelsås, 0411 Oslo, Norway, [10]Institute of Meteorology and Geophysics, University of Innsbruck, Innrain 52, A-6020 Innsbruck, Austria, [11]Department of Chemistry, University of Bern, Freiestrasse 3, CH-3012 Bern, Switzerland, [12]Department of Hydrobiology, Charles University, Vinicna 7, CZ 128 44 Prague 2, Czech Republic.

Remote mountain lakes have no catchment influences and are among the most undisturbed and sensitive ecosytems in Europe. Consequently, they are especially useful as indicators of impacts from atmospheric deposition of pollutants. Spheroidal carbonaceous fly-ash particles (SCPs) are produced only from high-temperature combustion of fossil fuels. In mountain lake systems, they therefore provide an unambiguous indicator of atmospheric deposition and their temporal and spatial distributions are known to be well correlated to other atmospherically transported and deposited pollutants such as S, heavy metals (especially Hg and Pb) and polycyclic aromatic hydrocarbons (PAHs).

In order to compare depositional fluxes of SCPs between mountain areas experiencing a variety of depositional regimes, intensive sampling over a fifteen month period was undertaken at lake sites representing six mountainous regions across Europe as part of the EU funded research program "MOLAR." The selected sites were Øvre Neådalsvatn (mid-Norway), Gossenköllesee (Austrian Alps), Estany Redo (Spanish Pyrenees), Lochnagar (Cairngorms, Scotland), Starolesnienske Pleso (Slovakian Tatras), and Jorisee (Swiss Alps).

Bulk atmospheric deposition collectors were sampled regularly (weekly or fortnightly) in order that an annual estimate of SCP deposition per unit area could be calculated and an estimate of depositional episodicity could be made. In addition, at Redo, a comparison of SCP in wet, dry, and bulk deposition was made. Wet and dry deposition appeared to contribute similar numbers of SCP to this site over the sampling period. Atmospheric fluxes were compared with depositional fluxes to the sediments using deepwater sediment traps and radiometrically dated sediment cores. These, combined with soil core data, allowed estimates of sediment focusing to be determined at each of the sites as well as the relative amounts of storage within lake sediments and catchment soils. SCP inventories in the lake sediments were found to show a good correlation with inventories of Hg and Pb.

Atmospheric fluxes, sediment core and soil core SCP data all showed similar patterns, i.e., that the sites of highest contamination were Lochnagar, Starolesnienske Pleso, and Estany Redo with Gossenkollesee and Jorisee intermediate and Øvre Neådalsvatn the site of lowest contamination. A high proportion of the total accumulated SCPs were found to be stored in the catchment soils suggesting that significant soil erosion, possibly as a result of future climate change, could lead to the input of large quantities of SCPs and associated pollutants such as Hg, Pb, and PAHs to the lake ecosystem. The main source of SCPs to the lake is undoubtedly direct deposition to the lake surface, while movement of SCPs from the littoral to the deepwater areas is also established. Deposition at the sites was found to be episodic with elevated levels of SCPs showing a correlation with higher concentrations of acid ions in deposition, such as sulfate and nitrate.

CONTINENTAL CRUST AS A CONSEQUENCE OF COLLISION GEODYNAMICS: SOME PRECAMBRIAN AND PHANEROZOIC EXAMPLES.

O. M. Rosen[1] and V. S. Fedorovsky[2], [1]Institute of the Lithosphere, Staromonetny per., 22, Moscow 109180, Russia (roseno@ilsan.msk.ru), [2]Geological Institute, Pyzhevsky per., 7, Moscow 109017, Russia (west45@glasnet.ru)

Any initial crust-forming process such as island arc, active continental margin formation, etc., should finish with continental collision to form a recurrent supercontinent. The main petrologic mark of that collision is a granite melt generation. Three depth levels of granite process in collisional crust are demonstrated below.

The Siberian Craton appears to be a result of the amalgamation of Archean granulite-gneiss and granite-greenstone terranes (Fig. 1) joined together through collisional shear zones. That zones demonstrate two metamorphic events and granite generation at 1.9 and 1.8 Ga. The both are accompanied with the areal granulite grade metamorphic events in the terranes occurring nearby. That lower crust level of a collisional mountain building was cropped out at 1.65 Ga after erosion of the upper crust probably composed of granites come from the collisional shear zones above.

The upper crust granite layer, thickness of 10 km, crops out in the Caledonian collision system of the western Baikal region. It was formed under collisional thrusting of the Paleozoic island arc volcanic terranes. Granite subliquids substance together with granite veins formed cupolas under intralayer convection. The process ended in shear deformation and oblique thrusting onto the Siberian craton [1].

In the recent collisional thickened crust the granite melt layer of ~10-km thickness is situated at 10–15-km depth (Himalayas, Caucasus). The Caucasus collision is a result of underthrusting northwards of the Trans-Caucasian plate below the Scythian plate. The Tyrnauz granite, intruded into the the uppermost folded complex 10 km above the granite layer, came from the

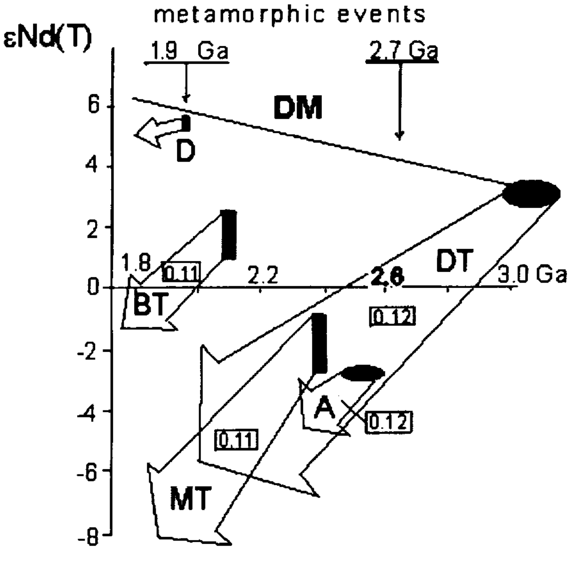

Fig. 1. Samarium-neodymium-isotopic evolution diagram for the northeastern Siberian Craton. DT, MT, BT = the Archean terranes, A = anorthosites, D = dolerite dike, and DM = depleted mantle. Numbers in quadrangles are averages of $^{147}Sm/^{144}Nd$ ratio. Black ovals = age determined by Sm-Nd whole-rock isochrone; black quadrangles = by another methods. "Metamorphic events" mark the collisional epochs.

TABLE 1. Chondrite normalized REE ratios of the Tyrnaus granite melt out modeling.

	Ce/Yb	Tb/Yb	Eu/Eu*
Source: Andes. crust [2]	4.1	1.2	0.88
Calculated melts out (%)			
5%	12.6	1.4	0.36
15%	10.8	1.4	0.40
30%	8.9	1.4	0.46
Tyrnauz granite melt	10.4	1.4	0.35
Calculated restites (%)			
95%	4.1	1.2	0.92
85%	3.6	1.2	1.00
70%	2.9	1.2	1.14
Restite: Lower crust [2]	2.7	1.1	1.07

15% partial melting of the Mesozoic island arc volcanics of the Trans-Caucasian plate probably of average andesitic composition. Separation of that granite is assumed to result to depletion of the source in the lower crust (Table 1).

Acknowledgments: This study is supported by RBRF grants 97-05-64463 and 99-05-68642.

References: [1] Fedorovsky V. S. (1997) *Geotectonics, 31,* 483–493. [2] Taylor S. R. and McLennan S. M. (1985) Blackwell, Cambridge, Mass., 312 pp.

SALT SEEPAGE INTO LAKE KINNERET, ISRAEL: CAN $\delta^{37}Cl$ HELP?

J. M. Rosenbaum[1], A. Nishri[2], M. Stiller[3], and M. Gophen[2], [1]University of Reading, Postgraduate Research Institute for Sedimentology, Whiteknights, Reading RG6 6AB, UK (j.rosenbaum@rdg.ac.uk), [2]Israel Oceanographic and Limnological Research Ltd., P.O. Box 345, Tiberias 14102, Israel, [3]Weitzmann Institute of Science, Environmental Sciences and Energy Research, P.O. Box 26, Rehovot, Israel.

Introduction: The threat of saltwater infiltration into freshwater aquifers is a problem of worldwide concern. We are developing a simple, quantitative approach to assess the mechanism and rate of brine infiltration into freshwater systems using a combination of chemical and stable isotope data. Our goal is to gain better knowledge of the mechanisms and rate of salt contamination of freshwater systems, a necessity before coherent remediation strategies can be chosen. We have chosen Lake Kinneret (Sea of Galilee) in northeastern Israel for our field test.

Background: Lake Kinneret provides 25% of the freshwater consumed annually in Israel. The lake overturns annually, and is surrounded by hot and cold springs with Cl concentrations up to 3300 ppm. The springs were diverted from the Lake in 1964, resulting in a continuous drop in salinity and Cl/Br ratio in the lake waters [1,2]. Previous studies have established that there is still at least one source of salt currently infiltrating the lake from below because lake salinity remains higher than that of its freshwater sources [2–6]. Data from sediment cores suggest that pore water/sediment reactions are negligible and show that strong gradients in Cl/Br ratios exist with depth in certain regions of the lake and are absent in others [1].

Methodology: We have undertaken a detailed chemical and Cl-O-H stable isotopic study of porewaters from two new ~3-m sediment cores from two different regions of the lake, historical lake waters dating back to 1968, porewaters from cores taken in 1979, and the surface springs in the region surrounding the lake. This work builds on the recent studies of Stiller [1,4,5], Nishri [2], Nativ [3,6], and coworkers, using the same samples previously analyzed wherever possible.

Preliminary Results: Our porewater analyses show measurable gradients in the major ions in solution. The two sediment cores display very different chemical trends with depth reflecting the difference in the waters underlying the sediments, e.g., Na/Cl increases in one core and decreases in the other. While some of the chemical trends can be attributed to a combination of advection and diffusion, porewater δD data is very complex and does not follow a regular pattern with depth suggesting water/sediment reactions are occurring. The pattern of the data for the historic lake samples suggests a major change in the source of Cl or mechanism of Cl introduction into the lake occurred between 1980 and 1982 (Fig. 1). The Cl-isotopic gradients in the porewaters show that brine input increases the isotope composition of the lake water (Fig. 1). The increase in the $\delta^{37}Cl$ value of the lake water over time suggests an increase in the relative importance of internal sources of salinity to the lake.

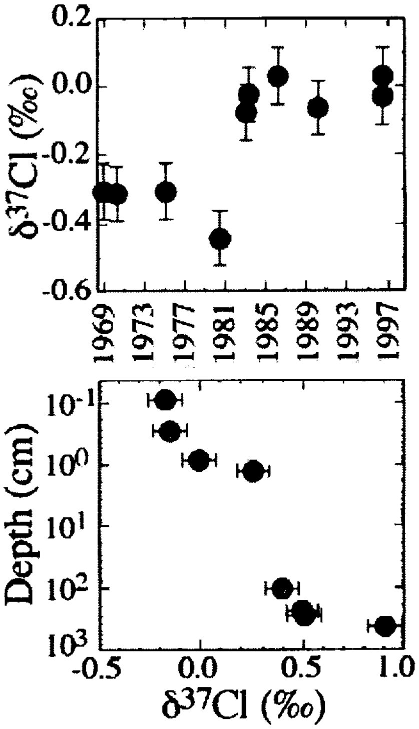

Fig. 1. For Kinneret lake waters (upper) and porewaters (lower) as a functions of time and depth. The lower panel is a composite profile of data from three cores.

Acknowledgments: This research is supported by the National Environmental Research Council grant GR9/03633 and the Israeli Water Commission.

References: [1] Stiller M. and Nissenbaum A. (1996) *Israel. J. Earth Sci., 45,* 153–160. [2] Nishri A. et al. (1999) *Chem. Geol.,* in press. [3] Bergelson G. et al. (1998) *Ground Water, 36,* 409–417. [4] Stiller M. et al. (1975) *EPSL, 25,* 297–304. [5] Stiller M. (1994) *Israel. J. Earth Sci., 43,* 179–185. [6] Bergelson G. et al. (1999) *Appl. Geochem., 14,* 91–118.

THE RESPONSE OF MARINE SEDIMENT BACTERIA TO ORGANIC CARBON INPUT.

R. Rosselló-Mora[1], B. Thamdrup[2], H. Schäfer[3], and R. Amann[1], [1]Max-Planck-Institute for Marine Microbiology, Bremen, Germany, [2]Institute of Biology, Odense University, Odense M, Denmark, [3]Netherlands Institute for Sea Research, Den Burg, The Netherlands.

Cyanobacterial biomass was added to anaerobic sediment of the Black Sea to simulate the natural input of complex organic substrate that occurs in nature after algae blooms. Sediments were incubated at 0°, 8°, and 15°C for 13 d. Metabolic changes were followed by the analysis of total C mineralization, sulfate reduction, and ammonium production rates. Microbial community dynamics were measured by several techniques of molecular biology applied to microbial ecology analyses (i.e., fluorescence *in situ* hybridization, FISH; denaturing gradient gel electrophoresis, DGGE; and sequencing of 16S rDNA PCR products). The addition of organic material resulted in significant changes in the composition of the microbial community at all temperatures tested. Sulfate reduction was the main mineralization process detected. However, fermentative organisms of the *Cytophaga-Flavobacterium* phylogenetic cluster showed to be the dominant fraction of active organisms. In the present communication we will show how the combination of both biogeochemical process measurements, and molecular microbial ecology analyses can improve our understanding of the function of the microbial communities in ecosystems like marine sediments. The main purpose of our presentation is to encourage the combined use of all these type of analyses, which may give a much accurate picture of what is really happening in natural environments.

QUANTIFYING ELEMENTAL SULFUR (S^0), BISULFIDE (HS^-), AND POLYSULFIDES (S_x^{2-}) USING A CYCLIC VOLTAMMETRY METHOD.

T. F. Rozan, S. M. Theberge, and G. W. Luther III, College of Marine Studies, University of Delaware, 700 Pilottown Road, Lewes DE 19958, USA (trozan@udel.edu; theberge@udel.edu; luther@udel.edu).

Introduction: Sulfur cycling is critical to our understanding of trace-metal cycling in marine and freshwater sediments. However, distinguishing the different S species is a complex and arduous undertaking [1]. Recent advancements using voltammetric methods have made possible the reliable and sensitive analysis of bisulfides (HS^-) and elemental S (S^0) [2]. Unfortunately, these methods are unable to differentiate between HS^- and S^0 and the intermediate polysulfide species (S_x^{2-}). Since polysulfides are involved with the formation of pyrite [3] and form strong complexes with class B metals [4,5], knowing the abundance of these species is an important step in our understanding in Fe and trace metal cycling.

The goal of this study was to develop a simple voltammetric method that could identify the different S species through the use of extremely high scan rates (>200 mV/s).

Methods: The voltammetric measurements were performed using an Analytical Instruments Systems Inc. Model DLK-100 voltammetric analyzer in conjunction with an EG&G Model 303A static Hg electrode in the hanging drop Hg electrode (HDME) mode. All solutions used an initial deposition step at −0.1 V for 5 s. After an additional 5-s quiet time, potentials were scanned between ±0.1 V with a vertex potential at −1.5 V.

To avoid any impurities, pure Na_2S_4 was prepared by the method of Rosen and Tegman except that premixing of the elemental S and sodium sulfide was found to improve the integrity of the product. The purity of the product was confirmed by X-Ray diffraction (XRD) and differential scanning colorimetry (DSC) analysis, and the products are typically >99% pure. Standard solutions of S^{2-} were made using A.C.S. reagent grade $Na_2S\ 9H_2O$ (Aldrich). Solutions of S^0 were prepared by dissolving 99.998% pure elemental S (Aldrich) in HPLC grade methanol. All laboratory prepared solutions were made with Milli-Q water that had been purged with N_2 for 1 h. The N_2 was first passed through a pyrocatechol trap, which lower O_2 concentrations $<0.2\ \mu M$.

Porewaters were measured *in situ* using microelectrodes [6]. The *in situ* method prevented any separation of HS^- and S^0, which is generally achieved upon acidification.

Results: Using scan rates >200 mV/s, in conjunction with an acid titration, HS^-, S^0, and S_x^{2-} were individually identified in both laboratory prepared solutions and natural porewaters from estuarine sediments.

Laboratory solutions were used to test the validity of high scan rates. In both single and multispecies solution different polysulfides were differentiated from HS^- and S^0. At high scan rates, the polysulfides gave two current peaks at different potentials. The reduction of the polysulfide from the Hg drop appears to be a two-step process: (1) breaking the Hg-S bond (reaction 1), and (2) reducing the S_4^{2-} to HS^- (reaction 2), resulting in the two current peaks

$$\text{Hg-S-S-S-S} + 2e^- \rightarrow \text{Hg} + S_4^{2-} \tag{1}$$

$$4H^+ + S_4^{2-} + 6e^- \rightarrow 4HS^- \tag{2}$$

Iron and NH_4^+ both can shift the second more negative current peak to more positive potentials eliminating peak separation. The NH_4^+ appears to provide a source of protons allowing the formation of HS^- to proceed more rapidly, while iron polysulfides appear to be less stable. At $NH_4^+ > 500\ \mu M$, no peak separation was observed. Iron polysulfides were observed to have peak separation of ~70 mV, which allowed species identification.

Porewaters collected from estuarine sediments were observed to follow a similar pattern. In the suboxic zone, only S^0 and iron polysulfides were observed. However, directly above the H_2S zone, porewaters were observed to have free polysulfides, iron polysulfides, and HS^-/S^0. This transition from the S^0 and iron polysulfides to H_2S occurred over a 1-cm interval.

References: [1] Luther G. W. III et al. (1985) *Limnol. Oceanogr., 30,* 727–736. [2] Wang F. et al. (1998) *Limnol. Oceanogr., 43,* 1353–1361. [3] Wilkin R. T. and Barnes H. L. (1996) *GCA, 60,* 4167–4179. [4] Thompson R. A. and Helz G. R. (1994) *GCA, 58,* 2971–2983. [5] Chadwell S. et al. (1999) *Aquatic Geochem.,* in press. [6] Luther G. W. III et al. (1998) *Limnol. Oceanogr., 43,* 325–333.

TRACE-ELEMENT CHARACTERIZATION OF METAMORPHIC ZIRCONS.

D. Rubatto[1], I. S. Williams, and D. Günther[2], [1]Research School of Earth Sciences, Australian National University, Canberra ACT 0200, Australia (daniela.rubatto@anu.edu.au), [2]Institut für Anorgansiche Chemie, Eidgenössische Technische Hochschule Zürich, Universitätsstrasse 6, CH-8092 Zürich, Switzerland.

Zircon is a mineral occurring in many magmatic and metamorphic rocks, that can be dated precisely by U-Pb. However, the correct interpretation of zircon U-Pb ages from metamorphic rocks is limited by the difficulty in relating zircon growth to metamorphic events. Zircon can record metamorphism by (1) overgrowth on detrital or inherited cores during high-temperature metamorphism and anatexis; (2) crystallization from a metamorphic fluid; or (3) recrystallization of a preexisting magmatic or detrital crystal during low-temperature, high-pressure metamorphism.

Zircon formed in these different metamorphic setting has been analyzed for trace elements (U, Th, and REE) using laser ablation inductively coupled plasma mass spectrometry (LA-ICP-MS) and ion microprobe (SHRIMP). Zircons from granulite grade metasediments of the Reynolds Range group (central Australia) have metamorphic rims that have overgrown detrital cores of magmatic origin. Metamorphic zircon rims have crystallized in both the leucosome and the metapelites. They have steep REE patterns with strong

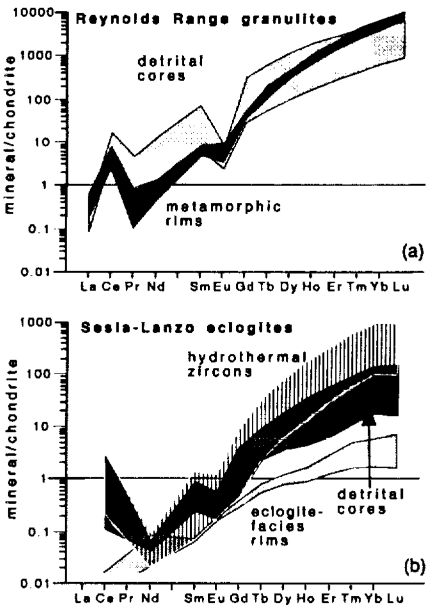

Fig. 1. Rare-earth-element patterns of zircons from (a) granulitic rocks of the Reynolds Range, and (b) eclogite-facies metasediments of the Sesia-Lanzo zone. Chondrite values according to [2].

enrichment in HREE, moderate negative Eu anomaly and strong positive Ce anomaly (Fig. 1a). The cores have more variable REE patterns, relatively flat in the HREE, with strong negative Eu anomaly and positive Ce anomaly. The metamorphic rims differ from the detrital cores also in having systematically lower Th/U ratios (<0.1). Similar REE concentrations and patterns of the zircon rims from the leucosomes and the metapelites suggest that both reached equilibrium with the melt. The negative Eu anomaly reflects the present of feldspar during zircon formation, whereas the strong enrichment in HREE documents the absence of garnet in the assemblage. Therefore, the zircon rims crystallized after the breakdown of white mica to form K-feldspar + sillimanite + melt.

An eclogite facies metasediment of the Sesia-Lanzo Zone (Western Alps) contains zircon with detrital magmatic cores surrounded by metamorphic rims with low Th/U ratios (<0.1). The detrital cores have higher U, Th, and REE contents than the rims and steeper REE patterns with strong negative Eu anomaly (Fig. 1b). On the other hand, the metamorphic zircon rims are characterized by extremely low contents in U, Th, and REE. Their REE patterns show only moderate enrichment in HREE, and no Eu anomaly. Flat REE patterns reflect the presence of garnet. The absence of Eu anomaly indicates zircon rim recrystallization after the high-pressure breakdown of plagioclase. These data demonstrate that the zircon rim formed during eclogite facies metamorphism.

Hydrothermal zircons from a metamorphic vein found within the eclogitic micaschist of the Sesia-Lanzo Zone are rich in U and REE and poor in Th (Th/U <0.1). Their REE patterns (Fig. 1b) indicate that they grew in equilibrium with feldspar and in the absence of garnet. This implies that the zircons crystallized prior to the formation of the present eclogite-facies assemblage, during prograde greenschist facies. This conclusion is supported by the U-Pb age of the zircons in the vein being 10 m.y. older than that of the zircon rims in the eclogitic micaschist [1].

In conclusion, low Th/U ratios characterize metamorphic zircon and distinctive REE patterns make it possible to link zircon formation with metamorphic stages. This correlation is the key to the precise dating of metamorphic events.

References: [1] Rubatto D. et al. (1999) *EPSL, 167,* 141–158. [2] Sun S. S. and McDonough W. F. (1989) *Geol. Surv Spec. Publ., 42,* 313–345.

EVIDENCE FOR A MAFIC, RUTILE-BEARING RESERVOIR IN THE EARTH.

R. L. Rudnick, M. Barth, W. F. McDonough, and I. Horn, Department of Earth and Planetary Sciences, Harvard University, 20 Oxford Street, Cambridge MA 02138, USA (rudnick@eps.harvard.edu).

Introduction: From a geochemical point of view, continental crust is generally assumed to be complementary to depleted mantle (DM or MORB source): elements depleted in the DM are enriched in the continental crust and visa versa. However, this does not hold for Nb and Ta, two refractory, lithophile, high-field strength elements, predicted to be in chondritic proportions to one another as well as to other refractory lithophile elements (e.g., REE) in the bulk silicate Earth. The Nb/La ratios in both the DM and the continental crust are subchondritic [1], as are their Nb/Ta ratios [2]. In addition, mass-balance calculations indicate that if the mass of DM represents 0.4 of the mass of the silicate Earth or greater (as the crustal abundances of many incompatible elements suggest), then there is a deficit of Al and Ca in the silicate portion of the Earth that is not accounted for by continental crust (Fig 1).

Nature of the Mafic Reservoir: These observations suggest that an additional reservoir exists in the silicate Earth, containing appreciable Ca and Al and high Nb/La and Nb/Ta. This reservoir must be intimately linked to formation of the continents and DM. Subducted oceanic crust fits these criteria. The mass of the mafic reservoir is best estimated from Al and Ca mass-balance arguments, which place it at anywhere between 1% and 7% of the mass of the bulk silicate Earth, depending upon the degree of depletion of the DM. This is on the order of the mass of oceanic crust that is likely to have been recycled through Earth history, assuming the present-day thickness, area, and recycling rates of oceanic crust extend through 3.5 Ga of Earth history.

Eclogite Compositions: In order to test this hypothesis, we have undertaken geochemical studies of samples that may derive from this reservoir. Although most subducted oceanic crust passes well beyond the reach of direct sampling by geologists, there is mounting evidence (primarily from stable isotopes) that eclogite xenoliths carried in kimberlites may be fragments of ocean floor that stranded (via collisional tectonics?) in the lithosphere of Archean cratons.

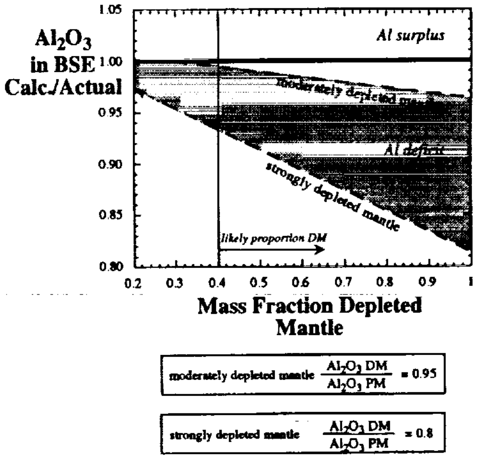

Fig. 1. Mass balance showing that an Al deficit exists in the silicate Earth if the fraction of the DM is 0.4 or greater. The amount of deficit depends on the degree of depletion of the DM. "DM" = depleted mantle, "PM" = primitive mantle, and "BSE" = bulk silicate Earth.

We have measured the Nb, Ta, and other lithophile and siderophile element contents of rutiles, ilmenites, garnets, and omphacites from eclogitic xenoliths from west Africa and Siberia by laser ablation inductively coupled plasma mass spectrometry (LA-ICP-MS). The oxide phases contain the majority of Nb and Ta in the whole rock, giving rise to high Nb/La in many of the reconstructed whole-rock compositions [3]. Most importantly, the Nb/Ta of the majority of eclogitic rutiles is super-chondritic; Nb/Ta ranges from 4 to 340, with a median of ~30 — approximately 2× the chondritic ratio. This contrasts with rutiles from continental crustal rocks, which have Nb/Ta between 6 and 39, with a median of 16 (i.e., chondritic). In addition, the eclogitic rutiles have significant W, Mo, and Sn abundances (median values of 8, 8, and 18 ppm respectively). Given a modal abundance of ~1%, rutile in eclogite, the mafic reservoir could hold 2–20% of the bulk silicate Earth budget of these elements.

Summary: The observations presented here suggest that a mafic, eclogitic reservoir, 1–7% by mass of the bulk silicate Earth, resides at deep levels within the Earth. The mass of this reservoir is on par with that of the continental lithospheric mantle, from which our xenolithic eclogites derive. The overall scarcity of eclgoites within the lithospheric mantle requires that the vast majority of recycled oceanic crust was transported to the convecting mantle. Our observations suggest that little of this mafic component has been remixed into the depleted mantle and therefore must reside as a distinct component in the deep Earth, perhaps at the core-mantle boundary.

References: [1] McDonough W. F. (1992) *Phil. Trans. R. Soc. London, 335,* 407–418. [2] Jochum et al. (1997) *Eos Trans. AGU, 78,* F805. [3] Barth M. et al., this volume.

ASSESSING REACTIVE SURFACE AREA DURING MICA DISSOLUTION WITH X-RAY PHOTOELECTRON SPECTROSCOPY AND REAL-TIME, *IN SITU* ATOMIC FORCE MICROSCOPY OBSERVATIONS.

E. Rufe and M. F. Hochella Jr., Department of Geological Sciences, Virginia Polytechnic Institute and State University, Blacksburg VA 24061, USA (erufe@vt.edu; hochella@vt.edu).

Introduction: Models describing the kinetics of water-rock interactions depend fundamentally on the measurement of surface area and its reaction variability. Yet this so-called "reactive surface area" remains an elusive parameter. This study combines atomic force microscopy (AFM) and X-ray photoelectron spectroscopy (XPS) to examine the relative reactivity of different mica surfaces during dissolution in acidic to circumneutral solutions.

Mica minerals are ideally suited for this study because surfaces with greatly varying reactivity can easily be identified. Dissolution of phyllosilicates is thought to be dominated by an edge attack mechanism, where cations are selectively removed from exposed (hk0) edges, while the (001) surfaces remain inert.

Materials and Methods: Samples of muscovite and phlogopite were cut to ~1 cm^2 and cleaved to reveal atomically smooth (001) surfaces. These samples were pre-etched by exposure to HF solution, creating shallow, crystallographically controlled etch pits. Phlogopite etch pits are triangular and bounded by (010) and (110) faces. Muscovite etch pits are irregularly shaped. Subsequent XPS and low-energy electron diffraction (LEED) analysis indicates that no significant compositional or structural alteration is induced by this pretreatment. Samples were imaged using a Digital Instruments Nanoscope IIIa atomic force microscope (AFM). *In situ* imaging was performed in solution in tapping mode AFM (TM-AFM) using oxide sharpened Si_3N_4 tips. *Ex situ* imaging was performed in air in contact mode using oxide sharpened tips, and in tapping mode using etched Si probes. X-ray photoelectron spectroscopy (XPS) spectra were collected using a Perkin-Elmer 5400 (PHI) X-ray photoelectron spectroscopy system, using non-monochromatic Al Kα radiation (hv = 1486.7 eV). Static charge referencing was performed relative to the adventitious C 1s photoline (BE = 284.6 eV) or the Au $4f_{7/2}$ photoline (BE = 84.0 eV) of Au deposited on the sample surface.

Results and Discussion: *In situ* and *ex situ* AFM observations reveal that dissolution of phlogopite and muscovite proceed by removal of material from (hk0) edges that form etch pit walls. New etch pits are not observed forming on mica (001) surfaces, attesting the inert nature of these surfaces. During phlogopite dissolution, step retreat of all (hk0) faces occurs at the same rate, suggesting these (010) and (110) faces have the same reactivities in this case. However, different muscovite (hk0) surfaces retreat at different rates, indicating the different muscovite edges have different reactivity in the range of conditions examined.

X-ray photoelectron spectroscopy analyses were performed on phlogopite samples reacted in pH 2 HCl solution and pH ~5.7 dd-H_2O for periods ranging from 4 to 132 h. Dissolution is characterized by a rapid reduction in the Mg/Si, Al/Si, and K/Si atomic ratios. These values reach maximum depletion in 24 h, then remain fairly constant with increased reaction time. Angle-resolved X-ray photoelectron spectroscopy (AR-XPS) measured surface compositions show the top ~20 Å of the (001) surface are enriched in Si and O, and severely depleted with respect to Al, Mg, and K. Long-term *in situ* AFM observations of phlogopite dissolution at pH 2 show the top sheet thickness increases from 10 Å to 18 Å between 39 h and 63 h, and then collapses to 12 Å between 87 h and 127 h. Analysis of photopeak shape and binding energy indicates the near surface of the sample undergoes structural alteration simultaneously with selective leaching of interlayer and octahedral cations. Silicon 2p and O 1s binding energies and full-width half-maximum (FWHM) show a progressive increase with increased reaction time. Additionally, Si 2p and O 1s binding energies increase from values typical of phyllosilicates to values typical of quartz and amorphous silica. These findings are consistent with the general model for leached layer development and suggest that the (001) surfaces of micas participate in the dissolution process during acid dissolution under these conditions.

Conclusions: The results of this study illustrate the heterogeneous nature of the reactivity of different mica surfaces during dissolution. Such variability probably applies to other silicate minerals as well. This suggests that microscopic characterization of silicates is necessary to determine the relative reactivity of different crystallographic faces with respect to overall dissolution flux.

Acknowledgments: Support for this research was provided by Petroleum Research Fund grants PRF-31598-AC2 and PRF-34326-AC2. The mineral samples were obtained from the Mineralogical Museum at Virginia Tech (phlogopite: HB-1246) and T. N. Solberg (muscovite).

OSMIUM CONCENTRATIONS AND ISOTOPIC COMPOSITION OF THE LOWER CRUST IN MEXICO.

J. Ruiz[1], J. T. Chesley, and K. Righter [2], Department of Geosciences, University of Arizona, Tucson AZ 85721, USA (jruiz@geo.arizona.edu), [2]Lunar and Planetary Laboratory, University of Arizona, Tucson AZ 85721, USA.

Introduction: Mexico represents an ideal area to study the composition of the lower crust since Proterozoic and Phanerozoic lower crust samples can be acquired through lower crustal xenoliths brought to the surface by Miocene or younger alkalic basalt, and exposed lower sections of Mesozoic accreted terranes..

Geology of Mexico: Mexico consists of a many terranes that were accreted at different in the Phanerozoic. The final assembly of the country occurred during the breakup of Pangea with the accretion of the Guerrero terrane, which is one of the largest juvenile terranes of the north American Cordillera. The other half of Mexico, approximately, is underlain by Proterozoic rocks of Grenville age. Exposures of these rocks are found in Oaxaca, southern Mexico and Tamaulipas, northern Mexico. These exposures consist of granulite-facies para- and orthogneisses with peak metamorphic pressures of ~8 kbar and temperatures of ~750°C. Lower crustal xenoliths in central Mexico include two-pyroxene, pyroxene-plagioclase, and pelitic granulites. The metapelites consist of garnet, quartz, feldspar, and pyroxene. The lower crustal xenoliths in general yield slightly higher pressures and temperatures than the exposed granulite massifs. The model Nd ages for the exposed granulites ranges between 1.3 and 1.6 Ga. Lower crustal xenoliths also yield predominantly 1.5-Ga model ages, but some samples report younger model ages.

In the accreted terranes of western Mexico, the lower crust consists of basalt with mid-ocean ridge chemical characteristics overlain by metamorphosed, recycled Proterozoic sediments. Above the metasedimentary rocks lies a thick sequence of calc-alkalic andesitess. The model Nd ages for the metasediments is also ~1.5 Ga. All other lithologies have juvenile Nd-isotopic values.

Osmium Isotopes: The present day $^{187}Os/^{188}Os$ ratios of the measured lower crustal metasedimentary and granulite lithologies from both accreted terranes and in nuclear Mexico range between 0.5 and 1.0. The metabasalt of the accreted terranes have $^{187}Os/^{188}Os$ values between 1 and 2. The Os concentration of all lower crustal lithologies ranges between 10–70 ppt. Upper crustal granitoids have $^{187}Os/^{188}Os$ between 0.8 and 1.2 with Os concentrations between 1–3 ppt. The data presented here indicate that the lower crust has higher Os concentrations than previously thought and that it can be relatively unradiogenic. These data also indicate that the lower crust is a more likely contaminant in the evolution of mantle-derived magmas than previously believed.

MODERN FORMATION PROCESSES FOR FOSSIL BRINES IN THE GREAT AUSTRALIAN BIGHT.

J. L. Russell and the ODP Leg 182 Shipboard Science Party, Scripps Institution of Oceanography, 9500 Gilman Drive, La Jolla CA 92093-0208, USA.

Through an accident of geography and meteorology, the physical oceanography of the South Australian Shelf contributes to the formation of very dense, high-salinity water. The longshore wind pattern on the continental shelf also produces a series of convergences and divergences of mass which are quasi-permanent features. The resulting geostrophic onshelf and offshelf transports extend into the deep ocean as coastal waves. These mass exchanges with the open ocean include an important contribution from the high-salinity outflow water produced through excess evaporation near the Eyre Peninsula. This shelf circulation pattern may explain the formation and transport of brines in the carbonate banks of the South Australian Shelf. We will present hydrographic data and analyses of porewater from sediment cores obtained during ODP Leg 182.

MAJOR- AND TRACE-ELEMENT ABUNDANCE DATA IN THE CIRCA 2.2-Ga HEKPOORT PALEOSOL.

R. Rye, Mail Code 170-25, Geological and Planetary Sciences Division, California Institute of Technology, Pasadena CA 91125, USA (rye@gps.caltech.edu).

The Hekpoort paleosol has long been interpreted to be a regional paleoweathering profile developed on ~2.2-Ga basaltic andesite lavas at the top of the Hekpoort Formation of the Pretoria group, Transvaal supergroup, South Africa [1]. In five separate profiles, from outcrops along road cuts near Waterval Onder and the Daspoort Tunnel and in three drill cores from the Bank Break area (BB3, BB8, and BB14), the top of the paleosol is a sericite-rich zone. The sericite zone grades downward into a chlorite-rich zone. In core BB8 and in the road cut at the Daspoort Tunnel we sampled the underlying or parent basaltic andesite into which the chlorite zone grades. We did not obtain samples of the parent material at Waterval Onder and in cores BB3 and BB14, but chemical analyses indicate that the chlorite and sericite zones in these profiles derive from underlying lavas similar to the ones we sampled in core BB8 and at the Daspoort Tunnel. The presence of rip-up clasts of the paleosol in the overlying ironstones of the Strubenkop Formation in the cores from Bank Break rule out the notion that most of the alteration was a result of interactions with hydrothermal fluids. Desiccation cracks at the top of the paleosol that were filled with sand during the deposition of the overlying sediments at Waterval Onder point to a subaerial weathering origin.

Aluminum, Ti, Zr, Cr, and V were apparently immobile during weathering and all subsequent alteration. We have calculated retention factors for these elements in each profile, assuming that Al was perfectly immobile. In core BB8, which is the most complete profile we have, our calculations indicate that between 95 and 100% of the Ti, Zr, Cr, and V were retained in the soil profile. Thus, there was no significant loss of any of these elements from the soil as a whole. The coefficients of variation of Ti/Al, Zr/Al, Cr/Al, and V/Al are all very low with each soil profile, indicating that the elements were not significantly redistributed within the soil. Aluminum, Ti, Zr, and Cr are typically immobile during weathering. Vanadium is somewhat mobile during aerobic weathering and its retention indicates that atmospheric O levels were low when the Hekpoort paleosol formed.

The vertical distribution of Fe, Mg, Mn, Ni, and Co indicates that these elements were largely removed from the top of the soil during weathering. The values of the ratios Fe/Al, Mg/Al, Mn/Al, Ni/Al, and Co/Al in some samples at or near the top of the soil fall below 10% of the value of these ratios in the parent material. However, the retention factors for Fe (0.3–1.0), Mg (0.1–0.5), Mn (0.3–0.9), Co (0.2–1.0), and Ni (0.8–1.3) indicate that a significant fraction of the complement of these elements was lost from the top subsequently reprecipitated in the lower portions of the soil.

Previous work indicated that the distribution of Fe and Mg in chlorites in the Hekpoort paleosol were consistent with the formation of pedogenic Fe^{2+}-rich smectite rather than pedogenic $FeCO_3$ in the lower portions of this soil [2]. Divalent cations such as Mn^{2+}, Ni^{2+}, and Co^{2+} would readily substitute into such a smectite.

The distribution of Fe^{2+} should be best preserved in core samples, which have not been subjected to modern, O-rich weathering. The molar ratio Ni^{2+}/Fe^{2+} is typically highest near the top of the Bank Break core profiles. This ratio decreases with increasing depth until its value is similar to that found in the parent material. Co^{2+}/Fe^{2+} is generally fairly constant. Mn^{2+}/Fe^{2+} generally increases toward the bottom of the profiles as does the ratio Mg^{2+}/Fe^{2+}. The variations in these molar ratios are inconsistent with the wholesale introduction of these elements by a hydrothermal solution since the composition of such a fluid was probably uniform over the length scale of each of these profiles. Experimental data on the distribution of divalent cations between solution and a trioctahedral smectite [3] indicate that the present distribution of these divalent cations is best interpreted as resulting from their release during weathering and subsequent reprecipitation as constituents of pedogenic smectite.

The precipitation of pedogenic smectite rather than siderite indicates that atmospheric pCO_2 was less than 2×10^{-2} atm when the Hekpoort paleosol formed. At this CO_2 level, the loss of Fe from the top of the profile during weathering indicates that weathering occurred with atmospheric $pO_2 < 8 \times 10^{-4}$.

References: [1] Button A. and Tyler N. (1981) *Econ. Geol. 75th Anniv. Vol.*, 686–709. [2] Rye et al. (1995) *Nature, 378,* 603–605. [3] Decarreau A. (1985) *GCA, 49,* 1537–1544.

AMMONIUM PARTITIONING AND NITROGEN-ISOTOPIC FRACTIONATION DURING HIGH-TEMPERATURE METAMORPHIC FLUID-ROCK INTERACTIONS.

S. J. Sadofsky and G. E. Bebout, Department of Earth and Environmental Sciences, Lehigh University, 31 Williams Drive, Bethlehem PA 18015, USA (sjs8@lehigh.edu).

Introduction: Despite recent advances in N-isotopic geochemistry, our understanding of the behavior of this element in the solid earth remains limited by a lack of fundamental information regarding the partitioning of ammonium and isotopic fractionation of N among coexisting mineral phases and fluids. Study of N behavior in regionally metamorphosed rocks provides the opportunity to assess intermineral NH_4^+ partitioning and N-isotopic fractionation among coexisting micas during medium-P/T metamorphism and also allows the use of N as a tracer of fluid-rock interactions. Two studies of N behavior in metamorphic environments evaluate the utility of the N-isotopic system in understanding metamorphic processes. The outcrop at Townshend Dam, Vermont, provides a continuous section of amphibolite facies metamorphic rocks of varied protoliths [i.e., 1,2], allowing examination of both intermineral N-behavior and preservation vs. homogenization of N content and $\delta^{15}N$ across-strike on a relatively small scale. Metamorphic rocks from western Maine allow examination of the effect of varying peak metamorphic conditions [i.e., 3] on intermineral N partitioning and isotopic fractionation in pelitic rocks.

Techniques: Nitrogen was prepared for isotopic analysis by a sealed quartz tube technique (modified from [4,5]). The temperature required for full and rapid extraction of N from biotite and white mica mineral separates is ~1200°C. Samples were then analyzed by standard stable isotope methods in a viscous flow dual inlet mass spectrometer. Blanks for this technique are #0.025 µmol N_2, and 1σ (for $n = 2–6$) is <0.15‰ for replicates of N-rich mica separates.

Results: Mica samples from Townshend Dam show significant variability in $\delta^{15}N_{air}$ (3.3–11.9‰) and N content (9–1270 ppm) across the strike of the dominant foliation. Samples with coexisting biotite and white mica have similar, but somewhat variable, $\delta^{15}N$ values (21 biotite-white mica pairs, mean difference = 0.4‰, range –0.9‰ to +2.7‰). In rocks with two micas, white mica on average contains 0.47× as much N as biotite; consistent with the results of other studies of intermineral NH_4^+ partitioning in schists, gneisses, and granites [6–8]. Biotite in biotite-ankerite-quartz veins contains significant N (302–1270 ppm) with $\delta^{15}N$ values similar to adjacent rocks. Organic C content and $\delta^{13}C$ were analyzed for a subset of samples from Townshend Dam to attempt to explain the large range in $\delta^{15}N$ within a single formation. An inverse correlation of $\delta^{13}C$ and $\delta^{15}N$ suggests that if CO_2 and N_2 were the dominant C- and N-bearing fluid species, then varying extents of devolatilization may explain at least some of this within-formation range in $\delta^{15}N$ [cf., 9].

Samples from western Maine ranging in grade from garnet to K-feldspar + sillimanite contain 264–1820 ppm N in biotite and 170–773 ppm in muscovite. $\delta^{15}N_{air}$ ranges from 4.1‰ to 8.9‰ and is very similar in coexisting micas (7 pairs). Muscovite contains ~0.45× as much N as biotite on average.

Discussion: There appears to be no N-isotopic fractionation among micas that have reached amphibolite grade or higher temperatures and ammonium partitions systematically between biotite and white mica. However, there is significant scatter in $\Delta^{15}N_{biotite\text{-}white\ mica}$ at Townshend Dam and in ammonium partitioning in rocks from both localities. Several possible reasons for the variation in N behavior in coexisting minerals have been investigated, including varying white mica mineralogy (muscovite vs. paragonite) and unit cell dimension, and differential closure relationships during cooling. The samples from Townshend Dam most unlike the mean in both $\Delta^{15}N$ and ammonium partitioning contain more chlorite (chl/chl + btt >0.4); thus retrograde replacement of biotite by chlorite may have been accompanied by some fluid-mineral N exchange. The variability of intermineral ammonium partitioning ($N_{white\ mica}/N_{biotite}$) appears to be a compound effect of several factors: the chlorite content of the rock likely plays a role (as above); and samples with paragonite, or N-rich muscovite, are more variable in partitioning at Townshend Dam. Rocks from western Maine show less variability in ammonium partitioning than rocks from Townshend Dam, with some of the outlying data corresponding to greater chlorite content.

Overall, the variations in $\delta^{15}N$ of these two suites differ significantly. At Townshend Dam the rocks experienced uniform metamorphic P-T conditions, but there is extreme variability in $\delta^{15}N$ (probably related to protolith heterogeneity). Despite the abundance of N in metamorphic fluids (evidenced by abundant N in vein biotite), these rocks have not been homogenized with respect to $\delta^{15}N$ or N content. In western Maine, all rocks contain abundant N; a general trend of higher $\delta^{15}N$ and lower N content with higher grade is consistent with the expected effects of devolatilization.

References: [1] Chamberlain C. P. and Conrad M. (1993) *GCA, 57,* 2613–2629. [2] Kohn M. and Valley J. (1994) *GCA, 58,* 5551–5566. [3] Guidotti C. V. and Holdaway M. J. (1993) *GSA Guidebook, 2,* L1–L26. [4] Bebout G. E. and Fogel M. L. (1992) *GCA, 56,* 2839–2849. [5] Bebout G. E. (1997) *EPSL, 151,* 77–95. [6] Honma H. and Itihara Y. (1981) *GCA,* *45*, 983–988. [7] Duit W. et al. (1986) *Am. J. Sci., 286*, 702–732. [8] Boyd S. R. and Philippot P. (1998) *Chem. Geol., 137*, 57–66. [9] Bebout G. E. et al. (1999) *Am. Mineral.*, in press.

QUANTUM CHEMICAL MODEL FOR APATITE BIOMINERLIZATION ON SILICA BIOCERAMICS.

N. Sahai and J. A. Tossell, Department of Chemistry and Biochemistry, University of Maryland, College Park, MD 20742, USA (nsahai@glue.umd.edu).

Introduction: Silicon is considered to be an essential trace element for normal bone development [1,2]. Bioactive silica ceramics are used as prosthetic bone and dental implants because they promote *in vivo* biomineralization of apatite [$Ca_5(PO_4)_3OH$], as well as *in vitro* mineralization when immersed in simulated body fluid of composition similar to human blood plasma. Apatite formation occurs in stages but earlier studies disagree on the reaction sequence, summarized here as:

Scheme 1 [3]

$[>SiO^{-1}]_n + M^{+2} + H_mPO_4^{m-3} \rightarrow$ Stage I

$\{[>SiO]_n - OPO_3H_m\}^{m-n^{-3}} + M^{+2} \rightarrow$ Stage II

$\{[>SiO]_n - OPO_3H_m - M\}^{m-n^{-1}}$ Stage III

vs.

Scheme 2 [4]

$[>SiO^{-1}]_n + M^{+2} + H_mPO_4^{m-3} \rightarrow$ Stage 1

$\{[>SiO]_n - M^{-n+2}\} + H_mPO_4^{m-3} \rightarrow$ Stage 2

$\{[>SiO^{-1}]_n - M^{+2} - OPO_3H_m^{m-n^{-1}}\}$ Stage 3

where $[>SiO^{-1}]_n$ is a symbolic representation of a surface-bound, deprotonated silanol group, and m = 1,2.

Method: We used *ab initio* Hartree Fock theory to distinguish between these two proposed reaction sequences. We examined apatite biomineralization via the interactions of alkaline-earth metal ions ($M^{+2} = Ca^{+2}$, Mg^{+2}), $H_mPO_4^{m-3}$, and H_2O at model bioceramic surfaces. The silica surface was represented at different protonation levels by fully protonated [$(Si_3O_6H_6)$], partially protonated [$(Si_3O_6H_5)^{-1}$] and fully deprotonated [$(Si_3O_6H_3)^{-3}$] rings. Solvation and cluster-size effects were considered. Energies were calculated using effective core potentials and ^{29}Si, ^{31}P nuclear magnetic resonance (NMR) shieldings were obtained at the 3–21-G* level.

Results and Conclusions: Comparison of theoretical reaction energies and NMR shielding trends with experimental NMR trends suggests the formation of [$(SiO^{-1})^n - M^{+2} - OPO_3H^{-2}$] clusters consistent with scheme 2. Direct Si-O-P bonds (scheme 1) are unlikely. Energetic preference of Mg^{+2} over Ca^{+2} at each stage explains the observed inhibition of apatite precipitation by Mg^{+2}. At high pH, the monodentate attachment of HPO_4^{-2} to the sorbed cation at the fully deprotonated silica surface is favored whereas bidentate attachment of HPO_4^{-2} or $H_2PO_4^{-1}$ is favored at low pHs. The bidentate geometry of the surface cluster is similar to the local geometry of brushite ($CaHPO_4\ 2H_2O$). The results of this study indicate that quantum chemical molecular orbital calculations provide a previously under-exploited method for exploring reaction mechanisms and energetics of biomineralization.

References: [1] Carlisle E. M. (1986) in *Silicon Biochemistry*, Wiley, Chichester. [2] Birchall J. D. and Espie A. W. (1986) in *Silicon Biochemistry*, Wiley, Chichester. [3] Hench L. L. (1990) *Bioceramics, 3*, 43–45. [4] Hayakawa S. et al. (1996) *Phys. Chem. Glasses, 37*, 188–192.

GREENSTONE-GRANITE BELTS OF THE HEARNE DOMAIN, NUNAVUT, CANADA: EVOLUTION OF JUVENILE NEOARCHEAN OCEANIC CRUST.

H. A. Sandeman[1], B. Cousens[2], W. J. Davis[1], S. Hanmer[1], T. Peterson[1], J. Ryan[1], and S. Tella[1], [1]Geological Survey of Canada, 601 Booth Street, Ottawa ON, K1A 0E8, Canada (hsandema@nrcan.gc.ca), [2]Ottawa-Carleton Geoscience Center, Carleton University, 1125 Colonel By Drive, Ottawa ON, K1S 5B6, Canada.

The western Churchill Province of the northwest Canadian Shield contains some of the least studied yet areally extensive greenstone belts in North America. In the Hearne domain, these belts encompass over 68,000 km^2 and contain a number of significant Au deposits and base metal prospects. Previous bedrock mapping, together with more recent geochronological and geochemical investigations, has significantly enhanced the knowledge base for this region. Broadly temporally equivalent (2680–2710 Ma), generally northeast-trending greenstone belts in different areas have distinct geochemical traits but, on the basis of Sm-Nd-isotopic analyses (n = 66), are interpreted as being predominantly juvenile in character. The central and northeast belts record three distinct types of basaltic to andesitic volcanism. In volumetric order these are as follows: type 1 basalts having flat, extended incompatible element (~6H primitive mantle) patterns lacking negative HFSE anomalies; type 2, Th, and LREE-enriched basalts to andesites with negative HFSE anomalies and; type 3 basalts to basaltic andesites with convex-upward patterns culminating in La, Ce, and Nb. In the north and northwest belts type 3 rocks are absent. The northwest belt contains rocks of types 1 and 2, whereas the northern belt has rocks of type 1 and basalts that are incompatible element depleted with variably developed negative HFSE anomalies. The central and northeast belts also contain widespread intermediate to felsic tuff horizons intercalated with the predominant mafic volcanic rocks. Along the western margin of the Hearne domain, abundant type 1 basalts are intercalated with tholeiitic intermediate to silicic volcanic rocks having Th and LREE-enriched extended incompatible element patterns with negative HFSE anomalies. Overall, the rocks exhibit ε_{Nd_t} values (ranging from +4.0 to –1.0) that show a strong negative covariation with SiO_2, implying contamination from significantly older, MesoArchean crust.

Slightly younger (~2691–2679 Ma), I-type, arc-related plutonic rocks intruded the supracrustal packages throughout the Hearne domain. These granitoids have TTG geochemical characteristics, negatively-sloped extended trace element patterns with prominent negative Nb and Ta anomalies, depleted HREE abundances and mantle-like ε_{Nd_t} values (2.3: n = 20). The TTG rocks were accompanied by locally abundant dacitic to rhyolitic volcanic and volcaniclastic rocks including proximal flow-banded and autobrecciated rhyolites, crystal and lapilli tuffs, agglomerate and volcanic conglomerate. These volcanic rocks include a variety of geochemical types, the majority of which have whole-rock and Nd-isotopic compositions comparable to the volumetrically dominant TTG plutons.

A preponderance of mantlelike ε_{Nd_t} values and the absence of inherited zircons in all geochronological specimens (except from the southwest belt) indicates that the majority of the Hearne domain represents a block of juvenile, Neoarchean oceanic crust. Many recent investigations of Archean greenstone belts have ascribed an oceanic plateau model for their development, predominantly on the basis of geochemical arguments. Picritic and komatiitic rocks, common constituents of oceanic plateaux, are quite rare in the Hearne domain. Felsic to intermediate tuffs and pelitic and chemical sedimentary rocks (BIF) are widespread and are interbedded with the all of the observed types of mafic to intermediate lavas. These field observations imply that these belts record critical features that are incompatible with an oceanic plateau setting. The geological, geochronological, and geochemical data support development of the greenstone belts in intraoceanic island arc and back arc settings rather than as an oceanic plateau. The observed crustal contamination of supracrustal rocks in the southwestern belt implies that the western margin of the Hearne domain probably developed near older continental crust.

RHENIUM AND OSMIUM SYSTEM IN OPHIOLITIC COMPLEXES: IMPLICATIONS FOR CHROMITITE FORMATION AND OPHIOLITE PARAGENESIS.

R. A. Santos[1], K. Suzuki[2], B. Takano[1], Y. Tatsumi[2], Y. Miyata[3], and Y. Nozaki[3], [1]Department of Systems Sciences, Graduate School of Arts and Sciences, University of Tokyo, 3-8-1 Komaba, Meguro-ku, Tokyo 153, Japan (crsantos@komaba.ecc.u-tokyo.ac.jp), [2]Institute for Geothermal Sciences, Graduate School of Science, Kyoto University, Noguchibaru, Beppu, Oita 874-0903, Japan, [3]Ocean Research Institute, University of Tokyo, Japan.

Abstract: Ultramafic rocks and some chromitites from two Philippine Ophiolite complexes, the Palawan and Dinagat ophiolite complexes, have been analyzed for Re- and Os-isotopic composition. Both complexes host chromitite pods and layers of economic quantities and are hosted by depleted mantle rocks (harzburgite) with dunite selvage. Lenses of dunite in harzburgite are discernible in both complexes and apparently increases in frequency as major zones of chromitite deposits are approached.

Prior to the use of the Carius tube digestion technique in the isotope dilution methodology, two other digestion steps were taken into consideration: the microwave digestion and the fire-assay techniques. The former has the advantages of optimum homogenization of spikes in the sample and of faster digestion time, whereas the latter is efficient in the recovery of Os (and the platinum group elements) but poor in Re recovery. The Carius tube technique with single-bead separation procedure is found to have the lowest blank contribution. Duplicate analysis of SARM7 standard rock is at the level of 98%.

The $^{187}Os/^{188}Os$ ratios of chromitite samples yield present-day values that are supra-chondritic (0.1304–0.1570) whereas harzburgite at some distance from the chromitite zone have ratios mainly of subchondritic to chondritic (0.1197–0.1273) level. Regressing these ratios based on the chromitite isochron resulted in values suggestive of extensive melt depletion of the peridotite hosts. The chromitite Os ratios are suggestive of radiogenic Os introduction into the chromitite-producing system. An apparent "chromatographic effect" on $^{187}Os/^{188}Os$ ratios was delineated on samples proximal to chromitite and pyroxenite zones. These samples yield values (0.1325–0.1730) that are suggestive of radiogenic Os enrichment.

The chromitites in both complexes are generally Cr-rich (Cr# >68) though minor layers of chromitites are at the level of 55–60 (Cr#). Inclusion mineralogy and geochemistry show the dominance of pargasite and diopside with relative enrichment in Na, K, and Ti in comparison with those in the peridotite matrix. Whole-rock REEs of the chromitites revealed relative enrichment compared to the peridotite host.

The Os and Re systematics in combination with the peridotite and chromitite mineralogy and chemistry suggest for the possible formation of the Palawan and Dinagat ophiolite complexes in a supra-subduction setting. Chromitite formation might have resulted from the interaction of fluid-enriched melt derived from the dehydration of a subducting slab with depleted upper-mantle rocks.

References: [1] Shirey S. and Walker R. (1998) *Annu. Rev. Earth Planet. Sci., 26,* 423–500. [2] Brandon A. et al. (1996) *Science, 272,* 861–864.

SEAWATER pH CONTROL ON THE BORON-ISOTOPIC COMPOSITION OF CALCITE: INORGANIC COPRECIPITATION EXPERIMENTS.

A. Sanyal[1,2], M. Nugent[3], R. J. Reeder[3], and J. Bijima[1], [1]Alfred Wegener Institute for Polar and Marine Research, Bremerhaven, Germany, [2]Lamont Doherty Earth Observatory, Columbia University, Palisades NY, USA, [3]Department of Geosciences, State University of New York–Stony Brook, Stony Brook NY 11794-2100, USA.

The pH control on B-isotopic systematics in seawater has raised interest in using the foraminiferal record from marine sediments as a proxy for paleo-pH determination of seawater. Previous experiments [1] based on laboratory-cultured foraminifera suggested that some species exert a biogenic (vital) effect on B-isotopic fractionation with seawater. To provide a basis for comparison of the pH dependence of B-isotopic fractionation in biogenic systems, we have determined the isotopic composition of B coprecipitated with calcite grown inorganically using the pH-stat method. Growth was carried out in synthetic, Mg-free seawater solutions at room temperature, in which pH was adjusted to the desired value (7.9, 8.3, and 8.6); B-free calcite was used as seed material. The $^{11}B/^{10}B$ ratios were determined by negative thermal ionization mass spectrometry (NTIMS).

The results show a systematic increase in $\delta^{11}B$ values of the calcite with increasing pH of the solution, from ~–19.1‰ at pH 7.9 to –13.7‰ at pH 8.6. The curve through these values (Fig. 1) closely parallels the calculated isotopic composition of the aqueous $B(OH)_4^-$ species in seawater [2], but is offset below it by 2–3‰. The similarity of these trends supports earlier conclusions [3] that $B(OH)_4^-$ is the dominant species incorporated into the calcite, although the cause of the offset remains unclear.

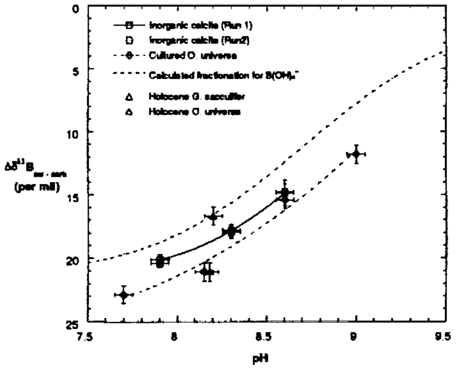

Fig. 1.

The $\delta^{11}B$ vs. pH curve for our inorganic calcites lies ~1‰ above the corresponding curve previously determined for cultured *O. universa* [1]. This suggests a slight biogenic (vital) effect on the B-isotopic fractionation between seawater and *O. universa*. Despite such a biogenic influence, the results indicate a comparable variation in $\delta^{11}B$ with pH for inorganic and foraminiferal calcite. This finding supports the use of this isotopic system in foraminifera as a reliable proxy for paleo-pH of seawater.

References: [1] Sanyal et al. (1996) *Paleoceanography, 11,* 513–517. [2] Kakihana et al. (1977) *Bull. Chem. Soc. Japan, 50,* 158–163. [3] Hemming N. G. and Hanson G. N. (1992) *GCA.*

COMPOUND-SPECIFIC HYDROGEN-ISOTOPIC MEASUREMENTS OF LACUSTRINE ORGANIC MATTER: A NOVEL TOOL FOR PALEOCLIMATOLOGY.

P. E. Sauer[1], J. M. Hayes[1], T. I. Eglinton[2], A. L. Sessions[3], and A. Schimmelmann[3], [1]Department of Geology and Geophysics, Woods Hole Oceanographic Institution, Woods Hole MA 02543, USA (psauer@whoi.edu), [2]Department of Marine Chemistry and Geochemistry, Woods Hole Oceanographic Institution, Woods Hole MA 02543, USA, [3]Department of Geological Sciences, Indiana University, Bloomington IN 47405, USA.

Introduction: We are investigating stable isotopic ratios of H (D/H) in sedimentary organic material as a new tool for paleoclimatic research. Stable isotopic ratios in precipitation (D/H and $^{18}O/^{16}O$) are established paleoclimate indicators in many parts of the world, correlating with climatic variables such as mean annual temperature or precipitation amounts [1]. Although paleoclimate records have been generated by isotopic analyses of ice cores, tree-rings, or carbonate in lake sediments and cave deposits, there remain many regions that lack material appropriate for these methods. In lake sediments, certain biomarker lipids are particularly good candidates as sourcewater D/H proxies because they are produced by a restricted range of organisms and therefore represent a distinct source signature. Compound-specific D/H analysis is a promising new approach for paleoclimatology because it allows the measurement of particular components of organic material which can be ascribed to a known source.

In addition to the analytical difficulties presented by molecular-level D/H measurements [2], there are a number of uncertainties embedded in sedimentary lipid D/H ratios that complicate their use as a paleoclimate proxy. It is important to separate aquatic and terrestrial organic matter due to evaporation from leaf surfaces or the use of different water sources [3]. Within single organisms, large D/H differences have been observed in different lipid moieties, and have been attributed to different synthetic pathways [4].

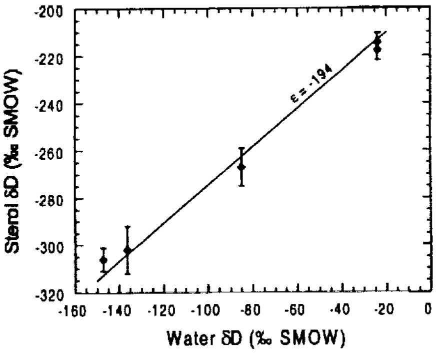

Fig. 1. δD of an algal sterol (24-methylcholest-5-enol) from surficial lacustrine sediments from a transect of lakes. Sites are located in eastern Massachusetts and eastern Canada.

To test the feasibility of using aquatic biomarkers in lake sediments, we analyzed a variety of lipids extracted from surface sediments from several lakes in eastern Massachusetts. These sites were chosen because dinoflagellates have been observed in the water column and dinosterol (4,23,24-trimethylcholsterol) is preserved in the surface sediments. Dinoflagellates are the only known source of dinosterol, making it an ideal aquatic biomarker. Using preparative capillary gas chromatography [5], we isolated individual stenol/stanol pairs for conventional D/H analyses, using off-line combustion with subsequent reduction of H_2O to H_2. We have also measured these samples using a new gas-chromatography/isotope-ratio monitoring system [2]. The results are identical within experimental error (presently 10–15‰). Isoprenoid lipids are depleted by 160–220‰ relative to source water, whereas n-alkyl lipids are depleted by 120–180‰.

However, single compounds exhibit a more restricted range of D/H fractionation. For example, in a transect of lakes with water D/H spanning –140‰ to –25‰, the D/H of free 24-methylcholest-5-enol is related to source water by a constant fractionation factor (ε) of –194‰ (Fig. 1). At these sites, 24-methyl-cholest-5-enol was not observed in terrestrial leave litter or soils, and is therefore interpreted as purely algal in origin. The higher plant sterol 24-ethylcholest-5-enol was enriched by ~30‰ relative to 24-methylcholest-5-enol at each site, suggesting it represents D-enriched terrestrial input.

References: [1] Dansgaard W. (1964) *Tellus, 16,* 436–468. [2] Burgoyne T. and Hayes J. (1998) *Anal. Chem., 70,* 5136–5141. [3] White J. W. C. et al. (1985) *GCA, 49,* 237–246. [4] Estep M. F. and Hoering T. C. (1980) *GCA, 44,* 1197–1209. [5] Eglinton T. I. et al. (1996) *Anal. Chem., 68,* 904–912.

DISSOLUTION OF ANALCITE UNDER CONDITIONS OF ALKALINE pH.

D. Savage[1], C. Rochelle[2], M. Mihara[3], Y. Moore[2], A. Milodowski[2], K. Bateman[2], and D. Bailey[2], [1]Quintessa Ltd. (davidsavage@quintessa.ltd.uk), [2]British Geological Survey (c.rochelle@bgs.ac.uk), [3]Japan Nuclear Cycle Development Institute, 4-49, Muramatsu, Tokai-mura, Naka-gun, Ibaraki 319-1194, Japan (mihara@tokai.jnc.go.jp).

Introduction: Many concepts for the deep disposal of radioactive wastes involve large quantities of cement and concrete. Groundwater will equilibrate with these materials and migrate under the local hydrogeological regime, and produce hyperalkaline pore fluids. Analcite is a framework aluminosilicate ($NaAlSi_2O_6$ H_2O) that has been identified from modeling and laboratory experimental studies to be an important solid product of the interaction of cement pore fluids with aluminosilicate minerals in the engineered barriers and host rock. This abstract summarizes a study to determine kinetic and thermodynamic data for analcite with a view to conduct more accurate mass-transfer modeling.

Experimental Procedure: A well-crystalline sample of analcite was obtained from Oregon, USA. This was carefully crushed and wet sieved, to produce grains lying in the 125–250-μm size range that were free of surface fines. Surface areas were determined by single point BET N adsorption. Analcite was reacted with pH buffer solutions in both batch and fluidized bed equipment at 25°, 50°, 70°, and 90°C.

Results: Analcite dissolution was highly nonstoichiometric, with Na being released in preference to Al and Si at pH 9–10, and Al being released in preference to both Na and Si at pH 13. The dissolution rate of analcite increased with increasing temperature and with increasing pH at each temperature (Fig. 1). The exception to this was that rates at 90°C were almost identical to those measured at 70°C. Absolute rates of dissolution ranged from 10^{-14} mol $cm^{-2}s^{-1}$ at pH 9.5 and at 25°C, to 10^{-11} mol $cm^{-2}s^{-1}$ at pH 12 at 70° and 90°C. The rate of dissolution at any temperature was pH-dependent, such that the rate could be described by $k(a_{H+})^n$, where k is the rate constant and n is –0.3 at 25°C, –0.4 at 50°C, –0.6 at 70°C, and –0.7 at 90°C. These data are in good agreement with that measured at 25°C [1] and those estimated from theoretical considerations of increasing surface charge on aluminosilicate minerals with increasing temperature [2,3].

In experiments involving K-based pH buffers, Na was apparently removed from the analcite structure by ion exchange for K, without involving dissolution and re-precipitation of the aluminosilicate framework. Scanning electron microscopy (SEM) of some reacted analcite grains showed pronounced surface cracking, which was parallel to the original analcite cleavage (Fig. 2). Analysis of the surfaces of the grains showed them to be rich in K relative to Na. These cracks appear to be a result of volume decrease due to substitution of K for Na ions and water molecules in the analcite structure to form leucite, $KAlSi_2O_6$. This occurred after only a few days at temperatures below 100°C.

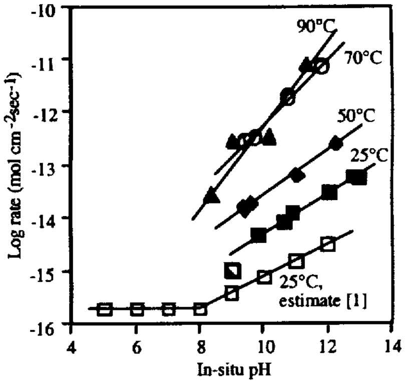

Fig. 1. Summary of analcite dissolution experiments.

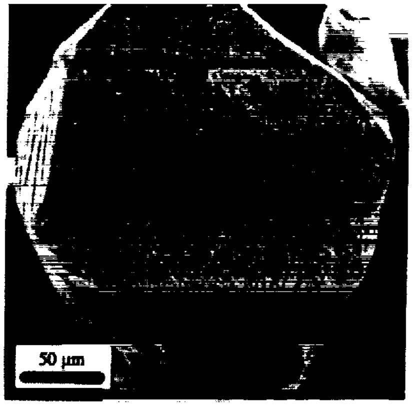

Fig. 2. Scanning electron microscope image of analcite grain reacted at 50°C and pH 13. Surface alteration to leucite shows extensive shrinkage and fine-grained Al oxyhydroxide precipitate.

Acknowledgments: The authors wish to thank the Japan Nuclear Cycle Development Institute for financial support. This abstract is published with the permission of the Director, British Geological Survey, National Environmental Research Council.

References: [1] Murphy W. M. et al. (1996) *Am. J. Sci., 296,* 128–186. [2] Brady P. V. and Walther J. V. (1989) *GCA, 53,* 2823–2830. [3] Walther J. V. (1996) *Am. J. Sci., 296,* 693–728.

COMPARISION OF EVOLUTION OF SAMARIUM-NEODYMIUM AND RUBIDIUM-STRONTIUM SYSTEMS IN METAMORPHIC COUNTRY ROCKS IN CONTACT ZONES OF INTRUSION: ELDORA STOCK, COLORADO (USA) AND OZERNAJA VARAKA, KOLA PENINSULA (RUSSIA).

V. M. Savatenkov and L. K. Levsky, Institute of Precambrian Geology and Geochronology, Makarova emb., 2, Saint-Petersburg, 199034, Russia (lev@ad.iggp.ras.spb.ru).

The main objects of our investigations were contact zones of the granitic intrusion Eldora Stock (Colorado) and alkaline-ultrabasic intrusion Ozernaja Varaka (Kola Peninsula). The country rocks from both zones experienced several episodes of regional metamorphism [1–3]. The fluid regime of contact metamorphism affecting these rocks is different in both cases and is defined by intrusion composition. New Sm-Nd and Rb-Sr whole-rock and mineral isotopic data on the considered objects briefly presented below.

Intrusions: Eldora Stock (E.S.) — quartz-monzonite intrusion (high H_2O/CO_2) t = 0.055 Ga, $\varepsilon_{Nd} = -20$.

Ozernaja Varaka (O.V.) - alkaline-ultrabasic intrusion (low H_2O/CO_2) t = 0.375 Ga, $\varepsilon_{Nd} = 6$.

Protolith's Age of the Country Rocks (Gneisses and Amphibolites): (E.S.) — Idaho Springs Formation: Sm-Nd (whole rock) t = 2.1 Ga, ε_{Nd} = 5.8; Rb-Sr (whole rock) was disturbed.

(O.V.) — Belomorian complex: Sm-Nd (whole rock) t = 2.8 Ga, ε_{Nd} = 2.6; Rb-Sr (whole rock) was disturbed.

Timing of Regional Metamorphism (Mineral Isochrones): (E.S.) — Sm-Nd (Px, Pl, Amph, Ap, Sph) 1.50–1.45 Ga; Rb-Sr (Pl, Amph) 1.45 Ga.

(O.V.) — Sm-Nd (Pl, Amph, Ep, Ap, Sph) 1.95–1.75 Ga; Rb-Sr (Pl, Amph) 1.75 Ga; Rb-Sr (KFsp, Pl) 1.69–1.60 Ga; Rb-Sr (Bt) 1.55 Ga.

Contact Metamorphism (Mineral Apparent Ages): (E.S.) — Five meters from contact: Sm-Nd (Pl, Amph, Ap, Bt) 1.0 Ga; Rb-Sr system was opened: there is influx of Rb in whole rock from the intrusion.

(O.V.) — Fifty meters from contact: Sm-Nd (Sph) 1.8 Ga; Sm-Nd (Ap) 1.6 Ga; Rb-Sr (Sph) 1.8 Ga; Rb-Sr (Bt) 0.65 Ga.; 200 m from contact: Sm-Nd and possibly Rb-Sr systems were opened. There was essential Sr and Nd influx from the intrusion.

The Sm-Nd-isotopic characteristics indicated in both cases on depleted mantle sourse of country rocks survived the reprinted regional metamorphic influences. The Rb-Sr whole-rock isotopic system in both cases was essentially disturbed and the Sm-Nd and Rb-Sr mineral isotopic systems were reequilibrated during of regional metamorphism [1.4–1.5 Ga (E.S.), 1.6–1.9 Ga (O.V.)].

Comparison of isotope data for the studied country rocks affected by contact metamorphism demonstrates obvious dependence of behavior of Sm-Nd-isotopic system from fluid regime of contact metamorphism. Essentially carbonatic fluid of alkaline-ultrabasic intrusion (O.V.) causes more Nd mobility rather aqueous fluid of granitic intrusion (E.S.).

References: [1] Hart S. R. (1964) *J. Geol., 75,* 493–525. [2] DePaolo D. J. (1981) *Nature, 291,* 193–196. [3] Savatenkov V. M. et al. (1996) *Geochem. Intl., 33,* 28–38.

SCAVENGING OF COBALT AND NICKEL BY IRON HYDROXIDE IN SUBMARINE HYDROTHERMAL PLUMES: EXPERIMENTAL MODELING.

A. V. Savenko, Department of Geography, Moscow State University, Vorobyovy Gory, Moscow 119899, Russia.

It is known that the main volcanogenic component of particulate matter in submarine hydrothermal plumes is Fe(III) hydroxide. When hydrothermal solutions discharge into the seawater, Fe(III) hydroxide is formed by oxidation of dissolved Fe(II). Many chemical elements are believed to be scavenged by iron hydroxide from hydrothermal plumes. However, the particulate matter of hydrothermal plumes also contains volcanogenic, biogenic, and terrigenic materials. Therefore it is difficult to use the data of field observations done for the estimation of the relative role of coprecipitation processes. The aim of this study was the experimental modeling of two important heavy metals, Co and Ni, coprecipitating with iron hydroxide in laboratory conditions.

The experiments were carried out with artificial 35‰ seawater having 0.25–20 μM Co and 0.6–20 μM Ni. The pH value was equal to 7.7–8.2. The addition of different quantities of 0.01 M $FeSO_4$ solution in the flasks with 200 mL of seawater containing Co and Ni caused iron hydroxide formation and removal of Co and Ni from solution. The suspensions were mixed during four days and after that dissolved Co and Ni were determined in filtrate by spectrophotometry.

The experiments demonstrated that the value of element (i)/Fe ratio in precipitated Fe(III) hydroxide is a hyperbole function of i/Fe ratio in initial solution

$$y = kx/(1 + bx)$$

where y is the i/Fe ratio in iron hydroxide, x is the i/Fe ratio in initial solution, i is Co or Ni, and k and b are the constant coefficients. The value of bx ≪1 in submarine hydrothermal plumes. Therefore, it is enough to know only the k coefficient. The values of the k coefficient for Co and Ni were determined to be 0.5 and 0.4, respectively.

The results of calculations based on the field measurements of hydrothermal solution composition [1–4] and experimental data give the i/Fe ratios in hydrothermal iron hydroxide of 1.7×10^{-5} to 2.7×10^{-4} and 6.6×10^{-5} to 1.1×10^{-3} for Co and Ni respectively. It is close to that obtained from analysis of hydrothermal plume particulate matter in the TAG region: Co/Fe = 2.5×10^{-4}, Ni/Fe = 2.7×10^{-4} [5,6]. Thus it may be concluded that the coprecipitation of Co and Ni with iron hydroxide is the main process controlling their scavenging in particulate matter of hydrothermal plume.

In contrast to the hydrothermal plumes, increased concentrations of Co and Ni in metalliferrous deposits only partially occurs through coprecipitation with hydrothermal iron hydroxide. Accumulation of a significant portion of Co and Ni in metalliferrous deposits apparently is caused by additional scavenging on MnO_2 from seawater. Formation of MnO_2 at these conditions occurs due to activity of bacteria, which are widespread in regions of underwater hydrothermal activity [7].

References: [1] German C. R. et al. (1991) *EPSL, 107,* 101–114. [2] Gurvich E. G. (1998) *Metalliferrous Sediments of the World Ocean,* Scientific World. [3] Tambiev S. B.et al. (1992) *Geochemistry, N2,* 201–213. [4] Trefry J. H. et al. (1994) *JGR, 99,* 4925–4935. [5] Trocine R. P. and Trefry J. H. (1988) *EPSL, 88,* 1–15. [6] Von Damm K. L. et al. (1985) *GCA, 49,* 2197–2220. [7] Von Damm K. L. et al. (1985) *GCA, 49,* 2221–2237.

ANALYSIS OF MICROBIAL DIVERSITY IN SEDIMENTS FROM THE BENGUELA UPWELLING SYSTEM SHOWING ANAEROBIC METHANE OXIDATION.

H. Schäfer[1], H. Fossing[2], T. G. Ferdelman[3], and G. Muyzer[1], [1]Netherlands Institute for Sea Research, P.O. Box 59, NL-1790 AB Den Burg, The Netherlands, [2]National Environmental Research Institute, DK-8600 Silkeborg, Denmark, [3]Max-Planck-Institute for Marine Microbiology, D-28359 Bremen, Germany.

The Benguela upwelling system belongs to the most productive marine regions. Part of the organic C is exported from the photic zone to the underlying sediments. Investigations of sediment cores retrieved from the continental margin have shown that near the sediment surface sulfate reduction is a dominant pathway of organic matter decomposition despite the lack of sulfate gradients in the same zone [1]. Furthermore, porewater profiles of sulfate, sulfide and methane, showed a distinct sulfate-methane transition (SMT) zone at depths of several meters. Near 1:1 stoichiometry of upward methane and downward sulfate fluxes in the SMT [2,3] suggest that anaerobic methane oxidation could be coupled to the reduction of sulfate, a process that might be biologically mediated by consortia of methanogens and sulfate-reducing bacteria [4] or by newly discovered Archaea related to the *Methanosarcinales* [5].

The aim of our study was to characterize the microbial communities of sediments from the Benguela upwelling area by molecular biological methods. Analyses concentrated on sediment samples taken from a 9-m-long gravity core at station GeoB 3703 obtained from 1300 m water depth on the continental slope off Namibia. Sediments at this station are characterized by high-organic C (5–7.5%) and high-surface sulfate reduction rates (20 nmol cm^{-3} d^{-1}). PCR products obtained from nucleic acid extracts of sediment samples from various depths were analyzed by genetic fingerprinting techniques. Mixed PCR products of bacterial populations were analyzed by denaturing gradient gel electrophoresis (DGGE) [6]. Comparison of DGGE banding patterns obtained from samples of different depths suggested a lower bacterial diversity at the SMT (with only two 16S rRNA sequence types) as compared to samples lying above or below the SMT. Thus far, some members of the bacterial assemblage could be identified by sequencing of excised bands or by hybridization analysis of DGGE profiles with probes targeting certain subgroups of the sulfate-reducing bacteria. At present archaeal populations are being analyzed by terminal restriction fragment length polymorphism (T-RFLP) [7]. Data obtained by the molecular approach should give further insight into the microbial diversity of these sediments, and might identify key players in deep-sea biogeochemical processes such as sulfate reduction and anaerobic transformation of methane.

References: [1] Ferdelman T. G. et al. (1999) *Limnol. Oceanogr.*, in press. [2] Niewöhner C. et al. (1998) *GCA, 62,* 455–464. [3] Fossing H. et al. (1999) *GCA,* submitted. [4] Hoehler et al. (1994). [5] Hinrichs et al. (1999) *Nature, 398,* 802–805. [6] Muyzer G. and Smalla K. (1998) *Antonie van Leeuwenhoek, 73,* 127–141. [7] Liu W. T. et al. (1997) *Appl. Environ. Microbiol., 63,* 4516–4522.

INFLUENCE OF TEMPERATURE ON NICKEL SORPTION ON CLAY MINERAL AND OXIDE SURFACES.

K. G. Scheckel and D. L. Sparks, University of Delaware, 147 Townsend Hall, Newark DE 19717-1303, USA.

Introduction: Many kinetic studies have shown that sorption of metals on natural materials results in the formation of metal precipitates. However, the influence of temperature on the kinetic formation of these metal precipitates has not been studied. The effect of temperature on reaction rates is well known and important in understanding reaction mechanisms. For most reactions, the increase in rate with increasing temperature is nonlinear and reaction-rate data obeyed the Arrhenius equation:

$$k = Ae^{-E_a/RT}$$

Energies of activation below 42 kJ mol^{-1} generally indicate diffusion-controlled processes and higher values represent chemical reaction processes [1]. For example, E_a values for gibbsite dissolution in various acid solutions ranged from 59 to 67 kJ mol^{-1} [2], while pesticide sorption on humic acid had an E_a value of 6.7 kJ mol^{-1} [3].

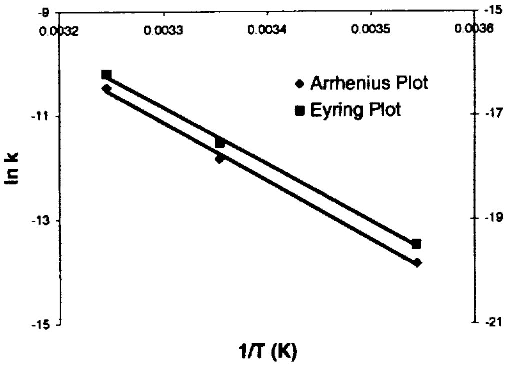

Fig. 1. Arrhenius and Eyring plots of first-order rate constants of Ni sorption on pyrophyllite at various temperatures.

TABLE 1. Summary of reaction parameters dervied from Arrhenius and Eyring equations for Ni sorption on clay mineral and oxide surfaces.

Surface	E_a (kJ/mol)	A (s^{-1})	$\Delta H^\ddagger$ (kJ/mol)	$\Delta S^\ddagger$ (J/mol)	$\Delta G^\ddagger$ (kJ/mol) at 25°C
Pyrophyllite	93.05	1.59E + 11	90.60	−38.70	102.23
Talc	95.35	1.75E + 11	92.90	−37.91	104.20
Silica	111.47	6.10E + 11	109.02	−27.51	117.22
Gibbsite	123.71	4.05E + 11	121.26	−30.90	130.47
Gibbsite/silica	95.09	4.54E + 11	92.64	−29.96	101.57

Additionally, one can determine the enthalpy, entropy, and free energy of formation by applying the Eyring equation

$$k = (k_bT/h)\ e^{-\Delta G\ddagger/RT} = (k_bT/h)\ e^{-\Delta S\ddagger/R}\ e^{-\Delta H\ddagger/RT}$$

Materials and Methods: Pyrophyllite and talc were employed in this research because they show very little deviation from the chemical formula of an ideal 2:1 clay. The structural difference between talc and pyrophyllite is that talc possesses three Mg^{2+} in its octahedral position while pyrophyllite has two Al^{3+} in the octahedral position. By using talc, Al^{3+} will not be present in the solution that is believed to be the driving mechanism behind the formation of mixed metal-Al surface precipitates. In addition, amorphous silica (SiO_2) (Zeofree® 5112), gibbsite [$Al(OH)_3$], and a stoichiometric combination of amorphous silica and gibbsite in similar molar ratios to pyrophyllite were employed. Silica (tetrahedral) and gibbsite (octahedral) make up the basic building blocks of phyllosilicate minerals.

For kinetic sorption studies, an initial Ni solution concentration of 3 mM [I = 0.1 M ($NaNO_3$), T = 9°, 25°, and 35°C], which was undersaturated with respect to the thermodynamic solubility product of β-$Ni(OH)_2$ [4], was reacted with a 10 g/L suspension of each of the minerals employing a pH-stat (pH 7.5) batch technique. The systems were purged with N_2 to eliminate CO_2.

Results: First-order kinetic plots of the sorption data yielded rate constants (k) used in determining temperature related parameters. Arrhenius and Eyring plots (Fig. 1) of the rate constants resulted in good linear fits with E_a and $\Delta H^\ddagger$ extrapolated from the slopes of the curves and A and $\Delta S^\ddagger$ calculated from the intercepts. From the free-energy relationship, $\Delta G^\ddagger$ was determined.

These data (Table 1) suggest a surface-controlled or associative mechanism for sorption based on the large E_a and negative $\Delta S^\ddagger$ values. Additionally, the large E_a values are within the range of mineral formation which supports previous findings of Ni precipitation on these mineral and oxide surfaces.

Conclusions: Sorption of Ni on the mineral phases results in the formation of mixed Ni-Al precipitates on pyrophyllite, gibbsite, and gibbsite/silica mixture and β-$Ni(OH)_2$-like products on talc and silica. By conducting temperature studies, we have shown that Ni sorption on these surfaces is surface-controlled as demonstrated by the large E_a and negative $\Delta S^\ddagger$ values.

References: [1] Sparks D. L. (1985) *Adv. Agron., 38,* 231–266. [2] Bloom P. R. and Erich M. S. (1987) *Soil Sci. Soc. Am. J., 51,* 1131–1136. [3] Khan S. U. (1973) *Can. J. Soil Sci., 53,* 429–479. [4] Scheidegger A. M. and Sparks D. L. (1996) *Chem. Geol., 132,* 157–164.

UPTAKE MECHANISMS OF RADIONUCLIDES ON CLAY SURFACES AS DETERMINED BY X-RAY ABSORPTION SPECTROSCOPY.

A. M. Scheidegger, R. Dähn, B. Baeyens and M. H. Bradbury, Waste Management Laboratory, Paul Scherrer Institute, Switzerland (andre.scheidegger@psi.ch).

The aim of the research activities in our laboratory is to develop and test models, and to acquire selected data in support of performance assessments of Swiss nuclear waste repositories. The work concentrates on the understanding of mechanisms and processes that govern the release of safety-relevant radionuclides from waste matrixes, and their transport through engineered barrier systems and the surrounding geosphere.

The work in the experimental program focuses on the determination of distribution coefficients of radionuclides on repository components and rock materials in order to compile specific and consistent sorption data bases to be used in safety assessment. For this reason, various sorption studies of radionuclides (Ni, Zn, Am, Sr, Cs, Th, and Eu) in clay systems have been performed. An extremely detailed study has been conducted on Ni sorption on montmorillonite. Montmorillonite is a 2:1 clay material with substantial isomorphic substitution. The clay material is a major component in the bentonite backfill for a high-level radioactive waste repository and an important mineral responsible for the retention of metals in the geosphere. The study examined the Ni sorption behavior over a wide range of reaction conditions (pH, ionic strength, initial metal concentration, and reaction time). Based on the sorption data and the macroscopic surface properties of the clay, a near-mechanistic surface complexation and cation exchage model was developed to predict the uptake of radionuclides and other environmental relevant metal ions [1–2]. However, to definitively prove the proposed surface complexation model, the macroscopic studies conducted need to be coupled with spectroscopic and microscopic investigations. Thus, X-ray absorption spectroscopy (XAS) and transmission electron microscopy (TEM) have become important analytical tools in our laboratory to gain an atomic/molecular level understanding of metal speciation and sorption processes occurring in natural mineral systems.

Recent XAS studies have shown that sorption of Ni on clay minerals can result not only in the binding of Ni to specific surface sites but also in the nucleation and growth of a Ni phase on the clay particles [3–5]. With montmorillonite, however, XAS measurements were limited to high-Ni concentrations due to the relatively high-Fe content in montmorillonite (up to 5% by weight) and the lack of a suitable fluorescence detector [4]. In the present paper we will show that nucleation of a new Ni phase on the clay surface can also occur at significantly lower Ni concentrations and illustrate how the sorption system is controlled by slow kinetic processes. Furthermore, we will demonstrate that the release of Ni from the Ni phase is strongly hindered in comparison with surface-sorbed Ni.

References: [1] Baeyens B. and Bradbury M. H. (1997) *J. Contam. Hydrol., 27,* 199–222. [2] Bradbury M. H. and Baeyens B. (1997) *J. Contam. Hydrol., 27,* 223–248. [3] Scheidegger A. M. et al. (1997). *J. Colloid Interface Sci., 186,* 118–128. [3] Scheidegger A. M. et al. (1998) *GCA, 62,* 2233–2245. [5] Towle S. N. et al. (1997) *J. Colloid Interface Sci., 187,* 62–82.

CALCIUM-RICH SILICA-UNDERSATURATED MELTS IN ISLAND ARCS.

P. Schiano[1,2], J. M. Eiler[1], and E. M. Stolper[1], [1]Division of Geological and Planetary Sciences, California Institute of Technology, Pasadena CA, USA (schiano@gps.caltech.edu), [2]Laboratoire Géochimie-Cosmochimie, IPG Paris, 4 place jussieu, 75252, Paris Cedex 05, France.

Island-arc basalts are generally thought to form by melting of the mantle wedge above subducted oceanic lithosphere, and their chemistry and melting environment is believed to reflect enrichment of the mantle wedge in water and other elements carried by aqueous fluids or silicate melts released from subducting oceanic crust. The mantle sources subjected to this metasomatic process are believed to be similar to the sources of MORBs (or perhaps more refractory peridotites). Here, we draw attention to primitive, nepheline-normative island-arc magmas that are characterized by remarkably high CaO contents (up to 19.0 wt%) and that cannot be simply reconciled with the standard model of arc petrogenesis,

Compilation of Silica-Undersaturated Calcic Melt Compositions: We compiled from the literature (and from our own analyses) the compositions of arc-related melts having CaO contents >13 wt%. Whole rocks and glass inclusions in Mg-rich olivine phenocrysts (Fo_{84-94}) with such high CaO contents are present in the Sunda, Luzon, Aeolian, New Guinea, Central America, Lesser Antilles, and Vanuatu arcs. Inclusions and lavas are indistinguishable in major-element variation diagrams and collectively define a compositionally distinct group when compared to other arc lavas (e.g, these inclusions and lavas are characterized by lower FeO concentrations at a given SiO_2 content than most arc lavas).

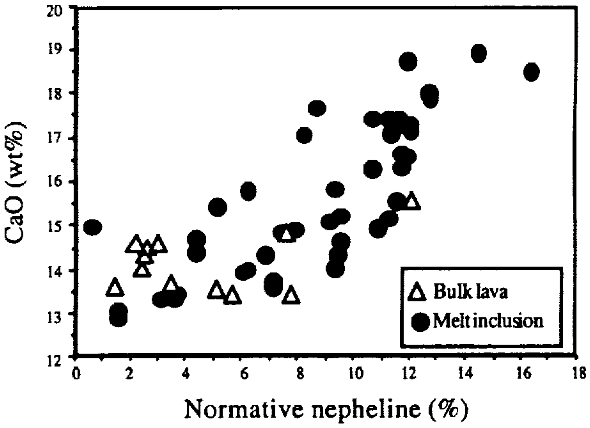

Fig. 1.

All of the high-CaO inclusions (after homogenization by high-T experiments) and lavas are nepheline normative (0.5–16.2%) and normative nepheline is positively correlated with CaO content (Fig. 1); CaO-rich whole rocks are characterized by high MgO (>6.5 wt%) and low silica (44–48 wt%) contents, and they are generally clinopyroxene-phyric (diopside-augite). The elevated CaO contents and silica-undersaturation are not due to accumulation of pyroxene in the case of the melt inclusions (i.e., they contain no pyroxene), but neither can these characteristics of the whole-rock lavas reflect clinopyroxene accumulation alone because the clinopyroxenes in these rocks are not nepheline normative. Excepting two inclusions from Aeolian Islands, all homogenized inclusions are characterized by high MgO (>7 wt%) contents.

Evolution of the Calcic Melts: Melt inclusions in olivine phenocrysts in a calc-alkaline basalt from Batan Island show a decrease of the CaO and MgO contents from 18.5 to 5.0 wt% and from 9.5 to 1.3 wt%, respectively, as SiO_2 increases from 44.3 to a 63.7 wt%, and a concomitant variation in the host olivine composition from Fo_{90} to Fo_{75}. These variations cannot be reconciled with olivine and clinopyroxene (the main phenocrysts of the host lava) crystallization alone, because of the nepheline-normative to quartz-normative evolution recorded by the melt inclusion compositions. The study of the major- and trace-element variations in the inclusions shows that the calcic, Si-undersaturated melts trapped in olivine have mixed with melts, which vary in their composition due to fractional crystallization of olivine, clinopyroxene and amphibole.

Origin of Silicon-undersaturated Calcic Melts: The CaO contents of experimental partial melts of fertile or depleted peridotites under dry conditions range up to 13–14 wt%; i.e., they are below the CaO contents of the calcic inclusions and lavas identified in this study. We also consider it unlikely that melting of peridotite in the presence of CO_2 is responsible for producing SiO_2-poor, CaO-melts melts, based on strong contrast between the incompatible-element geochemistry of melilitites/nephelinites (widely considered to be melts of carbonated peridotite) and the CaO-rich, Si-undersaturated arc magmas identified here.

The model compositions of partial melts of pyroxenite (based on thermodynamic calculations using MELTS) are comparable to those of the calcic, undersaturated melt considered here, suggesting that they could be evidence of a widespread contribution to arc magmas of partial melts of mafic material in the mantle wedge or arc lithosphere. The most likely source of the calcic melts is lower crustal pyroxenites common to the lithosphere of arc environment rather than mantle pyroxenite veins, because the former have higher CaO contents and may melt at lower temperatures due to the presence of minor amphibole.

QUANTIFICATION OF ORGANIC PARTICLES FROM FOSSIL-FUEL COMBUSTION IN SOILS.

M. W. I. Schmidt[1,*], H. Knicker[1], P. G. Hatcher[2], and I. Kögel-Knabner[1], [1]Lehrstuhl für Bodenkunde, Technische Universität München, 85350 Freising-Weihenstephan, Germany, [2]Department of Chemistry, Ohio State University, 100 West 18th Avenue, Columbus OH 43210, USA, (*present address: Max-Planck-Institut für Biogeochemie, P.O. Box 100 164, 07745 Jena, Germany; mschmidt@bgc-jena.mpg.de).

Introduction: Long-term dispersed atmospheric input of organic particles from fossil-fuel combustion (soot, char, and coke), and industrial processing of coal (coal dust) presumably accumulate in soils of industrialized areas. Such compounds are likely to have a drastic influence on quantity and chemical properties of soil organic matter. The objective of this study was to quantify the atmospheric input of organic particles in agricultural and forest soils neighboring industrialized areas. However, contamination was not visible macroscopically in all investigated soils.

Soils and Methods: Studied soils were situated 1–30 km downwind of possible sources of pollution in the Halle and Ruhr area, Germany. Bulk material and particle size fractions of A and B horizons were studied. Samples were investigated by elemental analysis (C, N), spectroscopy (CP MAS ^{13}NMR, Py-GC-MS), ^{14}C dating, microscopy, and magnetic measurements.

Results: Airborne organic particles increased C and N contents by factors of up to 10 and also magnetic susceptibility relative to natural reference soils. Pyrolysis products could be related to coal structures, while in natural reference soils lignin derived structures were more abundant. Organic particles are microscopically identified as coal dust, char, and coke particles (20–200 μm diameter), which increased C and N contents of these size fractions.

Structures of organic matter in these soils were characterized by high amounts of aliphatic or aromatic C, typical for coal and combusted particles. As examples, the ^{13}C CP MAS NMR spectra of two Phaeozem soils are presented in Fig. 1. The plowed A horizons of a noncontaminated (Ap) and a contaminated Phaeozem (Ap1) were compared to spectra of organic particles tentatively deposited in the Ap1 horizon, i.e., brown coal and combustion residues like soot [1]. The spectrum from the noncontaminated soil (Ap) revealed a typical pattern of organic matter commonly found in these soils, i.e., high intensities in the chemical shift regions assigned to carbohydrates (45–110 ppm), alkyl C (0–45 ppm), and carboxylic C (160–220 ppm). Aromatic compounds produced broad overlapping signals between 160 and 100 ppm. The spectrum of the contaminated Ap1 horizon showed a different pattern. It is dominated by signals in the alkyl C and aromatic C region. The spectrum of brown coal was similar, except for more distinct peaks for alkyl C and aromatic C. The spectrum of the soot sample reveals a distinct peak around 130 ppm, exemplifying the highly aromatic structure of soot. The striking similarities between spectra of the contaminated Ap1 horizon, brown coal and soot indicated that major proportions of organic particles from fossil fuel combustion have been accumulating in this soil.

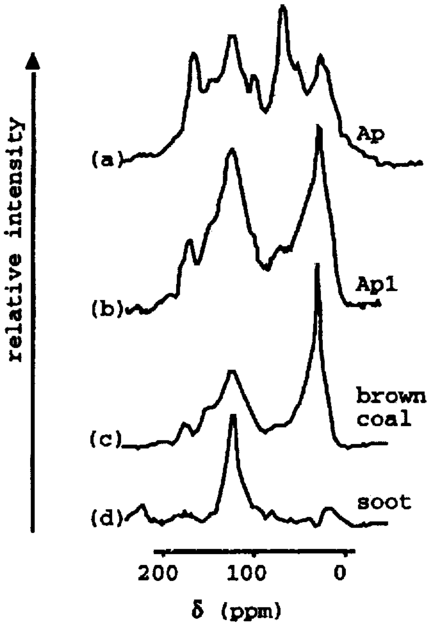

Fig. 1. Solid-state ^{13}C NMR spectra of the (a) noncontaminated and (b) contaminated horizon compared to (c) brown coal and (d) soot (spectrum d from [2]).

To quantify the organic particles from fossil fuel we used ^{14}C dating. Considering the elevated age of coals, compared to soils, in case of contamination a much higher ^{14}C age in the contaminated than in the natural soil should be expected, as a consequence of contamination by older material. Coal dust and combustion products are beyond the time covered by ^{14}C determination. The ^{14}C age of a natural reference soil was 1630 yr before present, which is an expected value. In contrast, the Ap1 horizon of the contaminated Phaeozem shows an unusually high ^{14}C age of 15,750 yr before present. Obviously brown coal dust and combusted particles contributed greatly to the measured ^{14}C age. Assuming both Ap horizons originally had the same ^{14}C age, we calculated the degree of contamination as 82% of the total organic C. Thus, the input of organic particles from fossil-fuel combustion into the Ap1 horizon was ~35 kg m^{-2}.

Conclusion: For the first time, the combination of a suite of complementary methods allowed to quantify the input of organic particles from fossil fuel combustion in soils. Disperse emissions of organic particles from fossil fuel combustion have accumulated for decades in soils of industrialized areas, altering quality and quantity of the organic matter. Presumably these particles also accumulated in other soils neighboring industrialized areas, but remain undetected due to low levels of contamination.

References: [1] Schmidt M. W. I. et al. (1996) *Org. Geochem., 25,* 29–39. [2] Sergides C. A. et al. (1987) *Appl. Spectr., 41,* 482–492.

CHAR FROM VEGETATION FIRES IN SOILS?

M. W. I. Schmidt[1,*], J. O. Skjemstad[2], and I. Kögel-Knabner[1], [1]Lehrstuhl für Bodenkunde, Technische Universität München, 85350 Freising-Weihenstephan, Germany, [2]Commonwealth Scientific and Industrial Research Organisation, Land and Water, Glen Osmond, SA 5064, Australia, (*present address: Max-Planck-Institut für Biogeochemie, PO 100 164, 07745 Jena, Germany; mschmidt@bgc-jena.mpg.de).

Introduction: Vegetation fires produce large amounts of char, which may increase the amount of aromatic C and contribute a relatively inert type of C to the SOM pool. Char may also affect soil organic matter composition, turnover, formation, and soil color. A color sequence of four German chernozemic soils was sampled to investigate the potential contribution of charred organic C (char) to these soils and a possible relationship between soil color and the chemical structure of soil organic matter.

Soils and Methods: The studied soils developed from almost identical parent material (loess), display similar chemical and physical properties, and are all under agricultural management with similar crop rotations. The striking difference was a gradual color change from black to gray. Soil samples represented a color-sequence changing from a black (soil 1) to gray (soil 4) color that developed on loess in the region south of Hannover, Germany [1].

The lignin content was detected by alkaline oxidation and char in soils was determined by a combination of high-energy ultraviolet photo-oxidation, scanning electron microscopy and solid-state ^{13}C NMR spectroscopy. Carbon-13 CP MAS NMR spectra were obtained before and after UV photo-oxidation. Previous studies showed that a number of materials found in soils, including wood, lignin, and humic acids, could all be destroyed by the high-energy photo-oxidation process, provided they were exposed to ultraviolet radiation in the presence of excess O. Charred organic matter, however, was not destroyed by this treatment [2,3].

Results: The spectra of soil 1 are shown as an example (Fig. 1). The spectrum before photo-oxidation shows several signals indicating the presence of a number of structures typically present in soil organic matter. We focus on the signals centered around 130 ppm with few additional peaks in the O-aryl C region, which is typical for the presence of char.

The presence of lignin units would have been indicated by signals around 130 ppm in combination with additional signals for O-aryl C structures (165 to 145 ppm) and aryl C (116 and 131 ppm), which are of minor importance

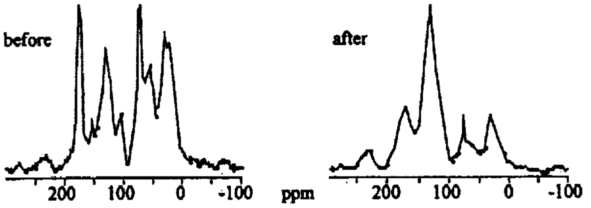

Fig. 1. Carbon-13 CP MAS NMR spectra of soil 1 obtained before and after UV photo-oxidation.

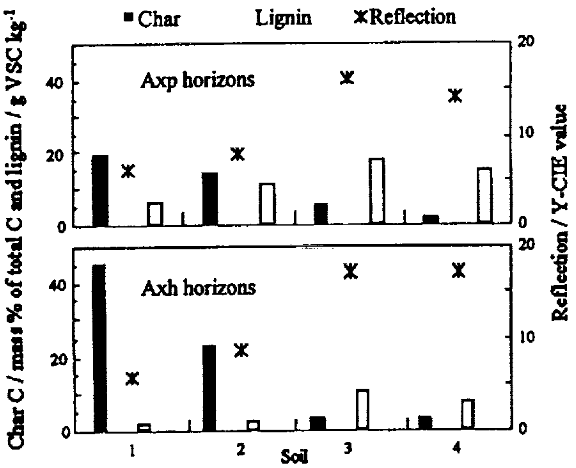

Fig. 2. Content of char C and lignin (normalized to organic C content) detected in the Axp and Axh horizons of soils 1 to 4 displayed as a color-sequence. Reflection is given as Y-CIE value that is an equivalent to the Munsell value.

here. After photo-oxidation the spectrum was dominated by an aryl C peak at 130 ppm, with spinning side bands (230, 30 ppm) and few other minor signals, indicating the presence of char. Together with data for mass balance and C content we then calculated the char content.

To visualize a potential interdependence between char and lignin content and soil color, data was displayed as a color sequence from black to gray colored soils in Fig. 2. As a trend, progressing from dark to light colored soils in the color-sequence (1) organic matter became less resistant to photo-oxidation, (2) contributions of char to the bulk soil C decreased, whereas (3) contributions of lignin to the bulk soil C increased. Contributions from char were always highest in the subsoils compared to the surface horizons, both normalized to organic C content and normalized to bulk soil mass.

Conclusion: The photo-oxidation method allows the identification of char C in German Chernozems. Char contributes up to 45% to the bulk soil organic C, which is equivalent to ~8 g/kg of the bulk soil. The color sequence of soils showed a strong relationship between color and the content of char, suggesting that the presence of char dominates color in these soils. In the Chernozems studied here, char is a major contributor to total organic C, but the origin of this fire-induced form of organic C remained unclear. Due to its recalcitrant nature, char can be preserved in the pedosphere for long periods of time. This has major implications for the processes of pedogenesis in Chernozemic soils and for the sequestration of C in these soils.

References: [1] Schmidt M. W. I. et al. (1999) *Eur. J. Soil Sci., 50,* in press. [2] Skjemstad J. O. et al. (1993) *J. Soil Sci., 44,* 485–499. [3] Skjemstad J. O. (1996) *Aust. J. Soil Res., 34,* 251–271.

AN EMPIRICAL ASSESSMENT OF "ULTRA" HIGH-PRECISION URANIUM-LEAD ZIRCON GEOCHRONOLOGY: ZIRCON AND SPHENE SYSTEMATICS OF THE FISH CANYON TUFF.

M. D. Schmitz and S. A. Bowring, Department of Earth, Atmospheric, and Planetary Sciences, Massachusetts Institute of Technology, 77 Massachusetts Avenue, Cambridge MA 02139, USA (mschmitz@mit.edu).

Uranium-lead zircon ages provide the the most precise and accurate absolute chronometers for the study of geological and evolutionary processes. The dating of volcanic ash beds by this method has been used to constrain the absolute timing and relative tempo of evolutionary change [1,2] and mass extinctions [3] with unprecedented resolution. These applications of "ultra" high-precision U-Pb zircon geochronology to young rocks push the limits of current analytical capability and challenge the traditional means of assessing analytical and geological uncertainty in U-Pb zircon age determinations. One means of assessing the limitations of U-Pb zircon geochronology is purely empirical and involves the collection of a very large dataset of single and multigrain zircon analyses from a well-characterized young volcanic tuff. We have obtained such a dataset using zircons from the Oligocene Fish Canyon Tuff, a well known $^{40}\text{Ar}/^{39}\text{Ar}$ geochronological standard.

Lead-206/uranium-238 dates (uncorrected for initial daughter disequilibria) of 23 of 24 single grains range from 28.24 to 28.55 Ma, with a weighted mean date of 28.42 ± 0.03 Ma (2σ uncertainty; MSWD 0.96). Lead-207/uranium-235 dates ranged from 28.33 to 28.70, with a weighted mean of 28.52 ± 0.05 Ma, slightly older than $^{206}\text{Pb}/^{238}\text{U}$ dates, resulting in analyses displaced slightly below and to the right of concordia (open ellipses in Fig. 1). A single grain yielded an anomalously old $^{206}\text{Pb}/^{238}\text{U}$ date of 29.34 Ma. The selection of zircon with inherited components was mostly avoided, indicating that inheritance of older zircon is negligible in this sample of Fish Canyon Tuff, and/or that inherited grains are easily avoided during the selection of grains for analysis. Errors on individual analyses directly correlate with the radiogenic to common Pb ratio of the analysis. In order to increase this ratio and thereby reduce the statistical uncertainty of each analysis, eight multigrain fractions of zircon (3–14 grains) were picked, abraded, and dissolved for analysis. Seven of these eight multigrain fractions (filled ellipses in Fig. 1) gave $^{206}\text{Pb}/^{238}\text{U}$ dates from 28.34 to 28.43 Ma, with a weighted mean date of 28.38 ± 0.02 Ma (MSWD 0.36). Only one analysis yielded an anomalously old $^{206}\text{Pb}/^{238}\text{U}$ date of 36.85 Ma. The $^{207}\text{Pb}/^{235}\text{U}$ dates of the seven coherent fractions ranged from 28.45 to 28.60 Ma, with a weighted mean of 28.52 ± 0.05 Ma (MSWD 0.65), again demonstrating the same consistent discordance exhibited by the single grain analyses.

These results are in close agreement with a previous single-grain zircon date of 28.41 ± 0.05 Ma for the Fish Canyon tuff [4], but is older than most published $^{40}\text{Ar}/^{39}\text{Ar}$ sanidine dates, which range from 27.8 to 28.1 Ma [5]. Notably, the weighted mean dates of single and multi-grain analyses, done in different experiments at different times, are within analytical uncertainty. Using this dataset, we will explore the sensitivity of individual and pooled zircon dates to the sources of analytical and geological uncertainty in zircon

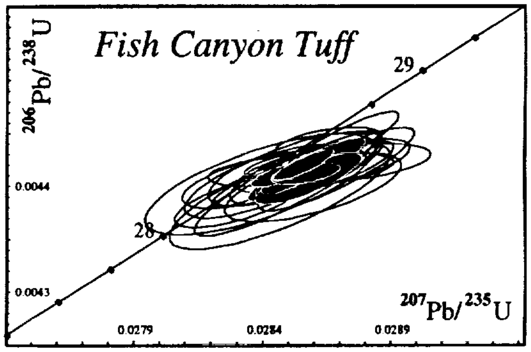

Fig. 1.

age determination, including familiar factors like Pb loss and inheritance, as well as commonly assumed or discounted factors including accurate common Pb corrections, spike calibrations, instrumental fractionation, and intermediate daughter product disequilibria. An additional dataset of single-grain sphene analyses which may aid in interpretation of the zircon data will also be presented.

References: [1] Bowring S. A. et al. (1993) *Science, 261,* 1293–1298. [2] Mundil R. et al. (1996) *EPSL, 141,* 137–151. [3] Bowring S. A. et al. (1998) *Science, 280,* 1039–1045. [4] Oberli F. (1990) *ICOG, 7,* 74. [5] Renne P. R. et al. (1994) *Geology, 22,* 783–786.

THE EVOLUTION OF CRATONIC GEOTHERMS: URANIUM-LEAD THERMOCHRONOMETRIC CONSTRAINTS FROM LOWER CRUSTAL XENOLITHS, LESOTHO, SOUTHERN AFRICA.

M. D. Schmitz and S. A. Bowring, Department of Earth, Atmospheric, and Planetary Sciences, Massachusetts Institute of Technology, 77 Massachusetts Avenue, Cambrige MA 02139, USA (mschmitz@mit.edu).

Crustal xenoliths entrained in the Cretaceous kimberlites of Lesotho provide a unique case study for examining the thermal evolution of Archean lower crust during later orogenesis. These kimberlites erupted through crust that is presumed to be underlain by Archean gneisses of the Kaapvaal Craton [1], and contain mantle xenoliths with Archean Re-depletion ages [2] and thermobarometry consistent with "cratonic" mantle geotherms [3]. Yet the lower crustal granulite and eclogite xenoliths from these kimberlites preserve "frozen" mineral equilibria consistent with formation under high-T orogenic crustal geotherms and have Proterozoic Nd- and Pb-isotopic systematics [1,3]. It seems apparent from this evidence that the Archean lower crust of the craton margin underwent an episode of thickening and heating during Proterozoic orogenesis culminating in granulite-facies metamorphic conditions, and subsequent decay of this perturbation — all the while underlain by a keel of Archean lithospheric mantle. However, prior to this study, modern high-precision geochronometric analysis has not been applied to these xenoliths to test this model.

We have applied high-precision ID-TIMS U-Pb thermochronometry to a suite of mafic and felsic granulite xenoliths from the Letseng, Matsoku, Mothae, and Liquobong kimberlites. Xenoliths contain a variety of accessory mineral thermochronometers, including zircon, monazite, titanite, rutile, and apatite, that can be used to constrain the P-T-t paths of these granulites. Zircon and monazite have nominal closure temperatures at or above the peak metamorphic conditions of these xenoliths [4,5], and commonly crystallize below their closure temperature, thus requiring careful interpretation in terms of their participation in various metamorphic reactions. The U-Pb systematics of titanite, rutile, and apatite are interpreted in light of their closure temperatures for Pb diffusion [6–8], as well as their metamorphic stability. Careful accessory mineral petrography, geochemical data, and zoning studies all aid in this intepretation.

Preliminary results from these xenoliths confirm the geochronologic framework of the model presented above. Zircons from the Lesotho granulites contain Archean (2.6-Ga) and Middle Proterozoic (1.7-Ga) cores documenting the age of their protoliths. These zircons also preserve multiple generations of metamorphic growth from 1050 to 1000 Ma, which, to first order, dates the episode of granulite facies metamorphism. Monazites from these same xenoliths also contain multiple generations of growth between 1005 and 1020 Ma. High-grade metamorphism of the lower crust of the craton margin is thus a Proterozoic phenomena related to Namaqua-Natal orogenesis. A more detailed interpretation of the zircon and monazite dates in the context of a temperature-time path for the lower crust will be presented based on tying crystallization of these phases to well-constrained T-dependedent metamorphic reactions.

Ongoing studies of titanite, rutile, and apatite from these xenoliths will constrain the lower temperature portion of the cooling path of the granulites. Ultimately, we hope to reconstruct the time-temperature path that these lower crustal granulites trace during the decay of a transient elevated orogenic geotherm to the cold cratonic geotherm of today.

References: [1] Rogers N. R. and Hawkesworth C. J. (1982) *Nature, 299,* 409–413. [2] Pearson D. G. et al. (1995) *EPSL, 134,* 341–357. [3] Griffen W. L. et al. (1977) *Proc. 2nd Intl. Kimberlites Conf., 2,* 59–86. [4] Cherniak D. J. and Watson E. B. (1998) *GSA Abstr. with Prog., 30,* A213. [5] Parrish R. R. (1990) *Can. J. Earth Sci., 32,* 1618–1642. [6] Cherniak D. J. (1993) *Chem. Geol., 110,* 177–194. [7] Cherniak D. J. (1998) *Eos Trans. AGU, 79,* 370. [8] Cherniak D. J. et al. (1991) *GCA, 55,* 1663–1673.

METHANE-BASED BIOSYNTHESIS IN FLORIDA ESCARPMENT ABYSSAL BRINE SEEPS.

M. Schoell[1], R. J. Hwang[1], C. K. Paull[2], and C. S. Martens[2], [1]Chevron Research and Technology Company, Richmond CA, USA, [2]University of North Carolina at Chapel Hill, Chapel Hill NC 27599, USA.

Introduction: Methane-rich seeps at the base of the Florida Escarpment nourish rich communities of heterotrophic organisms that are supported by chemosynthetic primary production [1–3]. The seeps form patches of black sulfide-rich sediments that are also rich in organic C. Methane, as one food source of symbiotic autotrophs, has a $\delta^{13}C$ of –80‰ and the $\delta^{13}C$ of tissues from heterotrophs range from –40‰ to –75‰, attesting to the C flow from methylotrops to heterotrophs. We conducted C-isotopic analyses on individual compounds analyzed in sediment extracts to identify compounds that can be directly linked to methylotrophs.

Sample description. We investigated the three different samples from within a seep patch (seep), from a transiton zone (mix), and several meters away from the seep (background).

Analytical methods for compound identification using a GC-MSD and compound specific isotope analysis with a IR-GC-MS are described elsewhere [4,5].

Results: All extracts contain n-alkanes between n-C_{16} and n-C_{35}, with a terrestrial origin of the n-C_{23} to n-C_{35} alkanes (pronounced OEP; $\delta^{13}C$ of

TABLE 1. Bulk analyses of samples.

Sample	Alvin No.	C_{org} (%)	$\delta^{13}C$ (‰)
Background	1761-C5	0.85	-32.8
Mix	1762-2B	1.68	-48.1
Seep	1763-1B	5.90	-64.3

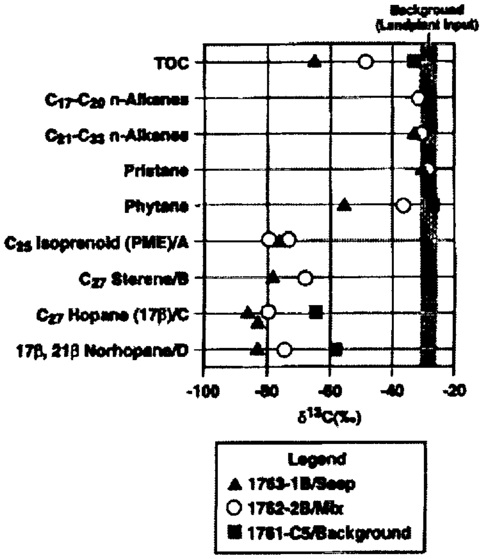

Fig. 1. Carbon-isotopic composition of individual compounds extracted from Florida Escarpment sediments in and around methane-rich brine seeps.

–27‰ to –32‰). Pristane is in all samples isotopically similar to the n-alkanes but phytane is ^{13}C-depleted in the Mix and Seep sample. There are conspicuous compounds in the GC trace that have been identified by mass spectra: i-C_{25} Pentamethyleicosane (PME); C_{27} Cholestene; C_{27} hopane (17β(H)-22,29,30 trisnorhopane); and C_{29} hopane (17β(H)-17β(H)-norhopane). The significant ^{13}C-depletion of these compounds (Fig. 1) links them directly or indirectly to the methylotropycally produced biomass.

Discussion: The isotopic data of pristane and the n-alkanes in the seep sediment are identical to those in the pelagic sediment and are all of terrestrial origin. The seep-related compounds that are different from those of the pelagic sediment are the isoprenoids phytane and PME isoprenoids, hopanes and surprisingly a unsaturated C_{27} sterene. What are their origins? The hopanes and the isoprenoids are known as direct biosynthesis products of methylotrophs [6]. Phytane ^{13}C-concentrations decrease from the pelagic to the seep sample, suggesting a mixture of terrestrial phytane with neo-formed bacterial phytane. Similar shifts in the hopanes indicate also a dual origin of these compounds in the pelagic sediment. However, sterenes are clearly of nonbacterial origin. An origin of these sterenes from mytilids is likely, as $\delta^{13}C$ of the bulk tissues of these animals is –74‰ [2].

One of the interesting observations in this study is that seep-related compounds are found in sediments that otherwise have characteristics of normal pelagic sediments. In this regard, these compounds can be used as pathfinders to seep environments. It is conceivable that moving animals spread these compounds around the seep area. Because of this unique labeling of these compounds, one may use isotopic analyses of individual compounds around the seeps for studies of the migration habits of seep-related animals.

References: [1] Paull C. K. et al. (1984) *Science, 226,* 965–967. [2] Paull C. K. et al. (1985) *Nature, 317,* 709–711. [3] Paull C. K. et al. (1989) *Nature, 342,* 166–168. [4] Schoell M. et al. (1992) *GCA,* 1391–1399. [5] Schoell M. et al. (1994) *Org. Geochem., 21,* 673–683, [6] Rohmer M. et al. (1989) *J. Gen. Microbiol., 130,* 1137–1150.

THE EFFECT OF VISIBLE LIGHT AND PHOSPHATE ON THE KINETICS OF PYRITE OXIDATION BY DISSOLVED MOLECULAR OXYGEN.

M. Schoonen[1] and D. Strongin[2], [1]Department of Geosciences, State University of New York–Stony Brook, Stony Brook NY 11794-2100, USA (mschoonen@notes.cc.sunysb.edu), [2]Department of Chemistry, Temple University, Philadelphia PA 19122, USA (dstrongi@nimbus.ocis.temple.edu).

Introduction: Pyrite oxidation by dissolved O_2 is an important reaction in the global cycles of S and Fe. Mining of sulfide ore and coal has greatly enhanced the global importance of this reaction and has created extremely acid and metal-rich environments. A large number of researchers, including Barnes and McKibben [1], have conducted experimental studies to determine the rate and mechanism of this process so that effective abatement strategies may be developed. Here the effect of illumination and addition of phosphate on the rate of pyrite oxidation is reported. Acid-cleaned, crushed pyrite was used. Experiments were conducted in a 1-L, water-jacketed, Pyrex, airtight vessel mounted on an optical bench. After preequilibrating the pyrite for 6–12 h in O_2-free water, pure O_2 gas was admitted. (The preequilibration is necessary to obtain reproducible results, we think that during this period intrinsic defects react with water; this notion is based on earlier UHV work [2]). The pH was kept constant using a pH-stat and the amount of NaOH added was used as a progress variable. Sulfate, Fe_{tot}, and PO_4 were periodically measured on aliquots. After establishing the reaction rate with the vessel covered with a black plastic sheet, the vessel was uncovered and illuminated with a 1000-W Xe lamp. The beam was cooled by passing it through a water filter. After establishing the rate under illumination, the vessel was covered again and the rate in the dark was remeasured. Experiments were carried out at pH 3, 4, 5, and 6. The temperature was closely monitored and all experiments were conducted at a temperature between 24° and 28°C. To evaluate the effect of PO_4 addition, two experiments were conducted at pH 4 and 6 in which the oxidation rate in the dark was measured as a function of PO_4 concentration.

Results and Discussion: Illumination accelerates the reaction rate by a factor of five at pH 3, 2.5 at pH 4 (see Fig. 1), 1.13 at pH 5, and 1.4 at pH 6. However, the rate of acid generation at pH 5 and 6 is nearly a factor of 10 higher than at pH 3 and 4. In all experiments, except the one at pH 5, a period of no acid generation was observed after the lamp was turned off. After this induction period, which lasted for 16 h at pH 3, the rate of acid production returned to approximately the same value as before the illumination. Illumination of the pyrite slurry raises the temperature in the vessel almost instantaneously a few degrees Celsius due to the fact that pyrite can absorb part of the radiation. This increase in heat cannot be efficiently dissipated even though the vessel is cooled by a constant temperature water bath. Given the high activation energy for pyrite oxidation, the rise in T can explain the slight acceleration at pH 5 and 6, but it cannot account for the acceleration observed at pH 3 and 4. In these most acid experiments, the relative rates of proton production and sulfate production also change when illuminated, suggesting a change in reaction mechanism. Experiments using XPS on single crystals may provide further insight.

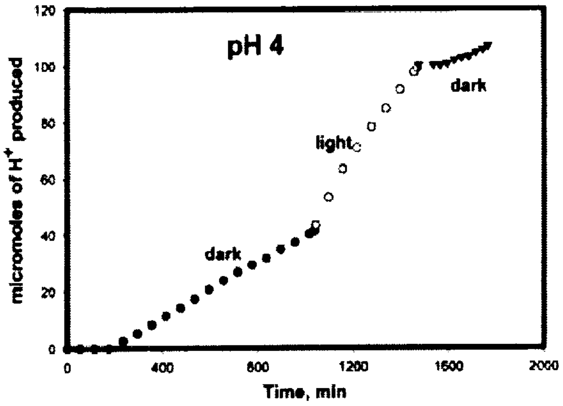

Fig. 1.

A radiation-induced acceleration of pyrite oxidation could lead to a diurnal effect in natural environments and it may explain some of the scatter in reported reaction rates. In general, illumination should be considered as a potentially important variable in any experimental study that involves semiconducting minerals.

Addition of phosphate decreases the oxidation rate significantly. The retardation effect on the oxidation rate appears to follow a Langmuir adsorption model. Earlier work in our group has shown that little phosphate sorbs on clean pyrite surfaces [3]. On oxidized pyrite surfaces PO_4 can also sorb onto Fe-(hydr)oxide patches. These patches are thought to facilitate electron transfer between the oxidant and the pyrite [2,4]. We postulate that sorption of PO_4 on these patches interferes with the electron transfer and that this is the cause for the retardation.

Acknowledgments: This work has been supported by DOE-BES.

References: [1] McKibben M. A. and Barnes H. L. (1986) *GCA, 50,* 1509–1520. [2] Guevremont J. M. et al. (1998) *ES&T, 32,* 3743–3748. [3] Bebie J. and Schoonen M. A. A. (1999) *EPSL,* in press. [4] Eggleston et al. (1996) *Am. Mineral., 81,* 1036–1056.

STRONTIUM ISOTOPES IN NEOPROTEROZOIC CAP CARBONATES FROM NAMIBIA: EVIDENCE FOR INTENSE CHEMICAL WEATHERING IN THE AFTERMATH OF A SNOWBALL EARTH.

D. P. Schrag[1], P. F. Hoffman[1], G. P. Halverson[1], S. A. Bowring[2], and K. Abbasi[2], [1]Department of Earth and Planetary Sciences, Harvard University, Cambridge MA 02138, USA (schrag@eps.harvard.edu), [2]Department of Earth, Atmospheric and Planetary Sciences, Massachusetts Institute of Technology, Cambridge MA 02139, USA.

The snowball Earth hypothesis proposes that Neoproterozoic glacial deposits and associated "cap" carbonates represent a series of global glaciations followed by extreme greenhouse conditions [1]. To study the cap carbonates in the context of the Snowball Earth hypothesis, we measured the Sr-isotopic composition ($^{87}Sr/^{86}Sr$) of carbonate rocks in Namibia from which we earlier obtained $\delta^{13}C$ data [1]. The data come from four sections located several hundred kilometers apart, and from different parts of the carbonate platform including the intra-shelf basin, the shelf rim, and the fore-shelf slope.

Regional variation in accumulation rate is inferred from the thickness of the basal dolomite member, and from the height of the C-isotopic excursion, and varies systematically with inferred water depth. The ^{87}Sr/^{86}Sr values in the carbonate rocks (500 m thick) underlying the glacial horizon climb range from 0.7072 to 0.7085. Above the glacial horizon, the data from all four sections show a similar pattern of variability. Initial postglacial values are between 0.708 and 0.710 before climbing steeply to >0.714. Peak values show substantial variations between sections from 0.714 to 0.724. Higher in the section, values drop more gradually and then stabilize to ~0.708. The stratigraphic extent of the positive anomaly varies with the inferred sedimentation rate, greatest in the shelf rim (150 m) and least in the fore-shelf slope (~20 m).

There are two possible frameworks for interpreting the Sr-isotopic data. First, it is possible that the entire pattern of isotopic variability was created by postdepositional diagenetic alteration, and that the extreme radiogenic values represent interaction with fluids from the granitic basement. However, there are several arguments against a diagenetic origin for these isotopic profiles. In all cases, the radiogenic anomaly occurs in the same statigraphic position above the glacial deposit (which is itself predominantly carbonate and not a source of radiogenic Sr). Moreover, the distance from basement, and the local structure, which could determine the direction of fluid flow, varies between these four sections. In addition, the isotopic excursion exists in sections where the dominant mineralogy is dolomite as well as calcite. Additional evidence against alteration includes the lack of strong correlation between ^{87}Sr/^{86}Sr and δ^{18}O values.

An alternative interpretation is that the Sr-isotopic data reflect primary values with some additional diagenetic overprint. If so, then the pattern requires an extraordinary explanation as it is impossible for the ^{87}Sr/^{86}Sr ratio of the whole ocean to change over the estimated duration for cap carbonate deposition (<10,000 yr!). The snowball Earth hypothesis asserts that a global glaciation occurred once the equatorward extent of sea ice crossed a critical threshold. As the tropical oceans froze rapidly, mean surface temperatures dropped by ~40°C. In the absence of a strong hydrologic cycle, the rate of chemical weathering of silicate minerals would be severely reduced, allowing accumulation levels of CO_2 in the atmosphere from volcanic outgassing over ~10 m.y. to eventually overcome the high planetary albedo. Melting sea ice near the equator would drive a runaway ice-albedo feedback in reverse, shifting the planetary climate to extreme greenhouse conditions in <100 yr with ~50°C surface temperatures at the equator. In the aftermath of the snowball Earth, the high surface temperatures and large surface area of fine grained silicate minerals, eroded by millions of years of glaciation and frost-shattering, would intensify silicate weathering, delivering alkalinity to seawater and driving rapid precipitation of cap carbonate in warm surface waters. In this context, it is possible that the ^{87}Sr/^{86}Sr excursion in the cap carbonate sequence reflects the response of the surface ocean to intense riverine input of radiogenic Sr derived from continental weathering. In the modern ocean, the delivery of Sr to the oceans by rivers is slow relative to the mixing rate between the surface and deep ocean, and hence the Sr-isotopic composition of the surface ocean is identical to the deep ocean. However, in the extreme conditions immediately following a global glaciation, if the riverine flux of Sr were high relative to the rate of mixing across the thermocline, the isotopic composition of the surface ocean would drift toward the composition of the input and away from the deep ocean. This effect would be amplified by stratification of the ocean caused by intense radiative heating by the greenhouse atmosphere and lowered salinity of the surface ocean from melting sea ice (~400 m thick upon termination). The ^{87}Sr/^{86}Sr ratio of the surface ocean would return to the whole ocean value once riverine inputs decreased and/or stratification of the surface ocean was reduced, yielding the stable ^{87}Sr/^{86}Sr values at the top of the sequence. A simple box model suggests that this mechanism can produce values of ~0.714 if an intense pulse of chemical weathering occurred over hundreds to thousands of years. However, this cannot explain the higher ^{87}Sr/^{86}Sr values in excess of 0.714 that are anticorrelated with carbonate content and are likely due to addition of clays with radiogenic Sr from decay of Rb.

References: Hoffman P. F. et al. (1998) *Science, 281,* 1342–1346.

URANIUM-SERIES DATING OF LAKE CARBONATES: THE LESSON FROM LAKE LISAN (PALEO-DEAD SEA).

A. Schramm[1], M. Stein[2], and S. L. Goldstein[3] [1]Max-Planck-Institut für Chemie, D-55010 Mainz, Germany, [2]Institute of Earth Sciences, The Hebrew University, Jerusalem, Israel, [3]Lamont-Doherty Earth Observatory and Department of Earth and Environmental Sciences, Columbia University, Palisades NY 10964, USA.

Lake Lisan, the last Glacial (~17–70 ka) precursor of the Dead Sea evolved through rapid changes in its water level. The lake history fluctuated between wetter and drier climatic conditions in the region. High-lake stand conditions (wet periods) were accompanied by development of a layered configuration and precipitation of aragonite from the upper layer. This layer also acted as a SO_4^{2-} accumulator during the lake's rise periods. The sulfate was removed, resulting in formation of prominent gypsum beds, upon climatic-induced (drier periods) mixing or even complete overturn of the lake. During low-lake stands, thick clastic layers were accumulated in the shallow shoulders of the lake basin.

Precise ^{230}Th-^{234}U ages were obtained by thermal ionization mass spectrometry (TIMS) on authigenic aragonite, which was deposited from the surface layer of the lake. It was discovered that the U-Th-isotopic system in Lisan aragonite is affected by the presence of initial aqueous Th as well as detrital U and Th. The composition of the authigenic and nonauthigenic components was determined by analyzing U- and Th-isotopic compositions and trace-element concentrations (e.g., Zr, Nb, Al, U, Th) in detrital and carbonate material from the Lisan section and in modern aragonite from the Dead Sea shore. The latter shows negligible detrital affects but contains initial Th, which corresponds to an apparent age of ~2.5 ka.

Thorium-230-uranium-234 ages were calculated by the isochron method and by correcting out detritus and initial aqueous ^{230}Th from individual samples. The two methods show excellent consistency and agree with the stratigraphic order of the samples. The ages range between 67 ka approximately 2 m above the base of Lisan Formation to 19 ka approximately 2 m beneath the top of the section at Perazim Valley. This age interval corresponds to stage 3 and parts of stages 2 and 4 in the marine isotopic record. The three members of the Lisan Formation at Perazim Valley are characterized by sedimentation rates of ~0.25, 1.76, and 0.80 mm/yr (bottom to top) respectively. Initial (^{234}U/^{238}U) activity ratios are 1.47 in the lower and upper members and 1.53 in the middle members.

The sedimentation rates and the U-isotopic compositions reflect the limnological history of the lake, which fluctuated between low and high lake stands due to the changing climatic conditions in the region. These changes are directly associated with the global history of the last glacial period. The low-stand clastic successions and gypsum layers are well correlated with the warming events in the global record while the high-stand aragonitic successions are correlated with the major cooling events. Finer structures in the mode of sedimentation appear throughout the section and can be correlated with shorter climatic cycles such as Dansgaard-Oeschger Events. It is concluded that the climate in the studied region is linked in finer details to the global climatic record.

FLUID EVOLUTION IN SHEAR-ZONE HOSTED MESOTHERMAL GOLD DEPOSITS: EXAMPLES FROM THE YILGARN CRATON AND LACHLAN FOLD BELT, AUSTRALIA.

P. K. Seccombe, S. C. Dick, and Z. Jiang, Department of Geology, The University of Newcastle, Callaghan, New South Wales 2308, Australia (psec@geology.newcastle.edu.au).

Structurally controlled mesothermal vein deposits represent major Au ± Cu resources in Archean and Paleozoic metamorphic terrains of Australia. Similarities in ore-fluid compositions and controls on Au deposition are evident, despite regional variations in host rock composition and metamorphic grades.

Gold mineralization at the Revenge mine in the Archean Yilgarn Craton of Western Australia is linked to dilation zones developed along second- and third-order, north-northwest-trending reverse faults propagating from the terrain-bounding Boulder-Lefroy Fault. Visible Au is confined to quartz breccia vein systems established within gabbroic host rocks, which are variably altered to assemblages dominated either by albite (proximal to veins), or biotite + albite or chlorite + biotite + calcite (distal alteration).

Ore-forming fluids at Revenge are typically multiphase H_2O-CO_2 mixtures of variable density and salinity. Fluid-inclusion microthermometry constrains depositional conditions for Au mineralization to the range P = 1675 to 2075 bars and T = 425°–525°C.

Interpreted fluctuations in fluid pressure at the time of trapping are consistent with a fault-valve model of fluid flow through the confining structures. Unmixing of CO_2-H_2O-NaCl fluids, due to episodic pressure decrease accompanying shear failure, was the dominant mechanism influencing Au deposition in quartz veins. Gold deposition was also influenced by sulfidation reactions in the gabbroic host rock.

Gold-copper ± (Zn-Pb-Ag) veins at the Peak mine, Cobar, in the Paleozoic Lachlan Fold Belt of eastern Australia, are confined to shear zones developed within a package of multiply deformed slates and metagraywackes of early Devonian age and along sheared contacts between metasediments and felsic metavolcanics (flow-banded and brecciated rhyolite).

Fluid-inclusion microthermometry at Peak indicates that both T and salinity increase during the paragenesis, corresponding to the introduction of Au-Cu followed by Pb-Zn ores. Fluids involved with the major Au-Cu event (stage 2 of the paragenesis) are hotter (ranging from 283° to 364°C) and more saline (6.0–8.6 wt% NaCl equivalent) than earlier, barren fluids. Temperatures of nearly 400°C are reached during deposition of the major Pb-Zn sulfide veins during stage 4 of the paragenesis.

Bulk analysis of inclusion fluids indicate a dramatic rise in the concentration of CO_2 during the initial Cu-Au event and the later Pb-Zn event at Peak. F^- and Cl^- levels are elevated in the fluids associated with the Pb-Zn event. By contrast, high CH_4 contents (and low CO_2/CH_4 ratios) characterize intervening and later stages of barren quartz deposition. Gas-phase compositions are confirmed by microthermometric data and laser Raman spectroscopy on individual fluid inclusions.

Fluid mixing is implicated as a control on ore deposition at Peak. Thermal and salinity cycles are likely to be linked to reactivation on the major thrusts and transient supply of fluid from basin and basement lithologies. An explanation for the additional base metals present in the Peak ores may involve differences in the host rocks among the two districts, rather than physicochemical factors during ore deposition.

HIGHLY RADIOGENIC UPPER CRUSTAL ROCKS OF CENTRAL IDAHO AND ITS BEARING ON ORE GENESIS.

K. P. Selvam[1], A. W. Macfarlane[1], G. Sen[1], and V. J. Salters[2], [1]Department of Geology, Florida International University, Miami FL 33199, USA, [2]National High Magnetic Field Laboratory, Florida State University, Tallahassee FL 32306, USA.

Many studies have posited deep, unexposed Paleozoic and Precambrian rocks as the sources of metals in hydrothermal ore deposits hosted by younger rocks in different parts of the world. The polymetallic ores of central Idaho are typical in this regard. The absence of Mesozoic sedimentary cover, as well as evidence for the existence of fossil hydrothermal systems coeval with the Cretaceous and Tertiary igneous activity and the mineralized nature of the Paleozoic sedimentary rocks exposed on the surface and in mine workings make central Idaho an ideal place for a careful evaluation of the role of host rocks in supplying the metals and other hydrothermal components.

While some previous studies of this region placed the source of metals mainly in the Paleozoic metasedimentary rocks, others favored deep unexposed sources below the metasediments. A major goal of our ongoing project is to determine the sources of Pb-Zn-Ag ores in central Idaho using Pb-isotopic ratios. In this report we present Pb-isotopic data on three principal groups of crustal rocks exposed in the area, including the Paleozoic metasedimentary rocks (e.g., Milligen and Dollarhide Formations) that host the ores. The two other crustal rocks include Proterozoic metasediments of the Yellowjacket Formation and Precambrian crystalline basement rocks of Shoup and Pioneer Mountain areas. Lead-isotopic compositions of these crustal rocks along with the ores are shown in Fig. 1.

Lead-isotopic compositions of ores and their host metasedimentary rocks overlap, which implies that most of the ore Pb was derived from the host rocks. Additionally, the data suggest that the Precambrian basement rocks could be the source of some radiogenic Pb found in the ores of central Idaho. The Paleozoic metasedimentary rocks of the Thompson Creek mine area with high Pb-isotopic ratios present a case for a radiogenic Pb source within the Paleozoic sedimentary sequence, and suggest that there may be similar units occurring in this region.

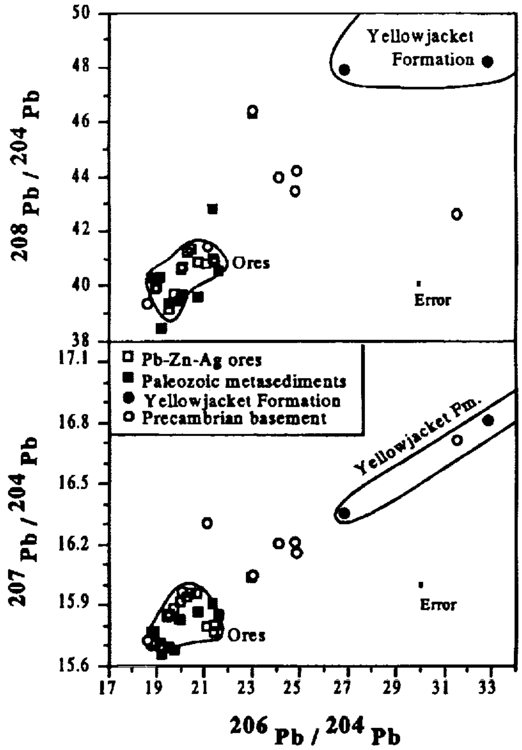

Fig. 1. Lead-isotopic composition of ores and host rocks of central Idaho in relation to other crustal rocks.

The Yellowjacket Formation, an equivalent of the Belt supergroup, hosts the Co-Cu mineralization in the Blackbird mine near Salmon. Both the ores and metasedimentary host rocks of the Blackbird mine have very high present-day Pb-isotopic ratios. Most of the ores hosted by the middle Proterozoic Belt supergroup of rocks in northern Idaho, western Montana, and southern British Columbia have less radiogenic Pb, but the Pb-isotopic composition of Belt rocks is not known. The results of this study do not support the generally held notion that the Proterozoic rocks of this region are less radiogenic in their Pb-isotopic composition. If this were the case, then the rocks and ores of Yellowjacket Formation must be unique among the Proterozoic metasedimentary rocks in having highly radiogenic Pb.

Metasediments of Yellowjacket Formation form a linear array on $^{206}Pb/^{204}Pb$-$^{207}Pb/^{204}Pb$ diagram and define an isochron age of 1.25 Ga. Most of the high-grade metamorphic rocks of the Shoup and Pioneer Mountains area also plot close to the lower end of this isochron, suggesting that the Yellowjacket Formation could have derived its sediments from Precambrian basement rocks similar to the ones exposed in this area.

HYDROGEN ISOTOPE RATIO MONITORING GAS CHROMATOGRAPH MASS SPECTROMETER.

A. L. Sessions[1], T. W. Burgoyne[2], A. Schimmelmann[2], and J. M. Hayes[1], [1]Department of Geology and Geophysics, Woods Hole Oceanographic Institution, Woods Hole MA 02543, USA (asessions@whoi.edu; jhayes@whoi.edu), [2]Departments of Chemistry and Geological Sciences, Indiana University, Bloomington IN 47405, USA (burgoyn@indiana.edu; aschimme@indiana.edu).

We have developed an analytical system capable of measuring $^2H/^1H$ (D/H) ratios in a wide range of individual organic compounds at the natural abundance level. Compounds are separated by a gas chromatograph (GC) using He carrier gas. The GC effluent is pyrolyzed to produce H_2 quantitatively and a portion is transmitted to an isotope-ratio mass spectrometer. An electrostatic filter suppresses transmission of scattered, low-energy $^4He^+$ to the mass-3 collector. Mass-2 and -3 ion currents are measured continuously and pointwise corrections are applied for contributions to the mass-3 beam from formation of H_3^+. Results are referred to the VSMOW scale by analysis of co-injected standards for which values of δD are known.

Production of H_2: At temperatures above 1450°C, pyrolysis of C-, O-, and H-bearing compounds yields H_2, CO, and graphite quantitatively [1]. The conversion requires a minimum residence time of ~300 ms within the heated zone. Production of methane is significant at lower temperatures and longer residence times and can lead to inaccurate results. Our system uses a SiC-resistive heating element to heat a 30 × 0.5 mm (i.d.) alumina tube, through which the sample stream flows. Tailing of peaks within the pyrolysis reactor is reduced by coating the inside with graphite.

Following pyrolysis, an open split transmits ~200 μL/min of He/H_2 to the mass spectrometer. Pyrolysis reduces H_2O background signals to <1 pA, lower than can be obtained with Nafion-based water removal systems. Therefore, no further water removal is employed.

Measurement of Ion Currents: The input of carrier gas produces a very large $^4He^+$ ion beam, a portion of which is scattered by inelastic collisions. $^4He^+$ ions that lose 25% of their energy have momentum equivalent to HD^+. To prevent these from reaching the mass-3 collector, an electrostatic lens was installed ~15 mm in front of the detector. The lens is held at ~80% of the 6.6-kV accelerating potential. With 200 μL He/min reaching the ion source, the m/z-3 ion current is >14 pA without the lens and <0.075 pA with the lens operating. The He flow rates accommodated are greater than those reported for a system using a wide-dispersion mass spectrometer [2,3].

The frequency response of the signal-processing pathways can limit the accuracy of D/H measurements. Accurate comparison of the ion beams requires close matching of the time constants of the amplifiers. Additionally, to allow accurate calculation of the extent of H_3^+ formation, the mass-2 amplifier must be fast enough to accurately reproduce changes in P_{H_2}. Calculations suggest that matched time constants <200 ms, not yet achieved in our system, will be required for optimal performance.

Correction for H_3^+: Collisions in the ion source produce H_3^+ by the reaction $H_2 + H_2^+ \rightarrow H_3^+ + H$. Unlike scattered $^4He^+$, the resulting H_3^+ has full kinetic energy and cannot be prevented from reaching the collector. As in conventional H-isotopic-ratio mass spectroscopy, a correction is applied for its contributions to the mass-3 signal. The formation of H_3^+ is proportional to $[H_2][H_2^+]$. In turn, the mass-2 ion current (i_2) is proportional to P_{H_2}. Accordingly, $i_{H_3} = K[i_2]^2$, where i_{H_3} is the H_3^+ ion current and K is the "H_3-factor." Two approaches have been proposed: a "pointwise" method in which each measurement of i_3 (typically 125 ms) is corrected based on the corresponding value of i_2 [4], and a "peakwise" method in which the heights of sample peaks are used as the basis for correcting the ratios of integrated peak areas [3,5,6]. Peakwise correction requires that all peaks have the same shape and underlying background. Pointwise correction is therefore required for GC analyses.

We examined two methods for determination of K: (1) the D/H ratio of a single sample of H_2 is measured at different values of P_{H_2}, and (2) K is chosen to minimize errors in δD in a series of GC peaks with widely varying height. Both methods gave similar values for K. The former method is more precise but the latter is more appropriate for continuous-flow conditions.

Performance: The performance of the system was evaluated using a homologous series of 15 n-alkanes for which values of δD had been determined conventionally. Two of the alkanes were used as isotopic reference compounds. For the remaining 13 the average standard deviation for measured values of δD was 3.6‰ (n = 10 injections). The root-mean-square deviation from the accurate value was 5.0‰ (n = 128 measurements), with no systematic errors due to peak size or retention time. Precision is currently limited by noise associated with the energy-filtering lens system.

References: [1] Burgoyne T. W. and Hayes J. M. (1998) *Anal. Chem., 70,* 5136–5141. [2] Prosser S. J. and Scrimgeour C. M. (1995) *Anal. Chem., 67,* 1992–1997. [3] Scrimgeour C. M. et al. (1999) *Rapid Comm. Mass Spec., 13,* 271–274. [4] Tobias H. J. et al. (1995) *Anal. Chem., 67,* 2486–2492. [5] Tobias H. J. and Brenna J. T. (1996) *Anal. Chem., 68,* 2281–2286. [6] Tobias H. J. and Brenna J. T. (1996) *Anal. Chem., 68,* 3002–3007.

ANCIENT-DEPLETED MANTLE UNDER A MODERN SPREADING CENTER: OSMIUM EVIDENCE FROM HYDROTHERMAL FLUIDS FROM JUAN DE FUCA RIDGE.

M. Sharma[1], A. W. Hofmann[1], G. J. Wasserburg[2], and D. A. Butterfield[3], [1]Max-Planck-Institut für Chemie, Postfach 3060, D-55020 Mainz, Germany, [2]Division of Geological and Planetary Sciences, California Institute of Technology, Pasadena CA 91125, USA, [3]Pacific Marine Environmental Laboratory, National Oceanic and Atmospheric Administration, Seattle WA 98115, USA.

Introduction: We present the first Os concentration and isotopic composition data for hydrothermal solutions from the Juan de Fuca Ridge in the Pacific Ocean. Conventional wisdom suggests that hydrothermal systems along mid-ocean ridges supply a large but unknown amount of Os to the oceans, derived from the alteration of mid-ocean-ridge basalts (MORB, $^{187}Os/^{188}Os$ ~0.125) [1]. That seawater reacts with hot oceanic crust to mobilize Os is borne out by Os-isotopic studies of metalliferous deposits precipitated from hydrothermal fluids in the TAG hydrothermal vent field in the Atlantic Ocean [2–3]. The data show sulfides/Fe-Mn crusts with $^{187}Os/^{188}Os$ ratios intermediate between that of seawater and MORB. We determined the Os concentration (C_{Os}) and isotopic composition of high-temperature ridge-crest fluids and the low-temperature fluids flowing out at the ridge-flanks. The results are intriguing as they have unexpectedly provided evidence of an ancient depleted domain within the upper mantle under the Juan de Fuca Ridge.

Samples: The Juan de Fuca Ridge, located ~500 km off the northwestern coast of the United States between the Blanco and Sovanco fracture zones, is a fast-spreading, sediment-free ridge. Extensive hydrothermal activity has been observed in three sections of the ridge: (1) Endeavour, (2) Axial Volcano, and (3) Cleft segment. Unfiltered fluid samples with low Mg contents, reflecting pure hydrothermal end members, were selected from these vent fields. These samples display a range of exit temperatures (265°–376°C) and Cl^- contents (148–1237 mmol kg^{-1}). Additionally, a sample of low-temperature off-axis fluid (50°C) was analyzed. This sample was collected from an ODP hole (leg 168, site 1026B) drilled on 3.5-Ma oceanic crust on the eastern flank of Juan de Fuca Ridge and possibly represents the warm reaction zone fluid supplying the springs (26°C) discovered recently in this area [4]. All samples were collected over the last 10 years with the submersible DSV Alvin.

Analysis: We utilize a procedure that converts Os existing in different oxidation states to OsO_4 in a closed system and results in a complete isotopic equilibrium between the sample and tracer [5]. The sample (30–50 mL) is taken in a large glass ampoule and frozen. Enriched ^{190}Os tracer and CrO_3-H_2SO_4 solution is then added to the ampoule. The ampoule is sealed and placed in an oven at 180°C for 40 h. The ampoule is then scoured open and OsO_4 distilled into chilled, concentrated HBr. The total ^{188}Os blank of this procedure is 0.013 ± 0.006 femtomol with $^{187}Os/^{188}Os$ = 0.27 ± 0.14. The total Os yield of this procedure is 90%. The Os isotopes were measured by negative thermal ionization mass spectrometry (NTIMS) using procedures given in [1].

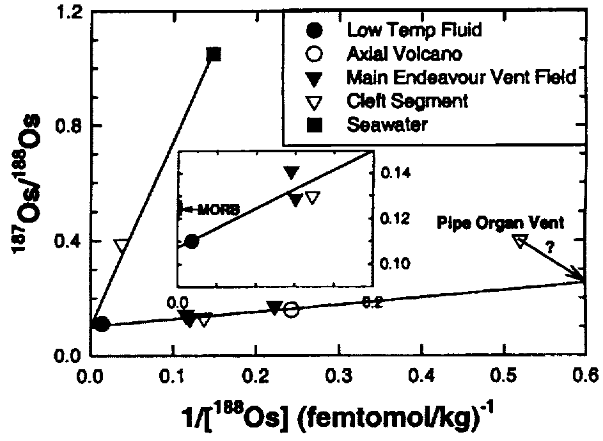

Fig. 1.

Results: The C_{Os} of the high-temperature hydrothermal fluids range from 15 to 202 femtomol kg^{-1} and the $^{187}Os/^{188}Os$ vary from 0.129 to 0.388. The C_{Os} of the low-temperature fluid is 518 femtomol kg^{-1}. Most remarkably, this sample has a $^{187}Os/^{188}Os$ ratio = 0.110 ± 0.001, much less than MORB or the upper mantle (~0.125) [6]. Such a low ratio has been measured in 2.7-Ga osmiridium samples from Witwatersrand [7]. Figure 1 plots the inverse of C_{Os} and $^{187}Os/^{188}Os$ ratios of the fluids. All data (except Pipe Organ, which is contaminated by ~22% seawater) plot along two mixing lines: (1) between a component with $^{187}Os/^{188}Os$ ratio = 0.11 and seawater, and (2) between two components with $^{187}Os/^{188}Os$ ratios of 0.11 and 0.2–0.3. The results point to a nearly complete overprinting of the seawater Os signal by a component with a $^{187}Os/^{188}Os$ ratio of 0.11. The model age of this component is 2.7 Ga. This observation is intriguing as it indicates the existence of an ancient depleted mantle component of unknown dimensions under the Juan de Fuca Ridge that has not mixed with the convecting MORB mantle.

Acknowledgments: California Institute of Technology Contribution 8642 (1033). DOE DE FG03-88ER-13851.

References: [1] Sharma M. et al. (1997) *GCA, 61,* 3287–3299. [2] Ravizza G. E. et al. (1996) *EPSL, 138,* 105–119. [3] Bruegmann G. E. et al. (1998) *Proc. ODP, 158,* 91–100. [4] Mottl M. J. et al. (1998) *Geology, 26,* 51–54. [5] Sharma M. et al. (1999) *GCA,* submitted. [6] Shirey S. B. and Walker R. J. (1998) *Annu. Rev. Earth Planet. Sci., 26,* 423–500. [7] Allègre C. J. and Luck J. M. (1980) *EPSL, 48,* 148–154.

THE CARBON DIOXIDE/HELIUM-3 SYSTEMATICS OF PLUME-, MID-OCEAN-RIDGE BASALT, AND ARC-TYPE LAVAS FROM THE MANUS BACK-ARC BASIN.

A. M. Shaw[1], D. R. Hilton[1], C. G. Macpherson[1,*], and J. M. Sinton[2], [1]Geosciences Research Division, Scripps Institute of Oceanography, La Jolla CA 92093-0244, USA (amshaw@ucsd.edu; drhilton@ucsd.edu), [2]Department of Geology and Geophysics, University of Hawai'i, Honolulu HI, USA (sinton@soest.hawaii.edu), (*present address: Southeast Asia Research Group, Department of Geology, Royal Holloway University London, Egham, Surrey, UK; c.macpherson@gl.rhbnc.ac.uk).

Introduction: The $CO_2/^3He$ ratio in magmatic volatiles has been used to provide constraints on the flux of CO_2 between mantle and exospheric reservoirs [e.g., 1]. The validity of any flux calculations is limited, however, by assumptions that $CO_2/^3He$ ratios measured in various media (basalt glasses, geothermal fluids, etc.) are representative of the underlying mantle source region. A recent study of Loihi Seamount [2] has shown that the $CO_2/^3He$ ratio can vary over 2 orders of magnitude, with magma composition coupled with degree and mode of degassing exerting the controlling influence on the measured $CO_2/^3He$ values. To assess further these potentially fractionating effects, we have analyzed a diverse suite of lavas from the Manus back-arc basin (Bismark Sea). These lavas span a broad compositional range and have plume-, MORB- and arc-type geochemical affinities [see 3]. Taken together, the Manus Basin lavas should allow a realistic assessment of the factors controlling the $CO_2/^3He$ ratio as well as characterization of the ranges in this parameter for the various petrogenetic types.

Setting and Samples: The Manus back-arc basin is located in the eastern Bismark Sea. Fresh volcanic glass was obtained from the Central Manus Spreading Center, the east-striking Extensional Transform Zone, and two rift zones: the Southern Rifts and the East Manus Rift. All glasses are tholeiitic and have been analyzed previously for major- and minor-element chemistry and radiogenic and He isotopes [see 3]. Based upon these analyses, the lavas are distinguished as MORB type-1, MORB type-2, back-arc-basin basalt (BABB), and arc-type. Plumelike $^3He/^4He$ ratios ($>12R_A$) characterize all types except for Arc lavas.

Analytical Approach: We analyzed for He, Ar, and CO_2 concentrations using stepped-heating protocols that permit resolution into vesicle and dissolved components. For CO_2, this distinction can be made on the basis of both the amount of gas released as a function of temperature and on $\delta^{13}C$ values (work in progress). For He and Ar, we used the gas yields at 800°C and 1200°C release steps, respectively, to represent these components. Crushing in vacuo established sample $^3He/^4He$ ratios [3].

Carbon Dioxide/Helium-3 Results: MORB-1 glasses (n = 5) have bulk-rock $CO_2/^3He$ ratios tightly constrained between $1–2 \times 10^9$ with a consistent pattern of lower values ($3–7 \times 10^8$) in the vesicle phase. In contrast, MORB-2 samples (n = 3) have higher total $CO_2/^3He$ values (2×10^9 to 2×10^{10}); again their vesicle ratios are consistently lower. BABBs (n = 4) show a similar range to MORB-2s, whereas arc-type lavas (n = 2) have significantly higher $CO_2/^3He$ ratios in both the bulk-rock and vesicle phases.

Degassing and Source Effects: The observation of lower $CO_2/^3He$ ratios in vesicles relative to the dissolved phase can be attributed to either (1) an equilibrium degassing case where the a factor [$= S_{He}/S_{CO_2} = (CO_2/^3He_{vapor})/(CO_2/^3He_{melt})$] <1; however, this is not consistent with degassing behavior anticipated for a tholeiitic magma [see 2]; or (2) a situation where vesicles gas is not in equilibrium with the dissolved gas, i.e., one or both phases may contain exsolved/residual gas from different volumes of magma. It is noteworthy, however, that vesicles have substantially higher $^4He/^{40}Ar^*$ ratios than coexisting glass — an observation opposite to that expected for equilibrium degassing.

In spite of indications of nonequilibrium degassing, can source $CO_2/^3He$ ratios still be identified? Higher H_2O contents in the sequence MORB-1, MORB-2, BABB, and arc lavas should lead to enhanced exsolution of CO_2 — consistent with the observation of higher $^4He/^{40}Ar^*$ ratios in the more evolved magma types — and more extreme (lower for a tholeiitic melt [2]) values of $CO_2/^3He$. This is not the case, and this suggests that the relative solubility characteristics of He and CO_2 cannot be the sole controlling influence on resultant $CO_2/^3He$ ratios. Therefore, a higher "initial $CO_2/^3He$ ratio" of all non-MORB-1 lavas (as anticipated for a subducted slab or arc crust input) and/or variations in magma chemistry (to decrease the a factor; [2]) are possible explanations. In an attempt to resolve this issue, ongoing studies will concentrate on (1) modeling the solubility behavior of CO_2 and He over the range of lava compositions encountered in the Manus Basin, and (2) utilizing the $\delta^{13}C$-isotopic composition of vesicle and dissolved CO_2 to identify crustal and/or slab additions to the CO_2 inventory.

References: [1] Marty and Tolstikhin (1998) *Chem. Geol., 145,* 233–248. [2] Hilton et al. (1998) *Nature, 396,* 359–362. [3] Macpherson et al. (1998) *Geology, 26,* 1007–1010.

ELEMENTAL FRACTIONATION AND EQUILIBRIUM PROCESSES.

D. M. Shaw, School of Geography and Geology, McMaster University, Hamilton ON, L8S 4M1, Canada (shawden@mcmaster.ca).

Goldschmidtian geochemistry delineated the behavior of individual elements, particularly the rarer ones, leading to the view that trace-element studies could be used to illuminate (some would say "to solve") geological problems, because of ideal behavior in low-concentration solutions, both liquid and solid.

After World War II, the theoretical groundwork laid by H. Neumann and by H. D. Holland and J. L. Kulp, based on Lord Rayleigh's 1902 theory, provided a base for trace-element studies in igneous and metamorphic petrology, while a seminal treatment of oxidation and reduction mechanisms by B. Mason did the same for aqueous media and sediments.

Improved analytical methods, augmented by resolution of contamination problems by continually decreasing the effective sample size, have led to better quantitative results for elemental studies, although not yet as good as for isotopic systems.

Element distributions in Earth materials are explained using heterogeneous phase equilibrium theory. One of the most useful concepts in that theory is that of the *equilibrium partition coefficient K(i)* of an element *i* between two phases, which has been extensively applied to fractionations in both melting and crystallization processes. But early hopes that Henry's Law, implying constant K(i), would govern trace-element distributions have been dashed, and partition coefficient studies now support many careers.

Nevertheless and paradoxically, the concept of the constant partition coefficient has been very useful in elaboration both of *continuous (dynamic) mantle melting* and of *crustal reaction melting.*

A quite different approach is used for *nonequilibrium melting.* Because of the great difference in diffusion kinetics for solid and liquid phases, this view contends that, at least over short periods, melting overrides partitioning and consequently both major and trace elements behave alike.

Unfortunately, however, few trace-element data arrays are sufficiently precise, or well-enough controlled geologically, to prove or disprove any of the models.

A HIGH-PRECISION BENTHIC FORAMINIFERAL STRONTIUM/CALCIUM RECORD OVER THE PAST 35,000 YEARS.

C.-C. Shen[1,2], S. R. Emerson[1], D. W. Hastings[3], T. Lee[2], C.-H. Chiu[2], and G. T. Shen[1], [1]School of Oceanography, WB-10, University of Washington, Seattle WA 98195, USA, [2]Institute of Earth Sciences, Academia Sinica, P.O. Box 1-55, Nankang, Taipei, Taiwan, China, [3]Department of Earth and Ocean Sciences, University of British Columbia, Vancouver BC, V6T 1Z4, Canada.

How constant was the Sr/Ca concentration ratio for seawater in the past thousands to millions of years? The answer is crucial for the reconstruction of past sea surface temperature (SST) using the temperature-sensitive partition of these two elements between coral skeleton and water. As the first step toward answering this difficult question, we have carefully developed, after extensive experimentation using modern core-top samples from Ontong-Java and Caribbean, a procedure to clean and measure Sr/Ca of benthic foraminifer *Cibicidoides wuellerstorfi*. Data for individual modern samples from the eastern equatorial Pacific appear to be normally distributed with a standard deviation (s.d.(1)) of 1.75%, far higher than the analytical uncertainty of 0.03%. Since both temperature and Sr/Ca of seawater should be nearly constant in deep ocean, the Sr/Ca of individual samples of this benthic species apparently cannot be used as a proxy for seawater Sr/Ca. On the other hand, the Sr/Ca for bulk samples consisting of large number of modern specimens (N = 8–25) were found to converge, and their standard deviation seemed to decrease according to $s.d.(N) = s.d.(I)/N^{0.5}$. Applying this to a core from the eastern equatorial Atlantic Ocean, we found that the bulk ratios (with estimated standard deviation from 0.12% to 0.39%) varied by as much as 3.5% over the past 35 k.y. If the Sr/Ca ratios of bulk samples of *C. wuellerstorfi* indeed reflect seawater Sr/Ca, then we have to suspect that seawater Sr/Ca was variable in the past. Such putative variation of seawater Sr/Ca would have significant implications on many fundamental issues in past global changes. For instance, it may reduce the coral-based estimate of tropical SST drop during the last glacial maximum (LGM) from 5°–6°C to 2°–3°C. But it would also raise the Sr/Ca-based SST estimates for the early Holocene to an almost unattainable level. Our results put the earlier speculation of such variations derived from less precise data on firmer grounds. It also accentuates the importance of exploring possible mechanisms to change seawater Sr/Ca on timescales shorter than the long residence time of these two elements in the ocean.

NEW INSIGHTS OF SULFIDE ORE GENESIS FROM AN OSMIUM-STRONTIUM-ISOTOPIC STUDY OF CHINKUASHI GOLD-COPPER DEPOSIT IN TAIWAN.

J. J. Shen[1], L. P. Tan[2], C. H. Chen[1], C. Y. Lan[1], and C. H. Chen[1], [1]Institute of Earth Sciences, Academia Sinica, P.O. Box 1-55, Nankang, Taipei, Taiwan, [2]Department of Geology, National Taiwan University, Taipei, Taiwan.

Differences between the geochemistry of Sr and Os mean that Os isotopes can yield insights into certain aspects of mantle and magma hydrothermal processes, where Sr-isotopic studies cannot. In particular, the distribution of Os and Sr in the continental crust differ significantly due to the differences in the partitioning of these elements between silicate partial melts and solid residue. Osmium behaves compatibly, thus partitioning strongly into the residue, while Sr behaves incompatibly. As a result, Os is concentrated in the mantle and deeper portions of the crust, whereas Sr is concentrated in the upper crust. Consequently, the Os concentration and isotopic composition of hydrothermal fluids may be sensitive to the depth of hydrothermal circulation, with deeply penetrating fluids carrying higher concentrations of less radiogenic Os than fluids associated with more superficial hydrothermal systems. Similarly, the fact that Os exhibits an active redox chemistry while Sr does not indicates that the behavior of Os along the flow path within a hydrothermal system will likely be influenced by evolving redox conditions.

The Miocene sediments of Chinkuashih in northeastern Taiwan contain abundant hydrothermal sulfide deposits rich in Au and Cu. The Au-Cu mineralization is associated with several small, late Pliocene-Pleistocene dacite-andesite intrusions. In two of the intrusions (Chiufen and Wutanshan), the ore is composed of pyrite, galena, sphalerite, marcasite, and native Au. In the Penshan intrusion enargite, luzonite and alunite are common. Seven sulfide samples (including pyrite, marcasite, sphalerite, enargite, and luzonite) have been analyzed for Re-Os recently. The preliminary data are shown in Fig. 1.

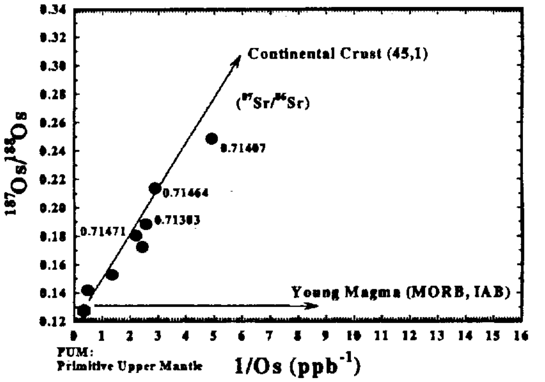

Fig. 1.

All sulfides show a narrow range of isotopic ratio for $^{187}Os/^{188}Os$ (from 0.139 to 0.249) but a large variation for $^{187}Re/^{188}Os$ (from 3.7 to 34.6). All Os data (Fig. 1) could be fitted by a two endmember mixing model in which the primitive upper mantle was contaminated by the continental crust. It is interesting that Chinguashih sulfides are dominated by mantle source on the Re-Os-isotopic system although there is no definitive evidence indicating mantle activity taking place in northern Taiwan.

The Sr-isotopic data for four sulfide samples from Chinkuashih area have also a very narrow range of isotopic ratio for $^{87}Sr/^{86}Sr$ (from 0.7130 ~ 0.7147) (Fig. 1). These ratios are well within the range spanned by those for typical Taiwan sediments. The Sr-Os data clearly showed that Sr was dominated by crustal sources while Os mainly came from the mantle.

The easiest way to interpret the mixing during Chinkuashih ore formation is that the Os in sulfides was transported by the hydrothermal fluid, which was originally meteoric water but penetrated along very deep faults to extract Os from the upper mantle. On the other hand, Sr mainly came from the shallow level when the hydrothermal fluid passed through the continental crust. Alternatively, Chinkuashih deposits were initially magmatic sulfide proto-ore formed by earlier magmatic activity. Then a relatively shallow hydrothermal circulation system brought the proto-sulfide-ore to the surface.

ION SOLVATION AND MOLECULAR DYNAMICS AT THE GOETHITE/WATER INTERFACE.

D. M. Sherman, Department of Earth Sciences, University of Bristol, Bristol BS8 1RJ, UK (dave.sherman@bris.ac.uk).

Introduction: Understanding the dielctric properties of water near mineral surfaces is essential before we can understand the behavior of water along grain boundaries and during mineral solution equilibria. The sorption of cations as either innersphere or outersphere complexes onto the surface of goethite is of fundamental importance in environmental chemistry. In the work reported here, I investigated the structure of water near the goethite (110) surface under both saturated and unsaturated conditions using molecular dynamical simulations. Subsequently, I investigated the solvation of NaCl by surface-sorbed water.

Molecular Dynamics Calculations: The calculations were based on the SPC/E model for water developed by Berendsen et al. [1]. The Na-O, Cl-O, and Cl-Cl short-range potentials of Smith and Dang [2] were used; these potentials were shown by Brodholdt [3] to give a very accurate description of the density of NaCl-water mixtures. The goethite (110) surface was modeled as a rigid framework with SPC/E charges on the O and H atoms and a charge of 1.27 for the Fe atoms. A 10.97 × 12.01-Å unit cell of goethite (110) was solvated by 16, 32, 60, and 144 water molecules. Calculations were run for 100 ps, with the first 10 ps used for thermal equilibration.

Dynamics of Water on Goethite (110): The first several monolayers of water are strongly oriented by the goethite surface and develop a structure different from that of bulk water. The self-diffusion constant of water decreases from 2.5×10^{-5} cm^2/s (bulk water) to 1×10^{-6} cm^2/s (four mono-

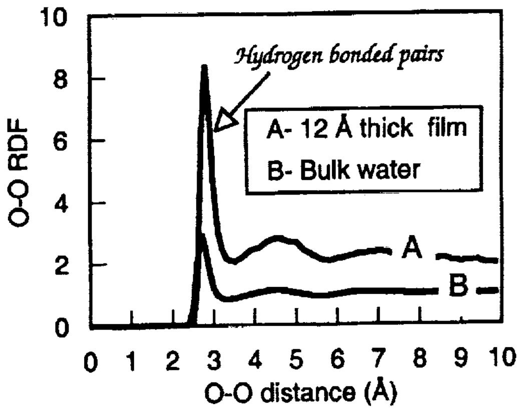

Fig. 1. Oxygen-oxygen RDF showing the enhanced H bonding between water molecules in the surface film of goethite.

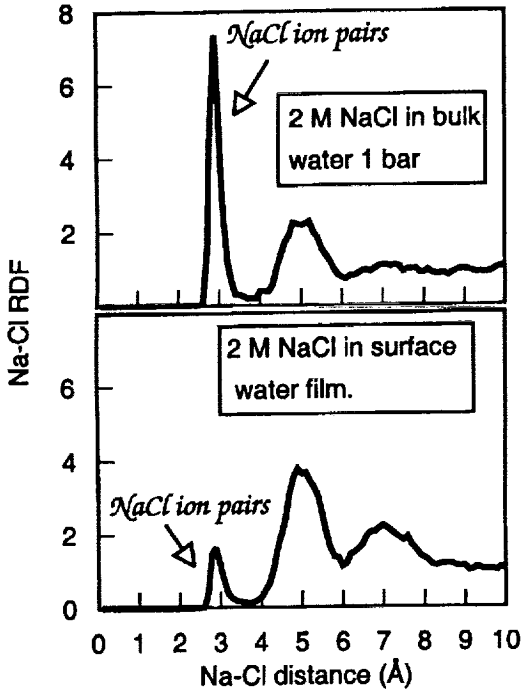

Fig. 2. Sodium chloride radial distribution functions showing decreased NaCl ion pairing in water sorbed onto the goethite surface.

layers on the goethite surface). Both the density and the degree of H bonding are enhanced in the surface water compared to that in bulk water. This effect is shown in the O-O radial distribution functions (Fig. 1) of bulk and surface water. The main peak at 2.9 Å corresponds to O-O pairs held together by H bonds. This effect is strongest, however, for surface films formed in unsaturated conditions.

Ion Association at the Goethite Surface: In concentrated NaCl solutions, a significant degree of ion pairing occurs. Near the goethite surface, however, the dielectric constant of water is increased due to the enhanced H bonding; this enhances the dissociation of NaCl ion pairs (Fig. 2). The effect on the goethite surface is comparable to that in bulk water at 5 kbar pressure.

Conclusions: The chemical behavior of water near mineral surfaces is different from that in bulk solution. Ionic dissociation will be enhanced near the mineral-solution interface and in aqueous films found in unsaturated conditions. These effects must be quantified before we can understand fluid-rock interactions.

References: [1] Berendsen H. J. C. et al. (1987) *J. Phys. Chem., 91,* 6269–6271. [2] Smith D. E. and Dang L. X. (1994) *J. Chem. Phys., 100,* 3757–3766. [3] Brodholdt J. P. (1998) *Chem. Geol., 151,* 11–19.

THERMODYNAMICS OF STRONTIUM, BARIUM, AND LEAD SOLID SOLUTION IN $CaSO_4$: RESULTS FROM ATOMISTIC SIMULATIONS.

D. M. Sherman, Department of Earth Sciences, University of Bristol, Bristol BS8 1RJ, UK (dave.sherman@bris.ac.uk.).

The divalent cations Ba^{2+}, Pb^{2+}, Cd^{2+}, and Sr^{2+} are significant toxic heavy metals and radionucliides in the environment. The aqueous concentrations of these ions in soil solution and groundwater may be limited by the formation of insoluble sulfate minerals. However, if these cations are incorporated via solid solution with Ca in anhydrite ($CaSO_4$) and gypsum, then the aqueous concentrations may be kept even below that determined by saturation of the pure sulfate end member. Before we can predict the effect of solid solution with CaSO4 on metal ion solubilities, we need to have activity composition relations along the $CaSO_4$-MSO_4 (M = Ba, Sr, Pb, and Cd) binaries.

Atomistic Simulations: Allen et al. [1] have derived a set of interatomic potentials for S-O, Ba-O(SO_4), Ca-O(SO_4), and Sr-O(SO_4) that give an accurate prediction of the structures and elastic constants of $SrSO_4$, $BaSO_4$, and $CaSO_4$. We can derive a potential for Pb^{2+}-O by fitting to the structure of anglesite, $PbSO_4$.

Calculated Mixing Parameters: The static-free energy of mixing can be estimated by averaging over the possible ionic configurations of a given composition using a 2 × 2 × 2 supercell of the Amam $CaSO_4$ structure. The resulting excess energies for Sr, Ba, and Pb in $CaSO_4$ are shown in Fig. 1. A regular solution model, such that $\Delta G_{excess} = \lambda X(X - 1)$, gives an excellent fit to the calculated energies of mixing. The calculated interaction parameters, l, are found to be 82.4, 29.7, and 24.1 kJ/mol for Ba, Pb, and Sr in anhydrite. The activity coefficients for the MSO_4 components in solid solution with $CaSO_4$ are $\gamma_A = \exp(\lambda(1 - X_M)^2/RT)$.

Calculated activity-composition relations for $BaSO_4$, $PbSO_4$, and $SrSO_4$ in anhydrite ($CaSO_4$) are shown in Fig. 2.

Aqueous Solubility of Barium, Lead, and Strontium in the Presence of $CaSO_4$: We can calculate the solubility of Ba, Sr, and Pb in the pres-

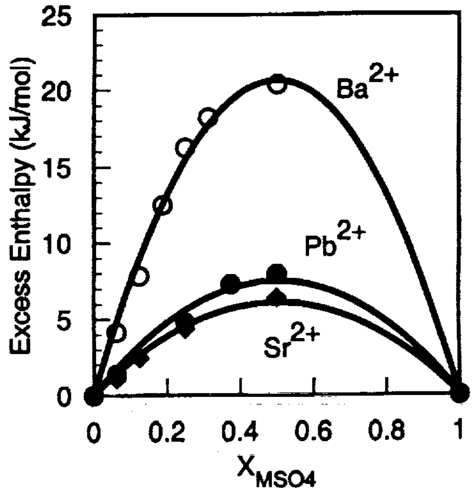

Fig. 1. Calculated mixing enthalpies fit to regular solution model.

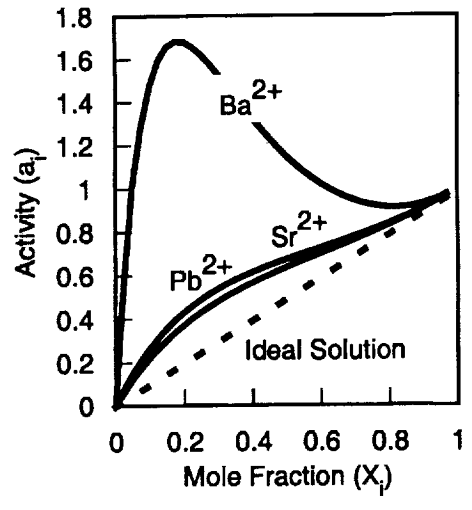

Fig. 2. Activity composition relations along the MSO_4-$CaSO_4$ binaries.

ence of anhydrite (ahy) given the interaction parameters and the solubility products of the endmember sulfate minerals. Consider the reaction

$$Ba^{2+}(aq) + CaSO_4(s) = BaSO_4(s, ahy) + Ca^{2+}(aq)$$

The equilibrium constant can be expressed

$$K = \frac{K_{sp}^{CaSO_4}}{K_{sp}^{BaSO_4}} = \frac{a_{Ca}^{aq}}{K_{Ba}^{aq}} X_{Ba}^{ahy} \exp(\lambda(1 - X_{Ba}^{ahy})^2/RT$$

In the limit where $X_{Ba} \ll 1$, we can write

$$K = \frac{K_{sp}^{CaSO_4}}{K_{sp}^{BaSO_4}} = \frac{a_{Ca}^{aq}}{K_{Ba}^{aq}} X_{Ba}^{ahy} \exp(\lambda/RT)$$

For reactive-transport modeling, we need a K_d to describe the partitioning of Ba between aqueous solution and solid anhydrite

$$K_d = \frac{[Ba^{2+}]}{X_{Ba^{2+}}} = \frac{K_{sp}^{BaSO_4}}{K_{sp}^{CaSO_4}} \frac{\gamma_{Ba}^{aq}}{\gamma_{Ca}^{aq}[Ca^{2+}]} \exp(-\lambda/RT)$$

The aqueous activity coefficients can be calculated using standard methods such as the Davies equation.

References: [1] Allen et al. (1993) *Faraday Discussions, 95,* 273–280.

RARE-EARTH-ELEMENT FRACTIONATION AND NEODYMIUM-ISOTOPIC VARIATION IN PACIFIC HYDROTHERMAL PLUMES AND METALLIFEROUS SEDIMENTS.

R. M. Sherrell[1], G. Ravizza[2], M. P. Field[1], and J. Blusztajn[2], [1]Institute of Marine and Coastal Sciences, Rutgers University, 71 Dudley Road, New Brunswick NJ 08901-8521, USA (sherrell@imcs.rutgers.edu), [2]Department of Marine Geology and Geophysics, Woods Hole Oceanographic Institution, Woods Hole MA 02543-1541, USA (gravizza@mail.whoi.edu).

We present results demonstrating that hydrothermal plume particles in Atlantic and Pacific plumes faithfully record ambient deepwater rare-earth-element (REE) composition with a constant light/heavy fractionation [1]. Armed with this finding, we explore the paleoceanographic utility of paired Nd-isotopic and precise REE pattern determinations in hydrothermal metalliferous sediments from the flanks of the southern East Pacific Rise (EPR). Previously, Nd-isotopic records (but not REE patterns) have been available chiefly from Fe-Mn crusts [2], which accrete at ~0.002 m/Ma and therefore have relatively poor temporal resolution.

Results and Discussion: Previous studies of REE systematics in an Atlantic hydrothermal plume showed increasing REE/Fe ratio with decreasing Fe as the plume dispersed, interpreted as continuous uptake of REE over time within the plume [3]. On the basis of new Pacific plume data (9°45'N on the EPR [1,4]); and a reinterpretation of the Atlantic (TAG; [3]) data, we now argue that REE systematics in plumes are not dictated by uptake kinetics, but by mixing of well-defined hydrothermal endmember particles with ambient background material. This behavior allows extrapolation to the composition of unmixed hydrothermal particles, which show light REE enrichment relative to seawater (factor of 1.8 in Nd/Er).

Previous studies have suggested that this signature would not be preserved in sediments, and that REE/Fe in southern EPR flank sediments increases with distance from the ridge crest due to continued long-term uptake. However, this enrichment likely reflects increasing fractions of other components (terrigenous particles and authigenic apatites) as the hydrothermal input decreases off-axis. By limiting our investigation to rapidly accumulating sediments proximal to the ridge axis, above the paleo-lysocline, we have avoided much of this complexity. Our results show no systematic change in REE/Fe with paleo-distance; REE/Fe and REE pattern shape closely match that of plume particles. Therefore, we interpret downcore variations in Nd/Er as changes in the REE composition of Pacific deepwater. Because negligible Nd is associated with nonhydrothermal sediment components, we also interpret downcore ε_{Nd} as a reflection of changing deepwater composition.

The downcore record from the SEPR shows variation in ε_{Nd} and Nd/Er exceeding the geographical/depth range in modern Pacific waters. The $\varepsilon_{Nd(0)}$ record is S-shaped in time; decreasing from –4.5 to –6.1 from 28 to 19 Ma, then increasing to a maximum of –3.0 at 8 Ma, then decreasing again to –4.5 at 1.5 Ma. The corresponding record of REE fractionation (as Nd/Er), shows inverse correlation to ε_{Nd} over 19–8 Ma, consistent with a shift of ~40% in Nd/Er to more continental (nonradiogenic and LREE depleted) signature. However, in the intervals 28–19 Ma and 8–1.5 Ma, ε_{Nd} decreases with time, while Nd/Er is little changed (≤10%). The range of Nd/Er values is less than or equal to the modern values recorded in plume particles, suggesting that deep Pacific water was LREE-depleted, relative to modern, through most of the last 28 m.y.

Prior records of ε_{Nd} in Fe-Mn crusts have generally been interpreted as reflecting variations in water mass mixing [2]. Our data suggest this inference is problematic, because Nd/Er changes are far too large to be consistent with ε_{Nd} changes driven by mixing modern Atlantic and Pacific deepwater. Rather it seems more likely that changes in REE sources within the Pacific basin may have altered quasi-independently of the ε_{Nd} and REE patterns of deepwater. Identification of such sources is difficult; indeed, the sources of radiogenic Nd to the modern Pacific remain unconstrained [5,6].

One intriguing hypothesis is that the net input of hydrothermal fluid REEs has varied over these timescales. The slow Fe(II) oxidation rate in the modern Pacific [7] may allow a large fraction of hydrothermal-source REE signature to escape the plume reaction zone and mix into the deep reservior, imprinting a more radiogenic Nd-isotopic signature to Pacific deep waters. We strees that this possibility is consistent with net removal of oceanic REEs by hydrothermal systems. Assuming relatively constant hydrothermal flux, varying influence of vent fluids on the deepwater REE signature could be driven by changes in pH and O_2, which set Fe(II) oxidation kinetics. Thus deepwater REE composition as recorded in these sediments may change as a result of variable "leakage" of hydrothermal REE signature from mid-ocean ridge systems.

References: [1] Sherrell R. M. et al. (1999) *GCA,* in press. [2] O'Nions R. K. et al. (1998) *EPSL, 155,* 15–28. [3] German C. R. et al. (1990) *Nature, 345,* 516–518. [4] Field M. P. and Sherrell R. M. (1998) *Anal. Chem., 70,* 4480–4486. [5] Bertram C. J. and Elderfield H. (1993) *GCA, 57,* 1957–1986. [6] Jeandel C. et al. (1995) *GCA, 59,* 535–547. [7] Field M. P. and Sherrell R. M. (1999) *GCA,* submitted.

BROWN COAL AS A DETOXICANT OF SOILS POLLUTED WITH HEAVY METALS.

A. V. Shestopalov, O. S. Bezuglova, and I. V.

Morozov, Department of Soil Science, Rostov State University, B. Sadovaya, 105, Rostov-on-Don 344006, Russia (besuglov@ic.ru).

Introduction: Brown coal (BC) has usually been used as fossil fuel, but there is the possibility that it may be used in other ways. The problem of purification of soils polluted with heavy metals (HM) can be solved though BC application.

Materials and Methods: Brown coal is a natural mineral-organic matter that has a large potential to bind the pollutants [1]. In our research the waste BC was used. This BC composition is almost similar to that of native BC. It contains humic acids (46%), which are of great importance for soil fertility. Humic acids can transform HM ions to ligands. BC can bind HM ions by physical absorption as well. BC capacity to absorb HM and to keep them inside was studied in model experiments. The upper horizon of ordinary calcareous chernozem (zonal soil) was mixed first with different forms of HM. After a month of incubation in vessels, it was mixed with different rates of BC. Upper layers (15 cm) of polluted urbanozems of Rostov-on-Don were mixed with different rates of BC. These soils were put into the glass vessels for the purpose of a long-term incubation at optimum temperature and humidity. The soil samples were taken out after a week, one month, and six months later accordingly. The amounts of HM mobile forms dissolved in acetate-ammonium extract with pH 4.8 were measured with the help of atomic absorption spectrometry.

Results and Discussion: The HM amounts were significantly decreased by BC application. In the chernozem the degree of detoxication depends on ion forms of HM; e.g., AcCu has maximum absorption by BC and minimum absorption was noted for CuO. BC absorbs AcCu and AcPb better than AcZn. The urbanozem 1 (~20 m from the highway) contained Pb 100 and Zn 45 mg kg^{-1}. Other HM were not detected. After six-month incubation with BC dose of 10 t ha^{-1} [here and below the soil layer (25 cm)] there was maximum absorption of HM. The Pb and Zn amounts were decreased to 31 and 37 mg kg^{-1} correspondingly. In our view, the BC dose of 10 t ha^{-1} was not sufficient for the final remediation of urbanozem 1. The urbanozem 2 (soil profile was laid in August 1998; the site not far from the chemical plant and 2 m from the highway) contained Zn 800, Mn 30.2, Cu 4.2, Cr 3.2, Co 3.2, Cd 2.2, and Ni 1.6 mg kg^{-1}. Lead was not detected. BC rates were 1, 5, 25, and 50 t ha^{-1}. In this experiment the soil samples were being taken out only after one week. With BC dose of 1 t ha^{-1}, there was maximum absorption of Zn. The Zn amount was decreased to 630 mg kg^{-1}. With BC rate of 5 t ha^{-1} there was maximum absorption of Cu. Copper amount was decreased to 2.9 mg kg^{-1}. In our investigation BC did not absorb small concentrations of HM, which is interesting as regards soil microelement condition. BC is characterized by lingering coupling with soil, therefore maximal absorption of HM would come after 3–5 months. The same urbanozem 2 (soil profile was laid in April 1999) contained Zn 1133 and Pb 109 mg kg^{-1}. The increase of Zn amount in this soil in 1999 in comparison with the previous year may be accounted for in two ways: the activity of chemical plant or the HM transformation from immobile to mobile forms. The formula below calculates the BC dose (191 t ha^{-1}) applied to this urbanozem. After three weeks incubation in vessels, the amounts of Zn and Pb were decreased to 565 and 59.5 mg kg^{-1} correspondingly. After five weeks incubation the amount of Zn was decreased to 371 mg kg^{-1} and the Pb amount was observed on previous level. It is possible that the BC dose for the remediation of soils contaminated with HM can be counted according to the following formula:

$$D = 0.0001\ S\ H\ d^{n} \sum_{i=1} Ci\ Ki$$

where D = dose of BC (t), S = polluted area (square meters), H = depth of polluted layer (centimeters), d = soil bulk density (gm cm^{-3}), C = concentration of HM mobile forms dissolved in acetate-ammonium extract with pH 4.8 (mg kg^{-1}) measured with the help of atomic absorption spectrometry, K = empiric coefficient. It is found that for Pb and Cu, K = 0.0044, and for Zn K = 0.0052. Possibly K-coefficient depends on electronegativity quantity (EN) of HM ions: EN >1.75, K = 0.0044; EN <1.75, K = 0.0052. If we use BC with other properties such as content of humic acids, ash percentage, etc., K-coefficient will change; however, the exemplary dose of BC can be counted according to the above-mentioned formula.

Conclusion: Brown coal can be used as a detoxicant of soils polluted with Pb, Cu, and Zn. It is worth noting that BC is a meliorant of humus condition as well.

References: [1] Bezuglova O. S. et al. (1996) *Eurasian Soil Sci., 29,* 1103–1106.

CARBON DIOXIDE FLUX DUE TO HYDROTHERMAL VENTING FROM BACK-ARC BASIN AND ISLAND ARC AND ITS INFLUENCE ON THE GLOBAL CARBON DIOXIDE CYCLE.

N. Shikazono and H. Kashiwagi, Department of Applied Chemistry, Keio University, 3-14-1, Hiyoshi, Kohoku-ku, Yokohama 223-0061, Japan (sikazono@applc.keio.ac.jp).

Several previous studies demonstrated that the CO_2 flux by hydrothermal solutions and volcanic gases from mid-ocean ridges plays an important role in the global CO_2 cycle and affects the level of atmospheric CO_2 [1]. Submarine volcanism and hydrothermal activity occur not only at mid-ocean ridges but also at back arcs and island arcs. The intense volcanic and hydrothermal activities at such tectonic settings suggest that the hydrothermal and volcanic CO_2 flux from such environments affects global CO_2 cycle. However, no such study has been carried out. This paper summarizes CO_2 concentration of hydrothermal solution venting from back-arc basins and island arcs, estimates CO_2 flux, and evaluates the influence of the CO_2 flux on the global geochemical cycle.

The summaries of the CO_2 concentrations show that the CO_2 concentrations in hydrothermal solutions from back-arc basins and mid-ocean ridges range from 30 to 200 mmol/kgH_2O and from 5 to 30 mol/kgH_2O, respectively, indicating that the CO_2 concentration of hydrothermal solution at back arc basins is higher than that at mid-ocean ridges.

Using these data on the CO_2 concentrations, seafloor production rates by Kaiho and Saito [2], and seawater/rock ratios by several methods, the hydrothermal CO_2 flux into the ocean from back-arc basins and mid-ocean ridges is estimated to be 0.2–6 × 10^{19} mol/m.y. and 0.4–9 × 10^{19} mol/m.y., respectively. It could be said from this estimate that the hydrothermal flux from back-arc basins has to be taken into account in considering the global CO_2 cycle.

At the convergent plate boundaries, CO_2 degasses not only from back-arc basins but also from island arcs by volcanic gases and hydrothermal solutions. The CO_2 flux from this setting is estimated to be 0.5–3 × 10^{18} mol/kg H_2O [e.g., 3], which seems to be comparable or less than that from back-arc basins and mid-ocean ridges.

Using the CO_2 fluxes from back-arc basins, island arcs, and mid-ocean ridges, the computations on the global CO_2 cycle were carried out. The calculations suggest that the hydrothermal CO_2 fluxes from subduction-related environmnets (back-arc basins and island arcs) are important for controlling the global CO_2 cycle and climate change.

References: [1] Javoy M. (1988) *Chem. Geol., 70.* [2] Kaiho K. and Saito S. (1994) *Terra Nova, 6,* 376–384. [3] Seward T. M. and Kerrich D. M. (1996) *EPSL, 139,* 105–113.

GEOCHEMICAL CONSEQUENCES OF PARTIAL MELTING AT THE CORE-MANTLE BOUNDARY.

N. Shimizu[1], K. Hirose[2], and Y. Fei[3], [1]Department of Geology and Geophysics, Woods Hole Oceanographic Institution, Woods Hole MA 02543, USA (nshimizu@whoi.edu), [2]Tokyo Institute of Technology, Tokyo, Japan, [3]Geophysical Laboratory, Carnegie Institution of Washington, Washington DC, USA.

Introduction: One of the important connections between deep-mantle seismic tomography and geochemical signatures observed in plume-derived ocean island basalts is the distribution of trace elements among lower-mantle mineral phases and their behavior during partial melting at the core-mantle boundary. For making a step toward the goal, the partitioning of 15 trace elements was determined among Ca-perovskite, Mg-perovskite, majorite, Ca-Al phase and melt on a natural basalt (MORB from MAR), and peridotite (KLB-1) compositions at 25 and 27 GPa. Experiments were conducted using a multi-anvil press at the Geophysical Laboratory, Carnegie Institution, and analytical work was made at Woods Hole using a Cameca IMS 3f-ion microprobe.

Results and Discussion: It was found that Ca-perovskite (Capv) is a very predominant carrier of all trace elements analyzed: Capv-melt partition coefficients vary from 1.2 for Ba, 2.9 for Sr, and 8.4 for Ce to more than 11.0 for other REE for the MORB composition at 27 GPa, 2450°–2500°C; for the KLB-1 composition at 25 GPa, 2450°C, they range from 10 for Ce to 19–25 for other REE. Mg-perovskite was found to be much less important as a repository of trace elements, with Capv/Mgpv ranging from 2 for Ti, Zr to more than 100 for Nd and Sm for the KLB-1 composition. The "bulk" solid-melt partition coefficients are greater than unity for most elements, without significant elemental fractionation for both peridotite and basalt compositions.

The results suggest that (1) if a rising plume "picks up" the solid phase assemblage because it is less dense than melt [e.g., 1], a trace-element-enriched plume mantle is easily created without changing elemental abundance patterns; and (2) if a Capv-bearing solid phase assemblage was involved in crystallization of a magma ocean, it would produce a trace-element-enriched mantle whose trace-element pattern would look very much like the chondritic precursor. It is implied that the integrity of geochemical signatures of shallow processes (e.g., hydrothermal alteration) could be maintained even if a subducted lithosphere undergoes partial melting at the core-mantle boundary.

References: [1] Hirose K. et al. (1999) *Nature, 397,* 53–56.

LARGE LEAD-ISOTOPIC VARIATIONS IN OLIVINE-HOSTED MELT INCLUSIONS IN A BASALT FROM THE MID-ATLANTIC RIDGE.

N. Shimizu[1], A. V. Sobolev[2], G. D. Layne[1], and O. P. Tsamerian[2], [1]Department of Geology and Geophysics, Woods Hole Oceanographic Institution, Woods Hole MA 02543, USA (nshimizu@whoi.edu), [2]Vernadsky Institute of Geochemistry, Russian Academy of Sciences, Moscow, Russia.

Introduction: Studies of high-Mg olivine-hosted melt inclusions have revealed that large chemical variations (in both major and trace elements) exist in single-lava melt inclusion suites and reflect variations in style and depths of melting and melt-rock reaction processes during melt migration [e.g., 1–3]. Analytical techniques developed at Woods Hole Oceanographic Institution [4] using a Cameca IMS 1270 ion microprobe enables *in situ* analysis of melt inclusions for Pb-isotopic compositions and have been applied to suites of HIMU-type ocean island basalts with the discovery of large isotopic variations in melt inclusions from individual lavas [5]. The same technology was used here to investigate whether primitive mid-ocean-ridge basalt (MORB) inclusions display isotopic variations that could be connected to source chemical characteristics. Of particular interest is a possible connection between trace-element garnet signatures and HIMU-type isotopic signatures, indicating involvement of garnet pyroxenites derived from recycled oceanic crust [e.g., 6,7]. We report here results on a melt-inclusion suite from a single lava (30/2) dredged from 14°N, MAR.

Analytical: A primary O^- ion beam with a current of ~40 nA was focused to a spot ~40 μm in diameter. With MRP = 3500, interferences of HREE, Hf-double oxides (e.g., $^{176}LuO_2$) and MREE-tripleoxides (e.g., $^{160}DyO_3$) are adequately resolved from Pb isotopes. Replicate analyses of basalt-glass standards (158-4 from Loihi [8] and DR4-2 from Tahiti [9]) demonstrate that $^{207}Pb/^{206}Pb$ and $^{208}Pb/^{206}Pb$ ratios can be determined with an in-run precision (σ) ~0.2% and $^{206}Pb/^{204}Pb$ with 0.4% in an analysis time of ~60 min. Results also demonstrate that mass fractionation is <0.15%/amu. For melt inclusions of this study, a precision for $^{207}Pb/^{206}Pb$ and $^{208}Pb/^{206}Pb$ ratios ranged from 0.25 to 0.5%.

Results and Discussion: Thirteen melt inclusions, one sulfide inclusion, and matrix glass were analyzed. Lead-207/lead-206 ratios vary from 0.8104 to 0.8535 (5%) and $^{208}Pb/^{206}Pb$ ratios vary from 1.991 to 2.075 (4%). These variations are greater than the entire range of variations observed for glasses from 12°24'N to 15°01'N across the geochemically anomalous segment of MAR [10–12]. In the $^{208}Pb/^{206}Pb$ vs. $^{207}Pb/^{206}Pb$ space, the observed variations form a quasilinear array ranging from "pure" DMM (0.857, 2.072) toward HIMU (0.725, 1.863). The results clearly demonstrate that melts derived from isotopically distinct sources "coexist" on small spatial and temporal scales; particularly significant is the occurrence of melts derived from the "pure" DMM source from this locality (14°N), because previous glass-based studies found that geochemical anomalies occur in close connection with bathymetry and implied an incipient mantle plume [11,12]. The present results suggest that recycled components occur on small spatial scales within peridotitic substrates and exert different magnitude of isotopic effects, depending on their abundance in individual melting systems in much the same way that "ubiquitous heterogeneities" were envisioned [13]. It is clear that isotopic analysis of high-Mg olivine-hosted melt inclusions will add a new dimension to geochemical studies of MORB.

References: [1] Sobolev A. V. and Shimizu N. (1993) *Nature, 363,* 151–154. [2] Sobolev A. V. and Shimizu N. (1994) *Mineral. Mag., 58A,* 862–863. [3] Shimizu N. (1998) *Phys. Earth Planet. Inter., 107,* 183–201. [4] Layne G. D. and Shimizu N. (1997) *Proc. SIMS XI,* 63–65. [5] Saal A. E. et al. (1998) *Science, 282,* 1481–1484. [6] Prinzhofer A. et al. (1989) *EPSL, 92,* 189–206. [7] Hirschmann M. M. and Stolper E. M. (1996) *Contrib. Mineral. Petrol., 124,* 185–208. [8] Garcia M. O. et al. (1995) *J. Petrol., 36,* 1647–1674. [9] Devey C. W. et al. (1990) *JGR, 95,* 5049–5066. [10] Bougault H. et al. (1988) *EPSL, 88,* 27–36. [11] Dosso L. et al. (1991) *EPSL, 106,* 29–43. [12] Dosso L. et al. (1993) *EPSL, 120,* 443–462. [13] Sleep N. H. (1984) *JGR, 89,* 10029–10041.

CARBON CYCLES STUDIED WITH FATTY-ACID BIOMARKERS AND A MIXED LAYER MODEL.

K. H. Shin[1,2], S. Noriki[2], N. Tanaka[2], and M. Ikeda[2], [1]International Arctic Research Center, University of Alaska, Fairbanks AK 99775-7320, USA, [2]Graduate School of Environmental Earth Sciences, Hokkaido University, Sapporo, 060-0810, Japan.

The concentration and production rate of the each particulate fatty acid is integrated in an euphotic layer. The mean values of these are determined in the periods of the summer (regenerated production period) and spring (new production period) in the subarctic ocean. Total fatty-acid production rates (mg C/m^2/d) were 46 in summer and 130 in spring.

The export rates of total fatty acids, which are the downward fluxes at 220 m depth, were 4.5 and 18 mg C/m^2/d, and the e-ratios of total fatty acids (export rates/production rates) were 0.098 and 0.14 in the summer and spring respectively. The e-ratio of each fatty acid varied strikingly, ranging from 0.006 to 0.91. The e-ratios of saturated and monounsaturated fatty acids showed generally high values, with the increasing C number in both seasons. However, the e-ratios of polyunsaturated fatty acids were much higher in the spring new-production period than those in the summer regenerated period. Conversely, the e-ratios of bacterial and zooplanktonic origin such as 17:0, 17:1, branched acids [1], and 18:1 (n-9) [2] were higher in summer than those in spring. The export ratio of each fatty acid shows significant variability due to the difference in the origin and lability of each fatty acids, and it is remarkably different between the new production period (bloom) and the regenerated production period (postbloom) in the subarctic ocean. This suggests that a change of ecosystem structure affects the composition and transport of fatty acid in the ocean.

In order to understand the settling processes, the turnover rate (production rate/integrated concentration) of each fatty acid was compared with the export rate normalized by integrated concentration of each fatty acid in the euphotic layer. The turnover rates of fatty acids varied considerably, but export rates normalized by integrated concentrations of fatty acids do not indicate any change among the fatty acids. It suggests no definite relation between turnover rates of fatty acids through photosynthesis and the formation processes of settling particles from the particulate matter in the euphotic layer. In the present study, C balance in the subarctic ocean was studied by a physical mixed layer model as well as biological processes.

References: [1] Volkman et al. (1980). [2] Wakeham (1984).

RHENIUM-OSMIUM AND OXYGEN-ISOTOPIC SYSTEMATICS OF DIAMONDIFEROUS AND NON-DIAMONDIFEROUS ECLOGITES FROM THE ROBERTS VICTOR KIMBERLITE, SOUTH AFRICA.

S. B. Shirey[1], U. Wiechert[2], R.W. Carlson[1], J. J. Gurney[3], and L. Van Heerden[3], [1]Department of Terrestrial Magnetism, Carnegie Institution of Washington, 5241 Broad Branch Road NW, Washington DC 20015, USA (shirey@dtm.ciw.edu), [2]Geophysical Laboratory, Carnegie Institution of

Washington, 5251 Broad Branch Road NW, Washington DC 20015, USA, [3]Department of Geological Sciences, University of Cape Town, Rondebosch 7700, South Africa.

Introduction: Eclogites make up a small fraction of the subcontinental lithopheric mantle (SCLM) [1], but they carry unique information about cratonic evolution. Eclogites are important diamond hosts, they can be Archean [2–4], and they can carry old surficial geochemical signatures. This Re-Os, O, and major-element study of Roberts Victor eclogites has been undertaken to refine their age, constrain the time of diamond formation and better understand prolith differences between the different eclogite types.

Roberts Victor: The Roberts Victor kimberlite, a 128 ± 15-Ma [5] group II kimberlite [6] situated in the Boshoff district east-northeast of Kimberley, is known for its abundant and texturally diverse eclogite suite [7,8]. Group I, group II, and diamondiferous eclogite types [8–10] are found here in addition to other unusual eclogite types. Group I eclogites have large, subhedral or rounded garnets in a matrix of clinopyroxene, higher Na_2O (>0.09 wt%) in their garnet, higher K_2O (>0.08 wt%) in their pyroxene, and higher $\delta^{18}O$ compared to the group II eclogites. Group II eclogites have irregular anhedral garnet and clinopyroxene in an interlocking fabric. Diamondiferous eclogites belong to group I using the Na_2Ogt and K_2Ocpx scheme [10].

Earlier isotopic studies [2,3,11] demonstrated a 2.5–2.7-Ga age for Roberts Victor eclogites that perhaps could be extended back to 3.2 Ga [11], with garnet and pyroxene in equilibrium up to the time of kimberlite eruption [2,12].

Analytical Methods: Rhenium-osmium-isotopic analyses used 2–3-g aliquots of sample, aqua regia in Carius tubes [13], solvent extraction into CCl_4 [14], microdistillation [15], anion exchange [16], and negative thermal ionization mass spectrometry (N-TIMS). Oxygen was released for isotopic analysis from clean garnet separates (1.5–2.0 mg) by evaporating with a CO_2 laser in a BrF_5 atmosphere [17,18].

Results: Rhenium contents of group I eclogites (0.78–3.4 ppb) are distinctly higher than group II eclogites (0.023–0.38 ppb), whereas Os contents on both groups are high (0.16–0.92 ppb) and overlap completely. Rhenium-187/osmium-188 ratios are controlled largely by Re abundance variations. $\delta^{18}O$ correlates strikingly with eclogite group and $^{187}Re/^{188}Os$; group I and diamondiferous eclogites have $^{187}Re/^{188}Os$ ranging from 3 to 20 and $\delta^{18}O$ ranging from 5.45‰ to 6.95‰, whereas group II eclogites have values of 0.7–2.50 and 3.65–5.20‰ respectively. Osmium-187/osmium-188 isotopic compositions at the kimberlite eruption age are strongly radiogenic (0.1412–1.159), in common with other eclogite suites. On a Re-Os isochron diagram, group II eclogites show poor age systematics and much less radiogenic $^{187}Os/^{188}Os$ due to their low $^{187}Re/^{188}Os$. Group I eclogites fall on an array with a 2.7-Ga slope in concert with previous Sm-Nd results [2]. The three diamondiferous samples fall on a 3.5-Ga Re-Os array similar to 15 diamondiferous eclogites from the Newlands kimberlite [19]. Two samples display severe recent Re gain (3.4 ppb) or loss (0.02 ppb).

Discussion: The Os concentration and MgO (11–17 wt%) content of Roberts Victor eclogites are signifincantly higher than basalt and previously studied Udachnaya eclogites [4], suggesting a picritic affinity. The large $\delta^{18}O$ range and heavy group I vs. light group II distinction agrees with earlier results [9] and is like the general $\delta^{18}O$ variations seen in oceanic crustal sections [20]. The correlation of $\delta^{18}O$ and $^{187}Re/^{188}Os$ and the Re control on Re/Os suggests that Re/Os fractionation in this eclogite suite occurred on the Archean seafloor and resulted from seawater-induced Re mobility. The high $^{187}Os/^{188}Os$ of the group I and diamoniferous eclogites results from their high $^{187}Re/^{188}Os$ and 2.7–3.5-Ga residence in the SCLM — not incorporation of radiogenic seawater Os. These data support a model whereby Roberts Victor eclogites formed by recycling of picritic oceanic crust shortly after ~3–3.4-Ga SCLM stabilization.

References: [1] Schulze D. J. (1989) *JGR, 94,* 4205–4212. [2] Jacob D. and Jagoutz E. (1994) *Proc. 5th Kimberlite Conf.,* 304–317. [3] Kramers (1979) *EPSL, 42,* 58–70. [4] Pearson et al. (1995) *Nature, 374,* 711–713. [5] Smith C. B. et al. (1985) *J. Geol Soc. S. Afr., 88,* 249–266. [6] Smith C. B. et al. (1985) *J. Geol. Soc. S. Afr., 88,* 267–280. [7] Hatton C. J. and Gurney J. J. (1987) in *Mantle Xenoliths* (P. H. Nixon, ed.), pp. 453–464. [8] MacGregor I. D. and Carter J. L. (1970) *PEPI, 3,* 391–397. [9] MacGregor I. D. and Manton W. I. (1986) *JGR, 91,* 14063–14079. [10] McCandless T. E. and Gurney J. J. (1989) *Proc. 4th Kimberlites Conf.,* 827–832. [11] Manton W. I. and Tatsumoto M. (1971) *EPSL, 10,* 217–226. [12] McCulloch M. T. (1989) *Proc. 4th Kimberlites Conf.,* 864–876. [13] Shirey S. B. and Walker R. J. (1995) *Anal. Chem., 67,* 2136–2141. [14] Carlson R. W. et al (1999) *Proc. 7th Kimberlites Conf.,* in press. [15] Birck J.-L. et al (1997) *Geostandards Newslett., 20,* 19–27. [16] Morgan J. W. and Walker R. J. (1989) *Anal. Chem. Acta, 222,* 291–300. [17] Sharp (1990) *GCA, 54,* 1353–1357 [18] Feibig J. et al. (1999) *GCA,* in press. [19] Menzies A. H. et al. (1999) *Proc. 7th Kimberlites Conf.,* in press. [20] Muehlenbachs K. (1986) *Rev. Mineral., 16,* 425–444.

TRACE ELEMENTS AND CARBON-ISOTOPIC COMPOSITION OF INCLUSION-FREE DIAMONDS.

A. A. Shiryaev, N. N. Dogadkin, and E. M. Galimov, Vernadsky Institute of Geochemistry and Analytical Chemistry, Russian Academy of Sciences, Kosygin Street 19, Moscow B-334, Russia (shiryaev@gmii.museum.ru; a_shiryaev@mail.ru).

Introduction: Conclusions about growth medium of diamonds are usually based on electron microprobe (EMP) analyses of silicate inclusions (size >5–10 μm) found in some crystals. Despite significant achievements, a number of important facts cannot be explained if one considers diamond growth from the silicate melts. One of the most serious questions is if silicate inclusions are representative samples of the diamond-growth environment.

Samples and Methods: Instrumental neutron activation analysis (INAA) was used to study bulk chemistry of diamonds. We investigated ~100 diamonds from different pipes and localities. Diamonds were characterized mineralogically and by fourier transform infrared (FTIR). Inclusions were extracted by crushing or burning, and inclusion-free chips (2–20 mg) were irradiated. Diamonds were cleaned in boiling AR + $HClO_4$ (or HF). Our Rutherford backscattering (RBS) studies show that this procedure effectively removes contaminants. Integral flux was 8×10^{17} neutrons/cm^2. γ-spectra were recorded with a Pb-shielded HpGe detector in three periods; duration of measurements was up to 8000 s. Spectra were processed with software; small peaks were hand-treated. $\delta^{13}C$ of diamonds was also studied.

Results: Level of impurities in the majority of the studied diamonds was very low (<1 ppm). In some samples much higher figures were found; this is related to mineral inclusions that were not detected optically. According to our data and literature [1,2], two elements, Na and Co, were present almost in every diamond. RBS results and the absence of correlation between sample mass and amount of these elements serve as a confirmation that they reside in the bulk of crystals and are not contaminants. Only a limited number of elements could be incorporated into diamond lattice. Cobalt-related photoluminescence was absent in our and in all natural diamonds studied to date. Therefore, we suggest that Co and Cu found in INAA studies reside in sulfide inclusions. Sulfides are the most common macroscopic inclusions in natural diamonds. INAA studies indicate that an absolute majority of natural diamonds contain submicroscopic sulfide inclusions.

Host for Na is not clear at present. There are at least two explanations for its omnipresence: (1) Na incorporation into diamond lattice, and (2) presence of Na-rich inclusions such as pyroxenes and/or Na-rich carbonates. Nothing conclusive can be said now about the first possibility. Presence of Na carbonates is doubtful since Ca is found rarely. Pyroxenes are common in eclogitic diamonds but are rare among inclusions in peridotitic. Following an early INAA work by Fesq et al. [2], we suggest that pyroxenes might be present in many diamonds as submicroinclusions.

No straightforward correlations were found between INAA data and FTIR or $\delta^{13}C$ results.

Discussion: Model of diamonds formation should explain overabundance of sulfides in diamonds in comparison to mantle petrology. Several mechanisms could be suggested:

1. Immiscible sulfide liquid segregates from silicate melts at the crystallization front [3]. Melting could be induced by C-bearing (metasomatic) fluid. The precipitation of C may result from the reaction of sulfide with CO_2 or CH_4 [4]. Trapping of a significant amount of microscopic pyroxenes might be explained by fractional crystallization of silicate melts where olivine crystals could grow to larger sizes by the momentum of the entrapment by growing diamond.

2. If diamonds grew in carbonate melts, then trapping of droplets of immiscible sulfide may occur while carbonate component will escape due to its extremely low viscosity.

3. Sulfide liquid could be in equilibrium with silicate melt. The position of dissolved C in silicates is unknown. A significant fraction of C likely resides in defects of silicate lattices. In principle, S may decrease C solubility in silicates, e.g., by replacement of C in defects. Diamond concentration in diamondiferous xenoliths reaches tens ppm. This is smaller but still in the same order of magnitude as C content of ordinary xenoliths [5]. This could be explained by "substitution" mechanism since no external C-bearing fluid is necessary for diamond formation. However, this scenario needs to be verified.

All three models could explain observed enrichment of diamonds in C^{12}. Models 1 and 2 may incorporate Rayleigh fractionation [6]. The "isotopic" part of the model 3 is based on the possible fractionation of C isotopes depending on the strength of its bonding in silicates. Depending on the degree of the S $\rightarrow$ C substitution, C with different isotopic composition will be released.

References: [1] Damarupurshad et al. (1997) *J. Radioanal. Nucl. Chem., 219,* 33–39. [2] Fesq et al. (1975) *Phys. Chem. Earth, 9,* 817–836. [3] Sharkov (1983) *Geokhimiya, 10,* 1399–1412. [4] Marx (1972) *Mineral. Mag., 38,* 636–638. [5] Deines (1992) in *Early Organic Evolution.* [6] Galimov (1991) *GCA, 55,* 1697–1708.

X-RAY INVESTIGATION OF PRINCIPAL NITROGEN-RELATED DEFECTS IN DIAMONDS AND THEIR MODELS.

A. A. Shiryaev[1], Yu. A. Klyuev[2], A. M. Naletov[2], and A. T. Dembo[3], [1]Vernadsky Institute of Geochemistry and Analytical Chemistry, Kosygin Street 19, Moscow B-334, Russia (shiryaev@gmii.museum.ru; a_shiryaev@mail.ru), [2]VNII Almaz, Gilyarovskii Street 65, Moscow, Russia, [3]Institute of Crystallography, Leninsky Prospekt 59, Moscow, Russia (dembo@saxslab.incr.msk.su).

Introduction: Nitrogen is the main elemental impurity in diamonds. It substitutes C atoms and forms IR-active defects. High-temperature-high-pressure treatment lead to aggregation [1] of single substitutional N atoms to more complicated structures: A and B defects (C $\rightarrow$ A $\rightarrow$ B). Usually it is assumed that A-center is the pair of substitutional N atoms [2] while B-defect is 4–8 N atoms in tetrahedral coordination around a vacancy. However, these models ("point defects") are not rigorously proved.

Based on correlation of IR absorption and intensity of X-ray diffuse scattering, Naletov et al. [3] and Klyuev et al. [4] suggest that B defects are spheroid (isometric) regions of diamond lattice with high concentration (~25 at%) of N atoms and diameter of 80–90 Å, while A center has diameter 40 Å and 6–18 at% of N. Recent work [5] confirms the existence of scattering centers of similar sizes.

In order to check validity of the cluster model of A and B centers, we have performed small-angle X-ray scattering (SAXS) investigations of natural type IaB and IA and synthetic IA diamonds. High-quality IIA diamond (N-less) was used as the reference.

Results: Figure 1 shows experimental SAXS curves. Scattering in type IIA diamond is negligible. It was subtracted together with background from curves of the other crystals. Diamonds with B defects scatter significantly. Assuming a monodisperse system, we calculated the size distribution of defects. Hard-sphere approximation gives the best results. Figure 2 shows the volume fraction of defects with corresponding radii. It is clearly seen that the principal scattering centers in diamonds with B defects are spheres with radius around 40–50 Å. Based on the present data and results of X-ray diffusive scattering, we support the model of B defects as spherelike regions in diamond lattice with diameter 80–100 Å enriched in N. Inside these regions N may form 4N + V complexes. Slight scattering in the size of these domains could be explained by different temperature of annealing in nature and/or different degree of aggregation. Diamonds with higher IR-absorption by B defects have larger X-ray scattering centers.

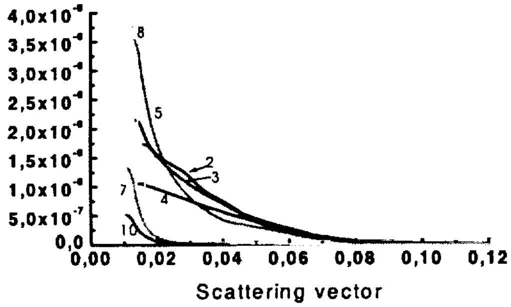

Fig. 1. Small-angle scattering curves.

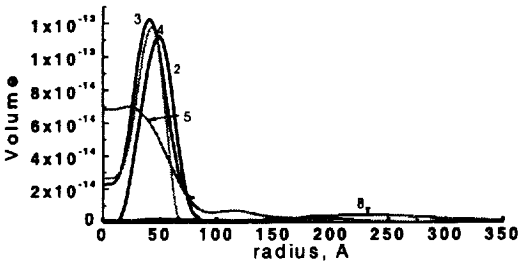

Fig. 2. Distribution of size of defects in diamonds with B centers.

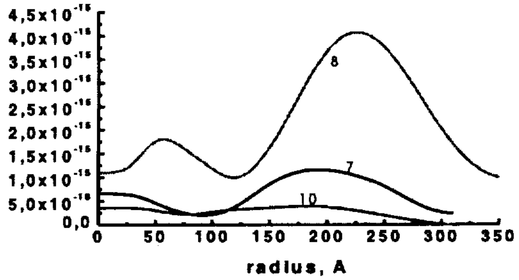

Fig. 3. Distribution of defects in diamonds with A centers.

Investigation of IA diamonds (Fig. 3) gave unexpected results: SAXS intensity is very small and comparable with that of IIA diamond. This may indicate that the model of A center as a point of defects could be correct, although it contradicts studies of diffuse scattering. In natural IA diamonds we do observe weak scattering from defects with R ~200 Å, which is not found in artificial stones. Therefore, we suggest that although optical manifestation of A center is similar in natural and synthetic stones, the structure could be somewhat different due to longer annealing in nature.

The impurity-diffusion rate and activation energy are strongly dependent on number of dislocations, vacancies, etc. From the cluster model of A and B defects we propose that after N incorporation as a single atom, stressed regions of the diamond lattice may serve as a sink for migrating N atoms. They began to form pairs that are optically active. Long annealing (some natural diamonds) leads to the formation of clusters of N pairs that is observable in SAXS. Nitrogen concentration in these regions is 6–18 at%. (A defect). Further annealing produces large defects (B centers) that could be regarded as nuclei of the new phase. Kinetics of N aggregation should be described by the Avraami equation.

References: [1] Evans T. (1992) in *Properties of Diamond.* [2] Sobolev E. V. et al. (1968) *Sov. Phys. Dokl., 12,* 665–668. [3] Naletov A. M. et al. (1977) *Fiz. Tverdogo Tel., 19,* 1529–1531. [4] Klyuev et al. (1977) *Sov. Phys. Solid State, 19,* 7–10. [5] Ramanan et al. (1998) *Acta Cryst., A54,* 163–171.

THE ESTUARINE CHEMISTRY OF RARE EARTH ELEMENTS: COMPARISON OF THE AMAZON, FLY, SEPIK, AND GULF OF PAPUA SYSTEMS.

E. Sholkovitz[1] and R. Szymczak[2], [1]Department of Marine Chemistry and Geochemistry, Woods Hole Oceanographic Institution, Woods Hole MA 02543, USA, [2]Radiochemical Oceanography Group, Australian Nuclear Science and Technology Organization, PMB 1, Menai NSW 2234, Australia.

By comparing and contrasting the estuaries of the Amazon, Fly, and Sepik Rivers (Papua, New Guinea), and the Gulf of Papua, we will explore degrees to which the estuarine chemistry of the rare earth elements (REE) is shaped by hydrographic, morphologic, and sedimentological differences. The chemical properties of the REE make this series of trace elements into unique probes of important geochemical processes operating in the boundary between rivers and the ocean.

There are two distinct processes operating on dissolved REE in estuaries. There is removal in the low (0–8) salinity region and release to the mid- to high-salinity region. Fractionation of the dissolved REE during these two processes operate in different directions. The order of removal follows LREE > MREE > HREE and the order of release follows HREE > MREE > LREE where L, M, and H refer to light (La, Ce, and Nd), middle (Sm, Eu, Gd, Tb, and Dy), and heavy (Er, Yb, and Lu) REE respectively. Large-scale removal and fractionation in the low salinity regions of all four estuaries is the result of salt-water induced coagulation of river borne colloids.

The increase of dissolved REE in the mid- to high-salinity regions of the Amazon, Fly, and Gulf of Papua estuaries implies that there is a source of dissolved REE to the outer regions. Resuspended sediment and/or bottom sediment are the mostly likely sources. The lack of REE increases in the Sepik River estuary helps to strengthen this explanation as the mixing zone of the Sepik River estuary is located over a deep shelf where little contact between bottom sediment and estuarine water occurs. In marked contrast, the other three estuaries are dominated by the continuous resuspension and deposition of bottom sediments where active chemical diagenesis is occurring. Release and its accompanying fractionation, we speculate, results from the complexation of REE with carbonate ions during the reaction of seawater with suspended particles and/or bottom sediment.

Hence, estuarine reactions not only markedly reduce river REE fluxes to the oceans but also modify the relative abundance of dissolved REE reaching the oceans. Removal and release during estuarine mixing lead to an "effective" river REE composition (that reaching the ocean after modification in estuaries) that is evolved toward the REE composition of seawater, which has a heavy REE-enriched composition when normalized against the REE composition of the Earth's continental crust. Last, the processes of removal and release must be considered when estimating the residence time of REE in the oceans and when explaining the regional variations in the Nd-isotopic composition of seawater in the ocean basins.

ANOMALOUS LEAD ISOTOPES AND SOURCES OF LEADS IN THE UPPER MISSISSIPPI VALLEY ZINC-LEAD DISTRICT, USA.

A. A. Sicree[1] and H. L. Barnes[2], [1]Earth and Mineral Sciences Museum, Pennsylvania State University, 122 Steidle Building, University Park PA 16802, USA (sicree@geosc.psu.edu), [2]Department of Geosciences, Pennsylvania State University, 122 Steidle Building, University Park PA 16802, USA (barnes@geosc.psu.edu).

Introduction: The Upper Mississippi Valley (UMV) Zn-Pb district is one of the most radiogenic Pb deposits in the world. The UMV's J-type leads are more anomalous than those of all other Mississippi Valley-type districts. Models for the deposition of Pb in the UMV must account for both the regional and the paragenetic variations observed in the district's Pb isotopes.

Sources of Radiogenic and Normal Lead: Regional zoning of ^{206}Pb/^{204}Pb, ^{207}Pb/^{204}Pb, and ^{208}Pb/^{204}Pb ratios in galenas from the UMV region indicates that UMV leads are most radiogenic to the northeast and least radiogenic south of the district [1]. This zonation requires two sources of Pb: one more radiogenic than the regional maximum, and the other less radiogenic than the regional minimum. However, such zoning does not require two ore-forming fluids.

Lead-isotopic values correlate not with thicknesses of underlying possible source strata of the UMV region but with depth to the Precambrian basement, implying that the Precambrian basement was a major source of the radiogenic Pb. Calculations show that all of the district's more-radiogenic Pb could be extracted from the top 0.26–32 m of the underlying granites and rhyolites of the Precambrian Eastern Granite-Rhyolite Province.

Upper Cambrian arkosic sandstones are the probable source for the normal or less-radiogenic Pb having sufficient Pb with compatible isotopic ratios. Such Pb probably contributed somewhat more than 30% of the district's total Pb. Calculations show that only 20–62 m of the Mt. Simon Sandstone over the area beneath the UMV district are required to produce the mass of required normal Pb. Causes of zoning can be due to differences in relative geochemical mobility of the radioactive precursors of ^{206}Pb, ^{207}Pb, and ^{208}Pb, particularly the soluble or volatile Ra and Rn intermediate daughter radioisotopes. Radium is highly soluble in reduced solutions and the comparative enrichment in ^{206}Pb over ^{207}Pb in the UMV correlates with the longer half-life of ^{226}Ra over ^{223}Ra.

Paragenetic Zoning of Lead Isotopes: A core-to-rim ion microprobe traverse of a galena crystal from the South Hayden orebody, in Lafayette County, Wisconsin, shows paragenetic zoning of both ^{207}Pb/^{206}Pb and ^{208}Pb/^{206}Pb vs. cumulative deposited mass profiles in which the core (accounting for ~30% of the total mass of Pb) has the most radiogenic Pb. Later, Pb-isotopic ratios drop to a steady-state value that persists (~41% of mass) until near the outer rim of the crystal where there is an abrupt, but minor (~3% of mass) return to more radiogenic Pb. In general, the history of Pb-isotopic deposition in the UMV is one of decreasing overall radiogenic character of the Pb, accompanied by a relative increase in thorogenic Pb followed by an abrupt, terminal increase in radiogenic character. All of the salient characteristics of lead isotopes in the UMV district and vicinity may be caused by a single, deep basinal brine as the ore-forming fluid.

Conclusions: Lead-isotopic zoning in the Upper Mississippi Valley Pb-Zn district fits an ore formation model in which a single ore fluid originated south of the district in the Illinois Basin and migrated northeastward through the district. Initially, the ore fluid carried less-radiogenic Pb but in the vicinity of the UMV district it extracted more-radiogenic Pb from the basal Cambrian sandstones and the underlying Precambrian basement granitic rocks and their erosion products, and thus became progressively more radiogenic across the district.

References: [1] Millen T. M. et al. (1995) *U. S. Geol. Surv. Bull., 2094-B,* 1–13.

THERMODYNAMIC MODELING OF BROMINE PARTITION BETWEEN SEAWATER AND ITS SOLIDS.

M. G. Siemann and M. Schramm, Technische Universität Clausthal, Fachgebiet Mineralogie, Geochemie, Salzlagerstätten, A.-Roemer-Strasse 2A, 38678 Clausthal-Zellerfeld, Germany (siemann@immr.tu-clausthal.de; schramm@immr.tu-clausthal.de).

Introduction: The abundance and partitioning of Br between chloride minerals and hypersaline brines is of prime importance in the system of marine evaporites. The distribution of Br between solid and solution depends mainly on the composition of the aqueous solution. This parameter varies over a large range when seawater is evaporated. Hence, a very large set of experimentally determined D_{Br} values for each step of seawater evaporation would be necessary, which is not transferable to other systems. Therefore, we have developed a new generalized mode for the calculation of Br partitioning where the incorporation of a trace element into a crystal is described as an extreme form of a solid solution formation.

Experiments: All evaporation experiments were done in a thermoconstant incubator box at 25° ± 1°C. To avoid the incorporation of fluid inclusions, a new crystallization method was developed. Nearly saturated brines with different contents of Br were evaporated using Erlenmeyer flasks.

Experimental results. Our experimental results differ significantly in several points from those given by other authors, e.g., the distribution coefficient for halite significantly increases for Br concentrations between 100 and 1000 μg/g. For higher concentrations D_{Br} reaches a rather constant value with a mean of 0.172 ± 0.004 (s), which is 12% higher than previous data. During nearly the whole precipitation of halite from seawater the concentrations of Br are in a range where the distribution coefficient is not constant. The concentration gaps of previous papers are closed and the distribution coefficient for low Br concentrations is documented by a larger set of experimental data now.

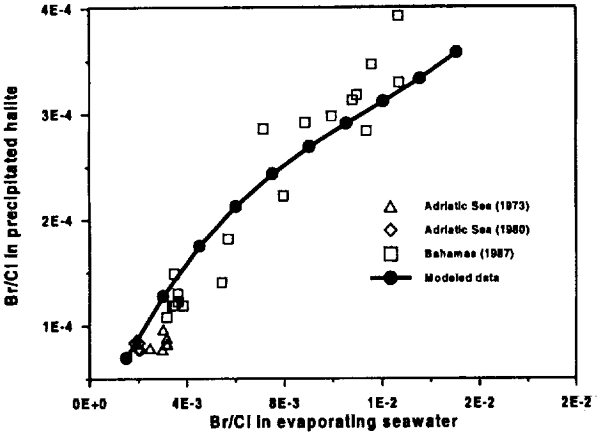

Fig. 1. Bromine/chlorine ratios in the evaporating seawater and the precipitated halite crystals.

Thermodynamic Developments: To use the experimentally developed data of trace-element concentrations in the brines for the thermodynamic modeling of a solid solution system or its extreme ends, a link between concentrations and activities had to be found. For very small values of X_{trace} the activity coefficient of the trace component λ^{te} can be given as a function of the partition coefficient D_{Br}

$$\lambda_{te} = \frac{1}{D_{Br}} \frac{\Pi a_i^{\upsilon_i}}{K_L^{te}} \frac{1}{m_{trace}}$$

$$\frac{\Sigma m_i M_i}{\left(X_{trace} M_{trace} + X_{major} M_{major} + \Sigma\left(\frac{1}{\upsilon_{trace}} n_{f\,ne} M_{f\,ne}\right)\right)}$$

where a is the activity of the aqueous components, ν the stoichiometric factor, m the molality, X the mole fraction, and M the molecular mass; i always refers to the aqueous and ∠ to the solid component.

Due to the fact that all previously known solid solution models fit the experimental data unsatisfactory, a new generalized solid solution model was developed that is able to describe the behavior of trace-element partitioning in crystals growing from brines. The basis of the new model is the assumption that the activity coefficient of the trace component in a solid solution system can be fitted satisfactory by the function

$$R\,T \log \lambda_{trace} = p_1\, X_{major}^2 + p_2\, X_{major}^{p_3}$$

where p_1 to p_3 are model parameters. The formalism was implemented into the source code of EQ3/6.

Results: The influence of alkali and Earth alkali cations in aqueous solutions on the distribution coefficient was modeled. At a concentration of ~1% in the aqueous solution, the distribution coefficient of Br in halite is reduced ~10% by K, 9.9% by Ca, 7% by Li, 4.5% by Rb, 3.5% by Sr, and 2.5% by Mg. For brines with lower Br contents the distribution coefficient is far away from the region of constancy.

Model validation. The model was validated by a comparison of thermodynamically modeled values for the Br concentration in halite precipitated from evaporating seawater and field observations of different authors. The thermodynamically calculated data are in good agreement with the experimental data as well as with the data from salt works (Fig. 1).

INFERENCES FROM URANIUM-SERIES DISEQUILIBRA ON MAGMA ORIGIN AND MIGRATION BENEATH THE IZU ARC.

O. Sigmarsson[1,2], J. B. Gill[2], P. Holden[2], and C. C Lundstrom[2], [1]Centre National de la Recherche Scientifique, Université Blaise Pascal, 63038 Clermont-Fd., France, [2]Earth Sciences Department, University of California, Santa Cruz CA 95064, USA.

Studies of U-series nuclides in arc lavas often reveal linear correlations on the (^{230}Th/^{232}Th)-(^{238}U/^{232}Th) isochron diagram. Such a correlation from historical lavas in the SVZ of south Chile was interpreted as an isochron reflecting the time elapsed between a U addition by fluids to the mantle source and magma eruption, being ≈20 k.y. These lavas have a uniform ^{87}Sr/^{86}Sr implying a relatively homogeneous magma source. Elsewhere, samples forming such correlation have variable Sr-, Nd-, and Pb-isotopic ratios, which may indicate that the linear variations are rather mixing lines than isochrons. Moreover, young arc lavas such as those from the SVZ have ^{226}Ra-excess over ^{230}Th that may result from the most recent fluid addition recorded by the lava compositions.

The amount of fluids from dehydration of a subducting oceanic lithosphere is likely to be related to the age of the slab that may determine both its thermal structure and degree of hydration. This is supported by a fair correlation between the maximum observed (^{238}U/^{230}Th) for a given arc and the age of the subducting oceanic crust. In contrast, the minimum (^{238}U/^{230}Th) for each setting is relatively constant regardless of the ocean crust maturity.

Melts of subducted sediments with rutile and garnet in the residue should have (^{230}Th/^{238}U), (^{226}Ra/^{230}Th), and (^{231}Pa/^{235}U) higher than 1, which upon mixing with a fluid enriched mantle melt (with U and Ra enriched relative to Th and Pa) would generate a mixing line on the isochron diagram. Excess ^{226}Ra are indeed observed in lavas with (^{230}Th/^{238}U) lower, equal or higher than unity. The maximum transfer time for primary arc magmas would then be <8 k.y.

The ideas above are being tested against new results on U-series nuclides in Recent basalts to basaltic andesites from the Izu-arc (south of Japan). The Th abundances in these lavas range from 0.169 to 0.412 ppm, whereas (^{230}Th/^{232}Th), (^{238}U/^{230}Th), and (^{231}Pa/^{235}U) vary between 0.96–1.80, 1.37–1.56, and 1.09–1.33 respectively. Large variability is observed for (^{226}Ra/^{230}Th), corrected for posteruptional decay, which ranges from 1.56 to 3.60.

The (^{231}Pa/^{235}U) of the Izu-arc samples fall on the lower end of the global island arc correlations between (^{231}Pa/^{235}U) and Th abundances, and (^{231}Pa/^{235}U) and (^{230}Th/^{238}U), from Pickett and Murrell (1997). In addition to large ^{238}U excess, the relatively low (^{231}Pa/^{235}U) suggest important proportions of U-rich fluid that is consistent with the high age of the subducting Pacific plate. The Izu-arc lavas form a linear array on the (^{230}Th/^{232}Th)-(^{238}U/^{232}Th) isochron diagram with a steeper slope than the equiline, excluding this correlation to represent an isochron. Moreover, a correlation of Th- and Nd-isotopic ratios, which are unlikely affected by a slab derived fluid component, suggests a binary mixing relationship. A covariation is also observed between (^{238}U/^{230}Th) and (^{226}Ra/^{230}Th)o in these samples, indicating a simultaneous and very recent addition of U and Ra to the magma source by fluids.

Current knowledge of the stability of hydrous phases in a peridotite and the solidus of water-saturated pelagic sediments suggests that concurrent dehydration and sediment melting may occur at an approximate depth of 120 km. An addition of a hydrous-rich sediment melt to the mantle wedge could provoke partial melting and fully account for the U-series observed in the Izu-arc lavas, if the time elapsed between melting and eruption is less than a few thousand years. Such a short timescale for magma transfer beneath an island arc is realistic for a predominant channel flow mechanism and magma velocity of <5 × 10^{-7}m/s.

MODELING CRUSTAL GROWTH USING A SAMARIUM-NEODYMIUM DATABASE OF SHALES.

F. Simien[1], E. Lewin[1], C. J. Allègre[1], and A. N. Dia[2], [1]Laboratoire de Géochimie et Cosmochimie, Institut de Physique du Globe de Paris, URA Centre National de la Recherche Scientifique, NRS 1758-UFR Sciences de la Terre, Université Paris VII Denis Diderot, 4 Place Jussieu, 75252 Paris Cedex 05, France, [2]Géosciences Rennes Campus de Beaulieu, 263 Avenue du Général Leclerc, 35042 Rennes Cedex, France.

Introduction: Crustal growth is a fundamental problem of understanding Earth evolution. Antagonistic models have tried to better understand whether the present mass of continents was formed early in the Earth's history [1] or if the crust has been continuously extracted from the mantle [2,3].

Recent discussions about the existence of an early depleted mantle reservoir put on the light evidences of primitive crust in several areas. On the other hand, crustal recycling into the mantle has been more and more accepted in the last 20 years. Thus the debate of crustal growth must be reexamined.

Studying shales with the Sm-Nd-isotopic system may bring important chronological information about crustal growth as shales integrate the diversity of mecanically eroded rocks and as this isotopic system is left undisturbed by surface processes. The Nd-isotopic composition of shales reflects a balance between juvenile inputs from the mantle by volcanism and reworked inputs from the continental crust. However, this signal is a biased mean of the different sources. For example, preexisting sediments and young mountains are more readily eroded. This bias parameter can be estimated and therefore corrected.

In order to have a view of the present day outcropping crust, we made a compilation of ~1000 Sm-Nd analysis of shales. We excluded samples containing a volcanogenic component in order to have a good representativity. This database does not reflect exactly the whole continental crust, but it represents a record of the upper continental crust at large scale since 4 Ga. Nethertheless, it must be noted that some areas like Europe and North America are oversampled.

Statistics from the Database: This database confirms that the ^{147}Sm/^{144}Nd ratio is constant during the earth's history [4]. The episodicity of orogenies comparated to the geologic evolution is also discussed. In the same way, we discuss the evolution of the heterogeneity of the shale's reservoir. Assuming that the Nd-isotopic system in shales reflects the whole continental crust, it appears, at a first order, that this reservoir evolved approximatively in a closed system with an apparent ^{147}Sm/^{144}Nd ratio of ~0.1809. This ratio is completely different from the present-day value directly measured in shales (0.1157). Therefore, the mantle and crust reservoirs evolved like an open system. Applying a model [4], we give an estimate for the net growth of the continental crust during the geologic times.

References: [1] Amstrong (1968) *Rev. Geophys. Space Phys., 6,* 175–179. [2] Hurley et al. (1962) *JGR, 67,* 5315–5334. [3] Allègre (1982) *Tectonophys., 81,* 109–132.[4] Allègre and Rousseau (1984) *EPSL, 67,* 19–34.

VARIATION IN THE SOURCES AND FLUXES OF ATMOSPHERIC POLLUTANTS PROXIMAL TO MONTRÉAL (QUÉBEC), CANADA, AS INFERRED FROM A YEAR'S LEAD- AND STRONTIUM-ISOTOPIC RECORD FOR PRECIPITATIONS.

A. Simonetti[1], C. Gariépy[1], L. Poissant[2], and J. Carignan[3], [1]Centre de Recherche en Géochimie Isotopique et en Géochronologie, Université du Québec à Montréal, CP 8888 succ. Centreville, Montréal H3C 3P8, Canada (c3204@er.uqam.ca), [2]Environment Canada, 100 Alexis-Nihon Boulevard, St. Laurent H4M 2M8, Canada, [3]Centre de Recherches Pétrographiques et Géochimiques-Centre National de la Recherche Scientifique, 15 rue Notre-Dame des Pauvres, BP 20, 54501 Vandoeuvre-lès-Nancy Cedex, France.

Precipitation samples (snow, freezing rain, and/or rain) representing either single, individual events retrieved primarily during the 1998 winter season or integrated over ~2-week intervals, were collected during the period December 1997 to January 1999 at the meteorological stations of St. Anicet and L'Assomption. The station at St. Anicet is located within a rural setting at ~100 km southwest of Montréal, whereas L'Assomption is situated in a semi-urban setting at ~40 km northeast of Montréal. The samples at both stations were retrieved using fully automated B200 (CAPMoN type) precipitation samplers equipped with Environment Canada "low-blank" polyethylene bags. This automated sampling system virtually eliminates the collection of aerosols during "dry" deposition since samples may only be taken upon detection of a precipitation event.

Abundances for a variety of trace elements, including heavy metals, and Pb- and Sr-isotopic ratios have been determined for precipitation samples (n = 50) from the two meteorological stations. The aims of this study are to examine the seasonal variation (if present) in the sources of atmospheric pollution using Pb- and Sr-isotopic data for the precipitations. In addition, long-term wind trajectory analyses indicate that the predominant wind directions in this region of North America parallel the orientation of the St. Lawrence river valley, i.e., they originate from the west, southwest, and south [e.g., 1]. The station of L'Assomption is situated in a downwind position with respect to the urban activity associated with Montréal, whereas St. Anicet is located in an upwind position with respect to the latter. Therefore, a comparison of the chemical and isotope data for samples for the identical precipitation event or integrated period of time from both stations may help establish the possible influence of the Montréal "pollution plume" on surrounding areas.

Median enrichment factors, relative to upper crustal abundances, for Cd, Cu, Mn, Pb, and Zn for most precipitation samples at both stations are similar. They range from ~30 (Mn) to ~14,000 (Cd), which are indicative of an anthropogenic origin. Moreover, their respective levels remain relatively constant throughout the year. However, winter precipitations collected at St. Anicet are characterized by slightly more elevated enrichment factors for Zn and Cd compared to those from L'Assomption for the same events.

Lead-206/lead-207 values exhibit a large seasonal variation at both stations, in particular at St. Anicet, with the most radiogenic values recorded during the winter months (1.170–1.190) and the lowest during the summer season ($\ll$1.150). Strontium-87/strontium-86 values also demonstrate a seasonal variation at both stations with the least radiogenic values recorded during the winter months (<0.7085), whereas for the remaining months the values are either relatively constant (0.7085–0.7088) at L'Assomption or variable (0.7085–0.710) at St. Anicet. The relatively "unradiogenic" nature of the ^{87}Sr/^{86}Sr ratios (<0.7085) recorded for winter precipitations at both stations are possibly related to atmospheric emissions from coal-fired power plants located in the western and midwestern regions of the United States. However, the nearly consistent nature of the ^{87}Sr/^{86}Sr values for nonwinter precipitations collected at L'Assomption possibly reflect Sr anthropogenic emissions from Montréal, such as those associated with cement-producing industries.

Comparison of Pb-isotopic data for the same, individual precipitation events (n = 7) from both stations do not systematically yield similar values. This indicates that air mass/scavenging processes may not be homogeneous at a scale of 100 km. With the exception of the 1998 summer samples from St. Anicet, which are defined by the least radiogenic ^{206}Pb/^{207}Pb values ($\ll$1.150), the Pb-isotopic systematics for the remaining precipitation samples from both stations may be explained by a mixture of anthropogenic emissions from US ($\approx$1.20) and Canadian ($\approx$1.15) sources. The relatively unradiogenic Pb-isotopic ratios for the summer precipitation samples from St. Anicet may be attributed to atmospheric emissions from the adjacent western regions (predominant upwind direction), possibly related to smelting activities at Sudbury Ontario.

A comparison between the chemical and Pb- and Sr-isotopic data obtained here to those for core samples of snowpack retrieved from adjacent regions in northeastern North America collected during the 1997 and 1998 winter seasons reveal some intriguing features. Of importance, the chemical and isotopic compositions from the latter represent a "naturally"-weighted sample of the wet and dry atmospheric aerosols deposited over 3–5 months. With the exception of the 1998 summer samples from St. Anicet, the entire variation in Pb- and Sr-isotopic ratios defined for the remaining samples analyzed in this study overlap with those measured in snowpack. The same is true for the enrichment factors for the various heavy metals, with the exception of those for Zn, which are systematically higher in the samples of snowpack; this possibly indicates an important contribution of Zn in periods of dry deposition.

References: [1] Matthieu et al. (1995) *Environ. Canada Rpt.*

GEOCHEMISTRY OF FLOOD PLAIN SEDIMENTS OF THE KAVERI RIVER, SOUTHERN INDIA.

P. Singh and V. Rajamani, School of Environmental Sciences, Jawaharlal Nehru University, New Delhi-110067, India (pramods@yahoo.com; vrm@jnuniv.ernet.in).

The geochemistry of sedimentary rocks has considerable importance to our understanding of the evolutionary history of Earth. Within their composition, sediments preserve a record of their source and consequently allow us to examine the relationship between the composition of upper crustal sources and the nature of sediments derived therefrom. Among ancient sediments, shales have been considered to be good proxy to the nature of exposed continental crust at the time of their formation. The main factors controlling their chemistry, however, are not well understood because of the difficulty in studying the petrography of shales. In modern sediments, geochemistry of channel sediments and their different size fractions have been used to evaluate their local source composition. But the difficulty with channel sediments is their limited application because they preserve the source characteristics only for a short distance of transport. Here we report that the flood plain sediments better preserve the source characteristics than other sediment load of a river, at least in areas where the rocks of the catchment region have been subjected to uplifts.

The flood plain sediments of Kaveri river in southern India are characterized by couplets of sandy and silty beds with mean size varying between 1.4Ø and 3.9Ø and between 4Ø and 4.7Ø units respectively. Silty beds show remarkable compositional uniformity within a vertical profile as well as for a distance of ~250 km downstream. This is so even in their REE geochemistry, both in abundance and patterns. Sandy beds, however, show more variability; they have lower REE abundance but very similar patterns all relative to silty beds. The geochemical variations seen in the two groups of sediments seem more likely due to the diluting effect of quartz than to the fractionation of any secondary minerals. Even the silty beds have low CIA values (average 55) suggesting not much chemical weathering of their source rocks. There is a slight decrease in SiO_2 concentration of silty beds downstream that may be due to sorting effect, retaining more quartz in the channel beds. This results in a slight increase of Fe, Mg, Cr, and Ni over the source rocks, although the average composition of the silty bed is found to be similar to charnockitic source rocks occurring as massive hills. Interestingly, the mean composition of the silty beds is also similar to PAAS (even in the –ve Eu anomaly) although their source rocks are predominantly Archean.

The REE in Kaveri flood plain sediments are found to be mainly hosted in silt and clay fractions; the sand fraction, however, is found to have lower abundance and +ve Eu anomaly. Heavy minerals, particularly zircon, appear to control the REE abundance in silt. Occasionally, concentration of heavy minerals in the fine silt fraction has led to higher abundance of REE in the silt relative to the clay fraction. Amorphous Fe oxy-hydroxides likely host the REE in the clay fraction. Thus if these two groups are separated out, i.e., clay and silt together in suspension and sand in the bed load, then they could have distinct chemistries that would be different from their common sources. However, in flood-plain sediments with a mean size of silt, clay + silt with higher abundance of REE are mixed with some amount of sand that dilutes it, resulting in lowering the concentration and making it almost similar to the source, especially the LREE; HREE may show slight enrichment due to heavy mineral concentration. It is known that during flooding hydrodynamically similar minerals are picked together and deposited as flood-plain sediments. Due to higher energy conditions during floods even particles up to fine sand are easily picked up in suspension and deposited. This process results in simultaneous deposition of both felsic and mafic minerals, causing a mineralogical remixing in the flood-plain sediments resulting in its compositional similarity to the source. We suggest the geochemistry of flood-plain sediments has the potential of unraveling the tectonic and climatic history of source regions and their exposed rocks.

REGIONAL ROCKY MOUNTAIN CLIMATE CHANGE RECORDED BY OXYGEN ISOTOPES OF HOLOCENE FERRICRETES.

D. J. Sjostrom[1], M. A. Poage[2], C. P. Chamberlain[1], and G. Furniss[2], [1]Department of Earth Sciences, Dartmouth College, Hanover NH 03755, USA (sjostrom@dartmouth.edu), [2]Department of Geology, University of Montana, Missoula MT 59812, USA.

Introduction: A recent study has suggested the O-isotopic composition of goethite [α-FeO(OH)] from Holocene ferricrete deposits can be used as a climate proxy [1]. As a continuation of this previous study, we sampled ferricrete deposits from two localities with distinct Holocene climate records in order to investigate the effects of regional climate change on the isotopic signature of ferricrete goethite.

Ferricrete Deposits: Iron oxyhydroxide cemented sediments (ferricretes) are commonly formed in drainages with naturally elevated metals concentrations and low pH as a result of the weathering of iron sulfide minerals. Rapid stream incision results in ancient ferricrete terrace deposits situated up to several tens of meters above current stream levels. The ferricrete deposits sampled for this study are exposed at Paymaster Creek, near Lincoln, west-central Montana and Cement Creek, outside of Silverton in the San Juan Mountains of Colorado.

The age of the ferricrete samples from Paymaster Creek was established using ^{14}C-dating of codeposited wood fragments that are commonly found within ferricrete deposits. The ferricretes range in age from 7.5 ka to present. Organic material suitable for dating has yet to be found at Cement Creek; relative stratigraphic ages were established by sample position above current stream base-level and maximum age of ferricrete deposits is assumed to be postglacial.

Rocky Mountain Climate: *Modern climate.* Modern seasonal precipitation in the Rocky Mountain region originates from one of two sources. Winter precipitation has its origin over the Pacific while summer precipitation is dominated by monsoonal moisture originating from the Gulfs of Mexico and California. The relative abundance of seasonal precipitation generally relies on geographic location and the position and intensity of the eastern Pacific subtropical high-pressure system. This system is in a northerly position in the summer, which causes summer drought in the northern Rockies and allows monsoonal moisture to move north into the southern Rockies. The southerly position of this high-pressure system in the winter results in relatively wet winters in the northern Rockies and dry conditions in the southern Rockies.

Holocene paleoclimate. In the early Holocene, 8% greater summer insolation caused the intensification of the east Pacific high-pressure system [2]. This resulted in drier summers in the northern Rockies and wetter summers in the southern Rockies with little change in winter precipitation

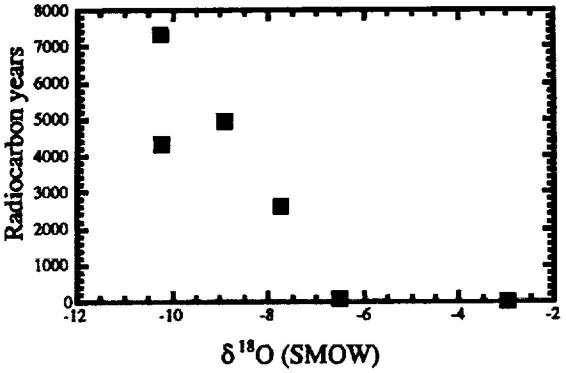

Fig. 1. $\delta^{18}O$ vs. age of ferricretes from Paymaster Creek, Montana.

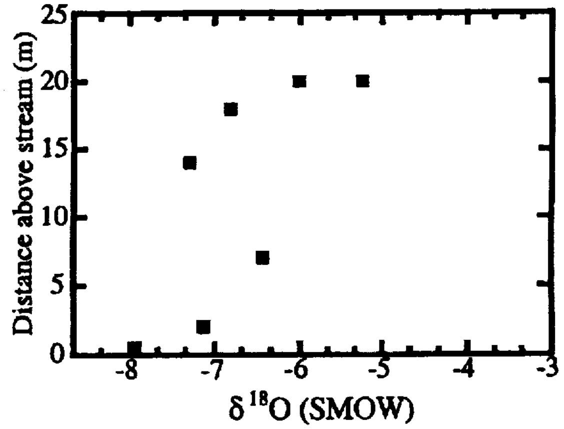

Fig. 2. $\delta^{18}O$ vs. stratigraphic position of ferricretes from Cement Creek, Colorado.

amounts relative to today. In general, relative amounts of seasonal precipitation have decreased throughout the Rocky Mountain region from the early Holocene to the present as summer insolation decreased to present intensity.

Results: $\delta^{18}O$ of ferricretes from Paymaster Creek, Montana, increased ~3‰ from the early Holocene to present (Fig. 1). At Cement Creek, Colorado, $\delta^{18}O$ of ferricrete samples decreases ~3‰ (Fig. 2). Due to the small temperature dependence of O-isotopic fractionation in the goethite-water system [3], we infer the $\delta^{18}O$ changes in our samples are the result of a change in isotopic composition of steam water. Specifically, we believe this data suggest an increase in the relative amount of summer precipitation in the northern Rockies and a relative increase in winter precipitation in the southern Rockies since the early Holocene. This interpretation is consistent with previous Holocene paleoclimate studies of the Rocky Mountain region [4,5]

Conclusions: The O-isotopic signature of ferricrete goethite appears to record regional climate signals. This method is potentially applicable to many sites throughout the Rocky Mountains, where few other climate proxies exist.

References: [1] Poage M. A. et al. (1997) *Mineralog. Mag., 62A,* 1188–1189. [2] Thompson et al. (1993) in *Global Climates Since the Last Glacial Maximum* (H. E. Wright et al.), pp. 468–513. [3] Yapp C. J. (1990) *Chem. Geol., 85,* 329–335. [4] Whitlock C. (1993) *Eco. Monographs, 63,* 173–198. [5] Friedman I. (1988) *Quat. Reasearch, 30,* 350–353.

THE DETERMINATION OF CHARCOAL IN SOILS.

J. O. Skjemstad, L. J. Janik, and J. A. McGowan, Commonwealth Scientific and Industrial Research Organisation, Land and Water, PMB 2, Glen Osmond 5064, South Australia (jan.skjemstad@adl.clw.csiro.au).

We have developed a technique for the estimation and isolation of charcoal C in soils based on selective oxidation using high energy ultraviolet photo-oxidation [1]. Soil samples are Na saturated and given a mild ultrasonic treatment to reduce the size of natural aggregates to <53 µm. The <53-µm fraction is then exposed to high-energy photo-oxidation in the presence of excess air for 2 h. Charcoal is highly resistant to this treatment, apparently through its chemical nature, and is concentrated in the fraction remaining while other soil organic substances are largely destroyed. Small amounts of physically protected C that are shielded from the ultraviolet light often survive the photo-oxidation treatment and are included in the residue. We have found little evidence for the presence of charcoal in the >53-µm fraction. Solid-state ^{13}C nuclear magnetic resonance (NMR) with cross-polarization and magic angle spinning (CP/MAS) can then be used to identify the nature of the organic materials remaining. Charcoal consists of extensively condensed or cross-linked aromatic ring structures that appear largely as an aromatic band at 130 ppm in NMR spectra. Quantification of char using CP/MAS ^{13}C NMR has proved unreliable due to the large proportion of C nuclei within the charcoal structure spatially isolated from protons. Bloch decay (BD) experiments show that on average only ~30% of the C nuclei present are observed by the CP/MAS technique, indicating the highly condensed nature of this material. In our work, we have assumed that the aromatic fraction represents the char unless there is evidence in the NMR spectra of lignin structures. If lignin structures are present, a correction to the aryl region based on the contribution of the O-aryl region is made. In our experience, these structures are rarely observed in samples following photo-oxidation.

In samples where the residue consists entirely of aromatic and carbonyl C, all organic structures must originate from char and perhaps also other tar-like products derived from the charring process. If other C nuclei are present, then a correction for the cross-polarization inefficiency must be made through an equation relating aryl C in CP spectra to that in BD spectra [2]. This technique has the advantage of allowing charcoal measurements to be made as well as isolating the charcoal material in a relatively "pure" state for further studies on chemical composition and morphology.

The described technique for charcoal analysis is time-consuming and expensive, requiring specialized equipment. More rapid techniques are required where a large number of estimates are required. In our laboratory, we have demonstrated that, using the described procedure as a "standard," charcoal C can be predicted in soils using a mid-infrared spectroscopic technique coupled with partial least squares (PLS) multivariate software [3]. Correlation with measured soils is good (R^2 = 0.88) and provides a rapid means of assessing charcoal contents for modeling and survey purposes. As part of the analysis, estimates of particulate organic C (POC, R^2 = 0.82) and total organic C (TOC, R^2 = 0.94) are also obtained at a rate of ~200 samples per day.

References: [1] Skjemstad, J. O. et al. (1996) *Aust. J. Soil Res., 34,* 251–271. [2] Skjemstad J. O. et al. (1999) *Commun. Soil Sci. Pl. Anal.,* in press. [3] Janik L. J. et al. (1998) *Aust. J. Exp. Ag., 38,* 681–696.

THE NATURE, DISTRIBUTION, AND IMPACT OF CHARCOAL IN SOILS.

J. O. Skjemstad, L. J. Janik, and L. R. Spouncer, Commonwealth Scientific Industrial Research Organisation, Land and Water, PMB 2, Glen Osmond 5064, South Australia (jan.skjemstad@adl.clw.csiro.au).

We have developed two techniques for the isolation and estimation of soil charcoal. The first technique, which relies on high energy photo-oxidation [1], can be used for both isolation and estimation but is slow and expensive. The second method utilizes infrared spectroscopy and can be used for the rapid quantification of charcoal carbon in soils [2].

Scanning electron microscopy shows that the highly aryl charcoal residues from photo-oxidation have a plantlike morphology. These charcoal particles can vary considerably in size and morphology and range from plant-like fragments in the 5–40-µm particle range to submicrometer particles that are often platey in nature and can be difficult to distinguish morphologically from clay. Virtually all of this finely divided charcoal appears to result from the burning of grasses and understorey vegetation in savannas and open woodlands. In Australia, burning of grasslands has been widespread for millennia and regular burning is an essential component for the functioning of some ecosystems.

Soils from all states in Australia and covering a wide range of environments have been separated and analyzed for their charcoal content through photo-oxidation and NMR analysis. All soils have a significant proportion of C remaining after photo-oxidation and in most cases, charcoal makes a major contribution to this fraction, often exceeding 80%. Although nearly all soils studied contain measurable amounts of charcoal, certain soil types always contain significant amounts. For example, soils that are dark in color but contain low amounts of organic C (<3%) invariably contain a high proportion of charcoal. It would appear that finely-divided charcoal is significant in determining soil color, at least in soils that have a low or moderate Fe content. Soils formed from alluvium with moderate or high clay contents also often contain significant amounts of charcoal. It is postulated that finely divided charcoal materials are mobile, behaving in a manner similar to clay and silt and hence accumulate in the same locations where clay and silt materials accumulate. Charcoal is therefore often found in high concentrations and to some depth in soils such as Vertisols, soils formed on riverine plains and deltas and in marine coastal sediments. The distribution of charcoal both laterally and vertically in soils is highly variable and appears to reflect the amount of above-ground biomass susceptible to fire and burning frequency, clay content as well as erosional and illuvial processes as described above.

The charcoal material in soils forms the basis of the inert or highly passive pools and has a significant influence on the dynamics of soil organic C. Under exploitive cultivation, soils high in charcoal appear to resist organic C decline, while those that are low decline more rapidly [3]. Exploitive cultivation therefore often results in an increasing trend in the aromaticity of the organic matter as more labile soil C pools decompose leaving the highly aromatic charcoal largely intact. As a result, effective soil organic C modeling can only be achieved if the charcoal content of the soil can be estimated reliably.

References: [1] Skjemstad J. O. et al. (1996) *Aust. J. Soil Res., 34,* 251–271. [2] Janik L. J. et al. (1998) *Aust. J. Exp. Ag., 38,* 681–696. [3] Skjemstad J. O. et al. (1998) *Aust. J. Exp. Ag., 38,* 667–680.

DISSOLUTION MECHANISMS OF HYDROGEN IN β-Mg_2SiO_4 (WADSLEYITE) USING HYDROGEN-1 MAGIC-ANGLE SPINNING NUCLEAR MAGNETIC RESONANCE.

A. E. Slesinger, B. J. Wood, and S. C. Kohn, Department of Earth Sciences, Wills Memorial Building, University of Bristol, Queens Road, Bristol BS8 1RJ, UK.

It has been established that β-Mg_2SiO_4 (wadsleyite) can dissolve up to 3.3 wt% water in its crystal structure [1–6]. Although Smyth [1] found that protonation of O1 is the principal dissolution mechanism of H, Downs [2] calculated that O2 might also be involved. In this study ^1H magic-angle spinning (MAS) NMR was used to provide information on the site(s) of protonation.

Hydrous wadsleyite was synthesized at 16 GPa and 1300°C in a 1000-ton multianvil press. Starting materials were mixtures of MgO, $Mg(OH)_2$, and SiO_2 that were welded into Pt capsules. These mixtures contained the equivalent of 0.3–3.3 wt% H_2O. The recovered samples were crushed and characterized using powder X-ray diffraction. ^1H MAS NMR spectra of a sample with 0.3 wt% H_2O show that only two local environments for H are present, whereas samples containing 1.6–3.3 wt% H_2O have at least four local environments for H. The results are consistent with O1 being the only O site that is protonated. At low H_2O concentrations, H appears to lie along both the O1–O3 and O1–O1 vectors (i.e., along the x and y directions only); at high H_2O concentrations H is also present along the two types of O1–O4 vectors (i.e., with a component parallel to the z-direction). This interpretation is consistent with XRD data [6] that show most Mg vacancies on M3.

References: [1] Smyth J. R. (1987) *Am. Mineral., 72,* 1051–1055. [2] Downs J. W. (1989) *Am. Mineral., 74,* 1124–1129. [3] Young T. E. et al. (1993) *Phys. Chem. Mineral., 19,* 419–422. [4] Inoue T. et al. (1995) *GRL, 22,* 117–120. [5] Kohlstedt D. L. et al. (1996) *Contrib. Mineral. Petrol., 123,* 345–357. [6] Kudoh Y. et al. (1996) *Phys. Chem. Mineral., 23,* 361–469.

THE NATURE AND REACTIVITY OF COMBUSTION SOOTS.

D. M. Smith and A. R. Chughtai, Department of Chemistry and Biochemistry, University of Denver, Denver CO 80208, USA.

An overview of results from two decades of research on black carbon particles in these laboratories is presented. Physical and chemical characteristics such as morphology, elemental composition, surface properties, spectra, PAH content, reactivity, and adsorption behavior are summarized.

The incomplete combustion of fossil fuels produces aggregated spheroidal particles with average ultimate particle diameter <100 nm, surface areas ranging from 60–90 m^2/g, significant pore structure, and surfaces with characteristic C-O functionalities. They react rapidly with oxidants such as ozone and oxides of N to produce surface groups that alter their subsequent reactivity. The kinetics of these reactions is summarized and the effects of simulated solar radiation on some of the reactions reported. Hydration of the black carbon particles as a function of relative humidity has been studied, largely through microgravimetry, and conclusions about the hydration process reached from the application of an isotherm to the data. The extent of hydration is a function of fuel type, combustion conditions, and such parameters as metal/mineral content and surface oxidation.

Studies of adsorption and adsorbate interaction (molecular O, oxides of N, O_2S, water vapor, and ammonia) have been carried out by a combination of electron paramagnetic resonance (EPR) spectroscopy and microgravimetry. The results show interaction between certain coabsorbates but not others.

These results are informing current work on the kinetics of reaction of black carbon (soot) particles in multicomponent systems.

GEOAVAILABILITY OF METALS IN A MINE-WASTE MATERIAL.

K. S. Smith[1], G. P. Meeker[1], R. W. Leinz[1], S. J. Sutley[1], H. L. O. Huyck[2], and G. A. Desborough[1], [1]Mail Stop 973, U.S. Geological Survey, Federal Center, Denver CO 80225-0046, USA (ksmith@usgs.gov), [2]P.O. Box 28161-16, Lakewood CO 80228, USA.

The concept of the availability of metals from natural materials, referred to as the geoavailability, is defined as that portion of a chemical element's or a compound's total content in Earth material that can be liberated to the surficial or near-surface environment (or biosphere) through mechanical, chemical, or biological processes. The geoavailability of a chemical element or a compound is related to the susceptibility and availability of its resident mineral phase(s) to alteration and weathering reactions [1]. Figure 1 illustrates the pathways from total metal content in an Earth material to toxicity. Geoavailability is an important step along these pathways. We present examples of geoavailability using mine-waste material. Detailed examination of the residence phase(s) of metals in the mine-waste material is necessary to understand the geoavailability of metals in mine-waste dumps. We use a combination of X-ray microanalysis and chemical-extraction techniques to determine metal residence phase(s) in the mine-waste materials. This information, combined with bulk chemical analysis and X-ray diffraction, can shed light on metal geoavailability and subsequent mobility from mine-waste material.

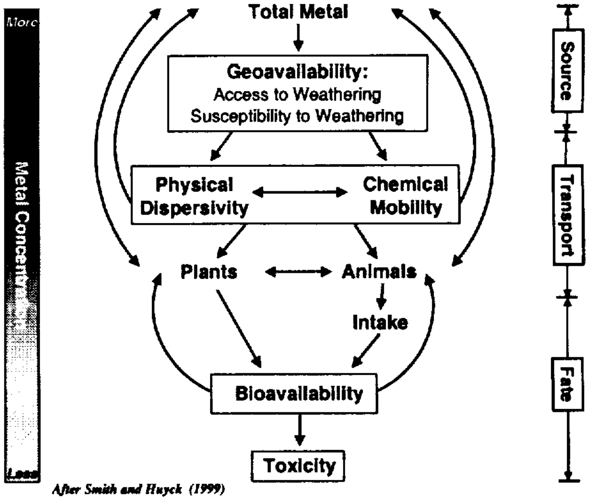

After Smith and Huyck (1999)

Fig. 1. Diagram illustrating the relationship between total metal content and bioavailability with geoavailability.

References: [1] Smith K. S. and Huyck H. L. O. (1999) *Rev. Econ. Geol., 6A,* 29–70.

RARE-EARTH-ELEMENT AND TRACE-ELEMENT TRENDS IN THE EVERGLADES AS TRACERS FOR SEDIMENTARY PROCESSES.

J. E. Sonke and V. J. M. Salters, Geochemistry Division, National High Magnetic Field Laboratory, Tallahassee FL 32306, USA (sonke@magnet.fsu.edu; salters@magnet.fsu.edu).

Ecological changes in the Everglades resulting from eutrophication can be directly related to the application of fertilizers in the Everglades Agricultural Area (EAA). We measured REE and trace elements in surface waters, plants, peat sediments, fertilizers, and bedrock from EAA, Environmental Nutrient Removal area (ENR) and Water Conservation Area (WCA), covering a range of human-influenced to pristine wetland ecosystems.

Results show decreasing P concentrations in sediments and waters toward pristine Everglades (Fig.1; F1 towards U3), and decreasing P concentrations with depth. Fertilizers applied in the EAA show distinct light-rare-earth-element (LREE) depleted patterns relative to North American shale. This is reflected in low Pr/Yb ratios of 0.78. Carbonate bedrock and clay minerals are LREE-enriched with Pr/Yb ratios of 2.7 and 2.8 respectively. Sediments, on average consisting of 86 wt% organic matter, 2 wt% clay, and 12 wt% carbonate, have Pr/Yb ratios of 3.8, suggesting the O.M. source to be enriched in LREE to an even larger extent. This is indeed reflected in living plants having Pr/Yb ratios of 7.8. The ability of plants to fractionate REE (higher LREE uptake relative to HREE) has been observed by other workers and must result in a LREE depletion of its uptake source. Praseodymium/ytterbium ratios of water average 0.36 and allow us to postulate an open ecosystem model in which plants fractionate LREE from waters, thereby enriching peat sediments and depleting the water source in LREE. Mass-balance calculations indicate 50–90% O.M. recycling in the upper 5 cm, assuming full retention of REE in O.M. upon decomposition. Increasing P and U concentrations toward surface peat layers correlate with decreasing Pr/Yb trends, indicating biological recycling as well as anthropogenic enrichment [1,2]. Using fertilizer trace-element characteristics we should be able to distinguish between these processes. Depth profiles in the sediments also show an increase

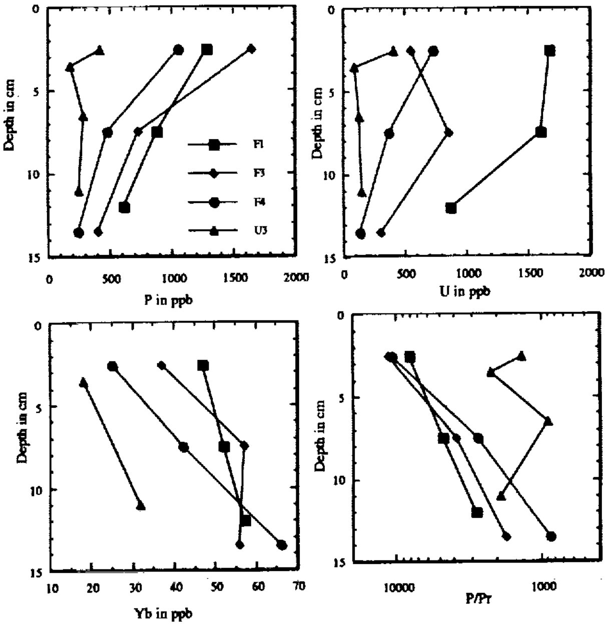

Fig. 1. Concentration profiles for WCA 2A sediments from different locations along the transect. The decrease in phosphorous and U with depth for all sites except U3 indicates the mobility and consumption of these elements as the sediments decompose. The P and U concentration in plants is expected to be constant (by first approximation) over the last two decades. Therefore, the decrease observed in the profile has to be associated with conservation in the upper layers through biological recycling.

in REE concentrations and in other relatively insoluble elements like Ti with depth (Fig. 1).

References: [1] Craft C. B. and Richardson C. J. (1993) *Biogeochemistry, 22,* 133–156. [2] Reddy K. R. et al. (1993) *Soil Sci. Soc. Am. J, 57,* 1147–1155.

$CaCO_3$ DISSOLUTION IN EQUATORIAL DEEP-SEA SEDIMENTS DURING INTERGLACIAL-GLACIAL TRANSITIONS.

J. Specht and A. Mangini, Heidelberger Akademie der Wissenschaften, INF 229 D-69120 Heidelberg, Germany (sp@uphys1.uphys.uni-heidelberg.de; mg@uphys1.uphys.uni-heidelberg.de).

Introduction: Archer and Maier-Reimer [1] had proposed an increased sediment organic C to $CaCO_3$ ratio to explain the observed lower atmospheric CO_2 during glacial times. In this scenario $CaCO_3$-dissolution events occur at interglacial-glacial transitions.

To examine those dissolution events we have studied 18 cores from the equatorial Atlantic and Pacific, where $CaCO_3$-fluxes were normalized against $^{230}Th_{ex}$.

Results: At most cores the interglacial-glacial transitions show $CaCO_3$-dissolution events. We define here the intensity of an event [%] as the relative drop in the $CaCO_3$-rain rate compared to the rain rates before and after the section with less $CaCO_3$. The intensity of the events is proportional to the drop of atmospheric CO_2 recorded in ice cores [2,3].

One may evaluate that on average the excess $CaCO_3$-dissolution during these events would deliver enough CO_3^{2-} to seawater to explain the atmospheric CO_2 drop.

In the scenario proposed by Archer and Maier-Reimer [1], oxidation of organic matter should explain most of the observed calcite dissolution. As to the cause of dissolution events, we examined $CaCO_3$-rain rates from cores taken from above and below the recent calcite lysocline at three different locations. This yields dissolution fluxes and especially the differences between the $CaCO_3$ fluxes at different depths. These values were applied to the equations describing calcite dissolution [4–6], which were solved numerically.

For example the difference between the sedimenting $CaCO_3$-fluxes at two depths during a dissolution event can be described by A_c(deep) – A_c(shallow) where $A_c = K_c\,([CO_3^{2-}]_{sat}(z) - ([CO_3^{2-}]_{BW} - RC_{org} - D))^{4.5}$; $\Delta \equiv D_{BW} + D_{C_{org}}$; A_c = $CaCO_3$-dissolution rate [µMol cm^{-2} a^{-1}]; K_c = rate coefficient: 1.2 µMol cm^{-2} a^{-1} per µMol kg^{-1} CO_3^{2-}-undersaturation [7]; $[CO_3^{2-}]_{sat}$ = saturation concentration of calcite at z; $[CO_3^{2-}]_{pw}$ = CO_3^{2-} porewater concentration; z = water depth, for the cores above or below the lysocline; Δ = additional CO_3^{2-} reduction during the dissolution event; Δ_{BW} = CO_3^{2-} reduction due to changes of the bottom-water chemistry during the dissolution event; $\Delta_{C_{org}}$ = additional CO_3^{2-} reduction due to changes of the rate of organic matter sedimentation during the dissolution event; and RC_{org} = CO_3^{2-} reduction due to organic matter oxidation.

We estimate an increase of 30% for the C_{org}-induced $CaCO_3$ dissolution. This is well below the 100% increase for equatorial regions required to explain the observed atmospheric CO_2, as estimated by Sigman et al. [7]. We conclude that the scenario proposed by Archer and Maier-Reimer [1] is improbable for equatorial regions in the Pacific and Atlantic Oceans.

References: [1] Archer D. and Maier-Reimer E. (1994) *Nature, 367,* 260–263. [2] Jouzel J. et al. (1993) *Nature, 364,* 407–411. [3] Fischer H. et al. (1999) *Science, 283,* 1712–1714. [4] Keir R. (1980) *GCA, 44,* 241–252. [5] Emerson S. and Bender M. (1981) *JMR, 39,* 139–162. [6] UNESCO (1987) *Unesco Techn. Pap. Mar. Sci.,* 51. [7] Sigman D. et al. (1998) *Global Biogeochem. Cycl., 12,* 409–427.

ISOTOPIC MODELING OF THE SIGNIFICANCE OF SULFATE REDUCTION FOR PHENOL ATTENUATION IN A POLLUTED AQUIFER.

M. Spence[1], S. Bottrell[1], S. Thornton[2], and D. Lerner[2], [1]School of Earth Sciences, University of Leeds LS2 9JT, UK, [2]Groundwater Protection and Restoration Group, Department of Civil and Structural Engineering, University of Sheffield, Sheffield S1 3JD, UK.

Introduction: An unconfined Triassic Sandstone aquifer in the W. Midlands, UK [1], has been polluted with phenolic hydrocarbons from a coal tar distillation plant. High (1-m) resolution groundwater sampling has identified a near-sterile plume core where the pollutant phenol concentration exceeds 6g/L, and a diluted upper margin where good evidence for bacterial sulfate reduction has been obtained. The pollution plume extends for a distance of ~500 m and reflects 50 yr of contaminant migration at a mean velocity of 10 m/yr. Nonaqueous phase contaminants persist in the subsurface below the site of the source term and these continue to leach phenolic compounds into the groundwater. The major pollutants, in order of decreasing concentration, are phenol, o/m/p- cresols, and xylenols. Data obtained from $\delta^{34}S$-SO_4 and $\delta^{18}O$-SO_4 stable isotopic analysis of plume groundwater have been used to inverse model the process of sulfate reduction and generate a mass balance for pollutant mineralization.

Groundwater Sampling and Isotopic Analysis: Conventional boreholes at the site source term were sampled with an inertial pump. Two high-resolution boreholes with a sampling interval of 1 m were also sampled using peristaltic pumps. Trace hydrogen sulfide was recovered from the high-resolution wells using a large sample volume N sparging apparatus [2]. Samples of groundwater were processed to remove the dissolved organic component prior to the precipitation of insoluble barium sulfate. Barium sulfate precipitates were converted to SO_2 and CO_2 prior to $\delta^{34}S$-SO_4 and $\delta^{18}O$-SO_4 determination by standard methods [3,4].

Results and Discussion: Isotopic analysis has revealed the presence of two sulfate reservoirs with distinct isotopic ratios. Natural groundwater sulfate ($\delta^{18}O$ = 3–4‰, $\delta^{34}S$ = 0‰) has mixed with a uniform pollutant sulfate reservoir ($\delta^{18}O$ = 10–12‰, $\delta^{34}S$ = 5‰). Sulfate O isotopes show simple linear mixing between these end members at the plume margin, but S isotopes have a superimposed shift toward heavier $\delta^{34}S$-SO_4 values (e.g., 26.6‰). This is a result of sulfate reduction modifying the S-isotopic composition of the plume sulfate. Sulfate in the plume core is isotopically similar to that recovered from the plume source term ($\delta^{18}O$ = 11.5‰, $\delta^{34}S$ = 5‰) indicating that no sulfate reduction has occurred in the center of the plume during migration.

Profiles of O-isotopic variation in the dissolved sulfate do not show evidence for sulfide reoxidation. This confirms the presence of a stable reservoir for reduced S. Reduced S could be stored as FeS or FeS_2 by reaction with sedimentary Fe oxides [5], although analysis of rock core shows no sulfide phases to be present. Dissolved HS^- with a $\delta^{34}S$ of 16.8‰ has been detected in association with isotopically heavy sulfate (26.6‰). This implies a fractionation factor of –9.8‰ for the sulfate reduction process. Prereduction sulfate concentration profiles have been calculated by inverse modeling the Rayleigh fractionation process. From these a mass balance for organic C degradation has been derived. This shows that 0.05% of the organic contaminant mass has been degraded by sulfate reduction. Above a total aromatic loading of 2400 mg/L sulfate reduction does not occur. Calculations suggest that sufficient sulfate is present to degrade a maximum of 2% of the organic pollutant loading.

Conclusion: The presence of an active colony of sulfate reducers within a contaminated aquifer has been inferred from enrichment in $^{34}SO_4$ characteristic of sulfate reduction [6] and a mass balance for pollutant degradation has been derived. The *in situ* degradation capacity is limited, however, due to the high contaminant load. If the plume continues to migrate in its present form, then mixing with uncontaminated groundwater will be negligible and the plume will migrate as a concentrated plug further into the aquifer. Results indicate that dilution would stimulate sulfate reduction by lowering the plume's toxicity, although additional sulfate would be required to make a significant impact on organic contaminant concentrations.

References: [1] Jackson D. and Lloyd J. W. (1983) *Quart J. Eng. Geol., 16,* 135–142. [2] Moncaster S. J. and Bottrell S. H. (1991) *Chem. Geol, 94,* 79–82. [3] Halas et al. (1982) *Isotopenpraxis, 18,* 11–13. [4] McCarthy et al. (1998) *Fuel, 77,* 677–682. [5] Canfield et al. (1992) *Am. J. Sci., 292,* 659–683. [6] Chambers L. A. and Trudinger P. A. (1979) *Geomicrobiology, 1,* 249–293.

STRONTIUM-ISOTOPIC RATIOS TRACE NATURAL ALKALINE ADDITION TO COAL MINE DRAINAGE.

S. L. Stafford[1], R. C. Capo[1], B. W. Stewart[1], A. Reynolds[1], and R. S. Hedin[2], [1]Department of Geology and Planetary Science, University of Pittsburgh, 321 EH, Pittsburgh PA 15260, USA, [2]Hedin Environmental, 195 Castle Shannon Road, Pittsburgh PA 15228, USA.

Abandoned mine drainage (AMD) from coal production has degraded water quality in 12,000 km of streams in the United States by reducing O levels, coating stream substrates, increasing turbidity levels, and increasing toxic metals [1]. It is the most significant water-quality problem in the Appalachian region. AMD contains significant amounts of Fe, SO_4, and Mn and may contain many trace metals such as Al. While AMD is often highly acidic (pH <3), it has recently been noted that some AMD is net alkaline or has geochemically evolved from acidic to net alkaline during the last 30 yr. An understanding of the geochemistry of naturally occurring alkaline mine waters will help optimize the use of passive wetland designs and to accurately predict the character of mine drainage in differing lithologies.

Alkaline mine drainage has been attributed to alkaline addition from calcareous overburden [2], weathering of silicate minerals [3], and cation exchange in clays [3,4]. We used elemental analysis and $^{87}Sr/^{86}Sr$ composition to constrain the contribution from these possible sources of alkaline addition to deep mines and to better understand the interaction of waters with the rocks in the mines. Mine waters were sampled at seven discharges from the abandoned coal mines of the Pittsburgh Coal in the Irwin syncline of southwestern Pennsylvania. Major and trace elements were analyzed by inductively coupled plasma atomic emission spectrometry (ICP-AES) and ion chromatography. The northern discharges were acidic with pH <3.5 and high concentrations of Al (1–13 ppm). The southern discharges were net alkaline with high amounts of Fe (13–78 ppm) and sulfate (296–1331 ppm). A positive correlation exists between Na and alkalinity at all sites. Strontium concentrations range between 0.7 and 2.6 ppm and exhibit a general increase from north to south in the syncline.

Freshwater limestone units overlying the coal are the most likely source of alkalinity in the AMD waters. In addition, the AMD may have interacted with calcareous shales and clay above the coal and within the coal. The $^{87}Sr/^{86}Sr$ composition of the freshwater limestone ranges from 0.7106 to 0.7111. Calcareous shales range from 0.7173 to 0.7269, and clay parting within the Pittsburgh Coal ranges from 0.7181 to 0.7298.

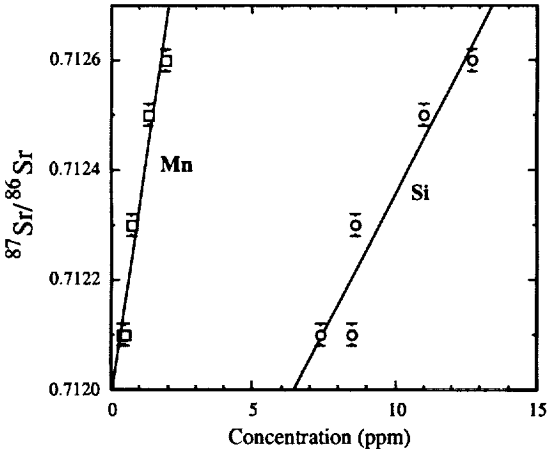

Fig. 1. Variations in [Mn] and [Si] with $^{87}Sr/^{86}Sr$ in alkaline mine drainage waters.

Abandoned mine drainage $^{87}Sr/^{86}Sr$ ratios range from 0.7121 to 0.7126. The isotopic composition of the mine waters suggests interaction of the waters both with the limestones and with the shales and clays within and directly above the coal seam. As noted in a previous study [4], the Na bicarbonate waters in these discharges could be produced by cation exchange reactions, as Ca in the water is replaced by Na in the overburden clay. These exchange reactions would increase the dissolution of calcium carbonate, allowing the accumulation of bicarbonate. Mass-balance calculations suggest that up to 25% of the Sr could be derived from interaction with clay minerals. A positive correlation of Fe, Mn, and Si concentrations with $^{87}Sr/^{86}Sr$ ratios in the net alkaline discharges is additional evidence of a silicate weathering component to the alkalinity of these mine waters (Fig. 1).

References: [1] Earle J. and Callaghan T. (1998) *Coal Mine Drainage Prediction and Pollution Prevention in Pennsylvania, 4,* 1–10. [2] Brady K. B. C. et al. (1988) *U.S. Bureau of Mines Information Circular 9183,* 33–43. [3] Brady K. B. C. et al. (1998) *Coal Mine Drainage Prediction and Pollution Prevention in Pennsylvania, 8,* 1–92. [4] Weaver T. J. (1998) *Geol. Soc. of Amer. Prog. Abstr., 30.*

MAJOR TRENDS IN THE MINERALOGY OF CARBONATE SKELETONS REFLECT OSCILLATIONS IN MID-OCEAN-RIDGE SPREADING RATES AND SEAWATER CHEMISTRY.

S. M. Stanley and L. A. Hardie, Department of Earth and Planetary Sciences, Johns Hopkins University, Baltimore MD 21218, USA (stanley@jhu.edu; hardie@gibbs.eps.jhu.edu).

The mineralogy of skeletal carbonates, like that of nonskeletal carbonates, has been profoundly influenced by changes in the chemical composition of seawater during the past half billion years. From study of oolites and early marine cements, Sandberg [1] showed that the Phanerozoic Eon has been characteried by three intervals of "aragonite seas" separated by two intervals of "calcite seas." Both aragonite and high-Mg calcite (>4 mol% Mg) precipitate in aragonite seas, including that of the present.

Changes in atmospheric pCO_2 have been invoked to explain transitions between aragonite and calcite seas, but the computer program PHRQPITZ predicts that calcite would precipitate from modern seawater at 25°C only within a narrow range of pCO_2 levels that are an order of magnitude higher than the present level. Furthermore, experiments show that high-Mg calcite, rather than low-Mg calcite, would precipitate at such high pCO_2 levels.

It has long been recognized that changes in the Mg/Ca ratio of seawater have the potential to cause shifts between aragonite and calcite seas. Experiments of Füchtbauer and Hardie [2] showed that for NaCl solutions the ionic strength of modern seawater at 28°C the shift from calcite to aragonite + high-Mg calcite occurs at a Mg/Ca ratio of $\sim$2. Spencer and Hardie [3] showed that small changes in the flux of Mg^{++} to, and Ca^{++} from, mid-ocean ridges can produce significant changes in the Mg/Ca ratio of seawater. Hardie [4] further showed that changes in total spreading rates along mid-ocean ridges, estimated from first-order sea-level curves, yield estimates for changes in the Mg/Ca ratio of seawater that correspond to Sandberg's transitions between aragonite and calcite seas.

Recognizing that certain groups of marine organisms have flourished throughout most of Phanerozoic time without major changes in skeletal mineralogy, we adopted a two-part strategy to search for temporal patterns of skeletal mineralogy corresponding to those of nonskeletal carbonates.

First, we examined taxa that have exhibited *hypercalcification*: taxa that have secreted unusually massive skeletons compared to those of closely related taxa or that have included populations engaging in rampant carbonate productivity. Such taxa may have required a favorable Mg/Ca ratio in seawater to flourish.

Second, we examined biologically simple taxa: ones that appear to engage in unsophisticated biomineralization and might therefore be strongly influenced by seawater chemistry; an extreme example would be an alga that simply induces calcification by extracting CO_2 from adjacent seawater for photosynthesis.

Reef-building taxa meet both criteria for a likely strong influence of the Mg/Ca ratio. They are hypercalcifiers and also tend to be simple organisms because competition for space on reefs is severe, and simple organisms, such as calcareous algae, sponges, and corals, are able to occupy space rapidly through vegetative or colonial growth.

Our search strategies reveal important links between seawater chemistry and skeletal mineralogy, connecting many previously puzzling phenomena with a single explanation. The dominant reef builders of calcitic seas, for example, have generally been calcitic and those of aragonitic seas have generally been aragonitic. The only conspicuous exception here is the success of the aragonitic scleractinian corals in Late Jurassic and Early Cretaceous time, but the Mg/Ca ratio of seawater at this time was near the boundary separating calcite and aragonite seas. Also, the high absolute concentration of Ca^{++} in calcite seas favors all secretors of $CaCO_3$. Furthermore, scleractinian corals assumed a subordinate role in reef building during the Late Cretaceous, when Hardie's calculations indicate that the Mg/Ca ratio of seawater descended to its lowest Phanerozoic level; despite the great warmth of Eocene seas, these corals failed to build large reefs again until the Oligocene Epoch when the Mg/Ca ratio had risen markedly.

Productivity of calcareous algae also reflects changes in the Mg/Ca ratio of seawater. *Halimeda*, which is aragonitic, produces 25–30% of recognizable carbonate grains of reefal lagoons in modern aragonite seas. Similarly, aragonitic dasycladacean algae flourished in the late Paleozoic-early Mesozoic aragonite seas; they have been regarded as the *Halimeda* of the Triassic. Massive calcitic chalk accumulated during the intervening Late Cretaceous interval of extreme calcite seas; calcareous nannoplankton were highly diverse before this time but failed to form chalk. Productivity of calcareous nannoplankton declined markedly during the Cenozoic, as the Mg/Ca ratio rose dramatically, and many taxa evolved smaller or less-robust coccoliths. Biologically simple animal taxa also exhibit evolutionary trends that reflect changes in the Mg/Ca ratio of seawater. For example, throughout their existence sponges and cheilostome bryozoans appear to have secreted skeletons with mineralogies corresponding to those of nonskeletal carbonates.

References: [1] Sandberg (1983, 1985). [2] Füchtbauer and Hardie (1976, 1980). [3] Spencer and Hardie (1990). [4] Hardie (1996).

THE PAN-AFRICAN PLUME EVENT AND THE GROWTH OF GONDWANA.

M. Stein, Institute of Earth Sciences, The Hebrew University, Givat Ram, Jerusalem, Israel (motis@vms.huji.ac.il).

Plumes and Continental Growth: Continental crust growth was conventionally viewed as subduction related process occurring along convergent plate boundaries. Yet the episodic nature of major orogenic events and the high rate of crust formation during these events that exceeds the present-day arc activity suggest that other processes such as plume magmatism are involved in continental crust formation [cf. 1]. Stein and Hofmann [2] proposed that the Earth history alternates between two modes of convection and dynamic evolution, one approximating a two-layer convective style, when plate tectonics operates in a "Wilsonian" manner, and continental crust forma-tion rates are low. The other mode, "MOMO," involves significant exchange of material between lower and upper mantle (Mantle Overturn) as well as high rate of continental crust formation (Major Orogenies). The lower mantle material is rising as large plume heads, which produce oceanic plateaus that are later accreted to the continents. Stein and Goldstein [3] argued that in many respects the differences between the "arc" and "plume head" growth models are a matter of emphasis because the transformation of the plume related-mantle material into continental crust and lithosphere is furnished by the subduction processes. Here, I discuss the growth of new lithospheric mantle and crust during the late Proterozoic Pan-African orogeny. I estimate the size of the juvenile lithospheric mantle and use it to estimate the size of its parental "plume mantle."

Alkali Magmas — Probes of the Lithospheric Mantle: Phanerozoic alkali-basalt erupted in different parts of the African-Arabian continent, along the East African rift, in North Africa, along the Trans-Antractic mountains, in Patagonia, east Brazil and along the Cameroon line. Many of these basalts show similar isotopic and geochemical characteristics (e.g., HIMU affinities), and are underlain by late Proterozoic crust.

Stein and Goldstein [3] suggested that the sources of the Phanerozoic alkali basalts from the ANS are distinct from the asthenospheric (MORB-type) mantle, both isotopically and chemically, but have been physically linked with the ANS since the late Proterozoic. They identified the sources as the lithospheric mantle located above the asthenospheric mantle and isolated from convective mixing. A similar linkage between lithospheric sources that were formed during the pan-African orogeny and the basalts can be established.

The Size of the Pan-African Plume Mantle: A rough estimate of the area covered by Phanerozoic basaltic fields suggests that the magmatic activity affected areas, which are at least 3–4× the size of the ANS. In turn, the "plume mantle" that was responsible for the growth of the Pan-African juvenile lithosphere occupied only the uppermost 150–200 km of the mantle. This result is compatible with Sr-isotopic constraints, which implies limited mass transfer between the lower and upper mantle during the plume episode.

Similar processes of plume upwelling and transformation of plume material into the continental lithosphere via subduction occurred throughout Earth's history and they appear to be the primary mean of continental growth.

References: [1] Reymer and Schubert (1984; 1986). [2] Stein and Hofmann (1994). [3] Stein and Goldstein (1996).

IN SITU ZIRCON TRACE-ELEMENT ANALYSIS BY HIGH-MASS-RESOLUTION SECONDARY ION MASS SPECTROMETRY.

R. A. Stern, J. C. Roddick Ion Microprobe Laboratory, Geological Survey of Canada, 601 Booth Street, Ottawa ON K1A 0E8, Canada (rstern@nrcan.gc.ca).

Introduction: The determination of U-Pb ages of sectioned zircon grains *in situ* is a technique carried out in a handful of laboratories with large radius ion microprobes. Although obtaining zircon U-Pb ages by secondary ion mass spectrometry (SIMS) is routine, the interpretation of ages from structurally complex zircons is not always clear in relation to crystallization of the protolith, metamorphic overprints, leucosome formation, or hydrothermal activity. Cathodoluminescence or back-scattered electron images are essential for identifying overall structures, and can be valuable in interpreting petrogenesis, but quantitative chemical data other than for Th, U, and Pb that could be used for fingerprinting and modeling the origin of specific zircon components are typically lacking. Our laboratory is developing ion microprobe methods to measure trace (REE, Y, and Ba) and Hf abundances in zircons to allow additional constraints to be placed on the origin of zircons.

Approach: Trace-element analysis of zircon has previously been carried out using both small and large radius ion microprobes [e.g., 1,2], utilizing energy filtering to reduce or eliminate isobaric interferences. Energy filtering is also necessary to reduce the differences in secondary ionization efficiency between the zircons and the synthetic silicate glass standards. The approach taken in this study utilizing the large radius SHRIMP II ion microprobe differs firstly in that high mass resolution rather than energy filtering is employed, permitting the highest possible secondary ion signal strengths, and secondly, that a natural zircon standard is being used for determining the relative secondary ion yields.

Zircon Standard: A 1-g cut gem zircon was obtained from A. Kennedy (Curtin University, Perth) and is believed to originate in Sri Lanka. The sectioned megacryst revealed no detectable variation in cathodoluminescence intensity, suggesting relatively good homogeneity in REE (especially Dy) contents. The sectioned megacryst was subsequently broken into several large pieces, and a subsample reduced to <350 µm. Further CL imaging of the small fragments revealed no variability, confirming the homogeneity of the sample.

Ion Probe Analysis: Sputtering employs a mass-filtered O^- primary ion beam. Positive secondary ions are focussed onto a 90-µm source slit and resolved with a 75-µm-wide collector slit. The mass resolution (1% definition) under these conditions is 7000, and the flat-tops on the peaks are 0.010 amu wide at mass 208. This working mass resolution eliminates all known isobaric interferences for the particular isotope species analyzed: ^{89}Y, ^{137}Ba, ^{139}La, ^{140}Ce, ^{141}Pr, ^{143}Nd, ^{147}Sm, ^{151}Eu, ^{155}Gd, ^{163}Dy, ^{165}Ho, ^{166}Er, ^{175}TbO, ^{175}Lu, ^{185}TmO, ^{189}YbO, $^{196}Zr_2O$, ^{196}HfO, ^{248}ThO, and ^{254}UO.

The ion microprobe trace-element analyses of the fragments of the zircon standard reveal a very high degree of homogeneity. Most of the inter-element ratios have one standard deviations of 2–5%. The exceptions are for ratios involving La and Ba, which are highly depleted and have relatively high analytical errors. The ratios of the isotopes when normalized to $^{196}Zr_2O$ show a similar dispersion. These data indicate that the standard is extremely homogeneous in the abundances of all the elements analyzed. Taking into account the contribution of counting errors to the data scatter, it is probable that the sample is homogeneous in trace elements to ±2%. Such homogeneity in a zircon standard has not been reported previously.

The absolute abundances of the major, minor, and trace elements in the zircon standard are being determined using the electron microprobe, isotope dilution, solution ICP-MS, and laser ablation ICP-MS. Once this information is available, the absolute abundances in unknown zircon samples can be calculated from the measured ratios. It is anticipated that the analytical uncertainties for most elements will be ±5% or better on typical spots 15–20 µm wide and 1 µm deep.

Applications: Application of the technique in the near future is focused upon (1) elucidating the mechanisms of oscillatory zoning in zircon, (2) determining the trace-element characteristics of altered zircon, and (3) determining the trace-element characteristics of 4.0-Ga terrestrial zircons and modeling the composition of the parent magmas.

References: [1] Hinton R. W. and Upton B. G. J. (1991) *GCA, 55,* 3287–3302. [2] Ireland T. R. and Wlotzka F. (1992) *EPSL, 109,* 1–10.

ANALYSIS OF VOLATILE ORGANIC COMPOUNDS OVER OCTOPUS SPRING, YELLOWSTONE NATIONAL PARK, USING OPEN-PATH FOURIER TRANSFORM INFRARED SPECTROSCOPY.

D. L. Stoner, J. G. Jolley, K. S. Miller, D. J. Fife, and W. F. Bauer, Chemical and Biological Sciences Department, Idaho National Engineering and Environmental Laboratory, P.O. Box 1625, Idaho Falls ID 83415-2203, USA (dstoner@inel.gov).

We report the use of open-path fourier transform infrared spectroscopy (OP-FTIR) to monitor volatile and semivolatile organic compounds emanating from the geothermal environment of Octopus Spring, Yellowstone National Park, Wyoming. OP-FTIR is a remote, nondestructive, optical-sensing technique that continuously collects infrared spectral data along a linear path in the open air. The system was deployed in the Octopus Spring area October 7–9, 1997. Infrared spectra were collected for one day over the microbial mats in the effluent channel area and for one day over the source pool. A weather station collected temperature, ambient light intensity, wind speed, wind direction, and barometric pressure data. The OP-FTIR data indicated that there were higher concentrations of some volatile and semivolatile organic compounds such as methyl acetate, acetate and methanol in the atmosphere over the mats than over the open spring. Dimethyl sulfide concentrations were slightly higher over the source pool than over the areas with microbial mats. The higher concentrations of organic acids and alcohols that were observed were indicative of a net flux of volatile organic acids out of the mats. Methane was at ambient concentration over the pool and the microbial mat areas. Interestingly, there were a few occasions in which the concentration of methyl mercaptan over the mats increased dramatically. These increases occurred simultaneously with decreases in methane concentration. There were no discernible trends that were attributable to light-dark periods. The results obtained in this study are rather thought provoking and raise a number of questions that merit further investigation. Nevertheless, this study demonstrated the use of a nondestructive optical-sensing technique for monitoring net flux of volatile organic compounds out of an ecosystem.

MAPPING AND CATALOGING MICROBIAL BIODIVERSITY WITHIN ITS GEOCHEMICAL ENVIRONMENT.

D. L. Stoner, M. C. Miller, L. J. White, J. A. Brizzee, R. L. Lee, and R. C. Rope, Idaho National Engineering and Environmental Laboratory, P.O. Box 1625, Idaho Falls ID 83415, USA (dstoner@inel.gov).

Research in recent years has indicated that there is microbiological diversity that has the potential for remarkable scientific and economic impact. In spite of the recent research activities, microbial diversity remains largely unknown and undiscovered. Furthermore, the information that has been obtained is scattered among a variety of published and unpublished documents. We report the development of a prototype Internet-accessible database and Geographic Information System (http://remus.inel.gov/ynp) that maps microorganisms and microbial activity in the context of their geochemical and geological environment and geographic position. The prototype system was constructed using microbiological and geochemical data and map layers for Yellowstone National Park. When fully implemented, scientists will be able to conduct database searches, construct maps that contain the information of interest, download files, and enter data over the Internet. The intended users of the database include microbiologists and geochemists; federal, state, and local natural resource managers; and science policy advisors planning the strategic direction of research. We are encouraging all potential users of the database to become involved with the development of the fully functional system. Users can get involved by (1) informing us of their scientific and information needs; (2) organizing, notifying us, and entering their data into the system; (3) sharing their expertise; and (4) writing complementary research proposals. Scientific investigators may also help by collecting Geographic Position System (GPS) coordinates and additional field data at their sampling locations. The fully developed system will enhance basic and applied research as well as resource management by promoting a comprehensive understanding of microorganisms within their geochemical environment.

THE ROLE OF GARNET-PYROXENITE IN THE SOURCE OF HAWAI'IAN BASALTS: HAFNIUM-NEODYMIUM-THORIUM-ISOTOPIC EVIDENCE.

A. Stracke[1], V. J. M. Salters[1], K. W. W. Sims[2], and J. Blichert-Toft[3], [1]Geochemistry Division, National High Magnetic Field Laboratory, Tallahassee FL 32306, USA, [2]Department of Geology and Geophysics, Woods Hole Oceanographic Institution, Woods Hole MA 02543, USA, [3]Laboratoire des Sciences de la Terre, Ecole Normale et Supérieure de Lyon, 69364 Lyon Cedex, France.

Introduction: Although a pyroxenitic component has often been suggested as the source of chemically and isotopically enriched isotopic signatures in oceanic basalts [1–4], its role in causing these variations remains controversial. Here, we report new Hf-isotopic and trace-element data for zero-age Hawai'ian basalts. We show that the combined Hf-Nd-Th-isotopic and trace-element data can distinguish between melts derived from peridotitic and pyroxenitic sources and exclude the existence of garnet-pyroxenite in the source of Hawai'ian basalts.

Hafnium-Neodymium-Thorium-isotopic Systematics: Hafnium, Nd, and Th isotopes correlate well with trace-element indexes of source enrichment and melting in the presence of garnet such as Th/U and $(Sm/Yb)_n$ respectively [5]. All samples have $(^{230}Th/^{238}U) > 1$ (parentheses denote activities) with Th excesses up to 30%. $\delta_{(Sm/Nd)}$ and $\delta_{(Lu/Hf)}$ parameters were defined by Salters and Hart [6]. $\delta_{(Lu/Hf)}$ is strongly affected by the amount of residual garnet, and $\delta_{(Sm/Nd)}$ is is an indicator of the degree of melting. $\delta_{(Sm/Nd)}$ and $\delta_{(Lu/Hf)}$ correlate well with Hf, Nd, and Th isotopes. The most enriched melts (low $^{176}Hf/^{177}Hf$) represent the highest degree of melting (low $\delta_{(Sm/Nd)}$)

and have the smallest garnet signature (low $\delta_{(Lu/Hf)}$). Amounts of ($^{230}Th/^{238}U$) are highest in low-degree melts with the largest garnet signature (high $\delta_{(Sm/Nd)}$ and high $\delta_{(Lu/Hf)}$). The most enriched melts (lowest $^{176}Hf/^{177}Hf$) have the smallest ($^{230}Th/^{238}U$).

Discussion: With partition coefficients most appropriate for melting of garnet-pyroxenite [7,8] and garnet-peridotite [9], melts from garnet-peridotite have smaller $\delta_{(Lu/Hf)}$ and significantly larger Th excesses than melts from a garnet-pyroxenite for similar degrees of melting. $\delta_{(Sm/Nd)}$ shows large variations with the degree of melting, but the variation is larger in garnet-peridotite melts than in garnet-pyroxenite melts. In addition, garnet-peridotite melts are expected to have a more depleted isotopic signature than garnet-pyroxenite melts. Based on these characteristics, garnet-pyroxenite melts are clearly distinguishable from garnet-peridotite melts in terms of $\delta_{(Lu/Hf)}$, $\delta_{(Sm/Nd)}$, ($^{230}Th/^{238}U$), $^{176}Hf/^{177}Hf$, and $^{143}Nd/^{144}Nd$. Due to its lower solidus temperature, garnet-pyroxenite begins to melt earlier than garnet-peridotite and is melted to a higher degree than the ambient peridotite at any depth of the melting regime [4]. The role of garnet-pyroxenite-derived melts in Hawai'ian basalts needs to be investigated in terms of mixing low-degree peridotite melts and high-degree pyroxenite melts. The lowest-degree melts should have the highest proportion of garnet-pyroxenite-derived melts in order to be consistent with melting of a garnet-pyroxenite-bearing source. If garnet-pyroxenite were present in the source of Hawai'ian basalts, we would thus expect the following: In low degree melts (high $\delta_{(Sm/Nd)}$), garnet-pyroxenite derived melts are most abundant, leading to high $\delta_{(Lu/Hf)}$, and low $^{176}Hf/^{177}Hf$, $^{143}Nd/^{144}Nd$, and ($^{230}Th/^{238}U$) values. With increasing degree of melting, the abundance of garnet-pyroxenite derived melts in the mixture decreases. Thus, $\delta_{(Sm/Nd)}$ and $\delta_{(Lu/Hf)}$ decrease, and $^{176}Hf/^{177}Hf$, $^{143}Nd/^{144}Nd$, and ($^{230}Th/^{238}U$) increase with increasing degree of melting. This leads to trends opposite to what is observed for the Hawai'ian basalts. In Hawai'ian basalts, low-degree melts (high $\delta_{(Sm/Nd)}$) are isotopically depleted, have large Th excesses and have the *smallest* proportion of garnet-pyroxenite-derived melt. The Th systematics in Hawai'ian basalts have been explained by variations in melting parameters (porosity, melting and upwelling rate) during melting of a garnet-peridotite source [10]. In the context of melting a mixed garnet-periodtite garnet-pyroxenite source, high ($^{230}Th/^{238}U$) melts of the Hawai'ian basalts (which are the smallest-degree melts) can only tolerate negligible amounts of garnet-pyroxenite melt to maintain their large Th excesses and depleted isotopic signatures, even with the most extreme values for melting parameters. We conclude that the trace-element and isotopic composition of the Hawai'ian basalts is inconsistent with melting of a garnet-pyroxenite-bearing source. This is consistent with previous studies on pyroxenites from peridotite massifs, suggesting that pyroxenite is not an appropriate source for oceanic basalts [e.g., 11–13].

References: [1] Zindler A. et al. (1979) *EPSL, 45,* 245–262. [2] Zindler A. et al. (1984) *EPSL, 70,* 175–195. [3] Allègre C. J. and Turcotte D. L. (1986) *Nature, 323,* 123–127. [4] Hirschmann M. M. and Stolper E. M. (1996) *CMP, 124,* 185–208. [5] Sims K. W .W. et al. (1995) *Science, 267,* 508–512. [6] Salters V. J .M. and Hart S. R. (1989) *Nature, 342,* 420–422. [7] Hauri E. et al. (1994) *Chem. Geol., 117,* 149–166. [8] LaTourette et al. (1993) *Science, 261,* 739–742. [9] Salters V. J. M. and Longhi J. (1999) *EPSL, 166,* 15–30. [10] Sims K. W. W. et al. (1999) *GCA,* submitted. [11] Blichert-Toft et al. (1999) *Science, 283,* 1303–1306. [12] Pearson et al. (1991) *EPSL, 102,* 289–301. [13] Reisberg et al. (1991) *EPSL, 105,* 196–213.

THE SULFUR-ISOTOPIC COMPOSITION OF PRECAMBRIAN SEDIMENTS: SEAWATER CHEMISTRY AND BIOLOGICAL EVOLUTION.

H. Strauss, Geologisch-Paläontologisches Institut, Westfälische Wilhelms-Universität Münster, Corrensstrasse 24, 48149 Münster, Germany (hstrauss@uni-muenster.de).

The sedimentary S cycle represents an important part of the exogenic cycle as it is directly linked to the C cycle and the evolution of O in the atmosphere-hydrosphere system. Reconstructing temporal variations through Earth's early history traditionally includes the use of stable isotopic ratio measurements of sulfate and sulfide. Results from modern marine settings as well as laboratory experiments are considered as reference for interpretation [1]. Prime questions address the temporal variation in the isotopic composition of seawater sulfate and the antiquity and operational mode of bacterial sulfate reduction, which represents the key process of anaerobic mineralization of organic matter in modern and Phanerozoic sedimentary systems.

More than 400 unpublished S-isotopic data, largely for sedimentary pyrite but also for marine evaporites, in addition to a substantial number of published data, are used to constrain the temporal variation of the sedimentary S cycle through the Precambrian. Thereby, different patterns exist for the Archean, the Archean-Proterozoic transition, the Proterozoic, and the Neoproterozoic and its transition into the Phanerozoic, suggesting a distinct temporal trend that is ultimately linked to the geological and biological evolution of the Earth and its lithosphere, hydrosphere, atmosphere, and biosphere.

The S-isotopic composition of Archean sedimentary pyrite displays a rather narrow range around 0‰, which resembles mantle S composition. In the absence of any substantial isotope fractionation, this record can be most readily interpreted as indicative of a hydrothermal source for sulfide S. However, an alternative biogenic origin has been proposed under specific environmental conditions [2].

Substantially larger variations, yet around an average value close to 0‰, characterize late Archean sediments, whereas early Palaeoproterozoic units display substantial variations including fairly strongly negative $\delta^{34}S$ values. This record is interpreted as being diagnostic of modern-style bacterial sulfate reduction, including a significant displacement of the isotopic composition in the resulting hydrogen sulfide.

Proterozoic sediments display a pattern in $\delta^{34}S$ that is indicative of bacterial sulfate reduction.

Quite variable S-isotopic values for pyrite have been recorded for Neoproterozoic sediments, with individual stratigraphic units displaying variations of more than 70‰.This pattern is interpreted to reflect sulfate limitation in the pore waters and a resulting unidirectional evolution of the S-isotopic budget as a consequence of rapid turnover of organic matter. Additional biologically mediated pathways have been suggested [3].

Due to the extremely fragmentary nature of the Precambrian evaporite record, our knowledge of the S-isotopic composition of seawater is largely confined to the Neoproterozoic with a few spotty data for earlier times [4]. The terminal Neoproterozoic, however, records a most substantial variation from values ~18‰ prior to the Varanger glaciation to average values near 30‰ after the terminal Neoproterozoic glacials and into the Cambrian [5].

Studying the S-isotopic composition of sedimentary S enables the reconstruction of geologically and biologically driven processes and their temporal variation throughout Earth history. Isotopic patterns observed in modern settings including laboratory culture experiments serve as a guideline for interpretation. Sometimes, this may limit the interpretation.

References: [1] Strauss H. (1997) *Palaeogeogr., Palaeoclimatol., Palaeoecol., 132,* 97–118. [2] Ohmoto H. et al. (1993) *Science, 262,* 555–557. [3] Canfield D. E. and Teske A. (1996) *Nature, 382,* 127–132. [4] Strauss H. (1993) *Precambrian Res., 63,* 225–246. [5] Shields G. et al. (1999) *J. Geol. Soc. London,* in press; Strauss H. et al. (1999) *Chem. Geol.,* in review.

RARE-EARTH-ELEMENT GEOCHEMISTRY OF FERROMANGANESE CONCRETIONS FROM THE BARENTS SEA AND THE WHITE SEA.

S. V. Strekopytov, E. L. Vinogradova, and A. V. Dubinin, Shirshov Institute of Oceanology, Russian Academy of Sciences, Nakhimovsky Prospekt, 36 Moscow 117851, Russia (geochem@geo.sio.rssi.ru).

Several types of Fe-Mn encrustations are known in the Arctic seas: ferromanganese concretions, ferruginous concretions, and crusts. Five samples of ferruginous flat concretions, one sample of crust from the Barents Sea and discoidal ferromanganese concretion from the White Sea (the Gorlo district) as well as two horizons (surface and subsurface) of associated sediments, were studied. Contents of 14 rare earth elements (REE) were determined by inductively coupled plasma mass spectrometry (ICP-MS) with VG Plasma Quad PQII STE [1]. In addition to bulk samples, labile fraction of concretions and sediments (1M $NH_2OH \times HCl$ + 25% CH_3COOH leachates) was analyzed.

The presence of both Fe^{2+} and Fe^{3+} and low content of Mn (<0.07%) in the surface sediments of the Barents Sea was observed, which reflects the suboxic conditions. The surface horizon of the White Sea sediments is fully oxidized. This difference in redox conditions results in the formation of different types of encrustations. Concretions from the central part of the Barents Sea are formed due to the upward Fe flux from the reducing zone

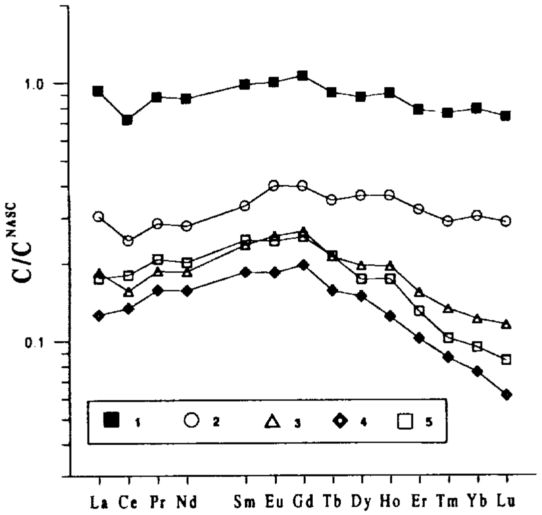

Fig. 1. Shale-normalized REE patterns of ferromanganese concretion from the White Sea (1), samples from the central part of the Barents Sea: ferruginous crust (2), reactive parts of concretion (3) and associated sediments [hor. 0–1 cm (4), and hor. 1–3 cm (5)].

of sediments and contain trace amounts of Mn (<0.15%), whereas discoidal concretions from the White Sea are enriched in this element (up to 8.8%).

Negative correlation found between Fe and Al contents in concretions is a result of the high portion of lithogenic material in their composition. Strong positive correlation between Fe and P contents (average molar P/Fe ratio is 0.15) is observed, which indicates the high role of phosphate-bound Fe and possible presence of iron hydroxophosphates.

Shale-normalized REE patterns of the Barents Sea sediments are characterized by a slight decrease in heavy REEs that is probably inherited from the source provenance rock composition. REE contents and patterns of the bulk samples of the Barents Sea concretions and sediments are similar, reflecting the origin of ferruginous concretions as the result of sediment grain cementation by iron oxyhydroxides. The REE pattern of the White Sea concretion (Fig. 1) is characterized by a distinct negative Ce anomaly and high contents of REE in comparison with the associated sands, which are poor in Fe and Mn.

The reactive part of sediments is characterized by a relative enrichment of middle REEs in the normalized pattern (Fig. 1). Possible carriers of REE in such sediments are iron oxyhydroxides and clay minerals.

The subsurface layer of sediments is usually enriched in REE relative to the surface-oxidized layer, so iron oxyhydroxides cannot dominate among REE carriers. A weak negative cerium anomaly is observed in the REE patterns of the reactive part of ferruginous concretions. Ferruginous crust from the Barents Sea has a REE pattern with a distinct negative Ce anomaly that is close to the pattern of the White Sea concretion.

A negative Ce anomaly is a characteristic feature of deep seawater. Though the data for the Barents Sea water are very limited [2], we assume that its REE pattern is close enough to the patterns of Atlantic and Arctic deep waters [3,4]. Near-bottom seawater can be an important source of labile REE of ferruginous and ferromanganese concretions.

References: [1] Dubinin A. V. (1993) *Geochem. Intl., 31,* 81–95. [2] Høgdahl O. T. (1967) *NATO Res. Grant 203, Semiann. Progr. Rpt. No. 5.* [3] Elderfield H. and Greaves M. J. (1982) *Nature, 296,* 214–219. [4] Westerlund S. and Öhman P. (1992) *Deep-Sea Res., 39,* 1613–1626.

STABLE ISOTOPIC INVESTIGATIONS OF THE CHLORINATED ALIPHATIC HYDROCARBONS.

N. C. Sturchio[1], L. J. Heraty[1], B. D. Holt[1], L. Huang[1,2], and T. Abrajano[1,3], [1]Argonne National Laboratory, ER-203, 9700 S. Cass Avenue, Argonne IL 60439-4843, USA, [2]present address: Environment Canada, Downsview, Ontario M3H 5T4, Canada, [3]present address: Rensselaer Polytechnic Institute, Troy NY 12180-3590, USA.

Introduction: Contamination of the terrestrial environment by anthropogenic chlorinated aliphatic hydrocarbons (CAHs, including chloroethenes, chloroethanes, and chloromethanes) is nearly ubiquitous. The application of stable isotopic ratio measurements (of H, C, and Cl) to understand the environmental behavior and fate of these compounds is a relatively new approach. We have developed new methods for the sampling and isotopic analysis of CAHs in air and water [1], and have applied these to measurements of isotopic fractionation of C and Cl during vapor-liquid partitioning [2] and microbial degradation in liquid cultures [3]. We have also performed several field studies of C and Cl isotopes in contaminated aquifers in which either natural or engineered degradation of CAHs has occurred [4].

Results and Discussion: *Vaporization studies.* A series of evaporation experiments was completed in which pure-phase CAH liquids were allowed to evaporate at room temperature, in a fume hood, as the mass and isotopic ratios of the residual liquid were periodically monitored [2]. These and additional new results are shown in Fig. 1.

Measured vapor-liquid fractionation factors, α, for $^{13}C/^{12}C$ and $^{37}Cl/^{35}Cl$ range from 1.00031 to 1.00160 and from 0.99819 to 0.99916, respectively. The inverse isotope fractionation effect for $^{13}C/^{12}C$ is observed in all cases, and there is an apparent systematic change in α values as the number of Cl atoms decreases in the chloromethane series, tetrachloromethane (CT) → trichloro-methane (TCM) → dichloromethane (DCM), and in the chloroethene series, tetrachloroethene (PCE) → trichloroethene (TCE). From these limited data generated to date, there also appears to be a general decrease of α values from chloromethanes → chloroethanes → chloroethenes. These systematic variations in α could be useful in interpreting volatilization effects for CAHs in the environment and distinguishing them from microbial degradation effects. The α values shown in Fig. 1 are near equilibrium but involve a significant kinetic isotope effect. Further measurements are in progress to establish equilibrium α values for vapor-liquid partitioning for pure-phase CAHs and for CAHs dissolved in water.

Microbial degradation studies. A series of microbial degradation experiments in liquid culture was completed. We investigated the kinetic isotope effects associated with aerobic degradation of DCM by MC8b, a gram-negative methylotrophic organism closely related to the genera *Methylobacterium* or *Ochrobactrum* [3]. The measured kinetic α values are 0.9576 ± 0.0015 for $^{13}C/^{12}C$ and 0.9962 ± 0.0003 for $^{37}Cl/^{35}Cl$. This isotope effect for C is extreme, twice that resulting from microbial oxidation of CH_4.

The large differences in characteristic α values for different processes (e.g., vaporization and microbial degradation have slopes with opposite signs on a $\delta^{13}C$ vs. $\delta^{37}Cl$ diagram) can be exploited for identifying and quantifying abiotic and biotic processes that affect the concentrations and isotopic characteristics of CAHs in soils, vadose zones, surface waters, and groundwaters.

Field studies. A number of field investigations of stable isotopic ratios of CAHs have been completed, and others are in progress. Our initial field study was of TCE contamination at the Paducah Gaseous Diffusion Plant in

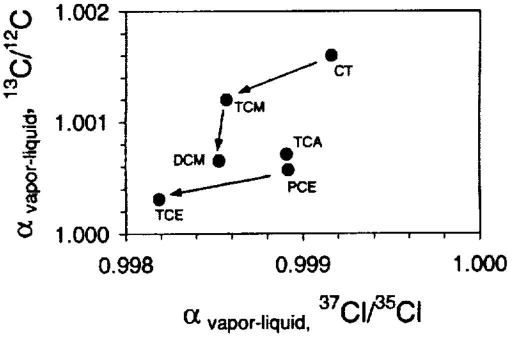

Fig. 1. Measured α values from CAH vaporization experiments conducted at 23° ± 1°C.

western Kentucky [4]. Stable isotopic data for Cl in TCE and dissolved inorganic chloride indicate that natural attenuation of TCE has occurred in the clays and silts overlying the regional aerobic gravel aquifer at the site, but no further attenuation is evident within the gravel aquifer [5].

Acknowledgments: This work was supported by the Environmental Management Science Program of the U. S. Department of Energy under contract W-31-109-Eng-38 to Argonne National Laboratory.

References: [1] Holt B. D. et al. (1997) *Anal. Chem., 69,* 2727–2733. [2] Huang L. et al. (1999) *Org. Geochem., 25,* in press. [3] Heraty L. J. et al. (1999) *Org. Geochem., 25,* in press. [4] Sturchio N. C. et al. (1998) *Environ. Sci. Tech., 32,* 3037–3042. [5] Sturchio N. C. et al. (1997).

MARINE SEDIMENTS: A BLACK CARBON RESERVOIR AND RECORD OF COMBUSTION.

D. Suman, Rosenstiel School of Marine and Atmospheric Science/MAF, University of Miami, 4600 Rickenbacker Causeway, Miami FL 33149-1098, USA (dsuman@rsmas.miami.edu)

Introduction: Black carbon (BC) deposited in ocean sediments provides regional and global information regarding vegetation and fossil-fuel-burning and transport mechanisms. BC's inert character permits its use as a tracer of past fire activity. Moreover, this stability suggests that BC may represent an important sink in the global C cycle.

Fluxes to Ocean Sediments: Black carbon fluxes to marine sediments may be functions of the magnitude of vegetation burning and fossil-fuel combustion, the distance from the burning source, and riverine and eolian transport mechanisms. Determinations of BC fluxes to surface sediments, largely from the Pacific Ocean, range between 0.002 and 3.6 µg BC cm^{-2} yr^{-1} for deep-sea sediments and 26 and 354 µg BC cm^{-2} yr^{-1} for sediments from the continental margins [1].

Global Black Carbon Cycle: The global BC cycle begins with the burning sources and involves a number of boxes in soils; lake, river, and ocean sediments; glaciers and ice sheets; and the atmosphere. Fluvial and eolian-transport mechanisms are both important in mobilizing BC between boxes. Global BC formation by vegetation fires may range between 50 and 270 Tg BC yr^{-1} with perhaps >80% of the BC remaining as soil residues [2]. Perhaps 6–28 Tg BC yr^{-1} is emitted into the atmosphere from vegetation burning. Emissions from all combustion sources may average 25 Tg BC yr^{-1}. About one third of the BC emitted to the atmosphere from continental sources is transported and deposited on the ocean surface. Global BC deposition to marine sediments in the deep ocean and continental margins is calculated using BC sediment flux data. About 10 Tg BC yr^{-1} is deposited in ocean sediments, largely in the coastal ocean. This may represent between 4 and 20% of the total BC produced by vegetation burning. BC deposition to the ocean surface is estimated from atmospheric BC concentration fields and is much more homogeneous across the global ocean than the BC fluxes to marine sediments. BC deposition to the ocean surface accounts for 7 Tg BC yr^{-1}. Rivers may transport 12 Tg BC yr^{-1} to the ocean, and this particulate matter is largely deposited in the coastal ocean sediments.

Temporal Records of Combustion: Several analyses of BC in near-shore sediment cores provide records of burning activities during the past 100–500 yr. BC fluxes to the Santa Barbara Basin (California) range from 9 to 38 µg BC cm^{-2} yr^{-1}, while BC fluxes to Saanich Inlet sediments (British Columbia) range from 43 to 122 µg BC cm^{-2} yr^{-1} [3]. BC fluxes to both sites may have remained constant or increased slightly during the past century. BC fluxes to Gulf of Panama sediments range from 94 to 165 µg BC cm^{-2} yr^{-1} with no obvious trends in the past two centuries [4]. BC fluxes to sediments of the Nicaraguan continental margin vary from 44 to 135 µg BC cm^{-2} yr^{-1} with a decrease toward the present, suggesting a decrease in burning activities on the adjacent land [5].

Black carbon records in deep sea sediment cores extend to the early Cenozoic (65 Ma) [6]. BC fluxes were generally low (0.001–0.01 µg BC cm^{-2} yr^{-1}) in the Palaeogene period (26–65 Ma) and increased significantly with the beginning of the Neogene. By the end of the late Neogene, BC fluxes were two or three orders of magnitude greater than those of the Palaeogene (0.1–10 µg BC cm^{-2} yr^{-1}). Low fluxes in the early Tertiary may be attributed to abundant tropical vegetation resulting from the warm, humid climate and low zonal wind strengths. With climate deterioration in the Cenozoic and the emergence of drier temperate forests and grasslands, more vegetation fuel may have been available for combustion.

References: [1] Suman D. O. et al. (1997) in *Sediment Records of Biomass Burning and Global Change* (J. S. Clark et al., eds.), pp. 271–293. [2] Kuhlbusch T. A. J. and Crutzen P. J. (1995) *Global Biogeochem. Cycles, 9,* 491–501. [3] Griffin J. J. and Goldberg E. D. (1975) *Limnol. Oceanogr., 20,* 456–463. [4] Suman D. O. (1986) *Environ. Conserv., 13,* 51–60. [5] Suman D. O. (1991) in *Global Biomass Burning* (J. S. Levine, ed.), pp. 512–518. [6] Herring J. R. (1985) in *The Carbon Cycle and Atmospheric CO_2* (E. T. Sundquist and W. S. Broecker, eds.), pp. 419–442.

2-METHYLHOPANOIDS: BIOMARKERS FOR CYANOBACTERIA AND FOR OXYGENIC PHOTOSYNTHESIS.

R. E. Summons[1], L. L. Jahnke[2], J. M. Hope[1], and G. A. Logan[1], [1]Australian Geological Survey Organisation, P.O. Box 378 Canberra, ACT 2601, Australia, [2]Exobiology Branch, NASA Ames Research Center, Moffett Field CA 94035, USA.

Summary: This paper reports new biomarker and C-isotopic data for cultured cyanobacteria, cyanobacterially dominated ecosystems, and ancient sediments and petroleum. We found that cyanobacteria are the predominant source of a distinctive membrane lipid biomarker, namely 2-methylbacteriohopanepolyol (2-Me-BHP). We then sought evidence for a geochemical record of the fossil hydrocarbon analogs of these compounds (2-methylhopanes) and found a trend toward their increased relative abundance in marine sediments going back through geological time to 2500 Ma. We conclude that cyanobacteria were the dominant form of phytoplankton and source of molecular O in the Proterozoic ocean. Extending the geological record of cyanobacteria further to the Archean is now a matter of finding a suitably preserved rock record.

Results and Discussion: Samples of cultured cyanobacteria and naturally occurring cyanobacterial mats were analyzed using an established protocol [1] illustrated in Fig. 1. Approximately 43% of the cultured samples contain 2-Me analogs (6 and 8). Four of five mats from the Yellowstone National Park hydrothermal environment had significant contents of 2-Me-BHP, although none of the five samples from hypersaline environments of Shark Bay did. While our present sample set represents a limited number of modern environments, the cultured organisms were a taxonomically diverse suite.

When hopanoids from bacteria enter the sediments, they undergo diagenetic and catagenetic conversion to the C_{27}-C_{35} geohopane series (3 in Fig. 1). The burial fate of 2-Me-BHP is virtually identical to BHP except that the 2β-methyl configuration of the original biochemicals (2 in Fig. 1) is progressively converted to more thermodynamically stable 2α-Me configuration (4 in Fig. 1)

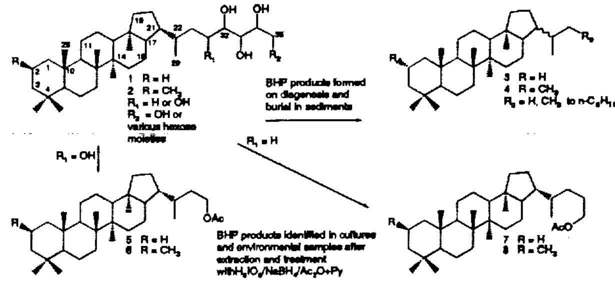
OH
OH
R
1
2
3
4
10
11
14
16
17
19
21
22
25
29
32
35
R₁
OH
R₂
1 R = H
2 R = CH₃
R₁ = H or OH
R₂ = OH or various hexose moieties
BHP products formed on diagenesis and burial in sediments
R₄
3 R = H
4 R = CH₃
R₃ = H, CH₃ to n-C₅H₁₁
R₃
R₁ = OH
R₁ = H
R
OAc
5 R = H
6 R = CH₃
BHP products identified in cultures and environmental samples after extraction and treatment withH₅IO₆/NaBH₄/Ac₂O+Py
R
AcO
7 R = H
8 R = CH₃

Fig. 1. Structures of bacteriohopanepolyols (1,2) typical of those found in cyanobacteria and their geohopane analogs recognized in sediments and petroleum (3,4). The studies of biological samples were conducted using a procedure first developed by Rohmer et al. [1]. Periodic acid oxidation cleaves the hydrophilic portion of the molecule at the first gem-diol to yield tractable and volatile hopanol acetates of the type 5–8 and that are amenable to routine gas chromatography (GC) and gas chromatography mass spectrometry (GC-MS) analysis. BHP lacking a gem-diol function evades detection.

in the 2-Me geohopane series. Our study of the relative abundances of 2-methylhopanes in sediments, bitumen, and oil reveals patterns connected to source-rock lithology, maturity, and paleoenvironmental setting. Higher relative abundances of 2-methylhopanes, expressed as a 2-methylhopane index, are a distinctive feature of oils and bitumens derived from carbonate rocks. Moreover, there are higher relative abundances of 2-methylhopanes in Proterozoic sediments of all lithologies compared to their Phanerozoic counterparts.

Environmental Studies: Analyses of various microbial mats from Yellowstone National Park reveal relatively simple patterns of lipid biomarkers that are appropriate for isotopic analyses at the molecular level. These data can be used to understand which compounds are produced by cyanobacteria, by *Chloroflexus*, and by other groups. They also allow some delineation of how environmental parameters such as pCO_2 and growth temperature influence the biosynthesis of certain types of lipid. The history of O and the history of cyanbacteria are intimately linked. This is the only group of prokaryotes capable of oxygenic photosynthesis, i.e., using the energy of sunlight to release the reducing power of water for fixation of CO_2 and O_2 production. Although debate still exists as to the timing and sequence of evolutionary events that led to oxygenic photosynthesis, and consequent oxygenation of the atmosphere and oceans, it is clear that the appearance of the cyano-bacteria is a crucial event that could be followed using their distinctive hydrocarbon biomarkers [2].

References: [1] Rohmer M. et al. (1984) *J. Gen. Microbiol., 130,* 1137–1150. [2] Summons R. E. et al. (1999) *Nature,* in press.

MOLECULAR MODELING OF CESIUM-SMECTITE HYDRATES.

R. A. Sutton and G. Sposito, Earth Sciences Division, Lawrence Berkeley National Laboratory, Berkeley CA 94720-3110, USA.

Recent evidence of groundwater contamination linked to colloidal transport of $^{137}Cs^+$ from a nuclear test site fuels a search for understanding the basic molecular mechanisms governing Cs^+ adsorption to clay mineral surfaces. Monte Carlo (MC) and molecular dynamics (MD) modeling techniques were applied to Cs-smectite systems (Cs-hectorite, -montmorillonite, and -beidellite) in order to interpret a variety of experimental data, as well as to evaluate the quality of the interaction potentials used in the simulations. Spectroscopic methods and surface chemistry techniques that attempt to differentiate interlayer water from water residing in micropores have provided data suggesting that, in stable 12-Å Cs-smectite hydrates, the interlamellar water content is less than a monolayer. Convergence profiles in MC (NσT) simulations were examined to estimate reasonable interlayer water contents of 1/3 and 2/3 water monolayer for these hydrates, with 1/3 monolayer as the most likely stable water content. Molecular dynamics (NVT) simulations (800 ps) of the MC-stable Cs-smectite systems revealed interlayer Cs^+ to be strongly bound to surface charge sites while exhibiting jump diffusion, especially in the 2/3 monolayer systems. The strongly adsorbed Cs^+ can be associated with a species identified in ^{133}Cs NMR studies of hydrated smectites. Published bulk diffusion coefficients are also consistent with strong adsorption of Cs^+. Our simulations thus demonstrate Cs-smectite system stability with interlamellar water contents of less than a monolayer, as suggested by experiments, and can be used to interpret NMR and other spectroscopic data concerning Cs^+ species adsorbed to 2:1 clay mineral surfaces.

THE INFLUENCE OF SULFIDES ON SOLUBLE IRON(III) IN ANOXIC SEDIMENT POREWATERS.

M. Taillefert[1], S. M. Theberge[1], V. Hover[2], and G. W. Luther III[1], [1]College of Marine Studies, University of Delaware, Newark DE 19958, USA, [2]Department of Geological Sciences, Rutgers University, Piscataway NJ 08901, USA.

Solid or colloidal Fe oxides are commonly involved in the mineralization of natural organic matter in sediments. However, more readily available soluble Fe(III) could accelerate the mineralization rate of natural organic matter. Experiments with synthetic solutions showed that soluble Fe(III) (i.e., <50 nm diameter) reacts at a Hg voltammetric electrode at circumneutral pH if it is complexed by an organic ligand. Aggregation proceeds upon aging of Fe(III), and its molecular weight increases. Simultaneously, the reduction potential of this species shifts negatively. The reactivity of soluble Fe(III) with sulfides is dramatically increased compared to its solid equivalent (e.g., amorphous hydrous Fe oxides or goethite). Here we report data from a natural system that confirm the existence of soluble Fe(III) in sediments and its interaction with sulfides.

Sediment porewaters from two different creeks of the Hackensack Meadowlands District (New Jersey) were analyzed at the millimeter scale with solid-state Hg/Au [O_2, ΣH_2S, Fe(II), and Fe(III)] and pH microelectrodes. The chemical profiles in these two anoxic sediments show the interaction between the Fe and S systems during early diagenesis. Soluble Fe(III) and Fe(II) are dominant in a creek where sulfide is negligible. This dominance suggests that the reductive dissolution of Fe(III) goes through the dissolution of solid Fe(III) and then reduction to Fe(II). In contrast, in a creek sediment where sulfide occurs in significant concentration, the reductive dissolution of Fe(III) is followed by formation of colloidal FeS, which further precipitates. In both cases, soluble Fe(III), probably complexed by an organic ligand, may play a significant role in the mineralization of natural organic matter. Soluble Fe(III) reactivity is probably enhanced in the sediment, accelerating mineralization processes, and its mobility may result in the shifting of local reactions at depths where other electron acceptors are used.

OXYGEN-ISOTOPIC AND RARE-EARTH-ELEMENT COMPOSITIONS OF QUARTZ VEINS WITHIN XINGZI GROUP OF LUSHAN, SOUTHEAST CHINA: IMPLICATIONS FOR THE ORIGIN OF METAMORPHIC FLUIDS.

H. F. Tang and C. Q. Liu, Institute of Geochemistry, Chinese Academy of Sciences, Guiyang, 550002, China (hftang@ms.gyig.ac.cn).

Abundant quartz veins occurring in many metamorphic rocks, especially metasedimentary ones, provide ideal samples for studying the origin of metamorphic fluids, because most such veins are the direct products of the fluids. Previous studies on metamorphic quartz veins have focused mainly on their mineral, major-element, and O-isotopic composition [1–4], and two different hypotheses have been advanced to account for their genesis [4]. Therefore, vein-forming metamorphic fluids may also have two different origins. However, the origin of metamorphic fluids remains controversial. In this paper, we inquire into the origin of metamorphic fluids forming the quartz veins within the Xingzi group of Lushan, southeast China, by using O-isotopic and rare-earth-element (REE) methods.

Xingzi Group of Lushan, which crops out within the central part of late Proterozoic orogen along the southeastern margin of Yangtze block, consists chiefly of metamorphosed pelitic and sandy rocks. Its metamorphic grade is amphibolite facies, and peak temperatures and pressures range from approximately 420° to 570°C and 5.3 to 5.7 GPa respectively [5]. Within this group, there are many quartz veins with different width (0.1 m to <1 m) and length (1 m to several meters). The metamorphic quartz veins distribute along the schistosity of their host rocks, and their mineral assemblages are quartz (>98%) and a few other minerals.

Oxygen-isotopic compositions of quartz separates from both veins and matrix of host rocks are determined using the conventional BrF_5 method and analyzed in a MAT-252 mass spectrometer. All values of $\delta^{18}O$ are reported as per mil (‰) relative to SMOW and accurate to ±0.2‰. $\delta^{18}O$ values range from 12.3‰ to 13.5‰ for vein quartzes and 11.0‰ to 12.9‰ for quartz separates from the matrix of host rocks, and the average $\delta^{18}O$ value of vein quartzes is 12.8 ± 0.5‰ (n = 10). These show that quartz veins are isotopically similar to their host metamorphic rocks, and suggest that the vein quartzes are redistributed from the wall rocks on a relatively local scale [3].

REE compositions of quartz veins and their host rocks are determined by solution inductively coupled plasma mass spectrometry (ICP-MS). The results show that quartz veins and their host rocks have much similar REE patterns with enrichment of LREE relative to HREE and an obviously negative Eu anomaly. Additionally, the average REE composition and pattern of the host rocks (n = 15) are almost the same as those of PAAS. Average vein REE composition (n = 10) is much lower than that of the host rocks, and average vein La_N and Yb_N are 3.50 and 0.62, respectively. Because no REEs can substitute for Si of quartz, REEs of quartz veins are surely included in fluid inclusions and/or other minor minerals trapped in quartzes when they precipitated from the metamorphic fluids. Consequently, the REE composition of quartz veins reflects that of metamorphic fluids. The similar REE patterns between the fluids and host rocks suggest that the metamorphic fluid within the Xingzi Group was directly derived from its wall rocks.

Combining the results described above, we can certainly consider that the metamorphic fluid studied was formed by devolatilization during the regional metamorphism of the Xingzi group. Oxygen-isotopic and REEs of metamorphic quartz veins were transported from their host rocks by the fluid. In addition, the metamorphic fluid must have been moved over distances on the order of meters or longer because no Si-depleted selvage can be recognized in the immediate wall rocks of individual quartz veins. However, it is now not sure whether the transport mechanism of the fluid was by diffusion or advection. In this study, REE mobility to some extent during regional metamorphism also is shown.

Acknowledgments: This work was supported by the National Science Foundation of China for Outstanding Young Scientists (Grant No. 49625304).

References: [1] Yardley B. W. D. (1975) *Geol. Mag., 112,* 183–190. [2] Ague J. J. (1994) *Am. J. Sci., 294,* 1061–1134. [3] Yardley B. W. D. and Bottrell S. H. (1992) *J. Metamorphic Geol., 10,* 453–464. [4] Van Haren J. L. M. et al. (1996) *GCA, 60,* 3487–3504. [5] Ye Y. et al. (1996) *J. Zhejiang Univ. (Natural Sci.), 30,* 600–609 (in Chinese).

MAKING CONTINENTAL CRUST BY CRUSTAL DELAMINATION IN SUBDUCTION ZONES, AND COMPLEMENTARY ACCUMULATION OF THE EMI COMPONENT IN THE DEEP MANTLE.

Y. Tatsumi, Institute for Geothermal Sciences, Kyoto University, Beepu 874-0903, Japan (tatsumi@bep.vgs.kyoto-u.ac.jp).

The continental crust possesses an andesitic composition [1,2], although basaltic magmas dominate the magmatisn on modern Earth. This may be the greatest dilemma facing those interested in the origin of the continental crust. It has been proposed that magmas with such andesitic compositions can form in subduction zones by processes including (1) differentiation of high-Mg andesite magmas that can be generated by melting of hydrous mantle [3]; (2) partial melting of the subducting oceanic crust [4,5]; (3) reaction of mantle/slab-derived melts with mantle peridotites [6]; and (4) basaltic underplating, remelting of such basaltic crusts, and subsequent delamination of mafic lower-crustal materials [7]. The first two mechanisms may not have been of considerable importance, because (1) such HMA-derived andesites or their plutonic equivalents may be volumetrically small in Archean cratons, and (2) a slab-derived silicic melt may not reach the surface without modification of its composition by reaction with mantle peridotites. Thus the last two explanations remain as plausible processes [6,8] and demand further examination.

An interesting assessment for the origin of continental crust may be to aim a comprehensive understanding of formation of continental crust and evolution of the mantle, because the continental crust is believed to be derived in principal by partial melting of the upper mantle, forming a complementary geochemical reservoir to the Earth's mantle [9]. It has been well established [10] that at least four geochemical reservoirs, in addition to the primitive mantle, may be required for explaining isotopic variations observed for ocean island and mid-oceanic ridge basalts, i.e., EMI, EMII, HIMU, and DMM. Among these, the origin of enriched components may be essential in understanding dynamics and evolution of the deep mantle, because such components typify magmas rising from deep-seated hotspots. It has been repeatedly emphasized that accumulation of sinking [11,12] and oceanic crusts [12–14], both experiencing compositional modification during subduction processes, may contribute to forming EMII and HIMU reservoirs respectively. These suggestions have been experimentally confirmed [15–17]. In contrast, the origin of EMI is still controversial. Some workers favor involvement of pelagic sediments [12,18], whereas others emphasize the recycling of the continental lower crust or the metasomatized subcontinental upper mantle [10,19].

Geochemical modeling suggests that partial melting of the subducting oceanic crust and subsequent melt-mantle reactions cannot yield andesitic magmas with trace-element compositions identical to the andesitic continental crust. The most striking difference between such andesite compositions is the lack of Pb spike in slab-derived melts. Instead, anatexis of the initial basaltic crust, which was created by underplating of basaltic magmas produced by overprinting of hydrous subduction component via slab dehydration, can reasonably account for the bulk continental crust composition, either leaving pyroxenitic or eclogitic restite. Separation of such mafic restites from the initial crust via delamination process must have taken place for building the present continental crust. Examination of isotopic evolution of delaminated components demonstrates that the pyroxenite component, which formed at 3.0–3.5 Ga and probably was stripped off shortly after its formation, possesses Sr-Nd-Pb isotopic compositions identical to the EMI component, one of the enriched geochemical reservoirs located in the deep mantle. Formation of the continental crust and complementary accumulation of the EMI reservoir in the deep mantle took place simultaneously in the Archean subduction factory.

References: [1] Rubnick R. L. and Fountain D. M. (1995) *Rev. Geophys., 33,* 267–309. [2] Taylor S. R. and McLennan S. M. (1995) *Rev. Geophys., 33,* 241–265. [3] Shirey S. B. and Hanson G. N. (1984) *Nature, 310,* 222–224. [4] Martin H. (1986) *Geology, 14,* 753–756. [5] Drummond M. S. and Defant M. J. (1990) *JGR, 95,* 21503–21521. [6] Kelemen P. B. (1995) *Contrib. Mineral. Petrol., 120,* 1–19. [7] Turcotte D. L. (1989) *AGU Geophys. Monogr. Ser., 51,* 321–329. [8] Rudnick R. L. (1995) *Nature, 378,* 571–578. [9] Hofmann A. W. (1988) *Plan. Sci. Lett., 90,* 297–314. [10] Zindler A. and Hart S. (1986) *Annu. Rev. Earth Plan. Sci., 14,* 493–571. [11] Devey C. W. et al. (1990) *JGR, 95,* 5049–5066. [12] Weaver B. L. (1991) *EPSL, 104,* 381–397. [13] Chauvel C. et al. (1992) *EPSL, 110,* 99–119. [14] Hauri E. H. and Hart S. R. (1993) *EPSL, 114,* 353–371. [15] Brenan J. M. et al. (1995) *Nature, 378,* 54–56. [16] Kogiso T. et al. (1997) *EPSL, 148,* 193–206. [17] Aizawa Y. et al. (1999) *The Island Arc, 8,* 38–46. [18] Woodhead J. D. et al. (1993) *Nature, 362,* 809–813. [19] Tatsumoto M. and Nakamura Y. (1991) *GCA, 55,* 3697–3708.

FORMATION OF SOIL FROM WEATHERED GRANITE: INSIGHTS INTO INORGANIC AND BIOGEOCHEMICAL PROCESSES FROM MINERALOGICAL, MICROBIOLOGICAL, AND BULK CHEMICAL ANALYSES.

A. E. Taunton, S. A. Welch, and J. F. Banfield, Department of Geology and Geophysics, University of Wisconsin-Madison, 1215 W. Dayton Street, Madison WI 53706, USA (razrback@geology.wisc.edu).

Introduction: Geochemical data from the newly exposed lower portion of a granite weathering profile provided mineralogical and geochemical information about the early stages of weathering of granite under predominantly inorganic conditions [1,2]. In this study, we analyzed weathering reactions occurring in the upper profile (close to the soil zone) and within the soil zone in order to understand the inorganic and biochemical weathering processes leading to soil formation.

Methods: Samples collected in 1983 were obtained from the lowest portion of a granite weathering profile (~6 m below the soil zone) exposed by a newly created road cut in the Bemboka granodiorite, southeastern New South Wales, Australia. In contrast, samples collected in 1998 and 1999 came from within 2 m of the soil zone or were collected from the soil zone (the soil zone is distinguished by loss of granite texture and higher abundance of organic debris). Samples were characterized by field-emission scanning electron microscopy (FESEM), energy-dispersive X-ray spectrometry (EDS), electron microprobe (EMP) analysis, epifluorescence optical microscopy, and X-ray fluorescence analysis (XRF).

Results: The abundance of Fe_2O_3 proved to be an effective measure of the degree of weathering, as gauged by sample appearance and concentrations of readily solubilized elements. Consequently, we have analyzed bulk chemical data by plotting elemental abundances against the abundance of Fe_2O_3 (the isovolumetric approximation used for analysis of the lower profile is inappropriate for very highly weathered rock and soils). In the lower profile, the relative Si loss rate is slightly slower than the average rate of loss of mass. In contrast, samples weathered to an equivalent degree in the upper profile show a relative Si loss rate that is much faster than average. Mn, which is immobile in the lower region (demonstrated by isovolumetric analysis), is strongly leached from the upper profile and soil zone. The rates of K and Mg loss are slightly enhanced in the upper, compared to the lower, profile, and elements such as Zr and Ti (normally considered immobile), exhibit a variable degree of loss in the upper profile and overlying soil zone. Finally, in contrast to the lower profile, samples from the upper profile show loss of all lanthanides except Ce. Together, these data indicate that the geochemistry of weathering of the lower and upper profiles is quite different. Cerium abundances are either consistent with this element being essentially immobile (up to ~1.5× the original weight-based abundance) in the lower and upper weathered profile or highly concentrated (up to 12× abundances of fresh granite in the soil zone). Cerium is concentrated in a subset of secondary phosphates (common in the upper profile), but almost undetectable in others (especially in the lower profile). Abundant bacteria and fungi are associated with secondary lanthanide phosphates in the upper weathered profile. In the soil zone, EDX analyses show that Ce-oxides are concentrated in pits formerly occupied by apatite and secondary phosphates.

Discussion: Geochemical data indicate that the profile can be subdivided into three distinctive weathering zones: (1) the lower profile, where weathering is essentially inorganic (chemical) and isovolumetric; (2) the upper rock profile, consisting of a zone 1–2 m thick, where weathering is still essentially isovolumetric but penetration by roots and abundant microorganisms is evident in more highly weathered regions. We suggest that biological processes are responsible for the enhanced loss of Si, K, Mn, and Mg (possibly due to plant uptake), as well as enhanced solubilization of Ti and Zr; and (3) the soil zone, where evidence of biological impact is abundant, grain size is significantly smaller, and granitic texture is lost.

In prior work [3], we attributed lanthanide concentrations at the bottom of the profile to biologically mediated secondary phosphate solubilization driven by phosphate limitation in the upper profile. Results of the current study suggest that the Ce content of secondary phosphates is an indicator of their genesis conditions. Phosphates that form early from lanthanides transported from adjacent allanite weathering sites under relatively reduced conditions have typical granitic LREE abundance patterns (i.e., are Ce-rich). Cerium-poor phosphates form in the lower profile from lanthanides released by biological dissolution of secondary phosphates in the upper profile. Cerium is oxidized in the upper profile and precipitates as insoluble Ce^{4+}-oxides. Thus, Ce is fractionated from the rest of the lanthanides. The up-to-12× Ce enrichment in the soil zone can most logically be attributed to loss of >90% of the mass present in an original granite volume (and associated compaction). This value places some constraint on the relative rates of weathering and erosion in this profile.

References: [1] Banfield J. F. (1985) M.S. thesis, Australian National University, Canberra Australia, 229 pp. [2] Banfield J. F. and Eggleton R. A. (1989) *Clays Clay Minerals, 37,* 113–127. [3] Taunton A. E. et al. (1999) *J. Alloys Coll.*, in press.

THE DEPENDENCE OF PLAGIOCLASE DISSOLUTION AND STRONTIUM RELEASE RATES ON SOLUTION SATURATION STATE.

A. S. Taylor[1], J. D. Blum[2], and A. C. Lasaga[1], [1]Department of Geology, Yale University, P.O. Box 208109, New Haven CT 06520, USA (aaron.taylor@yale.edu), [2]Department of Earth Sciences, Dartmouth College, 6105 Fairchild Hall, Hanover NH 03755, USA.

Whether as a proxy for silicate weathering through geologic time or as a tracer of nutrient fluxes in ecosystems, Sr isotopes are frequently used as indicators of chemical weathering. In spite of this widespread use, there are few data relating the kinetics of Sr release to the kinetics of mineral dissolution [1,2]. Establishing a more quantitative link between silicate weathering and Sr release will allow Sr isotopes to be used as a more effective proxy and should significantly improve our understanding of the relationship between the marine Sr-isotopic record, global weathering rates, and atmospheric CO_2 concentrations.

As the most common Ca-Mg silicate and an important source of Sr to continental runoff, plagioclase weathering plays a central role in both the Sr and C cycles. Brantley et al. [1] made the first measurements of Sr release rates during plagioclase weathering and found that the initial Sr flux during bytownite weathering is both nonstoichiometric and has an $^{87}Sr/^{86}Sr$ ratio that is higher than the overall mineral. We have expanded on this work by measuring plagioclase ($An_{38}Ab_{62}$) weathering rates under a wide variety of weathering solution saturation states. The saturation state of a weathering solution has been shown to significantly reduce albite dissolution rates [3]. In addition to decreasing the overall dissolution rate, changes in the solution saturation state could affect the relative weathering rates of minerals. In this case, the Sr-isotopic ratio of a weathering solution in contact with a rock could be affected by changes in the saturation state of the solution. We have performed plagioclase dissolution experiments in column reactors to determine the functional relationship between the dissolution and Sr-release rates of plagioclase and the saturation state of the weathering solution.

The dissolution rate for a given set of reaction conditions (25°C, pH ~3, $An_{38}Ab_{62}$) can be described with the equation

$$\text{Rate}_{\text{diss}} = -k\, f(\Delta G_r)$$

where k is the reaction rate constant (mol/m²/s) for the specific reaction conditions and $f(\Delta G_r)$ is a function relating the Gibbs free energy of reaction (ΔG_r) to the overall dissolution rate. Under far-from-equilibrium conditions, weathering solution compositions are such that $f(\Delta G_r) = 1$ and the dissolution rate is independent of solution chemistry. As species' concentrations increase in solution, $f(\Delta G_r)$ and therefore the dissolution rate decrease until equilibrium is reached and $\text{Rate}_{\text{diss}}$ becomes zero.

Under conditions that were far from equilibrium we observed stoichiometric Sr release during plagioclase dissolution after the initial stages of the experiment (500 h). We did not, however, find any significant variation in the $^{87}Sr/^{86}Sr$ ratio during the initial phases of our experiments, and the ratios of both the initial and later output solutions were the same as the reacting mineral. In addition, the $^{87}Sr/^{86}Sr$ ratio of the mineral did not change during the experiment. These results differ somewhat from those of Brantley et al. [1].

For ΔG_r between 0.0 and −6.0 kcal/mol, the overall dissolution and Sr-release rates become dependent on the solution composition. In spite of the decreased dissolution rate, the Sr release remains essentially stoichiometric. Furthermore, the $^{87}Sr/^{86}Sr$ of the output solutions is not affected by the increased saturation state of the solution. The $^{87}Sr/^{86}Sr$ ratio of Sr released during plagioclase weathering is equivalent to the mineral and independent of time or weathering conditions.

Elevated saturation states in weathering solutions lead to decreased plagioclase dissolution rates and Sr-release rates but do not affect the $^{87}Sr/^{86}Sr$ ratio of the output solutions. In a natural weathering environment, mineral weathering rates, CO_2 consumption, and Sr fluxes could all decrease as the weathering solution evolves chemically and plagioclase dissolution becomes suppressed.

References: [1] Brantley S. L. et al. (1998) *GCA, 62,* 1493–1500. [2] Taylor A. S. (1999) *GCA*, submitted. [3] Burch T. E. et al., *Chem. Geol., 105,* 137–162.

DIAMOND: JUST ANOTHER METAMORPHIC MINERAL?

L. A. Taylor, G. A. Snyder, and A. Camacho, Planetary Geosciences Institute, University of Tennessee, Knoxville TN 37996, USA (lataylor@utk.edu).

The once-held concept that diamonds are minerals crystallized from silicate melts within the upper mantle has been steadily changing. There is mounting evidence that many diamonds are products of metamorphism, more specifically metasomatism. This is particularly true for many eclogitic diamonds collected from kimberlitic xenoliths. In this paper, we will present much of the evidence and thought along these lines. Due to lack of space, we will omit some references, for which we apologize.

Diamondiferous eclogites are now generally considered to be mainly the products of subduction and metamorphism of oceanic crust [e.g., 1–4]. The evidence supporting this theory is (1) Gt and Cpx $\delta^{18}O$ values outside of mantle (5.5 ± 0.4‰), indicating a crustal component; (2) +Eu anomalies in Gt and Cpx, both within eclogites and as inclusions in diamond, certifying the involvement of plagioclase; (3) $\delta^{13}C$ values of +5‰ to −34‰ in eclogitic diamonds, possibly of biogenic origin; (4) $\delta^{34}S$ values of +15‰ to −14‰ in sulfide inclusions in diamonds; (5) elevated $^{87}Sr/^{86}Sr$, best explained by interactions with seawater; (6) ε_{Nd} values up to 250, attributed to effects of partial melting upon subduction; (7) bulk compositions of many diamondiferous eclogites representative of restites rather than magmas; and (8) the Archean TTG suite as a logical product of crystallization of the partial melt extracted from eclogites upon subduction [5]. However, since their transport to diamond P-T conditions by subduction of crustal protoliths, it is probable that most diamondiferous eclogites, collected from kimberlites (particularly

Group B/C of Shervais et al. [6]), have never experienced a major melt stage. How then could the diamonds in these eclogites be magmatic?

Mineral inclusions in diamonds, the "time capsules" of Bulanova [7], are thought to provide us with pristine mineral chemistry relating to the P-T-x conditions during the time of the diamond formation. A check of this assumption is that many diamond inclusions (DIs) are similar to those same minerals in the host eclogites [8]. In contrast, there is an increasing body of data indicating notable differences among multiple DIs from the same diamond [e.g., 5,7,9–14]. In fact, compositions of multiple DIs can differ so markedly that they may indicate mixed inclusion paragenesis (peridotite + eclogite) within a single diamond [15–16]. It appears that DI chemistry and diamond stratigraphy represent changes in the chemical environment as crystallization of the diamond progressed. These changes resulted in the observed discontinuous growth and chemical variations of the diamonds and their inclusions (but without presence of silicate magma). The evolution of compositions of the Cpx DIs from core to rim is contrary to that expected from igneous crystallization [14]. Indeed, it is probable that later growth of the outer portions of the diamond formed long after the present xenolith crystallization and involved C- and N-bearing fluids, such as those suggested by Deines and Harris [17], Stachel and Harris [18], and Taylor et al. [14].

In a quest to further understand diamonds and their host eclogites, our research group [19–21] has recently performed three-dimensional, X-ray tomography and continues a detailed "pull-apart" of a diamondiferous eclogite from Yakutia, found to contain 30 macrodiamonds. The diamonds are associated with zones of Cpx alteration, indicating possible paths of fluid flow. The Cpx and Gt inclusions of each diamond are different in major- and trace-element compositions and are not the same as those of the host eclogite. Even multiple diamond inclusions in the same diamond are different. Cathodoluminescence of polished surfaces of the diamonds reveals complex growth patterns representing alternating episodes of crystallization and resorption, accompanied by extreme fluctations in N aggregation states, possibly indicating grossly different residence times in the mantle for cores vs. rims of the diamonds.

It would appear that each diamond represents a different environment during its formation. There is not even evidence that the diamonds grew in the presence of the present host minerals. This eclogite is but the last residence place of the diamonds. This is the first such detailed dissection of diamondiferous eclogite, with greatly unexpected results. Is this xenolith the exception or the rule among eclogites?

References: [1] MacGregor and Manton (1986) *JGR, 91.* [2] Taylor and Neal (1989) *J. Geol., 97.* [3] Beard et al. (1996) *Contrib. Mineral. Petrol., 125.* [4] Snyder et al. (1997) *J. Petrol., 38.* [5] Ireland et al. (1994) *EPSL, 128.* [6] Shervais et al. (1988) *GSA Bull., 100.* [7] Bulanova (1995) *J. Geochem. Explor., 53.* [8] Taylor et al. (1996) *EPSL, 142.* [9] Bulanova et al. (1986) in *P, P, and M of Nat. D.* [10] Bulanova et al. (1996) *Contrib. Mineral. Petrol., 124.* [11] Griffin et al. (1993) *Lithos., 29.* [12] Sobolev et al. (1996) *Eos Trans. AGU,* S-287. [13] Sobolev et al. (1998) *Intl. Geol. Rev., 40.* [14] Taylor et al. (1998) *Intl. Geol. Rev., 40.* [15] Prinz et al. (1995) *Phys. Chem. Earth, 9.* [16] Wang (1998) *EPSL, 160.* [17] Deines and Harris (1994) GS Conf., Edinburgh. [18] Stachel and Harris (1997) *Contrib. Mineral. Petrol., 129.* [19] Keller et al. (1998) *7th Intl. Kimberlites Conf.* [20] Keller et al. (1999) *Proc. 7th Intl. Kimberlites Conf.* [21] Keller et al. (1999) *Geology.*

ON THE DIFFICULTIES OF MAKING EARTH-LIKE PLANETS.

S. R. Taylor, Department of Geology, Australian National University, Canberra 0200, Australia.

Although we have only one habitable planet in our solar system, the discovery of extra-solar system planets has raised popular hopes of finding Earth-like planets elsewhere. In order to investigate such scenarios, I examine the course of events in our solar system that resulted in the formation of our own planet to see how it arrived at its present useful site for *Homo sapiens*.

The question turns on whether this planet formed as an inevitable and natural consequence of planetary-building processes, or whether its formation and history were dominated by chance events. If the first scenario is true, then duplicate copies of our planet, although lacking in our system, can be expected to be common elsewhere. If the formation and evolution of our planet has been dominated by random processes, then our present situation may be unique. Among the many events that led to the formation and evolution of our planet are the initial size and angular momentum of the fragment that separated from a molecular cloud. These are crucial in determining whether a planetary system or a double star develops from the resulting nebula. Then there must be an adequate concentration of heavy elements to provide the 2% "rock" and "ice" components of the original nebula. An essential step in forming rocky planets in the inner nebula is loss of gas and depletion of volatile elements due to early solar activity, which is linked to the mass of the central star.

The lifetime of the gaseous nebula controls the formation of gas giants. In our system, Jupiter had to form in a few million years before the gas in the nebula was depleted. Although Uranus and Neptune eventually formed cores large enough to capture gas, they missed out and ended as ice giants. The early formation of Jupiter is responsible for the existence of the asteroid belt (and our supply of meteorites) and the small size of Mars, while the gas giant now acts as a gravitational shield for the terrestrial planets.

The Earth and the other inner planets accreted long after the giant planets in a gas-free inner nebula from volatile-depleted planetesimals that were probably already differentiated into metallic cores and silicate mantles. The accumulation of the Earth from such planetesimals was essentially a stochastic process, accounting for the differences among the four rocky inner planets, including the great contrast between those two apparent twins, Earth and Venus. The origin of our unique Moon by a single massive impact with the Earth by a body larger than Mars accounts for the obliquity (and its stability) and spin of the Earth in addition to explaining the angular momentum, orbital characteristics, and unique composition of the Moon.

Plate tectonics, unique among the terrestrial planets, led to the development of the continental crust on the Earth, an essential platform for the evolution of *Homo sapiens*. Random major impacts have punctuated the geological record, accentuating the directionless course of evolution. This sequence of events that resulted in the formation and evolution of our planet was thus unique within our system. The individual nature of the eight planets is repeated among the 60-odd satellites: no two seem identical.

This survey of our solar system raises the question whether the random sequence of events that led to the formation of the Earth are likely to be repeated in detail elsewhere. The discovery of other planetary systems has removed the previous belief that they would consist of a central star surrounded by an inner zone of rocky planets and an outer zone of giant planets beyond a few astronomical units. Jupiter-sized bodies in close orbits around other stars probably formed in a manner similar to our giant planets at several AU from their parent star and subsequently migrated inward, becoming stranded in close-but-stable orbits as "hot Jupiters," when the nebula gas was depleted. Such events would prevent the formation of terrestrial-type planets in such systems.

MEASUREMENT OF FLUXES AND CONCENTRATIONS OF HEAVY METALS IN SEDIMENT POREWATERS USING DIFFUSIVE GRADIENTS IN THIN FILMS.

P. R. Teasdale, W. Davison, and J. Hamilton-Taylor, Environmental Science, Lancaster University, Lancaster LA1 4YQ, UK.

The Principle of Operation of Diffusive Gradients in Thin Films (DGT): DGT is a recently developed technique in which analyte species are fractionated and concentrated with an assembly deployed *in situ* in natural waters. Analytical measurements are made after retrieval using sensitive laboratory instrumentation. The DGT assembly comprises a binding agent, such as a resin selective to the analyte ions in solution, immobilized in a thin layer of hydrogel (the binding gel). This is separated from solution by an ion-permeable hydrogel (diffusive gel) and a membrane filter (0.45-μm pore size), with a known total thickness, Δg. The diffusion coefficients of the analyte ions in the diffusive gel are a known fraction (usually >0.8) of their diffusion coefficient in water, D.

Within a few minutes of deployment, a steady-state linear concentration gradient is established between the bulk solution (analyte concentration, C) and the binding gel, where the concentration of the analyte species in solution is effectively zero. By exploiting this steady-state condition, DGT can be used to measure fluxes (J) *in situ*. The flux of an ion through the gel is described by Fick's first law of diffusion, and equates to $J = M/At$, where M is the mass of analyte species measured in the binding gel, A is the surface area of the DGT assembly, and t is the deployment time. If the concentration of analyte, C, in the bulk solution remains effectively constant, then it can also be estimated using $C = M\Delta g/DAt$. The principles of DGT have been verified in the laboratory [1]. Linear relationships are obtained between M and t, and M and $1/\Delta g$. Fractionation also occurs based on the kinetic availability of species, i.e., whether they dissociate during the time taken to diffuse to the binding gel. DGT thus measures a labile fraction of the analyte species in solution.

Diffusive Gradients in Thin Films in Sediments: The interpretation of DGT measurements in sediments is not as straightforward as in solution. Porewaters are not usually well mixed, and consequently the concentration adjacent to the DGT device may become depleted. Concentrations interpreted using the above equation may therefore underestimate porewater concentrations. For this reason DGT measurements under these conditions are usually given as time-averaged fluxes from the porewater to the DGT device [2,3]. This situation has been modeled and three different cases have been identified [4]. Independent measurements of porewater concentrations (e.g., peepers) or multiple DGT measurements are needed to ascertain which case is relevant.

1. In the sustained case, porewater concentrations adjacent to the DGT device are maintained at the bulk porewater concentration throughout the deployment. This can occur when solute transport rates in the sediment are rapid, i.e., through tidal pumping or bioirrigation, or if the rate of resupply from the solid phase to solution is fast compared to the rate of removal to the DGT device. Concentrations can be estimated using DGT under these conditions.
2. The only resupply of solutes to the porewaters is by diffusion and the flux to the device becomes progressively depleted with time. This situation has been modeled. For typical 24-h deployments, the diffusion-only DGT flux is about one-tenth of the sustained DGT flux.
3. Some resupply from the solid phase occurs but it is insufficient to sustain the porewater concentrations. Under these conditions, DGT is able to measure the flux limited by this solid-phase resupply.

Experimental Measurements of Solid Phase to Solution Fluxes: Recently measurements have been made to test our understanding of DGT deployments in sediments. DGT devices using a Chelex impregnated binding gel with a range of diffusive gel-layer thicknesses, and dialysis samplers (peepers) were deployed in a mesocosm of sediment taken from Esthwaite Water. These measurements demonstrate that different metals experience different resupply behavior in the sediment. For example, Co seems to experience no resupply, Ni partial resupply, and Cd close to sustained resupply. Other information was also obtained. A close correlation was observed between the Co and Mn profiles, suggesting that similar processes determine their local porewater concentrations, and there were similarities between the profiles for other trace metals as well. The effect of sediment heterogeneity was also important, particularly for short-term studies (up to 24 h). Profiles were observed to become less susceptible to heterogeneity over longer deployment periods (e.g., weeks), indicating that local structure may reflect short-term processes.

References: [1] Zhang H. and Davison W. (1995) *Anal. Chem., 67,* 3391–3400. [2] Zhang H. et al. (1995) *GCA, 59,* 4181–4192. [3] Davison W. et al. (1994) *Environ. Sci. Technol., 28,* 1623–1632. [4] Harper M. P. et al. (1998) *GCA, 62,* 2757–2770.

X-RAY SPECTROSCOPY INVESTIGATIONS OF LEAD(II) DISTRIBUTIONS WITHIN BIOFILMS FORMED ON METAL-OXIDE SURFACES.

A. S. Templeton[1], T. P. Trainor[1], J. D. Ostergren[1], S. J. Traina[2], A. M. Spormann[3], S. R. Sutton[4], M. Newville[4], and G. E. Brown Jr.[1], [1]Department of Geophysical and Environmental Sciences, Building 320, Stanford University, Stanford CA 94305, USA (templeton@stanford.edu), [2]Ohio State University, School of Natural Resources, Columbus OH 43210, USA, [3]Department of Civil Environmental Engineering, Stanford University, Stanford CA 94305, USA, [4]GSECARS, Building 434A, Argonne National Laboratory, Argonne IL 60439, USA.

Introduction: The development of microbial biofilms at mineral surfaces may have a dramatic effect on metal sorption and precipitation reactions in soils and aquatic environments. The relative contributions of biotic and abiotic factors to trace-metal sorption should depend strongly on the solution conditions within microenvironments, the availability of reactive mineral surface sites, and the abundance of strongly complexing organic functional groups within the biofilm. However, due to the complexity of these interrelationships and the difficulty in probing these microenvironments, the distribution, speciation, and local structure of metal sorption complexes at the mineral-biofilm interface are poorly understood

Our current research is directed toward clarifying the role of biofilms in the sorption of Pb(II) at mineral surfaces. We are developing quantitative methods for determining the partitioning of Pb(II) between biofilms and a variety of metal-oxide surfaces as a function of substrate characteristics, such as biofilm coverage and mineral-surface reactivity and structure, and environmental conditions such as pH, pCO_2, and metal concentration. Using a variety of spectroscopic approaches, such as extended X-ray absorption fine-structure spectroscopy (EXAFS) and grazing-incidence EXAFS, X-ray standing waves (XSW), and X-ray microprobe techniques, we have been able to examine directly the spatial distribution and speciation of Pb sorbed to biofilm-coated minerals.

Results: In our experiments, Pb was sorbed to biofilms generated by *Burkholderia cepacia* grown in the presence of α-Al_2O_3 and α-FeOOH. Pb L_{III}-EXAFS spectra data were collected for *B. cepacia*-mineral aggregates reacted with varying Pb concentrations at near-neutral pH. A quantitative measure of the fraction of Pb sorbed to the biofilm vs. the mineral components was obtained by fitting the EXAFS data with linear combinations of the EXAFS spectrum of Pb sorbed to *B. cepacia* and the spectrum of Pb sorbed to the clean mineral surface. In general, the linear-combination fitting results show that the fraction of Pb sorbed to the mineral surface is strongly dependent on the total Pb concentration. For example, Pb is partitioned almost equally between the biofilm and the α-Al_2O_3 surface at low Pb concentration (3 µM) and is increasingly concentrated within the biofilm at higher Pb concentrations (>85% Pb is sorbed to the biofilm at 30-µM Pb). The partitioning of Pb is also strongly dependent on the reactivity of the mineral substrate. For example, when Pb is sorbed to biofilm-coated α-Al_2O_3 and α-FeOOH under comparable solution conditions, Pb is predominantly sorbed to the FeOOH surface relative to the biofilm, whereas Pb is strongly partitioned into the biofilms formed on Al_2O_3 surfaces. Given the sensitivity of this approach, we have used EXAFS spectroscopy to quantitatively explore the solution conditions (pH, Pb) under which there exist large variations in the role of the biofilm vs. the mineral surface in the uptake of Pb.

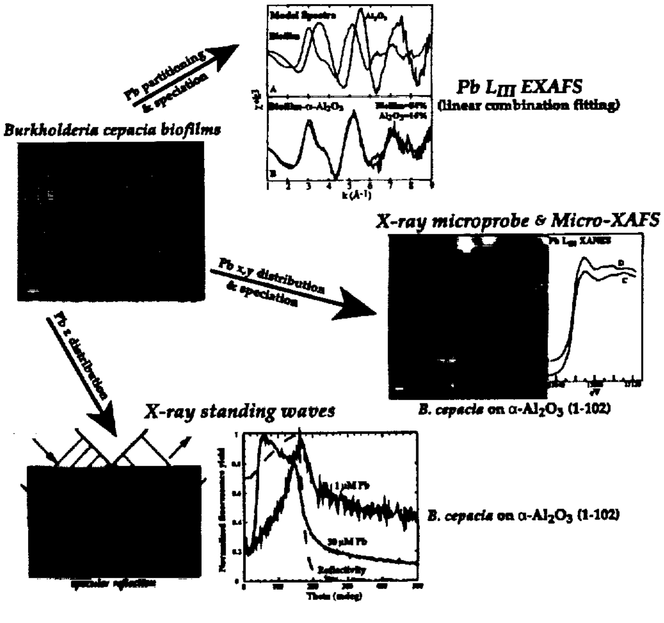
Burkholderia cepacia biofilms
Pb partitioning & speciation
Model Spectra
Biofilm
Al2O3
A
Biofilm-α-Al2O3
B
k(Å-1)
Pb LIII EXAFS
(linear combination fitting)
X-ray microprobe & Micro-XAFS
Pb x,y distribution & speciation
Pb LIII XANES
D
C
B. cepacia on α-Al2O3 (1-102)
Pb z distribution
X-ray standing waves
specular reflection
1 µM Pb
30 µM Pb
Reflectivity
Theta (mdeg)
B. cepacia on α-Al2O3 (1-102)

Fig. 1. Schematic diagram of the spectroscopic techniques used to obtain bulk and spatially resolved information on the distribution and speciation of Pb sorbed to biofilm-coated minerals.

X-ray standing waves fluorescence-yield data provide a complementary probe for examining the partitioning of Pb between the biofilm and the mineral surface. X-ray standing waves measurements have been used to map the vertical distribution of Pb within biofilms grown on single-crystal α-Al_2O_3 (1–102) and (0001). Preliminary *ex situ* XSW data show strong evidence for variations in the vertical distribution of Pb on the α-Al_2O_3 (1–102) surface as a function of Pb concentration. At low $[Pb]_T$, Pb is located predominantly at the mineral surface. In contrast, at higher $[Pb]_T$, the majority of Pb is distributed within the biofilm. However, the XSW fluorescence-yield profiles for Pb sorbed to biofilms formed on α-Al_2O_3 (0001) show a much smaller dependence on the $[Pb]_T$, and Pb is strongly partitioned into the biofilm even at low $[Pb]_T$. Thus, the strong affinity for Pb shown by the (1–102) surface relative to the (0001) surface in biofilm-free systems [1] remains important even in the presence of a biofilm, which again suggests that the structure and reactivity of the underlying mineral substrate exerts a strong influence on the initial partitioning of Pb between the biofilm and the mineral surface.

We will show that both bulk and spatially resolved synchrotron-based spectroscopic techniques are sensitive to the redistribution of Pb at the biofilm-mineral interface under varying solutions conditions. Preliminary modeling of the XSW distribution profiles will be presented, and quantitative information on the partitioning of Pb between biofilms and α-Al_2O_3 or α-FeOOH surfaces will be shown. These results will provide unique insights about the competition between biofilms and mineral surfaces during Pb uptake.

References: [1] Bargar J. R. et al. (1996) *GCA, 60,* 3541–3547.

THE FUNDAMENTALS OF CALCITE MINERALIZATION: SURFACE PROCESSES OF SPIRAL GROWTH.

H. H. Teng[1,*], P. M. Dove[1], and J. J. DeYoreo[2], [1]School of Earth and Atmospheric Sciences, Georgia Institute of Technology, Atlanta GA 30332, USA (*present address: Argonne National Laboratory, ER-203, 9700 Cass Avenue, Argonne IL 60439, USA), [2]Department of Chemistry and Materials Science, Lawrence Livermore National Laboratory, Livermore CA 94550, USA.

The mineralization of $CaCO_3$ is currently the focus of intense research due to its importance in both geological and biological environments. In particular, the possibility of using biorganic molecules as control agents has led to great interest in understanding the mechanisms that underlie biomineralization. One of the critical issues in controlling growth rates and morphologies is an understanding of how to solve the roles of kinetics and thermodynamics. Using *in situ* fluid-cell atomic force microscopy (AFM), we investigated the surface processes of calcite crystallization and characterized the fundamental kinetic and thermodynamic parameters that govern calcite growth in both inorganic and aspartic acid (ASP)-bearing solutions using direct measurements of microscopic properties of growth spirals.

Growth experiments were conducted on $\{10\bar{1}4\}$ faces of calcite in solutions with well-characterized chemistry and saturation state ($\sigma = \ln[(aCa^{2+})(aCO_3^{2-})/K_{sp}]$). Results were obtained for a σ range of 0.04–1.42. Using single-sourced, single spirals, we measured the dependence of step speed, v_s, on step length, L, as well as the dependence of critical step length, Lc (see Fig. 1), on σ for any system. As predicted by the Gibbs-Thomson relstionship, Lc exhibits a linear dependence on $1/\sigma$ to give values for the step-edge energies, α, of 4.41×10^{-5} and 3.44×10^{-5} erg/cm for the two-step directions, $<\bar{4}41>\pm$. A detailed analysis of the contributions to α from different step segments shows that corner sites have much higher free energies than straight portions of the steps. The large energy penalty of creating corner sites explains why calcite step edges are straight during growth. The value of Lc went to zero at approximately $\sigma = 5$, which indicates the supersaturation where growth undergoes a kinetic roughening with a free-energy barrier to 1-D nucleation at step edge of 2×10^{-6} erg. Once the magnitude of L reached Lc, v_s increased to its final value at a length that was short compared to that predicted by the BCF model, leading to anomalously small terrace widths. The addition of aspartic acid dramatically affects growth morphology by expressing a new crystallographic direction with reduced step-edge free energy. This suggests that the primary effect of Asp on calcite crystallization is to alter the thermodynamics of the growth surface.

Fig. 1.

Examining the dependence of v_s upon the deviation of equilibrium activity, $(a-a_e)$ shows that, at higher values of $(a-a_e)$, v_s is faster along positive directions. Under this condition, the spiral hillocks assumes a normal geometry. As $(a-a_e)$ decreases to $\sim 3 \times 10^{-5}$, v_s of the two directions becomes equal and a pseudo-isotropic hillock is formed. A novel inversion in hillock geometry is seen when $(a-a_e) < 3 \times 10^{-5}$, as the positive directions assume the slower step speed. The complex step kinetic behavior exhibits a form agreeing with models for impurity effect and is supported by observations of step pinning at low σ. Taking these effects into account, we derived values for the kinetic coefficients of step advancement of 0.54 and 0.30 cm/s for the two directions. In the presence of Asp, v_s shows a similar dependence upon $(a-a_e)$ for both directions, indicating that Asp may interact with steps by a similar mechanism irrespective of step orientations. However, a comparison of the kinetic data in Asp-free and Asp-bearing solutions suggests that, unlike other impurities reported in the literature, Asp is not a growth inhibitor for calcite crystallization. This result further supports the conclusion that the controls of Asp on calcite mineralization occur through interactions with the surface to change the energetics of growth.

KINETICS OF CALCITE GROWTH: ANALYSIS OF SURFACE PROCESSES AND RELATIONSHIPS TO MACROSCOPIC RATE LAWS.

H. H. Teng[1,*], P. M. Dove[1], and J. J. DeYoreo[2], [1]School of Earth and Atmospheric Sciences, Georgia Institute of Technology, Atlanta GA 30332, USA (*present address: Argonne National Laboratory, ER-203, 9700 Cass Avenue, Argonne IL 60439, USA), [2]Department of Chemistry and Materials Science, Lawrence Livermore National Laboratory, Livermore CA 94550, USA.

Calcite is the most abundant carbonate mineral and occurs in a wide variety of natural inorganic and biological systems. Although there is an enormous body of literature reporting investigations of carbonate crystallization, a review of the current knowledge suggests that two uncertainties may hinder further advances in controlling or directing the growth of carbonate minerals: (1) the microscopic surface processes that control the macroscopic manifestations of overall growth rate of crystal faces, and (2) the dependence of growth mechanism upon supersaturation. This study explores these uncertainties by comparing experimental evidence with the fundamental theoretical growth models to show where popular macroscopic growth expressions that are based upon chemical affinities (ΔG) of precipitation reactions hold or break down. Answers to these questions establish the knowledge base for constructing general models that quantify growth in complex mixtures of organic and inorganic constituents. They also establish relationships between microscopic processes and macroscopic growth rates determined by what is known as "bulk" methods throughout the scientific literature.

Using *in situ* atomic force microscopy (AFM), we conducted growth experiments to (1) determine the supersaturation ($\sigma = \ln[(aCa^{2+})(aCO_3^{2-})/$

Fig. 1.

K_{sp}]) range where growth occurs only by spiral formation; (2) determine the critical supersaturation that marks the activation of growth by a surface nucleation mechanism; (3) measure step-flow rates, v_s, and the corresponding slopes of growth hillocks, ρ; (4) calculate the overall or normal growth rates of single spirals using the measurements of v_s and ρ; and (5) analyze the dependence of overall growth rate, R_m, upon the dislocation source structure. We found that, at lower values of σ from 0 to 0.8, growth is initiated solely by surface imperfections including screw dislocations. Thus, crystal defect-originated growth, in particular spiral growth, is the only manifested mechanism. When $\sigma > 0.8$, two-dimensional nucleation becomes increasingly important with increasing σ. The magnitude of R_m for $\{10\bar{1}4\}$ faces grown by single spirals was estimated from the product of v_s and ρ measured at each σ. The results indicated a superlinear dependence of R_m upon ΔG.

Atomic force microscopy observations demonstrate that calcite growth by hillocks initiated at complex dislocation sources (see Fig. 1) is the dominant growth mode. This means that rate expressions that describe spiral growth must account for the effects of different types of dislocation source structures. General surface process-based rate expressions were derived by analyzing the dependence of ρ upon dislocation source structures using the BCF theories of crystal growth. These expressions have a complex dependence upon ΔG and can only be approximated by the second-order affinity-based rate laws under the special conditions that (1) growth proceeds only by the development of single-sourced, single spirals; and (2) growth occurs at the very-near-equilibrium conditions where spiral formation is the only operative mechanism. This suggests that experiments that measure temporal changes in solution chemistry yield an average growth rate by different types of hillocks. Hence, chemical affinity-based rate laws do not generally give meaningful interpretations of spiral-growth kinetics and, therefore, it is not appropriate to deduce growth mechanisms from macroscopic kinetic measurements. By combining direct observations with macroscopic methods that monitor temporal changes in solution chemistry during crystal growth, improved rate laws with greater predictive capabilities may be possible.

A CENTURY-LONG RECORD OF ANTHROPOGENIC NUTRIENT LOADING PROVIDED BY δ^{15}N VALUES IN SEDIMENT FROM A EUTROPHIC LAKE.

J. L. Teranes[1] and S. M. Bernasconi[2], [1]Department of Geological Sciences, University of Michigan, 2534 C. C. Little Building, Ann Arbor MI 48104, USA (jteranes@umich.edu), [2]Geological Institute, Swiss Federal Technological University-Eidgenössische Technische Hochschule, CH-8092, Zurich, Switzerland (stefano@erdw.ethz.ch).

Introduction: The N-isotopic composition of organic matter has become a valuable tool for reconstructing past productivity and changes in the nutrient availability in ocean surface waters [1]. Yet nutrient utilization and paleoproductivity have not been as successfully inferred from N isotopes in lake sediments. This is because P, and not N, commonly limits primary productivity in lakes. Under conditions of unlimited supply of nitrate, phytoplankton can continue to preferentially uptake ^{14}N.

In addition, factors other than primary productivity can influence the N-isotopic composition of lacustrine organic matter. For example, the N-isotopic composition of dissolved inorganic N (DIN) in lakes can significantly increase through time by external nitrate loading (i.e., anthropogenic eutrophication) and/or by water column denitrification in low-O environments. Nitrate derived from human and animal waster is enriched in ^{15}N (δ^{15}N = 10–20‰ [2]).

Changes in the source of organic matter, due to either shifts in species composition of phytoplankton or addition of organic matter from heterotrophs, can also overwhelm any δ^{15}N-productivity signal.

In this study, we present N-isotopic data from individually sampled light and dark annual laminae from a century-long (1885–1993) sediment record recovered from Baldeggersee, a small lake in central Switzerland. Due to dramatic and well-monitored changes in anthropogenic nitrate loading and environmental conditions during this century, Baldeggersee provides an ideal system to quantitatively document and evaluate the N-isotopic response of nutrient loading, nitrate utilization, and N limitation.

Results: Nitrogen-isotopic ratios in Baldeggersee organic matter are significantly higher than other reports of N isotopes in lake sediment (e.g., reported average values of 1–5‰ [3]). δ^{15}N values increase generally from the beginning of the record (δ^{15}N ~6–7‰) to the top of the core (δ^{15}N ~10–11‰; Fig. 1). Several abrupt positive N-isotopic excursions are superimposed on the increasing trend. A 6‰ positive δ^{15}N shift occurred between 1972 and 1976, coincident with the time of maximum P-loading, meromixis in the water column, strongest N-limitation of phytoplankton, and maximum extent of the anoxia hypolimnion [4]. Another abrupt N-isotopic increase (4‰) occurred in the most recent few years, when δ^{15}N values in the light layers again reached values >13‰.

Discussion: Nitrogen isotopes measured in the uppermost core samples were compared with surface water [NO_3^-] for the period of 1976–1993. The abrupt positive δ^{15}N shifts occurred when large seasonal phytoplankton blooms significantly decreased surface water [NO_3^-], thus providing conclusive evidence that N isotopes in organic matter can record NO_3^- utilization by phytoplankton.

The first-order increase in δ^{15}N values (~6‰ over the period 1885–1993) cannot be explained exclusively by nitrate utilization in response to increased primary productivity. Rather, the increasing trend dominantly reflects pro-

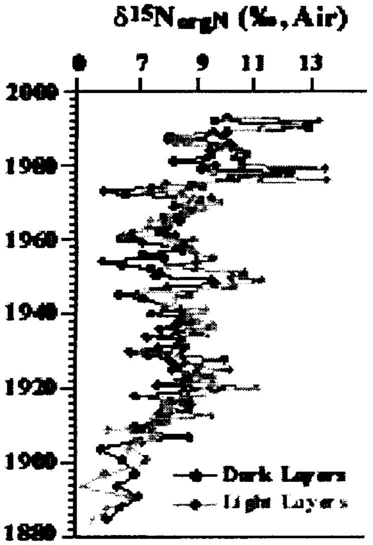

Fig. 1. Stratigraphic plot of δ^{15}N from the Baldeggersee laminated sequence.

gressive ^{15}N-enrichment of the Baldeggersee DIN pool due to external N-loading from animal manure in the watershed and/or increase of denitrification processes in the anoxia hypolimnion over the last 100 yr.

References: [1] Altabet M. A. and Francois R. (1994) *Global Biogeochem. Cycles, 8,* 103–116. [2] Kendall C. (1998) *Isotope Tracers in Catchment Hydrology,* 519–576. [3] Meyers P. A. (1997) *Org. Geochem., 27,* 213–250. [4] Wehrli B. et al. (1997) *Aquat. Sci., 59,* 285–295.

DISTRIBUTION AND MOBILITY OF LEAD IN ROADSIDE SOILS.

N. Teutsch[1], Y. Erel[1], and L. Halicz[2], [1]Institute of Earth Sciences, The Hebrew University of Jerusalem, 91904 Jerusalem, Israel, [2]Geological Survey of Israel, 30 Malkhei Yisrael Street, 95501 Jerusalem, Israel.

The emission of anthropogenic Pb in the last few decades has introduced large amounts of this toxic metal into the environment. A main source of the contamination in Israel and other countries is petrol-Pb. The conventional wisdom is that anthropogenic Pb emitted to the atmosphere is trapped in the upper part of the soil, and will reside there for centuries to come. However, in the last few years there has been a growing body of evidence which suggests that Pb mobility in soils is in fact more significant than previously estimated.

Soil samples were collected from soil profiles adjacent to the Jerusalem-Tel-Aviv highway and from soil profiles 500 m away. The concentrations and isotopic composition of Pb in the soils are used to determine the contribution of petrol-Pb relative to the soil, to quantify the distribution of rock-derived vs. anthropogenic Pb in different soil fractions, and to determine the rates of anthropogenic Pb infiltration into the soil. This project is one of the first to utilize Pb isotopes to distinguish between the detailed behavior and the mobility of rock-derived vs. anthropogenic Pb in soils, and is the first study to do so in semi-arid soils in general and in Israeli soils in particular.

Based on a comparison between samples collected in 1982 and 1996–1997 and changes in the isotopic composition within the soil profile, it is estimated that the migration velocity of anthropogenic Pb in the soil is 0.3–0.5 cm/yr, which is a much faster rate than previously estimated. In the most contaminated soil profiles there is a lower concentration of Pb in the top 1 cm compared with deeper horizons, which might reflect the gradual transition to unleaded petrol in Israel.

In this study, a selective sequential dissolution procedure [1] was adjusted to the clean laboratory in order to distinguish between rock-derived vs. petrol-Pb in different soil fractions (carbonates, Fe oxides, organic matter, and aluminosilicates). The distribution of petrol-Pb within the soil is unlike that of natural Pb. In uncontaminated soils, only 1% of the Pb is associated with the carbonate fraction, while the portion of Pb in carbonates in contaminated soils is much larger (up to 60%). Anthropogenic Pb is mostly associated with carbonates and Fe-oxides (50–80%), while natural Pb is primarily associated with aluminosilicates (~70%). The anthropogenic Pb penetrating the soil eventually replaces all the natural Pb including Pb associated with aluminosilicates.

References: [1] Han F. X. and Banin A. (1995) *Commun. Soil Sci. Plant Anal., 26,* 553–576.

IDENTIFYING METAL SULFIDE COMPLEXES IN FRESHWATERS USING LASER DESORPTION MASS SPECTROSCOPY.

S. M. Theberge, T. F. Rozan, and G. W. Luther III, College of Marine Studies, University of Delaware, 700 Pilottown Road, Lewes DE 19958, USA (theberge@udel.edu; trozan@udel.edu; luther@udel.edu).

Introduction: Metal sulfide complexes have been shown to exist and play an important role in trace metal transport in natural waters [1–4]. However, these results have come from indirect measurements of sulfide concentrations using square wave voltammetry (SWV) [5]. In this study, solutions containing different metals and sulfide (CuS, FeS, PbS, and ZnS) as well as the sulfide minerals chalcocite, covellite, FeS_{am}, galena, sphaelerite, and pyrite were analyzed using laser desorption mass spectroscopy. This technique allowed for the determination of the stoichiometry of each different metal sulfide complex from the isotopic distributions. These results were then compared to both similar analyses of conventionally filtered (<0.45 µm) and ultrafiltered (<1000 MW) river water to directly determine if any metal sulfides complexes existed in the oxic water.

Methods: All analyses were conducted on a Finnegan FTMS 2000 laser desorption mass spectrometer run in a negative ion mode. The laser source is a CO_2 laser with a 10.6-µm output. The ionization delay was set at either 1 or 5 s.

Metal stock solutions were prepared daily in N_2 purged water (Nanopure) with reagent grade metal salts and sulfide solutions that were made with washed crystals of Na_2S $9H_2O$. All mixture concentrations were in the micromolar range, exceeding all individual solubility products. Additionally, some Cu and Zn sulfide solutions were passed though a sphedax column to remove spectator ions.

Metal sulfide minerals were crushed to powder and rinsed with distilled water (Nanopure) prior to analysis.

River water samples were conventionally filtered using a 0.2-µm Nucleopore polycarbonate filter. Several samples were further ultrafiltered using a Filtron ultracassette with a 1000-MW cut-off. All filtered water was then concentrated by freeze-drying to dryness.

Electrochemical methods were conducted following the procedure given in [1]. In summary, sulfide was voltammetrically determined using cathodic stripping square-wave voltammetry (CSSWV) during an acid titration. Individual S species were identified depending on the pH and increases in sulfide concentrations.

Results: The resulting spectrum provided collaborating results to those observed by voltammetry. Copper, Fe, Pb, and Zn sulfide complexes were all observed to have 1:1 stoichiometries. Additionally, Cu and Zn were observed to form a second complex with a stoichiometry of 2:3. Copper formed sulfide complexes with a wide variety of metal:sulfide ratios.

River water samples were found to contain Cu sulfides with 2:3 stoichiometries. Samples collected at high river discharges (and high suspended particulate matter loads) had spectra similar to covellite. Samples collected at lower discharges were found to resemble to laboratory solutions of Cu sulfides with a 2:3 stoichiometry. A similar spectrum was observed for the low flow ultrafiltered samples, indicating that these complexes were truly dissolved.

Surprisingly, in the low-flow samples, Fe sulfides with a 1:2 stoichiometry similar to pyrite were observed. However, these complexes were observed in both the conventional filtrate and ultrafiltrate. No FeS was observed, even though trace amounts were measured using CSSWV.

References: [1] Rozan T. F. et al. (1999) *Environ. Sci. Technol.,* submitted. [2] Rozan T. F. and Benoit G. (1999) *GCA,* in press. [3] Luther G. W. III and Tsamakis E. J. (1989) *Mar. Chem., 27,* 165–177. [4] Theberge S. M. et al. (1997) *Deep-Sea Research II, 44,* 1381–1390. [5] Luther G. W. III et al. (1996) *Environ. Sci. Technol., 30,* 671–679.

OXYGEN-ISOTOPIC SYSTEMATICS OF REYKJANES RIDGE MID-OCEAN-RIDGE BASALT: CONSTRAINTS ON THE ORIGIN AND COMPOSITION OF ICELANDIC PLUME MANTLE.

M. F. Thirlwall[1], R. N. Taylor[2], D. P. Mattey[1], C. G. Macpherson[1], M. A. M. Gee[1], and B. J. Murton[2], [1]Department of Geology, Royal Holloway University of London, Egham, Surrey TW20 0EX, UK, [2]Southampton Oceanography Centre, Empress Dock, Southampton SO14 3ZH, UK (matthewt@gl.rhbnc.ac.uk).

The Iceland plume is one of the most productive current mantle plumes, responsible for the island of Iceland and the anomalously shallow ocean floor in the vicinity. Recent seismic tomographic work [1] has indicated that the plume originates at the core-mantle boundary and hence Icelandic magmas have the potential to record some of the chemical properties of this region, e.g., elevated ^{186}Os [2]. Many modern Icelandic tholeiites possess low $\delta^{18}O$ relative to upper mantle values (e.g., 3–4.2‰ for olivine [3], compared to 5.15‰ in xenolith olivine [4]), which has frequently been interpreted as the result of crustal contamination of the plume melts by low-$\delta^{18}O$ basaltic crust. This interpretation is supported by AFC-type relationships and decreased ^{230}Th disequilibrium, but it is difficult to define $\delta^{18}O$ of the mantle component. This has led to suggestions that $\delta^{18}O$ as low as 3‰ may be present in the plume mantle. Alternatively, if the plume mantle $\delta^{18}O$ value is indeed similar to upper mantle values, the large bulk-mass assimilation inferred would effectively eliminate the use of Icelandic lavas as indicators of core-mantle boundary chemistry.

Assuming a contamination model, the uniquely low $\delta^{18}O$ of Icelandic lavas compared with other ocean island basalts is regarded as a consequence of the alteration of Icelandic crust by very low-$\delta^{18}O$ high-latitude meteoric water in hydrothermal systems. Such a mechanism is clearly restricted to areas that have been exposed to meteoric fluid circulation, and is precluded from operating on the mid-ocean ridges adjoining Iceland below Pleistocene minimum sea level. The Reykjanes Ridge from 60°–63°N shows clear high-precision Pb-isotopic evidence [5] of binary mixing between enriched Icelandic plume mantle and a MORB-like source not seen in Iceland. We have determined $\delta^{18}O$ by laser fluorination on olivine, glass, and plagioclase from 20 Reykjanes Ridge lavas to define the $\delta^{18}O$ value of enriched Icelandic plume mantle. South of 62.4°, $\delta^{18}O$ for olivine is identical to the average upper-mantle value, apart from two samples at 58° that have anomalously high ^3He and Icelandic Sr-Nd-Pb isotopes. From 62.4°–63.0°, olivine $\delta^{18}O$ reduces to 4.5‰ and shows a strongly curved hyperbolic correlation with $^{143}Nd/^{144}Nd$. Such a relationship is very unlikely to be explained by crustal contamination, for although the oceanic crustal thickness increases toward Iceland, correlation with crustal thickness is much weaker than correlation with indices of plume mantle mixing, such as Nb/Zr and $^{143}Nd/^{144}Nd$. Further, since low-$\delta^{18}O$ meteoric water cannot penetrate to the >200 m below sea-level depths of these samples, there is no reason why other ocean-ridge sectors, or ocean islands, should not show similarly low $\delta^{18}O$. Finally, where crustal contamination has been invoked as the cause of low $\delta^{18}O$ in Iceland, there is no correlation observed or expected with $^{143}Nd/^{144}Nd$.

The hyperbola requires substantially higher Nd/O ratios, and hence Nd content, in the Icelandic plume component. Lead-strontium-neodymium-isotopic relationships dictate that $^{143}Nd/^{144}Nd$ in the plume component is significantly lower than the northernmost Reykjanes Ridge samples analyzed, defining olivine $\delta^{18}O$ in the plume component to be 3–4‰. Use of the observed Nd contents of Reykjanes Ridge and enriched Icelandic primitive lavas (Nd_I/Nd_{RR} = 3.5) to model the hyperbola does not yield sufficient curvature, implying that mixing along the Reykjanes Ridge involves mixing between mantle reservoirs, not melts. Source Nd_I/Nd_{RR} of ~14 is required to generate the curvature, indicating that Icelandic lavas represent ~4× greater mean melt fractions than southern Reykjanes Ridge lavas, consistent with a northward increase in crustal thickness from ~7–28 km.

Low $\delta^{18}O$ in some Hawai'ian magmas has been attributed [6] to incorporation of recycled lower ocean crust, the only known major low-$\delta^{18}O$ reservoir, into the plume mantle source. However, minimum $\delta^{18}O$ values observed for this are close to the estimated $\delta^{18}O$ of enriched Icelandic plume mantle, requiring an unacceptably large contribution from this in view of observed Os-isotopic ratios. Further, $\delta^{18}O$-radiogenic isotopic relationships are opposite to those seen in Hawai'i; it is not plausible that recycled lower oceanic crust would generate relatively enriched radiogenic isotopic ratios. An alternative mechanism for generating low $\delta^{18}O$ may be found at the core-mantle boundary. Theoretical calculations based on iron-silicate O fractionation, and observed $\delta^{18}O$-^3He relationships, suggest that $\delta^{18}O$ at the core-mantle boundary may be some 1‰ lower than in the upper mantle [7]. If so, the bulk $\delta^{18}O$ and Os isotopes of plumes originating here could be dominated by the core-mantle interaction, while their Sr-Nd-Pb-isotopic compositions were dominated by reycled components.

References: [1] Bihwaard H. and Spakman W. (1999) *EPSL, 166,* 121–126. [2] Brandon A. D. et al. (1998) *Science, 280,* 1570–1573. [3] Gee M. A. M. et al. (1998) *J. Petrology, 39,* 819–839. [4] Mattey D. P. et al. (1994) *EPSL, 128,* 231–241. [5] Thirlwall M. F. et al. (1998) *Mineral. Mag., 62A,* 1507–1508. [6] Lassiter J. C. and Hauri E. H. (1998) *EPSL, 164,* 483–496. [7] Macpherson C. G. et al. (1999) in preparation.

PROTACTINIUM-231/URANIUM-235–THORIUM-230/URANIUM-238 SYSTEMATICS OF YOUNG VOLCANIC ROCKS FROM CENTRAL AMERICA: CONTRASTING BEHAVIOR RELATED TO SUBDUCTION FLUXES?

R. B. Thomas[1], M. M. Hirschmann[1], H. Cheng[1], R. L. Edwards[1], and M. K. Reagan[2], [1]Department of Geology and Geophysics, University of Minnesota, Minneapolis MN 55455, USA (rebecca.b.thomas-1@umn.edu), [2]Department of Geology, University of Iowa, Iowa City IA 52242, USA.

Recent work has shown that ^{231}Pa is strongly fractionated from ^{235}U in arc lavas [1,2], indicating that $^{231}Pa/^{235}U$ may be a useful tracer for mass transfer processes in the source regions of arcs. Important mantle transfer processes in arcs include melting and fluid mobilization from the subducting slab. To better understand the interplay between these variables, we are investigating $^{231}Pa/^{235}U$-$^{230}Th/^{238}U$ systematics in Central America, where the slab input varies geographically. Subduction fluid influence on Costa Rican (CR) lavas is inferred to be much less than on Central Nicaraguan (CN) lavas, and lavas from southern Nicaragua have slab influence intermediate between those from CN and those from CR [3]

We have combined new thermal ionization mass spectrometry (TIMS) ^{231}Pa measurements with $^{230}Th/^{238}U$ measured by alpha counting spectroscopy [4] for eight young volcanic rocks from CR and Nicaragua (Fig. 1). All are from historical eruptions or from eruptions with known young ages. Data for CR volcanos and the two southernmost Nicaraguan samples cluster in the upper right quadrant, where both ^{230}Th and ^{231}Pa are in excess relative to their parent U nuclides. Samples from CN show a different trend, with similar ($^{231}Pa/^{235}U$) to those observed in CR, but ^{230}Th activities that are less that their ^{238}U activities. Previous workers have attributed ^{231}Pa excesses in arcs to the effects of partial melting. Thorium-230 excesses are generally believed to result from partial melting in the presence of garnet. In contrast, ($^{230}Th/^{238}U$) <1 in arcs is believed to be a result of preferential migration of U from the slab. Thus, the Pa/Th/U data from CR are likely to be primarily the result of strong fractionation in the presence of garnet during melting, with little or no influence of an U-rich slab fluid. This is consistent with evidence from stable trace elements and long-lived isotopic systems that generally suggest that subducted sediments and associated fluids play a minor role in CR [4,5]. The strong ^{231}Pa excesses are difficult to explain by simple melting processes unless melt fractions are restricted to below ~0.1%, indicating a likely role for some form of ingrowth, percolative flow, or both.

The CN data are more difficult to explain than those from CR. Although the observed ^{230}Th deficits are consistent with substantial addition of U from slab-derived fluid, as previously inferred for CN [2–4], $^{231}Pa/^{235}U$ excesses should be similarly affected (i.e., addition of U from the slab should reduce both $^{230}Th/^{238}U$ and $^{231}Pa/^{235}U$). However, the ($^{231}Pa/^{235}U$) excesses in CN are nearly as large as those in CR. This is particularly puzzling because of the positive correlation between $^{231}Pa/^{235}U$ and $^{230}Th/^{238}U$ observed from a worldwide survey of arc lavas [1].

Several possible factors singly or in combination may explain the differences between CN and CR Pa/Th/U systematics:

1. The ^{231}Pa excesses in CN were affected by a U-rich slab fluid, and so would otherwise have been larger than those from CR. This explanation is more attractive if some time passed between fluid addition from the slab and melting (i.e., there is some ^{231}Pa ingrowth in the solid prior to melting) and can be made consistent with simple quantitative models of fluid addition and melting, but requires that melt fractionation of $^{231}Pa/^{235}U$ is little reduced or even enhanced by fluid addition.

2. Protactinium is mobilized in the fluid. This is appealing because it is the simplest model that explains how $^{230}Th/^{238}U$ decreases while $^{231}Pa/^{235}U$ remains high. But it is difficult to reconcile this model with the global positive correlation between $^{231}Pa/^{235}U$ $^{230}Th/^{238}U$ in arcs [1], which has generally been attributed to reduction of $^{231}Pa/^{235}U$ by fluid addition.

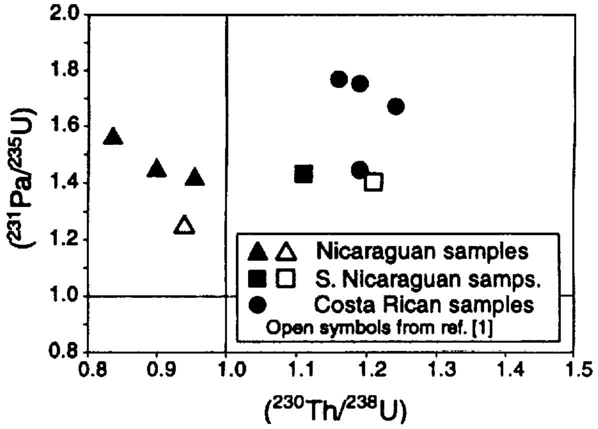

Fig. 1. Symbol heights reflect approximate error in $^{231}Pa/^{235}U$ measurements. Errors in $^{230}Th/^{238}U$ (by α counting) are ~5% or 10% in samples with low U concentrations [4].

3. There is little or no garnet in the source region of CN lavas. In this case, low $^{230}Th/^{238}U$ is generated in part by the greater compatibility of Th relative to U in cpx, which may or may not be true for cpx's in arc source regions. Regardless, this model requires an explanation for why the fluid-rich CN source would lack garnet, whereas the fluid-poor CR source clearly has garnet. This may possibly be attributable to prior removal of garnet from the CN source due to melting from extensive fluid fluxing.

References: [1] Pickett and Murrell (1997) *EPSL, 148,* 259–271. [2] Thomas et al. (1998) *Eos Trans. AGU, 79,* 1003. [3] Herrstrom et al. (1995) *Geology, 23,* 617–620. [4] Reagan et al. (1994) *GCA, 58,* 4199–4212; Reagan, unpublished data. [5] Carr et al. (1990) *CMP,* 369–380.

A MULTIMETHOD APPROACH TO CORRELATING BENTONITES FROM THE SILURIAN OF THE WELSH BASIN.

J. Thorogood[1], N. J. G. Pearce[1], C. A. Bendall[1], D. K. Loydell[2], R. Cave[1], and J. A. Evans[3], [1]Institute of Geography and Earth Sciences, University of Wales Aberystwyth, Ceredigion, Wales SY23 3DB, UK, [2]University of Portsmouth, Burnaby Building, Burnaby Road, Portsmouth PO1 3QL, UK, [3]Isotope Geosciences Laboratory, National Environmental Research Council, Keyworth, Nottingham NG12 5GG, UK.

Bentonites are common in the Silurian of Wales and the Welsh Borderlands and can be used to correlate diverse facies (deep-water graptolitic and shallow-water shelly) that occur in the Welsh Basin. Bentonites occur in both facies, and are essentially isochronous as they were deposited in a matter of days or weeks [1]. Their correlation may also identify the potential diachroneity of graptolite biozones across the basin [2]. Volcanic arc sources have been postulated for these deposits, although no direct proximal or distal source has been identified [3]. Isotope and geochemical analysis have been used here to provide a signature for bentonites from the Llandovery and Wenlock to enable correlations across the Welsh Basin (and possibly beyond) and place constraints on their source(s).

The discrimination diagram of [4] indicates the <2-μm clay fraction derived from a silicic, mostly subalkaline source(s) ranging from andesite to rhyolite (Fig. 1). Results suggest changing/evolving source(s) from volcanic arc in the early Silurian to within plate in the Wenlock [5]. The clay fraction shows light REE enrichment and negative Eu anomalies.

Apatites were separated from the bentonites and analyzed by laser ablation inductively coupled plasma mass spectrometry (LA-ICP-MS). Applying the discrimination diagram of [6] to the single-grain data revealed several magma sources in operation at any time, mostly from intermediate to alkaline sources. Comparing trace- and rare-earth-element data obtained from single apatite grains has provided a series of tentative correlations (e.g., Fig. 2). Continuing factor analysis on both clay and grain analyses is being applied to further substantiate these correlations.

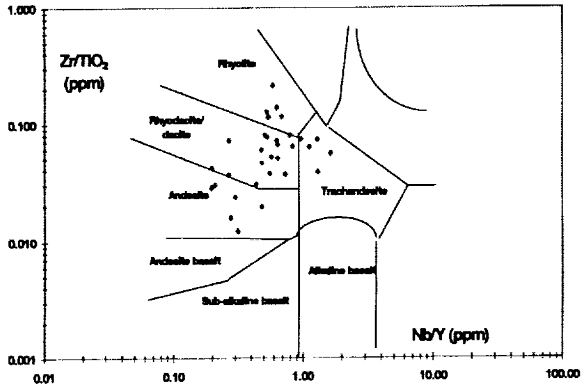

Fig. 1. Typical data from the <2-μm clay fraction from some Welsh bentonites.

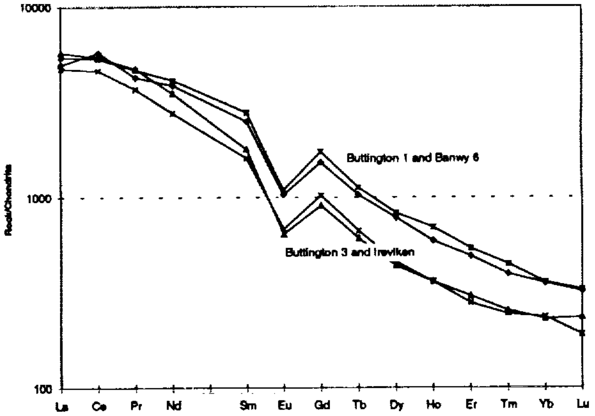

Fig. 2. Selected REE plots for single-grain apatite analysis.

References: [1] Bergström S. M. et al. (1998) *Temas Geoloigo-Mineros ITGE, 23,* 54–56. [2] Loydell D. K. (1993) in *High Resolution Stratigraphy* (E. A. Hailwood and R. B. Kidd, eds.), pp. 323–340, The Geological Society. [3] Fortey N. J. et al. (1996) *Trans. Royal Soc. Edinburgh: Earth Sciences, 86,* 167–180. [4] Winchester J. A. and Floyd P. A. (1977) *Chem. Geol., 20,* 325–343. [5] Pearce J. A. et al. (1984) *J. Petrology, 25,* 956–983. [6] Fleischer M. and Altschuler Z. S. (1986) *Neues Jahbruch Mineralogische Monatshafte, 10,* 467–480.

STRONTIUM AND NEODYMIUM ISOTOPES IN APATITES: THEIR APPLICATION TO THE STUDY OF BENTONITES FROM THE WELSH BASIN.

J. Thorogood[1], N. J. G. Pearce[1], J. A. Evans[2], D. K. Loydell[3], and R. Cave[1], [1]Institute of Geography and Earth Sciences, University of Wales Aberystwyth, Ceredigion, Wales SY23 3DB, UK, [2]Isotope Geosciences Laboratory, National Environmental Research Council, Keyworth, Nottingham NG12 5GG, UK, [3]University of Portsmouth, Burnaby Building, Burnaby Road, Portsmouth PO1 3QL, UK.

Bentonites have a bimodal grain size distribution, comprising clays (mostly mixed layer illite/smectite) and detrital and pyroclastic grains. In the Welsh Basin bentonites, the pyroclastic grains include euhedral heavy minerals such as zircon, apatite, and sphene, apparently unaltered by the local low-grade metamorphism during the closure of the Tornquist Sea and Iapetus Ocean [1,2].

Strontium-87/strontium-86 and $^{143}Nd/^{144}Nd$ have been measured for apatites from Silurian bentonites from Wales and the Welsh Borderland. Strontium and Nd concentrations determined by thermal ionization mass spectrometry (TIMS) are in good agreement with results from the laser ablation inductively coupled plasma mass spectrometry (LA-ICP-MS) study of single grains. However, despite the fact the Sr isotopes show a range of values that could be construed as magmatic, they show inconsistent behavior and spread toward radiogenic Sr enrichment. Strontium disturbance is supported by a Rb-Sr biotite age of 386.4 ± 5.4 Ma (Devonian), indicative of Sr disturbance during the Acadian Orogeny as widely recorded by igneous rocks from Wales [3].

Figure 1 shows ε_{Sr} against ε_{Nd} values. Most samples fall within the ε_{Nd} range of Welsh, Belgian, and Nova Scotian volcanic provinces (–3 to +4) [3–5]. There is no clear relationship between stratigraphic position and the isotopic ratios, rather, it suggests numerous magma sources operating through time. Single-grain apatite analysis by LA-ICP-MS also identifies the same groups using an apatite discrimination plot (Fig. 2. La + Pr + Ce atomic% vs. La/Nd atomic after [6]). Apatites from alkaline sources have higher LREE concentrations than those from a more siliceous source.

The ranges of ε_{Nd} values and magma types indicated are influenced by several factors: actual amount of contamination, relative concentrations of Nd in melt and contaminant, and isotopic composition of melt and contaminant [3].

References: [1] Samson S. D. et al. (1988) *Geology, 16,* 444–447. [2] Samson S. D. et al. (1995) *GCA, 59,* 2527–2536. [3] Evans J. A. (1989) Unpublished Ph.D. thesis, London University. [6] Fleischer M. and Altschuler

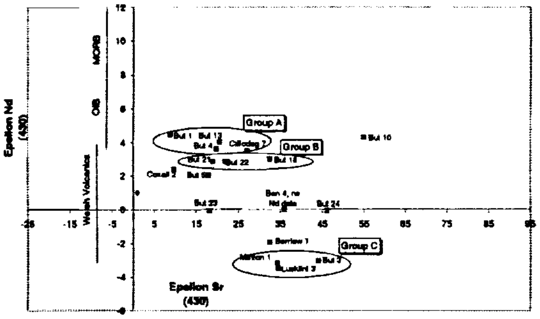

Fig. 1. $\varepsilon_{Nd_{430}}$ against $\varepsilon_{Sr_{430}}$ for apatites from Welsh bentonites.

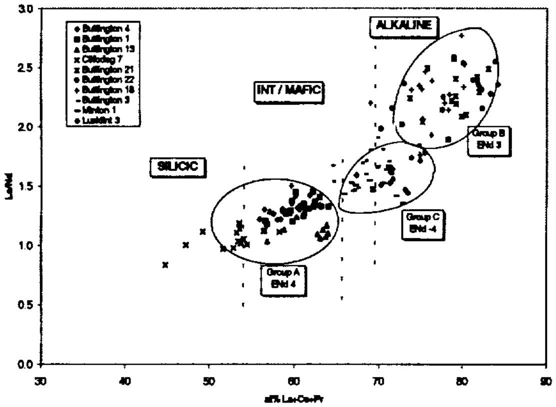

Fig. 2. Apatite discrimination diagram based on single-grain laser ablation ICP-MS analysis.

Z. S. (1986) *Neues Jahbruch Mineralogische Monatshafte, 10,* 467–480. [4] Noble S. R. et al. (1993) *Geol. Mag., 130,* 835–846. [5] Keppie J. D. et al. (1997) *Geol. Mag., 134,* 425–447.

CHEMICAL COMPOSITION OF CRETACEOUS SEAWATER: RESULTS FROM ENVIRONMENTAL SCANNING ELECTRON MICROSCOPE-ENERGY DISPERSIVE X-RAY SPECTROMETRY ANALYSES OF FLUID INCLUSIONS IN MARINE HALITES.

M. N. Timofeeff [1], T. K. Lowenstein[1], and L. A. Hardie[2], [1]Department of Geological Sciences and Environmental Studies, State University of New York at Binghamton, Binghamton NY 13902, USA (bf21297@binghamton.edu; lowenst@binghamton.edu), [2]Department of Earth and Planetary Sciences, Johns Hopkins University, Baltimore MD 21218, USA (hardie@gibbs.eps.jhu.edu).

Fluid inclusions in halites from three Cretaceous evaporites were analyzed via environmental scanning electron microscopy-energy dispersive X-ray spectrometry (ESEM-EDS) to test the hypothesis that seawater chemistry has fluctuated in the past, in rhythm with rates of ocean crust production and mid-ocean ridge hydrothermal activity [1]. The results indicate Cretaceous seawater differed significantly from modern seawater, enriched in Ca and K, depleted in SO_4, Mg, and Na, with Ca>SO_4. This is not unexpected because the Cretaceous was the time of maximum mid-ocean crust production during the Phanerozoic Eon.

Sixteen fluid inclusions from Cretaceous halite, Congo Basin, seven fluid inclusions from the Sergipe Basin, coastal Brazil, and 22 fluid inclusions in halite from the Khorat Plateau region of Thailand and Laos were analyzed using the ESEM-EDS technique. Lower Cretaceous (Aptian) evaporites from the Congo Basin and Brazil are about the same age (113–119 Ma.) [2] and were formed during early rifting and separation of South America and Africa [3]. They both lack $MgSO_4$ salts and contain the very rare $CaCl_2$-bearing mineral tachyhydrite [3]. A huge Late Cretaceous evaporite, the Maha Sarakham Formation, carrying bedded sylvite, carnallite, and tachyhydrie underlies an area of 60,000 km^2 on the Khorat Plateau, northeastern Thailand and Central Laos [4].

Results from the ESEM-EDS analyses of fluid inclusions were obtained for Mg, K, and Ca; Na and Cl were computed for halite saturation using the Harvie-Moller-Weare (H-M-W) computer program [5]. SO_4 was always below detection. The major question to be addressed is whether the fluid inclusions analyzed contained evaporated seawater. This is particularly important for the Cretaceous halites from Brazil and Congo because they accumulated during the early rifting phase of the south Atlantic Ocean and therefore might have received inflow waters other than seawater. One way to evaluate a seawater parentage is to plot fluid-inclusion chemistries from several geographically separated basins of about the same age. If each basin contains halite with fluid inclusion compositions that fall along a distinctive evaporation path, and if the paths for the various basins of the same age overlap one another, then the implication is that the parent water had a uniform "global" seawater chemistry. Additionally, the effects of nonmarine inflow and syndepositional recycling were not strong enough to greatly modify the overlapping evaporation paths.

The results from our ESEM-EDS analyses plotted on molality diagrams show: (1) a well-defined evaporation path for the major elements for each deposit that confirms that fluid inclusions analyzed are primary and formed from evaporating surface waters; and (2) that overlapping evaporation pathways of the major elements from all three deposits suggests a common parent water, seawater, and minimal influence of nonmarine inflow and recycling.

Cretaceous seawater chemistry was determined using the H-M-W computer program and assuming m_{Cl} Cretaceous = m_{Cl} modern seawater. The major-element concentrations in Cretaceous seawater were calculated to best fit the evaporation path defined by the Cretaceous fluid inclusions. The calculated Cretaceous seawater chemistry shows that K was ~40% greater and Mg was 30–40% lower than modern seawater. Calcium was enriched in Cretaceous seawater, and Ca was greater than SO_4, but the amounts of each cannot be determined from chemical analyses of fluid inclusions in halite. Precipitation of gypsum during evaporative concentration of seawater removes Ca and SO_4 in equal molar amounts. The amount of gypsum precipitated is unknown and therefore the initial concentrations of Ca and SO_4 in seawater before evaporation and precipitation of gypsum is unknown. If we assume modern seawater SO_4 concentrations, Cretaceous Ca was ~300% of that in modern seawater. If Cretaceous SO_4 was half the modern concentration, Cretaceous Ca was ~200% above modern seawater Ca.

Recently, Hardie [1] predicted changes in the chemical composition of Phanerozoic seawater controlled by relative changes in the amount of river influx and mid-ocean-ridge hydrothermal water flux. The H-M-W computer program was used to "evaporate" Hardie's predicted Cretaceous seawater [1] (enriched in Ca and K and depleted in Mg, Na, and SO_4 relative to modern seawater), and this calculated evaporation path closely matches the major-element chemical composition of fluid inclusions in Cretaceous halite (except K). These results strongly support the hypothesis that seawater has undergone significant changes in major-element composition in the past.

References: [1] Hardie L. A. (1996) *Geology, 24,* 279–283. [2] Palmer A. R. (1983) *Geology, 11,* 503–504. [3] Wardlaw N. C. (1972) *Econ. Geol., 67,* 156–168. [4] Hite R. J. and Japakasetr T. (1979) *Econ. Geol, 74,* 448–458. [5] Harvie C. E. et al. (1984) *GCA, 48,* 723–751.

CHEMICAL COMPOSITION OF PERMIAN SEAWATER: RESULTS FROM ENVIRONMENTAL SCANNING ELECTRON MICROSCOPE-ENERGY-DISPERSIVE X-RAY SPECTROMETRY ANALYSES OF FLUID INCLUSIONS IN MARINE HALITES.

M. N. Timofeeff[1], T. K. Lowenstein[1], and L. A. Hardie[2], [1]Department of Geological Sciences and Environmental Studies, State University of New York at Binghamton, Binghamton NY 13902, USA (bf21297@binghamton.edu; lowenst@binghamton.edu), [2]Department of Earth and Planetary Sciences, Johns Hopkins University, Baltimore MD 21218, USA (hardie@gibbs.eps.jhu.edu).

Fluid inclusions in marine halites from the Permian Salado Formation, New Mexico, and the San Andres Formation, Texas, analyzed using environmental scanning electron micrscopy–energy-dispersive X-ray spectrometry (ESEM-EDS) show that Permian seawater was different in major element chemical composition than modern seawater, enriched in K and depleted in Mg and SO_4. The ESEM-EDS technique involves chemical analysis of individual primary fluid inclusions >30 μm in size. Thirteen fluid inclusions from the Salado Formation and 52 inclusions from the San Andres Formation analyzed via ESEM-EDS were compared with 49 fluid inclusion analyses from the Salado halites [1] and 20 analyses from the Zechstein evaporites of Poland [2].

The latest Permian Salado evaporites (Ochoan Series) display m-scale shallowing upward cycles and contain halite with the $MgSO_4$ salts polyhalite and kieserite [3]. The evaporites of the San Andres Formation, Palo Duro basin in the Texas panhandle, are from the late Permian Guadalupian series [4]. They are cyclical carbonate/anhydrite/halite deposits that lack potash salts and formed in a marginal marine setting [4,5]. Halites from the lowest (Z1) of four large-scale stratigraphic cycles of the Polish Zechstein evaporites [2] are ~251–258 Ma, close in age to the Salado and San Andres evaporites.

Results from the ESEM-EDS analyses of fluid inclusions were obtained for Mg, K, and SO_4; Na and Cl were computed for halite saturation using the Harvie-Moller-Weare (H-M-W) computer program [6]. Calcium was always below detection. Several questions must be addressed before interpreting the analytical results. Assuming fluid inclusions contain trapped surface waters, then proving these waters are related to evaporated seawater is difficult because halite can form in a variety of nonmarine settings. One way to evaluate a seawater parentage is to plot fluid inclusion chemistries from several basins of about the same age. If each basin contains halite with fluid inclusion compositions that fall along a distinctive evaporation path, and if the paths for the various basins of the same age overlap one another, then the implication is that the parent water had a uniform "global" seawater chemistry. Additionally, the effects of nonmarine inflow and syndepositional recycling were not strong enough to greatly modify the overlapping evaporation paths.

The results from our ESEM-EDS analyses and the data of [1,2] plotted on molality diagrams show (1) a well-defined evaporation path for the major elements for each deposit, which confirms that fluid inclusions analyzed are primary and formed from evaporating surface waters; and (2) that overlapping evaporation pathways of the major elements from all three deposits suggest a common parent water, seawater, and minimal influence of nonmarine inflow and recycling.

Permian seawater chemistry was determined using the H-M-W computer program and assuming m_{Cl} Permian = m_{Cl} modern seawater. The major-element concentrations in Permian seawater were calculated to best fit the evaporation path defined by the Permian fluid inclusions. The calculated Permian seawater chemistry shows that K was ~50% greater and Mg was 15–20% lower than modern seawater. Calcium was less than SO_4 in Permian seawater but the amounts of each cannot be determined from chemical analyses of fluid inclusions in halite. Precipitation of gypsum during evaporative concentration of seawater removes Ca and SO_4 in equal molar amounts. The amount of gypsum precipitated is unknown and therefore the initial concentrations of Ca and SO_4 in seawater before evaporation and precipitation of gypsum are unknown. If we assume modern seawater Ca concentrations, Permian SO_4 was about half that in modern seawater. If Permian Ca was twice the modern concentration, Permian sulfate was ~15% below modern seawater sulfate.

Recently, Hardie [7] predicted changes in the chemical composition of Phanerozoic seawater controlled by relative changes in the amount of river influx and mid-ocean ridge hydrothermal water flux. The H-M-W computer program was used to "evaporate" Hardie's predicted Permian seawater [7] (enriched in Ca and K and depleted in Mg and SO_4 relative to modern seawater), and this calculated evaporation path closely matches the major-element chemical composition of fluid inclusions in Permian halite. These results strongly support the hypothesis that seawater has undergone significant changes in major-element composition in the past.

References: [1] Horita J. et al. (1991) *GCA, 55,* 417–432. [2] Peryt T. M. and Kovalevich V. M. (1996) *Geol. Palaontol. Teil.,* 337–356. [3] Lowenstein T. K. (1988) *GSA Bull., 100,* 592–608. [4] Hovorka S. (1987) *Sedimentology, 34,* 1029–1054. [5] Fracasso M. A. and Hovorka S. D. (1986) *Bur. of Econ. Geol. Rep. of Investigations, No. 156,* Texas Bur. of Econ. Geol., 48 pp. [6] Harvie C. E. et al. (1984) *GCA, 48,* 723–751. [7] Hardie L. A. (1996) *Geology, 24,* 279–283.

STRATIGRAPHIC RECORDS OF BLACK CARBON FROM LAKE SEDIMENTS AS ARCHIVES OF CONTINENTAL ENVIRONMENTAL CHANGE.

W. Tinner and F. S. Hu, Department of Plant Biology, 265 Morrill Hall, University of Illinois, Urbana IL 61801, USA (fshu@life.uiuc.edu).

Introduction: The abundance and size distribution of charcoal in lake sediments are commonly used by paleoecologists to inferfire history in relation to natural (e.g., vegetation and climate) and anthropogenic changes. For this purpose, various techniques have been developed to quantify charcoal in lake sediments in the past two decades. This presentation will provide an overview of charcoal in lake sediments as a paleoenvironmental indicator, followed by a discussion on the strengths and limitations of major existing techniques for charcoal analysis. Two case studies from North America and Europe will then be examined to illustrate interactions among fire, vegetation, climate, and human disturbance during the late Glacial and Holocene. These case studies represent two different biome types where fires play an essential role in vegetation structure, ecosystem function, and biogeochemical cycling, but the relative importance of climatic vs. anthropogenic factors differs greatly in controlling fire occurrence between the two systems.

Results and Discussion: Wien Lake (64°20'N, 152°16'W) is located in the modern closed boreal forests of central Alaska, where fire occurrence during the late Quaternary was primarily driven by climate and vegetation variations. Microscopic charcoal analysis of a lake-sediment core from this lake shows increasing charcoal abundance from 12,200 to 11,000 yr ago, suggesting that *Betula* shrub tundra in the region became increasingly fire-prone in response to biomass increases and dry climatic conditions. A marked decrease in charcoal influx 9800–10,800 yr ago suggests a reduction of shrub-tundra fires, which was probably caused by a climatic cooling during the Younger Dryas. Following an early-Holocene increase, charcoal influx rates decrease substantially 7200–8500 yr ago, likely reflecting a transitory decrease of boreal forest fires during an episode of climatic cooling. Charcoal influx rates increase with the establishment of modern closed boreal forests dominated by *Picea mariana* ~6500 yr ago. This charcoal record provides strong evidence that climate change exerted a deterministic control over fire occurrence.

Lago di Origlio (46°03'N, 8°57'E) is a lake in the southern Swiss Alps surrounded by temperate chestnut-oak forests and small patches of cultivated land. Microscopic charcoal analysis of the sediments reveals that charcoal abundance 9300–14,500 yr ago is similar to that of the same period at Wien Lake. A marked decrease of charcoal influx also occurs 9800–10,800 yr ago at Lago di Origlio, suggesting that the Younger Dryas cooling diminished forest fire incidence. Charcoal influx increases during the early Holocene but then decreased to reach a minimum ~7500 yr ago. Subsequently human activities gradually replaced climatic factors as the dominant control over the regional fire regime. During the Neolithic (3900–6500 yr ago) natural forests were greatly altered by anthropogenic fires, and certain natural vegetation species (e.g., *Abies alba*) disappeared partially or completely in favor of fire-tolerant species that expanded to form new fire-adapted vegetation types. The charcoal record from Lago di Origlio documents the central role of forest fires as a human tool for land use.

In addition to paleoecological applications, charcoal analysis of lake sediments offers information on the biogeochemical significance of black carbon in terrestrial systems. For example, charcoal influx rates at Wien Lake are broadly consistent with those from other boreal sites in North America and Europe, with a range of 0.1–2.8 mm^2 cm^{-2} yr^{-1}. By making various assumptions, we have estimated the abundance of black carbon in boreal lake sediments and soils. Our results suggest that the mean mass influx rate of black carbon is ~42,000 g km^{-2} yr^{-1}, with a wide range of 3500–98,000 g km^{-2} yr^{-1} in Alaska, Quebec, and Finland. If the modern boreal forests of the world became established ~7000 yr ago on average, this influx rate is equivalent to an accumulation of 3.528 × 10^{12} g black carbon in boreal sediments and soils during this period. This black-carbon pool represents only a small fraction of organic C in the boreal system. Given the high frequencies of forest fires in boreal regions, the fraction of biomass and soil organic matter converted to CO_2 during fire events, and the associated release of nutrients likely play a greater role in biogeochemical cycling than does the pool of largely recalcitrant black carbon.

LITHIUM-ISOTOPIC GEOCHEMISTRY OF MONO LAKE, CALIFORNIA.

P. B. Tomascak, N. G. Hemming, and S. R. Hemming, Lamont-Doherty Earth Observatory, Columbia University, Route 9W, Palisades NY 10964, USA (tomascak@ldeo.columbia.edu; hemming@ldeo.columbia.edu; sidney@ldeo.columbia.edu).

Introduction: Mono Lake is the modern vestige of Pleistocene Lake Russell and is one of the major long-lived closed-basin lakes of the Great Basin of the western United States. It is extremely alkaline and saline. Lake level over the last ~13 ka has fluctuated by ~180 m [1]. Many previous lake high stands are marked by deposits of carbonate (tufa), much of which has been dated [1,2]. Although ~85% of its water budget derives from Sierran streams [3], our data indicate that springs currently provide the bulk of the Li to the lake. This report is part of a larger project with the goal of using modern isotope and elemental distribution between lake water and carbonate precipitates to trace the geochemistry of the lake back through the Holocene and perhaps the Quaternary. Hence, an understanding of the modern Li-isotopic budget of Mono Lake is essential.

The Li concentration of Mono Lake is very high, and the isotopic composition is considerably heavier than those of any of the representative measured inputs. The Li-isotopic composition of lake water does not vary with depth nor does it show temporal or seasonal variability over the ~2.5-yr period of our sampling (δ^7Li ~20). Thermal and groundwater springs sampled in 1996 supply water with δ^7Li of 7.8, although the two have appreciably different Li concentrations. The ~12‰ offset between the Li-isotopic compositions of lake and spring waters is broadly similar to the present isotopic offset between oceanic and ambient riverine Li [4]. Water samples from the dominant Sierran stream to the lake, Rush Creek, are also lighter isotopically than lake water, and demonstrate little temporal variability (δ^7Li = 12.2 for Fall 1996 sample, 11.0 for Spring 1999).

Lake bottom sediments are dominated by silt- and clay-size detrital silicates of granitic and felsic-intermediate volcanic provenance, and clay minerals are rare [5]. Carbonate makes up 6–15% of lake bottom sediments. The spectacular tufa towers at Mono Lake are known to result from the interaction of alkaline lake water and cation-rich spring water. Interestingly, although the tufa examined is Li rich, its formation appears unimportant in terms of the Li-isotopic budget of the lake. It has δ^7Li slightly heavier than lake water (22.5). This tufa crystallized within months if not days of sampling, so it is unlikely that its isotopic composition has been corrupted by postcrystallization processes. Thus, it is anticipated that tufa will record Li-isotopic compositions of past lake water and that these measurements can be linked to hydrologic and/or climatic changes within the paleolake system.

Given the ~10^3× concentration difference, it is not remarkable that mixed lake-spring water 1.5 m from the spring orifice is dominated by lake Li and that its δ^7Li is within uncertainty of lake water (21.3), similar to tufa that crystallized in this zone. Whereas tufa is not enriched in ^{6}Li, the light Li sink remains to be discovered. Clay minerals have exchange properties that make them attractive candidates for producing the observed mass fractionation. However, in as much as lake sediments contain only minor proportions of clay minerals, the predominant agent of fractionation is likely not to be clays. This condition is analogous to that of the contrast in composition between the world's oceans relative to river and hydrothermal inputs. Due to the small size of Mono Lake (~180 km^2), we are optimistic that the fractionation mechanisms here can be discovered, and that the same process may be important on a global scale.

TABLE 1.

Sample (year-number)	Sample Type	Li (ppm)	δ^7Li
mono 96-2	Rush Creek	n.d.	12.2
mono 99-2	Rush Creek	0.002	11.0
mono 96-9	thermal spring	0.30	7.8
mono 96-13	groundwater spring	0.032	7.8
mono 96-10	lake water (8 m)	11.5	20.1
mono 96-10	lake water (24 m)	12.7	19.3
mono 99-10	lake surface water	10.3	19.8
replicate			20.3
mono 99-15B	lake-spring mix	0.76	21.3
mono 99-15D	fresh tufa	14.1	22.5

Isotope measurements by MC-ICP-MS at LDEO and at the Carnegie Institution of Washington (reproducibility ±1.1‰, 2σ population [5]). Lithium concentrations determined by flame atomic absorption spectrometry (AAS) (estimated uncertainty ±1.5%, 2s). n.d. = not determined.

References: [1] Benson L. V. et al. (1998) *Quat. Res., 49,* 1–10. [2] Stine S. W. (1987) Ph.D. thesis, Univ. California, Berkeley, 614 pp. [3] Neumann K. and Dreiss S. J. (1995) *Water Resources Res., 31,* 3183–3193. [4] Huh Y. et al. (1998) *GCA, 62,* 2039–2051. [5] Newton M. S. (1994) *SEPM Spec. Pub., 50,* 143–157. [6] Tomascak P. B. et al. (1999) *Chem. Geol., 158,* 145–154.

GOLD ADSORPTION ON GOETHITE AND HUMIC ACID-COATED GOETHITE.

T. Tosiani, Instituto de Ciencias de la Tierra, Universidad Central de Venezuela, Aptdo. 47509, Los Chaguaramos 1041-A, Caracas, Venezuela (ttosiani@strix.ciens.ucv.ve).

Natural organic matter (NOM) in surficial or groundwater exists as a variety of molecular sizes and complex mixture of polyfunctional organic compounds. Adsorption of these organic compounds onto inorganic colloids can alter the physicochemical properties of the solid. Although many classical adsorption models have been developed, little consideration has been given to desorption modeling, so that in environmental systems it may be inappropriate to consider a completely reversible or irreversible reaction [1].

Increasing evidence attests that various physical and chemical processes can mobilize and redistribute Au on surface environments. Dissolution of elemental Au with the aid of many inorganic and organic ligands, and subsequent transport and deposition in response to changes in various physicochemical parameters has been extensively studied. Adsorption of Au is probably an important process in determining the extent of gold mobilization and secondary dispersion in natural environment. Previous studies related with the adsorption of Au complexes on many mineral surfaces have been carried out; some more recent are related to the adsorption of Au on goethite [2]. However in the nature the presence of humic acids in soils and

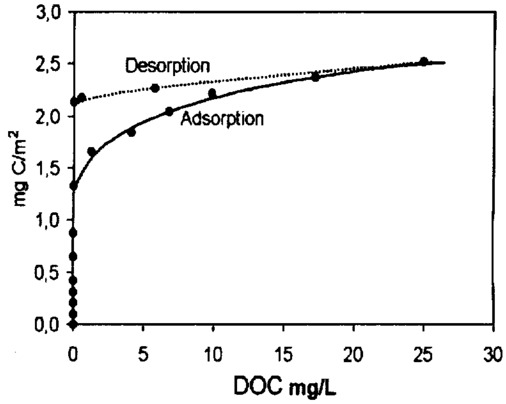

Fig. 1. Humic acid adsorption and desorption on goethite (20 g/m^2) at pH = 4–5 and NaCl = 0.01 N.

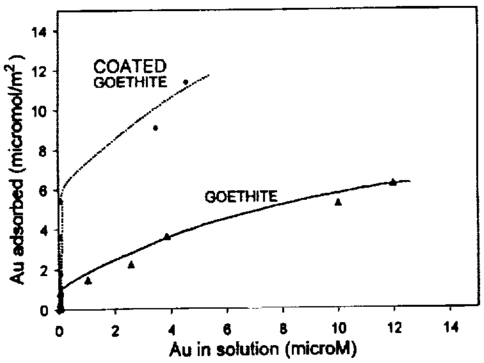

Fig. 2. Gold adsorption on goethite and goethite coated with NOM, at pH = 4.0–4.5 and $NaNO_3$ = 0.01 N.

natural waters, play an important role on change the surface characteristics of these iron oxihydroxides. The objective of this preliminary study was to verify and extend the previous studies by investigating the adsorption of Au(III)-chloride by goethite and NOM-coated goethite.

The humic acids used in these experiments come from the Paragua River (Venezuela), extracted using successive freezing and later liophilization [3]. The goethite was synthesized starting from ferric nitrate and potassium hydroxide at 60°C during 8 d, resulting in a well-crystallized goethite with a surface area of 20 m^2/g. The experiments of adsorption of humic acids on the goethite indicate a maximum adsorption of 2.5 mg C/m^2 at pH 4–5 with a very high histeretic behavior, where the desorption is very small, with a final concentration of 2.2 mg C/m^2 (Fig. 1). The goethite color is ocher, and after the adsorption of the humic acids, it takes a brown coloration in spite of the successive washing with water. The adsorption of humic acids is more efficient at pH = 2, while at pH = 10–12 the adsorption is almost null.

The adsorption of gold ($AuCl_4^-$) was measured in suspensions of pure goethite and coated goethite, both to a concentration of 0.5 g/L, at pH = 4.0–4.5 with an ionic strength of $NaNO_3$ = 0.01 N. The results indicate a enhanced capacity of Au adsorption from 4 to 6× when the goethite is coated with humic acids (Fig. 2)

In conclusion, the high adsorption and the histeretic behavior of NOM on the goethite at pH = 4–5, especially in tropical regions, could be the common surface characteristic of these oxihydroxides, and this property may contribute to enhance the secondary dispersion of Au near ore mineral deposits.

References: [1] Boaohua G. et al. (1995) *GCA, 59,* 219–229. [2] Machesky L. et al. (1991) *GCA, 55,* 769–776. [3] Martinez E. and López E. C. (1995) *Proceeding of III Int. Cong. Of Energy, Envir. and Tech. Innovation,* 293–298.

THEORETICAL EVIDENCE FOR COPPER THIOARSENITE COMPLEXING.

J. A. Tossell, Department of Chemistry and Biochemistry, University of Maryland, College Park MD 20742, USA (tossell@chem.umd.edu).

Introduction: To obtain an atomistic understanding of the structure and stability of the copper thioarsenite complex characterized experimentally by Clarke and Helz (UMCP) we have carried out quantum mechanical calculations on several isomers of that complex, a number of related complexes and the corresponding uncomplexed ligands. Using an ab initio molecular orbital approach which includes electron correlation (second order Moller-Plesset perturbation theory using a polarized double zeta valence orbital basis and effective core potentials) we calculate the lowest energy isomer to be CuS(SH)As(OH) (with bonds from Cu to S, SH and As) which has a calculated enthalpy of formation [from $Cu^+(aq)$ and AsS(SH)(OH)-(aq)] of about –110 kJ/mol. If entropic effects are ignored, this gives a log K value at room T of about 19.1 for the formation constant, (fortuitously) close to the value of 19.8 determined experimentally. More significantly, our method reproduces the experimental trend in log K values for the formation of the simpler complexes $CuCl_2^-$, $Cu(SH)_2^-$ and $Cu(CN)_2^-$ and allows us to understand why the CuS(SH)As(OH) complex is so stable. We find that the complexes of Cu^+ with $AsS(SH)_2^-$, $AsS(SH)(NH_2)^-$ and $AsS(SH)(CH_3)^-$ are also very stable (log K from 15.3–19.3), while the complexes with related As(V), P(III) and P(V) S-containing ligands are considerably less stable (log K from 4.6 to 9.3). For the complex formed from the purely oxidic ligand $AsO(OH)_2^-$, the calculated log K value is –9.2. The determining chemical characteristic of the strongly complexing ligands is the presence of two coordinating S atoms (one –S and one –SH) and an electron-rich As center. When the OH group on As is replaced by the strongly electron withdrawing F, the Cu-As bond is broken and the stability of the complex is greatly reduced. We have also calculated deprotonation enthalpies and estimated acid-dissociation constants for $As(OH)_3$, $As(SH)(OH)_2$, $As(SH)_2(OH)$ and $AsO(OH)_3$. In agreement with expectation, we calculate $AsO(OH)_3$, $As(SH)(OH)_2$ and $As(SH)_2(OH)$ to be much more acidic than $As(OH)_3$. Thus, $As(SH)_2(OH)$ is strongly deprotonated near neutral pH and its anion complexes very strongly with $Cu^+(aq)$, while $As(OH)_3$ exists mainly as the neutral molecule, and neither it nor its anion complexes significantly with Cu^+. Preliminary studies indicate similar strong complexation with thioarsenites for other "soft" cations, such as Ag^+.

ARGON IN MID-OCEAN-RIDGE BASALTS AND LOIHI GLASSES AND IMPLICATIONS FOR THE EVOLUTION OF THE EARTH'S MANTLE.

M. Trieloff[1], M. Falter[1], and E. K. Jessberger[2], [1]Max-Planck-Institut für Kernphysik, Saupfercheckweg 1, D-69117 Heidelberg, Germany (trieloff@pluto.mpi-hd.mpg.de), [2]Institut für Planetologie, Wilhelm-Klemm-Strasse 10, D-48149 Münster, Germany.

Noble-gas geochemistry is a tool of growing importance to obtain information on the early history and composition of the Earth that otherwise is inaccessible. As contamination of mantle-derived rocks by atmospheric-type noble gases is the most severe problem in elucidating the isotopic state of the mantle, we pursued a three-fold strategy to unravel the isotopic composition of Ar in MORB and Loihi glasses. (1) We separated mantle and atmospheric components by high-resolution step-heating and step-crushing, e.g., by gas extraction in 15–22 heating steps instead of typically three. (2) We selected mantle samples that were already demonstrated to be most pristine.

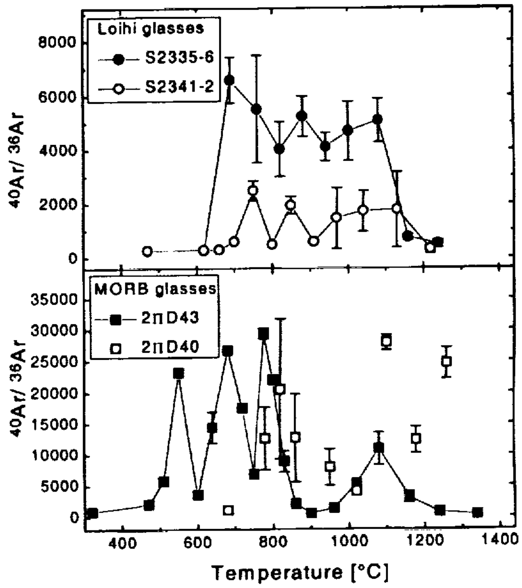

Fig. 1. Argon-40/argon-36 ratios vs. extraction temperature determined in selected MORB and Loihi glass samples. Maxima represent the current best values for the isotopic state of the mantle source.

We analyzed submarine basalt glasses with the highest ^{20}Ne/^{22}Ne and ^{40}Ar/^{36}Ar ratios previously determined, including the prominent "popping rock" 2ΠD43 [1–3] and glasses dredged in 3–5 km depth at the southern rift zone of Loihi seamount [4]. (3) We monitored the components that are dissolved in the glass by a novel approach, step-heating after neutron irradiation. Neutron induced ^{39}Ar, ^{37}Ar, and ^{38}Ar are derived from K, Ca, and C$^+$, respectively. Their release pattern characterize Ar components that are homogeneous within the glass. Heterogeneously distributed Ar then is identified by different degassing characteristics.

Our results clearly demonstrate that mantle Ar is partitioned between vesicles and basalt glass depending on vesicularity. In high-vesicular glasses, mantle Ar prefers to reside in vesicles, whereas in low-vesicular glasses a large fraction is homogenously dissolved in the glassy matrix. Atmospheric Ar generally is heterogeneously distributed and most probably introduced at eruption. The high-resolution step-heating and step-crushing analyses improved the definition of the isotopic state of the Earth's upper mantle (um) and the Hawai'ian plume reservoir (pl) to ^{40}Ar/^{36}Ar ≈ 30,000 and ≈ 6,000 (Fig. 1), respectively.

In addition, we find the remarkable relationship: $(^{40}\text{Ar}/^{36}\text{Ar})_{\text{um}}/(^{40}\text{Ar}/^{36}\text{Ar})_{\text{pl}} \approx (^{4}\text{He}/^{3}\text{He})_{\text{um}}/(^{4}\text{He}/^{3}\text{He})_{\text{pl}} \approx (^{21}\text{Ne}^{*}/^{22}\text{Ne})_{\text{um}}/(^{21}\text{Ne}^{*}/^{22}\text{Ne})_{\text{pl}}$ where ^{21}Ne* is nucleogenic ^{21}Ne. Such a relation between radiogenic (or nucleogenic) and primordial nuclides implies that the Earth's mantle He-Ne-Ar and K-Th-U compositions were homogeneous early in Earth history. While He and Ne were of solar type, Ar was dominated by a planetary or atmospheric component. The latter is indicated by the ^{36}Ar/^{38}Ar ratio [e.g., 5] as well as by the ^{20}Ne/^{36}Ar ratio [3]. Regarding evidence of atmospheric rather than planetary or solar composition of nonradiogenic Xe and Kr isotopes in MORB glasses [6,7], this indicates selective admixing of heavy atmospheric noble gas isotopes into the mantle very early in Earth's history. Such a scenario can be reconciled with (but does not require) steady-state models of the upper mantle.

References: [1] Staudacher T. et al. (1989) *EPSL, 96,* 119. [2] Burnard P. et al. (1997) *Science, 276,* 568. [3] Moreira M. et al. (1998) *Science, 279,* 1178. [4] Valbracht P. J. et al. (1997) *EPSL, 150,* 399. [5] Poreda R. and Farley K. (1992) *EPSL, 113,* 129. [6] Kunz J. et al. (1998) *Science, 280,* 877. [7] Kunz J. and Allègre C. J. (1999) *J. Conf. Abstr., 4(1),* 366.

HOW DOES QUARTZITE WEATHER? A GEOCHEMICAL STUDY OF PROTEROZOIC QUARTZITE IN THE SEMIARID REGIONS OF DELHI, INDIA.

J. K. Tripathi and V. Rajamani, School of Environmental Sciences, Jawaharlal Nehru University, New Delhi 110067, India.

Quartz is known to be the most resistant rock-forming mineral during surface weathering. However, a quartzite, a rock containing more than 98% quartz, is shown to have many weathering features that resemble those in limestones [1]. The nature of quartzite weathering and the mechanism for the formation of geomorphic features in quartzite are not understood. In the area around Delhi and Haryana, middle to late Proterozoic, metamorphosed quartzite occurs as a series of subparallel ridges. Hard, compact, and bouldery quartzite occurs on top of the ridges as tars and domes. On the flanks, the rocks have undergone extensive weathering in and around fractures, oriented subparallel to the surface, through infiltration of meteoric water. In extensively weathered zones, the quartzite has become friable reddish sands which are mined for construction works. Large boulders left over within the weathered zones and on top of the ridges show the development of one-half to one meter thick, color and texture zoned weathering rinds. Mineralogical and geochemical changes accompanying rind development within quartzite containing more than 98% quartz were studied to better understand the weathering mechanisms under semiarid conditions of Delhi region.

Unweathered quartzite includes a few grains of muscovite, biotite, feldspar, tourmaline, calcite, and pyrite, together making up to 2%. Occasionally large crystals of pyrite occur in visible concentrations, up to several percents. In the weathering rind, the fresh rock is followed by a white compact zone, then a pink less-compact zone, and finally by a red friable outer zone. The main secondary mineral formed in the white zone is a few percentages of kaolinite by the breakdown of all primary minerals with the exclusion of quartz. The progressive weathering resulted in the loss of Ca, Na, and K with accompanying increase in the Chemical Index of Alteration (CIA); REE and Al show an increase in the white zone because of illuviation processes; the REE show no fractionation as a result of weathering (i.e., the REE patterns remain invariant excepting a slight flattening because of the greater mobility of HREE); and the outer friable zone has gained Fe. We suggest that all the mineral and chemical changes were effected by the dissolution of pyrite by rainwater; sulfate-bearing acidic solution broke down the primary silicates and quantitatively mobilized the REE toward the clay-forming weathering front; Fe^{2+} in solution reacted with quartz grain surfaces to form hydrous ferrous silicate layers; these layers broke down in near-surface oxidizing conditions to form goethite (red-coatings), and the silica was released to the solution [2]. Therefore, the outer part became friable and gained Fe as ferric oxi-hydroxide coatings. Thus the presence of sulfides, albeit present in small amounts, makes quartzite weatherable even under semi-arid conditions for the terrain to acquire a rugged topography.

References: [1] Wray R. A. L. (1997) *Earth Sci. Rev., 42,* 137–160. [2] Morris R. C. and Fletcher A. B. (1987) *Nature, 330,* 558–561.

NON-CONSERVATIVE MOLYBDENUM BEHAVIOR IN SEAWATER.

C. B. Tuit[1] and G. E. Ravizza[2], [1]Mail Stop 8, Woods Hole Oceanographic Institution, Massachusetts Institute of Technology/Woods Hole Oceanographic Institution Joint Program, Woods Hole MA 02543, USA (ctuit@whoi.edu), [2]Mail Stop 22, Department of Geology and Geophysics, Woods Hole Oceanographic Institution, Woods Hole MA 02543, USA.

Introduction: The current literature holds that Mo is conservative in seawater, despite its role as a critical micronutrient [1,2]. Molybdenum is utilized in both nitrogenase, the enzyme responsible for N fixation, and nitrate reductase, the enzyme required for denitrification. Cells that are actively fixing N require 125× more Mo than cells with access to a N source [3]. This implies that regions of active N-fixation may exhibit Mo depletions. Nitrate reductase requires 30-fold less Mo than nitrogenase, but it is an extremely common enzyme, required by all organisms that use nitrate as a N source [4]. In suboxic regions, where nitrate becomes the terminal electron acceptor, the nitrate reductase activity may became large enough to drawdown dissolved Mo from the water column. Previous measurements of Mo profiles in the North Pacific, a region where water-column denitrification is common, hint at subtle variations in the upper 300 m, though Collier determined the profile was conservative within sample precision [1]. This study reexamines Mo water-column profiles in regions of active N-fixation and denitrification using a high-precision method in an attempt to reveal water-column variations not resolvable by previous techniques.

Methods: Molybdenum seawater samples were preconcentrated using an ion exchange method and concentrations were determined by isotopic dilution. Isotopic ratios were measured via inductively coupled plasma mass spectrometry (ICP-MS). Five- to 15-mL seawater samples were spiked with a known mass of ^{95}Mo, 100 µL of H_2O_2 and gently heated for 12 h to ensure isotopic equilibration. After spiking, Mo was concentrated and separated from sea salts using a chelex ion exchange resin. Procedural column blanks are <0.13% of the total analyte. Sample reproducibility is limited by uncertainty in the measured ratio associated with instrumental mass bias (preferential detection of the heavy ions) that ranges from 0.5 to 3.0%/amu. Spectra free of isobaric interferences and ratio standard errors less than ±0.4% allow us to correct for mass bias on a sample by sample basis. The mean difference between duplicate and triplicate analyses was ±0.5%.

Results: This method was used to examine the Mo vertical profile at a station in the Sargasso Sea (SS) and another in the Eastern Equatorial Pacific (EEP).

Sargasso Sea. This site was chosen to look for Mo drawdown associated with active N-fixation. This profile was collected in March 1998, at 25°60'N 70°04'W. Based on the observance of Trichodesmium, an important N-fixing cyanobacterium, and nearly complete depletion of nitrate + nitrite in the surface waters [5], this site is thought to support active N-fixation. The Mo profile at this site, however, is conservative at the 1% level. The salinity normalized mean Mo concentration (n = 17, excluding 1 outlier) is 107 nM ± 0.5% (1 s.d.). The lack of dissolved Mo depletion in these surface waters argues against the use of Mo as a sensitive tracer of N-fixation; however, a conservative profile may still allow us to set upper limits on the amount of N-fixation possible.

Eastern Equatorial Pacific. High-precision Mo analyses of seawater collected in November 1992 at 2°S, 95°W reveal Mo water-column variations on the order of 5 nM. These variations are consistent in both size and shape with those reported by Collier [1]. This station is in a high-nutrient, low-chlorophyll region with ample nitrate in the surface waters, implying little or no N-fixation. The water column has a broad O-depleted zone. The Mo maximum occurs within the O-depleted zone, directly below the nitrite maximum, which is consistent with Mo utilization by denitrifying bacteria followed by remineralization. This data, however, are qualitative and cannot preclude particle uptake by other processes, such as Mo cycling with Mn oxides either *in situ* or in waters advected from the continental margin. The salinity normalized mean Mo concentration for samples below 200 m (n = 8) was 108.5 nM ± 0.8% (1 s.d.).

Conclusions: There is excellent agreement between these data and that of Collier [mean concentration = 107 nM ± 2.3% (1 s.d.)], attesting to the accuracy of these data. The lack of significant variation in the SS data, and the strong resemblance between the EEP and Collier [1] profiles, argues against explaining the EEP variability in terms of random errors. Based on the relationship of the Mo and nitrite peaks, we argue that the Mo variations are the result of uptake due to dissimulatory nitrate reduction followed by rapid regeneration.

The long-standing belief that Mo is conservative in seawater has led to the neglect of this important micronutrient. Molybdenum water-column variations may provide insight into enzyme systems important to the N cycle. Molybdenum, like Fe, does not appear to fit the nutrient/scavenged/conservative paradigm so prevalent in marine chemistry. We suspect that Mo profiles may not be modeled using a single Mo:C ratio (a pseudo-Redfield approach) but will be influenced by specific enzymatic processes.

References: [1] Collier R. W. (1985) *Limnol. Oceanogr., 30,* 1351–1354. [2] Morris A. W. (1975) *Deep Sea Res., 22,* 49–54. [3] Sprent J. I. and Raven J. I. (1985) *Proceed. Royal Soc. Edinburgh, 85B,* 215–237. [4] Raven J. A. (1988) *New Phyto., 109,* 279–287. [5] Cavender-Barnes K. K. (1999) Ph.D thesis, Massachusetts Institute of Technology.

EXPERIMENTAL STUDY OF THE ALTERATION PROCESS OF BASALTIC GLASS UNDER HIGH PARTIAL PRESSURE OF CARBON DIOXIDE.

S. Utsunomiya and T. Murakami, Mineralogical Institute, University of Tokyo, 7-3-1 Hongo, Bunkyo-ku, Tokyo 113-0033, Japan (utu@min.s.u-tokyo.ac.jp).

Introduction: In the Archean, the interaction among rocks, water, and atmosphere played an important role for long-term stabilization of the Earth surface's environments. A large amount of CO_2 in the early Earth's atmosphere was consumed by weathering of submarine basalt and continental silicates containing Ca and Mg resulting in carbonate precipitation. There are a few experimental studies about the interaction between basalt and water under high partial pressure of CO_2. A 16-fold increase CO_2 content (P_{CO_2} of $10^{-2.3}$ atm) in solution raised a dissolution rate by a factor of 2. However, the pH of the solution varied during the dissolution [1]. We carried out an experiment of basaltic glass dissolution under high P_{CO_2} (2 atm) at a constant pH using our newly developed apparatus for this study, in order to elucidate the dissolution rate and the process of basaltic glass alteration under high P_{CO_2} compared to those under the present CO_2 level. The temperature of the early Archean ocean (~3.8 Ga) is estimated to be close to 100°C [2] and the pH moderately acidic [3]. The conditions of the experiment of this study were set to be similar to the Archean conditions.

Methods: Starting material for the basaltic glass was made of the natural basaltic lava in Miyake Island, Japan. It was crushed into the powder, melted at 1400°C, and then quenched. The product glass was crushed, sieved into 106 < diameter < 212 μm, and then ultrasonically washed in acetone. The average chemical composition (wt%) of the glass is SiO_2 58.95, Al_2O_3 15.64, *FeO 8.74, CaO 8.76, MgO 3.62, Na_2O 2.12, K_2O 0.65, TiO_2 1.10, MnO 0.35, *all Fe as FeO. The surface area of the specimen was measured to be 0.0910 m²/g by BET method. The hydrothermal experiment was done in a teflon batch equipped with P_{CO_2} controlling aperture [4]. The partial pressure of CO_2 was kept at 2.0 atm, which is equivalent to $10^{3.8}$ PAL (present atmospheric level). Super pure water with a lithium acetate (0.03 mol/L)-acetic acid was used as an initial solution and pH was adjusted to 5.0 at room temperature. The ratio of surface area to solution (cm²/mL) was adjusted to 10. The temperature was 100°C and the duration was 1–32 d. Cation concentrations after reaction were analyzed by inductively coupled plasma atomic emission spectrometry (ICP-AES), and by inductively coupled plasma mass spectrometry (ICP-MS). Secondary minerals were observed by field emission scanning electron microscopy (FE-SEM) with electron-dispersive X-ray spectrometry (EDX) and analyzed by powder X-ray diffraction (XRD).

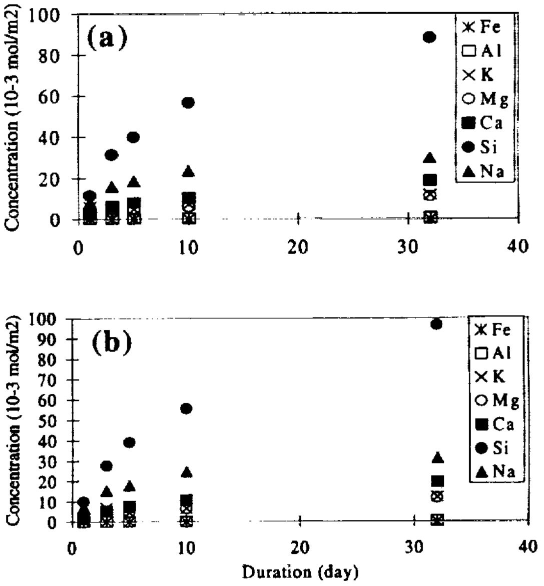

Fig. 1.

Results and Discussion: Figures 1a and 1b shows cations concentration vs. duration under P_{CO_2} = $10^{-3.5}$ and 2.0 atm respectively. These figures show that there is no difference in releasing major elements between two partial pressures of CO_2. Each dissolution rate of basalt was calculated based on the released Na during the period from 3 to 10 d. The rates were evaluated to be 1.57 and 1.94 (g/m²/d) at P_{CO_2} of $10^{-3.5}$ and 2.0 atm, respectively. These values do not have a significant difference if the errors during the analysis are considered. XRD analyses did not provide any information about secondary minerals. However, secondary minerals were observed by SEM to be precipitated over the fresh basaltic glass from 1 d under both P_{CO_2}. Two types of secondary minerals were observed; a large amount of ball-shaped materials (a few tens of nanometers in diameter) directly on the fresh glass, and aluminum (-oxy)-hydroxide (several micrometers). There wasn't any difference in the weathering processes between the two P_{CO_2} during 32 d. These results suggest high P_{CO_2} in the atmosphere does not affect on the dissolution rate and the weathering process of basaltic glass. This indicates that the alteration process of a sea-floor basalt in the Archean was same as that in the present time.

References: [1] Brady P. V. et al. (1997) *GCA, 61,* 965–973. [2] Kating J. F. et al. (1986) *Science, 234,* 1383–1385. [3] Grotzinger J. P. et al. (1993) *J. Geol., 101,* 235–243. [4] Utsunomiya S. et al. (1999) *Mineral. J., 21,* 1–8.

CARBONATITES AT 200 KILOMETERS: QUENCHED MELT INCLUSIONS IN MEGACRYSTALLINE LHERZOLITE XENOLITHS, SLAVE CRATON, CANADA.

E. van Achterbergh[1], W. L. Griffin[1], K. Kivi[2], N. J. Pearson[1], and S. Y. O'Reilly[1], [1]National Key Centre for the Geochemical Evolution and Metallogeny of Continents, Department of Earth and Planetary Science, Macquarie University, NSW 2109, Australia (evachter@laurel.ocs.mq.edu.au), [2]Kennecott Canada Exploration Inc., 1300 Walsh Street, Thunder Bay ON P7E 4X4, Canada.

Introduction: Megacrystalline lherzolite xenoliths from the A154 kimberlite (Slave Craton) were derived from the lower lithosphere (~1235°C and 60 kbar) and contain abundant inclusions of quenched carbonatite melt.

This study presents the first major- and trace-element data for a deep-seated carbonatite melt, which was shielded from interaction with mantle and crustal wall-rock by the clinopyroxene (cpx) host as it traveled to the surface.

Sample Description: Globular carbonate-rich inclusions (0.8–5.8 mm in diameter) occur within large (>2 cm) crystals of Cr-diopside. Orthopyroxene (opx) exsolution parallels the cleavage planes of the host cpx and the opx lamellae extend to the edges of the inclusions, indicating that the entrapment of the globules preceded the opx exsolution. The inclusions consist of Ti-rich phlogopite (phl), Cr-spinel (sp), radiating "spinifex" olivine (ol), and rare perovskite set in a matrix of fresh calcite (Fig. 1). Calcite occurs as two microstructural types: elongate randomly-oriented euhedral crystals (cc-1) and interstitial calcite (cc-2). The globular shape of the inclusions indicates that they were molten when trapped in the cpx; this entrapment probably occurred at >1235°C, as suggested by the presence of opx exsolution in the cpx. The quenched microstructures and the thermodynamic instability of calcite at the calculated mantle pressures imply that the constituent phases crystallized during transport in the kimberlite, calcite crystallizing last at low pressure.

Similar cpx megacrysts from the same locality also contain trapped globules of ultramafic silicate composition (kimberlite?), and some of these show unmixing of silicate and carbonate into concentric rings. In some cases, globules of ultramafic silicate, sulfide, and carbonate composition occur together in the same cpx grain.

Carbonatite Composition: Carbonatite melt compositions were calculated for each inclusion using electron microprobe analyses of the constituent phases and modal abundances derived from image analysis. This yields a wide range of compositions along the join between calcium- and magnesium carbonatites. The variation may reflect initial heterogeneity of the carbonatite melt and/or sampling of different volumes of the melt during sectioning. The average melt composition (in wt%) is SiO_2 = 12.0, TiO_2 = 0.22, Al_2O_3 = 0.88, Cr_2O_3 = 0.29, FeO = 2.6, MnO = 0.17, MgO = 12.5, CaO = 37.1, Na_2O = 0.03, K_2O = 0.72, NiO = 0.05, Cl = 0.002, F = 0.02, SrO = 1.2, BaO = 1.8, P_2O_5 = 0.15, and CO_2 = 30.5. The ca# varies from 40.7 to 87.2, reflecting the modal abundance of olivine. In contrast, the mg# is constrained between 88.4 and 90.2, consistent with equilibrium between the carbonatite melt and mantle peridotite. The calcite does not contain any $Mg(CO_3)$; all Mg and Fe in the original melt is concentrated in the olivine and phlogopite.

Strontium and Ba are concentrated in cc-1, depleting the late interstitial cc-2 in these elements. Preliminary trace-element analyses indicate that the carbonatite is depleted in Nb and rare earth elements compared with carbonatites associated with alkaline igneous complexes. Olivine in the inclusions is depleted in Ni (average = 1160 ppm).

Discussion: This carbonatite is enriched in Si and depleted in Na compared with those produced experimentally by partial melting of carbonated peridotite. Its association with globules of ultramafic silicate melts suggests that the carbonatite was derived from an asthenospheric silicate-carbonate melt [e.g., 1] that unmixed near the base of the lithosphere. These unusual samples offer new insights into the processes that produce both kimberlites and carbonatites, and on their metasomatic effects in the lithosphere.

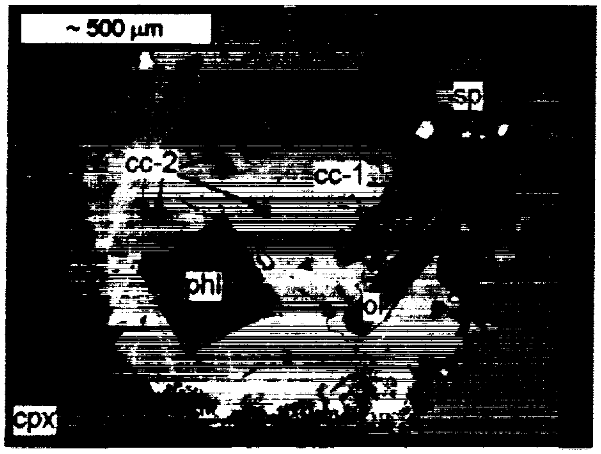

Fig. 1. Backscattered electron image of a carbonatite melt inclusion within a megacrystalline cpx grain; abbreviations as in the text.

Reference: [1] Wyllie P. J. (1980) *JGR, 85,* 6902–6910.

GLITTER: ONLINE INTERACTIVE DATA REDUCTION FOR THE LASER ABLATION INDUCTIVELY COUPLED PLASMA MASS SPECTROMETRY MICROPROBE.

E. van Achterbergh[1], C. G. Ryan[2,1], and W. L. Griffin[1,2], [1]National Key Centre for the Geochemical Evolution and Metallogeny of Continents, Department of Earth and Planetary Science, Macquarie University, NSW 2109, Australia (evachter@laurel.ocs.mq.edu.au), [2]Commonwealth Scientific and Industrial Research Organisation, Exploration and Mining, 51 Delhi Road, North Ryde, NSW 2113, Australia.

Introduction: The laser-ablation ICP-MS microprobe (LAM-ICP-MS), with its capability for rapid, sensitive, spatially resolved *in situ* trace-element analysis, will have the same impact on the geosciences as the spread of the electron microprobe (EMP) did in the 1970s. Until now, however, it has lacked the online, real-time data reduction that was a major factor in the rapid spread of EMP laboratories. To meet this need, GEMOC has developed GLITTER, the GEMOC Laser ICP-MS Total Trace Element Reduction software package. It gives the analytical results within seconds of data acquisition, and lets the operator use that input to guide further analytical strategy. GLITTER also features linked graphics and analysis tables, allowing rapid assessment of data quality.

The Structure of GLITTER: GLITTER consists of five main interactive user interfaces (windows): (1) The "GLITTER" window, containing the main menu options and the table of results; (2) the "Standards" window, where the user enters the values of the internal standard(s); (3) the "Review" window, where the time-resolved signals are viewed and integration intervals are selected; (4) the "Options" window, which selects customized calculation options (e.g., the type of yield interpolation across the standards or the background-fitting procedures); and (5) the "Plot" window(s), where data are visualized in various ways.

Theory: Trace-element concentrations are calculated using the following relationships

$$\mathrm{conc}_{ni} = (\mathrm{cps}_{nij}/\mathrm{abundance}_j)/(\mathrm{yield}_{ni})$$

where conc_{ni} = concentration of element i in analysis n, cps_{nij} = mean count rate (background-subtracted) of isotope j of i in analysis n, $\mathrm{abundance}_j$ = abundance of isotope j, and yield_{ni} = cps/ppm of i in analysis n, calculated by

$$\mathrm{yield}_{ni} = \mathrm{yield}_{ns} \times {}^{\mathrm{Int}(n)}(\mathrm{yield}_i/\mathrm{yield}_s)^{\mathrm{std}}$$

where yield_{ns} = cps/ppm of the internal standard s in analysis n, ${}^{\mathrm{Int}(n)}(\mathrm{yield}_i/\mathrm{yield}_s)^{\mathrm{std}}$ = the ratio of the yield of i to the yield of s in the standards, interpolated to analysis n. The results, as well as error estimates, minimum detection limits, fractionation trends, chondrite normalized values, etc., are displayed on demand in the table or plots and can be written to a text file.

The "Review" Window: Selection of background and signal intervals from the time-resolved signal is the key to rapid and accurate online analysis: this is done in GLITTER's unique "Review" window (Fig. 1). Two displays in "Review" show the time-resolved signals of the current analysis. The upper display consists of rows of pixels, each row representing the variation of the signal with time for a single isotope, with intensity shown by color brightness (shades of gray in Fig.1). This gives an immediate and highly visible indication of any spikes in the data, or heterogeneity in the sample, for one or more isotopes. The lower display shows the time-resolved signal for a single isotope, selected using the horizontal marker in the upper display.

GLITTER initially calculates the results with default integration intervals, using a simple algorithm to avoid obvious heterogeneity and large spikes. Users can reselect the integration intervals for each analysis by simply dragging any of the four vertical markers in the "Review" window. As the markers are moved, the data are dynamically recalculated and updated in the results

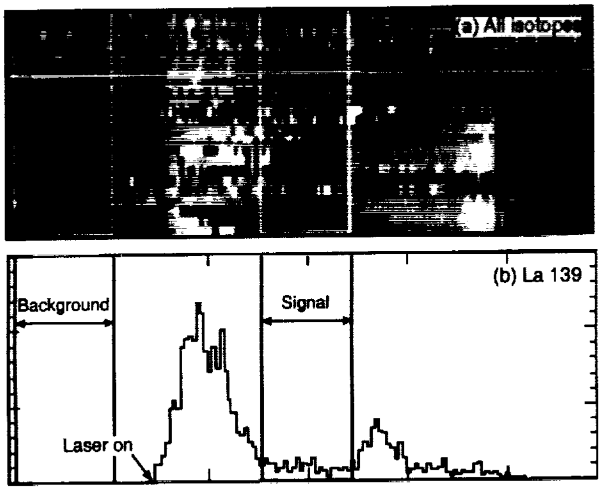

Fig. 1. GLITTER's "Review" window showing the time-resolved signals (x-axis = time, y-axis = count rate) for an orthopyroxene grain where a REE-rich inclusion was ablated near the start of the analysis. Note the high intensity area in the top half of (a), where the signals for the rare earth elements are shown. The integration interval was selected to avoid this part of the signal. The lower window (b) shows the signal for ^{139}La.

table and in any open "Plot" window(s). The use of GLITTER has led to a marked increase in the productivity of the LAM-ICP-MS by allowing assessment of results before selection of the next point and eliminating off-line processing. More details are available at www.es.mq.au/GEMOC/.

HYDROGEOCHEMISTRY OF MADEIRA ISLAND.

C. H. van der Weijden[1], J. P. G. Loch[1], and F. A. L. Pacheco[2], [1]Department of Geochemistry, Utrecht University, P.O. Box 80.021, 3508 TA Utrecht, The Netherlands (chvdw@geo.uu.nl; jpgl@geo.uu.nl), [2]Department of Geology, Universidade de Tras-os-Montes e Alto Douro, 5000 Vila Real, Portugal (fpacheco@utad.pt).

Introduction: In the summer of 1997, surface waters and groundwaters were sampled on Madeira. The objective was to explain the composition of these waters.

Geography: Madeira, situated in the north Atlantic Ocean 900 km southwest of Lisbon, is made up of Pliocene to Pleistocene lava flows and pyroclastic deposits. The island rises steeply from the sea; the highest point (1862 m) lies at a distance of only 11 km from the southern shore and 7 km from the northern shore. A great range of climatic conditions exists. The temperature gradient between sea level and the mountains is 10°C. The annual precipitation ranges from 500 (southern coast) and 1000 (northern coast) to 3000 mm in the highlands. At altitudes between 1200 and 1500 m, misty conditions prevail, but already from 500 m and up, it can be cloudy during daytime. The integrated annual precipitation is ~750 Mm^3, the storage capacity is estimated to be 200 Mm^3. This indicates short contact times between water and rocks.

Petrology: In the areas of sample collection, alkali olivine basalts/basanites and hawaiites are the dominant rocks, with intercalation of pyroclastic units. In some places, altered ash layers overlie the surface. Volcanic ashes and tuffs are severely weathered, whereas the massive lava flows are more weathering resistant. Phenocrysts consist predominantly of olivine and pyroxene. In the groundmass, plagioclase, augite, olivine, and dark minerals prevail.

Soils: In our sampling area, the soils are mostly haplic and umbric andosols, and chromic and dystric cambisols. Major inorganic components are Al-allophane, silico-aluminous and ferruginous amorphous materials, kaolinite-group minerals, gibbsite, vermiculite/chlorite and micas. At pH ≤ 5, Al-organic complexes can be formed. The relative abundances of the soil components depend on the composition of the parent rock, weathering stage, and hydrological conditions.

Sampling and Analysis: We collected 48 water samples, they were analyzed by inductively coupled plasma atomic emission spectroscopy (ICP-AES) for Ca, Mg, K, Na, Si, Fe, and Al, by ion-chromatography for Cl, SO_4, and NO_3, and by titration for alkalinity. Overall quality was checked by the charge balance (<10% off). In some samples δD and $\delta^{18}O$ were analyzed by mass spectrometry.

Results and Discussion: Waters with the lowest conductivities occur in the central highlands. The relative contribution of marine aerosols to the water compositions decreased from lower to higher altitudes, whereas the relative as well as the absolute contributions by water-rock interactions increased. Despite efforts to avoid inclusion of waters affected by agriculture, quite a few samples had NO_3 concentrations above background values. The Al and Fe concentrations were practically all below the detection limits, indicating their immobility in the weathering processes and in accordance with the described soil mineralogy. The δD and $\delta^{18}O$ values decreased significantly with increasing altitude (lower T's). The pCO_2 values, calculated on the basis of alkalinity, field-pH, and *in situ* T, were above the atmospheric value. Corrections for the marine contributions on the basis of the Cl concentrations showed that there were only minor excesses in SO_4 concentrations.

Using a clustering program, introduced by [1], on the residual composition, 10 subgroups of water samples were identified. They are primarily defined by differences in their alkalinities, but are also expressed in differences of molar ratios of the various components. The marked differences between ratios of HCO_3^- and $H_2SiO_3^0$ are indicative of the degree of weathering of the parent rocks. Differences in Ca/Na are partly due to compositional variations in plagioclases. Rather high Mg concentrations and small variations in Ca/Mg indicate that these waters are not in equilibrium with smectite, one of the incipient products of weathering of olivine and plagioclase.

Conclusion: Apart from the marine contributions, the water chemistries are mainly the result of weathering of olivine, pyroxene, and Ca-rich plagioclase and formation of soil components representative of severe weathering as described above.

References: [1] Pacheco F. and van der Weijden C. H. (1996) *Water Resour. Res., 32,* 3553–3570.

HIGH-RESOLUTION LEAD AND NEODYMIUM RECORDS OF NORTHEAST INDIAN OCEAN SEDIMENTS OVER THE PAST 150 ka: FLUCTUATIONS IN THE MONSOON AND HIMALAYAN WEATHERING ASSOCIATED WITH NORTHERN HEMISPHERE GLACIATION.

D. Vance[1] and K. W. Burton[2], [1]Department of Earth Sciences, The Open University, Walton Hall, Milton Keynes, MK7 6AA, UK (d.vance@open.ac.uk), [2]Département des Sciences de la Terre, UMR 6524 Centre National de la Recherche Scientifique, Université Blaise-Pascal, 5 Rue Kessler, 63038 Clermont-Ferrand, France.

Introduction: The radiogenic isotopes of Sr, Nd, and Pb have long been used to investigate the provenance of marine sedimentary products. More recently, it has been realized that the record of short residence-time elements, such as Nd and Pb in ferromanganese crusts, preserve information on the long-term variability of continental weathering and oceanic circulation. Furthermore, we have recently shown that the high-resolution record of Nd available from foraminifera records the short-term response of continental weathering rates [1] and hydrographic regime [2] to recent climate fluctuations associated with glaciation. For example, foraminifera from the past 150 ka from ODP site 758A in the northeast Indian Ocean record changes in the Nd-isotopic composition of surface water on the order of 2 ε units. These fluctuations are in phase with the global O-isotopic record, with more unradiogenic Nd obtained during interglacials and radiogenic values characterizing glacials. These variations have been attributed to changes in the rate of runoff from the Himalaya in response to fluctuations in the strength of the southwest monsoon. Here we present Nd and high-precision Pb-isotopic data, the latter obtained by multiple collector inductively coupled plasma mass spectrometry (MC-ICP-MS) [3], on the carbonate-rich bulk sediments from

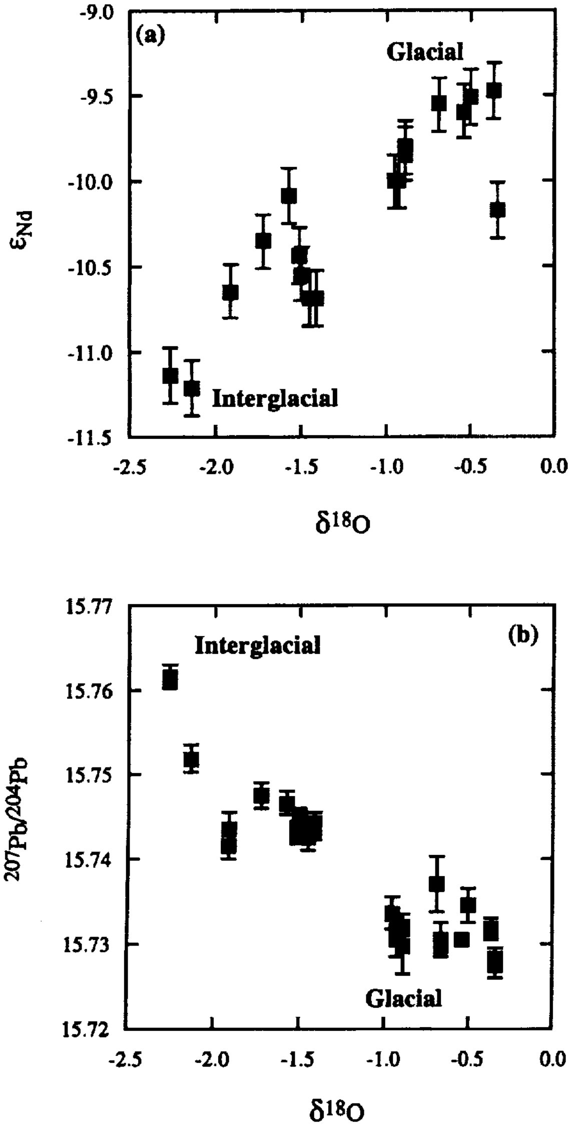

Fig. 1. Neodymium- and Pb-isotopic composition of 758A bulk sediments for the past 150 ka plotted against $\delta^{18}O$ in *G. sacculifera* from the same horizons.

this site that further document rapid fluctuations in weathering due to climate change over the past 150 ka.

Results: The Nd data for the bulk sediments (Fig. 1a) show an identical pattern of change to the foraminifera except that it is shifted to Nd-isotopic compositions about 1–2 ε units lower. Glacial sediments are characterized by ε_{Nd} of about −9.5 whereas interglacial values are around −11.5. The Pb data (Fig. 1b) also show similar patterns of change such that interglacial periods are characterized by Pb with high $^{208}Pb/^{204}Pb$, $^{207}Pb/^{204}Pb$ (Fig. 1b), and $^{206}Pb/^{204}Pb$, and low $^{207}Pb/^{206}Pb$. It is important to note, however, that the total variation in the Pb-isotopic compositions is small. For example, the range in $^{207}Pb/^{204}Pb$ is about the same as a typical error on a thermal ionization mass spectrometry (TIMS) Pb analysis. However, the resolution with the new plasma-source instruments is more than an order of magnitude better so that these small differences can be resolved.

Discussion: The Himalaya are characterized by radiogenic Pb and unradiogenic Nd similar to the values reported here for interglacial sediments. Thus these data further document the influence of monsoonal fluctuations associated with northern hemisphere glaciation on the supply of material from the Himalaya to the northeast Indian Ocean. The nature of the source of the material characterizing the glacial periods remains uncertain, but the Nd-and Pb-isotopic compositions of these sediments during glacial times is very similar to those characteristic of deep water in the open Indian Ocean over the past 5 m.y.

References: [1] Burton K. W. and Vance D. (1999) *Science,* submitted. [2] Vance D. and Burton K. W. (1999) *Science,* submitted. [3] Vance D. and van Calsteren P., this volume.

PRECISE LEAD-ISOTOPIC ANALYSIS BY MULTIPLE COLLECTOR INDUCTIVELY COUPLED PLASMA MASS SPECTROMETRY: LONG-TERM REPRODUCIBILITY AND COMPARISON WITH DOUBLE-SPIKE MEASUREMENTS.

D. Vance[1] and P. van Calsteren[1], [1]Department of Earth Sciences, The Open University, Walton Hall, Milton Keynes, MK7 6AA, UK (d.vance@open.ac.uk).

Introduction: Lead-isotopic analysis by thermal ionization mass spectrometry (TIMS) has traditionally been rendered difficult by the inability to internally normalize to an invariant isotopic ratio. However, two developments have ameliorated this situation. Firstly, the advent of double spikes has allowed an internal normalization procedure to be developed for thermal analyses [1,2]. Secondly, the advent of multiple collector inductively coupled plasma mass spectrometry (MC-ICP-MS) instruments, for which mass discrimination is indepedent of the chemistry of the analyte, now permits a normalization to be performed using an element with an overlapping mass range such as Tl [3–5]. In this paper we report data for Pb-isotopic analyses of SRM 981 and 982, as well as for geological samples, using a Nu Instruments MC-ICP-MS in order to assess long-term reproducibility of two different Pb-isotopic standards and to compare the data with recent measurements using double spikes.

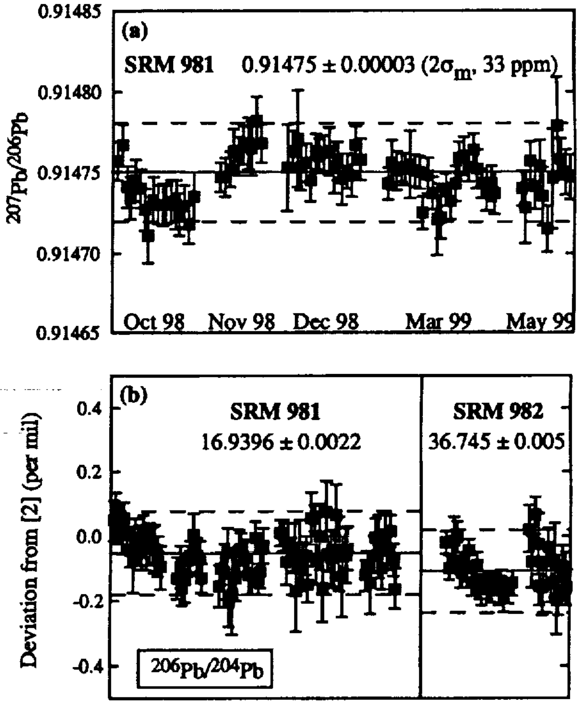

Fig. 1. (a) Lead-207/lead-206 ratios for SRM 981 normalized to a single $^{205}Tl/^{203}Tl$. Solid line: mean of all the analyses. Dashed lines ±2 standard deviations of all the data. (b) Measured $^{206}Pb/^{204}Pb$ for SRM 981 and 982, normalized to the same Tl-isotopic compostion and plotted as deviations from recent double-spike measurements [2].

Analytical Procedure: Solutions of SRM 981 and SRM 982 were analyzed more than 150 occasions over an eight-month period on a Nu Instruments mass spectrometer equipped with an MCN 6000 nebulizer. Typical sample use was 200–300 ng Pb, which gave total Pb beams of 30–50 pA for a 20-min analysis time. Raw data were corrected on line for Hg interference and mass fractionation using the measured ^{205}Tl/^{203}Tl ratio and an exponential law. In agreement with other studies [3–5], we have found that a ^{205}Tl/^{203}Tl-isotopic ratio higher than the generally accepted value is required to adequately normalize the Pb data. The ^{205}Tl/^{203}Tl ratio to which all the data in Fig. 1 is normalized is 2.38826 — about 500 ppm higher than the accepted value. This specific value for the Tl-isotopic composition was used to obtain a ^{207}Pb/^{206}Pb ratio that agrees with the most recent double-spike measurements of SRM 981 [2].

Results: There are three principal observations from this study: (1) The long-term reproducibility of Pb-isotopic measurements on MC-ICP-MS instruments is comparable with those achievable using double spikes. Figure 1a shows that the reproducibility for ratios involving the major Pb isotopes, in this case ^{207}Pb/^{206}Pb, is ~30 ppm and comparable to those achieved where an internal normalization is available (e.g., Sr, Nd). Reproducibility of the ratios involving ^{204}Pb are not as good (100–200 ppm) but are also comparable with double-spike analyses. (2) The second principal observation is that the Tl-isotopic composition required to normalize the ^{207}Pb/^{206}Pb ratio [2] is also adequate for the ^{207}Pb/^{204}Pb and ^{206}Pb/^{204}Pb ratios for 981 (e.g., Fig. 1b). In addition, this Tl-isotopic composition adequately reproduces the ratios for 982 (Fig. 1b) given by Todt et al. [1]. However, no Tl-isotopic composition can reproduce the Pb-isotopic compositions of Todt et al. [1] for both 981 and 982. (3) The exception to this are ratios involving ^{208}Pb. For the Tl-isotopic composition required to adequately normalize the isotopic ratios discussed above, the ^{208}Pb/^{204}Pb and ^{208}Pb/^{206}Pb ratios of both SRM 981 and SRM 982, measured by MC-ICP-MS, are consistently 200–400 ppm lower than those obtained in recent studies using double spikes [2]. The reason for this is unclear at present, but we note that a similar observation has been made by two other studies using two different MC-ICP-MS instruments [4,5].

References: [1] Galer S. J. G. and Abouchami W. (1998) *Mineral. Mag., 62A,* 491–492. [2] Todt W. et al. (1996) *Geophys. Monogr., 95,* 429–437. [3] Hirata T. (1996) *Analyst, 121,* 1407–1411. [4] Belshaw N. S. et al. (1999) *Int. J. Mass Spec. Ion Processes,* in press. [5] Rehkämper M. and Halliday A. N. (1999) *Int. J. Mass Spec. Ion Processes,* in press.

DISTRIBUTION OF CARBON AMONG ORGANIC-MINERAL FRACTIONS OF VERTISOLS AND ZONAL SOILS AS INFLUENCED BY BIOGEOCHEMICAL CONDITIONS.

A. Ya. Vanyushina[1,2], L. S. Travnikova[2], and R. C. O. Gaiego[1], [1]Moscow State University, Soil Science Faculty, Vorobievy Gory, Moscow, Russia (a_vanyushina@yahoo.com), [2]Dokuchaev Soil Institute, Pyzhevsky Per. 7, Moscow, Russia.

Introduction: The problem of C transformation in soils is hardly solved without studying its distribution over different organo-mineral (OM) soil components. This is because the character of mineral-phase impacts on the properties of these organic moieties and the rate of their mineralization.

Aim: To reveal the influence of bioclimatic and some geochemical soil-forming factors on the accumulation and quality of organic matter (OM) of Vertisols and zonal soils.

Objects: Vertisols and associated zonal soils from three climatic zones were considered. They include (1) temperate zone of (a) the pre-Caucasus, Stavropol'e — Pellic Vertisols (Vp) under native steep vegetation ("gilgai" complex), and arable Calcic Chernozem (Ck), (b) Moldova — arable Vp and Ck; (2) subtropical zone of the Trans-Caucasus, Georgia — arable Vp and Chromic Cambisol (Bc); and (3) tropical zone of Cuba — Vp under pasture, sugar corn, and forest and arable Rendzina (E).

Methods: Particle size and densimetric method of soil fractionation [1] is used for separation of OM of mineral soils into fractions. These fractions differ considerably in their association with clay minerals, turnover times, and hence their importance for C turnover. Two groups of products of OMin interactions, which include nearly whole totality of soil OM and subdivided into 3 fractions, have been separated from studying soils: light fraction (LF) group (LF1, density <1.8 g cm^{-3} and LF2, 1.8–2.0 g cm^{-3}), which is OM chemically unbounded with clay minerals, and clay group (CF) (particles <1 m 10^{-6}), which includes organo-clayey complexes. Carbon content and humic-fulvic acid (HA/FA) composition were determined for fractions. FTIR-spectroscopy was applied for analysis of the main fractions — LF1 and clay.

Results and Discussion: *Accumulation and distribution of carbon of organo-mineral fractions.* Carbon accumulation in LF of montmorillonitic Vp with equal amount of clay decreases from temperate to subtropical and tropical zones (from 1.2 through 0.33 to 0.11 g 100 g^{-1} soil), and C concentration in LF increases (38.0–46.3 to 32.4 and 31.4 g 100 g^{-1} fraction). Car-bon concentration in CF is low and varies slightly in these soils (1.2–1.97 g 100 g^{-1} fraction).

In comparison with zonal soils, the Vp of the different bioclimatic zone is characterized by several similar features: low level of C accumulation associated with LF as well as its quota in total C (0.33 g 100 g^{-1} soil and 27 g 100 g^{-1} C_t in Vp as compared to 0.74 and 37 in Bc). This is related to contrast hydrothermal regime and Na content in soil solutions.

Within each zone, arable and pasture Vp have lower levels of C accumulation associated with CF and LF and a low quota of C LF (4–11 g 100 g^{-1} C_t) as compared to natural Vertisols (14 g 100 g^{-1} C_t) as well as zonal soils (13.0 g 100 g^{-1} C_t). This is related to the differences in the intensity of mineralization between agricultural and natural soils in general, and a more intensive rate of LF mineralization in Vp as compared to zonal soils.

Peculiarity of fraction organo-mineral composition. For almost all soil pairs, the HA content in OM of LF of zonal soils exceeds that of Ve. On the contrary, the HA content of both LF and CF of Ve is closer than in zonal soils where the HA content of LF and CF differs dramatically (e.g., 80% and 83%; 41%, and 99% accordingly for LF and CF of Vp and E).

Fourier transform infrared (FTIR) spectra of clay fractions are similar, but the clay OM differs from LF OM with more homogenous composition. In LF of Ck the greater part of organic COO$^-$ bounds with Me-ions or the bound is stronger than in Vp (the shift of 1620–1610 cm^{-1} band in Vp to 1595 cm^{-1} [2]). LF of Vp is depleted with carbohydrates in comparison to Ck of the same land use (the 1050 cm^{-1} band).

Comparison of LF of soils of different land use. OM of soils under natural vegetation is enriched with carbohydrates and phenol compounds (the 1270 cm^{-1} and 1030–1100 cm^{-1} bands of gilgai Vp respectively) originating from plant residues.

LF of deep horizons. OM of the lowest parts of humic horizons seems to be more aromatic than that of the upper ones. This follows from the greater HA/FA ratio and intensive aromatic –C = C– stretching of samples from deep horizons.

Conclusions: The clay-bounded OM is controlled mainly by clay mineralogy of parent material, whereas free OM of LF by bioclimatic conditions. OM LF Ve is mineralized more intensively under agricultural use than those of zonal soils.

References: [1] Shaymukhametov M. Sh. et al. (1984) *Pochvovedeniye, 8,* 131–141. [2] Celi L. et al. (1997) *Soil Sci., 162,* 189–197.

DISSOLVED ORGANICS IN FORMATION WATERS FROM THE PANNONIAN BASIN, HUNGARY.

I. Varsanyi[1], Z. Karpati[2], J. M Matray[3], L. O. Kovacs[4], and A. Klopp[2], [1]Department of Mineralogy, Geochemistry and Petrology, University of Szeged, Hungary (varsanyi@geo.u-szeged.hu), [2]National Institute of Hygiene, Budapest, Hungary, [3]Department Stockage, ANTEA, BRGM, Orleans, France, [4]Hungarian Geological Survey, Budapest, Hungary.

Introduction: Different organic compounds in major or trace amounts are dissolved in waters. In shallow groundwater, the proportion of humic substances to total dissolved organics is up to 90%, mostly ~40%. In oil field waters, the dominant dissolved organic species up to 90% are short chain monocarboxylic acids [1,2]. Phenolic compounds as minor components were also identified in a detailed study on organic geochemistry of formation waters [3]. Thermal waters in the Pannonian Basin contain humic and fulvic acids, aliphatic hydrocarbons (C_{21}-C_{29}), alkylphenols, alkylbenzens, alkylnaftalens, light polycyclic aromatic hydrocarbons (PAH), and fatty acids [4]. The aim of the present work is to identify organic compounds dissolved in formation water and to establish their origin and history.

Geology: The study region is the southeastern part of Hungary, which represents the central part of the Pannonian Basin. The Pannonian Basin is filled with Neogene sediments. The Paleozoic-Mesozoic basement is overlain by 1000–3000-m-thick lower to middle Miocene layers formed in a marine to brackish environment, and by 1000–3000-m-thick Late Miocene (M_3Pa) lacustrine sediments. Infilling of the basin was continued by lacustrine and

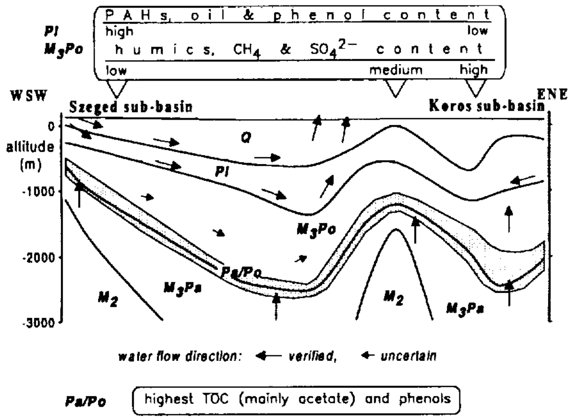
PAHs, oil & phenol content
high
low
humics, CH4 & SO4 2- content
low
medium
high
Pl
M3Po
WSW
ENE
Szeged sub-basin
Koros sub-basin
0
altitude (m)
-1000
-2000
-3000
Q
Pl
M3Po
Pa/Po
M2
M3Pa
M2
M3Pa
water flow direction: verified, uncertain
Pa/Po
highest TOC (mainly acetate) and phenols

Fig. 1.

deltaic sedimentation in the Pontian (M_3Po), and lacustrine and fluvial sedimentation in the Pliocene (Pl). During the Pleistocene (Q), fluvial sedimentation took place over the study area. As a result of tectonic events, the total thickness of sediments varies from 250 to 6000 m. In the M_3Po and Pl formations, oil and gas accumulations have been found [5].

Results: The water samples were collected in the depth interval of 75–2500 m with temperature ranging between 16° and 98°C. The study area was devided into three parts: the Szeged and Koros sub-basins and a high between them. The samples from the Pa/Po boundary (the deepest studied lithostratigraphic position) are considered as a separate group [6].

Both inorganic C and organic C (OC) contents contribute to the total dissolved C (TDC). In the Szeged sub-basin, the mean proportion of OC to TDC is 3.7%; this is 4.6% above the high, 7.7% in the Koros sub-basin, and 27.4% at the Pa/Po boundary. Humic substances, acetate, and propionate are present as major organics, alkylphenols and oil as minor organics, and PAH, benzene, alkylbenzene, and phenol as trace organics. In the shallower samples, the Q and Pl, layers in the Szeged sub-basin, and above the high, where the temperature is between 16° and 56°C, it is supposed that microbiological processes occur that form CO_2, humic substances and methane. In the deeper samples, between 65° and 135°C, monocarboxylic acids, phenol, alkylphenols, alkylbenzenes, and PAHs are formed, besides CO_2, humic substances, and methane, during thermal decomposition of the sediment organic material. PAHs, phenol, and oil are characteristic organic compounds in the Szeged sub-basin, and humic substances and methane in the more confined Koros sub-basin. At the Pa/Po boundary the dissolved organics are essentially represented by acetate + propionate with minor concentrations of PAHs, phenols, and methane.

Acknowledgments: This work was supported by the Hungarian Research Fund (OTKA T 026241).

References: [1] Willey L. M. et al. (1975) *GCA, 39,* 1707–1711. [2] Carothers W. W. and Kharaka Y. K. (1980) *GCA, 44,* 323–332. [3] Macleod G. et al. (1993) in *Geofluids* (J. Parnell et al., eds.), pp. 18–20, Geol. Soc., London. [4] Karpati Z. et al. (1996) *Egeszsegtudomany, 40,* 356–364. [5] Hetenyi M. (1992) *J. Petrol. Geol., 15,* 87–96. [6] Varsanyi I. et al. (1999) *Chem. Geol., 156,* 25–39.

INVESTIGATION OF THE ROLE OF NATURAL ORGANIC MATTER IN THE SORPTION OF COPPER IN AN OXISOIL PROFILE.

F. Vasconcelos[1], B. D. Honeyman[1], D. Macalady[2], and J. Ranville[2], [1]Division of Environmental Science and Engineering, Colorado School of Mines, Golden CO 80401, USA (fvasconc@mines.edu), [2]Department of Chemistry and Geochemistry, Colorado School of Mines, Golden CO 80401, USA.

Introduction: Oxisoils and sediments from lakes, rivers, and estuaries are among the natural systems with substantial fractions of Fe and Al (oxy)hydroxides. Laboratory studies of trace-metal sorption on to pure metal-(oxy)hydroxides and the subsequent surface complexation modeling (SCM) of these has received considerable attention over the last two decades. In spite of the vigorous overall activity in this area, there has been little application of SCMs to metal sorption by natural mineral assemblages [2,3]. Among the many factors that make the broad application of SCMs difficult is the presence of natural organic matter (NOM) [4].

In this study, the influence of NOM on the sorption of Cu by soil assemblages was investigated for a profile of a well-drained Typic Acriustox soil (i.e., Oxisoil) in a flat, undisturbed area in the Brasília National Park in Brazil. Soil samples were characterized at each horizon according to their mineralogy, organic C content, and percentage of Al_2O_3, Fe_2O_3, SiO_2, and TiO_2. Three samples from three different horizons (Hr) (i.e., A_1 = 19 cm, BW_2 = 197 cm, and C_2 = 540 cm) were chosen for detailed study. Samples were treated with NaOCl to remove NOM.

Experiments: Figures 1 and 2 show fractional Cu sorption by untreated oxisoil isolates and those with NOM removed, for two different soil horizons. Copper sorption to unaltered Hr A_1 is greater than for Hr BW_2. NOM removal decreases Cu sorption to Hr A_1 (Fig. 1) and enhances sorption to Hr. BW_2 (Fig. 2) and has no effect for Hr C_2 (data not shown). These results suggest that the role of soil organic matter in metal-ion sorption to mineral assemblages is complex, and that it may be difficult to generalize the behavior observed in more simpler systems [1] (i.e., monomineralic/dissolved organic

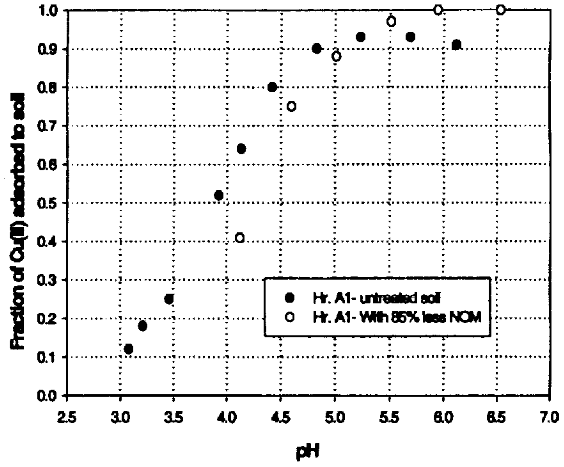

Fig. 1. Copper(II) adsorption edge onto soils from Hr. A1 before and after NaOCl treatment I = 0.01 M Cu(II) = 1 × 10^{-5} M soil/solution = 3.3 g/L.

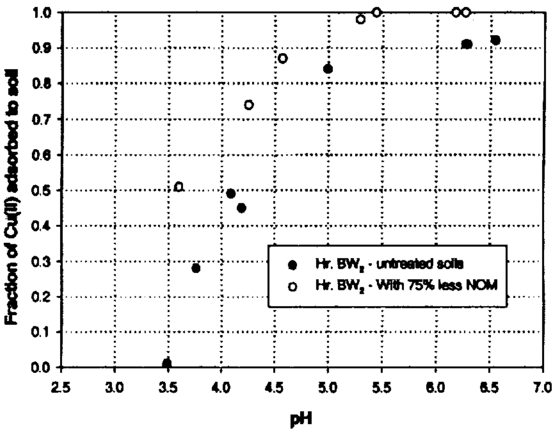

Fig. 2. Copper(II) adsorption edge onto soils from Hr. BW_2 before and after NaOCl treatment I = 0.01 M Cu(II) = 1 × 10^{-5} M soil/solution = 3.3 g/L.

matter/metal-ion systems). The diffuse double-layer model (DDLM) was used to simulate unaltered and altered experimental systems.

References: [1] Davis J. A. and Kent D. B. (1990) in *Minerals and Water Interface Ch. 5,* Mineralogical Society of America. [2] Davis J. A. et al. (1998) *Earth Sci. Tech., 32,* 2820–2828. [3] Weng X. et al. (1998) *Earth Sci. Tech., 32,* 870–875. [4] Tessier A. et al. (1996) *GCA, 60,* 387–404.

ISOTOPIC GEOCHEMISTRY OF SHARK TEETH AS INDICATORS OF ENVIRONMENTAL CONDITIONS.

T. W. Vennemann[1], E. Hegner[1], G. Cliff[2], and G. W. Benz[3], [1]Institute of Geochemistry, University of Tübingen, D-72076 Tübingen, Germany (torven@uni-tuebingen.de), [2]Natal Sharks Board, Private Bag 2, 4320 Umhlanga Rocks, South Africa, [3]Tennessee Aquarium, One Broad Street, Chattanooga TN 37401, USA.

The potential for using chemical and isotopic analyses of biogenic phosphates for paleoenvironmental reconstructions was recognized many years ago [1–3]. In contrast to biogenic carbonates, relatively little is known about species-specific fractionation effects for biogenic phosphate from fish, or variations in the isotopic composition as a function of changes in habitat and diet. These effects are important for fish, as they are nektic. In an attempt to address such effects, we have examined the O-, C-, Sr-, and Nd-isotopic compositions of teeth from ten different species, belonging to five different families and four different orders of sharks. The sharks were recently caught off the coast of Durban, South Africa, as well as from Prince William Sound (PWS), Alaska, and Victor Bay, Canada. Among marine phosphates, shark teeth are of particular interest because their record extends well back into the geologic past, they are readily classified on a taxonomic level, many fossil species have modern counterparts, the enameloid and dentine of such teeth are highly crystalline, and the teeth are continually replaced and hence are abundant in marine sediments.

The $\delta^{18}O$ values of tooth phosphate ($\delta^{18}O_P$) range from 20.4‰ to 22.8‰ (n = 45) for sharks caught off Durban. For each species, though, $\delta^{18}O_P$ values always agree to within 0.6‰, a variation that is just outside the analytical error of ±0.2‰. For samples where the dentine and the thin outer layer of enameloid were analyzed separately, no differences in the $\delta^{18}O_P$ values were observed. The isotopic data tend to reflect preferred habitat of the different species and hence the thermal structure of the water column. There are exceptions within one family, opening up the possibility of existence of species-specific fractionation effects. Temperatures calculated from phosphate-water fractionations correspond to those recorded for the Indian Ocean off Durban at depths between 10 and 300 m (24° to 16°C, annual variation ~2°C; salinity = 35‰).

In contrast to the O-isotopic composition of the phosphate, the C- and O-isotopic compositions of the carbonate in the apatite vary considerably. The $\delta^{18}O_C$ values are on average ~8.9‰ higher than the corresponding $\delta^{18}O_P$ values, but they may differ from this value by more than 1‰ (n = 30; 1σ = 0.9‰). The average fractionation of 8.9‰ is in good agreement with expected equilibrium fractionation between carbonate and coexisting phosphate [2]. The $\delta^{18}O_C$ values vary substantially within individual teeth, with values for enameloid and dentine varying non-systematically by up to 1‰.

Differences in the isotopic composition of C within a tooth are systematic, with enameloid always being enriched in ^{13}C compared to dentine. The difference in $\delta^{13}C$ values between carbonate in enameloid and dentine can be as large as 8‰. $\delta^{13}C$ values measured for enameloid (1.6–4.8‰) approach those that would reflect equilibrium with dissolved inorganic C in seawater (~1.5‰), while those for the dentine are substantially lower (between −6.4‰ and −2.3‰), the latter probably reflecting the diet of the particular shark species. The difference in $\delta^{13}C$ values between enameloid and dentine suggests derivation of C from different sources with a possible introduction or exchange of C after first formation of the enameloid.

The average $\delta^{18}O_P$ and $\delta^{18}O_C$ values of teeth from Greenland sharks (25.2‰ and 35.1‰ respectively) and Pacific Sleeper sharks (24.4‰ and 31.9‰) are very homogenous and significantly higher than those of teeth from sharks caught off Durban, reflecting significantly lower ambient water temperatures. $\delta^{13}C$ values for carbonate vary between −9.0‰ and −10.8‰.

The $^{87}Sr/^{86}Sr$ ratios of the teeth from Durban as well as PWS and Victor Bay are very homogenous and average 0.709165 with a 2σ standard deviation of 0.000012. Strontium contents vary from 1270 to 2100 ppm, and are very similar to those in well-preserved fossilized teeth [e.g., 4]. Seawater Sr is thus clearly incorporated during formation of the teeth. Concentrations of Sm and Nd were too low to obtain accurate isotopic ratios. This finding contrasts with much higher concentrations measured in fossilized teeth, supporting a postmortem incorporation of REEs in apatite of the teeth, presumably during early diagenesis.

References: [1] Longinelli A. (1965) *Nature, 207,* 716–719. [2] Longinelli A. and Nuti S. (1973) *EPSL, 19,* 373–376. [3] Kolodny Y. et al. (1983) *EPSL, 64,* 398–404. [4] Vennemann T. W. and Hegner E. (1998) *Palaeogeogr., Palaeoclimatol., Palaeoecol., 142,* 107–121.

HAFNIUM-ISOTOPIC COMPOSITION OF THE CRUST AND MANTLE DURING THE ARCHEAN: CONSTRAINTS ON CRUST-MANTLE EVOLUTION.

J. D. Vervoort[1], P. J. Patchett[1], F. Albarède[2], J. Blichert-Toft[2], M. E. Barley[3], T. S. Blake[3], C. W. Brauhart[3], M. G. Green[4], and R. J. Thériault[5], [1]Department of Geosciences, University of Arizona, Tucson AZ 85721, USA (vervoort@geo.arizona.edu), [2]Ecole Normale Supérieure de Lyon, 69364 Lyon Cedex 7, France, [3]University of Western Australia, Nedlands, WA 6907, Australia, [4]University of Sydney, Sydney, NSW 2006, Australia, [5]Geological Survey of Canada, 601 Booth Street, Ottawa ON K1A 0E8, Canada.

Important constraints on crust-mantle evolution have come from the Nd-isotopic record, which shows that the Earth differentiated into high Sm/Nd (depleted mantle) and low Sm/Nd (crust) reservoirs beginning early in its history. The timing and extent of this differentiation and the evolution of the different reservoirs, however, have been obscured by noise in the Nd record resulting from the inclusion of samples, particularly Archean, with poor age constraints and also by samples whose isotopic systems have not remained closed throughout their history. Establishing an accurate isotopic record of the Earth is crucial for refining models for mantle depletion and crustal growth through time.

The ability of multiple collector inductively coupled plasma mass spectrometry (MC-ICP-MS) to analyze Hf isotopes routinely in a wide range of samples now allows us to use a combined Sm/Nd-Lu/Hf-isotopic approach to resolve the complexities of this isotopic record. An integrated Hf- and Nd-isotopic approach is a powerful method because Sm/Nd- and Lu/Hf-isotopic systems behave coherently in nearly all crust and mantle environments. This has produced, over Earth's history, positively correlated arrays for both mantle and crustal rocks that are identical to a first-order approximation [1]. A decoupling of these two systems, when it occurs, is a strong indicator that there has been a disturbance to either (or both) systems.

We have analyzed a diverse collection of whole-rock samples from the Canadian Shield and the Pilbara Craton of Western Australia in order to evaluate the Archean record. The Canadian samples include low-grade basalts, komatiites and evolved rocks from the Abitibi, Wawa, and Wabigoon subprovinces of the Superior Province, and gneisses from the Churchill Province [2]. These range in age from ~2.7 (Abitibi and Wawa) to ~3.1 Ga. (Churchill). All samples are dominated by positive ε_{Hf} values (Abitibi and Wawa: +3.3 to +5.3 at 2.7 Ga; Wabigoon: +2.4 to +4.7 at 2.9 to 3.0 Ga). The ages of the Churchill samples are not well constrained, but ε_{Hf} values are all positive at 3.12 Ga.

The samples from the Pilbara, in contrast, do not have a dominantly depleted mantle character. A suite of 10 samples from the 3.24-Ga Panorama Formation [3] has consistent slightly negative initial ε_{Hf} values (8 samples −0.9 to −0.2; 2 samples at 1.8 and 2.4). Two suites of well-preserved, low-grade ~3.5-Ga basalts from the Pilgangoora belt [4] also have initial ε_{Hf} values close to zero. Basalts from the Coonterunah Group (3515 Ma) [5] have dominantly positive ε_{Hf} values (1.6 to 2.9; one sample at −2.3), whereas basalts from the slightly younger Warrawoona Group (3462 Ma) [5] are dominantly negative (−0.9 to −0.2; one sample at 2.4). A suite of samples from the Fortescue Group in the Nullagine basin of the Pilbara [6] has a wide range of initial ε_{Hf} values (−4.5 to +2.0) at 2.77 to 2.71 Ga, indicative of older crust involvement in the generation of these basalts.

The differences in the isotopic character of these two Archean cratons seem to be easily explained by the presence of significant volumes of older crust in the Pilbara and the paucity of older crust in the Superior Province, even though mantle differences cannot be discounted. It seems possible that the mantle may be quite heterogeneous on a global scale throughout the Archean. The majority of juvenile rocks of the Superior Province have been derived from a mantle that is fairly homogenous (with initial ε_{Hf} values of 3 to 5 at 3.0–2.7 Ga.). The mantle sources for the Pilbara may be considerably less depleted and more heterogeneous. This is consistent with the Pb-isotopic compositions of galenas in Pilbara's volcanogenic massive sulfide deposits that are more evolved and heterogeneous than their Superior Province counterparts [7].

Similar differences exist in the early Archean. Hafnium-isotopic data from both whole rocks [8] and zircons [9] from the 3.7–3.8-Ga Amîtsoq gneisses of West Greenland require a degree of mantle depletion (initial ε_{Hf} of 3–4) higher than the time-integrated rate for the depleted mantle reservoir. In contrast, Hf-isotopic compositions of detrital zircons from the Narryer Gneiss Complex in Western Australia do not have a depleted mantle character but seem to have been derived from a chondritic to evolved source [10].

References: [1] Vervoort J. D. et al. (1999) *EPSL, 168,* 79–99. [2] Thériault R. J. et al. (1994) *Geol. Surv. Can. Curr. Res., 1994-F,* 37–42. [3] Brauhart C. W. et al. (1998) *Econ. Geol., 93,* 292–302. [4] Barley M. E. (1993) *Precambrian Res., 60,* 47–67. [5] Buick R. (1995) *Nature, 375,* 574–577. [6] Blake T. S. (1993) *Precambrian Res., 60,* 185–241. [7] Thorpe R. I. (1992) *Univ. W. Austr., Publ. 22,* 395–407. [8] Vervoort J. D. and Blichert-Toft J. (1999) *GCA,* in press. [9] Vervoort J. D. et al. (1996) *Nature, 379,* 624–627. [10] Amelin Y. et al. (1999) *Nature,* in press.

LOW δ^{18}O DESPITE INVOLVEMENT OF SUBDUCTED CONTINENTAL MATERIAL IN THE BANDA ARC.

P. Z. Vroon[1,4], D. Lowry[1], M. J. van Bergen[2], A. Boyce[3], and D. Mattey[1], [1]Department of Geology, Royal Holloway University of London, Egham Hill, Egham, Surrey TW20 0EX, UK, [2]Faculty of Earth Sciences, Utrecht University, P.O. Box 80.021, 3508 TA Utrecht, The Netherlands, [3]Isotope Community Support Facility, Scottish Universities Research and Reactor Centre, East Kilbride, Glasgow G75 0QU, UK, [4]Faculty of Earth Sciences, Free University, De Boelelaan 1085, 1081 HV, Amsterdam, The Netherlands.

Introduction: The Banda Arc represents an extreme case of source contamination by subducted continental material (SCM), as evidenced by isotopic and trace-element signatures [1,2]. Correlations between Hf isotopes and trace-element ratios suggest that the transfer to the mantle wedge largely occurred by melts, and to a minor extent by fluids, both derived from SCM. There is no evidence that (altered) oceanic crust plays a significant role.

We investigated O-isotopic systematics of volcanics and sediments in front of the arc to further constrain contributions from the mantle wedge, subducted sediment, and the arc crust. Since the abundance of O is high in a fluid (<88%) and lower in a melt (~50%), correlations between O isotopes, radiogenic isotopes, and incompatible trace-element ratios could help to identify the mode of transfer between the subducted slab and the mantle wedge.

Results: Oxygen-isotopic ratios were obtained from phenocrysts (ol, cpx, opx, hbl, and bi), using the laser fluorination technique at RHBNC [3]. The $\delta^{18}O_{min}$ values have been converted to melt values applying theoretical $\Delta_{min\text{-}melt}$ values. The results are displayed in Fig. 1 and show only limited spread of $\delta^{18}O_{melt}$ (5.5–6.4‰), close to accepted mantle values (5.2–6.8‰) [4]. Only Serua shows relatively high $\delta^{18}O$ (6.1–7.5‰). These values correlate with radiogenic isotopes, which could be interpreted as resulting from assimilation of arc crust. All other volcanos plot close to the bulk mixing line between MORB and sediments in front of the arc ($\delta^{18}O_{WT}$ = 12.9–24.2‰).

Discussion: Low $\delta^{18}O_{melt}$ values appear to be an important characteristic of the Banda-Arc volcanics. It should be noted that other sediment tracers (Pb-Nd isotopes) indicate the involvement of 1–5% of SCM, the highest percentage observed in active island arcs. Figure 1 demonstrates that fluid derived from sediments is an unlikely end member in Nd-O mixing models. Sediment-derived melt is clearly a more appropriate end member. Some volcanos plot even below the sediment melt-MORB mixing curve, which can be attributed to AFC-type processes [5] in the mantle wedge (Fig. 1).

Conclusion: Given the important role of subducted continental material in the Banda Arc, our findings suggest that elevated $\delta^{18}O$ values in any arc magma are difficult to explain without arc-crust assimilation.

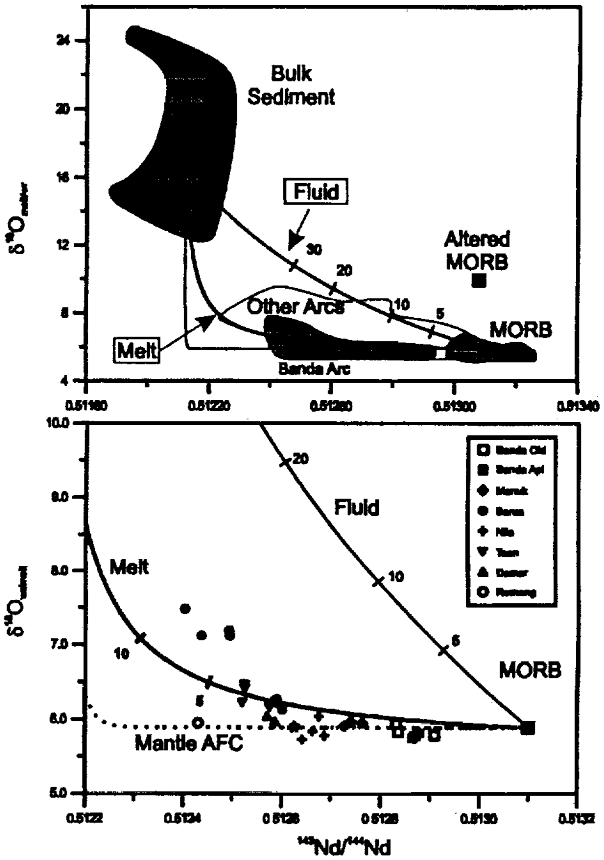

Fig. 1. Mixing between MORB mantle and (1) fluid, and (2) melt derived from sediment. End members: MORB: $\delta^{18}O$ = 5.89‰, $^{143}Nd/^{144}Nd$ = 0.51310, Nd = 0.73 ppm, O = 44.2%. Sediment: $\delta^{18}O$ = 16.5‰, $^{143}Nd/^{144}Nd$ = 0.51212. Fluid: Nd = 2.97ppm, O = 88.9%. Melt: Nd = 27ppm, O = 50.2%. AFC model (sediment melt assimilates MORB mantle) with r = 0.999 [5].

References: [1] Vroon P. Z. et al. (1993) *JGR, 98,* 22349–22366. [2] Vroon P. Z. et al. (1995) *GCA, 59,* 2573–2598. [3] Mattey D. P. and Macpherson C. G. (1993) *Chem. Geol., 105,* 305–318. [4] Eiler J. M. et al. (1997) *GCA, 61,* 2281–2293. [5] Kelemen P. B. et al. (1992) *Nature, 358,* 635–641.

GEOCHEMISTRY OF CARBON AND OXYGEN ISOTOPES OF CARBONATITES FROM THE WESTERN PART OF ALTAY-SAYAN FOLDING SYSTEM.

V. V. Vrublevsky[1], B. G. Pokrovsky[2], V. N. Kuleshev[2], I. F. Gertner[1], V. P. Parnachov[1], and G. N. Anoshin[3], [1]Tomsk State University, Lenin Avenue 36, 634050, Tomsk, Russia (petro@nggf.tsu.ru), [2]Geological Institute, Pyzhevsky Lane, 7, 109017, Moscow, Russia, [3]United Institute of Geology, Geophysics and Mineralogy, Koptug Avenue, 3, 630090, Novosibirsk, Russia.

Carbonatites in folding regions are of smaller scale and contain less mineralization than in platforms, where a majority of carbonatite-bearing magmatic rocks is formed. In contrast to platforms, carbonatites in folding regions are formed episodically.

The composition and metallogeny of carbonatites is controlled mainly by the degree of mantle matter participating in the rock-forming process. The mantle matter is dominated in the carbonatite of alkaline-ultrabasic complexes of platforms. In contrast, crust matter has participated to a large extent in the

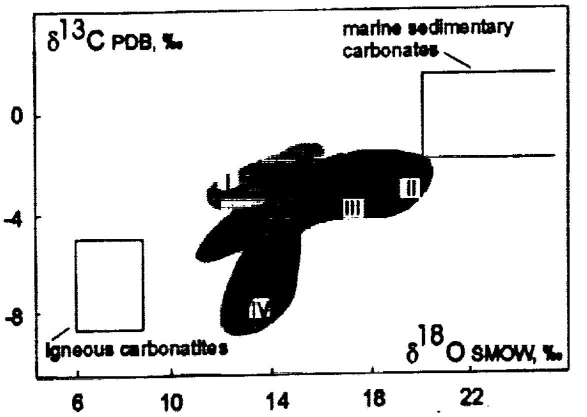

Fig. 1.

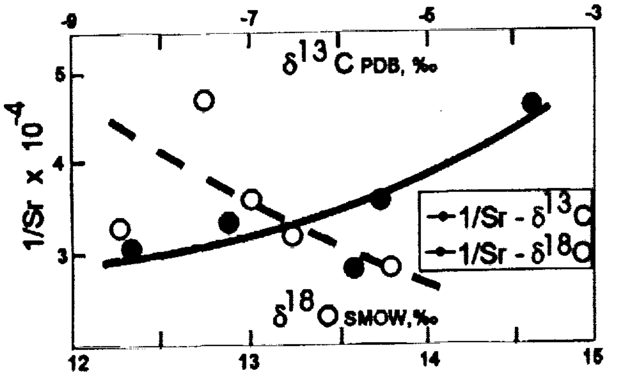

Fig. 2.

development of carbonatites of folding belts due to peculiarities of the tectonic structure of the lithosphere in folding belts. Commonly, such interaction is revealed by a trend in change of isotopic composition of carbonatites [1]. We have attempted to estimate a scale of this process, analyzing isotopic composition of C and O of 43 samples from endogenic carbonate rocks collected in some areas in the Altay-Sayany Folding Belt and in South Mongolia. These endogenic rocks were interpreted as carbonatites based on their mineralogy and geochemistry. Mafic complexes Edelveis in Gorny Altay and Mushugai-Huduk in Mongolia belong to K-alkaline differentiated series, whereas Verhnepetropavlovsky (Kuznezky Alatau Range) and Harlinsky (South Tuva) basic alkaline complexes reveal K-Na specifics of geochemistry.

Stable isotopic values of the analyzed carbonatites range between $\delta^{13}C$ –8.4‰ and –2.0‰ (PDB) and $\delta^{18}O$ 11.5‰ and 20.4‰ (SMOW), which corresponds to an intermediate area between the fields of the typical magmatic carbonatites [2] and sea-deposited carbonate. There is an obvious correlation trend between the stable isotopes. Individual trends, which characterize local specifics of carbonatite development, cause variation of the $\delta^{13}C$ and $\delta^{18}O$ values (Fig. 1: I = Kuznezky Alatau, II = Mongolia, III = Tuva, and IV = Gorny Altay). According to [3,4], such slope in trend is controlled by the change in CO_2/H_2O ratio in a postmagmatic fluid and by the degree of interaction between fluid (F) and rock (R) rather than by temperature regime of the carbonatite system. Such interaction has been revealed for the carbonatites of Gorny Altay. Observed correlation between the values of 1/Sr, $\delta^{13}C$, and $\delta^{18}O$ (Fig. 2) compared with the results of modeling allows us to assume high concentration of H_2O in fluids accompanied by an increasing F/R ratio due to an interaction with meteoric water enriched with light isotopes of O. In this case such interaction seems to complicate the contamination of the carbonatite system with the CO_2 of a crustal origin.

References: [1] Bell K., ed. (1989) *Carbonatites: Genesis and Evolution,* Unwin Hyman, London, 601 pp. [2] Javov M. et al. (1986) *Chem. Geol., 57,* 41–62. [3] Chacko T. et al. (1991) *GCA, 55,* 2867–2882. [4] Santos R. V. and Clayton R. N. (1995) *GCA, 59,* 1339–1352.

IMPROVEMENT OF LOW-LEVEL TRACE-ELEMENT ANALYSIS WITH THE ELECTRON MICROPROBE FOR RECORDING MANTLE PROCESSES.

C. Wagner[1] and M. Fialin[2], [1]Laboratoire de Pétrologie, European Space Agency, 7058-Centre National de la Recherche Scientifique, Université Paris 6, 4 Place Jussieu, 75952 Paris Cedex 05, France (cw@ccr.jussieu.fr), [2]Centre de Microanalyse CAMPARIS, European Space Agency, 7058-Centre National de la Recherche Scientifique, Université Paris 6, 4 Place Jussieu, 75952 Paris Cedex 05, France (fialin@ccr.jussieu.fr).

Introduction: Information related to geochemical processes is recorded at a microscale in minerals. Clinopyroxenes and amphiboles, for example, are of particular interest for petrogenetic interpretation of mantle processes. In peridotites, clinopyroxenes are the main trace-element carriers, and their composition can be used to constrain the relative importance of partial melting, metasomatism, or mixing in the upper mantle. Amphiboles, which are rarer phases in peridotites, testify for modal metasomatism and record the metasomatic agent imprint.

In recent years, microbeam techniques have thus become essential tools in distinguishing the signatures of complex processes. Among these techniques, the electron microprobe (EMP) may be used to provide reliable information on the elemental distribution among or within minerals at concentration levels as low as a few tenths of parts per million, by using an improved analytical procedure.

Analytical Procedure: The measurements were carried out with a CAMECA SX50 electron microprobe. The procedure is based on the "multisite" analytical mode [1,2], i.e., high excitation conditions (35 kV, 500 nA), long total counting time (4000 s) fractionated into subsets of 10–20 s count, each acquired from different sites to reduce possible damage due to prolonged irradiation, and statistical processing of each set of counts. All elements were analyzed with the Lα lines, as measured with a LIF_{200} monochromator for LREE and a PET monochromator for Sr, Zr, and Y. The improvement deals with the method of error calculation: stastistical and systematic errors are distinguished and the latter is eliminated by a careful measurement of the background curvature on a blank. The lack of knowledge of the background curvature can induce error as large as 100% on the weight percent concentration. In the proposed protocol, the shape of the continuum is represented by a parabola, the coefficients of which are determined experimentally on the selected blank, i.e., an olivine [3].

Results: We present EMP analyses for LREE, Sr, Y, and Zr in clinopyroxenes and amphiboles in three peridotites (SD30, 43, 68) from the French Massif Central. Those elements are useful tracers: for example, mantle enrichment is reflected in the clinopyroxene composition by an increase of the LREE contents with common 20–50 ppm concentrations, a range of values that can be measured by the EMP analysis.

The observed detection limits are as low as 11–13 ppm for LREE, 17 ppm for Sr, 18 ppm for Zr, and 12 ppm for Y using the given operating conditions. Precision (±2σ) on the weight percent concentrations is then 25% at 20 ppm and 12% at 50 ppm. Data are in good agreement with secondary ion mass spectrometry (SIMS) values.

The LREE and Sr contents reflect different degrees of enrichment; e.g., in clinopyroxenes, Lα ranges from chondritic values in sample SD30 up to 20× the chondritic values in sample SD68. Similar or higher enrichment (10–40×) has been previously reported in clinopyroxenes from a "composite" lherzolite nodule crosscut by an horblendite selvage [4]: the high abundances close to the selvage decrease as a function of increasing distance from it, recording the imprint of a metasomatic fluid emanating fom the dike. The presented data suggest that the enrichment of the clinopyroxenes in the studied noncomposite nodules may be due to "cryptic effects" of a similar metasomatizing melt.

Concluding Remarks and Perspective: Electron microprobe is thus useful in revealing the presence of some trace elements at a few tenths of parts-per-million level with a good spatial resolution and therefore may help selecting samples for other techniques with lower detection limits but less accessibility (e.g., SIMS, LA-ICP-MS, etc.).

References: [1] Fialin M. et al. (1999) *Am. Mineral., 84,* 70–77. [2] Wagner C. and Fialin M. (1999) *Proc. EMAS'99,* 354. [3] Fialin M. (1992) *X-Ray Spectrom., 21,* 175. [4] Wagner C. et al. (1998) *Mineral. Mag., 62A,* 1621–1622.

PLATINUM-RHENIUM-OSMIUM DISTRIBUTION AT 10 GPa IN IRON-NICKEL-SULFUR-PHOSPHORUS.

D. Walker, Lamont-Doherty Earth Observatory, Columbia University, Palisades NY 10964, USA (dwalker@ldeo.columbia.edu).

Fractionation of Pt, Re, and Os during growth of the solid inner core from the liquid outer core can potentially affect the long-term evolution of ^{187}Os/^{188}Os and ^{186}Os/^{188}Os in the outer core [1]. To set anticipated limits of the effects on the Pt/Os and Re/Os ratios, D(solid/liquid metal) for Pt, Re, Os, Fe, and Ni were determined at 10 GPa as a function of Fe-Ni-S-P liquid composition. Liquid compositional changes were introduced by variations in the bulk composition and temperature of the experiment. Multianvil methods were used to process samples in presintered MgO capsules at 1350°–1500°C at 10 GPa; electron microprobe methods were used to analyze phase compositions of quenched samples. Traveling solvent zone refining was used to digest refractory siderophile element starting materials into the liquid phase from which equilibrium solid-metal crystals were reprecipitated. This approach eliminated the nugget problem previously encountered. As a byproduct of this approach, rise-response profiles preserved in accumulating the solid show that the order of diffusivities in the liquid state is Pt ≫ Re > Os. Partitioning systematics of P-free and P-bearing experiments were both dependent on the S content of the liquid as at low pressure [2] but in slightly different ways from each other and from low pressure. D_{Os} and D_{Re} become more siderophile with increasing S in the liquid, and to even higher D values with P present. Platinum becomes, by contrast, distinctly less siderophile in the presence of P. Phosphorus-free systematics were less noisy and roughly consistent with those inferred from the fractionation seen in meteorite suites [3]. Atomic D_{Os}/D_{Re} ~1.3 and D_{Os}/D_{Pt} ~4 for (P-free) atomic S from 18% to 25%. The presence of ~3 at% P reduces D_{Os}/D_{Re} to indistinguishable from ~1 and raises D_{Os}/D_{Pt} above 10–15 in this same range of at% S. These results provide permissive evidence (at low P contents) that substantial fractionations of Pt, Re, and Os may have occurred during inner-core crystallization.

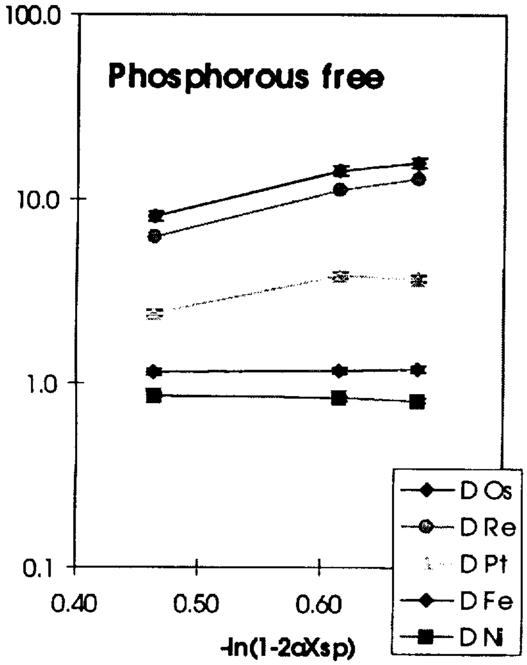

Fig. 1.

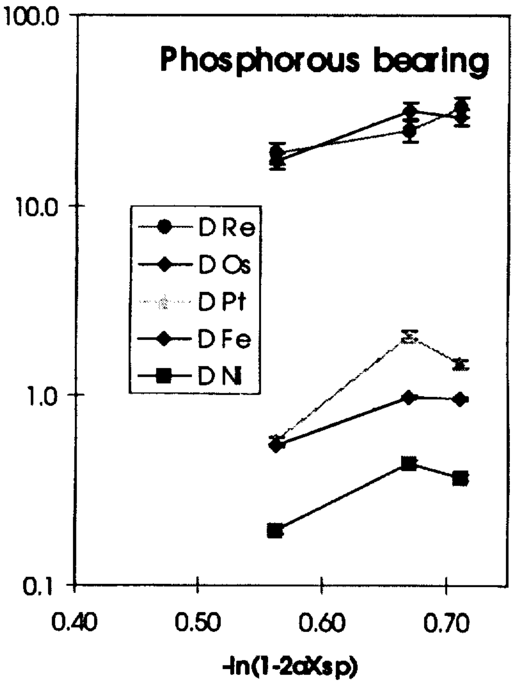

Fig. 2.

References: [1] Walker R. J. et al. (1995) *Science, 269,* 819–822. [2] Jones J. H. and Malvin D. J. (1990) *Metall. Trans. 21B,* 697–706. [3] Pernicka E. and Wasson J. W. (1987) *GCA, 51,* 1717–1726.

THE α_0*K_0 = CONSTANT FORM FITS HOT COMPRESSION OF B2 KCl, RHOMBOHEDRAL $KClO_3$, ORTHORHOMBIC $KClO_4$, and O_2 GAS TO 96 kbar CALIBRATED AGAINST B1 NaCl.

D. Walker[1], S. M. Clark[2], M. C. Johnson[3], and R. L. Jones[2], [1]Lamont-Doherty Earth Observatory, Columbia University, Palisades NY 10964, USA (dwalker@ldeo.columbia.edu), [2]Central Laboratory of the Research Council, Daresbury Laboratory, Warrington WA4 4AD, UK, [3]Geography and Geological Engineering, U.S. Military Academy, West Point NY 10996, USA.

B2 KCl was cocompressed with NaCl and simultaneously heated in the multianvil device on Station 16.4 Daresbury. The B2 KCl equation of state was measured by *in situ* XRD measurements of both phases. B2 KCl, calibrated against Boehler and Kennedy's [1] NaCl hot compression data and fit to an equation of state (e.o.s.) in the thermal Birch form (α_0*K_0 constant [2]), then served as an internal pressure standard for the compression and decomposition of rhombohedral $KClO_3$ and orthorhombic $KClO_4$. Thermodynamic manipulation allows the volume of O_2 gas to be computed along the decomposition curves of the chlorates that are encountered just below 600°C. All crystalline phases' hot compressions are well described by a thermal Birch equation of state. Oxygen-2 gas can also be adequately described in this way over a more limited T range (22–96 kbar, 550°–600°C).

Features of note include the contrasting K_0 values for high P forms B2 KCl and R $KClO_3$. R $KClO_3$ has the highest K_0 as expected for a high P form. Intriguingly, B2 KCl has K_0 marginally *lower* than even B1 KCl (sylvite) instead of being substantially higher. This confirms by volume measurements

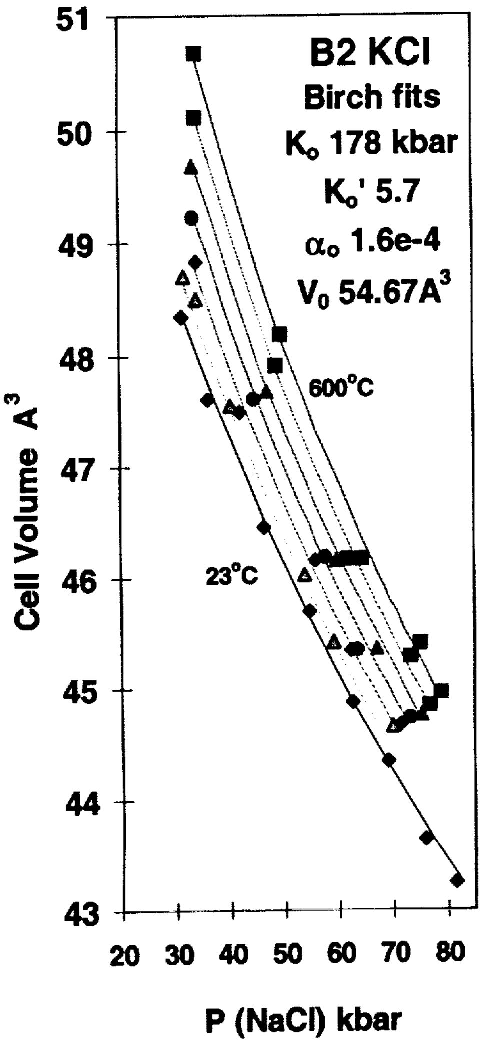

Fig. 1.

TABLE 1.

Phase	K_o kbar	K_o'	α_o/K	V_o A^3	ΔV(22–96 kb)/V_o
B2 KCl	178	5.7	1.6e-4	54.7* [Z = 1]	0.182
R $KClO_3$	260	3.5	1.6e-4	239* [Z = 3]	0.185
O $KClO_4$	181	7.1	1.8e-4	363 [Z = 4]	0.176
O_2 gas	120	16	←(at 600°C for 22–96kb)		0.169

* Metastable value from e.o.s. fit.

Boehler's prediction that this should be so, which was in turn supported by Hofmeister's [3] infrared study of several B1 to B2 transformations. A new high symmetry, noncubic form of $KClO_4$ was encountered at 20 kb above 600°C, but otherwise the low P form was observed over the P,T range investigated. Oxygen-2 gas compresses more easily at first (low K_o) and stiffens more rapidly (high K_o') than the crystalline phases reflecting its transition to a condensed phase. Moreover, the total compression sustained by O_2 gas is resolvably smaller in this P range than for crystals. This is a compositional effect. When covalently bonded molecular O_2 becomes a fully condensed fluid, it is less compressible than the crystals that are populated by relatively soft K and Cl ions.

References: [1] Boehler R. and Kennedy G. C. (1980) *J. Phys. Chem. Solids, 41,* 517–523. [2] Birch F. (1986) *JGR, 91,* 4949–4954. [3] Hofmeister A. M. (1997) *Phys. Rev. B 56,* 5835–5855.

SURPRISINGLY SMALL OXYGEN-2 GAS VOLUMES FROM 22–96 kbar AT 600°C ARE CONFIRMED FROM DECOMPOSITION OF ORTHORHOMBIC $KClO_4$.

D. Walker[1], S. M. Clark[2], M. C. Johnson[3], and R. L. Jones[2], [1]Lamont-Doherty Earth Observatory, Columbia University, Palisades NY 10964, USA (dwalker@ldeo.columbia.edu), [2]Central Laboratory of the Research Council, Daresbury Laboratory, Warrington WA4 4AD UK, [3]Geography and Geological Engineering, U.S. Military Academy, West Point NY 10996, USA.

Recently we reported O_2 gas volumes derived from decomposition of rhombohedral $KClO_3$ to B2 KCl by *in situ* X-ray diffraction (XRD) multianvil methods at Station 16.4 Daresbury [1]. Although the data appeared well behaved, we were surprised by the resulting volumes, because they appeared unreasonably low compared to mineralogical experience and also compared to shockwave results in the same pressure range [2] that do conform to min-

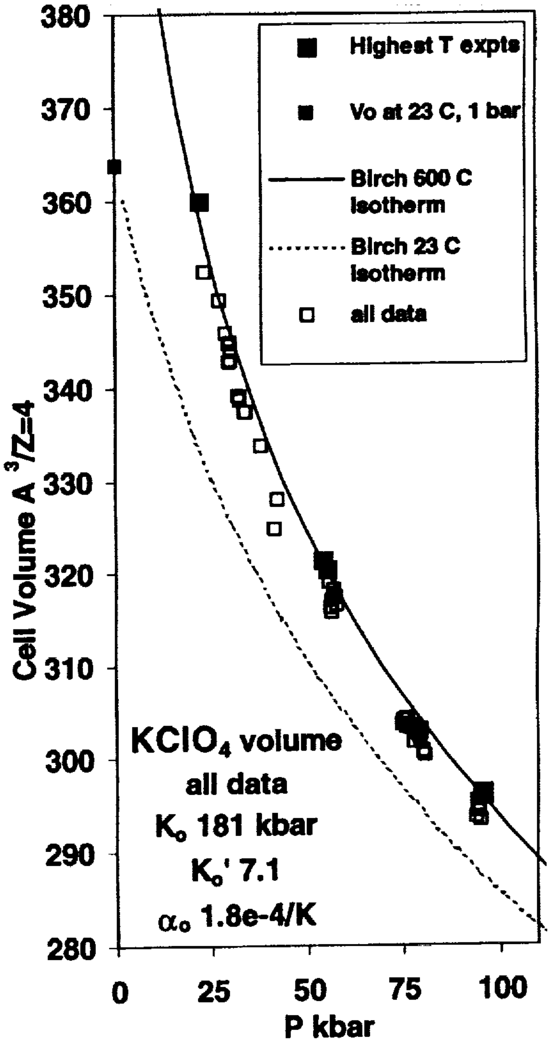

Fig. 1.

eralogical expectations. We therefore refined our experimental techniques, improved our calibrations and resolutions, reexamined the $KClO_3$ equilibrium, and explored the alternate related reaction of orthorhombic $KClO_4$ to B2 KCl and O. Crystalline phase volumes were obtained by synchrotron XRD at reaction P,T. Because the $KClO_4$ equilibrium, like the $KClO_3$ decomposition, varies by only ~20°C over the 22–96 kbar of the experiments, O volume may be computed directly from the difference between reactant and product crystal volumes. Any correction to the O volumes for nonzero dT/dP is limited to <1% of the values even for unreasonably large estimated bounds on the reaction ΔS (unknown because S for B2 KCl unknown). Because the $KClO_4$ decompositions occur only ~20°C above those for $KClO_3$, the two reactions afford an excellent cross-check on each other. Thermodynamic analysis indicates that $KClO_3$ decomposition is metastable with respect to $KClO_4$, but the metastable equilibrium still produces a valid O volume estimate. The results of technique improvement and study of new equilibria change our initial estimates by at most ±2%. Oxygen volumes vary by ~18% over the pressure range studied, so we confirm our previously reported low volumes [1]. At 600°C, O_2 volumes are 11.1 cc/mol at 22 kbar, 9.87 cc/mol at 53.5 kbar, and 9.21 cc/mol at 96 kbar. These values are compatible, after modest extrapolations in T from 200° to 600°C, with impulsively stimulated scattering data on liquid O_2 in diamond anvil cells.[3]. But our values are 30–50% below those derived from shock waves, a discrepancy that could be resolved if Hugoniot temperatures (unconstrained by measurement) approach 10**4 K higher than thought. Low volumes for O_2 may be a consequence of the more compact electronic structure of the O_2 molecule compared to the $O^=$ anion of mineralogical experience.

References: [1] Johnson M. C. et al. (1997) *Eos Trans. AGU, 78,* S313. [2] Nellis W. J. and Mitchell A. C. (1980) *J. Chem. Phys., 73,* 6137–6145. [3] Abramson E. H. et al. (1999) *J. Chem. Phys.,* in press.

OSMIUM-ISOTOPIC CONSTRAINTS ON THE EARLY EVOLUTION OF THE MANTLES OF THE EARTH, MOON, AND MARS.

R. J. Walker[1], B. Asuquo[1], H. M. Prichard[2], and A. D. Brandon[1], [1]Department of Geology, University of Maryland, College Park MD 20742, USA (rjwalker@geol.umd.edu) [2]University of Wales, Cardiff, CF1 3YE, UK.

Introduction: The ^{187}Re-^{187}Os-isotopic system provides important constraints on the origin of the highly siderophile elements (HSE) in the mantles of the terrestrial planets. The determination of Os-isotopic compositions can be used to monitor the time-integrated elemental Re/Os of materials derived from mantle reservoirs. These ratios may then be used to assess the impact of core segregation and late accretionary veneers on the HSE contained in planetary mantles.

Terrestrial Mantle: The Os-isotopic composition of the Earth's convecting upper mantle can be constrained via examination of several types of materials ultimately derived from it, including MORB, abyssal peridotites, and the ultramafic portions of ophiolites. Although there are problems associated with extracting an accurate picture of the Os-isotopic composition of the convecting upper mantle from each of these materials, several aspects of the compositions may enable a well-constrained estimate of this upper-mantle composition. Of note is the fact that the most radiogenic compositions of abyssal peridotites, and the least radiogenic compositions of MORB overlap at $^{187}Os/^{188}Os$ of 0.127–0.129 [1–3]. For reasons that will be discussed, we believe this is a good approximation of the ^{187}Os composition of the convecting upper mantle. Indeed, ophiolites suggest a similar present-day composition for the convecting upper mantle. We have analyzed chromites (n >40) from the mantle sections of 16 ophiolites ranging in age from 1.1 Ga to recent (Fig. 1). On a time vs. Os-isotopic composition plot, the data regress to give a modern $^{187}Os/^{188}Os$ of 0.1289 ± 19 (2σ), consistent with the overlapping composition range of MORB and abyssal peridotites. It is also interesting to note that this composition is essentially identical to the Os-isotopic composition (0.1290 ± 10) of a hypothetical undepleted or primitive upper mantle (PUM), that was estimated via extrapolations from ancient melt-depleted portions of the subcontinental lithospheric mantle (SCLM) [4]. The concurrence of data suggests that the convecting upper mantle is not measurably depleted in Re relative to PUM. Consequently, Re removal into the crust must largely be balanced via creation and isolation of Re-depleted SCLM, and the recycling of most oceanic crust back into the convecting upper mantle.

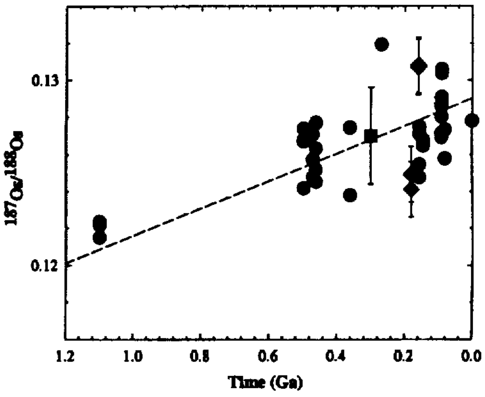

Fig. 1. Plot of initial Os-isotopic compositions for chromites (circles) from 15 ophiolites vs. time. Most data plot within ±2% of the evolution of the proposed primitive upper-mantle composition of [1] (dashed line; with ±2% uncertainty shown for square). Martian samples are shown as diamonds and plot within the ophiolite data array.

As we have noted previously [5], if this estimate of the $^{187}Os/^{188}Os$ of the upper mantle is accurate, then the time-integrated Re/Os of the upper mantle falls well within the range of chondritic meteorites, and more specifically, within the range of ordinary and enstatite chondrites. This match between the upper mantle and some types of chondrites argues most strongly that the HSE in the terrestrial upper mantle were set by the late accretion of chondritic materials subsequent to core segregation. High-pressure metal-silicate equilibrium, e.g., at the base of a magma ocean, can account for the Os composition only if distribution coefficients for Re and Os are virtually identical.

Mantles of Mars and the Moon: We previously reported Os data for Apollo 16 green glass [5], finding that the lunar mantle reservoir from which the green glass originated had evolved for nearly 1 b.y. with an essentially chondritic Re/Os. The data, however, provide less precise constraints than are available for the Earth and Mars because of the very low concentrations (high uncertainly in Re), and the fact the glasses are 3.6 b.y. old and, consequently, their mantle source evolved for much less time than the terrestrial mantle.

Whole-rock Re-Os analyses of meteorites (ALH 77005, LEW 88516, and EETA 79001A and B) of presumed martian origin have yielded results that overlap with the ophiolite array (Fig. 1). These meteorites generally have low Re/Os and relatively high Os concentrations.

These results suggest that the lunar and martian mantles may have obtained their HSE compositions via a similar late accretionary period as the Earth.

References: [1] Roy Barman M. et al. (1994) *GCA, 58,* 5043. [2] Schiano P. et al. (1997) *EPSL, 150,* 363. [3] Snow J. and Reisberg L. (1995) *EPSL, 136,* 723. [4] Meisel T. et al. (1996) *Nature, 383,* 517. [5] Walker R. J. et al. (1998) *LPSC XXIX,* 1271.

OSMIUM-186–OSMIUM-187-ISOTOPIC SYSTEMATICS OF MANGANESE NODULES AND MARINE SEDIMENTS.

R. J. Walker[1], S. R. Hemming[2], H. Becker[1], and M. Hodgson[1], [1]Department of Geology, University of Maryland, College Park MD 20742, USA (rjwalker@geol.umd.edu), [2]Lamont-Doherty Earth Observatory, Palisades NY 10964, USA.

Introduction: Previous studies have teamed the ^{87}Rb-^{87}Sr-isotopic system with the ^{187}Re-^{187}Os system in studies of the chemical evolution of the oceans [1,2]. Both systems display large fractionations of parent from daughter between the mantle and continental crust. Consequently, with time, the continental crust has evolved to much more radiogenic $^{187}Os/^{188}Os$ and $^{87}Sr/^{88}Sr$ compositions. The long residence times of Sr and Os in the oceans

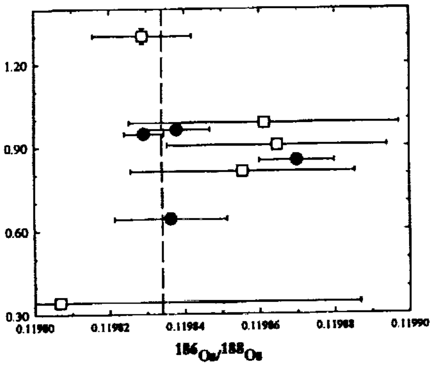

Fig. 1. Plot of $^{186}Os/^{188}Os$ vs. $^{187}Os/^{188}Os$ for Mn nodules (circles) and marine sediments (squares). The vertical dashed line delineates the modern $^{186}Os/^{188}Os$ of chondrites.

permit the assessment of globally integrated changes of input relative to local events occurring within one particular oceanic basin. The evolution of ^{187}Os-isotopic variations in seawater with time, in tandem with ^{87}Sr variations, has proved useful in constraining the contributions of continental crustal materials to the oceans. For example, recent strong increases in $^{187}Os/^{188}Os$ with $^{87}Sr/^{88}Sr$ are consistent with increased chemical weathering of continental materials, perhaps as a result of the uplift of the Himalayan and Cordilleran chains. Nonetheless, differences between the ^{187}Os and ^{87}Sr records of seawater during some time intervals are difficult to evaluate and require substantial changes in the types of materials that provide Os and Sr to oceans.

To examine these issues, we have begun work in applying the ^{190}Pt-^{186}Os tracer system. This system, like the ^{187}Re-^{187}Os system, may provide important constraints on the origin of Os added to seawater. The Pt-Os system is less sensitive to changes in parent/daughter ratios because ^{190}Pt is a very minor isotope of Pt and has a small decay constant. Nonetheless, with recent advances in high-precision measurement techniques of ^{186}Os [3], the system may have significant use in "fingerprinting" different terrestrial, especially crustal reservoirs.

Because the budget of Pt relative to Os is poorly determined for continental crustal materials, the application of this system to understanding oceanic inputs is still only loosely constrained. Several aspects of the system are noted. First, a study of the initial ^{186}Os-isotopic compositions of ores from the 1.85-Ga Sudbury Igneous Complex [4] indicates that at least some felsic crust has nearly chondritic to moderately suprachondritic Pt/Os. Basalts, in contrast, have very fractionated Pt/Os as a consequence of their mantlelike Pt concentrations, but a factor of ~100–1000 depletion of Os. Consequently, ancient basalts must have ^{186}Os-rich compositions relative to the mantle. Thus, we predict a significant difference in $^{186}Os/^{188}Os$ between ancient basaltic crust and felsic crust of any age. Although some sediments greatly concentrate Re, leading to huge fractionations in Re/Os, no large fractionations between Pt and Os have been observed [5]. Consequently, ancient sediments should not develop significantly suprachondritic $^{186}Os/^{188}Os$.

Methods: Approximately 30–50 ng of highly purified Os must be extracted from a rock in order to make the highest-quality $^{186}Os/^{188}Os$ measurement [3]. To achieve this, we utilize a Ni-sulfide fire-assay concentration technique to extract Os from 50–100 g aliquots of powder [6]. Where necessary, the final aliquots are combined to obtain sufficient Os for high-precision measurements.

Results: We have examined a variety of deep-sea Mn nodules and marine sediments. Because of their slow rate of formation, Mn nodules are less desirable than pelagic sediments for constraining the evolution of Os in seawater. Nonetheless, they contain considerably more Os than sediments, and have thus yielded the most precise data.

All but one of the Mn nodules and sediments have compositions consistent with a precursor that evolved with long-term chondritic Pt/Os (Fig. 1), although the less-precise data for the sediments also permit an interpretation of more radiogenic compositions. Additional aliquots will be analyzed to improve the quality of the data. An aliquot of Mn nodule V21-D5, however, has a distinctly suprachondritic composition. The $^{187}Os/^{188}Os$ of this sample (0.850088) suggests an average formation age of ~10 Ma, and may indicate substantial addition of Os derived from ancient basaltic crust at that time.

References: [1] Ravizza G. (1993) *EPSL, 118,* 335. [2] Peucker-Ehrenbrink B. et al. (1995) *EPSL, 130,* 155. [3] Walker R. et al. (1997) *GCA, 61,* 4799. [4] Morgan J. W. et al. (1997) *Eos Trans. AGU, 78,* F782. [5] Ravizza G. and Pyle D. (1997) *Chem. Geol., 141,* 251. [6] Brandon et al. (1998) *Science, 280,* 1570.

IMPROVING THE ACCURACY OF POTASSIUM-ARGON DETERMINATIONS ON ORGANOCLAYS.

J. M. Wampler[1], W. C. Elliott[2], S. K. Sears[3], and S. Shata[3], [1]School of Earth and Atmospheric Sciences, Georgia Institute of Technology, Atlanta GA 30332-0340, USA, [2]Department of Geology, Georgia State University, Atlanta GA 30303, USA, [3]Department of Earth and Planetary Sciences, McGill University, Montréal, H3A 2A7, Québec, Canada.

Introduction: Exchange of interlayer K ions by long-chain alkylammonium ions provides important opportunities for those who study K-Ar relationships in clays [1,2]. The organoclays produced by such treatment also provide several special challenges for those who determine the K and Ar isotopes in such materials: (1) Gases, formed by decomposition of an unusually large amount of organic matter during fusion of the clay to release Ar, may overwhelm getters — getters that have sufficient capacity for *ordinary* clay samples. (2) Certain volatile organic compounds, if not completely gettered, cause mass-spectrometric interference in the mass range of the Ar isotopes, which increases the uncertainty in the correction for atmospheric Ar. It could also lead to an overestimate of the amount of atmospheric Ar and thus an underestimate of the amount of radiogenic Ar. (3) The increase in mass of clay attendant upon exchange of massive organic ions for less-massive inorganic ions makes it difficult to interpret the effect of the treatment in terms of the amounts of K and radiogenic Ar released during treatment (although it does not affect the calculated K-Ar ages). We have developed techniques to minimize these problems in determining the Ar isotopes and K in clays that have been treated with long-chain alkyl-ammonium ions.

The Techniques: The techniques that are specifically important in K-Ar work with organoclays are described in the following. (Not all of these are new techniques.)

Minimizing gas formation. Because of the small size of the particles, Ar can be extracted completely from illite by heating at a temperature below that at which the material fuses. Heating at 1000°C for 15 min is sufficient to release all the radiogenic Ar from most clay samples. Consequently, clay samples may be heated sufficiently for Ar extraction in a fused-quartz tube from which the heavier organic products of decomposition may be condensed before they have much opportunity to decompose further by interaction with hot surfaces.

Destruction of volatile organics. The more volatile organic compounds created by decomposition of organoclay can mostly be eliminated by reaction with hot copper oxide. The main products of the reaction, water and CO_2, are easily trapped.

Cold trapping. Organic compounds having volatilities close to that of CO_2 (propane and propylene) have a sufficient vapor pressure at 77 K such that cold trapping with boiling liquid N is not sufficient to prevent interference by three-C organic ions in mass-spectrometric measurement of the Ar isotopes. A trap cooled by melting solid N (63 K) lowers the vapor pressures of these compounds by about two orders of magnitude from their values at 77 K.

Determining loss on ignition. The mass of organic matter added by treatment with alkylammonium ions can be determined approximately by determining the difference in mass loss on ignition of treated and untreated clays. Correction is required for the mass of the oxides of the inorganic cations that were replaced by organic ions, since those oxides are not present in the ignition residues of treated clays. If samples for Ar determination are enclosed in appropriate metal capsules, loss on ignition can be determined from the difference in mass of a capsule and its contents before and after Ar extraction at 1000°C.

Results: We have extracted Ar from two dozen clay-sized samples of 2:1 layer silicates that had been treated to replace exchange cations and some of the interlayer K ions with octadecylammonium ions ($n_C = 18$). These samples were encapsulated in copper foil for Ar extraction and for later determination of the mass loss on ignition. For 12 of the samples, the corresponding untreated samples were prepared and analyzed in the same way. The loss on ignition determined after Ar extraction is somewhat uncertain because a little of the Cu vaporizes during heating at 1000°C to extract Ar. It also may be that the conditions for Ar extraction (1000°C, vacuum) are not optimum for determining loss on ignition. Nevertheless, the differences in loss on ignition for treated and untreated submicrometer-sized fractions of illite/smectite-rich clays indicate that the increase in mass attendant upon treatment by octadecylammonium ions can be several tens of percent. (These results need to be compared to results obtained by ignition in air of samples in Au-foil capsules.) A dozen of the ignition residues were later fused in an Ar extraction line to demonstrate that all of the radiogenic Ar had been extracted at 1000°C.

References: [1] Sears S. K. et al. (1998) *Canadian Mineral., 36,* 1507–1524. [2] Chaudhuri S. et al. (1999) *Clays Clay Minerals, 47,* 96–102.

SPECTROSCOPIC PROBES OF DEGRADATION REACTIONS PROMOTED BY METAL OXIDE SURFACES.

D. Wang[1], W. E. Dubbin[2], J. Y. Shin[3], M. Zavarin[4], M. A. Cheney[3], T. G. Spiro[1], and G. Sposito[5], [1]Department of Chemistry, Princeton University, Princeton NJ 08544-1009, USA, [2]Department of Mineralogy, Natural History Museum, London SW7 5BD, UK, [3]Department of Environmental Science, Cook College, Rutgers University, New Brunswick NJ 08901-8551, USA, [4]Mail Stop L-219, Lawrence Livermore National Laboratory, Livermore CA 94551, USA, [5]Ecosystem Sciences, Hilgard Hall #3110, University of California, Berkeley CA 94720-3110, USA.

Introduction: Herbicide degradation by enzymatic catalysis in soil environments is well known, but little information exists as to the role of oxide mineral surfaces in this process. We have applied spectroscopic techniques to elucidate the degradation reactions of two herbicides of current environmental concern. Glyphosate, a broad-spectrum herbicide widely used in agriculture and forestry, was reacted with microcrystalline gibbsite, an aluminum hydroxide mineral, and investigated with extended X-ray absorption fine-structure (EXAFS) spectroscopy to discern the nature of the surface complex formed. Atrazine, the agricultural herbicide most frequently detected in shallow groundwater bodies of the United States, was reacted with vernadite, a manganese oxide, and investigated with ultraviolet resonance Raman (UVRR) spectroscopy to follow the pathway of its abiotic dealkylation on the mineral surface, a process discovered recently by Cheney et al.[1].

Experimental: Gibbsite and vernadite were synthesized and characterized in the laboratory following standard procedures.

Copper-glyphosate-gibbsite surface complexes were prepared by first adjusting a gibbsite suspension to pH 5.5, then adding sufficient Cu-glyphosate solution to produce a surface coverage near $1 \mu m/m^2$. After a 24-h reaction, the suspension was centrifuged, and the resulting paste was mounted onto a sample holder for study by EXAFS spectroscopy. Copper K-edge X-ray absorption spectra were collected in fluorescence mode at the Stanford Synchrotron Radiation Laboratory. Normalization and background subtraction to obtain EXAFS spectra were performed according to established procedures. Phase and amplitude functions needed for interpreting the spectra were extracted from spectra of well-characterized model compounds in conjunction with calculations using the FEFF software package.

Reagent-grade atrazine dissolved in diethyl ether was deposited onto vernadite, followed by evaporation of the solvent at 0°C and incubation of the sample at 30°C for up to 96 h [1]. After various periods of reaction, the sample was extracted with methanol and the extracts were examined by UVRR spectroscopy (excitation at 229 nm). Volatile products were quantified by gas chromatographic analysis of head-space gas above the incubated samples. Incubations were performed under N gas as well as in air. A least-squares method of deconvolution was used to quantify the reaction products based on a calibration file generated with standard solutions of atrazine and its three principal dealkylated forms.

Results: Copper K-edge EXAFS spectra of Cu-glyphosate complexes in solution at pH 5.5 revealed 1:1 Cu complexation by the phosphonate group of the herbicide. Formation of a ternary surface complex after introducing gibbsite was accompanied by the loss of phosphonate from the coordination sphere of Cu, thus indicating adsorption of this group to the oxide surface by ligand exchange [2]. The EXAFS spectra of Cu in the ternary complex matched closely the corresponding spectra of Cu-glycine and Cu-methylglycine complexes, suggesting Cu complexation in the ternary surface complex by the glyphosate carboxyl O and amine N, both of which remained detached from the gibbsite surface, extending into the aqueous solution phase. The amine N is therefore accessible to extracellular enzymes, allowing the rapid biodegradation of glyphosate in soil environments, as observed frequently, despite the well-known strong adsorption of the herbicide by oxide minerals.

Synoptic UVRR spectra showed a rapid loss of atrazine over the first 5 h of incubation and a corresponding increase in monodealkylated triazines, which reached maxima at 12 h, then in the fully dealkylated product. In the presence of N gas, mass balance was achieved among these four compounds, and olefin products were detected in the sample headspace. In the presence of air, the four compounds accounted only for ~70% of the initial mass, with CO_2 making up the rest along with aldehyde and ketone oxidation products of the olefins produced. Thus atrazine was efficiently dealkylated by vernadite irrespective of the presence of O.

Acknowledgments: W. E. Dubbin expresses gratitude to NSERC (Canada) for a fellowship. Support by DOE contracts DE-AC03-76SF00098 and DE-FG02-97ER14755 and NIH grant GM22576 is appreciated.

References: [1] Cheney M. A. et al. (1998) *Colloids Surfaces, A137,* 267. [2] Laiti E. et al. (1995) *J. Colloid Interface Sci., 175,* 230.

GEOCHEMISTRY AND METALLIZATION OF MYLONITE-HOSTED GOLD DEPOSIT IN SOUTHERN CHINA.

H. N. Wang, J. Chen, J. F. Ji, and C. Y. Sun, Nanjing University, China (wanghn@990.net).

Introduction: Many large Au deposits have a close genetic relationship to ductile shear zones. These Au deposits can be divided into three types: (1) mynolite-hosted, (2) crush belt-hosted, and (3) quartz vein. In recent years, the mynolite-Hosted Au deposit has been found to be one of the largest Au deposits in South China.

Ore Deposit Geology: Gold deposit is contained within a ductile shear zone. The ores occur as veins or as lenticular bodies within altered mylonite and ultramylonite host rocks. Native Au is disseminated in silicified, pyritized, and sericitized phyllonites. The auriferous shear zone has undergone two stages of evolution. The early stage was characterized by ductile deformation, duing which auriferous mylonite containing n × 10^6 Au was formed. The later stage was developed in brittle-ductile and brittle environments in which magmatic hydrothermal mineralization was superimposed, resulting in local Au enrichments or auriferous quartz vein.

The Features of Gold in Dislocation Wall: Based on the study of transmission electron microscopy (TEM), dense dislocations can be seen under bright field transmission. The Au-concentrated bright spots are regularly arranged in the dislocation wall.

Gold deposits in ductile shear zone have an obvious cause of structural formation. During ductile shearing, the large quantities of quartz that exist in a shear zone form the dynamic dislocation walls that are the important structures for Au to migrate to the shear zone and for increasing the total Au content of the shear zone.

Trace-Element and Isotopic Geochemistry: The auriferous silicified mylonite is similar in geochemical characteristics of REE and trace elements to the country rock, which may have provided ore-forming materials for the first stage of mineralization. The chemical and isotopic characteristics of the fluid inclusions from the auriferous quartz veins indicate that the ore-forming fluid responsible for the second stage of mineralization came from meteoric water or a magmatic hydrothermal source. The S and Pb isotopes of ores reflect the fact that the ore-forming materials originated mainly from a wall-rock source.

Gold Enrichment by Ductile Shearing: The geological characteristics, ore-body occurrences, and Au existence forms all indicate that ductile shearing leads to Au enrichment in mylonite belts. This conclusion is supported by the following observations: (1) The orebodies occur in the mylonite belts and are assocated with phyllonite and ultramylonite. The occurrence of ore bodies correlates directly with the occurrence of the mylonite belts. The scale of ore bodies is positively proportional to the scale of the mylonite belts and the strength of shearing strain. The dip and angle of ore bodies are basically consistent with those of the shear zone. (2) Native Au is disseminated in alternated mylonite ores. In polished section, native Au grains are oriented along phyllonite cleavages. (3) A large quartz subgrain with some bright Au-concentrated area is regularly arranged in the dislocation wall. (4) regional geochemical sections show that the metamorphosed rocks and migmatite that underwent ductile shearing have a preliminary Au enrichment.

MOLECULAR MODELING OF THE INTERLAYER STRUCTURE AND DYNAMICS IN HYDROTALCITE.

J. Wang[1], A. G. Kalinichev[1], R. J. Kirkpatrick[1], R. T. Cygan[2], and X. Hou[1], [1]Department of Geology, University of Illinois at Urbana-Champaign, Urbana IL 61801, USA (jwang7@uiuc.edu, kalinich@uiuc.edu), [2]Geochemistry Department, Sandia National Laboratories, Albuquerque NM 87185-0750, USA (rtcygan@sandia.gov).

Introduction: Sorption and exchange are fundamental processes in many geological and environmental systems, and the molecular-scale dynamics of the ions and water molecules involved is key to their microscopic understanding. Forcefield-based molecular-mechanics simulations, guided by experimental data and based on accurate potential functions, provide significant insight into the structural and dynamical interpretations of these processes [1]. Phases of the hydrotalcite group are among the few minerals with permanent anion adsorption and exchange capacity, and stand in contract to clay minerals, which have dominantly cation adsorption and exchange capacity. Their crystal structures are similar to that of brucite, $Mg(OH)_2$, but develop permanent positive charge from the isomorphic substitution of, e.g., Al^{3+} for Mg^2. The positive charge is balanced by interlayer anions that have associated water molecules. This paper focuses on the study of the structure and dynamics of interlayer species in hydrotacite-like compounds.

Forcefield-based Simulation: Molecular dynamics simulations were applied to hydrotalcite, $[Mg_2Al(OH)_6]Cl\ 1.5H_2O$ and $[Mg_2Al(OH)_6]_2CO_3\ 3H_2O$ [2–4], to model the structure and molecular dynamical behavior of interlayer species (Cl^-, CO_3^{2-}, and H_2O). The simulation cell consists of 6 × 3 × 1 crystallographic unit cells of hydrotalcite. A modification of the consistent valence force field (CVFF) for ionic species was used for all ion-ion and ion-water interactions and a flexible version of simple point charge potential was used for water [1,5]. In addition to the interlayer anions and water molecules, all atoms of the hydroxide layer were also treated as completely movable. Isothermal-isobaric molecular dynamical simulations in the NPT ensemble allowed us to leave the size and shape of the simulation cell unconstrained as well. The resulting crystal lattice parameters are in good agreement with measured data [2].

Interlayer Structure: Molecular-dynamics simulations for $[Mg_2Al(OH)_6]Cl\ 1.5H_2O$ hydrotalcite reveal significant positional and orientational disorder of the interlayer anions and water molecules. The interlayer species are located at three layers along the [001] direction, chlorides are at the middle between two octahedral layers, and about half of the water molecules are above the chloride layer and the other half below the chloride layer. The positions of Cl^- are relatively fixed with respect to the Mg^{2+} and Al^{3+} in the octahedral layers. Chloride ions are coordinated by the H of water molecules and OH groups of the octahedral layer. The water molecules undergo dynamical reorientation in the interlayer, and the rotation axis tends to be perpendicular to the layer plane because of the attraction between positively charged octahedral layers and the water. This reorientation is consistent with the ^1H nuclear magentic resonance (NMR) observations of hydrotalcite [6].

Molecular Dynamics: Power spectra of translational, librational, and vibrational motions of interlayer anions and H_2O molecules were calculated as Fourier transforms of the velocity autocorrelation functions for each species. The Cl^- power spectrum of hydrotalcite is more similar to that of Cl^- in bulk solution and on the surface of the hydrotalcite than in the hydrocalumite ($Ca_2Al(OH)_6Cl\ 2H_2O$) interlayer [5], consistent with the disordered interlayer structure. Strong electrostatic attraction between interlayer water molecules and octahedral Mg atoms make the M-O bond direction the preferable axis for H_2O librations (hindered rotations). However, due to the interlayer disorder, molecular librational spectra of H_2O in hydrotalcite resemble those of bulk liquid water [7] much more than that of the interlayer water of hydrocalumite.

References: [1] Molecular Simulations Inc. (1998) Cerius^2 User Guide. [2] Bellotto M. et al. (1996) *J. Phys. Chem.*, *100*, 8527–8534. [3] Titulaer M. K. et al (1996) *Clay Minerals*, *31*, 263–277. [4] Costantino U. et al. (1998) *Eur. J. Inorg. Chem.*, 1439–1446. [5] Kalinichev A. G. et al. (1999) *Am. Mineral.*, in preparation. [6] Pol A.V. D. et al. (1994) *J. Phys. Chem.*, *98*, 4050–4054. [7] Kalinichev A. G. and Heinzinger K. (1992) *Adv. Phys. Geochem.*, *10*, 1–59.

CARBONATE ROCK WEATHERING AND PEDOGENESIS IN THE SOUTH OF CHINA.

S. J. Wang, H. B. Ji, Z. Y. Ouyang, and D. Q. Zhou, The State Key Laboratory of Environmental Geochemistry, Institute of Geochemistry, Chinese Academy of Sciences, Guiyang 550002, China (hdh@public1.gy.gz.cn).

Based on a detailed field investigation, the five typical soil profiles developed on the bedrock dolomitite and limestone and morphologically located in upland karst terrain in the central, west, and north areas of Guizhou and the west area of Hunan, China, were selected. Through acid-dissolved extraction experiment of bedrock carbonate rock and mineralogical and trace-element geochemical study, the five soil profiles were proved to be *in situ* weathering and pedogenetic products of carbonate rock. Carbonate rock weathering and pedogenesis were suggested as the main sources for soils widely overlying on bedrock carbonate rocks in south China.

Except that pyrite became iron oxide and hydroxide, mineral compositions of HCl leachates of bedrock carbonate rock were the same as those of soils overlying on it in the five studied soil profiles. This implied that soil could be the weathering product of the underlying bedrock carbonate rock. It was important to note that volcanic secondary minerals, glassy detrital matter, and heavy minerals usually existed in loess were not found in different sizes of samples, implying that there existed no eolian matter in soil profile.

Concentrations of REE for the bedrock, transition zone, and soil samples were different; the latter was 10–1000× higher than the former. But the distribution patterns of REE for samples were similar, showing that the evolution characteristics of REE in soil have an obvious heritage to the parent rock. The four separate smooth curves (La-Ce-Pr-Nd, Pm-Sm-Eu-Gd, Gd-Tb-Dy-Ho, and Er-Tm-Yb-Lu), i.e., "M type" tetrad effect, existed in the distribution patterns of REE for bedrock and transition-zone samples, corresponding to those observed in marine carbonate and its products of water-rock interaction [1]. All of those features demonstrated that the studied profiles were *in situ* weathering profile of carbonate rock.

In Nb vs. TiO_2 and Zr vs. TiO_2 diagram, all samples of each profile had good linear relation, correlation coefficient of 0.969–0.998, demonstrating that the soil were derived from the underlying bedrock carbonate rock. In U/Pb vs. Th/Pb diagram, the ratios of U/Pb and Th/Pb of each soil profile evolved from the lower to higher values, and those of the parent rock and weathered rock were concentrated in the left lower parts. Samples from the three studied soil profiles distributed along the line of Th/U = 3.8 defined by UCC, and samples from the other two profiles along the simulated line of Th/U = 1.76. These differences could reflect distinction of weathering intensity of the studied profile [2].

According to the above research, it was suggested that the process of carbonate rock weathering and pedogenesis be divided into two stages: dissolution residue of carbonate rock weathering accumulated to form soil in the first stage and the second stage for chemical weathering of the residuum. The latter is similar to the weathering process of the other kinds of rocks.

Acknowledgements: The research is jointly supported by the Chinese National Science Foundation Committee (grant No. 4980003), Chinese national key basic research project (grant No. 95-pre-39), and Guizhou Science Foundation Committee.

References: [1] Liu C. Q. et al. (1993) *Chem. Geol.*, *106*, 359–374. [2] Dupre B. et al. (1996) *GCA*, *60*, 1301–1321.

GEOCHEMISTRY OF THE ORE FLUID IN THE JINJITAI CARBONATE ROCK-HOSTED GOLD DEPOSIT, SICHUAN, CHINA.

X. C. Wang and Z. R. Zhang, Institute of Geochemistry, Chinese Academy of Sciences, 73 Guanshui Road, Guiyang, Guizhou 550002, China.

Different ore types and their complex geochemical association reflect the parental fluid, the composition of the host rocks, and the condition of ore formation. The feature of ore fluids can give fundamental information to elaborate a metallogenic model and provide important criteria for ore exploitation in each deposit. This contribution aims to determine the composition of the ore fluid for the Jinjitai carbonate rock-hosted Au deposit in Sichuan China, and to discuss its metallogenic mechanism and elaborate some be used in a more rational exploitation of metals.

Geological Setting of the Deposit: The Jinjitai Au deposit is situated 20 km west of the town of Shimian in Sichuan Province. It was discovered in the 1980s and has a proven total reserve of more than 3 t of Au. It is located in the Longmenshan-Jinpingshan Cenozoic intracontinental orogenic belt at the western margin of the Yangtze Craton [1]. The ore grade ranges from 5 to 6 ppm, and the highest grade reached 25 ppm. The geological setting consists of marble, dolostone and clastic rocks (Devonian, Permian, and Triassic ages), migmatite (Archaeozoic), and diabase dikes (Cenozoic). Gold occurs disseminated or in shear fractures and is associated with quartz, sericite, dolomite, pyrite, tetrahedrite, chalcopyrite, galena, sphalerite, and arseno-pyrite within Middle Devonian dolostone and marble. Interstratified fractured zones controlled Au ore bodies strictly [2].

Element Geochemistry: Multi-element (major-, minor-, and trace-element) geochemical analyses in whole rock were carried out on selected samples from the deposit. The analyses of the ore paragenesis reveal the following results: (1) Gold: Au (72.94–98.42%), Ag (0.33–17.01%), with fineness 771–990, showing the existence of native Au and electrum with composition $Au_{0.77}Ag_{0.23}$; (2) Pyrite: Fe (46.30–46.29%), Cu (0.01–0.02%), S(51.11–51.45%), As (0.317%); (3) Tetrahedrite: Cu (39.10–42.27%), Fe(1.24–7.78%), Zn (0.39–7.06%), As(5.41–17.40%), Sb(2.70–20.46%), Ag (0.02–0.44%), S(24.94–27.35%), showing the complete isomorphous replacement of Fe-Zn and As-Sb.

Geochemical data in whole rock to the ore show a positive correlation between Au and As-Sb-Bi-Cu-Zn-Ag-Ba. REE geochemical data reveal that Au ore, calcite, and Triassic slate, as well as Devonian dolostone, have similar REE patterns that are different from that of diabase.

Isotopic Geochemistry: The $\delta^{34}S$ values of pyrite, tetrahedrite and chalcopyrite range from approximately –2.44‰ to +21.98‰, averaging 10.84‰. The $\delta^{13}C_{PDB}$ value of calcite ranges from approximately –2.70‰ to –0.66‰, averaging –1.15‰, which is similar to those of Devonian dolostone (–2.37 ~ –0.09‰, averaging –1.23‰). The δD and O values for the ore fluids range from –90 ~ –80‰, and from 0.75 ~ 4.82‰ respectively, which are plotted in the geothermal range on the diagram of D vs. ^{18}O for various fluids. The ratios of $^{206}Pb/^{204}Pb$, $^{207}Pb/^{204}Pb$, $^{208}Pb/^{204}Pb$ for sulfide minerals (pyrite and tetrahedrite) are 18.051~24.527, 15.522~15.870, and 38.292~38.828 respectively; those for diabase are 18.262~18.480, 15.351~15.603, and 37.781~38.593 respectively; and those for regional Devonian and Triassic rocks are 18.446~19.803, 15.600~15.818, and 38.580~38.932 respectively.

Fluid Inclusion Geochemistry: The inclusion study reveals that the Au ore was formed at 80°~300°C (average 240°C) by alkalescent fluids (pH 7.65 ~ 8.04) with salinity of 5.6 ~ 20.0 wt% NaCl, and density of 0.862~ 0.965 g/cm^3 under reductive environment (Eh –1.10 ~ –0.61 V).

Discussion and Conclusion: The present study reveals the deposit contains enough Cu and Ag that can be as a byproduct. In other words, there is a potential for these two metals. The presence of the association Au-As-Sb-Bi-Cu-Zn-Ag-Ba reflects the signature of the parental fluid and improves a new constraint to the genetic model. This geochemical association points to an important contribution of geothermal fluids to the ore-forming fluids to the ore-forming system,which is in accord with the H- and O-isotopic data.

The REE and S-, C-, and Pb-isotopic data suggest that the S and C in the ore fluid were derived chiefly from ore-hosted strata,and the metallic materials were not only supplied by the Middle Devonian and Triassic Strata, but also supplied by the Archaeozoic migmatite. The deposit may be formed during Cenozoic intracontinental orogeny [1,3].

Acknowledgments: A major program of Chinese Academy of Sciences (research on gross low-temperature metallogenic domains in southwestern China) financially supports the study.

References: [1] Luo Y. N., ed. (1995) *Contributions to Geology and Mineral Resources in Intracontinental Orogenic Belt*, Sichuan Press of Science and Technology, Chengdu, 360 pp. (in Chinese). [2] Wang X. C. (1993) *Acta Geologica Sichuan, 13,* 296–303 (in Chinese). [3] Wang X. C. (1994) in *Geochemistry of Ore Deposits* (R. Z. Hu, ed.), pp. 158–161, Seismological Press, Beijing.

GEOCHEMISTRY OF THE TRIASSIC BASALT IN THE LUHUO-DAOFU REGION, SOUTHWESTERN CHINA, AND ITS TECTONIC SIGNIFICANCE.

X. C. Wang and Z. R. Zhang, Institute of Geochemistry, Chinese Academy of Sciences, 73 Guanshui Road, Guiyang, Guizhou 550002, China.

Studies of volcanic rock geochemistry have made important contributions to interpretations of tectonic setting as well as estimates of average deep crust composition and its evolution. The present abstract aims to document geochemical data for the Luhuo-Daofu Triassic basalt in western Sichuan, China, and to compare them with those from known distinct tectonic settings elsewhere, in an attempt to evaluate their type of tectonic setting.

Geological Setting: The Luhuo-Daofu region is situated in central part of the Bayankala-Kekexili basin in which the Triassic strata are widespread. It is chiefly different from the remaining parts of Bayankala-Kekexili basin in its development of basic volcanic rocks, calcareous breccias, and associated ophiolitic ultrabasic intrusives. The basic volcanic rocks consist mainly of basalt, basic volcanic breccias, and tuffs. The basalts exhibit amygdaloidal, pillow and pelletoidal structures, and porphyritic, spherulitic textures. They are associated with radiolaria-bearing silicalite, syngenetic tectosedimentary breccias and flysch clastic rocks.

Major-element Geochemistry: Basalts collected from the Luhuo-Daofu region exhibit a large variation in their major compositions. They are plotted in the tholeiite range on the AFM diagram [1], in the ocean tholeiite range on the TiO_2-K_2O-P_2O_5 diagram [2], and in the MORB range on the FeO*-MgO-Al_2O_3 and FeO*/MgO-TiO_2 diagrams [3]. They are high in TiO_2, similar to the basalts collected from the modern mid-ocean ridge [4], and are also high in FeO + Fe_2O_3 and MgO. Especially their contents of FeO + Fe_2O_3 increase rapidly with decreasing MgO content. It shows a typical MORB evolution trend [5].

Trace-element Geochemistry: On the Ti/100-Zr-Y × 3, Zr/Y-Zr, and Ti-Zr diagrams [6–8], the Luhuo-Daofu basalts are plotted in the MORB range. REE analyses of basalts show that the samples have smooth chondrite-normalized REE abundance patterns, and are slightly rich in LREE. Their average ΣREE is 95.62×10^{-6}, with $(La/Yb)_N$ of 4.35, positive Eu anomaly (δEu = 1.19), and negative Ce anomaly (δCe = 0.29). Most of them possess the characters of tholeiite, and their mantle source regions belongs to that of the transitional-type mantle [9].

Lead-isotopic Geochemistry: The $^{206}Pb/^{204}Pb$, $^{207}Pb/^{204}Pb$, and $^{208}Pb/^{204}Pb$ ratio for a sample of basalt are 18.76, 15.52, and 39.36 respectively. In $^{207}Pb/^{204}Pb$- $^{206}Pb/^{204}Pb$ plot for different types of mantle rocks [1], it is located in the MORB range, showing the mixing feature of DMM and EMII.

Discussion and Conclusion: Rock-association types of the basalts in the Luhuo-Daofu region are mainly pillow basalt, vesicle-amygdaoidal basalt, and massive basalt. They are dominated by tholeiite with respect to their chemical composition. Major and trace elements and Pb isotopes indicate their MORB character. The authors think that the initial ocean basin where the Luhuo-Daofu basalts were formed is an immature marginal ocean basin located in the Tethys island-sea pattern. Its formation mechanism is related to the activity of thermal mantle plumes in different parts in the opening process of Tethys ocean. In Late Triassic the immature marginal ocean basin began subducting owing to continuous northeastward movement of the Indian Plate. Tectonic emplacement of ophiolitic shell components occurred and are kept on the secondary rifting belts as what we have seen at present.

Acknowledgments: A preselection program of Chinese National Climb Plan (fundamental research concerning the searching of super-large mineral deposits) financially supports the study.

References: [1] Irvine T. N. and Baragar W. R. A. (1971) *Can. J. Earth Sci., 8,* 523–548. [2] Pearce T. H. et al. (1975) *EPSL, 24,* 419–426. [3] Pearce T. H. et al. (1977) *EPSL, 36,* 121–132. [4] Dmitriev L. V. et al. (1989) *Abstracts of 28th International Geological Congress, 1,* 399. [5] Condie K. C. (1989) *Plate Tectonics and Crustal Evolution,* 3rd ed., New York, pp. 310–350, Pergamon Press. [6] Pearce J. A. and Cann J. R. (1973) *EPSL, 19,* 290–300. [7] Pearce J. A. (1982) in Orogenic andesites (R. S. Thorps and J. Chichester, ed.), pp. 525–548, Wiley, New York. [8] Pearce J. A. and Norry M. J. (1979) *Contrib. Mineral. Petrol., 69,* 33–47.[9] Le Roex A. P. (1983) *J. Petrol., 24,* 267–318. [10] Zindler A. and Hart S. R. (1986) *Annu. Rev. Earth Planet. Sci., 14,* 493–571. [11] McDonough W. F. and Sun S. S. (1995) *Chem. Geol., 120,* 223–253.

FIRST DATA ON RARE-EARTH-ELEMENT DISTRIBUTIONS IN THE CHANGJIANG ESTUARY: RELATIVELY LOW CONCENTRATIONS AND CONSERVATIVE BEHAVIOR AT LOW-SALINITY REGIONS.

Z.-L. Wang[1], C.-Q. Liu[1], and J. Zhang[2], [1]State Key Laboratory of Environmental Geochemistry, Institute of Geochemistry, Chinese Academy of Sciences, Guanshui Road 73, Guiyang 550002, China (zlwang@ms.

gyig.ac.cn), [2]Department of Environmental Biology and Chemistry, Faculty of Science, Toyama University, Gofuku 3190, Toyama 930-8555, Japan.

Introduction: Estuaries are both chemically and physically dynamic systems that act as buffers between the land and the ocean. The net flux of riverine materials to the open ocean depends on their estuarine reactivity. There have been many studies of the geochemistry of the rare earth elements (REEs) in estuaries with the objective both to elucidate the physical, chemical, and biological processes that determine the fate of the REEs and to estimate the net riverine contribution to the REE budget of the world oceans. Large-scale removal of REEs has been reported both in field research for many estuaries of the world and laboratory experiments. It has been firmly established the REE removal is a common feature of the mixing process in estuaries [1]. Changjiang is the third biggest river in the world; therefore, REE distributions in the Changjiang water and Changjiang estuary play an important role to interpret geochemistry of the REEs of the East China Sea and the West Pacific.

Sampling and Analysis: Water samples collected in surface waters across 80 km along the salinity gradient from 0‰ to 20‰ salinity of the Changjiang Estuary at November 5, 1998. The samples used for "dissolved" REE determinations were filtered through 0.1-μm hollow fibers (Millipore) immediately after collection and acidified to pH <1.5 and stored in acid-cleaned, 2-L high-density polyethylene bottles before analysis. Unfiltered water samples for measurements of the "total" acid-soluble REE concentrations were also collected, acidified by Q-HCl to pH <1.5 and filtered through 0.22-μm filters before analysis. Additional samples were also obtained at each station to measure salinity, pH, temperature, dissolved O, major anions, and cations.

Major cations were determined by graphite furnace atomic absorption spectroscopy (GFAAS) and anions by an ion chromatography. The analysis of REE and Y was performed by the inductively coupled plasma mass spectrometry (ICP-MS) method described in Shabani et al. [2], after preconcentrated and purified by solvent extraction and back extraction using HDEHP and H_2MEHP in heptane. Indium was used as an internal standard to monitor the quantitativeness of the chemical procedure, and Cd was used to monitor the stability of the ICP-MS determination. The blanks for the entire procedure and reagents were measured in parallel with the samples; they were 4% for La, 5% for Ce, and 2–3% for other REEs and Y. The accuracy and precision of REE measurements were better than ±3%. The entire procedure accomplished in Class-100 laboratory and Millipore-Q water and high-purity reagents were used.

Results: The most striking aspect of the data is the "dissolved" REE concentrations in Changjiang estuary gradually decreased slightly with increasing salinity at the lower estuary indicating that just slightly REE removal occurs during estuarine mixing at low salinity. This conservative behavior is very rare compared with the large-scale removal of REEs in other estuaries. But the "total" REE concentrations show a strongly removal (>90%) at same region. From 5‰ salinity to salinity 20, both the "dissolved" and "total" REE distributions increased linearly exhibiting non-conservative behavior. HREEs enrichment for "dissolved" REE and LREEs and MREEs enrichment for "total" REE observed throughout the estuary.

Another marked aspect of the REE distribution in Changjiang estuary is that the very low absolute abundance of REE than other estuaries. The same low REE concentrations obtained in the Changjiang mainstream waters in 1998 by Zhang et al. [3]. This also agrees with the results of lower concentrations of the other trace metals in Changjiang mainstream and Changjiang estuary waters. These low metal levels probably duo to the short residence time of the water and/or abundant suspended solids in it.

References: [1] Elderfield H. et al. (1990) *GCA, 54,* 971–991. [2] Shabani M. B. et al. (1990) *Anal. Chem., 62,* 2709–2714. [3] Zhang J. et al. (1998) *Goldschmidt Conference, Toulouse, Mineral. Mag., 62A,* 1693–1694.

BACTERIALLY PROMOTED CALCIUM CARBONATE PRECIPITATION AND SOLID-PHASE CAPTURE OF STRONTIUM AND UO_2.

L. A. Warren, N. Parmar, and F. G. Ferris, Department of Geology, Earth Sciences Centre, University of Toronto, 22 Russell Street, Toronto, ON M5S 3B1, Canada (lwarren@zircon.geology.utoronto.ca).

Introduction: A wide variety of soil and aquatic bacteria can degrade urea, deriving ammonia for metabolic requirements. Given sufficient microbial activity, this microbiological process also can affect solution chemistry through increases in both alkalinity and pH:

$$CO(NH_2)_2 + 2H_2O + H^+ \rightarrow 2NH_4^+ + HCO_3^- \qquad (1)$$

potentially promoting the precipitation of carbonates in the process

$$2HCO_3^- + Ca^{2+} \rightarrow CaCO_{3(s)} + CO_2 + H_2O \qquad (2)$$

Ongoing work has demonstrated that $CaCO_3$ precipitation can be successfully coupled to urea degradation by the common groundwater, gram-positive bacteria, *Bacillus pasteurei*:

$$2CO(NH_2)_2 + 3H_2O + 2H^+ + Ca^{2+} \rightarrow CaCO_{3(s)} + CO_2 + 4NH_4^+ \qquad (3)$$

Moreover, significant solid-phase capture of Sr and UO_2 can be achieved through this biologically mediated process, providing a potential bioremediation strategy for contaminated aquifers.

The objectives of the current study were to quantitatively examine the $CaCO_3$ precipitation dynamics in conjunction with solid-phase capture of Sr and UO_2, over time, during 4-d batch experiments, and compare the results to those from control *B. pasteurei* systems.

Methods: To quantify $CaCO_3$ precipitation over time, batch experimental systems were set up under three treatments: bacterial control, Sr treatment, and UO_2 treatment. All three experimental systems included a *B. pasteurei* cell density equivalent to an $OD_{600nm} = 0.4$; BHI media amended with 330 mmol urea ($CO(NH_2)_2$); 25 mmolar HCO_3^- (added as $NaHCO_3$) and Ca^{2+} (added as $CaCl_2$). A total of 1 mM Sr or UO_2 was added to the contaminant systems. All solutions were made with ultra-sterilized H_2O (USW) and filter sterilized before adding to the experimental systems, which were pH adjusted to 6 and then transferred to an anaerobic chamber and monitored for 96 h. Solution pH was monitored, filtered samples (0.2-μm sterile acrodisc filters with supor membrane) for NH_4^+, Ca^{2+}, Sr, and UO_2, and nonfiltered samples for total contaminant concentrations, image and spectral analyses scanning electron microscopy (SEM) and electron diffraction spectroscopy (EDS), and mineralogy X-Ray powder diffraction (XRD) were collected at half-hour intervals for the first 6 h, then at 24 and 96 h. Cell viability of the three experimental systems was monitored during the experiment by use of a molecular probe (BacLight Viability Kit and Molecular Probes) and direct cell counts using epifluorescence microscopy.

Results and Discussion: The pH values increased rapidly in all three systems reaching a value over 8 within minutes, and over 9 by 24 h. NH_4^+ concentrations also increased rapidly in all three systems indicating active urea degradation (7–8 mmol hr^{-1}) by *B. pasteurei,* such that approximately 85–90% of the urea had been degraded within 24 h in all three treatments. No differences in system pH or NH_4^+ concentrations were observed between control and contaminant systems indicating no toxic effects of 1 mmol Sr or UO_2 for *B. pasteurei.* This result was confirmed through direct cell counts of stained samples for viability analyses using epifluorescence microscopy. In both control and contaminant systems, more than 90% of the cells were still viable after 24 h.

Ca^{2+} concentrations showed different time trends among the three systems. In the control (no contaminants) system, 95% of the 25 mM Ca initially added was precipitated within 1 h. In contrast, in the presence of Sr or UO_2, solution Ca concentrations decreased much more slowly, reaching a 95% Ca precipitation rate only after 6 h. These differing results for Ca incorporation may reflect coprecipitation of Sr and UO_2 in the carbonates.

Solid-phase capture of Sr and UO_2 also showed different patterns. Solid associated Sr increased linearly over time to ~95% of the total Sr added by 24 h. In contrast, solid UO_2 concentrations initially increased rapidly then remained static for about 6 h at ~30% of the total UO_2 added, but decreased to about 7% by 24 h.

Visual inspection by SEM of the precipitates being formed throughout the experiment indicated that both authigenic precipitation was occurring directly at bacterial cell surfaces as well as homogeneously in solution in all three systems. Spectral analyses by EDS indicated clear Sr and U peaks associated with the carbonates indicating solid-phase capture. Further, the morphology of the $CaCO_3$ precipitates differed both among the three treatments as well as within each treatment system as time progressed. We are currently working on identifying the $CaCO_3$ as well as any Sr and UO_2 precipitates occurring over time in these systems by XRD.

CHROMIUM(III) SORPTION AND OXIDATION ON MANGANITE (γ-MnOOH) AS OBSERVED WITH FLUID-CELL ATOMIC FORCE MICROSCOPY AND X-RAY PHOTOELECTRON SPECTROSCOPY.

R. W. Weaver and M. F. Hochella Jr., Department of Geological Sciences, 4044 Derring Hall, Virginia Polytechnic Institute and State University, Blacksburg VA 24061, USA (rweaver@vt.edu; hochella@vt.edu).

This study presents new microscopic and spectroscopic observations of the interaction of Cr(III) solutions with manganite (γ-MnOOH). Manganese oxide surfaces are known to be active sorbents and oxidants of heavy metals in natural environments. Furthermore, in the case of Cr, Mn-oxides are believed to be the only naturally occurring oxidants capable of oxidizing Cr(III) to Cr(VI). Although the macroscopic sorptive and oxidative behavior of Mn oxides is well known from field and laboratory observations, the actual mechanism(s) responsible for this behavior remain unresolved. Past studies have suggested that various surface and bulk features such as redox-active Mn surface-sites, microtopography, ordered vacancies, and defects may all be sites where reactions occur with preference. However, many of these suggestions are based on observations from bulk solution studies that are not completely able to interpret the mechanism(s) of a microscopic surface reaction.

To provide a clearer picture of the role that surface features (e.g., steps, kinks terraces) play in promoting or inhibiting Cr(III) sorption and oxidation under specific solution conditions, this study utilizes microscale observations obtained from fluid-cell atomic force microscopy (AFM), scanning electron microscopy (SEM), and X-ray photoelectron spectrometry (XPS). The capability of the AFM to image a mineral surface at the nanometer level while it is reacting with a contacting solution is a particularly important advantage in understanding surface reactions in that the extent and spatial distribution of the reaction can be directly observed.

In situ, fluid-cell AFM observations of manganite surfaces reacted with Cr(III) solutions [0.1–4000 ppm Cr(III), pH 3–8] reveal that the reaction is heterogeneous involving both local dissolution (acidic and reductive) of manganite and Cr adsorption and/or surface microprecipitation. For example, within seconds of exposure to a pH 4.5, 50 ppm Cr(III) solution, Cr-bearing microprecipitates measuring <7 nm high by <20 nm wide and dissolution pits measuring <7 nm deep by <15 nm wide form. Over reaction periods exceeding several hours dissolution pits up to 3 μm wide and highly eroded step edges are visible in some areas of SEM images. Interestingly, other areas only a few micrometers away show that little to no dissolution has occurred. This suggests that the solution conditions are locally more aggressive at certain surface features.

X-ray photoelectron spectroscopy analysis of manganite surfaces exposed to pH 3.3, 4000 ppm Cr(III) solutions for 10 h reveal the microprecipitates to be dominantly Cr-bearing with a $Cr2p_{3/2,1/2}$ spin-orbit splitting of 9.7 eV. This spin-orbit splitting is identical to that reported for several Cr(III) oxides and oxyhydroxides. On-going experiments are focused on the determination of the oxidation state(s) of the microprecipitates and their rate and extent of accumulation over varied solution conditions.

RACEMIZATION ISOCHRONS FOR THE UNITED STATES ATLANTIC COASTAL PLAIN QUATERNARY: INDEPENDENT CALIBRATION AND GEOCHEMICAL IMPLICATIONS OF RESULTS FROM MARGINAL MARINE UNITS, CENTRAL FLORIDA.

J. F. Wehmiller[1], L. L. York[1], D. S. Jones[2], and R. W. Portell[2], [1]Department of Geology, University of Delaware, Newark DE 19716, USA (jwehm@udel.edu), [2]Florida Museum of Natural History, University of Florida, P.O. Box 117800, Gainesville FL 32611, USA.

Amino-acid racemization (AAR) is a widely employed method for estimation of relative or numerical ages in Quaternary deposits. Aminostratigraphy and aminochronology require adherence to two fundamental principles: (1) that D/L values increase with increasing sample age for samples with similar temperature histories, and (2) that D/L values in samples of equal age increase with increasing temperature or decreasing latitude. These principles appear to be violated in some cases when AAR data from Pleistocene units of the United States Atlantic margin are interpreted within a framework of local, independent chronological calibration. Reconciliation of AAR data with these controls requires rejection of some amino-acid results (because of unrecognized diagenetic effects), or that temperature histories for coastal plain sites have not been uniformly consistent with present latitudinal gradients of temperature, and/or that existing information for racemization rate constant temperature sensitivity be revised. These conclusions imply that the age resolution capabilities of AAR in Atlantic coastal plain deposits are not as precise as assumed in all prior AAR studies in this region, in spite of the fact that excellent precision is usually observed when multiple analyses are obtained from a single site.

Amino-acid racemization data and U-series thermal ionization mass spectrometry (TIMS) dates (coral) from sites in Virginia, South Carolina, and Georgia [2,3], combined with AAR data from Leisey Pit, Ruskin, Florida [3], provide new insights for regional aminostratigraphic models. AAR data for *Chione* from the superposed section at Leisey Pit conform to the local stratigraphic control provided by the section. The aminochronologic age estimate for the Fort Thompson unit at Leisey could be as young as marine isotopic stage 5 (MIS 5) if calibrated with *Chione* data from the Pacific coast of North America [4]; this age estimate appears inconsistent with the middle Pleistocene age estimate for this unit derived from Sr-isotopic and paleontological data from the unit [3], but it is in reasonable agreement with U-series calibrated AAR data from South Carolina and Georgia. Alternatively, a middle Pleistocene age (perhaps MIS 9-11-13) for the Leisey Fort Thompson unit appears consistent with most Florida AAR data [5–7] and the Sr-isotopic age estimate for the unit [3], but it is difficult to reconcile with AAR data from calibrated sites to the north unless temperature and/or geochemical anomalies are invoked. The Leisey section is an important sequence to understand in the ongoing effort to develop a reliable aminostratigraphic framework for the United States Atlantic coastal plain.

References: [1] Wehmiller J. F. et al. (1997) *GSA Abstr. Prog., 29(6)*, A-346. [2] Simmons K. R. et al. (1997) *Eos Trans. AGU, 78(46)*, F788. [3] Jones et al. (1995) *Bull. Fla. Mus. Nat. Hist.*, *37*, 93–105. [4] Wehmiller J. F. and Emerson W. K. (1980) *The Nautilus, 94*, 31–36. [5] Mitterer R. M. (1975) *EPSL, 28*, 275–282. [6] Hollin J. T. and Hearty P. J. (1987) *GSA Abstr. Prog., 19(7)*, 705. [7] Karrow P. F. and Belknap D. F. (1987) *GSA Abstr. Prog., 19(7)*, 722.

EVIDENCE FOR A CONTINENTAL COMPONENT AT ELAN BANK FROM LEG 183-SITE 1137 ON THE KERGUELEN PLATEAU.

D. Weis[1], J. Barling[2], D. Damasceno[1], F. A. Frey[3], K. Nicolaysen[3], and the Leg 183 Shipboard Scientific Party, [1]Earth and Environmental Sciences, Université Libre de Bruxelles, CP 160/02, Av. F. D. Roosevelt, 50, B-1050 Brussels, Belgium (dweis@ulb.ac.be), [2]Earth and Environmental Sciences, University of Rochester, Hutchison Hall 227, Rochester NY 14627, USA, [3]Department of Earth, Atmospheric and Planetary Sciences, Massachusetts Institute of Technology, Cambridge MA 02139, USA.

Introduction: The Kerguelen Plateau-Broken Ridge (KP-BR) is, with the Ontong-Java Plateau (OJP), one of the largest large igneous provinces or LIPs ($>2 \times 10^6$ km^2) formed during the Cretaceous period and probably resulted from the initial "impact" of a mantle plume at the base of the lithosphere. At ~115 Ma, after continental breakup, the Kerguelen Plume initiated formation of the KP-BR LIP as a subaerial plateau in a young oceanic basin. This is a very different tectonic setting from that of the Icelandic-North Atlantic LIP or that of OJP. The 115-m.y. volcanic record of the Kerguelen Plume is one of the best long-lived records of plume volcanism with most of the KP-BR representative of the plume head, a 5000-km-long hotspot track (the 82–38-Ma Ninetyeast Ridge) and OIB volcanism on the Kerguelen Archipelago and Heard Island from 40 to 0 Ma. The Kerguelen Plume has a very distinct enriched geochemical signature and carries the Dupal anomaly. The recent ODP Leg 183 drilled eight sites in the KP-BR to define spatial variations in age and geochemistry of the volcanic basement [1].

Setting: Site 1137 lies at a water depth of 1016 m on Elan Bank, a large western salient of the KP that is flanked on three sides by presumed Cretaceous oceanic crust of the Enderby Basin. The major basement objectives at Site 1137 were to characterize the age, petrography and compositions of the lavas. The position of Elan Bank, intermediate between the ~110-Ma southern KP and the ~85–95-Ma Central KP, is critical to the understanding of temporal and geochemical variations of this giant LIP.

Samples: Ten units were defined in the 151.7-m basement section at site 1137, including seven tholeiitic to transitional, sparsely to highly porphyritic, basaltic flow units (units 1–4, 7–8, 10) with interbedded volcaniclastic sandstone (5), conglomerate (6) and crystal-vitric tuff (9). The uppermost six basement units were emplaced subaerially, whereas the seventh unit was emplaced in a wet sediment. Basement units 5 (sandstone/siltstone) and 6 (conglomerate) are fluvial. The conglomerate has clasts (well-rounded granules to small boulders) of a wide variety of rock types: trachyte, flow-banded rhyolite, and various basalts. The most unexpected clasts in this oceanic setting are a garnet-biotite gneiss and granitoids. The altered crystal-vitric tuff is composed of ~40% coarse crystals of sanidine and contains <5% lithic clasts in a green matrix.

Geochemistry and Isotopes: Site 1137 basalts are only slightly to moderately altered in the interiors of the units (LOI <1.6 wt%). They are slightly quartz-normative tholeiitic basalts with MgO contents between 4.4 and 7.4 wt%. Compared to the other Cretaceous igneous basement, site 1137 basalts are more enriched in highly to moderately incompatible trace elements, especially high Zr, Nb, Ce for comparable Y contents. Site 1137 basalts have the highest Zr/Ti and Zr/Y. Downhole variations show an overall decrease in Nb/Ce, Nb/Zr, and Zr/Y. On a plot of Nb/Y vs. Zr/Y [2], site 1137 basalts plot outside the plume-related field, in a trend parallel to that of basalts from site 738 at the southern tip of the KP [3]. These trends point toward the average composition of upper continental crust.

The most interesting variations of site 1137 basalts are the isotopic compositions that vary nearly regularly downhole from 0.7049 to 0.7060 for ^{87}Sr/^{86}Sr, 0.51259 to 0.51244 for ^{143}Nd/^{144}Nd, and 15.594 to 15.654 for ^{207}Pb/^{204}Pb for ^{206}Pb/^{204}Pb at ~18.0 ± 0.4. These isotopic variations correlate well with the downhole TE abundance ratio variations. Relative to the basalts, the felsic volcanic rocks preserved as clasts in the conglomerate (6) and the volcanic lithic sandstone (5) have higher ^{87}Sr/^{86}Sr (up to 0.7322), higher ^{207}Pb/^{204}Pb (up to 15.820), and lower ^{143}Nd/^{144}Nd (down to 0.51222). The felsic clasts have ^{87}Sr/^{86}Sr of 0.7104 at 95 Ma, their inferred age from a two-point whole-rock isochron. The garnet-biotite gneiss clast has even higher Sr, lower Nd, and more radiogenic Pb ratios, and it has the isotopic characteristics of old upper continental crust.

Conclusions: (1) Petrographic, geochemical and isotopic characteristics of clasts in a fluvial conglomerate at site 1137 constitute the first unequivocal evidence of the presence of upper continental crust in the Elan Bank, part of the KP oceanic plateau. (2) Felsic volcanic rocks were emplaced at the same time as, or slightly earlier than, site 1137 basalts and result from an AFC process. They may derive from the same mantle source that has produced the basalt, but with stronger fractionation and contamination by the crustal component. (3) The continental crust component was also incorporated in the magmas that crystallized to form the basaltic basement at site 1137, altough its importance decreases with decreasing eruption age of the basalts. (4) Site 1137 basalts formed by partial melting of the Kerguelen Plume. The uppermost, least contaminated 1137 lavas have Sr and Nd ratios that overlap with 85% of the Kerguelen Archipelago lavas, in the field representative of the Kerguelen Plume [4].

Additional Information: The Leg 183 Shipboard Scientific Party includes M. Antretter, N. Arndt, F. Boehm, M. Borre, M. Coffin, H. Coxall, J. Damuth, H. Delius, R. Duncan, H. Inokuchi, L. Keszthelyi, J. Mahoney, L. Moore, R.D. Müller, C. Neal, M. Pringle, D. Reusch, P. Saccocia, D. Teagle, V. Wahnert, P. Wallace, S. Wise, and X. Zhao.

References:[1] Frey et al. (1999) *Science*, submitted. [2] Fitton et al. (1997) *EPSL, 153*, 197–208. [3] Mahoney et al. (1995) *Chem. Geol., 120*, 315–345. [4] Weis D. et al. (1998) *Mineral. Mag., 62A*, 1643–1644.

TRACING SOURCES OF CHANNEL AND NORTH SEA POLLUTION AEROSOLS ABOVE THE STRAITS OF DOVER USING LEAD-ISOTOPIC GEOCHEMISTRY.

D. Weis[1], K. Deboudt[2], and P. Flament[2], [1]Earth and Environmental Sciences, Université Libre de Bruxelles, CP 160/02, Av. F. D. Roosevelt, 50, B-1050 Brussels, Belgium (dweis@ulb.ac.be), [2]Université du Littoral-Côte d'Opale, LISE-ELICO (UPRES-A CNRS 8013), Station Marine, BP 59, F-62930 Wimereux, France.

Introduction: Anthropogenic Pb remains the most important input of Pb in the troposphere today. It is now important to take sources other than automobile emissions (e.g., Pb smelters, ferrous and nonferrous metal manufacturing plants, fossil fuel combustion, waste incinerators, etc.) into account in evaluating the Pb content of atmospheric aerosols to discriminate the origins of pollution aerosols. The capability of Pb isotopes to study the sources and transport of pollution aerosols [1] is demonstrated here above the Straits of Dover. We collected atmospheric aerosols above the Eastern Channel and the Southern Bight of the North Sea between March and November 1995. During the same period, to define more local contributions, we characterized the Pb-isotopic signatures of the main industrial sources on the French coast, near the Straits of Dover. Urban and automobile-derived aerosols were also collected.

Background and Results: The urban isotopic composition (^{206}Pb/^{207}Pb = 1.158 ± 0.003) has become more radiogenic in recent years [2]. This composition is also highly variable because of seasonal variations in the emissions (coal and oil burning in the winter, summer holidays with less industrial and automobile activities). On a regional scale, major industrial emissions that represent 67% of the industrial dust emissions in the Nord-Pas de Calais area [3] have a well-defined isotopic composition (1.13 < ^{206}Pb/^{207}Pb < 1.22), distinctly more radiogenic than the petrol-Pb signature (1.06 < ^{206}Pb/^{207}Pb < 1.12). These results, together with those measured near the main coastal highway (above the highway, on the lee and weather sides at 0 and 400 m), show that the automobile source has become a minor component of particulate Pb in air due to the phasing out of Pb in gasoline. On a local scale, Dunkerque, the most urbanized and industrialized area along the Straits of Dover, may transiently control elevated Pb concentrations.

The isotopic compositions of Pb aerosols collected above the Straits of Dover vary between 1.11 < ^{206}Pb/^{207}Pb < 1.14 for the Southern Bight samples and between 1.12 < ^{206}Pb/^{207}Pb < 1.17 for the Eastern Channel samples. These latter values are more radiogenic and associated with higher Pb concentrations.

Discussion and Conclusions: On the French coast of the Straits of Dover, automobile Pb appears today as a minor component of this metal in the air. This conclusion is supported by (1) the general reduction in atmospheric aerosol Pb contents above the Eastern Channel [4]; (2) the isotopic composition of Pb collected near the main coastal highway (1.13 < ^{206}Pb/^{207}Pb < 1.15), significantly different from gasoline values in Northern France and surrounding countries (1.06 < ^{206}Pb/^{207}Pb < 1.12); and (3) the urban signature (measurements near a main arterial street in Lille: ^{206}Pb/^{207}Pb = 1.158 ± 0.003) distinct from the petrol-Pb signature.

The radiogenicity of the urban signal has increased since Pb has been banned from gasoline. Nevertheless, it is not possible yet to fingerprint a French urban source, because all the current major urban contributors are not precisely known. In contrast, major industrial signatures can be defined on the French coast of the Straits of Dover (1.13 < ^{206}Pb/^{207}Pb < 1.22), particularly for the larger Pb smelter in Europe, where the emitted dusts contain 21 wt% Pb [2] (1.132 < ^{206}Pb/^{207}Pb < 1.135). These industrial sources have a median signature significantly different from the French and British petrol-Pb values.

The extent to which local and regional sources may explain Pb concentrations on the Straits of Dover can be assessed by sampling above the marine zone. The occurrence of medium range pollution episodes, related to semi-remote sources located in southeast England, can be shown. For air masses cyclonically transported over the North Atlantic, the isotopic signature technique traces remote sources, but uncertainties in calculations of air-mass trajectories over the Atlantic Ocean due to the lack of wind data limit the possibilities of source identification. For continental air masses, the isotopic measurements display a significant difference between high radiogenic Eastern European aerosols (1.145 < ^{206}Pb/^{207}Pb < 1.169) and low radiogenic Pb aerosols originating from Western Europe (1.111 < ^{206}Pb/^{207}Pb < 1.142). Evidence for a long-range transport of Eastern European Pb emissions may be related to the common use of leaded gasoline in Central and Eastern Europe (the former "Eastern countries"). The significance of this impact must be better documented and related to antipollution initiatives of Western European governments to limit the Pb emissions in the atmosphere.

References: [1] Véron et al. (1999) *Atmos. Environ.*, in press. [2] Hopper et al. (1991) *Tellus, 43B*, 45–60. [3] DRIRE (1997) *French Environ. and Industrial Authorities Tech. Rpt.*, 344 pp. [4] Flament P. et al. (1996) *Sci. Total Environ., 192*, 93–206.

ROLE OF MICROORGANISMS AND MICROBIAL METABOLITES IN APATITE AND BIOTITE DISSOLUTION KINETICS.

S. A. Welch, A. E. Taunton, and J. F. Banfield, Department of Geology and Geophysics, University of Wisconsin–Madison, 1215 W. Dayton Street, Madison WI 53706, USA (swelch@geology.wisc.edu; razrback@geology.wisc.edu; jill@geology.wisc.edu).

Introduction: Phosphorus is essential for all organisms and is often a limiting nutrient in many environments. In soils and weathered rock, the primary source of inorganic phosphate is apatite. Organisms can accelerate the rate of phosphate release from apatite by producing inorganic or organic acids or possibly other compounds (e.g., extracellular polymers or enzymes). Mineral dissolution experiments were conducted in solutions of organic acids and in microbial cultures to determine the effects of microbes and their metabolites on apatite and biotite dissolution.

Results: In the organic-acid experiments, apatite was dissolved in batch reactors in 1 mM solution of acetate, oxalate, and NaCl over a range of pH (initial pH 2–10). Dissolved phosphate was used as an indicator of mineral dissolution. Dissolution rates were calculated from the increase in phosphate concentration over time. In all batch experiments, initial release of phosphate was rapid and then decreased with time due to the consumption of protons and the approach to solution saturation. Apatite dissolution rates in the inorganic solutions decreased as pH increased from acidic to near neutral from $\sim 10^{-12}$ to 10^{-16}mol PO_4^{-3}/cm^2 s, and can be described by $r = ka_{H+}{}^n$ where n, the pH dependence of the dissolution rate, is ≈0.8. At initial pH 2, apatite dissolution rate in the oxalate and acetate solution is slightly lower than in the inorganic solution. However at higher pH, the organic acids increased apatite dissolution, and the relative rates, $r_{organic}/r_{inorganic,}$increase with increasing pH, reflecting the formation of Ca-organic complexes. The solution chemistry is not stochiometric in the oxalate experiments. This is attributed to the precipitation of secondary mineral phases, presumably Ca oxalates. Scanning electron microscopy (SEM) imaging of mineral samples after reaction showed submicrometer scale secondary minerals and extensive etching to form elongated spires parallel to c.

In the biological experiments, biotite and apatite were dissolved in solutions of microbial cultures. Experiments were designed so microorganisms would be limited by soluble inorganic nutrients. There were three treatments: biotite and dissolved phosphate (bio), biotite plus apatite (b + a), and apatite (ap). One of the microbial assemblages was grown from a mineral sample collected from the bottom of the soil zone and contained bacteria and eukaryotes. The other was from a weathered rock sample and contained primarily bacteria. In both experiments with biotite (bio and b + a), the microbes produced tens to hundreds of micromoles of low molecular weight organic acids, lowered solution pH to 3–4, and increased biotite dissolution by a factor of 2–10× compared to abiotic controls. Biotite dissolution was greater in the b + a experiments than in the biotite alone experiments. Phosphate release from apatite was 2 orders of magnitude higher than in the abiotic controls. In the apatite experiment (ap), phosphate release from apatite was again 2 orders of magnitude greater than for the abiotic control. However, solution pH remained near neutral and much lower concentrations of low molecular weight organics were detected in solution. SEM analysis of the mineral samples showed secondary precipitates and microbial colonization of the mineral surfaces. Apatite etched to form roundedelongated features parallel to c that are morphologically distinct from the sharp spires formed in the abiotic experiments.

OXYGEN-ISOTOPIC COMPOSITION OF CONODONT APATITE: A POTENTIAL PROXY FOR PALEOZOIC MARINE WATER TEMPERATURES AND SALINITIES.

B. Wenzel[1], W. Buggisch[1], M. M. Joachimski[1], P. Königshof[2], and C. Lécuyer[3], [1]Institut für Geologie und Mineralogie, Universität Erlangen, Schlossgarten 5, D-91054 Erlangen, Germany (bwenzel@geol.uni-erlangen.de), [2]Forschungsinstitut und Naturmuseum Senckenberg, Senckenberganlage 25, D-60325 Frankfurt, Germany, [3]Laboratoire de Sciences de la Terre, Centre National de la Recherche Scientifique-UMR 5570, Ecole Normale Supérieure de Lyon, 46 Allée d'Italie, 69364 Lyon Cedex 7, France.

Introduction: Recently developed phosphate microsampling techniques [1–3] enable O-isotopic analyses on very small samples of Paleozoic conodonts as potential new indicators for marine water temperatures and salinities. Due to the wide geographic distribution and excellent stratigraphic resolution of conodonts, it should be possible to construct marine $\delta^{18}O$ records with a much higher resolution than previously obtained with biogenic carbonates. But unlike the fairly extensive investigated carbonate O-isotopic system [4], much less is known about the phosphate O-isotopic paleothermometer.

Crucial for the use of conodonts as new proxies for Paleozoic paleoceanography is to evaluate (1) the potential influence of secondary diagenetic alteration on $\delta^{18}O_{phosphate}$, and (2) whether conodont animals precipitated apatite in isotopic equilibrium with ambient seawater.

Results: (1) Individual populations of conodonts usually show very homogenous $\delta^{18}O_{phosphate}$ values with standard deviations close to the analytical precision (±0.2‰). Coeval upper Devonian palmatolepids from the Rheinisches Schiefergebirge and Harz mountains (Germany) do not show a correlation between $\delta^{18}O_{phosphate}$ and maximum thermal alteration of the host rock. Even specimens from contact metamorphosed areas (CAI 7) show $\delta^{18}O_{phosphate}$ values similar to that of modern tropical marine invertebrates that suggests well preserved primary marine values.

In contrast, hydrothermally altered conodonts may reveal scattered isotopic values and significantly depleted ^{18}O contents. Such conodonts are frequently characterized by significantly altered apatite microstructures. It is concluded that thermal alteration during burial diagenesis does not necessarily alter $\delta^{18}O_{phosphate}$ of conodonts, but conodont apatite can be altered in hydrothermal diagenetic environments. Most Silurian, Devonian, and Carboniferous conodonts analyzed by us so far do not show evidence for hydrothermal alteration and reveal $\delta^{18}O_{phosphate}$ similar to those of modern tropical biogenic apatites. It can therefore be assumed that they reflect well-preserved primary isotopic signatures.

(2) Since conodont animals became extinct in the Triassic, it is difficult to determine wether they precipitated apatite in isotopic equilibrium with ambient seawater. As a test, we compared Devonian conodonts and fish teeth (Rheinisches Schiefergebirge) and Silurian conodonts and calcitic brachiopod shells (Gotland) from identic stratigraphic horizons. Fish teeth and conodonts show very similar $\delta^{18}O_{phosphate}$ values. Modern fish precipitate tooth apatite close to isotopic equilibrium with seawater [5]. Therefore, it can be assumed that Devonian fish teeth and conodonts also reflect equilibrium values.

Silurian conodonts and coeval brachiopods from Gotland also show significantly correlated $\delta^{18}O$ values, but reveal variable offsets between $\delta^{18}O_{phosphate}$ and $\delta^{18}O_{calcite}$. Whereas most calcitic brachiopods from Gotland show lower $\delta^{18}O$ values than their modern counterparts [6], conodonts reveal $\delta^{18}O$ values similar to modern and Mesozoic tropical biogenic apatites. The data suggest that either brachiopod shell calcite was diagenetically altered or that Silurian brachiopods did not precipitate shell calcite in isotopic equilibrium with seawater.

Conclusions: Our preliminary data suggest that conodont apatite can be used as an indicator for Paleozoic marine $\delta^{18}O$ variations. Although conodonts may be altered in hydrothermal diagenetic environments, secondary thermal alteration during burial diagenesis does not generally seem to affect $\delta^{18}O_{phosphate}$. Comparison of Devonian conodonts and fish teeth suggests that conodonts did precipitate apatite close to O-isotopic equilibrium with seawater.

References: [1] Holmden C. et al. (1997) *GCA, 61,* 2253–2263. [2] Wenzel B. et al., this volume. [3] Atudorei V. and Sharp Z. D. (1997) *Terra Nova (Abstract Supplement), 7,* 445. [4] Marshall J. D. (1992) *Geol. Mag., 129,* 143–160. [5] Kolodny Y. et al. (1983) *EPSL, 64,* 389–404. [6] Wenzel B. and Joachimski M. M. (1996) *Palaeogeogr., Palaeoclimatol., Palaeoecol., 122,* 145–166.

PHOSPHATE-OXYGEN-ISOTOPIC MICROANALYSIS BY INFRARED LASER ISOTOPE RATIO MONITORING GAS CHROMATOGRAPHY MASS SPECTROMETRY.

B. Wenzel, M. M. Joachimski, J. Rauch, and W. Buggisch, Institut für Geologie und Mineralogie, Universität Erlangen, Schlossgarten 5, D-91054 Erlangen, Germany (bwenzel@geol.uni-erlangen.de; joachimski@geol.uni-erlangen.de)

Introduction: The determination of the O-isotopic composition of the PO_4-group in apatitic microfossils (small fish teeth, conodonts) or intra-tooth $\delta^{18}O$-variations of vertebrate tooth phosphate has previously been hampered by relatively large sample sizes required for conventional offline isotope analyses (>10 mg). We present an improved version of the laser isotope-ratio monitoring gas chromatography with mass spectrometry (irm-GCMS) technique [1] such that the O-isotopic composition of very small samples of natural and synthetic phosphates (0.1 mg) can be precisely determined.

Method: A modified Finnigan Precon (pre-GC concentration device) system, connected on line via a gaschromatograph (GC) and an open-split interface to a Finnigan MAT 252 mass spectrometer was used for stable isotope analysis. The extraction unit consists of a CO_2-laser and a sample chamber made of Pyrex glass. Carbon dioxide is produced by laser heating of silver phosphate (Ag_3PO_4)/graphite mixtures and is transferred on line to the MS in a He stream.

Results: We observe that *in situ* laser heating of untreated natural apatites [1] frequently results in scattered $\delta^{18}O$ values and nonsystematic offsets of isotopic values compared to specified values. Experiments with conodonts, natural tooth enamel and mixtures of synthetic phosphates with variable amounts of carbonate suggest that adsorbed H_2O as well as lattice-bound CO_3^{2-}, OH^-, H_2O negatively influence $\delta^{18}O_{phosphate}$ analyses. These problems can be circumvented by purifying natural phosphates as Ag_3PO_4 [2]. Laser heating of Ag_3PO_4/graphite mixtures gives well-reproducible $\delta^{18}O_{phosphate}$ values ($1\sigma = 0.2‰$), irrespective of phosphate/graphite ratios. Our phosphate-purification technique allows samples as small as ~0.1 mg to be precisely analyzed. Analysis of various reference materials and natural apatites shows that laser generated $\delta^{18}O_{phosphate}$ values are constantly offset by −2.5‰ compared to conventional obtained data.

Conclusions: The combination of phosphate purification as Ag_3PO_4 followed by laser irm-GCMS allows precise $\delta^{18}O$ analyses on small samples of natural or synthetic phosphates without potential influences of other O-bearing compounds.

Compared to other phosphate microanalysis techniques [3], our method has the advantages that it is rapid (about 20 samples can be analyzed per day), relatively easy to use, and reasonably precise for paleoclimate investigations. With the described method, small samples of conodonts (2–10 elements) can be analyzed to obtain high-resolution Paleozoic marine $\delta^{18}O$ records.

References: [1] Sharp Z. D. and Cerling T. E. (1996) *GCA, 60,* 2909–2916. [2] O'Neil J. R. et al. (1994) *Israel. J. Earth Sci., 43,* 203–212. [3] Holmden C. et al. (1997) *GCA, 61,* 2253–2263.

MAGNETITE SURFACE PROTONATION TO 290°C FROM ACID/BASE TITRATIONS WITH *IN SITU* pH MEASUREMENT.

D. J. Wesolowski[1], M. L. Machesky[2], D. A. Palmer[1], and L. M. Anovitz[1], [1]Oak Ridge National Laboratory, P.O. Box 2008, Oak Ridge TN 37831-6110, USA (dqw@ornl.gov), [2]Illinois State Water Survey, 2204 Griffith Drive, Champaign IL 61820-7495, USA (machesky@sws.uiuc.edu).

Introduction: The proton-induced charge on mineral surfaces affects rates of dissolution/precipitation as well as the adsorption of trace elements and contaminants. Hydrogen electrode concentration cells developed at Oak Ridge National Laboratory enable highly accurate and precise measurement of the H^+ concentration of an aqueous solution relative to that of a reference solution of known stoichiometric H^+ molality at temperatures of 0°–300°C. We have recently applied this capability to studies of the protonation and point of zero charge (pH_{pzc}) of mineral surfaces, with rutile (TiO_2) being the first phase ever studied by direct pH titrations above 95°C [1,2]. Here we present preliminary results on the surface protonation of magnetite (Fe_3O_4).

Results: H^+ sorption isotherms (micromoles H^+/m^2 vs. pH) were obtained by acid titration of basic 0.03 and 0.30 molal sodium trifluoromethanesul-fonate (NaTr) solutions that contain 1–2 g of powdered magnetite, from 50° to 290°C. The micromoles of *excess* (or *deficit*) H^+ in solution at each point in the titration, calculated from the solution compositions and measured H^+ concentration, normalized to the mineral surface area (m^2), can be converted to net proton charge density (σ_H) with the relation $\sigma_H = -F$ (micromole solution excess H^+/m^2), where F is the Faraday constant in Coulombs/m equivalent.

Even in the "noncomplexing" NaTr electrolyte medium, the sorption isotherms exhibit sharp downturns below pH values of about 5 (290°C) to 6.5 (50°C) due to dissolution of magnetite, which consumes H^+ and releases Fe^{2+} into solution. At higher pH, dissolution does not affect the isotherms, but they are significantly steeper than the equivalent isotherms for rutile (relative to the respective pH_{pzc} values), which suggests much stronger Na^+ binding on magnetite surfaces.

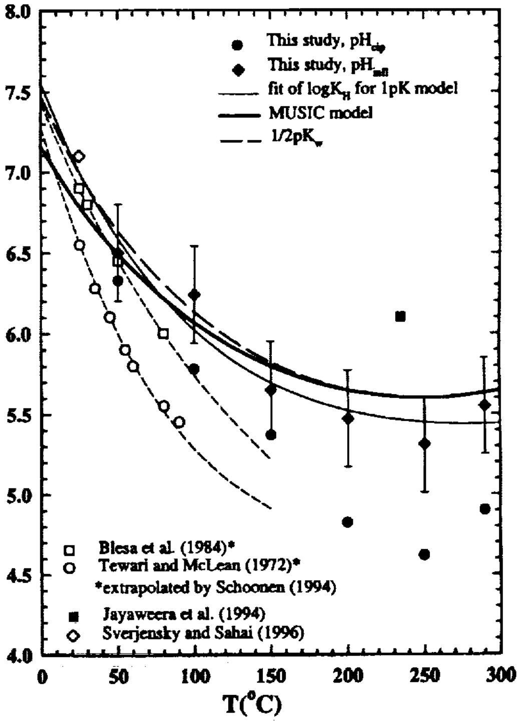

Fig. 1. pHpzc estimates for magnetite.

The isotherms in 0.03 and 0.30 molal NaTr exhibit a common intersection point (pH_{cip}) of 6.3, 5.8, 5.4, 4.8, 4.6, and 4.9 at 50°, 100°, 150°, 200°, 250°, and 290°C respectively. Such pH_{cip} are typically interpreted as approximating the pH_{pzc}. However, strong cation binding can shift the pH_{cip} well below the pristine pH_{pzc} [3]. Examination of the 0.03 molal isotherms indicates inflection points (pH_{infl}) at about 6.5, 6.2, 5.7, 5.5, 5.3, and 5.5 at 50°, 100°, 150°, 200°, 250°, and 290°C, respectively, which may be better estimates of the pristine pH_{pzc}. The figure compares these estimates of the magnetite pH_{pzc} with various literature estimates [4–8], as well as an independent calculation based on a temperature extrapolation of the MUSIC model [9]. The sorption isotherms can be adequately modeled using either a 1 pK approach, with the proton binding constant (K_H) equated to the pH_{infl}, or the MUSIC model, together with a basic Stern EDL configuration involving variable capacitance and cation binding constants.

References: [1] Machesky M. L. et al. (1994) *GCA, 58,* 5627–5632. [2] Machesky M. L. et al. (1998) *J. Coll. Int. Sci., 200,* 298–309. [3] Lyklema J. (1984) *J. Coll. Int. Sci., 99,* 109–117. [4] Blesa M. A. et al. (1984) *J. Coll. Int. Sci., 101,* 410–418. [5] Jayaweera P. et al. (1994) *Coll. Surf., A85,* 19–27. [6] Schoonen M. (1994) *GCA, 58,* 2845–2851. [7] Sverjensky D. A. and Sahai N. (1996) *GCA, 60,* 3773–3797. [8] Tewari P. H. and McLean A. W. (1972) *J. Coll. Int. Sci., 40,* 267–271. [9] Hiemstra T. et al. (1996) *J. Coll. Int. Sci., 184,* 680–692.

DEVELOPMENT OF QUATERNARY PEDOGENIC CALCITE AND DOLOMITE ON THE ISLAND OF HAWAI'I.

C. E. Whipkey[1], R. C. Capo[1], and O. A. Chadwick[2], [1]Department of Geology and Planetary Science, University of Pittsburgh, Pittsburgh PA 15260, USA (rcapo+@pitt.edu), [2]Department of Geography, University of California at Santa Barbara, Santa Barbara CA, USA.

Most studies of calcrete development involve continental soils, where cations derived from eolian dust can play a major role in secondary carbonate formation [1]. We investigated the development of soil carbonates on the semi-arid northwestern part of the island of Hawai'i, which receives minimal eolian dust input. These sites have been isolated from groundwater and direct seawater influence throughout their history. The soils have developed on volcanic flows with similar basaltic compositions that range in age from ~5 to ~350 ka [2]. The carbonates are found as powdery coatings, vesicle fillings, laminated layers, and lining fractures that serve as pathways for infiltration of soil water. Horizons of indurated calcareous cement surrounding volcanic clasts are found on older flows.

Secondary soil carbonate precipitates primarily from soil porewaters, whose cation content is derived from weathering parent material and from the atmosphere in the form of eolian dust, the dissolved fraction of precipitation and, near the coast, sea-spray aerosols. In Hawai'i, eolian dust (primarily Asian loess) is identifiable by the presence of quartz and mica grains, and in these dry sites plays a minimal role in providing cations for pedogenic carbonate accumulation. Soil water cations are therefore derived primarily from precipitation, sea spray, and volcanic parent material. Because these potential sources have distinct Sr-isotopic signatures (parent material ^{87}Sr/^{86}Sr = 0.7035–0.7039 and precipitation/sea spray ^{87}Sr/^{86}Sr = 0.7092), the proportion of cations derived from each source can be determined. Strontium-87/strontium-86 ratios of the soil carbonates range from 0.70378 to 0.70483, indicating that >80% of the Sr is derived from weathering of volcanics, even on the oldest, most weathered flows. Mineralogically, the older flows generally contain increasingly magnesian carbonates: low-Mg calcite (<4% $MgCO_3$; LMC) and high-Mg calcite (HMC) are present on Mauna Loa flows (5–10 ka), HMC on Mauna Kea (70–100 ka) and Kohala Hawi flows (170 Ka), and dolomite on Mauna Kea (~150 ka), Hawi (~170 Ka), and Kohala Pololu (~350 ka) flows. Dolomite is the only carbonate mineral identified in the oldest (Pololu) samples, where its stoichiometry increases with depth, from ~56% $CaCO_3$ at 100 cm to 50% $CaCO_3$ at 350 cm. SEM images reveal a very fine grain size (<1 µm) in some of the Mauna Kea calcite. Hawi dolomite can be found as subspherical ~50–100-µm aggregates of ~5-µm blocky grains. Pololu fracture-lining dolomite reveals a similar blocky morphology consisting of 1–10-µm units comprising smaller individual crystals. No systematic age-related trends in carbonate grain size were noted. Trace-element analysis by inductively coupled plasma–atomic emission spectroscopy (ICP-AES) indicates up to 1900 µg g^{-1} Na in the carbonates, which could be partly due to sea-spray influence. Differences in concentrations of other trace elements (Sr, Ba, Mn, and Fe) appear to be reflective of variations in parent material chemistry, rather than carbonate mineralogy or outside influence. For example, Sr, Ba, and Mn concentrations decrease between the Hawi and Pololu carbonates, while Fe increases. The same trends are seen in the parent lavas.

Molar Mg/Ca ratios of the volcanic flows range from ~0.8 to 1.5. Early weathering of volcanic glass and Mg-rich minerals, such as olivine, could have led to similar Mg/Ca ratios in soil porewaters, thus favoring magnesian carbonate formation. Sea spray and/or precipitation, which supplied up to 20% of Sr to the carbonates, have a Mg/Ca ratio of 5.2 and thus could significantly raise the Mg/Ca of soil porewaters. Although dolomite is thermodynamically more stable than calcite, rapid crystallization typical of semiarid soils favors magnesian calcite rather than dolomite formation [3], and dolomite was not observed in the younger (<100-ka) flows. The dolomite found on older flows could have formed by replacement of early-formed LMC and HMC under continued infiltration of high Mg/Ca soil waters. This dolomitization process culminated in the appearance of stoichiometric dolomite in soils on the oldest (350-ka) flow.

References: [1] Gile L. H. et al. (1981) *Soils and Geomorphology in the Basin and Range Area of Southern New Mexico — Guidebook to the Desert Project,* Mem. 39, N.M. Bur. Mines and Min. Res., Socorro. [2] Wolfe E. W. and Morris J. (1996) Geologic map of the island of Hawaii, USGS Map I-2524-A. [3] Folk R. L. and Land L. S. (1975) *AAPG Bull., 59,* 60–68.

HAFNIUM-ISOTOPIC GEOCHEMISTRY OF THE GALAPAGOS.

W. M. White[1] and J. Blichert-Toft[2], [1]Department of Geological Sciences, Cornell University, Ithaca NY 14853, USA (white@geology.cornell.edu), [2]Laboratoire des Sciences de la Terre, Ecole Normale Superieure de Lyon, 46, Allee d'Italie, 69364 Lyon Cedex 7, France (jblicher@ens-lyon.fr).

Introduction: The Galapagos Islands are among the most volcanically active regions of the world. Because Galapagos volcanism is spread over a wide area rather than confined to a single island, as is the case in Hawai'i and most other hotspots, it provides a unique opportunity to investigate spatial compositional variation in the mantle below. White et al. [1] found that lavas with "enriched," or plumelike, isotopic and trace-element compositions were confined to a horseshoe-like region on the periphery of the Galapagos Platform with "depleted" compositions occurring within the horseshoe in the center of the platform. White et al. [1] concluded that these isotopic variations were due primarily to mixing of the plume with entrained asthenosphere and secondarily to heterogeneity within the Galapagos mantle plume. This heterogeneity is geographic, with the north limb of the plume being isotopically distinct from the south limb. Here we report new Hf-isotopic ratios on 47 Galapagos lavas. These data, when combined with new and previously published Sr-, Nd-, and Pb-isotopic analyses, provide new insights into the nature of the Galapagos mantle plume.

Results: Hafnium-isotopic ratios were determined using the Plasma 54 multiple collector inductively coupled plasma mass spectrometer (MC-ICP-MS) at ENS Lyon [2]. Additional Sr-, Nd-, and Pb-isotopic ratios were determined by thermal ionization mass spectrometry (TIMS) at Cornell. The data are illustrated in Figs. 1 and 2. Though there are reasonable correlations between Hf- and the other isotopic ratios, correlations are notably poorer than in other oceanic islands, such as Hawai'i [3,4]. The weakness of the corre-

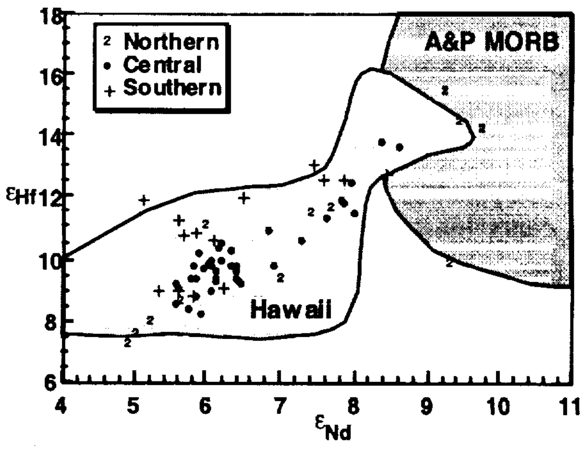

Fig. 1. ε_{Hf} vs. ε_{Nd} in Galapagos lavas.Lavas from southern islands have higher ε_{Hf} for a given ε_{Nd} than lavas from northern islands.

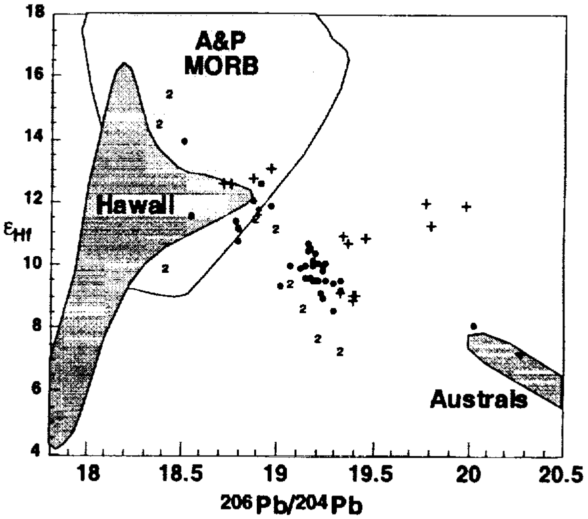

Fig. 2. ε_{Hf} vs. ^{206}Pb/^{204}Pb in Galapagos lavas.

lations implies that if the isotopic variations are due to mixing, more than two components must be involved.

Discussion: Though isotopic ratio-isotopic ratio correlations are relatively weak, when any three of the six isotopic ratios are plotted in three dimensions, a plane is readily apparent. The planar nature of the dataset is confirmed by factor analysis, which reveals that 93% of the variance in the Galapagos isotope data is explained by just 2 factors. The first of these, which we identify with proportion of entrained asthenosphere in the mixture, accounts for 82% of the variance. The second factor, which we associate with north-south heterogeneity in the plume, accounts for 11% of the variance. Hafnium-isotopic ratios provide strong confirmation that the Galapagos plume is laterally heterogeneous.

The main component of the Galapagos mantle plume is compositional similar to FOZO or "C," postulated to represent much of the lower mantle [5]. The southern component, however, appears to be unique and not been identified in any other oceanic island.

References: [1] White W. M. et al. (1993) *JGR, 93,* 19533. [2] Blichert-Toft et al. (1997) *Contrib. Mineral. Petrol., 127,* 935. [3] Stille P. et al. (1986) *GCA, 50,* 2303–2320. [4] Blichert-Toft J. et al. (1999) *Science,* submitted. [5] Hart S. R. et al. (1992) *Science, 256,* 517. [6] Hanan B. B. and Graham D. W. (1996) *Science, 272,* 991.

THE COORDINATION CHEMISTRY OF SIDEROPHORES WITHIN SOILS.

C. F. Whitehead and A. T. Stone, Johns Hopkins University, 313 Ames Hall, Baltimore MD 21218, USA (astone@jhu.edu).

Siderophore-Facilitated Iron Uptake: Siderophores facilitate Fe uptake in three steps: (1) Dissolved $\mathrm{Fe^{III}}$-siderophore complexes are formed by either capturing $\mathrm{Fe^{III}}$ from other $\mathrm{Fe^{III}}$-ligand complexes, or by adsorption of siderophore molecules and subsequent dissolution of the underlying $\mathrm{Fe^{III}}$ (hydr)oxide; (2) $\mathrm{Fe^{III}}$-siderophore complexes are transported back to the organism via diffusion; (3) $\mathrm{Fe^{III}}$-siderophore complexes are recognized by receptor sites on cell membranes and assimilated.

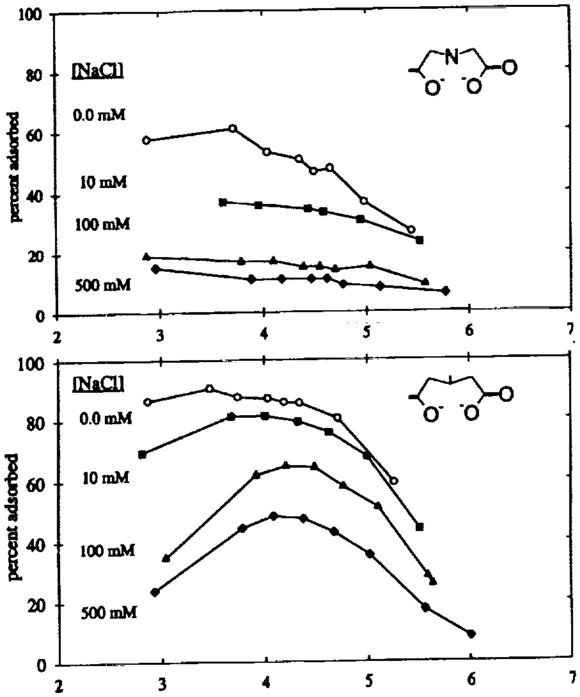

Fig. 1. One hundred micromole N-phenyliminodiacetic acid (top) and 110 µM 3-phenylglutaric acid (bottom) adsorption onto 1.1 g/L FeOOH (goethite) in 1.0 mM acetate.

Influence of Prevalent Geochemical Conditions: As far as step 1 is concerned, siderophore molecules in solution are seldom "free," but are instead coordinated to protons ($\mathrm{H^+}$), naturally occurring metal ions (e.g., $\mathrm{Mg^{II}}$, $\mathrm{Ca^{II}}$), and contaminant metal ions (e.g., $\mathrm{Ni^{II}}$). As a consequence, $\mathrm{Fe^{III}}$-siderophore complex formation requires proton- and metal ion-exchange.

Adsorbed siderophore molecules may exist in different proton levels, in ternary complexes involving other metal ions, and in different conformations. Different topological features on the surface may be more or less susceptible toward dissolution. Hence, the relationship between adsorption and siderophore-assisted dissolution may be complex.

As far as step 2 is concerned, $\mathrm{Fe^{III}}$-siderophore complexes may re-adsorb onto (hydr)oxide surfaces or partition into particulate natural organic matter. Both processes interfere with transport via diffusion.

Siderophore Functional Group Effects: The identity, number, and arrangement of ligand-donor groups determine which complex formation, adsorption/desorption, dissolution, and partitioning reactions control siderophore speciation. In a particular geochemical setting, one siderophore structure may be much more effective than another in facilitating Fe uptake. In order to make predictions about siderophore speciation and efficacy, structure-activity relationships must be developed.

Illustrative Example: Surrogate ligands are used to explore functional group effects on complex formation and adsorption. In solution, N-phenyliminodiacetic acid is much more effective at binding $\mathrm{Fe^{III}}$ than 3-phenylglutaric acid. N-phenylimino-diacetic acid possesses a central N atom can be used to form two stable five-membered chelate rings with $\mathrm{Fe^{III}}$. Without this N, 3-phenylglutaric acid can only form one energetically unfavorable eight-membered chelate ring.

Under the conditions employed in our adsorption experiments (see below), the ranking of the two ligands is reversed. 3-Phenylglutaric acid adsorption reaches 90%, while N-phenyliminodiacetic acid adsorption only reaches 60%.

In the case of N-phenyliminodiacetic acid, participation of the central N atom in adsorption may be less than in analogous solution complexes. In the case of 3-phenylglutaric acid, the distance between the two carboxylic acid groups is a liability for forming solution complexes, but an asset in adsorption, since it facilitates bridging between neighboring surface sites.

N-phenyliminodiacetic acid adsorption is more sensitive to changes in ionic strength and less sensitive to changes in pH than 3-phenylglutaric acid adsorption. As the pH decreases, N-phenylacetic acid undergoes one shift (dianion → monoanion), while 3-phenylglutaric acid undergoes two shifts (dianion → monoanion → neutral species) in speciation. Long-range electrostatic interactions that are sensitive to changes in protonation level exert a significant effect on adsorption.

GEOCHEMISTRY OF ECLOGITES FROM ALP DE TRESCOLMEN, ADULA NAPPE, CENTRAL ALPS, SWITZERLAND.

R. A. Wiesli[1], L. A. Taylor[1], J. W. Valley[2], M. J. Spicuzza[2], G. A. Snyder[1], A. Camacho[1], and M. Kurasawa[3], [1]Planetary Geosciences Institute, Department of Geological Sciences, University of Tennessee, Knoxville TN 37919, USA, [2]Department of Geology and Geophysics, University of Wisconsin–Madison, Madison WI 53706, USA, [3]Institute of Geosciences, Tsukuba University, Tsukuba, Japan.

In the central Swiss Alps, the former continental basement rocks from the European margin underwent subduction during the early Eocene [1]. Metamorphism of these rocks is considered to have followed a clockwise P-T-t path with burial to eclogite facies conditions followed by exhumation. In the Penninic Adula nappe complex, the eclogite facies overprint is of regional character and shows an increase in metamorphic grade from the northern part of the nappe (450°–550°C, 10–13 kbar at Vals) to the southern part of the nappe (750°–900°C, 18–35 kbar at Alpe Arami) [2]. Minor metabasic rocks occur throughout the nappe and may have been derived from a MORB source [3].

It is of interest to obtain information about fluid-rock interaction during the subduction process since it may help understand dehydration or metasomatic processes in the down-going slab. Garnet in the eclogite most likely grew during burial, as well as during the early stages of exhumation. The

Fig. 1. Calcium X-ray map of a garnet from Trescolmen. The lighter color indicates higher Ca-content.

zonation in major elements in garnet may be of help to constrain the P-T path as well as the nature of fluid-rock interaction.

At Alp de Trescolmen, located in the middle part of the Adula nappe, mafic boudins with cores of eclogites are exceptionally well exposed. Most of the eclogite boudins are found interspersed in the metapelitic host rocks. The eclogites at Alp de Trescolmen experienced temperatures and pressures in the range of 550°–650°C and 15–22 kbar respectively [4].

A detailed investigation has been initiated to study the geochemistry of the eclogites and the surrounding metapelites at Alp de Trescolmen and other localities in the Adula nappe, including a mineralogic-petrologic study, electron microprobe (EMP) analyses of major elements, O-isotopic analyses of mineral separates from eclogites and metapelites, and inductively coupled plasma mass spectrometry (ICP-MS) analyses of trace elements in the eclogites to unravel the fluid-rock interaction during subduction and exhumation between the eclogites and the surrounding metapelites.

Compositional X-ray maps of garnets from Alp de Trescolmen show two stages of growth. Garnets from the least retrogressed eclogites reveal complex zonation patterns, as can be seen in Fig. 1. The inner region of the garnet has a composition of 67% almandine, 13.5% pyrope, 17.6% grossular, and 1.7% spessartine. The Ca-rich region, which surrounds a low-Ca region in the center, has a composition of 48% almandine, 25.07% pyrope, 25.9% grossular, and 1% spessartine. These different garnet domains reflect changing P-T conditions of the crust during subduction followed by exhumation. The inner portion, with higher almandine content, suggests growth during prograde metamorphism, whereas the Ca-rich region possibly grew under peak metamorphic conditions.

In addition, laser ICP-MS analyses were carried out to determine if variations in trace elements reflect those in the major elements. Garnets show the typical LREE-depleted pattern, but the HREE show an unusually large variation of up to 1 order of magnitude in a single garnet. Clinopyroxenes exhibit a consistent trend of MREE enrichment.

Stable-isotopic compositions of mineral separates from eclogites and metapelites were analyzed using the CO_2 laser probe system at the University of Wisconsin. Internal mineral zonation was investigated using a thin saw blade technique that allowed a spatial resolution of ~0.5 mm [5]. Garnets from fresh eclogites have O-isotopic values between 5.2‰ and 5.9‰. Garnets from smaller eclogite boudins, which are often retrogressed to amphibolite exhibit $\delta^{18}O$ values ~6.5‰. Garnets from the surrounding metapelites have values in the range of 7.2–7.8‰. Quartz analyses reveal O-isotopic values in the range of 9.5–10.5‰. The fluid that retrogressed the eclogites was able to elevate the O values of the garnets. The variation in a single zoned garnet from an eclogite can be up to 0.6‰, as big as the variation in the entire boudin.

References: [1] Schmid S. M. et al. (1996) *Tectonics, 15,* 1036–1064. [2] Heinrich C. A. (1986) *J. Petrol., 27,* 123–154. [3] Santini L. (1991) Ph.D. dissertation, Univ. Lausanne. [4] Meyre C. (1997) *JMG, 15,* 687–700. [5] Elsenheimer D. and Valley J. W. (1993) *GCA, 57,* 543–557.

PARTITIONING OF TRACE METALS IN ANOXIC BLACK SEA SEDIMENTS.

R. T. Wilkin[1] and M. A. Arthur[2], [1]National Risk Management Laboratory, U. S. Environmental Protection Agency, Ada OK 74820, USA (wilkin.rick@epa.gov), [2]Department of Geosciences, Pennsylvania State University, University Park PA 16802, USA (arthur@geosc.psu.edu).

Introduction: Black shales commonly contain trace metals in concentrations more than a hundred times their average crustal abundance. Metal partitioning among sedimentary organic and mineral components as well as the physicochemical mechanisms of trace metal enrichment both remain as important research topics. The partitioning of transition metals into sedimentary iron sulfide minerals has been extensively studied because of the potential as environmental indicators and because sediments enriched in transition metals may eventually become sources of contamination during oxidative weathering, or during the processing of coals and oil shales. In this study we present a sequential extraction strategy to evaluate the mode of occurrence of trace metals in Black Sea sediments and to test hypotheses about the temporal and chemical evolution of the Black Sea water column.

Methods: Numerous studies indicate that sediment bound trace metals can be associated with several geochemical phases. The principal phases are metal oxides and oxyhydroxides, clays, organics, carbonates, and sulfides. In order to assess the partitioning of trace metals in Black Sea sediments, we have carried out a sequential extraction experiment on core GC59 retrieved from a depth of 600 m. The extraction procedure includes three steps to evaluate the amount of trace metals associated with sediment-reactive components (cold 1 N HCl, 24 h), iron sulfides (hot 1 M $CrCl_2$ + HCl), and organics (H_2O_2, 24 h). Before and after each extraction step, sediment samples were analyzed for major (Fe, Al) and trace elements (P, Mn, Mo, Ni, V, Ni, U, and Th) after complete microwave digestion in concentrated HF, HNO_3, and HCl. Trace elements were determined after dilution by inductively coupled plasma mass spectrometry (ICP-MS), and major elements were determined by inductively coupled plasma-atomic emission spectrometry (ICP-AES). Accuracy and precision of the analyses were between 5 and 10%. Accuracy was evaluated by parallel digestion and analysis of NIST standard reference materials 1646a, 2704, and 1633b.

Results: The elements Ni, V, Cu, and Th are dominantly (~50%) contained in the residual, non-extractable fraction, suggesting a significant detrital flux of these elements to the sediment-water interface. Molybdenum is unique in that >90% of the total amount is accounted for by the sequential extraction procedure (Fig. 1). In laminated unit I and unit II sediments, ~20% of the total Mo is present in the HCl extractable component; this fraction abruptly increases in sediments below the unit II-unit III boundary although

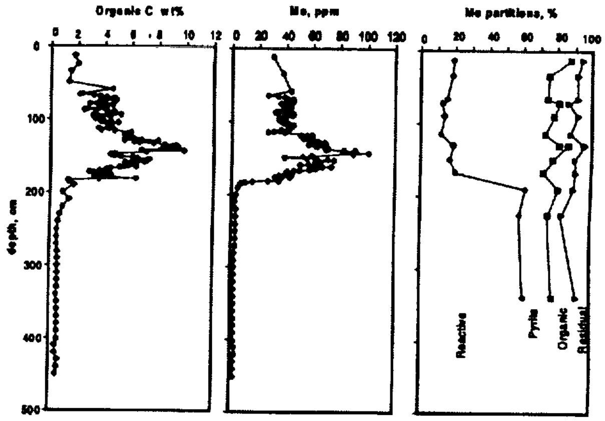

Fig. 1. Depth distribution of organic C, Mo, and Mo partitions in core GC59 (600 m).

the abundance of Mo dramatically decreases (Fig. 1). Iron sulfides apparently are the dominant sites of Mo incorporation in unit I and II, a result in agreement with the findings of Volkov and Fomina [1]. This result, however, is somewhat surprising considering the excellent correlation between Mo and OC ($r^2 = 0.92$) and the generally poor relationship between Mo and pyrite ($r^2 = 0.16$). The strong correlation but non-association between Mo and OC suggests that the abundance of each component respond to the same forcing factors. Because both Mo and OC concentrations increase toward the basin center where sedimentation rates are the lowest, we propose that diffusion to and adsorption processes on iron sulfides principally control sediment Mo concentrations. In deep-basin sediments the pyrite burial flux primarily originates above the sediment water interface [2]. Depleted Mo values in sediment trap materials [3] suggest that Mo is fixed dominantly below the sediment-water interface by diffusion of Mo from the overlying anoxic waters.

Note: This is an abstract of a proposed presentation and does not necessarily reflect EPA policy.

References: [1] Volkov I. I. and Fomina L. S. (1972) *Am. Assoc. Petrol. Geol. Mem., 20,* 456–477. [2] Wilkin R. T. et al. (1997) *EPSL, 148,* 517–525. [3] Crusius J. et al. (1996) *EPSL, 145,* 65–78.

THE CHEMICAL AND MINERALOGICAL RESPONSE OF ALLANITE TO HYDROTHERMAL ALTERATION, CASTO GRANITE, IDAHO.

S. A. Wood[1] and A. Ricketts[2], [1]Department of Geology and Geological Engineering, University of Idaho, Moscow ID 83844-3022, USA (swood@iron.mines.uidaho.edu), [2]311 South Skyline Drive, Idaho Falls ID 83402, USA.

Introduction: The effect of hydrothermal alteration on the mineral allanite, $(Ca, Mn, Ln)_2(Fe^{2+}, Fe^{3+}, Al)_3(SiO_4)_3OH$, where Ln = rare earth elements, has relevance to performance assessment of nuclear waste materials and to the use of REE and Nd isotopes as petrogenetic tracers. The response of allanite to hydrothermal activity in the Eocene Casto Pluton granite of central Idaho has been investigated using optical microscopy, quantitative electron microprobe analysis, and scanning electron microscopy (backscattered-electron imaging, X-ray elemental mapping, and qualitative energy-dispersive analysis). Evidence of hydrothermal alteration of the samples examined in this study includes sericitization of feldspar, chloritization of biotite, corrosion and replacement of allanite, and the presence of fluorite veins.

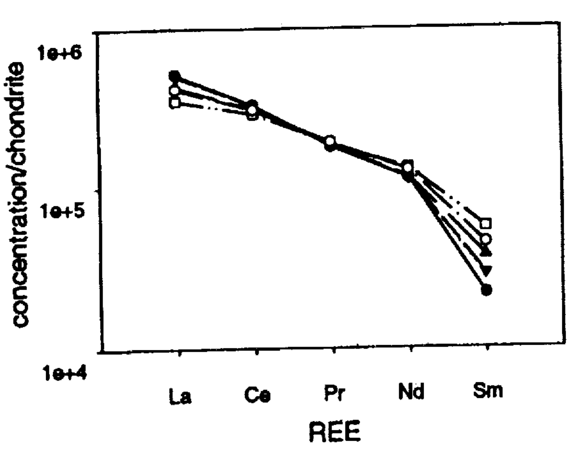

Fig. 1. Chondrite-normalized REE contents of selected allanite grains from the Casto Pluton.

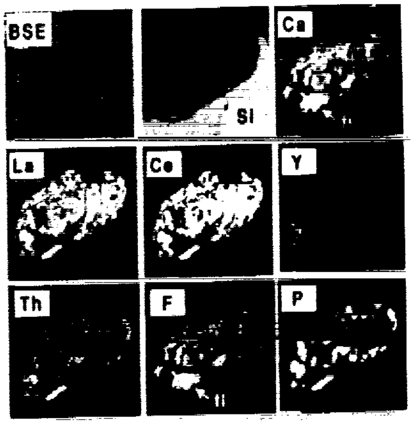

Fig. 2. Backscattered electron image and elemental X-ray maps of the most altered allanite grain found in this study. Note large portions of allanite grain altered to fluorite (elevated Ca, F) and a REE-phosphate (elevated La, Ce, Th, and P).

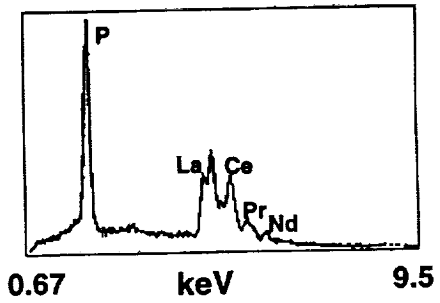

Fig. 3. Energy-dispersive spectroscopy spectrum of P-rich area from the allanite grain shown in Fig. 2.

Unaltered Allanite: Unaltered allanite from the Casto Pluton is characterized by a fairly narrow range of compositional variation (Fig. 1), with little or no zoning. A representative empirical formula, based on the composition of the least altered allanite grain, is

$$(Ln_{0.83}Ca_{1.07}Th_{0.04}Mn^{2+}_{0.06})(Ti^{4+}_{0.11}Mg^{2+}_{0.04}Fe^{2+}_{0.99}\,Fe^{3+}_{0.48}Al_{1.38})$$
$$(Si_{3.00}O_{12})(OH_{0.95}F_{0.05})$$

where $Ln = (La_{0.14}Ce_{0.41}Pr_{0.05}Nd_{0.17}Sm_{0.03}Y_{0.03})$

The small amount of compositional variation observed is consistent with the following two coupled substitutions: $Ca^{2+} + Th^{4+} \leftrightarrow 2Ln^{3+}$ and $Ln^{3+} + Fe^{2+} + Mg^{2+} \leftrightarrow Ca^{2+} + Al^{3+} + Fe^{3+}$.

Altered Allanite: Slightly altered allanite grains exhibit rims in which Th is enriched, and La and Ce are depleted. Increasing degrees of alteration lead to extensive corrosion and replacement of allanite by fluorite, a REE-, Th- and P-rich phase, possibly monazite or rhabdophane, and a Th-rich phase, probably thorianite (see Figs. 2 and 3).

Conclusions: In spite of strong alteration by a F-rich hydrothermal solution which destroyed large portions of allanite grains, the REE and Th were not mobilized very far before they were fixed in secondary phases such as monazite (or rhabdophane) and thorianite. A rough mass balance of the REE in the original allanite and in the secondary phases, together with whole-rock REE analyses, confirm that most of the REE remained in the rock after alteration. The lack of mobility of the REE in this environment may be due to buffering of F activity to low values by fluorite, and the ready availability of PO_4^{3-}.

THE EFFECT OF FULVIC ACID ON THE EXTENT AND RATE OF DISSOLUTION OF OBSIDIAN.

S. A. Wood[1], L. M. Anovitz[2], J. M. Elam[3], D. R. Cole[2], L. R. Riciputi[2], and P. Bénezeth[2], [1]Department of Geology and Geological Engineering, University of Idaho, Moscow ID 83844-3022, USA (swood@iron.mines.uidaho.edu), [2]Chemical and Analytical Sciences Division, Oak Ridge National Laboratory, Oak Ridge TN 37831-6110, USA, [3]Department of Anthropology, University of Tennessee, Knoxville TN, USA (anovitzlm@ornl.gov).

Introduction: An indicator of the age of obsidian artifacts is the extent of surface hydration, as water diffuses deeper into the glass with time [1,2]. Such dating is compromised if dissolution removes a significant portion of the surface layer. This effect is probably not significant in pure water at room temperature. However, it has been suggested that organic acids (e.g., fulvic acid) may complex Si and increase the solubility of silica [3,4]. As these acids are present in most soils, their effect may need to be taken into account when using the extent of hydration to date obsidian artifacts. Thus, we have conducted an experimental study of the effect of fulvic acid (FA) on the dissolution of obsidian.

Methods: Experiments were conducted at 30°C in 0.03 molal NaCl solutions. Obsidian (Pachuca source, Sierra de las Navajas, Mexico) was reacted for up to four months with solutions with various FA (Suwannee River) concentrations and pH values. Twelve solutions with pH 5.0, 5.4, and 6.1, and FA concentrations of nominally 0, 50, 150, and 600 mg/kg, were prepared. Two grams of powdered obsidian and 30–40 mL of solution were placed in 50-mL polyethylene syringes mounted on a rotating rack in a constant temperature bath. Samples were withdrawn at approximately one-month intervals, forced through a 0.2-μm filter, and analyzed by inductively coupled plasma-atomic emission spectrometry (ICP-AES) for Si, Al, Fe, Mg, K, and Ca. The pH was measured using a combination glass electrode calibrated on the H^+ concentration scale.

Results and Discussion: Concentrations of K, Mg, Ca, and Al in solution were very close to those of blank solutions of FA, with no clear variation with FA concentration. The concentrations of Si increased with time at all pH values and FA concentrations. At pH 5.4 (not shown) and 6.1 (Fig. 1), Si concentration is relatively constant with increasing FA concentration except at the highest FA concentration, where it increases. At pH 5.0 (not shown), the Si concentration is relatively high at the three lowest FA concentrations and then decreases at the highest FA concentration. In no case does the Si concentration exceed the solubility of amorphous silica at 30°C in pure water (~61 mg/L). These results suggest that FA may affect the rate of dissolution of obsidian, increasing the rate at pH >5, and decreasing it at pH = 5. However, it appears that any complex formed by Si and FA is relatively weak and does not affect solubility, in agreement with a recent study on amorphous silica solubility [5].

Fulvic acid apparently has a strong influence on the concentration of Fe leached from the obsidian, when FA is present in concentrations >100 mg/L. This may be due to complexation and/or reduction of Fe by FA. Additional experiments are in progress using a peat FA to determine whether the effect of FA depends on its composition. However, FA does not appear to increase the solubility of obsidian significantly and should not enhance removal of the hydrated layer assuming attainment of equilibrium.

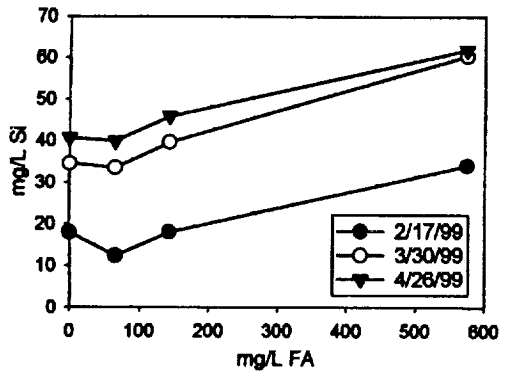

Fig. 1. Silicon concentration vs. FA concentration for obsidian dissolution experiments at pH = 6.1.

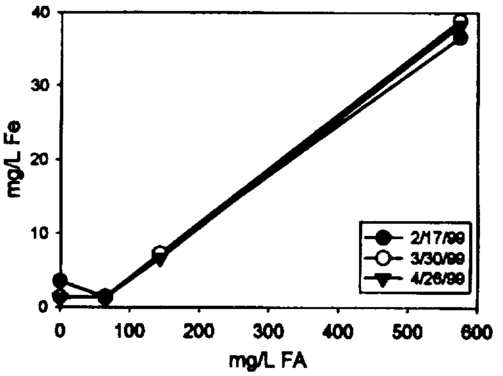

Fig. 2. Iron concentration vs. FA concentration for obsidian dissolution experiments at pH = 6.1.

References: [1] Friedman I. and Smit R. (1960) *Am. Antiquity, 25,* 476–522. [2] Anovitz L. M. et al. (1999) *J. Arch. Sci.,* in press. [3] Bennett P. C. (1991) *GCA, 55,* 1781-1797. [4] Bennett P. C. and Sigel D. I. (1987) *Nature, 326,* 684–686. [5] Pokrovski G. S. and Schott J. (1998) *GCA, 62,* 3413–3428.

DETERMINATION OF THE SOLUBILITY OF CRYSTALLINE NEODYMIUM $(OH)_3$ IN SODIUM TRIFLATE SOLUTIONS FROM 30° TO 250°C WITH *IN SITU* pH MEASUREMENT.

S. A. Wood[1], D. A. Palmer[2], D. J. Wesolowski[2], and P. Bénezeth[2], [1]Department of Geology and Geological Engineering, University of Idaho, Moscow ID 83844-3022, USA (swood@iron.mines.uidaho.edu), [2]Chemical and Analytical Sciences Division, Oak Ridge National Laboratory, Oak Ridge TN 37831-6110, USA (ddp@ornl.gov; dqw@ornl.gov; 72b@ornl.gov).

Introduction: An improved database for the solubility of rare-earth-element (REE) phases and the thermodynamics of REE complexation in hydrothermal solutions is crucial to (1) the use of REE patterns and Nd isotopes as petrogenetic tracers in hydrothermally altered rocks, (2) a better understanding of the origin of hydrothermal REE deposits, and (3) performance assessment of geologic repositories of nuclear waste. There is considerable disagreement in the literature on the solubilities of solid REE hydroxides and the thermodynamics of the hydrolysis of trivalent REE ions even at room temperature [1–5], and few data exist at elevated temperatures [1]. A systematic investigation of the solubility of $Nd(OH)_3(s)$ as a function of temperature, pH, and ionic strength is under way in our laboratories, and preliminary results are reported here. We have chosen Nd due to the importance of its isotopes as petrogenetic tracers and its similar chemical behavior to the actinide americium.

Methods: Crystalline $Nd(OH)_3(s)$ was synthesized by reacting pure $Nd_2O_3(s)$ with deionized, degassed water at 200°C for several weeks. Care was taken throughout to exclude CO_2. The solid was characterized both before and after the solubility experiments using X-ray diffraction (XRD), thermal gravimetric analysis (TGA), fourier transform infrared (FTIR) spectroscopy, and scanning electron microscopy (SEM).

Experiments were carried out in a H electrode concentration cell fitted with a sampling line and a magnetic stir bar. The noncomplexing salt, sodium trifluoromethanesulfonate (triflate), was employed to maintain constant ionic strength. Two pumps permitted the addition of acid or base during solubility runs, and solubility was reversed by approach from both under- and oversaturation. Solution samples were separated from the solid via a Pt-frit inside the reaction cell and a 0.2-μm membrane filter outside the cell. Analysis of samples for Nd was accomplished using inductively coupled plasma atomic

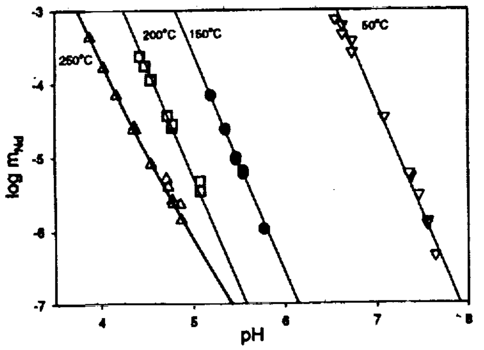

Fig. 1. Plot of log m_{Nd} vs. pH for the solubility of $Nd(OH)_3(s)$ in 0.03 molal Na-triflate media.

emission spectrometry (ICP-AES), inductively coupled plasma mass spectrometry (ICP-MS), and ion chromatography, depending on the concentration.

Results and Discussion: The results obtained at 0.03 molal ionic strength are shown in Fig. 1. The majority of the data shown in this plot at each temperature conform to lines with slopes of 3, implying that the dominant solubility controlling reaction is

$$Nd(OH)_3(s) + 3H^+ \leftrightarrow Nd^{3+} + 3H_2O(l) \qquad (1)$$

The equilibrium quotients for reaction (1) can be fit to a simple van't Hoff relation: log $Q_{s0} = -5.712 + 7270.0/T(K)$, with an $r^2 = 0.9979$. A preliminary determination of log Q_{s0} at 30°C using glass electrodes results in values identical to those predicted by this equation. Between 30° and 200°C there is no evidence of hydrolysis over the range of pH investigated thus far, but at 250°C there is evidence for the formation of $Nd(OH)^{2+}$ at pH >4.5 (Fig. 1). Modeling of the data at 250°C yields log $Q_{h1} = -4.33$ for the reaction: $Nd^{3+} + H_2O \leftrightarrow Nd(OH)^{2+} + H^+$(2), which indicates approximately 2 orders of magnitude less tendency toward hydrolysis than indicated by theoretical predictions [6,7]. Measurements at more alkaline pH and over a wider range of ionic strength are currently in progress. With these data, it will be possible to determine stability constants for Nd^{3+}-complexes with ligands such as chloride, acetate, sulfate, EDTA, etc.

References: [1] Deberdt S. et al. (1998) *Chem. Geol., 151,* 349–372. [2] Diakonov I. I. et al. (1998) *Chem. Geol., 151,* 327–347. [3] Rao L. et al. (1996) *Radiochim. Acta, 72,* 151–155. [4] Rizkalla E. N. and Choppin G. R. (1991) *Handbook on the Physics and Chemistry of Rare Earths, 15,* 393–442. [5] Wood S. A. (1990) *Chem. Geol., 82,* 159–186. [6] Haas J. R. et al. (1995) *GCA, 59,* 4329–4350. [7] Wood S. A. (1990) *Chem. Geol., 88,* 99–125.

PLATINUM GROUP ELEMENTS IN SUBDUCTION ZONE MAGMAS: ANION EXCHANGE PRECONCENTRATION INDUCTIVELY COUPLED PLASMA MASS SPECTROMETRY ANALYSES OF LESSER ANTILLES AND IZU-BONIN MAGMAS.

S. J. Woodland[1], D. G. Pearson[1], J. A. Pearce[1], and M. F. Thirlwall[2], [1]Department of Geological Sciences, University of Durham, South Road, Durham DH1 3LE, UK (s.j.woodland@durham.ac.uk), [2]Department of Geology, Royal Holloway University of London, Egham, Surrey TW20 OEX, UK.

Introduction: Platinum-group-element (PGE) data has been obtained on a suite of lavas and associated cumulates from the island of Grenada, Lesser Antilles. The analyzed suite ranged from highly magnesian picrites to andesites in composition and represents the first complete evaluation of PGE (Os, Ir, Ru, Pt, Pd, and Re) abundances in an intra-oceanic arc. In addition, boninitic samples from the Izu-Bonin fore-arc region (ODP Leg 125, Site 786B) have been investigated as a comparison of relative PGE abundances in these two contrasting subduction environments.

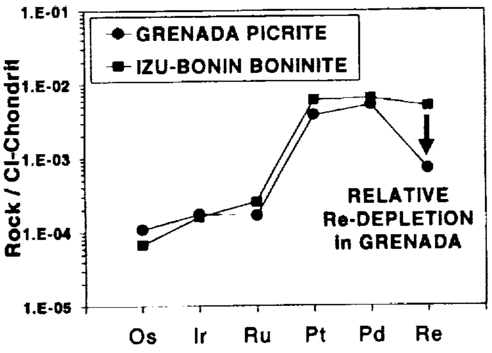

Fig. 1.

Analytical Procedure: Initial trials with isotope dilution Ni-S fire assay proved it inadequate for analysis of sub-part-per-billion PGE concentrations typical of arc volcanics, particularly as both Re and Os were required [1]. Samples were thus prepared using a Carius tube digestion technique, coupled with solvent extraction of Os and anion-chromatography preconcentration of the other PGEs [2,3]. Analysis is carried out using an Elan 6000 inductively coupled plasma mass spectrometer (ICP-MS). In conjunction with the ICP-MS, use of a CETAC Direct Injection Nebulizer (DIN) permits low-memory Os analysis. A CETAC ARIDUS desolvating nebulizer is used to minimize ZrO + HfO interferences on the PGEs. This low-blank technique allows analysis of low abundance samples, as blanks are typically <5 pg for Os, Ir, and Re, <10 pg for Ru and Pd, and <25 pg for Pt [2].

Platinum-Group-Element Signatures of Grenada Suite: PGE patterns have positive slopes (except for Re depletion) and become steeper as fractionation proceeds, e.g., picrite Pd/Ir = 25, andesite Pd/Ir = 216. Osmium and Ir are <0.2 ppb (picrites) and <0.02 ppb (andesites). Platinum and Pd are <4 ppb (picrites) and <2 ppb (Pt) and <1 ppb (Pd), in andesites. Overall abundance for all PGEs (excluding Re) decreases as fractionation proceeds. The PGEs do not appear to behave as a coherent group during arc-lava fractionation and are variably affected by fractionation of different mineral phases. The M-C series of Grenada [4] have anomalously high Re, Os, and Pd compared to other Grenada samples.

Platinum-Group-Element Signatures of Izu-Bonin Suite: Average PGE concentrations in boninites are Os 0.04 ppb, Ir 0.087 ppb, Ru 0.19 ppb, Pt 6.02 ppb, Pd 3.55 ppb, and Re 0.25 ppb. Average Pd/Ir of boninites is 42. The andesite contains slightly lower Os (0.023 ppb), Ir (0.025 ppb), and Pt (3.31 ppb) but higher Ru (0.24 ppb) and Pd (7.22 ppb). This implies mildly incompatible behavior for Ru, Pt, and Pd during initial fractionation, but compatible behavior for Os and Ir. Fractionation of andesite to rhyolite results in a significant decrease in all PGE concentrations (except Re), possibly due to initiation of magnetite fractionation [5].

Comparison of Izu-Bonin Boninite and Grenada Picrite Platinum-Group-Element Signatures: There is remarkable similarity between PGE abundance and shape of the PGE patterns of the primitive rocks (boninites and picrites) from both regions. This is surprising considering the alkalic nature of the Grenadian picrites and depleted nature of the boninites. The picrites (M-series [4]), however, are slightly enriched in Os and significantly depleted in Re, relative to the boninites.

Implications for Platinum-Group-Element Behavior in Subduction Zones: Within the two suites studied, it appears that the PGEs are relatively unaffected by variations in subduction-zone petrogenetic conditions, such as degree of melting and differential fluid/sediment input to their mantle sources. Higher Os concentrations in the more-hydrous Grenada magmas, compared to the boninites, lend support to the theory that Os may be mobilized by Cl-rich aqueous fluids [6]. Recognition of variable Re depletion and enrichment within Grenada picrites supports independent Os-isotopic evidence [7] that ancient Re-depleted mantle may exist beneath Grenada.

References: [1] Woodland S. J. and Pearson D. G. (1999) *Royal. Soc. Chem. Spec. Pub., 234,* 267–276. [2] Pearson D. G. and Woodland S. J.

(1999) *Chem. Geol.*, in press. [3] Pearson D. G. and Woodland S. J., this volume. [4] Thirlwall M. F. et al. (1996) *GCA, 60,* 4785–4810. [5] Murton et al. (1992) *Proc. ODP, 125,* 211–235. [6] Brandon A. D. et al. (1996) *Nature, 272,* 861–864. [7] Parkinson I. J. et al. (1998) *AGU Abstract-V41D-11,* F1012.

AN EXPERIMENTAL STUDY OF COPPER(I) CHLORIDE SOLUBILITY IN WATER VAPOR AT TEMPERATURES FROM 360° TO 400°C AND WATER-VAPOR SATURATED PRESSURE.

Z. Xiao[1], A. E. Williams-Jones[1], and C. H. Gammons[2], [1]Department of Earth and Planetary Sciences, McGill University, Montréal, Québec H3A 2A7, Canada (zhifeng@eps.mcgill.ca), [2]Department of Geological Engineering, Montana Tech of the University of Montana, Butte MT 59701, USA.

The solubility of $CuCl_{(s)}$ in vapor was measured in a vapor-saturated H_2O-NaCl-HCl (NaCl/HCl; 9:1) system at temperatures ranging from 360° to 400°C and total chloride concentration from 0.01 to 5 mol. For experiments at 360°C, $CuCl_{(s)}$ was dissolved directly into the liquid. At higher temperatures (380°C and 400°C), $CuCl_{(s)}$ was separated from the liquid by a quartz-glass tube, but reacted with vapor. Foils of metallic Cu were added as a redox agent.

At 360°C, the experiments measure partitioning between liquid and vapor, and the Cu concentration in vapor is controlled by its concentration in liquid. Data collected from these experiments show that the Cu solubility in vapor is independent of the total chloride concentration in the liquid or the vapor density. This indicates that Cu is dissolved as $CuCl_{(v)}$ in the vapor phase and thus the partitioning can be described by the reaction $CuCl_{(aq)} = CuCl_{(v)}$. The equilibrium relationship for this reaction can be represented as $K_C \approx m_{CuCl(v)}/m_{CuCl(aq)}$, where $m_{CuCl(v)}$ and $m_{CuCl(aq)}$ are the concentrations of CuCl in vapor and $CuCl^0$ in liquid, respectively, and the log K_C at 360°C is about –2.65.

At 380° and 400°C, the experiments measure solubility in saturated vapor. The Cu concentration correlates negatively with total chloride concentration. As data from Bischoff [1] on the NaCl-H_2O system show that increasing the NaCl concentration will decrease vapor density, it is believed that Cu solubility in the vapor is controlled mainly by vapor density through the following reaction:

$$CuCl(s) + 4\ H_2O = CuCl(H_2O)_4$$

Following Armellini and Tester [2], the equilibrium relationship for the above reaction can be written as $K_C \approx m_{CuCl(v)}/d^4_{H_2O(v)}$, where $m_{CuCl(v)}$ is the molality of Cu in the vapor phase and $d_{H_2O(v)}$ is the density of water vapor. The log K_C values for these experiments at 380° and 400°C are 0.22 and 1.17 respectively.

The partition coefficients for Cu between vapor and liquid were calculated for the CuCl-NaCl-HCl-H_2O system at 400°C and water-vapor saturated pressure at NaCl concentrations from 0.5 to 2.3 mol and a HCl concentration of 0.001 mol. The results indicate that the partition coefficients for Cu are nearly identical to those of Na under the same conditions [cf. 1]. This suggests that NaCl partitioning data can be used to estimate Cu(I) chloride partition coefficients at conditions for which no data for Cu are available.

The partition coefficients referred to above have been used to predict Cu concentration in a simple system where $T = 400°C$, $p = 500$ bar, pH was fixed by muscovite-K-feldspar-quartz, f_{S_2} and f_{O_2} were fixed by the assemblage pyrite-magnetite-hematite, NaCl/KCl = 4, and the total chloride concentration was up to 2.5 mol. With the help of a modified Eq3/6 computer program, we have estimated that ~0.002 mol Cu will be transported by the vapor. Partition coefficients decrease with increasing salinity, due to the increase in the solubility of Cu in the liquid phase. However, Cu solubility in the vapor changes little as the total chloride concentration increases from 0.5 to 2.5 mol. This suggests that even in a system with very high salinity, such as a porphyry Cu, the concentration of Cu in vapor could be high enough for vapor to transport appreciable Cu.

References: [1] Bischoff J. L. (1991) *Am. J. Sci., 291,* 309–338. [2] Armellini F. J. and Tester J. W. (1993) *Fluid Phase Equilibria, 84,* 123–142.

USING LINEAR FREE-ENERGY RELATIONSHIP TO PREDICT STABILITY CONSTANTS OF AQUEOUS METAL COMPLEXES/CHELATES.

H. Xu[1] and Y. Wang[2], [1] Department of Earth and Planetary Sciences, University of New Mexico, Albuquerque NM 87131, USA (hfxu@unm.edu), [2]Sandia National Laboratories, 115 North Main Street, Carlsbad NM 88220, USA (ywang@sandia.gov).

Metal complexation with various inorganic or organic ligands in aqueous solutions directly controls the solubility, sorption, and toxicity of toxic metals, including radionuclides, in natural environments. The quantitative calculations of metal complexation thus have been routinely used in predicting the fate and impact of heavy metals in natural environments. The effectiveness of these calculations depends heavily on the completeness and quality of the thermodynamic databases on which the calculations are based. Unfortunately, the thermodynamic data for many metal complexes, especially those with radionuclides, are currently either unknown or poorly constrained. Therefore, there is a need for (1) developing a method to predict the unknown thermodynamic data based on a limited number of the existing measurements, and (2) using this method to check the internal consistency of the thermodynamic databases that are used in the calculations.

We extend the Sverjensky-Molling relationship to predict the Gibbs free energies of formation or stability constants for a family of metal complexes and chelates with a given complexing ligand.

The linear free-energy relationship is a function of nonsolvation energy and inonic radii of cations. The relationship can be applied to both inorganic and organic metal complexs/chelates. The discrepancies between the predicted and experimental data are generally less than 1 log unit. The use of this linear free-energy correlation can significantly enhance our ability to predict the speciation, mobility, and toxicity of heavy metals in natural environments.

NITROUS OXIDE EMISSIONS FROM AGRICULTURAL SOIL IN GUIZHOU PROVINCE, SOUTHWESTERN CHINA.

W. B. Xu[1], Y. T. Hong[1], X. H. Chen[2], and C. S. Li[3], [1]State Key Laboratory of Environmental Geochemistry, Institute of Geochemistry, Chinese Academy of Sciences, Guiyang 550002, China (lmsei@public.gy.gz.cn), [2]Soil and Fertilizer Institute, Guizhou Academy of Agricultural Sciences, Guiyang 550013, China, [3]Institute for the Study of Earth, Oceans, and Space, University of New Hampshire, Durham NH, USA.

Nitrous oxide (N_2O) is an important trace gas in the atmosphere and in the cycling of N within the soil-atmosphere system. The purpose of this study is to assess N_2O emissions from cultivated agricultural soil in the Guizhou Province, southwestern China, and to study the potential influences of variations in climate and farming practices on N_2O emissions. This was done through seasonal measuring of N_2O fluxes from corn-rape rotation fields, soybean-winter wheat rotation fields, and fallow plots at the Soil and Fertilizer Institute, Guizhou Academy of Agricultural Sciences, and by comparing daily N_2O flux simulated by the Denitrification-Decomposition (DNDC) model [1–3] with field measurements.

Measurement results showed that diurnal regular variation of N_2O flux was similar at the above three fields, the time when daily N_2O flux reached the highest was 2 or 3 h later at corn and soybean fields than at rape and winter-wheat fields, and that temperature was the key factor influencing the diurnal regular variation of N_2O flux. N_2O fluxes from corn-rape rotation, soybean-winter wheat rotation, and fallow land were in the range 9.8~433.1, 4.0~18.4, and 9.7~282.0 mg N m^{-2} h^{-1} respectively; N_2O emissions were much higher than from cultivated agricultural soil in north China. Furthermore, the seasonal variation of N_2O fluxes was homologous at the three fields. N_2O flux pulses were driven by rainfall events directly, the relativity between N_2O flux and precipitation and soil's moisture were positive remarkably, but the relativity was not important between N_2O flux and temperature.

The Denitrification-Decomposition (DNDC) model [1] is a process-oriented, biogeochemical model of the N and C cycles in soil to assess N_2O emissions from agricultural soil using information on soil properties, agricultural practices, and weather variables as inputs. The structure, equations, and heritage of the DNDC model have been described in detail by [1]. Based on the success of test and validation exercises of measured and DNDC-modeled N_2O emission and several associated variables from the above study fields, which exhibited similar trends and magnitudes, we expanded the DNDC model to estimate N_2O emissions from entire agricultural soil at the county scale in Guizhou in 1995. Total N_2O emissions from agricultural lands in Guizhou counties ranged from 0.00349×10^6 kg N yr^{-1} to 0.218×10^6 kg N yr^{-1}. The total N_2O emission from all counties was 4.4×10^6 kg N yr^{-1}, with ~80% of N_2O emission from eight counties and 31.7% of N_2O emission from cornlands. The DNDC model was run with and without manure additions, fertilizer additions, and tillage to estimate the relative contribution of individual agricultural practice on total N_2O emission. The additions of manure, fertilizer, and tillage increased the total N_2O emission in Guizhou by 55%, 37%, and 33% respectively.

The DNDC model was also used to systematically assess the potential effect of changing climate and farming practices in future on N_2O emissions from Guizhou agricultural soil. The baseline conditions for the sensitivity studies were typical of climate condition, soil properties, and farming practices in the above fields. The effect of each climate variable or farming practice on N_2O emissions was tested by varying the single factor and holding all other parameters at baseline values. The 158 scenarios tested indicated that nitrated pollution in rainfall, additions of manure and fertilizer, and tillage may be especially significant anthropogenic factors that have increased N_2O emission from soil in the Guizhou Province, southwestern China.

From a policy perspective, a program to mitigate N_2O emissions from Guizhou agriculture could focus on a relatively limited area of the province and on cornlands and would involve a combination of measures including reductions in additions of manure and fertilizer and in tillage times.

Referrences: [1] Li C. S. et al. (1992) *JGR, 97,* 9759–9776. [2] Li C. S. et al. (1994) *Chemosphere, 28,* 1401–1415. [3] Li C. S. et al. (1996) *Global Biogeochem. Cycles, 10,* 297–306.

QUANTIFICATION OF QUENCH RATES IN WATER, AIR, AND LIQUID NITROGEN.

Z. Xu and Y. Zhang, Department of Geological Sciences, University of Michigan, Ann Arbor MI 48109-1063, USA (zhengjiu@umich.edu).

When red-hot lava enters water, what is the cooling rate of the lava from the surface to the interior? We investigated this problem based on the relation between cooling rate and the final molecular H_2O and OH species concentrations obtained from this laboratory [1,2]. A large chunk (irregular shape with each side ≥8 mm) of hydrous rhyolitic glass containing 0.8 wt% total H_2O was heated to 748°C for 5 min and then dropped into water. Calculated diffusive H_2O loss from the exposed surface affects only a distance of ~0.03 mm. A wafer is sectioned from the chunk of glass near the center and doubly polished. The molecular H_2O and hydroxyl bands at 5230 cm^{-1} and 4520 cm^{-1} are determined by infrared spectroscopy as a function of distance away from an original surface during quench in water. From the measurement, the apparent equilibrium temperature for the species reaction can be calculated. Within 0.4 mm of the surface, the apparent equilibrium temperature is close to 748°C, implying that within this distance the quench rate is high enough (>400°C/s) to preserve the species concentration at the experimental temperature of 748°C. Further away, the apparent equilibrium temperature is less because of the slower quench rate. When the apparent equilibrium temperature is <748°C by at least 20°C (preferentially by 50°C), it is possible to estimate the quench rate from quenched species concentrations (or infrared band intensities) using an experimentally determined relation between quench rate, species concentrations, and total H_2O concentrations [1,2]. The quench rates estimated in this manner at distances of 0.7–2.0 mm are less than those calculated from the 1-D semi-infinite heat conduction equation by assuming the surface temperature instantaneously becomes the room temperature (i.e., assuming quench rate at the surface is infinity) and using a heat diffusivity of 0.7 mm²/s [3]. The experimentally determined slower rate is expected because the surface temperature cannot instantaneously cool to room temperature. A vapor layer would form near the hot surface, which prevents the surface from instantaneous cooling. At distances >2.0 mm, the two experimental and calculated quench rates are similar. The similarity is also expected because the effect of the boundary condition on the interior temperature decreases as distance away from the boundary increases.

We also determined quench rate for a glass cooled in air and in liquid N from 750°C using the same technique. For air quench, the apparent equilibrium temperature at the surface and interior (to ~4 mm) is nearly constant (~620°C), implying that cooling at the outside surface is slow so that cooling in the interior can keep pace with the surface. The inferred cooling rate is ~11°C/s. For cooling in liquid N, the surface cooling rate is only ~50% higher than that in air, and at least 20× lower than that in water. This order of quenching efficiency is consistent with the results of [4].

To our knowledge, our study represents the first quantification of the surface and interior quench rates. Besides quantifying quenching rates of magma and rocks, the determination of interior quench rate will help theoreticians model heat conduction for cooling in water and in air.

References: [1] Zhang et al. (1997) *GCA, 61,* 2167. [2] Zhang and Xu, this volume. [3] Bagdassarov and Dingwell (1994) *JVGR, 60,* 179. [4] Dyar and Birnie (1984) *J. Non-Cryst. Sol., 67,* 397.

GEOCHEMICAL AND ISOTOPIC CONSTRAINTS FOR THE EVOLUTION OF THE SLAVE PROVINCE.

K. Yamashita[1,2] and R. A. Creaser[2], [1]Department of Earth and Planetary Sciences, Harvard University, 20 Oxford Street, Cambridge MA 02138, USA (kyamash@fas.harvard.edu), [2]Department of Earth and Atmospheric Sciences, University of Alberta, 126 ESB, Edmonton AB T6G2E3, Canada (robert.creaser@ualberta.ca).

Introduction: Various models for the tectonic development of the Slave province have been proposed over the past two decades. These include the intracontinenal rift model [1,2], arc-continent collision models [3], and combinations of these processes [4]. Over the past five years, we have undertaken a detailed isotopic and geochemical study of the main lithotectonic units in the Slave province in order to provide a firm basis for establishing a refined tectonic model. We have examined (1) selected exposures of pre-2.8-Ga basement granitoids/gneisses, (2) ~2.72–2.65-Ga Yellowknife supergroup (YKSG) volcanic and sedimentary rocks, and (3) ~2.6-Ga syn- to post-deformation granitoids from the western Slave province.

Results: Our main results are summarized below.

1. The U-Pb zircon age of the basement in the Hanikahimajuk Lake (HL) area (Northern Slave; 3378 Ma) is very similar to the age of the Kangguyak gneisses to the north, and that of a major metamorphic overprint in the Acasta gneisses to the southwest [5 and references therein].

2. Low $\varepsilon_{\mathrm{NdT}}$ values of YKSG volcanic rocks in the HL, Winter Lake (WL; Central Slave) and Yellowknife (S. Slave) areas document contamination by pre-2.8-Ga basement, indicating that the volcanic package was built on or in the vicinity of the basement.

3. Yellowknife supergroup mafic-intermediate volcanic rocks in the HL area can be classified into two associations based on trace-element characteristics: (1) depleted, tholeiitic type, and (2) calc-alkaline type. These two groupings are also found in the Yellowknife and Indin Lake areas of the southwest Slave province [2,6,13]. Given the geochemical evidence for basement contamination of (1), we do not envisage an origin in a typical mid-oceanic ridge setting.

4. The low $\varepsilon_{\mathrm{NdT}}$ of some YKSG sediments from the HL and WL areas show that part of the basement was exposed at the time of YKSG sediment deposition.

5. Through careful investigation of geochemical and isotopic signature of the Burwash Formation turbidites (Yellowknife area), we conclude that the source of these turbidites is a mixture of (1) YKSG volcanic rocks variably contaminated by pre-2.8-Ga basement, and (2) little-contaminated granitic rocks. The westerly derivation of these turbidites implies the existence of little-contaminated, pre-2.66-Ga granitic rocks west of Yellowknife and, therefore, provenance regions not underlain or weakly influenced by the basement.

6. Geochemistry of late-Archean granitoids indicates that ~2.61-Ga syn- and ~2.59-Ga postdeformation granitoids are derived mainly through partial melting of mafic crustal protoliths with local mantle input and partial melting of metasedimentary rocks respectively.

7. The geochronological and isotopic signatures of the pre-2.8-Ga basement seem to appear strongly in two areas: (1) the Acasta River area (westernmost Slave) and (2) along the N-S trending volcanic belt encompassing Arcadia Bay (northernmost Slave), HL, Point Lake, WL, Sleepy Dragon Complex, and Yellowknife [7,8].

In addition to these conclusions, the following summarizes points made by previous researchers that must also be taken into consideration: (1) Known pre-2.8-Ga basement is restricted to the western Slave province [5 and references therein]; (2) volcanic belts in the west-central Slave province are typically mafic dominated, whereas those in the east-northeast Slave province are felsic dominated [9]; and (3) 2625–2640-Ma igneous rocks have not yet been documented from the eastern or western Slave province [10].

Discussion: Integrating these observations, we propose a revised model for the evolution of the Slave craton, which is compatible with most field, isotopic, and geochemical features. We argue that the mafic-intermediate volcanic rocks of the western Slave province can be generated in a single ensialic back-arc system. In modern-day analogs, such as the Japan arc, depleted tholeiitic and calc-alkaline volcanic rocks (as well as felsic volcanic rocks) are both generated in the same back-arc system [11]. It is also noteworthy that YKSG mafic volcanic rocks near Point Lake, overlying the 3.15-Ga Augustus granite, are also interpreted to have formed in a back-arc setting [12]. The basement blocks of the western Slave are interpreted to be remnants of this rifted continental block. In this model, the two mafic-dominated volcanic belts in the western Slave province, i.e., (1) Grenville Lake-Indin Lake-Ghost/MacNaughton Lake, and (2) Arcadia Bay-HL-Point Lake-WL-Sleepy Dragon complex-Yellowknife, may represent the margin of a (now collapsed and shortened) ensialic back-arc.

References: [1] Henderson J. B. (1981) in *Plate Tectonics in the Precambrian*, pp. 213–235, Elsevier, Amsterdam. [2] MacLachlan K. and Helmstaedt H. (1995) *CJES, 32,* 614. [3] Kusky T. M. (1989) *Geology, 17,* 63. [4] Bleeker W. et al. (1997) *Lithoprobe Rpt., 56,* 36. [5] Bleeker W. and Stern R. A. (1997) *Lithoprobe Rpt., 56,* 32. [6] Isachsen C. E. and Bowring S. A. (1994) *Geology, 22,* 917. [7] Thorpe R. et al. (1992) *GSC Open file, 2484,* 179–184. [8] Davis W. J. and Hegner E. (1992) *Contrib. Mineral. Petrol., 111,* 493. [9] Padgham W. A. (1985) *Geol. Assoc. Can. Spec. Paper 28,* 133. [10] Villeneuve M. E. et al. (1997) *GSC, Current Res.* 1997-F, 37. [11] Miyake Y. (1994) *Geochem. J., 28,* 431. [12] Corcoran P. L. and Dostal J. (1997) *Lithoprobe Rpt., 56,* 205. [13] Pehrrson, personal communication.

POSSIBLE RELATIONS OF FELSIC MAGMAS TO ORE METALS IN VOLCANOGENIC MASSIVE SULFIDE DEPOSITS: GEOCHEMICAL EVIDENCE FROM THE BATHURST MINING CAMP, IBERIAN PYRITE BELT, ABITIBI BELT, AND THE HOKUROKU DISTRICT.

K. Yang and S. D. Scott, Scotiabank Marine Geology Research Laboratory, Department of Geology, University of Toronto, 22 Russell Street, Toronto M5S 3B1, Canada (kaihui@quartz.geology.utoronto.ca; scottsd@zircon.geology.utoronto.ca).

Volcanogenic massive sulfide (VMS) deposits hosted by felsic volcanic rocks of bimodal suites show considerable variations in composition, e.g., Cu ± Zn deposits in the Noranda camp; Cu-Zn ± Pb deposits in the Kamiskotia camp in Canada and the Hokuroku district in Japan; and Pb-Zn ± Cu deposits in the Bathurst mining camp in Canada and the Iberian Pyrite Belt in Spain and Portugal. The formation of these types of deposits is generally considered to be dominated by the footwall stratigraphy [1,2], where the hydrothermal fluids leached ore metals, and by felsic magmatic systems, in the form of subvolcanic intrusions, that provided heat (temperature up to 900°C [3]). Such intrusions may have directly contributed volatiles and ore metals into the hydrothermal systems by magmatic degassing [4]. Of these factors, the felsic volcanic rocks are believed to be essential, but to what extent the magmatic system has an influence on the proportion of ore metals remains unknown. The answer to this issue is crucial not only for metallogenic models but also for exploration for VMS deposits.

We have searched for a link between felsic magmas and the ore metals of VMS deposits by using trace-element geochemistry. A detailed investigation was carried out on the Ordovician felsic volcanic rocks associated with the VMS deposits in the Bathurst mining camp, New Brunswick, which comprise a bimodal suite thought to have formed in a continental back-arc basin. The large volume of felsic volcanic rocks is preponderantly subalkalic rhyolitic in composition, and these rocks are similar to those in the Iberian (Devonian), Abitibi (Archean), and Hokuroku (Miocene) regions.

Based on trace-element geochemistry, the felsic volcanic rocks from all the four regions can be categorized into low-Th, mid-Th, and high-Th rhyolites, which are correlative with the ore metals of the associated VMS deposits. The low-Th rhyolites host Noranda-type (Cu-rich) VMS deposits, and are probably fractionated from tholeiites of a primitive volcanic arc or oceanic back-arc setting, a case similar to the Manus back-arc basin in the western Pacific [5]. The mid-Th rhyolites are associated with Kuroko-type (Zn-Cu-Pb) VMS deposits, and are products of partial melting of mafic rocks in a mature island arc setting. The high-Th rhyolites contain Bathurst-type (Zn-Pb-Cu) VMS deposits, as typified by the Bathurst mining camp and the Iberian Pyrite belt. These high-Th rhyolites result from partial melting of continental crust in an intercontinental back-arc basin.

The geochemical correlation of felsic volcanic rocks with different kinds of VMS deposits implies a genetic link between the chemistry of the "pregnant" magmas and the ore metals of the deposits. In particular, low Th/Th* and low La_n/Yb_n values of the felsic volcanic rocks correspond with low Pb + Zn/Cu ratios of the associated Noranda-type VMS deposits, while medium to high Th/Th* and high La_n/Yb_n values of the volcanic rocks are correlative with medium to high Pb + Zn/Cu ratios of the associated Kuroko and Bathurst-type VMS deposits. Such a relationship suggests that the ore metals of the deposits are controlled by the types of felsic magmas. In accordance with this conclusion, results of recent melt/fluid inclusion studies on the felsic volcanic rocks that host the PACMANUS massive sulfides in the eastern Manus Basin, West Pacific [4], and the VMS deposits in the Bathurst mining camp [6] demonstrate the presence of ore-metal-bearing fluid in the felsic magmas. These magmatic fluids could have contributed large quantities of volatiles and ore metals to the hydrothermal systems that formed the large VMS deposits. The ore-metal content of this fluid is so high (2.3 wt% Zn, 7.2 wt% Cu, 2.7 wt% Fe) [4] that only a few percent is needed. These data suggest that felsic magmatism might be directly responsible for the formation of VMS deposits, particularly the large ones, in addition to providing a heat source for the circulation of seawater.

References: [1] Franklin J. M. et al. (1981) *Econ. Geol., 75th Ann. Vol.,* 485–627. [2] Lydon J. W. (1988) *Geosci. Can., 15,* 43–66. [3] Barrie C. T. (1995) *Geology, 23,* 169–172. [4] Yang K. and Scott S. D. (1996) *Nature, 383,* 420–423. [5] Scott S. D. and Binns R. A. (1995) *Geol. Soc. London, Spec. Pub., 87,* 191–205. [6] Yang K. and Scott S. D. (1999) *Econ. Geol.,* in review.

MILANKOVITCH THEORY REVIEWED FROM ARID CLOSED-BASIN LACUSTRINE CALCITE IN DEATH VALLEY, CALIFORNIA.

W. Yang[1] and T. K. Lowenstein[2], [1]Department of Earth and Planetary Sciences, Harvard University, 20 Oxford Street, Cambridge MA 02138, USA (yang@eps.harvard.edu), [2]Department of Geological Sciences, State University of New York at Binghamton, Binghamton NY 13901, USA.

Stable O- and C-isotopic data were obtained from 152 arid closed-basin lacustrine calcite samples from a 186-m-long saline sediment core (DV93-1) in Death Valley, California. The $\delta^{18}O$ and $\delta^{13}C$ values varied from –8.6 to +2.4‰ V-PDB and –1.7 to +5‰ V-PDB, respectively. The $\delta^{18}O$ record for calcite had similar excursions to those found for soluble sulfate in the DV93-1 core, marine carbonate (SPECMAP), and polar ice in the Summit ice core, Greenland. The $\delta^{18}O$ variations indicate noteworthy paleoclimatic changes during the past 200,000 yr. The $\delta^{18}O$ record had similar excursions to those found for sulfate in the Death Valley core, marine carbonate (SPECMAP), and polar ice in the Summit ice core, Greenland. The Death Valley record also shows periods of 96,000, 39,000, 21,000, 14,000, and 8000 yr based on fourier transform analysis that are generally consistent with those of the Earth-orbital variations. Of particular interest in these records is the controversy over the timing of glacial termination II, which is placed at 120 ± 3 ka in Death Valley, at 128 ± 3 ka in the SPECMAP record, at 135 ± 15 ka at Summit, and at 140 ± 3 ka in Devil's Hole. The SPECMAC termination at 128,000 yr is in phase with changes in solar insolation resulting from orbital variations (the Milankovitch theory). A termination at 120,000 yr is at the edge of being in phase with orbital variations, whereas a termination at 140,000 yr is out of phase with orbital variations.

FRACTAL ANALYSIS OF GOLD GRADE IN CANGSHANG GOLD DEPOSIT, NORTHWESTERN JIAODONG, CHINA.

Z. S. Yang, H. Y. Li, Z. M. Gao, Z. J. Ding, and T. Y. Luo, Institute of Geochemistry, Chinese Academy of Sciences, Guiyang 550002, China (zjding@ms.gyig.ac.an).

The concept of fractals has provided a means of quantifying the scale invariant processes or phenomena in geosciences such as the distribution of ore grade, topographic relief, fracture strength of rocks, earthquake magnitude, etc. [1–4]. Studies on the Au grade in the Cangshang Au deposit show that the distribution of Au grade is a multifractal.

The Cangshang Au deposit, located in the northwestern part of Jiaodong Peninsula, Shandong Province, China, is the wall-rock alteration type of Au deposits. The ore bodies are controlled by the fracture zone of a northeast strike fault named the Sanshandao-Cangshang Fault with the Neo-Archean Jiaodong Group as the hanging wall in the southeast and the Linglong Monzonitic Granite as the lying wall in the northwest. The extensive hydrothermal alteration can be divided into K-feldsparization, phyllic alteration, and silicification zones from the wall rock to the ore body. A large number of veinlets with different mineral assemblages that can be divided into five stages were superimposed on the silicification zone and parts of the phyllic alteration zone in the ore body during mineralization period [5].

The data on Au grade were collected from 13 exploration lines in the –50-m level and 11 exploration lines in the –80-m level. If the number of samples N with a grade greater than T is related to T by $N \sim T^{-D}$, the distribution of Au grade is a fractal, and D is the fractal dimension. In the log (N)-log (T) plots for different levels and exploration lines, linear relation was always obtained within two scale ranges. This indicates that the distribution of Au grade is a multifractal, and suggests that Au concentration occurs in two processes — silicification with disseminated pyrite and veinlet mineralization.

The fractal dimensions of the –50-m level are 0.225 and 1.690 within the scale ranges of $0.01 \times 10^{-6} \sim 2.57 \times 10^{-6}$ and $2.57 \times 10^{-6} \sim 50.00 \times 10^{-6}$, respectively, while those of the –80-m level are 0.326 ($0.01 \times 10^{-6} \sim 4.47 \times 10^{-6}$) and 2.308 ($4.47 \times 10^{-6} \sim 50.00 \times 10^{-6}$). The low values of the fractal dimensions indicate the distribution of Au grade is relatively uniform [6] in the low-grade range. This implies that Au is dispersed into the altered rock by intensive silicification, especially in the –50-m level. The high values of the fractal dimensions show that the distribution of Au grade is close to the dendritic distribution (D = 1.5) [7] or more complex. This suggests that Au is largely concentrated in the veinlets by crevasse filling, and implies that the period of veinlet development is the main period of mineralization.

The fractal dimensions of each exploration line vary between 0.045 and 0.388 within the low-scale range, and between 0.848 and 3.110 within the high-scale range. This variety indicates that the spatial distribution of Au grade is extremely complex, and also suggests that the intensity of alteration, the pattern of veinlets, and the density of fissures are at variance in the different parts of the ore body).

References: [1] Bölviken B, et al. (1992) *J. Geochem. Expl.*, *43*, 91–109. [2] Burrough P. A. (1981) *Nature, 294*, 240–242. [3] Turcotte D. L. (1986) *Econ. Geol.*, *81*, 1528–1532. [4] Chiles J. P. (1988) *Math. Geol.*, *20*, 631–654. [5] Yang Z. S. et al. (1999) *Geoscience*, *13*, 73–77 (in Chinese). [6] Shen W. et al. (1998) *Scientia Geologica Sinica*, *33*, 234–243 (in Chinese).

COMPARISON OF SIZE-EXCLUSION CHROMATOGRAPHIC GELS FOR THE CHARACTERIZATION OF POLYMERIC SILICA.

D. M. Yates[1] and P. J. Heaney[2], [1]Department of Materials Science and Engineering, University of Pennsylvania, Philadelphia PA 19104, USA, [2]Department of Geosciences, Pennsylvania State University, University Park PA 16802, USA.

A number of investigators have used size-exclusion chromatography (SEC) to characterize the formation of silica polymers in solution [1–4]. Recent developments in chromatography, however, have led to the replacement of the traditional cross dextran or "soft gel" types used in these studies with "rigid sphere" gels, which offer greater flow rates and higher resolution. An accurate study of the polymerization of silica by SEC requires that the measurements be conducted with a pH 3 buffer solution because solutions at this pH effectively "freeze" the polymerization reaction and allow for a more accurate determination of polymer size [4]. Furthermore, altering the ionic strength or composition of the SEC-buffer solution from that of the aqueous solution used in the polymerization experiment (~0.01–0.2 M) may bring about unwanted changes in the polymers during the analysis. The purpose of the present study was to assess the applicability of several rigid-sphere gels for the study of silica polymers within this narrow range of solution compositions.

Our experiments were conducted by combining monomeric silica solutions with 0.1 M NaCl solutions at pH 7. The solutions were sealed in 50-mL centrifuge tubes and allowed to equilibrate for 24 h. The solutions were then filtered through a 0.1-µm Millipore filter, acidified to pH 3 with 1 M HCl, and analyzed by inductively coupled plasma-atomic emission spectrometry (ICP-AES), the silico-molybdate method, and SEC. The columns used for the SEC analyses were packed with either the soft gel, Sephadex G200 (Pharmacia, fractionation range: 5000–600,000) or the rigid-sphere gels Superdex 200 (Pharmacia, fractionation range: 10,000–600,000), Sephacryl S300 (Pharmacia, fractionation range: 10,000–1,500,000), Cellufine GCL2000 (Amicon, fractionation range: 10,000–3,000,000) or Toyopearl HW-55F (Tosohaas, fractionation range: 1,000–700,000) and equilibrated with a 0.1-M NaCl buffer solution maintained at pH 3. Analyses were performed by injecting 1 mL sample solution into the SEC and collecting 3-mL fractions from the eluent stream to be analyzed by ICP-AES.

Size-exclusion chromatography analyses with Sephadex yielded good separation of monomer and polymer fractions in solution. Analyses conducted with Cellufine, Superdex, and Sephacryl gels, however, resulted in 100% adsorption of the silica polymers and yielded only monomeric silica peaks. Initial analyses conducted with the Toyopearl gel produced distinct monomer and polymer peaks; however, after ~4 experiments this gel produced results similar to the other rigid-sphere gels, yielding only a monomer peak. The rigid-sphere gels used in this study consisted of either pure cellulose (Cellufine) or of dextrans bonded together with rigid molecules such as agarose (Superdex) or N,N-methylenebisacrylamide (Sephacryl), whereas the soft gel, Sephadex, consisted only of cross-linked dextrans. The contrasting results of the soft vs. rigid gels in the present study appear to indicate that polymeric silica adsorbs to the binding molecules in the rigid-sphere gels. Use of various chromatographic gels for SEC analyses in the biological sciences was preceded by a great deal of research focused at optimizing the pH and composition of the SEC buffer solutions to minimize the adsorption of analyte species to the gel matrix. However, due to the narrowly constrained composition of the SEC buffer solution necessary for silica analyses, this type of optimization is not possible. We therefore conclude that the soft gel, Sephadex, at present is the most suitable media for SEC analyses of polymeric silica.

References: [1] Tarutani T. (1970) *J. Chrom.*, *50*, 523–526. [2] Shimada K. and Tarutani T. (1979) *J. Chrom.*, *168*, 401–406. [3] Shimada K. and Tarutani T. (1982) *Mem. Fac. Sci.*, *Kyoshi University*, *Ser. C 13*, 311–322. [4] Crerar D. A. et al. (1981) *GCA*, *45*, 1259–1266.

THE NIOBIUM-92-ZIRCONIUM-92 p-PROCESS CHRONOMETER.

Q. Z. Yin[1], I. Horn[1], W. F. McDonough[1], J. Zipfel[2], S. B. Jacobsen[1], and R. L. Rudnick[1], [1]Department of Earth and Planetary Sciences, Harvard University, 20 Oxford Street, Cambridge MA 02138, USA (yin@fas.harvard.edu), [2]Max-Planck-Institut für Chemie, Abteilung Kosmochemie, P.O. Box 3060, 55020 Mainz, Germany.

Introduction: ^{92g}Nb ($\tau_{1/2}$ = 36 Ma) is a shielded "p-only" nuclide. It decays by electron capture to ^{92}Zr. Its potential as one of the four p-process extinct chronometers (the other three being ^{53}Mn-^{53}Cr, ^{97}Tc-^{97}Mo, and ^{146}Sm-^{142}Nd) has long been recognized. Earlier efforts to detect the signature of ^{92g}Nb decay in bulk meteorite samples have been unsuccessful [1]. Recently a ^{92}Zr anomaly was reported in a rutile separated from Toluca (IAB) and presented as evidence for the presence of live ^{92g}Nb in the early solar system [2]. We have renewed this search as part of our ongoing effort to understand better the Nb-Zr-Mo-Tc-Ru region of the N-Z chart with the advancement of new analytical techniques.

The Sample: Rutile is a rare mineral occasionally reported in type IAB and related iron meteorites. It is typically observed in both silicate-bearing and silicate-free sulfide inclusions. The sample used for this study (Zagora) is an IAB iron with silicate inclusions. The original slab from the MPI collection showed a large (2 × 1-cm), incomplete troilite-rich silicate inclusion. The inclusion consists mainly of troilite enclosing fine-grained individual silicate grains or silicate aggregates. Four rutile grains were found in the entire inclusion. Each grain is associated with silicate aggregates and the host troilite. Grain sizes vary from 40–150 µm. Niobium (~9000 ppm) and Zr (~5000 ppm) with Nb/Zr ratios above 30× chondritic is observed. Manganese-53-chromium-53 systematics of two alabandite grains, analyzed in the same section, show no excess of ^{53}Cr from decay of ^{53}Mn ($\tau_{1/2}$ = 3.7 Ma) [3].

Analytical Techniques: The Harvard University Laser Ablation (HULA) facility Web page (http://www-eps.harvard.edu/la-icp-ms.html) interfaced with a Micromass IsoProbe multicollector magnetic sector inductively coupled plasma mass spectrometer (ICP-MS) recently installed at Harvard was used to determine the Zr-isotopic composition *in situ* in terrestrial and ex-

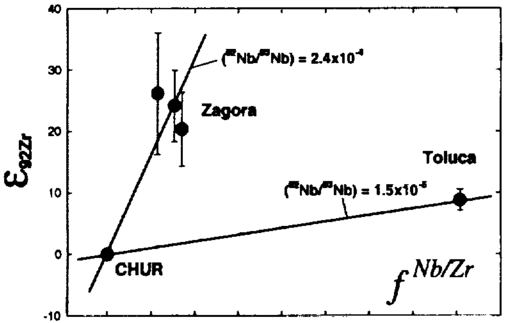

Fig. 1.

traterrestrial rutiles. The multicollecting Faraday cups in this instrument allowed simultaneous integration on masses ^{90}Zr, ^{91}Zr, ^{92}Zr, ^{93}Nb, ^{94}Zr, ^{95}Mo, ^{96}Zr, and ^{97}Mo in static mode. Niobium-93 was measured to obtain the Nb/Zr ratio simultaneously and to correct for mass 93 tail on mass 92 (abundance sensitivity <10 ppm). Both ^{95}Mo and ^{97}Mo were measured to monitor the potential Mo isobaric interferences, and their contributions were found to be negligible. Zirconium-90 signals ranging from 0.7 to 2 × 10^{-11} A were obtained from the meteoritic rutile samples depending on Zr content and laser spot size. The signal lasted only 40–80 s because of limited thickness of the thin section (~30 μm). The system was calibrated and tuned with the terrestrial in-house rutile standard. This standard was then measured for its isotopic composition using a time-resolved procedure in which gas blank was measured, then the laser turned on and the Zr, Nb, and Mo isotopes measured by multicollection. An exponential mass bias correction was applied assuming ^{90}Zr/^{91}Zr = 4.5845 [4]. Meteoritic rutiles were measured under the same conditions.

Results and Discussion: The measured ^{93}Nb/^{91}Zr ratio was used to derive the elemental Nb/Zr ratio, and our results are consistent with electron microprobe data (Zipfel, unpublished). The ^{92}Zr/^{91}Zr ratio measured in the terrestrial rutiles agrees with the reference value determined by thermal ionization mass spectrometry (TIMS) [4] within 0.5–3ε units. Three Zagora rutile grains reveal 2–26ε excesses relative to the terrestrial rutile in the ^{92}Zr/^{91}Zr ratio with an uncertainty of 6–10ε. Zagora data are plotted together with the published Toluca rutile result [2] in a ε^{92}Zr vs. $f^{Nb/Zr}$ plot. The smaller (8.8ε) effect in [2] was for a bulk sample of all 60 rutile grains that was processed through wet chemistry. The apparent initial $^{92\varepsilon}$Nb/^{93}Nb abundance is obtained using the CHUR reference point. The high apparent initial ^{92}Nb/^{93}Nb of 2.4 × 10^{-4} for Zagora suggests that bulk meteorite samples with $f^{Nb/Zr}$ over 1, ^{92}Zr* anomalies over 1ε are expected. This is well within the resolution of modern mass spectrometry.

References: [1] Minster J.-F. and Allègre C. J. (1982) *GCA, 46,* 565–573. [2] Harper C. L. (1996) *Astrophys. J., 466,* 437–456. [3] Hutcheon I. D. et al. (1992) *LPS XXIII,* 565–566. [4] Nomura M. et al. (1983) *Int. J. Mass Spec. Ion Physics, 50,* 219–227.

PRECISE AND ACCURATE CALIBRATION OF OSMIUM SPIKE.

Q. Z. Yin, C.-T. Lee, W. F. McDonough, I. Horn, R. L. Rudnick, and S. B. Jacobsen, Department of Earth and Planetary Sciences, Harvard University, 20 Oxford Street, Cambridge MA 02138, USA (yin@fas.harvard.edu).

Introduction: Since the introduction of high-precision negative thermal ionization mass spectrometry for Re- and Os-isotopic measurements in 1991 [1–3], two problems persisted in obtaining an absolute chronology with the Re-Os system. The first problem centers on the precision and accuracy of Os-spike calibration. The main difficulties arise from (1) the absence of stoichiometric Os metal or salts of high purity to serve as primary standards and (2) the lack of isotopic equilibrium between Os of different oxidation states and of different chemical forms in the spike and standard. Re-Os isochrons have been determined to per-mil-range precision in both slope and initial [4–6]. But because the accuracy of Os spike is currently limited to 0.5–1.6%, the isochron may be horizontally off by ~1.6%. This will have a significant effect on the calculated initial Os-isotopic composition. The second problem is that the half-life of ^{187}Re is only known to ~3% based on the direct measurement [7]. Any age calculated from the slope of an isochron has an uncertainty of ~3%. The uncertainty of the ^{187}Re half-life ultimately depends on the accuracy of the Os-spike calibration. It is thus clear that this is an area that needs further improvement, so that the Re-Os chronometer as an absolute dating tool can be applied to its fullest potential.

Reviews of Previous Osmium Spike Calibration: Lindner et al. [7] used certified pure ammonium hexachloroosmate, $(NH_4)_2OsCl_6$ as a standard; X-ray crystallographic analysis reveals that this salt is of high purity and of the proper substance. However, unsatisfied with consistent bias of 2.5% between two spikes, the Os content of the standard solution was checked again for accuracy by potentionmetric titration. This method cannot be considered absolute, however, because the reagent itself had to be standardized with an independent source of a chloroosmate (hence a "bootstrap" procedure) or chloroplatinate. At best the method provides an indication of confidence on accuracy at the precision level of the Plasmaquad inductively coupled plasma mass spectrometer (ICP-MS) that was used in Lindner's work [7].

Morgan et al. [4] used the same $(NH_4)_2OsCl_6$ standard to calibrate the same Os spike repeatedly and pooled the results, obtaining $2\sigma_m$ precision at the level of 0.23–0.36%. The accuracy of the Os-spike, however, was ascertained to 1% or better based on weight loss differences after cumulative heating at 140°C for 24 h.

Shen et al. [5] used two Os metal chips with 0.2–0.4% impurities. These metals were dissolved, converted to hexachloroosmate, dried, and redissolved in 4N H_2SO_4 as stock solution. The resulting Os-spike concentration varied from 0.39 to 1.3% (Metal I) and –0.33 to –1.41% (Metal II). The offset between the two metals was 1.6%, which probably results from O and C impurities in the Os metals.

Our Approach: In order to calibrate an Os spike precisely and accurately, two or more weighable, pure, nonhygroscopic, nonvolatile compounds of uniform composition of Os are required. Solid OsO_4 and Os metal sponge are not stoichiometric [4,8] up to the 5% level. In reviewing the literature, dissolving stable Os chloro- or bromo-compounds in HCl and HBr with minimal processing still appears to be the best option. We were able to obtain freshly manufactured anhydrous $(NH_4)_2OsCl_6$, K_2OsCl_6, Na_2OsCl_6, and $(NH_4)_2OsBr_6$ with stated purity of 99.999% shipped under Ar gas. Upon receipt, the first two compounds were immediately dissolved in HCl as stock solution, with two dissolutions being made for each compound.

In previous efforts, the Os-spike-normal isotopic equilibrium is achieved either by alkaline fusion or Carius tube technique. In this work, we used the Micromass IsoProbe multiple collector ICP-MS for the Os-isotopic analyses of the spike-normal mixtures. Preliminary tests show that nebulization and especially ionization in a 6500–8000 K plasma do not discriminate Os of different oxidation states and chemical forms. By simply mixing the Os spike with the standard, and diluting to the desired concentration for ICP analysis, the measured ^{190}Os/^{188}Os ratio of the mixture is good to 0.01% and reproducible. The mixture solution is doped with natural Ir and ^{191}Ir/^{193}Ir is used for the mass-bias correction of the Os mixture. Preliminary results based on two mixtures show that the Os-spike concentration calibrated against $(NH_4)_2OsCl_6$, and K_2OsCl_6 agree to 0.4%. We will complete the measurement of 12 spike-normal mixtures we have prepared. A Johnson-Matthey $(NH_4)_2OsCl_6$ standard prepared by QZY in Mainz and the LLNL $(NH_4)_2OsCl_6$ standard used for ^{187}Re half-life determination provided by M. Lindner will also be used to calibrate the Os spike, and the results will be compared for consistency.

References: [1] Creaser et al. (1991) *GCA, 55,* 397–401. [2] Yin et al. (1991) *Terra 3,* 491. [3] Voelkening et al. (1991) *Intl. J. Mass Spec., 105,* 147–159. [4] Morgan et al. (1995) *GCA, 59,* 2331–2344. [5] Shen et al. (1996) *GCA, 60,* 2887–2900. [6] Birck and Allègre (1998) *MAPS, 33,* 647–653. [7] Lindner et al. (1989) *GCA, 53,* 1597–1606. [8] Birck et al. (1997) *Geostandards Newslett., 20,* 19–27.

MOLYBDENUM- AND TUNGSTEN-ISOTOPIC SIGNATURES IN THE EARLY SOLAR SYSTEM.

Q. Z. Yin, K. Yamashita, and S. B. Jacobsen, Department of Earth and Planetary Sciences, Harvard University, 20 Oxford Street, Cambridge MA 02138, USA (yin@fas.harvard.edu).

Introduction: The ^{182}Hf-^{182}W and ^{97}Tc-^{97}Mo systems are ideal chronometers to address the problems related to the timescale of planetary accretion and metal-silicate differentiation (core-mantle fractionation at a planetary scale). These elements are refractory and significant parent/daughter fractionation is expected to take place during the segregation of metal phase from the chondritic reservoir. In principle, the segregation of metal before the extinction of ^{182}Hf and ^{97}Tc will produce a deficit and excess ^{182}W and ^{97}Mo in the iron meteorites. Such coupled effects were reported for the Toluca (IAB) iron meteorite [1,2].

Results and Discussion: We have extended this investigation further to several groups of iron meteorites with a wide range of Re/Mo ratios (used as proxy for Tc/Mo ratio). Sikhote-Alin (IIB-An) and Cape of Good Hope (IVB) show similar ^{97}Mo/^{96}Mo excess comparable to that of Toluca. However, in spite of high Re/Mo ratios, Henbury (IIIA) and Negrillos (IIA) show no resolvable difference from the terrestrial standards. This may imply that fractional crystallization in the inner/outer core, which produced the observed range of Re/Mo ratio of igneous groups of iron meteorites, occurred after the extinction of ^{97}Tc.

We have started W-Mo-isotopic studies of bulk chondrites and refractory CAIs from Allende. CAIs are believed to have formed very early in the history of the residual nebula and represent the oldest known class of non-presolar objects in meteorites [3]. Redox-dependent fractionation in subsets of these objects has generated significant depletions of W, Mo, and Ru relative to Re. Hafnium/tungsten fractionations up to 4× (relative to the solar Hf/W ratio) are also present in CAIs. The major goal of Mo-isotopic study in CAIs is to establish the solar nebular initial abundance of ^{97}Tc, so as any chronological information derived from ^{97}Tc-^{97}Mo system is placed on an absolute timescale. First Mo-isotopic results on CAI "A44A" indicate Mo-isotopic anomalies in both ^{95}Mo and ^{100}Mo in addition to ^{97}Mo.

For the bulk chondrites, two carbonaceous chondrites Allende (AL) and Murchison (MU) were initially chosen because these meteorites have been widely used to characterize chondritic composition. Like the A44A, the Mo-isotopic composition in both AL and MU is not normal. When normalized to pure s-process nuclide ^{96}Mo, both whole-rock Allende-2 (AL-WR2) and MU exhibit positive $\varepsilon^{95}\mathrm{Mo}_{(r,\,s)}$ (1~2), $\varepsilon^{97}\mathrm{Mo}_{(r,\,s)}$ (~1), and $\varepsilon^{100}\mathrm{Mo}_{(r)}$ (~2). These figures are comparable to the r-process residuals after subtraction of s-process from the solar abundance (i.e., $N_r(^{95}\mathrm{Mo}) = 2.13 \pm 0.24$, $N_r(^{97}\mathrm{Mo}) = 0.87 \pm 0.15$, $N_r(^{100}\mathrm{Mo}) = 2.42 \pm 0.13$; (Si = 10^5)) [4]. With the 2.5ε excess on p-process ^{94}Mo in AL-WR2, it is tempting to consider that ε^{97}Mo excess could be at least partly coming from $^{97}\mathrm{Tc}_{(\text{pure-p})}$ decay. Interestingly, however, the ^{97}Mo/^{96}Mo and ^{94}Mo/^{96}Mo ratios of AL-WR1-S (powdered AL from Smithsonian) plot on the s-process trend defined by Mo isotopes of presolar SiC and graphite grains from MU [5]. The positive ε^{95}Mo does not plot on the same trend, which may mean the powder contains a significant amount of CAI with Mo-isotopic signatures similar to that in A44A. It is noteworthy that the Cr-isotopic composition in the bulk the AL and MU as well as Nd-isotopic composition in AL are shown to be anomalous relative to terrestrial [6, unpublished data]. If the current result for Mo could be substantiated, it is clear that neither AL nor MU could be used to characterize bulk chondritic reservoir isotopic composition

Although there are extensive W-isotopic data on iron meteorites (εW = −3 to −5; [1,7–9]), the current precision of ~0.5–1ε does not allow us to see the possible differences in W-isotopic composition among different groups of iron meteorites. We have shown that improved mass spectrometry technique and controlled fractionation will allow us to achieve even higher precision [10]. Completed measurement on Sikhote-Alin and Negrillos appear to be tightly clustered around −3.1ε, which is indistinguishable from Toluca. We are continuing our studies on more iron meteorites from a variety of groups to bring the matter into a conclusion. The W-isotopic composition of bulk as well as mineral separates from a few selected chondrites will be measured by two different available techniques [negative thermal ionization mass spectrometry (N-TIMS) and multiple collector inductively coupled plasma mass spectrometry (MC-ICP-MS)].

References: [1] Yin Q. Z. and Jacobsen S. B. (1998) *LPS XXIX,* Abstract #1802. [2] Jacobsen S. B. and Yin Q. Z. (1998) *LPS XXIX,* Abstract #1852. [3] Allègre C. J. et al. (1995) *GCA, 59,* 1445. [4] Käppeler F. et al. (1989) *Rep. Prog. Phys., 52,* 881. [5] Nicolussi G. K. et al. (1998b) *GCA, 62,* 1093. [6] Rotaru M. et al. (1992) *Nature, 358,* 465. [7] Lee D.-C. and Halliday A. N. (1995) *Nature, 378,* 771. [8] Harper and Jacobsen (1996) *GCA, 60,* 1131. [9] Horan M. F. et al. (1998) *GCA, 62,* 545. [10] Yin et al. (1999) *LPS XXX,* Abstract #2049.

COMPARISON BETWEEN FIELD AND LABORATORY RATES OF RHYOLITE WEATHERING.

T. Yokoyama[1] and J. F. Banfield[2], [1]Mineralogical Institute, University of Tokyo, Hongo, Bunkyo-ku, Tokyo 113, Japan, [2]Department of Geology and Geophysics, University of Wisconsin–Madison, Madison WI 53706, USA.

Introduction: Several studies based on watershed mass-balance revealed a significant discrepancy (several orders of magnitude) between field and laboratory dissolution. Often this has been attributed to difficulties in determination of reactive surface area in the field [1]. The goal of the current study is to directly determine rhyolite weathering rates through analysis of weathering progress in lavas of known age and to test the hypothesis that, if reactive surface areas are well constrained, field rates should closely match laboratory rates. Previous studies of the Kozu island rhyolites indicate that the chemical compositions of the lavas have been constant over the last several tens of thousands of years [2]. Porous rhyolites were chosen because of their simple mineralogy (>86% glass), high porosity and permeability [3], and limited change in reactive surface area. The very high porosity and abundant cooling joints in the lava domes allow deep water penetration. Consequently, the rhyolitic rocks investigated here have characteristics of homogeneous deep-weathering [3]. This allows determination of element loss directly from changes in measured chemical compositions as a function of time. The ages of lava domes have been variously constrained: Mt.Tenjo at ~1100 yr ago by historic records, Mt. Kobe by hydration layer analysis at ~2600 yr ago, Mt. Osawa by C dating at 20,000 yr ago, and Mt. Awano-mikoto at ~40,000 yr ago by hydration layer analysis [3].

Dissolution Rate and Discussion: Analysis of fresh glass using electron probe microanalysis (EPMA) indicates that initial chemical compositions of the four lavas are approximately equal. Bulk compositions were determined by X-ray fluorescence analysis (XRF) in order to estimate rates of loss of elements from the glass. The change in chemical composition per cubic centimeter indicates some gain of normally insoluble components (Al_2O_3, FeO, TiO_2) with weathering. This may be due to slight compaction or colloidal transport. Observations using scanning electron microscopy (SEM) indicate alteration products on the glass surfaces of the ~20,000 and ~40,000-yr-old rocks. Given that EPMA maps reveal that Fe, and possibly Ti, are condensed in alteration products, we assumed Fe (and Ti) conservation. The effect of this correction on the determined rate is small.

A rate of Si release of ~10^{-18} mol/cm²/s was calculated from the specific surface area, age, and slopes of the linear trends revealed when the change in chemical composition (corrected) is plotted against time (Fig. 1). Both model calculations, based on change of chemical composition, and SEM observations indicate 0.3 cm³ of altered products per cubic centimeter of ~40,000-yr-old rock. Based on this result, the precipitation rate was estimated and the true dissolution rate was calculated. The resulting rate is ~2×10^{-18} mol/cm²/s. This value is ~10^3 lower than the experimental dissolution rate of rhyolitic glass, measured at 25°C and pH = 6.2 in a closed system [4].

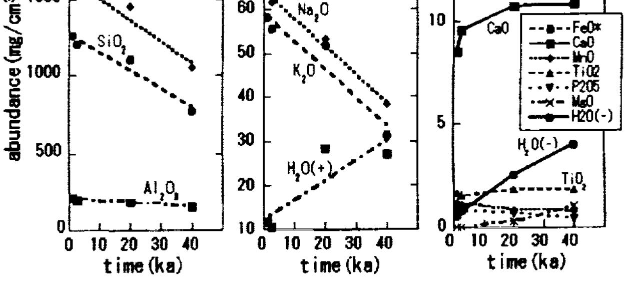

Fig. 1. Changes in chemical abundance with elapsed weathering time (corrected for Fe conservation).

The historic mean temperatures around Kozu island range between 23° and 27°C over the past 25,000 yr [5]. Consequently, the discrepancy between field and laboratory rates is probably not attributable to temperature. Rainfall is high, and given the high porosity and permeability, restricted access of fluids to glass surfaces is probably not a major factor.

One explanation for the comparatively slow rate of natural rhyolite glass dissolution may be that solutions are close to saturation relative to the experiment. When it rains, water penetrates into lava dome along cooling joints and then into the finer-scale porosity, where it is retained, reacts with glass surfaces, reaches saturation, and precipitates secondary aluminosilicate phases. The dependence of rates on saturation state is well known. Given that we can rule out most other factors, we attribute the significant difference between laboratory and field rates to this effect.

References: [1] Velbel M. A. (1985) *Am. J. Sci., 285,* 904–930. [2] Taniguchi H. (1977) *Bull. Volcanol. Soc. Japan, 22,* 133–147. [3] Oguchi T. et al. (1994) *Geogr. Rev. Japan., 67A,* 775–793. [4] White A. F. (1983) *GCA, 47,* 805–815. [5] Sawada K. and Handa N. (1998) *Nature, 392,* 592–595.

SOURCE TRACING OF ARCHAEOLOGICAL COPPER SMELTING ORE BY *IN SITU* ISOTOPIC MEASUREMENTS BY LASER ABLATION INDUCTIVELY COUPLED PLASMA MASS SPECTROMETRY USING QUADRUPOLE AND MULTICOLLECTOR TECHNIQUES.

S. M. M. Young[1], I. Horn[2], D. Miller[3], J. Cantle[4], F. Keenan[4], and I. Bowen[4], [1]Archaeometry Laboratories, Peabody Museum, Harvard University, Cambridge MA, USA, [2]Earth and Planetary Science Department, Harvard University, Cambridge MA, USA, [3]Archaeology Department, University of Cape Town, Cape Town, South Africa, [4]V. G. Elemental, Ion Path, Road Three, Winsford, Cheshire, UK.

Drierivier is a very complete precolonial Cu-smelting site located along the Oanob River in Rehoboth, central Namibia. In Sandlowsky's excavation of this site, three furnaces still containing slag and Cu prills were found, as well as numerous small samples of malachite ore. Copper artefacts were found by European explorers in the 18th centrury, but only rumors about ore bodies and itinerant smiths who dwelt in the central highlands existed. Thus, this is a very important archaeological site and we are in the process of metallographically, chemically, and isotopically analyzing the material to learn as much as possible about the precolonial smelting technology and sources of raw material. The materials found in the archaeological site display a very distinct and uncommon Pb-isotopic distribution. All samples are exceptionally high in content of ^{206}Pb.

An inductively coupled plasma mass spectrometry (ICP-MS) technique of simultaneous solution nebulization and laser ablation has been developed on the VG PQII ICP-MS with homemade laser optics and excimer (193-nm) laser at Harvard. It allows precise ^{207}Pb/^{206} Pb measurements for accessory minerals without the use of a matrix-matched calibration standard. A solution of known amounts of natural Tl spike is nebulized. The ^{205}Tl/^{203}Tl allows precise mass-bias correction of the Pb/Pb ratios. This is a powerful tool for *in situ* isotopic determinations. We obtain precision and accuracy of better than 2% RDS (2σ) both on Harvard standard zircons and on malachite samples containing <1 ppm of Pb.

Lead-207/lead-206 of the Cu prills from the furnace was 0.154; of the slag it was 0.113, and of the malachite at the site it was 0.114. We have analyzed malachite samples from mines all over Namibia and the Richtersveld region of northwest South Africa. Swartmodder, a malachite mine in central Namibia, has been found to be a formation containing very old Pb. The Swartmodder vein is ~2 km in length running north to south with an eastern side branch of ~0.5 km near the center. We obtain ^{207}Pb /^{206} Pb ratios ranging from of 0.088 for samples from the northern area of the mine to 0.285 for the southern end of the mine. This gives us Pb/Pb ages of the Pb deposited in the malachite ranging from 2 to 3 Ga. All other ore samples have common (or close to common) Pb-isotopic distribution ^{207}Pb/^{206}Pb of 0.806 ± 0.153. The Swartmodder deposit is the only malachite over a very vast region containing very ancient Pb. This is definitive evidence that it is the source used in the pre-colonial smelting site of Drierivier.

This ancient signature is related either to a 1.7–2.7-Ga craton, part of the original core of the continent of Africa, or it may lie on an "ancient" arc, which may be obducted seafloor. The source of the Pb itself is as ancient as the craton. The malachite may not be. Lead- and U-isotopic data were measured on the VG Axiom. The multiple-collector technique improves the precision of the isotope ratio by 1–2 orders of magnitude. The Pb-isotopic data will confirm and tighten with greater precision and accuracy the previous work done on the VG PQII at Harvard. The U-isotopic data will date the deposition of the malachite.

GEOLOGIC ASSESSMENT OF THE BIOGEOCHEMICAL FEEDBACK RESPONSE TO THE CLIMATIC AND CHEMICAL PERTURBATIONS OF THE LATE PALEOCENE THERMAL MAXIMUM.

J. C. Zachos[1] and G. R. Dickens[2], [1]Department of Earth Sciences, University of California, Santa Cruz CA 95064, USA (jzachos@es.ucsc.edu), [2]School of Earth Sciences, James Cook University, Townsville QLD 4811, Australia (jerry.dickens@jcu.edu.au).

Introduction: A growing body of evidence supports the hypothesis that a very large mass of C was rapidly added to the ocean or atmosphere during the Late Paleocene thermal maximum (LPTM) ca. 55 Ma. This evidence includes an abrupt C-isotopic (δ^{13}C) anomaly in all major C reservoirs of at least 2.5‰ and pronounced dissolution of carbonate in deep marine environments [1–4]. Thermal dissociation of marine-gas hydrates and subsequent oxidation of CH_4 to CO_2 is the most plausible explanation for the inferred C input, given the apparent rate (<10 k.y.) and magnitude of the δ^{13}C excursion [4]. However, enhanced outgassing of CO_2 associated with rifted margin volcanism [5] cannot be fully excluded with available information.

Gas Hydrates: A 1200-gigaton (Gt) input of C during the LPTM is conservative [4]. This suggestion assumes a gas hydrate source greatly enriched in ^{12}C (δ^{13}C of –60‰) and a minimum magnitude for the global δ^{13}C excursion of 2.5‰. If the C source was more enriched in ^{13}C (e.g., volcanos or ice/volatile objects), or the excursion were greater, the amount of C released during the LPTM would increase accordingly. In any scenario for the LPTM, the mass of C involved is immense, and an outstanding question is "what happened to all of the C?"

Geochemical Feedbacks: We assume the late Paleocene global C cycle prior to the LPTM was broadly similar to that before the industrial revolution ca. 1740 A.D. The system was in steady state, with rapid (<3 × 10^3 yr) C exchange between all ocean, atmosphere, and terrestrial C reservoirs, and with long-term (100–200 × 10^3 yr) C exchange between these reservoirs and the rock record. Thus, regardless of the source or location of C input, excess C supplied during the LPTM should have been (1) rapidly transferred to all ocean, atmosphere, and terrestrial C reservoirs, and (2) eventually purged as carbonate and organic matter [6]. The global nature and overall shape of the C-isotopic excursion are consistent with these two inferences. However, such an interpretation involves a number of biogeochemical feedbacks to remove C, including some that are poorly understood.

Addition of CO_2 (or oxidized CH_4) from an external source to any C reservoir of the ocean or atmosphere will increase the CO_2 of all ocean reservoirs and the pCO_2 of the atmosphere. This rationale should extend to the terrestrial reservoir: Elevated pCO_2 in the atmosphere is expected to increase the size of standing biomass and soil C. Intuitively, one would expect the standing biomass and soil C reservoirs to expand (beyond that noted above) because the accommodation space on continents would grow with increased warmth and precipitation. However, because forests and C-rich soils already extended well into the high latitudes of North America and Eurasia prior to the LPTM, expansion effects would be limited. Also, as is expected with future global warming, while some regions became wetter during the LPTM, other regions probably became drier. Terrestrial C reservoirs most likely expanded during the LPTM but were a minor and transient sink for excess C.

Addition of massive quantities of CO_2 from any source to any C reservoir in the ocean or atmosphere should increase pCO_2 in all deep-ocean reservoirs. Such an increase in pCO_2 should enhance $CaCO_3$ dissolution on the seafloor and raise the alkalinity. Although deep-sea sediment sequences show evidence for this dissolution, the interval of dissolution is short, and massive storage of C as DIC in the oceans was a temporary phenomena.

The permanent sink for the excess C must have been the rock record via silicate weathering and deposition of carbonate and organic C. Higher pCO_2

will increase chemical weathering rates, which in turn will stimulate several other processes that effectively extract C from the system. For one, higher chemical weathering, in combination with enhanced fluvial discharge, would significantly increase ocean inputs of dissolved ions and nutrients, including Fe and Si. This increase in chemical fluxes should have increased production of organic C as well as opal, especially in coastal upwelling regions where the inputs of NO_3^- and PO_4^{3-} are high. In addition, despite higher atmosphere pCO_2, increased ion concentrations in shelf waters would lead to supersaturation and deposition of carbonate.

The Sediment Record: The marine-sediment record documents the effects of a biogeochemical feedback response consistent with massive C input as outlined above. Deep-sea environments show evidence of increased carbonate dissolution and lower productivity (i.e., clay layers with low organic C content) at the peak of the LPTM [3,7] followed by a gradual recovery occurring over a period of >150 k.y. In contrast, neritic environments show evidence of enhanced carbonate accumulation or preservation and/or higher productivity and C burial [8,9]. The differential response/recovery between the deep sea and shelves suggests the increased dissolved load of rivers was being removed largely on the shelves. Biogeochemical decoupling of these systems is supported by a post-LPTM increase in C-isotopic gradients from neritic to pelagic environments [8–10]. The exact cause of this decoupling remains unknown.

References: [1] Kennett J. P. and Stott L. D. (1991) *Nature, 353,* 225–229. [2] Koch P. L. et al. (1992) *Nature, 358,* 319–322. [3] Bralower T. J. et al. (1997) *Geology, 25,* 963–967. [4] Dickens G. R et al. (1997) *Geology, 25,* 259–262. [5] Thomas E. and Shackleton N. J. (1996) *Geol. Soc. London Spec. Pub., 101,* 401–441. [6] Walker J. C. G. and Kasting J. F. (1992) *Paleogeogr., Palaeoclimatol., Palaeoecol., 97,* 151–189. [7] Thomas D. et al. (1999) *Paleoceanogr.,* in press. [8] Thomas E. et al. (1997) *Eos Trans. AGU, 78,* F363. [9] Gibson T. et al. (1993) *Paleoceanogr., 8,* 495–514. [10] Charisi S. D. and Schmitz B. (1998) *Paleoceanogr., 13,* 106–118.

CARBON DIOXIDE CYCLING: CLIMATE, IMPACTS, AND THE FAINT YOUNG SUN.

K. J. Zahnle and H. H. Sleep, NASA Ames Research Center, Moffett Field CA 94035, USA.

Evidence for relatively mild climates on ancient Earth and Mars has been a puzzle in light of the faint early Sun. The geologic evidence, although far from conclusive, would appear to indicate that the surfaces of both planets were, if anything, warmer ca. 3–4 Ga than they are now. The astrophysical argument that the Sun ought to have brightened ~30% since it reached the main sequence is hard to refute. There results a paradox between the icehouse we expect and the greenhouse we think we see [1]. The usual fix has been to posit massive CO_2 atmospheres, although reduced gases (e.g., NH_3 or CH_4) have had their partisans [2]. Evidence against siderite in paleosols dated 2.2–2.75 Ga sets a rough upper limit of 30 PAL (present atmospheric levels) on pCO_2 at that time [3]. This is an order of magnitude short of what is needed to defeat the fainter Sun. We present here an independent argument against high pCO_2 on early Earth that applies not only to the Archean but yet more forcefully to the Hadean era.

Much or most of Earth's CO_2 is currently in the mantle. A recent estimate is 170 bar [4]. The second large reservoir (60 bar) is provided by carbonates on continental platforms. The atmospheric (0.0003 bar) and hydrospheric (0.02 bar) reservoirs are small. On 100-Ma timescales, pCO_2 may be controlled by weathering or precipitation of carbonate rocks. But on long timescales the mantle becomes important. The current CO_2 mantle outgassing rate, ~2.5ε 12 mol/yr [4], would double the 60-bar surface carbonate inventory in 3 b.y.

Carbonitization of oceanic crust is probably important to closing this cycle [5–7]. Much of the CO_2 in low-temperature hydrothermal systems is removed from seawater to form carbonates [7]. Based on Schultz and Elderfield [6], we deduce that the ocean cycles through low-temperature hydrothermal systems in 2 m.y. and that current carbonitization is 1.65ε 12 mol/yr; based on Sansone et al. [7], the cycle time would be 8–20 m.y. and the current CO_2 sink 4–10× smaller. The estimate by Staudigel et al. [5] is comparable to the higher estimate. Some of the carbonatized basalt is eventually subducted with the oceanic crust. A detailed study of a volcano in the Kurile arc puts the subducted fraction at 64–84% [8]. If we assume that 74% is subducted, the flux of CO_2 to the mantle at 1 PAL would be between 1.2ε 11 and 1.2ε 12 mol/yr.

Carbonitization is directly proportional to the amount of CO_2 in the oceans and, like the mantle-outgassing rate, directly proportional to the creation of oceanic crust. For Archean heat flows 2–3× higher than today and corresponding crustal creation rates 4–9× higher, both outgassing and ingassing are faster (thus timescales drop to 300–700 m.y.) but the balance is unchanged; to second approximation, the hotter Archean mantle promotes partial melting to greater depth, which could increase outgassing by as much as a factor of 2. A rough upper limit on oceanic CO_2 is obtained by equating outgassing to ingassing, which for the numbers given here, implies that the ocean cannot hold much more than 4–40× the CO_2 it holds today. If ocean pH is assumed constant, the upper limit on pCO_2 is 4–40 PAL. This agrees with Rye et al. [3] while falling well short of what is required to combat the faint Sun.

Prospects for atmospheric CO_2 are worse in the Hadean, when impact ejecta were important sediments [9]. Impact ejecta are relatively easily chemically weathered and more mafic than more conventional sediments. With more buffering by basic and ultrabasic rocks and more weathering occurring at relatively low temperatures, the CO_2 sink would have been greater and the pH likely higher. Thus impact ejecta tend to draw down CO_2 more than the ocean crust working alone, and the least CO_2 would be left after the largest impacts. The net effect is that we expect relatively little CO_2 in the atmosphere, and so, in the absence of other greenhouse gases (e.g., methane), the oceans freeze over and the planet is cold indeed.

References: [1] Ringwood (1961) *GCA, 21,* 295. [2] Sagan and Mullen (1972) *Nature.* [3] Rye et al. (1995) *Nature, 378,* 603. [4] Zhang and Zindler (1993) *EPSL, 117,* 331. [5] Staudigel et al. (1989) *GCA, 53,* 3091. [6] Schultz and Elderfield (1997) *Philos. Trans. R. Soc. London, A355,* 387. [7] Sansone et al. (1998) *GCA.* [8] Fischer et al. (1998) *EPSL, 160,* 81. [9] Koster van Groos (1987) *JGR, 93,* 8952.

DYNAMICAL SIGNATURES OF LIVING SYSTEMS.

M. Zak, Mail Stop 126-347, Jet Propulsion Laboratory, 4800 Oak Grove Drive, Pasadena CA 91109-8099, USA.

One of the main challenges in modeling living systems is to distinguish a random walk of physical origin (for instance, Brownian motions) from those of biological origin, and that will constitute the starting point of the proposed approach. As conjectured in [1], the biological random walk must be nonlinear. Indeed, any stochastic Markov process can be described by the linear Fokker-Planck equation (or its discretized version); only that type of process has been observed in the inanimate world. However, all such processes always converge to a stable (ergodic or periodic) state, i.e., to the states of a lower complexity and high entropy. At the same time, the evolution of living systems is directed toward a higher level of complexity if complexity is associated with a number of structural variations. The simplest way to mimic such a tendency is to incorporate a nonlinearity into the random walk; then the probability evolution will attain the features of a diffusion equation: the formation and dissipation of shockwaves initiated by small, shallow wave disturbances. As a result, the evolution never "dies"; it produces new and different configurations that are accompanied by an increase or decrease of entropy (the decrease takes place during formation of shockwaves, the increase during their dissipation). In other words, the evolution can be directed "against the second law of thermodynamics" by forming patterns outside of equilibrium in the probability space. Due to that, a specie is not locked up in a certain pattern of behavior: it still can perform a variety of motions, and only the statistics of these motions is constrained by this pattern. It should be emphasized that such a "twist" is based upon the concept of reflection, i.e., the existence of the self-image (adopted from psychology).

The model consists of a generator of stochastic processes that represents the motor dynamics in the form of nonlinear random walks, and a simulator of the nonlinear version of the diffusion equation that represents the mental dynamics.

It has been demonstrated that coupled mental-motor dynamics can simulate emerging self-organization, prey-predator games, collaboration and competition, "collective brain," etc.

References: [1] Zak M. (1999) *Phys. Lett.,* in press.

HYDROLOGIC CONSTRAINTS ON THE LOCALIZATION OF SEDIMENT-HOSTED GOLD ORE BODIES OF SOUTHWESTERN GUIZHOU, CHINA.

C.-B. Zhang and Z.-R. Zhang, Chinese Academy of Sciences, Institute of Geochemistry, 73 Guanshui Road, Guiyang, Guizhou 550002, China.

More than 100 sediment-hosted Au deposits and occurrences of southwestern Guizhou lie near the southern edge of the Yangtze craton, which is composed of crystalline rocks of Proterozoic age overlain mainly by Paleozoic and lower to middle Triassic shallow-marine platform and reef facies carbonates grading southward and eastward into a thick section of interbedded siltstones and turbidite sandstones whose deposits were from the Yunkai Old Land and the Jiangnan Old Land respectively. The rocks were folded and faulted during the Yanshanian orogeny, 65–190 Ma. The south is topographic highs during the Jurassic and Cretaceous. Mineral deposits were mainly located in the breccia horizon at the base of the Longtan Formation of upper Permian, underlain by the massive gray limestone of lower Permian with a kast unconformity at the high-angle fault zones in the Triassic argillaceous limestone interlayered with shale, arkose, and fine-grained turbidite sandstone. No igneous rocks are exposed in the vicinity of the deposits, but vitrinite reflectance measurements for Permian rocks indicate that the rocks were heated to temperatures in the range of 100°–300°C. Primary deposits were formed predominately during Indonesian-Yanshan orogenies, climax period being ~100 Ma or slightly later. Ore-forming fluids were mainly from meteoric water. Hydrologic characteristics show that Longtan Formation is the major impermeable barrier, and lower Trassic shale is secondary, beneath which superhydrostatic regime may develop. Many hydraulic extension fractures are recognized. Numerical simulations suggest that confined aquifer may be formed at the kast unconformity, and ore-bearing hydrothermal solution can flow along fault into the Triassic and then precipitate the metals in the fault zones or the local Triassic aquifers.

References: [1] Ashly R. P. et al. (1991) *Ore Geol. Rev., 6,* 133–151. [2] Baskov E. A. (1987) in *The Fundementals of Paleohydrogeology of Ore Deposits,* Springer-Verlag, Berlin. [3] Cunningham C. G. et al. (1988) *Econ. Geol., 83,* 1462–1467. [4] Garven G. (1995) *Rev. Earth Planet. Sci., 23,* 89–117. [5] Garven G. and Raffensperger J. P. (1997) in *Geochemistry of Hydrothermal Ore Deposits* (H. L. Barnes, ed.), pp. 125–190, Wiley, New York. [6] Srerjensky D. A. and Garren G. (1992) *Nature, 356,* 481–482.

SUBCHRONIC TOXICITY OF RARE EARTH ELEMENTS AND ESTIMATED DAILY INTAKE ALLOWANCE.

H. Zhang, W. F. Zhu, and J. Feng, State Key Laboratory of Environmental Geochemistry, Institute of Geochemistry, Chinese Academy of Sciences, Guiyang 550002, China (zhanghui@ms.gyig.ac.cn).

Introduction: Some important REE toxicological data were obtained previously based on acute- and subchronic toxicity experiments on animals, but these results were indirect and suspectable. This paper focuses the bioeffects of REE on populations from two typical REE-high areas in South Jiangxi, China (region A is a HREE-enriched area and region B is a LREE-enriched area), and also on the estimation of daily REE intake allowance in terms of REE content and distribution in food chains.

Results: The population averages of intelligence quotient of children were 87.43 ± 21.60, 96.78 ± 12.28, and 109.40 ± 19.55 from regions A, B, and C (region C is the normal area), respectively. The significant differences between A and C ($P < 0.01$) and between B and C ($P < 0.05$) were obtained according to t testing. There were not significant differences in latency and interpeak latency of auditory brainstem electric response (ABR) between adults from REE-high area and from the normal area ($P > 0.05$), but different latencies and amplitudes of somatosensory evoked potential (SEP) were observed ($P < 0.05$) [1]. The fact that 15 of 25 adults from region A and 23 of 62 adults from region B had arteriosclerosis of grade I and II indicated that significant difference existed between A and C ($P < 0.01$) and between B and C ($P < 0.05$) [2]. The blood biochemical indices suggested that samples from region B showed an apparent decrease in total serum protein (TSP), albumin (AL), glutamic-pyruvic trabsaminase (GPT), and immunoglobulin A (IgA), and an increase in cholesterol (CHO); samples from region A showed an decrease in TSP, β-globulin (β-G) and an increase in CHO, immunoglobulin M (IgM), as compared with those from region C. The REE contents of water and vegetables from the two REE-high areas and region C were also significantly variable. The average daily intake of REE by an adult was 6.67, 5.98, and 3.33 mg from regions A, B, and C according to the adult recipes of local population [3].

Conclusions: Thus it can be seen from the above that REE will exert effects on central nervous, cardiovascular, and immune systems of the human body. Lanthanum can prevent the nerve ending from taking in glutamic acid in a noncompetitive mode and also inhibit the activity of Ca- and Mg-activated ATP enzymes [4]. These were probably the main factors leading to a significant decrease in the intelligence quotient of children, as well as to the shortening of adult nerve conduction from the median nerve to the thalamus. Since increasing incidence of atherosclerosis (AS) was accompanied with CHO in REE-high areas, it was believed that AS results from REE replacement of the Ca of Ca modulator CaM), interfering with the activity of various CaM-catalyzed enzymes and thus influencing the normal metabolism of fat and protein in liver, spleen, pancreas, and intestine [4]. From the above, we can conclude that the populations who take in 6–6.7 mg REE from food chains per day will suffer from subchronic toxicity, but those who take in 3.33 mg REE per day are relatively normal. Therefore, we define 4.2 mg REE as the daily intake allowance.

References: [1] Zhu W. F. et al. (1997) *Biol. Trace Element Res., 57,* 71–77. [2] Zhu W. F. et al. (1998) *Biol. Trace Element Res., 59,* 93–98. [3] Zhang H. et al. (1999) *Biol. Trace Element Res.,* in press. [4] Evans C. H. (1990) in *Biochemistry of the Lanthanides,* 1st Ed., Plenum Press, New York.

COULD THE LATE PERMIAN, DEEP OCEAN HAVE BEEN ANOXIC?

R. Zhang, M. J. Follows, J. Grotzinger, and J. C. Marshall, Department of Earth, Atmospheric and Planetary Sciences, Room 54-1419, Massachusetts Institute of Technology, Cambridge MA 02139, USA (rong@plume.mit.edu).

It has been suggested that a long-term, deep-sea anoxic event straddled the Permo-Triassic boundary 250 m.y. ago and was indicative of global biogechemical shifts implicated in the end-Permian mass extinction. Here, models of ocean circulation and biogeochemical cycling are used to provide insight into the processes required to induce deep-sea anoxia across the P/T boundary and a physical/biogeochemical context for mass extinction hypotheses. Two possible modes of late Permian ocean thermohaline circulation are identified — a vigorous "thermal mode" driven by cooling in southern polar latitudes and a weaker "haline mode" driven by evaporation from the subtropics. The "haline mode," which may exist in climates with enhanced hydrological cycles and weak diapycnal ocean mixing, can support widespread anoxia in the Panthalassic deep ocean, but the "thermal mode" more typical of climates such as our own cannot. The haline mode is inherently unstable and flips back and forth between the thermal mode with a period of a few thousand years, providing a mechanism for the repeated overturn of anoxic bottom water, as seen, for example, in the anoxic-oxic cycles of the Mid-Cretaceous. Though our calculations suggest a possible mechanism by which a deep stagnant Permian ocean could have become periodically anoxic, it is less clear how that state could have persisted for millions of years.

EXPERIMENTAL DETERMINATION OF THE DEPENDENCE OF WATER SPECIATION ON CONTROLLED COOLING RATE.

Y. Zhang and Z. Xu, Department of Geological Sciences, University of Michigan, Ann Arbor MI 48109-1063, USA (youxue@umich.edu).

This report is a continuation of our earlier study [1] on how H_2O speciation depends on cooling rate and how to quantify the dependence as a geospeedometer. Our earlier work covers cooling rate from 0.01 to 55°C/min and total H_2O content from 0.5 to 3.0 wt%. In this study, we expand the quench rate to 5,000°C/min and total H_2O content to 7.6%. Both for avoiding bubble growth at high H_2O and for generating high controlled quench rates, a piston-cylinder apparatus is used to conduct the experiments at 2–5 kbar. Previous experiments [2] have shown that a pressure of $\leq$5 kbar does not significantly affect the equilibrium speciation. In this study we confirm these results. We tried to improve the pressure reading and the procedure for

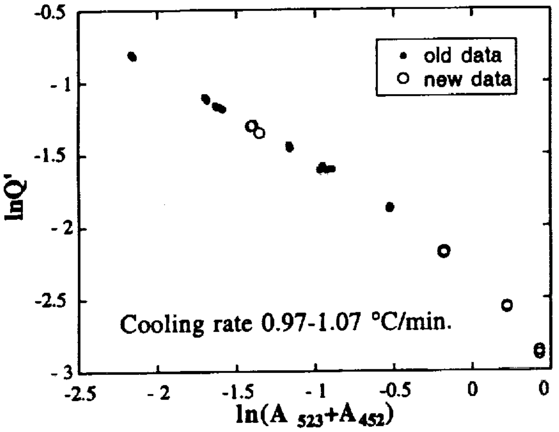

Fig. 1.

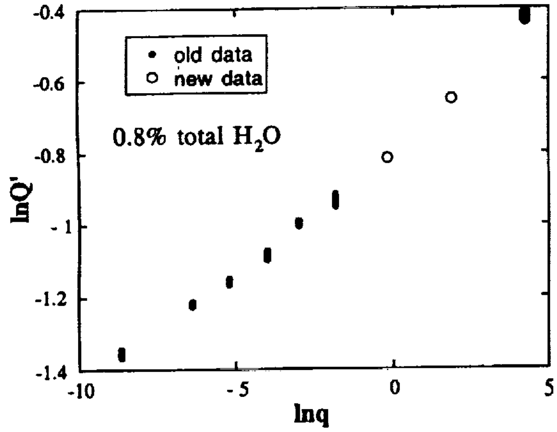

Fig. 2.

generating low pressures (2–5 kbar) in the piston-cylinder apparatus. Cooling rate is obtained from temperature recorded by a computer.

We previously showed [1] that for a given quench rate, there is an excellent linear relation between lnQ' and $\ln(A_{523} + A_{452})$ (where A_{523} and A_{452} are the absorbance of the infrared bands at 5230 and 4520 cm^{-1}/mm sample thickness, $A_{523} + A_{452}$ is a proxy for total H_2O content, and $Q' = A_{452}^2/A_{523}$ is a proxy for the species equilibrium constant K) when total H_2O is ≤3.0%. With new data at high H_2O, the linear relation does not hold anymore (Fig. 1). Furthermore, the linear relation between lnQ' and lnq (q is quench rate in K/s) does not hold at high q (Fig. 2). Hence, extrapolation of the geospeedometry model of Zhang et al. [1] may have large errors, and a new geospeedometry model using data covering a wide range of quench rate and total H_2O is necessary.

Our new data and previous data together cover all natural total H_2O ranges (up to 7.6%), and all currently accessible controlled quench rates (almost 6 orders of magnitude). The data are used to update the geospeedometry model for predicting quench rates of natural hydrous volcanic glasses. Furthermore, quench rates in water, air, and liquid N are quantified using our geospeedometer [3].

References: [1] Zhang et al. (1997) *GCA, 61,* 2167. [2] Zhang (1993) *Eos Trans. AGU, 74F,* 631. [3] Xu and Zhang, this volume.

COMPARATIVE STUDIES OF RARE EARTH ELEMENTS IN GROUNDWATERS AND AQUIFER MATERIALS FROM THE SOUTHERN GREAT BASIN.

X. Zhou[1], K. H. Johannesson[2], K. J. Stetzenbach[1], C. Guo[1], and I. M. Farnham[1], [1]Harry Reid Center for Environmental Studies, University of Nevada, Las Vegas NV 89154-4009, USA (xiaopinz@nevada.edu), [2]Department of Ocean, Earth, and Atmospheric Sciences, Old Dominion University, Norfolk VI 23529-0276, USA (kjohanne@odu.edu).

The rare earth elements (REEs), with their unique and chemically coherent behavior, have been used extensively as sensitive tracers of geochemical processes in rocks, seawater, rivers, and estuarine systems. Recently, REE concentrations and behavior have also been studied in several aquifers [1–3]. These studies have demonstrated that groundwaters can inherit their REE signatures from the rocks or aquifer materials with which they interact [4,5].

In southern Nevada and eastern California, many groundwater samples from springs and wells have been analyzed. Based on different REE signatures, these groundwaters have been classified into carbonate groundwaters and volcanic groundwaters [3]. Some of these groundwaters appear to be mixtures of two of more types of waters from different aquifers [6,7]. Groundwaters from the volcanic rock aquifers of the region, such as Tippipah and Topopah springs on the Nevada Test Site, exhibit distinctive LREE enrichments and substantial negative Eu anomalies for their shale-normalized patterns; however, they do not exhibit Ce anomalies. The carbonate groundwaters have relatively low concentrations of REEs (up to two orders of magnitude lower than volcanic aquifer groundwaters) and show a flat or HREE-enriched pattern after shale-normalization. Also, the carbonate groundwaters, unlike the volcanic groundwaters, have more diverse shale-normalized REE patterns. Some carbonate groundwaters, such as those from Ash Meadows and Death Valley springs, have no or slightly negative Ce anomalies and possibly minor negative Eu anomalies. The shale-normalized REE profiles of both Ash Meadows and Death Valley springs are fairly flat, although slight enrichments of HREEs are observed. Other carbonate groundwaters, such as those from the Spring Mountains, Pahranagat Valley, and Cane Spring, have strong negative Ce anomalies, substantial shale-normalized HREE enrichments, and minor Eu negative anomalies that closely resemble those of seawater [8].

In order to compare REEs in groundwater with those in aquifer materials, and to address the relationship between them, more than 50 rock samples were analyzed for the REEs. These rock samples are representative of rock types from aquifers in southern Nevada and eastern California. Tertiary felsic volcanic rocks from the Nevada Test Site show a fairly strong shale-normalized LREE enrichments with substantial Eu depletion, and no Ce anomalies. The lower Paleozoic (Cambrian and Ordovician) dolomites and dolomitic limestones from Frenchman Mountain, Mercury, Nevada, and Fossil Ridge in the lower Sheep Range, have similar shale-normalized REE patterns except for slight difference in concentrations. None of these lower Paleozoic dolomitic rocks exhibit negative Ce anomalies, and most do not have Eu anomalies. Instead, the shale-normalized REE patterns for these carbonate rocks are quite flat, with only slight LREE or HREE enrichments. However, the upper Paleozoic (Permian) limestones exhibit strong shale-normalized HREE enrichments with large Ce depletions. The shale-normalized REE patterns of these upper Paleozoic limestones are essentially identical to shale-normalized patterns for modern seawater [9,10].

In addition to measuring REE concentrations in the rocks and groundwaters, batch tests were conducted in the laboratory to examine how different rock types may affect the concentration of REEs in the solution. Five types of rock samples (shale, sandstone, limestone, dolomite, and pumice) and pure distilled water (pH = 7) were chosen for this study. The data show that both individual REE concentrations and total REE concentrations in the leachate solutions are very low, ranging from 5×10^{-3} pmol/kg to 40×10^{-3} pmol/kg, and from 0.26 pmol/kg to 6.75 pmol/kg respectively. The solution that reacted with pumice had the highest REE concentrations, whereas the solutions that reacted with Ordovician limestone and with Cambrian dolomite have the lowest REE concentrations. Normalized to shale, the REEs for most of the leachate solutions show fairly flat patterns. However, the leachate solution that reacted with pumice exhibits a slight enrichment in HREEs, while the solution leached from Cambrian sandstone shows a weak MREE enrichment. These batch studies suggest that different types of rocks can impart REE signatures to groundwaters that reflect the original rock REE signatures.

Comparisons of the REE concentrations and behaviors in both groundwaters and aquifer rocks demonstrate that the shale-normalized REE patterns of the carbonate groundwaters and those of the volcanic rock groundwaters resemble the shale-normalized REE patterns of the respective rock types through which they flow. Keeping these results in mind, the REE patterns of groundwaters from Ash Meadows and Death Valley springs suggest that these groundwaters are from lower carbonate aquifer that is chiefly composed of dolomite and dolomitic limestone, whereas the groundwaters from Spring Mountains and Pahranagat Valley are probably from upper carbonate aquifer that is composed of limestones. The negative Ce and Eu anomalies are also correlative between groundwaters and aquifer rocks. In other words, these anomalies reflect the relative Ce and Eu concentration of the whole-rock samples.

References: [1] Smedley P. L. (1991) *GCA, 55,* 2767–2779. [2] Johannesson K. H. et al. (1994) *JH, 154,* 271–289. [3] Johannesson K. H. et al. (1997) *Ground Water, 35,* 807–819. [4] Gosselin D. C. et al. (1992) *GCA, 56,* 1494–1505. [5] Sholkovitz E. R. (1995) *Aquatic Geochem., 1,* 1–34. [6] Winograd I. J. and Thordarson W. (1975) *U.S. Geological Survey Prof. Paper 712-C,* 126 pp. [7] Johannesson K. H. et al. (1997) *GCA, 61,* 3605–3618. [8] Fleet A. J. (1984) in *REE Geochemistry,* pp. 343–373. [9] Elderfield H. and Greaves M. J. (1982) *Nature, 296,* 214–219. [10] Bertram C. J. and Elder-field H. (1993) *GCA, 57,* 1957–1986.

NATURAL VARIATIONS OF IRON AND COPPER ISOTOPES DETERMINED BY PLASMA SOURCE MASS SPECTROMETRY: APPLICATIONS TO GEOCHEMISTRY AND COSMOCHEMISTRY.

X. K. Zhu, N. S. Belshaw, Y. Guo, and R. K. O'Nions, Department of Earth Sciences, University of Oxford, Parks Road, Oxford OX1 3PR, UK.

The determination of natural variations in stable isotopic abundances have provided profound insights into processes operating during the formation of the solar system and the evolution of the Earth. The potential offered by the isotope variations of transitional metals, such as Fe and Cu, however, has been little exploited largely due to the analytical difficulties. The introduction of multiple collector plasma source mass spectrometry has changed the situation dramatically. It is anticipated that important information about the early evolution history of the solar system, biological evolution, and low-temperature processes operating near the Earth's surface offered by the isotopic variations of Fe and Cu are now accessible. We report here the results of a study on Fe and Cu isotopes using multiple collector plasma source mass spectrometry (MC-ICP-MS).

Iron isotopes are measured relative to the IRMM-14 Fe-isotopic standard and are expressed as ε^{57}Fe, which expresses the difference of ^{57}Fe/^{54}Fe ratios between sample and standard in part per 10^4. The external precision for the techniques used is better than 1ε at 2σ level. Iron-rich samples from both terrestrial and extraterrestrial environments have been studied, and an overall variation of 38 in ε^{57}Fe units is observed. Iron meteorites studied ranging from type IA to type IIID are rather homogeneous in Fe-isotopic compositions with ε^{57}Fe values between 0.5 to 3. In contrast, the terrestrial samples studied show large Fe-isotopic variations with ε^{57}Fe values ranging from −27 to +11. It has also been observed that samples of siderite, ferromanganese crust, and chalcopyrite from black smoker sulphide chimneys show ^{57}Fe depletion relative to iron meteorites, whereas samples of hematite, magnetite, and continental chalcopyrite display ε^{57}Fe values that range from positive to negative.

Copper isotopes are determined relative to NIST-976 standard material and are express in ε values as well. The external precision for the techniques used is 0.6ε at 2σ level. A range of samples including native Cu, Cu-carbonate, and chalcopyrite from terrestrial and marine environments have been analyzed. An overall variation of 21 ε units is observed. The variations in ε^{65}Cu values display some interesting regularities. Those samples involving formation through low temperature aqueous solutions show large differences in ε^{65}Cu values event at a single locality, whereas chalcopyrite samples hosted in igneous rocks show similar Cu-isotopic composition worldwide. This indicates that the ε^{65}Cu variation arise principally through mass fractionation in low-temperature aqueous processes, rather than through source heterogeneity.

The natural variations of Fe and Cu isotopes observed in this study are more than 30× the 2σ analytical uncertainties of the techniques employed, and thus demonstrate the great potential for using stable isotopes of Cu and Fe as tracers in geological and planetary processes. These new capability for Cu- and Fe-isotopic measurements is expected to have a major impact across disciplines ranging from cosmochemistry and planetary geochemistry to biogeochemistry and biochemistry.

TERTIARY SEAWATER CHEMISTRY: IMPLICATIONS FROM FLUID INCLUSIONS IN HALITE.

H. Zimmermann, Department of Earth and Planetary Sciences, Harvard University, 20 Oxford Street, Cambridge MA 02138, USA (zimmermann@eps.harvard.edu).

Most reconstructions of the chemistry of seawater during the Phanerozoic are based on the mineralogy of marine evaporites or on the composition of fluid inclusions in such evaporites. This paper reviews and adds to the data for the composition of fluid inclusions in halite from Tertiary marine evaporites in an effort to define the composition of seawater during the past 35 m.y.

Three sets of fluid inclusion data are currently available. The analyses from the oldest Tertiary halites are from the Oligocene (35 Ma) evaporites of the Mulhouse Basin in France [1]. A second set is from the Badenian (15 Ma) evaporites from Eastern Europe [2–4]. The third set derives from Messinian (5 Ma) halites in the Red Sea, in Spain, and in Sicily [5,6].

The composition of none of the inclusion fluids in these evaporites can be explained in terms of the evaporation of modern seawater. Many inclusion brines have been involved in potash mineral precipitation or recycling of evaporites. About one third of the fluid inclusion analyses can be interpreted as evaporated seawater depleted in $MgSO_4$.

The Oligocene inclusion fluids indicate a Mg depletion of 35–38%, which agrees well with the mineralogy of the potash zones in these evaporites. The Badenian inclusion fluids show a Mg depletion of 11–22%, and the Messinian inclusion brines a Mg depletion of 11–17%, which is consistent with the composition of the potash zones in these evaporites.

The $MgSO_4$ depletion of these inclusion fluids is either due to the dolomitization of limestone during the evaporative concentration of modern seawater or to changes in the composition of seawater during the Tertiary, or a combination of these effects. Analyses of fluid inclusions containing nonevaporated seawater are needed to decide on the cause of the observed $MgSO_4$-depletion. Fluid inclusions in marine calcite cements may help to resolve the issue.

References: [1] Canals A. et al. (1993) *Org. Geochem., 20,* 1139–1151. [2] Veigas J. G. et al. (1997) *Slovak Geol. Mag., 3,* 181–186. [3] Galamay A. R. et al. (1997) *Slovak Geol. Mag., 3,* 165–171. [4] Kovalevich V. M. and Petrichenko O. I. (1997) *Slovak Geol. Mag., 3,* 173–180. [5] Kovalevich V. M. et al. (1997) *N. Jb. Mineral. Mh. 1997, 10,* 433–450. [6] Garcia-Veigas J. et al. (1995) *Bull. Soc. Geol. France, 166(6),* 699–710.

STABILITY OF POLYCYCLIC AROMATIC HYDROCARBONS IN THE SOLAR NEBULA.

M. Yu. Zolotov and E. L. Shock, Department of Earth and Planetary Sciences, Washington University, St. Louis MO 63130, USA (zolotov@zonvark.wustl.edu; shock@zonvark.wustl.edu).

Introduction: Polycyclic aromatic hydrocarbons (PAHs) are believed to be among the most abundant organic molecules in space. These compounds have been identified in carbonaceous chondrites [1–2], interplanetary dust particles (IDPs) [3], and presolar grains [4]. PAHs are probably present on the surfaces of asteroids and in the nuclei of comets, and can be the major group of organic compounds in interstellar molecular clouds [5]. In stellar nebulae, PAHs can form in Fischer-Tropsch (FT) type reactions from CO and H_2 on mineral grains [6–9] and in pyrolysis of other hydrocarbons [10]. Some of these processes can also be responsible for PAH synthesis in meteorite parent bodies (asteroids) and their surfaces. Although the relative contribution of each process remains unknown, the nebular FT-type grain-catalyzed synthesis is among the most plausible. Here we first evaluate the stability of condensed PAHs in the solar nebula with respect to FT-type reactions. We explore the effects of pressure, temperature, and the abundances of CO(g) and H_2O(g). Calculated stabilities for PAHs are compared with the observations from meteorites and IDPs.

Model: PAHs and other hydrocarbons are unstable with respect to graphite and methane, and may only exist as metastable phases if the formation of graphite and methane is prohibited [11]. In the solar nebula, such an inhibition could have provided conditions for hydrocarbon synthesis [7,8]. To evaluate the stability of PAHs, we calculate the saturation conditions for P, T, and fugacities of gases for the net equilibria

$$a\ H_2(g) + b\ CO(g) = PAH(\text{solid or liquid}) + b\ H_2O(g) \qquad (1)$$

We assume the activity of condensed hydrocarbons is unity, and the gases behave ideally. The partial pressure of H_2 roughly equals total pressure, and solar-based nominal H_2/CO and H_2/H_2O ratios are 1.4×10^2 and 1.8×10^2 respectively. We considered variations in these ratios based on the composition of comets and changes in the abundances of gases during chemical and physical processes. Two distinct models for P-T conditions for the nebular plane [12,13] are taken into account. To compare with the PAHs, we also evaluate the stability of condensed n-alkanes with respect to reactions like equation (1). Thermodynamic data for hydrocarbons are from [14,15].

Results and Discussion: The calculations show that there is a thermodynamic drive to form PAHs within the stability field of graphite and under conditions where CH_4 would predominate over CO if stable equilibria were reached. At the nominal abundances of CO and H_2O, PAHs can form metastably at temperatures below ~450 K at pressures below ~3×10^{-5} bar depending on the P-T model adopted for the nebula. Low temperatures, high pressures, high-CO abundances, and low-H_2O contents favor hydrocarbon synthesis. A decrease in the abundance of $H_2O(g)$ through ice formation at distances >5.2 AU favors PAH formation. However, taking a lower limit for the CO/H_2O ratio of 0.035, corresponding to the nucleus of Comet Halley [16], hydrocarbons cannot form. Nebular models [12,13] give similar results for hydrocarbon stability.

The energetic drive to form PAHs increases with an increase in C/H ratio in the species. For example, pyrene ($C_{16}H_{10}$) has a higher saturation temperature than either naphthalene (C_8H_{10}) or chrysene ($C_{18}H_{12}$). Pyrene is more stable than methylated pyrenes, but for lower molecular weight compounds (e.g., naphthalene) methylated species have a similar stability with the parent PAH. However, the conditions for PAH saturation are close to one another. Therefore, the formation of a metastable mixture is more likely than formation of a single PAH. Our calculations are consistent with the elevated abundance of pyrene and with the higher degree of alkylation of light PAHs in the Murchison meteorite [1].

The saturation temperatures for PAH are slightly higher than effective temperatures of FT reactions [6,8]. It is likely that the saturation temperatures are high enough to consume a few percent of CO on the surface of Fe-Ni grains during the period of over which the nebula existed (10^5–10^7 yr). The n-alkanes we consider have saturation temperatures 25°–40°C below those of the PAHs, suggesting that their formation could have been inhibited. This is consistent with the predominance of PAHs over other hydrocarbons in meteorites and IDPs. We conclude that there was a thermodynamic drive for FT-type synthesis in the solar nebula that provided an abiotic source for PAHs in solar system.

Acknowledgments: This work was sponsored by the NSF grant CHE-9714060 and NASA grant NAG5-7696.

References: [1] Krishnamurthy R. V. et al. (1992) *GCA, 56,* 4045–4058. [2] Cronin J. R. and Chang S. (1993) in *The Chemistry of Life's Origins,* pp. 209–258. [3] Clemett S. J. et al. (1993) *Science, 262,* 721–723. [4] Messenger S. et al. (1998) *Astrophys. J., 502,* 284–295. [5] Allamandola L. J. et al. (1989) *Astrophys. J., 71,* 733–775. [6] Anders E. et al. (1973) *Science, 182,* 781–790. [7] Prinn R. G. and Fegley B. Jr. (1989) in *Origin and Evolution of Planetary and Satellite Atmospheres,* pp. 78–136. [8] Fegley B. Jr. (1993) in *The Chemistry of Life's Origins,* pp. 75–147. [9] Llorca J. and Casanova I. (1998) *MAPS, 33,* 243–251. [10] Morgan W. A. Jr. et al. (1991) *Science, 252,* 109–112. [11] Eck R. V. et al. (1966) *Science, 153,* 628–633. [12] Lewis S. J. (1974) *Science, 186,* 440–443. [13] Cameron A. G. W. (1995) *Meteoritics, 30,* 133–161. [14] Richard L. and Helgeson H. C. (1998) *GCA, 62,* 3591–3636. [15] Helgeson H. C. et al. (1998) *GCA, 62,* 985–1081. [16] Eberhardt P. (1998) in *Asteroids, Comets, Meteors 1996,* COSPAR Coll. 10.